

Flow Measurement Engineering Handbook

THIRD EDITION



RICHARD W. MILLER

LIST OF SYMBOLS

Symbol and meaning	U.S. units	SI units†
a Constant in Hall-Yarborough equation of state		
a Constant in specific-heat equation	Btu/(lb _m ·mol·°R)	J*/(kg·mol·K)
a Constant in gas viscosity equation		
a_s Acceleration along a stream tube	ft/s ²	m/s ²
A Area	ft ²	m ²
A_a Annular area between float and tapered wall of a variable-area flowmeter	ft ²	m ²
A_p Deadweight-tester piston area	in ²	mm ²
A_t Throat area of a critical nozzle	ft ²	m ²
A_f Effective area of float in a variable-area flowmeter	ft ²	m ²
A_p Pipe area	ft ²	m ²
Acc Accuracy, combined precision and bias errors	%	%
(Acc) _{ref} Reference-condition accuracy	%	%
A_{plate} Plate area in viscosity derivation equation	ft ²	m ²
A Constant in Redlich-Kwong equation of state		
A Constant in Ostwald power-law equation		
A_L Constant in liquid viscosity equation		
b Constant in Hall-Yarborough equation of state		
b Constant in equation for specific heat at constant pressure		
b Constant in general form of discharge-coefficient equation		
b_c Slope constant in liquid-bulk-modulus equation		
b_p Frequency coefficient for pulsating flow		

†Except for dimensionless or defined SI unit symbols, as in T_K , symbols that apply to SI units are shown in the text with a superscript asterisk, as in F_a^* .

Symbol and meaning	U.S. units	SI units†
B Second virial coefficient in an equation of state		
B Directional bias error	%	%
B_{var} Directional bias error, where subscript var (variable) is denoted as q , G_F , G_b , Z , etc.		
$\pm B$ Bias-error range	%	%
B_{allow} Allowable bias error in a comparison test		
$\pm B_{\text{var}}$ Bias-error range, where subscript var (variable) is denoted as q , G_b , G_F , Z , etc.		
B_C Directional bias error in the discharge coefficient		
B_f Magnetic flux density	G	T
B_{ij} Binary mixture term in AGA-8 equation		
B Constant in Redlich-Kwong equation of state		
B_L Constant in liquid-viscosity equation		
c Constant in liquid-density equation	(°F) ⁻¹	
c Constant in Hall-Yarborough equation of state		
C_p Specific heat at constant pressure	Btu/(lb _m ·mol·°R)	J*/(kg·mol·K)
$(C_p)_i$ Specific heat at constant pressure for ideal gas	Btu/(lb _m ·mol·°R)	J*/(kg·mol·K)
$C_{p,\text{mix}}$ Specific heat at constant pressure of a gas mixture	Btu/(lb _m ·mol·°R)	J*/(kg·mol·K)
$(C_p)_p$ Specific heat at constant pressure of a perfect gas	Btu/(lb _m ·mol·°R)	J*/(kg·mol·K)
C_p/C_v Ratio of specific heats of a real gas		
$(C_p/C_v)_i$ Ratio of specific heats of an ideal gas		
$(C_p/C_v)_p$ Ratio of specific heats of a perfect gas		
C_v Specific heat of a gas at constant volume	Btu/(lb _m ·mol·°R)	J*/(kg·mol·K)
C Discharge coefficient, true flow rate divided by theoretical flow rate		
C_c Coefficient of contraction		
C_∞ Discharge coefficient at infinite Reynolds number		

†Except for dimensionless or defined SI unit symbols, as in T_K , symbols that apply to SI units are shown in the text with a superscript asterisk, as in F_a^* .

Symbol and meaning	U.S. units	SI units†
C_{DH} Discharge coefficient for a drain (vent) hole through a primary element		
C_N Discharge coefficient at normal flowing conditions		
C_{cond} Discharge coefficient following a nonstandard installation condition		
C_{max} Discharge coefficient at $R_D = 10^4$ for an eccentric orifice		
C_{min} Discharge coefficient at $R_D = 10^4$ for an eccentric orifice		
C_{mp} Mean molecular heat of a pure gas	(°F) ⁻¹	(°C) ⁻¹
$C_{mp,\text{mix}}$ Mean molecular heat at constant pressure of a gas mixture	(°F) ⁻¹	(°C) ⁻¹
C_{WA} Temperature correction factor in Hall-Yarborough equation of state	°R	K
d Constant in Hall-Yarborough equation of state		
d Bore of differential producer at flowing conditions $d = F_{ad} d_{\text{meas}}$	in	mm
d_f Bore of differential producer at flowing conditions corrected for both temperature and pressure, $d = F_{ad} F_{\Delta p} d_{\text{meas}}$	in	mm
$d_{f,\text{equiv}}$ Equivalent bore for a segmental orifice at flowing conditions	in	mm
d_h Pressure-tap-hole diameter	in	mm
d_{meas} Bore of a differential producer <i>measured</i> at a reference temperature, usually 68°F (20°C)	in	mm
d_w Diameter of a thermal well or other protrusion into a pipe	in	mm
d_T Target (disk) diameter	in	mm
d_{DH} Diameter of a drain or vent hole	in	mm
d_M Differential producers bore at flowing conditions		m
D Internal pipe diameter at flowing conditions $= F_{aD} d_{\text{meas}}$	in	mm
D_c Diameter of circle containing the segment of a segmental orifice	in	mm
D_f Pipe diameter at flowing pressure and temperature	in	m
D_F Bore of differential producer at flowing conditions $D_F = F_{aD} d_{\text{meas}}$	ft	
D_{meas} Pipe diameter (or upstream venturi inlet diameter) <i>measured</i> at a reference temperature, usually 68°F (20°C)	in	mm

†Except for dimensionless or defined SI unit symbols, as in T_K , symbols that apply to SI units are shown in the text with a superscript asterisk, as in F_K^* .

Symbol and meaning		U.S. units	SI units†
D_M	Bore of differential producer at flowing conditions $D_M^* = F_{aD}^* D_{M, \text{meas}}^*$		m
e	Enthalpy	Btu/lb _m	J*/kg
e_s	Magnetic-flowmeter signal voltage	V	V
E	Velocity-of-approach factor, $1/\sqrt{1 - \beta^4}$		
E_p	Modulus of elasticity for the pipe material	lb _f /in ²	Pa
E_{PE}	Modulus of elasticity for the primary-element material	lb _f /in ²	Pa
f	Friction factor in Darcy-Weisbach equation		
f	Constant in Hall-Yarborough equation of state		
f_f	Fanning friction factor		
$(f)_c$	Ryan-Johnson critical friction factor for power law fluids		
f_{Hz}	Frequency	Hz	Hz
$(f_{Hz})_{CW}$	Constant wave frequency	Hz	Hz
$(f_{Hz})_{DN}$	Downstream frequency of sonic pulses	Hz	Hz
$(f_{Hz})_{UP}$	Upstream frequency of sonic pulses	Hz	Hz
Δf_{Hz}	Frequency difference	Hz	Hz
F	Function used in Newton's solution		
F'	Derivative of function in Newton's solution of a zero root equation		
F_a	Thermal-expansion-factor correction for differential producers	in/(in·°F)	mm/(mm·°C)
F_{ad}	Thermal expansion factor for the bore of the primary element		
F_{aD}	Thermal expansion factor for the pipe diameter		
F_k	Correction for real gas in an isentropic expansion		
F_g	Specific-gravity factor in gas-factor equation, $\sqrt{1/G}$		
F_{Gr}	Specific-gravity factor in gas factor equation, $\sqrt{1/G_r}$		
F_p	Correction for liquid compressibility, ρ_f/ρ_F		
F_{pv}	Supercompressibility factor, $Z_b/\sqrt{Z_f}$		

†Except for dimensionless or defined SI unit symbols, as in T_K , symbols that apply to SI units are shown in the text with a superscript asterisk, as in F_a^* .

Symbol and meaning	U.S. units	SI units†
$F_{pv,Gr}$	Supercompressibility factor based on real gravity G_r , $\sqrt{Z_b/Z_f}$	
F_B	Bias-error correction factor, $(1 + B/100)^{-1}$	
$F_{B,var}$	Bias-error correction factor, where subscript var (variable) is denoted as q , G_b , G_F , Z , etc.	
F_C	Bias error correction for a differential producer	
F_K	Flow-coefficient Reynolds-number correction, K/K_{ref}	
F_L	Local gravity correction, g_i/g_c	lb _f /lb _m
F_M	Manometer correction factor	
F_P	Flow-rate correction for pulsating flow	
F_T	Target (disk) force, target flowmeter	lb _f
F_Y	Gas-expansion-factor correction, Y/Y_N	
F_{Dp}	Flowing pressure correction factor for pipe diameter	
F_{DH}	Drain-hole (vent-hole) correction factor	
F_{EL}	Elevation correction for gas-filled leads	
F_{FB}	Buoyancy correction factor for force determination	
F_{MB}	Buoyancy correction factor for mass determination	
F_{MC}	Meter coefficient factor, including all unmeasured variables	
F_{pb}	Pressure base correction factor gas factor equation, $14.73/p_b$	
F_{PB}	Pressure base correction in gas factor equation, $14.69595/p_b$	
F_{RF}	Recovery factor for dynamic pressure	
$F_{\rho b}$	Pressure base correction factor gas factor equation, $14.73/p_b$	
F_{PB}	Pressure base correction in gas factor equation, $14.69595/p_b$	
F_{tb}	Temperature base correction factor in gas factor equation, $T_b/519.67$ or $T_{kb}/288.7056$	
F_{TB}	Base-temperature correction factor in gas-factor equation, $T_b/518.67$ or $T_{kb}/288.15$	

†Except for dimensionless or defined SI unit symbols, as in T_K , symbols that apply to SI units are shown in the text with a superscript asterisk, as in F_{a^*} .

Symbol and meaning		U.S. units	SI units†
F_{tf}	Temperature correction factor in gas factor equation, $\sqrt{519.67/T_{f1}}$ or $\sqrt{288.7056/T_{K1}}$		
F_{TF}	Flowing-temperature correction factor in gas factor equation, $\sqrt{518.67/T_f}$ or $\sqrt{288.15/T_K}$		
F_{TP}	Factor correcting static pressure to total pressure		
F_{VA}	Factor correcting variable-area-flowmeter reading from design conditions to flowing conditions		
$F_{WV,dry}$	Factor converting wet-gas volume to dry-gas volume		
$F_{WVM,dry}$	Factor converting wet-gas mass to dry-gas mass		
F_X	Wet-steam or saturated-liquid quality correction factor		
F_{ARC}	Pen-arc correction for a radial planimeter		
$F_{N,l}$	Net force exerted by a liquid	lb _f	N
$F_{N,m}$	Net force exerted by a mass	lb _f	N
F_{plate}	Plate force in viscosity derivation equation	lb _f	N
$F_{\Delta p}$	Orifice plate correction for applied differential		
$F_{\gamma p}$	Correction for pressure to specific heat at constant pressure		
$F_{\gamma R}$	Real-gas correction factor to ratio of specific heats		
$F_{\mu\rho}$	Viscosity pressure-correction factor for an oil or gas		
g	Constant in Hall-Yarborough equation of state		
g_c	Dimensional conversion constant, 32.17405 lb _m ·ft/(lb _f ·s ²) or 1 kg·m/(N·s ²)	lb _m ·ft/(lb _f ·s ²)	kg·m/(N·s ²)
g_{calib}	Local gravity at which a device is calibrated	ft/s ²	m/s ²
g_l	Local gravitational constant	ft/s ²	ms/s ²
g_0	Standard acceleration due to gravity, 32.17405 ft/s ² or 9.806650 m/s ²	ft/s ²	m/s ²
G	Gas (vapor) specific gravity, $M_{w,gas}/M_{w,air}$		
G_b	Liquid base specific gravity, $\rho_b/(\rho_w)_{60,g_0}$		

†Except for dimensionless or defined SI unit symbols, as in T_K , symbols that apply to SI units are shown in the text with a superscript asterisk, as in F_o^* .

Symbol and meaning		U.S. units	SI units†
G'_b	Liquid base specific gravity at a hydrometer temperature other than 60°F (15.6°C)		
G_f	Flowing specific gravity of a liquid, $\rho_f/(\rho_w)_{60,g0}$		
G_{fl}	Specific gravity of float in a variable-area flowmeter, $\rho_{fl}/62.3663$ or $\rho_{fl}^*/999.012$		
G_{wv}	Specific gravity of water vapor, 0.6220		
G_{dry}	Specific gravity of dry gas in a gas-water vapor mixture		
G_{mix}	Specific gravity of a gas mixture, $M_{w,mix}/M_{w,air}$		
G_{wet}	Specific gravity of a gas mixed with water vapor		
G_F	Flowing liquid specific gravity uncorrected for pressure, $\rho_F/(\rho_w)_{60,g0}$		
G_R	real specific gravity of a gas, ρ_{gas}/ρ_{air}		
G_{SM}	Shear modulus of a solid	lb _f /in ²	N/m ²
h	Frontal width of an Annubar	in	m
h_i	Permanent pressure loss in inches of water	in	
h_s	Step height between mating pipe	in	mm
h_w	Differential pressure in inches of water at 68°F, 14.696 psia, and $g_0 = 32.17405 \text{ ft/s}^2$		
$h_{w,60^\circ}$	Differential pressure in inches of water at 60°F, 14.696 psia, in and $g_0 = 32.17405 \text{ ft/s}^2$		
$(h_w)_g$	Differential produced by gas phase in two-phase (or two-component) flow	in	
$(h_w)_{ss}$	Steady-state differential pressure in pulsating flow	in	
$(h_w)_{ind}$	Indicated differential pressure, uncorrected for fluid head in lead lines	in	
$(h_w)_{max}$	Maximum differential-pressure amplitude in pulsating flow	in	
$(h_w)_{min}$	Minimum differential-pressure amplitude in pulsating flow		
$(h_w)_N$	Differential pressure at normal operating flow rate	in	

†Except for dimensionless or defined SI unit symbols, as in T_K , symbols that apply to SI units are shown in the text with a superscript asterisk, as in F_a^* .

Symbol and meaning	U.S. units	SI units†
$(h_w)_{URV}$ Upper-range value of differential pressure corresponding to upper-range flow rate	in	
h_F Vortex-element barrier width	ft	m
H Manometer reading	ft	
H_0 Null hypotheses for test result due to chance		
H_1 Outside specification set by null hypotheses		
H_s Segmental-orifice segment height	in	mm
H_L Pressure loss in feet of flowing fluid	ft	
H_{EL} Elevation above a datum	ft	m
H_{LL} Lead-line pressure-tap elevation above a dry- or wet-type differential-pressure measuring device	ft	m
HP Horsepower	500 ft·lb _f /s	
i i th data point in a series of points		
I_i Indicated value of a measurement		
I_t True value of a measured variable		
$(I\%)_i$ Percentage difference between indicated value and average of indicated values	%	%
I Average of indicated values		
I_P Pulsation index		
I_{PT} Threshold pulsation index		
J Joules: energy, work, quantity of heat	ft·lb _f /Btu	N·m
k Isentropic exponent for a real gas		
k_i Ideal-gas isentropic exponent $(C_p/C_v)_i$		
k_p Perfect-gas isentropic exponent $(C_p/C_v)_p$		
k_1, k_2, k_3, \dots Constants		
k_{FS} Combined constant for a falling-sphere viscometer		
K Flow coefficient, $C/\sqrt{1-\beta^4} = EC$		
K_∞ Flow coefficient at infinite Reynolds number		
K_{ref} Flow coefficient at reference Reynolds number		
K_N Flow coefficient at normal operating Reynolds number		
K_{BM} Liquid bulk modulus	lb _f /in ²	N/m ²

†Except for dimensionless or defined SI unit symbols, as in T_K , symbols that apply to SI units are shown in the text with a superscript asterisk, as in F_a^* .

Symbol and meaning		U.S. units	SI units†
\bar{K}_{BM}	Liquid average bulk modulus	lb _f /in ²	N/m ²
K_{BMO}	Liquid bulk modulus at zero pressure, zero intercept	lb _f /in ²	N/m ²
K_{FC}	Permanent pressure-loss coefficient for flow conditioners in inches of water	(in·ft·s ²)/lb _m	
$K_{FC,H}$	Permanent pressure-loss coefficient for flow conditioners, in feet of flowing fluid	(lb _f ·s)/(ft ² ·lb _m)	
$K_{FC,\Delta P}$	Permanent pressure-loss coefficient for flow conditioners		
K_{LT}	Permanent pressure-loss coefficient for a target flowmeter	1/in ²	1/m ²
K_{UF}	Flow coefficient for ultrasonic flowmeter		
$K_{F,v}$	K factor for pulse-type flowmeter; subscript v may be gal, ft ³ , m ³ , l, etc.	pulses/ v	pulses/ v
$\bar{K}_{F,v}$	Mean K factor for pulse-type flowmeter; subscript v may be gal, ft ³ , m ³ , l, etc.	pulses/ v	pulses/ v
$(K_{F,v})_{\text{calib}}$	Laboratory determined K factor for pulse-type meter; subscript v may be gal, ft ³ , m ³ , l, etc.	pulses/ v	pulses/ v
$(K_{F,v})_{\text{flow}}$	K factor at flowing conditions	pulses/ v	pulses/ v
$(K_{F,v})_{\text{max}}$	Maximum value of K factor over designated linear range	pulses/ v	pulses/ v
$(K_{F,v})_{\text{min}}$	Minimum value of K factor over designated linear range	pulses/ v	pulses/ v
$K_{MF,v}$	Meter factor for pulse-type meter; subscript v may be gal, ft ³ , m ³ , l, etc.	v /pulse	v /pulse
$(K_{MF,v})_{\text{max}}$	Maximum value of meter factor over designated linear range	v /pulse	v /pulse
$(K_{MF,v})_{\text{min}}$	Minimum value of meter factor over designated linear range	v /pulse	v /pulse
$\bar{K}_{MF,v}$	Mean meter factor for pulse-type flowmeters; subscript v may be gal, ft ³ , m ³ , l, etc.	v /pulse	v /pulse
K_0, K_1	Constants in API 2054 liquid-petroleum equation		
K_{Pitot}	Pitot tube coefficient		
K_{VA}	Flow coefficient for a variable-area flowmeter		
l_1	Upstream tap length at a reference temperature	in	m

†Except for dimensionless or defined SI unit symbols, as in T_K , symbols that apply to SI units are shown in the text with a superscript asterisk, as in F_a^* .

Symbol and meaning		U.S. units	SI units†
l_2	Downstream tap length at a reference temperature	in	m
l_{1f}	Upstream tap length corrected for flowing temperatures	in	m
l_{2f}	Downstream tap length corrected for flowing temperature	in	m
\bar{L}	Linearity percentage about mean K factor	%	%
L	Development length for velocity profile	ft	m
L_p	Path length for a sonic pulse in an ultrasonic flowmeter	ft	m
L_s	Length of straight pipe following a step between two pipes	ft	m
LC	Lu-diagram ordinate value for liquid-compressibility determination		
L_1	Dimensionless ratio l_{1f}/D_f for upstream tap location		
L_2	Dimensionless ratio l_{2f}/D_f for downstream tap location		
m	Mass	lb _m	kg
m	Exponent in specific-heat equation		
m	Exponent in Ostwald power-law fluid equation		
m_i	Mass of liquid	lb _m	kg
M	M factor in Reynolds-number correction factor F_{RD} with discharge coefficient C		
M_K	M factor in Reynolds-number correction factor F_{RD} with flow coefficient K		
M_w	Molecular weight	lb _m /(lb _m ·mol)	kg/(kg·mol)
$M_{w,\text{air}}$	Molecular weight of air, 29.96247	lb _m /(lb _m ·mol)	kg/(kg·mol)
$M_{w,\text{gas}}$	Molecular weight of a gas	lb _m /(lb _m ·mol)	kg/(kg·mol)
$M_{w,\text{mix}}$	Molecular weight of a gas mixture	lb _m /(lb _m ·mol)	kg/(kg·mol)
MV	Measured variable; pressure, temperature, flow rate, etc.		
$(MV)_{\text{LRV}}$	Lower-range value of measured variable		
$(MV)_{\text{URV}}$	Upper-range value of measured variable		
n	Number of moles		

†Except for dimensionless or defined SI unit symbols, as in T_K , symbols that apply to SI units are shown in the text with a superscript asterisk, as in F_a^* .

Symbol and meaning	U.S. units	SI units†
n Exponent in gas viscosity equation		
n Exponent in specific heat equation		
n Exponent in power-law velocity profile equation		
n Number of data points		
n Coefficient in Pai velocity profile equation		
N Exponent in Goldhammer density equation		
N_t Time correction for hours planimeter, chart hours ÷ planimetered hours		
N_{vG} N factor for flowing volume with specific-gravity determination, liquids		
N_{vp} N factor for flowing volume with density determination, liquids and gases (vapors)		
N_{vhp} N factor for flowing volume in gas-factor equation		
N_{vpT} N factor for flowing volume in p_vT equation		
N_{MG} N factor for mass flow with a specific-gravity determination, liquids		
N_{Mp} N factor for mass flow with a density determination, liquids and gases (vapors)		
N_{Mhp} N factor for mass flow, gas-factor equation		
N_{MpT} N factor for mass flow, p_vT equation		
N_{VG} N factor for base volume with specific-gravity determination; liquids at 60°F (15.6°C) and 14.696 psia (101.325 kPa)		
N_{vp} N factor for base volume with density determination, liquids and gases (vapors)		
N_{vhp} N factor for standard (ISO 5024) gas base volume, gas factor equation; $p_b = 14.69595$ psia ($p_b^* = 101.325$ kPa), $T_b = 518.67^\circ\text{R}$ ($T_{kb} = 288.15$ K)		

†Except for dimensionless or defined SI unit symbols, as in T_K , symbols that apply to SI units are shown in the text with a superscript asterisk, as in F_u^* .

Symbol and meaning	U.S. units	SI units†
$(N_{V_{hp}})_b$	N factor for nonstandard base volume at selected base pressure and temperature, gas-factor equation	
N_{vpT}	N factor for standard (ISO 5024) gas base volume, pvT equation; $p_b = 14.69595$ psia ($p_b^* = 101.325$ kPa), $T_b = 518.67^\circ\text{R}$ ($T_{kb} = 288.15$ K)	
$(N_{vpT})_b$	N factor for nonstandard base volume at selected base pressure and temperature, pvT equation	
p_b	Base absolute pressure for gas volume	lb _f /in ² kPa
p_c	Critical absolute pressure of a substance	lb _f /in ² kPa
$p_{c,\text{atm}}$	Critical pressure, in atmospheres	
p_{ca}	Pseudocritical absolute pressure, Hall-Yarborough equation of state	lb _f /in ² kPa
p_d	Pressure of dry gas in a wet gas mixture	lb _f /in ² kPa
p_f	Absolute pressure at flowing conditions	lb _f /in ² kPa
p_{f1}	Upstream-tap absolute pressure at flowing conditions	lb _f /in ² kPa
$p_{f1'}$	Upstream pressure before upstream pressure tap	lb _f /in ² kPa
p_{f2}	Downstream-tap absolute pressure at flowing conditions	lb _f /in ² kPa
$p_{f2'}$	Downstream pressure after pressure recovery	lb _f /in ² kPa
p_{f3}	Fully recovered downstream pressure	lb _f /in ² kPa
$(p_f)_{\text{des}}$	Absolute pressure at design flowing conditions	lb _f /in ² kPa
p_{pc}	Gas (vapor) mixture pseudocritical absolute pressure	lb _f /in ² kPa
p_{pr}	Gas (vapor) mixture pseudocritical reduced pressure ratio, p_f/p_{pc}	
p_r	Reduced absolute pressure of a gas (vapor), p_f/p_c	
p_t	Critical-nozzle throat absolute pressure	lb _f /in ² kPa
p_v	Vapor pressure	lb _f /in ² kPa

†Except for dimensionless or defined SI unit symbols, as in T_K , symbols that apply to SI units are shown in the text with a superscript asterisk, as in F_a^* .

Symbol and meaning		U.S. units	SI units†
p_{wv}	Absolute pressure of water vapor in gas-water vapor mixture	lb _f /in ²	kPa
p_{sat}	Saturation pressure corresponding to flowing temperature	lb _f /in ²	kPa
p_{rsat}	Reduced saturation pressure, p_{sat}/p_c		
p_B	Barometric pressure	lb _f /in ²	kPa
p_G	Gauge pressure, $p_f - p_B$	lb _f /in ²	kPa
$(\Delta p^*)_g$	Differential pressure of gas phase in two-phase or two-component flow		kPa
$(\Delta p^*)_l$	Permanent pressure loss		kPa
$(\Delta p^*)_N$	Differential pressure at normal operating conditions		kPa
$(\Delta p^*)_{\text{URV}}$	Upper-range value of differential pressure corresponding to upper-range flow rate		kPa
P_f	Absolute pressure at flowing conditions	lb _f /ft ²	Pa
$P_{f,\text{Pa}}$	Flowing pressure, in pascals		Pa
P_{f1}	Upstream-tap absolute pressure at flowing conditions	lb _f /ft ²	Pa
P_{f2}	Downstream-tap absolute pressure at flowing conditions	lb _f /ft ²	Pa
$P_{f1'}$	Upstream-tap absolute pressure at lead-line evaluation H_{LL}	lb _f /ft ²	Pa
$P_{f2'}$	Downstream-tap absolute pressure at lead-line evaluation H_{LL}	lb _f /ft ²	Pa
$P_{\text{sat,Pa}}$	Saturation pressure corresponding to flowing temperature, in pascals		Pa
P_{vap}	Vapor pressure	lb _f /ft ²	Pa
P_t	Critical-nozzle throat absolute pressure	lb _f /ft ²	Pa
$(P_{\text{rdg}})_{MV}$	Measured-variable planimeter reading; pressure, temperature, flow rate, etc.		
$(P_{\text{rdg}})_0$	Circular-chart inner-radius planimeter reading		
P_B	Barometric pressure	lb _f /ft ²	Pa
P_D	Dynamic pressure, $\rho_f V_p^2/2g_c$ or $\rho_f^* V_p^{*2}/2$	lb _f /ft ²	Pa
P_G	Gauge pressure, $P_f - P_B$	lb _f /ft ²	Pa

†Except for dimensionless or defined SI unit symbols, as in T_K , symbols that apply to SI units are shown in the text with a superscript asterisk, as in F_a^* .

Symbol and meaning		U.S. units	SI units†
P_T	Total (stagnation) pressure, $P_f + P_D$	lb _f /ft ²	Pa
ΔP	Differential pressure, $P_{f1} - P_{f2}$	lb _f /ft ²	Pa
$(\Delta P)_{\text{ind}}$	Indicated differential pressure, $P'_{f1} - P'_{f2}$	lb _f /ft ²	Pa
$(q)_{\text{URV}}$	Flow-rate upper-range value in mass or volume units		
$q_{\text{gpm, Equiv}}$	Equivalent water flow-rate in flowing gallons per minute	gal/min	
q_{ind}	Indicated flow rate		
q_{true}	True flow rate corrected for directional bias		
q_v	Volumetric flow rate at flowing conditions; subscript v may be cfs, cfh, gpm, lpm, etc.		
$q_{\text{acfs}}, q_{\text{acfm}},$ $q_{\text{acfh}}, q_{\text{acfd}}$	Gas (vapor) volumetric flow rate at flowing conditions	ft ³ /s, ft ³ /min, ft ³ /h, ft ³ /24h	
$q_{\text{acms}}^*, q_{\text{acmm}}^*,$ $q_{\text{acmh}}^*, q_{\text{acmd}}^*$	Gas (vapor) volumetric flow rate at flowing conditions		m ³ /s, m ³ /min, m ³ /h, m ³ /24h
$q_{\text{alps}}^*, q_{\text{alpm}}^*,$ $q_{\text{alph}}^*, q_{\text{alpd}}^*$	Gas (vapor) volumetric flow rate at flowing conditions		L/s, L/min, L /h, L/24h
$q_{\text{bps}}, q_{\text{bpm}},$ $q_{\text{bph}}, q_{\text{bpd}}$	Liquid volumetric flow rate at flowing conditions	bbl/s, bbl/min, bbl/h, bbl/24h	
$q_{\text{cfs}}, q_{\text{cfm}}, q_{\text{cfh}},$ q_{cfd}	Liquid volumetric flow rate at flowing conditions	ft ³ /s, ft ³ /min, ft ³ / h, ft ³ /24h	
$q_{\text{cms}}^*, q_{\text{cmm}}^*,$ $q_{\text{cmh}}^*, q_{\text{cmd}}^*$	Liquid volumetric flow rate at flowing conditions		m ³ /s, m ³ /min, m ³ /h, m ³ /24h
$q_{\text{lps}}^*, q_{\text{lpm}}^*,$ $q_{\text{lph}}^*, q_{\text{lpd}}^*$	Liquid volumetric flow rate at flowing conditions		L/s, L/min, L/h, L/24h
$(q_v)_{\text{av}}$	Average of maximum and minimum volumetric flow rates in pulsating flow		
$(q_v)_{\text{max}}$	Maximum volumetric flow rate in pulsating flow		
$(q_v)_{\text{min}}$	Minimum volumetric flow rate in pulsating flow		
q_M	Mass flow rate: subscript M may be PPH, KPD, KPS, etc.		
$q_{\text{KPS}}^*, q_{\text{KPM}}^*,$ $q_{\text{KPH}}^*, q_{\text{KPD}}^*$	Liquid, gas (vapor) mass flow rate		kg/s, kg/min, kg/h, kg/24h
$q_{\text{PPS}}, q_{\text{PPM}},$ $q_{\text{PPH}}, q_{\text{PPD}}$	Liquid, gas (vapor) mass flow rate	lb _m /s, lb _m /min, lb _m /h, lb _m /24h	
$(q_M)_{\text{TC}}$	Mass flow rate of two-component or two-phase liquid-gas (vapor) mixture; subscript may be PPS, PPH, KPS, etc.		

†Except for dimensionless or defined SI unit symbols, as in T_K , symbols that apply to SI units are shown in the text with a superscript asterisk, as in F_u^* .

Symbol and meaning	U.S. units	SI units†
q_v	Volumetric flow rate calculated at standard (gas) or base (liquid) temperature and pressure	
$(q_v)_b$	Gas (vapor) volumetric flow rate calculated at selected base pressure and temperature	
$q_{BPS}, q_{BPM},$ q_{BPH}, q_{BPD}	Liquid volumetric flow rate at $T_F = 60^\circ\text{F}$ and $p_b = 14.696$ psia	bbl/s, bbl/min, bbl/h, bbl/24h
$q_{CFS}, q_{CFM},$ q_{CFH}, q_{CFD}	Liquid volumetric flow rate at $T_F = 60^\circ\text{F}$ and $p_b = 14.696$ psia	ft ³ /s, ft ³ /min, ft ³ /h, ft ³ /24h
$q_{GPS}, q_{GPM},$ q_{GPH}, q_{GPD}	Liquid volumetric flow rate at $T_F = 60^\circ\text{F}$ and $p_b = 14.696$ psia	gal/s, gal/min, gal/h, gal/24h
$q_{LPH}^*, q_{LPM}^*,$ q_{LPH}^*, q_{LPD}^*	Liquid volumetric flow rate at $T_c = 15.6^\circ\text{C}$ and $p_b^* = 101.3$ kPa	L/s, L/min, L/h, L/24h
$q_{SCFS}, q_{SCFM},$ q_{SCFH}, q_{SCFD}	Standard gas (vapor) volumetric flow rate at ISO-5024 base; $T_b = 518.67^\circ\text{R}$ and $p_b = 14.69595$ psia	ft ³ /s, ft ³ /min, ft ³ /h, ft ³ /24h
$\left. \begin{matrix} (q_{SCFS})_b, \\ (q_{SCFM})_b, \\ (q_{SCFH})_b, \\ (q_{SCFD})_b \end{matrix} \right\}$	Standard gas (vapor) volumetric flow rate at selected base temperature and pressure	$\left\{ \begin{matrix} \text{ft}^3/\text{s}, \\ \text{ft}^3/\text{min}, \\ \text{ft}^3/\text{h}, \\ \text{ft}^3/24\text{h} \end{matrix} \right\}$
$q_{SCMS}^*,$ $q_{SCMM}^*,$ q_{SCMH}^*, q_{SCMD}^*	Standard gas (vapor) volumetric flow rate at ISO-5024 base: $T_{kb} = 288.15$ K and $p_b^* = 101.325$ kPa	m ³ /s, m ³ /min, m ³ /h, m ³ /24h
$\left. \begin{matrix} (q_{SCMS})_b, \\ (q_{SCMM})_b, \\ (q_{SCMH})_b, \\ (q_{SCMD})_b \end{matrix} \right\}$	Standard gas (vapor) volumetric flow rate at selected base temperature and pressure	$\left\{ \begin{matrix} \text{m}^3/\text{s}, \\ \text{m}^3/\text{min}, \\ \text{m}^3/\text{h}, \\ \text{m}^3/24\text{h} \end{matrix} \right\}$
$q_{SLPS}^*, q_{SLPM}^*,$ q_{SLPH}^*, q_{SLPD}^*	Standard gas (vapor) volumetric flow rate at ISO-5024 base: $T_{kb} = 288.15$ K and $p_b^* = 101.325$ kPa	L/s, L/min, L/h, L/24h
$\left. \begin{matrix} (q_{SLPS})_b, \\ (q_{SLPM})_b, \\ (q_{SLPH})_b, \\ (q_{SLPD})_b \end{matrix} \right\}$	Standard gas (vapor) volumetric flow rate at selected base temperature and pressure	$\left\{ \begin{matrix} \text{L/s}, \\ \text{L/min}, \\ \text{L/h}, \\ \text{L/24h} \end{matrix} \right\}$
Q	Total mass or volume units	
Q_v	Total flow in volume units at flowing conditions; subscript v may be gal, ft ³ , m ³ , etc.	
Q_{acf}	Gas (vapor) total volume at flowing conditions	ft ³

†Except for dimensionless or defined SI unit symbols, as in T_K , symbols that apply to SI units are shown in the text with a superscript asterisk, as in F_a^* .

Symbol and meaning		U.S. units	SI units†
Q_{acm}^*	Gas (vapor) total volume at flowing conditions		m^3
Q_{bbl}	Liquid total volume at flowing conditions	bbl	
Q_{cf}	Liquid total volume at flowing conditions	ft^3	
Q_{cm}^*	Liquid total volume at flowing conditions		m^3
Q_{gal}	Total volume at flowing conditions	gal	
Q_l^*	Total volume at flowing conditions		L
Q_M	Total flow in mass units; subscript may be lb_m , kg, g, etc.		
Q_{kg}^*	Total mass		kg
Q_{lbm}	Total mass	lb_m	
Q_v	Total volume at standard (gas) or base (liquid) temperature and pressure	ft^3	m^3
$(Q_v)_b$	Gas (vapor) total volume at selected pressure and temperature	ft^3	m^3
Q_{BBL}	Liquid total volume at $T_F = 60^\circ F$ and $p_b = 14.696$ psia	bbl	
Q_{GAL}	Liquid total volume at $T_F = 60^\circ F$ and $p_b = 14.696$ psia		gal
Q_L^*	Liquid total volume at $T_c = 15.6^\circ C$ and $p_b^* = 101.3$ kPa		L
Q_{SCF}	Gas (vapor) total volume at ISO-5024 base: $T_b = 518.67^\circ R$ and $p_b = 14.69595$ psia	ft^3	
$(Q_{SCF})_b$	Gas (vapor) total volume at selected base temperature and pressure	ft^3	
Q_{SL}^*	Gas (vapor) total volume at ISO-5024 base: $T_{kb} = 288.15$ K and $p_b^* = 101.325$ kPa		L
$(Q_{SL}^*)_b$	Gas (vapor) total volume at selected base temperature and pressure		L
Q_{SCM}	Gas (vapor) total volume at ISO-5024 base: $T_{kb} = 288.15$ K and $p_b^* = 101.325$ kPa		m^3
$(Q_{SCM}^*)_b$	Gas (vapor) total volume at selected base temperature and pressure		m^3

†Except for dimensionless or defined SI unit symbols, as in T_K , symbols that apply to SI units are shown in the text with a superscript asterisk, as in F_a^* .

Symbol and meaning		U.S. units	SI units†
$(Q_{SCF})_{wet}$	Total volume of wet gas at standard conditions	ft ³	
$(Q_{SCM}^*)_{wet}$	Total volume of wet gas at standard conditions		m ³
$(Q_{lbm})_{TC}$	Total mass of two-component gas mixture	lb _m	
$(Q_{lbm})_s$	Total mass of dry gas in a two-component mixture	lb _m	
r	Radius to a point	in	mm
r_b	Elbow radius at centerline	in	mm
r_p	Pipe radius	in	mm
R_s	Universal gas constant for BWR state equation		atm dm ³ /(mol K)
R_d	Bore Reynolds number at flowing conditions using corrected pipe diameter, $d = F_{ad}d_{meas}$		
R_{temp}	Resistance of a metal at measured temperature	Ω	Ω
R_{ref}	Reference resistance value at 0°C	Ω	Ω
R_0	Universal gas constant, 10.73151 psia·ft ³ /(lb _m ·mol·°R) or 8.31441 J*/(g·mol·K)	Ω	Ω
R_{og}	Universal gas constant, in energy units 1.985862662 Btu/(lb _m ·mol·°R) or 8314.41 J/(kg·mol·K)		
R_D	Pipe Reynolds number at flowing conditions using corrected pipe diameter, $D = F_{aD}D_{meas}$		
R_{Df}	Pipe Reynolds number using corrected pipe diameter D_f		
$(R_{GA})_c$	Govier-Aziz critical Reynolds number for a Bingham fluid		
R_{MR}	Metzner-Reed Reynolds number for a power-law fluid		
$(R_{MR})_c$	Metzner-Reed critical Reynolds number for a power-law fluid		
RH	Relative humidity, p_{wv}/p_{set}		
s	Coefficient in Pai profile equation (5.16)		
S	Strouhal number, $f_{Hz} \cdot h_F / V_{free}$		
S_s	Fluid shear stress	lb _f /ft ²	N/m ²
$(S_s)_w$	Fluid wall shear stress	lb _f /ft ²	N/m ²
$(S_s)_y$	Bingham-fluid yield shear stress	lb _f /ft ²	N/m ²
\dot{S}	Fluid shear rate	s ⁻¹	s ⁻¹
\dot{S}_w	Fluid shear rate at wall	s ⁻¹	s ⁻¹
dS	Differential displacement in direction of flow	ft	m

†Except for dimensionless or defined SI unit symbols, as in T_K , symbols that apply to SI units are shown in the text with a superscript asterisk, as in F_a^* .

Symbol and meaning		U.S. units	SI units†
S_M	Sizing factor for differential producer, a constant		
SH	Specific humidity, ρ_{wv}/ρ_{dry}		
t	Time	s	s
t_{min}	Minimum orifice plate thickness to prevent yielding	in	m
t_p	Pipe wall thickness	in	m
t_{tF}	Time for test fluid to flow through a capillary viscometer	s	s
t_{ref}	Reference time for a capillary viscometer	s	s
t_{DN}	Time for a sonic pulse to travel downstream	s	s
t_{FS}	Time for sphere to fall in a falling-sphere viscometer	s	s
t_{PE}	Thickness of the primary element	in	m
t_{RA}	Admiralty Redwood seconds, viscosity determination	s	s
t_{RS}	Standard Redwood seconds, viscosity determination	s	s
t_{ST}	Student's t statistic		
t_{UP}	Time for a sonic pulse to travel upstream	s	s
t_{SSF}	Saybolt Furol seconds, viscosity determination	s	s
t_{SSU}	Saybolt universal seconds, viscosity determination	s	s
T_b	Base absolute temperature for a gas volume	°R	
T_c	Critical temperature of a substance	°R	K
T_{ci}	Critical temperature of the i th component in a binary mixture	°R	K
$T_{d,ref}$	Reference temperature for bore measurements	°R	K
T_f	Flowing absolute temperature, $T_F + 459.67$	°R	
T_{f1}	Flowing absolute temperature measured at upstream tap	°R	
$T_{f1'}$	Upstream temperature measured in a pipe	°R	K
T_{f2}	Flowing absolute temperature measured at downstream tap	°R	
$T_{f2'}$	Downstream temperature measured in a pipe	°R	K
T_{fi}	Indicated flowing absolute temperature	°R	

†Except for dimensionless or defined SI unit symbols, as in T_K , symbols that apply to SI units are shown in the text with a superscript asterisk, as in F_a^* .

Symbol and meaning		U.S. units	SI units†
T_{ij}	Binary mixtures reduced temperature, AGA-8 equation		
T_r	Reduced temperature of a gas (vapor), T_f/T_c		
$(T_p)_{des}$	Flowing absolute temperature at design conditions	°R	
T_{pc}	Pseudocritical temperature of a mixture of gases	°R	K
T_{pr}	Pseudocritical reduced temperature of a mixture of gases, T_f/T_{pc}		
T_{stag}	Stagnation temperature	°R	K
T	Reciprocal of reduced temperature, $1/T_{pr}$		
T	Period of oscillation in pulsating flow	s	s
T_B	Boiling point, absolute temperature	°R	K
T_c	Temperature in degrees Celsius		°C
$T_{D,ref}$	Reference temperature for a pipe measurement	°R	K
T_F	Flowing temperature in degrees Fahrenheit	°F	
ΔT_F	Difference in temperature, $T_F - 60$	°F	
T_K	Flowing absolute temperature, Kelvin scale		K
T_{K1}	Absolute temperature measured at upstream tap		K
T_{K2}	Absolute temperature measured at downstream tap		K
T_{Kb}	Base absolute temperature for a gas volume		K
T_{Kc}	Critical temperature, in kelvins		K
T_R	Absolute temperature in degrees Rankine	°R	
T_{WB}	Wet-bulb temperature	°F	°C
u	Internal energy	Btu/lb _m	J*/kg
U_{RSS}	Root-sum-squared value for the overall uncertainty		
v	Specific volume, $1/\rho$	ft ³ /lb _m	m ³ /kg
$V_{C,mol}$	COSTALD equation characteristic molar volume (critical volume)		m ³ /(kg·mol)
v_f	Flowing specific volume	ft ³ /lb _m	m ³ /kg
v_{mol}	Molar volume	ft ³ /(lb _m ·mol)	m ³ /(kg·mol)

†Except for dimensionless or defined SI unit symbols, as in T_K , symbols that apply to SI units are shown in the text with a superscript asterisk, as in F_a^* .

Symbol and meaning	U.S. units	SI units†
v_{r0} COSTALD equation spherical molecule function		$\text{m}^3/(\text{kg} \cdot \text{mol})$
v_{rb} COSTALD equation deviation molecule function		$\text{m}^3/(\text{kg} \cdot \text{mol})$
v_{wv} Specific volume of water vapor	ft^3/lb_m	m^3/kg
$V_{f/B}$ Fluid velocity with respect to blade for turbine flowmeters	ft/s	m/s
V_p Point velocity along pipe radius	ft/s	m/s
V_{free} Free-stream velocity, no confining walls	ft/s	m/s
V_{max} Maximum (centerline) velocity	ft/s	m/s
\bar{V}_f Average pipe velocity	ft/s	m/s
$(\bar{V}_f)_{\text{av}}$ Average of minimum and maximum velocities in pulsating flow	ft/s	m/s
$(\bar{V}_f)_C$ Critical velocity for transition to turbulent flow for Bingham fluid	ft/s	m/s
$(\bar{V}_f)_{\text{max}}$ Maximum average pipe velocity in pulsating flow	ft/s	m/s
$(\bar{V}_f)_{\text{min}}$ Minimum average pipe velocity in pulsating flow	ft/s	m/s
$(\bar{V}_f)_{VC}$ Average velocity at minimum flow area (vena contracta) of an orifice	ft/s	m/s
V_{mol} Molar volume		$\text{dm}^3/\text{mol}, \text{m}^3/\text{mol}$
\bar{V}_t Average throat velocity for a contoured-inlet primary element	ft/s	m/s
\bar{V}_{soft} Sonic velocity at throat of a critical nozzle	ft/s	m/s
$V_{\text{soft,calib}}$ Sonic velocity of calibration gas for a gas densitometer	ft/s	m/s
ΔV_{plate} Velocity difference between two parallel plates	ft/s	m/s
V_B Turbine-flowmeter blade velocity	ft/s	m/s
V_p Plug velocity in flow of a Bingham fluid	ft/s	m/s
V_{SO} Velocity of sound in a liquid	ft/s	m/s
V Volume	ft^3	m^3
ΔV Change in volume with pressure	ft^3	m^3
V_0 Liquid volume at zero pressure	ft^3	m^3
V_l Liquid volume	ft^3	m^3
V_m Volume of a standard mass	ft^3	m^3
V_{fl} Volume of float in a variable-area flowmeter	ft^3	m^3
V_{dry} Volume of dry gas in a wet (water) gas mixture	ft^3	m^3

†Except for dimensionless or defined SI unit symbols, as in T_K , symbols that apply to SI units are shown in the text with a superscript asterisk, as in F_a^* .

Symbol and meaning		U.S. units	SI units†
V_{wet}	Volume of wet (water) gas in a wet gas mixture	ft ³	m ³
W	Energy	W	W
W	Weight force	lb _f	N
W_i	Weighting function along the sonic path of an ultrasonic flowmeter	lb _f	N
W_s	Annular-slot width for corner-tapping	in	mm
W	Work	Btu/lb _m	J*/kg
x	Mole fraction in gas (vapor) phase		
x_m	Mass fraction, mass of component ÷ mass of total mixture		
x_p	Differential-pressure amplitude ratio in pulsating flow		
x_1	Pressure ratio based on upstream tap pressure, $\Delta p/p_1$		
x_2	Pressure ratio based on downstream pressure, $\Delta p/p_2$		
X	Sensitivity coefficient of a measured variable		
X_{var}	Sensitivity coefficient, where subscript var (variable) is denoted as G_b , G_f , Z , etc.		
X	Mixture quality, mass of gas phase ÷ mass of total mixture		
y	Elevation above sea level	ft	
\bar{y}	Mole fraction in liquid phase		
\bar{y}	Distance from pipe wall to point of average velocity	in	mm
Y	Gas expansion factor		
Y_1	Gas expansion factor based on upstream pressure		
$Y_{1,0.66}$	Gas expansion factor at pressure ratio of 0.66		
$Y_{1,0.77}$	Gas expansion factor at pressure ratio of 0.77, for pipe taps		
Y_2	Gas expansion factor based on downstream pressure		
Y_N	Gas expansion factor at normal flowing conditions, usually design conditions		
Y_{CR}	Critical flow function		
ΔY	Spacing between parallel plates	ft	
Y_{Arn}	Critical flow function derived by Arnberg	$\frac{\text{lb}_m}{\text{lb}_f \cdot \text{s}} \sqrt{^\circ\text{R}}$	
Z	Gas (vapor) compressibility factor		

†Except for dimensionless or defined SI unit symbols, as in T_K , symbols that apply to SI units are shown in the text with a superscript asterisk, as in F_a^* .

Symbol and meaning		U.S. units	SI units†
Z_b	Gas (vapor) compressibility factor at base temperature and pressure		
Z_c	Gas (vapor) compressibility factor at critical point		
Z_f	Gas (vapor) compressibility factor at flowing conditions		
Z_{pc}	Gas (vapor) pseudocritical compressibility factor for a mixture		
Z_{wu}	Water-vapor compressibility factor in a wet gas		
Z_{air}	Compressibility factor for air		
Z_{dry}	Compressibility factor of dry components in a wet gas		
Z_{wet}	Compressibility factor of a wet gas		
Z_L	Liquid compressibility factor		
Z_{MBWR}	Modified Benedict-Webb-Rubin equation of state compressibility factor		
$Z_{R/K}$	Redlich-Kwong equation-of-state compressibility factor		
$(Z_{R/K})_f$	Redlich-Kwong equation-of-state compressibility factor calculated at flowing conditions		
$(Z_{R/K})_{des}$	Redlich-Kwong equation-of-state compressibility factor calculated at design conditions		
Z_{SV}	Standardized variable for a statistical population in a hypotheses test		
Z^0	Edmister-Pitzer simple fluid compressibility factor		
Z^1	Edmister-Pitzer compressibility-factor correction for deviation from simple fluid		
α	Waveform coefficient for pulsating flow		
α_{ann}	Thermal expansion factor for an annubar	in/(in. °F)	mm/(mm. °C)
α_b	Thermal-expansion coefficient in API-2540 liquid-petroleum density equation		
α'_b	Derivative of thermal-expansion coefficient in API-2540 liquid-petroleum density equation		
α_H	Hydrometer cubical coefficient of expansion	(°F) ⁻¹	(°C) ⁻¹

†Except for dimensionless or defined SI unit symbols, as in T_K , symbols that apply to SI units are shown in the text with a superscript asterisk, as in F_a^* .

Symbol and meaning		U.S. units	SI units†
α_{HO}	Thermal-expansion coefficient for meter housing	in/(in·°F)	mm/(mm·°C)
α_p	Thermal-expansion coefficient for pipe material	in/(in·°F)	mm/(mm·°C)
α_{PE}	Thermal-expansion coefficient for primary-element material	in/(in·°F)	mm/(mm·°C)
β	Beta ratio, d/D		
β_{ann}	Beta ratio $h/$ for an Annubar		
β_c	Segment beta ratio for a segmental orifice, $\beta/0.98$		
β_f	Differential producer's beta ratio d_f/D_f at flowing conditions		
$\beta_{f,V-Cone}$	Beta ratio for a V-Cone meter		
β_T	Target or annular-orifice beta ratio, d_T/D		
β_{Wedge}	Beta ratio for a wedge flowmeter		
δ_d	Drive mode deflection in a Coriolis meter	in	mm
δ_F	Deflection resulting from a Coriolis force in a Coriolis mass flowmeter	in	mm
ε_i	Energy parameter for i th component in a gas mixture	°R	K
γ	Benedict-Webb-Rubin equation constant ($1/\rho_c^2$)	ft ⁶ /lb _m ²	m ⁶ /kg ²
γ_f	Specific weight of a fluid, liquid, or gas (vapor), $(g/g_c)\rho_f$	lb _f /ft ³	N/m ³
ε	Average depth of pipe-wall roughness	in/in	mm/mm
Γ_{mix}	Gas mixtures energy parameter	ft ⁶ /(lb _m ·mol) ²	m ⁶ /(kg·mol) ²
Γ_{Pitot}	Isentropic compression factor for a Pitot or impact tube		
η	Efficiency of motor and pump		
θ	Sonic-path angle for an ultrasonic flowmeter	degrees	degrees
μ_{app}	Apparent viscosity, S_s/\dot{S} , absolute viscosity units	lb _f ·s/ft ²	cP‡
$(\mu)_a$	Absolute viscosity at atmospheric pressure	lb _m /(ft·s)	cP‡
$(\mu)_p$	Absolute viscosity corrected for pressure	lb _m /(ft·s)	cP‡
μ_{cP}	Absolute viscosity in centipoises		cP‡
μ_{cP}^o	Viscosity of a gas at low pressure		cP
$\mu_{cP,app}$	Apparent absolute viscosity of a two-phase mixture		cP

†Except for dimensionless or defined SI unit symbols, as in T_K , symbols that apply to SI units are shown in the text with a superscript asterisk, as in F_a^* .

‡The poise (P) and the stokes (St) are cgs metric units, not SI metric; 1 P = 0.1 Pa·s; 1 St = 0.0001 m²/s.

Symbol and meaning	U.S. units	SI units†
$\mu_{cP,l}$ Viscosity of saturated liquid		cP
$\mu_{cP,mix}$ Absolute viscosity of a mixture in centipoises		cP‡
$\mu_{cP,ref}$ Reference viscosity for a capillary viscometer		cP‡
μ_{mix} Absolute viscosity of a mixture	lb _m /(ft·s)	cP‡
$(\mu_f)_e$ Absolute English-system viscosity, force units	lb _f ·s/ft ²	
$(\mu_m)_e$ Absolute English-system viscosity, mass units	lb _m /(ft·s)	
μ_P Absolute viscosity in poises		P‡
μ_p Poisson's ratio for pipe material	in/in	m/m
μ_{PE} Poisson's ratio for primary element material	in/in	m/m
μ_{Pas} Absolute viscosity in pascal seconds		Pa·s
ν_e Kinematic viscosity in English units	ft ² /s	
ν_{cSt} Kinematic viscosity in centistokes		cSt‡
ν_{St} Kinematic viscosity in stokes		St‡
ρ_b Density at base conditions: liquids, 60°F (15.6°C) and 14.7 psia (101.3 kPa); gases, 59°F (15°C) and 14.69595 psia (101.325 kPa); or at other selected base values	lb _m /ft ³	kg/m ³
ρ_{air} Air density at time of calibration	lb _m /ft ³	kg/m ³
$\rho_{air,c}$ Air density for calibrating a weigh tank	lb _m /ft ³	kg/m ³
ρ_f Density at flowing conditions	lb _m /ft ³	kg/m ³
ρ_{f1} Upstream density at flowing conditions	lb _m /ft ³	kg/m ³
ρ_{f2} Downstream density at flowing conditions	lb _m /ft ³	kg/m ³
$\rho_{f,ind}$ Indicated density from a vibrating densitometer	lb _m /ft ³	kg/m ³
$(\rho_f)_{des}$ Density at design conditions	lb _m /ft ³	kg/m ³
ρ_f Density of float in a variable-area flowmeter	lb _m /ft ³	kg/m ³
ρ_{ft} Density at throat of a critical flow nozzle	lb _m /ft ³	kg/m ³
ρ_{g1} Upstream density of gas in a two-component or two-phase flow	lb _m /ft ³	kg/m ³
ρ_l Density of liquid in a two-component or two-phase flow	lb _m /ft ³	kg/m ³

†Except for dimensionless or defined SI unit symbols, as in T_K , symbols that apply to SI units are shown in the text with a superscript asterisk, as in F_a^* .

‡The poise (P) and the stokes (St) are cgs metric units, not SI metric; 1 P = 0.1 Pa·s; 1 St = 0.0001 m²/s.

Symbol and meaning		U.S. units	SI units†
ρ_m	Manometer-fluid density	lb _m /ft ³	kg/m ³
ρ_{meas}	Density of a standard mass	lb _m /ft ³	kg/m ³
ρ_{mol}	Molar density	lb _m ·mol/ft ³	kg·mol/m ³
ρ_v	Density of water vapor at saturation	lb _m /ft ³	kg/m ³
ρ_r	Reduced density ρ/ρ_c		
ρ_{r0}	Initial estimate for Hall-Yarborough reduced density	lb _m /ft ³	kg/m ³
ρ_{ref}^*	Fluid reference density in a falling-sphere viscometer		kg/m ³
ρ_s	Manometer seal-fluid density	lb _m /ft ³	kg/m ³
ρ_{aph}^*	Sphere density in a falling-sphere viscometer		kg/m ³
ρ_{wet}	Density of a wet gas	lb _m /ft ³	kg/m ³
ρ_F	Density of fluid at flowing conditions, uncorrected for pressure	lb _m /ft ³	kg/m ³
ρ_{Hg}	Density of mercury	lb _m /ft ³	kg/m ³
ρ_{MBWR}	Density via modified Benedict-Webb-Rubin equation of state		kg/m ³
ρ_{TP}	Effective density of a two-phase flow of same substance in liquid and gas phases	lb _m /ft ³	kg/m ³
$(\rho_w)_{T, g0}$	Density of water at standard gravity (32.174) and any temperature	lb _m /ft ³	kg/m ³
$(\rho_w)_{68, g0}$	Density of water at 68°F, standard gravity, and atmospheric pressure: 62.31572 lb _m /ft ³ (998.2019 kg/m ³)	lb _m /ft ³	kg/m ³
$(\rho_w)_{60, g0}$	Density of water at 60°F, standard gravity, and atmospheric pressure: 62.36630 lb _m /ft ³ (999.0121 kg/m ³)	lb _m /ft ³	kg/m ³
σ	Standard deviation	%	%
σ_c	Cavitation number		
$(\sigma_c)_i$	Incipient cavitation number		
σ_{sp}	Lennard-Jones separation parameter	ft/(lb _m ·mol) ^{1/3}	
σ_y	Yield stress of a material	lb _f /in ²	Pa
σ_p	Precision, $t_{ST}\sigma$	%	%
σ_{1-2}	Sampling distribution of differences in means		
ϕ	Degrees latitude		
$(\phi)_e$	Coefficient of rigidity for a Bingham fluid	lb _f ·s/ft ²	

†Except for dimensionless or defined SI unit symbols, as in T_K , symbols that apply to SI units are shown in the text with a superscript asterisk, as in F_a^* .

Symbol and meaning		U.S. units	SI units [†]
ϕ_{sat}	Saturation reduced-pressure term in COSTALD equation		
ψ	Angle of swirl	degrees	degrees
ω	Acentric factor, Edmister-Pitzer diagram		
ω_{pc}	Pseudoacentric factor for a gas mixture		
ω_{mix}	Acentric factor of a gas mixture		
Ω	Angular frequency	rad/s	rad/s
Ω_d	Angular drive frequency in a Coriolis mass flowmeter	rad/s	rad/s

[†]Except for dimensionless or defined SI unit symbols, as in T_K , symbols that apply to SI units are shown in the text with a superscript asterisk, as in F_a^* .

FLOW MEASUREMENT ENGINEERING HANDBOOK

The purpose of this handbook is to provide flow measurement engineers with a single reference for engineering equations, physical-property data, accuracy estimation, and installation requirements for the most commonly used industrial flowmeters, in both United States customary (U.S.) and SI units. Equations are developed for sizing and flow-rate calculations for differential producers and linear-output flowmeters. This information is presented in tables and in graphical form for ready reference. Orifices, nozzles, venturis, elbow flowmeters, area averaging, "V" cone, Gilflo, wedge meters, pitot tubes, integral orifices, target flowmeters, critical-flow nozzles and orifices, and positive-displacement, turbine, vortex, magnetic, variable-area, laminar flow elements, ultrasonic, and Coriolis mass and thermal mass flowmeters are covered. Separate chapters are devoted to accuracy, measurement units, flowmeter selection, fluid properties, and influence quantities such as cavitation and pulsating flow.

OVERVIEW

The handbook is organized into three distinct sections: the first deals with factors common to all flowmeters, and the second with specific flowmeters; the third section is a physical properties appendix applicable to all flowmeters. The reader is first introduced to fluid properties, measurement units, accuracy calculations, and common influence quantities. The principle of operation for each flowmeter is then briefly explained, and the reasons for selecting a particular flowmeter are given. Differential producers are next introduced and explained. Engineering equations are developed, and examples presented. Design information and graphical information for sizing primary elements and fixed-geometry devices conclude the section on differential producers. Critical flowmeters are then discussed, and equations are developed for both gases (vapors) and choked liquid flow. Linear flowmeters are introduced and grouped according to the equations used to calculate flow rate. Their principle of operation is explained, and practical considerations are discussed. Flow equations are tabulated, and examples are presented along with the necessary graphical material.

The ISO/ASME/ANSI† discharge coefficient equations are used throughout. Methods and graphs pertaining to this equation and to other ISO/ASME/ANSI

†International Standards Organization/American Society of Mechanical Engineers/American National Standards Institute.

recommendations are developed into working engineering equations for both U.S. and SI units. Additionally, installation and design requirements given in ISO and ANSI standards are presented. Equations are given for calculating pressure loss and energy cost.

The β_0 method, which simplifies the sizing calculation for differential producers (orifices, nozzles, Lo-Loss tubes, venturis, etc.) is introduced. This method is then used with either an iteration or with Newton's solution for a zero-root equation to exactly size these primary devices.

In the chapter on critical flowmeters, equations are developed, design information is presented, and detailed calculations are given. There is also a section on choked liquid flow.

Reference installation conditions and primary constants are defined. These primary constants are then used to develop the flow-rate-equation constants to seven places. This eliminates the calculation errors associated with previous equation constants that were often rounded to three significant figures. Nonnewtonian fluids, pulsating flow, and cavitation are also discussed.

Information is presented on area averaging, "V" cone, Gilflo, wedge meters, pitot tubes, magnetic flowmeters, ultrasonic flowmeters, and Universal Venturi Tubes. The accuracy chapter simplifies the calculations required by present standards. These are tabulated, with examples given in subsequent chapters.

Organization

Throughout, the text material is organized for ready reference to equations and physical data in both U.S. and SI units. The individual chapters are organized as follows:

- In Chap. 2, the fluid properties used in the calculation of flow rate for all flowmeters are discussed, the equations are developed, and the use of the appendix data is discussed and exemplified.
- In Chap. 3, the measurement of pressure and temperature is explained, the relationship between U.S. and SI flow-rate units is discussed, and the subscripting system to be followed in the handbook is described.
- In Chap. 4, flow measurement accuracy is defined, and single-point accuracy and accuracy over a range are discussed in detail; sensitivity coefficients are derived and, through an example, used to calculate bias and accuracy.
- In Chap. 5, the conditions required for reference measurement accuracy are presented; the influence of nonnewtonian fluids, pulsating flow, and cavitation on flowmeter performance is described.
- In Chap. 6, the principles of operation, reasons for selection, and a selection guide are presented for flowmeters covered in the handbook, and pressure-cost and energy-cost equations are given.
- Chapter 7 is a brief introduction to the many flowmeters classified as differential producers.
- In Chap. 8, installation requirements for differential producers are given and recommended practice for installing lead lines is detailed.
- In Chap. 9, the volumetric and mass flow-rate equations are developed; primary constants, correction factors, Reynolds-number equations, and procedures for bore sizing and flow-rate calculations are given, along with examples for liquid, gas (vapor), and quality (wet) steam measurements.

- In Chap. 10, design requirements for the differential producer are presented, along with examples for devices that require graphical solutions and graphs based on the equations developed in Chap. 9.
- In Chap. 11, fixed-geometry flowmeters, for which the differential or target force must be determined, are described and their equations are tabulated; these devices include arithmetic-progression orifices, target flowmeters, integral orifices, area averaging, “V” cone, Gilflo wedge meters, pitot tubes, and elbow flowmeters.
- In Chap. 12, measured and unmeasured variables are defined; measurement equipment is then described for analog computers, digital flow computers, and for planimetering charts to calculate total flow.
- In Chap. 13, engineering equations for critical nozzle venturis and thick-orifice flowmeters are developed and tabulated, and the critical-flow function for many common gases is given in tables; liquid choked-flow equations for restrictive venturis and orifices are also presented, along with examples.
- In Chap. 14, the principles of operation, flow equations, and examples are given for turbine, vortex, and positive-displacement pulse-output-type meters. Magnetic, ultrasonic, Coriolis mass, thermal mass, and variable-area flowmeters are discussed, and measurement practices and equations are given for these devices.
- In Chap. 15, the *influence quantities* that affect all flowmeters are presented in tables and in graphs that illustrate the effect on meter performance. Some of these influence quantities include the effects of the upstream piping, multicomponent fluids, and pulsating flow on metering accuracy.

Open-Channel Measurement

Open-channel measurement is almost a separate field from closed-conduit flow measurement. The terminology, equations, and theory, although similarly based on hydraulics, are completely different. Many open-channel flowmeters (weirs, flumes) must be fabricated in situ; and they often require on-site hydraulic engineering to assure suitable results. This part of the field of flow measurement is rapidly changing, with newer technology being used to obtain more accurate results. For these reasons, open-channel measurement is not discussed in this book. However, texts have been written on the more traditional meters, and numerous technical publications have appeared in the literature over the last 10 years. The reader is referred to the following texts and standards for the proper use of open-channel flow measurement devices:

Bureau of Reclamation: *Water Measurement Manual*, U.S. Department of the Interior, Bureau of Reclamation, catalog no. I 27.19/2:W29/2/974, U.S. Government Printing Office, Washington, D.C., 1975.

National Bureau of Standards: *A Guide to Methods and Standards for the Measurement of Water Flow*, NBS Special Publication 421, U.S. Department of Commerce/NBS, code XNBSAV, 1975.

Ackers, P., W. R. White, J. A. Perkins, and A. J. M. Harrison: *Weirs and Flumes*, Wiley, New York, 1978.

Bos, M. G., J. A. Replogle, and A. J. Clemmens: *Flow Measuring Flumes and Open Channel Systems*, Wiley, New York, 1984.

ISO Standard 1438, *Liquid Flow Measurement in Open Channels Using Thin Plate Weirs and Venturi Flumes*, ISO 1438-1975(E), Geneva, 1975.

FLOWMETER DEFINITION

Defining a flowmeter is almost as difficult as classifying flowmeters. The only standard definition available is that given in ASME-IM (1991), ISO 4006 (1991). In it, the following definitions are given:

Flowmeter. A device that measures the rate of flow or quantity of a moving fluid in an open or closed conduit. It usually consists of both a primary and a secondary device.

Note: It is acceptable in practice to further identify the flowmeter by its applied theory, such as differential pressure, velocity, area, force, etc., or by its applied technology, such as orifice, turbine, vortex, ultrasonic, etc. Examples include turbine flowmeter, magnetic flowmeter, etc.

Flowmeter primary device. The device mounted internally or externally to the fluid conduit which produces a *signal* with a defined relationship to the fluid flow in accordance with known physical laws relating the interaction of the fluid to the presence of the primary device.

Note: The primary device may consist of one or more *elements* necessary to produce the primary device signal.

Flowmeter secondary device. The device that responds to the signal from the primary device and converts it to a display or to an output signal that can be translated relative to flow rate or quantity.

Note: The secondary device may consist of one or more *elements* as needed to translate the primary device signal into standardized or nonstandardized display or transmitted units (recorder, indicator, totalizer, etc.).

By these definitions, the primary device of an orifice flowmeter includes upstream and downstream piping, flow conditioner, orifice plate, and pressure taps. The differential-pressure transmitter, manifold valves, and connecting tubing are elements of the secondary device. The combination of these two devices is the orifice flowmeter.

FLOWMETER CLASSIFICATION

Flowmeters have been classified in numerous ways; in the most common classification system, meters are separated into quantity (total-flow) and rate meters and then further subdivided by operating principle. This essentially divides meters into those that measure discrete volume (positive-displacement meters) and those that directly or indirectly utilize the movement of the fluid to actuate a secondary element. Although this system reasonably describes the two meter classes, in practice rate meters are often used as quantity meters (vortex, turbine, orifice, etc.), and quantity meters are sometimes used as rate meters.

For the purpose of calculating flow rate or total flow, the classification of meters as either square-root (differential-producer) or linear meters is more convenient since, in general, all meters for which the flow is not a function of the square root of the differential pressure are essentially linear-scale meters. This grouping gives the same engineering equations for all meters in each group and avoids much confusion in flow calculations. Although linear meters have completely different operating principles from square-root meters, scaling to base volume and to mass flow are the same for both types.

REFERENCE

ASME MFC-1M *Glossary of Terms Used in the Measurement of Fluid Flow in Pipes*, ASME, New York, 1991.

ISO Standard 4006 *Measurement of fluid flow in closed conduits—Vocabulary and symbols* Geneva, 1991.

FLUID PROPERTIES

Data on physical properties is often required for calculations of base flow rates and pipe Reynolds numbers, and to predict the properties of a gas (vapor) after an expansion. The physical properties of liquids and gases change with pressure and temperature, and whether corrections need to be considered depends on the design objective. In many cases, properties are assumed constant at design conditions, and corrections are not applied. While there is no substitute for experimental data, estimates of the properties of a mixture may often have to be used in calculations. This requires theory, common sense, and experience.

Accuracy in predicting the properties of pure substances is considerably better for liquids and gases than for mixtures. In many applications, particularly for high inert mole fractions in natural gas, large errors can occur, and the estimated value should first be properly verified by test.

This chapter is a discussion of the most commonly used fluid properties and the estimation of these properties at various pressures and temperatures, for both pure substances and mixtures. For illustrative purposes shaded areas on graphs in this chapter are expanded and are not scaled.

THE p v T RELATIONSHIP

The p v T Behavior of a Pure Substance

Fluid density can be measured with a liquid or gas densitometer, but it is more common to use temperature and pressure measurements to calculate density. The reciprocal of the specific volume is the fluid's mass density, and it can be determined from pressure and temperature measurements using the p v T relationship. The interrelationships of pressure, temperature, and specific volume are also important because of the law of corresponding states. From these relationships, the fluid state can be defined, or the density of an unknown mixture can be calculated.

Depending on temperature and pressure, a substance may be either a solid, a solid-liquid mixture, a liquid, a liquid-vapor mixture, a vapor, or a gas. The words *vapor* and *gas* are often used interchangeably because they are thermodynamically identical. Historically, the term *vapor* has been used to designate a substance, such as water, that exists as a solid or liquid at room temperature and atmospheric pressure, and the term *gas* to designate a substance that exists in the gaseous state under the same conditions (air, oxygen, etc.). At and above the saturated-vapor line, all substances are thermodynamically gases and contain no liquid, as the term *vapor*

implies. The term *vapor* has also been used for gases in the region between the saturated-vapor line and the critical isotherm, where gases are more compressible.

Figure 2.1a shows the pressure-temperature diagram for water. The well-known characteristics of water will be used to explain the relationships among pressure, temperature, and specific volume.

Three regions, corresponding to fluid states, are shown separated by heavy lines in Fig. 2.1a. Ice at atmospheric pressure (14.7 psia) and 28°F is indicated by point A. When heat is added, water remains in the solid phase (ice) until the temperature reaches 32°F (point B). The temperature remains at 32°F (point B on the heavy line) until sufficient heat has been added to convert all the ice into liquid (water) at 32°F; liquid and solid coexist as a mixture to this point, with the percentages of solid and liquid determined by the exchange of heat to or from the external environment. If the amount of ice decreases, the amount of liquid must increase to maintain the initial mass.

When the temperature rises above 32°F, the solid phase completely disappears, leaving only liquid. Additional heat brings the temperature to 212°F, shown at point C on the second heavy line. At this point, some of the liquid is transformed into a vapor (gas). As long as the temperature remains at point C, two phases, liquid and gas, coexist. When the liquid disappears, the fluid is in the saturated-vapor (gas) phase.

Increasing the temperature to the critical temperature of 705.5°F (point D) brings the saturated vapor (gas) through the vapor region. In this region no liquid is present, and, although it is called a vapor, the fluid acts like a *real gas*. (If the pressure is increased to 3198 psia, the ice-to-liquid temperature at point B is not significantly changed.) At 705.5°F (374°C), it is impossible to discern where the liquid phase ends and the gas phase begins. At this point, the specific volumes (or densities) of the two phases are identical.

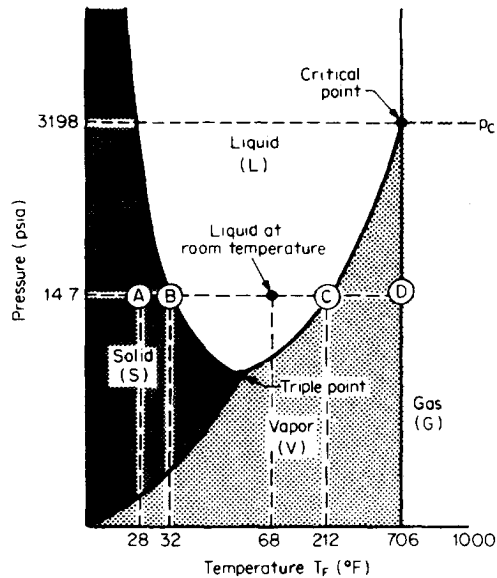
The point of equal specific volumes is referred to as the *critical point*. The temperature and pressure at the critical point are the critical temperature T_c and critical pressure p_c ; these are the values used to correlate fluids on a single diagram. The point indicated as the *triple point* is where solid, liquid, and gas are all present in varying amounts.

Figure 2.1b shows the pressure-specific volume diagram, with fluid-density values given below the specific-volume axis. The points A, B, C, and D denote regions of changing density. This figure also shows the *thermodynamically* defined vapor region between the saturated-vapor line and the critical-temperature isotherm.

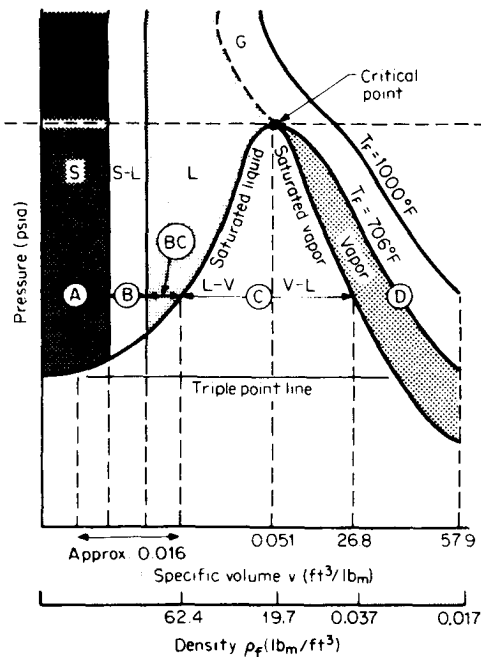
In a single phase (solid, liquid, or gas), density can be defined through pressure and temperature measurements. For a single phase, any two of pressure, temperature, and specific volume are independent, but any two will define the third. In the two-phase region, temperature and pressure are interdependent; pressure cannot be changed without changing temperature, and the state of the fluid cannot be defined by these measurements alone.

Two-phase mixtures contain differing amounts of each phase, and each has a substantially different density from the other. In two-phase pipe flows, liquid and vapor may be moving at different velocities, or they may occupy differing volumes of the pipe at different locations. This is a flow region to be avoided when possible, because of problems in calculating density and in separating the effects of the two phases on flowmeter performance.

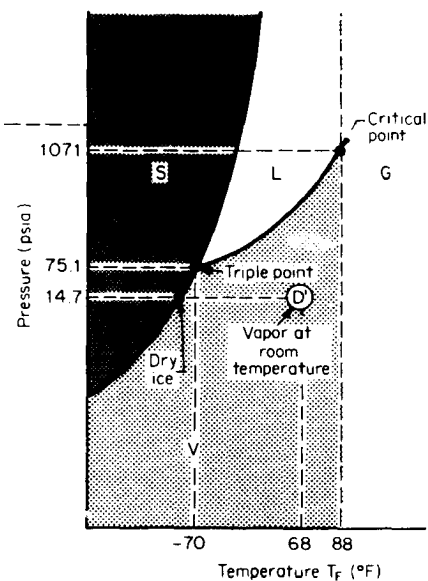
The phase diagram of carbon dioxide is shown in Fig. 2.1c. This diagram is similar in appearance to the water diagram, but the critical pressure and temperature are substantially lower [1070 psia (7380 kPa) and 88°F (31.1°C)]. At room temperature and atmospheric pressure, the fluid is in the vapor phase (point D'). For



(a)



(b)



(c)

Figure 2.1 Pressure-temperature and pressure-volume diagrams. (a) Water. (b) Water. (c) Carbon dioxide.

this reason, carbon dioxide is usually referred to as a gas, although by thermodynamic definition it should be called a vapor because it is below the critical isotherm at 68°F (20°C).

Thermodynamically, there is no difference between point *D* on the water diagram and point *D'* on the carbon dioxide diagram. Note that dry ice (solid carbon dioxide) at atmospheric pressure does not pass through the liquid region but *sublimates* from a solid directly into a gas.

All fluids (except helium, which has no defined triple point) exhibit phase diagrams and pressure-volume-temperature diagrams similar to those in Fig. 2.1.

Law of Corresponding States

First premised by Van der Waals, the *law of corresponding states* allows experimental data on some fluids to be used to approximate the properties of all fluids. At their critical points, the two fluids shown in Fig. 2.1*a* and *c* would be in corresponding states, although they would have different temperatures, specific volumes, and pressures. With critical temperature and pressure as correlating parameters, properties are reduced to corresponding states by defining the reduced temperature, pressure, and volume as

$$p_r = \frac{p_f}{p_c} \quad (2.1)$$

$$T_r = \frac{T_f}{T_c} \quad (2.2)$$

$$v_r = \frac{v_f}{v_c} \quad (2.3)$$

where p_c , T_c , and v_c are the respective values of pressure (in pounds per square inch absolute), temperature (in degrees Rankine), and specific volume (in cubic feet per pound-mass or per pound-mass-mole) at the critical point.

In Fig. 2.2, 10 fluids are shown on a plot of the compressibility factor *Z* versus the reduced pressure and temperature for each. (The compressibility factor, which is a correction factor applied to the ideal-gas equation to adjust for real-gas effects, will be discussed in more detail later.) The previous examples, carbon dioxide and water, are included on this curve.

The region between the critical pressure ratios of 0 and 1 has been enlarged in Fig. 2.3, to show the water and carbon dioxide points of Fig. 2.1. At room temperature and atmospheric pressure, the reduced pressure and temperature for water places point *B* in the shaded liquid region. Increasing the temperature brings the fluid to the saturated-liquid line. In the two-phase region denoted by line *C*, it is impossible to determine the proportions of the mixture from any diagram, since the reduced pressure and temperature will locate the two phases everywhere along line *C*. The fluid could be a saturated liquid, a saturated vapor (gas), or any mixture of the two.

When the reduced temperature is above the point where the reduced-temperature isotherm intercepts the saturated-vapor line, the state of the fluid is again defined by its temperature and pressure. Increasing the temperature further to 1000°F (538°C) brings the fluid to point *D*, in the superheated region.

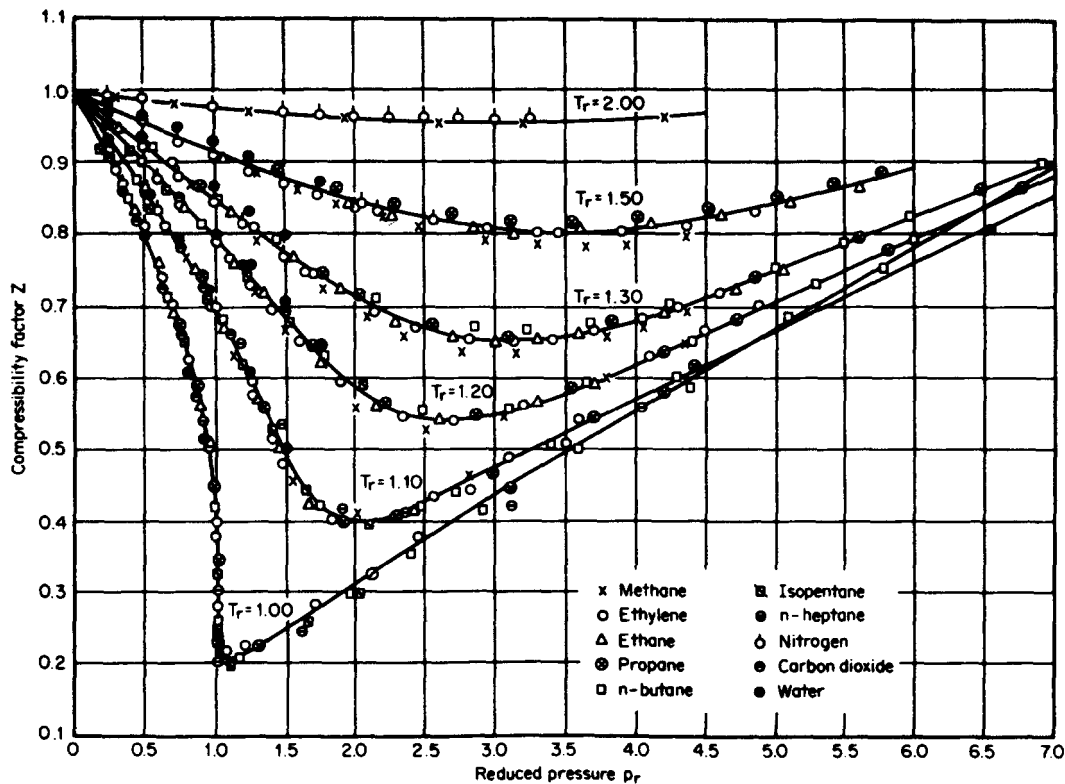


Figure 2.2 Generalized compressibility diagram showing data for various gases. (From Obert, 1948.)

Carbon dioxide has a higher reduced pressure at atmospheric pressure, and the reduced temperature places it in the vapor region. Methane (point *E*) is shown as a third example; at room temperature and atmospheric pressure, it is a gas.

Example 2.1. Propane is at 2000 psia (13,790 kPa) and 50°F (10°C). Determine whether it is a liquid or a gas. If it is a liquid, at what temperature, with the same pressure, will it become a gas?

From Table D.1, the critical properties are

$$p_c = 615.8 \text{ psia} \quad T_c = 665.6^\circ\text{R}$$

The reduced pressure and temperature are calculated with Eqs. (2.1) and (2.2) as

$$p_r = \frac{2000}{615.8} = 3.24$$

$$T_r = \frac{459.67 + 50}{665.6} = 0.766$$

These are shown as point *P* in the liquid region in Fig. 2.3. In this region, for the change from a liquid to a gas, the critical temperature must be reached; from Eq. (2.2),

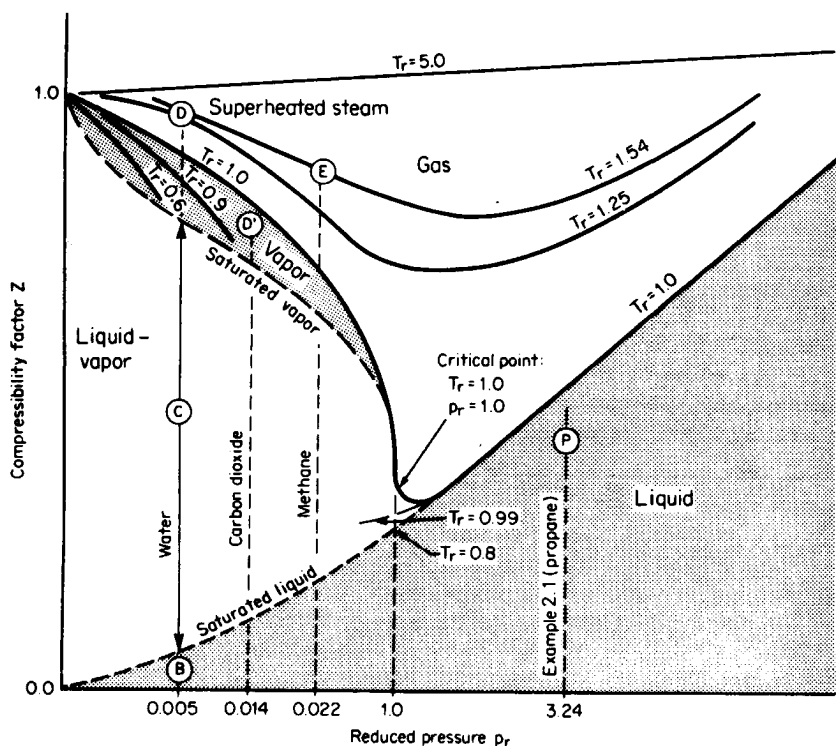


Figure 2.3 Corresponding states for water, carbon dioxide, and methane at room temperature and pressure.

$$T_r = \frac{459.67 + T_F}{665.6} = 1.0$$

and the required temperature is

$$T_F = 205.9^\circ\text{F} \text{ (96.6}^\circ\text{C)}$$

The p_vT Gas-Density Equation

The pressure, temperature, and volume relationship for a real gas can be expressed as

$$p_f V = n Z_f R_0 T_f \quad (2.4)$$

In the equation, n is the number of moles, and a mole is defined as a mass of gas equal to its molecular weight. A pound-mole of methane thus has a mass of 16.043 lb_m (the molecular weight), and a pound-mole of air has a mass of 28.963 lb_m. Note that a mole of one gas has a different mass than a mole of another gas (16.043 versus 28.963 lb_m, for example). The mole is, then, a mass unit that defines the same number of molecules; 1 mol of methane contains the same number of molecules as 1 mol of nitrogen. For this reason, it is the most convenient mass unit to use, particularly when the densities of gas mixtures are to be considered. In addition, use of the mole eliminates the need for determining individual gas constants, and the *universal* gas constant R_0 can be used in the English engineering system:

$$R_0 = 10.73151 \frac{\text{psia} \cdot \text{ft}^3}{\text{lb}_m \cdot \text{mol} \cdot ^\circ\text{R}} \quad (2.5)$$

The relationship among the number of moles, the pounds-mass of gas, and the molecular weight of the gas is

$$n = \frac{m}{M_w} \quad (2.6)$$

The factor Z in Eq. (2.4) is the compressibility factor, which corrects the equation for real-gas effects. When the compressibility factor is 1.0, the gas is called either *ideal* or *perfect*. If the specific heat at constant pressure is assumed independent of temperature and pressure, the gas is called perfect. When the specific heat is assumed to be only temperature-dependent, the gas is referred to as ideal.

By defining the ideal specific gravity as the ratio of the molecular weight of the gas to that of air, Eq. (2.4) may be rearranged into a density equation. The *specific gravity* of a gas (sometimes referred to as the *ideal specific gravity* or *relative density*) is defined as

$$G = \frac{M_{w,\text{gas}}}{M_{w,\text{air}}} \quad (2.7)$$

Substituting Eqs. (2.6) and (2.7) into Eq. (2.4) gives

$$p_f V_f = \frac{m}{GM_{w,\text{air}}} Z_f R_0 T_f \quad (2.8)$$

which, when rearranged to a density equation, becomes

$$\rho_f = \frac{m}{V_f} = \frac{GM_{w,air}p_f}{Z_f R_0 T_f} \quad (2.9)$$

Substituting the universal gas constant R_0 from Eq. (2.5) and the molecular weight of air into Eq. (2.9) (Jones, 1978) gives the density equation

$$\rho_f = \frac{28.96247}{10.73151} \frac{Gp_f}{Z_f T_f} = 2.698825 \frac{Gp_f}{Z_f T_f} \quad (2.10)$$

in U.S. units and

$$\rho_f^* = \frac{28.96247}{8.31441} \frac{Gp_f^*}{Z_f T_K} = 3.483407 \frac{Gp_f^*}{Z_f T_K} \quad (2.11)$$

in SI units.

Equations (2.10) and (2.11) are used to derive all flow equations that calculate flow rate from temperature T_f , pressure p_f , specific gravity G , and compressibility Z .

GAS SPECIFIC GRAVITY

Real and Ideal Specific Gravity

Historically, two almost identical specific-gravity values have been used in Eq. (2.10). The early definition of specific gravity was the ratio of gas density to air density when both are at the same temperature and pressure; this is now called the *real* specific gravity in the natural gas industry. The *ideal* specific gravity now in use is defined as the ratio of the molecular weights.

Specific-gravity measurement devices determine the density ratio at pressures and temperatures close to atmospheric conditions. It had been assumed that the measurement would be correct for any pressure and temperature. However, where improved accuracy is required, the slight effects of compressibility Z on both gas and air must be considered.

The real specific-gravity equation is

$$G_R = \left(\frac{\rho_{\text{gas}}}{\rho_{\text{air}}} \right)_{T,p} \quad (2.12)$$

where T and p are close to ambient temperature and pressure. Substituting the density equation (2.10) or (2.11) into Eq. (2.12) gives the relationship between ideal and real specific gravity as

$$G = \left[\left(\frac{ZT}{p} \right)_{\text{gas}} \left(\frac{p}{ZT} \right)_{\text{air}} \right]_{T,p} G_R \quad (2.13)$$

If a real specific-gravity measurement is made, the specific gravity G must be calculated with Eq. (2.13) before substitution into Eq. (2.10) or (2.11).

In most practical applications, the temperature and pressure of the sampled gas and the air are the same within the specific-gravity measuring device, and Eq. (2.13) reduces to

$$G = \left(\frac{Z_{\text{gas}}}{Z_{\text{air}}} \right)_{T,p} G_R \quad (2.14)$$

In this equation, the compressibilities of the gas and the air are calculated at the same pressure and temperature.

Specific-Gravity and Density Measuring Devices

Figure 2.4 shows several real specific-gravity measuring devices and a vibrating-type densitometer. In the buoyancy gas balance, illustrated in Fig. 2.4a, a displacer is first balanced in air, and the pressure and temperature are recorded. Air is then purged from the chamber using the unknown gas, and a new balance is obtained by adjusting the gas pressure. The ratio of the pressures is used to infer the specific gravity of the unknown gas. Obviously, this laboratory device is not well suited for on-line measurements.

For continuous recording, the gravitometer shown in Fig. 2.4b is used. A steady flow of the unknown gas is passed through a fixed-volume float that is balanced by a float of equal volume filled with a reference gas, with the two floats regulated to the same pressure. The difference between the densities of the reference gas and the sample gas causes an imbalance that is recorded on a calibrated specific-gravity chart.

The two rotating drums shown in Fig. 2.4c provide an on-line specific-gravity measuring device. Air is drawn in by the upper drum, and the lower drum brings in the gas sample. The two drums rotate in opposite directions. Adjacent to each impeller is a torque wheel that picks up the momentum of the spinning gas and transmits it to a lever. Since momentum is a direct function of density, for constant rotor speed the torque difference is a measure of specific gravity. With suitable linearization, the torque difference is recorded as real specific gravity.

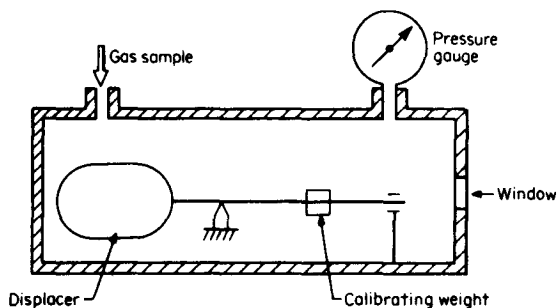
Example 2.2. Calculate the density of hydrogen at 588 psia (4054 kPa) and -10°F (-23°C). Also determine the reading of a device being used to measure the real specific gravity of hydrogen when the pressure and temperature of the hydrogen and air are 14.7 psia (101.3 kPa) and 80°F (26.7°C).

From Table G.6, at $p_f = 588$ psia and $T_f = 459.67 - 10 = 449.67$, the compressibility factor is $Z_f = 1.0264$. From Table D.1, $(M_w)_{\text{H}_2} = 2.0158$. Then, from Eq. (2.7),

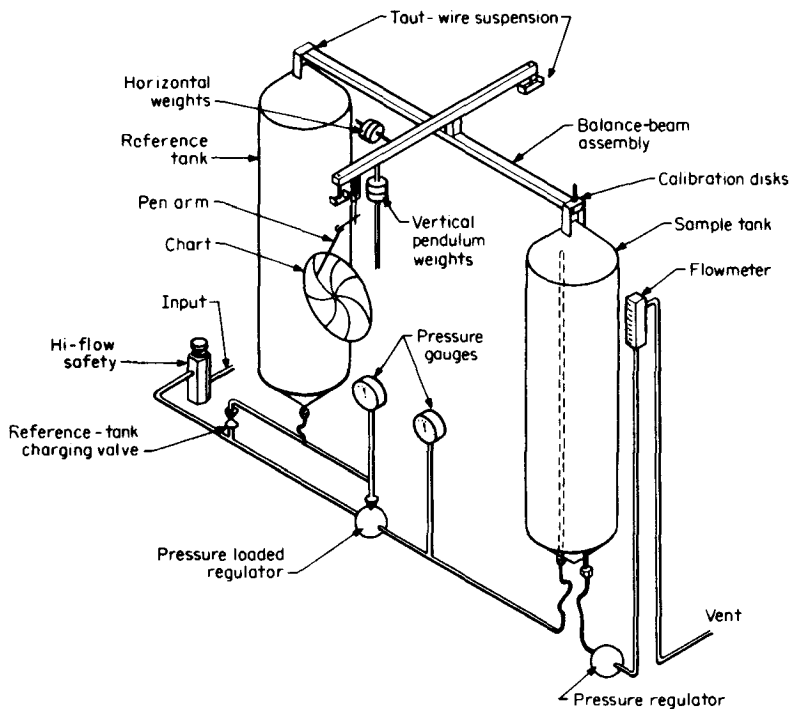
$$G = \frac{2.0158}{28.963} = 0.06960$$

The density is calculated from Eq. (2.10) as

$$\rho_f = 2.6988 \frac{(0.06960)(588)}{(1.0264)(449.67)} = 0.2393 \text{ lb}_m/\text{ft}^3$$

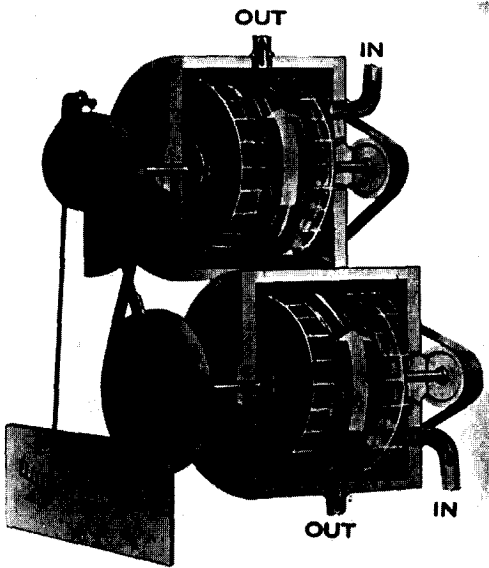


(a)

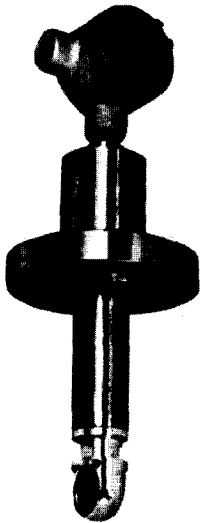


(b)

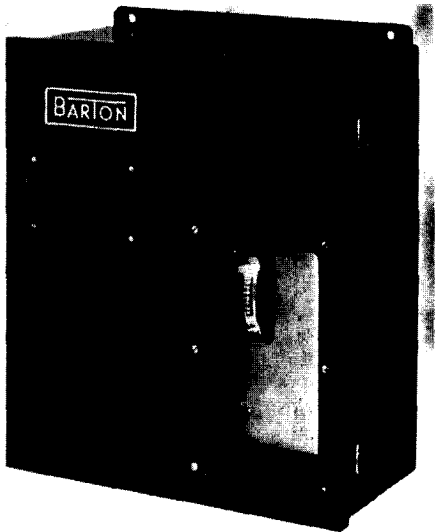
Figure 2.4 Density and specific-gravity measuring devices. (a) Buoyancy gas balance. (Courtesy UGC Industries, Inc.) (c) Momentum gravimeter: Ranarex Gas Analyzer. (Courtesy Permutit Co., Inc.) (d) Densitometer. (Courtesy ITT Barton.)



(c)



DENSITY PROBE



ELECTRONICS

(d)

Figure 2.4 (Continued)

The real specific gravity reading is calculated by rearranging Eq. (2.14) as

$$G_R = \frac{Z_{\text{air}}}{Z_{\text{gas}}} G = \frac{0.9999}{1.0006} 0.06960 = 0.06955$$

where Z_{air} and Z_{gas} are the values at 14.7 psia and 80°F.

The densitometer, shown in Fig. 2.4d, employs a thin rectangular plate in a cylindrical support structure as the density-sensing element. The mechanical components are assembled into a probe that is readily inserted through the pipe wall such that the reasoning plate is exposed to the process gas. In operation, the plate oscillates in simple harmonic motion, which accelerates the surrounding gas. By a closed feedback system utilizing a detector, an amplifier, and a driver coil, the plate is driven to maximum amplitude. The mass of surrounding fluid that vibrates with the plate varies with density, and the plate resonant frequency decreases with increasing gas density. The feedback-system resonant frequency then indicates the fluid density. Although the relationship between frequency and diversity is nonlinear, electronic linearization provides a standardized output. The device can be calibrated for use with both liquids and gases.

Jaescke and Hinze (1987) reported that when measuring natural gas using a resonant densitometer, an error of up to 0.6 percent could occur if the measurement were not corrected for the sound speed of the gas. The correction for the speed of sound differences between the calibration and flowing gas is

$$\rho_f = \frac{1 + (k_{\text{meter}}/V_{\text{son,calib}})^2}{1 + (k_{\text{meter}}/V_{\text{son,gas}})^2} \rho_{f,\text{ind}} \quad (2.15)$$

where k_{meter} is the densitometer constant, $V_{\text{son,calib}}$ is the velocity of sound of the calibration gas, $V_{\text{son,gas}}$ is the velocity of sound of the flowing gas, and $\rho_{f,\text{ind}}$ is the indicated density.

COMPRESSIBILITY VERSUS DENSITY DETERMINATION

Traditionally the units of measurement for gas flow have been volume (q_{SCFH} , q_{NCMH}) and those for vapor flow have been mass (lb_m/h, kg/h). For this reason the industries that meter gas exclusively (natural gas, air, etc.) developed their flow equations using a compressibility factor Z_f , and those that meter vapor flows (steam, ammonia, etc.) developed working equations based on density ρ_f . As can be seen from Eq. (2.10), density can be calculated from compressibility, or compressibility can be calculated from density when the gas composition, temperature, and pressure are known.

Numerous equations of state have been proposed that either calculate compressibility from pressure and temperature or calculate density directly. The equation or graphical solution selected depends on the desired accuracy and usually the preferred industrial practice.

Equations of state can conveniently be grouped as either generalized or specific. The generalized equation may have two or three parameters. Pressure and temperature are ratioed to a particular gas's or vapor's critical temperature T_c and pressure p_c , and the two reduced parameters p_r and T_r are used to predict the compressibility factor Z_f (see Fig. 2.2). A third parameter, the acentric factor ω , is introduced to

improve the prediction accuracy by accounting for the nonspherical nature of the molecules.

Specific equations of state are used where metering accuracy and other thermodynamic properties, such as enthalpy or the velocity of sound, require that the state equation be exact. These equations are based on accurate data which, by regression methods, is used to determine the virial coefficient constants.

The two most recognized specific equations of state are the *Manual for the Determination of Supercompressibility for Natural Gas* (1962), commonly referred to as the NX-19 state equations, and the *1967 IFC Formulation for Industrial Use* steam tables, referred to as the *1967 ASME Steam Tables*. Improved equations are now widely used for these fluids (AGA-8, GERG, and IAPS). These equations require iterative solutions, while the earlier forms are used to calculate the density or compressibility directly.

Virial Equation

Analytical state equations are derived using statistical mechanics and consideration of the intermolecular forces between gas molecules. The solution, representing the p_vT surface, is presented in terms of temperature-dependent *virial coefficients* and may be developed to solve for density ρ_f or compressibility Z_f . These equations are called *virial equations* and are written in the form

$$\frac{p_f}{R_0 T_f} = \rho_{\text{mol}} + B \rho_{\text{mol}}^2 + C \rho_{\text{mol}}^3 + D \rho_{\text{mol}}^4 + \dots \quad (2.16)$$

where p_f is in psia, T_f in degrees Rankine, R_0 in $\text{psia} \cdot \text{ft}^3 / (\text{lb}_m \cdot \text{mol})$, v_{mol} in $\text{ft}^3 / (\text{lb}_m \cdot \text{mol})$, and ρ_f in $\text{lb}_m \cdot \text{mol} / \text{ft}^3$. The constants B , C , D , . . . are known as the second, third, fourth, . . . *virial coefficients*.

In many applications the flowing density is less than one-half the critical density, and truncating the solution for density using only the second virial yields good accuracy (<0.25 percent).

The second virial molar density equation [Eq. (2.16)] is written, in SI units, as

$$\rho_{\text{mol}}^{*2} + \frac{1}{B} \rho_{\text{mol}}^* - \frac{P_f^*}{B R_{0E}^* T_K} = 0 \quad (2.17)$$

Equation (2.17) is a quadratic equation and may be solved for density by

$$\rho_{\text{mol}}^* = -\frac{1}{2B} - \frac{1}{2} \sqrt{\frac{1}{B^2} + \frac{4P_f^*}{B R_{0E}^* T_K}} \quad (2.18)$$

where ρ_{mol}^* has the units $\text{kg} \cdot \text{mol} / \text{m}^3$, the second virial B has the units $\text{m}^3 / \text{kg} \cdot \text{mol}$, the pressure P_f^* is in pascals, the universal gas constant R_{0E}^* has the units $\text{J} / (\text{kg} \cdot \text{mol} \cdot \text{K})$, and the temperature T_K is in kelvins. The density (kg / m^3) is

$$\rho_f^* = M_w \rho_{\text{mol}}^* \quad (2.19)$$

AIChE Virial Coefficient Equation. The Design Institute for Physical Property Data (AIChE, 1986) publishes an extensive data book on the properties of 1000 fluids. Equations are presented in a *generic* form, with equation constants selected from a data sheet.

The AIChE second virial coefficient, for a gas/vapor, is given as

$$B = a + \frac{b}{T_K} + \frac{c}{T_K^3} + \frac{d}{T_K^8} + \frac{e}{T_K^9} \quad (2.20)$$

where B has the units $\text{m}^3/\text{kg}\cdot\text{mol}$. The constants a , b , c , d , and e for some fluids are given in Table 2.1. Molar density is calculated by Eq. (2.18), and flowing density is calculated by Eq. (2.19).

Example 2.3. Gaseous methane is flowing at 200 psia (1.38 Mpa) and 50°F (10°C). Use the AIChE equation to calculate the density.

From the AIChE data compilation (Table 2.1) the constants for the second virial coefficient are

$$a = 5.438\text{E} - 02 \quad b = -2.714\text{E} + 01 \quad c = -2.135\text{E} + 05$$

$$d = 9.203\text{E} + 14 \quad e = -7.85\text{E} + 16$$

with $T_K = (50 + 459.67)/1.8 = 283.15$ K. Substitution into Eq. (2.20) yields the second virial as

$$\begin{aligned} B &= 5.438 \text{ E} - 02 + \frac{-2.714\text{E} + 01}{283.15} + \frac{-2.135\text{E} + 05}{(283.15)^3} + \frac{9.203\text{E} + 14}{(283.15)^8} \\ &\quad + \frac{-7.85\text{E} + 16}{(283.15)^9} \\ &= -0.05086 \text{ m}^3/\text{kg}\cdot\text{mol} \end{aligned}$$

The pressure, in pascals, is $P_f^* = 6.894757\text{E} + 03 \times 200 = 1.379\text{E} + 06$, where the conversion constant for pounds per square inch absolute to pascals is from App. C, Table C.1. The density is then, from Eq. (2.18),

TABLE 2.1 AIChE Second Virial Equation Constants

	Methane CH ₄	Ethylene C ₂ H ₄	Ethane C ₂ H ₆	Propadiene C ₃ H ₄	Propylene C ₃ H ₆
<i>a</i>	5.4380E - 02	7.1560E - 02	8.0950E - 02	8.5200E - 02	1.0010E - 01
<i>b</i>	-2.7140E + 01	-4.6270E + 01	-6.1710E + 01	-8.6500E + 01	-8.7450E + 01
<i>c</i>	-2.1350E + 05	-1.5023E + 06	-1.4350E + 06	-4.8200E + 06	-4.0140E + 06
<i>d</i>	9.2030E + 14	-1.8540E + 16	6.7600E + 16	-1.2780E + 18	-1.9460E + 17
<i>e</i>	-7.8500E + 16	1.2640E + 18	-9.7400E + 18	-2.7320E + 20	-4.9100E + 19
	Propane C ₃ H ₈	1,2-Butadiene C ₄ H ₆	Isobutene C ₄ H ₈	<i>n</i> -Butane C ₄ H ₁₀	Benzene C ₆ H ₆
<i>a</i>	1.1250E - 01	1.2450E - 01	1.3110E - 01	1.4164E - 01	1.4380E - 01
<i>b</i>	-1.0000E + 02	-1.1900E + 02	-9.9210E + 01	-1.3566E + 02	-1.7980E + 02
<i>c</i>	-4.3140E + 06	-9.2060E + 06	-1.1371E + 07	-1.0664E + 07	-2.4151E + 07
<i>d</i>	-1.8000E + 16	3.9570E + 18	-1.5410E + 18	-9.7300E + 17	-4.0000E + 17
<i>e</i>	-1.6500E + 19	-9.3200E + 20	6.3800E + 19	9.8400E + 16	-2.2670E + 21

Note: E in this table stands for *engineering notation*. For example, E + 07 = $\times 10^7$ and E - 07 = $\times 10^{-7}$, etc.

$$\rho_{\text{mol}}^* = -\frac{1}{(2)(-0.05086)} - \frac{1}{2} \sqrt{\frac{1}{(-0.05086)^2} + \frac{(4)(1.379\text{E} + 06)}{(-0.05086)(8314.4)(283.15)}}$$

$$= 0.6043 \text{ kg}\cdot\text{mol}/\text{m}^3$$

From App. D, Table D.1, the molecular weight M_w of methane is 16.043 kg/(kg·mol). The density, in kg/m³, is then, by Eq. (2.19)

$$\rho_f^* = M_w \rho_{\text{mol}}^* = (16.043)(0.6043) = 9.695 \text{ kg}/\text{m}^3 \text{ (0.6053 lb}_m/\text{ft}^3)$$

GAS COMPRESSIBILITY

Compressibility-Factor Diagrams

Deviation from the ideal gas law is taken into account with a multiplying factor called the compressibility factor, which can be found in tables, calculated from several available equations of state, or determined through generalized diagrams. For desk calculations, the generalized Nelson-Obert reduced two-parameter diagram is widely used. For improved accuracy, the three-parameter Edmister-Pitzer diagrams are used.

Nelson-Obert Diagram. Using experimental data for 26 single-component gases, Nelson and Obert (1954) developed the reduced two-parameter temperature and pressure diagram illustrated in Fig. 2.5a. For these gases, the smoothed curves fitted to within 1 percent. When used for other gases, except those near the critical point or strongly polar fluids, the accuracy of the diagram ranges approximately from 1 to 2 percent for compressibility factors greater than 0.6 and from 4 to 6 percent for factors in the range of 0.3 to 0.6. This diagram is not recommended for helium, hydrogen, or neon.

Edmister-Pitzer Diagrams. The Nelson-Obert diagram is based on a single two-parameter correlation. To improve the prediction, Pitzer (1955) introduced the *acentric factor* ω as a third parameter, to correct for the nonspherical nature of the molecular force field. The acentric factor is zero for the defined spherical simple fluids argon, krypton, and xenon. The Pitzer correlation yields good results for slightly polar and nonpolar gases, with an accuracy of approximately ± 1 percent when the compressibility factor ranges from 0.6 to 1.0, and ± 3 percent for factors in the range 0.2 to 0.8.

Edmister (1974) graphically presented Pitzer's results on two separate reduced-parameter diagrams. The first is the *simple-fluid* diagram illustrated in Fig. 2.5b; this is similar to the Nelson-Obert diagram, except that the reduced pressure axis has a logarithm scale. The second diagram is the *generalized compressibility correction for deviation from a simple fluid*. Assuming fluids with the same acentric factor have the same pvT relationship, and further assuming that the deviation function can be used in a linear manner to adjust for the acentric nature of the fluid, the compressibility can be calculated as

$$Z = Z^0 + \omega Z^1 \quad (2.21)$$

The acentric factors for many fluids are given in Table D.1. The two Edmister-Pitzer diagrams are presented in Figs. G.7 and G.8.

$$\rho_{\text{mol}}^* = -\frac{1}{(2)(-0.05086)} - \frac{1}{2} \sqrt{\frac{1}{(-0.05086)^2} + \frac{(4)(1.379 \times 10^6)}{(-0.05086)(8314.4)(283.15)}}$$

$$= 0.6043 \text{ kg} \cdot \text{mol} / \text{m}^3$$

From App. D, Table D.1, the molecular weight M_w of methane is 16.043 kg/(kg·mol). The density, in kg/m³, is then, by Eq. (2.19)

$$\rho_f^* = M_w \rho_{\text{mol}}^* = (16.043)(0.6043) = 9.695 \text{ kg} / \text{m}^3 \quad (0.6053 \text{ lb}_m / \text{ft}^3)$$

GAS COMPRESSIBILITY

Compressibility-Factor Diagrams

Deviation from the ideal gas law is taken into account with a multiplying factor called the compressibility factor, which can be found in tables, calculated from several available equations of state, or determined through generalized diagrams. For desk calculations, the generalized Nelson-Obert reduced two-parameter diagram is widely used. For improved accuracy, the three-parameter Edmister-Pitzer diagrams are used.

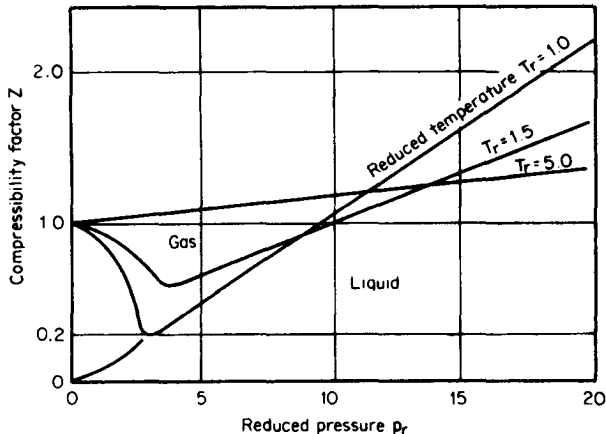
Nelson-Obert Diagram. Using experimental data for 26 single-component gases, Nelson and Obert (1954) developed the reduced two-parameter temperature and pressure diagram illustrated in Fig. 2.5a. For these gases, the smoothed curves fitted to within 1 percent. When used for other gases, except those near the critical point or strongly polar fluids, the accuracy of the diagram ranges approximately from 1 to 2 percent for compressibility factors greater than 0.6 and from 4 to 6 percent for factors in the range of 0.3 to 0.6. This diagram is not recommended for helium, hydrogen, or neon.

Edmister-Pitzer Diagrams. The Nelson-Obert diagram is based on a single two-parameter correlation. To improve the prediction, Pitzer (1955) introduced the *acentric factor* ω as a third parameter, to correct for the nonspherical nature of the molecular force field. The acentric factor is zero for the defined spherical simple fluids argon, krypton, and xenon. The Pitzer correlation yields good results for slightly polar and nonpolar gases, with an accuracy of approximately ± 1 percent when the compressibility factor ranges from 0.6 to 1.0, and ± 3 percent for factors in the range 0.2 to 0.8.

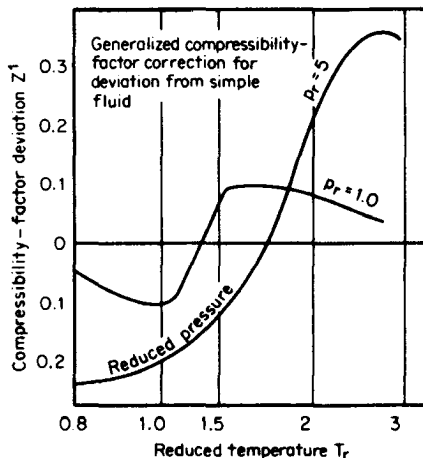
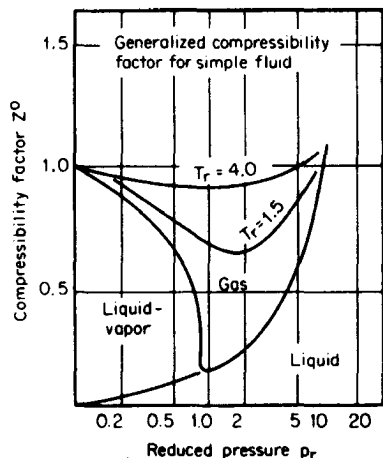
Edmister (1974) graphically presented Pitzer's results on two separate reduced-parameter diagrams. The first is the *simple-fluid* diagram illustrated in Fig. 2.5b; this is similar to the Nelson-Obert diagram, except that the reduced pressure axis has a logarithm scale. The second diagram is the *generalized compressibility correction for deviation from a simple fluid*. Assuming fluids with the same acentric factor have the same p_vT relationship, and further assuming that the deviation function can be used in a linear manner to adjust for the acentric nature of the fluid, the compressibility can be calculated as

$$Z = Z^0 + \omega Z^1 \quad (2.21)$$

The acentric factors for many fluids are given in Table D.1. The two Edmister-Pitzer diagrams are presented in Figs. G.7 and G.8.



(a)



(b)

Figure 2.5 Generalized compressibility diagrams (not to scale). (a) Nelson-Oberst (see Figs. G.1 through G.6). (b) Edmister (see Figs. G.7 and G.8).

Edmister (1974) proposed an equation for estimating the acentric factor from critical pressure, critical temperature, and boiling temperature as

$$\omega = \frac{3}{7} \frac{\log(p_c/14.7)}{T_c/T_B - 1} - 1 \quad (2.22)$$

This relationship correlates well with measured values and is especially useful in determining the compressibility factor of a gas mixture based on molar values.

Example 2.4. Calculate the density of methane at -99.7°F (-73.2°C) and 1470 psia (10,135 kPa) using (1) the Nelson-Oberst diagram and (2) the Edmister-Pitzer diagrams.

From Table D.1, for methane,

$$p_c = 667.2 \text{ psia} \quad (M_w)_{\text{CH}_4} = 16.043 \text{ lb}_m/\text{lb}_m \cdot \text{mol}$$

$$T_c = 343.1^\circ R \quad \omega = 0.008$$

The reduced parameters are then, from Eqs. (2.1) and (2.2),

$$p_r = \frac{1470}{667.2} = 2.20 \quad T_r = \frac{459.67 - 99.7}{343.1} = 1.05$$

1. *Nelson-Obert diagram.* From Fig. G.4, $Z = 0.365$. The specific gravity is, from Eq. (2.7),

$$G = \frac{16.043}{28.963} = 0.5539$$

The density is then, from Eq. (2.10),

$$\rho_f = (2.6988) \left[\frac{(0.5539)(1470)}{(0.365)(459.67 - 99.7)} \right] = 16.72 \text{ lb}_m/\text{ft}^3$$

2. *Edmister-Pitzer diagrams.* From Figs. G.7 and G.8, the simple-fluid compressibility and the correction for deviation from a simple fluid are

$$Z^0 = 0.372 \quad Z^1 = -0.08$$

Then, from Eq. (2.21),

$$Z = 0.372 + (0.008)(-0.08) = 0.371$$

The density is calculated with Eq. (2.11):

$$\rho_f = 2.6988 \frac{(0.5539)(1470)}{(0.371)(459.67 - 99.7)} = 16.45 \text{ lb}_m/\text{ft}^3$$

Calculating Compressibility

Numerous equations of state have been developed to relate pressure, temperature, and specific volume. Each has particular advantages and a range over which it can be applied. The more accurate equations require a change of constants for each gas and are most often used for thermodynamic studies and specific flow situations. In cases where mixture-combination rules are not available, a verification test is required if accuracy is important.

For many gas applications, the compressibility factor is seldom below 0.85, and it is most often between 0.95 and 1.0. Within this range, iterative solution of the equation of Redlich and Kwong (1949) is suggested for general gas applications. For natural gas the AGA† NX-19 (1963) equations, the AGA-8, the Pacific Energy Association equations (fitted to NX-19), or the Hall-Yarborough equation (fitted to the Standing-Katz diagrams) are commonly used.

†American Gas Association.

Redlich-Kwong Equation. Redlich and Kwong (1949) developed a two-parameter equation of state that can be rearranged to calculate the compressibility factor from the reduced pressure and temperature as

$$Z^3 - Z^2 - (B^2 + B - A)Z - AB = 0 \quad (2.23)$$

where
$$A = \frac{0.42748p_r}{T_r^{2.5}} \quad B = \frac{0.086647p_r}{T_r} \quad (2.24)$$

the constants are pure numbers; i.e.,

$$[(9)(2^{1/3} - 1)]^{-1} = 0.42748 \quad \frac{2^{1/3} - 1}{3} = 0.086647$$

Equation (2.23) is nonlinear, and an iterative solution is required. Newton's method for solving for the zero root of an equation is the simplest to use. Equation (2.23) is written in the function form given by Eq. (A.9) in App. A, and the estimates for the compressibility factor may be written as

$$Z_n = Z_{n-1} - \frac{F_{n-1}}{F'_{n-1}} \quad (2.25)$$

where Z_{n-1} is the initial estimate, F_{n-1} is

$$F_{n-1} = Z_{n-1}^3 - Z_{n-1}^2 - (B^2 + B - A)Z_{n-1} - AB \quad (2.26)$$

and the derivative of the function F_{n-1} is

$$F'_{n-1} = 3Z_{n-1}^2 - 2Z_{n-1} - (B^2 + B - A) \quad (2.27)$$

Figure 2.6 shows the percentage difference between compressibility factors computed with the Redlich-Kwong equation and the actual factors for argon, methane,

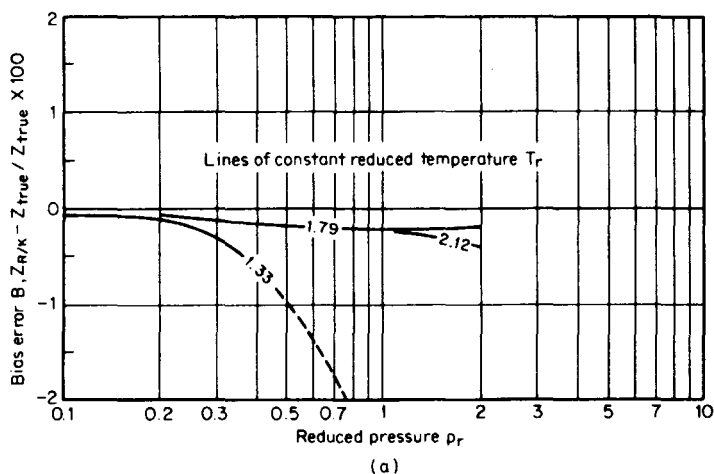


Figure 2.6 Bias error for Redlich-Kwong equations. (a) Argon. (b) Methane. (c) Oxygen.

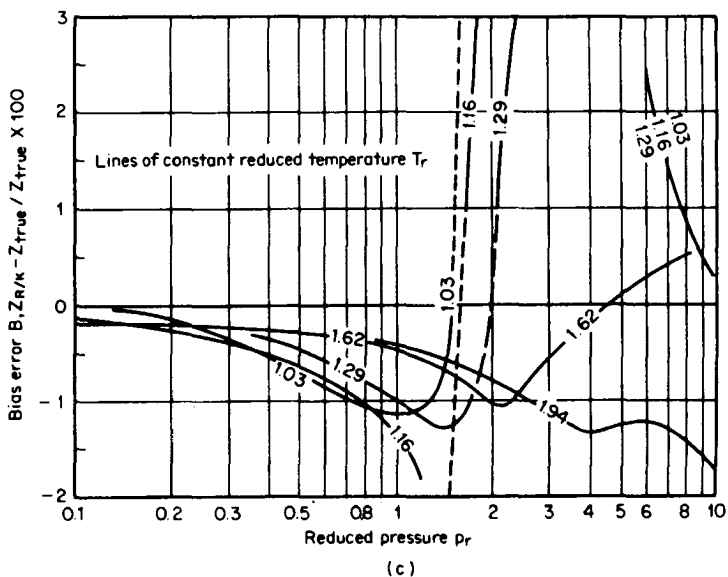
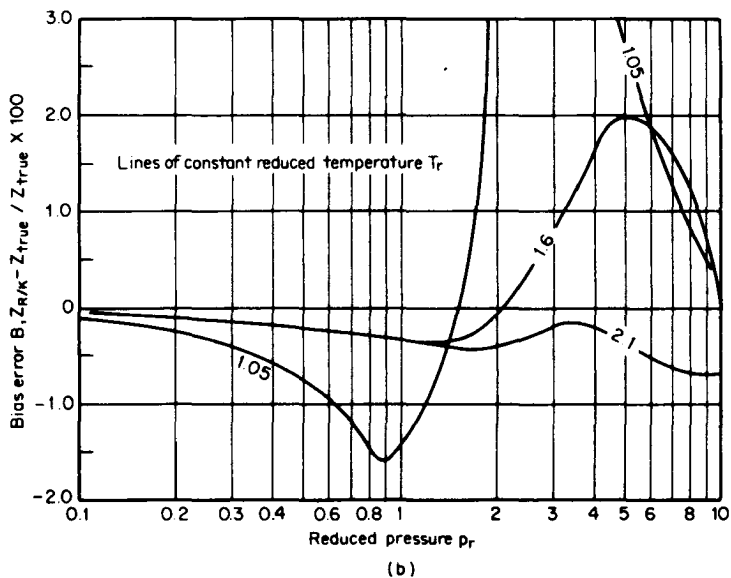


Figure 2.6 (Continued)

and oxygen. For reduced pressures below 0.6, the bias error is less than 1 percent. For lower reduced pressures, the error is 0.5 percent or less.

Interpolation Using the Redlich-Kwong Equation. When the compressibility factor is known from tables or by measurement at a given design-reduced pressure and temperature, the Redlich-Kwong equation can be used to predict operating values. For example, many on-site computers use a preset, dialed-in compressibility factor based on average daily pressure, temperature, and specific gravity. If the pressure or temperature varies from these values, a bias error will be introduced in the calculated flow rate.

If it is assumed that the compressibility factor calculated from the Redlich-Kwong equation is biased from the actual compressibility factor, then a ratio can be used to continuously adjust the dialed-in factor as follows:

$$Z_f = \frac{(Z_{R/K})_f}{(Z_{R/K})_{des}} Z_{des} \quad (2.28)$$

In Eq. (2.28) the tabular or measured compressibility factor Z_{des} is multiplied by the ratio of the compressibility factor calculated with the Redlich-Kwong equation at measured flowing temperature and pressure, to that calculated at the design conditions $(Z_{R/K})_{des}$.

In many gas (vapor) flow applications, density is read from tabular values at a design pressure and temperature. Under flowing conditions, the pressure and temperature are not always equal to design values, and the flow rate must be corrected. If the gas (vapor) is superheated and approximates an ideal gas ($Z = 1.0$), the correction is made with the ratio of pressure to temperature in accordance with Eq. (2.11). For real gas (vapor) and for accurate work, the compressibility of the gas should also be calculated at flowing conditions.

For computer applications, the Redlich-Kwong equation can be used to continually correct for the density at flowing conditions

$$\rho_f = \frac{(Z_{R/K})_{des}}{(Z_{R/K})_f} \frac{(T_f)_{des}}{T_f} \frac{P_f}{(P_f)_{des}} (\rho_f)_{des} \quad (2.29)$$

where the subscript *des* means design conditions, and the subscript *f* means flowing conditions. The Redlich-Kwong compressibility factor $(Z_{R/K})_{des}$ is calculated from design conditions for use in Eq. (2.29).

Example 2.5. The output of a vortex flowmeter is scaled to read steam flow in pounds-mass per hour at 400°F (204°C) and 120 psia (827 kPa), based on a density of 0.2452 lb_m/ft³ (3.928 kg/m³). Using the Redlich-Kwong equation with a single iteration ($Z_0 = 1$), calculate the bias error if the steam temperature and pressure change to 410°F (210°C) and 140 psia (965 kPa).

A vortex flowmeter measures volumetric flow at flowing conditions q_{acfh} . The calculated mass flow is then

$$(q_{PPH})_{des} = 0.2452(q_{acfh})_{vor}$$

at design conditions, and

$$(q_{PPH})_{true} = \rho_f(q_{acfh})_{vor}$$

at flowing conditions, where the subscript *vor* stands for vortex. The bias error is calculated by

$$B = \frac{(q_{PPH})_{des} - (q_{PPH})_{true}}{(q_{PPH})_{true}} = \frac{0.2452 - \rho_f}{\rho_f}$$

At design conditions of 400°F and 120 psia, the critical properties, from Table D.1, are

$$p_c = 3197.9 \text{ psia} \quad T_c = 1165.1^\circ\text{R}$$

and the reduced pressure and temperature are, from Eqs. (2.1) and (2.2),

$$p_r = \frac{p_f}{p_c} = \frac{120}{3197.9} = 0.037525 \quad T_r = \frac{T_f}{T_c} = \frac{459.67 + 400}{1165.1} = 0.73785$$

The Redlich-Kwong coefficients are, from Eq. (2.24),

$$A = \frac{0.42748 p_r}{T_r^{2.5}} = \frac{(0.42748)(0.037525)}{(0.73785)^{2.5}} = 0.03430$$

$$B = \frac{0.08665 p_r}{T_r} = \frac{(0.08665)(0.037525)}{0.73785} = 0.004408$$

With the initial estimate $Z_{n-1} = Z_0 = 1.0$, the function F_0 [Eq. (2.26)] becomes

$$F_0 = 1 - 1 - [(0.004408)^2 + (0.004408) - (0.03430)](1.0) \\ - (0.03430)(0.004408) = 0.03002$$

and the derivative of the function is, from Eq. (2.27),

$$F'_0 = (3)(1.0)^2 - (2.0)(1.0) - [(0.004408)^2 + (0.004408) - (0.03430)] \\ = 1.0299$$

From Eq. (2.25) the first iteration gives, with $Z_0 = 1$, the design value

$$(Z_{RK})_{des} = 1 - \frac{0.03002}{1.0299} = 0.9709$$

At flowing conditions, the reduced pressure and temperature are, from Eqs. (2.1) and (2.2),

$$p_r = \frac{p_f}{p_c} = \frac{140}{3197.9} = 0.043779 \quad T_r = \frac{T_f}{T_c} = \frac{459.67 + 410}{1165.1} = 0.74643$$

The Redlich-Kwong coefficients for flowing conditions are

$$A = 0.3979 \quad B = 0.005082$$

so that $F_0 = 0.03448$ and $F'_0 = 1.0299$ and the flowing compressibility becomes, from Eq. (2.25),

$$Z_f = 1.0 - \frac{0.3448}{1.0299} = 0.9665$$

From Eq. (2.28), the density at flowing conditions by the Redlich-Kwong equation is then

$$\rho_f = 0.2452 \frac{0.9709}{0.9665} \frac{459.67 + 400}{459.67 + 410} \frac{140}{120} = 0.2841$$

The bias error is calculated as

$$B_q = \frac{0.2452 - 0.2841}{0.2841} 100 = -13.7 \text{ percent}$$

Hall-Yarborough Equation. For general natural gas measurement, where the Standing and Katz (1942) compressibility diagram is used, the closed-form solution proposed by Hall and Yarborough (1973, 1974) is useful. The Hall-Yarborough has an accuracy of ± 0.3 percent for reduced temperatures above 1.05 and for very high reduced pressures. To derive the equation, a hard-sphere equation of state was modified by a generalized real-gas deviation function that fitted the Standing-Katz Z-factor diagram. The hard-sphere equation approximates real-gas characteristics at high pressures and temperatures and allows for a generalized closed-form equation, without specific constants for each gas.

To calculate the compressibility factor, two equations are required. The first is a zero-root equation that is iterated to find a reduced density value; from this, the compressibility factor is calculated.

First the mixture's pseudocritical temperature is calculated from known mole fractions as

$$T_{pc} = \sum x_i T_{ci} \quad (2.30)$$

This is corrected for the mole fraction of carbon dioxide and hydrogen sulfide content by computing

$$T_{ca} = T_{pc} - C_{WA} \quad (2.31)$$

$$\text{where } C_{WA} = 120[(x_{\text{CO}_2} + x_{\text{H}_2\text{S}})^{0.9} - (x_{\text{CO}_2} + x_{\text{H}_2\text{S}})^{1.6}] + 15(x_{\text{H}_2\text{S}}^{1/2} - x_{\text{H}_2\text{S}}^4) \quad (2.32)$$

The mixture's pseudocritical pressure is then determined as

$$p_{pc} = \sum x_i p_{ci} \quad (2.33)$$

which is adjusted for the mole fraction of carbon dioxide and hydrogen sulfide by computing

$$p_{ca} = \frac{p_{pc} T_{ca}}{T_{pc} + C_{WA} + x_{\text{H}_2\text{S}}(1 - x_{\text{H}_2\text{S}})C_{WA}} \quad (2.34)$$

The pseudocritical reduced temperature and pressure are then obtained using

$$T_{pr} = \frac{T_f}{T_{ca}} \quad p_{pr} = \frac{p_f}{p_{ca}} \quad (2.35)$$

The reduced density ρ_r is then calculated by Newton's method (see Sec. A.1) as

$$(\rho_r)_n = (\rho_r)_{n-1} - \frac{F_{n-1}}{F'_{n-1}} \quad (2.36)$$

where

$$F = -b + \frac{\rho_r + \rho_r^2 + \rho_r^3 - \rho_r^4}{(1 - \rho_r)^3} - c\rho_r^2 + d\rho_r^f \quad (2.37)$$

and

$$F' = \frac{1 + 4\rho_r + 4\rho_r^2 - 4\rho_r^3 + \rho_r^4}{(1 - \rho_r)^4} - 2c\rho_r + fd\rho_r^g \quad (2.38)$$

The constants in Eqs. (2.37) and (2.38) are derived from pseudocritical properties as

$$b = 0.06125p_{pr}T \exp a \quad f = 2.18 + 2.82T$$

$$c = 14.76T - 9.76T^2 + 4.58T^3 \quad g = 1.18 + 2.82T$$

$$d = 90.7T - 242.2T^2 + 42.4T^3$$

where

$$T = \frac{1}{T_{pr}} \quad \text{and} \quad a = -1.2(1 - T)^2$$

As the first estimate for the reduced density, the approximation

$$(\rho_r)_0 = b \quad (2.39)$$

is used. Three iterations are usually required to determine the reduced density to a closure accuracy of 0.1 percent. From this value the compressibility factor is calculated as

$$Z_f = \frac{b}{\rho_r} \quad (2.40)$$

Example 2.6. Calculate, using the Hall-Yarborough equation, the Standing-Katz compressibility factor for the mixture detailed below, at a flowing temperature of 100°F (37.8°C) and a pressure of 1000 psia (6895 kPa).

Component	Mole fraction x_i	Critical temperature T_{ci}^\dagger °R	$x_i T_{ci}$	Critical pressure p_{ci}^\dagger psia	$x_i p_{ci}$
Methane	0.6	343.1	205.9	667.2	400.3
Carbon dioxide	0.2	547.6	109.5	1069.9	214.0
Hydrogen sulfide	0.2	671.8	<u>134.4</u>	1269.2	<u>253.8</u>
			449.8		868.1

[†]From Table D.1.

From Eqs. (2.30) and (2.33), respectively,

$$T_{pc} = \sum x_i T_{ci} = 449.8 \quad p_{pc} = \sum x_i p_{ci} = 868.1$$

From Eq. (2.32),

$$C_{wA} = 120[(0.2 + 0.2)^{0.9} - (0.2 + 0.2)^{1.6}] + 15(0.2^{1/2} - 0.2^4) = 31.6^\circ\text{F}$$

The adjusted pseudocritical temperature is then, from Eq. (2.31),

$$T_{ca} = 449.8 - 31.6 = 418.2^\circ\text{R}$$

The adjusted pseudocritical pressure is, from Eq. (2.34),

$$p_{ca} = \frac{(868.1)(418.2)}{449.8 + 31.6 + (0.2)(1 - 0.2)(31.6)} = 746.3 \text{ psia}$$

The pseudocritical reduced temperature and pressure are, from Eq. (2.35),

$$T_{pr} = \frac{459.67 + 100}{418.2} = 1.338$$

$$p_{pr} = \frac{1000}{746.3} = 1.340$$

The Hall-Yarborough constants are, with $T = 1/T_{pr}$,

$$\begin{aligned} a &= -0.07658 & d &= -49.80 \\ b &= 0.05682 & f &= 4.288 \\ c &= 7.490 & g &= 3.287 \end{aligned}$$

The initial estimate for the reduced density is, from Eq. (2.39),

$$(\rho_r)_0 = 0.0952 \text{ lb}_m/\text{ft}^3$$

and the iterative solution is tabulated as follows:

Iteration n	Reduced density $(\rho_r)_{n-1}$	Function F_{n-1} [Eq. (2.31)]	Function F'_{n-1} [Eq. (2.32)]	Reduced density $(\rho_r)_n$ [Eq. (2.30)]
1	0.0952	0.0150	0.5890	0.0699
2	0.0699	-0.000759	0.6498	0.07105
3	0.0705	-0.000002	0.6462	0.07105

According to Eq. (2.40), the compressibility factor then is

$$Z_f = \frac{b}{(\rho_r)_n} = \frac{0.05682}{0.07105} = 0.7997$$

Pacific Energy Association Equations. Orifice flowmeters are used almost exclusively for the measurement of high-pressure natural gas. In developing the flow equation for calculating standard cubic feet per hour, a correction factor called the *AGA supercompressibility factor* was introduced for use in Eq. (9.68). For convenience it is derived as

$$F_{pv} = \frac{Z_b}{\sqrt{Z_f}} \quad (2.41)$$

In the natural gas industry the term *supercompressibility* is almost always used, even with reference to vortex, turbine, or other linear-output flowmeters. For these flowmeters, Eq. (2.41) is rewritten as

$$Z_f = \frac{Z_b}{F_{pv}^2} \quad (2.42)$$

For natural gas containing small amounts of inerts such as carbon dioxide and nitrogen, the supercompressibility factor may be found in the AGA (1963) tables. There are six volumes that cover pressures from 0 to 3000 psig (0 to 21,000 kPa). A seventh volume contains the corrections for nitrogen and carbon dioxide content. In the *Manual for the Determination of Supercompressibility Factors for Natural Gas* (AGA, 1963), the range is extended by computer calculations to a pressure of 5000 psig (34,475 kPa), temperatures of -40 to 240°F (-40 to 116°C), specific gravities of 0.554 to 1.000, and 15 percent carbon dioxide and nitrogen contents.

These tables and the manual computations are too extensive to publish in this handbook. For noncustody transfer flow calculations, the empirical equations and tabular corrections for inert constituent tables developed by the Pacific Energy Association (PEA, 1977) are used for computer computation. The supercompressibility factor is calculated from the generalized equation

$$F_{pv} = \sqrt{1 + \frac{k_1 p_G (10^{5+k_2 G})}{T_f^{3.825}}} \quad (2.43)$$

Values of k_1 and k_2 are specified for selected specific-gravity ranges, and these are given in Table 2.2.

TABLE 2.2 Constants for Natural Gas
Supercompressibility Equation; $p_f \leq 600$ psia

Range of specific gravity G	Constants	
	k_1	k_2
$0.600 \leq G$	2.48	2.020
$0.601 \leq G \leq 0.650$	3.32	1.810
$0.651 \leq G \leq 0.750$	4.66	1.600
$0.751 \leq G \leq 0.900$	7.91	1.260
$0.901 \leq G \leq 1.100$	11.63	1.070
$1.101 \leq G \leq 1.500$	17.48	0.900

Source: Pacific Energy Association (1977).

In Tables G.11 through G.16, values from Eq. (2.43) at 60°F (15.6°C) are listed. These must be adjusted for flowing temperature by first using Table G.17 and then algebraically subtracting the correction for inerts given in Table G.18.

Example 2.7. The specific gravity of a natural gas containing 5 percent by volume of carbon dioxide is measured as 0.73. The flowing pressure is 400 psig (2758 kPa), and the flowing temperature is 40°F (4.44°C). Assuming the base compressibility $Z_b = 0.9976$, determine the compressibility factor Z_f (1) by using the Pacific Energy Association equation and inert correction table and (2) from the tables given in App. G.

1. *By calculation and inert table.* From Table 2.2, $k_1 = 4.66$ and $k_2 = 1.600$. The supercompressibility factor is, from Eq. (2.43),

$$F_{pv} = \sqrt{1 + \frac{(4.66)(400)(10^{5+(1.6)(0.73)})}{(459.67 + 40)^{3.825}}}$$

$$= 1.063$$

From Table G.19, the correction for 5 percent CO₂ is -0.006, which is a subtractive correction; therefore,

$$F_{pv} = 1.063 - 0.006 = 1.057$$

The compressibility factor is then given by Eq. (2.42):

$$Z_f = \frac{0.9976}{(1.057)^2} = 0.893$$

2. *Tabular solution.* From Table G.13, $F_{pv} = 1.055$ at 400 psig and 60°F. Then, from Table G.17, the corrected value at 40°F is $F_{pv} = 1.064$. This value is corrected for 5 percent CO₂ by the subtraction of 0.006, so that

$$F_{pv} = 1.064 - 0.006 = 1.058$$

The compressibility factor is, again from Eq. (2.42),

$$Z_f = \frac{0.9976}{(1.058)^2} = 0.891$$

Natural Gas NX-19 Equation. The NX-19 (1963) natural gas state equations are widely used in custody transfer applications. Over most normal measurement ranges, 500 to 1500 psia (3.5 to 10.4 MPa) and -10 to 100°F (-23 to 38°C), the NX-19 equation will compute the gas compressibility factor to within 0.2 percent of the values computed by the newer AGA-8 state equation. Depending on contractual requirements, it is suitable for most applications, particularly since it is a closed form (noniterative) solution.

The ranges over which the NX-19 equation applies are

Pressure p_G	To 5000 psig (10.34 MPa, gauge)
Temperature T_F	-40 to 240°F (-40 to 116°C)
Specific gravity G	0.554 to 1.0
CO ₂ and N ₂	0 to 15%

Four methods are used to first obtain the adjusted temperature and pressure before entering the state equation.

Method 1. The *specific gravity method* calculates adjusted pressure and temperature from the mole fractions of carbon dioxide and nitrogen as

$$p_{\text{adj}} = \frac{156.47p_G}{160.8 - 7.22G_R + 100x_{\text{CO}_2} - 39.2x_{\text{N}_2}} \quad (2.44)$$

where x_{CO_2} and x_{N_2} are the mole fractions of carbon dioxide and nitrogen, respectively.

The adjusted temperature is defined by

$$T_{\text{adj}} = \frac{226.29(T_F + 460)}{99.15 + 211.9G_R - 100x_{\text{CO}_2} - 168.1x_{\text{N}_2}} \quad (2.45)$$

Method 2. Suggested for high-specific-gravity gas ($G_R > 0.75$), the *analysis method* requires a complete fractional analysis of the gas in order to determine the adjusted pressure and temperature, which are calculated by

$$p_{\text{adj}} = \frac{671.4p_G}{\sum x_i p_{ci}} \quad \text{and} \quad T_{\text{adj}} = \frac{359.46(T_F + 460)}{\sum x_i T_{ci}} \quad (2.46)$$

where p_{ci} is the critical pressure and T_{ci} is the critical temperature of each i th component.

Method 3. The *methane method*, also recommended for high-specific-gravity ($G_R > 0.75$) gases, requires the methane mole fraction and the two inert mole fractions of carbon dioxide and nitrogen fractions to be measured. The adjusted pressure p_{adj} and temperature T_{adj} are defined by

$$p_{\text{adj}} = \frac{671.4p_G}{891.11 - 172.56G_R + 443.04x_{\text{CO}_2} - 232.23x_{\text{N}_2} - 122.52x_{\text{CH}_4}} \quad (2.47)$$

$$T_{\text{adj}} = \frac{359.46(T_F + 460)}{327.77 + 214.82G_R - 144.12x_{\text{CO}_2} - 319.52x_{\text{N}_2} - 102.78x_{\text{CH}_4}} \quad (2.48)$$

Method 4. The *heating value method* uses the measured heating value [wet basis, Btu/(std ft³) at 14.73 psia and 60°F] and the mole fractions of nitrogen and carbon dioxide. The adjusted pressure and temperature are

$$p_{\text{adj}} = \frac{671.4p_G}{693 - 0.0209H_{\text{Btu,wet}} + 379x_{\text{CO}_2} - 201x_{\text{N}_2}} \quad (2.49)$$

$$\text{and} \quad T_{\text{adj}} = \frac{359.46(T_F + 460)}{124.7 + 0.2203H_{\text{Btu,wet}} + 384.99x_{\text{CO}_2} + 91.11x_{\text{N}_2}} \quad (2.50)$$

After calculating the adjusted pressure and temperature, the mixtures' pressure and temperature *correlation parameters* are calculated by

$$p = \frac{p_{\text{adj}} + 14.7}{1000} \quad T = \frac{T_{\text{adj}}}{500} \quad (2.51)$$

The compressibility factor is then calculated by first determining

$$m = 0.0330378T^{-2} - 0.0221323T^{-3} + 0.0161353T^{-5} \quad (2.52)$$

$$n = (0.265827T^{-2} + 0.0457697T^{-4} - 0.133185T^{-1})m^{-1} \quad (2.53)$$

$$B = \frac{3 - mn^2}{9mp^2} \quad (2.54)$$

$$b = \frac{9n - 2mn^3}{54mp^3} - \frac{E}{2mp^2} \quad (2.55)$$

$$D = [b + (b^2 + B^3)^{0.5}]^{1/3} \quad (2.56)$$

where E in Eq. (2.55) is a function of the pressure p and temperature T correlation parameters. The equations for E are given in Table 2.3 for the designated regions.

The flowing compressibility Z_f is determined by

$$Z_f = \frac{1}{B/D - D + n/3p} \quad (2.57)$$

TABLE 2.3 NX-19 Natural Gas Regions and E Equations

Ranges		
p	T	
0 to 2	1.09 to 1.40	E_1
0 to 1.3	0.84 to 1.09	E_2
1.3 to 2.0	0.88 to 1.09	E_3
1.3 to 2.0	0.84 to 0.88	E_4
2.0 to 5.0	0.84 to 0.88	E_5
2.0 to 5.0	0.88 to 1.09	E_6
2.0 to 5.0	1.09 to 1.32	E_7
2.0 to 5.0	1.32 to 1.40	E_8
$T_a = T - 1.09 \quad T_b = 1.09 - T$		
$E_1 = 1 - 0.00075p^{2.3} \exp(-20T_a) - 0.0011 T_a^{0.5} p^2 [2.17 + 1.4 T_a^{0.5} - p]^2$		
$E_2 = 1 - 0.00075p^{2.3} [2 - \exp(-20T_b)] - 1.317T_b^4 p (1.69 - p^2)$		
$E_3 = 1 - 0.00075p^{2.3} [2 - \exp(-20T_b)] + 0.455(200T_b^6 - 0.03249T_b$ $+ 2.0167T_b^2 - 18.028T_b^3 + 42.844T_b^4)(p - 1.3)[1.69(2)^{1.25} - p^2]$		
$E_4 = 1 - 0.00075p^{2.3} [2 - \exp(-20T_b)] + 0.455[200T_b^6 - 0.03249T_b + 2.0167T_b^2$ $- 18.028T_b^3 + 42.844T_b^4](p - 1.3)[1.69(2)^{1.25 + 80(0.88 - T)^2} - p^2]$		
$E_5 = E_4 - X \quad E_6 = E_3 - X \quad E_7 = E_1 - X \quad E_8 = E_7 - X_1^\dagger$		
$X = A(T - 2) + A_1(p - 2)^2 + A_2(p - 2)^3 + A_3(p - 2)^4$		
$X_1 = (p - 1.32)^2(p - 2)[3 - 1.483(p - 2) - 0.1(p - 2)^2 + 0.0833(p - 2)^3]$		
$A = 1.7172 - 2.33123T - 1.56796T^2 + 3.47644T^3 - 1.28603T^4$		
$A_1 = 0.016299 - 0.028094T + 0.48782T^2 - 0.78221T^3 + 0.27839T^4$		
$A_2 = -0.35978 + 0.51419T + 0.16453T^2 - 0.52216T^3 + 0.19687T^4$		
$A_3 = 0.075255 - 0.10573T - 0.058598T^2 + 0.14416T^3 - 0.054533T^4$		

† Set $p = 2.0$ when computing E_1 , E_3 , and E_4 .

When NX-19 is used for custody transfer applications, the base compressibility factor is calculated by

$$Z_b = \left(1 + \frac{0.00132}{T^{3.25}} \right)^{-2} \quad (2.58)$$

AGA 8. The Gas Research Institute (GRI, 1985) sponsored a major investigation to develop an equation of state to predict the compressibility of natural gas mixtures with higher inert contents (up to 50 percent N₂ and/or CO₂) and higher pressure and temperatures than the NX-19 equation is used for.

The region covered is from -200 to 400°F (-129 to 204°C) and 0 to 20,000 psia (138 MPa). Varying accuracy requirements for the molar density (or compressibility factor) were established for designated ranges. In the *custody transfer region*, where the temperature ranges from -60 to 180°F (-51 to 82°C) and the pressure from 0 to 1500 psia (0 to 10.4 MPa), the state equation has an estimated accuracy of 0.05 percent. Outside this region other accuracy requirements (up to 2 percent) are possible. In the region near the critical point no accuracy statement is given.

In the custody transfer region the equation of state also calculates the density of the pure components normally found in natural gas, such as methane, ethane, propane, and carbon dioxide, to within 0.2 percent. This makes it a most useful equation for many applications.

The AGA-8 (1992) molar density virial equation may be written as

$$\frac{p_f}{R_0 T_f} = \rho_{\text{mol}} + B \rho_{\text{mol}}^2 + C \rho_{\text{mol}}^3 + D \rho_{\text{mol}}^4 + E \rho_{\text{mol}}^6 + G \rho_{\text{mol}}^3 (1 + H \rho_{\text{mol}}^2) \exp(-H \rho_{\text{mol}}^2) \quad (2.59)$$

Equation (2.59) is written in U.S. customary units where the flowing pressure p_f is in psia, temperature T_f is in degrees Rankine, density ρ_{mol} is in lb_m·mol/ft³.

The universal gas constant R_0 for use with AGA-8 is given as 10.73164 psia·ft³/(lb_m·mol·°R)[8314.48 J/(kg·mol·K)].

Second Virial. The most important term in the state equation is the second virial B , since it contributed 90 percent of the final density or compressibility value. The second virial is determined by the exact virial binary mixing rule as

$$B = \sum_{i=1}^n \sum_{j=1}^n x_i x_j B_{ij} \quad (2.60)$$

where x_i and x_j are the component mole fractions and B_{ij} is the binary mixture's interaction virial coefficient term. The i and j subscripts represent methane, ethane, propane, or other components, and the combined subscript ij represents a binary mixture of the i and j components. For example, the second virial for a methane-ethane mixture would be written as

$$B = x_{\text{CH}_4} x_{\text{CH}_4} B_{\text{CH}_4, \text{CH}_4} + x_{\text{CH}_4} x_{\text{C}_2\text{H}_6} B_{\text{CH}_4, \text{C}_2\text{H}_6} + x_{\text{C}_2\text{H}_6} x_{\text{CH}_4} B_{\text{C}_2\text{H}_6, \text{CH}_4} + x_{\text{C}_2\text{H}_6} x_{\text{C}_2\text{H}_6} B_{\text{C}_2\text{H}_6, \text{C}_2\text{H}_6} \quad (2.61)$$

The term B_{ij} in Eq. (2.60) is calculated by

$$B_{ij} = [A_1 + A_2 T_{ij}^{-0.5} + A_3 T_{ij}^{-1} + A_4 T_{ij}^{-1.5} + A_5 T_{ij}^{-2} + A_6 T_{ij}^{-2.5} + A_7 T_{ij}^{-3.5}]$$

$$+ A_8 T_{ij}^{-4} + \frac{\omega_i + \omega_j}{2} (A_{20} T_{ij}^{-0.5} + A_{21} T_{ij}^{-2}) [\sigma_{spi} \sigma_{spj}]^{1.5} \quad (2.62)$$

The constants A_1, A_2, A_3, \dots are given in Table 2.4.

The Lennard-Jones separation parameter σ_{spi} or σ_{spj} for each pure substance is

$$\sigma_{sp} = \left(\frac{0.3189}{\rho_c} \right)^{1/3} \quad (2.63)$$

where ρ_c is the substance's critical density ($\text{lb}_m \cdot \text{mol}/\text{ft}^3$). Values for σ_{sp} are presented in Table 2.5.

The dimensionless binary mixture temperature T_{ij} is

TABLE 2.4 AGA-8 Equation-of-State Constants

$A_1 = 0.25837$	$A_8 = -0.28112$	$A_{15} = 21.35631$	$A_{22} = -4.82222$
$A_2 = 7.04794$	$A_9 = 2.62998$	$A_{16} = 14.15528$	$A_{23} = 12.22885$
$A_3 = -19.53600$	$A_{10} = 1.88315$	$A_{17} = 2.03047$	$A_{24} = -16.83781$
$A_4 = 14.43903$	$A_{11} = -7.15823$	$A_{18} = 9.96509$	$A_{25} = 0.55906$
$A_5 = -7.36355$	$A_{12} = 0.05833$	$A_{19} = 4.55053$	$A_{26} = 18.25211$
$A_6 = -0.18877$	$A_{13} = 18.02809$	$A_{20} = 6.51706$	$A_{27} = 11.79425$
$A_7 = 0.03392$	$A_{14} = -40.20412$	$A_{21} = -12.33577$	

TABLE 2.5 AGA-8 Equation Parameters

	Energy ϵ , °R	Size σ_{sp} , ($\text{ft}^3/\text{lb}_m \cdot \text{mol}$) ^{1/3}	Acentric ω
Methane	272.373	0.798064	0.0115
Ethane	436.514	0.910959	0.0915
Propane	528.651	1.010207	0.1520
<i>n</i> -Butane	607.766	1.092139	0.1957
Isobutane	583.324	1.103425	0.1760
<i>n</i> -Pentane	671.381	1.170828	0.2637
Isopentane	658.080	1.160552	0.2270
<i>n</i> -Hexane	725.117	1.229673	0.2988
<i>n</i> -Heptane	769.570	1.292305	0.3577
<i>n</i> -Octane	811.165	1.352288	0.4026
<i>n</i> -Nonane	849.815	1.404927	0.4342
<i>n</i> -Decane	879.774	1.444874	0.4980
Carbon dioxide	434.820	0.784121	0.1923
Carbon monoxide	189.963	0.780565	0.0402
Helium	7.418	0.663962	0.0000
Hydrogen	47.455	0.692463	0.0000
Hydrogen sulfide	533.439	0.795372	0.1000
Nitrogen	180.386	0.772480	0.0404
Oxygen	220.980	0.721091	0.0210
Water	925.228	0.658903	0.3440

$$T_{ij} = \frac{1.2593T_f}{W_{ij}(T_{ci}T_{cj})^{0.5}} = \frac{T_f}{W_{ij}(\epsilon_i\epsilon_j)^{0.5}} \quad (2.64)$$

where W_{ij} is the binary interaction parameter factor, which is set equal to 1 for binary mixtures not shown in Table 2.6 or for pairs of the same substance (methane-methane, ethane-ethane, etc.), ϵ_i and ϵ_j are energy parameters ($^{\circ}\text{R}$) for each pure substance in the assumed binary mixture. Values for ϵ are given in Table 2.5, and those for W_{ij} are given in Table 2.6.

Virial Terms (C, D, and E). The other terms in the state equation are defined in terms of the mixture's pseudoreduced temperature T_{pr} , the sixth power of the mixture's separation parameter ($\Gamma_{\text{mix}} = \sigma_{\text{mix}}^6$), and a mixture's acentric factor (ω_{mix}). These terms are

$$C = [A_9T_{pr}^{-0.5} + A_{10}T_{pr}^{-2} + A_{11}T_{pr}^{-2.5} + A_{12}T_{pr}^{-5} + \omega_{\text{mix}}(A_{22} + A_{23}T_{pr}^{-2})]\Gamma_{\text{mix}} \quad (2.65)$$

$$D = [A_{13}T_{pr}^{-0.5} + A_{14}T_{pr}^{-1} + A_{15}T_{pr}^{-1.5} + \omega_{\text{mix}}(A_{24}T_{pr}^{-2} + A_{25}T_{pr}^{-2.5})]\Gamma_{\text{mix}}^{1.5} \quad (2.66)$$

$$E = [A_{16}T_{pr}^{-1} + A_{17}T_{pr}^{-3} + A_{26}\omega_{\text{mix}}T_{pr}^{-1}]\Gamma_{\text{mix}}^{2.5} \quad (2.67)$$

$$G = [A_{18}T_{pr}^{-3} + A_{27}\omega_{\text{mix}}T_{pr}^{-3}]\Gamma_{\text{mix}} \quad (2.68)$$

$$H = A_{19}\Gamma_{\text{mix}} \quad (2.69)$$

The mixture's energy parameter Γ_{mix} is

$$\Gamma_{\text{mix}} = \sigma_{\text{mix}}^6 = \sum_{i=1}^n \sum_{j=1}^n x_i x_j \sigma_i^3 \sigma_j^3 V_{ij}^6 \quad (2.70)$$

Values for the binary size parameter V_{ij} are given in Table 2.6. The reduced pseudocritical temperature T_{pc} is determined from

$$T_{pc} = \frac{1}{\Gamma_{\text{mix}}} \sum_{i=1}^n \sum_{j=1}^n x_i x_j \sigma_i^3 \sigma_j^3 \epsilon_i^{1/2} \epsilon_j^{1/2} V_{ij}^6 U_{ij} \quad (2.71)$$

Values for the binary interaction energy parameter U_{ij} are given in Table 2.6.

The pseudoreduced temperature is

$$T_{pr} = \frac{T_f}{T_{pc}} \quad (2.72)$$

The mixture's pseudoacentric factor is

$$\omega_{\text{mix}} = \frac{1}{2T_{pc}^3} \sum_{i=1}^n \sum_{j=1}^n x_i x_j \epsilon_i^{1.5} \epsilon_j^{1.5} (\omega_i + \omega_j) U_{ij}^3 \quad (2.73)$$

Equation (2.59) is nonlinear in molar density ρ_{mol} and requires an iterative solution. From the molar density, the mass density, in conventional units, is obtained and, by Eq. (2.10), the compressibility at base Z_b or at flowing conditions Z_f may be calculated. The following computational procedure substantially reduces the required iteration time.

TABLE 2.6 AGA-8 Binary Pair Interaction Parameters

Pair	Energy U_{ij}	Size V_{ij}	Temperature W_{ij}
Methane/ethane	1.0414	0.9982	1.0015
Methane/propane	1.0014	1.0041	0.9904
Methane/isobutane	1.0000	1.0000	0.9779
Methane/ <i>n</i> -butane	1.0000	1.0000	0.9795
Methane/isopentane	1.0000	1.0000	0.9691
Methane/ <i>n</i> -pentane	1.0116	0.9738	0.9695
Methane/ <i>n</i> -hexane	1.1028	0.9681	0.9561
Methane/ <i>n</i> -heptane	0.9913	0.9793	0.9432
Methane/ <i>n</i> -octane	0.9673	0.9790	0.9321
Methane/ <i>n</i> -nonane	0.9433	0.9790	0.9205
Methane/ <i>n</i> -decane	0.9193	0.9789	0.9084
Nitrogen/methane	0.9555	1.0166	0.9757
Nitrogen/ethane	1.0751	1.0118	0.9707
Nitrogen/propane	1.0000	1.0000	0.9416
Nitrogen/isobutane	1.0000	1.0000	0.9274
Nitrogen/ <i>n</i> -butane	1.0000	1.0000	0.9297
Nitrogen/isopentane	1.0000	1.0000	0.9155
Nitrogen/ <i>n</i> -pentane	1.0000	1.0000	0.9161
Nitrogen/ <i>n</i> -hexane	1.0000	1.0000	0.8981
Nitrogen/ <i>n</i> -heptane	1.0000	1.0000	0.8806
Nitrogen/ <i>n</i> -octane	1.0000	1.0000	0.8656
Nitrogen/ <i>n</i> -nonane	1.0000	1.0000	0.8499
Nitrogen/ <i>n</i> -decane	1.0000	1.0000	0.8335
Nitrogen/carbon dioxide	1.0102	1.0494	1.0096
Carbon dioxide/methane	0.9642	1.0253	0.9559
Carbon dioxide/ethane	0.8614	1.0159	0.9159
Carbon dioxide/propane	0.7957	1.0126	0.8935
Carbon dioxide/isobutane	1.0000	1.0000	0.8454
Carbon dioxide/ <i>n</i> -butane	1.0000	1.0000	0.8517
Carbon dioxide/isopentane	1.0000	1.0000	0.8115
Carbon dioxide/ <i>n</i> -pentane	1.0000	1.0000	0.8131
Carbon dioxide/ <i>n</i> -hexane	1.0000	1.0000	0.7620
Carbon dioxide/ <i>n</i> -heptane	1.0000	1.0000	0.7124
Carbon dioxide/ <i>n</i> -octane	1.0000	1.0000	0.6698
Carbon dioxide/ <i>n</i> -nonane	1.0000	1.0000	0.6252
Carbon dioxide/ <i>n</i> -decane	1.0000	1.0000	0.5786

For all pairs, $U_{ji} = U_{ij}$, $V_{ji} = V_{ij}$, and $W_{ji} = W_{ij}$.

For pairs not shown (helium/nitrogen, methane/helium, carbon dioxide/carbon dioxide, methane/methane, ethane/ethane, etc.) $U_{ij} = V_{ij} = W_{ij} = 1.0000$.

Step 1. Calculate the compressibility factor using Redlich-Kwong or the NX-19 equation and then calculate the first estimate of the molar density as

$$\rho_{\text{mol},0} = \frac{P_f}{R_0 Z_{R/K} T_f} = \frac{P_f}{10.73164 Z_{R/K} T_f} \quad (2.74)$$

Step 2. Using Newton's method, calculate the function as, App. A.1,

$$F = \frac{p_f}{R_0 T_f} + \rho_{\text{mol}} + B\rho_{\text{mol}}^2 + C\rho_{\text{mol}}^3 + D\rho_{\text{mol}}^4 + E\rho_{\text{mol}}^6 + G\rho_{\text{mol}}^3(1 + H\rho_{\text{mol}}^2) \exp(-H\rho_{\text{mol}}^2) \quad (2.75)$$

Then calculate the derivative of the function by

$$F' = 1 + 2B\rho_{\text{mol}} + 3C\rho_{\text{mol}}^2 + 4D\rho_{\text{mol}}^3 + 6E\rho_{\text{mol}}^5 - G\rho_{\text{mol}}^2(2H^2\rho_{\text{mol}}^4 - 3H\rho_{\text{mol}}^2 - 3) \exp(-H\rho_{\text{mol}}^2) \quad (2.76)$$

Successive iterations for molar density are then, from App. A.1, Eq. (A.9),

$$\rho_{\text{mol},n} = \rho_{\text{mol},n-1} - \frac{F_{n-1}}{F'_{n-1}} \quad (2.77)$$

The density, in lb_m/ft^3 for molecular weight, is

$$\rho_f = M_{w,\text{mix}}\rho_{\text{mol}} \quad (2.78)$$

and with ideal specific gravity it is

$$\rho_f = 28.96247G\rho_{\text{mol}} \quad (2.79)$$

To calculate the compressibility factor, at either flowing or base conditions, use for flowing compressibility

$$Z_f = \frac{p_f}{R_0 T_f \rho_{\text{mol}}} = \frac{p_f}{10.73164 T_f \rho_{\text{mol}}} \quad (2.80)$$

and for base compressibility

$$Z_b = \frac{p_b}{R_0 T_b \rho_{b,\text{mol}}} = \frac{p_b}{10.73164 T_b \rho_{b,\text{mol}}} \quad (2.81)$$

The supercompressibility factor, used in some differential producers flow rate equations, is calculated by, for Eq. (9.66),

$$F_{pv} = \frac{Z_b}{\sqrt{Z_f}}$$

and for Eq. (9.68),

$$F_{pv} = \sqrt{\frac{Z_b}{Z_f}} \quad (2.82)$$

The mole fraction of all of the constituents of the mixture needs to be known in order to estimate gas density. In many installations a complete chromatographic analysis is not possible and alternate methods are used to estimate the mole fractions. These methods are:

1. Real gravity, carbon dioxide, and nitrogen mole fraction inputs (G_R , %CO₂, and %N₂)
2. Real gravity, heating value, carbon dioxide, and nitrogen mole fraction input ($HV_{\text{Btu/SCF}}$, G_R , %CO₂, and %N₂)
3. Real gravity, heating value, and carbon dioxide mole fraction input (G_R , $HV_{\text{Btu/SCF}}$, and %CO₂)
4. Heating value, carbon dioxide, and nitrogen mole fraction inputs ($HV_{\text{Btu/SCF}}$, %CO₂, and %N₂)
5. Real gravity, methane, carbon dioxide, and nitrogen mole fraction inputs (G_R , %CH₄, %CO₂, and %N₂)

The mole fractions are estimated by

$$x_i = a + bG_R + cHV_{\text{Btu/SCF}} + dx_{\text{CH}_4} + ex_{\text{N}_2} + fx_{\text{CO}_2} \quad (2.83)$$

Table 2.7 gives the values for the constants (a , b , c , d , e , and f) for each of the five methods. Mole fractions of hydrogen sulfide and water are assigned a value of zero. The sum of the pentanes is equally assigned to isopentane and n -pentane, and the sum of the hexanes is assigned in an 85, 12, and 3 percent proportion to n -hexane, n -heptane, and octane, respectively. Constituents not shown in Table 2.7 are assigned a value of zero.

GERG Natural Gas Equation. In Europe the Groupe European des Rechechés Gazieres (GERG) equation is widely used to compute the compressibility of natural gas. This equation was developed at the Van der Waals Laboratory to predict the compressibility of natural gas from test and available literature data (GERG, 1984). The compressibility is computed from mole fractions of the gas by

$$Z_f = 1 + \frac{1}{V_{\text{mol}}^*} \sum_{i=j=1}^{13} B_{ij}n_{ij} + \frac{1}{V_{\text{mol}}^{*2}} \sum_{i=j=1}^{13} C_{ijk}n_i n_j n_k \quad (2.84)$$

where n_i , n_j , and n_k are the mole fraction components, and V_{mol}^* is the molar volume (dm³/mol). Rearranging Eq. (2.4) yields the relationship between molar volume and compressibility,

$$Z_f = \frac{p_f^* V_{\text{mol}}^*}{R_0 T_K} \quad (2.85)$$

where $R_0 = 8.31441 \text{ J}^*/(\text{g} \cdot \text{mol} \cdot \text{K})$, and p_f^* is in pascals.

The molar density equation is then written, by substitution, as

$$\frac{p_f^*}{R_0 T_K} = \rho_{\text{mol}}^* + \left(\sum_{i=j=1}^{13} B_{ij} n_{ij} \right) \rho_{\text{mol}}^{*2} + \left(\sum_{i=j=k=1}^{13} C_{ijk} n_i n_j n_k \right) \rho_{\text{mol}}^{*3} \quad (2.86)$$

The i , j , k component of a mixture is as given in Table 2.8, the second virial coefficient B_{ij} is given in Table 2.9, and the third virial's C_{ijk} is given in Table 2.10.

The virial coefficients are functions of temperature and are determined by, for the second virial,

TABLE 2.7 Constants for AGA-8 Mole Fraction Estimation Methods

		$X_i = a + bG_R + cHV_{\text{Btu/SCF}} + dx_{\text{CH}_4} + ex_{\text{N}_2} + fx_{\text{CO}_2}$					
<i>i</i>	Method	<i>a</i>	<i>b</i>	<i>c</i>	<i>d</i>	<i>e</i>	<i>f</i>
CH ₄	1	1.63289	−1.1458	0.0	0.0	−0.59633	0.13596
	2	1.64569	−1.0159	−8.368E−05	0.0	−0.73631	−0.07449
	3	1.57921	−1.7003	−3.560E−04	0.0	0.0	1.02720
	4	1.73734	0.0	−7.3023E−04	0.0	−1.8295	−1.71810
	5	0.0	0.0	0.0	1.0	0.0	0.0
C ₂ H ₆	1	−0.31521	0.58160	0.0	0.0	−0.24416	−0.60593
	2	−0.32750	0.45690	8.0300E−05	0.0	−0.10982	−0.40397
	3	−0.32720	0.35260	1.3769E−04	0.0	0.0	−0.23790
	4	−0.35947	0.0	3.6249E−04	0.0	0.37820	0.33070
	5	1.73468	−0.85995	0.0	−1.2539	−0.98860	−0.42978
C ₃ H ₈	1	−0.18262	0.32360	0.0	0.0	−0.09545	−0.30510
	2	−0.18843	0.26480	3.7900E−05	0.0	−0.03213	−0.20981
	3	−0.19828	0.23790	6.2100E−05	0.0	0.0	−0.15790
	4	−0.22030	0.0	2.1399E−04	0.0	0.25520	0.22600
	5	0.11444	0.12969	0.0	−0.1907	−0.22830	−0.30270
<i>n</i> C ₄ H ₁₀	1	−0.05417	0.09540	0.0	0.0	−0.02983	−0.08920
	2	−0.05619	0.07500	1.3130E−05	0.0	−0.00789	−0.05618
	3	−0.06061	0.06920	2.0520E−05	0.0	0.0	−0.04300
	4	−0.06702	0.0	6.4690E−05	0.0	0.07420	0.06860
	5	−0.21867	0.21578	0.0	0.0977	0.02132	−0.10984
<i>i</i> C ₄ H ₁₀	1	−0.03223	0.05790	0.0	0.0	−0.02846	−0.05581
	2	−0.03245	0.05570	1.4200E−06	0.0	−0.02609	−0.05224
	3	−0.03237	0.03090	1.4990E−05	0.0	0.0	−0.01460
	4	−0.03521	0.0	3.4710E−05	0.0	0.03310	0.03530
	5	−0.13919	0.12532	0.0	0.0703	0.02361	−0.05272
ΣC ₅ H ₁₂	1	−0.02925	0.05200	0.0	0.0	−0.02169	−0.04805
	2	−0.02958	0.04860	2.2000E−06	0.0	−0.01802	−0.04252
	3	−0.03174	0.03220	1.3240E−05	0.0	0.0	−0.01580
	4	−0.03470	0.0	3.3770E−05	0.0	0.03450	0.03610
	5	−0.22604	0.18802	0.0	0.1219	0.05276	−0.06107
		<i>i</i> C ₅ H ₁₂ = 0.5 ΣC ₅ H ₁₂			<i>n</i> C ₅ H ₁₂ = 0.5 ΣC ₅ H ₁₂		
ΣC ₆ H ₁₄	1	−0.01503	0.02840	0.0	0.0	−0.02192	−0.02561
	2	−0.01690	0.00940	1.2200E−05	0.0	−0.00152	0.00506
	3	−0.01579	0.00730	1.2300E−05	0.0	0.0	0.00580
	4	−0.01644	0.0	1.6940E−05	0.0	0.00780	0.01750
	5	−0.11818	0.09655	0.0	0.0658	0.02376	−0.02962
		<i>i</i> C ₆ H ₁₄ = 0.85ΣC ₆ H ₁₄			<i>n</i> C ₆ H ₁₄ = 0.12ΣC ₆ H ₁₄		
N ₂	1	0.0	0.0	0.0	0.0	0.0	0.0
	2	0.0	0.0	0.0	0.0	0.0	0.0
	3	0.08728	0.92720	−5.9325E−04	0.0	0.0	−1.49840
	4	0.0	0.0	0.0	0.0	0.0	0.0
	5	0.0	0.0	0.0	0.0	0.0	0.0
		<i>i</i> C ₈ H ₁₈ = 0.03ΣC ₈ H ₁₈					
He	1	−0.00291	0.00440	0.0	0.0	0.04479	−0.00480
	2	0.01220	0.16020	−1.0008E−04	0.0	−0.12296	−0.25612
	3	0.00235	0.04680	−2.8300E−05	0.0	0.0	−0.07350
	4	−0.00175	0.0	1.3500E−06	0.0	0.04980	0.00170
	5	−0.06180	−0.04167	0.0	−0.0394	0.02480	0.00265

Note: E in this table stands for *engineering notation*. For example, E + 07 = 10⁷ and E − 07 = 10^{−7}, etc.

TABLE 2.8 Components and Ranges

<i>i, j, k</i>	Name	Component	Range % (mol)
1	Methane	CH ₄	>=50
2	Nitrogen	N ₂	
	Oxygen	O ₂	
	Argon	Ar	<=50
3	Carbon dioxide	CO ₂	
	Ethene	C ₂ H ₄	<=30
4	Ethane	C ₂ H ₆	<=20
5	Hydrogen	H ₂	<=10
6	Propane	C ₃ H ₈	
	Propene	C ₃ H ₆	<=5
7	Carbon monoxide	CO	<=3
8	Isobutane	C ₄ H ₁₀	
	Butane	C ₄ H ₁₀	<=1.5
9	Helium	He	<=0.5
10	2,2-Dimethylpropane	C ₅ H ₁₂	
	Isopentane	C ₅ H ₁₂	
	Pentane	C ₅ H ₁₂	
	Benzene	C ₆ H ₆	<=0.5
11	Isohexane	C ₆ H ₁₄	
	Hexane	C ₆ H ₁₄	
	Cyclohexane	C ₆ H ₁₂	
	Xylene(o)	C ₈ H ₁₀	<=0.5
12	Isoheptane	C ₇ H ₁₆	
	Heptane	C ₇ H ₁₆	
	Toluene	C ₇ H ₈	<=0.5
13	Octane	C ₈ H ₁₈	
	Nonane	C ₉ H ₂₀	
	Decane	C ₁₀ H ₂₂	<=0.5

$$B_{ij} = A + BT_K + CT_K^2 \quad (2.87)$$

and for the third virial by

$$C_{ijk} = A + BT_K + CT_K^2 \quad (2.88)$$

The density at the pressure and temperature of the gas is

$$\rho_f^* = M_{w,\text{mix}} \rho_m^* \quad (2.89)$$

Equation 2.86 is nonlinear in molar density and can be solved readily using Newton's method form given by Eq. (A.2) in App. A. The function F is defined by

$$F = -\frac{p_f^*}{R_0 T_K} + \rho_{\text{mol}}^* + \left(\sum_{i=j=1}^{13} B_{ij} n_i n_j \right) \rho_{\text{mol}}^{*2} + \left(\sum_{i=j=k=1}^{13} n_i n_j n_k \right) \rho_{\text{mol}}^{*3} \quad (2.90)$$

TABLE 2.9 GERG Equation Coefficients for Second Virial B_{ij}

i,j	A	B	C
1,1	-0.305530E+00	0.138050E-02	-0.167430E-05
1,2	-0.162897E-00	0.723055E-03	-0.796055E-06
1,3	-0.377721E+00	0.161771E-02	-0.190044E-05
1,4	-0.534311E+00	0.228510E-02	-0.270302E-05
1,5	-0.144562E+00	0.921030E-03	-0.135212E-05
1,6	-0.808030E+00	0.362500E-02	-0.455555E-05
1,8	-0.133598E+01	0.650241E-02	-0.857077E-05
1,1	-0.148583E+01	0.694054E-02	-0.866938E-05
1,11	-0.775140E+00	0.184050E-02	-0.400000E-06
1,12	-0.209989E+01	0.979707E-02	-0.125373E-04
1,13	-0.239409E+01	0.112199E-01	-0.143976E-04
2,2	-0.144600E+00	0.740910E-03	-0.911950E-06
2,3	-0.191944E+00	0.666407E-03	-0.537698E-06
2,4	-0.412214E+00	0.203558E-02	-0.270693E-05
2,5	-0.237582E-01	0.179302E-03	-0.194991E-06
2,6	-0.442660E-00	0.204986E-02	-0.261400E-05
3,3	-0.868340E-00	0.403760E-02	-0.516570E-05
3,4	-0.901431E-00	0.431802E-02	-0.577366E-05
3,6	-0.126372E+01	0.584661E-02	-0.747500E-05
3,8	-0.188108E+01	0.926431E-02	-0.124525E-04
3,10	-0.202135E+01	0.954081E-02	-0.121639E-04
4,4	-0.107320E+01	0.464810E-02	-0.560520E-05
4,5	0.266450E-02	-0.102765E-03	0.374149E-06
4,6	-0.142020E+01	0.575230E-02	-0.640000E-05
4,8	-0.283644E+01	0.136800E-01	-0.181244E-04
4,10	-0.331426E+01	0.152019E-01	-0.189007E-04
5,5	-0.175160E-02	0.849590E-04	-0.103660E-06
6,6	-0.259920E+01	0.119650E-01	-0.152910E-04
6,8	-0.435393E+01	0.213786E-01	-0.287483E-04
7,7	-0.130820E+00	0.602540E-03	-0.644300E-06
8,8	-0.708016E+01	0.363100E-01	-0.503829E-04
9,9	0.206740E-01	-0.513060E-04	0.724000E-07
10,10	-0.111580E+02	0.535740E-01	-0.684970E-04

The derivative of the function is then

$$F' = 1 + 2 \left(\sum_{i=j=1}^{13} B_{ij} n_i n_j \right) \rho_{\text{mol}}^* + 3 \left(\sum_{i=j=k=1}^{13} n_i n_j n_k \right) \rho_{\text{mol}}^{*2} \quad (2.91)$$

The estimates for the molar density are then, by App. A, Eq. (A.9),

TABLE 2.10 GERG Equation Coefficients for Third Virial C_{ijk}

	<i>A</i>	<i>B</i>	<i>C</i>
1,1,1	0.110140E-01	-0.492640E-04	0.683960E-07
1,1,2	0.950336E-02	-0.446604E-04	0.646311E-07
1,1,3	0.921537E-02	-0.326297E-04	0.384277E-07
1,1,4	0.471391E-02	0.131521E-04	-0.450064E-07
1,1,5	0.252725E-02	-0.904332E-05	0.115616E-07
1,1,6	0.145768E-01	-0.278502E-04	0.000000E-00
1,1,8	0.692768E-01	-0.214852E-03	0.000000E-00
1,1,10	0.892362E-01	-0.272925E-03	0.000000E-00
1,2,2	0.866892E-02	-0.424907E-04	0.635102E-07
1,2,3	0.900338E-02	-0.355487E-04	0.467680E-07
1,2,4	0.449508E-02	0.530233E-06	-0.152576E-07
1,2,5	0.360589E-02	-0.145437E-04	0.204722E-07
1,2,6	-0.187767E-01	0.142145E-03	-0.221855E-06
1,3,3	0.637108E-02	-0.747903E-05	-0.643736E-08
1,3,4	-0.176574E-02	0.597684E-04	-0.123785E-06
1,3,6	-0.623055E-01	0.459485E-03	-0.733765E-06
1,4,4	-0.180009E-01	0.187768E-03	-0.344478E-06
1,4,5	-0.116095E-02	0.263812E-04	-0.512600E-07
1,4,6	-0.992498E-01	0.713458E-03	-0.114420E-05
1,4,8	-0.992498E-01	0.713458E-03	-0.114420E-05
1,4,10	-0.992498E-01	0.713458E-03	-0.114420E-05
1,5,5	0.113514E-02	-0.101196E-05	-0.316717E-09
1,6,6	-0.107132E+00	0.711300E-03	-0.107919E-05
2,2,2	0.784980E-02	-0.398950E-04	0.611870E-07
2,2,3	0.776648E-02	-0.333367E-04	0.470391E-07
2,2,4	0.473374E-02	-0.715042E-05	0.165190E-08
2,2,5	0.335086E-02	-0.147638E-04	0.220414E-07
2,2,6	-0.139981E-01	0.106230E-03	-0.162413E-06
2,3,3	0.570471E-02	-0.127157E-04	0.865358E-08
2,3,4	-0.768174E-05	0.385226E-04	-0.817506E-07
2,3,5	0.269108E-02	-0.596904E-05	0.540142E-08
2,3,6	-0.301719E-01	0.222387E-03	-0.350693E-06
2,4,4	-0.113332E-01	0.123463E-03	-0.225648E-06
2,4,5	-0.297743E-03	0.168641E-04	-0.330680E-07
2,4,6	-0.506529E-01	0.363400E-03	-0.577241E-06
2,5,5	0.106796E-02	-0.252397E-05	0.310904E-08
2,6,6	-0.844178E-01	0.557418E-03	-0.835447E-06
3,3,3	0.205130E-02	0.348880E-04	-0.837030E-07
3,3,4	-0.109855E-01	0.133800E-03	-0.252624E-06

TABLE 2.10 (Continued)

	<i>A</i>	<i>B</i>	<i>C</i>
3,3,5	0.430967E-03	0.160191E-04	-0.345955E-07
3,3,6	-0.594074E-01	0.430798E-03	-0.691157E-06
3,4,4	-0.313527E-01	0.284509E-03	-0.508173E-06
3,4,5	-0.516317E-02	0.579276E-04	-0.105347E-06
3,4,6	-0.944235E-01	0.671721E-03	-0.108080E-05
3,5,5	0.522574E-04	0.693387E-05	-0.136454E-07
3,6,6	-0.149820E+00	0.994385E-03	-0.152037E-05
4,4,4	-0.621000E-01	0.508050E-03	-0.885260E-06
4,4,5	-0.185994E-01	0.163195E-03	-0.284869E-06
4,4,6	-0.144234E+00	0.101275E-02	-0.163277E-05
4,5,5	-0.370635E-02	0.390658E-04	-0.684792E-07
4,6,6	-0.216734E+00	0.143604E-02	-0.221182E-05
5,5,5	-0.932310E-05	0.283770E-05	-0.507540E-08
6,6,6	-0.270290E+00	0.171040E-02	-0.250010E-05
7,7,7	0.190870E-02	0.420040E-05	-0.156800E-07
9,9,9	-0.779620E-02	0.491760E-04	-0.774240E-07

$$\rho_{\text{mol},n}^* = \rho_{\text{mol},n-1}^* - \frac{F_{n-1}}{F'_{n-1}} \quad (2.92)$$

Measuring Compressibility

Several laboratory-type instruments have been designed to measure compressibility. These are shown schematically in Fig. 2.7. In the National Bureau of Standards apparatus (Bean, 1929) in Fig. 2.7*a*, a known gas volume *A* under pressure is repeatedly, and very carefully, discharged to a lower pressure in a fixed-volume burette *B*. This displaces mercury, under slight pressure, to an etch-marked position below burette *B*, which fixes the volume. The burette gauge pressure is then read on the adjacent manometer scale. The initial and final deadweight readings establish the initial and final gas sample conditions. By successive fixed temperature and volume reduction to measured lower pressure, the initial compressibility of the high-pressure gas sample is calculated.

In the U.S. Bureau of Mines-Burnett compressibility apparatus (Burnett, 1936), chamber *V*₁ is initially charged with the unknown gas, which then is repeatedly discharged into a chamber *V*₂ that is evacuated after each fill. If an ideal gas is expanded to an increased volume *V*₁ + *V*₂, and the temperature is returned to the original value, the ratio of final to initial pressure should be constant for successive expansions. This ratio is not constant for a real gas during the initial higher-pressure expansions, but the real gas does approach ideal-gas behavior at lower pressures. In a plotting of the ratio of initial pressure to reduced pressure versus initial pressure, a sloping line is obtained, rather than the horizontal line obtained for an ideal gas. By applying the real-gas equation, the compressibility factor at various pressures can be derived.

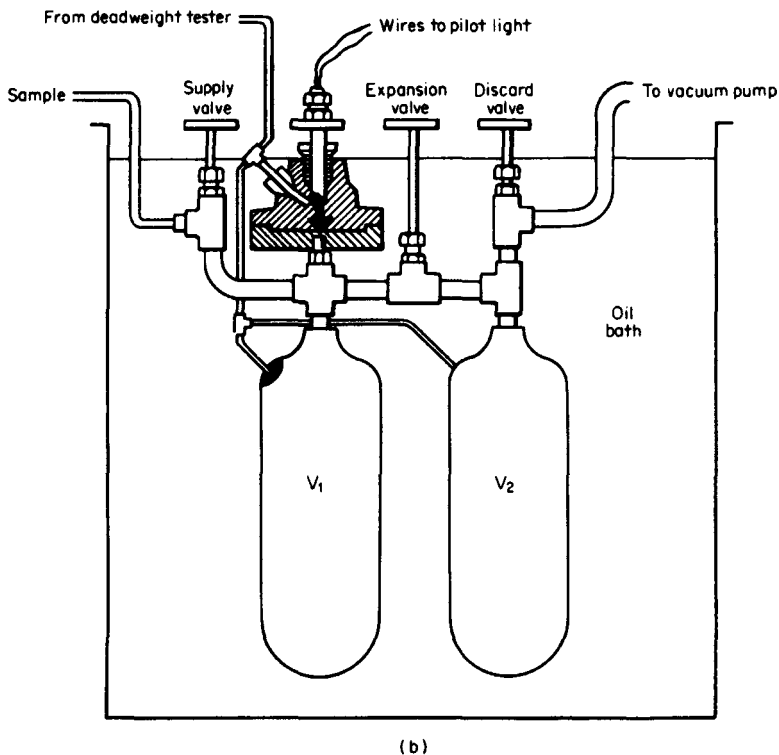
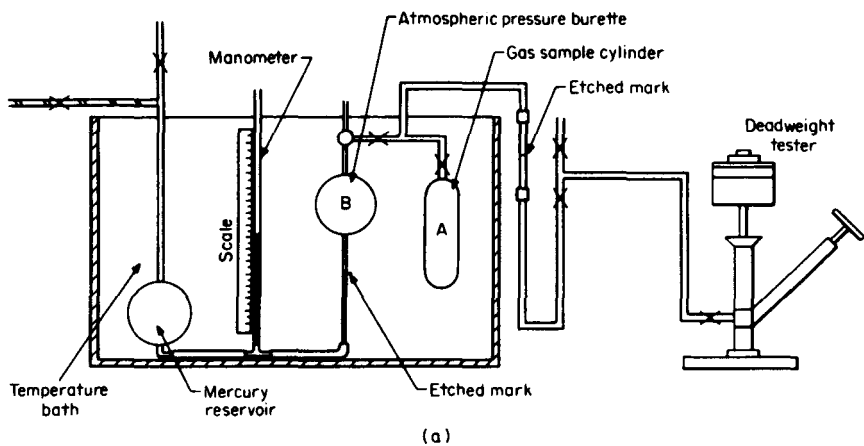


Figure 2.7 Compressibility-factor measuring devices. (a) National Bureau of Standards apparatus. (b) U.S. Bureau of Mines apparatus. (c) Automated pVT apparatus.

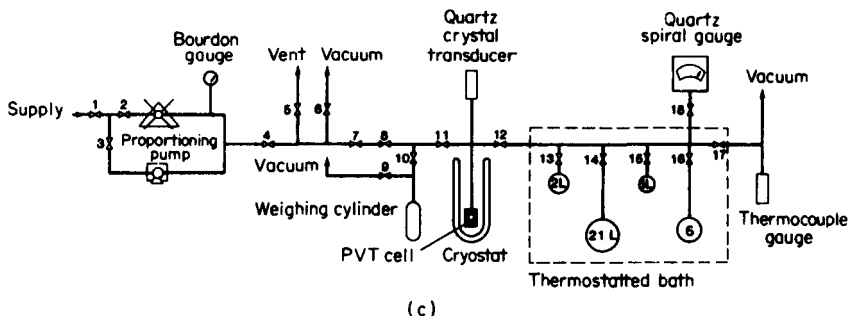


Figure 2.7 (Continued)

Figure 2.7c illustrates an automated *pvT* apparatus (Olien and Magee, 1988) for performing highly accurate pressure-volume-temperature isochoric measurements on pure fluids and mixtures. The apparatus has a precision of a few parts in 10^4 and an estimated accuracy of 0.1 percent over the temperature range of -280 to 350°F (100 to 450 K) with pressures up to 5000 psia (35 MPa).

GAS MIXTURES

Few tables or charts exist that can be used to determine density, or other fluid properties, for gas mixtures. The psychrometric charts for air and water and the supercompressibility tables for natural gas mixtures are two examples of tables that are available.

The density behavior of a flowing multicomponent gas is similar to that of a single-component gas, and the temperature and pressure are measured in the conventional manner. However, specific gravity and compressibility must be calculated on the basis of certain empirically determined combination rules. These are, in turn, based on certain mixture laws, and experimental evidence is often used to select one method over another. When no specific equations are given, the following may be used.

Specific Gravity

The number of moles in a mixture of gases is defined by

$$n = \sum n_i = n_1 + n_2 + n_3 + \dots \quad (2.93)$$

where n_1, n_2, n_3, \dots are the number of moles of each gas. The *mole fraction* of each component is defined as

$$x_1 = \frac{n_1}{n} \quad x_2 = \frac{n_2}{n} \quad x_3 = \frac{n_3}{n} \quad \dots \quad (2.94)$$

where the mole-fraction summation is further defined by

$$\sum x_i = 1 \quad (2.95)$$

The average molecular weight of the mixture is calculated by dividing the total mass, in pounds-mass, by the number of moles contained in the mixture; from Eq. (2.6),

$$M_{w,\text{mix}} = \frac{m}{n} \quad (2.96)$$

The mass of the total mixture is then the sum of the individual masses, which can be determined from the molecular weight of each gas with

$$m = \sum n_i M_{wi} = n_1 M_{w1} + n_2 M_{w2} + n_3 M_{w3} + \cdots \quad (2.97)$$

Substituting Eq. (2.97) into Eq. (2.96) yields

$$M_{w,\text{mix}} = \frac{\sum n_i M_{wi}}{n} \quad (2.98)$$

which can be reduced to a mole-fraction equation by using Eqs. (2.94):

$$M_{w,\text{mix}} = \sum x_i M_{wi} = x_1 M_{w1} + x_2 M_{w2} + x_3 M_{w3} + \cdots \quad (2.99)$$

The mole fraction of each component is obtained by either gravimetric or volumetric analysis, and the ideal specific gravity is calculated by dividing the mixture's averaged molecular weight by the molecular weight of dry air. From Eq. (2.99), this is

$$G_{\text{mix}} = \frac{\sum x_i M_{wi}}{M_{w,\text{air}}} = \frac{\sum x_i M_{wi}}{28.96247} \quad (2.100)$$

As an example, Table 2.11 presents the mole fractions and molecular weights of

TABLE 2.11 Composition of Dry Air and Computation of Average Molecular Weight

Component	Mole fraction x_i	Molecular weight M_{wi}	$x_i M_{wi}$
Nitrogen	0.78102	28.0134	21.87903
Oxygen	0.20946	31.9988	6.70247
Carbon dioxide	0.00033	44.0098	0.01452
Argon	0.00916	39.948	0.36592
Neon	0.00001818	20.179	0.00037
Helium	0.00000524	4.0026	0.00002
Krypton	0.00000114	83.80	0.00010
Xenon	0.000000087	131.30	0.00001
Hydrogen	0.000005	2.0158	0.00001
Methane	0.0000015	16.0426	0.00002
Nitrous oxide	0.0000003	44.0128	0.00001
Average molecular weight ($M_{w,\text{air}} = \sum x_i M_{wi}$)			28.96247

Source: Jones (1978).

the 11 constituents of *standard* dry air (Jones, 1978). The average molecular weight is shown calculated in accordance with Eq. (2.99).

Amagat's Volume Law

Amagat's volume law is derived under the supposition that the volume of a gas mixture can be divided into separable unique volumes, one for each gas, each volume existing at the mixture's pressure and temperature. The total volume is the sum of the individual volumes and is expressed as

$$V = \Sigma V_i = V_1 + V_2 + V_3 + \dots \quad (2.101)$$

For ideal gases, Eq. (2.101) may be rearranged to allow solution for the volume of each constituent, at the pressure and temperature of the mixture, as

$$V = \frac{nR_0T_f}{p_f} \quad V_1 = \frac{n_1R_0T_f}{p_f} \quad V_2 = \frac{n_2R_0T_f}{p_f} \quad V_3 = \frac{n_3R_0T_f}{p_f} \quad \dots \quad (2.102)$$

Since the ratio R_0T_f/p_f appears in each expression, the volumes of the components may be written as

$$V_1 = \frac{n_1}{n} V \quad V_2 = \frac{n_2}{n} V \quad V_3 = \frac{n_3}{n} V \quad \dots \quad (2.103)$$

The ratio of each volume to the total volume defines the mole fraction, so that

$$x_1 = \frac{n_1}{n} = \frac{V_1}{V} \quad x_2 = \frac{n_2}{n} = \frac{V_2}{V} \quad x_3 = \frac{n_3}{n} = \frac{V_3}{V} \quad \dots \quad (2.104)$$

For these equations, the ratios of volumes are experimentally determined by volumetric analysis, in which the gas is passed through various reagents that sequentially remove known constituents. By measuring the initial volume and the volume after each reduction, the ratios of volumes, and hence the mole fractions, are determined. Since this reduction takes place at atmospheric pressure, it is reasonable to assume negligible compressibility.

Dalton's Law of Partial Pressure

Rather than assume a unique volume for each constituent, Dalton assumed each gas occupies the total volume at the mixture's temperature. Under these conditions, the following relationships may be written for an ideal gas:

$$\frac{p_f V}{R_0 T_f} = \Sigma \frac{p_{fi} V}{R_0 T_f} = \frac{p_{f1} V}{R_0 T_f} + \frac{p_{f2} V}{R_0 T_f} + \frac{p_{f3} V}{R_0 T_f} + \dots \quad (2.105)$$

This equation reduces to

$$p_f = \Sigma p_{fi} = p_{f1} + p_{f2} + p_{f3} + \dots \quad (2.106)$$

Dalton's law of partial pressure states that *the pressure of a mixture of gases is equal to the sum of the partial pressures which each component of the gas would exert if it existed singularly in the mixture's volume at the mixture's temperature.*

If Dalton's law is applied to each component, a useful relationship between the partial pressures and mole fractions is derived:

$$n = \frac{p_f V}{R_0 T_f} \quad n_1 = \frac{p_{f1} V}{R_0 T_f} \quad n_2 = \frac{p_{f2} V}{R_0 T_f} \quad n_3 = \frac{p_{f3} V}{R_0 T_f} \quad \cdots \quad (2.107)$$

These equations reduce further to

$$p_{f1} = x_1 p_f \quad p_{f2} = x_2 p_f \quad p_{f3} = x_3 p_f \quad \cdots \quad (2.108)$$

Relationship between Mass (Gravimetric) and Volumetric Analysis

Two analyses are made to determine constituent percentages in a gas mixture. The volumetric analysis reports the results as a volume ratio, and the mass (gravimetric) analysis gives results based on mass determination, with the mass ratio defined by

$$x_{m1} = \frac{m_1}{m} \quad x_{m2} = \frac{m_2}{m} \quad x_{m3} = \frac{m_3}{m} \quad \cdots \quad (2.109)$$

where

$$m = \sum m_i = m_1 + m_2 + m_3 + \cdots \quad (2.110)$$

Example 2.8. A mixture of carbon dioxide and methane has a volumetric analysis of 5 and 95 percent, respectively. The line pressure is 500 psia (3450 kPa), and the temperature is 40°F (4.4°C). Assuming an ideal gas mixture, determine (1) the gravimetric analysis, (2) the mixture density, and (3) the pressure exerted by each component.

The molecular weights of carbon dioxide and methane are, from Table D.1, $(M_w)_{\text{CH}_4} = 16.043$ and $(M_w)_{\text{CO}_2} = 44.010$.

1. Gravimetric analysis. According to Eq. (2.104), the mole fraction is written

$$x_i = \frac{\text{moles (component)}}{\text{moles (mixture)}} = \frac{n_i}{n}$$

so that

$$x_{\text{CO}_2} = \frac{n_{\text{CO}_2}}{n} = 0.05 \quad x_{\text{CH}_4} = \frac{n_{\text{CH}_4}}{n} = 0.95$$

The masses of the components are *assumed*, from Eq. (2.6), to be

$$m_{\text{CO}_2} = (0.05)(44.01) = 2.201 \text{ lb}_m$$

$$m_{\text{CH}_4} = (0.95)(16.043) = 15.241 \text{ lb}_m$$

The total mass is then, by Eq. (2.110),

$$m = \sum m_i = 2.201 + 15.241 = 17.442 \text{ lb}_m$$

Finally, from Eq. (2.109), the gravimetric analysis is

$$(x_m)_{\text{CO}_2} = \frac{2.201}{17.442} = 0.126 = 12.6 \text{ percent}$$

$$(x_m)_{\text{CH}_4} = \frac{15.241}{17.442} = 0.874 = 87.4 \text{ percent}$$

2. *Density of mixture.* The specific gravity of the mixture is, according to Eq. (2.100),

$$G_{\text{mix}} = \frac{\sum x_i M_{wi}}{M_{w,\text{air}}} = \frac{\sum x_i M_{wi}}{28.96247}$$

Substituting the mole fractions x from part *a* and the molecular weights gives

$$G_{\text{mix}} = \frac{(0.95)(16.043) + (0.05)(44.01)}{28.96247} = 0.6022$$

The density of the mixture is then, from Eq. (2.10),

$$p_f = 2.698825 \frac{(0.6022)(500)}{(1.0)(459.67 + 40)} = 1.626 \text{ lb}_m/\text{ft}^3$$

where $Z_f = 1.0$ for an ideal gas.

3. *Pressure exerted by each component.* Dalton's law of partial pressure [Eq. (2.108)] gives

$$p_{\text{CO}_2} = (0.05)(500) = 25 \text{ psia}$$

$$p_{\text{CH}_4} = (0.95)(500) = 475 \text{ psia}$$

General Mixture Rules. When no specific mixture rules are given, the accepted rules for general applications are Kay's (1936) rule for the pseudocritical temperature, the modified Prausnitz and Gunn (1958) combination rule for the pseudocritical pressure, and the Joffe (1971) approximation for the acentric factor. With these pseudocritical properties, the Nelson-Obert, Edmister-Pitzer, or Redlich-Kwong state equation is used in the conventional manner to obtain the compressibility factor.

Kay's rule for the pseudocritical temperature is a mole-fraction average method that calculates values to within 2 percent of other proposed rules. This rule is

$$T_{pc} = \sum x_i T_{ci} = x_1 T_{c1} + x_2 T_{c2} + x_3 T_{c3} + \cdots \quad (2.111)$$

The pseudocritical pressure is calculated with the Prausnitz-Gunn combination rule as

$$p_{pc} = \frac{(\sum x_i Z_{ci}) R_0 T_{pc}}{\sum x_i V_{ci}} \quad (2.112)$$

where Z_{ci} and V_{ci} are, respectively, the compressibility factor and volume of each component at the critical temperature and pressure.

In using the Edmister diagram, the acentric factor is approximated with a mole-fraction average given by Joffe (1971):

$$\omega_{pc} = \sum x_i \omega_i = x_1 \omega_1 + x_2 \omega_2 + x_3 \omega_3 + \cdots \quad (2.113)$$

The pseudocritical reduced temperature and pressure are then calculated as

$$T_{pr} = \frac{T_f}{T_{pc}} \quad p_{pr} = \frac{p_f}{p_{pc}} \quad (2.114)$$

Example 2.9. Applying the mixture rules, use the Edmister diagrams to calculate the compressibility factor of the mixture of Example 2.6.

The pertinent data from Table D.1 are as follows:

Component	Mole fraction x_i	Critical temperature T_{ci}	Critical pressure P_{ci}	Critical volume V_{ci}	Critical compressibility factor Z_{ci}	Acentric factor ω
Methane	0.6	343.1	667.2	1.589	0.288	0.008
Carbon dioxide	0.2	547.6	1069.9	1.505	0.274	0.225
Hydrogen sulfide	0.2	671.8	1269.2	1.613	0.284	0.100

The pseudocritical properties of the mixture are, from Eq. (2.111),

$$T_{pc} = (0.6)(343.1) + (0.2)(547.6) + (0.2)(671.8) = 449.8^\circ\text{R}$$

and, from Eq. (2.112),

$$P_{pc} = \frac{[(0.6)(0.288) + (0.2)(0.274) + (0.2)(0.284)](10.7315)(449.8)}{(0.6)(1.589) + (0.2)(1.505) + (0.2)(1.613)} = 870.5 \text{ psia}$$

The acentric factor is found with Eq. (2.113):

$$\omega_{pc} = (0.6)(0.008) + (0.2)(0.225) + (0.2)(0.100) = 0.0698$$

The reduced pseudocritical pressure and temperature are, from Eq. (2.114),

$$T_{pr} = \frac{559.67}{449.8} = 1.244 \quad p_{pr} = \frac{1000}{870.5} = 1.149$$

The Edmister diagrams in Figs. G.7 and G.8 give

$$Z^0 = 0.792 \quad Z^1 = 0.095$$

The compressibility factor of the mixture is then, according to Eq. (2.21),

$$Z_f = 0.792 + (0.0698)(0.095) = 0.799$$

SPECIAL CASE OF A WET GAS

Water vapor in a gas stream is one component of a mixture's specific gravity, and it is measured as part of the total flow. In many cases, however, the volume or mass of dry gas must be calculated—for example, to establish heating value.

Psychrometric Principles

A gas mixed with a vapor behaves differently from a mixture of gases. Since a vapor is, by definition, a gas that lies between the saturated-vapor line and the

critical isotherm (see Fig. 2.1b), changes in pressure and temperature result in condensation or vaporization. When the vapor is water, the mixture may range between dry and saturated gas. A water vapor-gas mixture is referred to as a *psychrometric* mixture. Properties used to define gas-vapor mixtures are specific humidity, relative humidity, and dew point.

Specific Humidity. The *specific humidity* or *humidity ratio* is defined as the ratio of the mass of water vapor to the mass of dry gas. Under the assumption that the water vapor is an ideal gas at the low pressure existing in mixtures, Eq. (2.10) can be used to derive the following specific-humidity relationships for gas and vapor occupying the same volume:

$$\text{SH} = \frac{(\text{lb}_m)_{wv}}{(\text{lb}_m)_{\text{dry gas}}} = \frac{\rho_{wv}}{\rho_{\text{dry gas}}} \approx \frac{0.6220}{G_{\text{dry}}} \frac{p_{wv}}{p_f - p_{wv}} \quad (2.115)$$

Relative Humidity. The *relative humidity* is defined as the ratio of the water vapor pressure p_{wv} in the mixture to the water vapor pressure if the mixture were at saturation at the same temperature:

$$\text{RH} = \left[\frac{p_{wv}}{p_{\text{sat}}} \right]_T \quad (2.116)$$

Dew-Point Temperature. The water vapor in a gas may be superheated steam, or it may be at saturation. If the mixture is cooled at constant pressure, and if the vapor was superheated, each component will be cooled at constant partial pressure because the composition (mass) remains constant. At some reduced temperature the water vapor will reach saturation, and any further temperature decrease will result in condensation. The temperature at which liquid first appears is the *dew-point temperature*. Because the cooling takes place at constant pressure, the dew-point temperature is used to enter the steam tables to find the *partial pressure* of the water vapor in an unsaturated mixture; this partial pressure is the pressure corresponding to the saturation temperature, that is, the dew-point temperature.

Saturated and Unsaturated Gas

The quantity of water vapor in a gas can vary from zero to saturation. Shown in Fig. 2.8 are the pressure-volume (density) curves for carbon dioxide and water at saturation (Fig. 2.8a) and in an unsaturated state (Fig. 2.8b). These curves are useful in discussing saturation and nonsaturation.

Saturated Gas. Shown in Fig. 2.8a is the pressure-specific volume (density) diagram for carbon dioxide saturated with water vapor. The mixture pressure p_f is 100 psia (690 kPa) at a temperature of 100°F (37.8°C). The carbon dioxide pressure is, by Dalton's law, the mixture pressure less the pressure of the saturated water vapor. This vapor pressure is found in the steam tables and for 100°F (37.8°C) is 0.95 psia (6.6 kPa). The density shown for the dry carbon dioxide is calculated with Eq. (2.10) at a pressure of 99.05 psia. The ratio of the water vapor density to the density of the dry carbon dioxide is $0.0029/0.729 = 0.00398$, which is the specific humidity. Since the carbon dioxide is saturated, the relative humidity, which is the ratio of the water vapor pressure in the mixture to that at saturation, is 1.

2.48

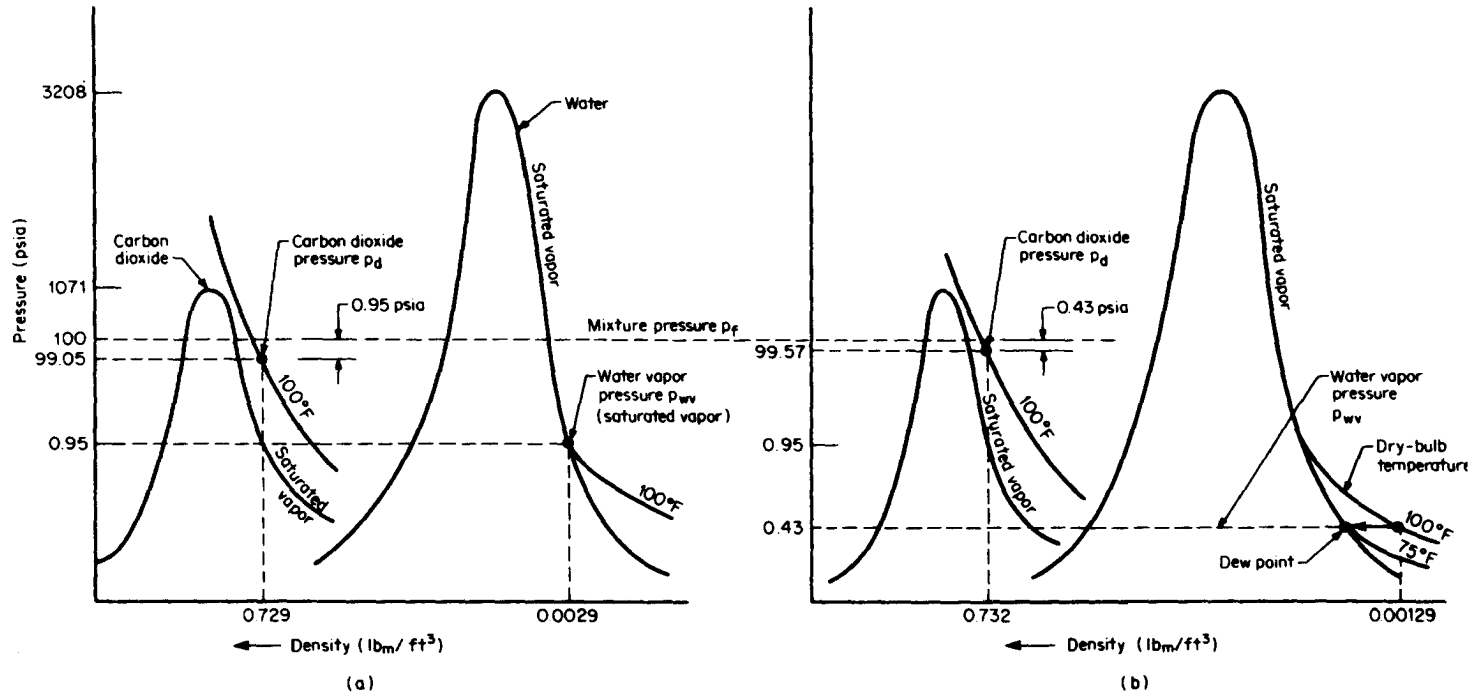


Figure 2.8 Pressure-density curves for carbon dioxide and water (not to scale). (a) Saturated mixture. (b) Unsaturated mixture.

Because the mixture is saturated, any further decrease in temperature results in condensation; therefore, the wet-bulb temperature is the temperature of the mixture [100°F (37.8°C)].

Unsaturated Gas. In Fig. 2.8*b* the mixture is shown unsaturated at the same 100°F (37.8°C) temperature. The arrow indicates cooling at constant pressure to the 75°F (23.9°C) dew-point temperature, at which liquid first appears. The pressure 0.43 psia (2.96 kPa) corresponds to the saturation pressure at 75°F (23.9°C) as found in the steam tables. Since the mixture is cooled at constant pressure, this is the *partial pressure* of the water vapor existing in the mixture at 100°F (37.8°C). Since the water vapor pressure is lower in the unsaturated case, the density of the dry carbon dioxide is higher; hence, the mass of water vapor per pound of dry gas, the specific humidity, is less than in the saturated case. The specific humidity is then $0.00129/0.732 = 0.00175$, and the relative humidity is $0.43/0.95 = 0.45$.

Equation Development

Under the assumption that water vapor is an ideal gas at the low saturation pressures existing in mixtures, the mole-fraction equation (2.108) can be substituted into Eq. (2.100) to yield the wet-gas specific gravity as

$$G_{\text{wet}} = \frac{p_f - p_{wv}}{p_f} G_{\text{dry}} + \frac{p_{wv}}{p_f} G_{wv} \quad (2.117)$$

The pressure difference in the first term is the partial pressure of the dry gas as defined by Dalton's law. The ratios of pressures in both terms are the respective mole fractions: dry gas and water vapor.

Since the specific gravity of water vapor is 0.6220, Eq. (2.117) may be rewritten as

$$G_{\text{wet}} = \left[1 + \frac{p_{wv}}{p_f} \left(\frac{0.6220}{G_{\text{dry}}} - 1 \right) \right] G_{\text{dry}} \quad (2.118)$$

The relationship between the water vapor pressure p_{wv} , dry-gas specific gravity G_{dry} , and wet-gas specific gravity G_{wet} is shown in Fig. 2.9. As the specific gravity of the dry gas approaches that of water vapor, the wet-gas specific gravity is well approximated by the dry-gas specific gravity. However, with gases such as hydrogen, where the specific gravity is significantly different, it is important that the relationship given by Eq. (2.118) be used.

The compressibility factor of the wet gas can be estimated with a simple mole-fraction average as

$$Z_{\text{wet}} = \left(1 - \frac{p_{wv}}{p_f} \right) Z_{\text{dry}} + \frac{p_{wv}}{p_f} Z_{wv} \quad (2.119)$$

In this equation, Z_{wv} is usually assumed to be 1.0 because the water vapor pressure is low.

To adjust a wet volume to a dry-volume basis, Amagat's volume law is first written as

$$V_{\text{wet}} = V_{\text{dry}} + V_{wv} \quad (2.120)$$

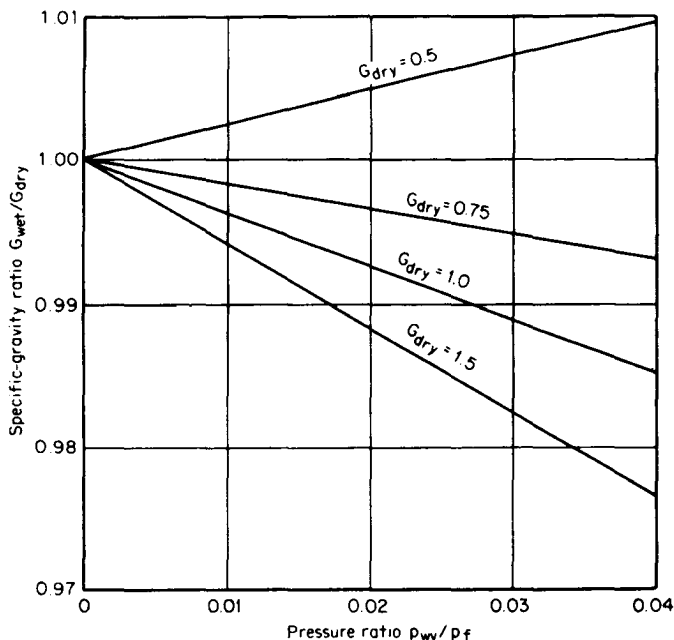


Figure 2.9 Ratio of dry-gas to wet-gas specific gravity.

When rearranged, this gives, as the relationship between the dry volume and wet volume,

$$F_{wv,dry} = \frac{V_{dry}}{V_{wet}} = 1 - \frac{V_{wu}}{V_{wet}} \quad (2.121)$$

which, after substitution of the relationships in Eqs. (2.104) and (2.108), reduces to

$$F_{wv,dry} = 1 - \frac{p_{wu}}{p_f} \quad (2.122)$$

To convert a volume of wet gas from one moisture condition to another, the partial pressure of the water vapor must be considered at the two differing temperatures. The pertinent relationship is

$$\frac{V_2}{V_1} = \frac{(1 - p_{wu}/p_f)_1}{(1 - p_{wu}/p_f)_2} \frac{p_{f1}}{p_{f2}} \frac{Z_{f2}}{Z_{f1}} \frac{T_{f2}}{T_{f1}} \quad (2.123)$$

where the subscript 1 refers to the measured or initial volume, and 2 to the converted volume.

For adjusting a wet-gas mass flow to a dry mass flow, a mass balance yields

$$(lb_m)_{wet} = (lb_m)_{dry} + (lb_m)_{wu} \quad (2.124)$$

This gives the relationship

$$F_{WVM,dry} = \frac{(\text{lb}_m)_{\text{dry}}}{(\text{lb}_m)_{\text{wet}}} = 1 - \frac{(\text{lb}_m)_{\text{wv}}}{(\text{lb}_m)_{\text{wet}}} \quad (2.125)$$

Rearranging Eq. (2.8) to solve for the mass of water vapor and for the mass of the wet mixture, and substituting the mole-fraction relationships given by Eq. (2.108), reduces Eq. (2.125) to

$$F_{WVM,dry} = 1 - \frac{0.6220}{G_{\text{wet}}} \frac{p_{\text{wv}}}{p_f} \frac{Z_{\text{wet}}}{Z_{\text{wv}}} \quad (2.126)$$

The following may be used to determine the density of a wet gas: the expression is

$$\rho_{\text{wet}} = \frac{2.698825 p_f G_{\text{wet}}}{Z_{\text{wet}} T_f} \quad \rho_{\text{wet}}^* = \frac{3.483407 p_f^* G_{\text{wet}}}{Z_f T_K} \quad (2.127)$$

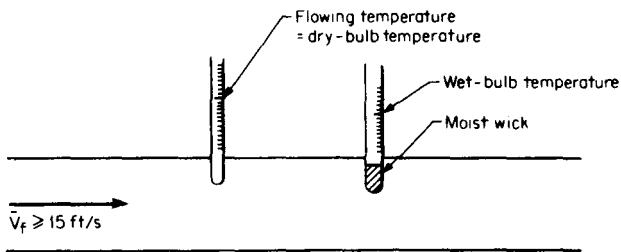
Moisture Determination

There are many humidity- and moisture-measuring devices. Generally, these devices either measure moisture content directly or infer moisture content from relative humidity, specific humidity, dew-point temperature, or hygrometer measurements. They may be summarized as follows:

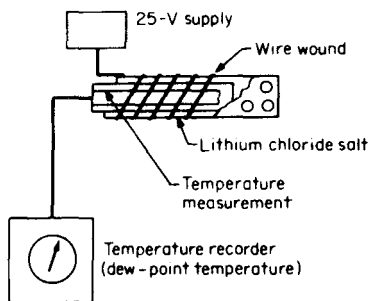
1. Inferential-measurement devices
 - a. Dew-point meters
 - (1) Vapor equilibrium meter
 - (2) Mechanized dew-point meter
 - (3) Fog chamber
 - (4) Electrolytic hygrometer
 - (5) Manually operated dew cup
 - b. Hygrometers
 - (1) Hair hygrometer
 - (2) Salt-conductivity hygrometer
 - c. Psychrometers
 - (1) Sling psychrometer
 - (2) Assman psychrometer
 - (3) Wet- and dry-bulb psychrometer
2. Moisture-measurement methods
 - a. Electric conductivity
 - b. Electric capacitance
 - c. Radio-frequency absorption
 - d. Microwave absorption
 - e. Infrared absorption
 - f. Equilibrium methods

Three commonly used devices are shown in Fig. 2.10.

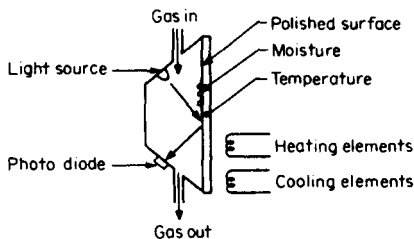
Wet- and Dry-Bulb Psychrometer. If two thermometers are inserted in the flow line (Fig. 2.10a), and one is covered with a continuously wetted wick, the temperature T_{WB} of the wet thermometer will be lower than that of the uncovered thermometer. If the line velocity is greater than 15 ft/s (4.6 m/s), the wetted thermometer will read the adiabatic saturation temperature.



(a)



(b)



(c)



(d)

Figure 2.10 Commonly used humidity-measuring devices. (a) Wet- and dry-bulb measurements. (b) Dewcel (Courtesy The Foxboro Co.) (c) Dew-point measuring device. (d) Dewscope. (Courtesy UGC Industries, Inc.)

Within the range of 32 to 100°F (0 to 38°C), the ratio of water vapor pressure to mixture pressure can be determined as

$$\frac{p_{wv}}{p_f} = \frac{p_{\text{sat}}}{p_f} - 0.000048C_{mp}(T_F - T_{WB}) \quad (2.128)$$

Values of the mean molecular heat C_{mp} are given in Table 2.12. The saturated vapor pressure p_{sat} is obtained from the steam tables using the line (wet-bulb) temperature T_{WB} .

If the mole fractions are known for a mixture of gases, the mean molecular heat can be calculated on a mole-fraction basis as

$$C_{mp,\text{mix}} = \sum x_i C_{mpi} = x_1 C_{mp1} + x_2 C_{mp2} + \cdots \quad (2.129)$$

Dewcel. The dew-point temperature, as well as the specific humidity and partial pressure of the water vapor, can be determined with the Dewcel shown in Fig. 2.10*b*. A thin metal tube is covered with a woven glass cloth that is saturated with lithium chloride. A voltage is applied to a double winding of silver wire over the glass cloth. The electrical conductivity between the wires is directly proportional to the moisture that the salt takes on from the surrounding gas. When the moisture is low, there is a small current flow, and the temperature rise within the cell due to Joule heating is low. When the moisture is high, there is a high current flow and the temperature is high. A thermometer placed inside the tube will measure the cell temperature and, therefore, the dew point or absolute humidity. The speed of response of the salt, in changing from moist (as a result of moisture in the stream) to dry is quite high.

Moisture-Condensation (Dew-Point) Instrument. If a small flow of moist gas is passed over a mirror whose temperature is controlled by refrigeration or heating (Fig. 2.10*c*), the moisture will just condense when the dew-point temperature is reached. This results in mirror fogging, which may be detected as a change in the output of a photocell and used in a feedback loop to control the mirror temperature. Figure 2.10*d* shows a commercially available dew-point instrument that operates in this way. Care should be taken in the case of natural gas, since the mirror may fog when hydrocarbons condense out before the water vapor.

TABLE 2.12 Mean Molecular Heats of Some Gases

Gas	Mean molecular heat C_{mp}
Acetylene	10.7
Air	7.7
Carbon dioxide	10.0
Carbon monoxide	7.7
Ethane	13.8
Ethylene	11.3
Hydrogen	7.7
Methane	9.4
Nitrogen	7.7

Example 2.10. The flow rate of a carbon dioxide and water vapor mixture is 20 lb_m/h (9.07 kg/h). The flowing temperature is 100°F (37.8°C), the flowing pressure is 100 psia (689 kPa), and the dew-point temperature is 75°F (23.9°C). What is the dry carbon dioxide flow rate?

Properties of dry gas. From Table D.1, $(M_w)_{\text{CO}_2} = 44.010$. The specific gravity of the dry gas is then, according to Eq. (2.7),

$$G_{\text{dry}} = \frac{44.010}{28.963} = 1.5195$$

The compressibility factor of the dry gas (carbon dioxide) is, from Table G.4, $Z_{\text{dry}} = 0.9699$.

Properties of water vapor. From the steam tables, the pressure of saturated steam (saturated vapor) at 75°F is $p_{\text{wv}} = 0.42964$ psia. Now, rearranging Eq. (2.10) for compressibility-factor determination and substitution yield

$$Z_{\text{wv}} = 2.69883 \frac{G_{\text{wv}} p_{\text{wv}}}{\rho_{\text{wv}} T_f} = 2.69883 \frac{(0.6220)(0.42964)(704.3)}{459.67 + 100} = 0.9076$$

where, from the steam tables,

$$\rho_{\text{wv}} = \frac{1}{v_{\text{wv}}} = \frac{1}{704.3} \text{ lb}_m/\text{ft}^3$$

Properties of wet gas. The compressibility factor of the wet gas is, from eq. (2.119),

$$Z_{\text{wet}} = \left(1 - \frac{0.42964}{100}\right) 0.9699 + \frac{0.42964}{100} 0.9076 = 0.9696$$

The specific gravity of the wet gas is then, from Eq. (2.118),

$$G_{\text{wet}} = \left[1 + \frac{0.42964}{100} \left(\frac{0.6220}{1.5195} - 1\right)\right] 1.5195 = 1.5156$$

The moisture correction factor for mass flow rate is given by Eq. (2.117):

$$F_{\text{WVM,dry}} = 1 - \frac{0.6220}{1.5156} \frac{0.42964}{100} \frac{0.9696}{0.9076} = 0.9982$$

The mass flow of dry gas is, then, by Eq. (2.126),

$$q_{\text{PPH,CO}_2} = F_{\text{WVM,dry}} q_{M,\text{wet}} = (0.9981)(20) = 19.97 \text{ lb}_m/\text{h}$$

Example 2.11. Manufactured gas has the dry-component volumetric analysis tabulated below. The flowing temperature is 100°F (37.8°C) at a mixture pressure of 25 psia (172 kPa). A wet-bulb reading of 72°F (22°C) is measured at a flow rate of 10,000 standard ft³/h (283 SCMH). Assuming an ideal gas mixture, what is the dry specific gravity and the dry-gas flow rate?

Required data from Tables D.1 and 2.3 are as follows:

Component	Mole fraction x_i	Molecular weight M_{wi}	Molecular heat C_{mpi}
Ethylene	0.004	28.054	11.3
Ethane	0.006	30.070	13.8
Methane	0.1139	16.043	9.4
Carbon monoxide	0.2024	28.011	7.7
Hydrogen	0.3790	2.016	7.7
Nitrogen	0.0083	28.013	7.7
Carbon dioxide	0.2863	44.010	10.0

The mean molecular heat of the mixture is, by Eq. (2.129),

$$C_{mp,mix} = \sum x_i C_{mpi} = 8.60$$

The specific gravity of the mixture, from Eq. (2.100), is

$$G_{mix} = \frac{\sum x_i M_{wi}}{28.96247} = 0.738$$

From the steam tables, the saturation pressure at 72°F is $p_{sat} = 0.39$ psia. Then, from Eq. (2.128),

$$\frac{p_{wv}}{p_f} = \frac{0.39}{25} - 0.000048(8.60)(100 - 72) = 0.0040$$

The moisture correction factor for volume flow rate is then, by Eq. (2.122),

$$F_{wv,dry} = 1 - \frac{p_{wv}}{p_f} = 1 - 0.004 = 0.996$$

The dry-volume flow rate is then, from Eq. (2.121),

$$q_{SCFH,dry} = F_{wv,dry} q_{SCFH,wet}$$

$$q_{SCFH,dry} = (0.996)(10,000) = 9960 \text{ standard ft}^3/\text{h}$$

DENSITY CALCULATION

BWR State Equation

The Benedict-Webb-Rubin (BWR) equation of state is widely used in the petroleum and in other related industries. In the BWR equation pressure is expressed as a function of density and temperature. The equation form is a power series, with the last term being an exponential term in density. There are eight empirical constants for each pure substance. These are listed in Table 2.13. The BWR equation is

TABLE 2.13 Coefficients for the BWR Equation for Pure Gases

Component	Formula	$A_o \times 10^{-1}$	$B_o \times 10$	$C_o \times 10^{-5}$	$a \times 10$	$b \times 10^2$	$c \times 10^{-4}$	$\alpha \times 10^4$	$\gamma \times 10^4$
Methane	CH ₄	0.18712416	0.43203053	0.23500139	0.69197996	0.39787382	0.30179295	0.96835765	0.57118125
Ethane	C ₂ H ₆	0.33694517	0.47836255	2.1242566	4.3040066	1.2548604	3.6099896	2.1688803	1.0970452
Propane	C ₃ H ₈	0.59995798	0.73771408	5.0824370	9.3265688	2.4228587	11.187364	4.8673088	1.8911758
Isobutane	C ₄ H ₁₀	0.99391990	1.3149901	9.0456865	23.336257	4.8755556	33.096106	9.9851955	3.4889348
Butane	C ₄ H ₁₀	1.0196945	1.2786628	9.9892910	19.385909	4.0737290	32.335018	10.442644	3.3385434
2,2-Dimethylpropane	C ₅ H ₁₂	1.29635	1.70530	12.73	34.905	6.68120	54.6	20	5
Isopentane	C ₅ H ₁₂	1.3850687	1.7226312	16.060581	31.995467	5.9691011	63.969012	19.622886	5.0483466
Pentane	C ₅ H ₁₂	1.1961292	1.2292766	17.211571	47.865495	9.2539518	69.983519	13.043829	4.3925926
2,2-Dimethylbutane	C ₆ H ₁₄	1.1842	1.9214	33.595	101.08	14.000	174.83	21.890	5.6500
2,3-Dimethylbutane	C ₆ H ₁₄	1.3828	0.9209	18.670	55.238	10.994	85.505	22.759	6.5044
3-Methylpentane	C ₆ H ₁₄	1.7973	1.7900	18.861	43.546	8.637	89.829	30.450	7.2131
Isohexane	C ₆ H ₁₄	1.4930	1.729	28.500	74.286	12.15	140	23.5	6.20
Hexane	C ₆ H ₁₄	1.7242174	2.1381624	32.118381	72.566978	11.287862	160.71350	26.553281	6.6797489
Isoheptane	C ₇ H ₁₆	1.5799	1.856	49.530	92.778	16.43	203.14	31.4	7.76
Heptane	C ₇ H ₁₆	1.7400941	2.1174513	51.337115	122.92505	17.644551	277.93572	33.896262	7.9043803
Octane	C ₈ H ₁₈	2.5770533	3.9840039	75.734303	148.23592	16.594366	450.73712	61.241114	10.301145
Nonane	C ₉ H ₂₀	3.4572536	5.5673163	107.48997	192.71408	21.684926	657.78328	75.142491	10.770395
Decane	C ₁₀ H ₂₂	3.9375142	6.1734390	133.85286	244.35467	26.569730	883.88508	101.13456	13.081063
Benzene	C ₆ H ₆	0.651013	0.503020	34.3016	557.047	7.66343	117.652	7.00159	2.93016
Hydrogen sulphide	H ₂ S	0.37652960	0.52078546	2.0278814	2.5665687	0.63514110	2.9086082	0.52722820	0.45739050
Sulphur dioxide	SO ₂	0.212054	0.261827	7.93879	84.4395	1.46542	11.3362	0.719604	0.592390
Ethene	C ₂ H ₄	0.333958	0.556833	1.31140	2.59000	0.8600	2.1120	1.78000	0.923000
Propene	C ₃ H ₆	0.611220	0.850647	4.39182	7.74056	1.87059	10.2611	4.55696	1.82900
1-Butene	C ₄ H ₈	0.895325	1.16025	9.27280	16.9270	3.48156	27.4920	9.10889	2.95945

1-Pentene	C ₅ H ₁₀	1.105967	1.279227	13.88744	22.62858	4.228689	45.37675	12.19270	3.594533
Argon	Ar	0.0823417	0.22282597	0.1314125	0.288558	0.215269	0.07982437	0.5558895	0.23382711
Helium	He	0.0040962	0.23661	0.00000162	-0.0057339	-0.00001973	-0.00000055	-0.072673	0.077942
Carbon dioxide	CO ₂	0.18367101	0.32014927	1.7602805	2.4204855	0.62536078	1.9008120	0.48784066	0.42808218
Carbon monoxide	CO	0.12211169	0.45809483	0.07683175	0.23439776	0.21683496	0.073332301	2.0968189	0.67019093
Hydrogen	H ₂	0.02099032	0.2361049	0.00051116	0.00502886	0.05531	281.1889	2.113289	0.3507597
Nitrogen	N ₂	0.12654834	0.47170114	0.04836143	0.23094543	0.25483185	0.05775574	0.98032114	0.52104571
Oxygen	O ₂	0.09508520	0.00000035	0.32643518	1.62689940	0.358834736	1.28273741	-39270.58894	3.01
Nitric oxide	NO	0.25441140	0.39458452	1.4794968	1.67741770	0.51001644	1.5946	0.25559433	0.48129414

$$p_{\text{atm}} = A\rho_{\text{mol}}^* + B\rho_{\text{mol}}^{*2} + C\rho_{\text{mol}}^{*3} + D\rho_{\text{mol}}^{*6} + E\rho_{\text{mol}}^{*3} + F\rho_{\text{mol}}^{*5}e^{-\gamma\rho_{\text{mol}}^{*2}} \quad (2.130)$$

The virial temperature-dependent coefficients are defined by

$$A = R_a T_K \quad B = B_0 R_a T_K - A_0 - \frac{C_0}{T_K} \quad C = (b R_a T_K - a)$$

$$D = a\alpha \quad E = \frac{c}{T_K^2} \quad F = \frac{c\gamma}{T_K^2}$$

where p_{atm} is the pressure in atmospheres, T_K is the temperature in degrees kelvin, $R_a = 0.08206 \text{ atm dm}^3/(\text{mol K})$ is the universal gas constant, and ρ_{mol} is the molar density (mol/dm^3).

Equation 2.130 is nonlinear in molar density and can be solved readily using Newton's method form given by Eq. (A.2) in App. A. The function F is defined by

$$F = -p_{\text{atm}} + A\rho_{\text{mol}}^* + B\rho_{\text{mol}}^{*2} + C\rho_{\text{mol}}^{*3} + D\rho_{\text{mol}}^{*6} + E\rho_{\text{mol}}^{*3} + F\rho_{\text{mol}}^{*5}e^{-\gamma\rho_{\text{mol}}^{*2}} \quad (2.131)$$

and the derivative of the function becomes

$$F' = A + 2B\rho_{\text{mol}}^* + 3C\rho_{\text{mol}}^{*2} + 6D\rho_{\text{mol}}^{*5} + 3E\rho_{\text{mol}}^{*2} + F(5 - 2\gamma\rho_{\text{mol}}^{*2})\rho_{\text{mol}}^{*4}e^{-\gamma\rho_{\text{mol}}^{*2}} \quad (2.132)$$

The estimates for the molar density are then, by App. A, Eq. (A.9),

$$\rho_{\text{mol},n}^* = \rho_{\text{mol},n-1}^* - \frac{F}{F'} \quad (2.133)$$

The density is then

$$\rho^* = M_w \rho_{\text{mol}}^* \quad (2.134)$$

Modified Benedict-Webb-Rubin Equation

The eight-constant Benedict-Webb-Rubin (1964) equation has been modified (MBWR) into a 32-term state equation that is extremely valuable in describing the thermodynamic pVT surface and for fitting experimental data. It is described by McCarty (1975). It is widely used to define heat capacities, density, and sound velocity for pure substances and mixtures (Younglove, 1982; Reynolds, 1979). The molar SI unit density equation is

$$P_f^* = A\rho_{\text{mol}}^* + B\rho_{\text{mol}}^{*2} + C\rho_{\text{mol}}^{*3} + D\rho_{\text{mol}}^{*4} + E\rho_{\text{mol}}^{*5} + F\rho_{\text{mol}}^{*6} + G\rho_{\text{mol}}^{*7} + H\rho_{\text{mol}}^{*8} + J\rho_{\text{mol}}^{*9} + [K\rho_{\text{mol}}^{*3} + L\rho_{\text{mol}}^{*5} + M\rho_{\text{mol}}^{*7} + N\rho_{\text{mol}}^{*9} + O\rho_{\text{mol}}^{*11} + P\rho_{\text{mol}}^{*13}] \exp(-\gamma\rho_{\text{mol}}^{*2}) \quad (2.135)$$

where, for SI units, the equation constants are

$$A = 8314.4T_K$$

$$B = A_1T_K + A_2T_K^{1/2} + A_3$$

$$C = A_6T_K + A_7 + A_8T_K^{-1}$$

$$+ A_4T_K^{-1} + A_5T_K^{-2}$$

$$+ A_9T_K^{-2}$$

$$D = A_{10}T_K + A_{11} + A_{12}T_K^{-1}$$

$$E = A_{13}$$

$$F = A_{14}T_K^{-1} + A_{15}T_K^{-2}$$

$$G = A_{16}T_K^{-1}$$

$$H = A_{17}T_K^{-1} + A_{18}T_K^{-2}$$

$$J = A_{19}T_K^{-2}$$

$$K = A_{20}T_K^{-2} + A_{21}T_K^{-3}$$

$$L = A_{22}T_K^{-2} + A_{23}T_K^{-4}$$

$$M = A_{24}T_K^{-2} + A_{25}T_K^{-3}$$

$$N = A_{26}T_K^{-2} + A_{27}T_K^{-4}$$

$$O = A_{28}T_K^{-2} + A_{29}T_K^{-3}$$

$$P = A_{30}T_K^{-2} + A_{31}T_K^{-3} + A_{32}T_K^{-4}$$

$$\gamma = \rho_c^{-2} = \text{constant}$$

Values of A_i for some fluids are given in Table 2.14.

Equation (2.130) is nonlinear in molar density and can be solved readily using Newton's method function form given by Eq. (A.2) in App. A. The function F is defined by

$$F = P_f^* + A\rho_{\text{mol}}^* + B\rho_{\text{mol}}^{*2} + C\rho_{\text{mol}}^{*3} + D\rho_{\text{mol}}^{*4} + E\rho_{\text{mol}}^{*5} + F\rho_{\text{mol}}^{*6} + G\rho_{\text{mol}}^{*7} + H\rho_{\text{mol}}^{*8} \\ + J\rho_{\text{mol}}^{*9} + [K\rho_{\text{mol}}^{*3} + L\rho_{\text{mol}}^{*5} + M\rho_{\text{mol}}^{*7} + N\rho_{\text{mol}}^{*9} + O\rho_{\text{mol}}^{*11} + P\rho_{\text{mol}}^{*13}] \exp(-\gamma\rho_{\text{mol}}^{*2}) \quad (2.136)$$

and the derivative of the function by

$$F' = A + 2B\rho_{\text{mol}}^* + 3C\rho_{\text{mol}}^{*2} + 4D\rho_{\text{mol}}^{*3} + 5E\rho_{\text{mol}}^{*4} + 6F\rho_{\text{mol}}^{*5} \\ + 7G\rho_{\text{mol}}^{*6} + 8H\rho_{\text{mol}}^{*7} + 9J\rho_{\text{mol}}^{*8} + VU' + UV' \quad (2.137)$$

$$\text{where} \quad V = \exp(-\gamma\rho_{\text{mol}}^{*2}) \quad V' = -2\gamma\rho^* \exp(-\gamma\rho_{\text{mol}}^{*2})$$

$$\text{and} \quad U = K\rho_{\text{mol}}^{*3} + L\rho_{\text{mol}}^{*5} + M\rho_{\text{mol}}^{*7} + N\rho_{\text{mol}}^{*9} + O\rho_{\text{mol}}^{*11} + P\rho_{\text{mol}}^{*13}$$

$$U' = 3K\rho_{\text{mol}}^{*2} + 5L\rho_{\text{mol}}^{*4} + 7M\rho_{\text{mol}}^{*6} + 9N\rho_{\text{mol}}^{*8} + 11O\rho_{\text{mol}}^{*10} + 13P\rho_{\text{mol}}^{*12}$$

The estimates for the molar density are then, by App. A, Eq. (A.9),

$$\rho_{\text{mol},n}^* = \rho_{\text{mol},n-1}^* - \frac{F_{n-1}}{F'_{n-1}} \quad (2.138)$$

ASME 1967 Steam Equation

The ASME Steam Tables (ASME, 1967) present tabulated results of the properties of steam over four specified reduced-pressure and -temperature regions. Within each region the specific state equation used to produce the tabular values is presented.

TABLE 2.14 Constants for MBWR Equation of State

Argon M_w 39.948 Gamma γ		Ethylene M_w 28.054 Gamma γ		Hydrogen M_w 2.01584 Gamma γ	
	0.0056		0.0172		0.0041
A_1	-6.569731294E+01	A_1	-2.14668436668300E+03	A_1	4.675528393416E+01
A_2	1.822957801E+04	A_2	1.79143372253400E+05	A_2	4.289274251454E+03
A_3	-3.649470141E+05	A_3	-3.67531560393000E+06	A_3	-5.164085596504E+04
A_4	1.232012107E+07	A_4	3.70717893466900E+08	A_4	2.961790279801E+05
A_5	-8.613578274E+08	A_5	-3.19828256670900E+10	A_5	-3.027194968412E+05
A_6	7.978579691E+00	A_6	5.80937977473200E+01	A_6	1.908100320379E+00
A_7	-2.911489110E+03	A_7	-7.89557082489900E+04	A_7	-1.339776859288E+02
A_8	7.581821758E+05	A_8	1.14862037583500E+07	A_8	3.056473115421E+04
A_9	8.780488169E+08	A_9	2.71377462919300E+10	A_9	5.161197159532E+06
A_{10}	1.423145989E-02	A_{10}	-8.64712431910700E+00	A_{10}	1.999981550224E-02
A_{11}	1.674146131E-02	A_{11}	1.61772726638500E+04	A_{11}	2.896370593560E+01
A_{12}	-3.200447909E-04	A_{12}	-2.73152749627100E+06	A_{12}	-2.257803939041E+03
A_{13}	2.561766372E-00	A_{13}	-2.67228364145900E+02	A_{13}	-2.287392761826E-01
A_{14}	-5.475934941E-01	A_{14}	-4.75238133199000E+03	A_{14}	2.446261478645E+00
A_{15}	-4.505032058E-04	A_{15}	-6.25563734621700E+06	A_{15}	-1.718186011190E+02
A_{16}	2.013254653E+00	A_{16}	4.57623496443400E+02	A_{16}	-5.465142603459E-02
A_{17}	-1.678941273E-02	A_{17}	-7.53483926932000E+00	A_{17}	4.051941401315E-04
A_{18}	4.207329271E+01	A_{18}	1.63817198220900E+04	A_{18}	1.157595123961E-01
A_{19}	-5.444212996E-01	A_{19}	-3.56309074074000E+02	A_{19}	-1.269162728389E-03
A_{20}	-8.004855011E+08	A_{20}	-1.83300078317000E+10	A_{20}	-4.983023605519E+06
A_{21}	-1.319304201E+10	A_{21}	-1.80507421737858E+12	A_{21}	-1.606676092098E+07
A_{22}	-4.954923930E+06	A_{22}	-4.79458791887400E+08	A_{22}	-1.926799185310E+04
A_{23}	8.092132177E+09	A_{23}	3.53194828942386E+12	A_{23}	9.319894638928E+05
A_{24}	-9.870104061E+03	A_{24}	-2.56257103915500E+06	A_{24}	-3.222596554434E+01
A_{25}	2.020441562E+05	A_{25}	1.04430825329200E+08	A_{25}	1.206839307669E+02
A_{26}	-1.637417205E+01	A_{26}	-1.69530336365900E+04	A_{26}	-3.841588197470E-02
A_{27}	-7.038944136E+04	A_{27}	-1.71033422495800E+08	A_{27}	-4.036157453608E+00
A_{28}	-1.154324539E-02	A_{28}	-2.05411446237200E+01	A_{28}	-1.250868123513E-05
A_{29}	1.555990117E+00	A_{29}	6.72755876666100E+03	A_{29}	1.976107321888E-04
A_{30}	-1.492178536E-05	A_{30}	-1.55716840332800E-01	A_{30}	-2.411883474011E-08
A_{31}	-1.001356071E-03	A_{31}	-1.22981473607700E+01	A_{31}	-4.127551498251E-08
A_{32}	2.933963216E-02	A_{32}	4.23432593857300E+01	A_{32}	8.917972883610E-07

Methane M_w 16.043		Nitrogen M_w 28.0134		Oxygen M_w 31.9988	
Gamma γ	0.0096	Gamma γ	0.0056	Gamma γ	0.0056
A_1	-1.895061186540000E+03	A_1	1.380297474656910E+02	A_1	-4.365859650E+01
A_2	1.047569871900000E+05	A_2	1.084506501348800E+04	A_2	2.005820677E+04
A_3	-1.574465116580000E+06	A_3	-2.471324064362090E+05	A_3	-4.197909916E+05
A_4	7.825446056550000E+07	A_4	3.455257980807090E+06	A_4	1.878215317E+07
A_5	-3.820999196230000E+09	A_5	-4.279707690665950E+08	A_5	-1.287473398E+09
A_6	8.580391931510000E+01	A_6	1.064911566997600E+01	A_6	1.556745888E+00
A_7	-5.029933949990000E+04	A_7	-1.140867079734990E+03	A_7	1.343639359E+02
A_8	8.814356513330000E+06	A_8	1.444902497287470E+01	A_8	-2.228415518E+05
A_9	-3.270989785940000E+09	A_9	1.871457567553270E+09	A_9	4.767792275E+08
A_{10}	-4.010879464170000E+00	A_{10}	8.218876886830790E-03	A_{10}	4.790846641E-02
A_{11}	2.703070512490000E+03	A_{11}	2.360990493347590E+02	A_{11}	2.464611107E+02
A_{12}	-3.080381911050000E+05	A_{12}	-5.144803081201350E+04	A_{12}	-1.921891680E+04
A_{13}	1.941230022610000E+01	A_{13}	4.914545013668030E+00	A_{13}	-6.978320847E-01
A_{14}	-1.981794735760000E+01	A_{14}	-1.151627162398930E+02	A_{14}	-6.214145909E+01
A_{15}	6.155290774530000E+05	A_{15}	-7.168037246649830E+04	A_{15}	-1.860852567E+04
A_{16}	-5.366268522030000E+01	A_{16}	7.616667619499810E+00	A_{16}	2.609791417E+00
A_{17}	1.542817877940000E+00	A_{17}	-1.130930066219500E-01	A_{17}	-2.447611408E-02
A_{18}	-1.114090492650000E+03	A_{18}	3.736831166830890E+01	A_{18}	1.457743352E+01
A_{19}	1.939315409660000E+00	A_{19}	-2.039851507580860E-01	A_{19}	-1.726492873E-01
A_{20}	3.915907312960000E+09	A_{20}	-1.719662008989660E+09	A_{20}	-2.384892520E+08
A_{21}	-1.600231661092744E+11	A_{21}	-1.213055199747770E+10	A_{21}	-2.301807796E+10
A_{22}	1.978574738144000E+07	A_{22}	-9.881399141427890E+06	A_{22}	-2.790303526E+10
A_{23}	1.681955331556445E+11	A_{23}	5.619886893510850E+09	A_{23}	9.400577575E+09
A_{24}	6.110415744050000E+04	A_{24}	-1.823043964118450E+04	A_{24}	-4.169449637E+03
A_{25}	3.814735912150000E+06	A_{25}	-2.599826498477050E+05	A_{25}	2.008497853E+05
A_{26}	1.272577968900000E+02	A_{26}	-4.191893423157420E+01	A_{26}	-1.256076520E+01
A_{27}	-3.481223354440000E+06	A_{27}	-2.596406670530230E+04	A_{27}	-6.406362964E+04
A_{28}	-5.481126166360000E-01	A_{28}	-1.258683201921190E-02	A_{28}	-2.475580168E-03
A_{29}	1.880817799350000E+02	A_{29}	1.049286599400460E+00	A_{29}	1.346309703E+00
A_{30}	7.809999067200000E-04	A_{30}	-5.458369305152010E-05	A_{30}	-1.161502470E-05
A_{31}	-2.906693238720000E-01	A_{31}	-7.674511670597170E-04	A_{31}	-1.034699798E-03
A_{32}	3.773109563890000E+00	A_{32}	5.931232870994390E-03	A_{32}	2.365936964E-02

Note: E in this table stands for *engineering notation*. For example, E+07 = 10^7 and E-07 = 10^{-7} , etc.

Region 2 covers the saturation and superheated steam region from 0 to 2400 psia (0 to 16,550 kPa). This is the range of pressures most commonly used in flow measurement applications, and the density equation is presented here.

The equation is a closed-form solution (noniterative) and is developed using reduced pressure p_r and temperature parameters T_r to define the reduced volume v_r . The reduced properties are

$$T_r = \frac{T_K}{T_{Kc}} = \frac{T_K}{647.3} \quad p_r = \frac{p_f^*}{P_c} = \frac{P_f^*}{22.12 \times 10^6}$$

$$v_r = \frac{v_{m^3/kg}}{v_c} = \frac{v_{m^3/kg}}{0.00317} \quad (2.139)$$

The saturation pressure boundary (region) is defined by

$$p_1 = l_0 + l_1 T_r + l_2 T_r^2 \quad (2.140)$$

The constants l_0 , l_1 , and l_2 are given in Table 2.15. With

$$x = \exp[0.7633333333(1 - T_r)] \quad (2.141)$$

the reduced-volume equation is written as

$$v_r = \frac{v}{v_c} = I_1 \frac{T_r}{p_r} - B_{11}x^{13} - B_{12}x^3 - 2p_r(B_{21}x^{18} + B_{22}x^2 + B_{23}x) \\ - 3p_r^2(B_{31}x^{18} + B_{32}x^{10}) - 4p_r^3(B_{41}x^{25} + B_{42}x^{14}) - 5p_r^4(B_{51}x^{32} + B_{52}x^{28} \\ + B_{53}x^{24}) - [6p_r^{-7}(B_{81}x^{24} + B_{82}x^{14})][p_r^{-6} + BB_{81}x^{54} + BB_{82}x^{27}]^{-2} \\ + 11 \left(\frac{p_r}{p_1} \right)^{10} (B_{90} + B_{91}x + B_{92}x^2 + B_{93}x^3 + B_{94}x^4 + B_{95}x^5 + B_{96}x^6) \\ - [4p_r^{-5}(B_{61}x^{12} + B_{62}x^{11})][p_r^{-4} + BB_{61}x^{14}]^{-2} \\ - [5p_r^{-6}(B_{71}x^{24} + B_{72}x^{18})][p_r^{-5} + BB_{71}x^{19}]^{-2} \quad (2.142)$$

The constants shown in these equations are given in Table 2.15. The density, in SI units, is calculated by

$$\rho_{kg/m^3}^* = (v_c v_r)^{-1} \quad (2.143)$$

and, for U.S. units, by

$$\rho_{lb/ft^3} = (16.01846 v_c v_r)^{-1} \quad (2.144)$$

IAPS Steam Equation

The ASME Research Committee (White, 1986) on the properties of steam has provided data on steam properties for over 50 years. This committee, working with the International Association for the Properties of Steam (IAPS), has led to the formulation of an equation (IAPS, 1985) for the properties of water based on the Helmholtz function. The density relationship is derived from the Helmholtz function as

TABLE 2.15 ASME 1967 Steam Equation Constants

$p_c = 22.12 \text{ MPa}$	$T_{Kc} = 647.3 \text{ K}$	$v_c = 0.00317 \text{ m}^3/\text{kg}$
$I_1 = 4.260321148$		
$l_0 = 15.74373327$	$l_1 = -34.17061978$	$l_2 = 19.31380707$
$K_1 = -7.691234564$	$K_2 = -26.08023696$	$K_3 = -168.1706546$
$K_4 = 64.23285504$	$K_6 = -118.9646225$	$K_6 = 4.16711732$
$K_7 = 20.9750676$	$K_8 = 1000000000$	$K_9 = 6$
$B_{11} = 0.066703759$	$B_{12} = 1.388983801$	$B_{21} = 0.08390104328$
$B_{22} = 0.02614670893$	$B_{23} = -0.03373439453$	$B_{31} = 0.4520918904$
$B_{32} = 0.1069036614$	$B_{41} = -0.5975336707$	$B_{42} = -0.08847535804$
$B_{51} = 0.5958051609$	$B_{52} = -0.5159303373$	$B_{53} = 0.2075021122$
$B_{61} = 0.1190610271$	$B_{62} = -0.09867174132$	$B_{71} = 0.1683998803$
$B_{72} = -0.05809438001$	$B_{81} = 0.006552390126$	$B_{82} = 0.0005710218649$
$B_{90} = 193.6587558$	$B_{91} = -1388.522425$	$B_{92} = 4126.607219$
$B_{93} = -6508.211677$	$B_{94} = 5745.984054$	$B_{96} = -2693.088365$
$B_{96} = 523.5718623$		
$BB_{61} = 0.4006073948$	$BB_{71} = 0.08636081627$	$BB_{81} = -0.8532322921$
$BB_{62} = 0.3460208861$		

$$p = \rho^2 \left(\frac{\partial \Psi}{\partial \rho} \right)_{T_K} \quad (2.145)$$

where the Helmholtz function Ψ is the summation of three functions: base function Ψ_1 , residual Ψ_2 , and ideal gas Ψ_3 , or

$$\Psi = \Psi_1 + \Psi_2 + \Psi_3 \quad (2.146)$$

The base function Ψ_1 is computed by

$$\begin{aligned} \Psi_1 = \frac{R_0 T_K}{M_w} \left[-\ln(1 - \rho_d) - \frac{1 - \beta}{1 - \rho_d} + \frac{\alpha + \beta + 1}{2(1 - \rho_d)^2} \right. \\ \left. + 4\rho_d \left(\frac{B}{b} - \rho_d \right) - \frac{\alpha - \beta + 3}{2} + \ln \frac{\rho R_0 T_K}{M_w P_0} \right] \end{aligned} \quad (2.147)$$

where $P_0 = 1.01325$ bars (1 atmosphere), with the dimensionless density ρ_d determined by

$$\rho_d = \frac{b\rho}{4} \quad (2.148)$$

The two molecular parameters, b and B , are temperature-dependent and defined by

$$b = b_1 \ln \frac{T_K}{647.073} + \sum_{j=0,1,3,5} b_j \left(\frac{647.073}{T_K} \right)^j \quad (2.149)$$

$$B = \sum_{j=0,1,2,4} B_j \left(\frac{647.073}{T_K} \right)^j \quad (2.150)$$

The coefficients b_j and B_j are listed in Table 2.16.

TABLE 2.16 IAPS Equations Base
Function Coefficients

$b_j(\text{cm}^3\text{g}^{-1})$	j	$B_j(\text{cm}^3\text{g}^{-1})$
0.7478629	0	1.1278334
-0.3540782	1	-0.5944001
0.0000000	2	-5.010996
0.007159876	3	0.0000000
0.0000000	4	0.63684256
-0.003528426	5	0.0000000

The residual function is a 40-term equation fit to experimental data. This equation is

$$\Psi_2 = \sum_{i=1}^{36} \frac{g_i}{k(i)} \left(\frac{647.073}{T_K} \right)^{l(i)} (1 - e^{-\rho})^{k(i)} + \sum_{i=37}^{40} g_i \delta_i^{l(i)} \exp(-\alpha_i \delta_i^{k(i)} - \beta_i \tau^2) \quad (2.151)$$

The quantities δ_i and τ_i are, respectively,

$$\delta_i = \frac{\rho - \rho_i}{\rho_i} \quad \tau_i = \frac{T_K - T_i}{T_i} \quad (2.152)$$

where $g(i)$, $k(i)$, and $l(i)$ are integers; these values and those for ρ_i and T_i are given in Table 2.17.

The ideal gas function for water is

$$\Psi_3 = -\frac{R_0}{M_w} \left[1 + \left(\frac{100C_1}{T_K} + C_2 \right) \ln \left(\frac{T_K}{100} \right) + \sum_{i=3}^{18} C_i \left(\frac{T_K}{100} \right)^{i-6} \right] \quad (2.153)$$

Coefficients C_i are listed in Table 2.18.

SATURATION TEMPERATURE AND PRESSURE

Except for an obstructionless flowmeter (magnetic or ultrasonic), the decrease in pressure as a liquid moves through the meter may result in flashing (liquid to vapor state) or in a damaging cavitation condition. The pressure at which this occurs is the vapor pressure corresponding to the fluid's upstream temperature. Vapor pressures may be found in tables or computed from vapor pressure equations. Several of these are given below.

Lee-Kessler

The Lee-Kessler equation (Reid et al., 1987) is a three-parameter corresponding states equation that yields good results for all fluids:

TABLE 2.17 Coefficients for Residual Function

i	$k(j)$	$l(i)$	$g(i)(Jg^{-1})$				
1	1	1	-5.3062968529023E02				
2	1	2	2.2744901424408E03				
3	1	4	7.8779333020687E02				
4	1	6	-6.9830527374994E01				
5	2	1	1.7863832875422E04				
6	2	2	-3.9514731563338E04				
7	2	4	3.3803884280753E04				
8	2	6	-1.3855050202703E04				
9	3	1	-2.5637436613260E05				
10	3	2	4.8212575981415E05				
11	3	4	-3.4183016969660E05				
12	3	6	1.2223156417448E05				
13	4	1	1.1797433655832E06				
14	4	2	-2.1734810110373E06				
15	4	4	1.0829952168620E06				
16	4	6	-2.5441998064049E05				
17	5	1	-3.1377774947767E06				
18	5	2	5.2911910757704E06				
19	5	4	-1.3802577177877E06				
20	5	6	-2.5109914369001E05				
21	6	1	4.6561826115608E06				
22	6	2	-7.2752773275387E06				
23	6	4	4.1774246148294E05				
24	6	6	1.4016358244614E06				
25	7	1	-3.1555231392127E06				
26	7	2	4.7929666384584E06				
27	7	4	4.0912664781209E05				
28	7	6	-1.3626369388386E06				
29	9	1	6.9625220862664E05				
30	9	2	-1.0834900096447E06				
31	9	4	-2.2722827401688E05				
32	9	6	3.8365486000660E05				
33	3	0	6.8833257944332E03				
34	3	3	2.1757245522644E04				
35	1	3	-2.6627944829770E03				
36	5	3	-7.0730418082074E04				
i	$k(i)$	$l(i)$	$p_i(g\text{ cm}^{-3})$	$T_i(K)$	$*i$	$*i$	$g_i(J\text{ g}^{-1})$
37	2	0	0.319	640.	34	20000	-0.225
38	2	0	0.319	640.	40	20000	-1.68
39	2	0	0.319	641.6	30	40000	0.055
40	4	0	1.55	270.	1050	25	-93.0

TABLE 2.18 Coefficients for Ideal Gas Function

<i>i</i>	<i>C_i</i>
1	1.93027101800E+01
2	2.09662681977E+01
3	-4.83429455355E-01
4	6.05743189245E+00
5	2.25602388500E+01
6	-9.87532442000E+00
7	-4.31355385130E+00
8	4.58155781000E+00
9	-4.77549018830E-02
10	4.12384606330E-03
11	-2.79290528520E-04
12	1.44816952610E-05
13	-5.64736587480E-07
14	1.62004460000E-08
15	-3.30382279600E-10
16	4.51916067368E-12
17	-3.70734122708E-14
18	1.37546068238E-16

$$p_r = \frac{p_f}{p_c} = \exp (A_1 T_r + \omega A_2 T_r) \quad (2.154)$$

where A_1 and A_2 are temperature-dependent terms, for A_1

$$A_1 = 5.92714 - \frac{6.09648}{T_r} - 1.28862 \ln (T_r) + 0.169347 T_r \quad (2.155)$$

and for A_2

$$A_2 = 15.2518 - \frac{15.6875}{T_r} - 13.4721 \ln (T_r) + 0.43577 T_r \quad (2.156)$$

where $T_r = T_f/T_c$ and ω is the acentric factor.

If the temperature, rather than the pressure, is to be calculated, Eq. (2.154) is nonlinear in temperature and can be solved readily using Newton's method form given by Eq. (A.2) in App. A. The function F is defined by

$$F = -p_r + \exp (A_1 T_r + \omega A_2 T_r) \quad (2.157)$$

The derivative of the function is then

$$F' = (A_1 + \omega A_2) \exp (A_1 T_r + \omega A_2 T_r) \quad (2.158)$$

The estimates for the reduced temperature are then, by App. A, Eq. (A.9),

$$T_{r,n} = T_{r,n-1} - \frac{F_{n-1}}{F_{n-1}} \quad (2.159)$$

The temperature is then

$$T_f = T_r T_c \quad (2.160)$$

AICHe Vapor Pressure Equation

The Design Institute for Physical Properties Data (AICHe, 1986) presents the constants to be used in a vapor pressure equation for over 1000 fluids. The AICHe is

$$P_{\text{vap}}^* = \exp \left[a + \frac{b}{T_K} + c \ln (T_K) + dT_K^e \right] \quad (2.161)$$

where P_{vap}^* is the vapor pressure in pascals, T_K is the temperature in degrees kelvin, and a , b , c , d , and e are constants; several of these are present in Table 2.19.

If the temperature, rather than the pressure, is to be calculated, Eq. (2.161) is nonlinear in temperature and can be solved readily using Newton's method form given by Eq. (A.2) in App. A. The function F is defined by

$$F = -P_{\text{vap}} + \exp a + \frac{b}{T_K} + c \ln (T_K) + dT_K^e \quad (2.162)$$

The derivative of the function is then

$$F' = \left(-\frac{b}{T_K^2} + \frac{c}{T_K} + deT_K^{e-1} \right) \exp \left[a + \frac{b}{T_K} + c \ln (T_K) + dT_K^e \right] \quad (2.163)$$

The estimates for the temperature are then, by App. A, Eq. (A.9),

$$T_{K,n} = T_{K,n-1} + \frac{F_{n-1}}{F_{n-1}} \quad (2.164)$$

Steam Saturation Temperature. The reduced saturation steam temperature is a function of the reduced saturation pressure:

$$\ln (p_r) = \frac{K_1 T + K_2 T^2 + K_3 T^3 + K_4 T^4 + K_5 T^5}{1 + (K_6 - 1)T + (K_7 - K_6)T^2 - K_7 T^3} - \frac{T}{K_8 T^2 + K_9} \quad (2.165)$$

where

$$T = 1 - \frac{T_K}{T_c} = 1 - \frac{T_K}{647.3} \quad (2.166)$$

Equation (2.165) is nonlinear in temperature, and Newton's method (App. A) can be used to solve for the reduced temperature, and hence the saturation temperature, by first defining the function F [App. A, Eq. (A.9)] as

$$F = -\ln (p_r) + \frac{K_1 T + K_2 T^2 + K_3 T^3 + K_4 T^4 + K_5 T^5}{1 + (K_6 - 1)T + (K_7 - K_6)T^2 - K_7 T^3} - \frac{T}{K_8 T^2 + K_9} \quad (2.167)$$

where K_1 , K_2 , \dots are found in Table 2.15. The derivative of the function is then

TABLE 2.19 AIChE Vapor Pressure Equation Constants

	Acetaldehyde C_2H_4O	Acetic acid $C_2H_4O_2$	Acetic anhydride $C_4H_6O_3$	Acetone C_3H_6O	Acrylic acid $C_3H_4O_2$
<i>a</i>	2.0607E+02	7.0230E+01	1.0506E+02	7.0720E+01	5.7992E+01
<i>b</i>	-8.4786E+03	-6.8465E+03	-8.8979E+03	-5.6850E+03	-7.2180E+03
<i>c</i>	-3.1548E+01	-7.0320E+00	-1.2162E+01	-7.3510E+00	-4.8813E+00
<i>d</i>	4.6314E-02	5.0210E-06	7.6561E-06	6.3000E-06	1.0060E-03
<i>e</i>	1.0000E+00	2.0000E+00	2.0000E+00	2.0000E+00	1.0000E+00
	Acrylonitrile C_3H_3N	Acetyl chloride C_2H_3ClO	Carbolic acid C_6H_6O	Carbon disulfide CS_2	Carbon tetrachloride CCl_4
<i>a</i>	8.7604E+01	1.8772E+02	5.9080E+01	6.2797E+01	7.8439E+01
<i>b</i>	-6.3927E+03	-8.7010E+03	-8.0500E+03	-4.7063E+03	-6.1281E+03
<i>c</i>	-1.0101E+01	-2.7926E+01	-4.8990E+00	-6.7794E+00	-8.5763E+00
<i>d</i>	1.0891E-05	3.7322E-02	2.8000E-04	8.0195E-03	6.8461E-06
<i>e</i>	2.0000E+00	1.0000E+00	1.0000E+00	1.0000E+00	2.0000E+00
	Cyclohexatriene C_6H_6	Chloroform $CHCl_3$	Cyclohexanol $C_6H_{12}O$	Decane $C_{10}H_{22}$	Diethyl carbonal $C_5H_{12}O$
<i>a</i>	7.8050E+01	1.3526E+02	1.1982E+02	6.5940E+01	8.6409E+01
<i>b</i>	-6.2755E+03	-7.4746E+03	-1.1155E+04	-7.7331E+03	-8.6747E+03
<i>c</i>	-8.4443E+00	-1.8700E+01	-1.3711E+01	-6.1174E+00	-8.8204E+00
<i>d</i>	6.2600E-06	2.1909E-02	3.6685E-06	1.1180E-06	7.2696E-18
<i>e</i>	2.0000E+00	1.0000E+00	2.0000E+00	2.0000E+00	6.0000E+00
	Dihydroxyethane $C_2H_6O_2$	Glycerital $C_3H_8O_3$	Glycol $C_2H_6O_2$	Hendecane $C_{11}H_{24}$	Hydrogen sulfate H_2O_4S
<i>a</i>	1.9464E+02	1.1205E+02	1.9464E+02	1.9583E+02	-1.6212E+01
<i>b</i>	-1.4615E+04	-1.4376E+04	-1.4615E+04	-1.2914E+04	-9.0687E+03
<i>c</i>	-2.5433E+01	-1.1871E+01	-2.5433E+01	-2.7327E+01	8.9959E+00
<i>d</i>	2.0140E-05	7.9537E-18	2.0140E-05	2.4106E-02	-2.5661E-02
<i>e</i>	2.0000E+00	6.0000E+00	2.0000E+00	1.0000E+00	1.0000E+00
	Karsan CH_2O	Maleic acid $C_4H_4O_4$	Mesityl oxide $C_6H_{10}O$	Methanol CH_4O	Methyl formate $C_2H_4O_2$
<i>a</i>	1.0151E+02	1.1641E+02	9.5024E+01	1.0993E+02	7.1570E+01
<i>b</i>	-4.9172E+03	-1.1403E+04	-8.1306E+03	-7.4713E+03	-5.4300E+03
<i>c</i>	-1.3765E+01	-1.2834E+01	-1.0716E+01	-1.3988E+01	-7.4848E+00
<i>d</i>	2.2031E-02	1.6965E-17	5.8708E-06	1.5281E-02	6.2200E-06
<i>e</i>	1.0000E+00	6.0000E+00	2.0000E+00	1.0000E+00	2.0000E+00

TABLE 2.19 AIChE Vapor Pressure Equation Constants (*Continued*)

	Methyl ketone C_3H_6O	Monochlorobenzene C_6H_5Cl	Nitric acid HNO_3	Nonane C_9H_{20}	1-Nonene C_9H_{18}
<i>a</i>	7.0720E+01	4.9642E+01	1.7014E+02	6.6184E+01	1.4445E+02
<i>b</i>	-5.6850E+03	-5.9408E+03	-1.0078E+04	-7.2370E+03	-9.6762E+03
<i>c</i>	-7.3510E+00	-3.9391E+00	-2.2769E+01	-6.2614E+00	-1.9446E+01
<i>d</i>	6.3000E-06	1.1417E-06	2.7300E-05	1.6668E-06	1.8031E-02
<i>e</i>	2.0000E+00	2.0000E+00	2.0000E+00	2.0000E+00	1.0000E+00

$$F' = \frac{vu' - uv'}{v^2} - \frac{K_9 - K_8T^2}{(K_8T^2 + K_9)^2} \quad (2.168)$$

where u , v , u' , and v' are calculated by

$$u = K_1T + K_2T^2 + K_3T^3 + K_4T^4 + K_5T^5$$

$$u' = K_1 + 2K_2T + 3K_3T^2 + 4K_4T^3 + 5K_5T^4$$

$$v = 1 + (K_6 - 1)T + (K_7 - K_6)T^2 - K_7T^3$$

$$v' = K_6 - 1 + 2(K_7 - K_6)T - 3K_7T^2$$

The value of T ($T = 1 - T_r$) is first determined by Newton's method as

$$T_n = T_{n-1} - \frac{F_{n-1}}{F'_{n-1}} \quad (2.169)$$

As the initial estimate for $T_{K,sat}$ in kelvins, use

$$(T_{K,sat})_0 = -\frac{4890}{\ln(P_f^*/10^6) - 10.7} \quad (2.170)$$

The saturation temperature ($T_{K,sat}$) is calculated by

$$T_{K,sat} = T_c(1 - T) = 647.3(1 - T)$$

LIQUID DENSITY AND SPECIFIC GRAVITY

Liquid density decreases with increasing temperature and, to a much smaller degree, increases with pressure. Depending on how the density is determined, corrections may be needed if the value at flowing conditions is to be obtained.

The density of a liquid is relatively easy and inexpensive to measure, and for most fluids at least one experimental data point is available. The density of a mixture of liquids is usually calculated on a molar volume-average basis, preferably with an experimentally determined point to ensure accuracy.

Water Density (Reference Equation)

The literature contains a number of slightly different values for the density of water at both 60 and 68°F. Since the density of water at these temperatures is a basic reference (for specific gravity at 60°F, and for the inch-of-water differential pressure unit at 68°F), it is important to select one source as the reference standard. In this handbook, the PTB (1991) equation will be used. This equation expresses mass density, in kilograms per cubic meter, as a function of temperature:

$$\begin{aligned}\rho_w^* &= 9.998395639 \times 10^2 + 6.798299989 \times 10^{-2}T \cdot c \\ &\quad - 9.106025564 \times 10^{-3}T^2 \cdot c + 1.005272999 \times 10^{-4}T^3 \cdot c \\ &\quad - 1.126713526 \times 10^{-6}T^4 \cdot c + 6.591795606 \times 10^{-9}T^6 \cdot c\end{aligned}\quad (2.171)$$

From this equation, the reference density of water at 60°F (15.6°C) and 14.696 psia (101.325 kPa) is

$$(\rho_w)_{60,14.696} = 62.36630 \text{ lb}_m/\text{ft}^3 \text{ (999.0121 kg/m}^3\text{)} \quad (2.172)$$

and at 68°F (20°C) and 14.696 psia (101.325 kPa) it is

$$(\rho_w)_{68,14.696} = 62.31572 \text{ lb}_m/\text{ft}^3 \text{ (998.2019 kg/m}^3\text{)} \quad (2.173)$$

These values will be used in developing all subsequent equations for which the density of water is a reference.

Liquid Specific Gravity

The liquid specific gravity (relative density) of a fluid is the ratio of the density of the fluid, at its temperature, to the density of water at a specified reference temperature. In scientific work, the reference is double-distilled water at 4°C (39.2°F); for general engineering work, the reference temperature is 60°F (15.6°C), with no specification as to the condition of the water (although distilled water is implied). ISO 5024 (1976) is standardized on 15°C (59°F) for petroleum liquids. However, API 2540 (1987) adopts 60°F (15.6°C) as the reference for density corrections [see Eq. (2.106)]. Since all published data, curves, and tables are based on 60°F (15.6°C), that temperature will be used in this handbook.

In flow measurement, two liquid specific gravities are used: the specific gravity at base conditions G_b and the specific gravity at flowing conditions G_F . Base conditions are defined as 60°F (15.6°C) and 14.696 psia (101.325 kPa), or standard atmospheric pressure. The base specific gravity is the ratio of fluid density to water density when both are at base conditions; it is written as

$$G_b = \left(\frac{\rho_b}{\rho_w} \right)_{60,14.696} = \left(\frac{\rho_b}{62.36630} \right)_{60,14.696} = \left(\frac{\rho_b^*}{999.0121} \right)_{15.6,101.33} \quad (2.174)$$

The flowing specific gravity is defined as the ratio of fluid density at line temperature to the density of water at base conditions and is defined by

$$G_F = \frac{\rho_F}{(\rho_w)_{60,14.696}} = \frac{\rho_F}{62.36630} = \frac{\rho_F^*}{999.0121} \quad (2.175)$$

Measurement of Specific Gravity and Density

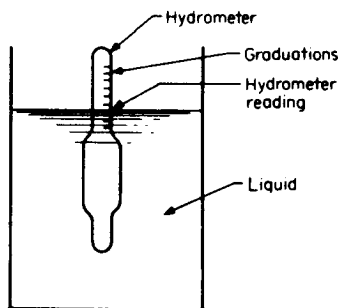


Figure 2.11 Liquid hydrometer.

Hydrometers. Hydrometers (Fig. 2.11) are the most convenient and widely used devices for determining the specific gravity of relatively transparent liquids. One-tenth of one percent accuracy is usually achievable with a calibrated device.

The hydrometer displaces a volume of the unknown liquid until an equilibrium is reached between upward buoyant force and downward hydrometer weight force. By suitable graduation, calibration with known fluids, and the addition of lead-pellet weights, the scale reading is calibrated to read either specific gravity or some related

unit (such as API degrees or Baumé degrees).

API Degrees. The scale of the American Petroleum Institute (API) hydrometer is calibrated in degrees API ($^{\circ}\text{API}$). The specific gravity at base conditions [60°F (15.6°C)] is calculated from the API hydrometer reading as

$$G_b = \frac{141.5}{131.5 + ^{\circ}\text{API}} \quad (2.176)$$

API-degree hydrometers read correctly only when the liquid temperature is 60°F (15.6°C), since the glass volume changes with changes in temperature. A correction for temperature is included in the tabular values given in Table 5A of ASTM Standard 2540.

Baumé Degrees. In 1768 the French chemist Baumé proposed two hydrometer scales—one for liquids heavier than water and the other for liquids lighter than water. These scales are widely used to measure the specific gravity of syrups, acids, and other light and heavy liquids. With 60°F (15.6°C) as the reference water density, the Baumé scales provide base readings via

$$G_b = \frac{140}{^{\circ}\text{Bé} + 130} \quad (2.177)$$

for lighter-than-water liquids and

$$G_b = \frac{145}{145 - ^{\circ}\text{Bé}} \quad (2.178)$$

for heavier-than-water liquids.

Westphal Balance. Shown in Fig. 2.12 is the Westphal balance, a specific-gravity-measuring instrument. Unlike the hydrometer, which floats in the liquid, the Westphal balance plummet is fully submerged. The cord tension is the difference be-

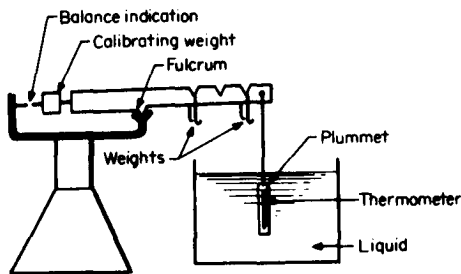


Figure 2.12 Westphal balance.

tween the downward plummet weight force and the upward buoyant force. The moment of this resultant force is balanced by placing calibrated rider weights in notches on the balance arm. Calibration with distilled water at 60°F (15.6°C) allows the instrument to be calibrated to read the specific gravity directly.

Glass Volumetric Correction. Hydrometers are designed and calibrated to read correctly at a specified base temperature. Usually this temperature is 60°F (15.56°C), but other base temperatures may be indicated.

To calculate the specific gravity at the test fluid temperature, the cubical expansion coefficient given in Table 2.20 can be used. The specific gravity G'_b based on the hydrometer reading is first calculated from the proper conversion equation [Eqs. (2.176) to (2.179)]; then G'_b is used in the following equation to calculate the specific gravity:

TABLE 2.20 Cubical Coefficients for Hydrometer Glass (Direct-Reading Hydrometers)

Hydrometer	Cubical coefficient α_H	
	(°F) ⁻¹	(°C) ⁻¹
Normal Pyrex	0.0000056	0.000010
Jena III, API†	0.0000128	0.000023
New hydrometers	0.0000139	0.000025
Sinkers	0.0000150	0.000027
Sinker no. 234	0.00000594	0.0000107

†For API-degree hydrometer correction, $G_F = [1 - 0.00001278(T_F - 60) - 0.000000062(T_F - 60)^2]G'_b$.

$$G_F = [1 - \alpha_H(T_F - 60)]G'_b \quad (2.179)$$

For the API-degree hydrometer, a more exact expression is

$$G_F = [1 - 0.00001278(T_F - 60) - 0.0000000062(T_F - 60)^2] \quad (2.180)$$

$$\times \frac{141.5}{131.5 + ^\circ\text{API}}$$

where $^\circ\text{API}$ is the hydrometer reading at temperature T_F .

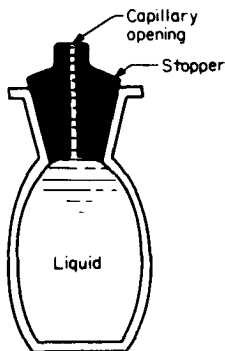


Figure 2.13 Pycnometer bottle.

Pycnometer. The most accurate way to determine specific gravity and density is by using a pycnometer bottle (Fig. 2.13). The bottle and stopper are weighed twice—first empty and then filled with distilled water—to determine the bottle volume. The bottle is then filled with the unknown liquid and weighed. The mass density is the recorded mass divided by the bottle volume, and the specific gravity is the ratio of the fluid mass to the distilled-water value. Care must be exercised to ensure that the temperature is recorded and used to adjust to the reference-density temperature. Measurement accuracy to the fourth decimal place (approximately 0.01 percent) is possible with this instrument. However, in measuring light hydrocarbons,

care must be taken to obtain a representative sample and to clean the bottle properly between tests.

Liquid Densitometer. Shown in Fig. 2.14 is an on-line liquid densitometer that provides continuous measurement of liquid density. The stainless steel sensor consists of a single, straight, unobstructed polished bore tube. Operating on the mass-resonance principle, the sensor is maintained in oscillation by self-contained electronics requiring ac power input. Density is measured as a function of sensor-liquid natural frequency. The transmitter provides either a current or voltage analog that is directly proportional to density.

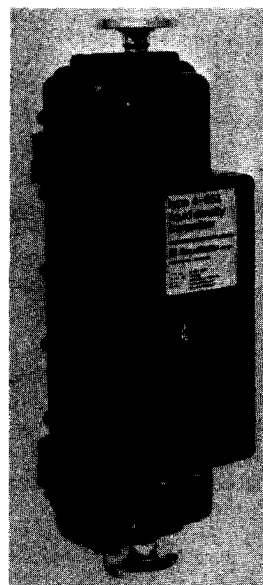
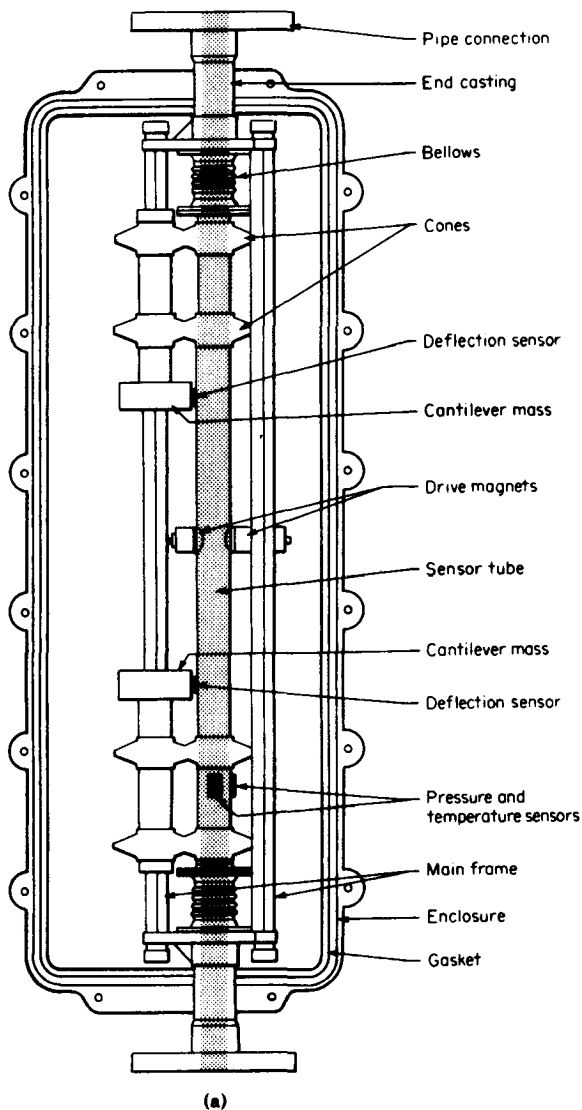
Calculating Liquid Density and Specific Gravity

When measurements are not available, it is sometimes necessary to estimate density. Several generalized equations are useful both for this purpose and for estimating the effect of a temperature change on the flow calculations. These equations usually provide estimates to within only 1 or 2 percent and should be used only in the absence of data.

Goldhammer Equation. The simplest extrapolation equation, based on the fluid's critical temperature T_c , is the early Goldhammer (1910) ratio equation, which is

$$\frac{(\rho_F - \rho_v)_{T_F}}{(\rho_b - \rho_v)_{60^\circ\text{F}}} = \left(\frac{T_c - T_f}{T_c - 519.67} \right)^{1/N} \quad (2.181)$$

where ρ_v is the density of the vapor at T_F and at 60°F (15.6°C). The value of N



(b)

Figure 2.14 Liquid densitometer. (Courtesy Bell & Howell.) (a) Physical construction. (b) Transmitter.

was found by Fishtine (1963) to vary slightly with compound type. Several values are given in Table 2.21.

Under the assumption that the vapor density, ρ_v is negligible at both base conditions and the flowing temperature, Eq. (2.181) reduces to

$$\rho_F = \rho_b \left(\frac{T_c - T_f}{T_c - 519.67} \right)^{1/N} \quad (2.182)$$

TABLE 2.21 Exponent Values for Goldhammer Equation

Compound type	Exponent N
Water and alcohol	4
Hydrocarbons and ethers	3.45
Other organic compounds	3.23
Inorganic compounds	3.03

Substituting Eqs. (2.174) and (2.175) into Eq. (2.182) gives the relationship between flowing and base specific gravity as

$$G_F = G_b \left(\frac{T_c - T_f}{T_c - 519.67} \right)^{1/N} \quad (2.183)$$

Goyal-Doraiswamy Equation. Goyal and Doraiswamy (1966) presented an equation for calculating density based on critical properties and molecular weight. The equation can be rearranged in terms of specific gravity as

$$G_F = \frac{p_c M_w}{T_c} \left(\frac{0.008}{Z_c^{0.773}} - 0.01102 \frac{T_f}{T_c} \right) \quad (2.184)$$

The compressibility factor Z_c is the value at the critical point, which is fluid-dependent; it may range from 0.22 for methyl alcohol to 0.312 for air. Values of p_c , T_c , M_w , and Z_c are given in Table D.1.

When no data is available on the critical compressibility factor, the relationship developed by Edmister (1974) can be used:

$$Z_c = 0.371 - 0.0343 \frac{\log(p_c/14.7)}{T_c/T_b - 1} \quad (2.185)$$

where T_b is the boiling-point temperature in degrees Rankine.

Numerous equations have been suggested for the computation of density using critical properties, based on atomic and structural contributions of the substances. These have an uncertainty of 1 to 5 percent and are used only when laboratory data is unavailable and flow measurement accuracy is not required. The works by Perry and Green (1984), Reid et al. (1987), and Smith and Van Ness (1987) present these equations in detail.

Thermal-Expansion Equation. For moderate temperatures [0 to 100°F (−18 to 38°C)], the density at atmospheric pressure can be approximated by

$$\rho_F = [1 - c(T_F - 60)]^2 \rho_b \approx [1 - 2c(T_F - 60)] \rho_b \quad (2.186)$$

and the specific gravity at flowing conditions by

$$G_F = [1 - c(T_F - 60)]^2 G_b \approx [1 - 2c(T_F - 60)] G_b \quad (2.187)$$

The constant c is given in Table 2.22 for various fluids.

TABLE 2.22 Thermal-Expansion Constant c for Some Fluids

Liquid	c	Liquid	c
Acetic acid	0.000298	Ether	0.00046
Acetone	0.000413	Glycerine	0.0001403
Amyl alcohol	0.000251	HCl, 33.2%	0.0001264
Ethyl alcohol	0.0003111	Mercury	0.0000505
Methyl alcohol	0.0003331	Olive oil	0.0002003
Benzene	0.000344	Potassium chloride, 24.3%	0.0000981
Bromine	0.0003144	Phenol	0.000303
Calcium chloride, 5.8%	0.0000694	Sodium chloride, 20.6%	0.000115
Calcium chloride, 40.9%	0.0001272	Sodium sulfate, 24%	0.000114
Carbon disulfide	0.000383	Sulfuric acid, 10.9%	0.0001075
Carbon tetrachloride	0.0003433	Sulfuric acid, 100%	0.000155
Chloroform	0.0003536	Turpentine	0.0002703

API 2540 Equation. The American Petroleum Institute, in a joint program with the National Bureau of Standards (NIST), developed a density equation based on 463 samples of five different oil products. The results of this work are incorporated into Chap. 11.1, "Volume Correction Factors," of API Standard 2540 (1987).

The density equation is based on the thermal-expansion coefficient of the product at 60°F (15.6°C) base temperature, which is calculated from the base density as

$$\alpha_b = \frac{K_0}{\rho_b^{*2}} + \frac{K_1}{\rho_b^*} \quad (2.188)$$

where the base density ρ_b^* is in kilograms per cubic meter. The empirically derived constants K_0 and K_1 for the five product groups are given in Table 2.23. The density of the product at flowing temperature is then calculated as

$$\rho_F^* = \rho_b^* \exp [-\alpha_b \Delta T_F (1 + 0.8\alpha_b \Delta T_F)] \quad (2.189)$$

where $\Delta T_F = T_F - 60$. The specific gravity at flowing or measured temperature is then

TABLE 2.23 Constants K_0 and K_1 for Five Product Groups

Product group	K_0	K_1
Crude oils and JP4†	341.0957	0.0
Jet fuels, kerosenes, solvents	330.3010	0.0
Gasolines and naphthenes	192.4571	0.2438
Lubricating oils	144.0427	0.1895
Diesel oil, heating oils, fuel oils	103.8720	0.2701

Note: Pentanes and hydrocarbons lower in the hydrocarbon chain are *not* covered by this data.

†API News Release 1987 added JP4.

$$G_F = G_b \exp [-\alpha_b \Delta T_F (1 + 0.8\alpha_b \Delta T_F)] \quad (2.190)$$

In many installations, the specific gravity or density is measured at flowing temperature, and the base specific gravity is required for the calculation of base volumes. Since Eq. (2.190) cannot be solved directly for base density, an iterative solution is required. Newton's method can be applied by rearranging Eq. (2.189) into a zero-root equation (see Sec. A.1) to give the function F as

$$F = \ln \rho_b^* - \ln \rho_F^* - \alpha_b \Delta T_F (1 + 0.8\alpha_b \Delta T_F) \quad (2.191)$$

The derivative of this function is

$$F' = \frac{1}{\rho_b^*} + \alpha_b' \Delta T_F + 1.6\alpha_b \alpha_b' \Delta T_F^2 \quad (2.192)$$

where

$$\alpha_b' = \frac{2K_0}{\rho_b^{*3}} + \frac{K_1}{\rho_b^{*2}} \quad (2.193)$$

The iteration for the base density is then

$$(\rho_b^*)_n = (\rho_b^*)_{n-1} - \frac{F_{n-1}}{F'_{n-1}} \quad (2.194)$$

where F and F' are the solutions of Eqs. (2.191) and (2.192), for an initial estimate of base density use

$$(\rho_b^*)_0 = \rho_F^* [1 + \Delta T_F \exp (0.0106 \times ^\circ\text{API} - 8.05)] \quad (2.195)$$

Example 2.12. For gasoline at a temperature of 80.5°F (26.9°C), the API hydrometer reading is 63.5°API. Using the API 2540 equations, determine (1) its specific gravity G_F at 80.5°F, (2) its specific gravity G_b at 60°F, and (3) its API-degree reading at 60°F (or API_{60/60}).

1. Flowing specific gravity. The flowing specific gravity, uncorrected for pressure, is obtained by correcting the hydrometer for volumetric expansion. From Eq. (2.180),

$$\begin{aligned} G_F &= [1 - (0.00001278)(80.5 - 60) \\ &\quad - (0.0000000062)(80.5 - 60)^2] \frac{141.5}{131.5 + 63.5} \\ &= 0.72545 \end{aligned}$$

2. Specific gravity of 60°F. Now, from Eq. (2.175), the density is

$$\rho_F^* = (0.72545)(999.012) = 724.73 \text{ kg/m}^3$$

The initial estimate of the base density is, by Eq. (2.195),

$$\begin{aligned} (\rho_b^*)_0 &= 724.73 \{1 + (80.5 - 60) \exp [(0.0106)(63.5) - 8.05]\} \\ &= 734.02 \text{ kg/m}^3 \end{aligned}$$

The next step is to calculate α_b and α_b' . From Table 2.23, $K_0 = 192.4571$ and

$K_1 = 0.2438$. Then, by Eq. (2.188),

$$\alpha_b = \frac{192.4571}{(734.02)^2} + \frac{0.2438}{734.02} = 0.0006893$$

and by Eq. (2.193),

$$\alpha'_b = \frac{(2)(192.4571)}{(734.02)^3} + \frac{0.2438}{(734.02)^2} = 0.0000014258$$

Now the function F and its derivative F' are calculated and used to compute a second estimate, as follows: Since $\Delta T_F = 80.5 - 60 = 20.5^\circ\text{F}$, Eq. (2.191) gives

$$\begin{aligned} F_0 &= \ln 734.02 - \ln 724.73 - (0.0006893)(20.5)[(1 + (0.8)(0.0006893)(20.5))] \\ &= -0.001553 \end{aligned}$$

and Eq. (2.192) gives

$$\begin{aligned} F' &= \frac{1}{734.02} + (0.0000014258)(20.5) \\ &\quad + (1.6)(0.0006893)(0.0000014258)(20.5)^2 \\ &= 0.001392 \end{aligned}$$

The second estimate of the base density is then, from Eq. (2.194),

$$(\rho_b)_1 = 734.02 - \frac{-0.001553}{0.001392} = 735.14$$

A second iteration provides an estimate that is different from this value by only 0.0001 percent. The specific gravity at 60°F is then, by Eq. (2.174),

$$G_b = \frac{735.14}{999.012} = 0.7359$$

3. API degrees at 60°F . Rearranging Eq. (2.176) and substituting yield

$$\text{API}_{60/60} = \frac{141.5}{G_b} - 131.5 = \frac{141.5}{0.7359} - 131.5 = 60.78$$

AIChE Liquid Density Equation. The Design Institute for Physical Property Data (AIChE, 1986) presents the constants to be used in a liquid density equation for 1000 fluids. The AIChE liquid density generic equation is

$$\rho_F^* = \frac{aM_w}{b^{1+(1-T_K/c)d}} \quad (2.196)$$

where a , b , c , and d are constants and ρ_F^* is the liquid density (kg/m^3) at the flowing temperature (Kelvin), and at low pressure. Values for these constants, for several fluids, are presented in Table 2.24.

TABLE 2.24 AIChE Liquid Density Equation Constants

	Methane CH ₄	Ethylene C ₂ H ₄	Ethane C ₂ H ₆	Propadiene C ₃ H ₄	Propylene C ₃ H ₆
<i>a</i>	2.8730E+00	2.1433E+00	1.8257E+00	1.5750E+00	1.5245E+00
<i>b</i>	2.8810E-01	3.8061E-01	2.7330E-01	2.6410E-01	2.7517E-01
<i>c</i>	1.9058E+02	2.8236E+02	3.0542E+02	3.9315E+02	3.6476E+02
<i>d</i>	2.7700E-01	2.8571E-01	2.8330E-01	2.7950E-01	3.0246E-01
	Propane C ₃ H ₈	1,2-Butadiene C ₄ H ₆	Isobutene C ₄ H ₈	<i>n</i> -Butane C ₄ H ₁₀	Benzene C ₆ H ₆
<i>a</i>	1.3937E+00	1.2190E+00	1.0182E+00	1.1103E+00	9.7619E-01
<i>b</i>	2.7744E-01	2.6696E-01	2.5685E-01	2.7881E-01	2.6701E-01
<i>c</i>	3.6982E+02	4.4400E+02	4.1790E+02	4.2518E+02	5.6216E+02
<i>d</i>	2.8700E-01	2.8570E-01	2.6700E-01	2.8377E-01	2.7357E-01

Note: E in this table stands for *engineering notation*. For example, E+07 = 10⁷ and E-07 = 10⁻⁷, etc.

Specific Gravity of a Mixture

When two or more liquids are mixed, the specific gravity of the mixture may be estimated by substituting pseudocritical properties into Eq. (2.184). With known mole fractions *y_i*, the pseudocritical pressure, temperature, and compressibility factor are calculated using Kay’s (1936) rule:

$$p_{pc} = \sum y_i p_{ci} = y_1 p_{c1} + y_2 p_{c2} + \cdots \tag{2.197}$$

for pseudocritical pressure,

$$T_{pc} = \sum y_i T_{ci} = y_1 T_{c1} + y_2 T_{c2} + \cdots \tag{2.198}$$

for pseudocritical temperature, and

$$Z_{pc} = \sum y_i Z_{ci} = y_1 Z_{c1} + y_2 Z_{c2} + \cdots \tag{2.199}$$

for the pseudocritical compressibility factor at the critical point. The average molecular weight can be estimated as

$$M_{w,mix} = \sum y_i M_{wi} = y_1 M_{w1} + y_2 M_{w2} + \cdots \tag{2.200}$$

Example 2.13. Using Goyal’s generalized equation, estimate the specific gravity of a 22 percent ethylene and 78 percent isobutane mixture at (a) 60°F (15.6°C) and (b) 105°F (40.6°C).

From Table D.1, the pertinent properties are as follows:

Property	Ethylene	Isobutane
<i>p_c</i>	730.4 psia	529.1 psia
<i>T_c</i>	508.3°R	734.6°R
<i>Z_c</i>	0.276	0.283
<i>M_w</i>	28.04	58.124

The pseudocritical properties of the mixture are then, from Eqs. (2.197) to (2.200),

$$p_{pc} = (0.22)(730.4) + (0.78)(529.1) = 573.4 \text{ psia}$$

$$T_{pc} = (0.22)(508.3) + (0.78)(734.6) = 684.8^\circ\text{R}$$

$$Z_{pc} = (0.22)(0.276) + (0.78)(0.283) = 0.282$$

$$M_{w,\text{mix}} = (0.22)(28.054) + (0.78)(58.124) = 51.509 \text{ lb}_m/(\text{lb}_m \cdot \text{mole})$$

1. *Specific gravity at 60°F (15.6°C).* From Eq. (2.184),

$$\begin{aligned} G_b &= \frac{(573.4)(51.509)}{684.8} \left(\frac{0.008}{(0.282)^{0.773}} - 0.01102 \frac{459.67 + 60}{684.8} \right) \\ &= 0.557 \end{aligned}$$

2. *Specific gravity at 105°F (40.6°C).* From Eq. (2.184),

$$\begin{aligned} G_F &= 43.13 \left(0.02128 - 0.01102 \frac{459.67 + 105}{684.8} \right) \\ &= 0.526 \end{aligned}$$

LIQUID COMPRESSIBILITY

Liquids are not normally considered compressible, and the values for density ρ_F or specific gravity G_F found in tables or measured at atmospheric pressure are seldom increased. There are cases, however, when compressibility must be considered, and a correction made. For example, a liquid becomes more compressible with increases in pressure and temperature; as the critical-temperature isotherm is approached, the liquid acts much like a gas and becomes quite compressible. This can occur for pentanes and lighter hydrocarbons.

The p_vT Relationship

Using water as an example, Fig. 2.15 illustrates the relationship among temperature, pressure, and density in the liquid region. Point A (Fig. 2.15a) lies on the saturated-liquid line, at a reduced temperature of 0.7 and a reduced pressure of 0.045. Increasing the pressure at constant temperature to a reduced pressure of 1.0 [3200 psia (22,000 kPa)] increases the density by approximately 2 percent (Fig. 2.15b). When the reduced pressure is further increased to 4.8 (point B), there is a 6 percent increase in density.

Compressibility is approximately linear over wide pressure ranges, and it can, with reasonable accuracy, be represented by the straight lines shown in Fig. 2.15b. With this figure, the relationship among pressure, temperature, and density is easily visualized. As the critical isotherm is approached ($T_r = 1.0$), the ratio of the density to the density at saturation increases substantially. For example, at a reduced temperature of 0.9 ($T_F = 590^\circ\text{F}$), there is an 18 percent density increase for the 10:1 pressure increase from 1400 to 15,500 psia (9700 to 107,000 kPa).

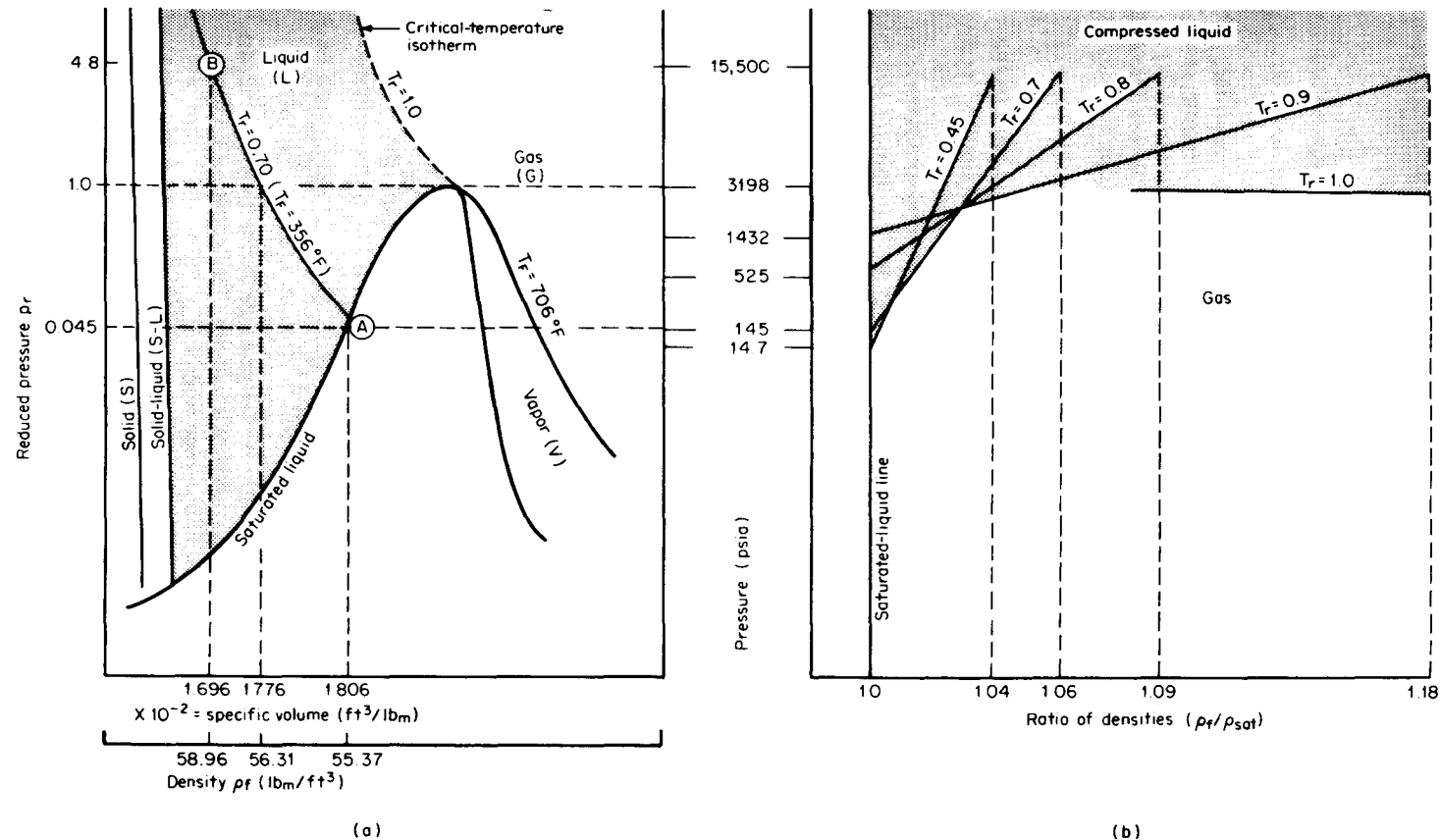


Figure 2.15 Effect of pressure and temperature on the density of water. (a) Pressure versus density. (b) Ratio of densities (not to scale).

Correction Methods

Four methods are suggested for estimating compressibility corrections:

1. Bulk-modulus method
2. Generalized reduced temperature and pressure curves of Lu
3. Generalized liquid compressibility factor
4. Average liquid hydrocarbon compressibility factor

Bulk-Modulus Method. The ratio of the pressure stress to the volumetric strain defines a fluid's bulk modulus of elasticity. The equation relating the pressure change to the volumetric change is then

$$K_{BM} = -\frac{V_0 \Delta P}{\Delta V} \quad (2.201)$$

where K_{BM} is the bulk modulus, and V_0 the initial, uncompressed volume. Unfortunately, the value of K_{BM} is a function of both temperature and pressure, as can be seen from Fig. 2.16a. At constant temperature, the change in the bulk modulus with pressures up to 15,000 lb/in² is well approximated by the tangent bulk-modulus equation (Hayward, 1967):

$$\bar{K}_{BM} = K_{BM0} + b_c p_f \quad (2.202)$$

where K_{BM0} is the zero-pressure intercept. Values for K_{BM0} and b_c are given in Table E.1 for various substances at 68°F (20°C).

By defining the liquid compressibility correction factor as the ratio of the density at line pressure to the density at atmospheric pressure, both at the same temperature, the following equation may be derived from Eq. (2.202):

$$F_p = \frac{\rho_f}{\rho_F} = \frac{G_f}{G_F} = \frac{\bar{K}_{BM}}{\bar{K}_{BM} - p_f} \quad (2.203)$$

where F_p is the *liquid compressibility correction factor*. Over the pressure ranges normally encountered in pipelines [up to 6000 lb/in² (41,400 kPa)], the effect of pressure on the bulk modulus is negligible, and Eq. (2.203) can be reduced to a simpler equation that includes a liquid compressibility factor Z_L :

$$F_p = 1 + \frac{p_f}{1000} Z_L \quad (2.204)$$

The liquid compressibility factor Z_L , derived by equating Eq. (2.203) to Eq. (2.204), is then

$$Z_L = \frac{1000}{K_{BM0} + (b_c - 1)p_f} \quad (2.205)$$

For moderate pressures [up to 2500 lb/in² (17,200 kPa)], the compressibility factor Z_L at the intercept is suggested for general use; this is defined by

$$Z_L = \frac{1000}{K_{BMO}} \quad (2.206)$$

Values of Z_L are given in Table E.1 for some fluids.

Lu Diagram. For estimating liquid density changes with pressure and temperature, when the critical pressure and temperature are known, the generalized curves of Lu (1959) can be used. These curves are presented in Fig. E.23 and illustrated in Fig. 2.16b.

If a density is known at a given temperature and pressure, the density at a second pressure and temperature can be calculated as

$$\rho_{f2} = \frac{LC_2}{LC_1} \rho_{f1} \quad (2.207)$$

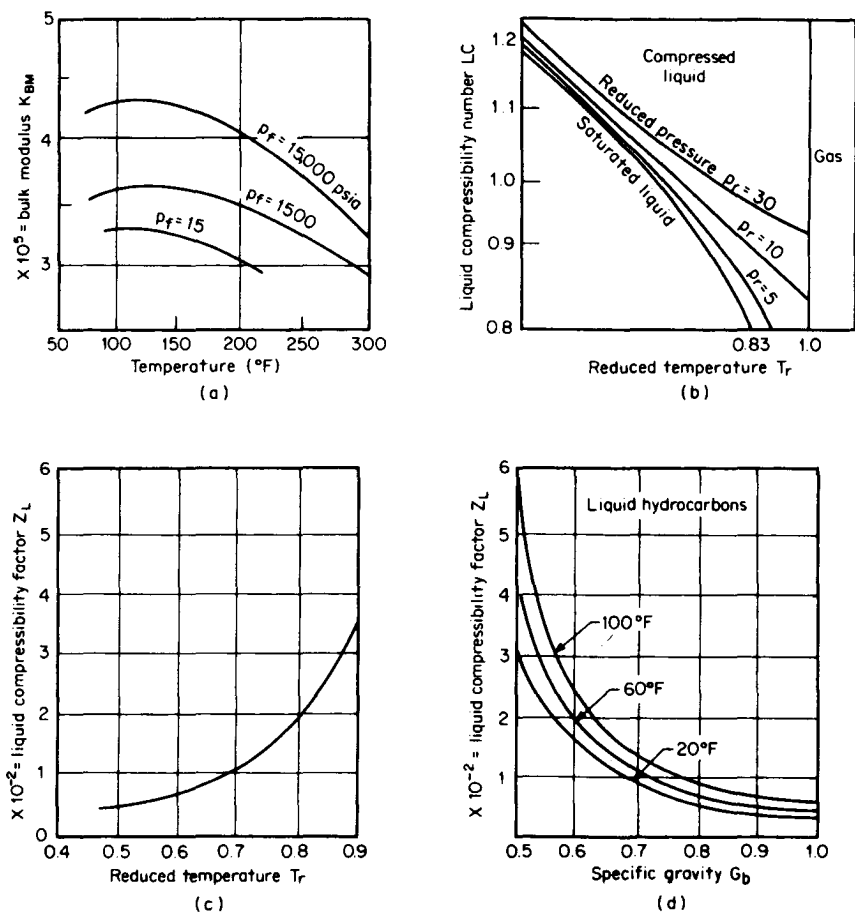


Figure 2.16 Liquid compressibility curves. (a) Bulk modulus for water (see Table E.1). (b) Lu's generalized diagram (see Fig. E.23). (c) Generalized liquid compressibility factor (see Fig. E.24). (d) Average liquid-hydrocarbon compressibility factor (see Fig. E.22).

where LC_2 and LC_1 are read from the appropriate curve intersections for the reduced temperature and pressure coordinates.

Generalized Liquid Compressibility Factor. The Lu generalized curves can be used to construct a generalized liquid compressibility factor curve. Under the assumptions that (1) the bulk modulus changes slightly with temperature up to the saturated-liquid line (Fig. 2.16b), and (2) the compressibility factor Z_L is independent of pressures up to 10,000 lb/in² (69,000 kPa), the liquid compressibility factor curve illustrated in Fig. 2.16c and presented in Fig. E.24 can be drawn for reduced temperatures up to 0.9. Equation (2.204) can then be rewritten in terms of the reduced pressure as

$$F_p = 1 + Z_L p_r \quad (2.208)$$

where Z_L is determined from Fig. E.24 or calculated with the series expansion formula

$$Z_L = 0.269T_r - 0.5163T_r^2 + 0.3521T_r^3 - 0.0461 \quad (2.209)$$

Liquid-Hydrocarbon Compressibility Curves. Compressibility test work on various liquid hydrocarbons has shown that generalized curves can be constructed (API 1101, 1960), based on base specific gravity G_b and temperature T_f . Illustrated in Fig. 2.16d and presented in detail in Fig. E.22 is the Z_L curve for liquid hydrocarbons. The value of Z_L is an average, and test data on the fluid should be obtained if accuracy is important.

API Chapter 11.1 Equations. The American Petroleum Institute (API), in its manual of petroleum measurement standards Chaps. 11.2.1 and 11.2.2 (API, 1984, 1987), gives equations for the density of liquid hydrocarbons (excluding lubricating oils) referenced to the density at the saturation pressure p_{sat} (bubble point pressure). The bubble point pressure may be obtained by test or estimated by using Eq. (2.110). In many applications the bubble point pressure ranges from 0 to 50 psia, and the results are not significantly affected (<0.1 percent) by assuming a zero value. Assuming the liquid density at the saturation pressure, corresponding to the flowing temperature, is equal to the density at atmospheric pressure, the liquid compressibility correction factor may be written as

$$F_p = \frac{\rho_f}{\rho_F} \approx \frac{\rho_f}{\rho_{\text{sat}}} = \frac{1}{1 - (p_f - p_{\text{sat}})Z_L} \approx \frac{1}{1 - Z_L p_f} \quad (2.210)$$

When the base specific gravity G_b is in the range of 0.35 to 0.637, the compressibility factor Z_L is calculated by

$$Z_L = \frac{1}{K_{BMO} + b_c(p_f - p_{\text{sat}})} \approx \frac{1}{K_{BMO} + b_c p_f} \quad (2.211)$$

Assuming that the bulk modulus K_{BMO} is temperature- but not pressure-dependent, the bulk modulus and the pressure slope factor of Eq. (2.205) are calculated by

$$K_{BMO} = A_1 + (A_2 + A_3 T_f)G_b + (A_4 T_f + A_5 T_f^2 + A_6 T_f^3)G_b^2 \\ + (A_7 T_f^2 + A_8 T_f^3)G_b^4 + A_9 T_f^6 G_b^6 + A_{10} T_f + A_{11} T_f^2 \quad (2.212)$$

TABLE 2.25 API Liquid Hydrocarbon
Compressibility Constants

Range	
$0.35 \leq G_b \leq 0.637$	
$0 < p_f \leq 2185 \text{ psia}$	
$-50 < T_f \leq 140^\circ\text{F}$	
$A_1 = -9.5495939\text{E}+04$	$A_9 = 2.8324481\text{E}-02$
$A_2 = 9.1311491\text{E}+05$	$A_{10} = 7.9552900\text{E}+02$
$A_3 = -5.1101580\text{E}+03$	$A_{11} = -2.1465891\text{E}-01$
$A_4 = 3.6458380\text{E}+03$	$A_{12} = 8.8384000\text{E}+01$
$A_5 = 1.5774390\text{E}+00$	$A_{13} = -2.0401600\text{E}+01$
$A_6 = 7.2900662\text{E}-03$	$A_{14} = 2.2112678\text{E}-01$
$A_7 = -1.0502139\text{E}+00$	$A_{15} = -6.0357667\text{E}-05$
$A_8 = -2.7769343\text{E}-02$	

Note: Constants to be double-precision.

$$b_c = A_{12}G_b + (A_{13} + A_{14}T_f)G_b^2 + A_{15}T_f^2 \quad (2.213)$$

Constants A_1 to A_{15} are given in Table 2.25.

It is important to note that the constants A_i are based on a conversion of degrees Fahrenheit to degrees Rankine by $T_f = ^\circ\text{F} + 459.7$ and not $T_f = ^\circ\text{F} + 459.67$. The equation applies for absolute temperatures T_f less than 0.96 of the critical temperature T_c , which is defined by

$$T_f \leq 0.96T_c = 0.96(621.418 - 22.686G_b + 1737.86G_b^2) \quad (2.214)$$

For base specific gravities in the range of 0.639 to 1.076, Z_L is defined by

$$Z_L = 10^{-5} \exp(-1.9947 + 0.00013427T_f + 0.79549G_b^{-2} + 0.0023306T_fG_b^{-2}) \quad (2.215)$$

where T_f is in degrees Fahrenheit.

COSTALD Equation

Numerous equations have been suggested for the estimation of the densities of pure compounds and mixtures. The COSTALD equation (corresponding state liquid density) gives improved accuracy (Hankinson and Thompson, 1979) for nonpolar substances over many of the previous methods (Yen and Wood, 1966; Rackett, 1970). The equation is widely used to predict the density of liquefied natural gas (LNG) and liquefied petroleum gas (LPG). The Hankinson and Thompson COSTALD equation model calculates the molar saturation volume [$\text{m}^3/(\text{kg}\cdot\text{mol})$] based on a three-parameter correlation. The COSTALD equation is

$$v_{\text{mol,sat}} = (1 - \omega v_{rb})v_{r0}v_{c,\text{mol}} \quad (2.216)$$

where v_{rb} is the spherical molecular function, v_{r0} is the deviation function, ω is the

acentric factor, and v_c is the critical molar volume. v_{r0} and $v_{r\delta}$ in Eq. (2.216) are defined by

$$v_{r0} = 1 + a(1 - T_r)^{1/3} + b(1 - T_r)^{2/3} + c(1 - T_r) + d(1 - T_r)^{4/3}$$

$$v_{r\delta} = \frac{e + fT_r + gT_r^2 + hT_r^3}{T_r - 1.00001} \quad (2.217)$$

where T_r is the reduced temperature. The values of the acentric factor ω , the critical volume $v_{c,\text{mol}}$, and the constants a, b, c, d, \dots are given in Table 2.26.

TABLE 2.26 COSTALD Equation and Constants for Some Fluids

$a = -1.52816$	$b = 1.43907$	$c = -0.81446$	$d = 0.190454$		
$e = -0.296123$	$f = 0.386914$	$g = -0.0427258$	$h = -0.0480645$		
$a_1 = -9.070217$	$b_1 = 62.45326$	$d_1 = 135.1102$	$f_1 = 4.79594$		
$g_1 = 0.250047$	$h_1 = 1.14188$	$j_1 = 0.861488$	$k_1 = 0.0344483$		
$v_{c,\text{mol}},$ $\text{m}^3/\text{kg} \cdot \text{mol}$	ω		$v_{c,\text{mol}},$ $\text{m}^3/\text{kg} \cdot \text{mol}$	ω	
Paraffins					
Methane	0.09939	0.0074	<i>n</i> -Nonane	0.5529	0.4478
Ethane	0.1458	0.0983	<i>n</i> -Decane	0.6192	0.4916
Propane	0.2001	0.1532	<i>n</i> -Undecane	0.6865	0.5422
<i>n</i> -Butane	0.2544	0.2008	<i>n</i> -Dodecane	0.7558	0.5807
Isobutane	0.2568	0.1825	<i>n</i> -Tridecane	0.8317	0.6340
Isopentane	0.3096	0.2400	Dodecane	1.5839	1.0561
Neopentane	0.3126	0.1975	Tricosane	1.6507	1.0477
<i>n</i> -Hexane	0.3682	0.3007	Octacosane	1.8972	0.8455
Olefins					
Ethylene	0.1310	0.0882	Pentene-1	0.2951	0.2824
Propylene	0.1829	0.1455	Hexene-1	0.3509	0.2850
Butene-1	0.2377	0.1921	Heptene-1	0.4113	0.2611
Isobutene	0.2369	0.1959	Octene-1	0.4710	0.3876
Aromatics					
Benzene	0.2564	0.2137	<i>p</i> -Xylene	0.3740	0.3216
Toluene	0.3137	0.2651	Styrene	0.3482	0.2420
<i>o</i> -Xylene	0.3673	0.3118	Cumene	0.4271	0.3277
<i>m</i> -Xylene	0.3740	0.3216	Heavy	2.2323	0.7619
Mercaptans					
Methyl	0.1508	0.1567	<i>n</i> -Butyl	0.3135	0.2781
Ethyl	0.2023	0.1915	<i>sec</i> -Butyl	0.3139	0.2494
<i>n</i> -Propyl	0.2572	0.2380	Isobutyl	0.3159	0.2496
Isopropyl	0.2606	0.2105	<i>tert</i> -Butyl	0.3162	0.2831

The compressed liquid density (kg/m^3), based on the Tait (1888) compressed liquid model, is derived as

$$\rho_f^* = \left\{ v_{\text{mol,sat}} \left[1 - (j_1 + k_1 \omega) \ln \left(\frac{B + p_f}{B + p_{\text{sat}}} \right) \right] \right\}^{-1} M_w \quad (2.218)$$

where B is determined by

$$B = [-1 + a_1(1 - T_r)^{1/3} + b_1(1 - T_r)^{2/3} + d_1(1 - T_r) + \exp(f_1 + g_1 \omega + h_1 \omega^2)(1 - T_r)^{4/3}] p_c \quad (2.219)$$

Values for a_1, b_1, c_1, \dots are presented in Table 2.26.

The saturation pressure p_{sat} in Eq. (2.218) may be obtained from a bubble point calculation or estimated from a generalized vapor pressure relationship. The Han-kinson et al. (1975) generalized relationship for the saturation pressure is

$$p_{\text{sat}} = 10^{p_{\text{rsat},0} + \omega p_{\text{rsat},1}} p_c \quad (2.220)$$

The two reduced saturation parameters in Eq. (2.220) are, for $p_{\text{rsat},0}$,

$$p_{\text{rsat},0} = 5.8031817 \log(T_r) + 0.07608141 \phi_{\text{sat}} \quad (2.221)$$

and for $p_{\text{rsat},1}$

$$p_{\text{rsat},1} = 4.86601[\log(T_r) + 0.03721754 \phi_{\text{sat}}] \quad (2.222)$$

where

$$\phi_{\text{sat}} = 35 - \frac{36}{T_r} - 96.736 \log(T_r) + T_r^6 \quad (2.223)$$

The COSTALD equation mixture rule for the pseudocritical mixture's temperature is

$$T_{c,\text{mix}} = \frac{\sum_i \sum_j x_i x_j v_{cij} T_{cij}}{v_{c,\text{mix}}} \quad (2.224)$$

The mixture's characteristic volume is calculated by

$$v_{c,\text{mix}} = 0.25[\sum x_i v_{ci} + 3(\sum x_i v_{ci}^{2/3})(\sum x_i v_{ci}^{1/3})] \quad (2.225)$$

and, for the characteristic volume i, j components, by

$$v_{cij} T_{cij} = (v_{ci} T_{ci} v_{cj} T_{cj})^{1/2} \quad (2.226)$$

The mixture's acentric factor is

$$\omega_{\text{mix}} = \sum x_i \omega_i \quad (2.227)$$

Example 2.14. Determine the density of water at 1500 and 15,000 psia (10,342 and 103,421 kPa) at 300°F (149°C) using (1) the bulk-modulus method, (2) the Lu diagram, and (3) the liquid compressibility factor derived from the Lu diagram.

From the steam tables, the following data is available:

- Saturated liquid: $\rho_f = 57.31 \text{ lb}_m/\text{ft}^3$ (300°F, 67 psia)
 - Compressed liquid: $\rho_f = 57.64 \text{ lb}_m/\text{ft}^3$ (300°F, 1500 psia)
 - Compressed liquid: $\rho_f = 60.24 \text{ lb}_m/\text{ft}^3$ (300°F, 15,000 psia)
1. *Bulk-modulus method.* From Table E.1, $Z_L = 0.00262$ at 68°F and 14.7 psia. At 1500 psia, the liquid compressibility factor is, from Eq. (2.204),

$$F_p = 1 + 0.00262 \frac{1500 - 67}{1000} = 1.0038$$

The flowing density at 1500 psia is then, by Eq. (2.203),

$$\rho_f = F_p \rho_F = (1.0038)(57.31) = 57.53 \text{ lb}_m/\text{ft}^3$$

which differs from the steam-table value by -0.2 percent.

At 15,000 psia the liquid compressibility factor is, from Eq. (2.204),

$$F_p = 1 + 0.00262 \frac{15,000 - 67}{1000} = 1.0391$$

The flowing density is, by Eq. (2.203),

$$\rho_f = F_p \rho_F = (1.0391)(57.31) = 59.55 \text{ lb}_m/\text{ft}^3$$

which differs from the steam-table value by -1.1 percent.

2. *Lu generalized diagram.* At 1500 psia the reduced pressure is, from Eq. (2.1),

$$p_r = \frac{1500}{3198} = 0.469$$

and the reduced temperature is, from Eq. (2.2),

$$T_r = \frac{459.67 + 300}{1165.1} = 0.652$$

In the Lu diagram (Fig. E.23), from the saturated-liquid line the ordinate is read as $LC_1 = 0.960$, and for the reduced properties $p_r = 0.469$ and $T_r = 0.652$, $LC_2 = 0.964$. The density at 1500 psia is now calculated from Eq. (2.207) as

$$\rho_{f2} = \rho_{f1} \frac{LC_2}{LC_1} = 57.31 \frac{0.964}{0.960} = 57.55 \text{ lb}_m/\text{ft}^3$$

which differs from the steam-table value by -0.2 percent.

At 15,000 psia the reduced pressure is

$$p_r = \frac{15,000}{3198} = 4.690$$

and the reduced temperature is

$$T_r = \frac{459.67 + 300}{1165.1} = 0.652$$

At these values, the Lu diagram gives

$$LC_1 = 0.960 \quad LC_2 = 0.998$$

and the density at 15,000 psia is, by Eq. (2.207),

$$\rho_{f2} = \rho_{f1} \frac{LC_2}{LC_1} = 57.31 \frac{0.998}{0.960} = 59.58 \text{ lb}_m/\text{ft}^3$$

which differs from the steam-table value by -1.1 percent.

3. *Liquid compressibility factor.* At 1500 psia, by Eqs. (2.209), (2.208), and (2.203),

$$Z_L = (0.269)(0.652) - (0.5163)(0.652)^2 \\ + (0.3521)(0.652)^3 - 0.0461 = 0.0074$$

$$F_p = 1 + (0.0074)(0.469) = 1.0035$$

$$\rho_f = F_p \rho_F = (1.0035)(57.31) = 57.51 \text{ lb}_m/\text{ft}^3$$

which shows a bias error of -0.2 percent.

At 15,000 psia,

$$F_p = 1 + (0.0074)(4.690) = 1.035$$

$$\rho_f = (1.035)(57.31) = 59.30 \text{ lb}_m/\text{ft}^3$$

for a bias error of -1.3 percent.

Example 2.15. Use the Goldhammer equation and the generalized liquid compressibility factor to estimate the density of water at 500 psia (3450 kPa) and 100°F (38°C). *Note:* The density of water of 500 psia (3450 kPa) and 100°F (38°C) is $62.07 \text{ lb}_m/\text{ft}^3$.

According to Eq. (2.182), the density at 100°F , with $T_c = 1165.1$ from Table D.1 and $N = 4$ from Table 2.6, is

$$\rho_F = 62.366 \left[\frac{1165.1 - (459.67 + 100)}{1165.1 - 519.67} \right]^{1/4} = 61.38 \text{ lb}_m/\text{ft}^3$$

The reduced temperature at 100°F is, from Eq. (2.2),

$$T_r = \frac{459.67 + 100}{1165.1} = 0.480$$

The liquid compressibility factor is then, by Eq. (2.209),

$$Z_L = (0.269)(0.480) - (0.5163)(0.480)^2 + (0.3521)(0.480)^3 - 0.0461 = 0.003$$

The reduced pressure at 500 psia, with $p_c = 3198$, is from Eq. (2.1),

$$p_r = \frac{500}{3198} = 0.156$$

The liquid compressibility factor is then, from Eq. (2.208),

$$F_p = 1 + Z_L p_r = 1 + (0.003)(0.156) = 1.0005$$

and Eq. (2.203) gives the density at flowing conditions as

$$\rho_f = F_p \rho_F = (1.0005)(61.38) = 61.41 \text{ lb}_m/\text{ft}^3$$

which shows a bias error of -1.1 percent.

Example 2.16. The gasoline of Example 2.12 is flowing in a 2-in (50-mm) line at 1000 psia (6895 kPa). Estimate the flowing density of the gasoline using (1) the liquid-hydrocarbon-compressibility curves and (2) the API chapter 12.2.1 equation.

1. Liquid-hydrocarbon-compressibility-curves. From Example 2.12:

$$\rho_f^* = 724.73 \text{ kg/m}^3$$

From App. E, Fig. E.22, the average liquid hydrocarbon compressibility is $Z_L = 0.0088$. The liquid compressibility correction factor is then, by Eq. (2.204),

$$F_p = 1 + Z_L \frac{p_f}{1000} = 1 + 0.0088 \frac{1000}{1000} = 1.0088$$

The flowing density is then, from Eq. (2.203),

$$\rho_f^* = F_p \rho_f^* = (1.0088)(724.73) = 731.12 \text{ kg/m}^3$$

2. API Chap. 11.2.1 equation. From Example 2.12, the base specific gravity is $G_b = 0.7359$. The API liquid compressibility factor, from Eq. (2.215), is

$$Z_L = (10^{-5}) \exp [-1.9947 + (0.00013427)(80.5) + (0.79549)(0.7359)^{-2} \\ + (0.0023306)(80.5)(0.7359)^{-2}] = 0.000008116$$

The liquid compressibility correction is then, from Eq. (2.203),

$$F_p = \frac{\rho_f}{\rho_F} = \frac{1}{1 - (0.00000811)(1000)} = 1.0082$$

The flowing density is then

$$\rho_f^* = F_p \rho_F^* = (1.0082)(724.73) = 730.67 \text{ kg/m}^3$$

VISCOSITY

Viscosity is the measure of a fluid's internal, or intermolecular, resistance to shear stress. For pipe flows this property causes a velocity profile which can affect flow-meter performance.

Absolute Viscosity

Figure 2.17a shows two parallel plates of equal area, separated by a small distance, with fluid between them. A constant force applied to the top plate causes both plate and fluid to move at constant velocity. The fluid in contact with the bottom fixed plate has no velocity. The relationship among applied force, plate area, and linear displacement is given by

$$F_{\text{plate}} = (\mu_f)_e A_{\text{plate}} \frac{\Delta V_{\text{plate}}}{\Delta Y} \quad (2.228)$$

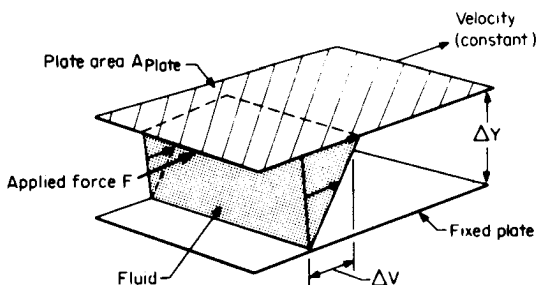
The constant $(\mu_f)_e$ is the fluid's *absolute viscosity*, which depends primarily on interactions among fluid molecules. For liquids such as molasses, its value can be quite high, and for gases very low.

The applied force divided by the plate area is the shear stress S_s . For newtonian fluids the relationship between shear stress and deformation rate is linear; the ratio of the two, the absolute viscosity, is constant. There are, however, fluids that are nonnewtonian, and their viscosities are not constant, as illustrated in Fig. 2.17b. These fluids are covered in more detail in Chap. 5.

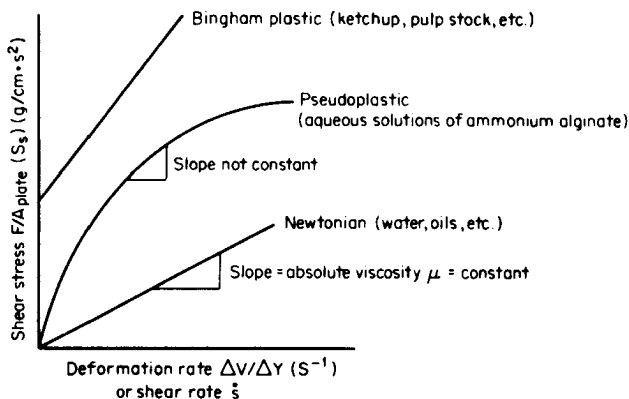
Absolute-viscosity units are derived from Eq. (2.228). In the English engineering system, two sets of units are often found in tables. One is based on the pound-mass, and the other on the pound-force. For clarity, these will be denoted by the subscripts m and f . The absolute viscosity in force units is defined as

$$(\mu_f)_e = \frac{F_{\text{plate}}}{A_{\text{plate}}} \frac{\Delta Y}{\Delta V_{\text{plate}}} = \frac{\text{lb}_f \cdot \text{s}}{\text{ft}^2} \quad (2.229)$$

and in mass units as



(a)



(b)

Figure 2.17 Fluid viscosity. (a) Newtonian fluid between parallel plates. (b) Newtonian and nonnewtonian fluids: shear stress versus shear strain rate (time-independent).

$$(\mu_m)_e = \frac{\text{lb}_m}{\text{ft} \cdot \text{s}} \quad (2.230)$$

The dimensional gravitational constant g_c converts force units to mass units:

$$(\mu_m)_e = g_c(\mu_f)_e = \frac{\text{lb}_m}{\text{lb}_f} \frac{\text{ft}}{\text{s}^2} \frac{\text{lb}_f \cdot \text{s}}{\text{ft}^2} = \frac{\text{lb}_m}{\text{ft} \cdot \text{s}} \quad (2.231)$$

In the SI system the absolute viscosity unit is the pascal second (Pa·s), which is defined dimensionally by

$$\mu_{\text{Pa} \cdot \text{s}} = \frac{F_{\text{plate}}^*}{A_{\text{plate}}^*} \frac{\Delta Y^*}{\Delta V_{\text{plate}}^*} = \frac{\text{N} \cdot \text{m}}{\text{m}^2(\text{m}/\text{s})} = \frac{\text{N} \cdot \text{s}}{\text{m}^2} = \text{Pa} \cdot \text{s} \quad (2.232)$$

The more commonly used viscosity unit is the poise (or centipoise), which has the units

$$\mu_P = \frac{g}{\text{cm} \cdot \text{s}} \quad (2.233)$$

Equations (2.232) and (2.233) indicate that no gravity correction is required in the SI system between force and mass absolute-viscosity units. While some texts continue to use both English viscosity units, the poise (or centipoise) is now widely used and eventually should replace the two English units.

Kinematic Viscosity

Mass is eliminated from the viscosity unit if the absolute viscosity is divided by the fluid density. The result is referred to as the *kinematic viscosity*. In the English engineering system, the absolute viscosity $(\mu_m)_e$ should be divided by the density in pounds-mass per cubic foot. The viscosity in poises divided by the density in grams per cubic centimeter gives the kinematic viscosity in *stokes*. It should be noted that the density in grams per cubic centimeter is *approximately* the fluid's specific gravity, and, for this reason, some conversion equations appear with specific gravity as the divisor.

The kinematic-viscosity unit in the English engineering system is

$$\nu_e = \frac{(\mu_m)_e}{\rho_f} = \frac{32.174(\mu_f)_e}{\rho_f} = \frac{\text{ft}^2}{\text{s}} \quad (2.234)$$

The SI kinematic-viscosity unit (stokes) is

$$\nu_{\text{St}} = \frac{1000\mu_P}{\rho_f^*} = \frac{1.00099\mu_P}{F_P G_F} \approx \frac{\mu_P}{G_F} = \frac{\text{cm}^2}{\text{s}} \quad (2.235)$$

Example 2.17. Steam tables give the absolute viscosity of steam at 800°F (427°C) and 1500 psia (10,340 kPa) in the English force system as $5.37 \times 10^{-7} \text{ lb}_f \cdot \text{s}/\text{ft}^2$. Convert this viscosity unit to centipoises and centistokes using the basic conversion equations.

1. **Viscosity in centipoises.** The viscosity in mass units is first calculated with Eq. (2.231) as

$$(\mu_m)_e = g_c(\mu_f)_e = (32.174)(5.37 \times 10^{-7}) = 1.72 \times 10^{-5} \text{ lb}_m/(\text{ft} \cdot \text{s})$$

From Table C.1, the conversion to the SI system is

$$\text{lb}_m \times 453.6 = g \quad \text{and} \quad \text{ft} \times 30.48 = \text{cm}$$

The viscosity in poises is then calculated by Eq. (2.233) as

$$\mu_P = 1.72 \times 10^{-5} \frac{453.6}{30.48} = 2.57 \times 10^{-4} \text{ g}/(\text{cm} \cdot \text{s})$$

and in centipoises it is

$$\mu_{cP} = 100\mu_P = 2.57 \times 10^{-2} = 0.0257 \text{ cP}$$

2. *Viscosity in centistokes.* The density from Table G.1 is $\rho_f = 2.299 \text{ lb}_m/\text{ft}^3$. From Table C.1, the conversion to SI units gives $\rho_f^* = (2.299)(16.02) = 36.9 \text{ kg}/\text{m}^3$. the kinematic viscosity in stokes is then, from Eq. (2.235),

$$\nu_{St} = \frac{1000\mu_P}{\rho_f^*} = \frac{(1000)(2.57 \times 10^{-4})}{36.9} = 0.00696 \text{ St}$$

and the viscosity in centistokes is

$$\nu_{cSt} = 100\nu_{St} = 0.696 \text{ cSt}$$

Liquid Viscosity

The estimation of liquid viscosity, except for simple cases, is based on empirical equations. Viscosity data at two points is necessary to predict the effects of both pressure and temperature. An increase in temperature reduces the viscosity while an increase in pressure increases the viscosity, but to a much lesser degree. Petroleum products and liquids with complex molecular structures, being relatively more compressible than other liquids, are more sensitive to pressure.

Pressure Correction for Liquid Hydrocarbons. In most flow applications, the effect of pressure on viscosity is not significant. The small change in viscosity affects only the Reynolds number, which, for most normal flow rates, has a slight effect on derived flow coefficients. For water, the viscosity at 5000 lb/in² (34,500 kPa) is 1.14 times the viscosity measured at atmospheric pressure, while for amyl alcohol it is 1.35 times higher.

For liquid hydrocarbons with $\mu_{cP} > 1.2$, the viscosity at high pressure can be estimated with Kouzel's (1965) relationship:

$$F_{\mu P} = \frac{(\mu_{cP})_P}{(\mu_{cP})_a} = 10^{(P_f/1000)[0.0239 + 0.01638(\mu_{cP})_a^{0.278}]} \quad (2.236)$$

where the absolute viscosity is in centipoises, and the subscripts P and a refer to the higher-pressure and atmospheric-pressure values, respectively. Figure 2.18a illustrates the pressure correction; a more detailed curve is presented in Fig. F.27.

Temperature Correction from Two Known Values. The absolute viscosities of liquids decrease with temperature, with the larger changes occurring for the more complex-structured fluids. Viscosity values are normally read from tables, graphs,

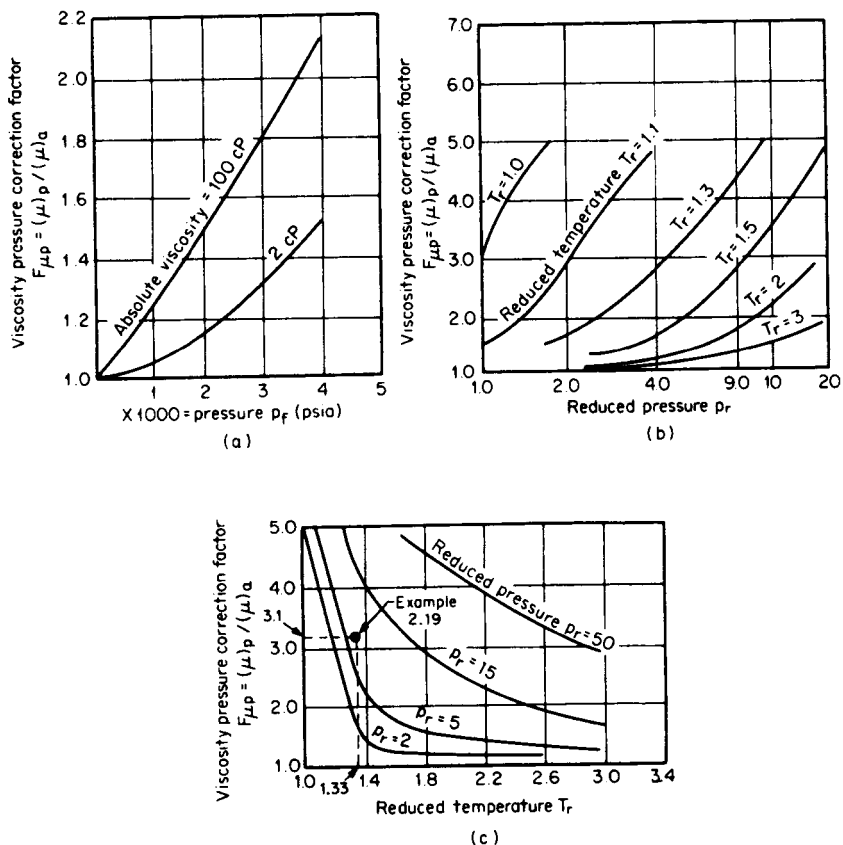


Figure 2.18 Effects of pressure on liquid-hydrocarbon viscosity and on gas viscosity. (a) Pressure correction for liquid hydrocarbons (see Fig. F.27). (b) Generalized curves for pressure corrections for gas viscosity (see Fig. H.17). (c) Cross-plot of part b for interpolation (see Fig. H.18).

or nomographs that relate viscosity to temperature, based on prior measurements for the more common fluids. When necessary, viscosity measurements of newtonian fluids are easily made.

When two viscosity values are known from either measurements or tables, Andrade's (1930) equation is commonly used to predict intermediate viscosities or for data extrapolation. Andrade's equation is

$$\mu = A_L \exp \frac{B_L}{T_R} \quad (2.237)$$

The constants A_L and B_L are calculated from two known viscosity values. With the subscripts 1 and 2 referring to the known values, the constants A_L and B_L can be calculated as

TABLE 2.27 AIChE Liquid Viscosity Equation Constants

	Methane CH ₄	Ethylene C ₂ H ₄	Ethane C ₂ H ₆	Propadiene C ₃ H ₄	Propylene C ₃ H ₆
<i>a</i>	-1.7220E+00	-2.4020E+00	-7.7480E+00	8.4279E+00	-4.4830E+01
<i>b</i>	8.4500E+01	1.9450E+02	3.0350E+02	-1.6383E+02	1.3370E+03
<i>c</i>	-1.7095E+00	-1.4576E+00	-5.0050E-01	-2.9373E+00	5.6710E+00
<i>d</i>	-9.0200E-24	0.0	-1.0000E-25	0.0	0.0
<i>e</i>	1.0000E+01	0.0	1.0000E+01	0.0	0.0

	Propane C ₃ H ₈	1,2-Butadiene C ₃ H ₆	Isobutene C ₄ H ₈	<i>n</i> -Butane C ₄ H ₁₀	Benzene C ₆ H ₆
<i>a</i>	-1.2832E+01	-9.0974E+00	-4.8766E+01	7.5000E-01	6.7640E+00
<i>b</i>	5.6634E+02	5.1905E+02	1.9070E+03	2.1870E+02	3.3640E+02
<i>c</i>	3.4688E-01	-2.1310E-01	5.9030E+00	-1.7882E+00	-2.6870E+00
<i>d</i>	-3.5111E-26	-9.8000E-28	-9.2000E-27	-4.0000E-27	0.0
<i>e</i>	1.0000E+01	1.0000E+01	1.0000E+01	1.0000E+01	0.0

Note: E in this table stands for *engineering notation*. For example, E+07 = 10⁷ and E-07 = 10⁻⁷, etc.

$$\mathbf{B}_L = \frac{T_{R1} T_{R2} \ln (\mu_1 / \mu_2)}{T_{R2} - T_{R1}} \quad (2.238)$$

and

$$\mathbf{A}_L = \frac{\mu_1}{\exp (\mathbf{B}_L / T_{R1})} \quad (2.239)$$

In these equations, the absolute viscosity can be in either the English or SI system of units, and the absolute temperature in degrees Rankine or kelvins. Over reasonable temperature limits, the kinematic viscosity ν_{cst} can be used, provided the change in specific gravity with temperature is small.

Work by Doolittle (1951) and others has shown that the constant \mathbf{A}_L is a function of the free molar volume of the fluid and the compressed molar volume. The constant \mathbf{B}_L has been related to the diffusional motion activation-energy level and the universal gas constant. These relationships are sometimes used to predict the combined effect of temperature and pressure. However, in most practical flow measurements, the additional complexity and required data do not warrant adjustment for the combined effect. Rather, a separate adjustment for pressure and then a temperature correction are suggested.

AIChE Liquid Viscosity Equation. The Design Institute for Physical Property Data (AIChE, 1986) data book generic equation for liquid viscosity is

$$\mu_{\text{Pa}\cdot\text{s}} = \exp \left(a + \frac{b}{T_K} + c \ln T_K + d T_K^e \right) \quad (2.240)$$

where $\mu_{\text{Pa}\cdot\text{s}}$ is the viscosity in pascal-seconds (Pa·s). Values for the constants *a*, *b*, *c*, *d*, and *e* for some fluids are presented in Table 2.27.

Temperature Correction from a Single Value. When only a single viscosity value is available, the best approximation of the viscosity at other temperatures is the curve illustrated in Fig. 2.19 and given in Fig. F.26. To use the curve, one locates the known viscosity value, in centipoises, on the vertical axis and then moves along the temperature scale to the *difference* between the desired temperature and the temperature for which the viscosity is known.

Mixtures. If no viscosity data is available for a mixture, Reid et al. (1987) recommend that the viscosity be calculated on the basis of mole fractions, as

$$\mu_{cP, \text{mix}} = \exp [\sum y_i \ln (\mu_{cP})_i] \quad (2.241)$$

where the $(\mu_{cP})_i$ are the viscosity values of the *pure* components at the mixture temperature. The bias errors to be expected with Eq. (2.241) may vary widely for chemically similar substances, but they are usually below 15 percent (Reid et al., 1987).

Example 2.18. The viscosity of an oil is measured as 20 cP at 50°F (10°C), and 2 cP at 198°F (92°C). Estimate the viscosity at 140°F (60°C), using (1) Andrade's equation and (2) the generalized curve given in Fig. 2.19, and (3) estimate the viscosity at 500 psia (3448 kPa) and 140°F (60°C).

1. Andrade's equation. Andrade's equation (2.237), written for centipoises, is

$$\mu_{cP} = A_L \exp \frac{B_L}{T_R}$$

The coefficients B_L and A_L are calculated from Eqs. (2.238) and (2.239) with $T_{R1} = 509.67$ and $T_{R2} = 657.67$:

$$B_L = \frac{(509.67)(657.67) \ln (20/2)}{657.67 - 509.67} = 5215$$

$$A_L = \frac{20}{\exp (5215/509.67)} = 0.00072$$

The viscosity at 140°F (599.67°R) is then, by Eq. (2.237),

$$\mu_{cP} = 0.00072 \exp \frac{5215}{T_R} = 0.00072 \exp \frac{5215}{599.67} = 4.31 \text{ cP}$$

2. Viscosity from generalized curve. The change in temperature is $\Delta^\circ\text{C} = 60 - 10 = 50$. For this change in temperature, the viscosity is read on Fig. 2.19 as $\mu_{cP} = 4.2$.

3. Viscosity at 500 psia and 140°F. The correction for pressure is given by Eq. (2.236):

$$\begin{aligned} F_{\mu p} &= 10^{(pf/1000)[0.0239+0.01638(\mu_{cP})_0^{0.278}]} \\ &= 10^{(500/1000)[0.0239+(0.01638)(4.31)^{0.278}]} \\ &= 1.057 \end{aligned}$$

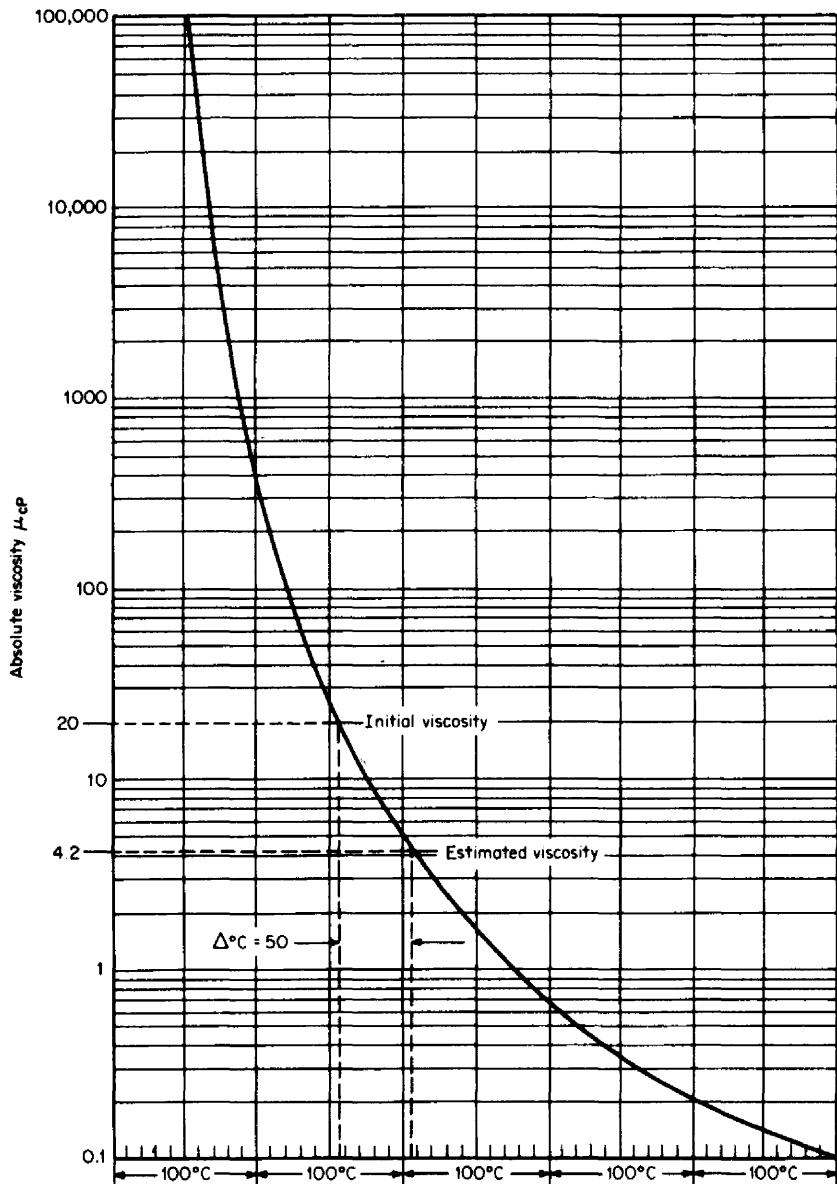


Figure 2.19 Curve for estimating viscosity from a single measured value. Values shown are for Example 2.18. (From Gambill, 1959.)

The viscosity is then, by Eq. (2.236),

$$(\mu_{\text{cP}})_p = F_{\mu p}(\mu_{\text{cP}})_a = (1.057)(4.31) = 4.56 \text{ cP}$$

Example 2.19. Estimate the viscosity of a liquid mixture of ethyl benzoate and benzyl benzoate at 77°F (25°C). The mole fraction of benzyl benzoate is 0.606. The following data is given:

- Ethyl benzoate: $(\mu_{\text{cP}})_1 = 2.01 \text{ cP}$
- Benzyl benzoate: $(\mu_{\text{cP}})_2 = 8.48$
- Measured viscosity: 4.95 cP

The mixture's viscosity is calculated with Eq. (2.241):

$$\mu_{\text{cP,mix}} = \exp [(1 - 0.606) \ln 2.01 + 0.606 \ln 8.48] = 4.81 \text{ cP}$$

Viscosities of Gases

With a temperature increase, the viscosity of a gas (vapor) increases; this behavior is opposite that of liquids. At very high pressures, however, the viscosity mechanism inverts, and gases behave like liquids. For most gases, classical kinetic theory and experimental results show little viscosity change for pressures up to 1500 psia (10,340 kPa). Viscosity changes are not of particular concern in most flow measurements, for which pressures do not reach this value. Additionally, gas flows are usually at very high Reynolds numbers, where even large viscosity changes are usually negligible in the flow computation.

Exponential Equation for Two Known Viscosities. Over normally encountered temperature ranges, an exponential equation can be used to interpolate or extrapolate to unknown viscosities. The simplest such equation is

$$\mu_{\text{cP}} = aT_K^n \quad (2.242)$$

where the values of n and a are derived from two known viscosities as

$$n = \frac{\ln [(\mu_{\text{cP}})_2 / (\mu_{\text{cP}})_1]}{\ln (T_{K2} / T_{K1})} \quad (2.243)$$

and

$$a = \frac{(\mu_{\text{cP}})_1}{T_{K1}^n} \quad (2.244)$$

Temperature Correction from a Single Value. When the viscosity is known at a single temperature, the viscosity at another temperature can be estimated by rewriting Arnold's (1933) correlations as

$$(\mu_{\text{cP}})_2 = \left(\frac{T_{R2}}{T_{R1}} \right)^{1.5} \frac{T_{R1} + 1.47T_B}{T_{R2} + 1.47T_B} (\mu_{\text{cP}})_1 \quad (2.245)$$

where the subscript 1 refers to the known value, and subscript 2 to the unknown value. In this equation, the temperature can be in either degrees Rankine or kelvins.

Equation (2.245) may also be written in terms of the critical temperature by substituting the approximate equation relating the boiling temperature T_b to the critical temperature T_c . That substitution gives

$$(\mu_{\text{cP}})_2 = \left(\frac{T_{\text{R}2}}{T_{\text{R}1}} \right)^{1.5} \frac{T_{\text{R}1} + 0.9T_c}{T_{\text{R}2} + 0.9T_c} (\mu_{\text{cP}})_1 \quad (2.246)$$

AICHe Gas (vapor) Viscosity. The Design Institute for Physical Property Data (AICHe, 1986) publishes an extensive data book on the properties of 1000 fluids. The generic equation for gas (vapor) viscosity is

$$\mu_{\text{Pa}\cdot\text{s}} = \frac{aT_k^b}{1 + c/T_k + d/T_k^2} \quad (2.247)$$

Table 2.28 presents values for the constants a , b , c , and d for some fluids.

Mixtures. The square-root rule used in the chemical industry provides the simplest and most useful equation for finding the viscosity of a mixture of gases. For 20 percent hydrogen-rich mixtures other equations are sometimes used, but for general flow measurements the square-root rule is adequate. This mixture rule is

$$\mu_{\text{mix}} = \frac{\sum x_i \mu_i M_{wi}^{1/2}}{\sum x_i M_{wi}^{1/2}} \quad (2.248)$$

Example 2.20. Ammonia has viscosities of 0.0108 cP at 100°F (37.8°C), and 0.0285 cP at 1000°F (538°C). Estimate its viscosity at 300°F (149°C) with (1) the exponential equation and (2) Arnold's equation.

1. Exponential equation. The exponential equation (2.242) is

$$\mu_{\text{cP}} = aT_K^n$$

TABLE 2.28 AICHe Gas (Vapor) Viscosity Constants

	Methane CH ₄	Ethylene C ₂ H ₄	Ethane C ₂ H ₆	Propadiene C ₃ H ₄	Propylene C ₃ H ₆
<i>a</i>	1.3230E-05	2.0789E-06	7.8170E-06	8.4350E-07	8.7900E-06
<i>b</i>	1.7980E-01	4.1630E-01	2.7300E-01	5.3270E-01	2.3200E-01
<i>c</i>	7.1800E+02	3.5270E+02	9.8100E+02	3.3200E+02	8.0000E+02
<i>d</i>	-8.9000E+23	0.0	-3.0300E+04	0.0	1.2000E+04
	Propane C ₃ H ₈	1,2-Butadiene C ₄ H ₆	Isobutene C ₄ H ₈	<i>n</i> -Butane C ₄ H ₁₀	Benzene C ₆ H ₆
<i>a</i>	2.2090E-06	5.6761E-07	7.6750E-06	1.0310E-05	3.3140E-08
<i>b</i>	3.8240E-01	5.5320E-01	2.6640E-01	2.0770E-01	9.6760E-01
<i>c</i>	4.0500E+02	2.1141E+02	9.8200E+02	1.0055E+03	7.9000E+00
<i>d</i>	0.0	0.0	0.0	8.1000E+03	0.0

Note: E in this table stands for *engineering notation*. For example, E+07 = 10⁷ and E-07 = 10⁻⁷, etc.

With $T_{K1} = 273.15 + 37.8 = 311$ K and $T_{K2} = 273.15 + 538 = 811$ K, the exponent n and coefficient a are, from Eqs. (2.243) and (2.244),

$$n = \frac{\ln(0.0285/0.0108)}{\ln(811/311)} = 1.012$$

$$a = \frac{0.0108}{(311)^{1.012}} = 0.0000324$$

The viscosity at 300°F (149°C) or $T_K = 273.15 + 149 = 422$ K is then

$$\mu_{cP} = (0.0000324)(422)^{1.012} = 0.0147 \text{ cP}$$

2. Arnold's equation. From Table D.1, the boiling temperature for ammonia is $T_B = 431.5^\circ\text{R}$. Also, for use in Arnold's equation (2.245),

$$T_{R1} = 459.67 + 100 = 560^\circ\text{R}$$

$$T_{R2} = 459.67 + 300 = 760^\circ\text{R}$$

Substitution then gives

$$(\mu_{cP})_{300^\circ\text{F}} = (0.0108) \left(\frac{760}{560} \right)^{1.5} \frac{560 + (1.47)(431.5)}{760 + (1.47)(431.5)} = 0.0146 \text{ cP}$$

Example 2.21. The mole fractions of a methane-ethane mixture are 0.7 and 0.3, respectively. Estimate the viscosity of the mixture at 80°F (26.7°C).

From the nomograph in Fig. H.1, at 80°F the viscosity of methane is $\mu_{cP} = 0.0108$, and that of ethane is $\mu_{cP} = 0.0093$. From Table D.1, for methane, $(M_w)_{\text{CH}_4} = 16.04$, and for ethane, $(M_w)_{\text{C}_2\text{H}_6} = 30.07$. The mixture's viscosity is then, from Eq. (2.248),

$$\begin{aligned} (\mu_{cP})_{\text{mix}} &= \frac{\sum x_i \mu_i M_{wi}^{1/2}}{\sum x_i M_{wi}^{1/2}} = \frac{(0.7)(0.0108)(16.04)^{1/2} + (0.3)(0.0093)(30.07)^{1/2}}{(0.7)(16.04)^{1/2} + (0.3)(30.07)^{1/2}} \\ &= 0.0102 \text{ cP} \end{aligned}$$

Pressure Correction. The effect of high pressure on a gas is to increase its viscosity. Below 1500 psia (10,340 kPa) this effect is negligible, but in high-pressure applications the viscosity may be increased 2 to 5 times, depending on the temperature; the largest increases take place at temperatures approaching the critical isotherm. Figure 2.18*b* and *c* illustrate the viscosity-pressure correction factor $F_{\mu p}$, based on critical temperature and pressure ratios (Perry and Green, 1984); detailed curves are presented in Figs. H.17 and H.18.

To use these curves, the reduced pressure and temperature are first calculated with Eqs. (2.1) and (2.2), and the viscosity-pressure correction factor is read. The viscosity at the high pressure is then obtained as

$$(\mu)_p = F_{\mu p}(\mu)_a \quad (2.249)$$

where the subscripts p and a refer to the pressure-corrected viscosity and the atmospheric-pressure viscosity, respectively.

Residual-Viscosity Equation. The viscosity of a gas (vapor) at high pressure is well estimated (Reid et al., 1987) by the residual viscosity function $(\mu - \mu^\circ)$, where μ is the dense (or flowing) gas viscosity and μ° is the viscosity of the gas at the same temperature but at a low pressure. This model gives accuracies of 1.8 percent for polar gases and 3.2 percent for nonpolar gases. For nonpolar gases (carbon dioxide, methane, ethane, propane, etc.) the viscosity at flowing conditions of pressure and temperature

$$\mu_{\text{cP}} = \mu_{\text{cP}}^\circ + \left[\frac{A - 1}{B} \right] 10^{-4} \quad (2.250)$$

where μ_{cP} is the viscosity in centipoises and A is a function of the reduced density ($\rho_r = \rho/\rho_c$) which is calculated by

$$A = (1.023 + 0.23364\rho_r + 0.58533\rho_r^2 - 0.40758\rho_r^3 + 0.093324\rho_r^4)^4 \quad (2.251)$$

B is calculated from

$$B = \frac{T_{Kc}^{1/6}}{M_w^{1/2} P_{c,\text{atm}}^{2/3}} = \frac{3.5 \times 10^{-4} T_r}{\mu_{\text{cP}}^\circ} \quad (2.252)$$

where T_{Kc} is the critical temperature of the gas in kelvins, T_r is the reduced temperature, $P_{c,\text{atm}}$ is the critical pressure in atmospheres, and M_w is the molecular weight.

The low-pressure gas (vapor) viscosity μ_{cP}° is estimated, for $T_r \leq 1$, by

$$\mu_{\text{cP}}^\circ = 3.5 \times 10^{-4} B^{-1} T_r^{0.965} \quad (2.253)$$

and for $T_r > 1$ by

$$\mu_{\text{cP}}^\circ = 3.5 \times 10^{-4} B^{-1} T_r^{0.71 + 0.29/T_r} \quad (2.254)$$

For polar fluids (ammonia, ethyl alcohol, freons, methyl alcohol, etc.), the residual correlation, for $\rho_r \leq 0.1$, is

$$\mu_{\text{cP}} = \mu_{\text{cP}}^\circ + 1.656 \times 10^{-4} \frac{\rho_r^{1.111}}{B} \quad (2.255)$$

For $0.1 < \rho_r \leq 0.9$ it is

$$\mu_{\text{cP}} = \mu_{\text{cP}}^\circ + 6.07 \times 10^{-6} \frac{(9.045\rho_r + 0.063)^{1.739}}{B} \quad (2.256)$$

and for $0.9 < \rho_r \leq 2.6$, it is

$$\mu_{\text{cP}} = \mu_{\text{cP}}^\circ + \frac{10^C}{10,000B} \quad (2.257)$$

C in Eq. (2.257) for $0.9 < \rho_r \leq 2.2$ is

$$C = 4 - 10^{0.6439 - 0.1005\rho_r + 4} \quad (2.258)$$

and for $2.2 < \rho_r \leq 2.6$ it is

$$C = 4 - 10^{0.6439 - 0.1005p_r - 4.75 \times 10^{-4}(\rho_r^3 - 10.65)^2} \quad (2.259)$$

Example 2.22. Estimate the viscosity of the methane-ethane mixture of Example 2.21 at 4000 psia (27,580 kPa).

Properties from Table D.1 and Example 2.21 are as follows:

Property	Methane	Ethane
x_i	0.7	0.3
p_c	667.2 psia	708.4 psia
T_c	343.1°R	549.7°R
V_c	1.589 ft ³ /(lb _m ·mol)	2.374 ft ³ /(lb _m ·mol)
Z_c	0.288	0.285

The pseudocritical properties of the mixture are then, from Eqs. (2.112) and (2.113),

$$T_{pc} = \sum x_i T_{ci} = (0.7)(343.1) + (0.3)(549.7) = 405.1^\circ\text{R}$$

$$p_{pc} = \frac{(\sum x_i Z_{ci}) R_0 T_{pc}}{\sum x_i V_{ci}} = \frac{[(0.7)(0.288) + (0.3)(0.285)](10.7315)(405.1)}{(0.7)(1.589) + (0.3)(2.374)} = 684.1 \text{ psia}$$

where $R_0 = 10.73151 \text{ psia} \cdot \text{ft}^3 / \text{lb}_m \cdot \text{mole} \cdot ^\circ\text{R}$. The reduced properties are then, from Eq. (2.115),

$$T_{pr} = \frac{459.67 + 80}{405.1} = 1.33 \quad p_{pr} = \frac{4000}{684.1} = 5.85$$

From the viscosity-pressure correction curve, the factor $F_{\mu p}$ is read as $F_{\mu p} = 3.1$. The viscosity at 4000 psia is then, by Eq. (2.249),

$$(\mu_{cP})_{4000} = F_{\mu p}(\mu_{cP})_a = (3.1)(0.0102) = 0.0316 \text{ cP}$$

Example 2.23. Estimate the viscosity of a 2000-psia (14-MPa) and 100°F (37.8°C) natural gas. The mole percent is 60-20-20 methane, propane, and ethane, and the density is 14.319 lb_m/ft³.

The mixture's pseudocritical properties are

$$T_c = \sum x_i T_{ci} = (0.6)(343.1) + (0.2)(549.7) + (0.2)(665.6) = 448.92^\circ\text{R}$$

$$p_{pc} = \sum x_i p_{ci} = (0.6)(667.2) + (0.2)(708.4) + (0.2)(615.8) = 665.16 \text{ psia}$$

$$Z_{pc} = \sum x_i Z_{ci} = (0.6)(0.288) + (0.2)(0.285) + (0.2)(0.281) = 0.286$$

and the mixture's molecular weight is

$$\begin{aligned} M_{w,\text{gas}} &= \sum M_{wi} = (0.6)(16.043) + (0.2)(30.0701) + (0.2)(44.0972) \\ &= 24.459 \text{ lb}_m / (\text{lb}_m \cdot \text{mol}) \end{aligned}$$

The specific gravity of the mixture is then

$$G = \frac{M_{w,\text{gas}}}{M_{w,\text{air}}} = \frac{24.459}{28.963} = 0.8445$$

where the values of T_{ci} , p_{ci} , Z_{ci} , and M_{wi} for methane, ethane, and propane are taken from App. D, Table D.1.

The pseudocritical density is then, from Eq. (2.10),

$$\rho_{pc} = (2.698825) \frac{(665.16)(0.8445)}{(0.286)(448.92)} = 11.808 \text{ lb}_m/\text{ft}^3$$

The pseudoreduced density, from Eq. (2.3), is

$$\rho_{pr} = \frac{v_{pc}}{v_f} = \frac{\rho_f}{\rho_{pc}} = \frac{14.319}{11.808} = 1.2127$$

The pseudocritical temperature, expressed in kelvins, is

$$T_{Kc} = T_{pc}/1.8 = 448.92/1.8 = 310.9 \text{ K}$$

and the pseudocritical pressure, in atmospheres, is

$$p_{pc,\text{atm}} = p_{pc}/p_{\text{atm}} = 665.16/14.696 = 45.261$$

The low-pressure viscosity may now be determined, from Eq. (2.253), as

$$\begin{aligned} \mu_{cp}^{\circ} &= (3.5 \times 10^{-4})(24.459)^{1/2}(45.261)^{2/3}(310.9)^{-1/6}(1.247)^{(0.71+0.29/1.247)} \\ &= 0.0104 \text{ cP} \end{aligned}$$

The constants A and B , for use in the residual-viscosity equation, are, from Eq. (2.251),

$$\begin{aligned} A &= [(1.023 + (0.23364)(1.2127) + 0.58533(1.2127)^2 - (0.40758)(1.2127)^3 \\ &\quad + (0.093324)(1.2127)^4)]^4 = 7.271 \end{aligned}$$

and, for B , from Eq. (2.252),

$$B = \frac{(3.5 \times 10^{-4})(1.247)}{0.0104} = 0.0419$$

The viscosity at the flowing pressure is then, in accordance with Eq. (2.250),

$$\mu_{cp} = 0.0104 + \frac{(7.271 - 1)(10^{-4})}{(0.0419)} = 0.0255 \text{ cP}$$

Viscosity-Measuring Devices

There are two common viscometer types and numerous special types for high-pressure tests, in-line measurement (Fig. 2.20), or rheology studies. The most common and inexpensive is the efflux type, in which a known volume of fluid is discharged through an orifice or capillary, and the measured time to discharge the volume is substituted into an empirical equation to calculate the viscosity. In the

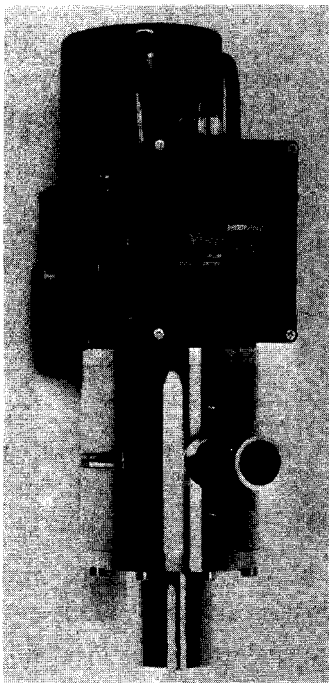


Figure 2.20 In-line viscometer. (*Courtesy Brookfield Engineering Laboratories.*)

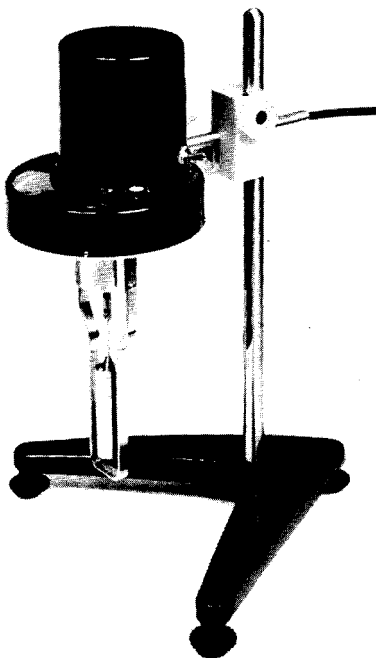


Figure 2.21 Rotational viscometer for rheology studies. (*Courtesy Brookfield Engineering Laboratories.*)

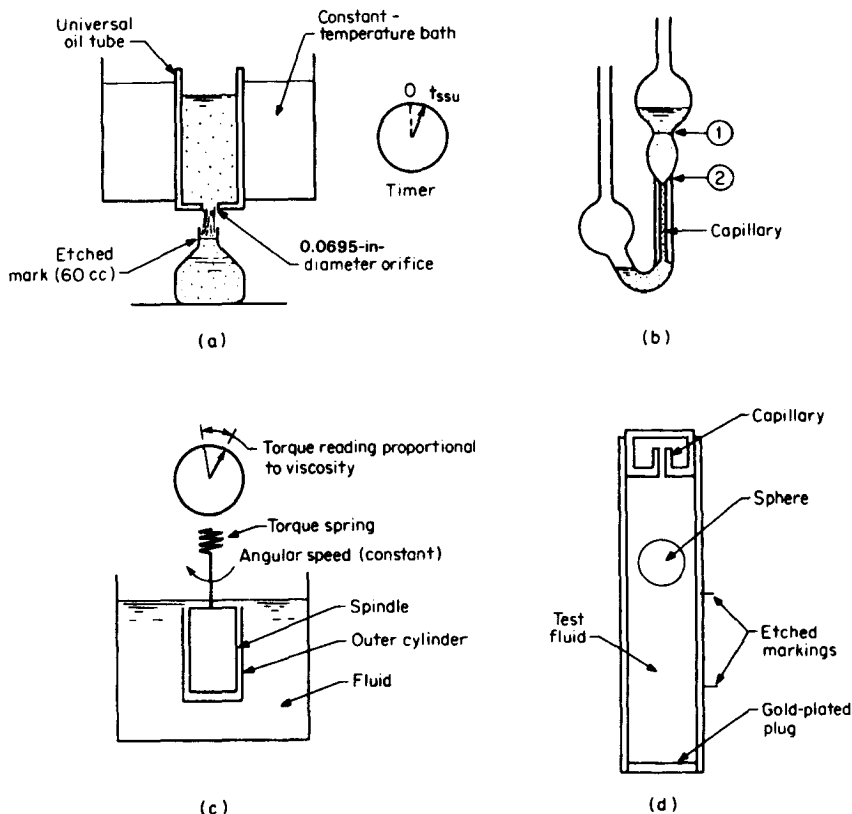


Figure 2.22 Viscometers. (a) Saybolt second. (b) Ostwald capillary. (c) Rotational. (d) Hoespler (liquid and gas).

second type, the measured torque on a constant-speed rotating cylinder (Fig. 2.21) or cone, immersed in the fluid, is taken as a direct indication of the viscosity of the fluid.

Of the special types, those that make use of a falling or rolling ball or the measured time for a bubble to rise through the liquid are the most common for field testing. Vibrating reeds, mixers with torque dynamometers, and plunger types are also used, either as continuous-measurement devices, for special measurements of inks and asphalt, or in the measurement of the softening characteristics of non-newtonian fluids.

Orifice-Efflux Viscometers. The most commonly used viscosity-measuring instrument in the United States is the Saybolt viscometer (see Fig. 2.22a). The sample fluid is held in a universal oil tube which is immersed in a controlled constant-temperature oil or water bath. The fluid is initially prevented from flowing by a small cork. When the temperature becomes constant, the cork is removed, and a 60-cm³ flask is filled by discharging the sample through a 0.0695-in (1.7-mm) orifice located at the bottom of the oil tube. The time required to fill the 60-cm³ flask is the viscosity in *Saybolt universal seconds*. The device should be used only

when laminar flow occurs in the tube, and for discharge times above 30 s. For very viscous oils a larger orifice is used, and the time unit is referred to as in the *Saybolt Furol Second*.

The following empirical equations relate the measured Saybolt universal times to the centistoke viscosity unit; exact relationships are given in ASTM D445-71 (1971):

$$\nu_{\text{cSt}} = 0.226t_{\text{SSU}} - \frac{195}{t_{\text{SSU}}} \quad \text{for } 32 \text{ s} < t_{\text{SSU}} < 100 \text{ s} \quad (2.260)$$

$$\nu_{\text{cSt}} = 0.220t_{\text{SSU}} - \frac{135}{t_{\text{SSU}}} \quad \text{for } t_{\text{SSU}} > 100 \text{ s} \quad (2.261)$$

For highly viscous fluids, Saybolt Furol times are substituted into the following equations to calculate centistoke viscosities

$$\nu_{\text{cSt}} = 2.24t_{\text{SSF}} - \frac{184}{t_{\text{SSF}}} \quad \text{for } 25 \text{ s} \leq t_{\text{SSF}} \leq 40 \text{ s} \quad (2.262)$$

$$\nu_{\text{cSt}} = 2.16t_{\text{SSF}} - \frac{60}{t_{\text{SSF}}} \quad \text{for } t_{\text{SSF}} > 40 \text{ s} \quad (2.263)$$

Other orifice-efflux-type viscometers include the Zahn, Cox, Scott, and Fordcup. These were designed either for simpler operation or for the viscosity measurement of special fluids such as paint, varnish, and tar. The Redwood viscosity scale is commonly used in Great Britain. The Redwood viscosity equations are similar in form to the Saybolt equations and are as follows:

Redwood No. 1 (Standard)

$$\nu_{\text{cSt}} = 0.26t_{\text{RS}} - \frac{179}{t_{\text{RS}}} \quad \text{for } 34 \text{ s} \leq t_{\text{RS}} \leq 100 \text{ s} \quad (2.264)$$

$$\nu_{\text{cSt}} = 0.247t_{\text{RS}} - \frac{50}{t_{\text{RS}}} \quad \text{for } t_{\text{RS}} > 100 \text{ s} \quad (2.265)$$

Redwood No. 2 (Admiralty)

$$\nu_{\text{cSt}} = 2.46t_{\text{RA}} - \frac{100}{t_{\text{RA}}} \quad \text{for } 32 \text{ s} \leq t_{\text{RA}} \leq 90 \text{ s} \quad (2.266)$$

$$\nu_{\text{cSt}} = 2.45t_{\text{RA}} \quad \text{for } t_{\text{RA}} > 90 \text{ s} \quad (2.267)$$

Capillary-Efflux Viscometers. Because of their short orifice length, orifice-efflux viscometers are not particularly well suited for rheological studies. End effects and the transition from laminar to turbulent flow within the tube or orifice are not easily analyzed or interpreted. For these reasons, a device with a well-defined capillary passage is best for high accuracy. The most familiar such device is the Ostwald viscometer tube, shown in Fig. 2.22*b*. As with the orifice type, the time required for a known volume of fluid to move from etched mark 1 to etched mark 2 is measured. This time is then compared to that for a fluid with known viscosity under the same conditions. For steady, incompressible flow, no wall slippage, a tube long

enough to negate end effects, and negligible thermal gradients and pressure changes, the unknown viscosity is calculated as

$$\mu_{cP} = \frac{\mu_{cP,ref} t_{tF} \rho_F^*}{t_{ref} \rho_{ref}^*} \quad (2.268)$$

where the subscript F refers to the test fluid, and ref to the reference fluid.

The use of capillary-type viscometers requires a knowledge of the rheological properties of fluids and the many specialized empirical and theoretical equations used to accurately determine the behavior of both newtonian and nonnewtonian fluids. Many specialized capillary viscometers are available; for further information, the reader is referred to the text by Van Wazer et al. (1963).

Rotating Viscometers. Rotating one cylinder inside another (Fig. 2.22c), with the fixed clearance space filled with the test fluid, creates a shear force proportional to the fluid viscosity. The torque, measured at constant rotational speed, is a direct indication of the viscosity; by suitable scaling and calibration with known fluids, the absolute viscosity may be read. Depending on the viscosity range, many combinations of cylinders, rotational speeds, and torque-measuring devices (often strain gauges) are available.

Falling-Sphere Viscometer. A ball falling through a fluid through the action of the difference between ball density and fluid density obeys Stokes' law relating downward velocity to viscosity. The Hoespler viscometer (Fig. 2.22d) can measure, to within ± 0.1 to ± 0.5 percent, the viscosities of gases or very viscous fluids (over a range of 0.01 to 1,000,000 cP) with the same tube, but with different calibrated spheres. The general equation for calculating the viscosity is

$$\nu_{cst} = k_{FS}(\rho_{sph}^* - \rho_F^*)t_{FS} \quad (2.269)$$

where k_{FS} is a combination constant determined with a known fluid, ρ_{sph}^* is the density of the sphere, ρ_F^* is the density of the test fluid, and t_{FS} is the measured time (in seconds) for the sphere to pass between the enclosing cylinder's two etched marks.

THE ISENTROPIC EXPONENT

Gases expand as they flow through the reduced area of a differential producer. The expansion to a lower pressure is assumed to follow a polytropic path, for which the relationship between pressure and volume is defined by

$$pV^n = \text{constant} \quad (2.270)$$

Because of the short expansion length and usually small pressure differences, an idealized one-dimensional isentropic expansion is assumed; the expansion is reversible, and there is no heat loss (adiabatic expansion). Under these assumptions, the relationship between the two pressures and volumes is

$$\frac{p_1}{p_2} = \left(\frac{V_2}{V_1} \right)^k = \left(\frac{\rho_{f1}}{\rho_{f2}} \right)^k \quad (2.271)$$

where the exponent k is the isentropic exponent. In the literature, three different exponents have been used in this equation; which one is selected depends on whether the gas is assumed to be perfect, ideal, or real.

Within the normal operating ranges of differential pressure, flowing pressure, and temperature, the flow equations are not particularly sensitive to the value of the isentropic exponent. The assumption of a perfect or ideal gas is therefore reasonable.

Perfect Gas

A *perfect* gas has a compressibility factor of 1, and its specific-heat ratio is assumed to be independent of both temperature and pressure. The relationship between the specific-heat ratio and the universal gas constant may be expressed as

$$(C_p - C_v)_p = 1.98586 \text{ Btu}/(\text{lb}_m \cdot \text{mol} \cdot ^\circ\text{R}) \quad (2.272)$$

Rearranging Eq. (2.272) and rounding the universal gas constant yield the following expression for the ratio of specific heats for a perfect gas:

$$k_p = \left(\frac{C_p}{C_v} \right)_p = \frac{(C_p)_p}{(C_p)_p - 1.986} \quad (2.273)$$

where $(C_p)_p$ refers to the specific heat of the gas at 14.696 psia (101.325 kPa) and 59°F (15°C).

It should be noted that many tables, nomographs, and other sources give the specific heat at constant pressure in terms of pounds-mass or kilograms, and not on a mole basis. These values should be multiplied by the molecular weight of the gas to satisfy the units of Eq. (2.273). For gas mixtures, the specific heat at constant pressure can be *approximated* by summing mole fractions as follows:

$$C_{p,\text{mix}} \approx \sum x_i C_{pi} \quad (2.274)$$

Ideal Gas

An *ideal* gas has a compressibility factor of 1, and its specific heat at constant pressure C_p is a function of temperature but no pressure. For an ideal gas, the isentropic exponent is

$$k_i = \left(\frac{C_p}{C_v} \right)_i = \frac{(C_p)_i}{(C_p)_i - 1.986} \quad (2.275)$$

where $(C_p)_i$ is a function of the absolute temperature. Data on many common gases has been fitted to equations that are given in Table I.2. Tables I.1 and I.2 list the specific heats $(C_p)_i$ for some gases.

AIChE Heat Capacity Equation. The Design Institute for Physical Property Data (AIChE, 1986) generic ideal heat capacity (specific heat) is

$$(C_p)_i = a + b \exp \left(-\frac{c}{T_K^d} \right) \quad (2.276)$$

$(C_p)_i$ has the units of J/(kg·mol·K). The constants a , b , c , and d for some fluids

are presented in Table 2.29. Constants for up to 1000 fluids may be obtained from the AIChE data book.

Example 2.24. Assuming air is an ideal gas mixture ($Z = 1.0$) consisting of 80 percent nitrogen and 20 percent oxygen, use the temperature-specific heat nomograph in App. I to calculate the isentropic exponent k_i for this ideal gas at (a) 68°F (20°C) and (b) 1000°F (538°C).

From Fig. I.17, at 68°F,

$$(C_p)_{N_2} = 0.25 \text{ Btu}/(\text{lb}_m \cdot ^\circ\text{F}) \quad (C_p)_{O_2} = 0.22 \text{ Btu}/(\text{lb}_m \cdot ^\circ\text{F})$$

and at 1000°F,

$$(C_p)_{N_2} = 0.27 \text{ Btu}/(\text{lb}_m \cdot ^\circ\text{F}) \quad (C_p)_{O_2} = 0.26 \text{ Btu}/(\text{lb}_m \cdot ^\circ\text{F})$$

From Table D.1,

$$(M_w)_{N_2} = 28.0134 \text{ lb}_m/(\text{lb}_m \cdot \text{mol}) \quad (M_w)_{O_2} = 31.998 \text{ lb}_m/(\text{lb}_m \cdot \text{mol})$$

and the mixture's molecular weight is, from Eq. (2.99),

$$M_{w,\text{mix}} = \sum x_i M_{wi} = (0.8)(28.013) + (0.2)(31.998) = 28.810 \text{ lb}_m/(\text{lb}_m \cdot \text{mol})$$

1. Ideal-gas isentropic exponent at 68°F. The mixture's specific heat at 68°F is approximated with Eq. (2.274):

$$C_{p,\text{mix}} = \sum x_i C_{pi} = (0.8)(0.25) + (0.2)(0.22) = 0.244 \text{ Btu}/(\text{lb}_m \cdot ^\circ\text{F})$$

The ideal-gas isentropic exponent for the mixture at 68°F is then, from Eq. (2.275) with M_w included for consistent units,

$$k_i = \frac{(0.244)(28.810)}{(0.244)(28.810) - 1.986} = 1.394$$

2. Ideal-gas isentropic exponent at 1000°F. The mixture's specific heat at 1000°F is, again from Eq. (2.274),

TABLE 2.29 AIChE Gas (Vapor) Heat Capacity Constants

	Methane CH ₄	Ethylene C ₂ H ₄	Ethane C ₂ H ₆	Propadiene C ₃ H ₄	Propylene C ₃ H ₆
<i>a</i>	3.3106E+04	3.2950E+04	3.8380E+04	3.4493E+04	4.4950E+04
<i>b</i>	9.9975E+04	1.1555E+05	1.7500E+05	1.5436E+05	1.9091E+05
<i>c</i>	2.3380E+03	1.2340E+03	8.4350E+02	2.9560E+02	8.7000E+02
<i>d</i>	1.1347E+00	1.0977E+00	1.0204E+00	8.9150E-01	1.0411E+00
	Propane C ₃ H ₈	1,2-Butadiene C ₃ H ₆	Isobutene C ₄ H ₈	<i>n</i> -Butane C ₄ H ₁₀	Benzene C ₆ H ₆
<i>a</i>	4.7497E+04	5.4949E+04	6.0100E+04	5.7380E+04	3.6007E+04
<i>b</i>	2.4670E+05	2.1120E+05	2.6215E+05	3.4240E+05	2.7294E+05
<i>c</i>	6.9858E+02	6.4380E+02	6.4730E+02	3.7050E+02	1.1744E+03
<i>d</i>	1.0074E+00	1.0028E+00	9.9770E-01	9.0700E-01	1.1386E+00

Note: E in this table stands for *engineering notation*. For example, E+07 = 10⁷ and E-07 = 10⁻⁷, etc.

$$C_{p,\text{mix}} = (0.8)(0.27) + (0.2)(0.26) = 0.268 \text{ Btu}/(\text{lb}_m \cdot ^\circ\text{F})$$

Then the isentropic exponent at 1000°F is, by Eq. (2.275), again with M_w included,

$$k_i = \frac{(0.268)(28.810)}{(0.268)(28.810) - 1.986} = 1.346$$

Real Gas

In the expansion of a *real* gas the effects of compressibility must be considered for correct prediction of the density change from upstream pressure and temperature measurements. Several isentropic flow models have been proposed (Sullivan, 1979) that predict the isentropic exponent from equations of state. Figures I.5 through I.16 present the isentropic exponents for many gases, based on these models.

A numerical solution that may also be used is based on the isentropic-exponent equation given in *Fluid Meters* (ASME, 1971); this equation is

$$k = \left\{ \frac{1}{1 - [(\partial Z/Z)/(\partial p/p)]_T} \right\} \frac{C_p}{C_v} = F_k \frac{C_p}{C_v} \quad (2.277)$$

A three-step calculation procedure is necessary to solve Eq. (2.277) numerically. The generalized diagrams for these steps are illustrated in Fig. 2.23; these diagrams are not to scale; Figs. I.1 through I.3 should be used for actual calculations. The appendix diagrams are for a simple fluid with acentric factor equal to 1.0. For other fluids, the diagrams presented in the text by Edmister (1974) or the following Redlich-Kwong solution are suggested for better accuracy.

Step 1: Pressure Correction. Shown in Fig. 2.23a is the Edmister (1974) generalized diagram that is used to correct the specific heat for pressure. This is an additive correction that approximates the pressure effect to within 5 to 10 percent for most fluids. The corrected (for pressure) specific heat is

$$C_p = (C_p)_i + F_{\gamma p} \quad (2.278)$$

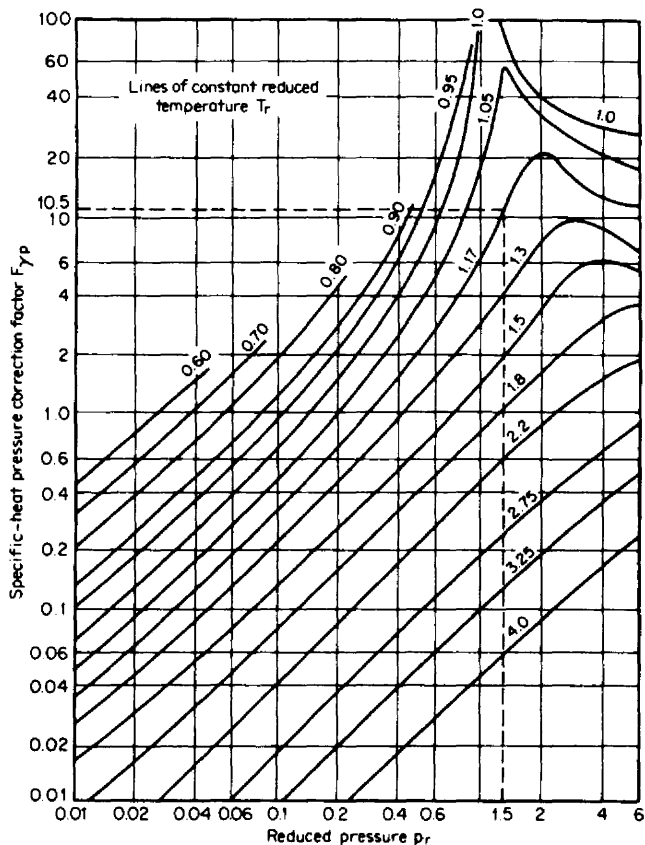
where C_p is the specific heat corrected for pressure, and $(C_p)_i$ is the specific heat of an ideal gas at the temperature of the subject gas.

For the graphical determination of the correction for pressure, the reduced temperature T_r and pressure p_r are first calculated; then the value of $F_{\gamma p}$ is read from the curve.

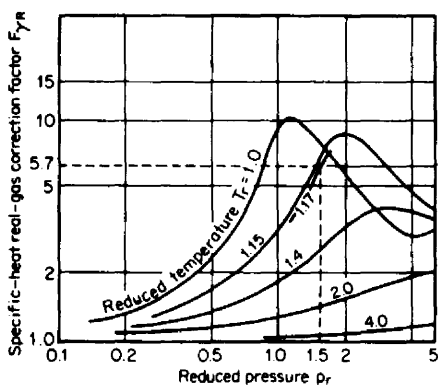
Step 2: Specific-Heat Real-Gas Correction $F_{\gamma R}$. Edmister's (1974) generalized-properties diagram, shown in Fig. 2.23b, corrects for the effect of compressibility. It can be viewed as a modification to the universal gas constant shown in Eq. (2.273). Note from the curves that as the reduced-pressure ratio p_r decreases, the real-gas correction factor approaches 1.0.

The reduced pressure and temperature are calculated, and the value of the real-gas correction factor is read from the appropriate curve. The specific-heat ratio, corrected for pressure and temperature, is then calculated as

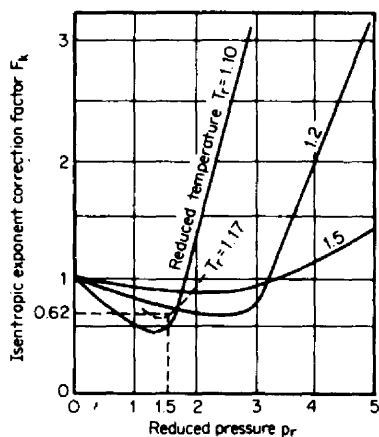
$$\frac{C_p}{C_v} = \frac{C_p}{C_p - 1.986F_{\gamma R}} \quad (2.279)$$



(a)



(b)



(c)

Figure 2.23 Generalized diagrams used to calculate the isentropic exponent (not to scale); dashed lines are for Example 2.25. (a) Pressure correction (see Fig. I.1). (b) Real-gas correction (see Fig. I.2). (c) Isentropic-exponent correction (see Fig. I.3).

Step 3: Isentropic-Exponent Calculation. Illustrated in Fig. 2.23c is a generalized-properties curve developed from the Hall-Yarborough equation of state by successively incrementing the pressure and calculating the compressibility change for an isothermal expansion in accordance with the term in braces in Eq. (2.277). The exact curve, given in Fig. 1.3, can be used to find F_k for the calculation of the isentropic exponent by substitution into Eq. (2.277):

$$k = F_k \frac{C_p}{C_v} \quad (2.280)$$

Redlich-Kwong Solution

The isentropic exponent for a real gas is defined by

$$k = \left(\frac{\partial p}{\partial \ln v} \right)_s = -\frac{C_p}{C_v} \left(\frac{\partial p}{\partial v} \right)_T \frac{v_f}{p_f} = -\frac{C_p}{C_v} \left(\frac{\partial p}{\partial v} \right)_T \frac{Z_f R_{0E} T_f}{p_f^2} \quad (2.281)$$

where C_p and C_v [Btu/(lb_m·mol·°R), J/(kg·mol·K)] are the heat capacities at constant pressure and temperature, respectively, evaluated at the flowing pressure and temperature, Z_f is the Redlich-Kwong compressibility factor [Eq. (2.23)], R_{0E} is the universal gas constant [Btu/(lb_m·mol·°R), J/(kg·mol·K)], T_f is the flowing absolute temperature (°R, K), and p_f is the flowing pressure (psia, Pa). In order to calculate the quantities given in Eq. (2.281), the Redlich-Kwong equation of state is differentiated in accordance with the following thermodynamic relationships (Hansen-Miller, 1988). The heat capacity (specific heat) at constant pressure and at flowing conditions is

$$C_p = (C_p)_i + \Delta C_p = (C_p)_i - R_{0E} T_f (T_f \phi'' + 2\phi') \quad (2.282)$$

where $(C_p)_i$ is the heat capacity at the flowing temperature of the ideal gas and ϕ' (°R⁻¹, K⁻¹) and ϕ'' (°R⁻², K⁻²) are the first and second derivatives of the fluid's fugacity coefficient Φ .

The heat capacity at constant volume, for a real gas, is

$$C_v = C_p - T_f \left(\frac{\partial p}{\partial T} \right)_v \left(\frac{\partial v}{\partial T} \right)_p = C_p - A_1 B_1 T_f \quad (2.283)$$

The term A_1 is calculated by

$$A_1 = \left(\frac{\partial p}{\partial T} \right)_v = \frac{p_f}{T_f} \left(\frac{1}{Z_f - B} + \frac{A}{2Z_f(Z_f + B)} \right) \quad (2.284)$$

and the term B_1 is calculated by

$$B_1 = \left(\frac{\partial v}{\partial T} \right)_p = \frac{R_{0E} T_f}{p_f} \left(Z_f' + \frac{Z_f}{T_f} \right) \quad (2.285)$$

Z_f is the Redlich-Kwong compressibility factor, and A and B are the Redlich-Kwong constants.

The derivative of the compressibility factor Z_f' is

$$Z'_f = \left(\frac{\partial Z}{\partial T} \right)_p = - \frac{3.5AB + (2B^2 + B - 2.5A)Z_f}{[3Z_f^2 - 2Z_f + A - B^2 - B]T_f} = \frac{U}{W} \quad (2.286)$$

The first and second derivatives of the fugacity coefficient ϕ require the second derivative of the compressibility factor, which is

$$Z''_f = \left(\frac{\partial^2 Z}{\partial T^2} \right)_p = \frac{U'W - W'U}{W^2} \quad (2.287)$$

The derivative of U , the numerator of Eq. (2.286), is

$$U' = (2B^2 + B - 2.5A)Z'_f - (4B^2 + B - 6.25A) \frac{Z_f}{T_f} - \frac{12.25AB}{T_f} \quad (2.288)$$

and the derivative of W , the denominator of Eq. (2.286), is

$$W' = 1.5A - B^2 + (2 - 3Z_p)Z_f + 2T_f(1 - 3Z_p)Z'_f \quad (2.289)$$

The term $(\partial p / \partial v)_T$ in Eq. (2.281) is then

$$-\left(\frac{\partial p}{\partial v} \right)_T = \frac{(\partial p / \partial v)_p}{(\partial T / \partial p)_v} = \frac{(\partial p / \partial T)_v}{(\partial v / \partial T)_p} = \frac{A_1}{B_1} \quad (2.290)$$

The fugacity coefficient ϕ is calculated by

$$\phi = \int_0^p (Z - 1) \frac{dp}{p} = Z_f - 1 - \ln(Z_f - B) - \frac{A}{B} \ln \left(1 + \frac{B}{Z_f} \right) \quad (2.291)$$

The derivative of fugacity ϕ' then becomes

$$\phi' = Z'_f - \frac{Z'_f + B/T_f}{Z_f - B} + \frac{A}{B} \left[\frac{1.5 \ln(1 + B/Z_f)}{T_f} + \frac{B}{Z_f} \left(\frac{Z''_f + Z'_f/T_f}{Z_f + B} \right) \right] \quad (2.292)$$

and the second derivative ϕ'' is derived as

$$\begin{aligned} \phi'' = Z'' - \frac{Z''_f - 2B/T_f^2}{Z_f - B} + \left(\frac{Z'_f + B/T_f}{Z_f - B} \right)^2 \\ + \frac{A}{B} \left[-\frac{3.75}{T_f^2} \ln D + \frac{D'}{D} \left(\frac{3}{T_f} + \frac{D'}{D} - \frac{D''}{D'} \right) \right] \end{aligned} \quad (2.293)$$

where D , D' , and D'' are

$$\begin{aligned} D &= 1 + \frac{B}{Z_f} & D' &= -\frac{B}{Z_f^2} \left(Z'_f + \frac{Z_f}{T_f} \right) \\ D'' &= \frac{2B}{Z_f^2} \left(\frac{Z_f}{T_f^2} + \frac{Z'_f}{T_f} + \frac{Z_f'^2}{Z_f} - \frac{Z''_f}{2} \right) \end{aligned} \quad (2.294)$$

Example 2.25. Assuming carbon dioxide is an ideal gas, use the equation given in Table I.3 to calculate the ideal isentropic exponent at 1000°F (538°C).

The specific heat at constant pressure is

$$(C_p)_i = 16.2 - \frac{6.53 \times 10^3}{T_R} + \frac{1.41 \times 10^6}{T_R^2}$$

At 1000°F, $T_R = 1459.7^\circ\text{R}$. Then substitution gives

$$(C_p)_i = 16.2 - \frac{6.53 \times 10^3}{1459.7} + \frac{1.41 \times 10^6}{(1459.7)^2} = 12.39 \text{ Btu}/(\text{lb}_m \cdot \text{mol} \cdot ^\circ\text{R})$$

The ideal isentropic exponent is then, by Eq. (2.275),

$$k_i = \frac{12.39}{12.39 - 1.986} = 1.191$$

Example 2.26. The expansion factor for gas flow through an orifice is discussed below. For an orifice for which $\beta = 0.75$, calculate the bias error in measuring the flow rate of methane at 1000 psia (6895 kPa) and -60°F (-51.1°C) if the gas is assumed to be (1) perfect and (2) ideal. The differential pressure h_w is 200 in (50 kPa).

The expansion factor for an orifice is

$$Y_1 = 1 - (0.41 + 0.35\beta^4) \frac{x}{k}$$

where
$$x = \frac{h_w}{27.73 p_{f1}} = \frac{200}{(27.73)(1000)} = 0.0072$$

Then,
$$Y_1 = 1 - [0.41 + (0.35)(0.75)^4] \frac{0.0072}{k} = 1 - \frac{0.00376}{k}$$

The flow-rate equation for an orifice is

$$q_{PPH} = F_{MC} Y_1 \sqrt{h_w p_{f1}}$$

at a measured differential pressure and density, the expansion-factor sensitivity coefficient is 1.0; $a \pm 1$ percent expansion-factor change represents $a \pm 1$ percent flow-rate bias error.

For methane, from Table D.1,

$$T_c = 343.1^\circ\text{R} \quad p_c = 667.1 \text{ psia}$$

From Eq. (2.115), the reduced properties are

$$T_r = \frac{459.67 - 60}{343.1} = 1.17 \quad p_r = \frac{1000}{667.1} = 1.50$$

From Table I.1, at 59°F ,

$$(C_p)_p = 8.45 \text{ Btu}/(\text{lb}_m \cdot \text{mol} \cdot ^\circ\text{R})$$

and at -60°F ,

$$(C_p)_i = 8.08 \text{ Btu}/(\text{lb}_m \cdot \text{mol} \cdot ^\circ\text{R})$$

Perfect gas. The isentropic exponent of the perfect gas is, by Eq. (2.273),

$$k_p = \frac{(C_p)_p}{(C_p)_p - 1.986} = \frac{8.45}{8.45 - 1.986} = 1.307$$

Its expansion factor is, then,

$$Y_1 = 1 - \frac{0.00376}{k_p} = 1 - \frac{0.00376}{1.307} = 0.9971$$

Ideal gas. For the ideal gas, the isentropic exponent is calculated from the specific heat at the flowing temperature of -60°F , using Eq. (2.275):

$$k_i = \frac{(C_p)_i}{(C_p)_i - 1.986} = \frac{8.08}{8.08 - 1.986} = 1.326$$

The expansion factor for the ideal gas is then

$$Y_1 = 1 - \frac{0.00376}{k_i} = 1 - \frac{0.00376}{1.326} = 0.9972$$

Real gas. The real-gas isentropic exponent is calculated using Eq. (2.277),

$$k = F_k \frac{C_p}{C_v}$$

where, from Eq. (2.279),

$$\frac{C_p}{C_v} = \frac{C_p}{C_p - 1.986F_{\gamma R}}$$

The specific heat corrected for pressure and temperature is, by Eq. (2.278),

$$C_p = (C_p)_i + F_{\gamma p}$$

From Fig. I.1, for $T_r = 1.17$ and $p_r = 1.50$, $F_{\gamma p} = 10.5 \text{ Btu}/(\text{lb}_m \cdot \text{mol} \cdot ^\circ\text{R})$. Then, at -60°F with $(C_p)_i = 8.08 \text{ Btu}/(\text{lb}_m \cdot \text{mol} \cdot ^\circ\text{R})$,

$$C_p = 8.08 + 10.5 = 18.58 \text{ Btu}/(\text{lb}_m \cdot \text{mol} \cdot ^\circ\text{R})$$

From Fig. I.2, the real gas correction for $T_r = 1.17$ and $p_r = 1.50$ is $F_{\gamma R} = 5.7$. The ratio of specific heats is then

$$\frac{C_p}{C_v} = \frac{18.58}{18.58 - (1.986)(5.7)} = 2.559$$

From Fig. I.3, the correction for a real gas is $F_k = 0.62$. The isentropic exponent is then, from Eq. (2.280),

$$k = F_k \frac{C_p}{C_v} = (0.62)(2.559) = 1.587$$

The expansion factor for the real gas is

$$Y_1 = Y_{\text{real}} = 1 - \frac{0.00376}{k} = 1 - \frac{0.00376}{1.587} = 0.9976$$

Bias error. The bias error is calculated as

$$B_{\%} = \frac{Y_{\text{ind}} - Y_{\text{true}}}{Y_{\text{true}}} 100$$

where it is assumed that $Y_{\text{true}} = Y_{\text{real}}$.

1. Perfect gas

$$B = \frac{0.9971 - 0.9976}{0.9976} 100 = -0.05 \text{ percent}$$

2. Ideal gas

$$B = \frac{0.9972 - 0.9976}{0.9976} 100 = -0.04 \text{ percent}$$

REFERENCES

- AGA: *Gas Measurement Manual*, American Gas Association, Washington, D.C., 1963.
- AGA: *Manual for the Determination of Supercompressibility Factors for Natural Gas*, American Gas Association, New York, 1963.
- AGA 8, *Compressibility and Supercompressibility for Natural Gas and Other Hydrocarbon Gases*, Transmission Measurement Committee Report No. 8, AGA Catalog No. XQ 1285, Arlington, VA., 1992.
- AIChE: *Data Compilation Tables of Properties of Pure Compounds*, Design Institute for Physical Property Data, AIChE, New York, 1986.
- Andrade, E. N. da C.: "The Viscosity of Liquids," *Nature*, vol. 125, pp. 309, 582, 1930.
- API: *Manual of Petroleum Measurement Standards*, 1st ed., chap. 11.2.1, "Compressibility Factors of Hydrocarbons: 0–90°API Gravity Range," American Petroleum Institute, Washington, D.C., 1984.
- API: *Manual of Petroleum Measurement Standards*, 1st ed., chap. 11.2.2, "Compressibility Factors of Hydrocarbons: 0.350–0.637 Relative Density (60°F/60°F) and –50°F to 140°F Meeting Temperature [GPA8286-86]," American Petroleum Institute, Washington, D.C., 1987.
- API Standard 1101, *Measurement of Petroleum Liquid Hydrocarbons by Positive Displacement Meter*, p. 52, American Petroleum Institute, Washington, D.C., 1960.
- API Standard 2540, *Manual of Petroleum Measurement Standards*, vol. 11, chap. 11.1, tables 5A, 5B, 6A, 6B, American Petroleum Institute, Washington, D.C., 1980.
- Arnolds, J.H.: *J. Chem. Phys.*, vol. 1, p. 170, 1933.
- ASME: *Fluid Meters*, 6th ed., ASME, New York, 1971.
- ASME: *ASME Thermodynamic and Transport Properties of Steam*, 3d ed., ASME, New York, 1967.
- ASTM Standard 445-71, ASTM, Washington, D.C., 1971.
- Bean, H. S.: "An Apparatus and Methods for Determining the Compressibility of a Gas and the Correction for 'Supercompressibility,'" *J. Res. Nat. Bur. Stand.*, vol. 4, pp. 645–661, 1929.
- Benedict, W. S., G. B. Webb, and L. C. Rubin: "An Empirical Equation for Thermodynamic Properties of Light Hydrocarbons and Their Mixtures," *Chem. Eng. Prog.*, vol. 47, p. 419, 1951; *J. Chem. Phys.*, vol. 8, p. 334, 1940, vol. 10, p. 764, 1964.
- Burnett, E. S.: "Compressibility Determination without Volume Measurements," *J. Appl. Mech.*, vol. 3, pp. A136–A140, 1936.

- Doolittle, A. K.: "Studies in Newtonian Flow," *J. Appl. Phys.*, vol. 22, p. 1471, 1951.
- Edmister, W. C.: *Applied Hydrocarbon Thermodynamics*, vol. 1, Gulf, Houston, Texas, 1974.
- : *Applied Hydrocarbon Thermodynamics*, vol. 2, Gulf, Houston, Texas, 1974.
- Eirich, F. R.: *Rheology—Theory and Application*, vol. 1, pp. 258, Academic, New York, 1956.
- Fishtine, S. H.: "Estimates of Saturated Fluid Densities and Critical Constants," *Ind. Eng. Chem. Fundam.*, vol. 2, no. 2, pp. 149–155, 1963.
- Gambill, W. R.: "How P and T Change Gas Viscosity," *Chem. Eng.*, p. 157, 1958.
- GERG: *Compressibility of Natural Gas Mixtures*, Groupe Européen des Recherches Gazières, Report 8410-3, October 1984.
- Goldhammer, D. A.: "Studien über die Theorie der übereinstimmenden Zustände," *Phys. Chem.*, vol. 71, p. 577, 1910.
- Goyal, P., and L. K. Doraiswamy: "Estimating Liquid Densities," *Hydrocarbon Process. Pet. Refiner*, vol. 45, p. 200, 1966.
- GRI: *Development of Improved Capabilities for Computation of Gas Supercompressibility Factors and Other Properties*, Gas Research Institute, Chicago, 1985.
- Hall, K. P., and L. Yarborough: "A New Equation of State for Z-Factor Calculation," *Oil Gas J.*, vol. 77, no. 25, pp. 82–92, 1973.
- Haar, L., J. S. Gallagher, and G. S. Kell: *NBS/NRC Steam Tables*, Hemisphere Publishing, McGraw-Hill Int. Book Co., 1984.
- Hankinson, R. W., and G. H. Thomson: "Calculate Liquid Densities Accurately," *Hydrocarbon process.*, pp. 277–283, September 1979.
- Hankinson, R. W., R. C. Estes, and T. A. Coker: "Physical Properties from a Modified Soave-Redlich-Kwong Equation of State in a Process System Environment," paper presented at the 68th Annual AIChE meeting, Los Angeles, 1975.
- Hansen, P. D., and R. W. Miller, private communications, 1988.
- Hayward, A. T. J.: *Compressibility Equations for Liquids—A Comparative Study*, National Engineering Laboratory, Ministry of Technology, East Kilbride, Scotland, 1967.
- IAPS: *IAPS Formulation 1985 for the thermodynamic Properties of Steam*, Release NIST (NBS), Gaithersburg, VA, Nov. 1985.
- ISO Standard 5024, *Petroleum Liquids and Gases—Measurement—Standard Reference Conditions*, International Standards Organization, Geneva, 1976.
- Jaeschke, M., and H. M. Hinze, "Using Densitometers in Gas Metering," *Hydrocarbon Processing*, vol. 66, no. 6, pp. 37–41, June 1987.
- Joffe, J.: "Combining Rules for the Third Parameter in the Pseudocritical Method for Mixtures," *Ind. Eng. Chem. Fundam.*, vol. 10, p. 532, 1971.
- Jones, F. E.: "The Air Density Equation and the Transfer of the Mass Unit," *J. Res. Nat. Bur. Stand.*, vol. 83, no. 5, pp. 419–428, 1978.
- Kay, W. B.: "Density of Hydrocarbon Gases and Vapors," *Ind. Eng. Chem.*, vol. 28, no. 9, pp. 1014–1019, 1936.
- Kouzel, B.: "How Pressure Affects Liquid Viscosity," *Hydrocarbon Process. Pet. Refiner*, vol. 44, no. 3, p. 120, 1965.
- Lu, B. C.: "Estimate Specific Liquid Volumes," *Chem. Eng.*, vol. 66, pp. 137–138, 1959.
- McCarty, R.D.: "Determination of Thermodynamic Properties from Experimental Thermodynamics," in N. Le Neindre and B. Vodar (eds.), *Experimental Thermodynamics of Non-Reacting Fluids*, vol. II, Butterworth, London, 1975.
- Nelson, L. C., and E. F. Obert: "Generalized pvT Properties of Gases," *Trans. ASME*, vol. 76, p. 1057, 1954.
- Obert, E. F.: *Thermodynamics*, McGraw-Hill, New York, 1948.
- Olien, N. A., and J. W. Magee: "Isochoric pvT Measurements on CO₂ and 0.98 CO₂ + 0.02 CH₄ from 225 to 400 K with Pressures to 35 MPa," *Int. J. Thermophys.*, 1988.
- PEA: *Tentative Standard for the Application of Gas Measurement Procedures to Computer Usage*, Pacific Energy Association Bulletin T.S.-622-77, Los Angeles, 1977.

- Perry, J. H., and D. W. Green: *Chemical Engineers' Handbook*, 6th ed., McGraw-Hill, New York, 1984.
- Pitzer, K. S., B. Z. Lippmann, and R. F. Curl: "The Volumetric and Thermodynamic Properties of Fluids," *J. Am. Chem. Soc.*, vol. 77, pp. 3427-3433, 1955.
- Prausnitz, J. M., and R. D. Gunn: "Volumetric Properties of Nonpolar Gaseous Mixtures," *AIChE J.*, vol. 4, pp. 430, 494, 1958.
- PTB: "Die Dichte des Wasser im internationalen Einheitensystem und der internationalen praktischen Temperaturskala von 1968," *PTB Mitt.*, vol. 81, no. 6, pp. 412-414, 1971.
- Rackett, H. G.: "Equation of State for Saturated Liquids," *J. Chem. Eng. Data*, vol. 15, p. 514, 1970.
- Redlich, O., and J. N. S. Kwong: "On the Thermodynamics of Solutions. V An Equation of State. Fugacities of Gaseous Solutions," *Chem. Rev.*, vol. 44, p. 233, 1949.
- Reid, R. C., J. K. M. Prausnitz, and B. R. Poling: *The Properties of Gases and Liquids*, 4th ed., McGraw-Hill, New York, 1987.
- Reynolds, W. C.: "Thermodynamic Properties in SI," Dept. of Mechanical Engineering, Stanford Univ., Stanford, CA 94305, 1979.
- Smith and Van Ness: *Introduction to Chemical Thermodynamics*, 4th ed. McGraw-Hill, New York, 1987.
- Standing, M. B., and D. L. Katz: "Density of Natural Gas," *AIIME Pet. Dev. Tech.*, vol. 146, pp. 140-149, 1942.
- Sullivan, D. A.: "Historical Review of Real-Fluid Isentropic Flow Models," Paper 79-WA-FM-1, ASME Winter Annual Meeting, New York, 1979.
- Tait, P. G.: "Physics and Chemistry of the Voyage of H.M.S. Challenger," vol. II, part IV, S. P. LXI, HMSO, London, 1888.
- Van Wazer, J. R., J. W. Lyons, K. Y. Kim, and R. E. Colwell: *Viscosity and Flow Measurement*, Interscience/Wiley, New York, 1963.
- White, H. J.: "Properties of Steam," *Mechanical Engineering*, ASME Magazine, pp. 36-37, August 1986.
- Yarborough, L., and K. P. Hall: "How to Solve Equation of State for Z-Factors," *Oil Gas J.*, vol. 78, pp. 86-88, 1974.
- Yen, L. C., and S. S. Wood: "A Generalized Equation for Computer Calculations of Liquid Densities," *AIChE J.*, vol. 12, p. 95, 1966.
- Younglove, B. A.: *Thermophysical Properties of Fluids. I. Argon, Ethylene, Para-hydrogen, Nitrogen, Nitrogen Trifluoride, and Oxygen*, AIChE, Nat. Inst. of Physics, and NBS, Washington, D.C., 1982.

MEASUREMENT

The purpose of this chapter is to present the basic measurement units used in flow measurement and to discuss typical temperature- and pressure-measuring devices. This information will be used in subsequent chapters in the development of the engineering flow equations.

MASS, FORCE, WEIGHT

The English Engineering System of Units

Table 3.1 summarizes the five fundamental systems of units that have been constructed from Newton's second law of motion to relate force F , mass m , length L , and time t . While any system can be developed from three fundamental quantities, the four quantities of the English engineering system—the foot (ft), pound-force (lb_f), pound-mass (lb_m), and second (s)—will be used here to develop the U.S. customary unit equations.

To relate the pound-force to the pound-mass, a proportionality equation can be written between the engineering and the absolute units. Using the definition that 1 lb_f will accelerate 1 lb_m at 32.17405 ft/s^2 , a dimensional conversion constant can be derived as

$$\mathbf{F} = \frac{1}{g_c} m a \quad (3.1)$$

$$\text{lb}_f = \frac{1}{\text{lb}_m \cdot \text{ft}/(\text{lb}_f \cdot \text{s}^2)} \text{lb}_m \frac{\text{ft}}{\text{s}^2}$$

The constant g_c has the same value as standard gravity g_0 , defined at sea level and 45° latitude, but it has the dimensions of $\text{lb}_m \cdot \text{ft}/(\text{lb}_f \cdot \text{s}^2)$. It is, therefore, a dimensional conversion factor to relate pounds-force and pounds-mass. Substituting local gravity (g_l) for acceleration a in Eq. (3.1) gives the relationship between mass and weight force as

$$W = \frac{g_l}{g_c} m \quad (3.2)$$

$$\text{lb}_f = \frac{g_l}{g_c} \text{lb}_m$$

TABLE 3.1 Dimensional Systems

System	Mass (m)	Force (F)	Length (L)	Time (t)
English				
Engineering (F, m, L, t)	pound-mass (lb _m)	pound-force (lb _f)	foot (ft)	second (s)
Absolute (m, L, t)	pound-mass (lb _m)	poundal (lb _m ·ft/s ²)	foot (ft)	second (s)
Technical (F, L, t)	slug (lb _f ·s ² /ft)	pound-force (lb _f)	foot (ft)	second (s)
Metric				
Absolute (m, L, t)	gram (g)	dyne (g·cm/s ²)	centimeter (cm)	second (s)
International				
SI (m, L, t)	kilogram (kg)	Newton (kg·m/s ²)	meter (m)	second (s)

The ratio of local gravity g_l to the dimensional constant g_c can be approximated to within 0.005 percent with an expression given by Benedict (1984):

$$F_L = \frac{g_l}{g_c} = 1 - 2.637 \times 10^{-3} \cos 2\phi - 9.6 \times 10^{-8}y - 5 \times 10^{-5} \text{ lb}_f/\text{lb}_m \quad (3.3)$$

where ϕ is the latitude in degrees, and y the altitude in feet above sea level.

Some confusion results from the fact that the word weight has long been used to mean both mass (lb_m) and force (lb_f). When weighted on a beam scale, an object is calibrated against a known mass. Since both are influenced by the same local gravity, the scale reading is corrected to the mass value and, hence, mass is measured. However, a spring scale calibrated with a 1-lb mass at sea level and 45° latitude (standard gravity) will indicate *one pound* for this mass only at this location. At other gravities ($g_l \neq g_0$) the 1-lb mass will not “weigh” 1 lb_f on this scale.

The SI System of Units

In the International System of units (SI), the force unit is the newton (N). It is the force that, when applied to a 1-kg mass, will cause an acceleration of 1 m/s². The relationship between force, mass, and acceleration is

$$\mathbf{F}^* = \frac{m^* a^*}{g_c^*} \quad (3.4)$$

$$1 \text{ N} = \frac{1 \text{ kg} \times 1 \text{ m/s}^2}{g_c^*}$$

or

$$g_c^* = 1 \frac{\text{kg} \cdot \text{m}}{\text{N} \cdot \text{s}^2}$$

The *weight* force in newtons of a 1-kg mass is then

$$W^* = \frac{g_l^*}{g_c^*} m^* = 9.80665 F_L m^* \quad (3.5)$$

The kilogram mass is, by international agreement, the mass of a certain bar of platinum-iridium located in Sevres, France. The pound-mass in the English engineering system is exactly 0.45359237 kg.

Buoyancy Correction for Mass Determination

Standard masses (kilogram, pound-mass) are used to calibrate scales and as force references. However, the volume of the mass displaces surrounding air, creating an upward buoyant force that reduces the applied force. Mass standards are usually corrected for air buoyancy to values in a vacuum; when a standard mass is placed on a scale at any location, the scale reading is corrected to read the value of the applied mass. The correction thus includes the effects of both buoyancy and local gravity. However, the correction will apply to an object other than the standard mass only if the object displaces the same volume of air as the standard mass. If the standard mass displaces more air than the object, the corrected scale reading must be increased; if less, it must be decreased.

A buoyancy force is not exerted on a fluid in a pipeline. Therefore, if a liquid is collected in a weigh tank, and the reading is compared to a flowmeter's mass-flow indication, a 0.1 to 0.3 percent bias-error correction should be made to account for the difference between flowing liquid density and the density of the standard masses used to calibrate the scale.

Figure 3.1a shows a 10-lb standard mass placed on a scale at any geographic location. The upward buoyant force reduces the weight force W , and the scale reading is adjusted to read 10 lb_m. The net force transmitted is then

$$\mathbf{F}_{N,m} = F_L m - F_L V_m \rho_{\text{air},c} \quad (3.6)$$

The first term in Eq. (3.6) is the force of the standard mass, its weight, and the second is the upward buoyant force created by displacing the volume of air occupied by the standard mass m . Equation (3.6) can be rewritten by substituting the density of the standard mass m as

$$\mathbf{F}_{N,m} = F_L m - F_L \frac{\rho_{\text{air},c}}{\rho_{\text{mass}}} m \quad (3.7)$$

where the subscript air, c refers to the density of air at the time of calibration.

Equation (3.6) can also be written as

$$\mathbf{F}_{N,m} = \left(1 - \frac{\rho_{\text{air},c}}{\rho_{\text{mass}}} \right) F_L m \quad (3.8)$$

If the weigh tank is filled with liquid (Fig. 3.1b), and the corrected scale reading is 10, the upward buoyant force is increased by the liquid volume, and the net force exerted by the liquid is

$$\mathbf{F}_{N,l} = \left(1 - \frac{\rho_{\text{air}}}{\rho_l} \right) F_L m_l \quad (3.9)$$

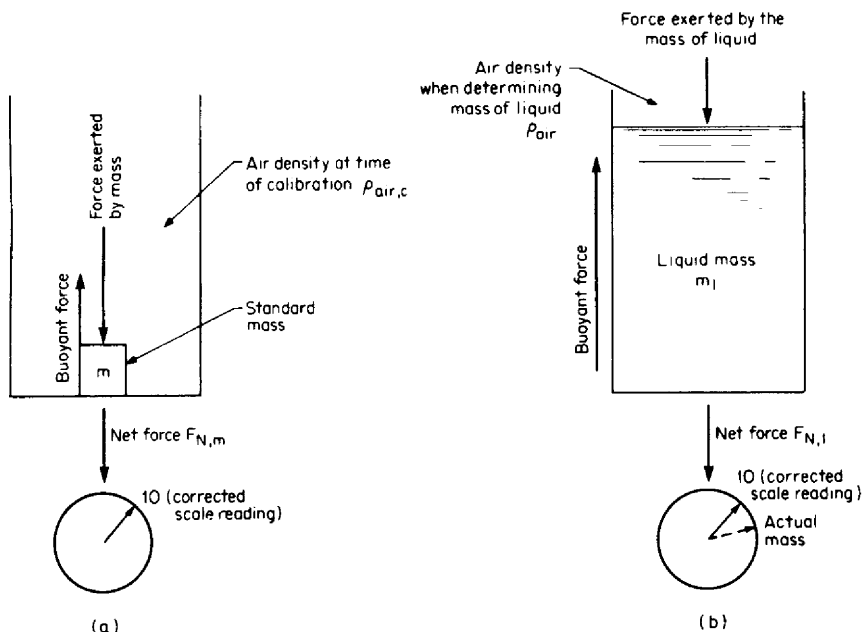


Figure 3.1 Effects of buoyancy in the determination of mass.

where the subscript air refers to the air density at the time the liquid mass is determined. Since the corrected scale readings are the same, Eq. (3.8) can be equated to Eq. (3.9), and the buoyancy correction becomes

$$F_{MB} = \frac{m_l}{m} = \left(\frac{\rho_{mass} - \rho_{air,c}}{\rho_l - \rho_{air}} \right) \frac{\rho_l}{\rho_{mass}} \quad (3.10)$$

The mass of the collected liquid is then related to the standard mass (in pounds-mass or kilograms) by

$$m_l = F_{MB} m \quad (3.11)$$

Buoyancy Correction for Force Determination

A buoyancy correction is also required when standard masses are used as a force reference. Figure 3.2 shows standard masses placed on a platform to produce a force on the piston of a dead-weight tester. The force exerted on the surface of the oil is given by Eq. (3.8), and the buoyancy correction is

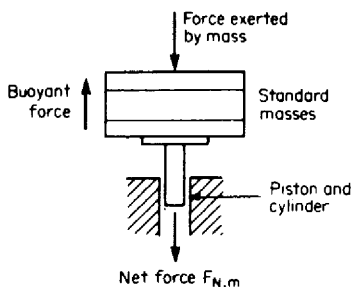


Figure 3.2 Effect of buoyancy when standard masses are used as a force reference.

$$F_{FB} = 1 - \frac{\rho_{air}}{\rho_{mass}} \quad (3.12)$$

The net force transmitted is then

$$\mathbf{F}_{N,m} = F_L F_{FB} m \quad (3.13)$$

In the SI system, the net force (in newtons) is

$$\mathbf{F}_{N,m}^* = 9.80665 F_L F_{FB} m^* \quad (3.14)$$

where m^* is the mass in kilograms.

Example 3.1. A gallon of alcohol is weighed on a scale that was calibrated with steel masses when the air density was $0.07500 \text{ lb}_m/\text{ft}^3$. At the time of the weighing, the air density is $0.07490 \text{ lb}_m/\text{ft}^3$, and the scale reading is 6.572 lb_m . Determine the density of the alcohol if the density of the steel masses is $489 \text{ lb}_m/\text{ft}^3$.

The volume of the alcohol is

$$\mathbf{V}_l = (231 \text{ in}^3/\text{gal})(\text{ft}^3/1728 \text{ in}^3) = 0.13368 \text{ ft}^3$$

The initial estimate for the density of the alcohol is

$$(\rho_l)_0 = \frac{m_l}{\mathbf{V}_l} = \frac{6.572}{0.13368} = 49.162 \text{ lb}_m/\text{ft}^3$$

The initial estimate for the buoyancy correction factor is, from Eq. (3.10),

$$F_{MB} = \frac{489 - 0.07500}{49.162 - 0.07490} \frac{49.162}{489} = 1.00137$$

The corrected mass of the alcohol is, from Eq. (3.11),

$$m_l = (1.00137)(6.572) = 6.581$$

A second iteration gives $(\rho_l)_1 = 49.230$, and, from Eq. (3.10),

$$F_{MB} = \frac{489 - 0.07500}{49.230 - 0.07490} \frac{49.230}{489} = 1.00137$$

as previously. The mass of alcohol is then $m_l = 6.581 \text{ lb}_m$, and its density is

$$\rho_l = \frac{6.581}{0.13368} = 49.230 \text{ lb}_m/\text{ft}^3$$

Example 3.2. In Fairbanks, Alaska, at a latitude of 65° north and an altitude of 5000 ft (1524 m) above sea level, a 10-lb_m (4.54-kg) mass is placed on a dead-weight tester. What is the applied force if the air density is $0.07458 \text{ lb}_m/\text{ft}^3$? (Assume steel masses, $\rho_{\text{mass}} = 489 \text{ lb}_m/\text{ft}^3$.)

The correction for local gravity is, by Eq. (3.3),

$$F_L = 1 - 2.637 \times 10^{-3} \cos 130 - (9.6 \times 10^{-8})(5000) \\ - 5 \times 10^{-5} = 1.00117 \text{ lb}_f/\text{lb}_m$$

and the correction for buoyancy is, by Eq. (3.12),

$$F_{FB} = 1 - \frac{0.07458}{489} = 0.99985$$

Net force in English engineering system. From Eq. (3.13),

$$F_{N,m} = (1.00117)(0.99985)(10) = 10.010 \text{ lb}_f$$

Net force in SI system. The mass in the SI system is

$$m^* = (0.4535924)(10) = 4.535924 \text{ kg}$$

and, from Eq. (3.14),

$$F_{N,m}^* = (9.80665)(1.00117)(0.99985)(4.535924) = 44.527 \text{ N}$$

PRESSURE

Definitions

Pressure is defined as intensity of force and is evaluated as the force exerted on a unit area. In the English engineering system of units, the pressure unit is the pound-force per square inch (lb_f/in^2). In the SI system, the unit is the newton per square meter (N/m^2) or pascal (Pa). From these units are derived such convenient units of measurement as the inch of water, bar, and standard atmosphere. Nine pressure terms are used to define pressure levels and pressure differences. These are discussed below and illustrated in Fig. 3.3.

Absolute Zero Pressure. If all molecules were removed from within a chamber, a perfect vacuum would exist, and no pressure forces would be exerted on the chamber walls. This idealized state defines the condition of zero pressure and is referred to as *absolute zero*.

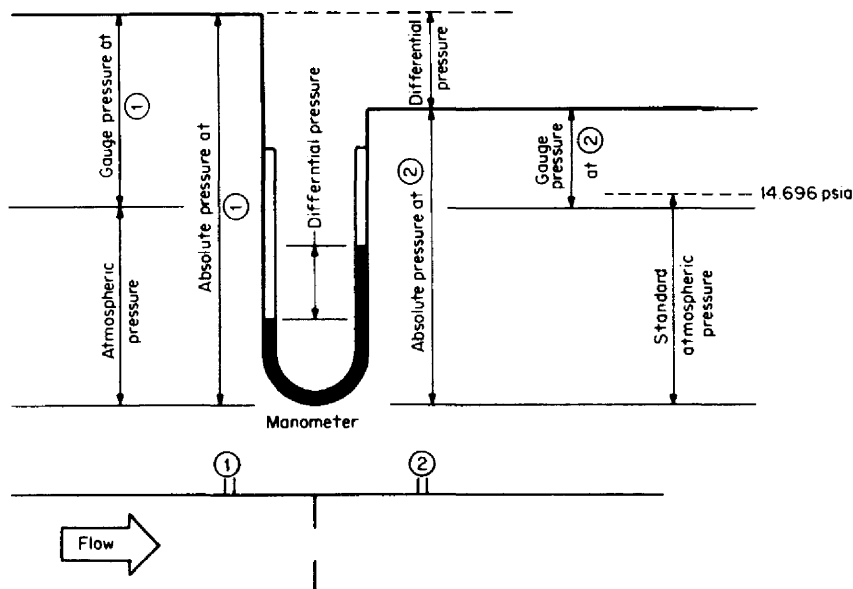


Figure 3.3 Pressure levels and terminology.

Absolute Pressure. The absolute pressure is the pressure above absolute zero. The static absolute pressure defines the molecular activity of a gas. It is the pressure used in the calculation of gas density.

Atmospheric Pressure. The pressure exerted by the atmosphere above absolute zero is defined as atmospheric pressure. Although this pressure varies with location, it is convenient to define a standard atmosphere of pressure at sea level as 14.696 psia (101.325 kPa) and to use this value as a reference in computing gas volumes.

Actual atmospheric pressure is measured with a barometer and varies with altitude. At 5000 ft (1524 m), it is approximately 12.3 psia (84.8 kPa); at 10,000 feet (3048 m), it is 10 psia (69 kPa).

Gauge Pressure. Pressure gauges measure the difference between the pressure inside a pressure element and the surrounding atmospheric pressure. To obtain absolute pressure, atmospheric pressure must be added to the gauge reading.

Vacuums. A vacuum-gauge reading is a reading below atmospheric pressure, usually expressed in inches of mercury (vacuum).

Differential Pressure. A differential pressure is the difference between two pressures. It is measured by either separating the two pressures with a diaphragm and measuring the force or motion of the diaphragm or by observing the height of a column of liquid in a manometer.

Piezometer Rings. Piezometer rings are used to average static pressure tap readings around the pipe wall. The standard ring shown in Fig. 3.4a is typically used; however, Blake (1976) has shown that the Triple-T design (Figure 3.4b) is theoretically more correct as an averaging ring. Piezometer rings reduce some of the effects of upstream fittings and orifice eccentricity on the discharge coefficient. Dirt and air in liquid lines are serious problem areas that need to be considered when installing piezometers.

Static Pressure. The actual pressure exerted by a fluid either at rest or in motion is its static pressure. Either a piezometer ring or a small radial hole in a pipe wall will allow the static pressure to be measured.

In obtaining the static pressure of a flowing fluid, it is important that the hole be drilled perpendicular to the pipe, with no burrs and no rounded corners. Rayle (1959) has shown (Fig. 3.5) that departure from recommended hole size, inclination, or edge condition results in bias errors of -0.5 to $+1.1$ percent of the dynamic pressure.

Ferron (1986) points out that countless static pressure measurements are in error because of poor pressure tap construction. Based on tests at the Alden Research Laboratories and the work of Rayle (1959) and Brunkalla (1985), he suggests a $\frac{1}{4}$ -in (6.4-mm) hole diameter for pipe sizes greater than 2 in (50 mm) and that:

Pressure taps should be drilled, and preferably reamed, such that the centerline of the hole meets the pipe centerline at right angles to the axial pipe centerline. The drilling should be done after all fittings for attaching the pressure tubing have been welded to the pipe.

In the pipe interior, the hole must be round and free of burrs or wire edges. The cleaning of burrs or wire edges must be performed in a manner to prevent any concave or convex surface surrounding the hole. If finished properly, the edge of the hole will be square with the inner pipe surface.

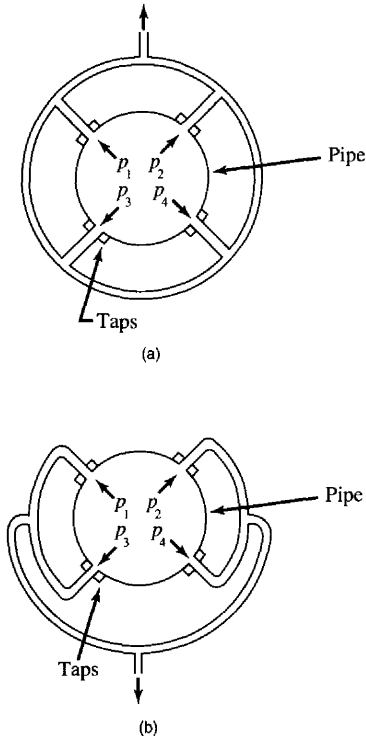


Figure 3.4 Piezometer rings. (a) Typical. (b) Triple-T-design.

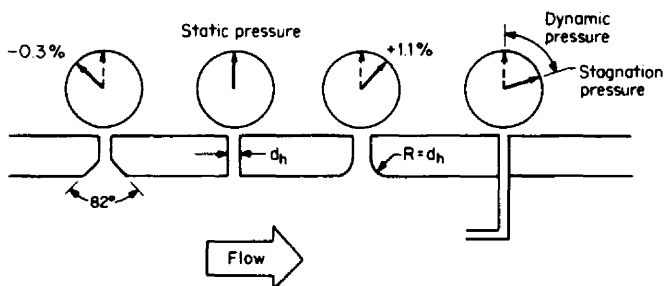


Figure 3.5 Bias error caused by edge condition of wall pressure-tap hole. (From Rayle, 1959.)

Dynamic Pressure. If a tube is bent perpendicular to a flow (Fig. 3.5), the static pressure is increased by the directed kinetic energy of the stream. At zero velocity the pressure reading is the same as the static pressure, but as the velocity increases the difference is observed to increase by the square of the velocity. This difference in pressure levels is due to *dynamic pressure*.

Total Pressure. The sum of the static and dynamic pressures is the stagnation, or total, pressure. The stagnation pressure may be read with a pressure gauge connected to a pitot tube as shown in Fig. 3.5.

Pressure Relations. Because of the many pressure units involved, it is important that a consistent set of units be used in conjunction with the following pressure relationships.

For flow-line pressure in pounds-force per square foot,

$$P_f = P_G + P_B \quad (3.15)$$

the total pressure (pounds-force per square foot) is the sum of the dynamic pressure and the static pressure; that is

$$P_T = P_f + P_D \quad (3.16)$$

where the dynamic pressure P_D may be expressed in terms of the fluid density and velocity as

$$P_D = \frac{\rho_f V_p^2}{2g_c} \quad (3.17)$$

The differential pressure between two pressure levels is

$$\Delta P = P_{f1} - P_{f2} \quad (3.18)$$

Units

Numerous units and pressure scales have been developed to express pressure. Some of the more common ones are as follows:

1. Atmospheric pressure

- Standard atmospheres (atm)
- Atmospheric pressure (atm)
- Millimeters of mercury at 0°C (mm Hg)

2. Absolute pressure

- Pounds per square inch absolute (psia)
- Bars (bar)
- Pascals (Pa, kPa)

3. Differential pressure

- Feet of flowing fluid
- Inches of flowing fluid
- Inches of water (in H₂O) at flowing temperature

- Inches of water (in H₂O) at 39.2°F, at 60°F, at 68°F
- Inches of mercury (in Hg) at 32°F, at 60°F, at 68°F
- Bars (bar)
- Pascals (Pa, kPa)
- Pounds per square inch, differential (psid)

4. General terms

- Pounds per square inch gauge (psig)
- Inches of mercury (in Hg) at 32°F, at 60°F, at 69°F
- Deciboyles
- Torr (torr)

The SI conversion factors between these units and the pascal are given in Table C.1. For conversion between two non-SI pressure units, the known units are first converted to pascals; then, by division, the desired conversion is obtained. For example, the conversion of inches of mercury at 32°F to kilograms-force per square centimeter would be expressed as

$$(\text{in Hg})_{32^\circ\text{F}}(3.38638\text{E} + 03) = \text{Pa} = (\text{kg}_f/\text{cm}^2)(9.806650\text{E} + 04)$$

$$\text{or } \text{kg}_f/\text{cm}^2 = \left(\frac{3.38638\text{E} + 03}{9.806650\text{E} + 04} \right) (\text{in Hg})_{32^\circ\text{F}} = (0.03453147)(\text{in Hg})_{32^\circ\text{F}}$$

Standards

The deadweight tester and simple manometer are the two basic pressure standards. The U-tube or cistern-type manometer is used from approximately 3 lb/in² (21 kPa) to 100 lb_f/in² (690 kPa) with an accuracy of ± 0.1 percent. Manometers can, however, be designed to be highly accurate. Shown in Fig. 3.6(b) is a high-accuracy, ± 0.0003 -in-Hg, ± 0.003 percent of reading, mercury manometer. The deadweight tester defines pressures from 0.01 to 10,000 psig (0.07 to 69,000 kPa) within an accuracy range of 0.01 to 0.15 percent, depending on design. A commercially available deadweight tester is shown in Fig. 3.7.

Manometer. Because of its inherent simplicity, the simple glass U-tube manometer (Fig. 3.6a) has been the basic pressure standard for many years. Manometers measure pressure by balancing pressure forces directly against a liquid column. The liquid selected depends on the pressure difference and may range from a light-fluid such as kerosene to a very dense liquid such as mercury.

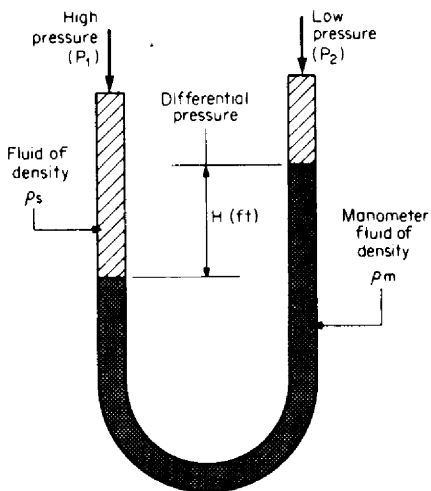
For the manometer shown in Fig. 3.6a, the indicated differential pressure is

$$\Delta P = \frac{g_l}{g_c} (\rho_m - \rho_s)H = F_L(\rho_m - \rho_s)H \quad \text{lb}_f/\text{ft}^2 \quad (3.19)$$

where H is in feet, ρ_m is the manometer-fluid density, and ρ_s is the fluid density in the high-pressure side. In the SI system, the differential pressure is given by

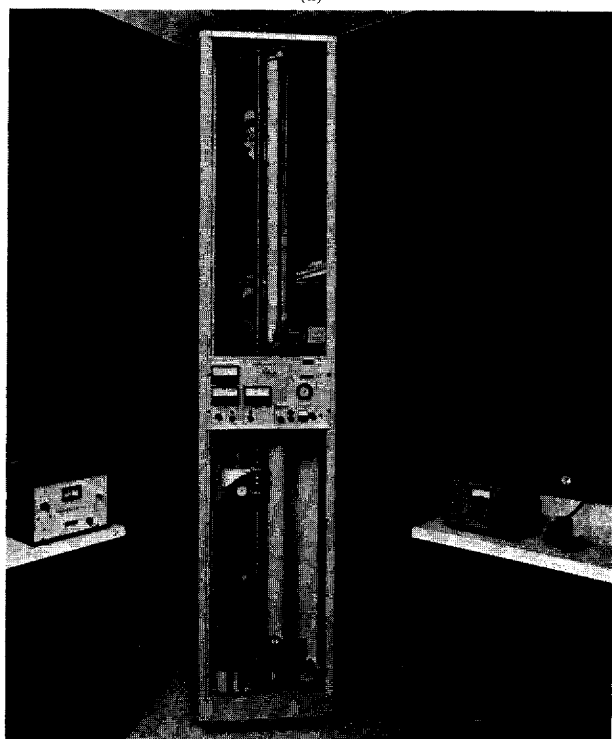
$$\Delta P^* = 9.806650 F_L(\rho_m^* - \rho_s^*)H^* \quad \text{Pa} \quad (3.20)$$

The *inch-of-water* differential-pressure unit is used in the differential-producer flow



$$P_1 - P_2 = F_L (\rho_m - \rho_s) H$$

(a)



(b)

Figure 3.6 (a) Basic U-tube-manometer principle. (b) High accuracy manometer. (Courtesy Schwien Engineering, Inc.)

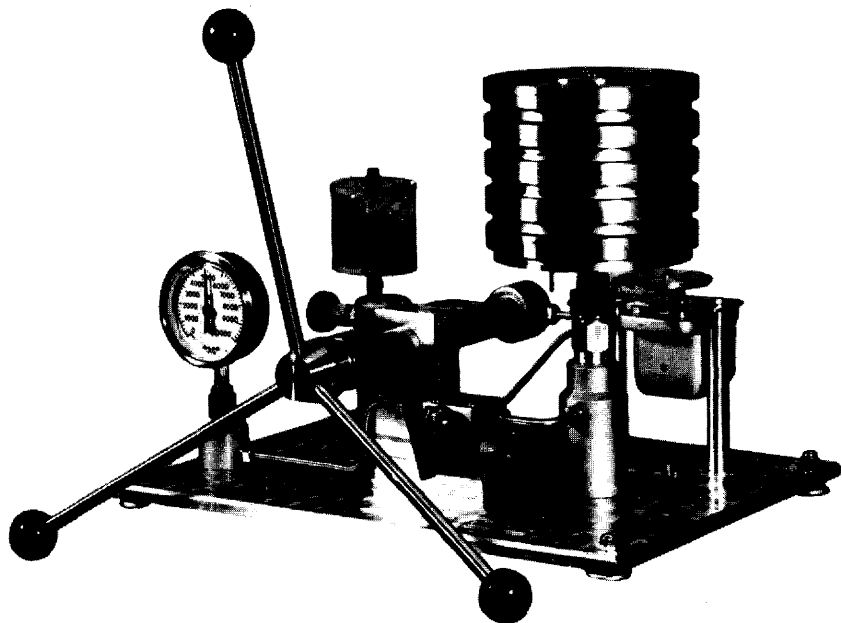


Figure 3.7 Precision deadweight tester. (Courtesy Chandler Engineering Co.)

equation. It is derived as the equivalent pressure read on a water-filled manometer at a specified temperature and at standard gravity (g_0) or, from Eq. (3.19),

$$\Delta P = \frac{g_l}{g_c} (\rho_w)_{T, g_0} H = (\rho_w)_{T, g_0} \frac{h_w}{12} \quad \text{lb}_f/\text{ft}^2 \quad (3.21)$$

Substituting the density of water at standard gravity, given by Eq. (2.77), yields the relationship between an inch of water (pressure) at 68°F and the differential pressure as

$$\Delta P = \frac{62.31572}{12} h_w = 5.192977 h_w \quad \text{lb}_f/\text{ft}^2 \quad (3.22)$$

Deadweight Tester. Shown in Fig. 3.8 are the basic elements of a deadweight gauge used to produce a reference calibration pressure. An accurately honed piston of known area is inserted into a cylinder, and standard masses are then placed on the platform. When the oil pump supplies sufficient pressure to raise the masses, the force exerted by the oil pressure over the piston area is balanced by the weight force. The pressure is then defined by

$$p_G = \frac{\mathbf{F}_{N,m}}{\text{piston area}} = \frac{\mathbf{F}_{N,m}}{A_p} \quad (3.23)$$

Deadweight testers using air instead of oil (Fig. 3.9) are also available, as well as compact portable pneumatic calibrators for field use.

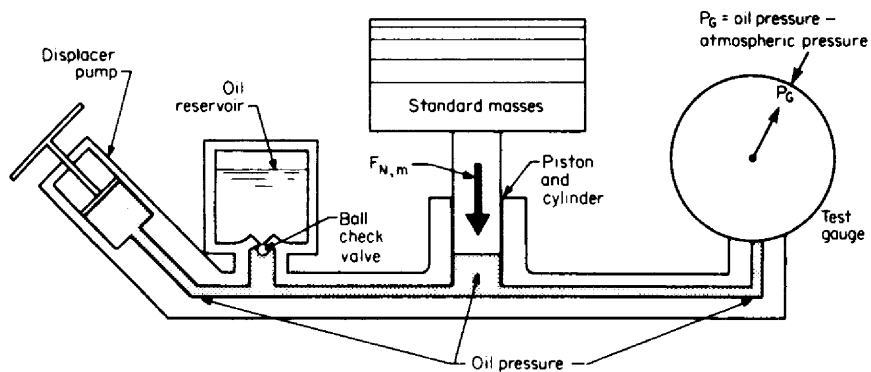


Figure 3.8 Oil deadweight tester.



Figure 3.9 Pneumatic deadweight tester. (Courtesy Ametek.)

When using deadweight testers, of either the oil or air type, it is important to apply all known corrections (bias errors) for local gravity, elevation, buoyancy, or thermal expansion of the piston, since these errors may be significant (>0.1 percent).

The deadweight tester (Fig. 3.9) uses the following correction factor for thermal, local gravity, and elevation effects.

$$p = \left\{ \frac{g_1(1 + 2.37 \times 10^{-7} H)}{g_{\text{calib}}[1 + 1.67 \times 10^{-5} (T_c - 23)]} \right\} p_{\text{weight}} \quad (3.24)$$

where H (in feet) is positive when the air tester is above the device being tested, p_{weight} is the pressure assigned to the weight, g_{calib} is the gravity value for which the tester is calibrated, and g_1 is the local gravity.

Differential Pressure. The dual-gas-operated deadweight tester (Fig. 3.10) is widely used to calibrate differential pressure transmitters at their operating static pressure. This device is used to determine bias error, usually used for correction purposes, at line static pressures up to 12,000 psia (83 MPa). The device first applies a common static pressure to the low- and high-pressure sides of the transmitter. The low-pressure side is then isolated, at the elevated pressure, and the high-pressure side then incremented upward over the desired differential range.

Accuracy is defined as the overall uncertainty in the measurement of the difference between two static pressures and a percentage of the differential pressure value, which depends upon the selected piston-cylinder and mass set (weights). Typically, at 1000 psia (7 MPa), the accuracy is estimated as ± 0.04 percent for a 10-psia (69-kPa) differential pressure.

Industrial Devices

The secondary devices used to measure differential pressure are commonly divided into two types—wet and dry. In the dry type (Fig. 3.11), the process fluid is isolated by a diaphragm; in the wet type, mercury usually is the separator. Mercury meters

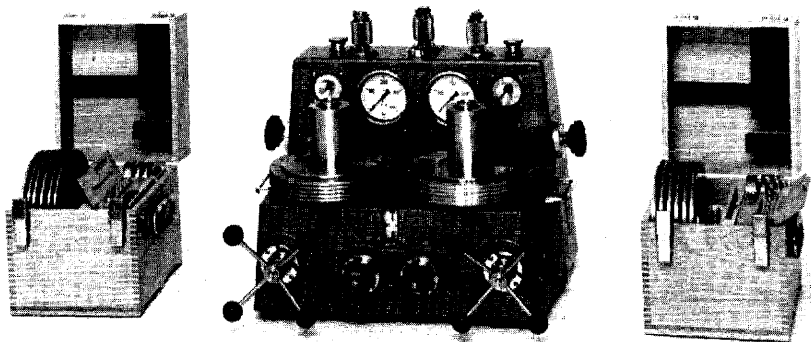


Figure 3.10 Differential pressure deadweight tester. (Courtesy DH instruments.)

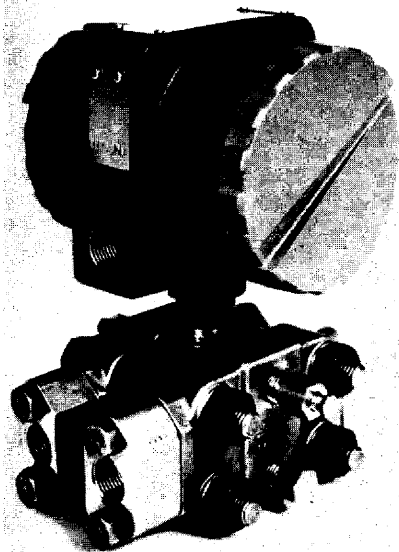


Figure 3.11 Dry-type differential-pressure transmitter. (Courtesy The Foxboro Co.)

were the mainstay of the process and natural gas industries for many years. However, they have been completely replaced by the dry type in the process industry, and dry-type bellows meter (Fig. 3.12), which requires no external power source, are rapidly replacing mercury meters in natural gas applications.

Dry Type. Dry-type devices are conveniently separated into motion and direct-measuring types. In the motion type (Fig. 3.12), the pressure difference across a diaphragm causes a bellows to move against a restraining spring. The motion, which can be recorded directly, is proportional to the differential pressure. In the direct-measuring type (Fig. 3.13a), small deflections of a diaphragm are either measured or restrained by a feedback force. The deflections may be detected via induction, capacitance, a strain gauge, or a taut resonating wire.

In the force-feedback device, the differential pressure is proportional to the feedback force. If the low-pressure side is evacuated, then the absolute pressure is measured (Fig. 3.14). Dry-type *transmitters* have an accuracy in the range of ± 0.1 to ± 1 percent of the upper range value (URV).

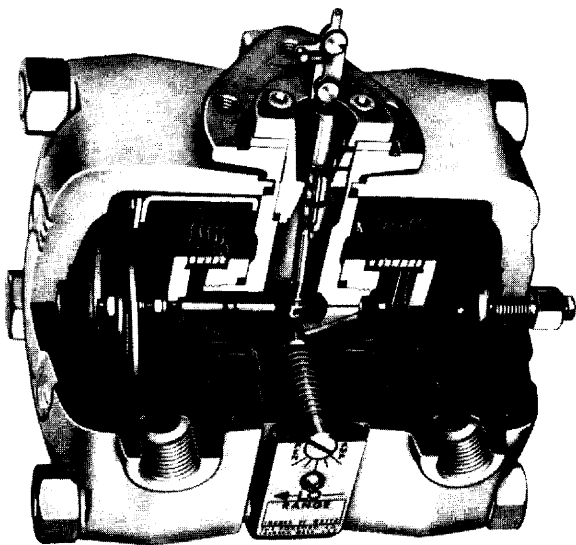


Figure 3.12 Bellows dry-type differential-pressure measuring device. (Courtesy The Foxboro Co.)

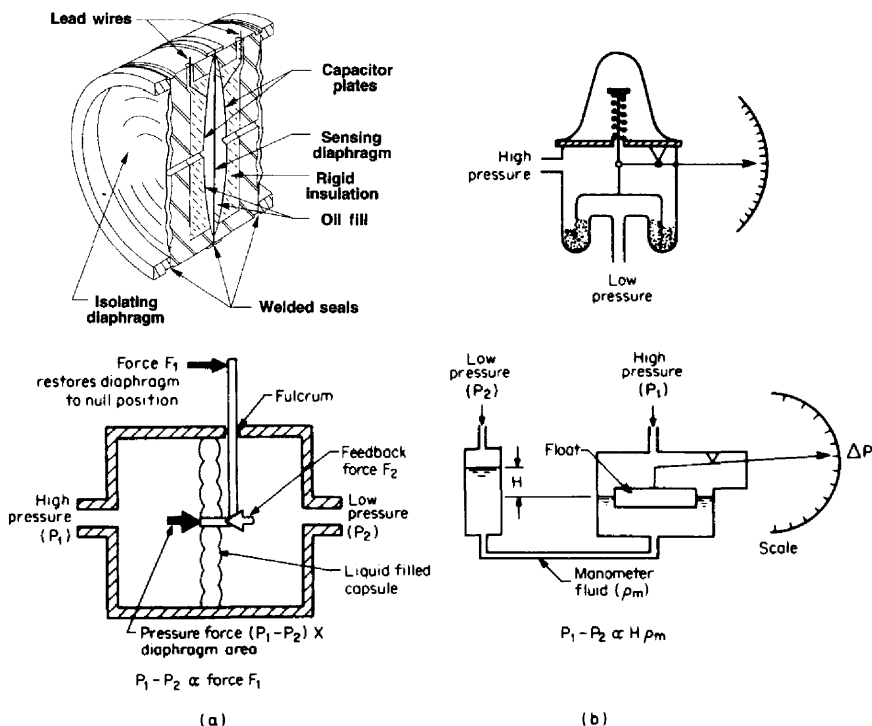


Figure 3.13 Dry and wet pressure or differential-pressure measuring devices. (a) Dry types. (Courtesy Rosemount, Inc.) (b) Wet types.

Table 3.2 lists the most common pressure transmitters, their relative accuracy, and basic operating principles, and Table 3.3 gives the typical ranges for differential pressure transmitters.

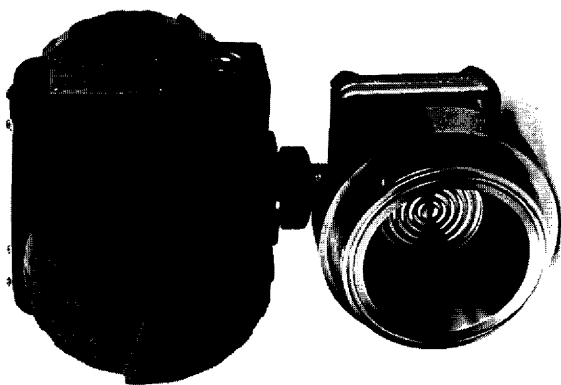
The *capacitance-type* transducers use a measuring diaphragm that moves relative to one or two fixed plates. An oscillator bridge circuit detects the changes in capacitance as the plate moves under the action of the applied force (pressure or differential). The very small mass, good frequency response, and high resolution yields excellent accuracy.

One of the most common pressure transducers are *strain gauges*. The gauges are usually mounted directly on the pressure sensor, supported by the sensing diaphragms, or bonded to cantilever springs which provide the restoring moment. The majority are unbonded wire, foil, or semiconductor techniques.

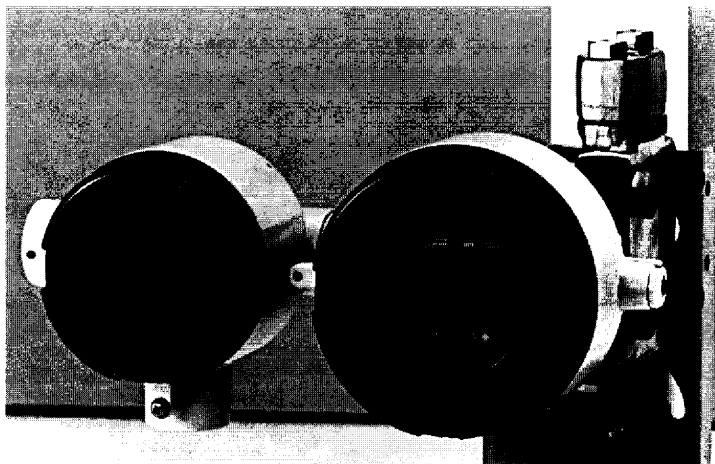
The *variable capacitance sensing module* (Fig. 3.13a) is a completely sealed module that allows direct electronic sensing of pressure-induced diaphragm deflection. Differential capacitance between the sensing diaphragm and the capacitor plates is electronically converted to a two-wire signal.

Pressure is transmitted through an isolating diaphragm, and oil fill fluid to a sensing diaphragm located in the center of the cell. The reference pressure is transmitted by the same method to the other side of the sensing diaphragm. The sensing diaphragm moves to a position that is proportional to the difference between the process and reference pressure.

Capacitance plates on both sides of the sensing diaphragm detect the position of the diaphragm. The capacitance between the sensing diaphragm and either capacitor is dependent upon, among other factors, the distance between the sensing diaphragm and the two capacitor plates. The capacitance-sensing element in the electronic requires an ac voltage to generate the capacitance signal. The ac voltage is supplied by an oscillator circuit. The signal from the oscillator circuit is capacitor-coupled to the transmitter case ground through the sensing capacitor. The difference in capacitance between the sensing diaphragm and each capacitor plate is converted to a proportional 4- to 20-mA signal.



(a)



(b)

Figure 3.14 Pressure measuring device. ((a) (Courtesy The Foxboro Co.)) ((b) Courtesy Johnson Yokogawa Corporation.))

The *piezoelectric* effect is caused when asymmetrical crystals are elastically deformed along specific axes, producing an electric potential within the crystal. This causes a flow of electric charge in the external electronic. This principle is widely used for measuring dynamic pressure, force and shock, or vibratory motion.

The *reluctive* types are distinguished primarily by the manner in which the exciting electric energy enters the system. In these devices, the energy is introduced as a magnetomotive force, which may be derived from a permanent magnet or from electromagnetism. In either case, it is the interaction of a magnetic field and an electric conductor to produce a current.

The linear-variable differential transformer (LVDT) is useful for laboratory measurements of growth, stress, thickness, vibration, shock, and contour. It is employed to provide electrical feedback for valves and actuators in servo control systems.

TABLE 3.2 Accuracy and Range for Pressure Transmitters

Principle	Accuracy, % _{URV}	Pressure element	Range
Strain gauge	0.1	Diaphragm with or without beam	0–20,000 psig
	0.1	Piezoresistive	0–5000 psig
Capacitive	0.1	Diaphragm	200 mmHg–10,000 psig
Piezoelectric	0.1	Distortion of crystal	0.1 mmHg–100,000 psig
Frequency change	0.2	Resonant wire	5–7 in H ₂ O
	0.025	Resonant crystal	0–20 psia
Potentionmetric	0.5	Bourdon tube	10–10,000 psig
	0.5	Diaphragm capsule	5–10,000 psig
Reluctive	0.25	Diaphragm	0 in H ₂ O–10,000 psig
	0.25	Bourdon tube	5 in H ₂ O–100,000 psig
Linear-variable differential transformer (LVDT)	0.15	Diaphragm	5 in H ₂ O–100 psi
	0.3	Bourdon tube	5 in H ₂ O–10,000 psig
Pneumatic	0.5	Bellows-null balance	0–15 psi
	0.5	Bellows-force balance	0–15 psi
Interferometric	†	Manometer	>0.029 psi

†Small fraction of a psi.

TABLE 3.3 Differential-Pressure Transmitter Ranges

Range	Differential pressure, in H ₂ O (kPa)	Static pressure, psi (MPa)
Low	0–5 to 0–25	500
	(0–1.2 to 0–6)	(3.5)
Medium	0–20 to 0–250	1500
	(0–5 to 0–62)	(10.5)
High	0–200 to 0–850	6000
	(0–50 to 0–210)	(42)

The advantages of the LVRT include an excellent linearity bobbin over long strokes (up to 24 in) and good temperature stability. A disadvantage is that the overall length must be double the stroke.

The *pneumatic* instruments combine a pressure-sensing element with a standard motion transmitter to detect the position of the pressure-sensing element and provide a linear 3- to 15-psi output signal. Best accuracy is achieved since the pressure-sensing element develops many times the 2-g force required for full-scale operation of the transmitter pilot.

Wet Type. Shown in Fig. 3.13*b* are the two basic wet-type meters—the inverted bell and the float type. In the inverted bell, the force developed by the differential pressure acting on the bell is opposed by a spring force. The motion of the bell is a direct measure of the differential pressure; and, with a sizeable bell, a considerable force can be developed and, hence, low differential pressures can be measured. Typical inverted-bell designs operate in the range of 0 to 10 in H₂O (0 to 2.5 kPa).

In the many float types, a cylindrical steel float chamber forms one side of a manometer and contains a steel disk floating on mercury. A cylindrical steel reference chamber forms the second side of the manometer. The area of this chamber is selected to give the desired mercury-level change for the operating differential pressure, which usually is from 20 to 200 in H₂O (5 to 50 kPa).

Intelligent Transmitters

The accuracies of standard industrial differential and pressure transmitters are specified at reference conditions for pressure and temperature. Deviation from these stated reference conditions results in additional error, usually a *bias error*. Depending on the desired measurement objective and operating conditions, these increased errors may or may not be present or acceptable.

Industrial instruments are designed to minimize thermal and static pressure errors; and for most noncritical applications, such as for control, these error sources do not warrant the additional cost for intelligent transmitters. However, for many applications the ability to change range and essentially eliminate pressure and temperature errors can be economically justified.

Shown in Fig. 3.11 is a differential pressure intelligent transmitter which may be configured with a hand-held terminal. This device has a primary *resonant wire* whose frequency is a function of the applied differential pressure. A microprocessor computes and transmits a digital or standardized 4- to 20-mA signal corrected to a reference calibration for differential pressure.

A hand-held configurator is used to change the upper range value (URV) or as a diagnostic aid. The stated accuracy for this secondary device is ± 0.1 percent URV.

Correction Factors

In practice, wet- and dry-type differential-pressure measuring devices are sometimes located a substantial distance above or below the pressure taps. The indicated pressure is then other than that at the taps, and an *elevation correction* is required. Bean (1957) gives an (extreme) illustration of the possible effects of elevation for a manometer located 50 ft (15.2 m) below an orifice. In this example, a +0.6 percent bias error is calculated.

For the wet type, the displacement of the manometer fluid by the lower-density process or seal fluid requires that a *manometer correction factor* be applied to the indicated reading. These two corrections are considered here.

Elevation Correction. The pressures at location H_{LL} below the pressure sources in Fig. 3.15 are

$$P_{f1'} = P_{f1} + \rho_{f1} F_L H_{LL} \quad P_{f2'} = P_{f2} + \rho_{f2} F_L H_{LL} \quad (3.25)$$

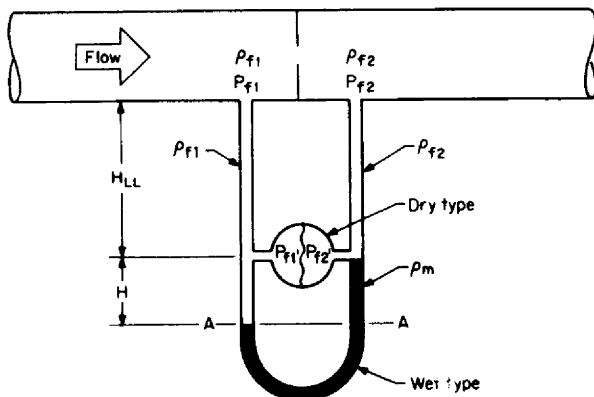


Figure 3.15 Schematic of wet- or dry-type device installation.

The relationship between the *true* and *indicated* differentials is then

$$\Delta P = (\Delta P)_{\text{ind}} - (\rho_{f1} - \rho_{f2}) F_L H_{LL} \quad (3.26)$$

For gas (vapor) and liquid flows with liquid-filled leads at the same temperature, no elevation correction is required ($\rho_{f1} = \rho_{f2}$). However, with gas-filled leads, the downstream lead is always at a lower density ($\rho_{f1} > \rho_{f2}$). Substituting the gas density equation (2.10) into Eq. (3.26) and expressing the pressure differences in inches of water h_w give the relationship between indicated and true differential pressure as

$$h_w = (h_w)_{\text{ind}} - 0.01874 \frac{F_L G H_{LL}}{Z_{f1} T_{f1}} h_w \quad (3.27)$$

An iterative solution is then necessary to calculate the true differential from the indicated reading. A negligible error is introduced, however, if it is assumed that the indicated and true differentials are equal; then

$$h_w = \left(1 - 0.01874 \frac{F_L G H_{LL}}{Z_{f1} T_{f1}} \right) (h_w)_{\text{ind}} \quad (3.28)$$

The elevation correction factor is then defined by

$$F_{EL} = 1 - 0.01874 \frac{F_L G H_{LL}}{Z_{f1} T_{f1}} \quad (3.29)$$

In this expression H_{LL} is positive for locations below the differential producer, and

negative for locations above. In the SI system, the elevation correction factor is similarly derived as

$$F_{EL}^* = 1 - 0.03416 \frac{F_L G H_{LL}^*}{Z_{f1} T_{K1}} \quad (3.30)$$

Manometer Factor. The manometer-factor correction is obtained by equating pressures at location AA as

$$P_{f1'} + F_L \rho_{f1} H = P_{f2'} + F_L \rho_m H \quad (3.31)$$

Rearranging yields

$$P_{f1'} - P_{f2'} = F_L \left(1 - \frac{\rho_{f1}}{\rho_m} \right) H \rho_m \quad (3.32)$$

Defining the pressure difference $P_{f1'} - P_{f2'}$ via Eq. (3.25) then yields

$$P_{f1} - P_{f2} = F_L F_{EL} \rho_m \left(1 - \frac{\rho_{f1}}{\rho_m} \right) H \quad (3.33)$$

Since wet-type devices are scaled to read in inches of water, the relationship between the true and indicated differential pressures becomes

$$h_w = F_{EL} F_M (h_w)_{ind} \quad (3.34)$$

for U.S. units, and

$$\Delta p^* = F_{EL}^* F_M^* (\Delta p^*)_{ind} \quad (3.35)$$

for SI units, where F_M is the *manometer factor* defined by

$$F_M = \left(1 - \frac{\rho_{f1}}{\rho_m} \right) F_L \quad (3.36)$$

for U.S. units, and

$$F_M^* = \left(1 - \frac{\rho_{f1}^*}{\rho_m^*} \right) F_L \quad (3.37)$$

for SI units.

In the development of these equations, the fluid density over the manometer is assumed to be that of the upstream process fluid. If a seal liquid is used, then its density ρ_s should be substituted into Eq. (3.33) or (3.34). For gases (vapors), density is calculated with Eq. (2.10) for U.S. units and with Eq. (2.11) for SI units.

If the manometer fluid is water, Eq. (2.171) can be used to calculate density. If the fluid is mercury, the density (ANSI/API 2530, 1991) is given by

$$\rho_{Hg} = [1 - 0.000101(T_F - 60)]846.324 \quad (3.38)$$

Example 3.3. A deadweight tester with weights *trimmed* at a location with a local gravity of 32.164 ft/s² is used to calibrate a pressure gauge at a location 2000 ft (609.6 m) above sea level and at 10° latitude. What is the actual pressure if 100-psig weights are used? (Assume the air-buoyancy correction is the same for both locations.)

At the new location, the local gravity correction is, by Eq. (3.3),

$$(F_L)_2 = 1 - 2.637 \times 10^{-3} \cos(2)(10) - (9.6 \times 10^{-8})(2000) - 5 \times 10^{-5} \\ = 0.99728 \text{ lb}_f/\text{lb}_m$$

At the original location, the local gravity correction is

$$(F_L)_1 = \frac{32.164}{32.174} = 0.99969 \text{ lb}_f/\text{lb}_m$$

Since weights of the same mass are used, the pressure at the new location can be obtained by combining Eqs. (3.13) and (3.23) as

$$\frac{(p_G)_1 A_p}{(F_L)_1 F_{FB} m_s} = \frac{(p_G)_2 A_p}{(F_L)_2 F_{FB} m_s}$$

Since the masses, buoyancy, and piston areas are the same,

$$(p_G)_2 = 100 \frac{0.99728}{0.99969} = 99.76 \text{ psig}$$

Example 3.4. A dry-type differential-pressure transducer is located 50 ft (15.2 m) above an orifice flowmeter measuring the natural gas of Example 2.7. If the indicated differential pressure is 100 in H_2O , what is the true differential pressure for lead lines at the same temperature as the process? (Use $g_f = 32.162 \text{ ft/s}^2$.)

From Example 2.7, $G = 0.73$, $Z_f = 0.878$, and $T_f = 499.7^\circ\text{R}$ (40°F). The location correction factor for density within the leads is, from Eq. (3.3),

$$F_L = \frac{32.162}{32.174} = 0.9996 \text{ lb}_f/\text{lb}_m$$

From Eq. (3.28) the true differential pressure is

$$h_w = \left[1 - 0.01874 \frac{(0.9996)(0.73)(-50)}{(0.878)(499.7)} \right] (100) = 100.16 \text{ in } \text{H}_2\text{O}$$

Example 3.5. A wet-type mercury-filled meter based on the manometer principle is manifolded at the same position as the dry-type transducer of Example 3.4. What is its reading?

The density of the gas over the mercury is calculated with Eq. (2.10) as

$$\rho_{f1} = 2.69883 \frac{(0.73)(400 + 14.7)}{(0.878)(499.7)} = 1.862 \text{ lb}_m/\text{ft}^3$$

The density of the mercury at 40°F is, by Eq. (3.38),

$$\rho_{\text{Hg}} = 846.324[1 - (0.000101)(40 - 60)] = 848.034 \text{ lb}_m/\text{ft}^3$$

Equation (3.34) can be written as

$$(h_w)_{\text{ind}} = \frac{h_w}{F_{EL} F_M}$$

where, from Eq. (3.36),

$$F_M = \left(1 - \frac{1.862}{848.03}\right)(0.9996) = 0.9974$$

Substitution then gives

$$(h_w)_{\text{ind}} = \frac{100.16}{(1.0016)(0.9974)} = 100.26 \text{ in H}_2\text{O}$$

TEMPERATURE

Scales

In 1968, the International Committee on Weights and Measures adopted several changes in the empirical temperature scale. This work is reported in "The International Practical Temperature Scale of 1968." In it, the kelvin (K) was adopted as the basic thermodynamic temperature unit.

Although this new scale better approximates the thermodynamic scale, it has yet to replace the empirical equations used to calculate absolute temperatures. These are

$$T_{\circ\text{R}} = T_{\circ\text{F}} + 459.67 \quad (3.39)$$

for degrees Rankine, and

$$T_K = T_{\circ\text{C}} + 273.15 \quad (3.40)$$

for kelvins, with the relationship between the Fahrenheit and Celsius scales being defined by

$$T_{\circ\text{F}} = \frac{9}{5}T_{\circ\text{C}} + 32 \quad (3.41)$$

and

$$T_{\circ\text{C}} = \frac{5}{9}(T_{\circ\text{F}} - 32) \quad (3.42)$$

The equation relating Rankine temperatures to the kelvin temperature scale is

$$T_{\circ\text{R}} = \frac{9}{5}T_K \quad (3.43)$$

Measurement

Many temperature-measuring devices are based on the thermal expansion of a solid, liquid, or gas, on a thermoelectric measurement in which a thermally induced electromotive force (emf) is used to infer temperature, or on the measurement of a resistance change in either a precision resistor or a thermistor. Of these, the most commonly used are the mercury-in-glass thermometer, the gas (or vapor) expansion thermometer, the thermocouple, and the resistance thermometer.

Mercury-in-Glass Thermometer. The mercury-in-glass thermometer (Fig. 3.16a) is widely used in both laboratory and industry because of its basic simplicity. The typical thermometer consists of a bulb-reservoir and a capillary. As heat is trans-

ferred into the bulb, the mercury rises due to thermal expansion and displaces a sealed inert gas. The temperature is then read on a scale calibrated in the units of interest.

It is important that the thermometer be used under the conditions that prevailed during calibration. Specifically, thermometers are calibrated either partially or completely immersed in a temperature bath. If they are used under other conditions, then a stem correction is required. Benedict (1984) gives several examples concerning stem correction. In one, a total-immersion thermometer immersed only to the 200°F (93°C) mark is in error by 4 percent when used to measure an 814°F (434°C) temperature.

Gas (or Vapor) Expansion Thermometer. This thermometer operates on the principle that a gas expands at constant volume as its temperature is increased. In the industrial device shown in Fig. 3.16*b*, a change in temperature at the sensor causes a change in gas pressure. This pressure change is transferred by the thermal-system capsule to a change in force on the force bar. The design of the force-balance mechanism allows the bar to pivot imperceptibly about a pair of cross-flexure fulcrums when the gas pressure changes. This small bar motion causes a change in the clearance between the nozzle and the top of the force bar, resulting in a change in the relay output pressure. In addition to changing the output signal of the trans-

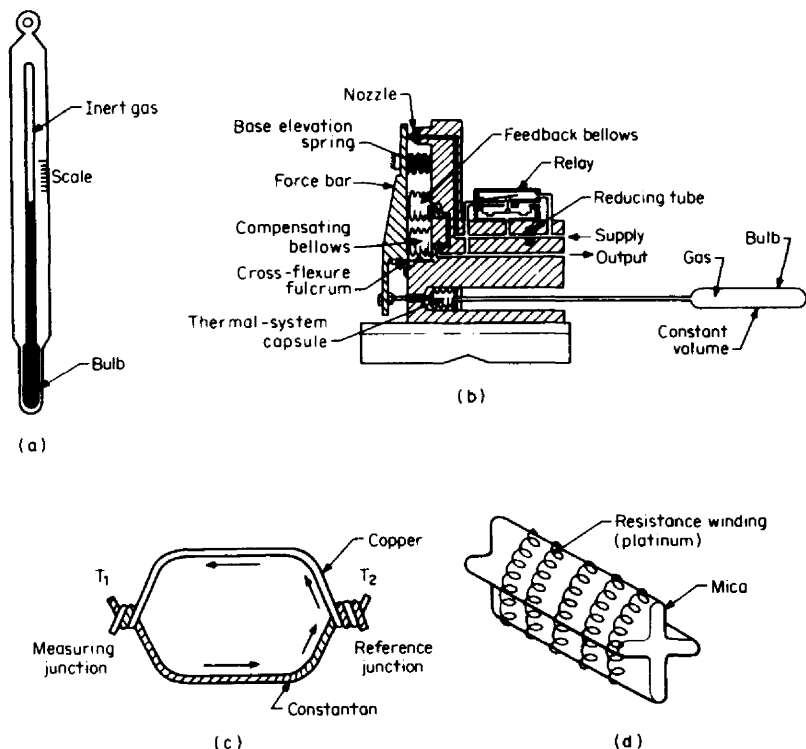


Figure 3.16 Thermometers. (a) Mercury in glass. (b) Gas-expansion thermometer (Courtesy The Foxboro Co.) (c) Simple thermocouple. (d) Platinum resistance thermometer.

mitter, this change in pressure is applied to the force bar by the feedback bellows. Thus the moments about the cross-flexure fulcrums are kept in equilibrium, and the output signal of the transmitter is proportional to the measured temperature.

Nitrogen is almost always used as the fill gas since it can be used over a wide temperature range and because it is available as a high-quality gas. The scale is nearly linear, and the temperature limits range from -350 to 1400°F (-220 to 760°C).

Since a fluid's vapor pressure depends only on the free-surface temperature of a liquid, a measured vapor pressure can also be used to indicate temperature. The *vapor-actuated* thermometer is similar to the gas thermometer, with the bulb casing being larger to contain all the liquid when the temperature is below that of the capillary and thermal-system capsule.

Thermocouples. The thermocouple provides a reliable and accurate temperature indication for many industrial applications. In its simplest form it consists of a pair of dissimilar conductors joined together at both ends, as shown in Fig. 3.16c. If the temperature is to be measured at T_1 , a reference temperature is maintained at T_2 , and the emf produced is related to the temperature by a polynomial fitting equation. Depending on the combination of conductors and the desired temperature range, the order of the polynomial may extend from second to ninth.

The temperature-emf characteristics of a thermocouple depend upon the materials used in the element of the thermocouple and the temperature to which they are subjected. The selection of materials for thermocouple elements is subject to at least the following requirements:

1. The materials should be able to withstand the extremes of the temperature to be measured, without significant deterioration, for a suitable period of time.
2. A relatively large emf should be developed per degree change in temperature so that the instrument can be used to determine small temperature changes.
3. The emf should increase with increasing temperature continuously over the range of use.
4. The materials should maintain their original temperature-emf characteristics for long periods. Consistency of calibration is largely dependent upon freedom from contamination and mechanical strains. These introduce nonhomogeneities in the thermocouple elements.
5. The materials should be homogeneous and capable of easy standardization. They should be commercially available to permit replacement without the necessity of recalibrating the temperature-measuring instrument.
6. The materials should be capable of being formed into an adequately strong thermocouple assembly to meet installation and application requirements.

The ISA designations, temperature ranges, and limits of error for several of the more common combinations of thermocouple conductors are presented in Table 3.4. In Fig. 3.17 are shown several thermocouple types.

Resistance Thermometers. The industrial resistance thermometer is widely used because of its accuracy and basic simplicity; temperature changes of 0.03°F (0.02°C) are easily detected in industrial processes. The measurement range of this instrument is about the same as that of the copper-constantan thermocouple, iron-constantan thermocouple, and expansion thermometer; these limits are approximately -300 to 1200°F (-184 to 689°C).

The resistance thermometer requires no reference junction, since it operates on a measured change in the resistance of a metal or semiconductor (thermistor) with temperature. Usually the metal is platinum, copper, or nickel, and the semiconductor of a metallic oxide.

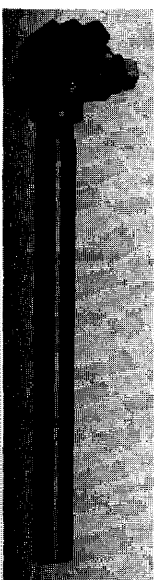
For a pure metal, the relationship between temperature and resistance is expressed as a series expansion in temperature with constant coefficients:

$$R_{\text{temp}} = (1 + aT_{\text{C}} + bT_{\text{C}}^2 + cT_{\text{C}}^3 + \cdots)R_{\text{ref}} \quad (3.44)$$

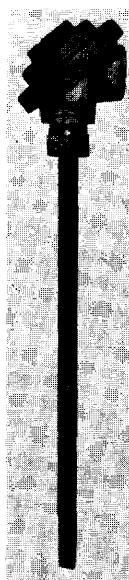
where R_{ref} is the resistance, in ohms, at a reference temperature, usually 0°C (32°F), and R_{temp} is the measured resistance. For many applications, an average coefficient of resistance is assumed, and all terms with powers higher than the first are assumed zero. For platinum, a second-order equation accurately predicts behavior at temperatures up to 1200°F (649°C). Copper sensors are less expensive than platinum sensors and quite linear. However, these are limited to temperatures up to 250°F

TABLE 3.4 Designations and Limits of Error of Thermocouples and Thermocouple Wires

ISA designation	Material (positive vs. negative element)	Temperature	Limit of error, %	
			°F	°C
Type T	Copper vs. copper-nickel	−328 to 32°F (−200 to 0°C)	± 2.7	± 1.5
	(copper-constantan)	32 to 700°F (0 to 350°C)	± 1.35	± 0.75
Type J	Iron vs. copper-nickel	32 to 1400°F (0 to 1400°C)	± 1.35	± 0.75
	(iron-constantan)			
Type E	Nickel-chromium vs. copper-nickel	−328 to 32°F (−200 to 0°C)	± 1.8	± 1.0
	(chromel-constantan)	32 to 2300°F (0 to 1250°C)	± 0.9	± 0.5
Type K	Nickel-chromium vs. nickel-aluminum	−328 to 32°F (−200 to 0°C)	± 3.6	± 2.0
	(chromel-alumel)	32 to 2300°F (0 to 1250°C)	± 1.35	± 0.75
Type R	Platinum 13% rhodium vs. platinum (Pt 13 Rh-Pt)	32 to 2700°F (0 to 1450°C)	± 0.34	± 0.25
Type S	Platinum 10% rhodium vs. platinum (Pt 10 Rh-Pt)	1600 to 3100°F (870 to 1700°C)	± 0.34	± 0.25
Type B	Platinum 30% rhodium vs. platinum 6% rhodium (Pt 30 Rh-Pt 6 Rh)	1600 to 3100°F (870 to 1700°C)	± 0.9	± 0.5



(a)



(b)



(c)

Figure 3.17 Thermocouple types. (Courtesy *The Foxboro Co.*) (a) Wire type. (b) PYOD type. (c) Minox type.

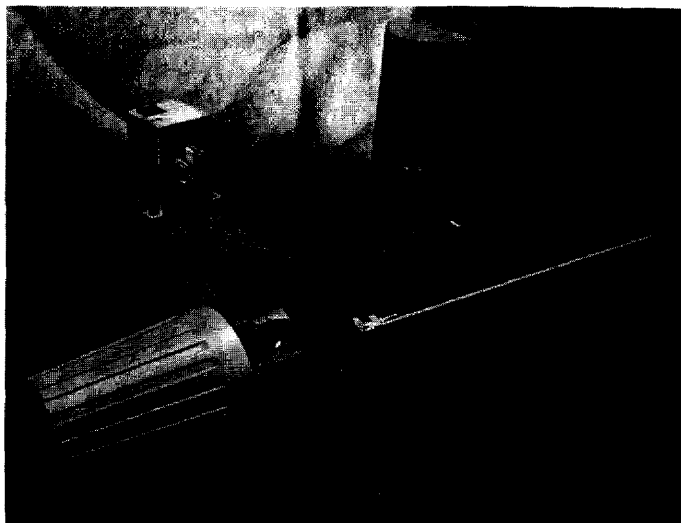


Figure 3.18 Industrial RTD temperature transmitter. (Courtesy *The Foxboro Co.*)

(121°C). Nickel is quite nonlinear and has an upper temperature limit of 600°F (316°C). Because of its inherent stability and linearity, the basic platinum resistance temperature detector (RTD), shown in Figs. 3.16*d* and 3.18, continues to dominate the field in resistance thermometers.

The thermistor is classified as a semiconductor because its electric conductivity falls between that of an insulator and that of a conductor. The name thermistor comes from *thermally sensitive resistor*—the resistance of a thermistor varies as a function of temperature.

The thermistor is a solid semiconductor with a high temperature coefficient of resistivity. The variation of resistance with temperature can be approximated with a simple exponential equation of the form

$$R_{\text{temp}} = a \exp \frac{b}{T_f} \quad (3.45)$$

where R_{temp} is the resistance at the measured absolute temperature T_f . The constants a and b are typically 0.06 and 8000, respectively.

Thermometer Wells

In numerous applications, it is neither desirable nor practical to expose a temperature sensor directly to a process material. Thermometer wells are, therefore, used to protect against damage from corrosion, erosion, abrasion, and high-pressure processes. A well is also useful in protecting a sensor from physical damage during handling and normal operation. When the ambient temperature is significantly higher than the flowing temperature or when the well is exposed to direct sunlight, heat conduction along the well can raise the indicated temperature by 2 to 3°F. In these cases, care must be taken to properly insulate the thermometer well.

Wells are provided in many configurations; some of these are depicted in Fig. 3.19. The open-end type can either be plain or have a lagging extension. A lagging length of 3 in (75 mm) is standard, but other lengths are available. For mounting purposes, there is a choice of external threads or process flanges. The external threads can be obtained in either NPT or SI metric sizes, and the process flanges are made to either ANSI or ISO specifications. The closed end of a well can have either a straight or tapered tip, or a straight tip with a reinforced neck. A sanitary well is also available for use in food industries. This special purpose well has a tapered tip but no external threads or flange. It is usually welded in a sanitary fitting, pipeline, or storage tank.

Temperature of a Moving Stream

It is important that the true static temperature at the location of the point of pressure measurement be used in the state equation for density. For other fluid properties, or for dimensional corrections for temperature, the temperature should be adjusted to the point of interest.

There are three corrections that need to be considered, all of which are quite small and usually considered negligible. However, for laboratory-type work or in custody transfer applications, where all errors need to be considered, corrections also should be considered.

True Temperature. The true (static) temperature of a moving fluid is recorded only if the thermometer is located in a large reservoir or is moving at the same velocity as the stream (see Fig. 3.20*a,b*). However, practical measurements are made with a thermometer at rest with respect to the fluid, and the mass flow impact on the measuring device gives a reading higher than the static temperature. The maximum difference would be observed for an isentropic compression of the fluid to the stagnation temperature (Fig. 3.20*c*). In practice, this maximum is seldom achieved because of thermometer losses, fluid frictional effects, thermometer well design, and other factors. The indicated temperature is then somewhere between the static and theoretical stagnation temperature (Fig. 3.20*d*).

For liquids the difference between static and theoretical stagnation temperatures is quite small. Benedict (1984) gives an example concerning 200°F (93°C) water

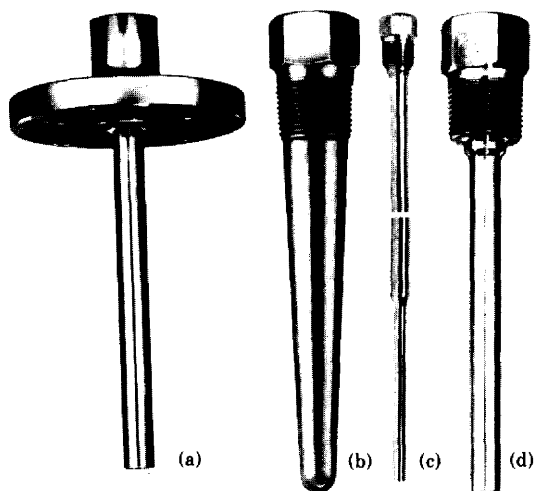


Figure 3.19 Thermometer wells. (Courtesy The Foxboro Co.) (a) Plain flanged solid. (b) Lagged threaded tapered. (c) Plain threaded welded. (d) Plain threaded solid.

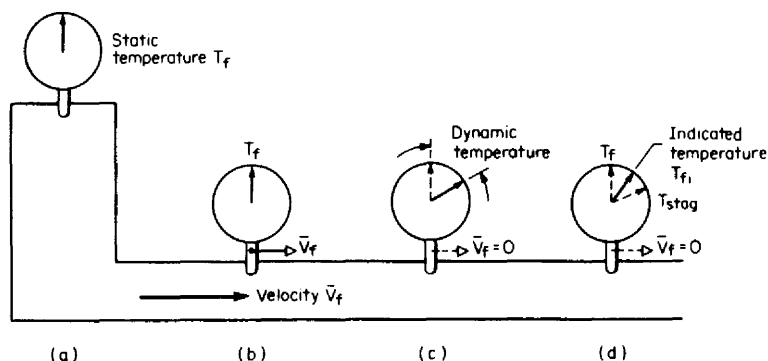


Figure 3.20 Temperatures of a moving stream.

flowing at 20 ft/s (6.1 m/s); the difference between static and indicated temperature is only 0.002°F (0.001°C). For gases, however, the effect is not always insignificant.

The correction is made by introducing a recovery factor expressed, in U.S. units, by

$$T_f = T_{fi} - \frac{M_w \bar{V}_f^2}{2g_c C_p J} F_{RF} \quad (3.46)$$

and, for SI units,

$$T_K = T_{Ki} - \frac{M_w \bar{V}_f^2}{2C_p} F_{RF} \quad (3.47)$$

where F_{RF} , which ranges from 0.9 to 1.0, is the recovery factor, T_{fi} (T_{Ki}) is the indicated temperature (°R, K), M_w is the molecular weight [$\text{lb}_m/(\text{lb}_m \cdot \text{mol} \cdot ^\circ\text{R})$, $\text{kg}/(\text{kg} \cdot \text{mol} \cdot \text{K})$], g_c is the U.S. dimensional conversion constant [$32.17405 \text{ lb}_m/(\text{lb}_f \cdot \text{s}^2)$], \bar{V}_f is the fluid velocity (ft/s, m/s), and J is the conversion (U.S. units) of $\text{ft} \cdot \text{lb}_f$ to Btu ($J = 778.16934 \text{ ft} \cdot \text{lb}_f/\text{Btu}$).

Gas (Vapor) Expansion Corrections

Figure 3.21 illustrates the temperature profile along a pipe axis when a flow conditioner (see Chap. 5) and a flowmeter that produces a differential pressure are installed. It is seen that the temperature depends upon the pressure gradient along the pipe axis.

In practice, the thermal well is located either 20 pipe diameters upstream of the primary element or 4 to 8 pipe diameters downstream (see Chap. 8). The pressure tap location may either be at the upstream tap (p_{f1}) or the downstream tap (p_{f2}) for a differential producer; for linear meters (vortex, turbine, etc.), the pressure tap location is defined by the manufacturer. A temperature directional bias error, and hence an error in density in the density calculation, then results.

The bias error is small and normally considered negligible. However, a correction based on an isentropic expansion, or an *isenthalpic expansion*, across the flowmeter after pressure recovery can be used to adjust the temperature from the thermal well location to the point of interest. This assumes that the pipe is lagged and thermally insulated (no heat transfer) and that no work enters or leaves the system.

Isenthalpic Expansion from Upstream Thermal Well to Primary Element. In the absence of heat transfer and work, the gas temperature is lowered by pipe friction and flow conditioner, if present, over the 20 pipe diameter length between thermal well and upstream pressure tap. The thermal gradient can be calculated by assuming isenthalpic conditions as

$$\frac{T_{f1'} - T_{f1}}{p_{f1'} - p_{f1}} = \left(\frac{\partial T}{\partial p} \right)_H = \frac{R_{0E} T_{f1}}{p_{f1} C_p} \left(\frac{\partial Z}{\partial T} \right)_p = \frac{Z' R_{0E} T_{f1}}{p_{f1} C_p} \quad (3.48)$$

where $T_{f1'}$ is the upstream temperature, T_{f1} is the temperature at the upstream tap, $p_{f1'} - p_{f1}$ is the pressure loss, R_{0E} is the universal gas constant [$\text{Btu}/(\text{lb}_m \cdot \text{mol} \cdot ^\circ\text{R})$, $\text{J}/(\text{kg} \cdot \text{mol} \cdot \text{K})$], p_{f1} is the pressure at the upstream tap (psia, Pa), C_p is the real gas

heat capacity at constant pressure [$\text{Btu}/(\text{lb}_m \cdot \text{mol} \cdot ^\circ\text{R})$, $\text{J}/(\text{kg} \cdot \text{mol} \cdot \text{K})$], and $(\partial Z/\partial T)_p$ is the partial derivative of compressibility.

Isentropic Expansion across the Primary Element. The minimum temperature is at the minimum pressure (downstream pressure tap). Assuming an isentropic expansion, the relationship between an upstream temperature measurement T_{f1} and the true temperature at a flange, corner, or $D/2$ (radius tap) is

$$\frac{T_{f1}}{T_{f2}} = \left(\frac{p_{f1}}{p_{f2}} \right)^{(k-1)/k} = \left(\frac{p_{f2} + h_w/27.73}{p_{f2}} \right)^{(k-1)/k} \quad (3.49)$$

where k is the isentropic exponent, T_{f1} is the temperature at the upstream tap, T_{f2} is the temperature at the downstream tap, h_w is the differential pressure, and p_{f1} and p_{f2} are the respective pressures.

Isenthalpic Expansion to a Downstream Thermal Well. The overall pressure loss (see Chap. 6) of the primary element results in a decrease in temperature at the downstream thermal well. An isenthalpic expansion results in the following relationship:

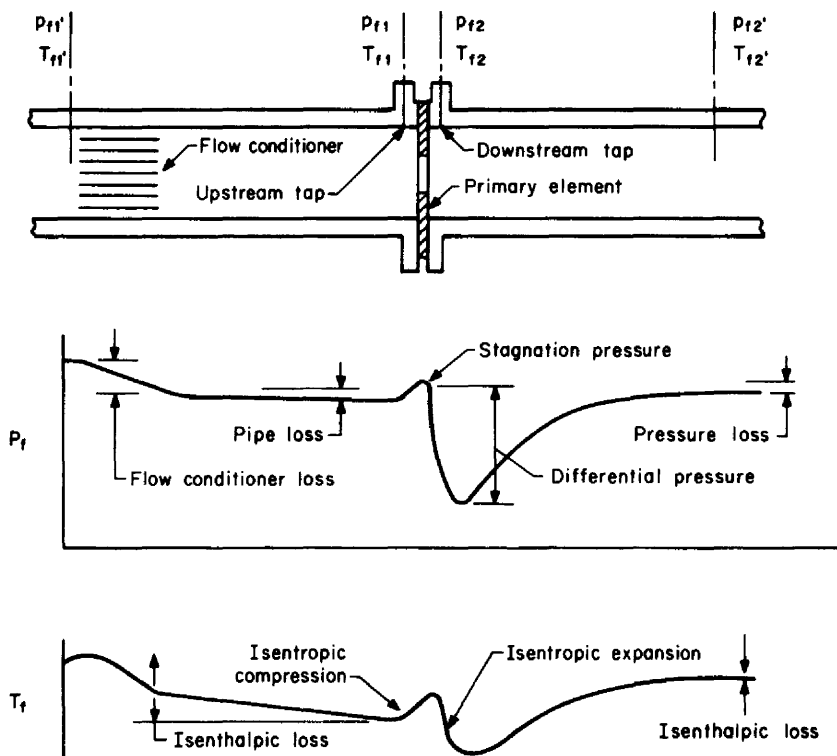


Figure 3.21 Pressure and temperature profile along a pipe (not to scale).

$$\frac{T_{f1} - T_{f2'}}{p_{f1} - p_{f2'}} = \left(\frac{\partial T}{\partial p} \right)_H = \frac{R_{0E} T_{f2'}}{p_{f2'} C_p} \left(\frac{\partial Z}{\partial T} \right)_p = \frac{Z'_f R_{0E} T_{f2'}}{p_{f2'} C_p} \quad (3.50)$$

Example 3.6. A 60 percent methane, 20 percent ethane, and 20 percent propane natural gas mixture is moving at 80 ft/s (26 m/s) in an 8-in (250-mm) pipe. A resistance thermometer (RTD) indicates a temperature of 100°F (37.8°C) when inserted in a thermal well 8 pipe diameters downstream of a 0.6 beta ratio orifice flowmeter. Assuming a thermal recovery factor of 0.9, estimate the temperature, correct (true) density at the downstream pressure tap, and directional density bias error when the flowing differential pressure is 100 in (25 kPa) and the overall pressure loss is 65 in (16 kPa).

The following data is available: Indicated density ρ_i based on a pressure of 2000 psia and a temperature of 100°F:

$$\rho_i = 14.3193 \text{ lb}_m/\text{ft}^3 \text{ at } p_{f2} = 2000 \text{ psia and } T_{f2i} \text{ of } 100^\circ\text{F}$$

$$M_w = 24.45926 \text{ lb}_m/(\text{lb}_m \cdot \text{mol} \cdot ^\circ\text{R}) \quad k = 2.285$$

$$C_p = 21.28373 \text{ Btu}/(\text{lb}_m \cdot \text{mol} \cdot ^\circ\text{R}) \quad Z'_f = (\partial Z / \partial T)_p = 1.853 \times 10^{-3} \text{ R}^{-1}$$

The true temperature at the thermal well $T_{f2'}$ (see Fig. 3.21) with the indicated temperature $T_{f2i} = (459.67 + 100) = 559.67$, by Eq. (3.46), is

$$T_{f2'} = T_{f2i} - \frac{M_w \bar{V}_f^2}{2g_c C_p J} F_{RF} = 559.67 - \frac{(24.45926)(80)^2(0.9)}{(2)(32.174)(21.284)(778.16)} = 559.5378$$

The temperature is first adjusted to the upstream pressure tap by Eq. (3.50) with $p_{f2'} = (2000 + h_w/27.73) = (2000 + 16/27.73) = 2002.344$ psia,

$$\frac{T_{f1} - T_{f2'}}{p_{f1} - p_{f2'}} = \frac{Z'_f R_{0E} T_{f2'}}{p_{f2'} C_p} = \frac{(1.853 \times 10^{-3})(1.9589)(559.54)}{(2002.344)(21.2837)} = 4.765 \times 10^{-5}$$

With $p_{f1} - p_{f2'} = 65/27.73 = 2.344$ psia, the upstream temperature T_{f1} is $T_{f1} = 559.54 + (4.765 \times 10^{-5})(2.344) = 559.5379^\circ\text{R}$

Note that the difference $(T_{f1} - T_{f2'})$ is only 0.0001.

The temperature at the downstream tap is now calculated, with Eq. (3.49):

$$\frac{T_{f1}}{T_{f2}} = \left(\frac{p_{f2} + h_w/27.73}{p_{f2}} \right)^{(k-1)/k} = \left(\frac{2000 + 100/27.73}{2000} \right)^{(2.285-1)/2.285} = 1.00101$$

The true temperature at the downstream pressure tap is then

$$T_{f2} = T_{f1}/1.00101 = (559.5379)/1.00101 = 558.8126$$

The true density ρ_i at the downstream tap, corrected for the true temperature T_{f2} , by ratioing Eq. (2.10), is

$$\rho_i = \frac{2.669 p_{f2} G / Z_{f2} T_{f2}}{2.699 p_{f2'} G / Z_{f2'} T_{f2'}} \rho_i = \frac{T_{f2'}}{T_{f2}} \rho_i \frac{559.67}{558.81} 14.319 = 14.341 \text{ lb}_m/\text{ft}^3$$

where $p_{f2} = p_{f2'}$ and $Z_{f2} \approx Z_{f2'}$.

With ρ_i denoting the indicated density and ρ_t the true density, the directional density bias error, with Eq. (4.5), is

$$B_\rho = \frac{\rho_i - \rho_t}{\rho_t} 100 = \frac{14.3193 - 14.34129}{14.34129} 100 = -0.15 \text{ percent}$$

SMART TRANSMITTERS

Intelligent or *smart* transmitters were initially differential and temperature transmitters but now include absolute pressure, gauge pressure, and a *smart* flow transmitter (Fig. 3.22) which combines all of the measured variables used to compute the flow rate. Vortex, electromagnetic, Coriolis, and other types of flowmeters are also designed as *smart* meters.

In the system shown in Fig. 3.23 the sensor signal is digitized and then linearized, reranged, engineering unit conversions obtained, and communication and diagnostics performed by the dedicated transmitter's microprocessor. System communication is accomplished by a remote hand-held terminal (HHT) that is attached into the standardized 4- to 20-mA loop at the desired location. Digital system communication is either carried out on the 4- to 20-mA loop or may be a total digital communication along the field bus.

Typically the transmitter's output, percentage of span (or upper range value), zero suppression, or elevation, model number, tag number, date of calibration, etc., can be displayed remotely. Digital transmitters (Bbullar, 1994) are generally used in applications that require a high level of performance in terms of stability, diagnostics, wide range, and accuracy.

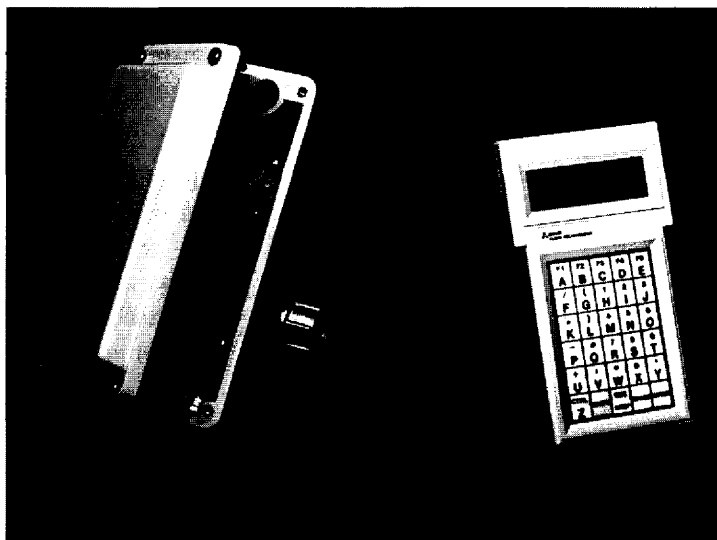
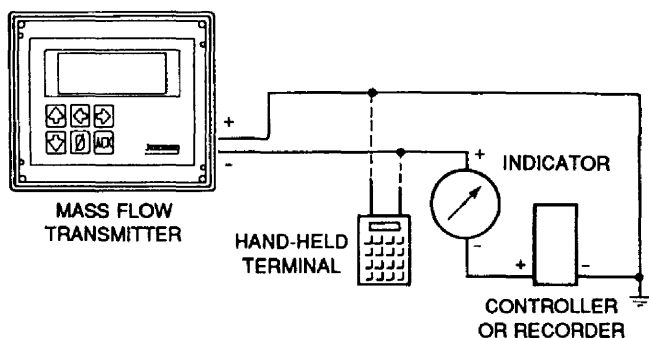


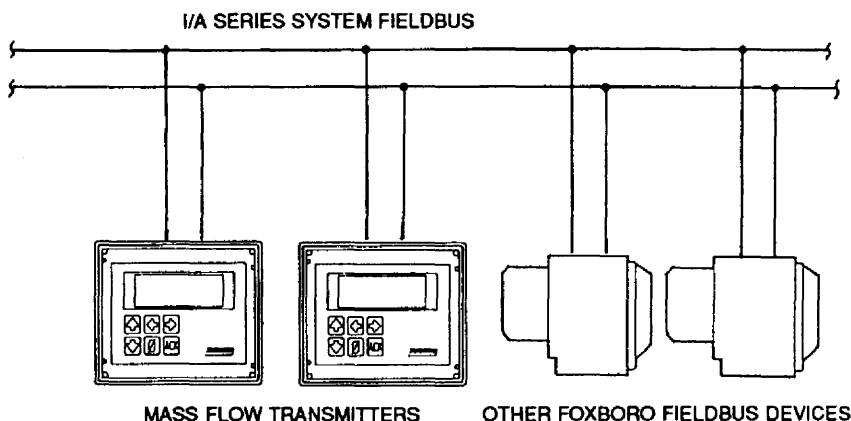
Figure 3.22 Smart flow transmitter. (Courtesy EG&G Flow Technology, Inc.)

A differential pressure transmitter that uses a resonant single-crystal silicon sensor is described in Nishikawa et al. (1993) and Larson (1994). The sensor and diaphragm are fabricated by three-dimensional micromachining techniques that ensure low hysteresis, stability, high sensitivity, and reproducibility. The *digital* frequency can be measured by a microprocessor with no A/D conversion that degrades accuracy. The transmitter measures differential as low as 0.4 in (100 Pa).

The *smart flow transmitter* shown in Figure 3.22 extends the versatility of the microprocessor to the field (McCoy, 1992). The transmitter processes the inputs from the flowmeter, temperature, and pressure transmitters and computes compensated volumetric or mass flow rate for all fluids. Viscosity and density corrections are performed within the software with a cubic spline, or linear interpolation is available for flow-rate linearization. Pressure and temperature inputs can be either 4 to 20 mA or voltage. The data from individual transmitters can be transmitted, either scaled or unscaled, to a control room for individual sensor observation.



(a)



(b)

Figure 3.23 Smart transmitter installation. (a) 4–20 mA output. (b) Digital output. (Courtesy The Foxboro Co.)

Flow rates are calculated in either mass or volumetric units. The mass flow-rate unit is time-dependent only—that is, in pounds-mass per hour, per second, or per day. However, the volumetric unit may be calculated in gallons, cubic feet, or cubic meters per unit time at flowing temperature or at a specified base temperature. To distinguish between mass-flow, base-volume, and actual volumetric units, an uppercase subscript will be used for mass-flow and base-volume units, and lowercase for flowing volumetric flow-rate units. Table 3.5 lists the symbols and subscripting that will be used in this book.

Liquid flow rates are almost always calculated in volume units (gallons per minute), and gas flows in standard cubic feet per hour. Vapor flows, such as of steam and ammonia, are usually calculated in mass units of pounds-mass per hour.

Fundamental Volumetric Flow-Rate Unit

In the English engineering system, the fundamental volume flow-rate unit is the cubic foot per second. Under the assumption that the velocity profile is one-dimensional and is represented by an average value (see Fig. 3.24), the flow rate may be calculated as

$$q_{cfs} = A_p \bar{V}_f = \frac{\pi}{4} \left(\frac{D}{12} \right)^2 \bar{V}_f = 5.454154 \times 10^{-3} D^2 \bar{V}_f \quad (3.51)$$

where D is in inches, and \bar{V}_f is in feet per second. In the SI system the corresponding equation is

$$q_{cms}^* = A_p^* \bar{V}_f^* = \frac{\pi}{4} \left(\frac{D^*}{1000} \right)^2 \bar{V}_f^* = 7.853982 \times 10^{-7} D^{*2} \bar{V}_f^* \quad (3.52)$$

where D^* is in millimeters and \bar{V}_f^* is in meters per second.

Relationship between Mass and Volumetric Units

Flowmeters may be grouped in four broad classes, depending on their principle of operation:

1. Velocity-measuring (vortex, turbine, ultrasonic, magnetic)
2. Discrete volume-measuring (positive displacement)
3. Velocity- and density-dependent (orifice, nozzle, venturi)
4. True mass flowmeters

Depending on the desired flow-rate unit, mass-flow continuity may be used to derive an equation relating a mass flow to a volumetric flow or base to flowing volume units. The relationship between the volumetric and mass flow-rate units for a density measurement is

$$q_{PPS} = \rho_f q_{cfs} \quad (3.53)$$

for the U.S. system, and

TABLE 3.5 Subscribing for Flow Rate and Total Flow

Symbols	Meaning	Units	
		U.S.	SI
Flow rate			
$q_{a\text{cfs}}, q_{a\text{cfm}}, q_{a\text{cfh}}, q_{a\text{cfd}}$	Gas (vapor) volumetric flow rate at <i>flowing</i> conditions	ft ³ /s, ft ³ /min, ft ³ /h, ft ³ /24h	
$q_a^* \text{ cms}, q_a^* \text{ cmm}, q_a^* \text{ cmh}, q_a^* \text{ cmd}$	Gas (vapor) volumetric flow rate at <i>flowing</i> conditions		m ³ /s, m ³ /min, m ³ /h, m ³ /24h
$q_a^* \text{ lps}, q_a^* \text{ lpm}, q_a^* \text{ lph}, q_a^* \text{ lpd}$	Gas (vapor) volumetric flow rate at <i>flowing</i> conditions		L/s, L/min, L/h, L/24h
$q_{b\text{pa}}, q_{b\text{pm}}, q_{b\text{ph}}, q_{b\text{pd}}$	Liquid volumetric rate at <i>flowing</i> conditions	bbl/s, bbl/min, bbl/h, bbl/24h	
$q_{c\text{fs}}, q_{c\text{fm}}, q_{c\text{fh}}, q_{c\text{fd}}$	Liquid volumetric flow rate at <i>flowing</i> conditions	ft ³ /s, ft ³ /min, ft ³ /h, ft ³ /24h	
$q_c^* \text{ ms}, q_c^* \text{ mm}, q_c^* \text{ mh}, q_c^* \text{ md}$	Liquid volumetric flow rate at <i>flowing</i> conditions		m ³ /s, m ³ /min, m ³ /h, m ³ /24h
$q_l^* \text{ ps}, q_l^* \text{ pm}, q_l^* \text{ ph}, q_l^* \text{ pd}$	Liquid volumetric flow rate at <i>flowing</i> conditions		L/s, L/min, L/h, L/24h
$q_{\text{KPS}}, q_{\text{KPM}}, q_{\text{KPH}}, q_{\text{KPD}}$	Liquid and gas (vapor) mass flow rate		kg/s, kg/min, kg/h, kg/24h
$q_{\text{PPS}}, q_{\text{PPM}}, q_{\text{PPH}}, q_{\text{PPD}}$	Liquid and gas (vapor) mass flow rate	lb _m /s, lb _m /min, lb _m /h, lb _m /24h	
$q_{\text{BPS}}, q_{\text{BPM}}, q_{\text{BPH}}, q_{\text{BPD}}$	Liquid volumetric flow rate at $T_F = 60^\circ\text{F}$, $p_b = 14.696$ psia	bbl/s, bbl/min, bbl/h, bbl/24h	
$q_{\text{CFS}}, q_{\text{CFM}}, q_{\text{CFH}}, q_{\text{CFD}}$	Liquid volumetric flow rate at $T_F = 60^\circ\text{F}$, $p_b = 14.696$ psia	ft ³ /s, ft ³ /min, ft ³ /h, ft ³ /24h	
$q_{\text{GPS}}, q_{\text{GPM}}, q_{\text{GPH}}, q_{\text{GPD}}$	Liquid volumetric flow rate at $T_F = 60^\circ\text{F}$, $p_b = 14.696$ psia	gal/s, gal/min, gal/h, gal/24h	
$q_{\text{LPS}}, q_{\text{LPM}}, q_{\text{LPH}}, q_{\text{LPD}}$	Liquid volumetric flow rate at $T_C = 15.56^\circ\text{C}$, $p_b = 101.3$ kPa	L/s, L/min, L/h, L/24h	

$q_{SCFS}, q_{SCFM}, q_{SCFH}, q_{SCFD}$	Standard gas (vapor) volumetric flow rate at <i>ISO</i> 5024 base, $T_b = 518.67^\circ\text{R}$, $p_b = 14.69595$	$\text{ft}^3/\text{s}, \text{ft}^3/\text{min}, \text{ft}^3/\text{h}, \text{ft}^3/24\text{h}$	
$(q_{SCFS})_b, (q_{SCFM})_b, (q_{SCFH})_b, (q_{SCFD})_b$	Standard gas (vapor) volumetric flow rate at <i>selected</i> base temperature and pressure	$\text{ft}^3/\text{s}, \text{ft}^3/\text{min}, \text{ft}^3/\text{h}, \text{ft}^3/24\text{h}$	
$q_{SCMS}^*, q_{SCMM}^*, q_{SCMH}^*, q_{SCMD}^*$	Standard gas (vapor) volumetric flow rate at <i>ISO</i> 5024 base, $T_{KB} = 288.15\text{ K}$, $p_b^* = 101.325\text{ kPa}$		$\text{m}^3/\text{s}, \text{m}^3/\text{min}, \text{m}^3/\text{h}, \text{m}^3/24\text{h}$
$q_{NCMS}^*, q_{NCMM}^*, q_{NCMH}^*, q_{NCMD}^*$	Normal gas (vapor) flow rate at normal base temperature and pressure, $T_{KB} = 273.15$, $p_b^* = 101.325\text{ kPa}$		$\text{m}^3/\text{s}, \text{m}^3/\text{min}, \text{m}^3/\text{h}, \text{m}^3/24\text{h}$
$(q_{SCMS}^*)_b, (q_{SCMM}^*)_b, (q_{SCMH}^*)_b, (q_{SCMD}^*)_b$	Standard gas (vapor) volumetric flow rate at <i>selected</i> base temperature and pressure		$\text{m}^3/\text{s}, \text{m}^3/\text{min}, \text{m}^3/\text{h}, \text{m}^3/24\text{h}$
$q_{SLPS}^*, q_{SLPM}^*, q_{SLPH}^*, q_{SLPD}^*$	Standard gas (vapor) volumetric flow rate at <i>ISO</i> 5024 base, $T_{KB} = 288.15\text{ K}$, $p_b^* = 101.325\text{ kPa}$		$\text{L}/\text{s}, \text{L}/\text{min}, \text{L}/\text{h}, \text{L}/24\text{h}$
$(q_{SLPS}^*)_b, (q_{SLPM}^*)_b, (q_{SLPH}^*)_b, (q_{SLPD}^*)_b$	Standard gas (vapor) volumetric flow rate at <i>selected</i> base temperature and pressure		$\text{L}/\text{s}, \text{L}/\text{min}, \text{L}/\text{h}, \text{L}/24\text{h}$
Total flow			
Q_{acf}	Gas (vapor) total volume	ft^3	
Q_{acm}^*	Gas (vapor) total volume		m^3

TABLE 3.5 Subscribing for Flow Rate and Total Flow (*Continued*)

Symbols	Meaning	Units	
		U.S.	SI
Q_{bbl}	Liquid total volume at flowing conditions	bbl	
Q_{cf}	Liquid total volume at flowing conditions	ft ³	
Q_{cm}^*	Liquid total volume at flowing conditions		m ³
Q_{gal}	Liquid total volume at flowing conditions	gal	
Q_{l}^*	Liquid total volume at flowing conditions		L
Q_{kg}^*	Total mass—liquid, gas (vapor)		kg
Q_{lb_m}	Total mass—liquid, gas (vapor)	lb _m	
Q_{BBL}	Liquid total volume at $T_F = 60^\circ\text{F}$, $p_b = 14.696$ psia	bbl	
Q_{L}^*	Liquid total volume at $T_{\text{c}} = 15.56^\circ\text{C}$, $p_b^* = 101.3$ kPa		L
Q_{NCM}^*	Gas (vapor) total volume at normal base temperature and pressure, $T_{\text{KB}} = 273.15$, 101.325 kPa		m ³
Q_{SCF}	Gas (vapor) total volume at <i>ISO 5024 base</i> , $T_b = 518.67^\circ\text{R}$, $p_b = 14.69595$ psia	ft ³	
$(Q_{\text{SCF}})_b$	Gas (vapor) total volume at <i>selected base</i> temperature and pressure	ft ³	
Q_{SL}^*	Gas (vapor) total volume at <i>ISO 5024 base</i> , $T_{\text{Kb}} = 288.15$ K, $p_b^* = 101.325$ kPa		L
$(Q_{\text{SL}}^*)_b$	Gas (vapor) total volume at <i>selected base</i> temperature and pressure		L
Q_{SCM}^*	Gas (vapor) total volume at <i>ISO 5024 base</i> , $T_{\text{Kb}} = 288.15$ K, $p_b^* = 101.3245$ kPa		m ³
$(Q_{\text{SCM}}^*)_b$	Gas (vapor) total volume at <i>selected base</i> temperature and pressure		m ³

$$q_{KPS}^* = \rho_f^* q_a^* \text{ cms} \quad (3.54)$$

for the SI system.

If density is calculated using the pvT equation, substitution of Eq. (2.10) into Eq. (3.53) gives the relationship for U.S. units as

$$q_{PPS} = 2.698825 \frac{GP_f}{Z_f T_f} q_{acfs} \quad (3.55)$$

A similar substitution of Eq. (2.11) into Eq. (3.54) yields the SI-unit relationship

$$q_{KPS}^* = 2.483407 \frac{GP_{af}^*}{Z_f T_k} q_a^* \text{ cms} \quad (3.56)$$

Flowing Gallons per Minute

The gallon is a volumetric unit defined as exactly 0.13368056 ft^3 (0.003785412 m^3). The flow rate in gallons per minute at flowing conditions is then defined in terms of the flowing volumetric flow rate in cubic feet per second as

$$q_{\text{gpm}} = \frac{60}{0.13368056} q_{\text{cfs}} = 448.8312 q_{\text{cfs}} \quad (3.57)$$

and in terms of the average pipeline velocity as

$$q_{\text{gpm}} = 2.447994 D^2 \bar{V}_f \quad (3.58)$$

Base Gallons per Minute

In the United States, liquid flow rates are often calculated in either gallons or barrels per unit time, referred to a base temperature of 60°F (15.6°C) rather than at the

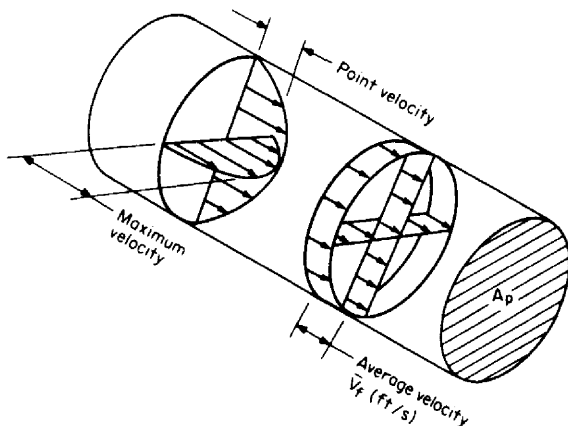


Figure 3.24 Average velocity used to derive volumetric flow-rate unit.

flowing temperature. ISO Standard 5024(1981) on petroleum liquids adopts 59°F (15°C) as the reference temperature, and it is expected that this will eventually replace 60°F (15.6°C).

A flowmeter can be scaled to either base or actual volumetric flow-rate units. The relationship between actual and base gallons is illustrated in Fig. 3.25. In Fig. 3.25a, the flowmeter is scaled to actual gallons per minute, and the tank level will indicate the same volume as the integrated flowmeter's output. This volume is, however, lower when the liquid temperature is reduced to a base of 60°F (15.6°C) (the values shown are exaggerated for emphasis). In Fig. 3.25b the flowmeter is scaled to indicate base volume. In this case, for a temperature higher than the base temperature, the tank level will always be higher than the integrated meter output. In both cases the base volume remains the same, provided the liquid has the same density at 60°F (15.6°C).

Equating the mass flow at flowing temperature to the mass flow rate at base temperature gives the following relationship between flowing and base volumes:

$$q_{PPS} = \rho_f q_{cfs} = \rho_b q_{CFS} \quad (3.59)$$

or, the base volume may be defined via the ratio of flowing to base density as

$$q_{CFS} = \frac{\rho_f}{\rho_b} q_{cfs} \quad q_{CMS}^* = \frac{\rho_f^*}{\rho_b^*} q_{c_{ms}}^* \quad (3.60)$$

Equation (3.60) is the basic equation that relates the measured flow rate to any base

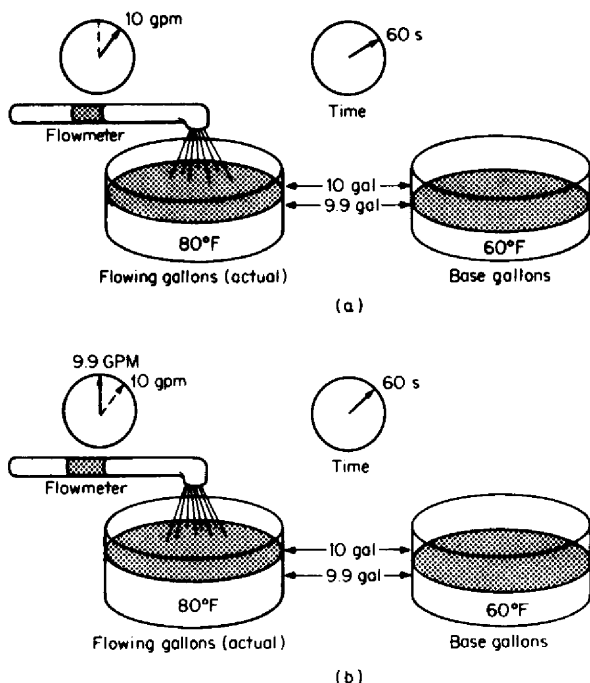


Figure 3.25 Flowmeters scaled to indicate flowing or base volumetric units. (a) Flowmeter scaled to flowing gallons per minute q_{gpm} . (b) Flowmeter scaled to base gallons per minute q_{GPM} .

volume, in both U.S. and SI units and for both liquids and gases (vapors). For base gallons per minute, the equation can be written in terms of density or specific gravity as

$$q_{\text{GPM}} = \frac{\rho_f}{\rho_b} q_{\text{gpm}} = \frac{G_f}{G_b} q_{\text{gpm}} = \frac{F_p G_F}{G_b} q_{\text{gpm}} \quad (3.61)$$

Provided consistent volume and time units are used, any volume units, such as barrels, cubic meters, or liters, can be used in Eq. (3.61) to convert between volume at flowing conditions and a selected base volume.

THE STANDARD AND NORMAL CUBIC FOOT (METER)

In the United States the standard cubic foot is the most commonly used gas volume unit. It is standardized in ISO 5024 (1981) for petroleum gas (natural gas) as the volume the flowing gas would occupy at a pressure of 14.69595 psia (101.325 kPa) and a temperature of 59°F (15°C). However, other pressures and temperatures are more commonly used for natural gas, oxygen, and nitrogen volumes. The base selected depends on the industry, the country long-term usage, and often contractual requirements. For example in Europe it is common to use either a *standard* cubic meter or a *normal* cubic meter as a volumetric unit. The standard cubic meter uses a temperature base of 60°F (15.56°C) with the normal cubic meter base temperature being 32°F (0°C) and the pressure base for both being 14.69595 psia (101.325 kPa).

If density is measured, the relationship between actual and standard volumetric flow at a selected base is defined by Eq. (3.60) as

$$(q_{\text{SCFS}})_b = \frac{\rho_f}{\rho_b} q_{\text{acfs}} = \frac{\rho_f}{\rho_b} q_{\text{cfs}} = \frac{q_{\text{PPS}}}{\rho_b} \quad (3.62)$$

In this equation, the lowercase subscript acfs has been added because gas flows are commonly referred to as *actual* cubic feet rather than as cubic feet, although technically there is no difference.

In the SI system, the flow in standard cubic meters per second at a selected base is calculated as

$$(q_{\text{SCMS}})_b = \frac{\rho_f^*}{\rho_b^*} q_{\text{a cms}}^* \quad (3.63)$$

If the density is calculated from the p_vT equation, the substitution of Eq. (2.10) into Eq. (3.62) gives the selected-base-volume flow rate as

$$(q_{\text{SCFS}})_b = \frac{Z_b}{Z_f} \frac{T_b}{T_f} \frac{p_f}{p_b} q_{\text{acfs}} \quad (3.64)$$

for U.S. units, and

$$(q_{\text{SCMS}})_b = \frac{Z_b}{Z_f} \frac{T_{Kb}}{T_K} \frac{p_f^*}{p_b^*} q_{\text{a cms}}^* \quad (3.65)$$

for SI units.

At the ISO Standard 5024 base of 14.69595 psia (101.325 kPa) and 59°F (15°C) Eqs. (3.64) and (3.65) become

$$q_{\text{SCFS}} = 35.29340 \frac{Z_b}{Z_f} \frac{P_f}{T_f} q_{\text{acfs}} \quad (3.66)$$

for U.S. units, and

$$q_{\text{SCMS}}^* = 2.843819 \frac{Z_b}{Z_f} \frac{P_f^*}{T_K} q_{\text{a cms}}^* \quad (3.67)$$

for SI units.

Primary Constants and Standard Conditions for Gas Flows

To make exact comparisons among mass-flow, flowing-volume, and standard-volume flow rates, it is necessary to specify the *standard* conditions selected for pressure, temperature, air density, and the primary constants used in the gas density equation. Table 3.6 lists those that will be used for gases in this handbook in the development of the engineering equations.

Example 3.7. The gasoline of Example 2.16(1) is flowing in a 2-in (50-mm) schedule-80 pipe. The measured flow rate is 100 gal/min (6.31 L/s) at base conditions. Determine (1) the flow rate in actual gallons per minute, (2) the flow rate in actual cubic feet per second, (3) the mass flow rate in pounds per day, and (4) the average pipeline velocity in feet per second. (See Examples 9.1 and 9.3 for the sizing of an orifice for these conditions.)

1. Actual gallons per minute. From Examples 2.12 and 2.16(1),

$$G_F = 0.7255 \quad G_b = 0.7359 \quad F_p = 1.0088$$

TABLE 3.6 ISO Standard Conditions and Primary Constants for Developing Gas Flow Equations

STANDARD CONDITIONS†	
Pressure	14.69595 psia (101.325 kPa)
Temperature	59°F (518.67°R, 15°C, 288.15 K)
PRIMARY CONSTANTS	
Universal gas constant‡	10.73151 psia·ft ³ /(lb _m ·mol·°R) [8.31441 J*/(g·mol·K)]
Acceleration of gravity <i>g</i> ₀	32.17405 ft/s ² (9.806650 m/s ²)
AIR AT STANDARD CONDITIONS	
Compressibility <i>Z</i> §	0.9995824
Molecular weight‡	28.96247 lb _m /(lb _m ·mol)
Density (dry)	0.0765002 lb _m /ft ³ (1.225416 kg/m ³)

†ISO 5024 (1981).

‡Jones (1978).

§Interpolated to seventh place using Redlich-Kwong equation of state.

Substitution into Eq. (3.61), rewritten to solve for flowing gallons per minute, gives

$$q_{\text{gpm}} = \frac{G_b}{F_p G_F} q_{\text{GPM}} = \frac{0.7359}{(1.0088)(0.7255)}(100) = 100.55 \text{ gal/min}$$

2. *Actual cubic feet per second.* With Table C.1, the conversion equation can be written as

$$q_{\text{cfs}}(2.831685\text{E} - 02) = q_{\text{cms}} = q_{\text{gpm}}(6.309020\text{E} - 05)$$

$$q_{\text{cfs}} = \frac{6.309020 \times 10^{-5}}{2.831685 \times 10^{-2}} q_{\text{gpm}} = (2.228009 \times 10^{-3})(100.55) = 0.22403 \text{ ft}^3/\text{s}$$

or Eq. (3.57) may be rearranged to yield

$$q_{\text{cfs}} = \frac{q_{\text{gpm}}}{448.8312} = \frac{100.55}{448.8312} = 0.22403 \text{ ft}^3/\text{s}$$

3. *Mass flow rate in pounds-mass per day.* From Eq. (3.53), $q_{\text{PPS}} = \rho_f q_{\text{cfs}}$. The flowing density ρ_f is, by Eqs. (2.203) and (2.175),

$$\begin{aligned} \rho_f &= F_p \rho_F = 62.3663 F_p G_F = (1.0088)(0.7255)(62.3663) \\ &= 45.6449 \text{ lb}_m/\text{ft}^3 \end{aligned}$$

$$\begin{aligned} \text{then } q_{\text{PPD}} &= (24)(3600)\rho_f q_{\text{cfs}} = (24)(3600)(45.6449)(0.22403) \\ &= 883,512 \text{ lb}_m/\text{day} \end{aligned}$$

4. *Average pipeline velocity.* From Table B.1, for 2-in schedule-80 pipe, $D = 1.939$; then, by Eq. (3.51) rearranged to solve for \bar{V}_f ,

$$\bar{V}_f = \frac{q_{\text{cfs}}}{(\pi/4)(D/12)^2} = \frac{0.22403}{(\pi/4)(1.939/12)^2} = 10.93 \text{ ft/s}$$

Example 3.8. Natural gas is flowing at 340 standard m^3/h (ISO Standard 5024 base) in a 52.50-mm (2.067-in) pipe. For the design information given below, determine (1) the actual flow rate in actual cubic meters per hour, (2) the mass flow rate in kilograms per hour, (3) the average pipeline velocity in meters per second, and (4) the standard cubic feet per hour. The design information is

$$p_f^* = 184 \text{ kPa} \quad T_K = 300 \text{ K} \quad G = 0.652$$

$$Z_f = 0.9995 \quad D^* = 52.50 \text{ mm} \quad Z_b = 1.0$$

1. *Actual cubic meters per hour.* Equation (3.63) can be rewritten for an hourly basis as

$$q_{\text{acmh}}^* = \frac{\rho_b^*}{\rho_f^*} q_{\text{SCMH}}^*$$

where ρ_f^* and ρ_b^* are calculated at flowing and base conditions using Eq. (2.11) as

$$\rho_f^* = 3.483407 \frac{Gp_f^*}{Z_f T_K} = 3.483407 \frac{(0.652)(184)}{(0.9995)(300)} = 1.39369 \text{ kg/m}^3$$

$$\text{and } \rho_b^* = 3.483407 \frac{Gp_b^*}{Z_b T_{Kb}} = 3.483407 \frac{(0.652)(101.325)}{(1.0)(288.15)} = 0.79864 \text{ kg/m}^3$$

Substitution then yields

$$q_{\text{acmh}}^* = \frac{0.79864}{1.39369} 340 = 194.83 \text{ m}^3/\text{h}$$

2. *Mass flow rate.* Equation (3.54) in hourly flow-rate units is

$$\begin{aligned} q_{\text{KPH}}^* &= \rho_f^* q_{\text{acmh}}^* \\ &= (1.39369)(194.83) = 271.54 \text{ kg/h} \end{aligned}$$

3. *Average pipeline velocity.* Rearranging Eq. (3.52) and substituting yields

$$\begin{aligned} \bar{V}_f^* &= \frac{q_{\text{cms}}^*}{(\pi/4)(D^*/1000)^2} \\ &= \frac{194.83/3600}{(\pi/4)(52.50/1000)^2} = 25.00 \text{ m/s} \end{aligned}$$

4. *Standard cubic feet per hour.* Table C.1 shows the conversion $(\text{ft}^3/\text{s})(2.831685 \text{ E} - 02) = \text{m}^3/\text{s}$. Then

$$\begin{aligned} q_{\text{SCFH}} &= \frac{q_{\text{SCMH}}^*}{2.831685 \times 10^{-2}} = \frac{340}{2.831685 \times 10^{-2}} \\ &= 12,007 \text{ standard ft}^3/\text{h} \end{aligned}$$

FLOW CALIBRATION STANDARDS

All flowmeters initially are tested using a flow-rate standard to establish the relationship between the meter indicated flow rate (or indicated total flow) and the *true flow rate*. The true rate is established in a flow laboratory that maintains reference standards traceable to national standards. In the case of the differential producers (orifice, nozzle, venturi, etc.) sufficient data has been accumulated to derive an equation that will predict, within acceptable accuracy limits, the discharge coefficient from measured dimensions. In the standards written by the codifying bodies (ASME, ISO, etc.) these equations are assigned an overall uncertainty value and a usable Reynolds number range.

A flowmeter should be flow-calibrated using accepted reference standards to achieve improved accuracy or confidence that the metering is within the desired limits. Since flow rate is not a single measurement, but a combination of several measurements, it is important that laboratory bias errors, procedures, and statistical documentation be scrupulously maintained.

Liquid Calibration

Two calibration standards are generally used for liquid meter calibration, the weighing (mass) and the volumetric methods. In both, the determination of mass or volume may be made either dynamically or statically. The weighing method is standardized in ANSI/ASME MFC-9M (1995) and in ISO 4185 (1985).

Static Weighing. In the static weighing method (Fig. 3.26a) the liquid, usually water, is diverted into a collection tank located on a weighing mechanism at the start of the test and then diverted back into the reservoir after a suitable collection of mass and other readings is obtained in order to meet accuracy objectives. The initial weight (tare) is subtracted from the final weight (gross) to obtain the net mass that passed through the meter under test. This net mass is divided by the measured diversion time to obtain the *true mass flow rate*.

Corrections are applied for buoyancy and diverter bias error to obtain a corrected mass flow rate. Since all readings are made under static conditions, the scale and timer readings are easily traced to national reference standards.

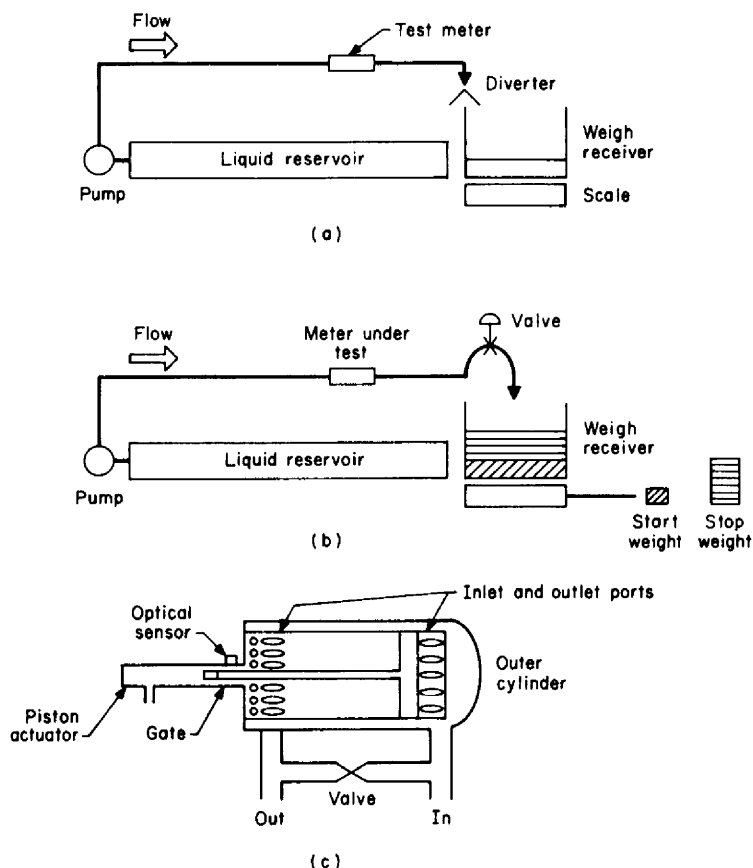


Figure 3.26 Liquid calibration standards. (a) Static weighing. (b) Dynamic weighing. (c) Ballistic prover.

Dynamic Weighing. The dynamic weighing method (Fig. 3.26*b*) requires that the mass measurement be made under steady flow-rate conditions into a receiver. When steady flow is indicated by the meter under test, the weigh tank drain valve is closed and mass begins to accumulate until the counterbalance weight is lifted. As the balance arm passes through a preset trigger, the timer starts and the test run begins. Additional mass is then added to the counterbalance. When the liquid mass entering the receiver equals the added mass, the timer is stopped, terminating the run. Since mass is continually changing as the receiver is filled, suitable dynamic corrections (Craft, 1986) need to be applied to the mass readings.

The accuracy of either the dynamic or the static weigh method is determined by an overall uncertainty analysis that includes bias and random errors associated with the mass standards, diverter or dynamic inertial effects, and the measured run time. Typically, this uncertainty is less than 0.1 percent in the mass flow-rate determination.

Volumetric. If the static or dynamic measurement is made volumetrically, rather than by collecting mass, the method is called volumetric. It is important that suitable bias error corrections be made for this method (ISO DIS 8316, 1987).

Ball or Ballistic Prover. In situ calibration is often required for custody transfer applications. The ballistic prover (Fig. 3.26*c*) is a compact defined-volume test device. The prover is often mounted on a small truck and brought to the measurement site. Larger provers that use a ball rather than a piston are permanently installed for routine meter proving.

The prover (ANSI/API MPMS4, 1979) operates on the principle of diverting all of the metered fluid through the prover and counting the meter pulses generated between a starting and a stopping trigger over the known volume between detectors. This volume is accurately known, and the pulse per unit volume is thereby determined.

Gas Calibration

Weighing and Volumetric. Similar to a liquid calibration, the gas passing through the meter under steady flow conditions may be measured with a mass or volume reference standard. In the weigh method the gas is accumulated and weighed on a beam balance (Fig. 3.27*a*) and the recorded value is divided by the run time to calculate the mass flow rate.

In the volume method (Fig. 3.27*b*) a precise known volume is filled or exhausted and the initial and final tank pressure and temperature are measured. From these measurements the initial and final mass may be calculated using the state equation for the flowing gas and the receiver or discharge tank known volume. The mass flow rate is calculated as the net calculated mass divided by the test interval.

Bell Prover and Piston Prover. Shown in Fig. 3.27*c* is the bell prover that is widely used for low-pressure calibrations of positive displacement and other meters. ISO DIS 8959 (1986) and ISO DIS 9695-1 (1992) gives the requirements for the accurate determination of gas volumes using this method.

The bell is either filled or lowered by opening and closing suitable valving. This displaces or fills a known calibrated volume over a measured time interval (for rate) as the bell rises or falls. Under carefully controlled conditions the bell prover has an estimated overall uncertainty (accuracy) of 0.1 to 0.2 percent.

Kirik and Peace (1992) present a detailed uncertainty analysis of an automated bell prover used for testing gas turbine meters. Errors are estimated for each system component, classified by type, and then combined into uncertainty levels for each calibrated volume. This analysis indicated that uncertainty varies with calibration conditions. The analysis indicated uncertainties in the order of $\pm 0.15\%$ are achievable for displaced volumes of 400 ft³ (11 m³).

Bellinga and Delhez (1993) redesigned a liquid piston prover to serve as a primary calibration standard for natural gas. The ultimate goal, after obtaining sufficient data, is to gain acceptance of the device as a primary standard for meter calibration.

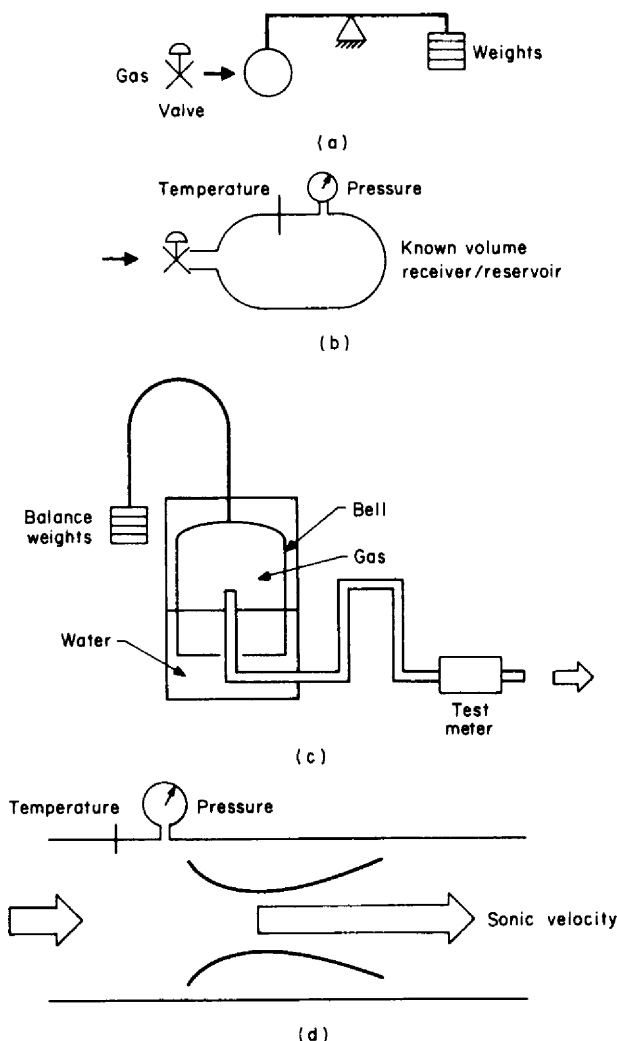


Figure 3.27 Gas calibration standards. (a) Weighing. (b) Volumetric. (c) Critical nozzle.

Critical Flow Nozzles. The critical flow nozzle (Fig. 3.27c) is increasingly being used as a secondary gas or vapor flow measurement standard. A sonic shock wave limits the flow rate in the nozzle's throat to the speed of sound for the fluid under test. Assuming an isentropic expansion from the inlet plenum to the throat, the mass flow rate is calculated from measured pressure and stagnation temperatures to an accuracy of 0.25 percent (ANSI/ASME MFC-7M, 1992, see chap. 13).

REFERENCES

- ANSI/API MPMS-4, *Manual of Petroleum Measurement Standards*, 1st ed., chap. 4, "Proving Systems," ANSI, New York, 1979.
- ANSI/API 2530, *Orifice Metering of Natural Gas*, American Gas Association, New York, 1991.
- ANSI/ASME MFC-2M, *Measurement Uncertainty for Fluid Flow in Closed Conduits*, ANSI, New York, 1995.
- ANSI/ASME MFC-7M, *Measurement of Gas Flow by Means of Critical Flow Venturi Nozzles*, ANSI, New York, 1992.
- Bbular, R.: "DP Transmitter Revisited," *Control*, pp. 38–41, September 1994.
- Bean, H.S.: "Correction Factors," *Gas*, vol. 27, pp. 48–50, August 1957.
- Bellinga, H., and F.J. Delhez.: "Experience with a High Capacity Piston Prover as a Primary Standard for High Pressure Gas Flow Measurement," *Flow Measurement and Instrumentation*, vol. 4, no. 2, pp. 85–90, April 1993.
- Benedict, R.P.: *Fundamentals of Temperature, Pressure, and Flow Measurement*, 2d ed., Wiley, New York, 1984.
- "The International Practical Temperature Scale of 1968," a committee report, *Metrologia*, vol. 5, p. 2, April 1969.
- Blake, K.A.: "The Design of Piezometer Rings," *J. Fluid Mech.*, no. 78, pp. 415–427, 1976.
- Brunkalla, R.L.: "Effects of Fabrication Technique on the Discharge Coefficient for Throat Tap Nozzles," *ASME Paper 84-JPGC-PTC-10*, October 1985.
- Craft, D.W.: "Dynamic Weigh Stand Flowmeter Calibrators—Corrections for Inherent Systematic Errors," *Proc. Int. Symp. Fluid Flow Meas.*, Session 13, AGA, 1986.
- Ferron, A.G.: "Construction of Static Pressure Taps," *Tech. Memo*, Alden Research Lab., Alden, Mass., September 1986.
- ISO 4185, *Measurement of Liquid Flow in Closed Conduits—Weighing Method*, ISO, Geneva, 1985.
- ISO Standard 5024, *Petroleum Liquids and Gases—Measurement—Standard Reference Conditions*, ISO, Geneva, 1981.
- ISO/DIS 8316, *Measurement of Liquid Flow in Closed Conduits—Method by Collection of the Liquid in a Volumetric Tank* (draft), ISO Standard, ISO TC30, Geneva, 1987.
- ISO 9368-1: *Measurement of liquid flow in closed conduits by the weighing method—Procedure for checking installations*, ISO, Geneva, 1990.
- ISO DIS 9695-1: *Measurement of gas flow rate—Volumetric method*, ISO, Geneva, 1992.
- Kirik, M.J., and D.W. Peace.: "Uncertainty Analysis of an Automated Bell Prover System," *Int'l Gas Research Conf.*, Orlando, Florida, 1992.
- Jones, F.E.: "The Air Density Equation and the Transfer of the Mass Unit," *J. Res. Nat. Bur. Stand.*, vol. 83, no. 5, pp. 419–428, 1978.
- Larson, K.: "Sizing Up Micro-machined Instruments," *Control*, p. 52, May 1994.
- McCoy, M.: "Sensor Data Integration for Improved Flow Data Accuracy," *Sensors*, pp. 8–14.
- Nishikawa, T., T. Kobayashi, T. Mikami, K. Yoshika, and H. Kuwayama: "Intelligent DP Transmitter Using a Resonant Single-Crystal Silicon Sensor," paper, ISA/1993.

CHAPTER 4

ACCURACY

Errors are inherent in all measurements. Even under ideal conditions, repeated measurements of a reference standard, such as a standard mass placed on a scale, will give slightly different instrument readings. These errors may be random or biased, stem from the reference standard, or change with time. Environmental factors, such as temperature, pressure, and relative humidity, can also affect measurements.

Accuracy, overall uncertainty, systematic error, bias error, repeatability, hysteresis, and reproducibility are but a few of the terms used by standardizing organizations and trade associations to define the many sources of error. Although called by different names, many of these have the same meaning. Because of the widespread use and understanding of the terms *accuracy*, *bias error*, and *precision*, they will be used exclusively in this book. Accuracy, which is the combination of bias and precision errors, will be defined in accordance with the author's interpretations of the available flow measurement uncertainty standards and current draft documents, including ANSI/ASME MFC-2M (1988), ANSI ASME PTC 19.1 (1985), and ISO 5168 (1979).

The measurement of flow rate requires not only a primary device but usually additional instruments to measure temperature, pressure, density, differential pressure, etc. To determine flow-rate measurement accuracy, the accuracy of the primary device must be combined with the individual accuracies of these additional measuring devices and then properly weighed in the flow-rate calculation.

The following brief introduction to the subject presents a simple procedure for calculating overall flow-rate accuracy. The combining of errors by statistical methods is now widely accepted. For engineering purposes, it is difficult to apply the rigorous and complex statistical approaches presented in the standards for the purpose of evaluating second- and third-order effects. In most cases a suitable accuracy statement can be derived through the use of simplifying assumptions, with the more complete determination reserved only for contractual use and for documentation of data for technical papers, etc.

FUNDAMENTAL CONSIDERATIONS

The International Organization for Legal Metrology (OIML, 1984) defines accuracy as "The closeness of agreement between the result of a measurement and the (conventional) true value of the measurand." OIML notes that "the use of the term precision for accuracy should be avoided."

By definition, an accuracy of 99 percent is an inaccuracy of 1 percent, and, as accuracy improves, inaccuracy is reduced. For convenience, however, inaccuracy has almost always been referred to as "accuracy."

Accuracy statements for industrial and laboratory instruments are usually given as a percentage of either the upper range value (URV; formerly called full-scale value) or the true value, rather than in terms of the units of measurement. Since percentages are easier to use, particularly in the calculation of flowmeter accuracy, they will be utilized here to derive the accuracy equation.

At a single measurement point, there are three sources of error. The average of many readings might be offset from the true value (bias error); the readings may be randomly scattered about the offset (precision error); and one reading might fall well outside the majority of the readings (illegitimate, or outlier error). It is the combination of the first two that establishes the *accuracy* or quality of the instrument.

Two methods are commonly used to specify accuracy over a range of values. In the first, a calibration curve is plotted over the intended range of use, and each reading is then corrected by reference to a correction curve (ISO DIS 7066, 1984). If desired, a mathematical correction-factor equation is derived by regression analysis, and subsequent corrections are calculated by computer. In the second method, an accuracy value based on typical calibration curves for production units is given. While the first method has the advantage of eliminating bias, the considerable expense of individually calibrating each instrument is seldom warranted. Many of today's industrial instruments are calibrated at several points, and a bias error correction is made by a microprocessor.

Flowmeters and auxiliary instruments are usually assigned two accuracies. The first is called the *reference-condition accuracy* and is obtained under laboratory conditions. A range of temperatures, pressures, supply voltages, flow conditions, etc., is specified over which the user can expect the device to be within a specified reference-accuracy envelope. The second refers to the effect of influence quantities on the reference accuracy. It applies when the device is used outside the referenced range for temperature, relative humidity, static pressure, flow-pulsation level, etc., and is usually specified as a *limit of error*, such as ± 1 percent per 100°F. For example, a pressure-measuring device would be within its ± 1 percent reference-accuracy envelope if used in an air-conditioned room, but a bias error, and possible increased precision error, might be observed if it were installed in the harsh temperature environment of a steel mill.

MEASUREMENT ACCURACY

Accuracy Components

As an illustration of the two separate errors that define accuracy, consider three temperature-measuring devices that have been placed in boiling water and have provided the readings given in Table 4.1. The three sets of temperature data are also shown plotted on targets in Fig. 4.1, where the bull's-eye is 212°F, the *true* value.

Data for the first device (Fig. 4.1a) are tightly clustered about an average value, but offset from the center. The difference between the average and true values is the instrument's bias error, and the scatter about the average is the precision error. Note that one point is significantly different from the rest. This is an outlier, because it is not part of the normal population. Statistical methods (ANSI/ASME MFC-

TABLE 4.1 Calibration Data for Three Temperature-Measuring Devices

Measurement	Reading		
	Device 1	Device 2	Device 3
1	210.1	210	212.0
2	210.0	213	212.2
3	209.8	212	212.1
4	210.2	214	212.0
5	209.9	210	211.8
6	200.0†		

†Possible illegitimate error or an outlier.

2M, 1988) are available for determining whether to reject it or include it in calculations.

A bias error is directional and must be added or subtracted from the instrument's reading to obtain the true value. A precision error is random about the bias. Precision can be improved only by selecting another measuring device, but bias error, if known, can be eliminated by correction. This particular device is considered precise but biased; it is not considered accurate without correction.

The second device (Fig. 4.1*b*) has a wide scatter about the bull's-eye. While the average is centered, indicating no significant bias, the inability to read values close to each other makes the device imprecise, or of poor precision; the chances of reading 212°F are quite poor. This device would not be considered accurate because of the large precision error.

The third device (Fig. 4.1*c*) is both precise and unbiased. The average of the five readings is 212°F, and there is little scatter. Because this device is both precise and unbiased, it is considered accurate.

This example suggests three distinct cases regarding accuracy:

1. Bias error is not negligible, but precision is good (device 1).
2. Bias error is negligible, but precision is poor (device 2).
3. Bias error is small and precision is good (device 3); this is an accurate device.

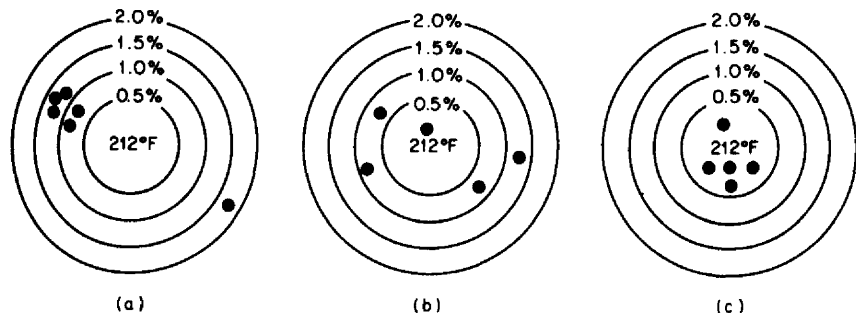


Figure 4.1 Targets showing data scatter with respect to true value. (a) Device 1. (b) Device 2. (c) Device 3.

Depending on how sensitive the flow-rate calculation is to the particular temperature that is being measured, device 1 could be used for control; devices 1 and 2 could be used for measurement and control if the temperature sensitivity of the flow calculation were negligible; and device 3 could be used for both measurement and control. In all cases, device 3 is to be preferred, unless economic considerations outweigh measurement needs.

Precision and bias errors must first be treated separately and then combined to obtain the final accuracy value. Precision errors follow the laws of chance, in that they are purely random in nature. The chance (probability) of reading either 211°F

or 213°F when a particular thermometer is placed in boiling water may be only 5 percent, but the chance of reading 212°F may be 20 percent. The chances of reading intermediate values increase as the readings approach the average; these chances follow the familiar bell-shaped curve of gaussian (normal) distribution, as illustrated in Fig. 4.2 for device 1. Using statistically derived equations, a range within which 95 percent of the readings would be expected to fall can be calculated. The 95 percent confidence range (or level) is used in the ISO 5168 (1978) ANSI/ASME MFC-2M (1988) and ANSI/ASME PTC 19.1 (1985) flow measurement standards.

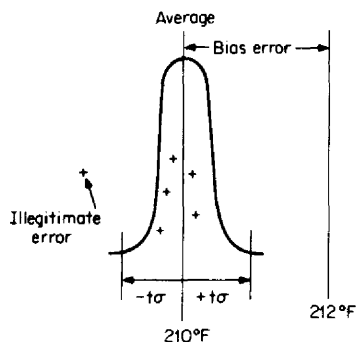


Figure 4.2 Data for device 1 shown on a bell curve.

Bias errors do not follow the laws of chance, and no confidence level can be derived for them. There are two types of bias errors, variable and constant. Typical sources are as follows:

Sources of Variable Bias Errors

1. Drift in the voltage of a standard cell used periodically to standardize a potentiometer
2. Progressive wear on the linkage of a recorder (a time-dependent wear function)
3. Progressive wear of the orifice edge in a dirty stream
4. An uncorrected zero shift in a differential-pressure transmitter (or other measuring device)

Sources of Constant Bias Errors

1. An unknown bias error in a reference standard that is used to calibrate secondary devices
2. Deadweight-tester weights not corrected for local gravity
3. Use of the assumption of an ideal gas
4. A scale used to determine mass but not corrected for liquid buoyancy
5. A flowmeter installed too close to an elbow or other flow disturbance
6. Incorrect measurement of an orifice or pipe bore

A source of error that can never be explained, calculated, or estimated (or overlooked) is the outlier (sometimes called human error, illegitimate error, or blunder)

that occurs when an operator records 221°F instead of 212°F, or when the water was not at the boiling point as readings were recorded, or when a known source of bias error was not considered—such as not correcting the boiling point of water for atmospheric pressure. Illegitimate errors should always be reported, since they might be indicative of a meaningful phenomenon. But, for engineering purposes, outliers must be discarded after a reasonable effort to locate their source. Several statistical methods for rejecting outliers are covered in ISO 5168 (1978), ANSI (MFC) (1988), and ANSI/ASME PTC 19.1 (1985).

Calculating Precision

Precision is the ability of a measuring device to give (repeat) the same readings for the same input. Because variations in readings are random, statistical theory can be used to calculate a precision value at the 95 percent confidence level from the variance of the readings.

To calculate the precision, an approximate standard deviation is first calculated for the readings (data points). This is multiplied by a correction factor derived from Student's t distribution for the 95 percent confidence level.

This factor depends on the number of data points and, for an infinite number of points, approaches 1.96. Student's t values are plotted in Fig. 4.3 versus sample size, and the values are given in Table 4.2.

The standard deviation, in percent, is

$$\sigma = \left[\frac{\sum (I_{\%})_i^2}{n - 1} \right]^{1/2} \quad (4.1)$$

where n is the number of data points, and $(I_{\%})_i$ is the percentage deviation of each data point I_i from the average \bar{I} of the indicated readings:

$$(I_{\%})_i = \frac{I_i - \bar{I}}{\bar{I}} 100 \quad (4.2)$$

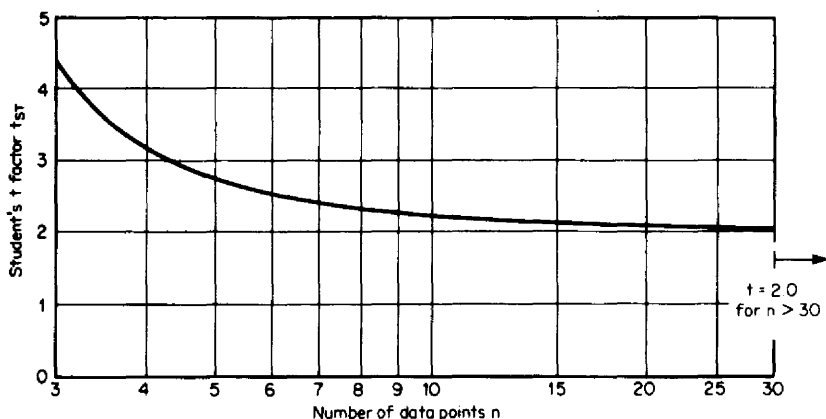


Figure 4.3 Student's t for the 95 percent confidence level.

TABLE 4.2 Two-Tailed Student's t Values for 95 Percent Confidence Level

Number of data points n	Degrees of freedom $(n - 1)$	t_{ST}	Number of data points n	Degrees of freedom $(n - 1)$	t_{ST}
2	1	12.706	18	17	2.110
3	2	4.303	19	18	2.101
4	3	3.182	20	19	2.093
5	4	2.776	21	20	2.086
6	5	2.571	22	21	2.080
7	6	2.447	23	22	2.074
8	7	2.365	24	23	2.069
9	8	2.306	25	24	2.064
10	9	2.262	26	25	2.060
11	10	2.228	27	26	2.056
12	11	2.201	28	27	2.052
13	12	2.179	29	28	2.048
14	13	2.160	30	29	2.045
15	14	2.145	31	30	2.042
16	15	2.131	32	31	2.0
17	16	2.120			

with

$$\bar{I} = \frac{\sum I_i}{n} = \frac{I_1 + I_2 + I_3 + \dots}{n} \quad (4.3)$$

The precision at the 95 percent confidence level is then

$$\sigma_p = t_{ST} \sigma \quad (4.4)$$

where t_{ST} is found in Table 4.2 or Fig. 4.3.

Calculating Bias Error

The difference between the most likely value (the average) and the *true* value, as established by a reference standard, is the bias error (see Fig. 4.2). While the true value is never exactly known (because of inherent reference-standard precision and bias errors), engineering practice is to assume that the reference standard has negligible error.

The difference between the average of the instrument's readings and the reference-standard reading gives the *directional bias error*, defined by

$$B = \frac{\bar{I} - I_t}{I_t} 100 \quad (4.5)$$

where the subscript t refers to the true, or reference-standard, value. With a positive bias, the instrument is said to be reading high, and with a negative bias reading low.

It is common to use a correction factor to adjust readings for known bias errors. This factor is derived in terms of the bias error as

$$F_B = \left(1 + \frac{B}{100}\right)^{-1} \quad (4.6)$$

and the correction for directional bias is made as follows:

$$I_i = F_B \bar{I} \quad (4.7)$$

An added complication enters the bias-error calculations because of the confidence associated with the average value. Confidence in the average of 1000 readings is higher than that for an average of only five readings. It has been shown that precision can be used to calculate a 95 percent confidence level for the average. This establishes a range centered on the average and determined as

$$\pm B = \frac{\sigma_p}{\sqrt{n}} \quad (4.8)$$

It can be seen from Eq. (4.8) that as the number of readings increases, the bias-error range $\pm B$ shrinks toward zero. For many devices, precision error is small ($\sigma_p < 0.10$ percent), and the bias-error range can be neglected in the accuracy calculation.

Accuracy at a Single Point

Accuracy is *closeness* to the true value, and it includes the effects of both precision and bias error. These are combined by considering the precision [Eq. (4.4)] and the bias-error range $\pm B$ [Eq. (4.8)] as random, adding their squares, and taking the square root of their sum. The directional bias error is then algebraically added, and the accuracy is calculated as

$$\text{Acc} = B \pm \sqrt{\sigma_p^2 + \frac{\sigma_p^2}{n}} = B \pm \sqrt{\left(1 + \frac{1}{n}\right) \sigma_p^2} \quad (4.9)$$

When the directional bias error is known, each reading should be corrected with Eq. (4.6). The accuracy calculation then reduces to

$$\text{Acc} = \pm \sqrt{\left(1 + \frac{1}{n}\right) \sigma_p^2} \quad (4.10)$$

Many devices have good precision (<0.1 percent), and for a reasonable number of data points ($n > 5$), Eq. (4.10) further reduces to

$$\text{Acc} = \pm \sigma_p \quad (4.11)$$

Equation (4.11), in which the accuracy is set equal to the precision of the device at the given test value, also includes the following assumptions:

1. The accuracy of the reference standard is 5 times better than that of the instrument whose accuracy is being determined.
2. All readings have been corrected for known directional bias errors.

Example 4.1. Determine the precision, directional bias error, correction factor, bias-error range, and accuracy for device 1 in Table 4.1.

Precision. With the outlier omitted, the calculation may be tabulated as follows:

i	I_i	$(I_{\%})_i, \%$ [Eq. (4.2)]	$(I_{\%})_i^2$
1	210.1	+0.048	0.0023
2	210.0	0.0	0.0
3	209.8	-0.095	0.0090
4	210.2	+0.095	0.0090
5	<u>209.9</u>	-0.048	<u>0.0023</u>
	1050.0		0.0226

In constructing the table, Eq. (4.3) was used to compute

$$\bar{I} = \frac{\sum I_i}{n} = \frac{1050}{5} = 210.0$$

The standard deviation is, by Eq. (4.1),

$$\sigma = \left(\frac{\sum (I_{\%})_i^2}{n-1} \right)^{1/2} = \left(\frac{0.0226}{5-1} \right)^{1/2} = \pm 0.0753 \text{ percent}$$

From Table 4.2 for $n = 5$, $t_{ST} = 2.776$. The precision is then, by Eq. (4.4),

$$\sigma_p = t_{ST} \sigma = \pm (2.776)(0.0753) = \pm 0.21 \text{ percent}$$

Directional bias error. The directional bias error is calculated with Eq. (4.5):

$$B = \frac{\bar{I} - I_t}{I_t} 100 = \frac{210 - 212}{212} 100 = -0.94 \text{ percent}$$

Correction factor. The correction factor can now be calculated with Eq. (4.6):

$$F_B = \left(1 + \frac{-0.94}{100} \right)^{-1} = 1.0095$$

Bias-error range. The bias-error range is, from Eq. (4.8),

$$\pm B = \frac{\pm 0.21}{\sqrt{5}} = \pm 0.094 \text{ percent}$$

Accuracy. The accuracy is, by Eq. (4.9),

$$\begin{aligned} \text{Acc} &= -0.94 \pm \sqrt{\left(1 + \frac{1}{5} \right) (0.21)^2} = -0.94 \pm 0.23 \\ &= -0.7 \text{ to } -1.2 \text{ percent} \end{aligned}$$

If each reading had been multiplied by the correction factor F_B , the accuracy would be calculated with Eq. (4.10) as

$$\text{Acc} = \sqrt{\left(1 + \frac{1}{5}\right)(0.21)^2} = \pm 0.23 \text{ percent}$$

ACCURACY OVER A RANGE

If a temperature-measuring device is calibrated with different inputs, directional bias errors and precision errors similar to those shown in Fig. 4.4 are obtained. A *calibration curve* may be drawn through the directional-bias-error points, and each reading corrected to the true value I_r . Then the calculation of accuracy reduces to the calculation of precision as in Eq. (4.11).

To establish a calibration curve for each instrument is usually economically unjustified. Instead, most instruments are type-tested to establish a reference *accuracy envelope* that incorporates precision, directional bias, and bias-error range

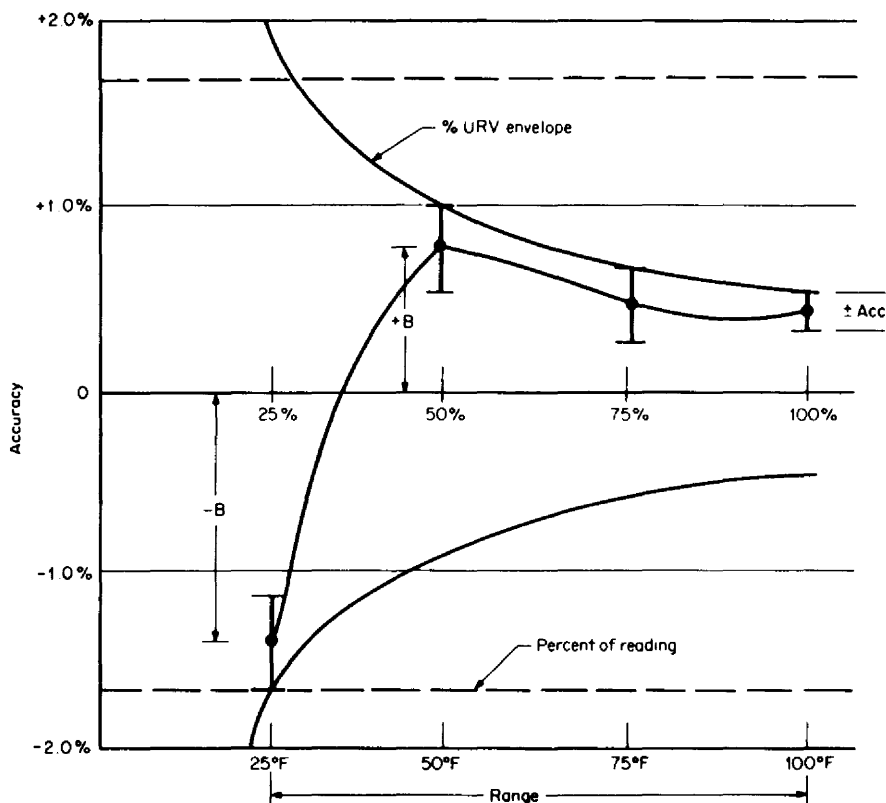


Figure 4.4 Accuracy envelopes over a range.

over a specified range of the measured variable. The limits of the envelope are expressed as a percentage of the upper range value (URV) or as a percentage of the reading. Accuracy envelopes are specified for reference conditions, and they apply within stated limits on ambient temperature, input power, relative humidity, etc. The accuracy envelopes for many industrial instruments have been substantially reduced by computer-calculating the bias-error correction based on test data obtained over the useful range.

Influence Quantities

If an installation's ambient temperature, relative humidity, etc., are outside the stated limits of the reference conditions for an accuracy envelope, additional bias or precision errors may result. These sources of errors are referred to as *influence quantities*, and they give rise to the most difficult errors to assess, because of their possible interrelationships. For example, an additional bias of ± 0.5 percent may be indicated on the basis of a separate test for temperature, and a -0.5 percent bias based on a similar relative-humidity test. Combined, these would indicate no additional error. However, if both effects are tested for simultaneously, the error might be -0.25 percent. In many cases, the effect of a particular influence quantity is to directionally bias the reading and not to significantly affect the precision. In some cases, these influences change the instrument's zero and have negligible effect on span. By zeroing under flowing conditions, these errors are then minimized.

The ANSI/ASME MFC-2M (1988) and ANSI/ASME PTC 19.1 (1985) standards and the ISO/TC30 (1987) draft of *Flow Measurement Uncertainty* suggest that, "When it is known that a bias results from a particular cause, special calibrations may be performed allowing the cause to perturbate through its complete range to determine the range of bias." They further suggest, "In practice most measurements will have many sources of bias limits from calibration (reference conditions), data acquisition and data reduction. As long as none of them are extremely large (10 to 1) relative to the others, the quadrature sum (root-sum-square) is a very good approximation of the combination of such errors."

For instruments, a limiting specification is usually given over a range, such as " ± 1.25 percent of the URV per 100°F temperature change." Within this range, the ± 1.25 percent may be assumed to be linearly related to the difference between reference and operating temperatures. And, if it is assumed that each influence quantity is independent of other influence quantities, the root-sum-square method can be used to combine the errors. The operating-condition accuracy is then calculated as

$$\text{Acc} = \pm (\text{Acc})_{\text{ref}} \pm \sqrt{B_T^2 + B_p^2 + B_{RH}^2 + \dots} \quad (4.12)$$

where the subscript ref refers to reference-condition accuracy, and the subscripts of T , p , and RH refer to the influences of temperature, pressure, and relative humidity. Other influences should be included as they may arise in a particular measurement situation.

In-Situ Testing

Testing a flowmeter on site (*in situ*) is sometimes necessary for either contractual reasons or to ensure that it is within uncertainty limits. This is particularly true for

large meters where there are few available laboratories, calibrations are prohibitively expensive, and laboratory calibration accuracy is often greater than ± 2 percent.

An in-situ test can be conducted using one of several of those below as a *secondary* meter:

- A ball, piston, or ballistic prover
- A critical flow-nozzle (gas only)
- A calibrated flowmeter located in series
- A tracer method (salt velocity, radioactive, etc.)
- Comparison to another uncalibrated series installed meter

In-situ testing cannot duplicate reference conditions that existed when a meter's published or standardized uncertainty value was established; therefore, before conducting an in-situ test an estimate should be made on the acceptable limit of error between meters being compared.

Several precautions must be observed before conducting a test so that reference conditions are approximated; some of these are:

- Flush (clean) piping prior to installing the meters.
- Ensure that a liquid system has no air, that a gas (vapor) system has no entrained liquids.
- Ensure that flow variations during testing are at a minimum, usually $< \pm 1$ percent.
- Ensure that there are no protruding gaskets upstream of the meter.
- Measure the piping to ensure that dimensions and finish are within standard limits.
- Ensure that all measurement equipment is installed in accordance with standards or to the manufacturer's recommendations.
- Avoid pulsating flow, cavitation, etc., to have meaningful results.

Means and Proportions Test. If two metering devices are installed in series, a *means and proportions* comparison test can be used to estimate the bias limit. This statistical test, called a test of significance, (Spiegel, 1975) assumes an initial *hypothesis* that the difference in the average of the first meter and that of the second is significant or is not significant within a bias limit based on the scatter (precision) of the flow-rate calculation for each meter. Tests of hypotheses and significance enable decisions to be made as to whether to accept or reject hypotheses that test results differ significantly from expected results.

In a comparative test between two populations (meter 1 and meter 2) there are two mean values and two random errors (precision):

1. The average flow rate for the first meter and the associated standard deviation
2. The average flow rate for the second meter and the associated standard deviation

Flow-rate variations occurring during testing can be estimated by the meter's reading and, assuming random variations, a standard deviation can be determined for each. These means and standard deviations are then used in the *means and proportions* computational steps as outlined below.

First define the hypotheses for the acceptable bias limit B_{allow} between meters:

- H_0 : if $B \leq B_{\text{allow}}$, the observed difference is due to chance, and the meters are within specification.
- H_1 : if $B > B_{\text{allow}}$, the observed difference is outside the allowable specification.

Determine the average flow rate for each meter as

$$q_{1,\text{avg}} = \frac{\sum q_{1,i}}{n} \quad (4.13)$$

$$q_{2,\text{avg}} = \frac{\sum q_{2,i}}{n} \quad (4.14)$$

where n is the number of test.

The standard deviation for each meter is then calculated by

$$\sigma_1 = \frac{t_{ST}}{1.96} \sqrt{\frac{\sum (q_{1,i} - q_{1,\text{avg}})^2}{n - 1}} \quad (4.15)$$

$$\sigma_2 = \frac{t_{ST}}{1.96} \sqrt{\frac{\sum (q_{2,i} - q_{2,\text{avg}})^2}{n - 1}} \quad (4.16)$$

where t_{ST} is the Student's t value from Table 4.2.

The estimated sampling distribution of difference in means is

$$\sigma_{1-2} = \sqrt{\frac{\sigma_1^2}{n} + \frac{\sigma_2^2}{n}} \quad (4.17)$$

Define the limits on the means (estimated bias error) by

$$q_{1,\text{test}} = q_{1,\text{avg}} \pm \frac{B}{100} q_{1,\text{avg}} \quad (4.18)$$

$$q_{2,\text{test}} = q_{2,\text{avg}} \pm \frac{B}{100} q_{2,\text{avg}} \quad (4.19)$$

Note: The sign of B is to minimize the difference between $q_{1,\text{avg}}$ and $q_{2,\text{avg}}$.

Compute the *standardized variable* Z_{SV} as

$$Z_{SV} = \frac{q_{1,\text{test}} - q_{2,\text{test}}}{\sigma_{1-2}} \quad (4.20)$$

- For a 95 percent confidence interval, change B (iterate) until $Z = 1.96$ (or -1.96)
- The estimated bias is then the value of B when $Z = 1.96$ (or $Z = -1.96$)
- If $Z_{SV} = 1.96$ when $B = 0$, there is no discernible difference between meters.

Example 4.2. A differential-pressure-measuring device has a reference-condition accuracy specification of ± 0.2 percent of the URV. For the reference and operating conditions given below, estimate the accuracy at an ambient temperature of 100°F (37.8°C) and a line static pressure of 1000 psia (6895 kPa).

	Reference condition	Operating condition
Temperature	75 ± 3°F	± 1.25% for 100°F (total error)†
Pressure	14.7 psia	± 0.5% to 3000 psia

†Includes a zero error which can be corrected for by “zeroing” at temperature (100°F).

The influence quantities are temperature and pressure. Their bias errors are computed with Eq. (4.5), assuming linear relationships. They are

$$B_T = \pm \frac{100 - 75}{100} 1.25 = \pm 0.31 \text{ percent URV}$$

for temperature, and

$$B_p = \pm \frac{1000 - 14.7}{3000} 0.5 = \pm 0.16 \text{ percent URV}$$

for pressure. The accuracy at operating conditions is then estimated with Eq. (4.12):

$$\text{Acc} = \pm 0.2 \pm \sqrt{(0.31)^2 + (0.16)^2} = \pm 0.55 \text{ percent URV}$$

Example 4.3. A 36-in (915-mm) and a 48-in (1220-mm) venturi flowmeter are installed in series in a water-pumping station. The meters were not calibrated, and it was decided to check the meters by comparison and to adjust the meters' readings to the estimated bias between them.

Set up a *worksheet* to determine

1. The test specification that the maximum allowable flow-rate variations are ≤ 1.5 percent
2. The hypotheses that the meters are within ± 2 percent
3. The adjusted meter factor for each meter

The following information is available: The 36-in meter will produce a differential of $h_w = 100.5$ in when the water flow rate is 64.8 million flowing gallons per day (mgpd) and the 48-in meter will produce a differential of $h_w = 235.5$ in at 125.28 mgpd.

The flow-rate equation, by Eq. (9.104), for the 36-in meter is

$$q_{36", \text{mgpd}} = F_{36", \text{MC}} \sqrt{h_w} = \left(\frac{64.8}{\sqrt{100.5}} \right) \sqrt{h_w} = 6.4639 \sqrt{h_w}$$

and for the 48-in meter it is

$$q_{48", \text{mgpd}} = F_{48", \text{MC}} \sqrt{h_w} = \left(\frac{125.28}{\sqrt{235.5}} \right) \sqrt{h_w} = 8.1637 \sqrt{h_w}$$

Two differential-pressure transmitters with a range of $h_{w, \text{URV}} = 100$ in were used to measure the differential pressure. The 4- to 20-mA transmitters were calibrated with a deadweight air tester and a correction applied; the correction equations, from Eq. (4.6) are, for the 36-in meter,

$$F_{36'',B} = 1 + 0.00367 \left(\frac{\text{mA} - 4}{16} \right)$$

and for the 48-in meter are

$$F_{48'',B} = 1 - 0.0025 \left(\frac{\text{mA} - 4}{16} \right)$$

The differential pressure is then, by Eq. (4.7), for the 36-in meter,

$$h_{w,36} = F_{36'',B} \left(\frac{\text{mA}_{\text{rdg}} - 4}{16} \right)$$

and for the 48-in meter is

$$h_{w,48} = F_{48'',B} \left(\frac{\text{mA}_{\text{rdg}} - 4}{16} \right)$$

The worksheet is shown below:

The hypotheses tests are:

H_0 : If $B \leq 2$ percent, the observed differences are due to chance and the meters are within limits.

H_1 : If $B > 2$ percent, the observed differences are not due to chance and the meters are outside limits.

For the 36-in meter the average flow rate, using Eq. (4.13), is

$$q_{36'',\text{avg}} = \frac{\sum q_{36'',i}}{n} = 39.479 \text{ mgpd}$$

and for the 48-in meter the flow-rate becomes

$$q_{48'',\text{avg}} = \frac{\sum q_{48'',i}}{n} = 40.362 \text{ mgpd}$$

The standard deviation for the 36-in meter is, by Eq. (4.15),

$$\sigma_{36''} = \frac{t_{ST}}{1.96} \sqrt{\frac{\sum (q_{36'',i} - q_{36'',\text{avg}})^2}{n - 1}} = \frac{2.262}{1.96} \sqrt{\frac{0.1771}{10 - 1}} = 0.162$$

where, for 10 observations (tests), $t_{ST} = 2.262$ from Table 4.2.

The standard deviation for the 48-in meter is similarly

$$\sigma_{48''} = \frac{t_{ST}}{1.96} \sqrt{\frac{\sum (q_{48'',i} - q_{48'',\text{avg}})^2}{n - 1}} = \frac{2.262}{1.96} \sqrt{\frac{0.1229}{10 - 1}} = 0.135$$

The *sampling distribution in means*, with Eq. 4.17, becomes,

$$\sigma_{36'' - 48''} = \sqrt{\frac{0.162^2}{10} + \frac{0.135^2}{10}} = 0.0667$$

	36-in meter						48-in meter					
	mA_{rdg}	$F_{36^\circ.B}$	mA	$h_{w,36^\circ}$	$q_{36^\circ,\text{mgpd}}$	delta_1^\dagger	mA_{rdg}	$F_{48^\circ.B}$	mA	$h_{w,48^\circ}$	$q_{48^\circ,\text{mgpd}}$	delta_2^\ddagger
1	9.970	1.001	9.984	37.398	39.529	0.002	7.900	0.999	7.895	24.345	40.280	0.007
2	9.890	1.001	9.903	36.896	39.263	0.047	7.960	0.999	7.955	24.719	40.589	0.051
3	10.000	1.001	10.014	37.586	39.628	0.022	7.900	0.999	7.895	23.345	40.280	0.007
4	10.000	1.001	10.014	37.586	39.628	0.022	7.920	0.999	7.915	24.470	40.383	0.000
5	9.930	1.001	9.944	37.147	39.396	0.007	7.930	0.999	7.925	24.532	40.435	0.005
6	9.980	1.001	9.994	37.461	39.562	0.007	7.910	0.999	7.905	24.407	40.332	0.001
7	9.970	1.001	9.984	37.398	39.529	0.002	7.890	0.999	7.885	24.283	40.228	0.018
8	9.890	1.001	9.903	36.896	39.263	0.047	7.890	0.999	7.885	24.283	40.228	0.018
9	9.990	1.001	10.004	37.523	35.595	0.014	7.920	0.999	7.915	24.470	40.383	0.000
10	9.930	1.001	9.944	37.147	39.396	0.007	7.940	0.999	7.935	24.594	40.486	0.015
			$q_{36^\circ,\text{avg}} =$	39.479	0.1771			$q_{48^\circ,\text{avg}} =$	40.362	0.1229		

$$^\dagger\text{delta}_1 = (q_{36^\circ,i} - q_{36^\circ,\text{avg}})^2$$

$$^\ddagger\text{delta}_2 = (q_{48^\circ,i} - q_{48^\circ,\text{avg}})^2$$

The limits on the means can now be defined by Eqs. (4.18) and (4.19) as

$$q_{36'',\text{test}} = \left(1 + \frac{B}{100}\right) q_{36'',\text{avg}} = \left(1 + \frac{B}{100}\right) 39.479$$

$$q_{48'',\text{test}} = \left(1 - \frac{B}{100}\right) q_{48'',\text{avg}} = \left(1 - \frac{B}{100}\right) 40.362$$

1. *The test specification that the maximum allowable flow-rate variations are $\leq \pm 1.5$ percent.* The flow-rate variation for the two meters are, for the 36-in meter,

$$\pm q_{36''} = \left(\pm \frac{1.96\sigma_{36''}}{q_{36'',\text{avg}}}\right) 100 = \left[\pm \frac{(1.96)(0.162)}{39.479}\right] 100 = \pm 0.92\%$$

and, for the 48-in meter,

$$\pm q_{48''} = \left(\pm \frac{1.96\sigma_{48''}}{q_{48'',\text{avg}}}\right) 100 = \left[\pm \frac{(1.96)(0.135)}{40.362}\right] 100 = \pm 0.66\%$$

Since both variations are < 1.5 percent, the test specification is met.

2. *The hypotheses that the meters are within ± 2 percent.* For no bias between meters, $Z_{\text{SV}} = 1.96$ when $B = 0$, or

$$Z_{\text{SV},B=0} = \frac{q_{48'',\text{avg}} - q_{36'',\text{avg}}}{\sigma_{36''-48''}} = \frac{40.362 - 39.479}{0.067770} = 13.2$$

Since $Z_{\text{SV},B=0} > 1.96$, there is a bias between the two meters. This bias is obtained by

$$Z_{\text{SV}} = 1.96 = \frac{\left(1 - \frac{B}{100}\right) q_{48'',\text{avg}} - \left(1 + \frac{B}{100}\right) q_{36'',\text{avg}}}{\sigma_{36''-48''}}$$

$$= \frac{(q_{48'',\text{avg}} - q_{36'',\text{avg}}) - (q_{48'',\text{avg}} + q_{36'',\text{avg}}) \frac{B}{100}}{\sigma_{48''-36''}}$$

Rearranging yields the bias error as

$$B = \frac{(q_{48'',\text{avg}} - q_{36'',\text{avg}}) - 1.96\sigma_{48''-36''}}{(q_{48'',\text{avg}} + q_{36'',\text{avg}})}$$

$$= \frac{(40.362 - 39.479) - (1.96)(0.0667)}{(40.362 + 39.479)} 100 = 0.942\%$$

The bias between meters is then ± 0.94 percent, and the meters are within the hypotheses assumption of ± 2 percent.

Since the 36-in meter is reading low, the estimated bias error using Eq. (4.5) is

$$B_{36''} = -0.942\%$$

and for the 48-in meter it is

$$B_{36''} = +0.942$$

3. The adjusted meter factors are calculated using Eq. (4.6). For the 36-in meter, the meter coefficient is

$$F_{36'',MC} = \left(1 + \frac{B}{100}\right)^{-1} \frac{64.8}{\sqrt{100.5}} = \left(1 + \frac{-0.942}{100}\right)^{-1} \frac{64.8}{\sqrt{100.5}} = 6.5253$$

and, for the 48-in meter,

$$F_{48'',MC} = \left(1 + \frac{B}{100}\right)^{-1} \left(\frac{125.28}{\sqrt{235.5}}\right) = \left(1 + \frac{+0.942}{100}\right)^{-1} \frac{125.28}{\sqrt{235.5}} = 8.0875$$

SENSITIVITY COEFFICIENTS

General

Flow measurement often requires that a number of measurements be combined. In the case of an orifice flowmeter measuring natural gas, for example, line pressure, differential pressure, temperature, and gravitometer measurements are combined in an equation to calculate the flow rate. The form of such an equation depends on the flowmeter's principle of operation; the mathematical relationships among the measured variables establishes the *sensitivity* of the final calculation to each of these variables.

Each measurement has a specific *sensitivity coefficient* that can be derived from a mathematical relationship, estimated from charts or tables, or be exactly calculated using a computer program for the complete flow-rate solution. It is the proper combination of these coefficients that allows individual accuracies to be included in an overall flow-rate accuracy value. Sensitivity coefficients are useful in determining what effect an individual instrument's directional bias has on the calculated flow rate and in deciding whether a more precise or accurate device is necessary. In reviewing suspected flow-rate measurement errors, the measurement that has the largest sensitivity coefficient should always be investigated first.

Mathematical Considerations

When an equation is used to calculate a quantity based on measured values of two or more variables, a mathematical entity called the *total differential* can be used to determine the individual effect of each variable on the final result. If the pertinent variables are independent, then the general functional relationship for the differential producer's flow-rate equation is

$$q = f(p, T, h_w, D, d, \dots) \quad (4.21)$$

The total differential is the sum of the partial differentials of the independent variables:

$$dq = \frac{\partial q}{\partial p} dp + \frac{\partial q}{\partial T} dT + \frac{\partial q}{\partial h_w} dh_w + \frac{\partial q}{\partial D} dD + \dots \quad (4.22)$$

Dividing Eq. (4.22) by the flow rate q and rearranging yield

$$\frac{dq}{q} = X_p \frac{dp}{p} + X_T \frac{dT}{T} + X_{h_w} \frac{dh_w}{h_w} + X_D \frac{dD}{D} + \dots \quad (4.23)$$

where X_p , X_T , X_{h_w} , X_D , \dots are the sensitivity coefficients for the variables, equal to the partial derivatives in Eq. (4.22). The terms they multiply in Eq. (4.23) represent relative changes in the variables. The percentage change in flow rate may thus be calculated as the sum of the products formed when each sensitivity coefficient is multiplied by the percentage change in its variable.

The variables in Eq. (4.21) are not, in general, independent. For example, the bore of a flow nozzle is a function of temperature and the thermal-expansion factor. Including these additional functional relationships significantly complicates the calculation but has little effect on calculational accuracy. An example ISO 5168 (1978) shows that the combined uncertainty (accuracy) differs by less than 0.01 percent between the simplified and more detailed calculations.

Determining Sensitivity Coefficients

As an illustration of the procedure for determining sensitivity coefficients, consider only the temperature, dimensional, and differential-pressure measurements used in calculating an airflow rate using a flow nozzle. Bernoulli's equation and the conservation of mass flow can be combined to give

$$q_{PPH} = \frac{F_{MC} d^2}{\sqrt{1 - (d/D)^4}} \sqrt{h_w \rho_f} \quad (4.24)$$

where F_{MC} is assumed to be constant with a known accuracy, d is the nozzle bore, and D is the pipe diameter. The density ρ_f can be calculated from the temperature T_f , pressure p_f , compressibility Z_f , and specific gravity G with Eq. (2.10):

$$\rho_f = 2.698825 \frac{G p_f}{Z_f T_f} \quad (2.10)$$

Substituting Eq. (2.10) into Eq. (4.24) yields

$$q_{PPH} = \frac{F_{MC} d^2}{\sqrt{1 - (d/D)^4}} \sqrt{\frac{h_w}{T_f}} \quad (4.25)$$

where F_{MC} now assumes a new value that includes the specific gravity G , compressibility factor Z_f , constant 2.698825, and a constant pressure p_f value.

In Eq. (4.25), the flow equation has been reduced to a form that includes only the effects of bore d , pipe size D , temperature T_f , and differential pressure h_w on the calculated mass flow. These will be referred to in this handbook as the *measured variables*.

First consider the sensitivity of the flow rate to temperature, which will be measured in degrees Fahrenheit. If the diameters d and D and the differential pressure h_w are temporarily assumed to be constant and the total differential of Eq. (4.25)

is taken with respect to temperature, the partial derivative of the mass-flow equation with respect to temperature is obtained as

$$dq_{\text{PPH}} = \frac{F_{\text{MC}} d^2 \sqrt{h_w}}{\sqrt{1 - (d/D)^4}} \left(-\frac{1}{2} \right) (459.67 + T_F)^{-3/2} dT_F \quad (4.26)$$

Dividing both sides of Eq. (4.26) by the mass flow [Eq. (4.25)] and multiplying by T_F/T_F yields an equation of the form of Eq. (4.23), from which the temperature sensitivity coefficient is found to be

$$X_{TF} = -\frac{1}{2} \frac{|T_F|}{459.67 + T_F} \quad (4.27)$$

The absolute-value symbol in the numerator of this equation indicates that the minus sign is to be removed from negative temperatures such as -60°F .

The sensitivity coefficient X_{TF} is multiplied by the temperature directional bias error to calculate the temperature bias error in mass flow, and by the temperature accuracy (\pm) to calculate the accuracy-range contribution of the temperature device. That is, for directional bias

$$(q_{\text{PPH}})_{\%} = X_{TF} B_{TF} \quad (4.28)$$

and for accuracy

$$\pm (q_{\text{PPH}})_{\%} = X_{TF} (\text{Acc})_{TF} \quad (4.29)$$

In the same way, sensitivity coefficients may be obtained as

$$X_D = -\frac{2\beta^4}{1 - \beta^4} \quad (4.30)$$

for pipe diameter D , where $\beta = d/D$;

$$X_d = \frac{2}{1 - \beta^4} \quad (4.31)$$

for flowmeter bore d , again with $\beta = d/D$;

$$X_{h_w} = \frac{1}{2} \quad (4.32)$$

for differential pressure h_w ; and finally

$$X_{\text{FMC}} = 1 \quad (4.33)$$

if F_{MC} is not constant as assumed.

Computer-Derived Sensitivity Coefficients

The sensitivity coefficients derived by neglecting second- and third-order derivatives are approximate, and an exact bias error correction is not possible. For exacting work, the complete solution for the flow-rate calculation should be programmed and the sensitivity coefficients for pressure, temperature, differential, etc., determined by incrementing each variable by 1 percent and calculating the percentage change in flow rate when all other variables remain fixed at the selected evaluation point.

Combining Sensitivity Coefficients

Sensitivity coefficients can be used for two purposes. First, if a measurement is made and a directional bias error is later found, the directional flow-rate bias can be calculated from the sensitivity coefficients. Second, the flow-rate measurement accuracy can be determined by properly combining the individual measuring-device accuracies with the sensitivity coefficients.

Directional Bias Errors. Directional bias errors are combined by summation:

$$B_q = X_{TF}B_{TF} + X_D B_D + X_d B_d + X_{hw} B_{hw} + \cdots \quad (4.34)$$

where B_q is the percent directional bias error in flow rate for directional bias errors in temperature, and B_{TF} , B_D , B_d , . . . are defined similarly. No "units" subscript is shown on the flow-rate bias error because all terms in Eq. (4.34) are dimensionless (percentages); the flow rate can be measured in any units.

Accuracy. If the directional bias of each instrument is corrected for, or each instrument is operating within its accuracy envelope, the accuracies of the various measuring instruments may be combined by the root-sum-square method to estimate the flow-rate measurement accuracy:

$$(\text{Acc})_q = \pm \{ [X_{TF}(\text{Acc})_{TF}]^2 + [X_D(\text{Acc})_D]^2 + [X_d(\text{Acc})_d]^2 + [X_{hw}(\text{Acc})_{hw}]^2 + \cdots \}^{1/2} \quad (4.35)$$

For engineering purposes, this is an extremely useful equation. It provides the combined effect of all influence quantities, including reference-condition accuracies and the sensitivities of the measured variables.

Example 4.4. Calculate the accuracy of a determination of mass flow using a flow nozzle, given the following accuracy statements:

Measurement	Indicated	Accuracy, %
Temperature T_F	60°F	± 0.5
Differential pressure h_w	100	± 0.2
Pipe diameter D	7.981 in	± 0.2
Nozzle bore d	5.5867 in	± 0.05
Flow constant F_{MC}	55	± 0.75

The calculation may be tabulated as follows:

Source	Sensitivity coefficient X	$[X(\text{Acc})]^2$
Eq. (4.27)	$X_{TF} = -\frac{1}{2} \frac{ 60 }{460 + 60} = -0.058$	$[(-0.058)(\pm 0.5)]^2 = 0.0008$
Eq. (4.32)	$X_{hw} = +\frac{1}{2}$	$[(+0.5)(\pm 0.2)]^2 = 0.0100$
Eq. (4.30)	$X_D = -\frac{(2)(0.7)^4}{1 - (0.7)^4} = -0.632$	$[(-0.632)(\pm 0.2)]^2 = 0.0160$
Eq. (4.31)	$X_d = +\frac{2}{1 - (0.7)^4} = +2.632$	$[(+2.632)(\pm 0.05)]^2 = 0.0173$
Eq. (4.33)	$X_{FMC} = +1.0$	$[(1.0)(\pm 0.75)]^2 = 0.5625$
		<u>0.6066</u>

The accuracy is then, from Eq. (4.35),

$$(\text{Acc})_q = \pm \{\Sigma [X(\text{Acc})^2]\}^{1/2} = \pm (0.6066)^{1/2} = \pm 0.78 \text{ percent}$$

Example 4.5. For Example 4.4, the true values obtained below were determined. Compute the correction factor to be applied to the flow rate that was calculated from the indicated values.

Variable	Indicated	True	Bias error, %
Temperature T_F	60°F	65°F	-7.69
Differential pressure h_w	100	99	+1.01
Pipe diameter D	7.981 in	7.9012 in	+1.01
Nozzle bore d	5.5867 in	5.6006 in	-0.25

The calculations may be tabulated as follows:

Variable	Sensitivity coefficient X^\dagger	Bias error B^\ddagger	XB
Temperature	-0.058	-7.69	+0.444
Differential pressure	+0.5	+1.01	+0.505
Pipe diameter	-0.632	+1.01	-0.638
Nozzle bore	+2.632	-0.25	-0.658
			-0.347

† From Example 4.4.

‡ From Eq. (4.5).

The bias error in the flow rate is then, from Eq. (4.34),

$$B_q = \Sigma XB = -0.35 \text{ percent}$$

and the correction factor is, from Eq. (4.6),

$$F_{B,q} = \left(1 + \frac{-0.35}{100}\right)^{-1} = 1.0035$$

Example 4.6. A flange tap orifice flowmeter is metering natural gas with the initial conditions shown in the worksheet below in row 1. Compute the sensitivity coefficient for each of the variables shown using computer software. The PC Software The FLOW CONSULTANT ‡ computes the flow rate for a +1 percent change in the variables shown, including the effect of pressure and temperature on the properties of natural gas. The computational sequence is as follows:

1. Compute the flow rate for the pressure, temperature, etc., values shown in row 1, $q_{\text{SCFH,ref}} = 1,000,000$.
2. Save the data and compute the flow rate for a 1 percent pressure increase (**bold type** above), $q_{\text{SCFH,press}} = 1,005,165$.

‡ The FLOW CONSULTANT $^\text{TM}$ is a registered trademark of R.W. Miller & Associates.

	Pressure, p_f	Temperature, T_f	Gravity, G	Nitrogen, %N ₂	Carbon dioxide, %CO ₂	Viscosity, μ_{cP}	Isentropic exponent, k	Diameter, D	Bore, d	Differential, h_w	Flow rate, q_{SCFH}	Sensitivity factor, $X_{i,var}$
1	100.00	60.00	0.60	1.00	1.00	0.0107	1.2895	12.5000	6.0908	100	1000000	
2	101.00	60.00	0.60	1.00	1.00	0.0107	1.2895	12.5000	6.0908	100	1005165	0.5165
3	100.00	60.80	0.60	1.00	1.00	0.0107	1.2895	12.5000	6.0908	100	999407	-0.0593
4	100.00	60.00	0.61	1.00	1.00	0.0107	1.2895	12.5000	6.0908	100	995104	-0.4896
5	100.00	60.00	0.60	1.01	1.00	0.0107	1.2895	12.5000	6.0908	100	999992	-0.0008
6	100.00	60.00	0.60	1.00	1.01	0.0107	1.2895	12.5000	6.0908	100	999997	-0.0003
7	100.00	60.00	0.60	1.00	1.00	0.0108	1.2895	12.5000	6.0908	100	1000002	0.0002
8	100.00	60.00	0.60	1.00	1.00	0.0107	1.3115	12.5000	6.0908	100	1000204	0.0204
9	100.00	60.00	0.60	1.00	1.00	0.0107	1.2895	12.6250	6.0908	100	998673	-0.1327
10	100.00	60.00	0.60	1.00	1.00	0.0107	1.2895	12.5000	6.1517	100	1021497	2.1497
11	100.00	60.00	0.60	1.00	1.00	0.0107	1.2895	12.5000	6.0908	101	1004864	0.4864

3. Enter the flow rate into the worksheet and to compute the sensitivity coefficient with Eq. (4.23) as

$$X_p = \frac{\% \Delta q}{\% \Delta p} = \frac{\left(\frac{1,005,165 - 1,000,000}{1,000,000} \right) 100}{1} = +0.5165$$

4. Retrieve the reference file and change the temperature by +1 percent, giving a flow rate of $q_{\text{SCFH,Temp}} = 999,407$, which, when entered into the worksheet, yields a temperature sensitivity coefficient of

$$X_T = \frac{\% \Delta q}{\% \Delta T} = \frac{\left(\frac{999,407 - 1,000,000}{1,000,000} \right) 100}{1} = -0.0593$$

Similar computations are performed for each variable. The computed sensitivity coefficients are shown in the last column of the worksheet.

Example 4.7. For Example 4.6 estimate the accuracy in the determination of flow rate for the uncertainty estimates shown in the worksheet below:

Variable	± Variable (var)	± Acc (%)	X_{var}	$X_{\text{var}} \text{Acc}_{\text{var}}$	$[X_{\text{var}} \text{Acc}_{\text{var}}]^2$
Pressure, p_f	0.5000 psia	0.50	0.5165	0.2583	0.0667
Temperature, T_f	1.0000°F	1.67	-0.0593	-0.0988	0.0098
Specific gravity, G	0.0015	0.25	-0.4896	-0.1224	0.0150
Percent nitrogen, %N ₂	0.0015	0.15	-0.0008	-0.0001	0.0000
Percent carbon dioxide, %CO ₂	0.0015	0.15	-0.0003	-0.0000	0.0000
Viscosity, μ_{cp}	0.0002 cP	2.00	0.0002	0.0004	0.0000
Isentropic exponent, k	0.0645	5.00	0.0204	0.1020	0.0104
Pipe diameter, D	0.0050 in	0.04	-0.1327	-0.0053	0.0000
Orifice bore, d	0.0005 in	0.01	2.1497	0.0176	0.0003
Differential pressure, h_u	0.2500 in	0.25	0.4864	0.1216	0.0148
Discharge coefficient, C		0.60	1.0000	0.6000	0.3600
Gas expansion factor, Y_1	Acc(%) = ± 0.144 h_u / p_f	0.14	1.0000	0.1440	0.0207
Last column sum = $\Sigma [(X_{\text{var}})(\text{Acc})]^2 = 0.4977\%$					

The estimated accuracy is then, by Eq. (4.35),

$$(\text{Acc})_q = \pm \sqrt{\Sigma [(X_{\text{var}})(\text{Acc})]^2} \pm \sqrt{0.4977} = \pm 0.71\%$$

ANSI/ISO UNCERTAINTY EQUATIONS

The ANSI and ISO flow measurement uncertainty standards [ANSI/ASME (1988), ANSI/ASME PTC 19.1 (1985), ISO 5168 draft (1987)] present two equations for estimating the coverage at the 95 and 99 percent uncertainty limits. These standards

specify, in detail, how the random (precision) and bias errors are to be calculated (or estimated) and then combined to arrive at the stated coverage values. Since bias errors are not random in nature, the term *coverage*, rather than *precision error*, is used to define the expected uncertainty limits.

The uncertainty equation, for 99 percent coverage, is

$$\text{Acc}_{99\%} = U_{\text{ADD}} = B + t_{ST,99}\sigma \quad (4.36)$$

where $t_{ST,99}$ is the Student's t value for the 99 percent confidence level and the equation for 95 percent coverage is

$$\text{Acc} = U_{\text{RSS}} = \sqrt{B^2 + \sigma_p^2} \quad (4.37)$$

In Eqs. (4.36) and (4.37) the bias error B is the combined root-sum-squared (RSS) error of all known or estimated bias errors traced to a national reference standard and the precision (σ_p) is determined by definitive statistical rules.

ISO 5168 and ASME uncertainty standards are currently being revised in accordance with an ISO directive that all standards follow the recommendations of ISO/TAG 4 (1993) in the preparation of ISO documents on the subject. The treatment of errors is similar to present usage but the latest version of these standards should be referenced. Other standards are also being prepared on *Methods of specifying flowmeter performance* (ISO/DIS 11631, 1994).

The following references give a more complete handling of uncertainty analysis for ISO documentation.

ISO/DIS 3534-1, *Statistics—Vocabulary and symbols—Part 1: Probability and general statistical terms*

ISO 3534-3, *Statistics—Vocabulary and symbols—Part 3: Design of experiments*

ISO 5725-1, *Accuracy (trueness and precision) of measurement methods and results; Part 1: General principles and definitions*

ISO 5725-2, *Part 2: The basic method for the determination of repeatability and reproduction of a standard measurement method*

ISO 5725-3, *Part 3: Intermediate measures on the precision*

ISO 5725-4, *Part 4: The basic method for determination of the trueness of standard measurement method*

ISO 5725-5, *Part 5: Measurement methods alternative to the basic methods for determining trueness and precision*

ISO 5725-6, *Part 6: The use in practice of accuracy values*

ISO 10 012-1, *Quality assurance requirements for measuring equipment—Meteorological confirmation systems for measuring equipment*

ISO 5725, 1986: *Precision of test methods—Determination of repeatability and reproducibility for a standard test method by inter-laboratory tests*

IEC 770, 1984: *Methods of evaluating the performance of transmitters for use in industrial-process control systems.*

REFERENCES

ANSI/ASME MFC-2M, *Measurement Uncertainty for Fluid Flow in Closed Conduits*, ANSI, New York, 1988.

ANSI/ASME PTC 19.1, *Measurement Uncertainty*, ANSI, New York, 1985.

ISO/TC30/SC9, *Measurement of Fluid Flow—Estimation of Uncertainty of a Flow Rate Measurement* (draft revision), ISO 5168, NEL, East Kilbride, Scotland, 1987.

ISO/TAG 4, *Guide to the Expression of Uncertainty in Measurement*, ISO, Geneva, 1994.

ISO 5168, *Measurement of Fluid Flow—Estimation of Uncertainty of a Flow Rate Measurement*, ISO 5168, Geneva, 1979.

ISO/DIS 7006/1, *Assessment of Uncertainty in Calibration and Use of Flow Measurement Devices. Part 1, Linear Calibration Relationships*, ISO, Geneva, 1984.

ISO/DIS 7006/2, *Assessment of Uncertainty in Calibration and Use of Flow Measurement Devices. Part 2, Non-linear Calibration Relationships*, ISO, Geneva, 1984.

ISO/DIS 11631, *Methods of Specifying Flowmeter Performance*, ISO, Geneva, 1994.

OIML: *International Vocabulary of Basic Terms in Metrology*, ISO, Switzerland, 1984.

Spiegel, M.R. *Probability and Statistics*, McGraw-Hill Book Co., NY, 1975.

INFLUENCE QUANTITIES

Accuracy statements for flowmeters are based on the steady flow of a homogeneous, single-phase newtonian fluid with an approach velocity profile that does not alter the coefficient obtained in long, straight runs of pipe. Departures from these reference conditions are called flowmeter *influence quantities*. Velocity-profile deviations, nonhomogeneous flow, pulsating flow, and cavitation are the four major influence quantities affecting all flowmeters. The errors associated with a particular influence quantity depend on the sensitivity of a particular flowmeter to that quantity and whether or not a calculation correction can be made. For newtonian fluids, velocity profiles can usually be brought into acceptable limits by the installation of sufficient straight pipe or, for shorter lengths, with flow conditioners. However, other influence quantities may require the installation of pulsating dampers or the use of a less sensitive flowmeter to achieve the desired degree of accuracy. The major influence quantities and their effects are discussed in detail in the following sections.

VELOCITY PROFILE

Velocity profile is probably the most important (and least understood) influence quantity. The effects of swirl, nonnewtonian fluids, and nonaxisymmetric profiles on a meter's performance are not only difficult to analyze, but they cannot easily be duplicated in a laboratory.

Newtonian Fluids

The rheological behavior of a fluid determines whether it is classified as newtonian or nonnewtonian. A newtonian fluid is defined as a fluid which, when acted upon by an applied shearing stress, has a velocity gradient that is solely proportional to the applied stress. The constant of proportionality is the absolute viscosity defined in Chap. 2. All gases, most liquids, and fine mixtures of spherical particles in liquids and gases are newtonian fluids.

The velocity profile established by a newtonian fluid is the basic reference condition for all flowmeters, and from this profile all corrections are made. Special laboratory tests are required to establish the effects of nonnewtonian fluids on flowmeters, and little published data is available because of the many types of nonnewtonian fluids.

Flow Characteristics. If there were no viscosity, the velocity of a flowing fluid would be uniform across a pipe section. The presence of even the small absolute viscosity of a gas induces a shearing action between adjacent fluid particles that reduces the velocity to zero at the pipe wall and thus forms a nonuniform velocity profile. Osborne Reynolds (Reynolds, 1883) observed that, in the absence of swirl, a newtonian fluid had two distinctly different velocity profiles.

In Reynolds' experiment, a dye stream was injected into a flow of water in a glass pipe. At low velocities the dye stream was observed to remain parallel to the pipe axis along the length of pipe. However, when the velocity was increased, the dye stream initially oscillated, but eventually mixed completely with the water, at some distance from the dye injection point. In the first profile (Fig. 5.1a), the fluid moves in layers, or laminae, with one layer sliding over another. In the second (Fig. 5.1b), dye mixes with the fluid, and turbulent agitation occurs. These profiles were observed to be separated by a transition regime where both laminar and turbulent conditions may exist at differing pipe radii.

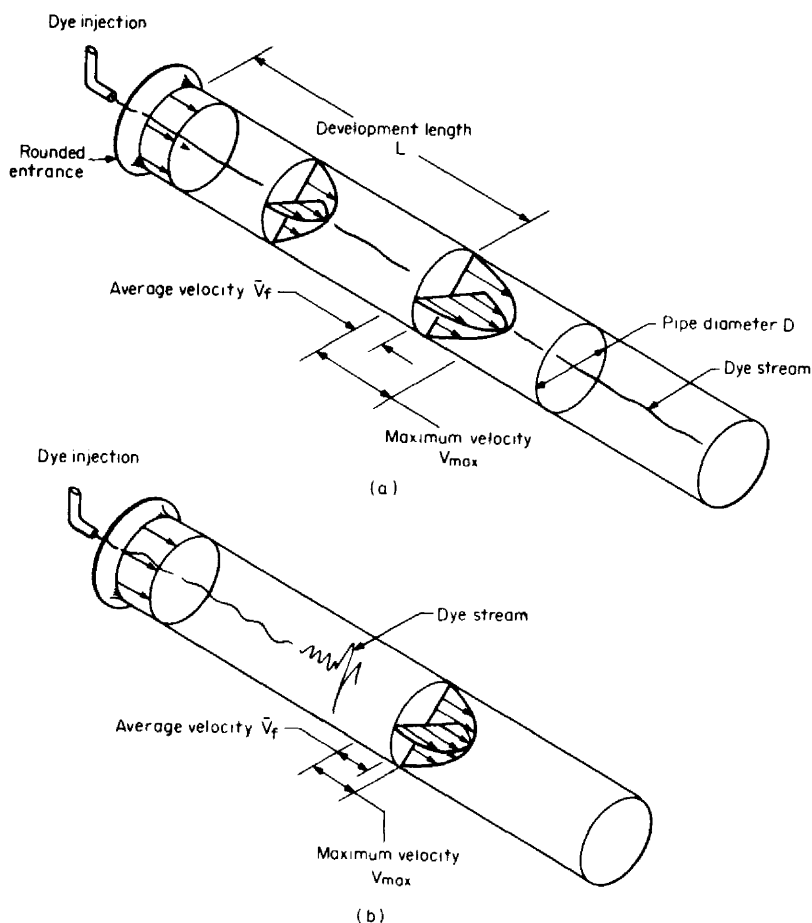


Figure 5.1 Laminar and turbulent profiles. (a) Laminar flow, $R_D \leq 2000$. (b) Turbulent flow, $R_D > 4000$.

At lower velocities, or for more viscous fluids, viscous forces restrain fluid particles into parallel-layer motion. At higher velocities, or for less viscous fluids, inertia forces overcome viscous forces and particles move in a turbulent, almost random manner. The laminar profile is easily analyzed, but turbulent profiles with their complex and random motions are not well understood.

In Reynolds' experiments, the ratio of inertia to viscous forces was observed to be dimensionless and related to viscosity, average pipeline velocity, and geometrically similar boundary conditions. For a homogeneous newtonian fluid, this dimensionless ratio is

$$R_D = \frac{\bar{V}_f D_F \rho_f}{(\mu_m)_e} = \frac{\bar{V}_f^* D_M \rho_f^*}{\mu_{Pa_s}} \quad (5.1)$$

Reynolds Number. From an engineering viewpoint, the many variables that affect velocity profile cannot be evaluated for all possible flowmeters and for all pipeline conditions. For this reason, steady flow and a fully developed flow profile, as defined by a newtonian, homogeneous fluid, are initially assumed. Coefficient variation can then be predicted with the dimensionless Reynolds number. This number has been found to be an acceptable correlating parameter that combines the effects of viscosity, density, and pipeline velocity. A flow coefficient that is obtained for water at a specified Reynolds number will be the same for oil or gas at the same Reynolds number.

Table C.4 presents equations for calculating pipe Reynolds numbers for various U.S. flow-rate and viscosity units, and Table C.5 lists similar equations for SI units. In some flowmeter correlations, the *bore* Reynolds number is used; this is calculated by replacing D in Eq. (5.1) with the bore d of the primary element.

The laminar and turbulent profiles shown in Fig. 5.1 are symmetric about diametral planes and are conveniently shown two-dimensionally as in Fig. 5.2. Experimental evidence indicates that they have the following characteristics.

Laminar Profile. The fully developed laminar flow profile is parabolic for pipe Reynolds numbers below 2000 and unaffected by wall roughness. The average pipeline velocity is one-half the centerline velocity, and the relationship between point and maximum velocities is given by

$$V_p = V_{\max} \left[1 - \left(\frac{r}{r_p} \right)^2 \right] \quad (5.2)$$

The average velocity is obtained by integration of Eq. (5.2):

$$\bar{V}_f = \frac{1}{2} V_{\max} \quad (5.3)$$

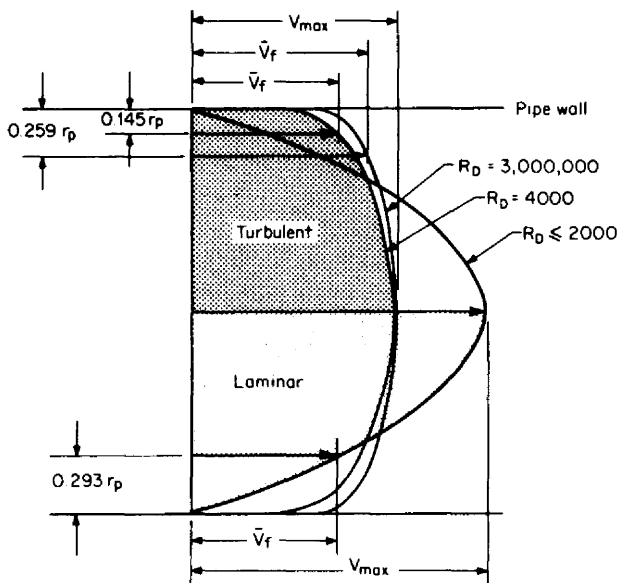
Substituting Eq. (5.3) into Eq. (5.2) yields the distance of the average velocity from the pipe wall as

$$\bar{y} = 0.293 r_p \quad (5.4)$$

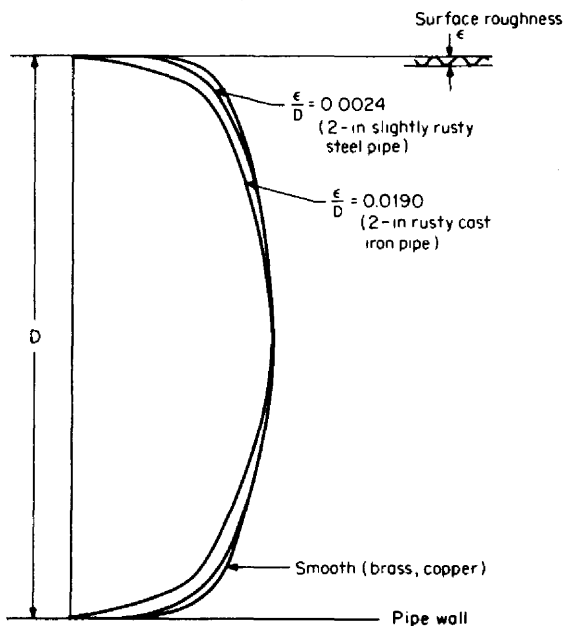
The laminar profile develops from an almost blunt profile to a fully developed parabolic shape in a development length (Govier and Aziz, 1977) of

$$L = 0.028 D R_D \quad (5.5)$$

For flow measurements to be taken in the laminar regime ($R_D < 2000$), sufficient upstream pipe must be available to provide the length defined by Eq. (5.5). Although laminar flow is unaffected by pipe roughness, pipe-entrance conditions



(a)



(b)

Figure 5.2 Velocity profiles in laminar and turbulent flow. (a) Smooth pipe. (b) Rough pipe.

(sharp edge versus rounded inlet) or other conditions may cause a need for additional length.

Turbulent Profile. At Reynolds numbers between approximately 2000 and 4000, a transition regime is crossed, and the parabolic geometry is altered. As shown in Fig. 5.2a, at Reynolds numbers of 4000 or larger the profile becomes blunter, and with increasing Reynolds number the profile becomes increasingly flatter until all particles, except at the walls, are moving at the same velocity. In practice, this profile is approached most nearly by gases at high velocities. This flat profile is referred to as the *infinite Reynolds-number profile*, the *rectilinear profile*, or sometimes the *plug-flow profile*.

The profile is complex and unstable in the narrow transition regime. Depending on whether the velocity is decreasing or increasing, it may be parabolic, blunt, or a combination of both. The Reynolds number for the onset of turbulence has been observed to range from 4000 to 7000, depending on whether the flow rate was slowly increased or decreased. Transition flow is a flow regime over which accurate flow measurement is quite difficult.

The turbulent profile is not of fixed geometry but rather changes with wall roughness and Reynolds number. The simplest equation for calculating the velocity at a point in *smooth* pipes is the empirical power-law equation,

$$V_p = V_{\max} \left(1 - \frac{r}{r_p} \right)^{1/n} \quad (5.6)$$

where the exponent n can be calculated with reasonable accuracy as

$$n = 1.66 \log R_D \quad (5.7)$$

Power-law profiles [Eq. (5.6)] adequately describe turbulent flow but do not allow exact calculation of the centerline or wall velocity.

For smooth pipe, the point of average velocity \bar{V}_f for Reynolds numbers larger than 10,000 is well approximated by

$$\bar{y} = \left[\frac{2n^2}{(n+1)(2n+1)} \right]^n r_p \quad (5.8)$$

As shown in Fig. 5.2b, a rough wall holds back additional fluid via increased shear at the wall. The *relative roughness* is defined as the ratio of average depth of pipe roughness ϵ to pipe diameter D . It is this ratio and the pipe Reynolds number that determine whether the turbulent profile is more or less blunted. Figure 5.2b shows that as the relative roughness increases, the profile becomes less blunt.

The ratio of average velocity to centerline velocity is graphed in Fig. 5.3. In smooth pipe, this ratio increases with increasing Reynolds number; the profile becomes increasingly blunt. For rough pipe, the ratio approaches a constant, which implies that the profile remains fixed above some minimum Reynolds number. Flows with Reynolds numbers above this minimum are said to be in the *complete-turbulence regime*.

Many equations have been proposed for calculating turbulent velocity profiles, using relative roughness and Reynolds number as correlating parameters. Many of these were developed from Nikuradse's (1933, 1960) smooth and sand-roughened pressure-loss data. Logan and Jones (1962), who supplemented this data, found no significant differences, except for very rough pipes.

The friction factor f , defined by the Darcy-Weisbach (1854) equation

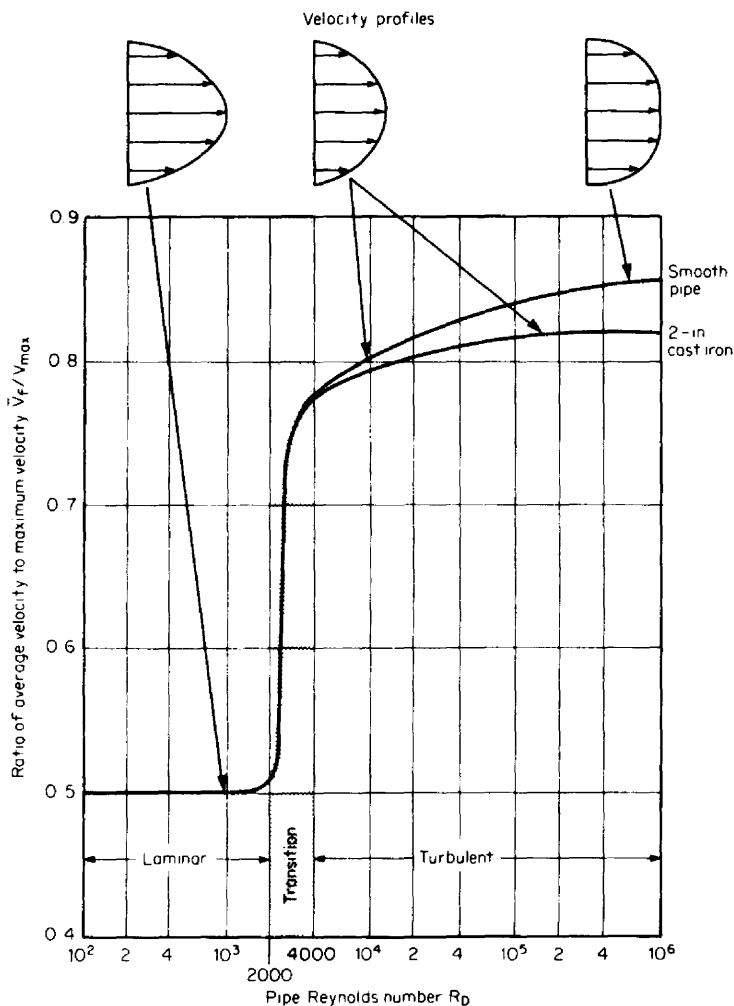


Figure 5.3 Ratio of average to maximum (centerline) velocity for smooth and rough pipe.

$$f = \frac{8g_c(S_s)_w}{\rho_f \bar{V}_f^2} = -\frac{dP}{dL_P} \frac{2g_c D_F}{\rho_f \bar{V}_f^2} = \frac{H_L}{L/D \bar{V}_f^2 / 2g_c} \quad (5.9)$$

is the usual correlating parameter between Reynolds number and point velocity. Friction factors are usually presented in graphical form, based on the work of Moody (1944) (see Fig. B.3). The Colebrook (1939) partially rough wall friction-factor equation is widely used for calculating friction factors. For parameters defined in accordance with Eq. (5.9), this equation is

$$\frac{1}{\sqrt{f}} = -2 \log \left(\frac{\epsilon/D}{3.7} + \frac{2.51}{\sqrt{f} R_D} \right) \quad (5.10)$$

Equation (5.10) is nonlinear; it can be solved with Newton's method (see Sec. A.1) by defining the function

$$F = -f^{-1/2} - 2 \log \left(\frac{\epsilon/D}{3.7} + \frac{2.51}{\sqrt{f} R_D} \right) \quad (5.11)$$

The derivative of the function is

$$F' = \frac{1}{2} f^{-3/2} + \frac{4.034}{(\epsilon/D) R_D f^{3/2} + 9.287 f} \quad (5.12)$$

and the friction factor is calculated by iteration as

$$f_n = f_{n-1} - \frac{F_{n-1}}{F'_{n-1}} \quad (5.13)$$

A single iteration will produce a result within ± 0.01 percent of the limit if the initial estimate is calculated as

$$f_0 = 0.25 \left[\log \left(\frac{0.2703 \epsilon}{D} + \frac{5.74}{R_D^{0.9}} \right) \right]^{-2} \quad (5.14)$$

Teyssandier (1975) found that the Pai (1953) profile equation best correlated empirical orifice-coefficient data. Pai's equation can be written for average pipeline velocity as

$$\bar{V}_f = \frac{V_{\max}}{1 + 1.44 \sqrt{f}} \quad (5.15)$$

and for point velocity as

$$V_p = \left[1 + \frac{s-n}{n-1} \left(\frac{r}{r_p} \right)^2 + \frac{1-s}{n-1} \left(\frac{r}{r_p} \right)^{2n} \right] V_{\max} \quad (5.16)$$

where

$$s = \frac{f R_D}{32 + 46.08 \sqrt{f}} \quad (5.17)$$

and

$$n = \frac{2 - f R_D / 32}{1.44 \sqrt{f} - 1} \quad (5.18)$$

Another widely used equation relating friction factor to average velocity is given by Pao (1961) as

$$\frac{V_p}{\bar{V}_f} = 1 + \left(1.43 + 2.15 \log \frac{y}{r_p} \right) \sqrt{f} \quad (5.19)$$

which provides the velocity ratio as a function of relative roughness after substitution of Eq. (5.14):

$$\frac{V_p}{\bar{V}_f} = 1 - \frac{0.715 + 1.075 \log (y/r_p)}{\log (0.2703 \epsilon/D + 5.74/R_D^{0.9})} \quad (5.20)$$

The location \bar{y} of the average velocity is obtained by setting $V_p/\bar{V}_f = 1.0$ in Eq. (5.19) to obtain

$$\frac{\bar{y}}{r_p} = 10^{-1.43/2.15} = 0.216 \quad (5.21)$$

In Fig. 5.4a the ratio of average to centerline velocity, based on the Pai profile, is plotted against pipe Reynolds number for various relative-roughness values. In Fig. 5.4b the effect of relative roughness on the location of the average velocity is shown. The location of the average pipe velocity was obtained by integration of the Pai profile and iteration to locate the average velocity. This figure shows that at a given Reynolds number the average velocity is located further into the pipe with increased roughness. Also, for a given relative roughness, it is located further into the pipe with increased Reynolds number.

In Fig. 5.5 the point of average velocity is shown for power-law and Pao profiles for pipes normally used in flow measurement. This curve explains why a velocity traverse is usually necessary to properly locate a single-point velocity-measuring device (pitot tube). The fixed location for pitot tube recommended by ISO/DIS 7145 (1981) for ± 3 percent accuracy is shown on this curve.

Nonnewtonian Fluids

Reynolds-number corrections are developed for newtonian fluids, for which the ratio of shear stress to shear rate is constant. This ratio is easily obtained with a single viscometer measurement. For nonnewtonian fluids, the ratio changes with stress; it is, therefore, called the *apparent viscosity*. Nonnewtonian fluids are subdivided into two major classifications—*time-independent* and *time-dependent*. Under constant stress, a time-independent fluid's apparent viscosity will not change with time, while the apparent viscosity of a time-dependent fluid will change with time.

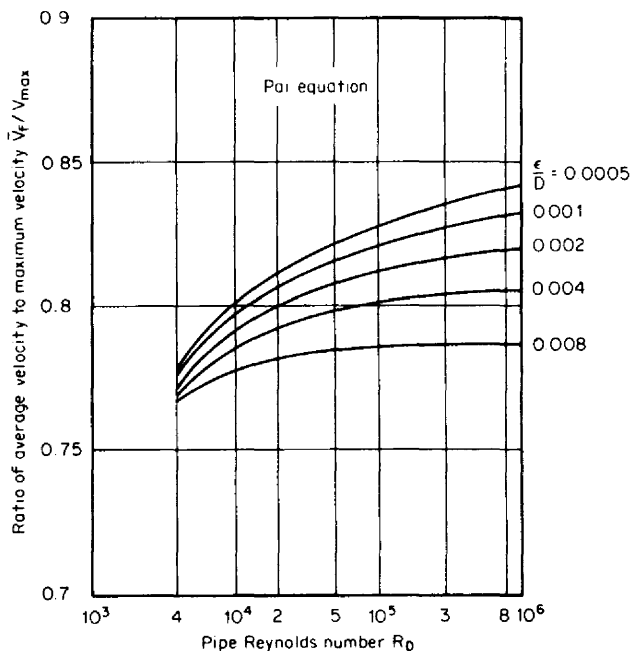
Vorwerk et al. (1994) present data on an optical laser doppler flowmeter that successfully measures centerline velocity for a nonnewtonian fluid and converts this information to volumetric flow rate using three models for the rheological flow curves to compute the apparent viscosity for several nonnewtonian fluids.

Among the more common time-independent nonnewtonian fluids are the following:

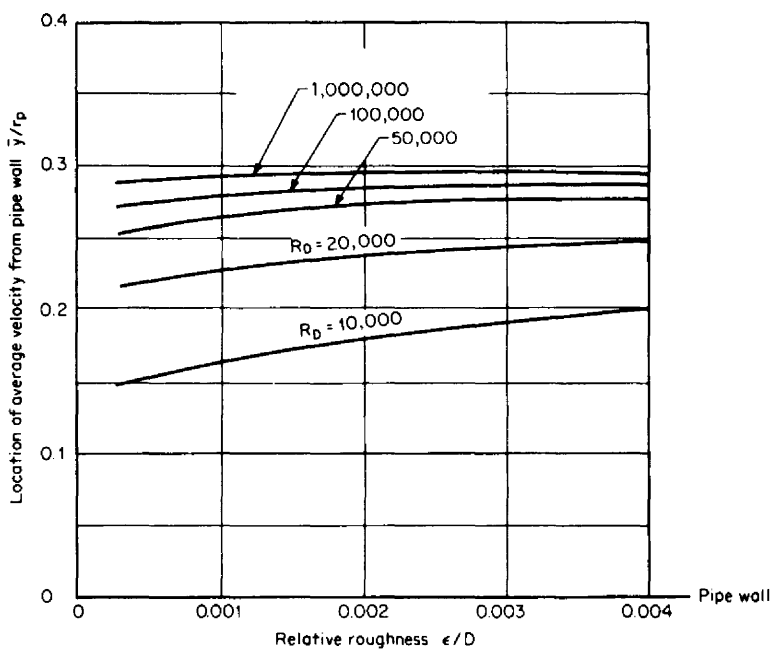
1. Plug-flow fluids

a. Bingham (or Bingham-like) fluids

- (1) Aluminum soap grease (at 250°F)
- (2) Some asphalts
- (3) Some bitumens
- (4) Calcium soap grease (at 250°F)
- (5) Cement rock (aqueous suspensions, 92 percent under 74 μm)
- (6) Chocolate
- (7) Some emulsions
- (8) Hydrocarbon grease, thickened
- (9) Catsup
- (10) Lithium stearate grease, 14G8
- (11) Luting (dispersion of synthetic wax in polyisobutane)
- (12) Mayonnaise
- (13) Drilling mud



(a)



(b)

Figure 5.4 Effect of pipe roughness on the location and ratio of average velocity to centerline velocity. (a) Velocity ratio. (b) Location of average velocity.

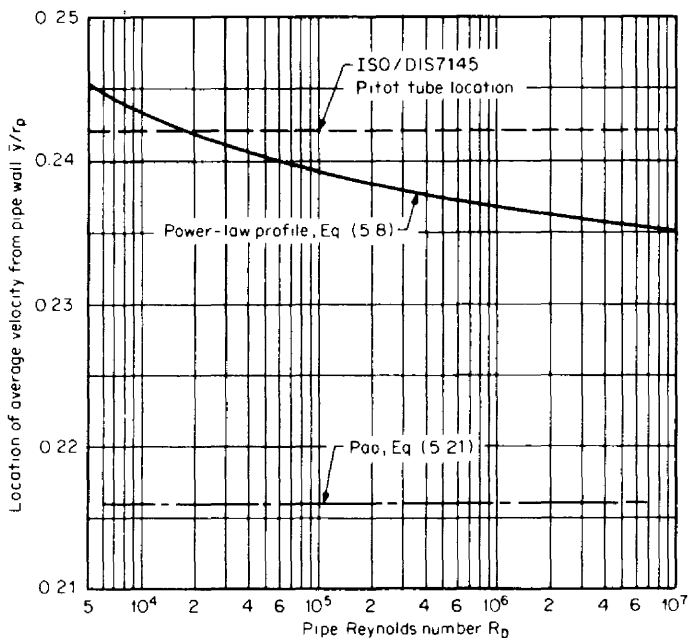


Figure 5.5 Location of average velocity from pipe wall.

- (14) Mustard
- (15) Ointments
- (16) Paint
- (17) Some long-chain polymers (carboxymethylene)
- (18) Paper pulp
- (19) Toothpaste
- (20) Water suspension of fly ash, clay (Milicz), coal char, finely divided minerals, kaolin, metallic oxides, paint, thorium oxide, titanium oxide, quartz, sewage sludge

b. Yield pseudoplastics

- (1) Carboxypolymethylene (Carbopol), water dispersions
- (2) Many Bingham-like suspensions at intermediate concentrations

2. Power-law fluids

a. Pseudoplastics ($m < 1$)

- (1) Ammonium alginate (aqueous solution)
- (2) Emulsions, e.g., incendiary bomb thickened with aluminum soaps and polymethyl methacrylate
- (3) Ethyl cellulose, 11 percent solution in cyclohexanone
- (4) 12 percent gel of aluminum soaps in gasoline
- (5) Blood plasma
- (6) Molten polyethylene [266°F (108°C)]
- (7) Water suspensions† of clay (Attasol), ferrosilicon, galena, latex, magnetite, titania

†Some of these may be classified as dilatant or newtonian in certain concentrations and at high shear rates.

- b. Dilatant fluids† ($m > 1$)
 - (1) Cornstarch in ethylene glycol
 - (2) Ethylene glycol-glycerine with small amount of water
 - (3) Starch in water
 - (4) Titania in 42-cP sucrose
 - (5) Titanium dioxide, 27 to 47 percent in water

The time-dependent nonnewtonian fluids include:

1. Thixotropic
 - a. Water suspensions of bentonitic clay
 - b. Some crude oils at low temperatures
 - c. Pseudoplastic emulsions of soaps
 - d. High polymers in gasoline
2. Rheopectic
 - a. Printer's ink
 - b. Saturated polyester ($M_w = 2000$)
3. Viscoelastic
 - a. Carbopol solutions
 - b. Flour dough
 - c. Some jellies
 - d. Nylon
 - e. Polymer solutions: carboxymethylcellulose (CMC), polyisobutylene in decalin, polyox, polyacrylamide, polyethylene oxide, sodium carboxymethyl cellulose

Nonnewtonian velocity profiles are not the same as newtonian profiles. The required zero wall velocity causes varying shear rates in a nonnewtonian fluid, and nonnewtonian fluids distribute the velocity differently among fluid layers. Although nonnewtonian profiles are not easily predicted, they are symmetrical, and the number of pipe lengths required to establish profiles are usually one-third to one-half those for a newtonian fluid.

In many applications, nonnewtonian fluids are in the laminar flow regime, and it is convenient to categorize their profiles in terms of departure from the newtonian laminar profile. In the turbulent regime, the distinction between profiles is not so great, and *the apparent viscosity may be used in Eq. (5.1) for the Reynolds number.*

Time-independent pseudoplastics have blunter laminar profiles than newtonian fluids, while dilatant fluids produce pronounced, almost conical, peaking profiles. The Bingham fluids produce almost rectilinear profiles. Time-dependent thixotropic and rheopectic fluids exhibit time-variable pseudoplastic or yield-pseudoplastic behavior. This results in profile changes with both flow rate and time. Viscoelastic fluids are the most complex, having partial elastic recovery and time-dependent viscous properties.

Flow-measurement data for nonnewtonian fluids in the laminar regime is almost nonexistent. In many applications, except for venturi measurements of slurry or sewage or where Reynolds-number corrections are not required, the magnetic flowmeter is used because its output is essentially an average of the profile.

Time-Independent Fluids. Newtonian, pseudoplastic, dilatant, and Bingham-plasticlike fluids are time-independent fluids whose apparent viscosity does not change with the duration of an applied stress. A graph of shear stress versus shear

†Observed only in certain concentration ranges of suspensions of irregularly shaped solids.

rate for these fluids is shown in Fig. 5.6. In the figure, all the fluids have the same *apparent viscosity* as water (0.0095 P) at an applied shear stress of 200 g/(cm·s²).

Apparent viscosity is the ratio of shear stress to shear rate. Figure 5.6 shows that, except for newtonian fluids, the apparent viscosity changes with the shear stress. For pseudoplastics the apparent viscosity decreases with increasing shear stress, while for dilatant fluids it increases. For Bingham plastics an initial stress must be applied to initiate motion. After this yield stress is reached, a Bingham fluid exhibits a linear relation between shear stress and shear rate, similar to newtonian fluids.

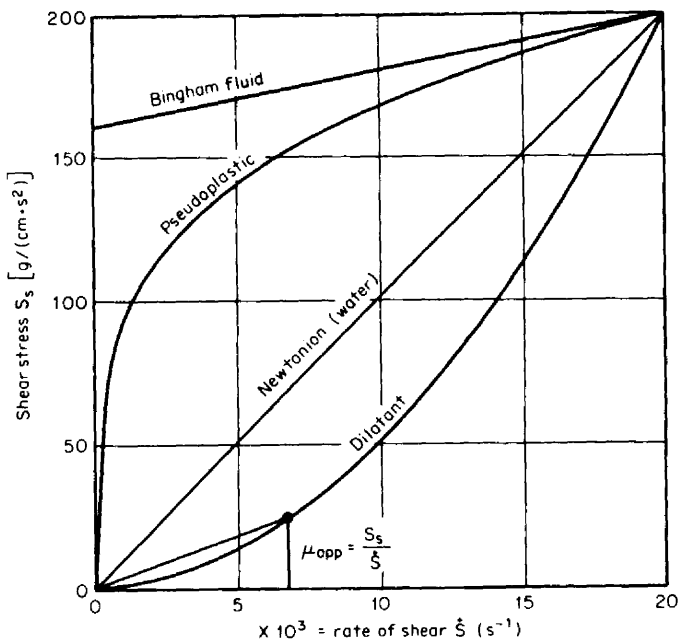


Figure 5.6 Shear stress versus shear rate for time-independent fluids.

If the shear stress is plotted against shear rate logarithmically, the straight-line relationships shown in Fig. 5.7 are obtained for dilatant and pseudoplastic fluids. That is, the shear stress is related to the shear rate raised to a power. The Ostwald equation is widely used in engineering calculations to describe the shear behavior of these *power-law* fluids. This equation is

$$S_s = A \dot{\gamma}^m \quad (5.22)$$

where the constant A and exponent m are called the *consistency index* (or *power-law coefficient*) and *flow-behavior index* (or *power-law exponent*). Both constants are determined by multiple viscosity measurements. Dilatant fluids have exponents greater than 1, newtonian fluids have an exponent of 1, and pseudoplastics have a power-law exponent smaller than 1. Table 5.1 presents typical constants for some power-law fluids.

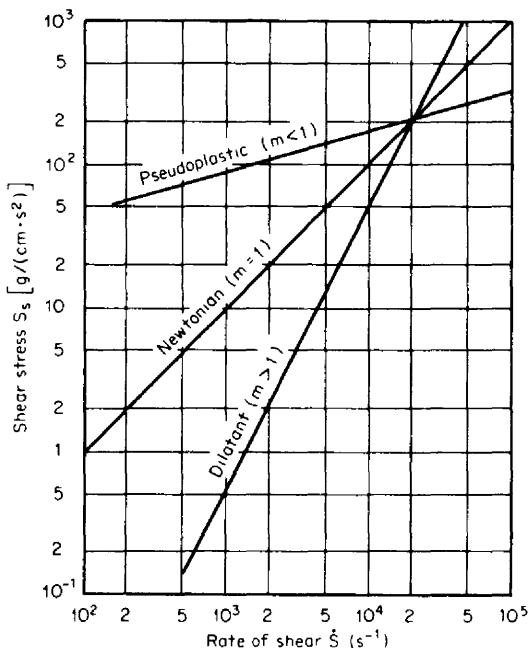


Figure 5.7 Logarithm plot of shear stress versus shear rate.

TABLE 5.1 Typical Constants for Power-Law Fluids

Fluid	Power-law constant A'	Power-law exponent $m' = m$
Water suspensions		
14.3% clay	0.0441	0.35
21.2% clay	0.0106	0.335
25% clay	0.0345	0.185
31.9% clay	0.0611	0.251
36.8% clay	0.1845	0.176
40.4% clay	0.4346	0.132
23% lime	0.1786	0.178
4% pulp	0.4611	0.575
Carboxymethylcellulose (3% water solution)	0.2146	0.566
10% napalm in kerosene	0.0995	0.520

Sources: Metzner and Reed (1955) and Govier and Aziz (1977).

By definition, the apparent viscosity is

$$\mu_{\text{app}} = \frac{S_s}{\dot{S}} \quad (5.23)$$

Substituting Eq. (5.22) into Eq. (5.23) yields the apparent-viscosity equation for power-law fluids as

$$\mu_{\text{app}} = A\dot{S}^{m-1} \quad (5.24)$$

For newtonian fluids, where $m = 1$, this equation reduces to the constant A —the absolute viscosity. Shown in Fig. 5.8 are apparent viscosities for the two power-law fluids involved in Fig. 5.7.

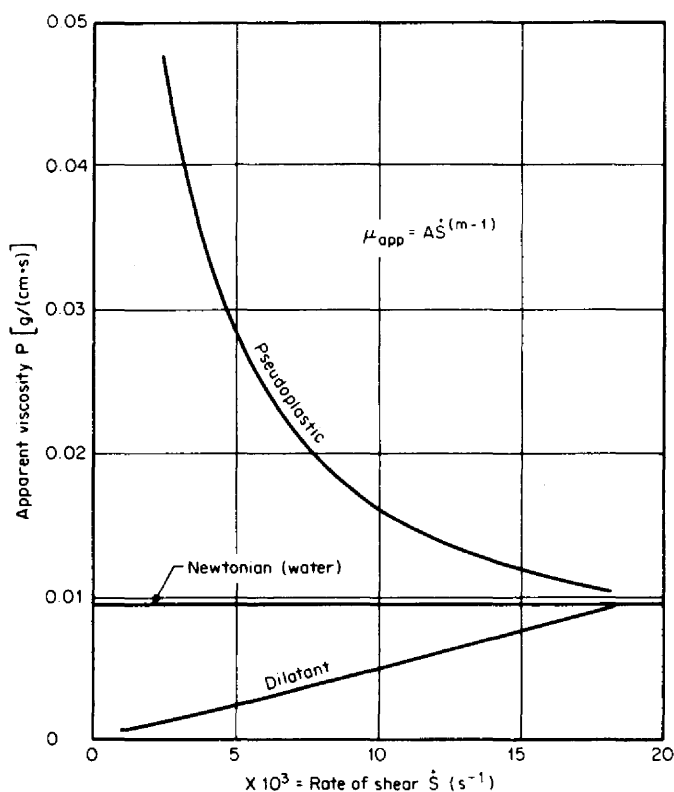


Figure 5.8 Apparent viscosity of power-law fluids.

Laminar Flow of Power-Law Fluids. Like newtonian fluids, nonnewtonian fluids exhibit a transition from laminar to turbulent flow profile with increasing Reynolds number. For newtonian fluids the transition begins at a Reynolds number of 2000; for power-law fluids the Metzner-Reed (1955) Reynolds number is used to predict the onset of turbulence.

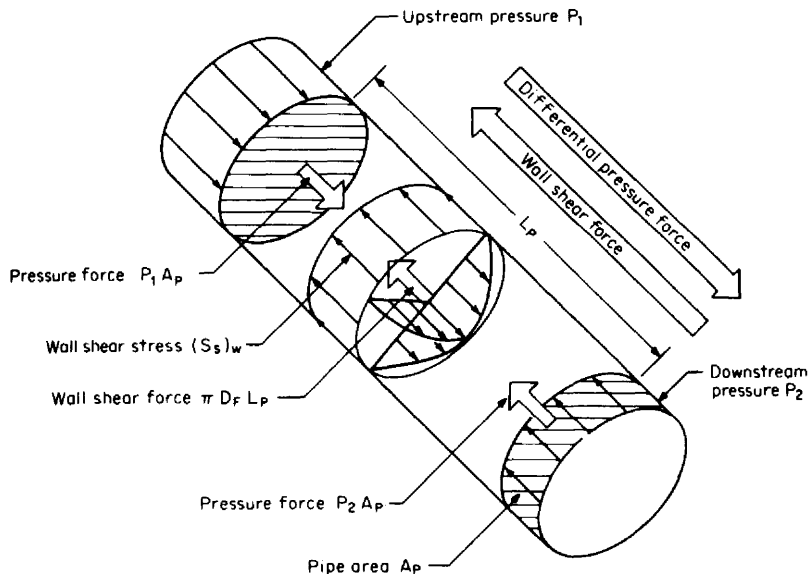


Figure 5.9 Wall shear and pressure force balance.

Figure 5.9 shows a section of flow pipe of known diameter with two pressure taps at a fixed spacing. A force summation can be used to find the wall shear stress $(S_s)_w$ in terms of the differential pressure, pipe diameter, and pipe length:

$$\pi L_p D_F (S_s)_w = \frac{\pi}{4} D_F^2 \Delta P \quad (5.25)$$

where the right-hand side is the pressure force required to overcome the wall fluid shear force (shear stress times wall area). Rearrangement of Eq. (5.25) yields

$$(S_s)_w = \frac{D_F \Delta P}{4 L_p} \quad (5.26)$$

The wall shear rate \dot{S}_w can be determined from a log-log plot of the measured differential pressure versus velocity as

$$\dot{S}_w = \frac{1 + 3m'}{4m'} \frac{8 \bar{V}_f}{D_F} \quad (5.27)$$

where m' is the slope of the plotted line. Combining Eqs. (5.23), (5.26), and (5.27) gives

$$\frac{D_F \Delta P}{4 L_p} = A' \left(\frac{8 \bar{V}_f}{D_F} \right)^{m'} = (S_s)_w \quad (5.28)$$

The term $8 \bar{V}_f / D_F$ is called the *Poiseuille flow index*, and the constants A' and m' are obtained from pressure-loss measurements. In laminar flow the Fanning friction factor f_f is related to Reynolds number and independent of wall roughness. If the

Reynolds number for nonnewtonian fluids is defined to be the Metzner-Reed Reynolds number, then the following relationship is developed:

$$f_f = \frac{16}{R_{MR}} = \frac{g_c D_F \Delta P}{2 \rho_f \bar{V}_f^2 L_p} \quad (5.29)$$

where f_f is by definition one-quarter of the Darcy-Weisbach friction factor generally used for pressure-loss calculations. Substituting Eq. (5.28) into Eq. (5.29) yields the Metzner-Reed Reynolds number as

$$R_{MR} = \frac{D_F^{m'} \bar{V}_f^{2-m'} \rho_f}{g_c A' 8^{m'-1}} \quad (5.30)$$

Equations (5.28) through (5.30) are written for the fundamental English engineering units of feet, pounds-force, pounds-mass, and seconds. If the pipe size D is in inches, then the Metzner-Reed Reynolds number is

$$R_{MR} = \frac{8 D_F^{m'} \bar{V}_f^{2-m'} \rho_f}{g_c A' 96^{m'}} \quad (5.31)$$

For power-law and newtonian fluids, m' equals m , and the relationship between the constants given in Eqs. (5.22) and (5.30) is

$$A' = \frac{A}{g_c} \left(\frac{1 + 3m}{4m} \right)^m \quad (5.32)$$

For the special case of newtonian fluids, $m = m' = 1$, and the relationship becomes

$$A' = (\mu_f)_e = \frac{(\mu_m)_e}{g_c} = \frac{A}{g_c} \quad (5.33)$$

That is, the absolute viscosity equals the constant A . The Metzner-Reed Reynolds-number equation then reduces to the familiar newtonian pipe Reynolds-number equation (5.1).

Figure 5.10 is a plot of Eq. (5.28) for a 118-cP newtonian fluid $[(\mu_f)_e = 0.00254]$ and a 23 percent lime in water power-law fluid. The values of A' and m' were selected from Table 5.1.

The Metzner-Reed Reynolds number was derived from the laminar friction-factor equation and, when it is combined with the Ryan-Johnson (1959) critical-friction-factor equation, an equation can be developed that will predict the onset of turbulence. The Ryan-Johnson critical friction factor is

$$(f_f)_c = \frac{1}{404} \frac{(1 + 3m')^2}{m'} \left(\frac{1}{2 + m'} \right)^{(2+m')/(1+m')} \quad (5.34)$$

For a newtonian fluid ($m' = 1.0$), equating Eq. (5.34) to Eq. (5.29) results in a pipe Reynolds number of 2099 for the onset of turbulence for a newtonian fluid. Use of the value 384 [rather than the 404 in Eq. (5.34)] to obtain the accepted Reynolds-number transition value of 2000 gives the critical Metzner-Reed Reynolds number as

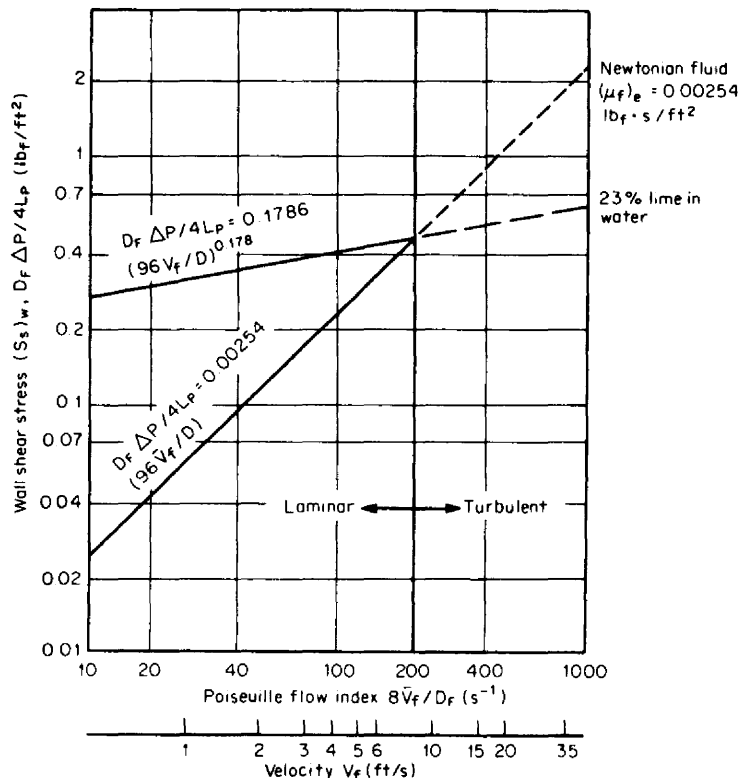


Figure 5.10 Poiseuille pressure and flow index for 4-in pipe flow of a newtonian and a power-law fluid.

$$(R_{MR})_c = \frac{6158m'(2 + m')^{(2+m')/(1+m')}}{(1 + 3m')^2} \quad (5.35)$$

The critical velocity for the onset of turbulence is then

$$(\bar{V}_F)_c = \left[770 \frac{g_c A' m'}{\rho_f} \left(\frac{8}{D_F} \right)^{m'} \frac{(2 + m')^{(2+m')/(1+m')}}{(1 + 3m')^2} \right]^{1/(2-m')} \quad (5.36)$$

The critical Metzner-Reed Reynolds number is plotted against the power-law exponent in Fig. 5.11.

Many flow measurements are made in small-diameter pipes for flows of high-apparent-viscosity fluids. The Metzner-Reed Reynolds number for such flows is, therefore, below the values shown in Fig. 5.11. For such fluids the relationship between point and average pipeline velocity is derived from the power-law-model equation as

$$V_p = \frac{3m + 1}{m + 1} \left[1 - \left(\frac{r}{r_p} \right)^{(m+1)/m} \right] \bar{V}_F \quad (5.37)$$

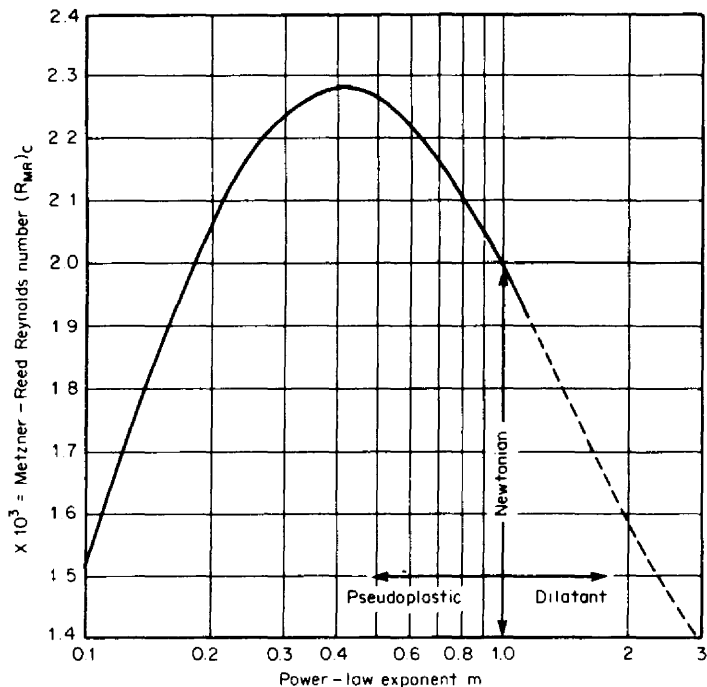


Figure 5.11 Critical Metzner-Reed Reynolds number for pseudoplastic and dilatant fluids.

Again, for a newtonian fluid ($m = 1$), this equation reduces to the parabolic velocity-profile Eqs. (5.2) and (5.3).

The ratio of point to average velocity is shown in Fig. 5.12. For pseudoplastics, the profile becomes increasingly blunt with decreasing power-law exponent, approaching a rectilinear profile. For dilatant fluids, the profile becomes conical in shape with increasing exponent. The location of the average velocity from the pipe wall is shown in Fig. 5.13.

Laminar Flow of Bingham Fluids. Bingham (or Bingham-like) fluids require some minimum stress to initiate motion between fluid layers. Until this *yield stress* is reached, adjacent layers retain a zero velocity gradient (shear rate).

Figure 5.14 shows shear stress plotted against shear rate for a typical Bingham fluid. The slope, as well as the yield shear stress, is seen to be a function of the volume fraction of solids. After the yield stress S_y is reached, the shear rate increases linearly. (For some fluids, called *yield-pseudoplastics*, this portion of the curve follows the power-law rather than a linear relationship.) The slope of the linear portion of the curve is defined as the *coefficient of rigidity* (ϕ_p), and, because it is linear, is sometimes referred to as the *plug-flow viscosity*.

Figure 5.15 illustrates the velocity profile and gives the coordinate system for the flow of a Bingham fluid. To initiate motion, a minimum pressure force is required to overcome the yield shear stress. Wall shear is transmitted only through a small fluid layer until equilibrium is reached between the pressure and the combined wall and fluid yield shear forces.

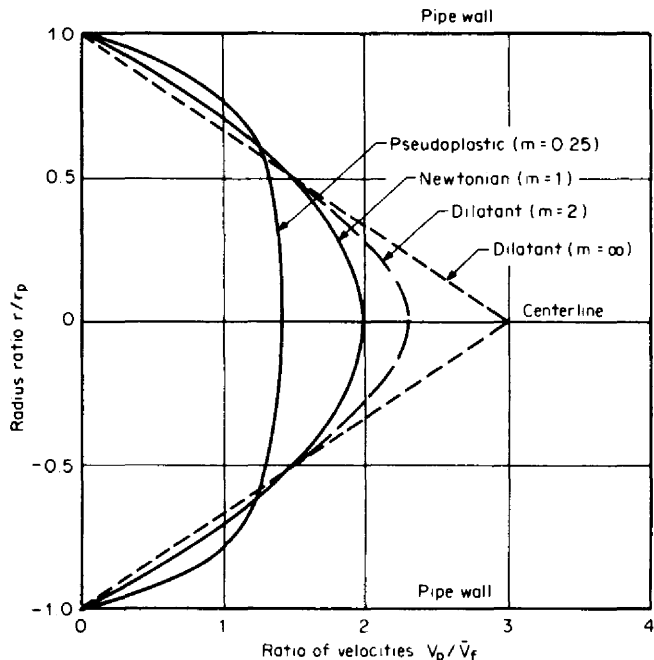


Figure 5.12 Velocity profile in laminar flow.

The velocity profile resembles a cylindrical plug of uniform-velocity fluid surrounded by a fluid annulus. An increase in the upstream pressure increases the plug velocity, which in turn increases the wall shear. This decreases the plug diameter until a laminar profile is approached.

The plug velocity \bar{V}_p , plug diameter D_p , velocity from the outside of the plug to the wall V_p , and average pipeline velocity \bar{V}_f are derived from the equation for shear stress in cylindrical coordinates and the rheological shear stress-shear rate equations for a Bingham fluid. For cylindrical coordinates and steady flow, the shear stress is defined by

$$S_s = -\frac{r}{2} \frac{dP}{dL_p} \quad (5.38)$$

The shear stress is also the sum of the yield shear stress $(S_s)_y$ and shear rate:

$$S_s = (S_s)_y + (\phi_p)_e \dot{S} \quad (5.39)$$

When the shear stress S_s is less than the yield shear stress $(S_s)_y$, the shear rate \dot{S} must be zero; no velocity gradients exist across the pipe section. Since the shear rate is the change in velocity divided by the incremental radius in cylindrical coordinates, the diameter of the plug can be derived from Eqs. (5.38) and (5.39) by setting shear rate equal to zero:

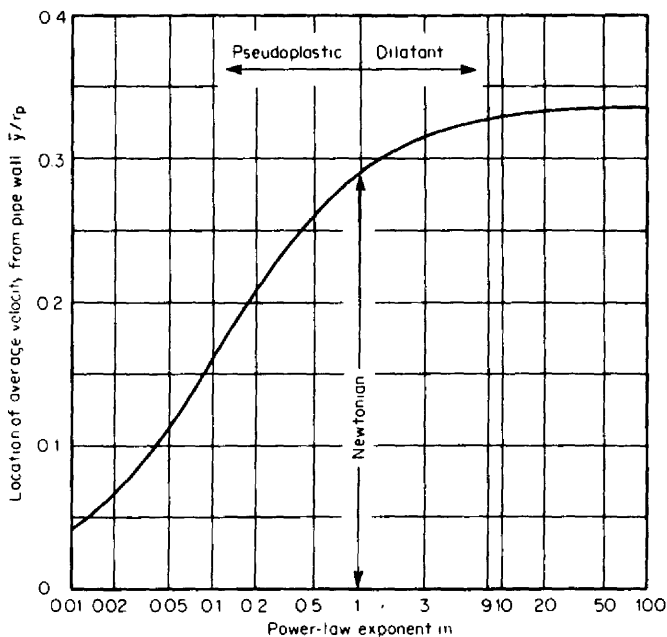


Figure 5.13 Location of average velocity from pipe wall in laminar flow.

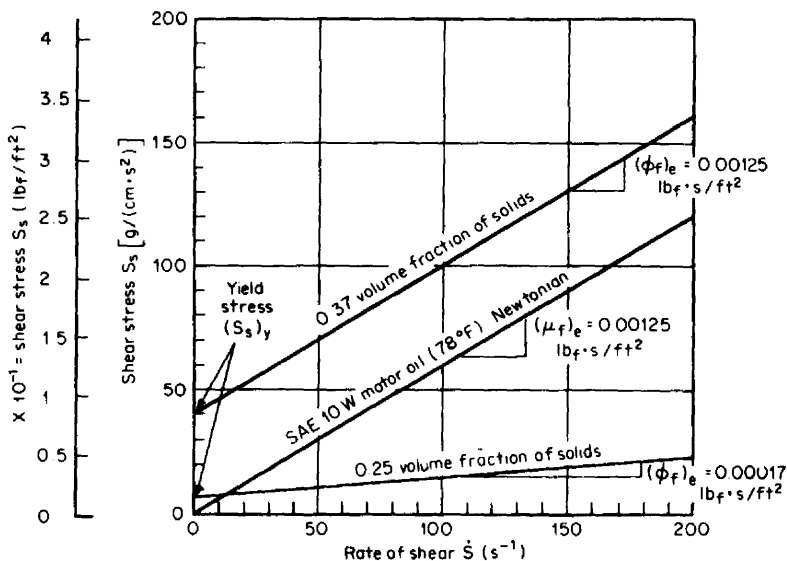


Figure 5.14 Shear stress versus shear rate for water suspensions of finely divided gallena. (Data from Govier and Aziz, 1977.)

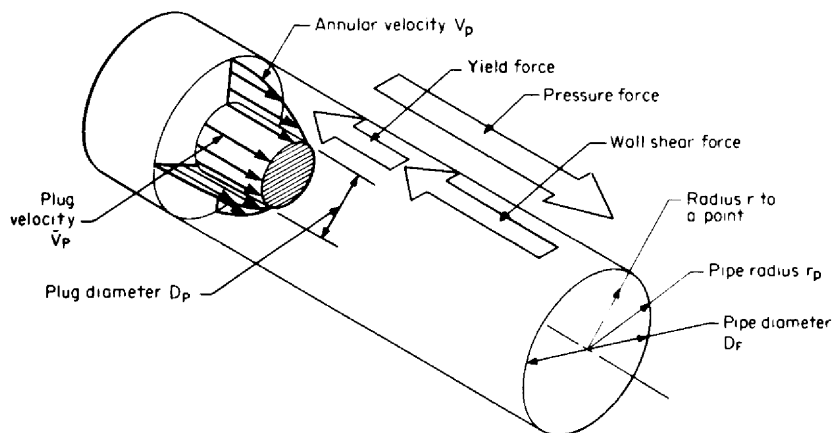


Figure 5.15 Pipe flow of Bingham or Bingham-like fluids.

$$D_p = \frac{4(S_s)_y}{\Delta P/L_p} \quad (5.40)$$

where $\Delta P/L_p$ is the measured pressure loss over a given length of pipe. The plug velocity then is

$$\bar{V}_p = \frac{(S_s)_y^2}{(\phi_f)_e \Delta P/L_p} \left(\frac{D_F}{D_p} - 1 \right)^2 \quad (5.41)$$

and, in the region outside the constant-velocity plug, the point velocity is

$$V_p = \frac{\Delta P/L_p}{4(\phi_f)_e} (r_p^2 - r^2) - \frac{(S_s)_y}{(\phi_f)_e} (r_p - r) \quad (5.42)$$

The average pipeline velocity is the sum of the plug flow and integrated annular flow divided by the pipe area and is expressed as

$$\bar{V}_f = \frac{D_F}{8} \frac{1}{(\phi_f)_e} \frac{D_F \Delta P}{L_p} \left[1 - \frac{4}{3} (S_s)_y \left(\frac{4L_p}{D_F \Delta P} \right) + \frac{(S_s)_y^4}{3} \left(\frac{4L_p}{D_F \Delta P} \right)^4 \right] \quad (5.43)$$

This turns out to be the Buckingham equation when it is rearranged in the form

$$q_{cfs} = \frac{\pi D_F^3}{32(\phi_f)_e} \frac{D_F \Delta P}{4L_p} \left[1 - \frac{4}{3} (S_s)_y \left(\frac{4L_p}{D_F \Delta P} \right) + \frac{(S_s)_y^4}{3} \left(\frac{4L_p}{D_F \Delta P} \right)^4 \right] \quad (5.44)$$

Figures 5.16 and 5.17 show wall shear stress versus the Poiseuille flow index for the Bingham fluids shown in Fig. 5.14.

The Reynolds number at the transition from laminar to turbulent flow can be estimated with the Reynolds number proposed by Govier and Aziz:

$$(R_{GA})_c = \frac{\rho_f (\bar{V}_f)_c D_F}{g_c (\phi_f)_e [1 + (S_s)_y D_F / 6(\phi_f)_e (\bar{V}_f)_c]} \approx 2100 \quad (5.45)$$

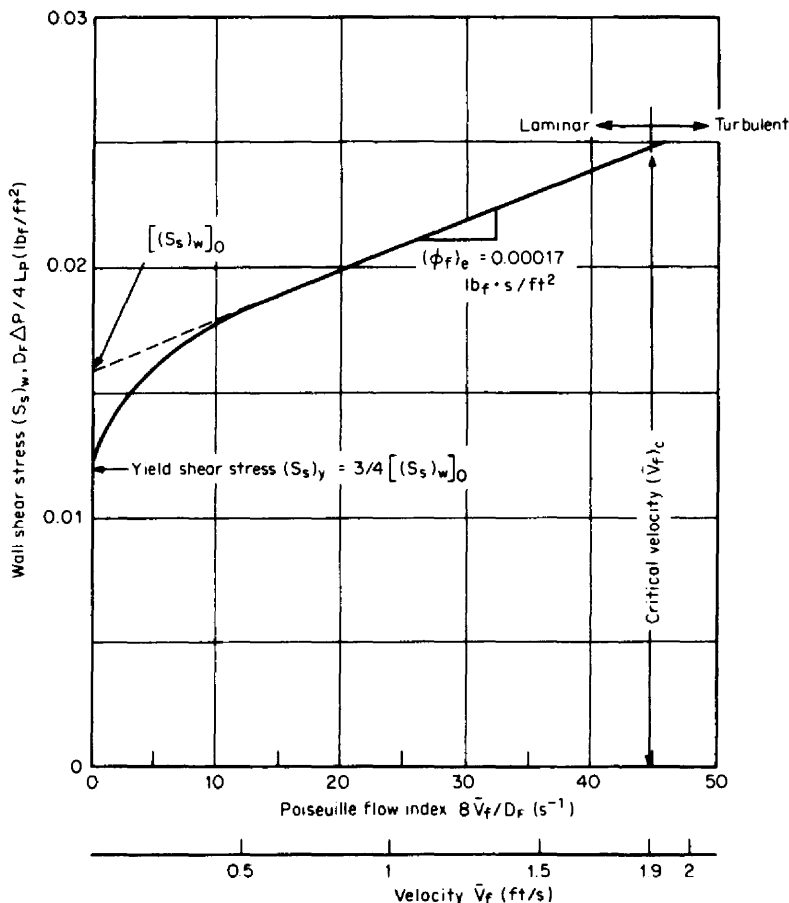


Figure 5.16 Flow with 0.25 percent volume fraction of solids in a 4-in pipe.

The bracketed term modifies the newtonian Reynolds number with the yield shear stress and coefficient of rigidity $(\mu_F)_e$. When the yield shear stress is zero, the coefficient of rigidity equals the absolute viscosity, and Eq. (5.45) reduces to the newtonian Reynolds-number equation.

For line sizes greater than 1 in, the bracketed term of Eq. (5.45) is greater than unity, and the critical velocity is well approximated by

$$(\bar{V}_F)_c = 106 \sqrt{\frac{(S_s)_y}{\rho_F}} \quad (5.46)$$

In this equation, the yield stress has the units of pounds-force per square foot. For most Bingham fluids, the flow remains laminar because the critical velocity exceeds 5 to 10 ft/s for yield stresses above approximately 0.1 lb_f/ft^2 .

Table 5.2 gives some typical values of coefficient of rigidity and shear stress for Bingham-like fluids. Table 5.3 gives the critical velocities for some line sizes based

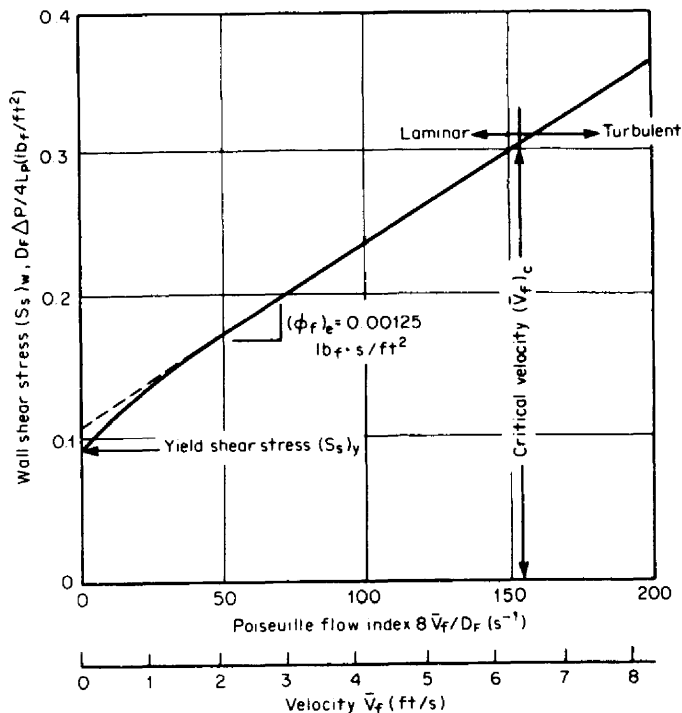


Figure 5.17 Flow with 0.37 percent volume fraction of solids in a 4-in pipe.

on Eq. (5.46). Some of the smaller line sizes shown are not normally used for Bingham-like fluids, but values are given to illustrate the fact that Bingham fluids require higher velocities than newtonian fluids to reach transition.

Prediction of the flow profile for a Bingham fluid is obviously more complex than for other time-independent fluids. The plug diameter D_p is a function of wall shear stress and coefficient of rigidity $(\phi_f)_e$. To illustrate the possible combinations, curves for two Bingham fluids with identical coefficients of rigidity but different yield shear stresses are shown in Fig. 5.18. In the region from point A to point C in Fig. 5.18, increasing pressure increases the velocity, and the profiles shown in Fig. 5.19a are successively produced for low-yield-stress fluids. For higher-yield-stress fluids (points A', B', C'), a larger plug diameter is formed for the same pipe velocity (Fig. 5.18b). For a fluid with zero yield stress (a newtonian fluid), the profile is parabolic.

The ratio of plug diameter to pipe diameter can be expressed in terms of the Poiseuille index as

$$\frac{8\bar{V}_f}{D_F} = \frac{(S_s)_w}{(\phi_f)_e} \left[1 - \frac{4}{3} \frac{D_p}{D_F} + \frac{1}{3} \left(\frac{D_p}{D_F} \right)^4 \right] \quad (5.47)$$

Ratios of plug to pipe diameter for various values of the ratio of yield shear stress to the coefficient of rigidity are shown versus the Poiseuille index in Fig. 5.20. For the low-yield-stress fluids the plug diameter rapidly decreases until, at 0.1 ft/s, the

TABLE 5.2 Yield Stress and Coefficient of Rigidity for Some Bingham (or Bingham-like) Fluids†

Substance	Metric units			English units			
	Specific gravity G_F	Yield stress (S_y) _y g·cm/s ²	Coefficient of rigidity ϕcP , g·cm/s	Yield stress (S_y) _y		Coefficient of rigidity ηR	
				lb _f /ft ²	lb _f /in ²	(ϕf) _e , lb _f ·s/ft ²	(ϕ_m) _e , lb _m /(ft·s)
Luting (dispersion of synthetic wax in polyisobutene)		15,700–19,600	1,000,000	32.8–40.9	0.227–0.284	20.8	670.0
Calcium soap grease (at 120°C)		7,100	6,500	14.8	0.103	0.136	4.37
Aluminum soap grease (at 120°C)		5,100	5,000	10.7	0.074	0.104	3.36
Lithium stearate grease, 14G8		6,500	100	13.6	0.094	0.0021	0.067
Flocculated aqueous china-clay, suspensions (80% under 1 μ m):							
No. 6	1.149	78	4.0	0.16	0.0011	0.000084	0.0027
No. 4	1.207	250	6.7	0.522	0.0036	0.00014	0.0045
No. 1	1.280	590	13.1	1.32	0.0086	0.00027	0.0088
Aqueous suspensions of Milicz clay ($d_{uv} = 70 \mu$ m):							
13.9 weight % solids		23	8.7	0.048	0.00033	0.00018	0.0058
16.8 weight % solids		53	13.6	0.111	0.00077	0.000284	0.0091
19.6 weight % solids		130	25.0	0.215	0.00189	0.000522	0.0168

Aqueous clay suspensions:								
No. V		1.36	66.5	19.4	0.139	0.00096	0.000406	0.0130
No. III		1.44	200	32.8	0.418	0.0029	0.000685	0.0220
No. I		1.49	345	44.7	0.721	0.0050	0.000834	0.0300
Aqueous suspensions of cement rock (92% under 74 μm), 54.3 weight % solids		1.52	38	6.86	0.0794	0.0055	0.000143	0.0046
Sewage sludges, 10 weight % solids:								
Chicago plant			6.7	52	0.0140	0.000007	0.00109	0.0349
Stuttgart plant			48	115	0.100	0.0007	0.00240	0.0773
Sludge No. 5 (Imhoff tank), 14 weight % solids		1.06	31	24.5	0.065	0.00045	0.000512	0.0165
Aqueous suspensions of coal char:								
Weight %								
Total solids	325-mesh solids							
45.5	28.6	1.23	20	31	0.055	0.00038	0.00065	0.0208
50.4	47.5	1.22	20	28	0.0418	0.00029	0.00058	0.0188

†Data from Govier and Aziz (1977).

TABLE 5.3 Critical Velocity by Line Size for Bingham (or Bingham-like) Fluids

Substance	Critical velocity (\bar{V}_p), ft/s; for line size D of:					
	0.5 in	1 in	1.5 in	2 in	3 in	4 in
Luting (dispersion of synthetic wax in polyisobutene)	$(\bar{V}_p)_c > 40$ ft/s					
Calcium soap grease (at 120°C)						
Aluminum soap grease (at 120°C)						
Lithium stearate grease, 14G8						
Flocculated aqueous china-clay, suspensions (80% under 1 μ m):						
No. 6	6.1	5.5	5.3	5.3	5.2	5.1
No. 4	10.5	9.6	9.4	9.2	9.0	9.0
No. 1	16.7	15.1	14.6	14.4	14.1	14.0
Aqueous suspensions of Milicz clay ($d_{av} = 70 \mu$ m):						
13.9 weight % solids	6.1	4.3	3.8	3.6	3.3	3.2
16.8 weight % solids	9.5	6.7	5.7	5.4	5.1	5.0
19.6 weight % solids	10.5	10.5	8.9	8.2	7.5	7.1
Aqueous clay suspensions:						
No. V	9.6	6.6	5.8	5.4	5.0	4.8
No. III	15.7	11.0	9.6	9.0	8.3	8.1
No. I	20.5	14.3	12.5	11.6	10.8	10.4
Aqueous suspensions of cement rock (92% under 74 μ m), 54.3 weight % solids	4.5	3.7	3.5	3.4	3.3	3.2
Sewage sludges, 10 weight % solids:						
Chicago plant	28.3	14.3	9.7	7.4	5.2	4.1
Stuttgart plant	>40	31.8	21.7	16.7	11.9	9.7
Sludge No. 5 (Imhoff tank), 14 weight % solids	13.4	7.7	6.0	5.3	4.5	4.2
Aqueous suspensions of coal char						
Weight %						
Total solids						
325-mesh solids						
45.4	28.6	14.2	7.9	5.9	5.0	4.2
50.4	47.5	12.9	7.1	5.3	4.5	3.7
3.8	3.4					

profile is essentially newtonian. For the higher-yield-stress Bingham fluids, the plug diameter remains at one-half the pipe diameter.

Time-Dependent Fluids. The profiles established by time-independent fluids are, at least to some degree, predictable. There are, however, two broad classes of non-newtonian fluids that change apparent viscosity with time. These time-dependent fluids are referred to as *thixotropic* if the apparent viscosity decreases with time,

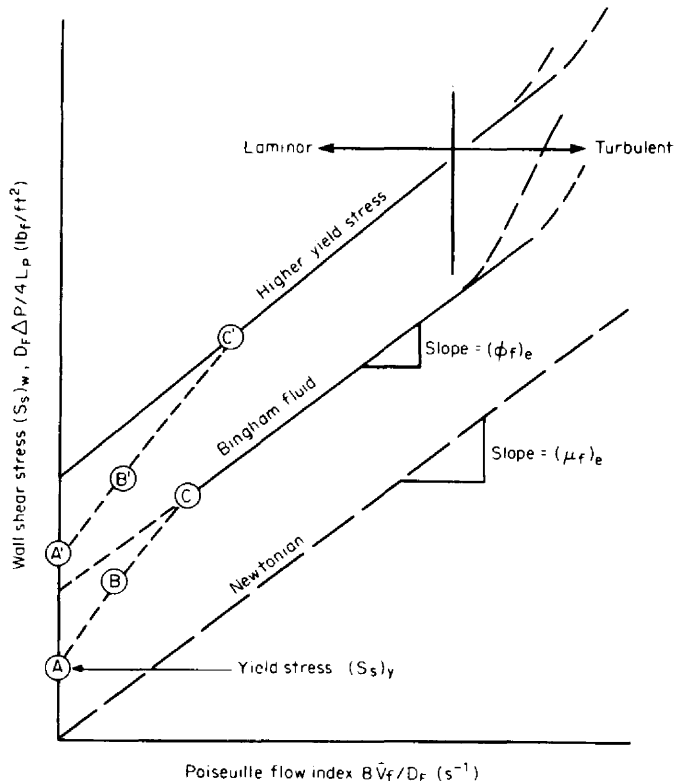


Figure 5.18 Typical pressure index versus Poiseuille index curve for Bingham fluids.

and *rheopectic* if the apparent viscosity increases with time. Thixotropic fluids become more pseudoplastic, and rheopectic fluids more dilatant, with time. In both cases shear stress-shear rate curves, although time-dependent, generally follow the power-law relationship of pseudoplastics; the exponent is less than 1. This results in profiles that approach, in time, the newtonian parabolic profile for rheopectic fluids, and blunter profiles for thixotropic fluids. Most thixotropic and rheopectic fluids have high apparent viscosities and, therefore, are in the laminar regime characterized in the earlier discussion of pseudoplastics.

Thixotropic Fluids. Thixotropic fluids have a structure that breaks down under constant shear. Low-temperature crude oils, drilling mud with the consistency of bentonitic clay in water, paints, ink, and mayonnaise are examples of thixotropic fluids.

In Fig. 5.21 is a generalized shear stress-shear rate curve for thixotropic fluids. As the shear rate is increased over a short period of time, the upper curve *AB* is followed. An immediate decrease in shear causes the fluid to follow the lower portion of the hysteresis curve, from *B* to *A*. This results in the flow-profile changes shown in the lower portion of Fig. 5.21.

If the shear rate is held constant at point *B*, the structure continually breaks down and undergoes an apparent viscosity decrease. Decreasing the shear rate from that at point *C* to zero can set up a yield-stress value at point *D*. The resulting

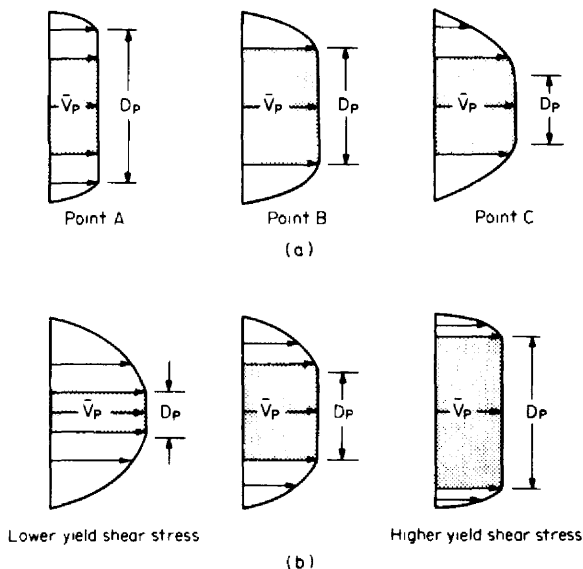


Figure 5.19 Velocity profiles for Bingham fluids. (a) Development of laminar profile. (b) Effect of yield stress on plug diameter at point B.

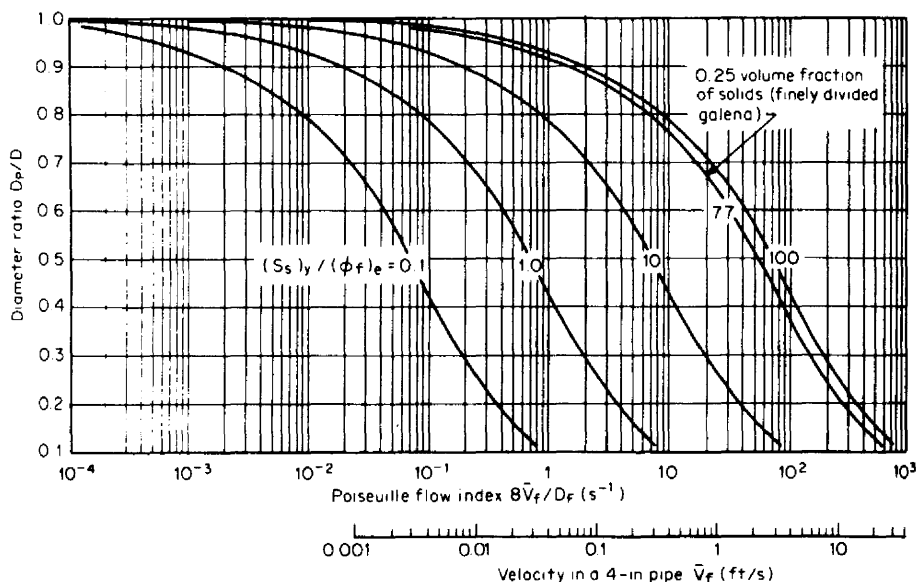


Figure 5.20 Ratio of plug to pipe diameter for the flow of a Bingham fluid.

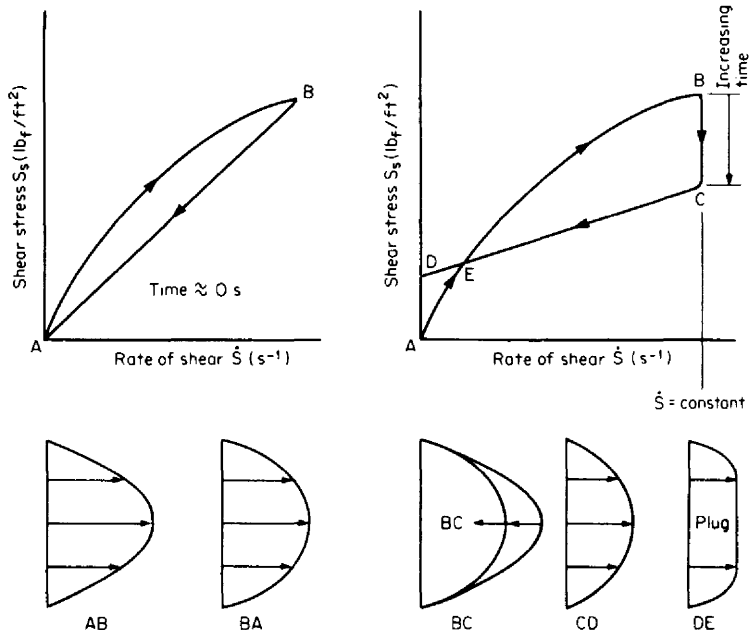


Figure 5.21 Characteristic shear stress-shear rate curves and possible velocity profiles for thixotropic fluids.

profiles can differ considerably at all flow rates, depending on whether the flow rate is increasing (A to B), remains fixed (B to C), or decreases (C to D). Most thixotropic fluids recover their original viscosity (point D to A) if allowed to stand for a sufficient length of time; some fluids require hours, and others restore within seconds. Figure 5.22 shows the decrease in apparent viscosity with constant shear rate of a thixotropic fluid.

Rheopectic Fluids. Time-dependent rheopectic fluids exhibit behavior opposite to that of thixotropic fluids in that, with constant stirring, the shear stress increases (Fig. 5.23). For this reason they are sometimes referred to as negative thixotropic fluids. As the slope of the shear stress-shear rate curve increases with time, these fluids become more dilatant.

In rheopectic fluids a small shearing motion accelerates the formation of a more rigid higher-apparent-viscosity fluid structure. If the shear rate is high, the viscosity may not increase, but, in general, the apparent viscosity increases with time to some limiting value. If the shear strain rate goes to zero, the initial viscosity and fluid structure are restored. In Fig. 5.24 is a shear stress-shear rate curve for a 2000-molecular-weight polyester that exhibits rheopectic behavior in some ranges. In Fig. 5.25 are the expected profile alterations for rheopectic fluids. At constant flow the profile becomes more newtonian.

Viscoelastic Fluids. Polymeric liquids, jellies, flour dough, and many fluids normally considered newtonian will, under certain conditions, not immediately return to a state of zero shear rate upon the removal of stress. This retention of shear stress accounts for the Weissenberg effect, in which flour dough climbs up the shaft of the stirrer due to stress buildup in the fluid, and the fact that an extruded polymer has a diameter that is larger than the die bore.

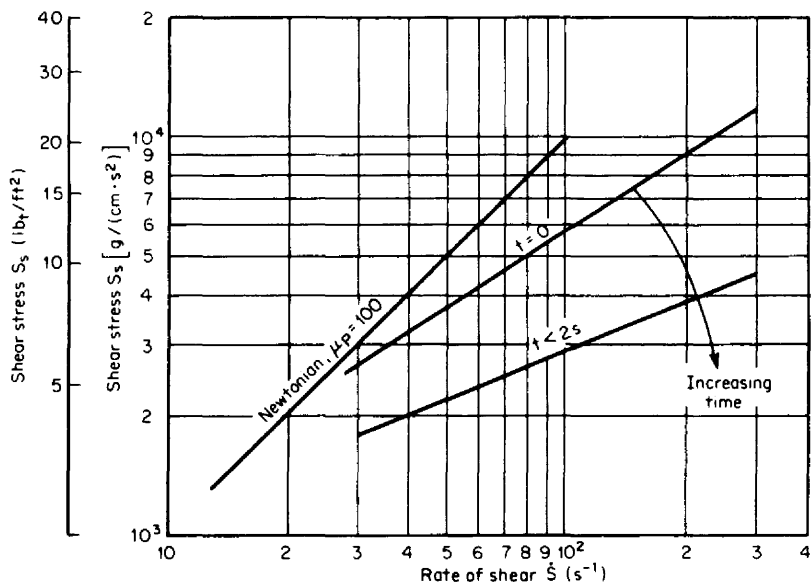


Figure 5.22 Thixotropy in an emulsion of soaps and higher polymers in gasoline. (Data from Govier and Aziz, 1977.)

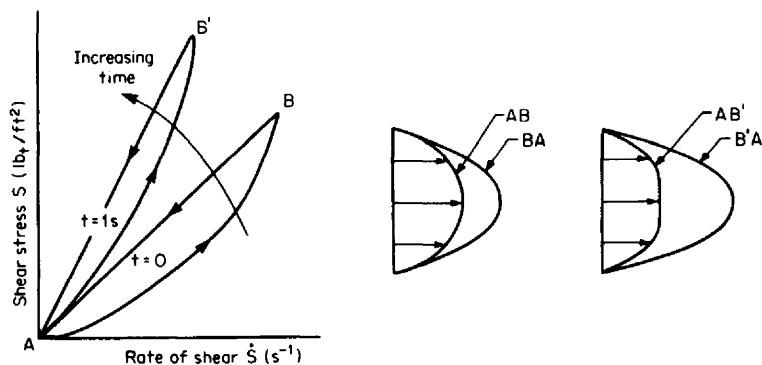


Figure 5.23 Characteristic shear stress-shear rate curves and possible velocity profiles for a rheopectic fluid.

In most fluids the energy of deformation is dissipated, but viscoelastic fluids retain energy, like an elastic solid. If a shear stress is applied to a solid (Fig. 5.25a), a defined deformation angle is observed. But for liquids, even a minute shear stress causes a continually increasing shear angle (strain) because viscous liquids cannot support shear. Unlike elastic solids, for which shearing resistance depends on deformation angle, the shearing resistance of a viscous fluid is proportional to the rate of deformation. For solids the angle is uniquely defined by Hooke's law relating shear stress to strain angle. But for nonviscoelastic fluids there can be no elastic behavior.

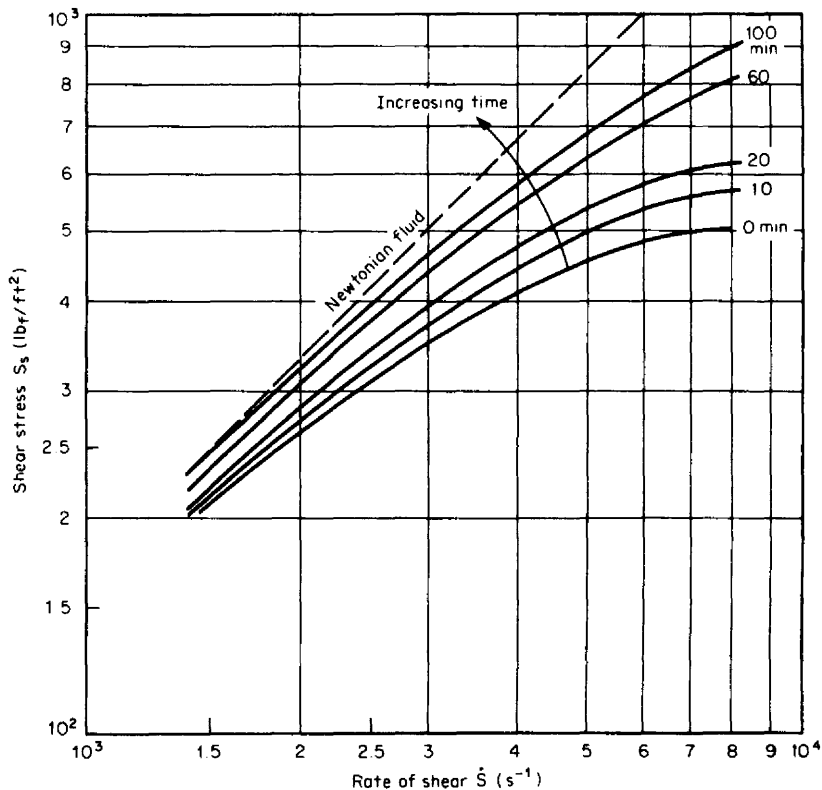


Figure 5.24 Time-dependent rheopectic fluid, a 2000-molecular-weight polyester. (Data from Govier and Aziz, 1977.)

Figure 5.25a and b presents a simplified illustration of the difference between a newtonian and a viscoelastic fluid under flowing conditions. For newtonian fluids, the only normal stresses are pressure-related, and wall shear-stress forces cannot induce elastic strain. But with viscoelastic fluids at the same velocity, a strain similar to that for a solid is present. This produces an additional normal stress within the fluid. At constant velocity, shear stress is constant, and both fluids exhibit newtonian flow behavior. When the flow rate is suddenly brought to zero, or in oscillatory flow, the change in shear stress is immediately accommodated by the newtonian fluid, and the normal pressure stresses are equalized. But, for the viscoelastic fluid, the strain energy resulting from elastic behavior requires time to dissipate. This time-dependent relaxation of both shear and normal stresses results in the liquid having both *viscous* and *elastic* properties.

The simplest mathematical model for this behavior is the Maxwell fluid equation, in which shear stress is separated into two terms:

$$S_s = (\mu_f)_e \dot{S} - k_1 \frac{dS_s}{dt} \quad (5.48)$$

The first right-hand term is the linear newtonian viscosity relationship, and the

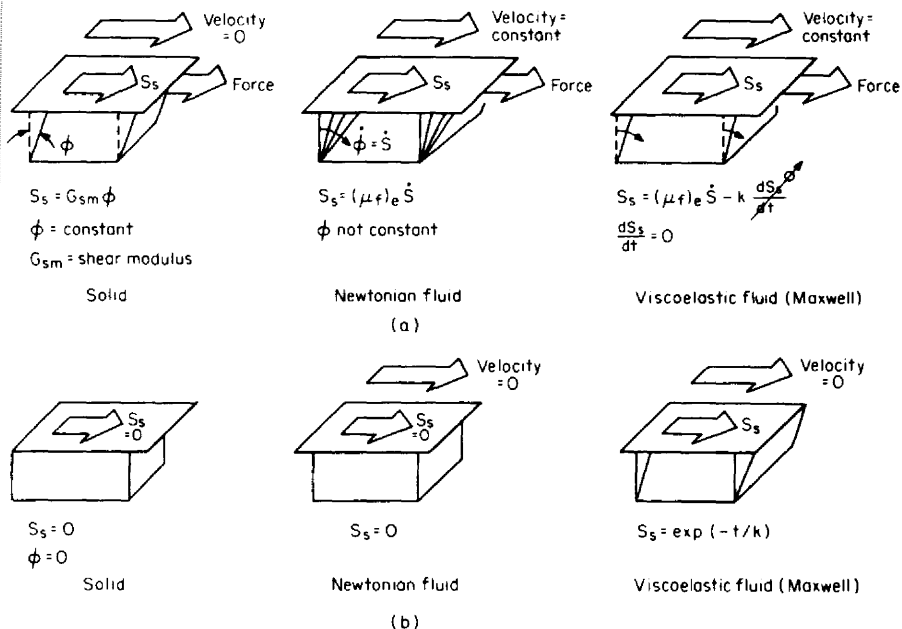


Figure 5.25 Effect of a force on a solid, newtonian fluid and on a viscoelastic fluid. (a) Application of force. (b) Removal of force.

second accounts for the relaxation of shear and normal stresses; k_1 is a constant that depends on viscosity and a rigidity modulus.

At steady flow the rate of change of shear stress dS_s/dt is zero (wall shear stress is constant), and the flow profile can be expected to be newtonian. If the flow rate is brought to zero (Fig. 5.25b), the shear rate S returns to zero, but the shear stress decays exponentially: Separating the variables in Eq. (5.48) gives

$$\frac{dS_s}{S_s} = \frac{-1}{k_1} dt \quad (5.49)$$

Upon integration, the shear stress is found to be

$$S_s = e^{-t/k_1} \quad (5.50)$$

The constant $1/k_1$ is called the *relaxation time*; it is the time constant for the exponential decay of normal stresses at constant strain.

Many modern fluids exhibit viscoelastic properties and have been the subject of extensive rheological investigation. Numerous equations have been proposed, of varying complexity. The reader is referred to the texts by Van Wazer et al. (1963) and Wilkinson (1960).

Profile Distortion

Pipe fittings, reducers, expanders, strainers, and elbows—necessary for normal plant piping—all affect profile. The many types and combinations of fittings result in

changes that are difficult to predict. Axial velocity vectors may be altered by one or a combination of the following:

1. A pure swirl that causes rotation about the pipe axis.
2. Secondary flows, such as two or more counterrotational vortices in a plane perpendicular to the pipe axis, or a bound, recirculating, secondary vortex flow caused by separation (a sudden enlargement in pipe size). These are usually in a plane parallel to the pipe axis.
3. An asymmetrical profile that peaks near the wall.
4. A symmetrical profile that has a high core velocity resulting from a sudden or too rapid reduction in pipe area.

In combination, these usually result in radial, tangential, and axial velocity vectors that are not symmetrical. While some flowmeters may be insensitive to radial velocity components (magnetic flowmeters), others are highly susceptible (single-path ultrasonic flowmeters). Also, insensitivity to tangential components (swirl) varies among flowmeters. For example, Fig. 5.26 shows the discharge-coefficient change (Kinghorn, 1977) for a venturi and an orifice when pure swirl is introduced into the line. In Fig. 5.26 a positive change means that the discharge coefficient is higher than without swirl.

The straight lengths of pipe required to eliminate swirl are different for gases and for liquids; the higher viscosities of liquids dissipate both swirl and profile distortion sooner, so liquids require shorter pipe lengths. Figures 5.27 and 5.28 show the pipe lengths required to dissipate an entry swirl angle at various Reynolds

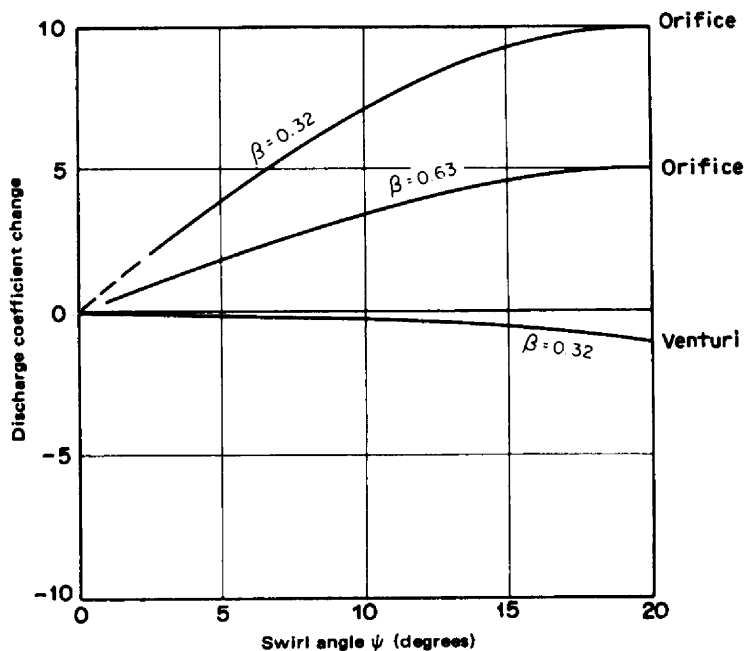


Figure 5.26 Bias error caused by swirl.

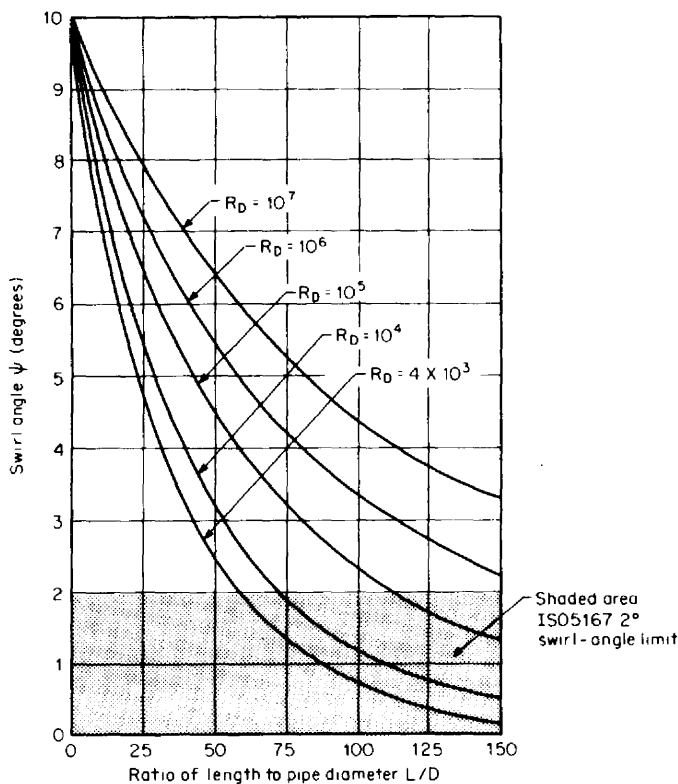


Figure 5.27 Pipe lengths to reduce 10° initial swirl angle.

numbers. These curves were derived from the equations presented by Kreith and Sonju (1965).

The reduction of swirl is a strong function of pipe roughness (Mottram and Rawat, 1986), with rough pipe decaying swirl in shorter straight runs. Halsey (1987) has shown, for a double bend in differing planes, that the swirl angle at a downstream location is well represented by

$$\psi = \psi_0 \exp \left(-\frac{6fL}{D} \right) \quad (5.51)$$

where ψ is the swirl angle downstream of the fitting, ψ_0 is the initial angle, f is the pipe friction factor, and L/D is the ratio of straight pipe length L to pipe internal diameter D .

In general, upstream fittings can be grouped into two broad categories: those that distort profile but produce little swirl and those that both distort and cause bulk swirl. A distorted profile can usually be brought into an acceptable form by adding sufficient straight lengths of pipe or by using flow conditioners in combination with reduced straight lengths.

A single elbow (Fig. 5.29) distorts the profile in the elbow plane, with the asymmetric profile progressively becoming double-peaked as the plane is rotated

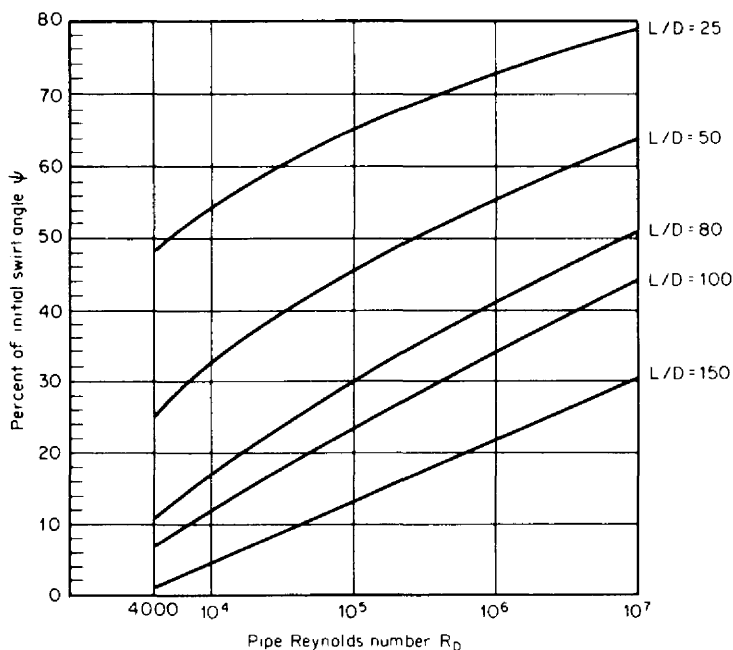


Figure 5.28 Pipe lengths to reduce initial swirl angle, percent.

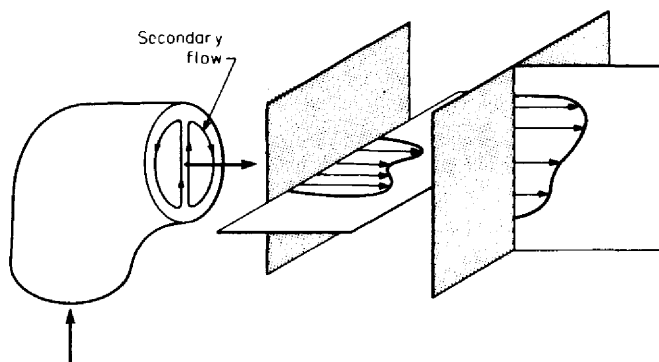


Figure 5.29 Velocity distribution following a single elbow.

into the horizontal. Secondary flows, consisting of double vortices, are also produced, and these give rise to a radial velocity component. A single elbow, or any fitting that produces an asymmetric profile, is considered to be in the first category—producing little swirl. A single bend, two elbows in the same plane or a partially opened valve will distort the profile but impart little rotation.

Installation of a Cheng rotary vane (Kosla and Mutsakis, 1992) upstream of an elbow eliminates the secondary flow and significantly reduces vibration at pumps. The pumps will operate at a higher flow rate with increased head, while consuming less electrical energy.

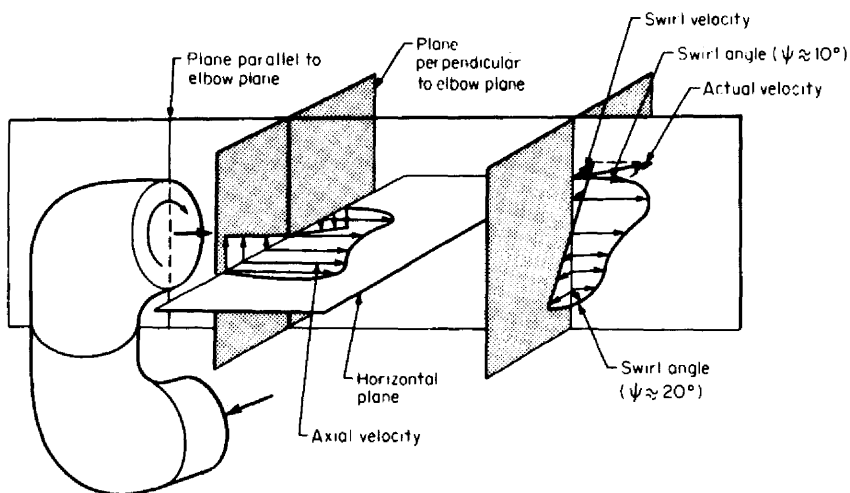


Figure 5.30 Velocity distribution following close-coupled elbows in different planes.

The helical fixed vanes look similar to a ship's propeller and alter the incoming flow to compensate for the turning effects of the elbow. Clarke (1994) reports lower pump maintenance and improved performance with these vanes installed upstream of elbows. Before the vanes were installed, vibration, caused by cavitation, was created by elbow turbulence and resulted in 10 pipeline failures a year.

If elbows are arranged such that the flow must change direction (Fig. 5.30), swirl is produced in addition to the asymmetric profile. This causes the profile to corkscrew down the pipe, as shown in Fig. 5.31. Swirl is caused by low-energy fluid moving from the inside of the first elbow to the inside of the second. When intersecting elbow planes form an angle between 30 and 90°, most of the low-energy fluid follows the shortest path, causing fluid rotation rather than producing secondary flows. The strongest swirl occurs when elbow planes are at 60° to each other. However, the addition of 2 to 5 (and preferably 10 to 30) diameters of straight pipe between elbows substantially reduces interaction and considerably reduces swirl.

Swirl and similar distorted profiles are also produced when a high-velocity stream is blended at right angles into a lower-velocity stream.

The analysis of such profiles is difficult. The swirl angle, profile distortion, and resulting three-component velocity vectors are related to the bend radius, entering profile, entering swirl, secondary flows, spacing between elbows, and angle between elbow planes. Figure 5.32 shows some typical fittings and piping conditions, grouped into the two flow-disturbance categories. In general, fittings that cause secondary flow in a plane parallel to the pipe axis produce higher fluid turbulence, which assists in recovering the profile in shorter lengths. Contoured fittings, such as a long sweeping bend, more strongly establish both secondary flows and profile distortion.

Mattingly and Yeh (1986), using laser velocimetry, are investigating the feasibility of predicting a meter's bias error based on a mathematical model of the meter. This model, combined with expressions for the decay of swirl and expected distorted profiles for various combinations of upstream fittings, will be used to estimate the error. These studies will assist in computer-aided design work and in estimating overall uncertainty for some installations.

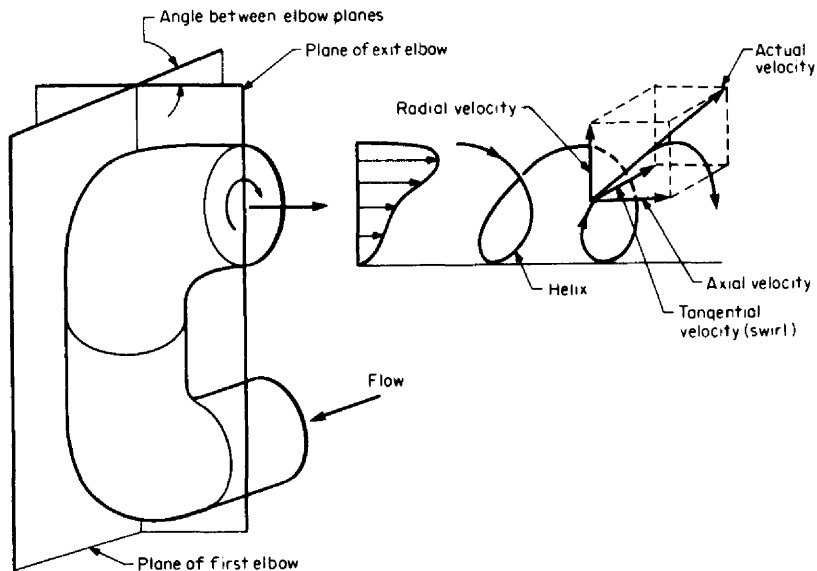


Figure 5.31 Velocity components in swirling flow following close-coupled elbows in different planes.

Initial turbine meter tests have been successful in predicting the bias error for a meter sensitive to swirl angle, but other mathematical models will be needed for meters that are sensitive to radial and severe profile distortion.

Flow Conditioners. In many installations it is impossible to provide sufficient lengths of straight pipe to remove swirl and to restore an acceptable reference profile geometry. For this reason, flow conditioners (Fig. 5.33) are used in combination with specified pipe lengths.

Shown in Fig. 5.34 are velocity and swirl angles measured at 1 pipe diameter upstream and 7.5 pipe diameters downstream of three flow conditioners. Distortion and swirl were produced by two close-coupled elbows in different planes, with flow conditioners located 1.5 pipe diameters downstream of the last elbow. The swirl is effectively removed by a four-tube-bundle conditioner, but the profile is not brought into symmetry. The swirl is eliminated by both the Zanker and Mitsubishi conditioners, and the profile is made more symmetric.

AGA-ASME tube-bundle conditioners (Fig. 5.35) are widely used because of their low cost, ease of fabrication, and low maintenance. The number of tubes is not specified, but, in general, four to eight tubes effectively remove swirl and secondary flows, and nineteen or more remove moderate distortion. Further increasing the number of tubes does not improve the profile-restoring capability.

Tube bundles effectively reduce swirl to 2° or less, the overall length not being a significant parameter in the removal of swirl. The AGA straightener (Fig. 5.35a) has less distortion downstream than the ISO straightener and a lower overall pressure loss. However, neither achieves an equivalent fully developed velocity profile in less than 11 pipe diameters. To achieve a fully developed profile it is important that the flow be blocked or restricted close to the wall, with the central core having the larger flow area.

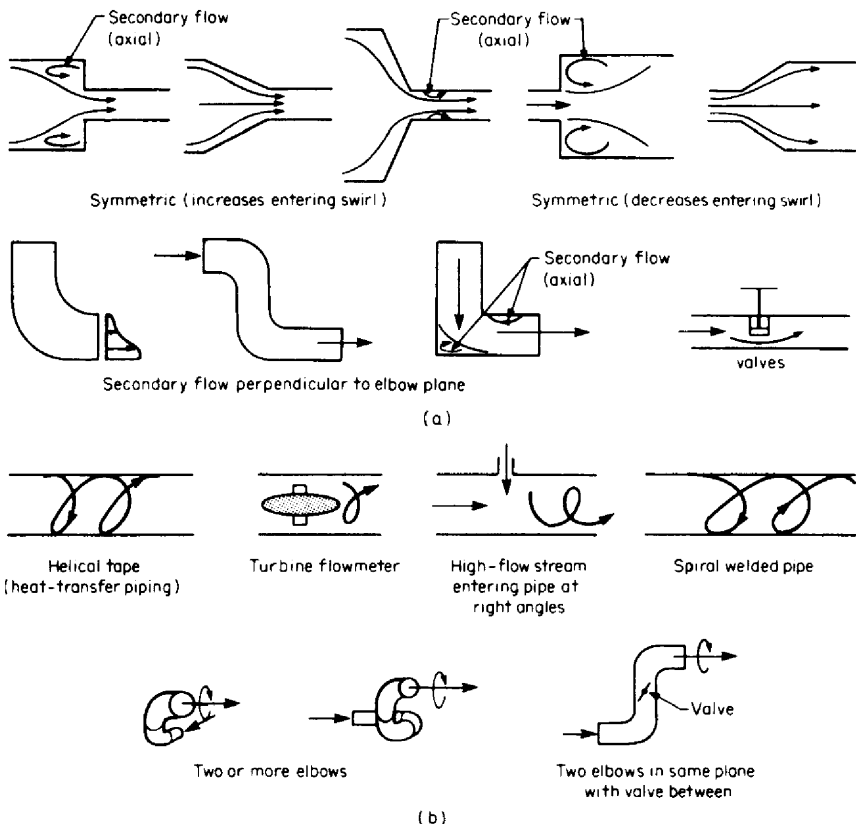


Figure 5.32 Fittings categorized by disturbance type. (a) Category 1: profile distortion and secondary flow. (b) Category 2: profile distortion, secondary flows, and swirl.

The Vortab conditioner (Fig. 5.35b) conditions the profile by removing both swirl and distortion with minimum overall pressure loss and required upstream straight pipe.

The hole size, spacing for the downstream construction of the Zanker (1969) conditioner are shown in Fig. 5.36. Laws and Ouzzone (1992) reported test results that showed that the thickness of the Zanker plate has an effect on the performance of the composite device, upstream perforated plate, and downstream honeycomb section to distorted flow. If the plate is sufficiently deep, the honeycomb section becomes redundant, and a single thick plate is satisfactory.

The construction details for the single-plate Mitsubishi conditioner (Akashi et al., 1979) are shown in Fig. 5.37a. Several thick perforated plates have been proposed based on the findings of Asashi. The K-Lab plate (Wilcox et al., 1990) and the Laws (1990) plate are similar in construction and are shown in Fig. 5.37b and c. These conditioners lower pressure loss and a fixed hole diameter and are easier to fabricate than the Zanker or Sprengle conditioner. The permanent pressure loss increases with the distortion that must be removed. Swirl conditioners (Fig. 5.33a) have the lowest pressure loss but require more straight pipe lengths than the higher-

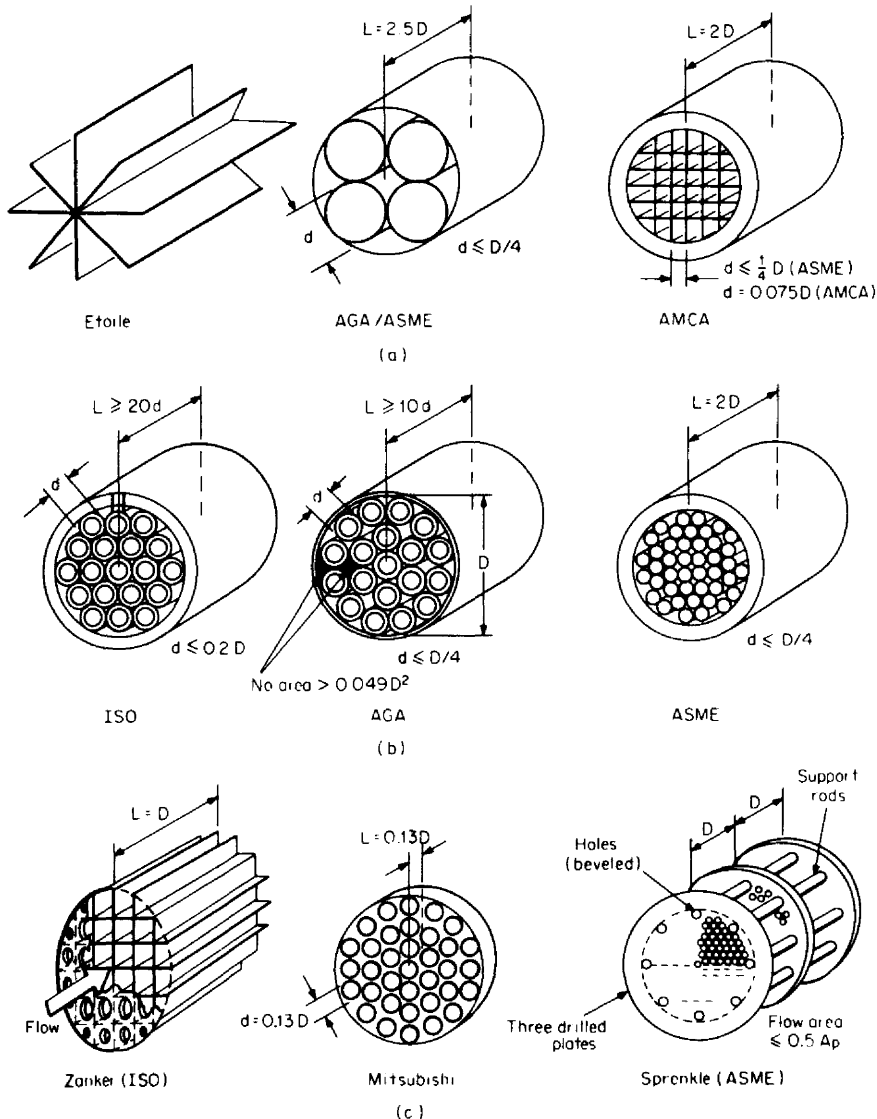


Figure 5.33 Flow conditioners. (a) Swirl. (b) Swirl and moderate distortion. (c) Swirl and distortion.

pressure-loss conditioners shown in Fig. 5.33c. The unrecoverable pressure loss for the conditioners shown in Fig. 5.33, expressed in terms of pipeline velocity, is

$$h_l = K_{FC} \rho_f \bar{V}_f^2 \quad (5.52)$$

in inches of water,

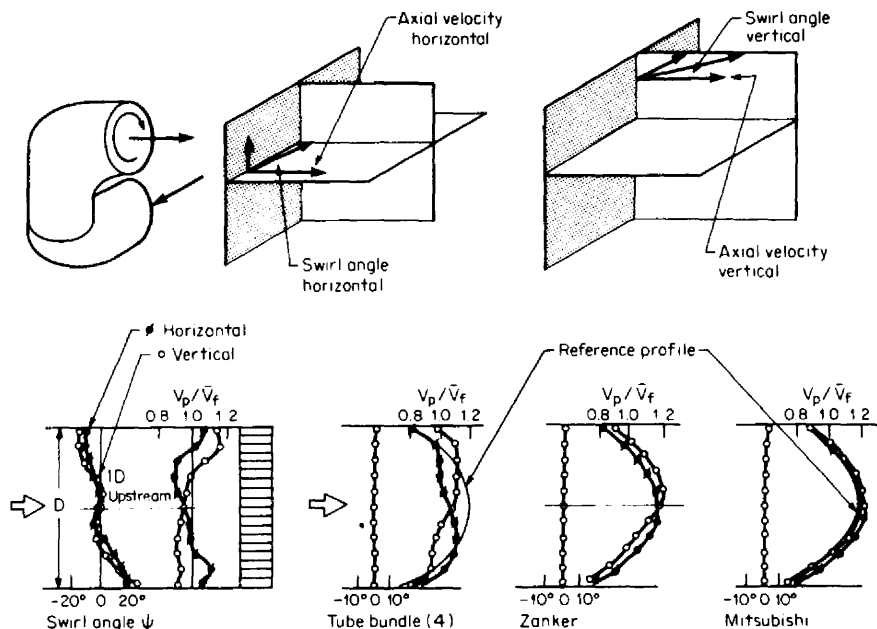


Figure 5.34 Velocity and swirl angle upstream and downstream of three flow conditioners. (From Akashi et al., 1979.)

$$H_L = K_{FC,H} \frac{\bar{V}_f^2}{2g_c} \quad (5.53)$$

in feet of flowing fluid, and

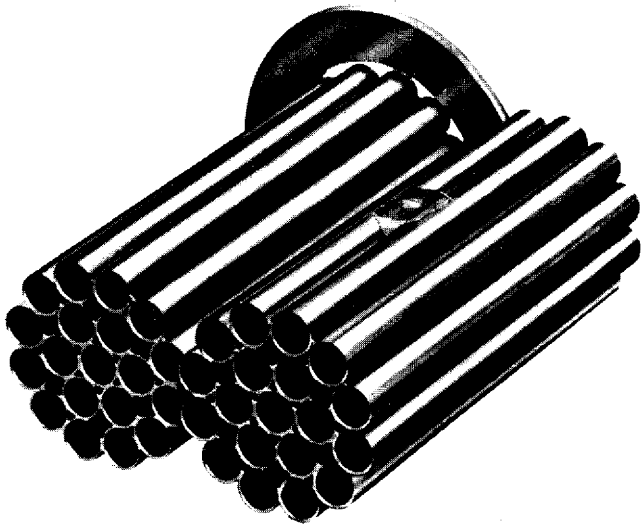
$$\Delta P = K_{FC,\Delta P} \frac{\rho_f \bar{V}_f^2}{2g_c} \quad (5.54)$$

in pounds-force per square foot. Pressure-loss coefficients for these equations are given in Table 5.4.

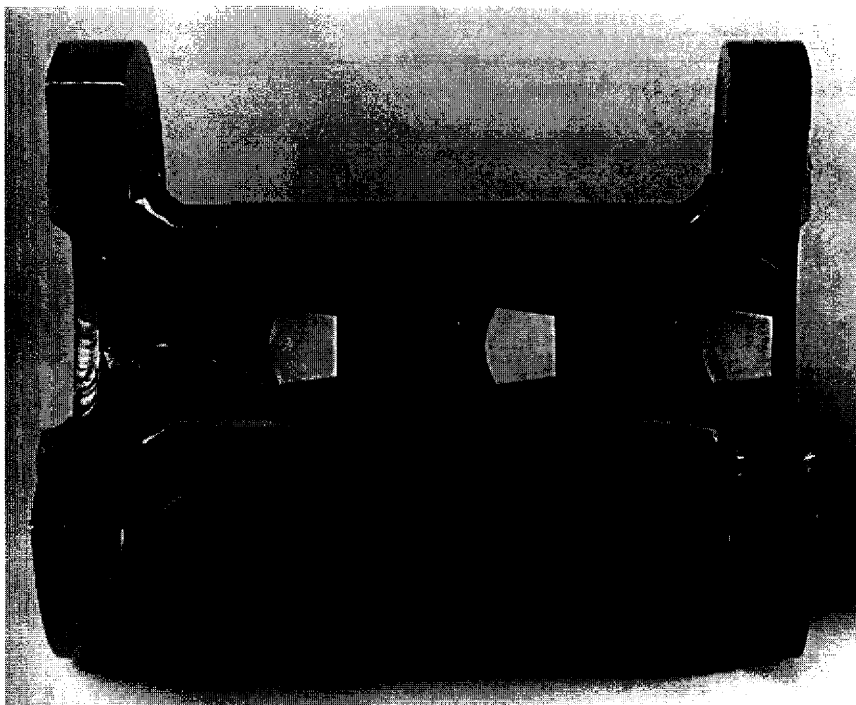
NONHOMOGENEOUS FLOWS

The theoretical and working flow equations for all flowmeters are based on homogeneous flows. Densities at specific cross sections within the flowmeter must be known from either calculations, direct measurements, or previously determined tabulated values. Depending on the flowmeter's principle of operation, the effect of a nonhomogeneous flow can be slight or quite significant.

It is convenient to group nonhomogeneous fluids into the following three broad categories:

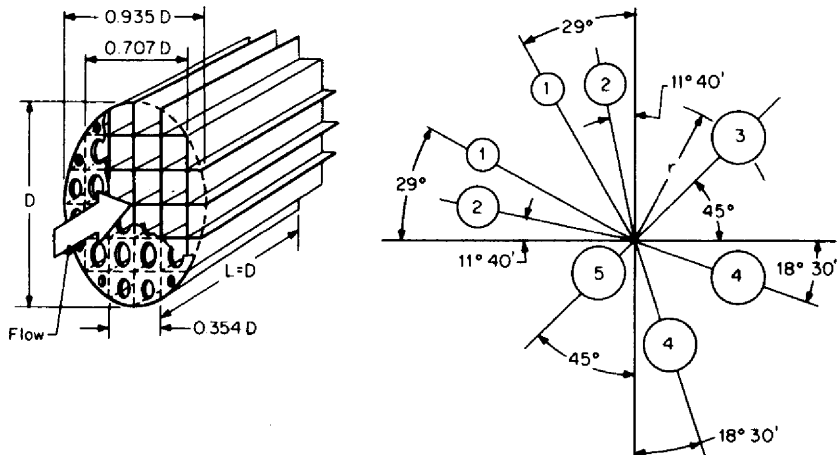


(a)



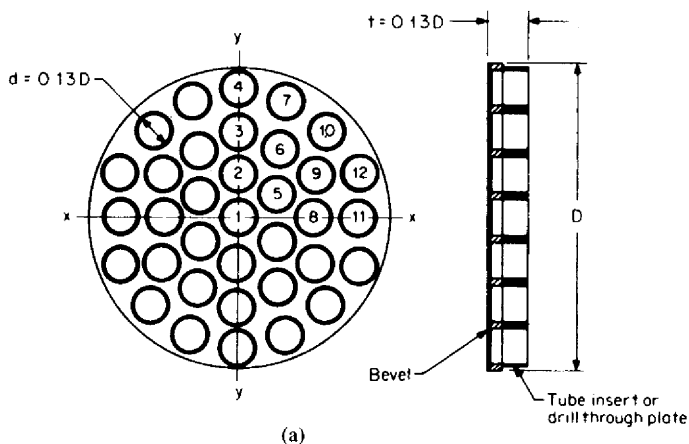
(b)

Figure 5.35 Flow conditioners. (a) AGA-ASME tube bundle. (Courtesy Daniel Industries, Inc.)
(b) Vortab.



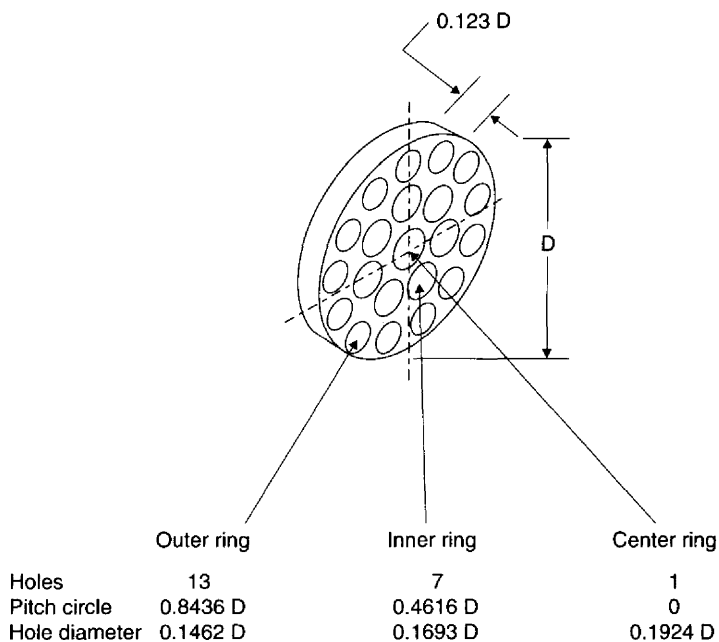
	Hole number				
	1	2	3	4	5
Hole diameter	0.077D	0.110D	0.1365D	0.139D	0.141D
Radius to hole (r)	0.45D	0.425D	0.375D	0.28D	0.125D
Number of holes	8	8	4	8	4

Figure 5.36 Zanker flow conditioner.

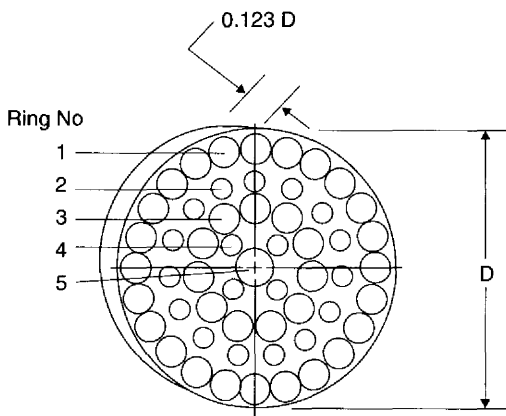


	Hole number											
Coordinate	1	2	3	4	5	6	7	8	9	10	11	12
x	0	0	0	0	0.129D	0.134D	0.156D	0.252D	0.255D	0.288D	0.396D	0.400D
y	0	0.142D	0.283D	0.423D	0.078D	0.225D	0.381D	0	0.146D	0.288D	0	0.151D
Number of holes	1	2	2	2	4	4	4	2	4	4	2	4

Figure 5.37 Thick plate flow conditioners for swirl and distortion. (a) Mitsubishi. (b) K-Lab. (c) Laws.



(b)



Ring	1	2	3	4	5
Holes	24	15	11	4	1
Hole diameter	$0.1071 D$	$0.0714 D$	$0.107 D$	$0.0714 D$	$0.1286 D$

(c)

Figure 5.37 (Continued)

TABLE 5.4 Unrecoverable Pressure-Loss Coefficients for Flow Conditioners

Flow conditioner	Unrecoverable pressure-loss coefficient	
	K_{FC}	$K_{FC,H}$ and $K_{FC,\Delta P}$
Tube bundle (4) (Etoile)	0.0035	1
Mitsubishi	0.006	2
Tube bundle (20) (Zanker)	0.017	5
Tube bundle (41) (AMCA†)	0.024	8
Sprenkle (50% flow area):		
Beveled holes	0.033	11
Square-edged holes	0.042	14

†Air Moving and Conditioning Association Standard 210-67 (1967).

1. Two-phase fluids
2. Fluids with two or more components
3. Two-phase fluids or fluids with two or more components that can be considered homogeneous

Two-phase fluids include *quality* steam and ammonia vapor flows, where the fluid is a single substance partially in a liquid state and partially in a gaseous state. Fluids with two or more components would be air in water, coal mixed with oil, pulp stock in water, or any combination of liquids, gases, and solids of differing substances in varying proportions. In many cases, if the second phase or one of two mixture components is finely dispersed and approximately of the same density as the other, the nonhomogeneous mixture is considered homogeneous, and the flow equations are used without additional secondary equipment to measure mixture percentage.

There are two significant differences between nonhomogeneous and homogeneous flows. First, the density is not easily determined; second, one phase or one or more of the components may not be moving at the same velocity as the main flow, and, in some cases, may actually be flowing along the bottom of the pipe. This is called *holdup* or *slip*. Slip is a complex function of viscosity, particle size, density differences, surface tension, and the *superficial* velocity of each component. The effects of gravity also alter flow patterns—horizontal, vertical, and inclined pipe cause differing relative velocities for the components.

While there is a large body of information on nonhomogeneous pressure loss, the added complexity of making a flow measurement has not been well addressed, either experimentally or theoretically. The reader is referred to the texts by Govier and Aziz (1977), Hewitt (1978), and Wasp et al. (1979) for detailed analysis of these complex flows. In this handbook, only fluids that can be considered homogeneous will be discussed.

When two-phase or multicomponent flows are metered, the void fraction, holdup, or percentage of each constituent needs to be determined in order to predict the quantity, or velocity, of each component. Several measurement methods are available. The reader is directed to a review paper on particle sizing techniques by Tayali

and Bates (1990) for additional information on the various methods, including details on optical methods.

Gamma Ray Gauging. Gamma rays are part of the electromagnetic spectrum (infrared, visible light, etc.) which can be sensed at a detector. Depending on composition, rays are absorbed, scattered, or passed through the pipe. These rays are detected, and their relative strength is an indication of the flowing density.

Gamma ray gauging requires a source, a detector, and usually a microprocessor to compute density based on stored algorithms for a particular fluid application (Nelson and Hendrick, 1985). Nuclear gauging is widely used, under carefully controlled conditions, for metering slurries, suspensions, multicomponent fluids, and fluids of variable compositions. Olatunbosun and Frith (1986) have recently reported on a versatile measurement system capable of nonintrusive multicomponent/multiphase flow measurement for monitoring and control.

A neutron radiography visualization method for multiphase flows is presented in detail by Takenaka et al. (1990). Visualizations by real-time neutron radiography are demonstrated for various flows of a nitrogen-water two-component flow in a stainless pipe, annular flow of water in a vertical pipe, and for other flow conditions. The method obtained photographs taken every 1/60 s by an image-processing method of the flow profiles.

Johansen and Froystein (1994) discuss the significance and limitations of gamma-ray imaging. They conclude that there is a need for faster-responding compact detectors and that scintillation crystals are the only practical gamma-ray absorbers over the range of interest. Kumar et al. (1995) have implemented a γ -rays void-fraction automatic scanner system capable of measuring fluidized beds and bubbly columns.

Capacitance Measurement. The measured electrical capacitance between two diametrically opposite electrodes is directly proportional to the permittivity of the flowing multicomponent mixture. Transducers whose operating principle is based on detecting the change in capacitance with changes in components of the flowing mixture, are increasingly being used.

The major problem with this technique (Beck et al., 1986) is the dependence of the concentration measurement on the flow regime in the pipe (bubbly, stratified, etc.). The difficulty is overcome by using helical sensors or rotating electrical fields. Capacitance transducers have been successfully used for measuring water concentrations in oil, gas, and void fractions in oil, and Beck et al. report on a three-component (oil, water, and air) apparatus.

Fiber Optic. The work described by Berthold et al. (1994) presents the first application of near-infrared absorption methods to void fraction measurements in two-component or two-phase flows. The primary problem with prior methods is the high degree of scattering from small bubbles or droplets in the visible wavelength band. By using two-wavelength compensation methods, the light scattering is significantly reduced. This fiber optic method measures void fraction in a small volume along a line across the pipe. Time averaging results in a good approximation of the flowing bubbles.

Microwave Absorption. El-Ayouty and Stepanek (1983) have demonstrated the feasibility of microwave absorption by water molecules in a concurrent gas-and-water-based liquid flow. In an upward flowing pipe, with both air and water and

with air and a corn syrup solution, the mean amplitude of the holdup fluctuations were a strong function of the gas and liquid flow rates and multicomponent flow regimes.

Ultrasound. Ultrasound (Xu et al., 1986) is attractive for gas/liquid flows because it offers the possibility of an external clamp on a detector/emitter mounting. Two transmitters are mounted a distance apart and are excited simultaneously by a periodic pulse. This produces a series of equispaced high-frequency ultrasonic waves passing through an upstream and downstream separated volume. As the bubbly air/water flows upward, the amplitude of the pulsed waves is modulated by the scattering caused by the entrained air.

PULSATING FLOW

Reference-condition accuracy is based on steady flow, which is defined by ISO Technical Report 3313 (1988) as "flow condition in a measuring section in which the flow does not vary in time." ISO 5167 (1995) notes that "This International Standard applies only to pressure differential devices in which the flow remains subsonic throughout the measurement section, is steady or varies only slowly with time." Although an ISO working group (1975) was established to characterize steady flow, and several draft documents were written, no international or national standards exist that define steady flow. Without a clear distinction between steady and unsteady flow, the user must decide whether a flow measurement standard does or does not apply.

It is important to recognize that flow is a dynamic process, and the dynamics of the pulsating fluid, turbulence intensity, and primary and secondary devices are interrelated in flow measurement. Fluctuating pressure within lead lines, the response to velocity-profile changes, vortex formation, and turbine-rotor inertia are but some of the influences arising from interrelationships between flow and flow-meter dynamics.

In the *ideal* flowmeter, variations in flow rate, pressure, and density are instantaneously sensed, and no error results. But in real flowmeters, the inertia, damping, and fluid-pressure forcing function, as well as profile alterations and pipeline resonant frequencies, affect secondary measuring devices. The response characteristics of each affect the resolution of the overall flow.

Pulsating flow has been the subject of numerous experimental and analytical investigations. This work covers four major investigation areas:

1. Pulsating and unsteady pipeline flow investigation
2. Development of correction factors to be applied to specific flowmeters
3. Definition of a *threshold pulsation index* below which a certain bias error is assumed
4. Design of passive filters, such as volume tanks and in-line restrictors, that reduce pressure fluctuations to acceptable limits for flow measurement

The following paragraphs citing Muller (1970) appeared in the proceedings of the symposium, *The Measurement of Pulsating Flow*:

The aim of the meeting was to make people aware of the influence of pulsations on the accuracy of measurement. He [Muller] observed that the problem had not really been solved since Hodgson's work. However, delegates will carry away with them important ideas now being developed in relation to the subject.

There are several glimmers of light although the practical solution of the problem at present is still to damp out fluctuations, as a suitable flowmeter for all flow conditions is awaited. Of necessity, measurement must come before control can be attempted and the limiting factor is in the former and not the latter; hence only one paper on pulsating flow control was presented.

R.C. Mottram (1994) further supports these observations with the following statement:

The only practical solution is supported by documented experimental data is to reduce the amplitude of the velocity pulsation by introducing damping into the system. Probably the best known and longest established damping scheme involves the placing of a single receiver between the pulsative source and the differential pressure type flowmeter. Another scheme uses a double chamber receiver with internal choke tube instead of a single chamber receiver. It is possible to derive theoretical criteria for both schemes for the determination of adequate damping involving a dimensionless group known as the Hodgson number.

Little has changed since this 1970 symposium, and although there is more insight into the problems of pulsating-flow measurement, the practical solution still is to *filter* pulsations prior to making a measurement. Jeffery (1986) indicates that predicting the effect of pulsations remains difficult. Jeffery's work has shown, for orifice meters, that the Hodgson number, long used as an aid for the design of damping components in the metering system, cannot guarantee that the measurement error will be less than 1 percent.

In the absence of standards, the threshold pulsation index I_p defined by Head (1956) is recommended. For index values below the threshold value, reference-condition accuracy applies. For greater index values, passive-type filters (such as restrictors), increased volume, or a combination of both should be used to bring flow variations below the threshold value.

Flow Characteristics

Typical flowmeter signals produce three distinct types of traces on a recorder. The pen may draw a random pattern (Fig. 5.38a), a defined oscillation period with a superimposed noise pattern (Fig. 5.38b), or a complex waveform (Fig. 5.38c).

The small-amplitude, rapid pen drawing is caused by the action of the fluid's turbulent intensity on the flowmeter and is referred to as *noise*. Noise is always present and is produced by throttling valves, fittings, slightly protruding gaskets, flow separation, and cavitation within the installation. Noise patterns are usually of smaller amplitude in laminar flow than in turbulent flow. Because they are usually of small amplitude, random, and similar to noise patterns in the laboratory in which the flowmeter accuracy was determined, they lead to no additional error.

A cycling flow rate results from fixed-speed pumps, compressors, and fans, oscillating control valves, and sometimes fixed-pipeline vibration frequencies. The time to complete one cycle may be hours or seconds, but the period is defined by

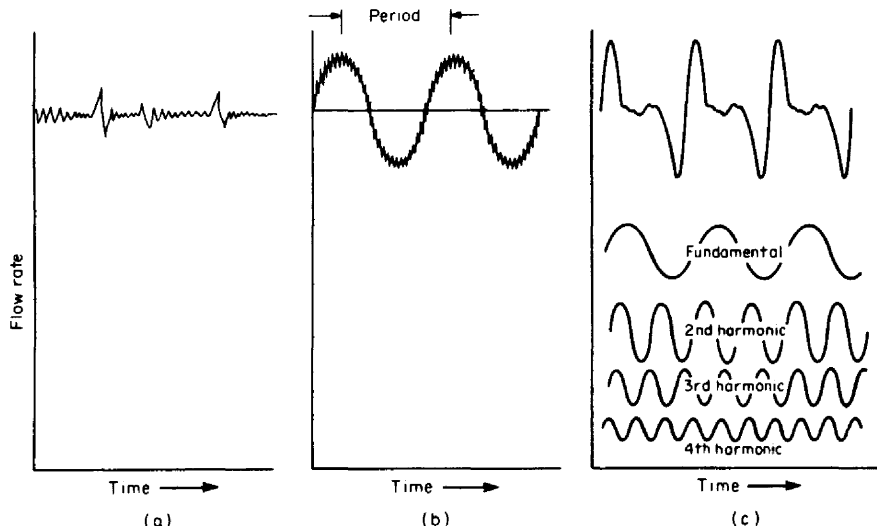


Figure 5.38 Typical recording of a flowmeter signal. (a) Noise. (b) Defined waveform. (c) Complex waveform.

a single value. For long periods and small flow-rate changes, all flowmeters usually follow these changes while remaining within their reference accuracy.

When reciprocating compressors are used to transport large quantities of high-pressure gas in reciprocating steam-engine flows, pressure and flow fluctuations are large and contain multiple frequencies (Fig. 5.38c). This results in observable, usually fixed waveforms with several harmonic frequencies of differing amplitudes.

Edwards and Wilkinson (1971) investigated the effect of changing frequency on laminar flow profiles (Fig. 5.39). At low amplitudes and frequencies the profile is unaffected, but with increasing frequency two symmetrical peaks develop that progressively move outward toward the wall. For turbulent flow (Fig. 5.40), Mizushima et al. (1975) show that a high-amplitude, low-frequency source distorts the profile throughout the pulsating period. The effects diminish with increasing frequency.

Shown in Fig. 5.41 are curves of typical integrated-velocity-profile flow rate, centerline velocity, and longitudinal pressure gradient in pulsating turbulent flow, as measured by Kirmse (1979). The integrated velocity profile (flow rate) is not in phase with either pressure gradient (pressure loss) or centerline velocity. In general, velocity and pressure frequencies are combinations of harmonic frequencies of varying amplitude. To fully identify their characteristics requires high-frequency-response velocity and pressure transducers, and a wave analyzer. Additionally, a restrictive device in the line, such as an orifice or vortex-element bluff body, alters the frequency spectrum in the critical measuring planes. In many applications, waveforms in gas pipelines are extremely complex and, as a result, have not been analyzed satisfactorily.

Threshold Pulsation Index

Head (1956) has shown that a pulsation intensity, defined as the ratio of the difference between maximum and minimum flow rate to the average flow rate (Fig.

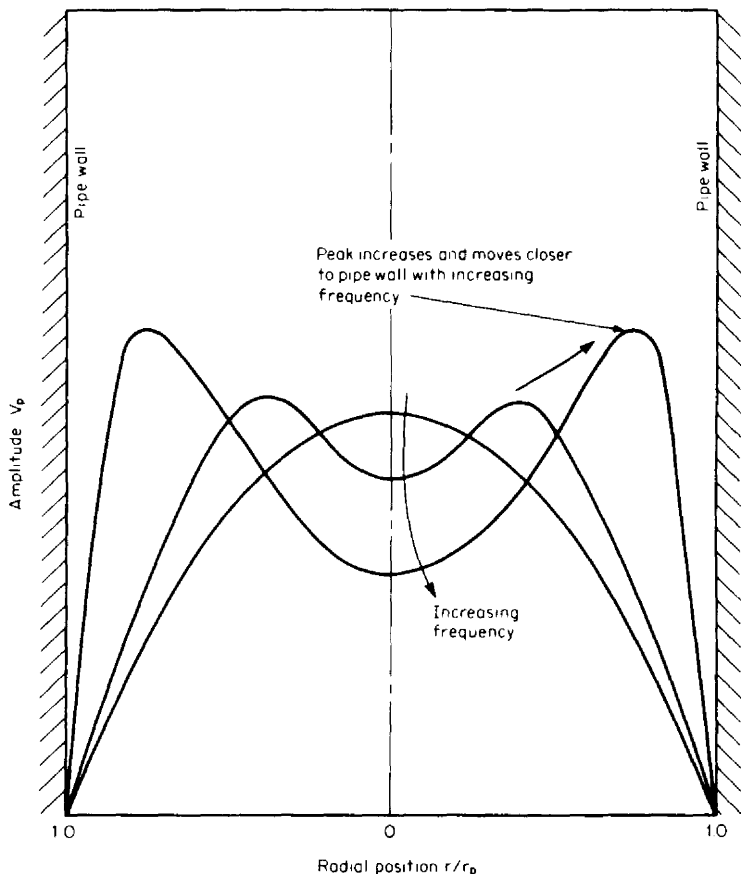


Figure 5.39 Effect of frequency on velocity amplitude in laminar flow.

5.42) can be used to estimate bias errors for a given class of flowmeters. The pulsation index is defined as

$$I_p = \frac{(\bar{V}_f)_{\max} - (\bar{V}_f)_{\min}}{2(\bar{V}_f)_{av}} = \frac{(q_v)_{\max} - (q_v)_{\min}}{2(q_v)_{av}} \quad (5.55)$$

The flow-rate correction factor based on this index is

$$F_p = \frac{\text{indicated flow}}{\text{average flow}} = (1 + 4\alpha b_p I_p^2)^n \quad (5.56)$$

In Eq. (5.56), α is a wave-shape coefficient determined by Fourier analysis of the harmonics contained in the various wave shapes shown in Fig. 5.42. The maximum known value of α is 0.25 for a rectangular flow fluctuation. The frequency coefficient b_p ranges from 0 to 1 and includes flowmeter-system damping and the effect of the pulsation frequency on the primary element. For a given wave shape,

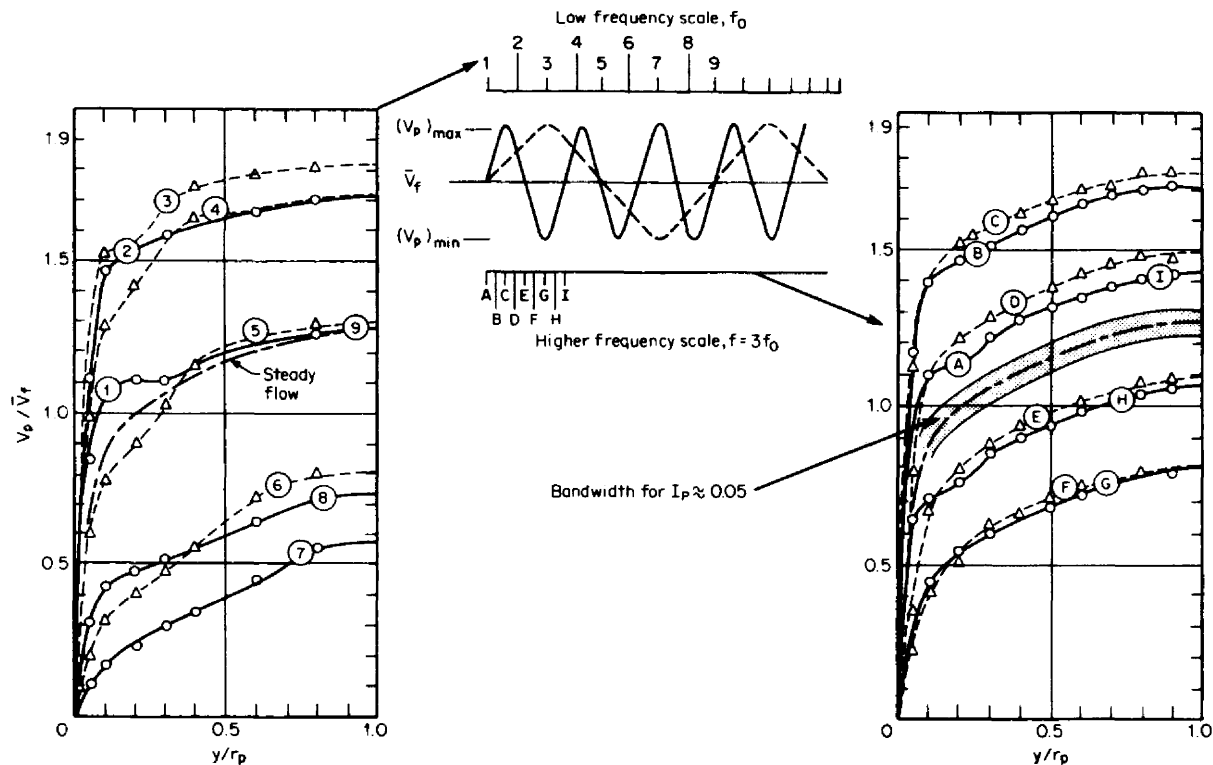


Figure 5.40 Effect of frequency on profile in turbulent flow.

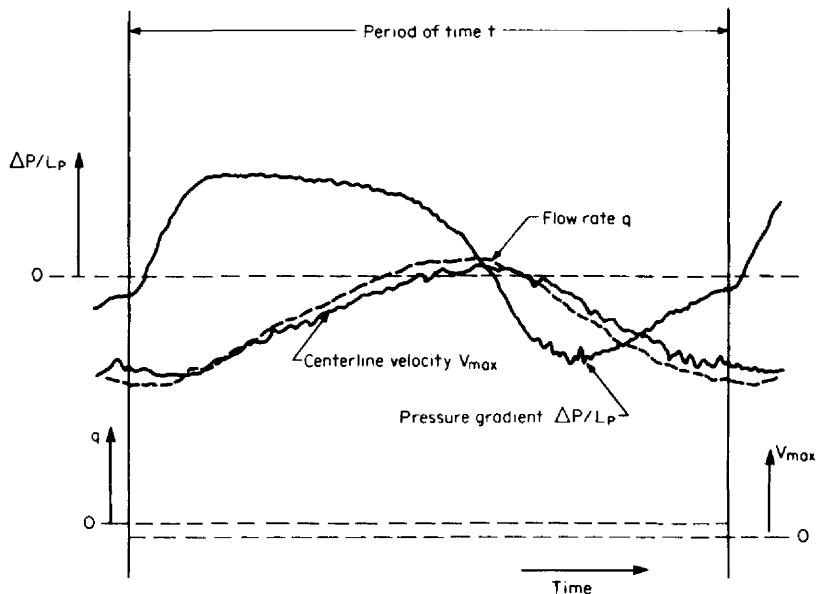


Figure 5.41 Typical fluctuations of discharge pressure gradient and centerline velocity for pulsating turbulent flow ($R_D = 10^5$).

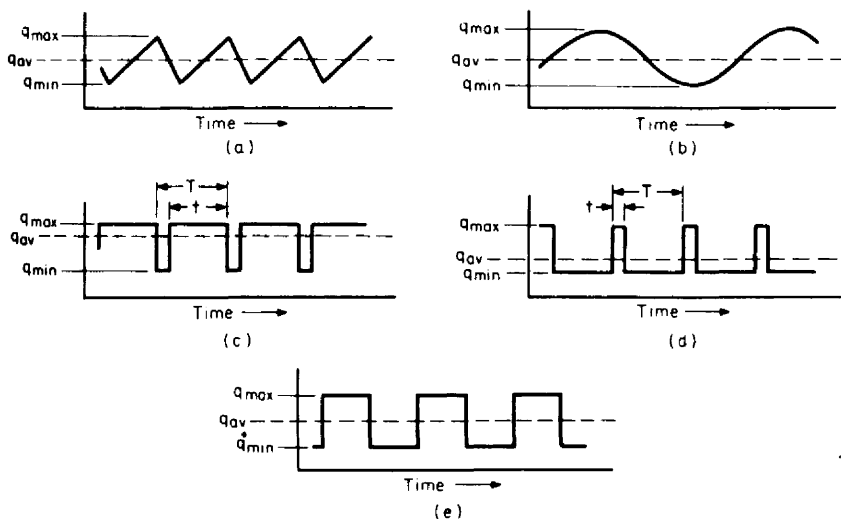


Figure 5.42 Waveform coefficients for some geometrical waveforms. (a) Sawtooth, $\alpha = 0.0833$. (b) Sinusoidal, $\alpha = 0.125$. (c) Dip, $\alpha = (t/T)(1 - t/T)$. (d) Spike, $\alpha = (t/T)(1 - t/T)$. (e) Rectangular, $\alpha = 0.25$, $t/T = 0.5$.

b_p is close to 0 (no error) over frequency ranges that flowmeters can follow. These ranges extend from 1 cycle/h to 10 Hz, depending on flowmeter and auxiliary equipment. At greater frequencies, flowmeters cannot follow rapid changes, and b_p approaches 1.0, resulting in maximum bias error.

In turbulent compressible flow, n in Eq. (5.56) is 0.5 for differential producers and 1.0 for linear meters; it is 0 for all flowmeters in laminar flow. In the laminar-to-turbulent transition regime, n may range from 0 to 0.5 for differential producers and from 0 to 1.0 for linear flowmeters. The maximum bias error then occurs when $n = 0.5$ for differential producers, when $n = 1.0$ for linear meters, and when $b_p = 1.0$.

The pulsation index is maximum for all flowmeters when $n = 1$, $\alpha = 0.25$, and $b_p = 1.0$. If $F_p = 1.001$ (bias = +0.1 percent) is selected as an acceptable correction-factor limit that includes normal variations among laboratories, then with these values for n , α , and b_p , Eq. (5.56) becomes

$$1.001 = 1 + I_{pT}^2 \quad (5.57)$$

where I_{pT} is the *threshold pulsation index* that defines steady flow at reference conditions, and

$$I_{pT} = 0.03 \quad (5.58)$$

This index allows for a ± 3 percent flow-rate change for a linear flowmeter (vortex, turbine, ultrasonic, etc.) and a ± 6 percent variation in differential pressure for differential producers.

Keyser (1981) empirically derived a maximum-bias-error equation that fits 90 percent of available unsteady-flow data for orifice flowmeters. This equation and the data are shown in Fig. 5.43. The bias error is calculated in terms of the threshold pulsation index as

$$B = 20 \exp [-(2.7 - 7.2I_{pT})^2] = 0.04 \text{ percent} \quad (5.59)$$

In a pulsation study on gas-turbine flowmeters, Lee et al. (1975) presented the data shown in Fig. 5.44. Substituting the threshold pulsation index into the maximum-bias-error equation gives

$$B = 69I_{pT}^2 = 0.06 \text{ percent} \quad (5.60)$$

This recent data and that presented in the original work by Head suggest that a threshold pulsation index of 0.03 is reasonable for the purpose of defining steady flow.

Pulsation Measurement

Severe flow pulsation is usually visually apparent from either a recording of the flowmeter signal, an audible steady rumble, or a sustained hum. For highly damped secondary devices, a visual observation or audible detection may not be sufficient.

If pulsating flow is suspected, a high-frequency-response pressure- or velocity-measuring device, located close to the primary device, should be used to characterize the unsteadiness. A linearized hot-wire anemometer with a light-beam recording oscillograph or an electronic strain-gauge pressure transducer can detect frequencies up to 10 kHz. Harmonics can then be determined using a wave analyzer, Fourier analysis, or spectrum analysis.

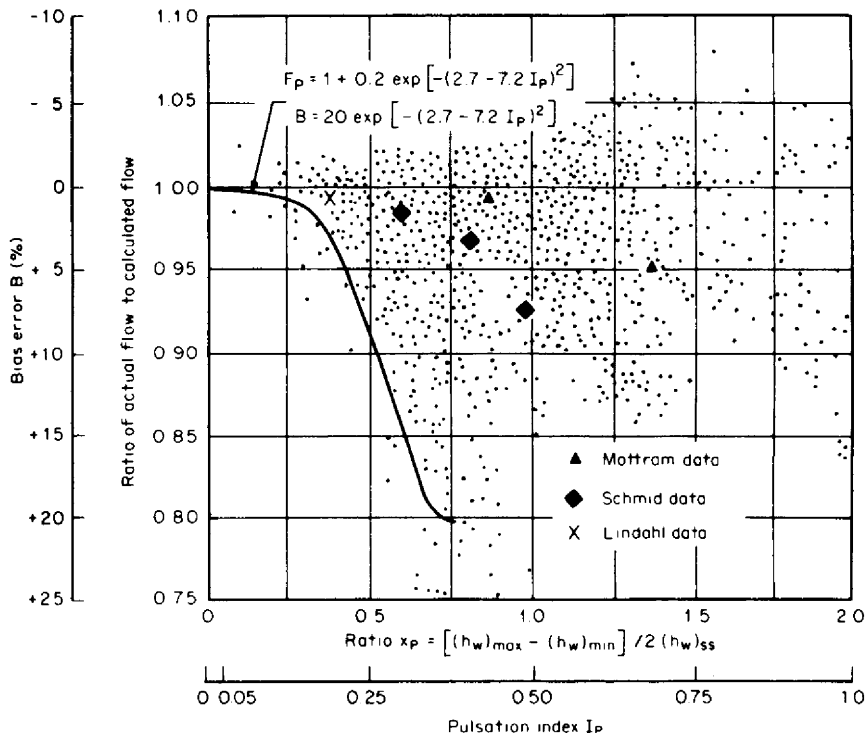


Figure 5.43 Orifice-flowmeter pulsation data.

Filters

If the threshold pulsation index has been exceeded, corrective action is necessary. Accepted practice is to install a low-pass in-line filter that cuts off all frequencies above the minimum determined value. The design of these filters depends on whether the fluid is a liquid or a gas. Since pulsation not only affects flow measurement but causes unacceptable pipeline vibration as well, pulsation dampers are usually part of the initial piping design. Figure 5.45a shows a typical volume-choke pulsation damper used for gas flows, and Fig. 5.45b a gas-filled surge chamber used for liquids. Industrial stabilizers are shown installed on the suction and discharge sides of a four-stage liquid pump in Fig. 5.46.

Numerous passive filter designs have been found effective for various pump types, pump speeds, etc. Location, volume, restrictor size, frequency range, and other parameters for passive filters are the subject of many texts, design brochures, and technical articles. The reader is referred to the works by Campbell (1958), Chilton and Handley (1955), Greer Hydraulics (1981), and Yeaple (1966).

CAVITATION/FLASHING

Cavitation occurs in two distinct stages. In the first stage voids or cavities are formed, and in the second stage these collapse or implode back into an all-liquid

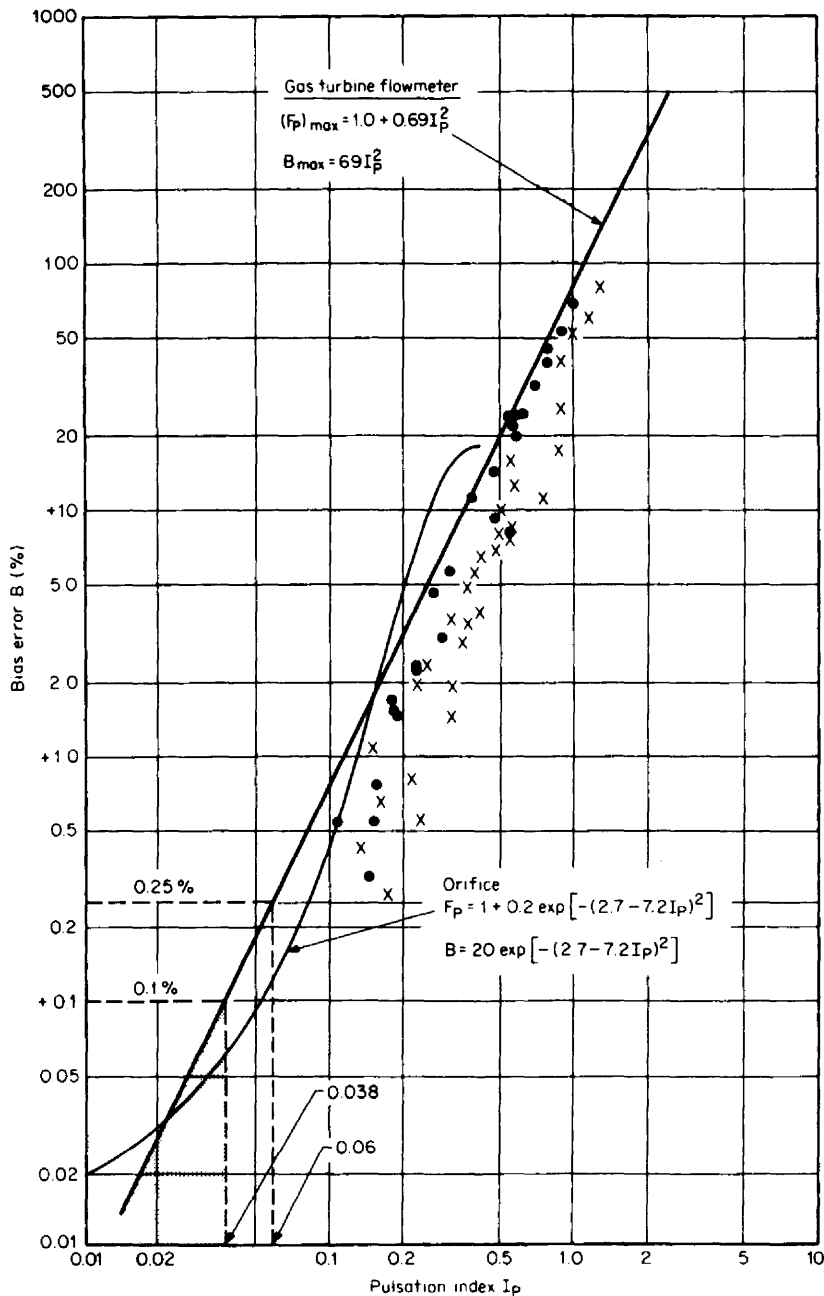
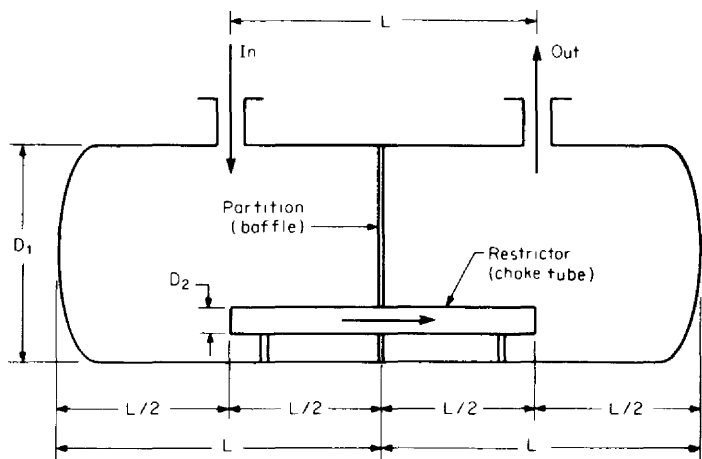
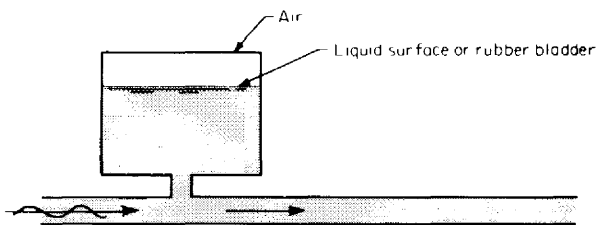


Figure 5.44 Gas turbine flowmeter pulsation data.



Flow rate $\times 10^3 =$ q_{SCFH}	Tank diameter D_1 (in)	Choke diameter D_2 (in)	Length L (in)
125	16	1.5	38
125 - 450	24	2	34
450 - 700	30	3	40

(a)



(b)

Figure 5.45 Typical passive filters for gas and liquid flows. (a) Gas. (b) Liquid.

state. Two types of cavitation may occur, gaseous or vaporous, with both types requiring a nucleating agent for inception. These nucleating points enlarge into finite cavities within the liquid.

Most liquids contain various solid contaminants so that necessary nuclei for *incipient cavitation* are almost always present. The inception of cavitation may be delayed significantly if the liquid has been carefully degassed, polymers added, or the liquid maintained under high pressures for a period of time for the gas to be completely dissolved.

If the cavitation process ceases before the second stage, so that vapor persists downstream of the region where bubble collapse normally takes place, the process

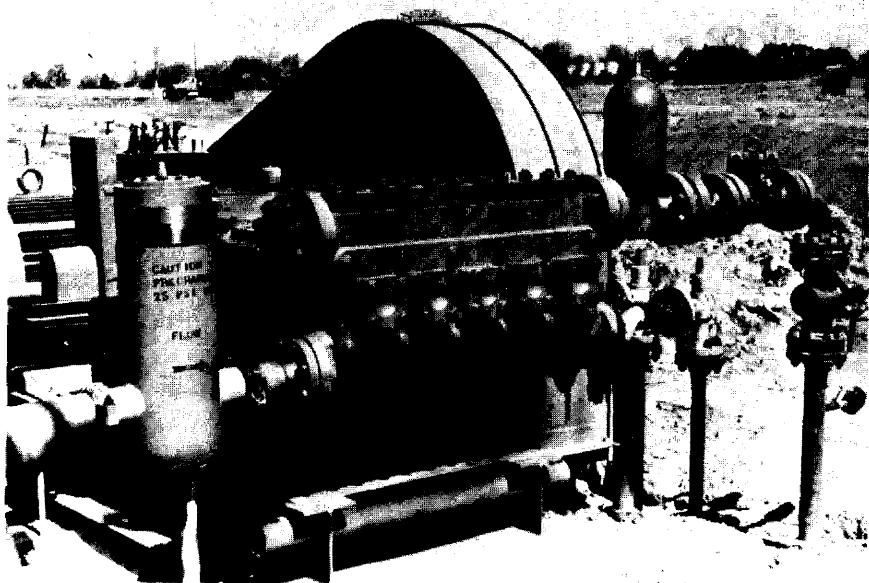


Figure 5.46 Suction and discharge stabilizers. (Courtesy Greer Hydraulics.)

is known as flashing. Since flashing is directly related to the first stage of cavitation, the theory of cavitation also apply to flashing.

Upstream of a nozzle, point 1 of Fig. 5.47a, the liquid has a pressure above its vapor pressure. The total energy level of the stream, neglecting potential energy (elevation), is then the sum of potential (pressure) and kinetic energy (velocity).

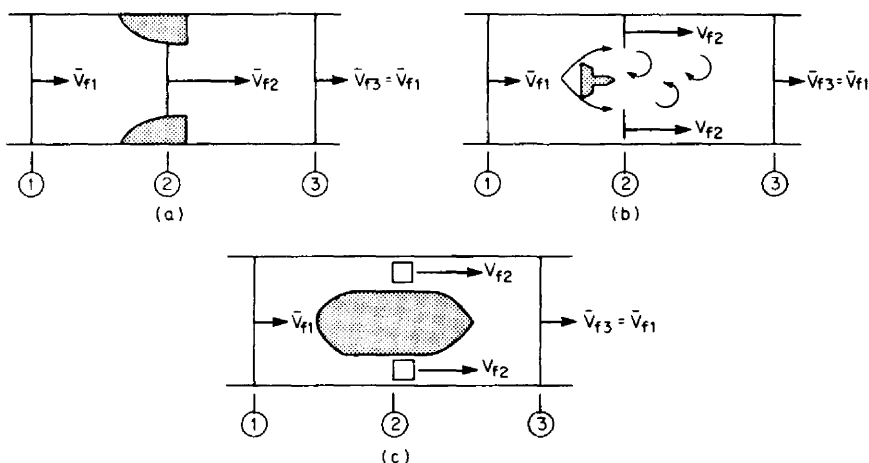


Figure 5.47 Location of maximum velocity and minimum pressure. (a) Differential producer. (b) Vortex flowmeter. (c) Liquid turbine flowmeter.

With no energy lost through the boundaries of the system in the form of work or heat, the total energy remains constant along a datum plane in the system.

As the fluid stream approaches the nozzle, or any restriction, the cross-sectional area decreases, and the velocity increases inversely proportional to the open area. Since the sum of the pressure and velocity heads remains constant, the liquid pressure decreases. If the velocity is increased until the pressure falls to the vapor pressure, voids are formed in the stream, resulting in the first stage of cavitation.

Further downstream from this minimum pressure point the fluid decelerates, resulting in an increase in pressure. This pressure recovery causes the bubbles formed to collapse or implode back into the liquid state, completing the cavitation process.

If the downstream pressure is at, or less than, the inlet vapor pressure, the downstream fluid would have an increasing percentage of vapor, the velocity would continually increase, and flashing rather than cavitation would occur. The following general definitions apply.

for cavitation:

- The inlet and outlet fluids are all liquid and do not exist upstream.
- Upstream liquid is subcooled; however, it is possible for cavitation to exist for a saturated liquid upstream.
- Outlet pressure is at or greater than the vapor pressure of the liquid.

and for flashing:

- The inlet and outlet fluids are all liquid and some vapor must be present downstream.
- The upstream liquid may be either saturated or subcooled.
- The downstream pressure must be at or below the vapor pressure of the liquid.

Cavitation

When decreased line pressure approaches the vapor pressure of a liquid in the line, cavitation begins. In essence, cavitation is boiling of the liquid caused by decreasing pressure rather than by increasing temperature. It is the formation and collapse (implosion) of vapor cavities. This imploding is responsible for the audible noise associated with cavitation, which can range from occasional popping to the sound of moving sand. Extensive cavitation destroys piping, restricts flow, ruins turbine blades, and produces unacceptable noise levels. Cavitation occurs in a system whenever pressure has been reduced sufficiently, by either friction, flow separation, or restrictors such as valves, vortex elements, or differential-producing flowmeters. Even in a well-designed piping system, cavitation can occur if control or relief valves are suddenly opened.

The physics that generates noise also creates vibration that can be a major problem. The vibration level depends on:

- The system mass
- The physical structure
- Whether instruments are vibration-sensitive

Material damage caused by cavitation can be quite serious. Under severe cavitation, extremely hard control valve components fail in a few hours. There are many examples where cavitation eroded holes completely through flowmeters, or downstream piping walls, and destroyed valve plugs and bodies.

No single metal's physical property has been found that correlates with experimental data for cavitation failures. In general, resistance to cavitation damage increases with increasing hardness, and some attempts at correlating resistance based on material properties such as tensile strength, modulus of elasticity, and strain energy in addition to hardness have been attempted. For hard materials damage appears as a rough cinder look, which is different from the usual smooth appearance.

The damaging cavitation effect always takes place in close proximity to the imploding bubbles. This is most probably caused by imploding pressures as high as 100,000 psi. High-pressure shock waves emanate from the implosion centers, and when these shock waves are at a solid boundary, they produce a very small concentrated hammerlike blow; this will fatigue the surface and remove the metal. Since implosion energy is absorbed by the flowing liquid, implosions away from surfaces are believed not to cause damage.

Dissolved gases and gas bubbles in liquids provide nucleative points and assist in the onset of cavitation. With gas concentrations in the range of 40 parts per million, fluids will cavitate at higher static pressures. Generally, cavitation begins at higher static pressures and lower velocities in larger line sizes; once started, it will continue at higher static pressures than the initiating pressure.

The number used for correlating cavitation data is the dimensionless *cavitation number*, defined as

$$\sigma_c = \frac{2g_c(P_{f2} - P_{v2})}{\rho_f \bar{V}_{f2}^2} \quad (5.61)$$

where the pressures P_{f2} and P_{v2} are in pounds-force per square foot, and the subscript 2 refers to the location of the maximum velocity within the flowmeter, as shown in Fig. 5.47. In Eq. (5.61) the difference between the static pressure P_{f2} and vapor pressure P_{v2} can be viewed as the force required to *collapse* the vapor bubbles. The velocity-squared term is the dynamic pressure required to *initiate* bubble formation. The cavitation number σ_c is then the ratio between the collapsing and forming forces.

Initially, cavitation begins with very small bubbles isolated in a small section of the flowmeter. As the cavitation number decreases, formation becomes more rapid, with bubble size usually increasing. For cavitation numbers below a certain value $(\sigma_c)_i$, called the *incipient* cavitation number, cavitation becomes increasingly destructive to both piping and flowmeters. The addition of very small amounts of a polymer has been shown by Oba et al. (1978) to reduce both the incipient cavitation number and the audible cavitation noise (Fig. 5.48).

In general, the incipient cavitation number ranges from 1.0 to 2.5 for abrupt obstructions and orifice, vortex, and flow nozzles, where downstream pressure recovery is abrupt. For contoured inlet and exit devices, such as the venturi, venturi nozzle, and Lo-Loss tube, the incipient cavitation number ranges from 0.2 to 0.5.

Three pressure locations are shown in Fig. 5.47. The upstream pressure P_{f1} is reduced to a minimum value P_{f2} at a minimum flow area, while the velocity is increased to a maximum value V_{f2} at approximately the same location. At location 2 the cavitation number is minimized, and cavitation will begin if the incipient cavitation number is reached. In some flowmeters, where there is a sudden change in a streamline ahead of a reduced area, separation may cause cavitation to begin

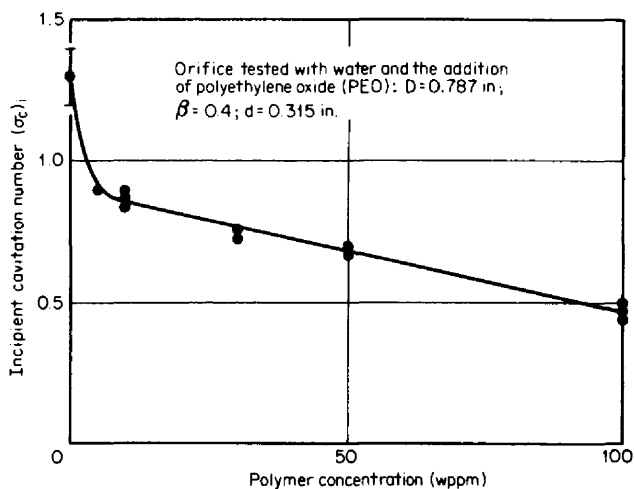


Figure 5.48 Reduction of incipient cavitation number with the addition of polyethylene oxide (WPPM = parts per million by weight).

slightly upstream of this minimum flow area. The flow will then recover to the full pipe area at location 3. The pressure P_{f3} will be close to P_{f1} , and the average velocity will return to the full-pipe-area value. The difference between the pressures at locations 1 and 3 is the permanent pressure loss; depending on how the flow recovers, it may be a significant percentage of the maximum pressure difference $P_{f1} - P_{f2}$ or it may be negligible.

For differential producers, the required minimum upstream or downstream pressure (back pressure) can be calculated from known incipient cavitation numbers (Table 5.5) by mass flow continuity and Bernoulli's equation. For turbine and vortex flowmeters, the point of minimum pressure depends on design, which obviously varies with line size and manufacturer. For these meters, a minimum back pressure is commonly specified. This minimum is calculated from the pressure loss $P_{f1} - P_{f3}$ and fluid vapor pressure with equations of the general form

$$(P_{f3})_{\min} = A(P_{f1} - P_{f3}) + BP_v \quad (5.62)$$

where P_{f3} is the minimum downstream pressure, and the constants A and B are determined experimentally. Any set of consistent pressure units may be used in Eq.

TABLE 5.5 Incipient Cavitation Numbers for Differential Producers

Flowmeter	Incipient cavitation number
Venturi	0.33
Nozzle venturi	0.55
Dall tube	1.0
Flow nozzle	1.8
Orifice	3.0

Source: Cousin (1977).

(5.62). For turbine and vortex flowmeters, conservative estimates are 3.0 for A and 1.5 for B ; however, the manufacturers should be consulted for actual values.

Figure 5.49a shows the bias error for a nozzle and a venturi as the cavitation number decreases below the incipient value. Although the bias error occurs at a

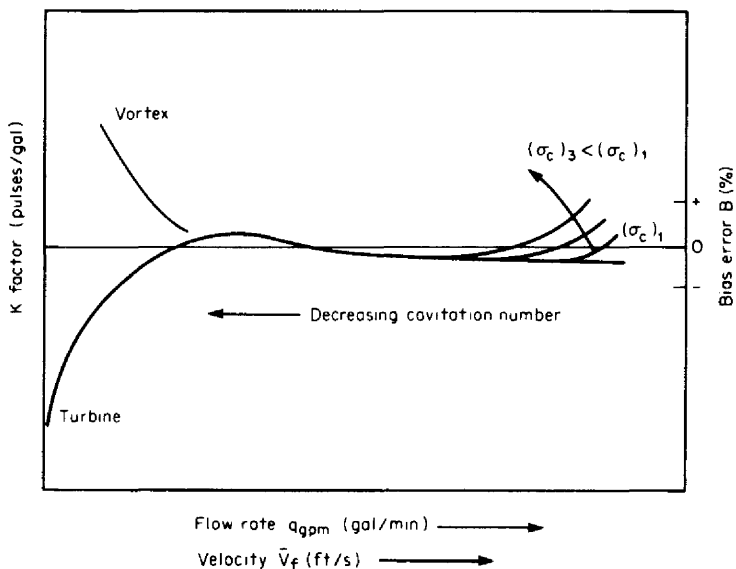
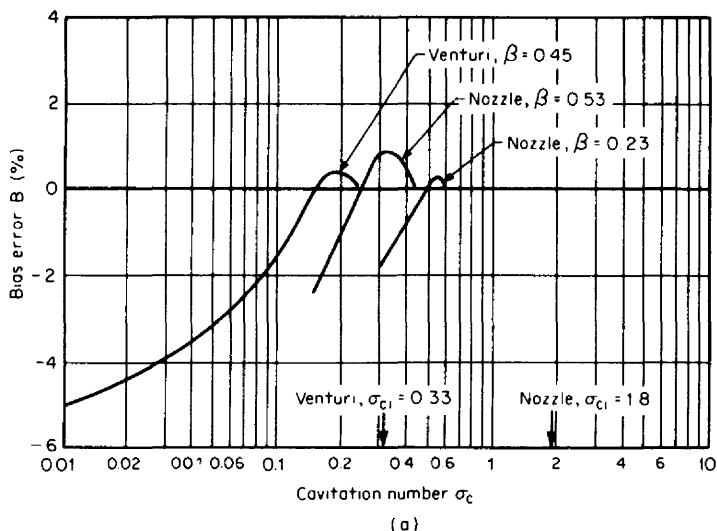


Figure 5.49 Effect of cavitation on flowmeters. (a) Nozzle and venturi. (b) Vortex and turbine flowmeters.

lower value than the incipient cavitation number $(\sigma_c)_i$, flowmeters should not be used in this range. When the line pressure across a section of the differential producer is the fluid's vapor pressure, the flow is *choked* (see Chap. 13), and increasing the upstream pressure will not increase the flow rate. The effect of cavitation on vortex and turbine flowmeters is shown in Fig. 5.49b. As the back pressure is reduced or the velocity is increased, cavitation results in a positive bias.

Flashing

In a flashing liquid, the volume of vapor is frequently greater than the volume of liquid, so the liquid droplets tend to achieve the high velocity of the vapor. These high-velocity particles impact on the surface, causing deformation and ultimately removal of the surface material.

Flashing causes both damage and decreased efficiency. Physical damage appears as a very smooth fine sandblasted surface. Physical damage resulting from flashing is usually in the downstream section, and downstream piping is often eroded or pitted. For liquids near saturation, flashing sometimes begins upstream and the entire flowmeter body can be affected.

Selection of proper materials usually solves most damage problems. The practice of specifying chromium-bearing steel reduces the incidence of the damage often referred to as *body washout*.

AIR ENTRAINMENT

No flowmeter can distinguish between pure liquid and a liquid containing air. Air entrainment can result in a large metering error even with small amounts of entrained gases. For accurate metering, air eliminators are installed to ensure that air, or entrained gas, is not present in the metered fluid.

Air eliminators reduce the velocity of the fluid in a stilling chamber (Fig. 5.50) to allow time for gases (vapor) to escape before reentering the pipeline. As gas accumulates, the liquid level falls, lowering a float that opens a vent to release the gas from the eliminator. It is important that a sufficient outlet back pressure be maintained to ensure a correct gas discharge rate.

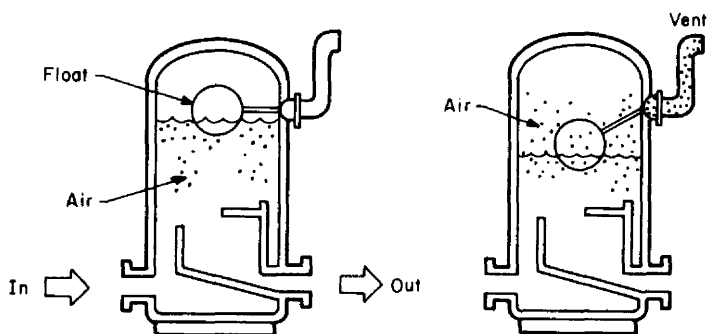


Figure 5.50 Air eliminator.

Gas Solubility

All gases are soluble to some degree in liquids at very high pressures or when the liquid is at or close to its critical temperature. The effect of the soluble gas is normally to lower the density and viscosity values that would have been measured or predicted via a state equation or other prediction methods for a pure substance or a mixture of substances. At normal operating pressures and temperatures, most gases are only slightly soluble in typical liquids and have negligible effects (<0.001 percent) on the flow measurement.

There is little reliable data on the effect of gas solubility on a liquid's fluid properties. Also, neither experimental data nor a reliable correlation method exists for predicting the effect of solubility. Katz et al. (1959) give an example of the solubility of reservoir natural gas on a 1.013 specific gravity crude oil at 108°F (42°C) and under a pressure of 1853 psia (12.8 MPa). At atmospheric pressure and temperature, over 666 standard cubic feet of gas per barrel of crude oil evolved.

REFERENCE CONDITIONS

Accuracy

Four methods are commonly used to establish the accuracy of the primary device; the method selected depends on economics, the accuracy required, and whether the primary and secondary devices can be separated. The accuracy statement for all four is based on specified reference conditions.

Draft standard ASME MFFCC SC15 (1988) details methods for reporting the influence of flow patterns on a flowmeter. This standard should be helpful when users compare different meters for a given application.

The four methods for establishing accuracy relative to reference conditions are:

1. The primary device is calibrated, with its associated piping configuration, in a hydraulic laboratory to determine the relationship between the actual and theoretically calculated flow rates. A calibration factor can usually be determined to an accuracy of ± 0.15 percent, and it is used to correct all future on-site flow-rate calculations. The flow-rate accuracy is then the combination of primary-device and secondary-equipment accuracy.
2. If the primary device has dimensional similarity, as does an orifice, flow nozzle, or venturi, the discharge coefficients obtained from many tests are used to establish an equation for calculating the coefficient based on dimensions. Twice the standard deviation of the data with respect to this equation, the *error of estimate*, defines the coefficient accuracy.
3. For some flowmeters it is difficult and costly to control either dimensions or other factors that affect the relationship between output and true flow rate. In these cases, the primary device is water-calibrated to determine an accuracy which is then statistically combined with that of the secondary device to obtain the overall *flowmeter* accuracy (magnetic flowmeter). In some cases, the flowmeter is calibrated as a system to establish a reference accuracy.
4. Based on theory and a fully developed velocity profile, an analog of the flowmeter response to actual flow rate is developed. This analog, combined with suitable dimensional measurements, is used to estimate the accuracy.

Whether theoretically or empirically established, reference flow conditions imply:

1. A fully developed laminar or turbulent velocity profile that is nonswirling (rotating) and axisymmetric (symmetric about the pipe centerline)
2. A newtonian fluid
3. A homogeneous single-phase fluid that completely fills the pipe
4. Steady flow
5. Flow-calculation correction for dimensional changes resulting from thermal, pressure, or other known bias errors

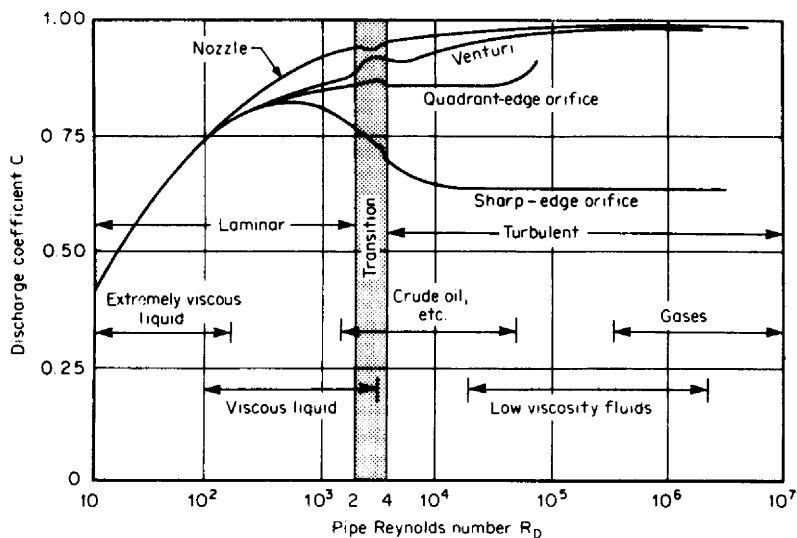
Flowmeter Signature Curve

Under reference conditions, all flowmeters exhibit a characteristic curve that is a function of velocity profile. This *signature curve* has approximately the same shape for all flowmeters of similar design but may vary in level (bias error), depending on how well each individual device is manufactured. For differential producers, the discharge coefficient C defines the relationship between the actual laboratory-determined flow rate and that calculated from the theoretical flow-rate equation. This coefficient is observed to change with pipe Reynolds number (profile). A similar Reynolds-number relationship is observed for other flowmeters. Shown in Fig. 5.51 are typical signature curves for differential producers and turbine and vortex flowmeters. The signature curve is established in a laboratory with long, straight runs of pipe to achieve fully developed reference profiles. Since these are seldom achievable in field installations, tests are conducted with selected upstream flow disturbances, with the primary device incrementally moved closer to the disturbance. The minimum downstream location at which a change occurs in either curve shape or bias defines the reference upstream piping length. If the device is located closer to the disturbance, swirl, secondary flows, and nonaxisymmetric profile result in additional errors.

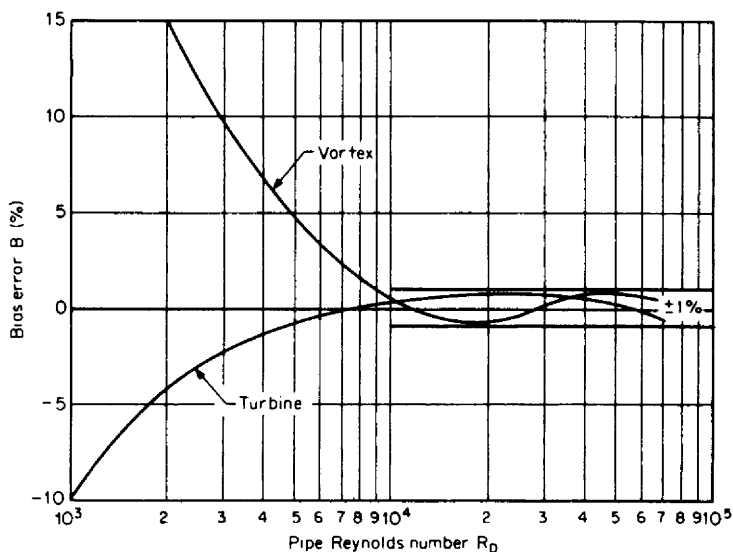
The various classes of flowmeters tolerate profile variations to differing degrees. Radial flow components from an elbow significantly change a single-path ultrasonic flowmeter output at 5 pipe diameters, but only slightly change a venturi's coefficient. The orientation of an ultrasonic path, the pressure connections for a differential producer, and the electrode axis of a magnetic flowmeter with respect to the distorted profile must be considered in establishing reference lengths.

Wall Roughness

In turbulent flow, relative roughness and Reynolds number establish the flow profile, and some criterion should be available to define *reference-condition piping*, from which profile corrections may be made. Unfortunately, relative roughness and flow profiles are not standardized. However, for a series of hydraulics-laboratory tests conducted with orifice flowmeters, the relative pipe roughness was estimated [in ISO Standard 5167 (1995)] to be 10×10^{-4} . The diameters and materials of pipes that satisfy this "criterion" are given in Table 5.6. Until standards become available, these pipes can be used as reference-condition pipes.



(a)



(b)

Figure 5.51 Typical flowmeter signature curves. (a) Differential producer. (b) Turbine and vortex flowmeters.

Length of Straight Pipe

ISO Standard 5167 (1995), which treats orifices, venturis, and flow nozzles, defines the general flow condition at the primary device as follows:

TABLE 5.6 Pipe Roughness and Acceptable Size Range for Reference Conditions†

Pipe material	Wall roughness	Pipe size D (reference conditions), in
Aluminum		
Asbestos cement, coated (new)		
Brass		
Copper	≤ 0.001	≥ 1
Glass		
Plastic		
Steel, cold-drawn seamless		
Asbestos cement (normal)		
Cast iron, bituminized (new)	≤ 0.002	≥ 2
Steel, bituminized (new)		
Steel, rolled seamless		
Steel, spirally welded	≤ 0.005	≥ 4
Steel, galvanized		
Cast iron, asphalt dipped		
Steel, bituminized (normal)	≤ 0.008	≥ 6
Steel, mildly rusty		
Cast iron (new)		
Galvanized iron	≤ 0.010	≥ 8
Steel (rusty)		

†Based on relative roughness of pipes used in orifice flowmeter coefficient test program (flanged D - and $D/2$ taps), ISO Standard 5167 (1995).

Swirl-free conditions at the primary can be taken to exist when the swirl angle over the pipe is less than 2 degrees. Acceptable velocity profile conditions can be presumed to prevail when at each point across the pipe cross-section the ratio of local axial velocity to the maximum axial velocity at the cross-section agree to within 5% with that which would be achieved in swirl-free flow at the same radial position at a cross-section located at the end of a very long straight length (over $100D$) of similar pipe.

This definition, although specifically for differential producers, is probably stringent enough to apply to all flowmeters. Without calibration data, a piping length (or the combination of a flow conditioner and piping length) that, by test, has met this definition can be considered a *reference piping length*.

REFERENCES

- AKASHI, K., H. Watanabe, and K. Kenichi: "Development of New Flow Rectifier for Shortening Upstream Straight Pipe Length of Flowmeter," *Tokyo Flow Symp., IMEKO*, Paper 12b-5, pp. 279-284, Society of Instrumentation and Control, Tokyo, 1979.

- ASME MFFCC SC15, *Standard Method for Establishing Installation Effects on Flowmeters* (draft) ASME, New York, 1988.
- Beck, M. S., E. A. Hammer, and R. Thorn: "On-Line Multicomponent Flow Measurement," *Int. Symp. Flowmetering and Proving in the Offshore Oil Ind.*, Institute of Measurement and Control, Aberdeen, Scotland, 1986.
- Berthold, J.W., S.E. Reed, and C.A. Nash: "Fibre Optic Sensor System for Void Fraction Measurements in Aqueous Two-Phase Fluids," *Flow Measurement and Instrumentation*, vol. 5, no. 1, pp. 3–13, January 1994.
- Campbell, D. P.: *Process Dynamics*, Wiley, New York, 1958.
- Chilton, E.G., and L.R. Handley: "Pulsation Absorbers for Reciprocating Pumps," *Trans. ASME*, vol. 77, pp. 225–230, 1955.
- Clarke, K.J.: "Curing Cavitation Saves Money; Cuts Vibration, Erosion Damage," *Chem. Processing*, February 1994.
- Colebrook, C.F.: "Turbulent Flow in Pipes with Particular Reference to the Transition Region between Smooth and Rough Pipe Laws," *J. Inst. Civ. Eng.*, vol. 11, pp. 133–136, 1938–1939.
- Cousin, T.: "The Effect of Cavitation and Air/Water Mixtures on the Discharge Coefficients of Differential Pressure Flowmeters," *IMEKO VII Congr.*, pp. BFL2411–2417, Institute of Measurement and Control, London, 1977.
- Darcy, H.: "Sur des recherches experimentales relatives au mouvement des eaux dans les tuyaux," *Comptes Rendu de l'Académie des Sciences de France*, vol. 38, pp. 1109–1121, 1854.
- Edwards, M.F., and M.A. Wilkinson: "Review of Potential Applications of Pulsating Flow in Pipes," *Trans. Inst. Chem. Eng.*, vol. 49, pp. 85–94, 1971.
- El-Ayouty, E., and J.B. Stepanek: "Use of Microwaves in the Measurement of Frequencies and Amplitudes in Liquid Hold-up Fluctuations," *Int. Conf. Phys. Modeling Multi-phase Flow*, Coventry, England, BHRA, 1983.
- Govier, G.W., and K. Aziz: "The Flow of Complex Mixtures in Pipes," Krieger, Huntington, N.Y., 1977.
- Greer Bulletins TR-1, 1500E, 1507, 5005, and 6500, Greer Hydraulics, Chatsworth, Calif., 1979–1981.
- Halsey, D.M.: "Flowmeters in Swirling Flows," *J. Phys. E; Sci. Instrum.*, vol. 20, pp. 1036–1040, 1987.
- Head, V.P.: "A Practical Pulsation Threshold for Flowmeters," *Trans. ASME*, vol. 78, pp. 1471–1473, 1956.
- Hewitt, G.F.: *Measurements of Two Phase Flow Parameters*, Academic, London, 1978.
- ISO: *Characterization of Steady Flow* (draft), Secretariat ANSI, ISP/TC30/SC2/WG7, doc.(secr.-3)7, 1975.
- ISO/DIS 7145, *Determination of Flowrate of Fluids in Closed Conduits of Circular Cross-Section—Method of Velocity Measurement at One Point of the Cross-Section*, ISO, UDC 532.542, Geneva, 1981.
- ISO Standard 5167, *Measurement of Fluid Flow by Means of Orifice Plates, Nozzles, and Venturi Tubes Inserted in Circular Cross-Section Conduits Running Full*, p. 19, ISO 5167-1980(E), Geneva, 1995.
- ISO Technical Report 3313, *Measurements of Pulsating Fluid Flow in a Pipe by Means of Orifice Plates, Nozzles or Venturi Tubes, in Particular in the Case of Sinusoidal or Square Wave Intermittent Periodic-Type Fluctuations*, ISO/TR 3313(E), 1988.
- Jeffery, B. J.: "The Hodgson Number as a Criterion for Limiting Metering Error under Pulsating Flow Conditions," *Int. Conf. Flow Meas. in Mid 80's*, paper 6.2, vol. 2, NEL, East Kilbride, Scotland, 1986.
- Johansen, G. A., and T. Froystein: "Gamma Detectors for Tomographic Flow Imaging," *Flow Measurement and Instrumentation*, vol. 5, no. 1, pp. 15–21, January 1994.
- Katz, D. L., D. Cornell, J. A. Vary, R. Kobayashi, J. R. Elenbass, F. H. Poettmann, and C. F. Weinaug: *Handbook of Natural Gas Engineering*, McGraw-Hill, New York, 1959.

Keyser, D. R.: "Unsteady Flow Measurement, Its Theory and Observations," in *Flow, Its Measurement and Control in Science and Industry*, vol. 2, Instrument Society of America, Research Triangle Park, N.C., 1981.

Kinghorn, F. C.: "Flow Measurement in Swirling or Asymmetric Flow—A Review," *Flowcon 77 Proc.*, pp. 45–71, Institute of Measurement and Control, Gatton & Kent, U.K., 1977.

Kirmse, R. E.: "Investigations of Pulsating Turbulent Pipe Flows," *J. Fluids Eng.*, vol. 101, pp. 436–442, 1979.

Kosla, L., and M. Mutsakis: "New In-Pipe Flow Conditioner Cuts Fluid Problems," *Chem. Eng.*, September 1992.

Kreith, F., and O. K. Sonju: "The Decay of a Turbulent Swirl in a Pipe," *J. Fluid Mech.*, vol. 22, pt. 2, pp. 257–271, 1965.

Kumar, S. B., D. Moslemian, and M. P. Dudukovic: "A γ -ray Tomographic Scanner for Imaging Voidage Distribution in Two-Phase Flow Systems," *Flow Measurement and Instrumentation*, vol. 6, no. 1, pp. 61–73, January 1995.

Laws, E. M.: "Flow Conditioning—A New Development," *Flow Measurement and Instrumentation*, vol. 1, no. 3, pp. 165–170, April 1990.

Laws, E. M., and A. Ouazzane: "Effect of Plate Depth on the Performance of a Zanker Flow Straightener," *Flow Measurement and Instrumentation*, vol. 3, no. 4, pp. 257–269, October 1992.

Lee, W. F. Z., M. J. Kirik, and J. A. Bonner: "Gas Turbine Flowmeter Measurement of Pulsating Flow," *J. Eng. Power*, vol. 97, pp. 531–539, October 1975.

Lindahl, E. J.: "Pulsation and Its Effect on Flowmeters," *Trans. ASME*, vol. 68, pp. 893–894, November 1946.

Logan, E. L., and J. B. Jones: "Flow in a Pipe Following an Abrupt Increase in Surface Roughness," ASME Winter Annual Meeting, Paper 62-Hyd-5, 1962.

Mattingly, G. E., and T. T. Yeh: "Flowmeter Installation Effects: A New Approach to an Old but Prevalent Problem," *Int. Conf. Flow Meas. in Mid 80's*, paper 6.3, vol. 2, NEL, East Kilbride, Scotland, 1986.

Metzner, A. B., and J. C. Reed: "Flow of Non-Newtonian Fluids—Correlation of the Laminar Transition and Turbulent-Flow Regions," *AIChE J.*, vol. 1, pp. 434–440, 1955.

Mizushima, T., T. Maruyama, and H. Hirasawa: "Structure of the Turbulence in Pulsating Pipe Flows," *J. Chem. Eng. Jpn.*, vol. 81, no. 3, pp. 210–216, 1975.

Moody, L. F.: "Friction Factors for Pipe Flows," *Trans. ASME*, vol. 66, p. 671, 1944.

Mottram, R. C.: "The Measurement of Pulsating Flow Using Orifice Plate Meters," in *Flow, Its Measurement and Control in Science and Industry*, vol. 1, pp. 197–208, ISA, Pittsburgh, 1974.

———: "Damping Criteria for Pulsating Gas Flow Measurement," *Flow Measurement and Instrumentation*, vol. 1, no. 1, pp. 15–22, January 1994.

Nelson, J. B., and W. G. Hendrick: "Industrial Gamma Ray Gauging—Applications and Pitfalls," *Proc. 40th Annual Symp. on Ind. & Proc. Industries*, Texas A&M, Texas, 1985.

Muller, E.: "The Measurement of Pulsating Flow," in *The Measurement of Pulsating Flow* (symp. Proc.), Institute of Measurement and Control, London, 1970.

Nikuradse, J.: *Gestzmassigkeiten der turbulenten Stromung in glatten Rohren*, Forschungsheft 356, VDI Verlag, Berlin, 1932.

———: *Stromungsgesetze in rauhen Rohren*, Forschungsheft 361, VDI Verlag, Berlin, 1933 (translated as NACA TM 1292, 1960).

Oba, R., Y. Ito, and K. Uranishi: "Effect of Polymer Additives on Cavitation Development and Noise in Water Flow through an Orifice," *J. Fluids Eng.*, vol. 100, pp. 493–499, 1978.

Olatunbosun, S., and B. Frith: "Two-Phase Flow Imaging using Gamma Scattering/Transmission Technique," *Int. Conf. Flow Meas. in Mid 80's*, paper 2.2, vol. 1, NEL, East Kilbride, Scotland, 1986.

Pai, S. I.: "On Turbulent Flow in a Circular Pipe," *J. Franklin Inst.*, vol. 20, no. 4, pp. 337–352, 1953.

Pao, R. H. F.: *Fluid Mechanics*, Wiley, New York, 1961.

Reynolds, O.: "An Experimental Investigation of the Circumstances Which Determine whether the Motion of Water Will Be Direct or Sinuous, and of the Law of Resistance in Parallel Channels," *Philos., Trans. R. Soc. London*, vol. 174, p. 935, 1883.

Ryan, N. W., and M. M. Johnson: "Transition from Laminar to Turbulent Flow in Pipes," *AIChE J.*, vol. 5, no. 4, pp. 433-435, 1959.

Takenaka, N., K. Fujii, A. Akagawa, K. Ono, K. Sonoda, K. Nishizaki, and H. Asano: "Application of Neutron Radiography to Visualization of Multiphase Flows," *Flow Measurement and Instrumentation*, vol. 1, no. 3, pp. 149-156, April 1990.

Tayali, N. E., and C. J. Bates: "Particle Sizing Techniques in Multiphase Flows: A Review," *Flow Measurement and Instrumentation*, vol. 1, no. 2, pp. 77-105, January 1990.

Teyssandier, R. G.: "Flow Coefficient Variation for Concentric Orifices from an Analysis of Turbulent Velocity Profiles," ASME Winter Annual Meeting, Paper 75 WA/FE-19, 1975.

Van Wazer, J. R., J. W. Lyons, K. Y. Kim, and R. E. Colwell: *Viscosity and Flow Measurement: A Laboratory Handbook of Rheology*, Interscience/Wiley, New York, 1963.

Vorwerk, J., R. Steger, M. Teufel, and P. O. Brunn: "Use of an Optical Meter to Measure the Flow Rate and Apparent Viscosity of Non-Newtonian Fluids," *Flow Measurement and Instrumentation*, vol. 5, no. 1, January 1994.

Wasp, E. J., J. P. Kenny, and R. L. Gandhi: *Solid-Liquid Flow Slurry Pipeline Transportation*, Gulf, Houston, Texas, 1979.

Wilcox, P. L., T. Werberg, and A. Erdal: "Stort Gas Metering Station Using K-Lab Flow Conditioner," A.G.A. Int'l Conference, Calgary, June 1990.

Wilkinson, W. L.: *Non-newtonian Fluids*, Pergamon, New York, 1960.

Yeaple, F.: *Hydraulic and Pneumatic Power and Control: Design, Performance, Application*, McGraw-Hill, New York, 1966.

Xu, L. A., R. G. Green, M. S. Beck, and A. Plaskowski: "A Pulsed Ultrasound Cross-Correlation System for Velocity Measurement in Two-Component Flow," *Int. Conf. Flow Meas. in Mid 80's*, paper 2.1, vol. 1, NEL, East Kilbride, Scotland, 1986.

Zanker, K. J.: "The Development of a Flow Straightener for Use with Orifice Flowmeters in Disturbed Flow," Paper D-2, *Symp. on Flow Measurement*, Scotland, 1969.

FLOWMETER SELECTION

The instrument engineer probably has a wider choice of devices when specifying a flowmeter than for any other process-monitoring application. It is estimated (Hayward, 1975) that at least 100 flowmeter types are commercially available, and new types are being continually introduced. Meters are chosen on the basis of cost, line size, the fluid being metered, its state (gas, vapor, or liquid), meter range, and desired accuracy.

Furness (1993) reviews the British Standard 7405 (1991) and summarizes as follows:

With so many different types of flowmeters available from so many sources of supply, flowmeter selection is becoming increasingly difficult. . . . The new BS 7405 classifies closed conduit flowmeters into 10 major groups and this grouping was used in the basic layout of the standard. More than 45 variables were identified as the most important factors in selection.

Clearly then, meter selection is difficult and requires a knowledge of the process as well as the basic principle underlying the more common meter types.

Only the more widely used general-purpose flowmeters—those listed in Table 6.1—are covered in this handbook. For these devices, operating principles, selection bases, and equations for the calculation of permanent pressure loss and yearly energy cost are summarized in this chapter.

DIFFERENTIAL PRODUCERS

The differential-producing flowmeters, sometimes called *head-class* flowmeters, are selected most frequently because of their long history of use in many applications. A number of primary elements belong to this class: The concentric orifice, venturi, flow nozzle, Lo-Loss tube, target flowmeter, pitot tube, and multipart-averaging are all differential producers. When some other flowmeter is selected, it is usually because of an obstructionless feature, wider range, or a tendency against freezing or condensate buildup in lead lines or because the fluid is abrasive, dirty, or made up of more than one component (slurry). It is probably true that all new flowmeters must, at least initially, compete in applications where the thin concentric orifice has proved less than satisfactory.

Although orifice flowmeters continue to account for 80+ percent of installed process plant meters, the past 8 to 10 years have seen a gradual shift in meter

Flowmeter	Pipe size, in (mm)	Gases (vapors)		Liquids					
		Clean	Dirty	Clean	Viscous	Dirty	Corrosive	Slurries	
								Fibrous	Abrasive

Square-root scale; maximum single range 4:1

Orifice									
Square-edged	> 1.5 (40)								
Honed meter run	0.5 - 1.5 (12 - 40)								
Foxboro IFOA									
Integral	< 0.5 (12)								
Quadrant/conic edge	> 1.5 (40)								
Eccentric	> 2 (50)								
Segmental	> 4 (100)								
Annular	> 4 (100)								
Target	> 0.5 - 4 (12 - 100)								
"V" Cone	> 0.5 - 72 (12 - 1800)								
Venturi	> 2 (50)								
Flow nozzle	> 2 (50)								
Lo-Loos	> 3 (75)								
Pitot	> 3 (75)								
Multiport averaging	> 1 (25)								
Elbow	> 2 (50)								
Wedge	0.5 - 24 (12 - 300)								

Linear scale; typical range 10:1

Laminar Flow	0.25 - 16 (6 - 400)								
Gilflo									
Magnetic	0.1 - 72 (2.5 - 1800)								
Mass flowmeter	0.1 - 72 (2.5 - 1800)								
Coriolis									
Positive-displacement	< 12 (300)								
Thermal mass									
Turbine	0.25 - 24 (6 - 600)								
Ultrasonic									
Time-of-flight	> 0.5 (12)								
Doppler	> 0.5 (12)								
Variable-area	≤ 3 (75)								
Vortex	0.5 - 16 (12 - 400)								

■ = designed for this application; ▒ = normally applicable; □ = not designed for this application.

TABLE 6.1 Flowmeter Selection Table (*Continued*)

Temperature, °F (°C)	Pressure, psig (kPa)	Accuracy, uncalibrated (including transmitter)	Reynolds number
Process temperature to 1000°F (540°C); transmitter limited to -20-350°F (-30-120°C)	To 6000 psig (41,000 kPa)		
		±1-2% URV†	$R_D > 2000$
		±1% URV	$R_D > 1000$
		±2-5% URV	$R_D > 100$
		±2% URV	$R_D > 200$
		±2% URV	$R_D > 10,000$
		±2% URV	$R_D > 10,000$
		±2% URV	$R_D > 10,000$
		±1% URV	$R_D > 10,000$
		±1.5-5% URV	$R_D > 100$
		±1-±2% URV	$R_D > 75,000$
		±1-±2% URV	$R_D > 10,000$
		±1.25% URV	$R_D > 12,500$
		±5% URV	No limit
		±1.25% URV	$R_D > 10,000$
		±4.25% URV	$R_D > 10,000$
		±2-4% URV	$R_D > 100$
Typical calibrated accuracy			
<200 (93)†	<100 (700)	±0.5-2% URV	$R_D < 2000$
<600 (315)†	<600 (4200)	±1% URV	$R_D > 10,000$
360 (180)	≤1500 (10,500)	±0.5% of rate to ±1% URV	No limit
<670 (300)	<2000	±0.2% to ±1% of rate	No limit
Gases: 250 (120) Liquids: 600 (315)	≤1400 (10,000)	Gases: ±1% URV Liquids: ±0.5% of rate	≤8000 cSt
<1000 (537)†	≤3000 (21,000)	±1% URV	No limit
-450-500 (-268-260)	≤3000 (21,000)	Gases: ±0.5% of rate Liquids: ±1% of rate	≤2-15 cSt
-450-500 (-268-260)			
-300-500 (180-260)	Pipe rating	±1% of rate to ±5% URV	No limit
-300-250 (-180-120)	Pipe rating	±5% URV	No limit
Glass: ≤400 (200) Metal: ≤1000 (540)	Glass: 350 (2400) Metal: 720 (5000)	±0.5% of rate to ±1% URV	To highly viscous fluids
≤750 (400)	≤1500 (10,500)	±0.5-1.5% of rate	>10,000

†URV = upper range value of the flow rate; formerly full-scale flow rate.

†refer to manufacturer for specification.

selection to the more advanced technologies (Flynn and Larson, 1994). The differential pressure transmitter and orifice are no longer routinely installed. Users are now more likely to consider alternative, proven technologies for many applications such as vortex, magnetic, ultrasonic, and mass flowmeters.

Basic Principle

The underlying principle for all differential-producing flowmeters is Bernoulli's streamline energy equation. When a flow is contracted (Fig. 6.1), either gradually or abruptly, kinetic energy increases at the expense of available potential energy (static pressure). The pressure difference between the taps located at the full pipe section (section 1 in Fig. 6.1) and in the vicinity of the contraction (section 2) is related to the square of the velocity at section 1 less the square of the velocity at section 2, to fluid properties, and to the abruptness of the contraction. Since the velocity times the pipe area is the volumetric flow rate, the basic flow equation may be written as a square-root relationship among measured differential pressure h_w , density ρ_f , and flow rate q as

$$q_{\text{efs}} = F_{MC} \sqrt{\frac{h_w}{\rho_f}} \quad (6.1)$$

The meter constant F_{MC} adjusts for dimensional units and includes a discharge coefficient that corrects for contraction characteristics, pressure-tap location, and velocity profile (Reynolds number). For a gas, the density differences caused by gas expansion between measurement taps requires an expansion-factor correction. This may be based on empirical data, as in the case of the square-edged orifice, or derived from thermodynamic considerations for the more gradually contracting elements (venturi and flow nozzle).

From Eq. (6.1) it is seen that, for example, if the differential pressure h_w decreases by a factor of 9, then the flow rate q decreases by a factor of 3. The accuracy of a fixed-upper-range differential pressure transmitter is therefore degraded. This is a basic reason for considering differential producers to have a maximum flow-rate range of 4:1.

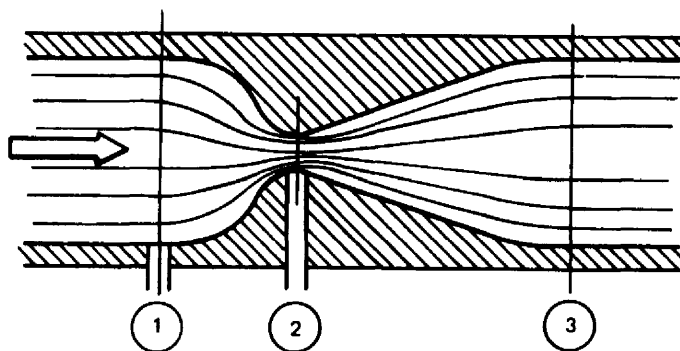


Figure 6.1 Basic principle of the differential producers.

The use of smart transmitters, which allow the differential pressure range to be changed by simply entering the appropriate reranged value, is now widely accepted. This concept coupled with on-line flow computation has extended in-situ flow-rate range to the limits of the estimated uncertainties (accuracy) for the installation.

The Orifice



Figure 6.2 Square-edged concentric orifice.

Square Edge. In 2-in (50-mm) and larger line sizes the concentric orifice (Fig. 6.2) is the most common restriction for clean liquids, gases, and low-velocity vapor (steam) flows. It is a sharp, square-edged hole bored in a flat, thin plate. The ratio of hole diameter d to pipe diameter D defines the beta ratio β . For most applications this ratio should be between 0.2 and 0.75, depending on desired differential; a high- β orifice produces less differential for the same flow rate than a small- β orifice.

Beta ratios greater than 0.75 are sometimes used where accuracy is unimportant.

Depending on upstream and downstream tap location, the flowmeter is referred to as a corner tap, a flange tap, a D -and- $D/2$ tap, a pipe tap ($2\frac{1}{2}D$ and $8D$), or a vena contracta tap-orifice flowmeter. Corner and D -and- $D/2$ taps are widely used in Europe, while flange taps predominate in the United States. Pipe taps ($2\frac{1}{2}D$ and $8D$) are sometimes used as bypass pump restrictors for natural gas or where the other tapping arrangements require drilling too close to the plate. Vena contracta taps have been replaced by D -and- $D/2$ taps because future changes in orifice bore require no tap relocation.

Several standards [ISO 5167 (1995), ASME MFC-3M (1995), and ANSI/API 2530 (1991) for natural gas and hydrocarbon fluids] have been written to detail installation requirements and construction and to estimate the overall uncertainty (accuracy). Overall accuracy ranges from ± 0.8 to ± 0.5 percent, depending on the fluid and the upstream piping configuration and whether corrections for Reynolds number, gas expansion factor, and other effects are included in the computation. While standards differ on the minimum pipe Reynolds number that permits this accuracy, a value of 10,000 is considered acceptable by most.

The maximum pipe Reynolds number R_D may be as high as 3.3×10^7 (Gorter and Rooji, 1977). However, a discharge coefficient rise of up to 1.56 percent for a 0.71 beta ratio orifice has been reported by Jones (1986) at bore Reynolds numbers R_d greater than 8×10^6 . This rise, at very high Reynolds numbers, may be explained by the work of Grose (1985) on the inviscid (zero viscosity) contraction coefficient change with beta ratio.

Quadrant and Conic Edge. When the pipe Reynolds number is below 10,000, the upstream orifice edge is either rounded (quadrant, Fig. 6.3) or conical (Fig. 6.4); these contours give a more constant and predictable discharge coefficient at lower Reynolds numbers. At low Reynolds numbers the coefficient of a square-edged

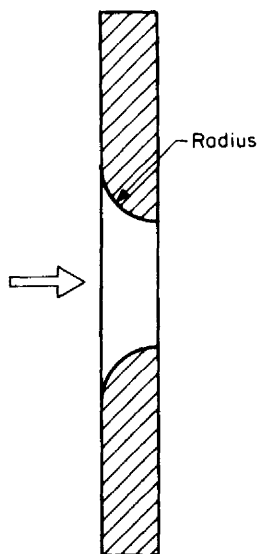


Figure 6.3 Quadrant-edged orifice.

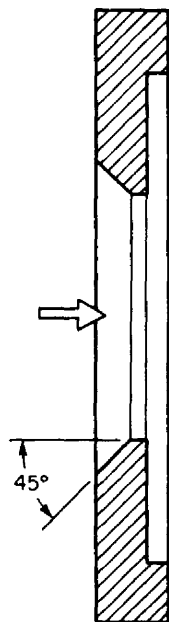


Figure 6.4 Conical orifice.

orifice may change by as much as 30 percent, but for these geometries the effect is only 1 to 2 percent, making a more usable flowmeter for viscous fluids. The quadrant plate is widely used in the United States, whereas the conic plate predominates in European applications.

Small Line Sizes. In $\frac{1}{2}$ - to $1\frac{1}{2}$ -in (12- to 40-mm) line sizes, the effects of pipe roughness, plate eccentricity, and edge sharpness are magnified, resulting in unpredictable coefficients. All indications are that coefficients must be experimentally determined, with selection of a square or quadrant edge depending on Reynolds number.

For these line sizes, corner pressure taps are preferred, since the downstream pressure tap lies beyond the vena contracta (location of minimum pressure). The Foxboro Integral Flow Orifice Assembly (IFOA), Fig. 6.5, The Rosemount Model 1195, or Taylor Jet Set supplies meter runs in line sizes of $\frac{1}{2}$ to $1\frac{1}{2}$ in (12 to 40 mm) that have experimentally determined coefficient prediction equations. The IFOA is available in standard or sized bore or with a quadrant edge for very low flows. Honed meter runs (ASME MFC-SC2, 1987, Filban et al., 1960) are also widely used in these sizes.

Integral Orifice. When the pipe size is $\frac{1}{2}$ in (12.7 mm) or smaller and the fluid is clean, it is common to select an orifice installed integrally with the differential-pressure transmitter (Fig. 6.6). This provides a compact installation in which overall accuracy, usually ± 2 to ± 5 percent uncalibrated, has been predetermined based on flow-calibrating reproducible fixed-size orifices.

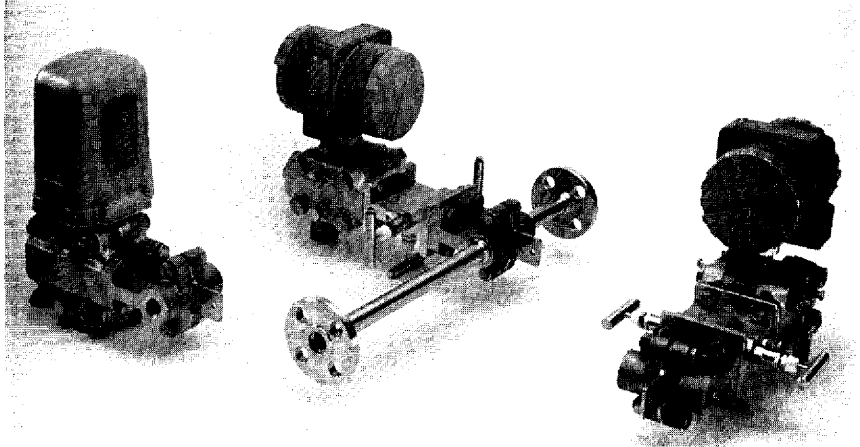
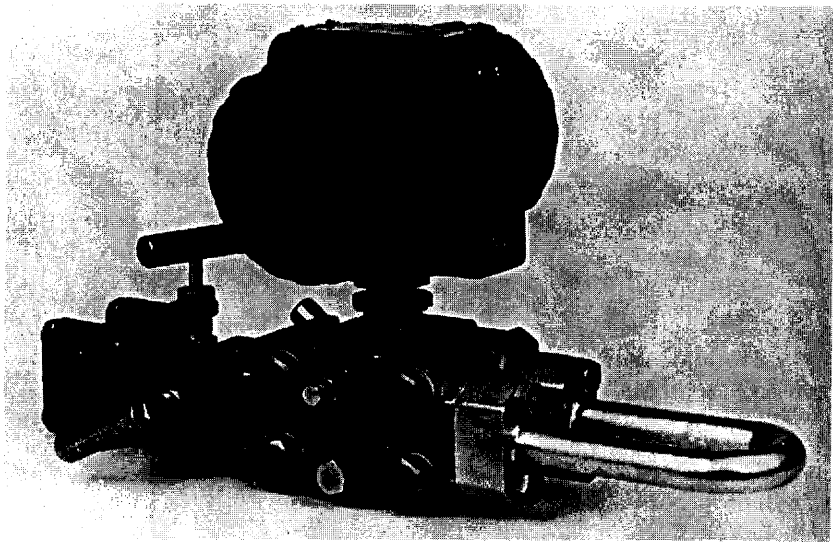


Figure 6.5 Integral orifice assembly. (Courtesy The Foxboro Co.)

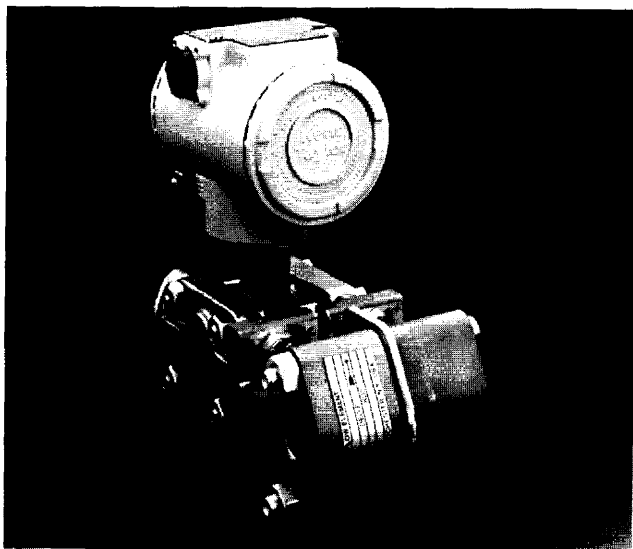


(a)

Figure 6.6 Integral orifice. (a) In-line. (Courtesy The Foxboro Co.) (b) U-bend. (Courtesy The Foxboro Co.) (c) In-line. (Courtesy ABB-KENT/Taylor.)



(b)



(c)

Figure 6.6 (Continued)

Eccentric and Segmental Orifices. If the orifice hole is placed at the bottom of the pipe for gases (Fig. 6.7), and at the top for liquids, entrained water or air will flow through the plate rather than build up in front of it. If a segmental opening (Fig. 6.8) is machined in the plate, passage of liquids, air, or particulate matter is also possible. Data for these orifice geometries is limited, but they provide low-cost alternatives for troublesome applications. Their uncalibrated coefficient accuracy is usually estimated as ± 2 percent.



Figure 6.7 Eccentric orifice.



Figure 6.8 Segmental orifice.

Wedge Meter

The Taylor wedge flow element (Fig. 6.9) is similar to a segmental orifice in that particulate matter or entrained gases easily pass through the meter. It is of a fixed-body design with double remote seals for the differential pressure measurement. Test results (Owen, 1979) have shown a constant discharge coefficient over a wide Reynolds number range.

The design makes it well suited for air or particulate entrained flows, viscous flows, and slurry flows. A PVC body also is available for chlorine and similar chemical applications. Estimated accuracy is in the range of 1 to 2 percent.

Venturi Tube

The tapered inlet and diverging exit of the classical Herschel venturi (Fig. 6.10) substantially reduces permanent pressure loss. Since dirt will not build up as it passes through the contoured sections (as it does in front of an orifice), this differential producer can be used for dirty flow applications. Initially designed for large-line-size [6 in (150 mm) or larger] water and waste applications, the venturi has become more popular in smaller line sizes with the introduction of the proprietary Universal Venturi Tube (Fig. 6.11), a flowmeter of reduced weight and shorter overall length having the advantages of the venturi principle (Halmi, 1974).

Several proprietary venturi-type flowmeters are widely used in the water and waste industry. These are designed to reduce overall weight and length, usually by reducing the overall throat length. Insert-type designs are also common with the throat pressure tap(s) connected to the outer pipe by either a solid plug or with a Bourdon tube connection to minimize thermal stress for high-temperature applications.

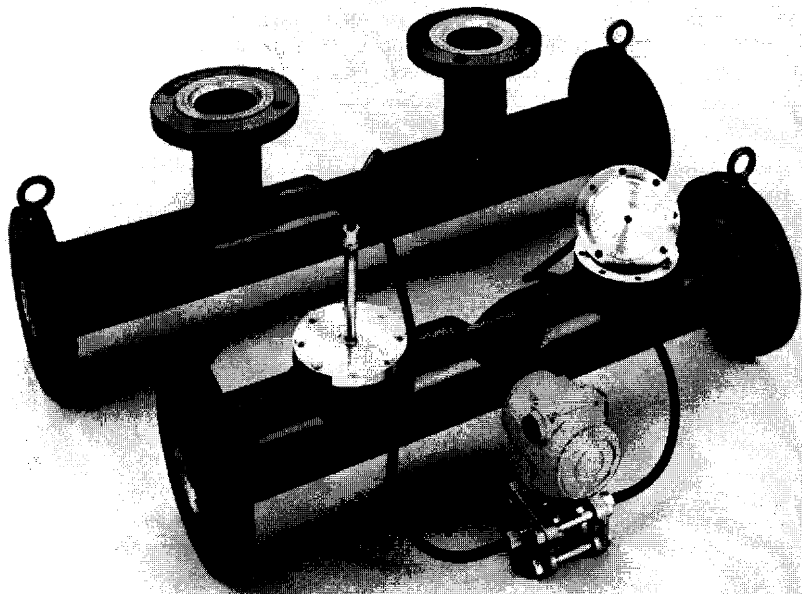


Figure 6.9 Wedge flowmeter. (Courtesy Taylor Instruments.)

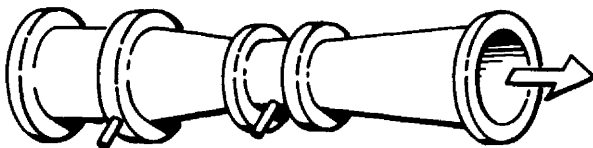


Figure 6.10 Classical venturi.

For pipe Reynolds numbers greater than 100,000, discharge coefficients for venturis are constant and predictable to within ± 0.5 to ± 2 percent, depending on design. Venturis are not normally used for lower Reynolds numbers without the acceptance of worsened coefficient accuracy. When pumping cost and/or shorter upstream installation length are important, the additional expense for a venturi design is usually warranted.

The venturi is increasingly being used for high-accuracy gas and vapor flows. The introduction of *smart* differential pressure transmitters and flow computers that increase rangeability have essentially negated the need to change the bore of the primary device.

Flow Nozzle

The flow nozzle (Fig. 6.12) has an elliptical (ASME) or a radius (ISA) entrance and is generally selected for steam (vapor) flows at high pipeline velocities [100

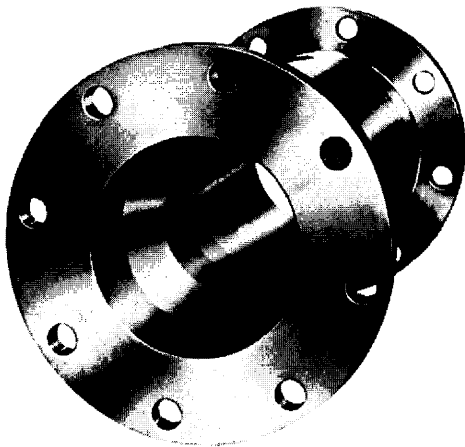


Figure 6.11 Universal Venturi Tube. (*Courtesy BIF.*)

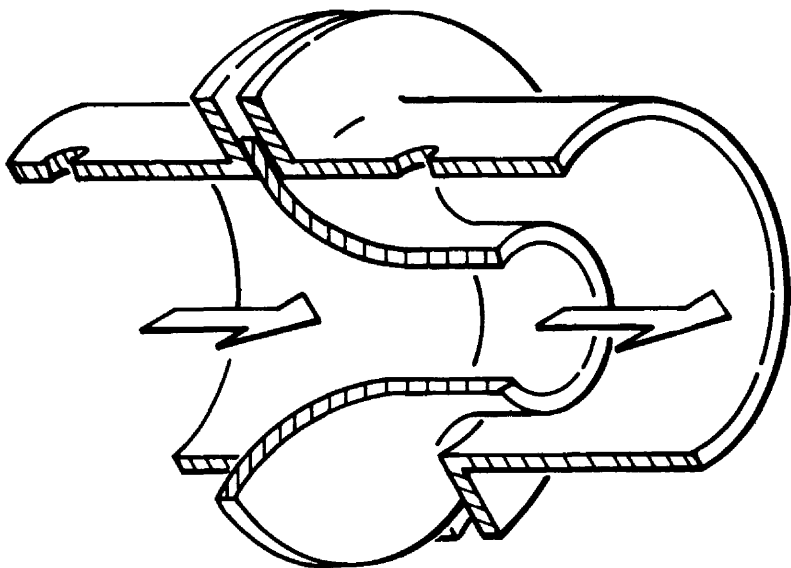


Figure 6.12 Flow nozzle.

ft/s (30.5 m/s)]. Because of its rigidity it is dimensionally more stable at higher temperatures and velocities than an orifice.

The initial cost of a flow nozzle is substantially higher than that of an orifice but lower than that of a venturi; however, its permanent pressure loss is significantly higher than that of a venturi. When both are sized to create the same differential

at the same flow rate, the pressure loss of a flow nozzle is approximately the same as for an orifice.

Flow nozzles and critical venturi nozzles (Fig. 6.13) are sometimes operated at critical (choked) flow for flow limiting or as secondary flow standards (Jones and Ferguson 1986). The most widely used nozzles are the ASME elliptical-inlet long-radius wall-tap nozzle and the ASME throat-tap nozzle for steam-turbine testing. In Europe the ISA 1932 nozzle is widely used. Standards used for construction, installation, and uncertainty (accuracy) are ISO 5167 (1991) and ASME MFC-3M (1995) and, for the critical flow nozzle, ANSI/ASME 7M (1987).

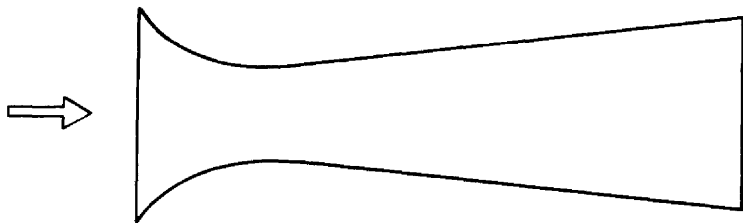


Figure 6.13 Critical-flow venturi nozzle.

Lo-Loss Permanent-Pressure-Loss Devices

Several proprietary designs (Fig. 6.14) have been introduced that produce high differentials with lower permanent pressure loss, lower weight, and shorter overall laying lengths. Coefficient information at high Reynolds numbers is not generally available for these designs. Also, little theoretical work (required for good extrapolation) is available, and the user is cautioned to stay within calibrated ranges. Support information remains proprietary, and the user should contact the manufacturer for the latest information.

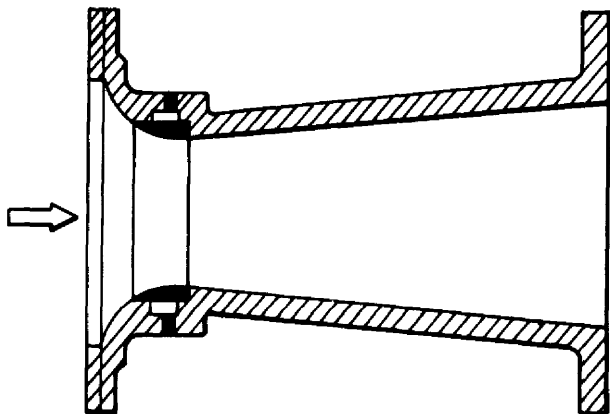


Figure 6.14 Lo-loss tube. (Courtesy Badger Meter, Inc.)

Elbow Flowmeter

As a fluid passes through a pipe elbow, the pressure at the outside radius of the elbow increases due to centrifugal force (Fig. 6.15). If pressure taps are located at the outside and inside of the elbow at either $22\frac{1}{2}^\circ$ or 45° , a reproducible measurement can be made. Taps located at angles greater than 45° are not recommended, because flow separation may cause erratic readings.

Elbow meters are inexpensive flowmeters, since many installations have elbows. Even when the elbow ID is measured, differences among elbows limit accuracy to ± 4 percent (Murdock et al., 1963), but precision (repeatability) is good (± 0.2 percent). The flow is unobstructed, however, with no additional permanent pressure loss. Several manufacturers offer proprietary machined elbow flowmeters for improved accuracy, but little data has been published on these devices. The major disadvantage of the elbow flowmeter is the very low differential pressure that is created, particularly for gas flows.

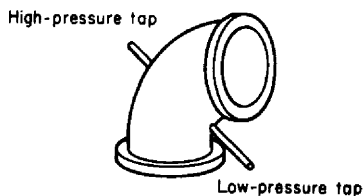


Figure 6.15 Elbow flowmeter.

Pitot Tube and Multiport Averaging Devices

The pitot tube (Fig. 6.16) is used for large pipe sizes when the fluid is a clean liquid or gas (vapor) and an inexpensive measurement is required. For this device, the difference between total (stagnation) pressure and static pressure follows the square-root relationship, with velocity being sensed at the insertion depth only. By traversing, an average-velocity point can be located and used to measure flow rate.

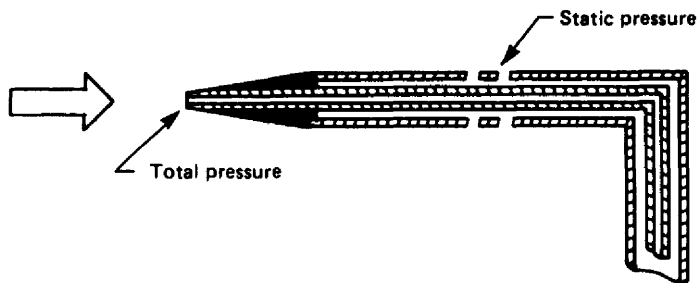
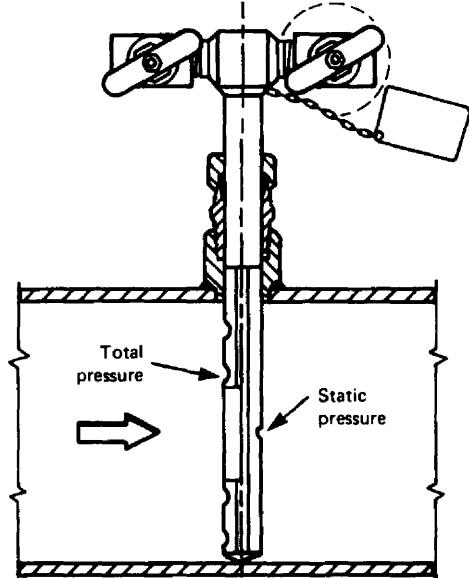
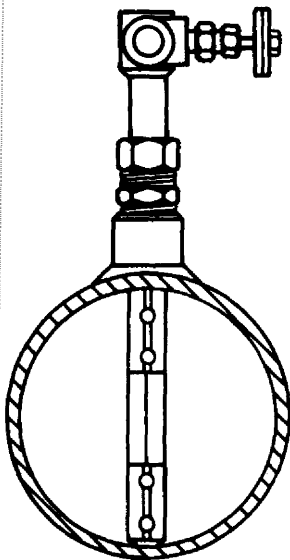


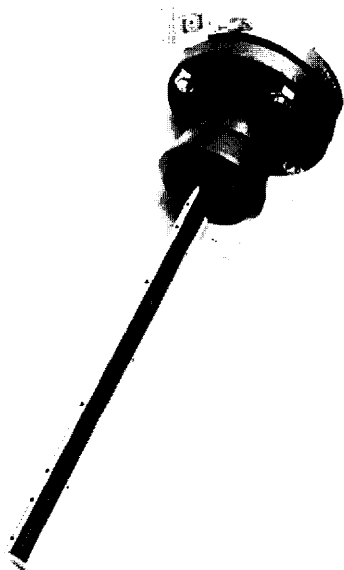
Figure 6.16 Pitot tube.

The multiport averaging pitot tube (Fig. 6.17) spans the pipe and has virtually replaced the pitot. Ease of installation, low cost, very low overall pressure loss, good performance, and hot-tapping capabilities make these devices competitive with other differential producers in many industrial applications.

There are several designs available, ranging from a cylinder to a diamond-shaped strut. These designs (Fig. 6.17a, b) increase the number of stagnation and static pressure-sensing ports with increasing line size, have extensively published data,



(a)



(b)

Figure 6.17 Multiport averaging flowmeters. (a) Annubar. (Courtesy Dietrich Standard Corp.) (b) Ellipse flow sensor. (Courtesy Presso, Ltd.)

and theoretically relate the coefficient to a blockage factor. ASME (ASME/MFC-SC16, 1995) is currently preparing a standard covering these devices.

Ease of installation, low cost, very low permanent pressure loss, and insertability into existing piping make these devices convenient for ducts and large-line-size measurements. The multiport averaging devices have essentially replaced the pitot tube for clean liquids, gases, and vapors (steam). Because total-pressure ports face the flow, a purging flow may be necessary for dirty-stream applications.

A variety of multiported designs is now available. Users should review individual manufacturers' support data before applying these devices outside ranges for which data is available.

Annular Flowmeters

Annular Orifice. The annular orifice (Fig. 6.18) was developed to overcome the problems of dirt buildup in front of an orifice in liquid streams and of liquid buildup in a moist gas stream. Total (stagnation) pressure taps and rearward facing taps produce a high differential for a given β , here redefined as the ratio of disk diameter to pipe diameter. Little data has been presented for line-size correlation. Only air data is available for the normally used beta ratios. A design that slips between flanges has reportedly been successfully used for air in 24-in (600-mm) and larger line sizes.

Target Flowmeter. The target flowmeter (Fig. 6.19a, b) has the features of the annular orifice without the disadvantages of freezing or plugging lead lines. The primary element consists of a sharp-leading-edge disk (target) fastened to a bar. The differential pressure produced by the reduced annular area creates a disk *drag force*. This is transmitted through a bar to a suitable force-measuring secondary device, and the flow rate is calculated as the square root of this output.

Target flowmeters are particularly well suited for dirty and low-Reynolds-number flows, but they are also used with clean fluids and for natural gas (Reinecke et al., 1966). Their uncalibrated accuracy ranges from ± 1 to ± 5 percent, depending on line size, beta ratio, and Reynolds number.

"V" Cone. The "V" cone produces a differential pressure as the fluid accelerates along a contoured annular cone as shown in Fig. 6.20. The differential is generally lower than other differential producers, but shorter upstream lying length requirements (2–5 PD), lower permanent pressure loss, and a constant coefficient over a wider Reynolds-number range are major claims. The strut-type mounting requires

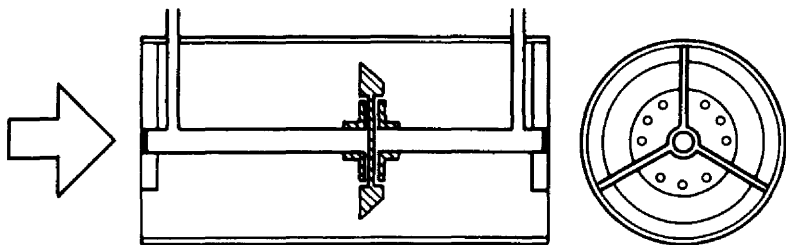


Figure 6.18 Annular orifice.

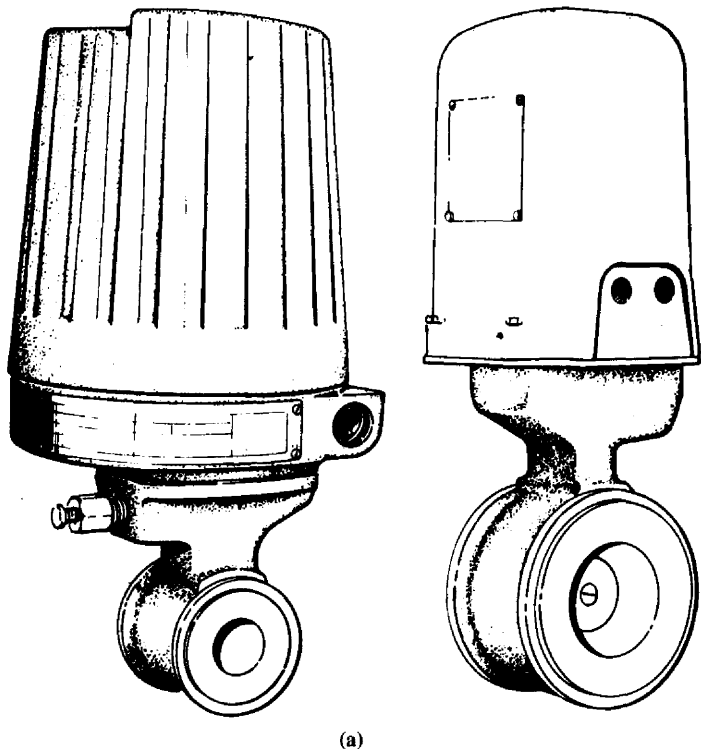


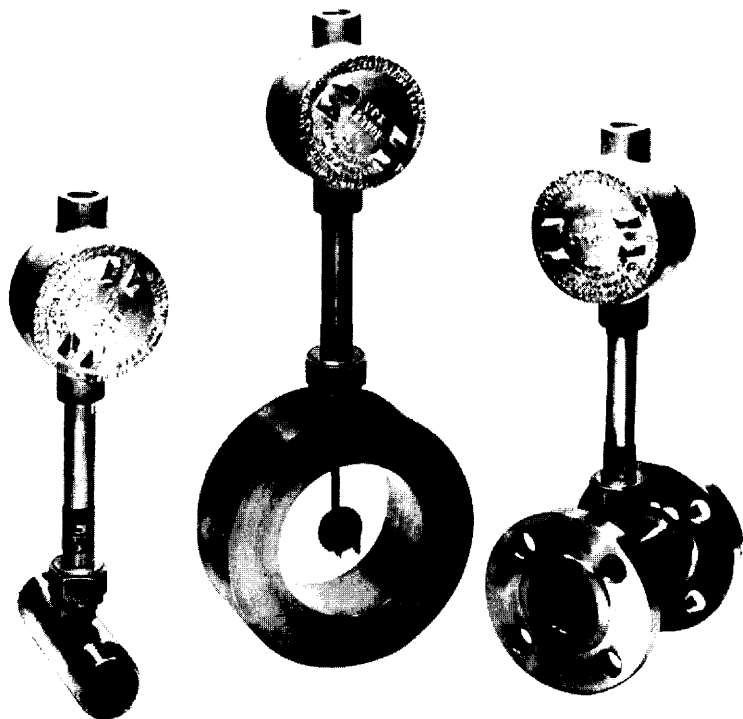
Figure 6.19 Target flowmeters. (a) Foxboro. (Courtesy The Foxboro Co.) (b) Ramapo. (Courtesy Hersey Measurement Co.)

that consideration be given to maximum flow rates to ensure minimum vibratory stress. The manufacturer should be made aware of possibilities for cavitating fluids, flashing, thermal loading, etc., as is typical of all flowmeters.

Linear Differential Producers

There are several differential producer designs that produce a differential pressure proportional to the flow rate and not to the square of the flow rate. These are discussed below.

Laminar Flow Element. Laminar flow occurs when the Reynolds number is below 2000. In this flow regime the pressure loss across a length of pipe is inversely proportional to the Reynolds number. Figure 6.21 shows a laminar flowmeter that consists of a large number of small-diameter channels. The flow through these parallel ducts is essentially at the entering pipeline velocity. If dimensions are reduced, laminar flow will occur within each duct section. The differential across the *laminar* element is then proportional to the flow rate (velocity) in accordance with the Hagan-Poiseuille law for laminar flow pressure drop. The flow rate for laminar meters can then be expressed as



(b)

Figure 6.19 (Continued)

$$q = \frac{k_1 \Delta P}{\mu} \quad (6.2)$$

where k_1 is a constant based on meter design, q is the volumetric flow rate, and μ is the absolute viscosity.

The overall pressure loss is the same as the produced differential, approximately 10 in (2.5 kPa) of water. Meters are normally used on gas flows, but the principle applies to liquids. Meters are calibrated to establish the k_1 factor to within ± 0.5 percent. The lower limit of the linear flow-rate range is the acceptable accuracy of the differential pressure measurement device. Since laminar flow is achieved by small passage areas, as small as 0.009 in (0.228 mm) in some meter sizes, the metered fluid must be clean. Accuracy of ± 0.25 percent is attainable with a precision of ± 0.1 percent (Weigand and Lombardo, 1989).

The laminar flow element is often used in pulsative flow applications because of its linear relationship, and the element itself introduces a damping action on the system. To minimize the error in the measurement of differential when large pulsative amplitudes are encountered, it is recommended that porous plug (or linear damping) devices be inserted in the differential pressure tap lead lines.

Laminar flow elements are widely used to meter the flow of clean low-pressure gases and are commonly used to measure air flow to internal combustion engines,

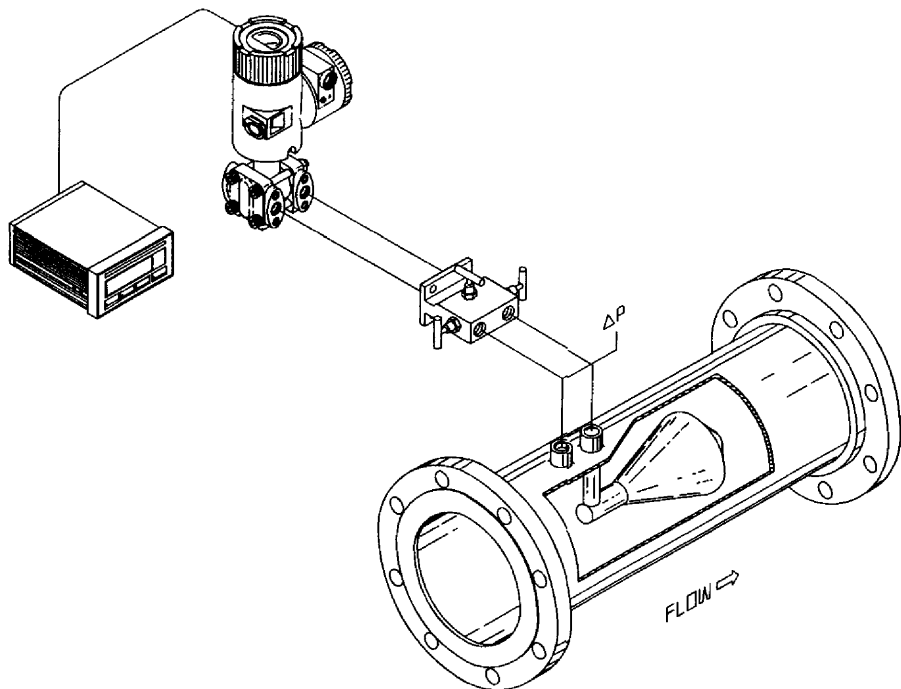


Figure 6.20 "V" cone. (Courtesy McCrometer Div. of Ketema.)

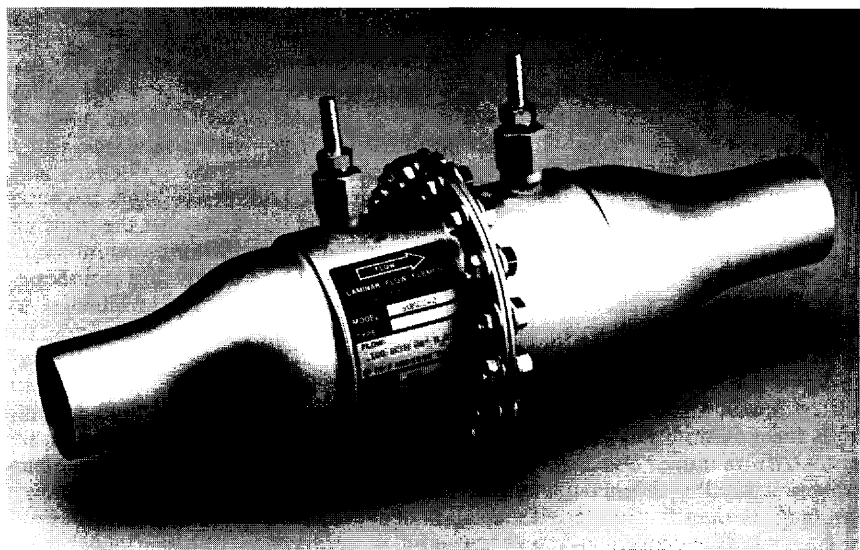


Figure 6.21 Laminar flowmeter. (Courtesy Meriam Instruments, Inc.)

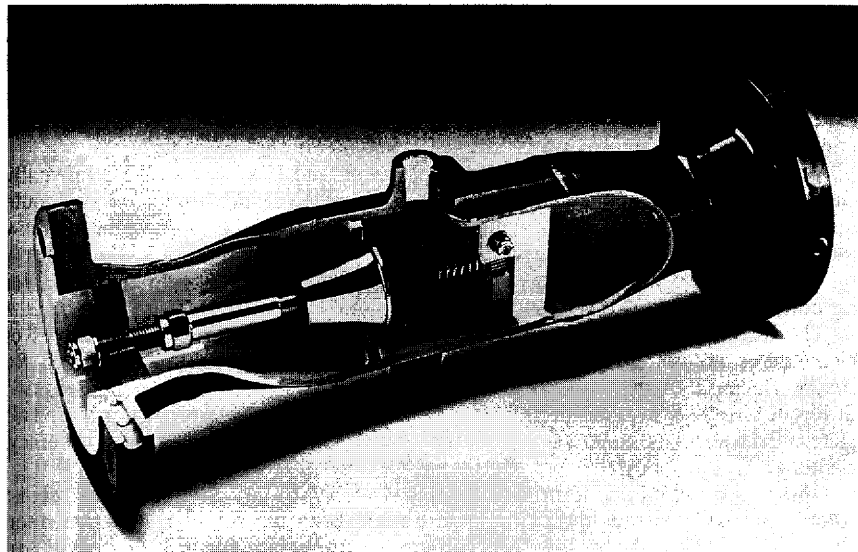


Figure 6.22 Gilflo flowmeter. (*Courtesy Spirax Metering, Inc.*)

where severe pulsative flow conditions occur. Other examples are air flow for fans, air motors, valves, and filters. The measurements of leakage rates from airplane cabins, home windows, and storm windows are other applications.

Gilflo. The Gilflo spring-loaded variable-area flowmeter (Fig. 6.22) claims to offer a 100:1 linear flow-rate range. The device operates on the spring-loaded variable-area principle in which the annular area is varied by the downstream motion of a cone with increasing flow rate. The cone moves axially against a heavy-duty precision spring. The resulting differential pressure, which is linear with flow rate, is measured by a differential pressure transmitter.

The meters are compact and the annular flow features minimize the required length of the upstream pipe. The meters are suitable for liquid, gases, and vapors and are commonly used in the metering of steam in large buildings where wide-range flow rates need to be metered for billing purposes.

LINEAR FLOWMETERS

Turbine Flowmeter

The speed of a turbine flowmeter's rotor increases linearly with flow velocity. Blade rotation is thus a measure of velocity and is detected by noncontacting external magnetic or other proximity detectors. The relationship between line velocity and rotor speed is linear (within ± 0.5 percent) over a wide flow range of 10:1 to 20:1. Liquid turbine flowmeters can attain an accuracy (uncertainty) of ± 0.25 percent and a precision (repeatability) of ± 0.05 percent over a 20:1 flow-rate range when all known influence quantity factors are applied or controlled (Rubin, 1991). Low-

velocity performance is affected by velocity profile, tip clearance, friction across the blades, bearing friction, and other retarding torques (Rubin et al., 1965). The major problems with liquid turbine flowmeters are the detrimental effects of overspeed when the liquid flashes or when slugs of vapor or air enter the line, shifts in calibration with blade wear, bearing friction, and large calibration shifts for liquids containing small amounts of air (Kinghorn and McHugh, 1981).

With a jet mixer installed upstream, Millington and King (1986) experimentally showed that, for up to 10 percent by volume of air in oil, mixing techniques could not reduce metering error (bias) to less than 3 percent regardless of the oil flow rate and gas content. For larger air concentration the meter overregistered at low oil flow rates and underestimated at the higher flow rates. The limit of error, for air concentrations of greater than 10 but less than 25 percent, was 15 percent.

The turbine flowmeter is used for accurate, wide-range flow measurements of clean gases and liquids, and some manufacturers offer flowmeters designed for steam. Because of the large density differences between liquids and gases, two different turbine flowmeter designs (Figs. 6.23 and 6.24) are required for these two states. Both designs are used in custody transfer applications requiring accuracy, range, and a pulse-train output.

The self-adjusting gas turbine flowmeter (Lee, 1986) has two rotors, the second rotor of which measures the exiting swirl angle from the primary upstream rotor. This allows for a self-checking and self-correcting feature for upstream swirl and retarding torque changes in the system.

Turbine flowmeters are calibrated in either a hydraulics or low-pressure-air laboratory. The laboratory-determined meter coefficient is either expressed as a *K factor* in units of pulses per gallon (pulses per cubic meter) or is given as a *meter*

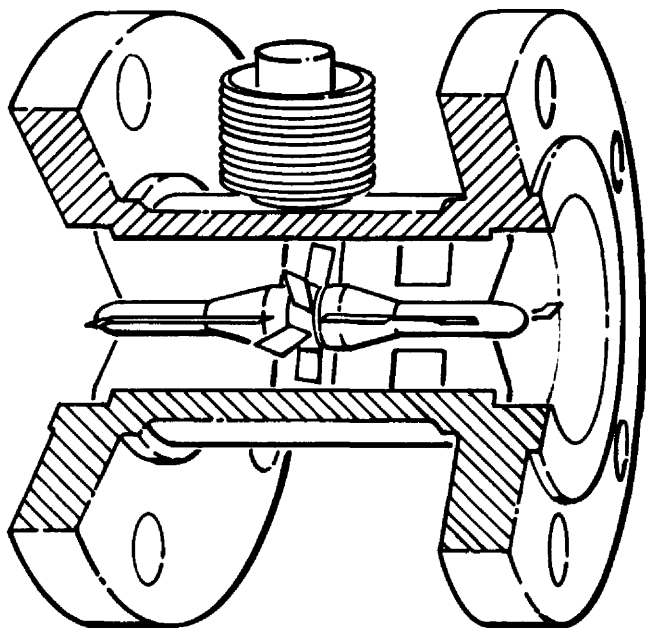
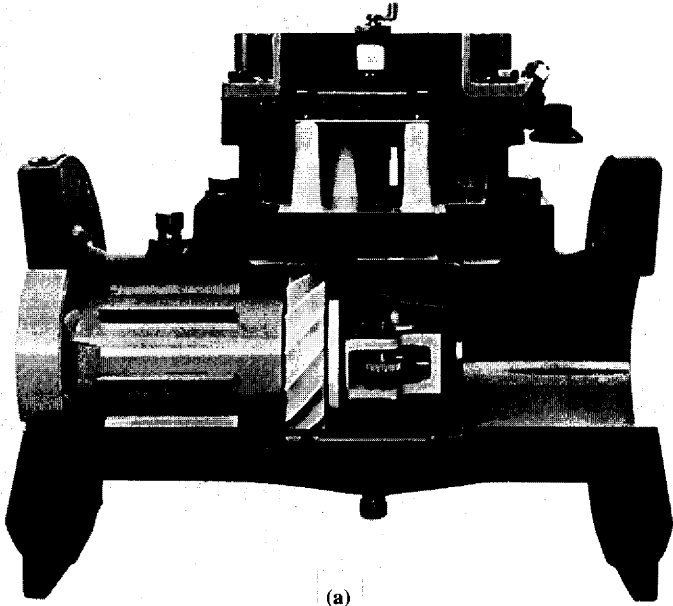
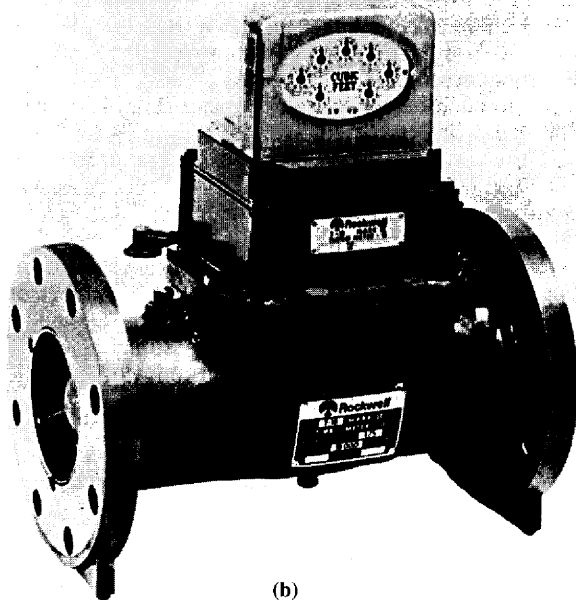


Figure 6.23 Liquid turbine flowmeter.



(a)



(b)

Figure 6.24 Gas turbine flowmeter. (Courtesy Equimeter, Inc.) (a) Internal mechanism. (b) Exterior.

factor in cubic feet per pulse (cubic meters per pulse). API Publication 2101 (1981) defines meter factor as prover volume divided by registered volume. For the metering of liquid hydrocarbons, the requirements of this manual must be strictly adhered to. Accuracy is claimed as ± 0.25 to ± 1 percent of indicated flow rate, depending on flow-rate range, viscosity, and installation conditions.

Since the turbine meter indicates actual volumetric flow, the accuracy of the secondary measurement equipment, such as pressure, temperature, or density, is combined to arrive at an estimated overall uncertainty (accuracy) for the measurement of mass flow (pound-mass, kilogram) or standard volumetric units (SCF, SCM, etc.). If the fluid is a gas (Bonner, 1993), ASME/ANSI 4M (1987), AGA Report No. 7 (1981), and ISO Standard 9951 (1992) present the standardized method for these computations.

Vortex Flowmeter

Vortex shedding is a common flow phenomenon that causes bridges to collapse and telephone wires to sing. The instability of the flow field after it splits into two paths around a bluff object causes vortices to shed from alternate sides of the object at a frequency linearly proportional to velocity. If the approximately sinusoidal pressure or velocity changes created by the moving vortices in the fluid are detected, the flow rate can be determined. The relationship between pipeline velocity and shedding frequency is linear and independent of fluid density over flow-rate ranges of 20:1 or 30:1.

The K, or meter, factor is the same for liquids, gases (vapors), and cryogenic fluids (Brennan et al., 1974), making this device an ideal all-purpose flowmeter. Vortex meters are well suited for steam (SIREP-WIB, 1985), natural gas (Miller et al., 1984), and liquid flows. They are now approved for custody transfer natural gas metering in some countries (Kastner, 1986).

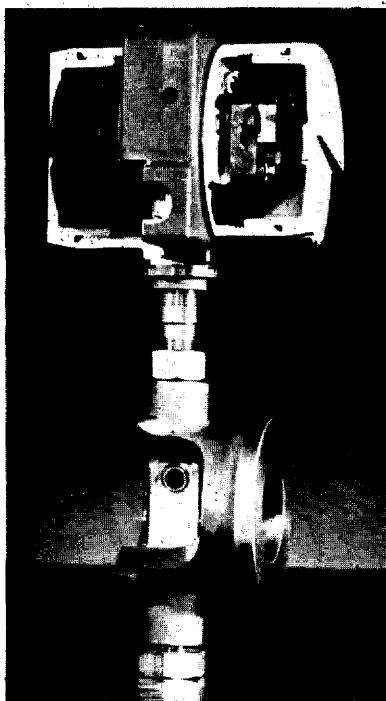
The barlike construction of the vortex flowmeter (Fig. 6.25) allows for the passage of dirt. The output frequency is lower for the same flow rate than that of a turbine meter, and the vortex device is without overspeed or moving-part problems. Experimental and theoretical information indicates that the calibration factor at moderate Reynolds numbers is not as sensitive to edge sharpness or dimensional changes as those of square-edged orifices and target flowmeters (Lomas, 1977).

Several manufacturers offer vortex flowmeters for line sizes from $\frac{1}{2}$ to 16 in (12 to 400 mm). Vortices are shed down to a pipe Reynolds number of 2000, but the shedding rate is nonlinear for Reynolds numbers from 2000 to 10,000; for this reason, a minimum Reynolds number of 10,000 is usually given.

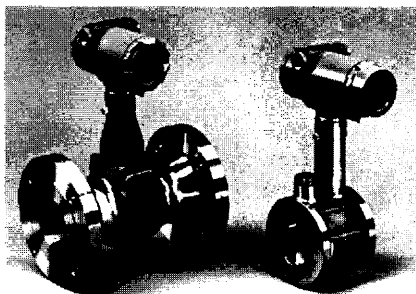
Meter geometry is highly reproducible for a given line size (Miller et al., 1977), and accuracy is normally ± 0.5 to ± 1 percent over a 15:1 or 20:1 flow-rate range. Vortex flowmeters are increasingly being used because of their accuracy, range, precision, and relative insensitivity to fluid properties. ANSI standard ANSI/ASME MFC-6M (1987) covers vortex flowmeters for liquid, gas, and vapor applications.

The *smart* vortex flowmeter shown in Fig. 6.25a transmits the alternating pressure impulses exerted on the bar to smart electronics. These meters communicate using the HART protocol, which uses an industry-standard Bell 202 frequency shift keying (FSK) technique. Remote communication is via a high-frequency signal on top of the standardized 4- to 20-mA output signal. The means of communications may vary with manufacturers.

Selecting the size of a vortex meter (Biles, 1991) requires a knowledge of the process variables and the manufacturer's limitations on pressure, temperature, pipe-



(a)



(b)

Figure 6.25 Vortex flowmeter. (a) The Foxboro meter. (Courtesy The Foxboro Co.) (b) Spool piece and waver vortex flowmeters. (Courtesy Rosemount, Inc.)

line velocity, and Reynolds number. Often two different-size meters could be used. The selected size depends on the operating pressure range for gases or vapors, and in general the smallest-size meter should be selected. However, for liquids the cavitation limits and overall pressure loss may require the larger-size meter. Manufacturers usually supply a sizing PC program that assists in the selection process.

Magnetic Flowmeter

Based on magnetic induction principles, the magnetic flowmeter (Fig. 6.26) provides an obstructionless flowmeter that essentially averages velocity over the pipe area (Shercliff, 1962). Fluids to be measured must have a conductivity of at least $2 \mu\text{S}/\text{cm}$ to be measurable. A voltage is generated by the flowmeter that is mutually perpendicular to flow direction and magnetic field and is detected by two flush-mounted electrodes on a diameter of a nonconducting pipe wall. The low-level millivolt signal is proportional to the average pipeline velocity, and, for this reason, magnetic flowmeters are ideally suited for all conductive fluids that operate in both the laminar and turbulent flow regimes.

Unlike the differential producer, for which fluid density enters into the volumetric flow equation, the magnetic flowmeter's operating principle makes it a *true* volumetric flow device. Entrapped air, foam, two or more component mixtures,

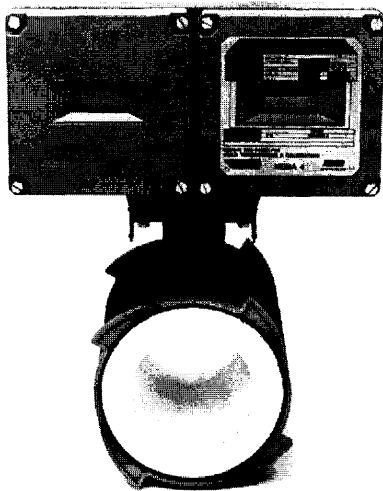


Figure 6.26 Electromagnetic flowmeters.
(Courtesy The Foxboro Co.)

aggregates, etc., if uniformly mixed and traveling at the pipeline velocity, are measured on a flowing-volume basis.

Usually a nonmagnetic material (stainless steel) provides the necessary structural integrity, while an inserted nonconducting liner of Teflon, rubber, or a ceramic electrically insulates the generated voltage from the supporting structure. Some meters are made wholly of fiberglass, but these have low pressure ratings. The meter housings are made of magnetic materials with coils installed inside and imbedded in a thick insulating liner. With properly selected liners, magnetic flowmeters are ideally suited for slurries, dirty flows, pulp stock, nonnewtonian fluids, corrosive liquids, and other liquids that are difficult to handle. Flowmeters are offered in sizes of from 0.1 to 96 in (2.5 to 2400 mm) with numerous secondary-device output options [4 to 20 mA, 3 to 15 psig (20 to 100 kPa), pulse train, etc.].

Two separate design approaches, based on magnetic-field excitation, are offered. In the first, ac mains directly power the electromagnetic coils; in the second (Fig. 6.27), the field is dc-energized for a short time duration. In the ac system, signal voltage is referenced to excitation voltage, to current, or to a field-measuring flux coil. In the dc system, electrode voltage is measured first with no magnetic field and then with a field. The measured voltage difference is the flow signal.

Magnetic flowmeters (both primary and secondary devices) are linear over a 10:1 range within an accuracy envelope of ± 0.5 to ± 1 percent of either actual or upper-range flow rate.

Area averaging makes magnetic flowmeters less sensitive to profile changes than many other meter types (Haacke, 1974). Magnetic flowmeters also have been developed to respond to transient flows (Lefebvre and Durgin, 1986) with a frequency response of 60 Hz.

Figure 6.28 shows a balanced electrode meter (Scarpa, 1993) that takes advantage of the fact that no flow-induced potentials exist in the same plane as the sensing

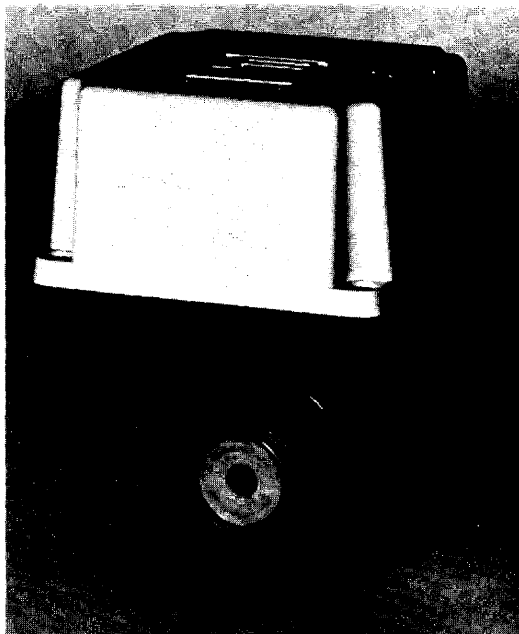


Figure 6.27 DC field electromagnetic flowmeter.
(Courtesy Fischer & Porter.)

electrodes, which are along a parallel axis to the induced magnetic field and rotated 90° from the sensing electrode. By installing ground electrodes at these locations, an averaging of the velocity profile will occur within the plane of the balancing electrodes. This feature will theoretically vector sum all out-of-phase flow-induced vectors for improved averaging of axisymmetric or skewed velocity vectors.

Smart magnetic flowmeters can be configured locally or remotely using a keypad and liquid-crystal display. The parameters that affect meter output, tag number, and other identifying information can be accessed and changed. These meters offer self-diagnostics that alert the user to problems within the transmitter, flowtube, or process. Remote interrogation can also be performed to simulate any desired signal. This capability allows testing of the output loop, receiving equipment, and the flowmeter. ASME-16M (1995) cover both the ac and dc type magnetic flowmeters.

Ultrasonic Flowmeters

There are two types of liquid ultrasonic flowmeters. In the first type (*time-of-flight* meters, Fig. 6.29), a high-frequency (approximately 1 MHz) pressure wave is beamed at an acute angle across the pipe. The time required for the wave to reach the opposite wall depends on whether it is moving with or against the flow and on the speed of sound through the liquid. Flow-rate information is obtained from the measured time. In the second type, referred to as the *Doppler* flowmeter, the pressure front does not traverse the pipe but is reflected back to a detector by particulate

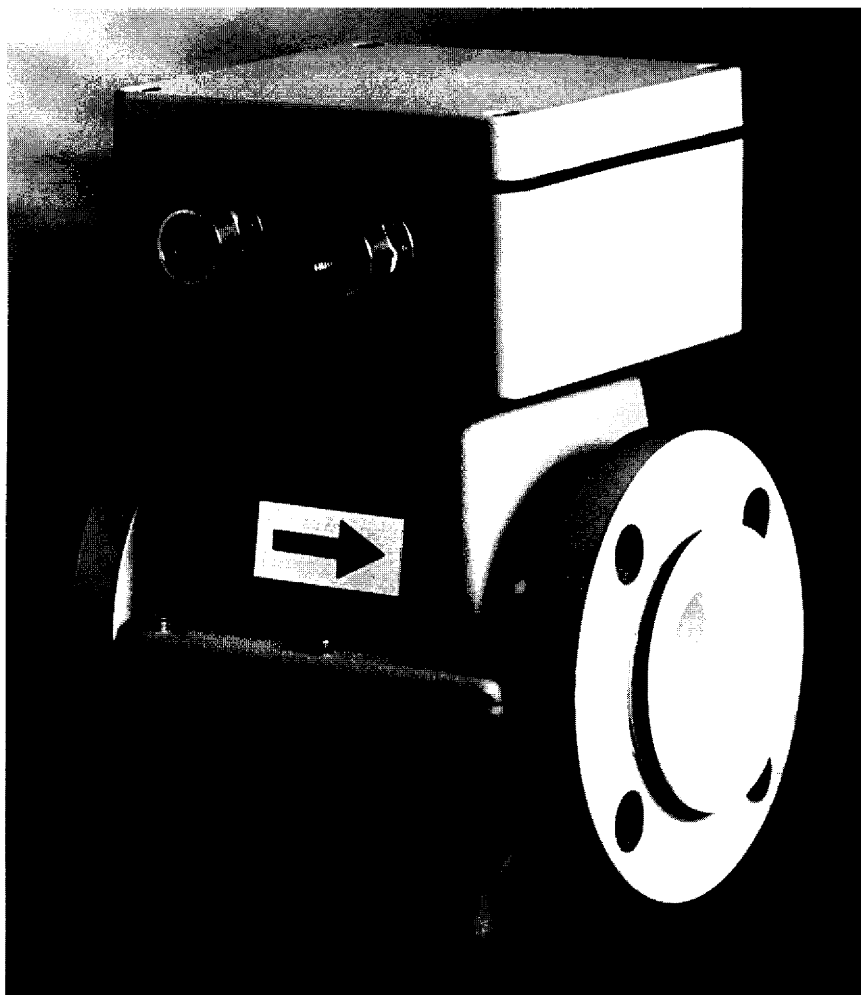


Figure 6.28 B.E.P. (Balanced Electrode Plane) electromagnetic flowmeter. (*Courtesy Hersey Measurement Company.*)

matter moving with the flow. The difference between reflected frequency and fixed transmitted frequency implies the flow rate.

There is a wide variety of time-of-flight ultrasonic flowmeters. The notable differences are usually in the number of beam paths across the pipe. A single beam averages profile along the beam and not across the pipe area. This makes the single-path measurement dependent on velocity profile. Multipath meters average along several paths, reducing profile dependency. Both single-path and multipath ultrasonic flowmeters are sensitive to swirl.

Time-of-flight flowmeters are generally used in clean liquid applications, where the ultrasonic beam is not attenuated or continuously interrupted by fluid particles. Some manufacturers claim success with rather dirty fluids, but then data interro-

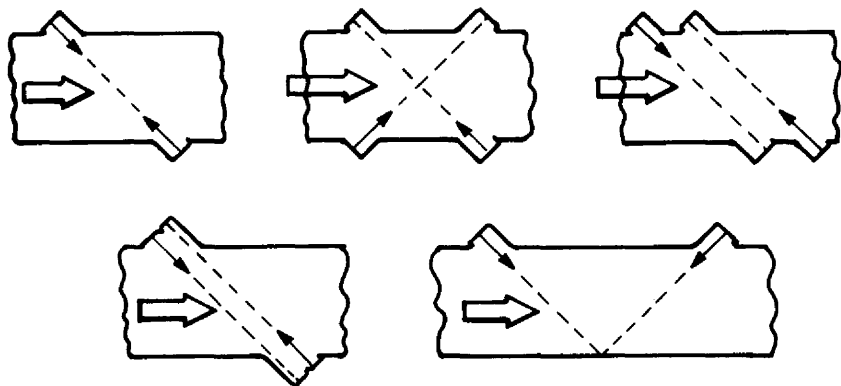


Figure 6.29 Ultrasonic flowmeter paths.

gation and data rejection, which reduce response time, are often necessary. Claimed accuracies range from ± 1 to ± 4 percent, depending on design. Specific, detailed laboratory flow-calibration data, either from manufacturers or independent laboratories, has not been widely published.

The Doppler-type flowmeter relies on small particles or impurities in the flow but has also been used successfully on many almost-clean as well as very dirty streams. Because of the velocity profile, accuracy depends on particle concentration and distribution. Accuracy is also influenced by the relative velocity between particles and fluid.

Clamp-on ultrasonic flowmeters are used in power plant water balances (Lynnworth and Adsmond, 1984) with an estimated accuracy of ± 5 percent of the upper-range flow rate. Field experience with the various types of meters is mixed. Doppler meters have had some repeatability problems (DeVries, 1986) because of the minimum required particulate concentration, or varying depth of beam penetration. Some users (Robinson, 1986) report poor results with all types, but others (O'Herron, 1985) report ease of installation and expected performance, following good transducer coupling procedures, in difficult installations. Nolan et al. (1986) have shown good results when metering natural gas with a four-path meter. ANSI standard ANSI/ASME MFC-5M (1985) covers transit time ultrasonic flowmeters.

Ultrasonic flowmeters that measure gas flow (Fig. 6.30) are available; similar meter designs are also widely used on flare gas mass flow applications. These may be multipath or of the reflective type. There is no overall pressure loss (obstructionless, fast response times, and wide operating ranges are claimed features). The transit time natural gas meter shown in Fig. 6.31b has sufficient response times to meter pulsating flows over a 50:1 turndown in line sizes 6 to 48 in (150 to 1200 mm). The flow computer computes the properties of natural gas either by the AGA-8 or NX-19 equations. In addition the average molecular weight of the flowing gas is obtainable.

Positive-Displacement Meters

Positive-displacement (PD) meters segregate the flow into discrete volumes and then sum total volume by counting *unit* volumes passing through the meter. Their major use is for metering household water, low-pressure natural gas, and gasoline. Mil-

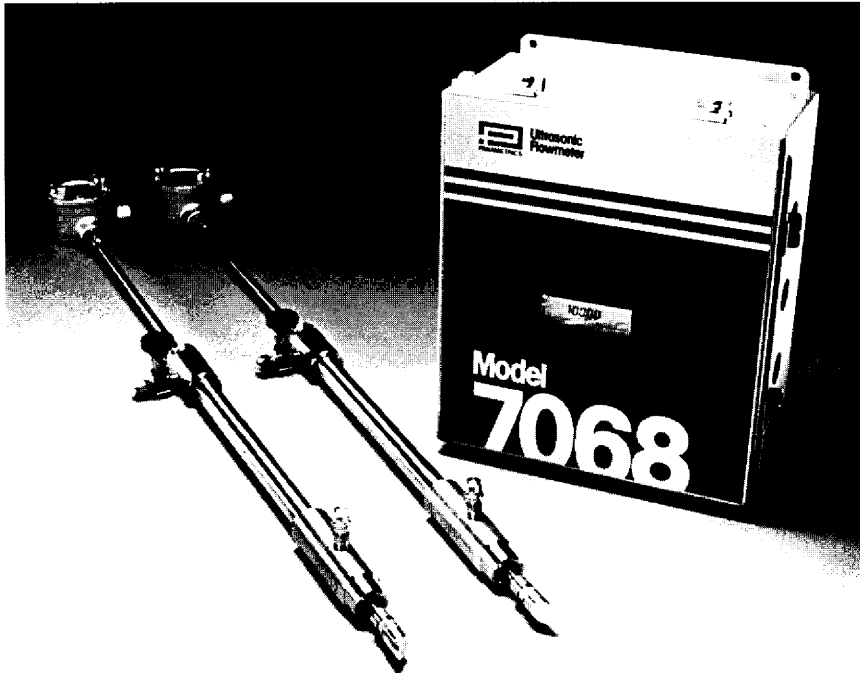


Figure 6.30 Gas ultrasonic flowmeter. (Courtesy Panametrics, Inc.)

lions of PD meters are in daily use, in greater quantities than all other flow measurement devices. In recent years, PD meters have been used increasingly in blending and loading applications where accuracy is required. Since PD meters have no time base, they are seldom used as rate flowmeters. Gas and liquid PD meters measure volume at line pressure and temperature; compensation to base volume or to total mass flow is accomplished by calculation or by mechanical ratioing.

Illustrated in Fig. 6.32 are several positive-displacement devices. As fluid enters a chamber, an impeller, a piston, a diaphragm, or a disk rotates or moves to accommodate the entering fluid, and a known volume is discharged. In the bellows type, four measuring compartments operate simultaneously, some filling while others are emptying. As each is filled and discharged, rotation is transmitted through suitable gearing to a counter that reads total volume. Seals were required to separate the volumes, and the pressure loss across the meter provides the energy to drive the moving parts. Because of the close tolerances required, the fluid temperature and viscosity affect the range as well as the accuracy. Manufacturers should be consulted on temperature, pressure, and viscosity limitations.

Numerous PD-meter designs are available for measuring both liquids and gases. They are ideal for viscous liquids and for batching and blending applications where wide range accuracy is required. Filters are normally installed upstream to prevent dirt from entering the meter, and periodic calibration is usually used to monitor mechanical wear.

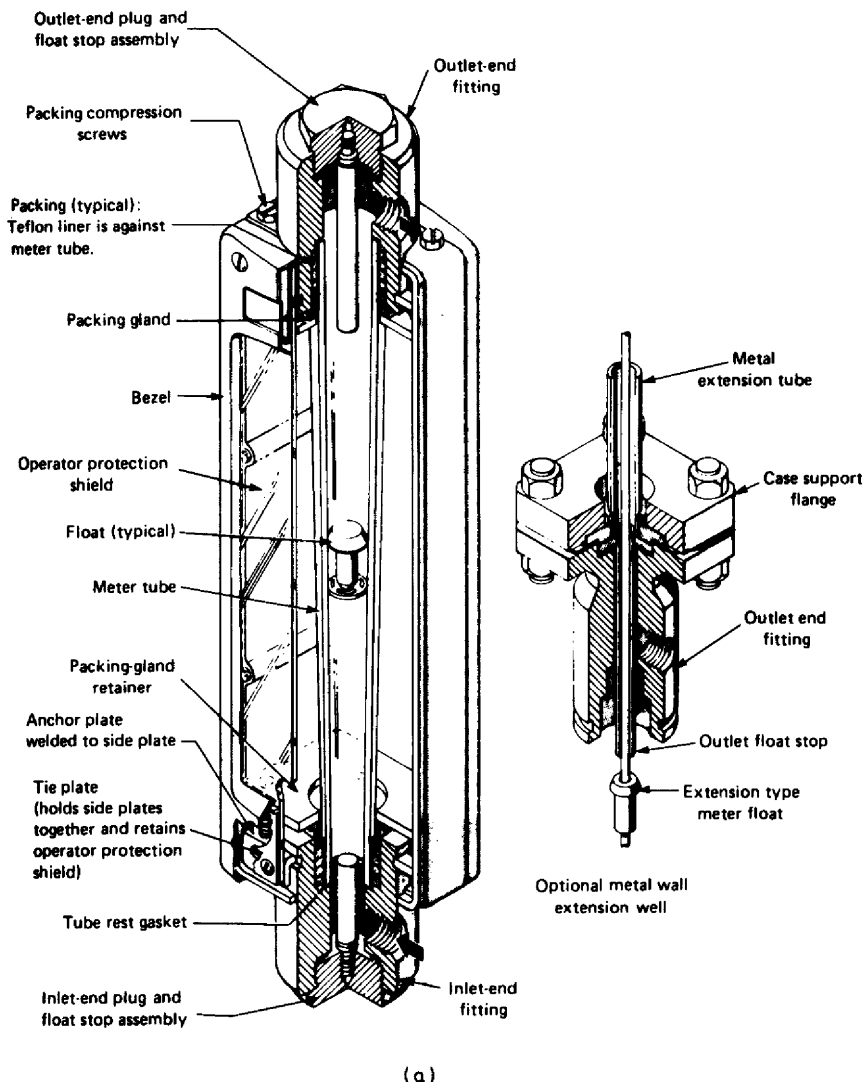


Figure 6.31 Variable-area meters. (Courtesy Fischer & Porter.) (a) Glass (internal). (b) Glass (exterior). (c) Armored throughflow (internal). (d) Armored throughflow (exterior).

Designs are available to handle pressures up to 1500 psig (10,300 kPa) and temperatures to 600°F (320°C) for liquids and 250°F (120°C) for gases. Flow-rate ranges are from 0.1 to 9000 gal/min (0.4 to 34,000 L/min) for liquids and up to 100,000 standard ft³/h (2831 standard m³/h) for gases. Measurement accuracy is 0.5 to 1 percent of the upper range value over typically 10:1 flow-rate ranges.

For gas flows the diaphragm meter is by far the most widely used. As capacity increases, these meters increase in size to the point where work crews are required to set them in place. Although maintenance is minimal, reported shift in accuracy over a 5-year period may be reading low by 1 percent (Loga, 1990). The rotary positive-displacement meters are smaller in size and are gaining increasing support from users in the gas distribution and transmission markets. In these industries the *permanent* accuracy feature is claimed as a distinct advantage. OIML R31 (1994) is an internal legal metrology standard covering diaphragm meters.

Variable-Area Meters (Rotameters)

Variable-area flowmeters are a special form of differential producer wherein the area of the flow restriction is varied to maintain constant differential pressure. The rotameter (Fig. 6.31) consists of a vertical tapered tube through which the fluid moves in an upward direction. A float, either spherical or cone-shaped, with a density higher than that of the fluid, creates an annular passage between its maximum circumference and the wall of the tapered tube. As the flow varies, the float rises or falls to vary the area so that the differential pressure across the float just balances the gravitational force on the float. The differential pressure is then maintained constant, and the float position is a measure of the rate of flow.

(b)

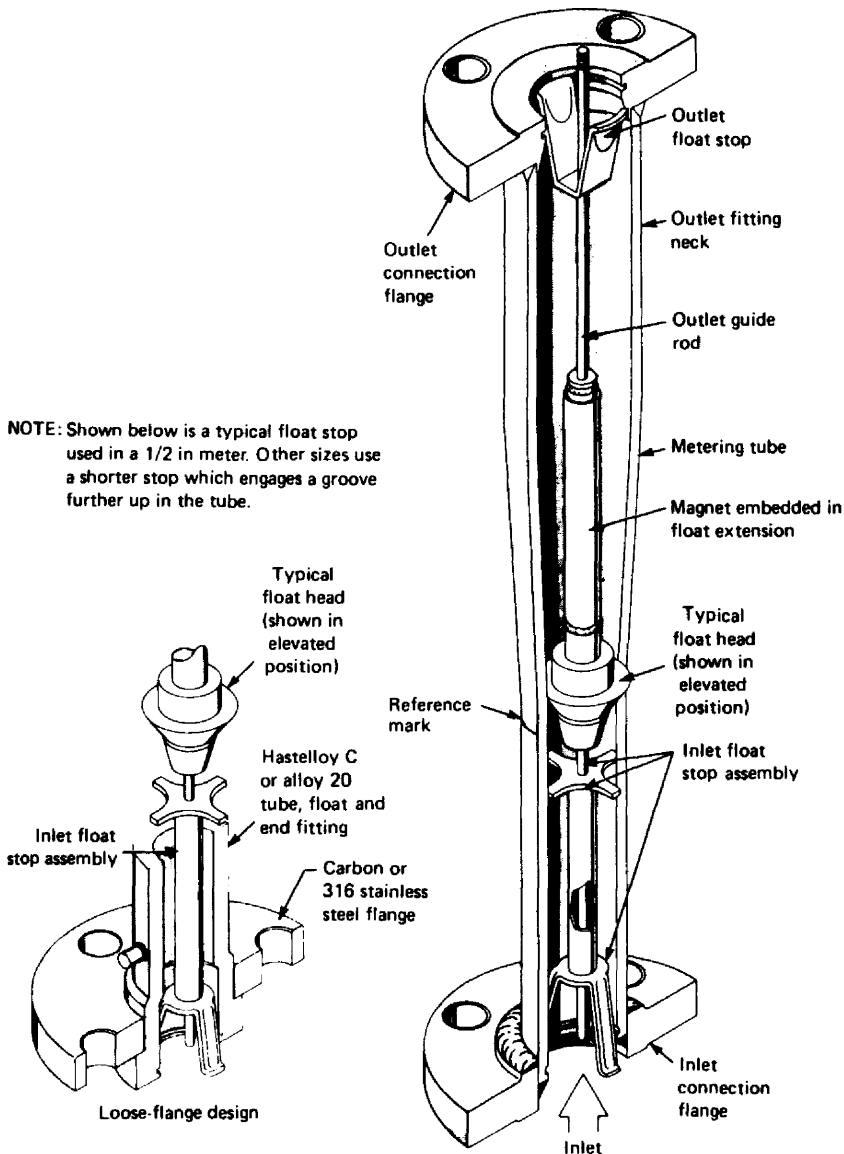
Figure 6.31 (Continued)

A float in a transparent tapered tube makes a very simple flowmeter. The proper taper can be selected to provide a linear flow scale. In applications where the float cannot be seen, as when the flow of an opaque liquid is being measured or when a metal tube must be used because of large flow volume or elevated pressure, the float position can be detected electrically or pneumatically for indication and/or control purposes.

A second type of variable-area meter consists of a mechanically variable restriction and a means for direct differential-pressure measurement across it. The area of the restriction is controlled either directly or through a servomechanism actuated by the differential pressure, so as to hold the differential pressure constant. The flow rate is then proportional to the effective area of the restriction. The output can be in the form of a motion that is derived from the motion which varies the restriction, or it may be an electrical or pneumatic signal proportional to the effective area.

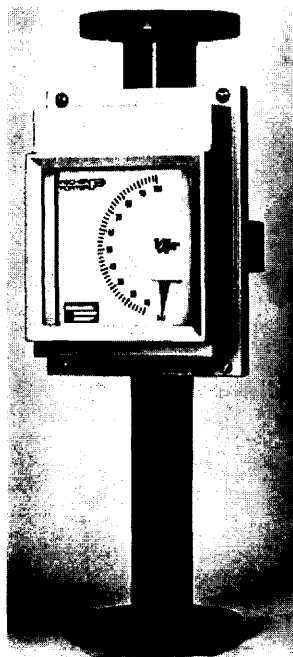
Variable-area meters are used for liquids, gases, and vapors (steam) with pressures up to 350 psig (2400 kPa) for glass tubes and up to 720 psig (5000 kPa) for metal tubes. Temperature limits range up to 400°F (205°C) for glass tubes and 1000°F (540°C) for metal tubes. Flow rates from 0.01 cm³/min to 4000 gal/min (15,000 L/min) can be measured over a 5:1 or 10:1 flow-rate range, with an accuracy of ± 0.5 percent of flow rate to ± 1.0 percent of the upper-range flow rate, depending on type, size, and calibration.

NOTE: Shown below is a typical float stop used in a 1/2 in meter. Other sizes use a shorter stop which engages a groove further up in the tube.



(c)

Figure 6.31 (Continued)



(d)

Figure 6.31 (Continued)

Mass Flowmeters

There are many reasons to measure mass. Chemical reactions are based on mass balance equations, combustion is based on the mass flow of the oxidant, accurate blending is a mass balance, and most products are sold by weight (mass). The metering of fluids by mass rather than volumetric is therefore becoming increasingly popular (Fusaro, 1993). Mass metering using Coriolis or thermal mass flowmeters now account for approximately 9 percent of the flowmeter market, with the projected use of these meters estimated to exceed magnetic and positive displacement by the year 2000.

There are three ways in which mass flow may be determined. The first is by calculating the mass flow *inferentially* by multiplying the flowing volumetric flow rate by density; the second is by using a mass flowmeter whose principle of operation is based on mass flow; and the third is by dividing the differential produced from a differential producer by the output of linear meter. The ratio is

$$q_M = \frac{k_1 q_v \rho_f}{k_2 q_v} = k_3 q_v \rho_f = k_4 \frac{\Delta p}{f_{Hz}} \quad (6.3)$$

where the numerator is the produced differential Δp and the denominator F_{Hz} is the output frequency from a linear meter. k_1 , k_2 , k_3 , and k_4 are the meter constants.

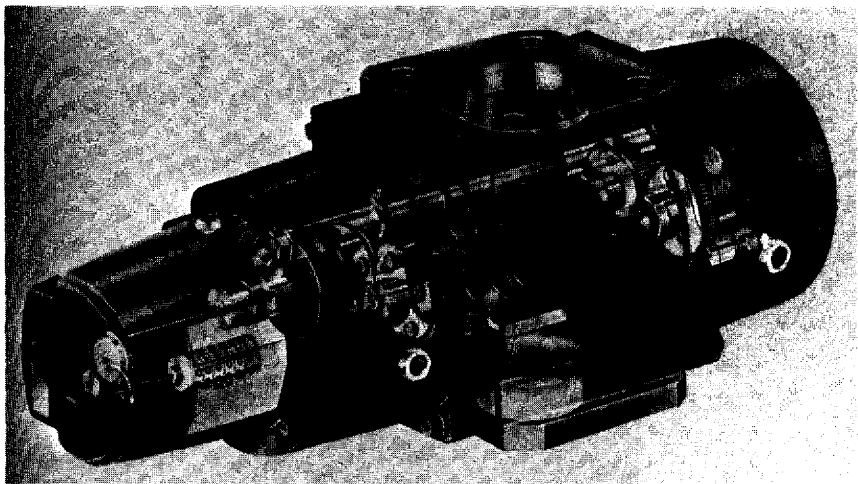
The inferential method is most commonly used, but for some applications the recently introduced Coriolis direct mass flowmeters are becoming popular. The ratio method has potential as a lower-cost, but not as accurate, solution.

In a Coriolis meter the fluid is caused to translate, move in a straight line, and rotate about a pivot point at the same time. This results in a Coriolis acceleration component that is mutually perpendicular to the rotational and translation direction vectors (Fig. 6.33a). The acceleration produces a force on the containment pipe (or tube) proportional to the mass flow rate. In the piping circuit shown (Fig. 6.33a), the flow is turned back on itself in the U-tube arrangement and creates a twisting couple on the structure. The angle of twist produced by this couple is a measure of the mass flow rate.

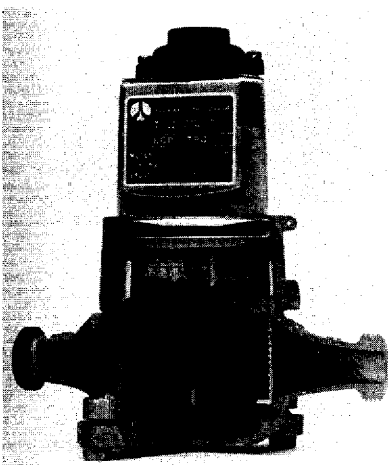
Several Coriolis mass flowmeters are commercially available for liquid flows and for high-pressure gas flows. Figure 6.33b shows the external construction of U-tube mass flowmeter.

Some meters have reported ± 2 percent errors for small void fractions of gas (1.5 percent) (Grumski and Bajura, 1984). Compatibility with process fluids (particularly those with free chloride), high overall pressure loss, potential leakage due to metal weld fatigue, and problems with two-component flows (liquid/gas) are reported for some meters (Gast and Furness, 1986).

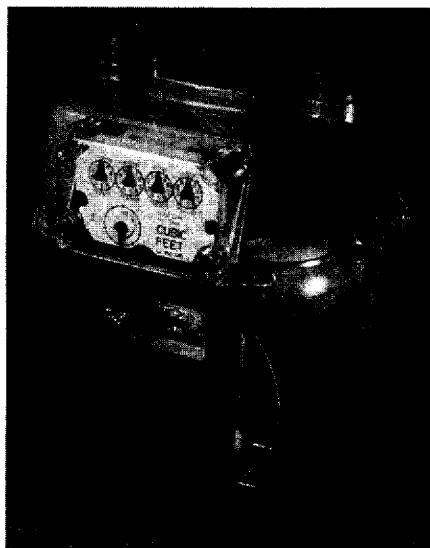
Although specifications vary, these meters have a mass-flow-rate accuracy of ± 0.15 to ± 0.4 percent. Reported results have been favorable for the intended applications, and OIML, ASME, and ISO are considering preparing a standard for their use.



(a)

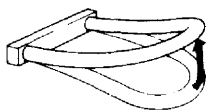


(b)

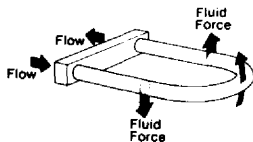


(c)

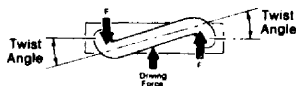
Figure 6.32 Positive-displacement meters. (a) ROOTS rotary gas meter. (Courtesy Roots Dresser.) (b) Oscillating-piston and piston-roller water meter. (Courtesy Equimeter, Inc.) (c) Domestic gas meter. (Courtesy Equimeter, Inc.)



1. Vibrating flow tube.



2. Fluid forces reacting to vibration of flow tube.



3. End view of flow tube showing twist.

(a)

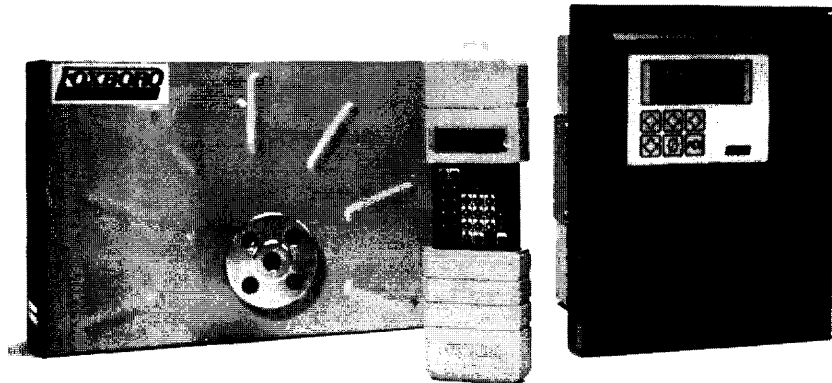


(b)

Figure 6.33 Coriolis mass flowmeter. (a) Forces. (b) Exterior. (Courtesy MicroMotions.) (c) Foxboro I/A meter. (Courtesy The Foxboro Co.)

Coriolis mass flowmeters are normally used to measure the mass flow of liquids but have been used for metering high-density gases. Thermal mass flowmeters are widely used to meter air or any single component gas (Fig. 6.34).

There are two basic types of thermal mass flowmeters. The first type measures the heat-loss rate that occurs when a liquid or gas flows over a heated element. The heated element may be a thermistor, thin film, or thermocouple. In the second type



(c)

Figure 6.33 (Continued)

the rise in the temperature of the fluid when it is heated by a coil or grid is a measure of the mass flow rate. In both types the mass flow rate may be computed from known properties of the fluid.

In the hot-wire type the wire is electrically heated and the temperature of the wire is determined from its resistance. The temperature of the wire may be kept constant by regulating the power. The mass flow rate is then a function of power. With this method the response is faster than with the alternate method of maintaining a constant current and measuring the resistance to obtain the mass flow-rate function.

If the flow rate (velocity) goes to zero, the current type often burns out the wire; in the power type this problem is not present. The hot-wire type is widely used in laboratories and is becoming increasingly popular for an array-type measurement across ducts. These effectively measure the average mass flow rate.

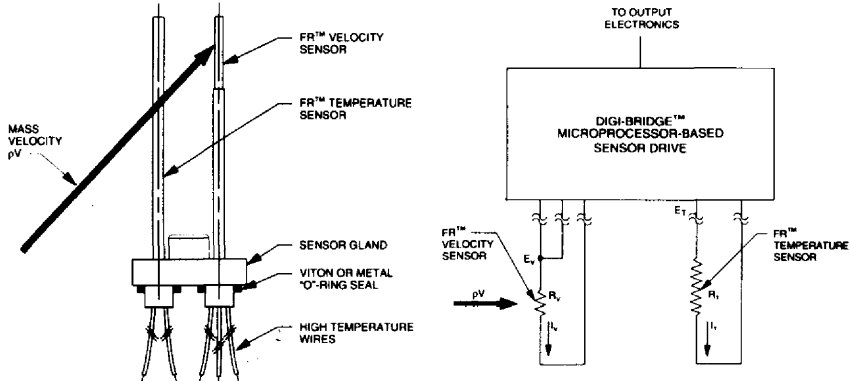
An immersible-type thermal mass flowmeter consisting of two sensors is shown in Fig. 6.35. The first sensor is the velocity sensor, and the second measures the stream temperature and automatically corrects for temperature changes. Each sensor is a reference-grade platinum resistance RTD wound on a ceramic mandrel. The computation for the unit shown is for a digital rather than an analog bridge. The mass flow rate at the measuring point is computed by

$$q_m = \left[\frac{1}{k_1} \left(\frac{E_v^2/R_v}{T_v - T} \right) - \frac{k_2}{k_1} \right]^{1/m} \quad (6.4)$$

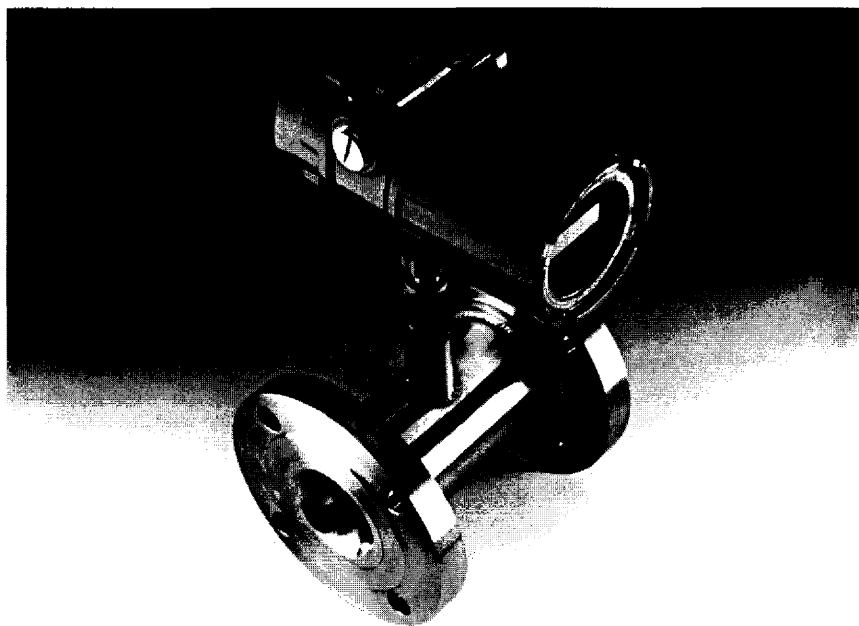
where k_1 , k_2 , and m are empirically constants. The temperature difference ($T_v - T$) is maintained constant by changing the electrical power (E_v^2/R_v).

Thermal mass flowmeters may employ a bypass from the main flow to infer the total mass flowrate (Fig. 6.35a, b). The main flow is split into two streams, with the small fraction stream flowing through the metering section. A laminar flow element provides the linear pressure drop that effectively ensures a proportional flow relationship between the two fluid paths. The mass flowrate is computed by

$$q_m = \left(1 + \frac{q_{m2}}{q_{m1}} \right) \frac{(Q_{\text{heat}} - Q_{\text{heat},0})}{C_p \Delta T} \quad (6.5)$$



(a)



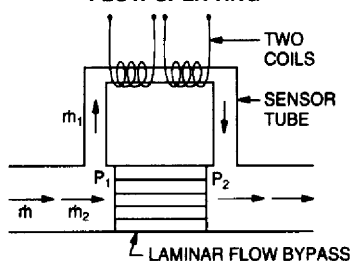
(b)

Figure 6.34 Immersible thermal mass flowmeter. (Courtesy Sierra Instruments, Inc.) (a) Operating principle. (b) Flowmeter.

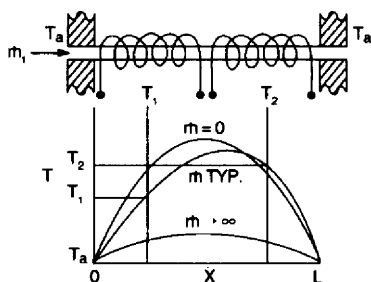
where q_{m1} is the mass flow rate through the bypass, q_{m2} is the mass flow rate through the body of the meter, the constant amount of heat is Q_{heat} , and $Q_{\text{heat},0}$ is the conducted heat transfer through the mounting block. C_p is the constant specific heat of the fluid.

Thermal mass flowmeters have been designed for liquids, slurries, powered solids, and gases. The insertion type has very low overall pressure loss and the bypass type has only 5 to 10 in (5 to 25 kPa) of water loss. They are widely used in the

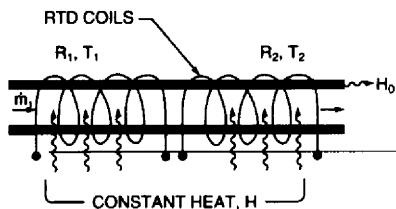
FLOW SPLITTING



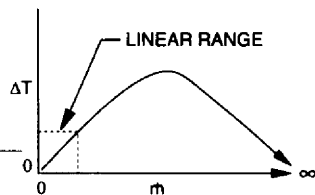
TEMPERATURE DISTRIBUTION



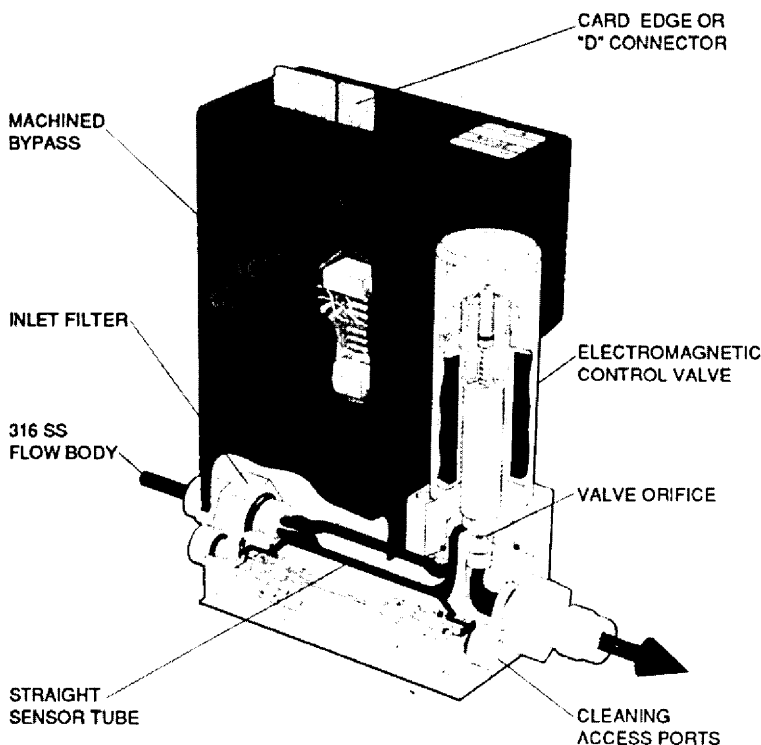
CAPILLARY-TUBE SENSOR



RAW OUTPUT



(a)



(b)

Figure 6.35 Capillary by-pass thermal mass flowmeter. (Courtesy Sierra Instruments, Inc.) (a) Operating principle. (b) Flowmeter.

aerospace industry, for duct flows, flare gas applications, and test purposes. Several standards have been written or are in the preparation stage; these are OIML R 105 (1993), OIML PS5D/RS10 (1993), ASME/ANSI MFC-11M (1994), and ISO TC30 SC12/WG5 (1994).

Insertion Meters

Insertion-type meters are an economical solution for many flow measurement applications. An insertion meter infers the overall flow by a velocity measurement located at a selected point within the pipe. The insertion meter may be a magnetic flowmeter, a pitot tube, a vortex meter, a hot film, or a turbine or be based on any available metering technology.

An insertion-type meter consists of the sensor, a support structure, suitable fittings, and pressure seals. In general, the meter may be hot-tapped and is usually less expensive to install than other types of meters. Since insertion-type meters are small, compared to the overall pipe area, their overall pressure losses are quite low.

Overall accuracy is a combination of meter accuracy, pipe diameter uncertainty, profile distortion error, position error, and blockage error. Ginesi (1987) estimates a ± 2 to 5 percent accuracy range for typical meters, and Scott and Davies (1983) indicate that ± 0.1 percent repeatability may be possible. They estimate an overall accuracy of ± 5 percent for fully developed pipe flow and for detailed traverses, ± 3 percent. This, however, requires a mathematical complex (spline routine) formulation to define the profile.

METER-SELECTION CONSIDERATIONS

General Guidelines

The choice of flowmeter for a given application depends upon the importance attached to various phases of the measurement problem. Hence, it must remain a matter of individual judgment based on engineering knowledge. The predominance of one class of flowmeter in a particular field with similar operating conditions is usually a good first guide.

It is obvious that an attempt to weigh and balance all qualifications without detailed knowledge of the specific application would be presumptuous. There are, however, five broad questions that are helpful in arriving at a flowmeter decision. There are limited tradeoffs in the first three, since they determine whether or not a particular meter is suitable. The last two are the most difficult because they involve the cost-versus-performance decision. The questions are as follows:

1. What type of fluid is to be handled?
 - a. Is the fluid a liquid, gas, or vapor?
 - b. Is the fluid clean, dirty, or a slurry?
 - c. Is the fluid corrosive?
2. What are the process conditions? The temperature and pressure limits?
3. What are the installation conditions?
 - a. Is an open-channel or closed-conduit measurement planned?
 - b. What is the line size?
 - c. What is the operating pipe Reynolds number?
 - d. Is adequate upstream length available?

- e. Can flow conditioners be used?
- f. Is there excessive pipe vibration?
- g. Will the flow be steady or pulsating?
- h. What are the ambient or room conditions of temperature and humidity?
- 4. What are the performance and general flow measurement requirements?
 - a. What overall accuracy is required, and over what range?
 - b. Is the flowmeter normally used at a specific flow rate or over a range of flows?
 - c. Is the flowmeter to be used for control only, and what frequency of response is necessary (0.1 s is usually required for small-line-size control)?
 - d. What is the range of flow rates to be measured, and what rates will occasionally be experienced?
- 5. What are the economics of installation and operation? Economic considerations include:
 - a. Initial cost of the primary and secondary devices and auxiliary equipment
 - b. Installation cost, including labor and piping
 - c. Energy cost to operate the flowmeter and pumping cost to compensate for the overall pressure loss
 - d. Reliability versus maintenance cost
 - e. Availability of parts and service facilities
 - f. Possible uses in future applications
 - g. The risks in trying a new flowmeter type

Table 6.1 lists information relative to these decision factors for the flowmeters covered in this handbook. In comparing the costs of flowmeters, several factors must be considered other than the actual purchase price. The effects of improved meter accuracy and range on plant efficiency and the quality of the product are important in any decision. Additionally, the costs of installation, long-term maintenance, and operating energy need to be assessed. It is difficult to rank initial purchase price, because material requirements and the need for additional secondary elements vary by meter type. However, as a guide, three relative purchase-price groupings are given in Table 6.2 for the meters listed in Table 6.1.

Overall Pressure Loss

Except for obstructionless meters (magnetic and ultrasonic), every meter has an overall permanent pressure loss greater than an equivalent straight length of pipe. The overall permanent pressure loss is calculated using the pressure loss coefficient, for U.S. units, by

$$\Delta P = \frac{K \rho_f \bar{V}_f^2}{2g_c} \quad (6.6)$$

where ΔP is in lb_f/ft^2 , ρ_f is the flowing density, in lb_m/ft^3 , and V_f is the average pipeline velocity, in ft/s .

For SI units the equation is

$$\Delta P^* = \frac{K \rho_f^* \bar{V}_f^{*2}}{2} \quad (6.7)$$

where ΔP^* is in pascals (N/m^2), ρ_f^* is the flowing density, in kg/m^3 , and V_f^* is the average pipeline velocity, in m/s^2 .

TABLE 6.2 Relative Purchase Price by Group†

Group 1 (low)	Group 2 (medium)	Group 3 (high)
Elbow	Vortex	Venturi
Pitot	Turbine [$D < 6$ in (300 mm)]	Magnetic
Multiport averaging	Variable-area (metal)	Ultrasonic (time of flight)
Variable-area (glass)	Lo-Loss	Positive-displacement ($D > 4$ in (100 mm))
Variable-area (metal) [$D < 2$ in (50 mm)]	Universal Venturi Tube	Mass flowmeter (Coriolis)
Orifice	Flow nozzle	Laminar flowmeter "V" cone
Target	Ultrasonic (Doppler)	
Gillflo thermal mass wedge "V" cone		
Positive- displacement [$D < 2$ in (50 mm)]		

†To be used as a guide only. Ranking may be the same within groups, or flowmeters may change groups because of line size, material of construction, auxiliary equipment, etc.

Figure 6.36 shows the loss coefficients for a square-edged orifice, the ISO flow nozzle, and the quadrant-edged orifice for low Reynolds-number flows (Alvi et al., 1978). Figure 6.37 shows the permanent pressure loss in percent of differential pressure for the differential producers when the Reynolds number is greater than 6000. Equations for calculating permanent pressure loss are given in Table 6.3 for U.S. units and in Table 6.4 for SI units. In Table 6.5 are the power and energy-cost equations for both U.S. and SI units.

The equations presented in Table 6.3 are expressions fitted to the ASME fluid meters (1971) curves (Fig. 6.37). For pipe Reynolds numbers R_D greater than 6000, the following equation (Alvi et al., 1978) may be used to calculate the overall pressure loss for quadrant- and square-edged orifices, and for nozzles in U.S. units:

$$h_l = \left[1 - \frac{2\beta^2 C^2}{1 - \beta^4} \left(\frac{1}{C_c} - \beta^2 \right) \right] h_w \quad (6.8)$$

For SI units, it is

$$\Delta p_l^* = \left[1 - \frac{2\beta^2 C^2}{1 - \beta^4} \left(\frac{1}{C_c} - \beta^2 \right) \right] \Delta p^* \quad (6.9)$$

where C is the discharge coefficient and C_c is the coefficient of contraction calculated, for square- and quadrant-edged orifices, by

$$C_c = \frac{C}{\sqrt{1 - \beta^4 + C^2 \beta^4}} \quad (6.10)$$

For nozzles, $C_c = 1.0$

The permanent pressure loss for Coriolis mass flowmeters depends upon tube geometry and tube size. Cascetta et al. (1992) presents water calibration data for

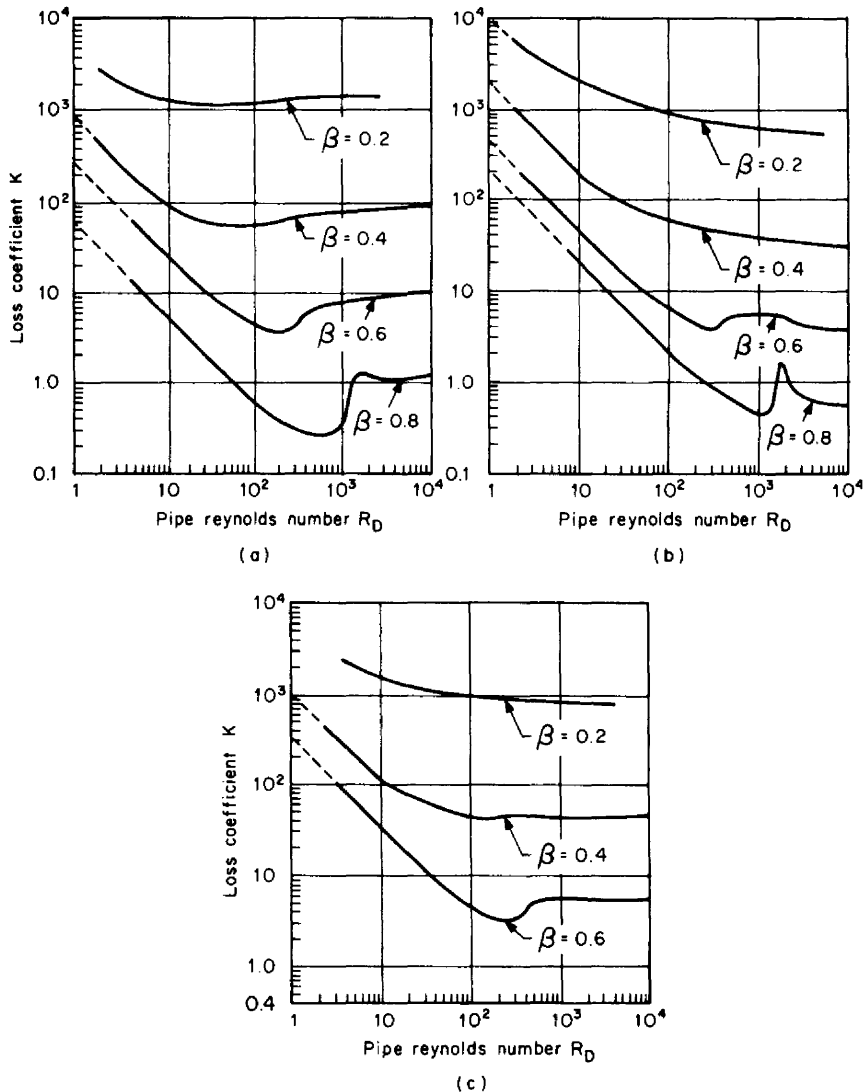


Figure 6.36 Pressure-loss coefficients. (a) Square-edged orifices. (b) Contoured inlet (nozzle, venturi, etc.). (c) Quadrant-edged orifice.

comparative purposes on several 1-in meters. These loss coefficients are presented in Table 6.6 and the pressure loss versus the mass flow rate are illustrated in Figs. 6.38 and 6.39. The effect of viscosity on the permanent pressure loss should be checked since increased viscosity will increase the pressure loss. The manufacturer should be consulted for the latest information.

Example 6.1. Calculate the overall pressure loss for a corner tap orifice flowing 40 base gallons per minute (q_{GPM}) of crude oil at 85°F (29.4°C) in a 2-in (50-mm) schedule 80 pipe. The beta ratio β is 0.5; the measured differential pressure is 100 in H_2O (25 kPa); and the crude oil base specific gravity G_b is 0.85.

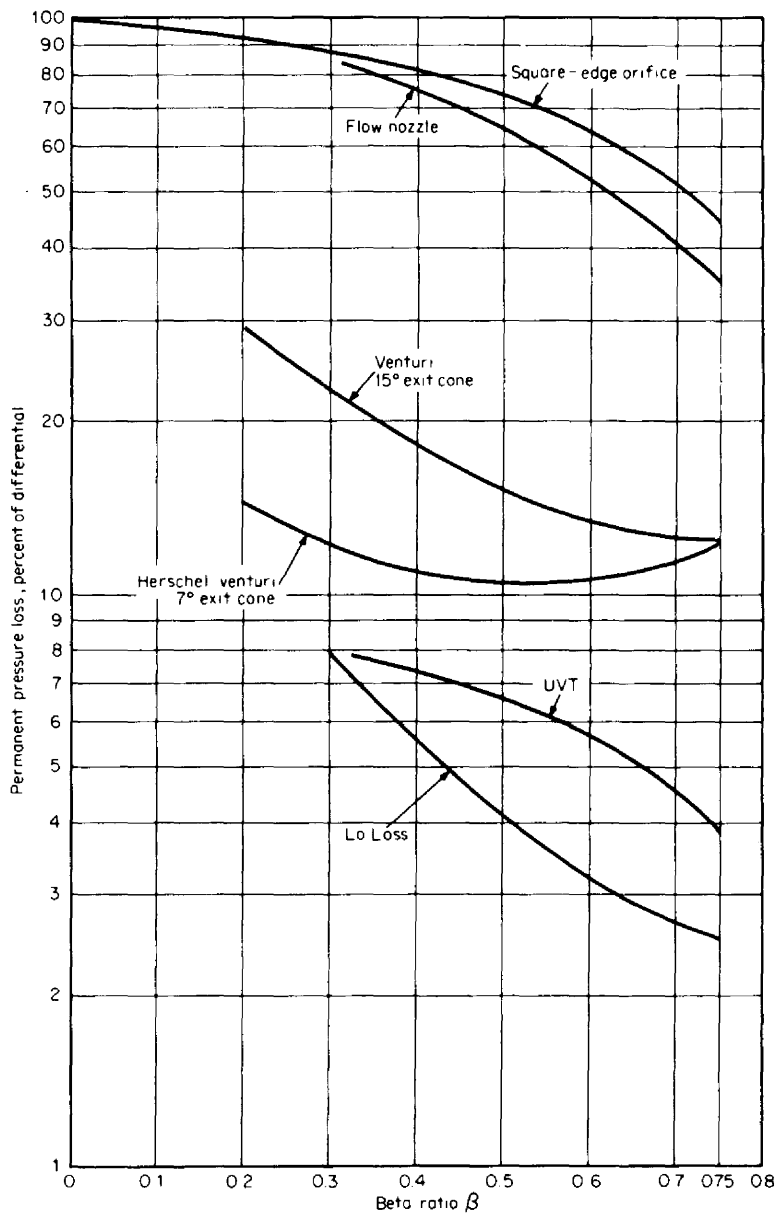


Figure 6.37 Permanent-pressure-loss curves for differential producers.

TABLE 6.3 Permanent Pressure-Loss Equations (U.S. Units)

Flowmeter		Liquid		Gas (vapor)		Liquid/gas (vapor); mass flow
Venturi:						
15° exit cone	————→			$h_l = (0.436 - 0.86\beta + 0.59\beta^2)h_w$	(a)	←————
7° exit cone	————→			$h_l = (0.218 - 0.42\beta + 0.38\beta^2)h_w$	(b)	←————
Universal Venturi Tube†	————→			$h_l = (0.065 + 0.092\beta - 0.167\beta^2)h_w$	(c)	←————
Lo-Loss tube‡	————→			$h_l = (0.151 - 0.304\beta + 0.182\beta^2)h_w$	(d)	←————
Nozzle	————→			$h_l = (1 + 0.014\beta - 2.06\beta^2 + 1.18\beta^3)h_w$	(e)	←————
Orifice	————→			$h_l = (1 - 0.24\beta - 0.52\beta^2 - 0.16\beta^3)h_w$	(f)	←————
Annubar:§				$h_l = \frac{k}{D} h_w$	(g)	
				Type 15/16 $k = 0.478$; 35/36 $k = 1.59$		
				25/26 $k = 1.11$; 45/46 $k = 2.55$		
Pitot	————→			$h_l = \frac{0.6}{D} h_w$	(h)	←————
Target¶	————→			$h_l = 0.000467 \frac{\rho_f \bar{V}_f^2}{(1 - \beta_f)^{2.75}}$	(i)	←————

TABLE 6.3 Permanent Pressure-Loss Equations (U.S. Units) (*Continued*)

Flowmeter	Liquid	Gas (vapor)	Liquid/gas (vapor); mass flow
	$h_l = \frac{F_p G_F}{(1 - \beta_T)^{2.75}} \left(\frac{q_{\text{gpm}}}{14.3D^2} \right)^2$	$h_l = \frac{Z_{f1} G_{Tf1}}{p_{f1}(1 - \beta_T)^{2.75}} \left(\frac{q_{\text{SCFH}}}{19,520D^2} \right)^2$	$h_l = \frac{1}{\rho_{f1}(1 - \beta_T)^{2.75}} \left(\frac{q_{\text{PPH}}}{909D^2} \right)^2$
	(j)	(q)	(v)
	$h_l = \frac{G_b^2}{F_p G_F (1 - \beta_T)^{2.75}} \left(\frac{q_{\text{GPM}}}{14.3D^2} \right)^2$		
	(k)		
Turbine [†]	$h_l = 0.00577 \rho_f \bar{V}_f^2$	$h_l = 0.0129 \rho_{f1} \bar{V}_f^2$	Liquid: $h_l = \frac{1}{\rho_{f1}} \left(\frac{q_{\text{PPH}}}{259D^2} \right)^2$
	(l)	(r)	(w)
	$h_l = F_p G_F \left(\frac{q_{\text{gpm}}}{4.08D^2} \right)^2$	$h_l = \frac{Z_{f1} G_{Tf1}}{p_{f1}} \left(\frac{q_{\text{SCFH}}}{3714D^2} \right)^2$	Gas (vapor): $h_l = \frac{1}{\rho_{f1}} \left(\frac{q_{\text{PPH}}}{173D^2} \right)^2$
	(m)	(s)	(x)
	$h_l = \frac{G_b^2}{F_p G_F} \left(\frac{q_{\text{GPM}}}{4.08D^2} \right)^2$		
	(n)		
Vortex [‡]	\longrightarrow	$h_l = 0.00554 \rho_{f1} \bar{V}_f^2$	\longleftarrow
	$h_l = F_p G_F \left(\frac{q_{\text{gpm}}}{4.17D^2} \right)^2$	$h_l = \frac{Z_{f1} G_{Tf1}}{p_{f1}} \left(\frac{q_{\text{SCFH}}}{5669D^2} \right)^2$	$h_l = \frac{1}{\rho_{f1}} \left(\frac{q_{\text{PPH}}}{264D^2} \right)^2$
	(o)	(u)	(y)
	$h_l = \frac{G_b^2}{F_p G_F} \left(\frac{q_{\text{GPM}}}{4.17D^2} \right)^2$		
	(p)		

[†]The manufacturer (BIF) should be consulted for exact information.

[‡]The manufacturer (Badger Meter Inc.) should be consulted for exact information.

[§]The manufacturer (Dieterich Standard Corp.) should be consulted for exact information.

[¶]Foxboro flowmeter gas-turbine flowmeter equation based on Rockwell literature; the manufacturer should be consulted for exact information.

TABLE 6.4 Permanent Pressure-Loss Equations (SI Units)

Flowmeter		Liquid	Gas (vapor)		Liquid/gas (vapor); mass flow
Venturi:					
15° exit cone	----->		$\Delta p_l^* = (0.436 - 0.86\beta + 0.59\beta^2)\Delta p^*$	(a)	←-----
7° exit cone	----->		$\Delta p_l^* = (0.218 - 0.42\beta + 0.38\beta^2)\Delta p^*$	(b)	←-----
Universal Venturi Tube†	----->		$\Delta p_l^* = (0.065 + 0.092\beta - 0.167\beta^2)\Delta p^*$	(c)	←-----
Lo-Loss tube‡	----->		$\Delta p_l^* = (0.151 - 0.304\beta + 0.182\beta^2)\Delta p^*$	(d)	←-----
Nozzle	----->		$\Delta p_l^* = (1 + 0.014\beta - 2.06\beta^2 + 1.18\beta^3)\Delta p^*$	(e)	←-----
Orifice	----->		$\Delta p_l^* = (1 - 0.24\beta - 0.52\beta^2 - 0.16\beta^3)\Delta p^*$	(f)	
Annubar:§			$\Delta p_l^* = \frac{k}{D^*} \Delta p^*$	(g)	
			Type 15/16 $k = 12.1$; 35/36 $k = 28.2$		
			25/26 $k = 40.4$; 45/46 $k = 64.8$		
Pitot	----->		$\Delta p_l^* = \frac{15.2}{D^*} \Delta p^*$	(h)	
Target¶	----->		$\Delta p_l^* = 0.0000779 \frac{\rho_f^* \bar{V}_f^{*2}}{(1 - \beta_r)^{2.75}}$	(i)	←-----

TABLE 6.4 Permanent Pressure-Loss Equations (SI Units) (*Continued*)

Flowmeter	Liquid	Gas (vapor)	Liquid/gas (vapor); mass flow
	$\Delta p_i^* = \frac{F_p G_F}{(1 - B_T)^{2.75}} \left(\frac{592 q_{\text{ipm}}^*}{D^{*2}} \right)^2$	(j) $\Delta p_i^* = \frac{Z_{f1} G T_{K1}}{p_{f1}^* (1 - \beta_T)^{2.75}} \left(\frac{2.05 q_{\text{SCMH}}^*}{D^{*2}} \right)^2$	(q) $\Delta p_i^* = \frac{1}{\rho_{f1}^* (1 - \beta_T)^{2.75}} \left(\frac{3.06 q_{\text{KPH}}^*}{D^{*2}} \right)^2$
	(k) $\Delta p_i^* = \frac{G_b^2}{F_p G_F (1 - \beta_T)^{2.75}} \left(\frac{5.92 q_{\text{LPM}}^*}{D^{*2}} \right)^2$		(v)
Turbine¶	(l) $\Delta p_i^* = 0.000964 \rho_f^* \bar{V}_f^{*2}$	(r) $\Delta p_i^* = 0.00216 \rho_{f1}^* \bar{V}_{f1}^{*2}$	(w) Liquid: $\Delta p_i^* = \frac{1}{\rho_{f1}^*} \left(\frac{11 q_{\text{KPH}}^*}{D^{*2}} \right)^2$
	(m) $\Delta p_i^* = F_p G_F \left(\frac{20.8 q_{\text{ipm}}^*}{D^{*2}} \right)^2$	(s) $\Delta p_i^* = \frac{Z_{f1} G T_{K1}}{p_{f1}^*} \left(\frac{10.8 q_{\text{SCMH}}^*}{D^{*2}} \right)^2$	(x) Gas (vapor): $\Delta p_i^* = \frac{1}{\rho_{f1}^*} \left(\frac{16.4 q_{\text{KPH}}^*}{D^{*2}} \right)^2$
	(n) $\Delta p_i^* = \frac{G_b^2}{F_p G_F} \left(\frac{20.8 q_{\text{LPM}}^*}{D^{*2}} \right)^2$		
Vortex¶	→	(t) $\Delta p_i^* = 0.000923 \rho_{f1}^* \bar{V}_{f1}^{*2}$	(u) ←
	(o) $\Delta p_i^* = F_p G_F \left(\frac{20.4 q_{\text{ipm}}^*}{D^{*2}} \right)^2$	(p) $\Delta p_i^* = \frac{Z_{f1} G T_{K1}}{p_{f1}^*} \left(\frac{7.06 q_{\text{SCMH}}^*}{D^{*2}} \right)^2$	(y) $\Delta p_i^* = \frac{1}{\rho_{f1}^*} \left(\frac{10.75 q_{\text{KPH}}^*}{D^{*2}} \right)^2$
	(p) $\Delta p_i^* = \frac{G_b^2}{F_p G_F} \left(\frac{20.4 q_{\text{LPM}}^*}{D^{*2}} \right)^2$		

†The manufacturer (BIF) should be consulted for exact information.

‡The manufacturer (Badger Meter Inc.) should be consulted for exact information.

§The manufacturer (Dieterich Standard Corp.) should be consulted for exact information.

¶Foxboro flowmeter gas-turbine flowmeter equation based on Rockwell literature; the manufacturer should be consulted for exact information.

TABLE 6.5 Power and Energy-Cost Equations (U.S. and SI Units)

Liquid		Gas (vapor)		Liquid/gas (vapor); mass flow	
U.S. units (horsepower)					
$hp = \frac{h_i q_{gpm}}{47,500 \eta}$	(a)	$hp = \frac{Z_{f1} T_{f1} h_i q_{SCFH}}{13.5 \times 10^6 \eta p_{f1}}$	(c)	$hp = \frac{h_i q_{PPH}}{3.8 \times 10^5 \eta p_{f1}}$	(d)
$hp = \frac{G_b h_i q_{GPM}}{47,500 \eta F_p G_F}$	(b)				
Energy cost (\$/year) = (0.746)(hp)(operating hours/year)(\$/kW·h) (e)					
SI units (watts)					
$W = \frac{\Delta p^* q_{LPM}^*}{60 \eta}$	(f)	$W = \frac{Z_{f1} T_{K1} \Delta p^* q_{SCMH}^*}{10.24 \eta p_{f1}^*}$	(h)	$W = \frac{\Delta p^* q_{KPH}^*}{3.6 \eta p_{f1}^*}$	(i)
$W = \frac{G_b \Delta p^* q_{LPM}}{60 \eta F_p G_F}$	(g)				
Energy cost (\$/year) = (W/1000)(operating hours/year)(\$/kW·h) (j)					

From the API 2540 equation the flowing specific gravity is calculated as 0.8399. The fluid's viscosity is 3.63 cP.

The discharge coefficient C is calculated from Eq. (f), Table 9.1:

$$C = 0.5959 + 0.0312 \beta^{2.1} - 0.184 \beta^8 + 91.72 \beta^{2.5} / R_D^{0.75}$$

The pipe Reynolds number R_D is calculated from the equation given in Table C.4, with $D = 1.939$ from Table B.1, as

$$R_D = \frac{3159.433 G_b q_{GPM}}{D \mu_{cP}} = \frac{(3159.433)(0.8399)(40)}{(1.939)(3.63)} = 15,080$$

Substitution into the discharge coefficient yields

$$C = 0.5959 + (0.0312) (0.5)^{2.1} - (0.184) (0.5)^8 + (91.72)^{2.5} / (15,080)^{0.75} = 0.6144$$

The coefficient of contraction C_c is, by Eq. (6.10),

$$C_c = \frac{C}{\sqrt{1 - \beta^4 + C^2 \beta^4}} = \frac{0.6144}{\sqrt{1 - (0.5)^4 + (0.6144)^2 (0.5)^4}} = 0.6267$$








Substitution into Eq. (6.8) gives the overall permanent pressure loss as

$$h_l = \left\{ 1 - \frac{(2)(0.5)^2 (0.6144)^2}{1 - (0.5)^4} \left[\frac{1}{0.6267} - (0.5)^2 \right] \right\} 100 = 72.91 \text{ in}$$

Energy Cost

In many instances, the additional energy cost resulting from permanent pressure loss is a factor in flowmeter selection. Pumping costs are sometimes significant in

TABLE 6.6 Loss Coefficients for 1-in (25 mm) Coriolis Mass Flowmeters†

	$K_{\text{psid}}, \text{psi}$	$K_{\text{bar}}, \text{bar}$
	0.4505	1.5099E-01
	0.3236	1.0846E-01
	0.2187	7.3299E-02
	0.1871	6.2715E-02
	0.1741	5.8351E-02
	0.1579	5.2912E-02
	0.0935	3.1349E-02
$\Delta p_{l, \text{psid}} = K_{\text{psid}} q_{\text{lb}_m/\text{s}}^2 \qquad \Delta p_{l, \text{bar}} = K_{\text{bar}} q_{\text{kg}/\text{s}}^2$		

†Manufacturers should be consulted for exact information.

Source: Cascetta et al. (1992)

larger line sizes and may justify the selection of a more expensive flowmeter that either has a lower permanent pressure-loss coefficient or is obstructionless.

Example 6.2. Calculate the yearly energy cost for an ASME long-radius nozzle and a flange-tap orifice measuring 30,000 lb_m/h (13,610 kg/h) in a 6-in (150-mm) pipe. The nozzle and orifice bore are sized to produce 100 in (25 kPa) at the upper-range flow rate (30,000 lb_m/h). Energy costs \$0.05/kW·h; the motor and pump efficiency is assumed to be 100 percent for a steam flow.

From Example 9.2, $\beta = 0.6085$ for the nozzle and $\beta = 0.7432$ for the orifice, and $\rho_{f1} = 0.3952 \text{ lb}_m/\text{ft}^3$.

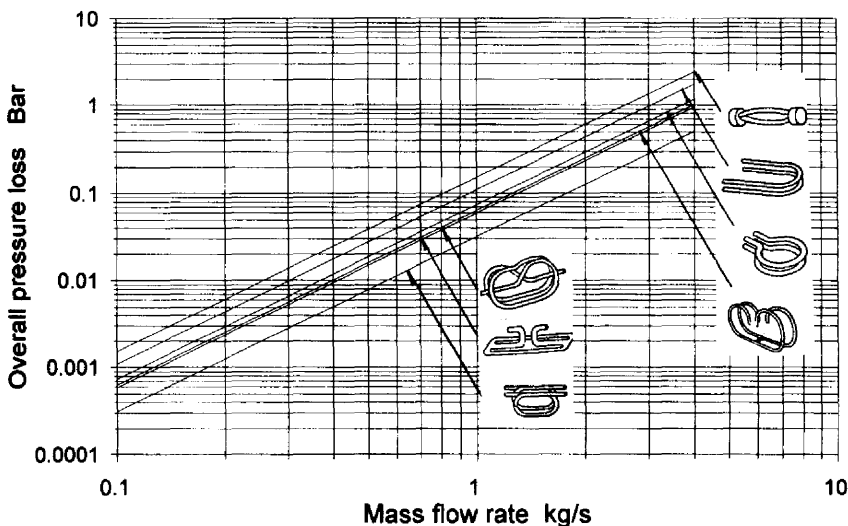


Figure 6.38 Overall pressure loss for a 1 in (25 mm) Coriolis mass flowmeter.

Energy cost for the nozzle. The permanent pressure loss is, from Eq. (e) of Table 6.3,

$$\begin{aligned}
 h_l &= (1 + 0.014\beta - 2.06\beta^2 + 1.18\beta^3)h_w \\
 &= [1 + (0.014)(0.6085) - (2.06)(0.6085)^2 \\
 &\quad + (1.18)(0.6085)^3](100) = 51.2 \text{ in}
 \end{aligned}$$

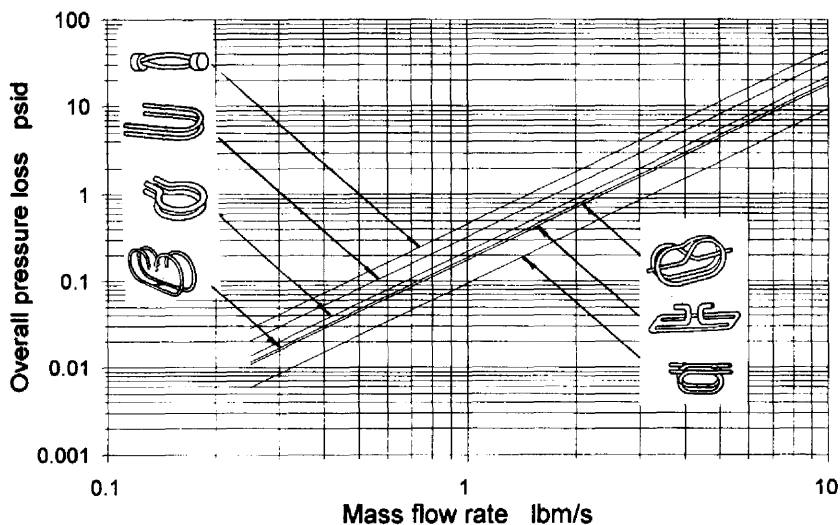


Figure 6.39 Overall pressure loss for a 1 in (25 mm) Coriolis mass flowmeter.

The required horsepower, from Table 6.5, is calculated with Eq. (d) of Table 6.5:

$$\text{hp} = \frac{h_f q_{\text{PPH}}}{3.8 \times 10^5 \eta \rho_{f1}} = \frac{(51.2)(30000)}{(3.8 \times 10^5)(1.0)(0.3952)} = 10.2 \text{ hp}$$

The yearly energy cost is then calculated with Eq. (e) of Table 6.5:

$$\begin{aligned} \text{Energy cost} &= (0.75)(\text{hp})(\text{operating hours/year})(\$/\text{kW}\cdot\text{h}) \\ &= (0.75)(10.2)(8760)(0.05) = \$3357/\text{year} \end{aligned}$$

Energy cost for the orifice. The permanent pressure loss is calculated with Eq. (f) of Table 6.3:

$$\begin{aligned} h_l &= (1 - 0.24\beta - 0.52\beta^2 - 0.16\beta^3)h_w \\ &= [1 - (0.24)(0.7432) - (0.52)(0.7432)^2 - (0.16)(0.7432)^3](100) = 46.9 \text{ in} \end{aligned}$$

From Eq. (d) of Table 6.5, the required horsepower is

$$\text{hp} = \frac{h_f q_{\text{PPH}}}{3.8 \times 10^5 \eta \rho_{f1}} = \frac{(46.9)(30000)}{(3.8 \times 10^5)(1.0)(0.3952)} = 9.4 \text{ hp}$$

The energy cost is then, by Eq. (e) of Table 6.5,

$$\begin{aligned} \text{Energy cost} &= (0.75)(\text{hp})(\text{operating hours/year})(\$/\text{kW}\cdot\text{h}) \\ &= (0.75)(9.4)(8760)(0.05) = \$3087/\text{year} \end{aligned}$$

Example 6.3. Calculate the yearly energy cost for a 200-mm Foxboro vortex flowmeter and for an orifice flowmeter measuring 38°C water flowing at 5.7 m³/min. For the orifice, $\beta = 0.689$, and the differential pressure is 50 kPa. Assume an 80 percent pump in motor efficiency and an energy cost of \$0.05/kW·h.

From Eqs. (2.165) and (2.175), the density and specific gravity of water at 38°C are

$$\rho_F^* = 992.96 \text{ kg/m}^3 \quad G_F = \frac{992.96}{999.012} = 0.9939$$

Energy cost for the vortex flowmeter. With negligible liquid compressibility the permanent pressure loss is found with Eq. (o) of Table 6.4:

$$\Delta p_l^* = F_p G_F \left(\frac{20.4 q_{\text{ipm}}^*}{D^{*2}} \right) = (1.0)(0.9939) \left[\frac{(20.4)(5.7)(1000)}{(193.68)^2} \right]^2 = 9.55 \text{ kPa}$$

where, for the Foxboro vortex flowmeter, $D^* = 193.68 \text{ mm}$. The required energy is then calculated with Eq. (f) of Table 6.5:

$$W = \frac{\Delta p^* q_{\text{ipm}}^*}{60 \eta} = \frac{(9.55)(5.7)(1000)}{(60)(0.8)} = 1134 \text{ W}$$

The yearly energy cost is, from Eq. (j) of Table 6.5,

$$\begin{aligned}\text{Energy cost} &= (W/1000)(\text{operating hours/year})(\$/\text{kW}\cdot\text{h}) = \frac{1134}{1000} (8760)(0.05) \\ &= \$497/\text{year}\end{aligned}$$

Energy cost for the orifice. The permanent pressure loss is found with Eq. (f) of Table 6.4:

$$\begin{aligned}\Delta p_l^* &= (1 - 0.24\beta - 0.52\beta^2 - 0.16\beta^3)\Delta p^* \\ &= [1 - (0.24)(0.689) - (0.52)(0.689)^2 - (0.16)(0.689)^3](50) = 26.8 \text{ kPa}\end{aligned}$$

The required energy is then, by Eq. (f) of Table 6.5,

$$W = \frac{\Delta p^* q_{lpm}^*}{60 \eta} = \frac{(26.8)(5.7)(1000)}{(60)(0.8)} = 3179 \text{ W}$$

The yearly energy cost is, from Eq. (j) of Table 6.5,

$$\begin{aligned}\text{Energy cost} &= (W/1000)(\text{operating hours/year})(\$/\text{kW}\cdot\text{h}) = \frac{3179}{1000} (8760)(0.05) \\ &= \$1393/\text{year}\end{aligned}$$

Natural Gas Measurement

In the custody transfer measurement of natural gas, the concentric square-edged orifice, with flange taps of $2\frac{1}{2}D$ and $8D$ (pipe taps), and the turbine flowmeter are used widely in the United States. In the United States, ANSI 2530 (1991) for orifice flowmeters and AGA 7 or ANSI/ASME MFC-4M (1987) for turbine flowmeters are usually specified in contracts. In Europe, turbine, orifice, and vortex flowmeters are used for custody transfer.

Usually, the pressure available is substantially higher than that required, and a pressure regulator is installed near the orifice flowmeter. Hence, a primary device having a higher pressure-recovery characteristic is seldom needed. In some cases, lower overall pressure-loss devices are used in *noncustody* transfer applications to reduce the sizable annual pumping cost required for orifice flowmeters.

REFERENCES

-
- AGA Report 7, *Measurement of Fuel Gas by Turbine Meters*, catalog no. X00580, American Gas Association, Arlington, Va., 1981.
- Alvi, S. H., K. Sridharan, and N. S. Lakshmana Rao: "Loss Characteristics of Orifices and Nozzles," *J. Fluid Eng.*, vol. 100, pp. 299–307, September 1978.
- ANSI/API 2530 *Orifice Metering of Natural Gas*, American Gas Association, New York, 1991.
- ANSI/ASME MFC-4M, *Measurements of Gas Flow by Turbine Meters*, ANSI, New York, 1987.
- ANSI/ASME MFC-5M, *Measurement of Liquid Flow in Closed Conduits Using Transit-Time Ultrasonic Flowmeters*, ANSI, New York, 1985.

- ANSI/ASME MFC-6M, *Measurement of Fluid Flow in Pipes Using Vortex Flow Meters*, ANSI, New York, 1987.
- ANSI/ASME MFC-7M, *Measurement of Gas Flow by Means of Critical Flow Venturi Nozzles*, ANSI, New York, 1987.
- API Publication 2101, chap. 12.2, American Petroleum Institute, Washington, D.C., 1981.
- ASME FLUIDMETERS Their Theory and Application, ASME, 1971.
- ASME MFC-3M, *Measurement of Fluid Flow in Closed Conduits Using Orifice, Nozzle, and Venturi*, ASME, New York, 1985.
- ASME/ANSI MFC-11M, *Measurement of Fluid Flow by Means of Coriolis Mass Flowmeters*, ASME, New York, 1994.
- ASME-16M, *Measurement of Fluid Flow in Closed Conduits by Means of Electromagnetic Flowmeters*, ASME, New York, 1995.
- ASME/MFC-SC2, *Small Bore Precision Orifices* (draft), ASME MFC, New York, 1986.
- ASME/MFC-SC16, *Multi-port Averaging Pitot Primary Device* (draft), ASME MFC, New York, 1987.
- Biles, R.: "Vortex Flowmeter Performance," *Measurement & Control*, September 1991.
- Bonner, J. A.: "A New International Standard, ISO 9951: The Measurement of Gas Flow in Closed Conduits—Turbine Meters," *Flow Measurement and Instrumentation*, vol. 4, no. 2, pp. 99–100, April 1993.
- Brennan, J. A., R. W. Stokes, C. H. Kneebone, and D. B. Mann: "An Evaluation of Selected Angular Momentum, Vortex Shedding and Orifice Cryogenic Flowmeters," U.S. Department of Commerce, NBS, Technical Note 650, 1974.
- British Standard 7405:1991, *Selection and Application of Flowmeters for the Measurement of Fluid Flow in Closed Conduits*, BSI, 1991.
- Cascetta, F., G. Cignolo, R. Gloria, G. Martini, A. Riveetti, and P. Vigo: "Experimental Intercomparison of Coriolis Mass Flowmeters," *Trans. Institute of Measurement & Control*, vol. 14, no. 2, pp. 98–107, 1992.
- DeVries, E. A.: "Experience with Ultrasonic Flowmeters," *Hydrocarbon Process.*, pp. 65–66, Gulf Pub., Houston, Texas, June 1986.
- Filban, T. J., and W. A. Griffin: "Small Diameter Orifice Metering," *J. Basic Eng.*, vol. 82, no. 3, p. 735, 1960.
- Flynn, R., and K. Larson: "A Changing of the Guard in Flowmeter Technology," *Control*, pp. 42–45, February 1994.
- Furness, R. A.: "BS 7405: The Principles of Flowmeter Selection," *Flow Measurement and Instrumentation*, vol. 2, no. 4, pp. 233–242, October 1993.
- Fusaro, D.: "Mass Measurement Trend Drives Coriolis, Thermal Meters," *Control*, pp. 30–33, January 1993.
- Gast, T., and R. A. Furness: "Mass Flow Technology," *Int. Conf. Flow Meas. in Mid 80's*, Paper 10.2, vol. 2, NEL, East Kilbride, Scotland, 1986.
- Ginesi, D.: "Try Insertion Flowmeters for Low Cost 'Hot-Tap' Installations," *Power*, vol. 131, no. 3, pp. 69–71, March 1987.
- Gorter, J., and D. G. de Rooij: "An Investigation in Widening the Reynolds Number Range for Flow Measurement in Closed Circuits by Means of Orifice Plates," *Fluid Flow Measurements in the Mid-1970's* (conf. proc.), vol. 1, pp. 3–23, Her Majesty's Stationery Office, Edinburgh, 1977.
- Grose, R. D.: "Orifice Contraction Coefficient for Inviscid Incompressible Flow," *Trans. ASME, J. Fluid Eng.*, vol. 107, pp. 36–42, March 1985.
- Grumski, J. T., and R. A. Bajura: "Performance of a Coriolis-Type Mass Flow Meter in the Measurement of Two-Phase (Air-Liquid) Mixtures," *Mass Flow Meas.* ASME WAM, pp. 75–83, Dec. 9–14, 1984.
- Haacke, A. C.: "Sensitivity of the Electromagnetic Flowmeter to Fluid Velocity Profile," *Pittsburgh Flow Symposium*, vol. 1, pt. 2, pp. 735–743, ISA, Pittsburgh, 1974.

Halmi, D.: "Metering Performance Investigation and Substantiation of the Universal Venturi Tube," pt. 1, "Hydraulic Shape and Discharge Coefficient," *J. Fluids Eng.*, ser. 1, vol. 96, no. 2, pp. 124–131, 1974.

Halmi, D.: "Metering Performance Investigation and Substantiation of the Universal Venturi Tube," pt. 2, "Installation Effect, Compressible Flow, and Head Loss," *J. Fluids Eng.*, ser. 1, vol. 96, no. 2, pp. 132–138, 1974.

Hayward, A. T. J.: "How to Choose a Flowmeter," *The Chartered Mechanical Engineer*, reprinted from *J. Mech. E.*, 1975.

ISO Standard 5167, *Measurement of Fluid Flow by Means of Orifice Plates, Nozzles and Venturi Tubes in Circular Cross-Section Conduits Running Full*, ISO 5167-1991(E) 1991.

ISO DIS 10790-2, *Measurement of Fluid Flow in Closed Conduits—Coriolis Mass Flowmeters*, ISO, Geneva, 1992.

ISO 9104, *Measurement of Fluid Flow in Closed Conduits—Method of Evaluating the Performance of Electromagnetic Flow-Meters for Liquids*, ISO, Geneva, 1991.

ISO 6817, *Measurement of Conductive Liquid Flow in Closed Conduits—Method Using Electromagnetic Flowmeters*, ISO, Geneva, 1992.

ISO Standard 9951, *Measurement of Gas Flow in Closed Conduits—Turbine Meters*, ISO, Geneva, 1992.

ISO TC 30, *Measurement of Fluid Flow by Means of Vortex Meters Inserted in Circular Cross Section Conduits Running Full*, ISO, Geneva, 1995.

ISO TC30 SC12/WG5, *Measurement of Fluid Flow in Closed Conduits—Direct Mass Flow Measurement Using Thermal Mass Flowmeters and Coriolis Mass Flowmeters*, ISO, Geneva, 1994.

Jones, E. H., and K. R. Ferguson: "Determination of the Basic Orifice Factors for Two Commercial 40.64 CM (16") Meter Runs at High Reynolds Numbers," *Proc. Int. Fluid Flow Meas.*, Session 12, Paper 3, AGA, Washington, D.C., November 1986.

Kastner, H. J.: "Officially Approved Gas Metering in W-Germany—The Establishment of the Vortex Meter," *Proc. Int. Fluid Flow Meas.* Session 5, Paper 1, AGA, Washington, D.C., November 1986.

Kinghorn, F. C., and A. McHugh: "The Performance of Turbine Meters in Two-Component Gas/Liquid Flow," in *Flow, Its Measurement and Control in Science and Industry*, vol. 2, ISA, Research Triangle Park, N.C., 1981.

Lee, W. Z.: "Performance of a Self-Adjusting Gas Turbine Meter," *Proc. Int. Fluid Flow Meas.*, Session 8, Paper 3, AGA, Washington, D.C., November 1986.

Lefebvre, P. J., and W. W. Durgin: "A Transient Electromagnetic Flowmeter," WAM Paper, ASME, Anaheim, Calif., 1986.

Loga, T. H.: "Rotary Positive Displacement Meters—Theory, Development, and Future Applications," 2d Int'l. Symp. on Fluid Flow Measurement, pp. 99–113, AGA, Calgary, 1990.

Lomas, D.: "Vortex, Turbine, Orifice—Which One Do I Choose," *Flow-Con 77* (symp. proc.), p. 25, Institute of Measurement and Control, Sussex, U.K., 1977.

Lynnworth, C., and J. L. Adsmond: "Clamp-on Flowmeter Surveys Powerplant Water Balance," *Power*, vol. 128, no. 1, pp. 118–119, January 1984.

Miller, R. W., C. Wilkes, and E. Jones: "Vortex and Orifice Metering of Natural Gas," *Mass Flow Meas.*, pp. 1–7, ASME WAM, FED-vol. 17, ASME, 1984.

Miller, R. W., J. P. DeCarlo, and J. T. Cullen: "Vortex Flowmeter Calibration Results and Application Experiences," *Flow-Con 77* (symp. proc.), pp. 341–371, Institute of Measurement and Control, Sussex, U.K., 1977.

Millington, B. C., and N. W. King: "The Performance of a Turbine Meter in a Gas-Liquid Flow with an Upstream Flow Conditioning," *Proc. Int. Conf. Flow Meas. in Mid 80's*, NEL, East Kilbride, Scotland, 1986.

Murdock, J. W., C. J. Foltz, and C. Gregory: "Performance Characteristics of Elbow Flowmeters," ASME Winter Annual Meeting, Paper 63-WA-17, 1963.

- Nissen, C. J.: "HPV Meter," *Meas. & Control*, issue 133, February 1989.
- Nissen, C. J.: "Solving Material Metering Problems," *Intec (ISA)*, April 1992.
- Nolan, M. E., J. G. O'Hair, and R. Teyssandier: "The Measurement of High Pressure Natural Gas Flows Using the Four-Path Ultrasonic Flowmeter Developed by British Gas," *Proc. Int. Fluid Flow Meas.*, Session 14, Paper 4, AGA, Washington, D.C., November 1986.
- O'Herron: "Performance Evaluation of Ultrasonic, Doppler Type," ISA, Paper 85-0633, Research Triangle Park, N.C., 1985.
- OIML R31 (Draft Revision), *Diaphragm Gas Meters*, OIML, 1994.
- OIML R 105, *Direct Mass Flow Measuring Systems for Quantities of Liquid*, OIML, 1993.
- OIML PS5D/RS10 (Draft Revision), *Type Evaluation Report Form*, OIML, 1993.
- OIML SP5D-Sr-9, *Vortex Meters Used in Measuring Systems for Fluids*, OIML, 1992.
- Owen, R. E.: "Segmental Wedge Flow Element," Taylor Instruments, Rochester, N.Y., 1979.
- Reinecke, M. E., W. G. Ragains, and R. W. Miller: "An Experimental Study of the Capability of Measuring Gas Mass Flow," *Flow Measurement Symp.*, pp. 232-252, ASME, New York, 1966.
- Robinson, C.: "Obstructionless Flowmeters: Smooth Sailing for Some, Rough Passage for Others," *Intech*, pp. 33-36, ISA, Research Triangle Park, N.C., December 1986.
- Rubin, M.: "How to Keep Turbine Meters Accurate," *Control*, June 1991.
- Rubin, M., R. W. Miller, and W. G. Fox: "Driving Torques in a Theoretical Model of a Turbine Meter," *J. Basic Eng.*, ser. D., vol. 87, no. 2, pp. 413-420, 1965.
- Scarpa, T. J.: "Magmeter Spotlights New Technology," *Intech Industry*, pp. 53-55, April 1993.
- Scott, M. J., and J. Davies: "A Practical Approach to Insertion Flow-metering Profiling," *Proc. Flow Metering and Proving Tech. in the Offshore Oil Ind.*, The Institute for Measurement and Control, Aberdeen, Scotland, pp. 49-56, 1983.
- Shercliff, J. A.: *The Theory of Electromagnetic Flow-Measurement*, Cambridge University Press, Cambridge, England, 1962.
- SIREP-WIB: *Investigation of a 6" Vortex Flowmeter*, Organization for Applied Science and Research, TNO, Breda, Netherlands, Evaluation Report E2482T85, May 1985.
- van Bakkum, J., M. M. Warffemius, and D. M. Oldenzil: "On the Hydrodynamical Stability of Electromagnetic Flowmeters," *Proc. 5th Int'l IMEKO Conf. on Flow Measurement*, pp. 135-142, VDI, Dusseldorf, 1989.
- Weigand, J., and L. Lombardo: "The Use of Laminar Flow Element in Computerized Flow Measurement," ISA paper 89-002, ISA, 1989.

INTRODUCTION TO THE DIFFERENTIAL PRODUCER

The differential-producing flowmeters are the most widely used in industrial process-measurement and control applications. The square-edged concentric orifice is selected for 80 percent of all liquid, gas, and vapor (steam) applications. This chapter contains a brief history of the differential producer and a look at the organization of Chaps. 8 through 12, which deal exclusively with differential producers.

HISTORICAL BACKGROUND

There are numerous examples of the early application of the principle of the differential producer. The hourglass and the use of the orifice during Caesar's time to measure the flow of water to householders are but two of many. But the developments which led to the design and widespread use of the various types of primary elements began in the seventeenth century.

At the start of the seventeenth century, Castelli and Torricelli laid the foundation for the theory of differential producers with the concepts that the rate of flow is equal to the velocity times the pipe area and that the discharge through an orifice varies with the square root of the head. Until recently all differential producers have been called *head-class* flowmeters because of this early work and that of Bernoulli, who, in 1738, developed the hydraulic equation for the calculation of flow rate.

In 1732, Pitot presented his paper on the pitot tube, and in 1797 Venturi published his work on a flowmeter principle that today bears his name. Venturi's work was developed into the first commercial flowmeter in 1887 by Clemens Herschel. Herschel's laboratory work defined the dimensions of the *Herschel venturi* and laid the foundation for future laboratory investigations to determine the relationships between geometry and differential pressure for the other differential producers.

In 1913, E. O. Hickstein (1915) presented early data on orifice flowmeters with pressure taps located $2\frac{1}{2}$ pipe diameters upstream and 8 pipe diameters downstream. This work, and that of others, led to several other pressure-tap locations, such as those for *D*-and-*D/2* and vena contracta taps.

In 1916, E. G. Bailey delivered a paper on the measurement of steam with orifice flowmeters, and in 1912 experimental work by Thomas R. Weymouth of the United Natural Gas Company was the basis for the use of the orifice flowmeter for measuring natural gas. For convenience, Weymouth used flange pressure taps located

1 in upstream and 1 in downstream of the faces of a conventional square-edged orifice. In Europe, orifice flowmeters using the corner tap location were being experimentally investigated.

Although the orifice was widely used for many different fluids, it wasn't until 1930 that a joint AGA/ASME/NBS test program obtained sufficient data to develop a coefficient-prediction equation. The Ohio State University (1935) test report and the Buckingham fitting equations for the various tapping arrangements have been used by ASME and AGA since 1935. The ability to predict coefficients from measured dimensions led to the full commercialization of the orifice flowmeter.

In the late 1950s, work in the United States was combined with European practice, and ISO Standards R541 (1967) for orifices and nozzles and R781 (1968) for venturis were issued.

In the mid-1960s, an ASME Fluid Meters Research Committee initiated a study to reevaluate the Ohio State data and to add new coefficient data. The objective of this study was to derive, by regression analysis, a simpler and more accurate coefficient-prediction equation for flange-tapped orifices. The results (Dowdell and Chen, 1970) were not encouraging; the Ohio State data had a ± 1.85 percent deviation (2σ) from the Buckingham equation. By limiting line sizes and beta ratios, ASME *Fluid Meters* (1971) changed the previous ± 0.55 percent coefficient accuracy statement to ± 1 percent.

In 1975, J. Stolz proposed a universal orifice equation to the ISO orifice flowmeter subcommittee. He proposed, based on logical rules, to combine the Ohio State data into a single dimensionless equation suitable for flange, corner, and D -and- $D/2$ taps. This equation was presented in a 1978 paper (Stolz, 1978). The orifice prediction equation appears in ISO Standard 5167 (1980), which combines Standards R541 and R781 into a single differential-producer standard. Based on the Dowdell and Chen (1970) investigation and subsequent papers by Miller et al. (1979), the ASME Fluid Meters Research Committee (1981) adopted the ISO 5167 (1980) equation, used in this handbook for all primary elements. Subsequently, ISO 5167 was developed into ASME MFC-3M (1995) as an engineering standard for orifice, nozzle, and venturi flowmeters.

The significance of the orifice flowmeter in the custody transfer of large quantities of natural gas led to extensive test programs to obtain data in both the United States and Europe. The American Petroleum Institute (API), The Gas Research Institute (GRI), The Gas Processors Association (GPA), and a special program under the sponsorship of the European Economic Community (EEC) have produced a significant body of data for use in formulating a new orifice discharge prediction equation. The U.S. data covers a pipe Reynolds-number range of 150 to 16,000,000 and contains over 20,000 data points (Fling, 1986).

Three prediction equations have been developed by regression of this data (ISO Report, 1994); they are:

- The ANSI/API-2530/AGA-3, 1991
- The Stolz II equation
- The NEL/TC28 equation

The ANSI/API-2530/AGA-3, 1991 is currently in use in ANSI 2530. The Stolz II and NEL/TC28 equations are being considered as a future replacement coefficient equation for both ANSI 2530 and ISO 5167. The NEL/TC28 equation has been approved by letter ballot as the equation for ISO 5167 (1991).

These equations are based on the same data set and, therefore, yield similar statistical results. The Stolz II *rational* equation is of the familiar form $C = C_{\infty} + b/R_D^n$ and is a more practical working equation for general plant and other computations. The NEL/TC-28 equation is considerably more complex. Both equations are presented in Chap. 9 for information purposes.

For the measurement of natural gas in the United States, AGA 3 (ANSI/API 2530, 1992) is usually required for contractual purposes; in it the equation for flange taps is presented. For this measurement the sizing, flow rate, and differential pressure equations developed in this handbook may be used by substituting the ANSI/API equation presented in Chap. 9.

The first investigation of a flow nozzle dates back to the nineteenth century (Froude, 1847). In 1930 Germany standardized on an ISA (1932) nozzle geometry. [The ISA (International Federation of National Standardizing Organizations) was replaced by the present International Organization for Standardization (ISO).] In the United States the long-radius flow nozzle was developed at Ohio State University (Beitler and Bean, 1948) primarily for the measurement of steam flows. The need for improved accuracy when testing steam turbines led to the development of the ASME throat-tap nozzle. The downstream pressure tap in this nozzle is in the cylindrical throat section.

The commercial success of the orifice, venturi, and nozzle led to the development of continually improved secondary measuring elements. This, coupled with test work and user familiarity, led to the further development of primary elements such as the segmental orifice, eccentric orifice, Lo-Loss tube, elbow, and annular orifice. These primary elements, combined with a wide variety of available secondary elements, are used to indicate, record, compute, and control the majority of flow measurements made today.

ORGANIZATION OF DIFFERENTIAL-PRODUCER INFORMATION

Flowmeter Elements

Figure 7.1a shows a differential-producer flowmeter. The meter consists of two separate devices that act in combination to measure flow rate. The first is the primary device (Fig. 7.1b). The geometry of the differential producer, the length and condition of the reference piping, and the pressure-tap location with respect to the primary element are properties of the primary device. Any change in these properties from reference conditions alters the differential pressure-flow rate relationship. Figure 7.1c shows the elements of the secondary device. The differential pressure is measured by transmitting pressure through lead lines to a secondary differential-pressure measuring element. The secondary device in this case consists of three elements: lead lines, valving, and manometer. Since the flow rate can be calculated from visual observation of the differential pressure, no further readout equipment is required. If the flow rate were to be calculated by a central processor or on-site computer or from a chart record, each of these would be an additional element of the secondary device.

As shown in Fig. 7.1a, the differential pressure depends on the pressure-tap locations and on whether the contraction is abrupt or gradual. The relationship between measured differential and flow rate is then a function of tap locations,

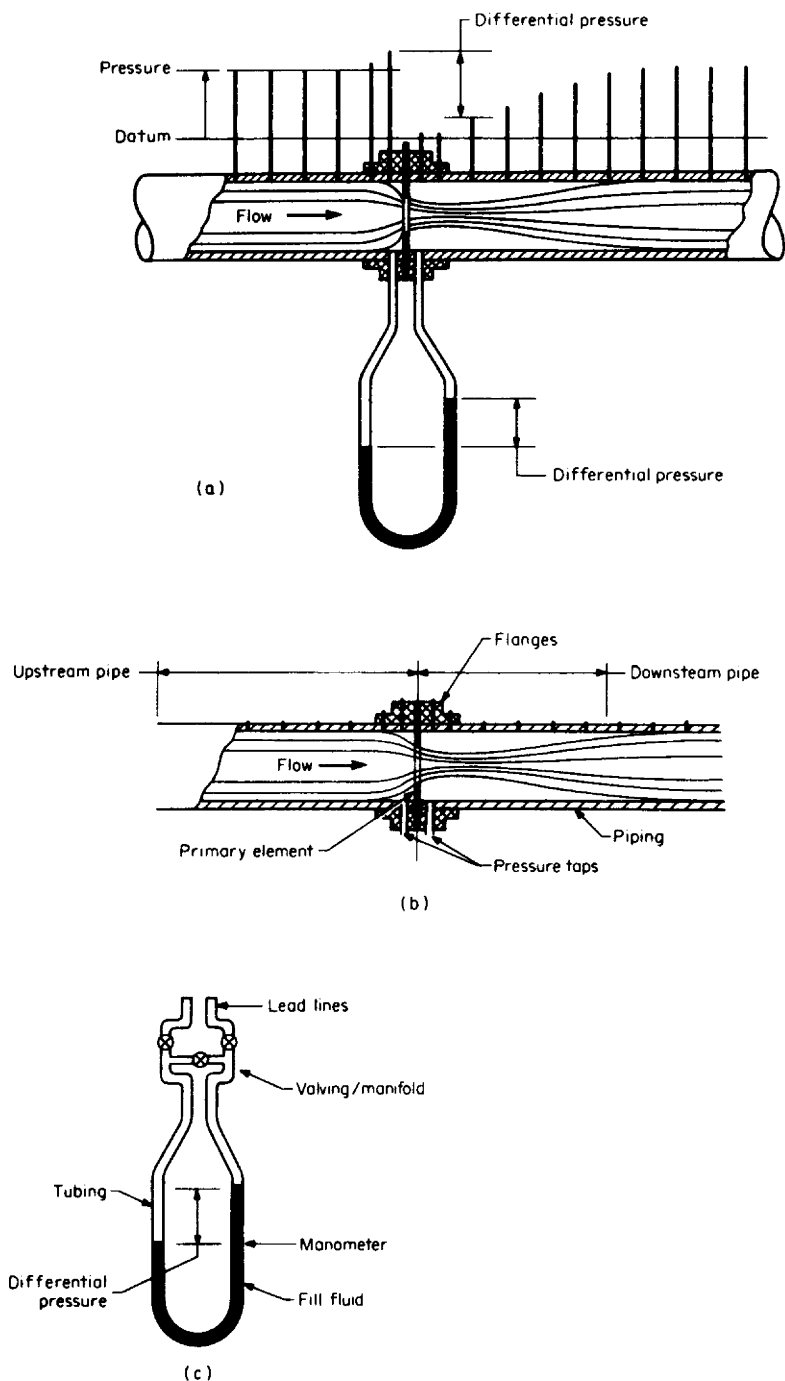


Figure 7.1 Differential-producer flowmeter. (a) Flowmeter. (b) Elements of the primary device. (c) Elements of the secondary device.

primary-element design, and associated upstream and downstream piping. These effects are included in the discharge coefficient, which relates the actual flow rate to the theoretically calculated flow rate.

Contents of Chapters 8 to 12

Obviously, with the number of differential producers that have both common and unique features, grouping is necessary to avoid repetition. These meters have, therefore, been separated into two broad groups for discussion. In the first group are those meters in which the bore is sized to produce a design differential—for example, 100 in (25 kPa) at 1000 gal/min (3800 l/min). In the second group are flowmeters in which geometry is fixed and the differential (or target force) must be calculated for a design flow rate. The content of the chapters are:

Chapter 8: Installation. In this chapter, pipe circularity, pressure-tap design, the location of thermal wells, lead lines, and installation piping are discussed.

Chapter 9: Engineering Equations. Here the engineering equations for sizing and for calculating flow rates in both U.S. and SI units are derived and presented in tables for primary elements that are sized to produce a design differential at a given flow rate. Procedural tables are presented along with examples that deal with sizing and the calculation of flow rates and accuracy.

Chapter 10: Design Information. Recommended designs for the various primary elements are presented in this chapter. For graphical sizing and flow-rate calculation, discharge-coefficient curves are provided—both based on equations given in Chap. 9 and for meters for which the coefficient has not been reduced to an equation. Thermal-expansion-factor and gas-expansion-factor curves are also given.

Chapter 11: Fixed-Geometry Devices. This chapter presents the geometry-factor equations that are substituted into the engineering equations of Chap. 9 to calculate differential pressure (or target force) for elements with fixed geometry (elbow, target, integral orifice, and arithmetic-progression orifice, etc.). This substitution-of-variables method allows the retention of the basic form of the equations given in Chap. 9. Tables and graphs are also given for flow-coefficient calculations.

Chapter 12: Computations. This chapter reviews the available computational methods for calculating either flow rate or total flow using chart integration and analog or digital flow computers.

Chapter 15, Meter Influence Quantities, presents graphically and in tables the influence of various departures from standard conditions on the performance of all flowmeters. The effect of upstream disturbances, edge roundness, accumulation of dirt, etc. are presented in this chapter.

REFERENCES

-
- AGA-ASME: *The Flow of Water Through Orifices*, Ohio State University Studies, Engineering Series, vol. IV, no. 3, Bulletin 89, 1935.
- ANSI/API 2530, *Orifice Metering of Natural Gas*, ANSI, New York, 1991.

- ASME: "The ASME-ISO Orifice Equation," *Mech. Eng.*, vol. 103, no. 7, 1981.
- ASME: *Fluid Meters*, 6th ed., ASME, New York, 1971.
- ASME MFC-3M, *Measurement of Fluid Flow in Pipes Using Orifice, Nozzle, and Venturi*, ASME, New York, 1995.
- Bailey, E. G.: "Stream Flow Measurement," *Power*, vol. 38, p. 250, 1916.
- Beitler, S. R., and H. S. Bean: *Research on Flow Nozzles*, Ohio State University Engineering Experiment Station Bulletin 131, 1948.
- Dowdell, R. B., and Yu Lin Chen: "A Statistical Approach to the Prediction of Discharge Coefficients for Concentric Orifice Plates," *J. Basic Eng.*, vol. 92, no. 4, p. 752, 1970.
- Fling, W. A., "The API/GPA Orifice Plate Database," *65th Annual GPA Conv.*, San Antonio, Texas, GPA, March 10–12, 1986.
- Froude, W.: "Discharge of Elastic Fluids under Pressure," *Proc. Inst. Civ. Eng. London*, vol. 6, pp. 356–399, 1847.
- Herschel, C.: "The Venturi Water Meter," *Trans. Am. Soc. Civ. Eng.*, vol. 17, p. 228, 1887.
- Hickstein, E.O.: "Flow of Air Through Thin-Plate Orifices," *Trans. ASME*, vol. 37, p. 765, 1915.
- ISA Bulletin 12, International Federation of National Standardizing Organizations, Geneva, 1932.
- ISO Report, *Report from the Joint ISO-TC30/SC2, ISO-TC-28/SC5 Working Group for a New Discharge Coefficient for Orifice Plates*, (Rev. 1 of 7), July 1994.
- ISO Standard R541, *Measurement of Fluid Flow by Means of Orifice Plates and Nozzles*, ISO, Geneva, 1967.
- ISO Standard R781, *Measurement of Fluid Flow by Means of Venturi*, ISO, Geneva, 1968.
- ISO Standard 5167, *Measurement of Fluid Flow by Means of Orifice Plates, Nozzles and Venturi Tubes Inserted in Circular Cross-Section Conduits Running Full*, ISO 5167-1980(E), Geneva, 1980.
- Miller, R. W.: "The Stolz and ASME-AGA Orifice Equation Compared to Laboratory Data," *J. Fluids Eng.*, vol. 101, no. 4, pp. 483–490, 1979.
- and G. A. Koslow: "The Uncertainty Values for the ASME-AGA and ISO 5167 Flange Tap Orifice Equation," ASME Winter Annual Meeting, Paper FM-5, 1979.
- Stolz, J.: *An Approach Toward a General Correlation of Discharge Coefficients of Orifice Plate Flowmeters*, ISO/TC30/SC2 (France 6) 654, 1975.
- : "A Universal Equation for the Calculation of Orifice Plates," in *FloMeko 1978, Groningen*, 1978, North-Holland, Amsterdam, 1978.
- Weymouth, Thomas R.: "Measurement of Natural Gas," *Trans. ASME*, vol. 34, p. 1091. 1912.

DIFFERENTIAL PRODUCERS: INSTALLATION

It is important that the installation of the primary element approach the standard or reference conditions which prevailed when the flow-coefficient information was obtained. The condition of the pipe, mating of pipe sections, pressure-tap design, straight lengths of pipe preceding and following the primary element, and lead lines that transmit the differential pressure to the secondary measuring element all affect measurement accuracy. While some of these may have a minor effect, others can introduce 5 or 10 percent bias errors. In general, these errors are not predictable, and attempts to adjust coefficients for the effect of nonstandard conditions have not been successful.

PIPING

Reference Piping

ISO Standard 5167† (1991) gives requirements for reference piping concerning the following items:

1. Visual condition of the outside of the pipe as to both straightness and circularity
2. Visual condition of the internal surface of the pipe
3. Reference-condition relative roughness for the internal surface (see Table 5.6)
4. Location of measurement planes and number of measurements for the determination of the average pipe diameter D
5. Circularity of a specified length of pipe preceding the primary element

†Subsequently ISO 5167 was developed into ANSI/ASME MFC-3M.

6. Maximum allowable step height for mating sections of upstream pipe
7. Limits on mating upstream-pipe step-height ratio (for addition of ± 0.2 percent to the discharge-coefficient accuracy)

These requirements are shown in Figs. 8.1 through 8.3.

A low-frequency far-field eddy current (FFEC) technique has been developed by the Southwest Research Institute (ASME, 1985) for application in the power, petrochemical, and paper industries. The probes help examine changes in wall thickness and localized thinning in the first 60 in (1.5 m) of curved or straight carbon-steel tubes found in power plants.

Pipe wall thickness, or wall thinning, may also be measured by ultrasonic techniques. The ultrasonic devices have a typical quoted accuracy of ± 0.001 in (0.025 mm) when measuring thickness in pipe (or tubing) in the 0.030- to 20-in (0.76- to 510-mm) size range.

Pressure Taps

Figure 8.4 illustrates the recommended geometry for wall static-pressure taps. Both pressure taps should be of the same diameter and, where the hole breaks through, should be square with no roughness, burrs, or wire edges. In Fig. 8.5 are shown typical pressure connections used for low- and high-temperature applications.

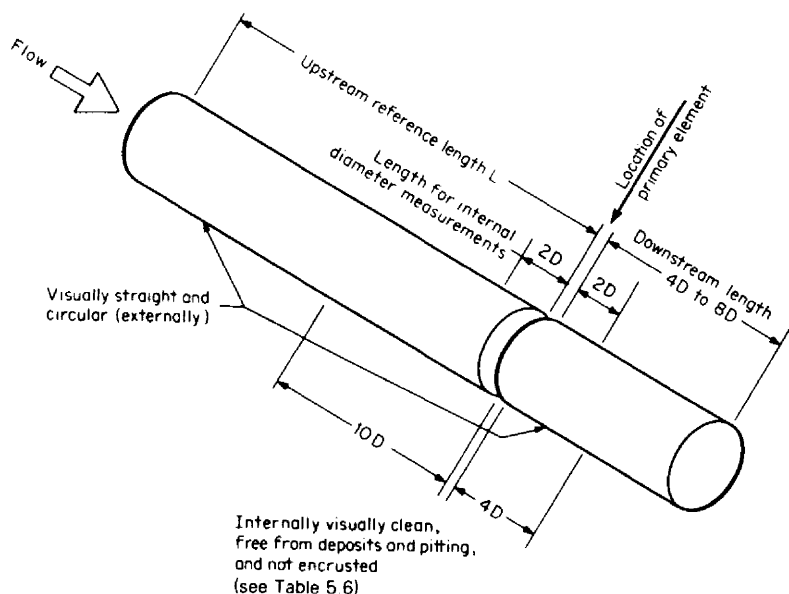
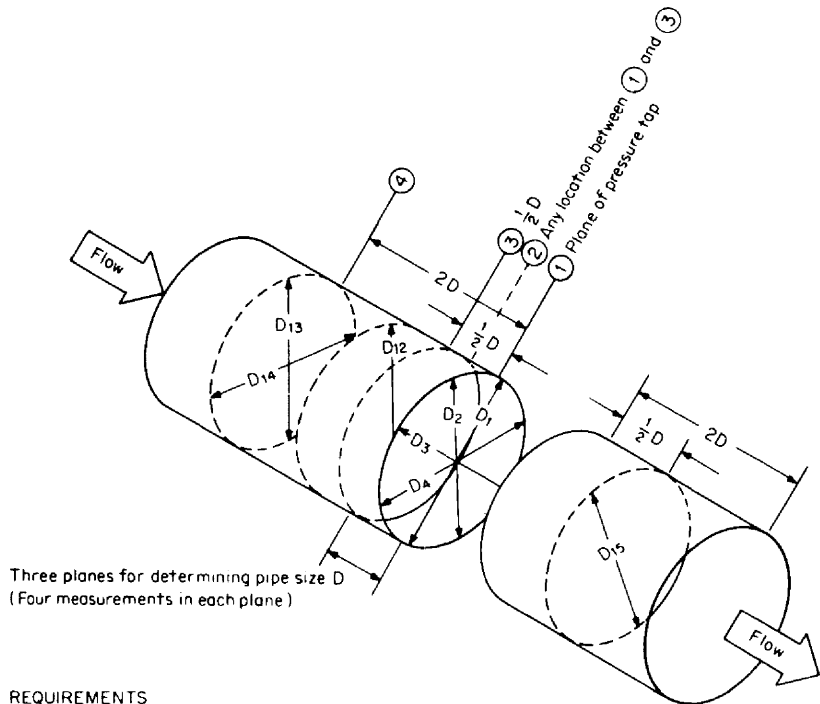


Figure 8.1 ISO visual requirements for pipe condition.



REQUIREMENTS

Upstream

Pipe diameter:

$$D = \frac{D_1 + D_2 + D_3 + \dots + D_{12}}{12}$$

at planes ①, ②, ③

Circularity: $0.997D \leq D_1, D_2, \dots, D_{14}, D_n \leq 1.003D$

at planes ①, ②, ③ and ④

where n = sufficient additional measurements to provide assurance between planes ③ and ④

Downstream:

Single diameter check:

$$0.97D \leq D_{15} \leq 1.03D$$

For classical venturi:

$D \leq \pm 1\%$ of entrance cylinder diameter

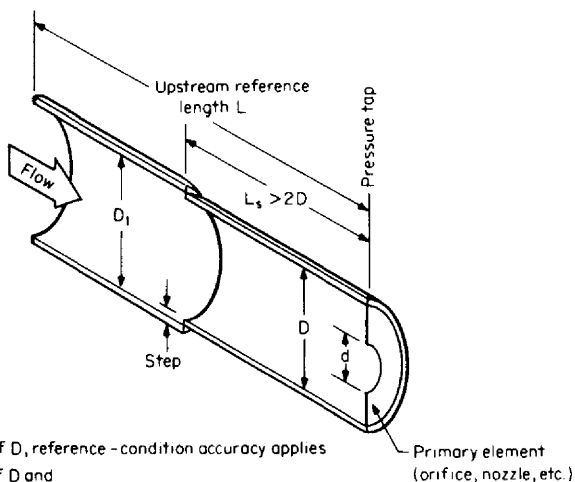
$D_1, D_2, D_3, \dots, D_n \leq \pm 2\%$ of entrance cylinder diameter

$D_{15} \geq 90\%$ of diameter at end of venturi divergent

Figure 8.2 ISO pipe-diameter measurement and circularity requirements.

Protrusions or Pockets

If a pocket or obstruction is present in the upstream or downstream pipe, the velocity profile will be affected. Depending on disturbance diameter, these should be located a sufficient distance from the primary element to ensure fully recovered flow. ISO Standard 5167 (1991) and ANSI/API 2530 (1991) specifications for the location of these devices are shown in Fig. 8.6. Although ISO allows for an upstream thermal well, it is good practice to locate these downstream to ensure minimum profile distortion.



$$h_s/D \leq 0.002 \frac{L_s/D + 0.4}{0.1 + 2.3\beta^4} \quad h_s/D \leq 0.05$$

with $\beta = d/D$ $h_s = D_1 - D$

then add 0.2% to discharge-coefficient accuracy.

Figure 8.3 ISO requirements for discharge-coefficient accuracy and for ± 0.2 percent addition for upstream pipe sections.

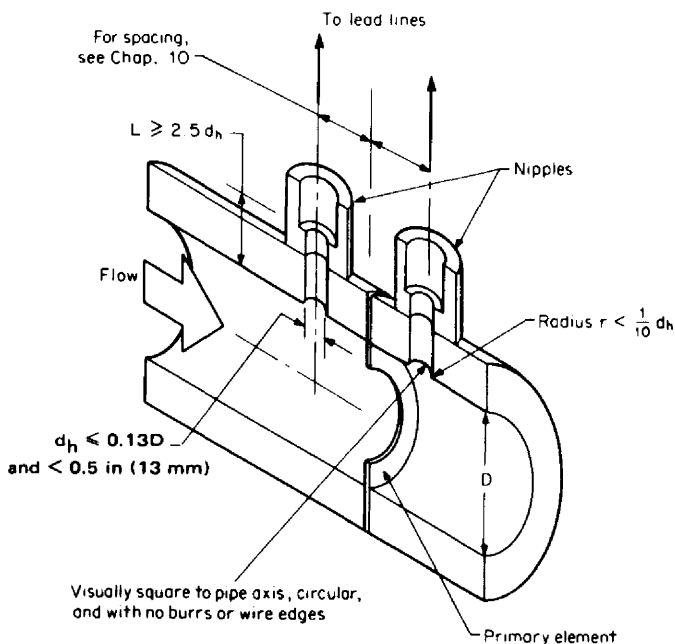


Figure 8.4 ISO pressure-tap design requirements.

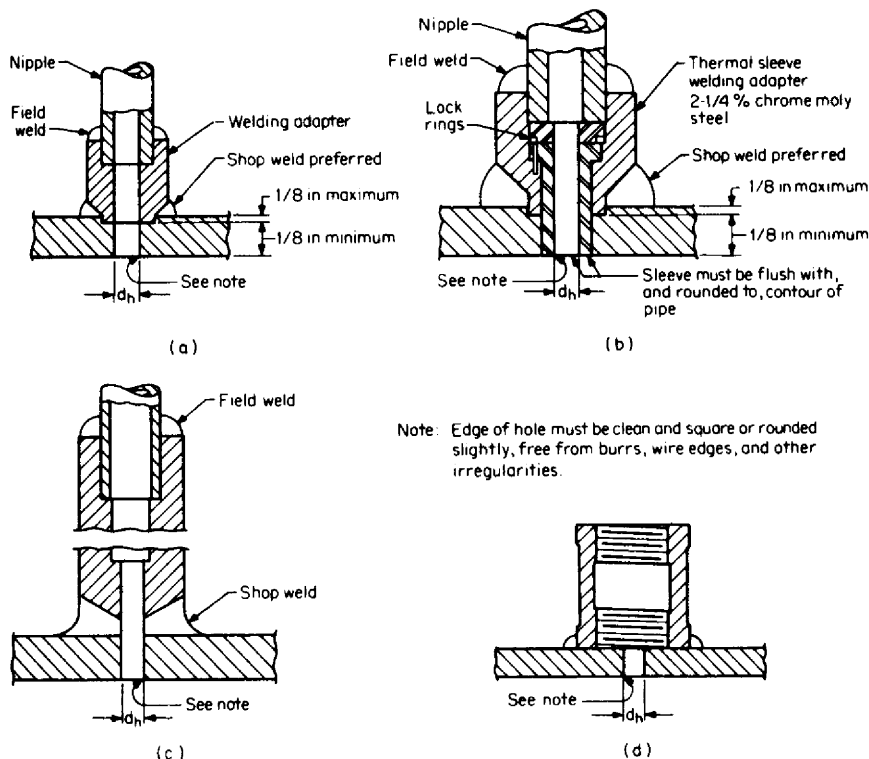


Figure 8.5 Methods of making pressure connections to pipe. (a) For temperatures up to 800°F. (b) For temperatures above 800°F and a secondary element with appreciable displacement. (c) Optional design where full-penetration weld is required. (d) For temperatures up to 400°F. (From ASME Fluid Meters; used with permission.)

Gaskets or weld beads that extend into the pipe tend to increase fluid turbulence and alter the profile. Welds should be ground smooth, and gaskets trimmed, so that no protrusion is evident on visual inspection.

Straight-Pipe Lengths

The required length of straight pipe preceding and following the primary element depends on the primary element and the type of upstream disturbance. Several U.S. and European test programs have provided data concerning the effects of specific upstream disturbances on orifices, nozzles, venturi nozzles, and venturis. This information has been used to establish *recommended* minimum pipe lengths. However, the recommended minimum lengths differ between U.S. sources (ANSI 2530, 1990 and ASME MFC-3M, 1995) and ISO Standard 5167 (1991), with the ISO recommendations being more conservative.

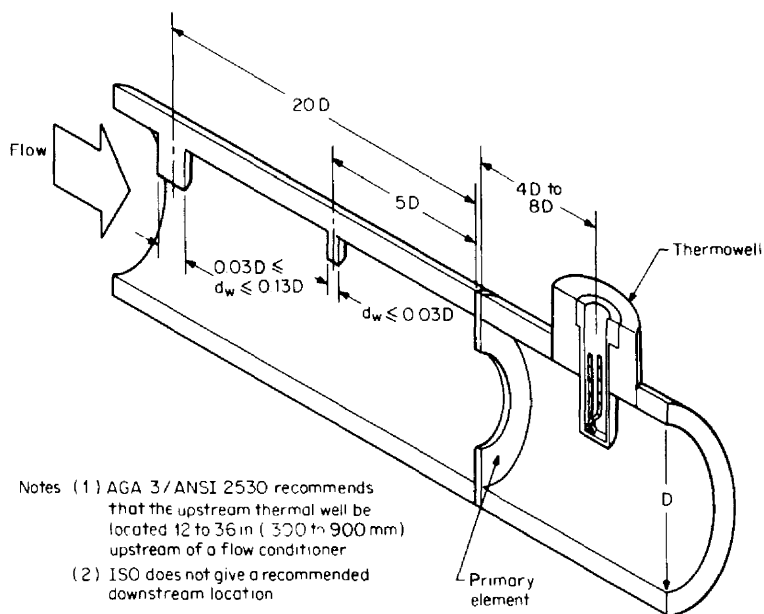


Figure 8.6 ISO- and AGA-recommended locations for thermal wells or pockets.

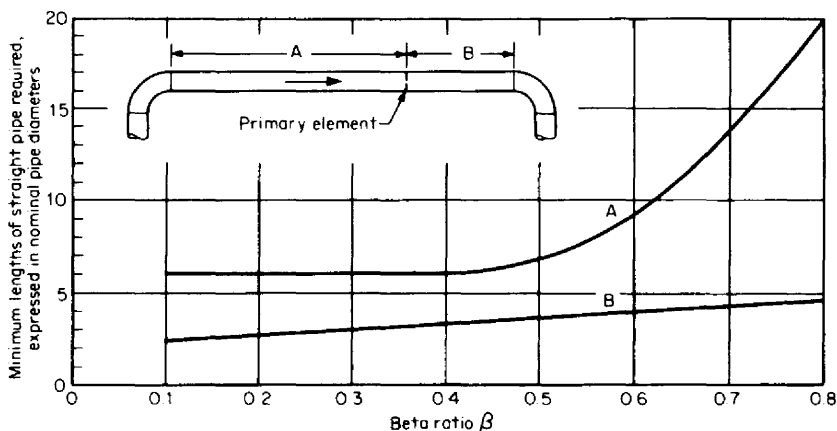


Figure 8.7 Installation lengths for primary elements preceded by an elbow in a single plane.

ANSI 2530 and Fluid Meters. In Figs. 8.7 through 8.11 are the ANSI 2530 and ASME *Fluid Meters* (1971) recommendations for straight pipe with and without a flow conditioner for orifices, nozzles, and venturis. *Fluid Meters* indicates that the diagram which corresponds closest to the actual piping arrangement should be used to determine the required length, and that minimum length is necessary to hold

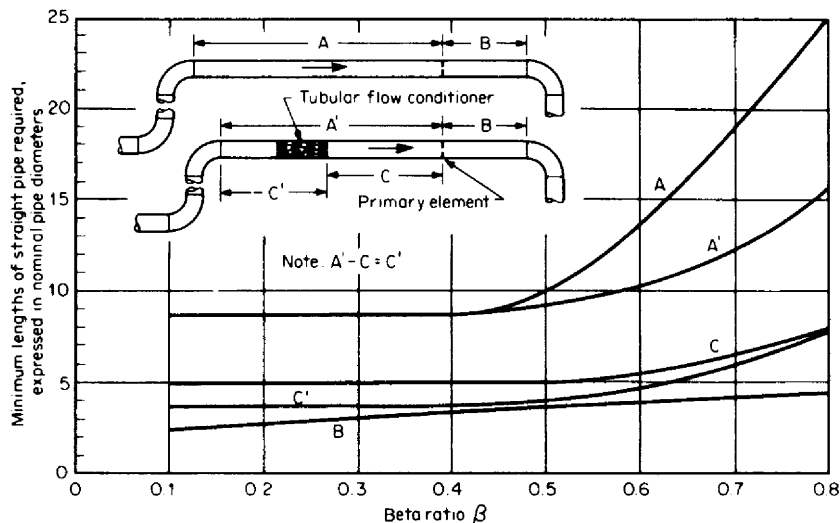


Figure 8.8 Installation lengths for primary element preceded by two elbows in one plane.

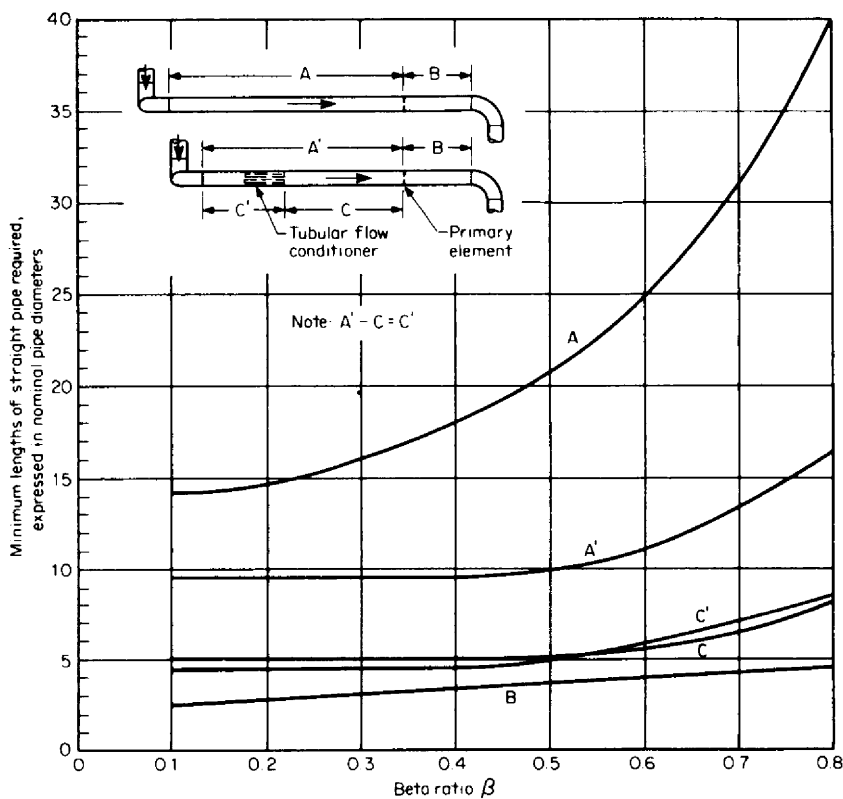


Figure 8.9 Installation lengths for primary element preceded by two elbows in different planes.

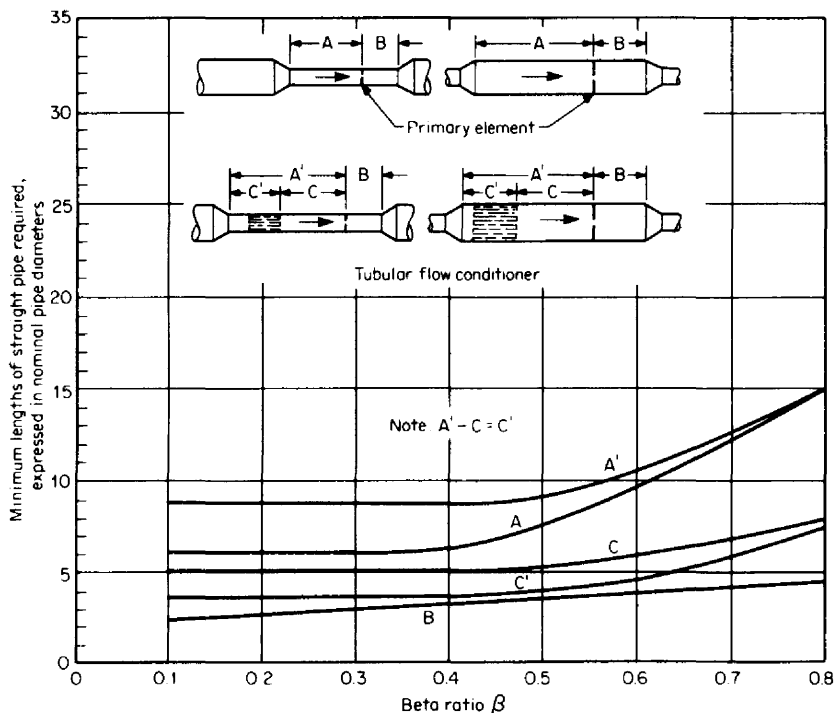


Figure 8.10 Installation lengths for primary element preceded by reducer or expander.

pipng bias errors, due to piping influence, to less than ± 0.5 percent. Further, it is recommended that for any decrease in length an additional ± 0.5 percent to be added to the flow-coefficient accuracy value.

ISO Standard 5167. ISO straight-length requirements for orifices, nozzles, venturi nozzles, and venturis are listed by beta ratio in Table 8.1. These lengths are generally twice the ANSI 2530 and *Fluid Meters* requirements. For lengths one-half those shown, an additional ± 0.5 percent is to be algebraically added to the coefficient accuracy given in Table 9.42. ISO recommends that a flow conditioner be installed 20 pipe diameters following the disturbance and that an additional 22 pipe diameters be installed between the conditioner and the primary element.

Proprietary Devices. Straight lengths have been standardized only for venturis, nozzles, venturi nozzles, and orifices. For proprietary devices, the user should follow the manufacturer's recommendations. In Table 8.2 are the recommendations for the annubar, and in Fig. 8.12 curves of bias error versus pipe length for the Lo-Loss tube.

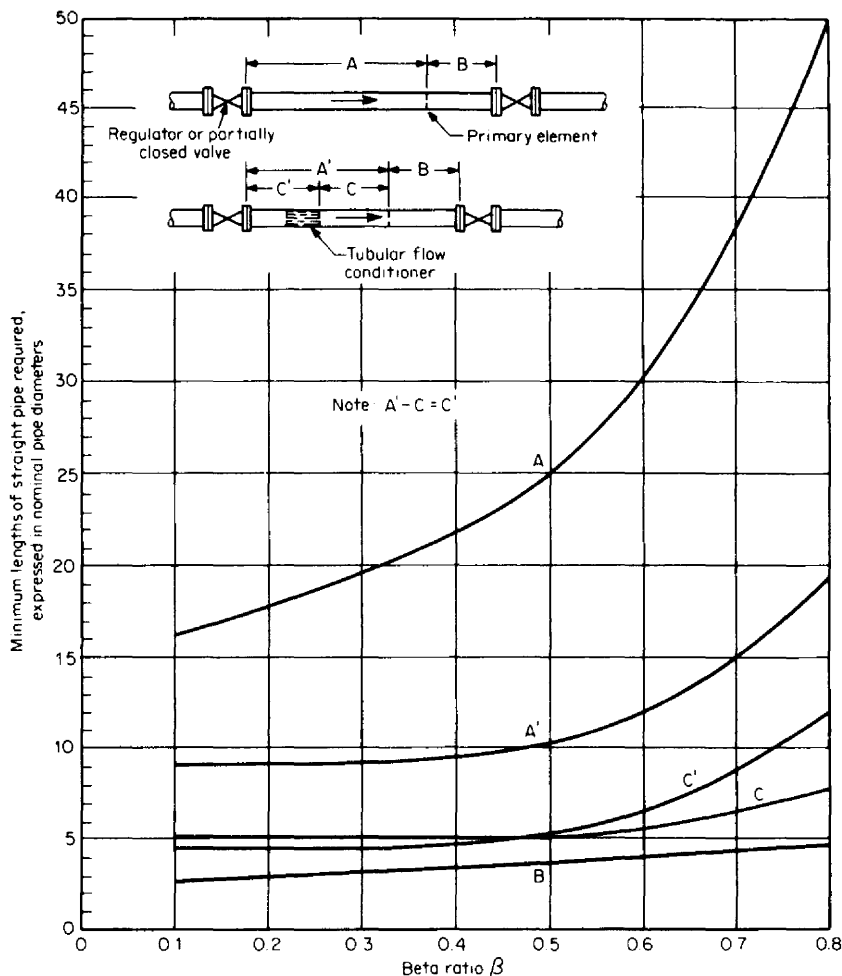
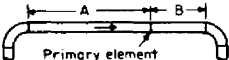
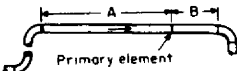
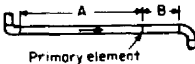
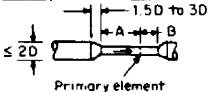


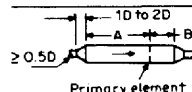
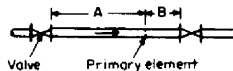
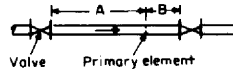
Figure 8.11 Installation lengths for primary element preceded by regulator or valve.

LEAD LINES

Lead lines connect the primary and secondary elements and transmit the process differential pressure to the secondary element. Prior to the introduction of dry-type differential-pressure transmitters, lead-line design was quite complex. Seal pots, condensation chambers, sediment chambers, and purge flows were required to ensure that volume changes within the wet-type meters would not affect the measurement or introduce sediment.

TABLE 8.1 ISO Standard 5167 Required Straight Lengths for Orifice, Nozzle, ISA Venturi Nozzle, and Venturi in Multiples of Pipe Diameter D

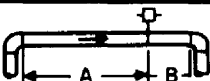
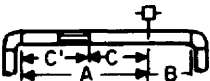
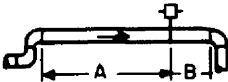
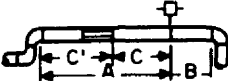
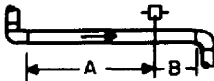
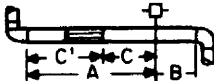
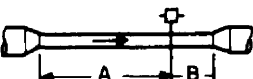

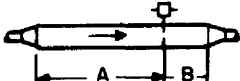
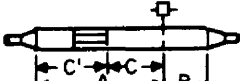
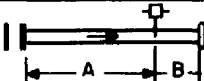
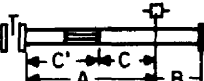
Upstream disturbance	Dimension	Device	β						
			0.2	0.3	0.4	0.5	0.6	0.7	0.75
 <p>Primary element</p>	A	Orifices Nozzles	10	10	14	14	18	28	36
Single elbow		Venturis		0.5	0.5	1.5	3	4	4.5
 <p>Primary element</p>	A	Orifices Nozzles	14	16	18	20	26	36	42
Two elbows in same plane		Venturis		1.5	1.5	2.5	3.5	4.5	4.5
 <p>Primary element</p>	A	Orifices Nozzles	34	34	36	40	48	62	70
Two elbows in different planes		Venturis†		0.5	0.5	8.5	17.5	27.5	29.5
 <p>Primary element</p>	A	Orifices Nozzles	5	5	5	6	9	14	22
Reducer		Venturis		0.5	2.5	5.5	8.5	10.5	11.5

 <p>Expander</p>	A	Orifices Nozzles	16	16	16	18	22	30	38
		Venturis		1.5	1.5	2.5	3.5	5.5	6.5
 <p>Globe valve, fully open</p>	A	Orifices Nozzles	18	18	20	22	26	32	36
		Venturis							
 <p>Gate valve, fully open</p>	A	Orifices Nozzles	12	12	12	12	14	20	24
		Venturis		1.5	2.5	3.5	4.5	5.5	5.5
Downstream length for all pictured disturbances	B	Orifices Nozzles	4	5	6	6	7	7	8
		Venturis		4d	4d	4d	4d	4d	4d

†Add ± 0.5 percent additional uncertainty.

- NOTES:
- For upstream and downstream lengths equal to one-half the values shown, add ± 0.5 percent to the accuracy values in Table 9.54.
 - Any flow conditioner shall be installed in the straight length between the primary element and the upstream disturbance, or the fitting closest to the element. The straight length between fitting and conditioner shall be at least $20D$, and the length between conditioner and element shall be at least $22D$.
 - Interpolate pipe diameters for intermediate beta ratios.

TABLE 8.2 Recommended Lengths for Annubars

Minimum diameters of straight pipe†	Upstream dimension					Downstream dimension B
	Without vanes		With vanes			
	In plane A	Out of plane A	A'	C	C'	
	7	9				3
			6	3	3	
	9	14				3
			8	4	4	
	19	24				4
			9	4	5	
	8	8				3
			8	4	4	
	8	8				3
			8	4	4	
	24	24				4
			9	4	5	

†Values shown are the recommended spacing in terms of internal diameters for normal industrial metering requirements.

Source: Dieterich Standard Corp.

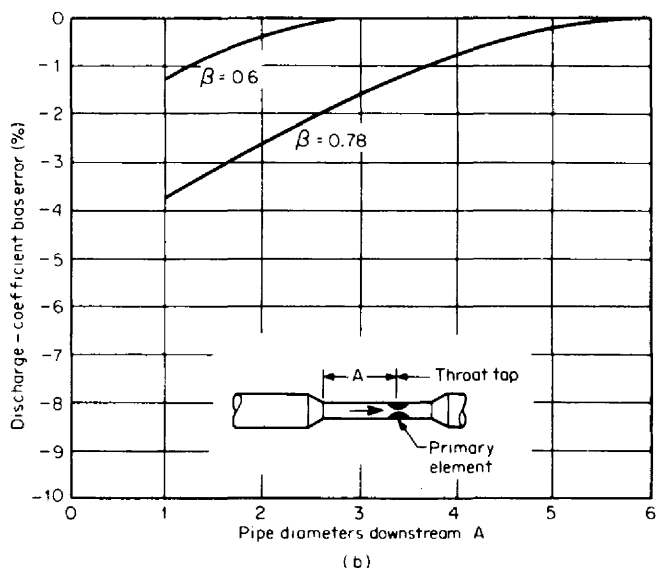
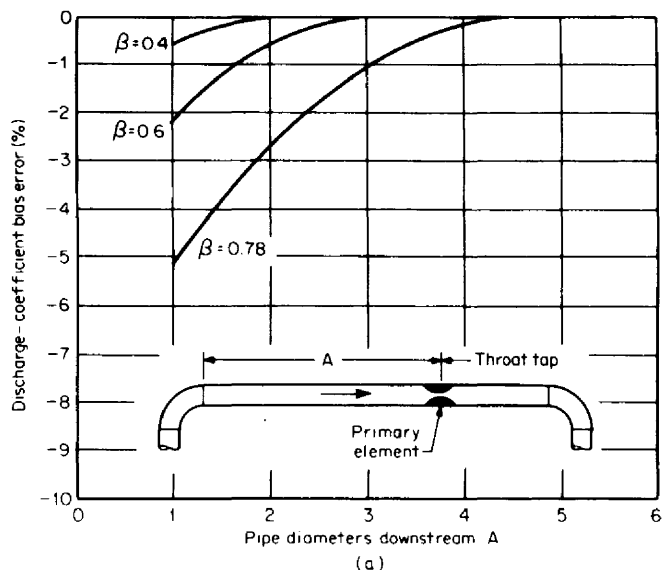


Figure 8.12 Recommended lengths for Lo-Loss tube. (Courtesy Badger Meter, Inc.) (a) Single elbow. (b) Reducer. (c) Tee.

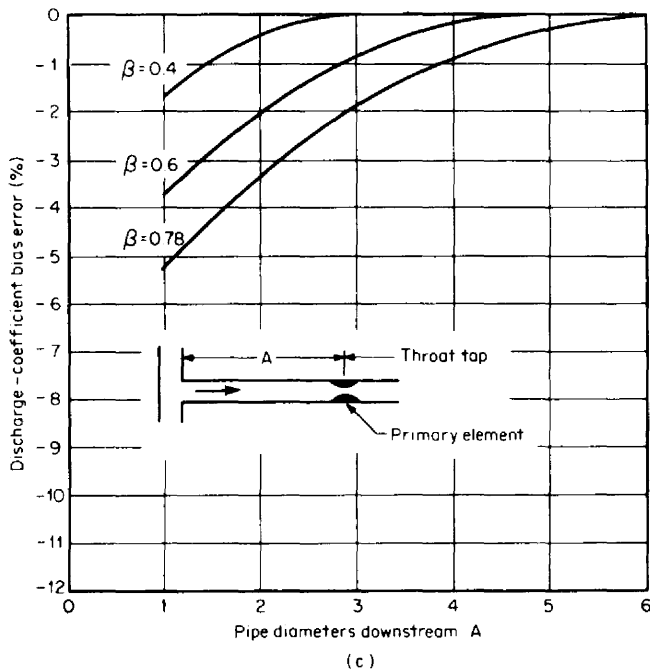


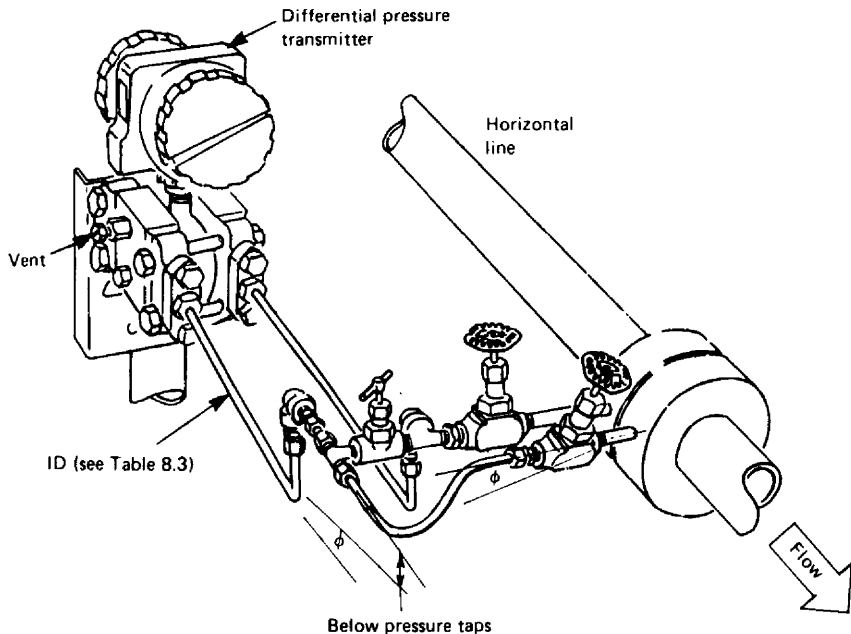
Figure 8.12 (Continued)

Dry-type meters have completely replaced mercury-filled meters in all but a few industries. The recognized hazards of mercury have led to a phasing-out program in the natural gas industry, and special safety precautions are required for laboratory use. Today many instrument manufacturers have discontinued the sale and repair of mercury-filled meters and offer only the dry type. Special high-accuracy mercury-filled manometers are still available, but these are usually used only in laboratories.

The following lead-line requirements, installation diagrams, and notes apply only to the dry-type differential transmitter. For information concerning the installation of wet-type meters, the reader is referred to ISO Standard 2186 (1973), or, for both wet and dry types, to ANSI/ASME MFC-8M (1995).

General Requirements

For liquid flows in a horizontal pipe (Figs. 8.13 and 8.14), the pressure taps should be located at the sides of the pipe, with no more than a $\pm 45^\circ$ orientation. For horizontal clean gas flows (Fig. 8.15), the pressure taps should be vertical; for vapors (steam, ammonia) and dirty or condensable gases (Fig. 8.16), the taps should



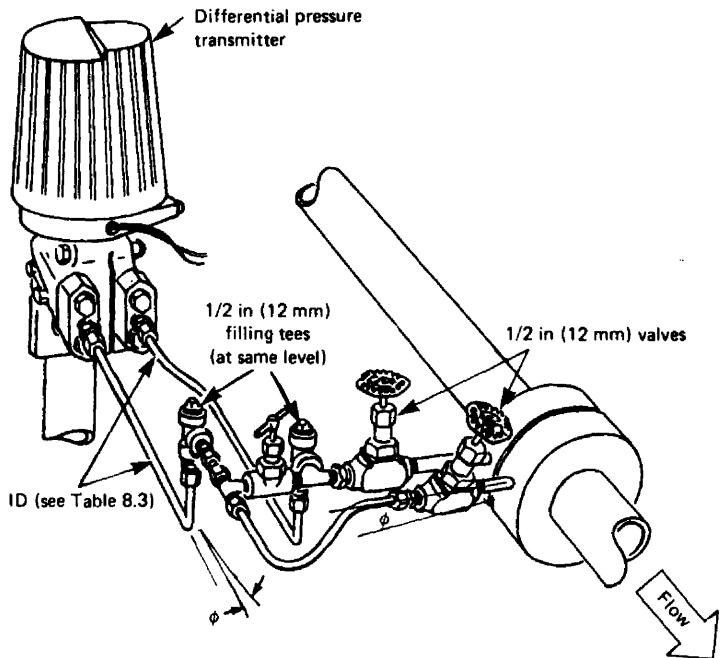
- Notes: (1) Slope upward, $\phi = 1$ in/ft (80 mm/m) for water;
 $\phi = 2$ to 4 in/ft (160 to 320 mm/m) for more viscous fluids.
 (2) Minimize all lead-line lengths.
 (3) For hot liquids, make unlagged lead lines long enough
 to minimize density changes.

Figure 8.13 Horizontal installation for clean fluids. (Courtesy The Foxboro Co.)

be located at the side. For vertical pipe installations, the pressure taps can be at any radial position around the pipe circumference (Figs. 8.17 through 8.20).

The differential-pressure transmitter should be located as close to the taps as possible. This improves the speed of response and reduces the possibility of resonance or attenuation within the leads. Prefabricated manifolds are available for easy close-coupled installation (Fig. 8.21).

Lead lines should be of the same bore, no less than 0.25 in (6 mm) in diameter for clean liquids. For condensable vapor flows, where gas bubbles may be liberated, the diameter should be no less than 0.4 in (10 mm). For long, liquid-filled lines, a gradient of 1 in/ft (80 mm/m) is recommended to allow gas bubbles to rise back into the flow line. If the fluid is of medium to high viscosity (5 to 100 cP), the slope should be increased to 2 to 4 in/ft (160 to 320 mm/m). The tubing bore should be increased to the ISO-recommended values given in Table 8.3 if long lead lines are necessary.



- Notes: (1) Slope upward, $\phi = 1$ in/ft (80 mm/m) for water;
 $\phi = 2$ to 4 in/ft (160 to 320 mm/m) for more viscous fluids.
 (2) Minimize all lead-line lengths.
 (3) For hot liquids, make unlagged lead lines long enough to minimize density changes.

Figure 8.14 Horizontal installation for dirty or corrosive fluids using a seal fluid. (Courtesy The Foxboro Co.)

The two lead lines should be close together and lagged, if necessary, to reduce density variations due to temperature differences. Any head difference between leads alters the differential, although zeroing under flowing pressure and temperature usually reduces this error.

For clean liquids and dry gases, lead lines are purged through transmitter vents. If the flowing gas or liquid must be isolated from the measuring element because of corrosion, dirt, sediment, or condensation, seal fluids are used. Several slack, flush-mounted diaphragm seals are also available for isolation.

A seal fluid serves two purposes—to isolate the process and to provide protection against freezing. The most common seal liquid for oils is a mixture of 50 percent water and 50 percent ethylene glycol or glycerine, or, for lower-temperature protection, a mixture with 60 percent ethylene glycol. The ethylene glycol mixture has a specific gravity of about 1.07; the glycerine, about 1.13. The 50 percent ethylene glycol mixture freezes at -35°F (-37°C), and the 60 percent mixture at

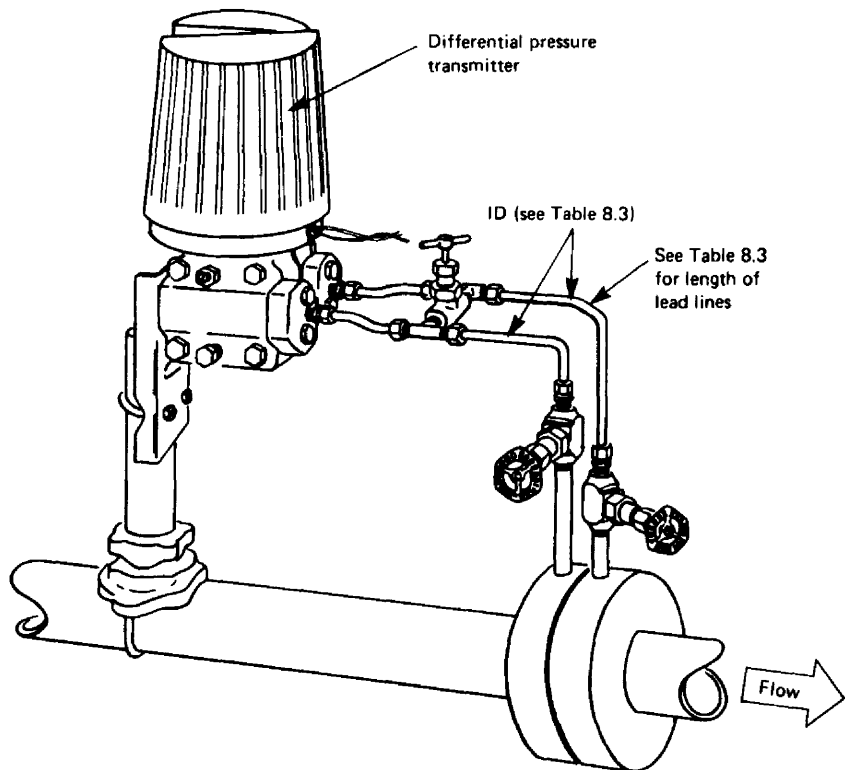


Figure 8.15 Horizontal installation for clean noncondensable gas. (Courtesy The Foxboro Co.)

-56°F (-50°C). The 50 percent glycerine mixture freezes at -9.4°F (-23°C) and the 60 percent at -56°F (-49°C).

For water and low-gravity aqueous solutions of salts and acids, dibutyl phthalate has been found highly satisfactory. Dibutyl phthalate has a specific gravity of 1.05, freezes at -31°F (-35°C), and has a boiling point of 612°F (322°C). For liquids with a specific gravity greater than 1.01 heavier seal fluids must be found. Chloronaphthalene or Halowax oil, various Arochlors, transformer sealing fluids, Kel-F oil (trifluorochloroethylene polymers), fluorolubes, and acetylene tetrabromide have been used, but many are toxic, highly viscous, or have other disadvantages. No really satisfactory sealing medium for large displacement secondary elements (wet-type meters) has been found for materials such as concentrated sulfuric acid, although lighter oils, such as Nujol or other acid and caustic treated oils, have been used. Use of an oil lighter than the flowing fluid introduces serious maintenance problems.

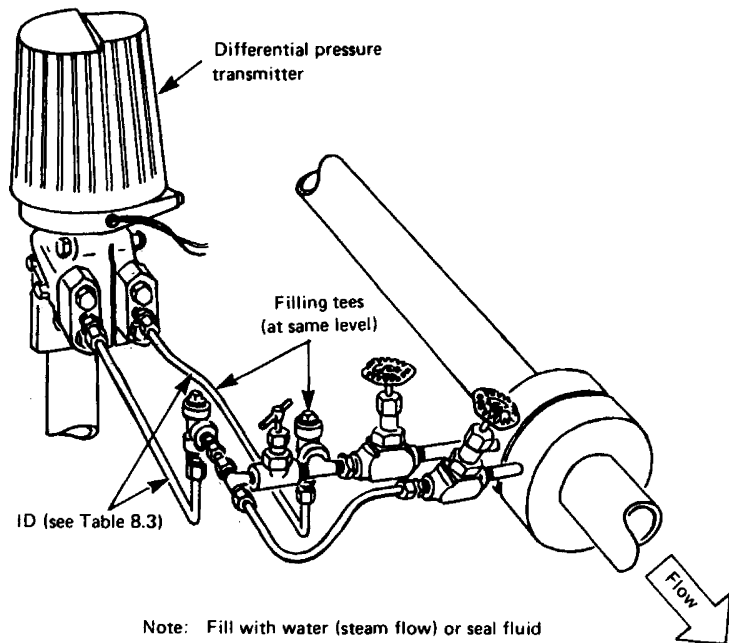


Figure 8.16 Horizontal installation for vapor (steam) or dirty or condensable gases. (Courtesy The Foxboro Co.)

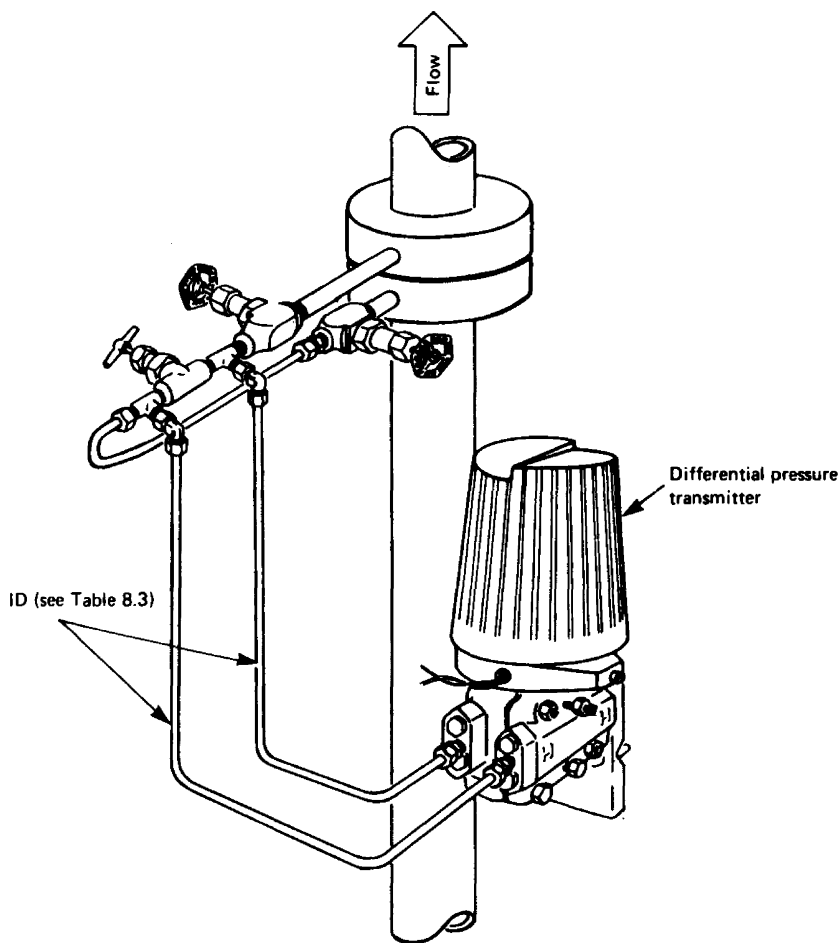
TABLE 8.3 Recommended Minimum Internal Diameters of Lead Lines

Lead-line length, ft	Fluid being metered			
	Water, steam, dry gas	Wet gas	Low- to medium-viscosity fluids	Dirty liquids or gases†
To 50	0.25 in (6 mm)	0.375 in (9 mm)	0.5 in (12.5 mm)	1.0 in (25 mm)
50–135‡	0.25 in (6 mm)	0.375 in (9 mm)	0.75 in (18.8 mm)	1.0 in (25 mm)
135–270	0.50 in (12.5 mm)	0.50 in (12.5 mm)	1.0 in (25 mm)	1.5 in (38 mm)

†Without seal fluid.

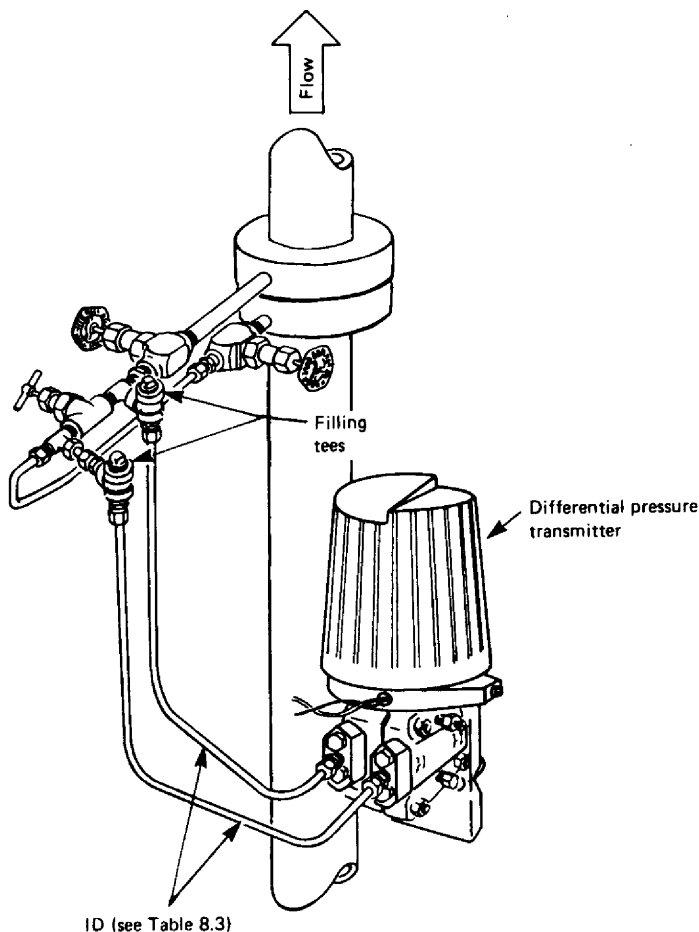
‡Lengths longer than 50 ft are not usually recommended and should be used only when absolutely necessary.

Source: ISO 2186 (1973).



Note: For temperature above 250°F (121°C),
lag leads to pipe.

Figure 8.17 Vertical installation for clean liquids. (Courtesy The Foxboro Co.)



- Notes: (1) Two filling tees must be at the same elevation as the high-pressure tap.
 (2) For temperatures above 250°F (121°C), lag leads to pipe.
 (3) Flow upward for liquids containing appreciable amounts of gas.
 (4) Flow downward if liquid contains small amounts of granular solids.

Figure 8.18 Vertical installation for dirty or corrosive liquids. (Courtesy The Foxboro Co.)

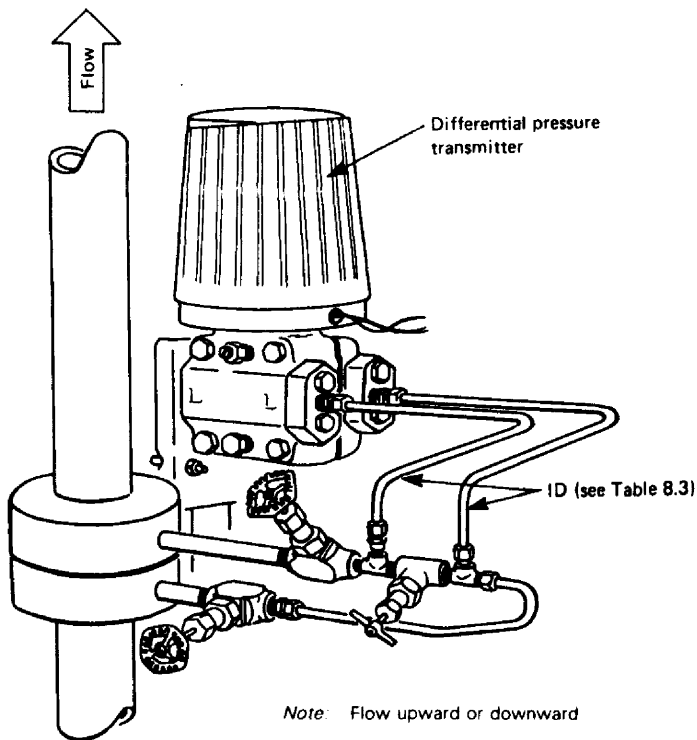
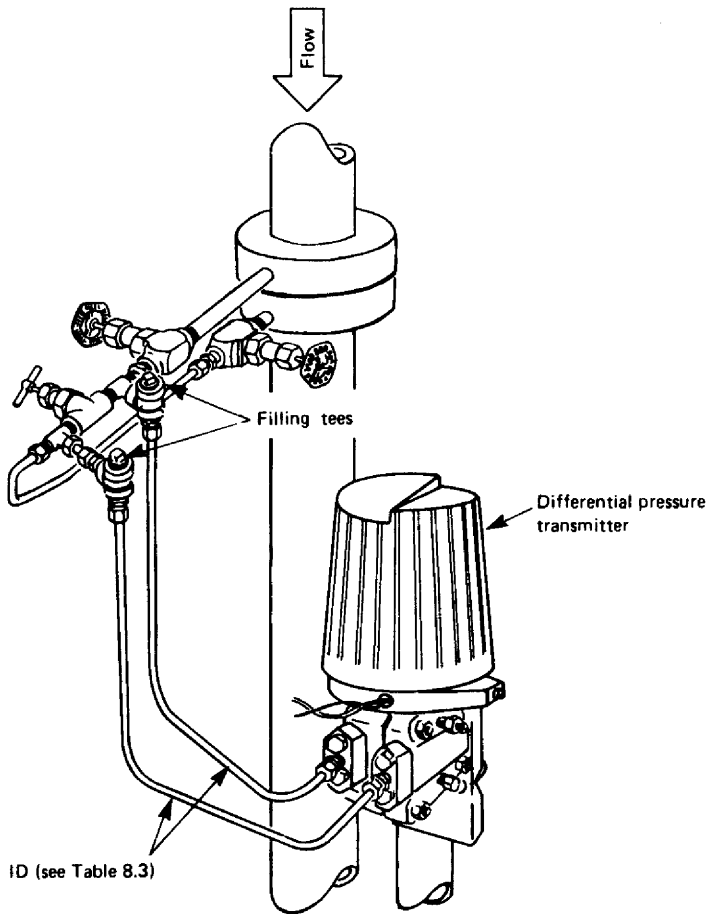


Figure 8.19 Vertical installation for clean noncondensable gases. (Courtesy The Foxboro Co.)

Pressure Taps

For gas and vapor flows a pressure-tap connection is required if a pressure compensation is to be made. The precautions outlined for the differential-pressure connection should be followed. The pressure transmitter is usually connected via a tee to either the upstream or downstream pressure lead line.

The tap selected depends on whether an upstream or downstream gas expansion factor is to be calculated. A second pressure tap is recommended when using meters that have a sizable change in volume as the differential increases (bellows, manometer type, etc.). The presence of pulsations, or severe line noise, may result in *cross talk* between the differential-pressure and pressure meters that can result in errors in both measurements.



Note: Fill with water (steam flow) or seal fluid for dirty or condensable gases.

Figure 8.20 Vertical installation for vapor (steam), condensable gases, or dirty gases. (Courtesy The Foxboro Co.)

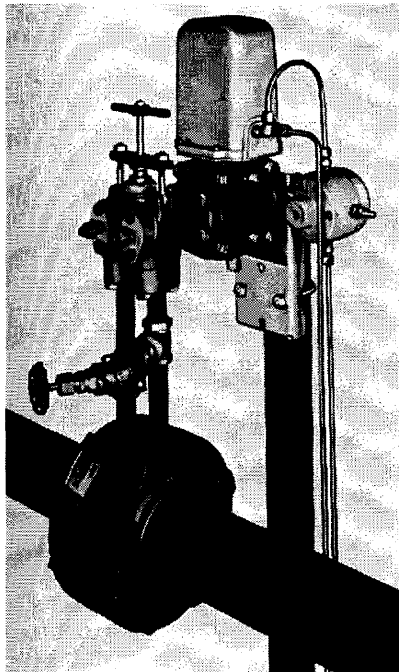


Figure 8.21 Valving manifold. (Courtesy The Foxboro Co.)

REFERENCES

- ANSI/ASME MFC-8M, *Measurement of Fluid Flow in Closed Conduits—Connections for Pressure Signal Transmission Between Primary and Secondary Devices*, ANSI, New York, 1995.
- ANSI/API 2530, *Orifice Metering of Natural Gas*, catalog no. XQ0178, American Gas Association, Arlington, Va., 1991.
- ASME: *Fluid Meters*, 6th ed., ASME, New York, 1971.
- ASME: "An FFEC Probe," *Mech. Eng.*, p. 55, August 1985.
- ASME MFC-3M, *Measurement of Fluid Flow in Pipes Using Orifice, Nozzle, and Venturi*, ASME, New York, 1995.
- ISO Standard 2186, *Fluid Flow in Closed Conduits—Connections for Pressure Signal Transmissions between Primary and Secondary Elements*, ISO 2186-1973, Geneva, 1973.
- ISO Standard 5167, *Measurement of Fluid Flow by Means of Plates, Nozzles and Venturi Tubes Inserted in Circular Cross-Section Conduits Running Full*, ISO 5167-1980(E), Geneva, 1991.

DIFFERENTIAL PRODUCERS: ENGINEERING EQUATIONS

The sizing and flow-rate equations for all differential producers are identical. They are developed from theoretical assumptions, modified by correction factors based on empirical evidence, and further altered based on geometric considerations relative to fixed-geometry devices. This chapter develops the engineering equations and presents them in tables for ease in preparing computer programs.

THEORETICAL FLOW-RATE EQUATIONS

Liquid Equation

The dynamic equation for *one-dimensional* flow of incompressible fluids is derived by applying Newton's second law to the fluid element shown in Fig. 9.1a. The sum of the three forces in the direction of flow is equated to the mass of the element times its acceleration.

The external forces acting on the fluid element in the direction of flow are:

1. The net driving force produced by the static pressure acting over the element's upstream and downstream areas
2. The body force (weight) for a nonhorizontal element
3. The viscous shear stress that acts on the circumference of the element

These forces are expressed in differential form, using the English engineering system of units, as

$$-\frac{\partial P_f}{\partial S} dS \, dA \quad (9.1)$$

for the net pressure force,

$$-\rho_f \frac{g_l}{g_c} dS dA \frac{\partial H}{\partial S} \quad (9.2)$$

for the body force, and

$$-2\pi r S_s dS \quad (9.3)$$

for the viscous shear force, where the minus signs indicate that pressure is decreasing in the direction of flow, the shear stress opposes the motion, and the body force is decreasing because of the elevation change. Applying Newton's second law of motion to the fluid element yields

$$-\frac{\partial P_f}{\partial S} dS dA - \rho_f \frac{g_l}{g_c} dS dA \frac{\partial H}{\partial S} - 2\pi r S_s dS = \frac{\rho_f}{g_c} dS dA a_s \quad (9.4)$$

with

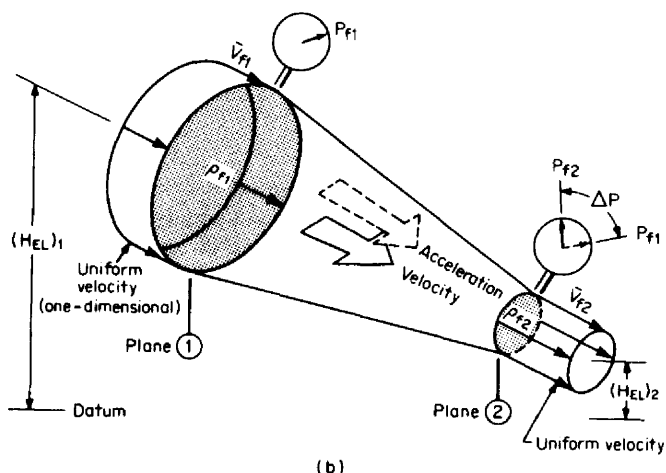
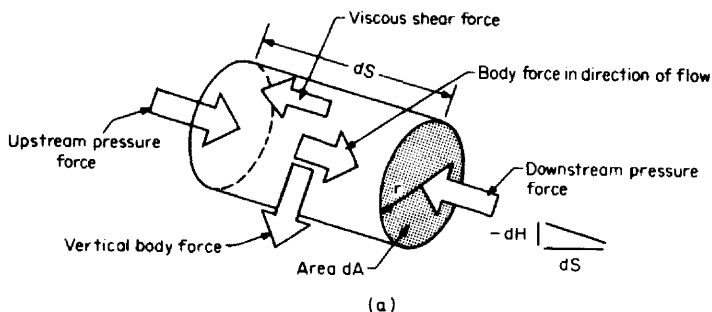


Figure 9.1 Incompressible fluid flow (liquid). (a) Streamline element. (b) Bernoulli's equation applied to the differential producer.

$$a_s = \frac{\partial}{\partial S} \left(\frac{\bar{V}_f^2}{2} \right)$$

this becomes, for a nonviscous fluid,

$$-\frac{\partial P_f}{\partial S} - \rho_f \frac{g_l}{g_c} \frac{\partial H}{\partial S} = \frac{\rho_f}{g_c} \frac{\partial}{\partial S} \left(\frac{\bar{V}_f^2}{2} \right) \quad (9.5)$$

The dynamic equation for one-dimensional flow per unit of fluid mass is obtained by dividing Eq. (9.5) by the mass density:

$$-\frac{1}{\rho_f} \frac{\partial P_f}{\partial S} - \frac{g_l}{g_c} \frac{\partial H}{\partial S} = \frac{1}{g_c} \frac{\partial}{\partial S} \left(\frac{\bar{V}_f^2}{2} \right) \quad (9.6)$$

This is known as *Euler's equation*.

Assuming constant density and integrating Eq. (9.6) along the streamline yield *Bernoulli's equation*:

$$\frac{P_f}{\rho_f} + \frac{\bar{V}_f^2}{2g_c} + \frac{g_l}{g_c} H_{EL} = \text{constant} \quad (9.7)$$

$$\frac{\text{ft} \cdot \text{lb}_f}{\text{lb}_m} + \frac{\text{ft} \cdot \text{lb}_f}{\text{lb}_m} + \frac{\text{ft} \cdot \text{lb}_f}{\text{lb}_m} = \text{constant}$$

Equation (9.7) is written in terms of energy per unit mass, and it indicates that *the energy along a streamline remains constant for an incompressible, nonviscous fluid*.

Bernoulli's equation can also be written for *specific weight* instead of mass density. With

$$\gamma_f = \frac{g_l}{g_c} \rho_f \quad \frac{\text{lb}_f}{\text{ft}^3}$$

Equation (9.7) becomes

$$\frac{P_f}{\gamma_f} + \frac{\bar{V}_f^2}{2g_l} + H_{EL} = \text{constant} \quad (9.8)$$

$$\text{ft} + \text{ft} + \text{ft} = \text{constant}$$

Each term in Eq. (9.8) has the dimensions of feet and, therefore, is a *head*. In some literature, the head equation (9.8) is used to develop the engineering equations, which is the reason for the name *head-class* meters.

The two forms of Bernoulli's equation are equally valid. Note, however, that density values taken from tables or derived from equations must be in units of pounds-mass per cubic foot and, therefore, must be corrected for local gravity.

In the SI system of units, Bernoulli's equation is written as

$$\frac{P_f^*}{\rho_f^*} + \frac{\bar{V}_f^{*2}}{2} + g_l^* H_{EL}^* = \text{constant} \quad (9.9)$$

$$\frac{\text{kg} \cdot \text{m}^2/\text{s}^2}{\text{kg}} + \frac{\text{kg} \cdot \text{m}^2/\text{s}^2}{\text{kg}} + \frac{\text{kg} \cdot \text{m}^2/\text{s}^2}{\text{kg}} = \text{constant}$$

$$\frac{J^*}{\text{kg}} + \frac{J^*}{\text{kg}} + \frac{J^*}{\text{kg}} = \text{constant}$$

Here, the unit of pressure is the pascal, the unit of velocity is the meter per second, the unit for local gravity is the meter per second per second, and the unit of elevation is the meter.

Figure 9.1*b* shows Bernoulli's equation as it applies to a converging stream tube. The density is constant at all sections, the velocity is uniform across each section, and the sum of the pressure energy, kinetic energy, and potential energy is constant. For steady flow, the velocity increases because of the area reduction from plane 1 to plane 2. To maintain an energy balance, the pressure energy is reduced and the kinetic energy is increased. If pressure measurements were made at the two locations, the downstream static pressure would be lower than the upstream pressure. Applying Bernoulli's energy equation between locations 1 and 2 gives

$$\frac{P_{f1}}{\rho_f} + \frac{\bar{V}_{f1}^2}{2g_c} + \frac{g_l}{g_c} (H_{EL})_1 = \frac{P_{f2}}{\rho_f} + \frac{\bar{V}_{f2}^2}{2g_c} + \frac{g_l}{g_c} (H_{EL})_2 \quad (9.10)$$

In practice, the elevation difference between pressure taps is corrected for by bringing the upstream and downstream lead lines to a differential-pressure measuring device that senses both pressures at a common elevation (see Sec. A.2). For a constant-density fluid, this reduces Eq. (9.10) to the form

$$\frac{P_{f1} - P_{f2}}{\rho_f} = \frac{\bar{V}_{f2}^2 - \bar{V}_{f1}^2}{2g_c} \quad (9.11)$$

Equation (9.11) is reduced to flow-rate units by applying the mass flow continuity equation between planes 1 and 2. This mass balance simply states that the mass of fluid entering plane 1 equals the mass leaving at plane 2 and stays within the confines of the stream tube; mathematically,

$$q_{PPS} = \rho_{f1} A_1 \bar{V}_{f1} = \rho_{f2} A_2 \bar{V}_{f2} \quad (9.12)$$

$$\text{lb}_m/\text{s} = \text{lb}_m/\text{s} = \text{lb}_m/\text{s}$$

and for a constant-density fluid

$$q_{cfs} = A_1 \bar{V}_{f1} = A_2 \bar{V}_{f2} \quad (9.13)$$

$$\text{ft}^3/\text{s} = \text{ft}^3/\text{s} = \text{ft}^3/\text{s}$$

Substituting Eq. (9.13) into Eq. (9.11) yields

$$\frac{P_{f1} - P_{f2}}{\rho_f} = \frac{[1 - (A_2/A_1)^2] \bar{V}_{f2}^2}{2g_c} \quad (9.14)$$

If planes 1 and 2 are circular, with pipe and bore diameters at flowing temperature of D_F and d_F in feet, Eq. (9.14) can be rewritten as

$$\frac{P_{f1} - P_{f2}}{\rho_f} = \frac{[1 - (d_F/D_F)^4] \bar{V}_f^{*2}}{2g_c} \quad (9.15)$$

Rearranging Eq. (9.12) to solve for the velocity at plane 2 in terms of the mass flow rate yields

$$\bar{V}_{f2} = \frac{q_{PPS}}{\rho_f A_2} = \frac{q_{PPS}}{\pi/4 d_F^2 \rho_f} \quad (9.16)$$

The theoretical mass flow rate equation for the differential producer is obtained by substituting Eq. (9.16) into Eq. (9.15) and rearranging to obtain

$$(q_{PPS})_{\text{theo}} = \sqrt{2g_c} \frac{\pi}{4} d_F^2 \sqrt{\frac{1}{1 - (d_F/D_F)^4}} \sqrt{\Delta P \rho_f} \quad (9.17)$$

The units in this equation are pounds-force, pounds-mass, feet, and seconds (English engineering system). With differential pressure in inches of water as defined by Eq. (3.22), and diameters D and d at flowing conditions in inches, the mass flow equation becomes

$$(q_{PPS})_{\text{theo}} = 0.09970190 \frac{d^2}{\sqrt{1 - (d/D)^4}} \sqrt{h_w \rho_f} \quad (9.18)$$

where the dimensional constant is exactly

$$\frac{\pi}{4} \left(\frac{1}{12} \right)^2 \left[\frac{2g_c(\rho_w)_{68^\circ\text{F}}}{12} \right]^{1/2} = 0.09970190 \text{ lb}_m^{1/2} \cdot \text{ft}^{3/2} \cdot \text{in}^{-5/2} \cdot \text{s}^{-1} \quad (9.19)$$

A similar derivation using the SI equation (9.9) yields

$$(q_{KPS}^*)_{\text{theo}} = \frac{\pi}{4} \sqrt{2} \frac{d_M^2}{\sqrt{1 - (d_M/D_M)^4}} \sqrt{\Delta P^* \rho_f^*} \quad (9.20)$$

With differential pressure in kilopascals and flowing conditions diameters D^* and d^* in millimeters, Eq. (9.20) becomes

$$(q_{KPS}^*)_{\text{theo}} = 3.512407 \times 10^{-5} \frac{d^{*2}}{\sqrt{1 - (d^*/D^*)^4}} \sqrt{\Delta P^* \rho_f^*} \quad (9.21)$$

where the constant is exactly

$$\frac{\pi}{4} \sqrt{2} \frac{\sqrt{1000}}{(1000)^2} = 3.512407 \times 10^{-5} \text{ kg}^{1/2} \cdot \text{m}^{3/2} \cdot \text{mm}^{-2} \cdot \text{kPa}^{-1/2} \cdot \text{s}^{-1} \quad (9.22)$$

The theoretical volumetric flow rate, in cubic feet per second at flowing conditions, is obtained as

$$(q_{\text{cfs}})_{\text{theo}} = \frac{q_{\text{PPS}}}{\rho_f} = 0.09970190 \frac{d^2}{\sqrt{1 - (d/D)^4}} \sqrt{\frac{h_w}{\rho_f}} \quad (9.23)$$

and, in SI units of cubic meters per second, as

$$(q_{\text{cms}}^*)_{\text{theo}} = \frac{q_{\text{KPS}}^*}{\rho_f^*} = 3.512407 \times 10^{-5} \frac{d^{*2}}{\sqrt{1 - (d^*/D^*)^4}} \sqrt{\frac{\Delta p^*}{\rho_f^*}} \quad (9.24)$$

Gas (Vapor) Equation

For gas (vapor) flows, the fluid density is not constant between planes 1 and 2 of Fig. 9.1b. As the gas pressure decreases to accommodate the increase in kinetic energy, the density decreases, and the assumption of constant density no longer applies. Only for very low differential pressures will Eq. (9.18) or (9.21) apply with any degree of accuracy.

To correct the equation for gas expansion, a *gas expansion factor* is developed from the thermodynamic steady-flow energy equation. This equation is, for U.S. units,

$$\mathbf{Q} - \mathbf{W} = J(u_2 - u_1) + \frac{P_{f2}}{\rho_{f2}} - \frac{P_{f1}}{\rho_{f1}} + \frac{\bar{V}_{f2}^2 - \bar{V}_{f1}^2}{2g_c} + \frac{g_l}{g_c} (H_{EL2} - H_{EL1}) \quad (9.25)$$

This equation expresses the energy balance between planes 1 and 2. For an adiabatic process, with no work \mathbf{W} entering or leaving the system, and for no elevation difference, Eq. (9.25) reduces to

$$\frac{\bar{V}_{f2}^2 - \bar{V}_{f1}^2}{2g_c} = e_1 - e_2 = - \int_{P_{f1}}^{P_{f2}} \frac{dP}{\rho} \quad (9.26)$$

where $e_1 - e_2$ is the enthalpy difference between measuring planes. The integral is evaluated by assuming an isentropic expansion from plane 1 to plane 2, expressed by

$$P \left(\frac{1}{\rho} \right)^k = \text{constant} \quad (9.27)$$

Upon integration, Eq. (9.26) yields

$$e_1 - e_2 = \int_{P_{f1}}^{P_{f2}} \frac{dP}{\rho} = \frac{P_{f1}}{\rho_{f1}} \frac{k}{k-1} \left[1 - \left(\frac{P_{f2}}{P_{f1}} \right)^{(k-1)/k} \right] \quad (9.28)$$

Substituting this equation into Eq. (9.26) and using mass flow continuity yields the form of the *theoretical adiabatic mass flow equation*. In U.S. units this is

$$(q_{\text{PPS}})_{\text{theo}} = 0.09970190 \frac{Y_1 d^2}{\sqrt{1 - (d/D)^4}} \sqrt{h_w \rho_{f1}} \quad (9.29)$$

where the Y_1 is the *adiabatic gas expansion factor* defined by

$$Y_1 = \left\{ \frac{[1 - (d/D)^4][k/(k-1)](p_{f2}/p_{f1})^{2/k}[1 - (p_{f2}/p_{f1})^{(k-1)/k}]}{[1 - (d/D)^4(p_{f2}/p_{f1})^{2/k}](1 - p_{f2}/p_{f1})} \right\}^{1/2} \quad (9.30)$$

The value of Y_1 depends on the ratio of diameters, the isentropic exponent, and the ratio between the measured downstream and upstream pressures. Equation (9.29) is, therefore, a dimensionless equation that may be written in SI units as

$$(q_{\text{KPS}})_{\text{theo}} = 3.512407 \times 10^{-5} \frac{Y_1 d^{*2}}{\sqrt{1 - (d^*/D^*)^4}} \sqrt{\Delta p^* \rho_{f1}^*} \quad (9.31)$$

For volumetric units in actual cubic feet per second, the equation becomes

$$(q_{\text{acfs}})_{\text{theo}} = \frac{q_{\text{PPS}}}{\rho_f} = 0.09970190 \frac{Y_1 d^2}{\sqrt{1 - (d/D)^4}} \sqrt{\frac{h_w}{\rho_{f1}}} \quad (9.32)$$

And in the SI system, in actual cubic meters per second, Eq. (9.29) becomes

$$(q_{\text{acms}}^*)_{\text{theo}} = 3.512407 \times 10^{-5} \frac{Y_1 d^{*2}}{\sqrt{1 - (d^*/D^*)^4}} \sqrt{\frac{\Delta p^*}{\rho_{f1}^*}} \quad (9.33)$$

By suitable algebraic manipulation, the steady-flow energy equation for compressible flow has thus been rearranged into the form of the incompressible mass flow equation. The single difference is that the compressible-flow equation contains the additional factor Y_1 . In both U.S. and SI units, the equation requires the determination of the upstream density (at plane 1); hence, when the pvT relationship is used to calculate density, the assumption is that the pressure, temperature, and compressibility are determined there as well. When a densitometer is used, the density and pressure at the upstream tap location are required.

To solve for the adiabatic gas expansion factor, the ratio of downstream to upstream pressure is required. For an upstream tap location, this ratio is calculated from the measured differential as

$$\frac{p_{f2}}{p_{f1}} = \frac{p_{f2}^*}{p_{f1}^*} = 1 - x_1 \quad (9.34)$$

where

$$x_1 = \frac{p_{f1} - p_{f2}}{p_{f1}} = \frac{\Delta p^*}{p_{f1}^*} = \frac{h_w}{27.73 p_{f1}} \quad (9.35)$$

When the downstream pressure is measured, this ratio is calculated from the measured downstream tap pressure, and the flow equation must be rewritten for a density determination at that location. With mass flow continuity between locations 1 and 2, this equation is

$$(q_{\text{PPS}})_1 = (q_{\text{PPS}})_2 \propto Y_1 \sqrt{h_w \rho_{f1}} = Y_2 \sqrt{h_w \rho_{f2}} \quad (9.36)$$

which, for the same differential pressure h_w becomes

$$Y_1^2 \rho_{f1} = Y_2^2 \rho_{f2} \quad (9.37)$$

Substituting the pvT density equation (2.10) into Eq. (9.37) yields

$$Y_2 = Y_1 \left(\frac{p_{f1}}{p_{f2}} \frac{Z_{f2}}{Z_{f1}} \frac{T_{f2}}{T_{f1}} \right)^{1/2} \quad (9.38)$$

The ratio of compressibility factors Z_{f2}/Z_{f1} could be calculated using the Redlich-Kwong extrapolation method presented in Chap. 2 or from available data. However, for most applications, the differential pressure is small compared to the static pressure, and the compressibility change and temperature change during expansion may be assumed to be negligible. This reduces Eq. (9.38) to

$$Y_2 = Y_1 \left(\frac{p_{f1}}{p_{f2}} \right)^{1/2} = Y_1 \left(\frac{p_{f1}^*}{p_{f2}^*} \right)^{1/2} = Y_1 \sqrt{\frac{1}{1-x_1}} = Y_1 \sqrt{1+x_2} \quad (9.39)$$

where

$$x_2 = \frac{p_{f1} - p_{f2}}{p_{f2}} = \frac{\Delta p^*}{p_{f2}^*} = \frac{h_w}{27.73 p_{f2}} \quad (9.40)$$

The mass flow equation for downstream tap measurements is then

$$(q_{PPS})_{\text{theo}} = 0.09970190 \frac{Y_2 d^2}{\sqrt{1 - (d/D)^4}} \sqrt{h_w \rho_{f2}} \quad (9.41)$$

for U.S. units, and

$$(q_{KPS}^*)_{\text{theo}} = 3.512407 \times 10^{-5} \frac{Y_2 d^{*2}}{\sqrt{1 - (d^*/D^*)^4}} \sqrt{\Delta p^* \rho_{f2}^*} \quad (9.42)$$

for SI units, where Y_2 is defined by Eq. (9.39), and the pressure ratio is derived from the downstream pressure as

$$\frac{p_{f2}}{p_{f1}} = \frac{p_{f2}^*}{p_{f1}^*} = \frac{1}{1+x_2} \quad (9.43)$$

The volumetric flow in actual cubic feet per second is, similarly,

$$(q_{acfs})_{\text{theo}} = \frac{q_{PPS}}{\rho_{f2}} = 0.09970190 \frac{Y_2 d^2}{\sqrt{1 - (d/D)^4}} \sqrt{\frac{h_w}{\rho_{f2}}} \quad (9.44)$$

and in SI units it is

$$(q_{acms}^*)_{\text{theo}} = \frac{q_{KPS}^*}{\rho_{f2}^*} = 3.512407 \times 10^{-5} \frac{Y_2 d^{*2}}{\sqrt{1 - (d^*/D^*)^4}} \sqrt{\frac{\Delta p^*}{\rho_{f2}^*}} \quad (9.45)$$

CORRECTIONS TO THE THEORETICAL EQUATIONS

The theoretical flow equation calculates the true flow rate only when all the assumptions used to develop it are valid. This is seldom the case, and the true flow rate is almost always less than the theoretically calculated value.

How closely the true flow rate can be calculated depends almost entirely on the geometry of the contraction. For a venturi or flow nozzle, where the area reduction is gradual (Fig. 9.2a), the agreement is within 1 to 3 percent. But for the square-edged orifice (Fig. 9.2b), the abrupt area reduction places the minimum-flow area a downstream of the plate at the plane of the vena contracta. Since the diameter of the vena contracta for an orifice cannot be measured, the theoretical equation includes the measured bore as the correlating diameter. Also, increased downstream turbulence results in an energy loss that is not accounted for by either Bernoulli's equation or the thermodynamic steady flow energy equation. These two factors result in the true flow being approximately 60 percent of the theoretically calculated value. The location of the two measuring taps is also important because it establishes the measured differential.

For both contoured and abrupt reductions, the assumption that the velocity profile is uniform is valid only at very high Reynolds numbers (see Chap. 5). With decreasing velocity or increasing viscosity, the Reynolds number decreases and the profile becomes more peaked, resulting in a further departure from the assumption of a rectilinear or one-dimensional profile. Expansion approaches the adiabatic as-

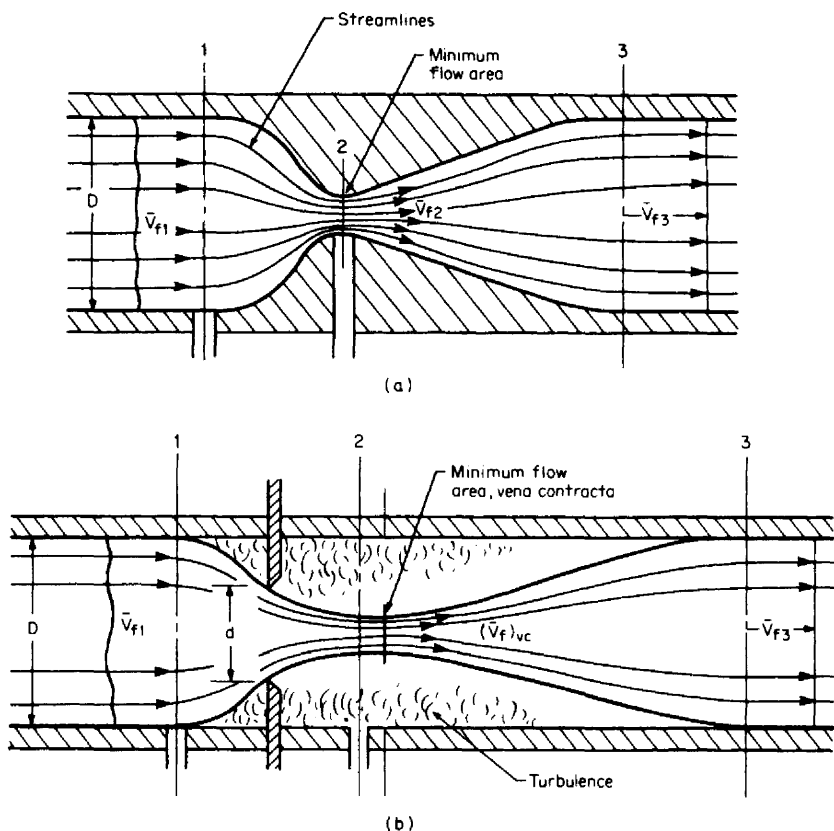


Figure 9.2 Contraction types. (a) Gradual. (b) Abrupt.

sumption for contoured elements, but not for the abrupt flow-streamline changes across an orifice, where both radial and axial expansion occur.

The theoretical equation is adjusted for these effects with two empirically determined corrections. The first is the *discharge coefficient* C , which corrects for velocity profile (Reynolds number), tap location, and contraction geometry; the second is an empirically derived *net expansion-factor equation* for orifice flowmeters.

Discharge Coefficient

For a given primary element, the discharge coefficient is derived from laboratory data by ratioing the true and theoretical flow rates. The true flow rate is determined by weighing or volumetric collection of the fluid over a measured time interval, and the theoretical flow rate is calculated with Eq. (9.18). The discharge coefficient is then defined as

$$C = \frac{\text{true flow rate}}{\text{theoretical flow rate}} \quad (9.46)$$

The discharge coefficient corrects the theoretical equation for the influence of velocity profile (Reynolds number), the assumption of no energy loss between taps, and pressure-tap location.

In some flow equations, the discharge coefficient is combined with the velocity of approach and redefined as the *flow coefficient*. For fixed-geometry primary devices, to simplify the equation, or where primary elements are available in a limited range of sizes, the flow coefficient is used in place of the discharge coefficient. The flow coefficient is defined as

$$K = \frac{C}{\sqrt{1 - (d/D)^4}} = \frac{C}{\sqrt{1 - (d^*/D^*)^4}} = \frac{C}{\sqrt{1 - \beta^4}} = EC \quad (9.47)$$

where $\beta = d/D$ and $E = 1/\sqrt{1 - \beta^4}$ is the velocity of approach factor.

Methods of Presenting the Discharge Coefficient

The discharge coefficient may be presented in four different ways:

Method 1. A discharge coefficient-Reynolds number curve, similar to Fig. 9.3a, is obtained from laboratory data. This is the most accurate method, since all dimensional effects and other influences on the primary device are included in the data points.

Method 2. A signature curve based on calibration data for many devices of the same geometry is given with an accuracy envelope (Fig. 9.3b). The flow coefficient is obtained graphically by reading the coefficient at the pipe Reynolds number.

Method 3. The flow coefficient for a fixed-geometry device is ratioed to a constant K_{ref} , which is usually the flow coefficient at a high Reynolds number (Fig. 9.3c). This ratio,

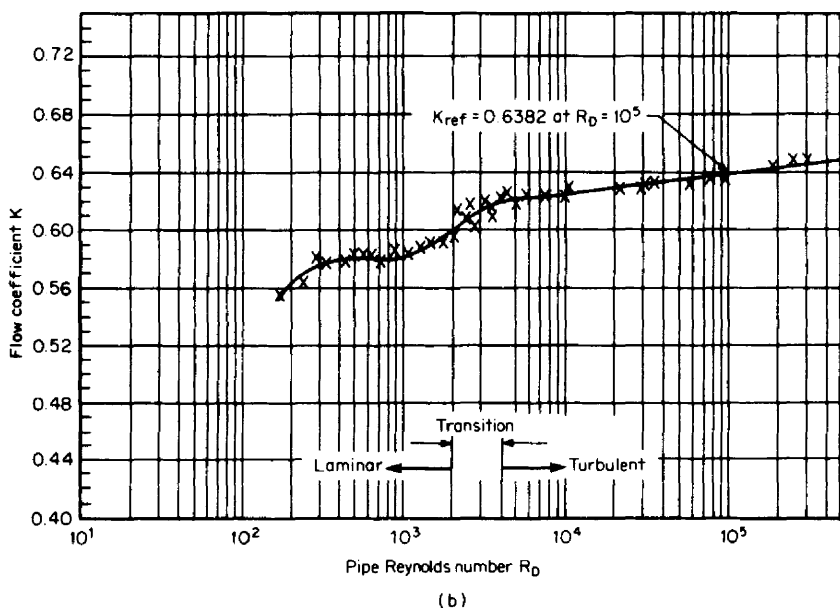
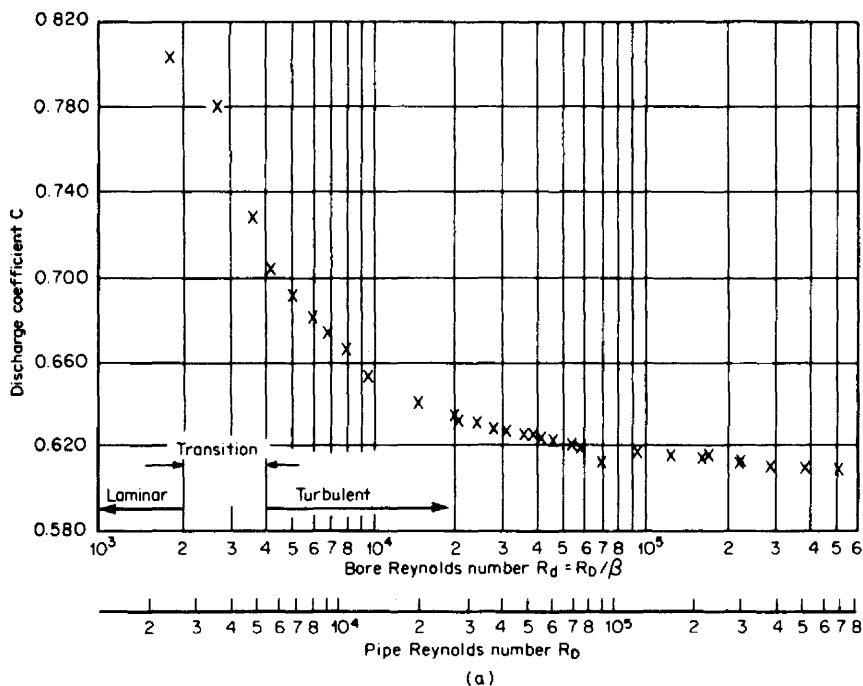


Figure 9.3 Methods of graphically presenting discharge- or flow-coefficient variations with pipe Reynolds number. (a) Flow-laboratory-determined orifice discharge coefficient $D = 4$ in (100 mm), $\beta = 0.73$. (b) Generalized flow-coefficient curve for a target flowmeter. (c) Reynolds-number correction factor F_K derived from part b. (d) Orifice discharge-coefficient curves.

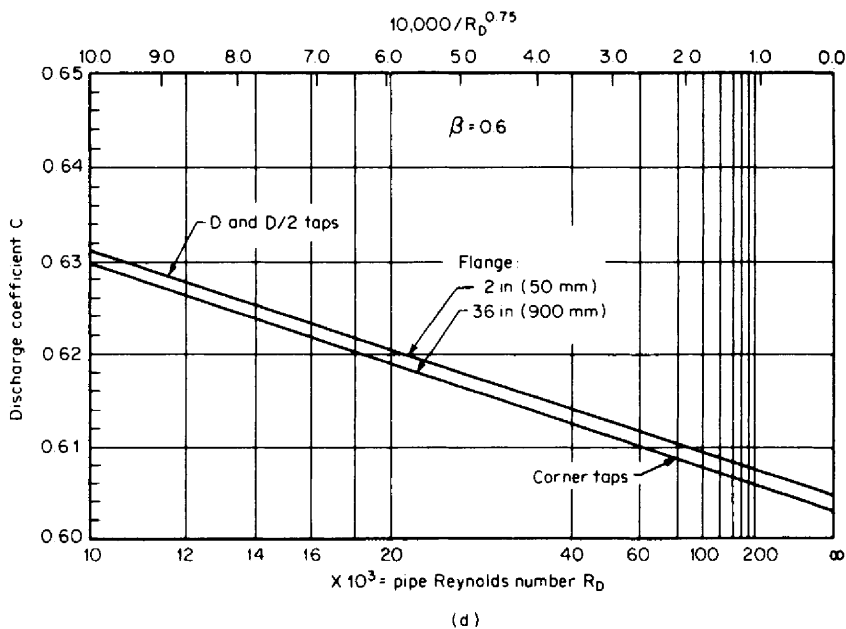
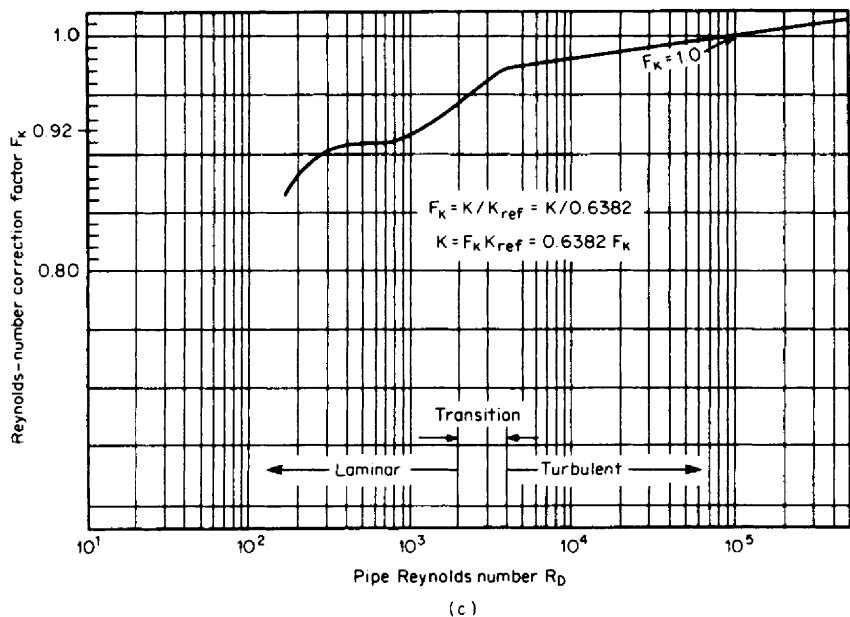


Figure 9.3 (Continued)

$$F_K = \frac{K}{K_{\text{ref}}} \quad (9.48)$$

is plotted against pipe or bore Reynolds number. The Reynolds-number scale may be either logarithmic or linearized. Curves or tables of F_K versus Reynolds number are used in graphical or tabular computations.

Method 4. For all standardized primary elements, numerous test points have been used to develop an empirical equation that predicts the discharge coefficient from bore and pipe-diameter measurements. The accuracy of these equations is usually acceptable, and a flow calibration is seldom performed. However, for Reynolds number, pipe size, etc., outside the specific range of the equation, a signature curve should be used to obtain the discharge coefficient.

In the turbulent flow regime ($R_D > 4000$), the discharge coefficient for all primary elements can be expressed with an equation of the general form

$$C = C_\infty + \frac{b}{R_D^n} \quad (9.49)$$

in which C_∞ is the discharge coefficient at an infinite Reynolds number, and b is the Reynolds-number correction term. For a graphical solution, the coefficient calculated by Eq. (9.49) is plotted versus Reynolds number. By scaling the Reynolds-number axis as the reciprocal of the Reynolds number raised to the exponent n , the change in discharge coefficient with Reynolds number is linearized, as shown in Fig. 9.3d.

Depending on the primary element, the infinite-Reynolds-number discharge coefficient may be a constant or a function of measured dimensions or tap location. The value of b may also be a function of dimensions, or it may be 0. The Reynolds-number exponent n is constant and depends on the primary element. The equations used for primary elements are presented in Table 9.1; the locations and names of the orifice taps are shown in Fig. 9.4.

Thermal Expansion Factors

At flowing conditions the pipe diameter will increase or decrease in size with pressure and temperature from the value measured at a reference temperature, usually 68°F (15.5°C). The effect due to pressure is usually considered negligible and only the thermal effect is considered. If a pressure effect is considered to be important, the equations presented under the Section "Generic Solution" in this chapter may be used.

It is important to note that all sizing, flow-rate, and differential-pressure equations are now written in terms of the flowing beta β and diameters d and D at flowing temperature. The diameters at the measured (bench) temperature of 68°F (20°C) are subscripted as d_{meas} and D_{meas} , respectively. The thermal expansion factor equations that appeared in prior editions of this text and in the standards no longer appear in the flow-rate, sizing, or differential-pressure equations. Rather, the correction for thermal expansion is now implemented prior to these computations.

The pipe and primary element material expands or contracts with temperature. The pipe and bore diameters are measured at room temperature but will be larger or smaller when used at other temperatures. These dimensions are used in the dimensional term $d^2/\sqrt{1 - (d/D)^4}$ and in the beta ratio-dependent terms for the

TABLE 9.1 Equations and Values for C_x , b , and n of Eq. (9.49)†

Primary device	Discharge coefficient C_x at infinite Reynolds number	Reynolds-number term	
		Coefficient b	Exponent n
Venturi			
Machined inlet	0.995	0	0
Rough cast inlet	0.984	0	0
Rough welded sheet-iron inlet	0.985	0	0
Primary flow signal venturi‡	0.990	0	0
Leopold venturi‡	0.968	0	0
Gerand venturi‡	0.888	0	0
Universal Venturi Tube‡	0.9797	0	0
Lo-Loss tube§	$1.005 - 0.471\beta + 0.564\beta^2 - 0.514\beta^3$	0	0
Nozzle:			
ASME long radius	0.9975	$-6.53\beta^{0.5}$	0.5
ASME throat tap§	$C = 1.0054 - \frac{0.185\beta^{0.2}}{R_D^{0.2}} \left[1 - \frac{361239\beta}{R_D} \right]^{0.8}$		
ISA	$0.9900 - 0.2262\beta^{4.1}$	$(-0.00175\beta^2 + 0.0033\beta^{4.15})10^{6.9}$	1.15
Venturi nozzle (ISA inlet)	$0.9558 - 0.196\beta^{4.5}$	0	0
Orifice:			
Corner taps	$0.5959 + 0.0312\beta^{2.1} - 0.184\beta^8$	$91.706\beta^{2.5}$	0.75
Flange taps (D in inches)			
$D \geq 2.3$	$0.5959 + 0.0312\beta^{2.1} - 0.184\beta^8 + 0.09 \frac{\beta^4}{D(1 - \beta^4)} - 0.0337 \frac{\beta^3}{D}$	$91.706\beta^{2.5}$	0.75
$2 \leq D \leq 2.3^d$	$0.5959 + 0.0312\beta^{2.1} - 0.184\beta^8 + 0.039 \frac{\beta^4}{1 - \beta^4} - 0.0337 \frac{\beta^3}{D}$	$91.706\beta^{2.5}$	0.75

Flange taps (D^* in millimeters)

$D^* \geq 58.4$	$0.5959 + 0.0312\beta^{2.1} - 0.184\beta^8 + 2.286 \frac{\beta^4}{D^*(1 - \beta^4)} - 0.856 \frac{\beta^3}{D^*}$					$91.706\beta^{2.5}$					0.75
$50.8 \leq D^* \leq 58.4$	$0.5959 + 0.0312\beta^{2.1} - 0.184\beta^8 + 0.039 \frac{\beta^4}{1 - \beta^4} - 0.856 \frac{\beta^3}{D^*}$					$91.706\beta^{2.5}$					0.75
D and $D/2$ taps	$0.5959 + 0.0312\beta^{2.1} - 0.184\beta^8 + 0.039 \frac{\beta^4}{1 - \beta^4} - 0.01584$					$91.706\beta^{2.5}$					0.75
$2\frac{1}{2}D$ and $8D$ taps	$0.5959 + 0.461\beta^{2.1} + 0.48\beta^8 + 0.039 \frac{\beta^4}{1 - \beta^4}$					$91.706\beta^{2.5}$					0.75
Eccentric orifice (flange taps)	$a + b\beta^{2.1} + c\beta^8 + d \frac{\beta^4}{1 - \beta^4} + e\beta^3$					$f + g\beta + h\beta^2 + i\beta^3 + j\beta^4$					0.75
180° taps	a	b	c	d	e	f	g	h	i	j	
$D \leq 4$ (100 mm)	0.5917	0.3061	0.3406	-0.1019	-0.2715	7.3	-15.7	170.8	-399.7	332.2	
$D > 4$ (100 mm)	0.6016	0.3312	-1.5581	0.6510	-0.7308	-139.7	1328.8	-4228.2	5691.9	-2710.4	
90° taps											
$D \leq 4$ (100 mm)	0.5866	0.3917	0.7586	-0.2273	-0.3343	69.1	-469.4	1245.6	-1287.5	486.2	
$D > 4$ (100 mm)	0.6037	0.1598	-0.2918	0.0244	-0.0790	-103.2	898.3	-2557.3	2977.0	-1131.3	
Eccentric orifice (vena-contracta taps)											
180° taps											
$D \leq 4$ (100 mm)	0.5925	0.3380	0.4016	-0.1046	-0.3212	23.3	-207.0	821.5	-1388.6	900.3	
$D > 4$ (100 mm)	0.5922	0.3932	0.3412	-0.0569	-0.4628	55.7	-471.4	1721.8	-2722.6	1569.4	

TABLE 9.1 Equations and Values for C_x , b , and n of Eq. (9.49)[†] (Continued)

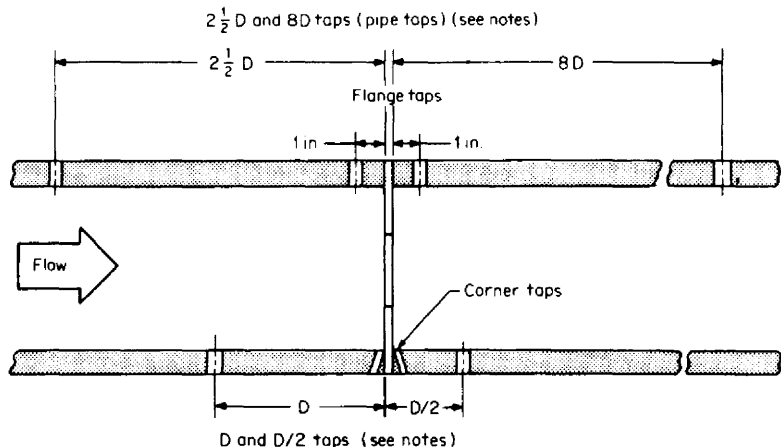
Primary device	Discharge coefficient C_x at infinite Reynolds number						Reynolds-number term			
							Coefficient b		Exponent n	
90° taps										
$D > 4$ (100 mm)	0.5875	0.3813	0.6898	-0.1963	-0.3366	-69.3	556.9	-1332.2	1303.7	-394.8
$D > 4$ (100 mm)	0.5949	0.4078	0.0547	0.0955	-0.5608	52.8	-434.2	1571.2	-2460.9	1420.2
Segmental orifice										
Flange taps										
$D \leq 4$ (100 mm)	0.6284	0.1462	-0.8464	0.2603	-0.2886		0			0
$D > 4$ (100 mm)	0.6276	0.0828	0.2739	-0.0934	-0.1132		0			0
Vena-contracta taps										
$D \leq 4$ (100 mm)	0.6261	0.1851	-0.2879	0.1170	-0.2845		0			0
$D > 4$ (100 mm)	0.6276	0.0828	0.2739	-0.0934	-0.1132		0			0
Quadrant (corner and flange taps) ^f										
$D \geq 1.5$ (40 mm)	$0.7746 - 0.1334\beta^{2.1} + 1.4098\beta^8 + 0.0675 \frac{\beta^4}{1 - \beta^4} + 0.3865\beta^3$						0		0	
Conic orifice										
$D \geq 1$ (25 mm)	$250\beta \leq R_D \leq 500\beta$				0.734		0		0	
	$5000\beta < R_D \leq 200,000\beta$				0.730					
Honed orifice meter runs										
Flange taps	$[0.5980 + 0.468(\beta^4 + 10\beta^{12})](1 - \beta^4)^{0.5}$						$(0.87 + 8.1\beta^4)(1 - \beta^4)^{0.5}$		0.5	
$\frac{1}{2} \leq D \leq 1\frac{1}{2}$										
Corner taps (D in inches)	$\left[\frac{0.5991 + \frac{0.0044}{D}}{(1 - \beta^4)^{0.5}} + \left(0.3155 + \frac{0.0175}{D} \right) (\beta^4 + 2\beta^{16}) \right]$						$\left[\frac{0.52}{D} - 0.192 + \left(16.48 - \frac{1.16}{D} \right) (\beta^4 + 4\beta^{16}) \right]$		$(1 - \beta^4)^{0.5}$	
$\frac{1}{2} \leq D \leq 1\frac{1}{2}$										

Corner taps (D^* in millimeters)	$\left[\frac{0.5991 + \frac{1.1176}{D^*} + \left(0.3155 + \frac{0.4445}{D^*} \right) (\beta^4 + 2\beta^{16})}{(1 - \beta^4)^{0.5}} \right]$					$\left[\frac{13.2}{D^*} - 0.192 + \left(16.48 \frac{29.46}{D^*} \right) (\beta^4 + 4\beta^{16}) \right] (1 - \beta^4)^{0.5}$					0.5
$\frac{1}{2} \leq D \leq 1\frac{1}{2}$											
Corner taps (D^* in millimeters)	$\left[\frac{0.5991 + \frac{1.1176}{D^*} + \left(0.3155 + \frac{0.4445}{D^*} \right) (\beta^4 + 2\beta^{16})}{(1 - \beta^4)^{0.5}} \right]$					$\left[\frac{13.2}{D^*} - 0.192 + \left(16.48 \frac{29.46}{D^*} \right) (\beta^4 + 4\beta^{16}) \right] (1 - \beta^4)^{0.5}$					0.5
Integral Flow Orifice Assembly											
Foxboro (IFOA)											
Quadrant-edged $D = \frac{1}{2}$ (12.5 mm)	$1.1126 - 99.13\beta^2 + 8006\beta^4 - 26900\beta^8$					$-10.72\beta^{1/2} + 3823\beta^{5/2} - 309,300\beta^{9/2}$					0.5
Square-edged $D = \frac{1}{2}$ (12.5 mm)	$0.6479 - 0.3505\beta^2 + 0.3853\beta^4 - 4.645\beta^8$					$-0.4356\beta^{1/2} + 33.49\beta^{5/2} - 88.33\beta^{9/2}$					0.5
Square-edged $D = 1$ (12.5 mm)	$0.6050 - 0.1837\beta^2 + 0.6615\beta^4 - 1.094\beta^8$					$1.646\beta^{1/2} + 2.394\beta^{5/2} - 4.899\beta^{9/2}$					0.5
Square-edged $D = 1\frac{1}{2}$ (40 mm)	$0.6122 - 0.1076\beta^2 + 0.3416\beta^4 - 0.684\beta^8$					$0.2368\beta^{1/2} + 14.3\beta^{5/2} - 12.86\beta^{9/2}$					0.5
Rosemount 1195IO‡											
Quadrant	1.005529					6.75					0.5
Square edge	$a_1 + b_1\beta + c_1\beta^2 + d_1\beta^3 + e_1\beta^4$					$f_1 + g_1\beta + h_1\beta^2 + i_1\beta^3 + j_1\beta^4$					0.5
	a_1	b_1	c_1	d_1	e_1	f_1	g_1	h_1	i_1	j_1	
$D = 1/2$ in (12.7 mm)	0.588423	-0.7817863	1.20573	-3.378356	2.8854437	3.146978	-17.54468	56.26178	-77.01062	52.11968	
$D = 1$ in (25.4 mm)	0.595342	-0.03890471	0.2588337	-0.346828	0.07300363	1.08031	0.6620094	-6.079081	12.1711	6.377415	
$D = 1\ 1/2$ in (38.1 mm)	0.6051001	-0.1111218	0.2830634	0.0403530	-0.3459831	2.337983	-13.71296	66.42804	-124.0909	89.79559	

†Detailed Reynolds-number, line-size, beta-ratio, and other limitations are given in Table 9.54.

‡The manufacturer should be consulted for exact coefficient information and limits on Reynolds number and size.

§Keyser-Murdock equation with beta term; ASME PTC-6 should be reviewed for latest standard computations.



Notes:

(1) $2\frac{1}{2}D$ and $8D$ pipe taps are not recommended in ISO 5167 or ASME Fluid Meters.

(2) D and $D/2$ are radius taps now used in place of vena contracta taps.

Figure 9.4 Orifice pressure-tap locations and their names.

discharge coefficient and the gas expansion factor. The pipe diameter at flowing conditions is calculated by

$$D = F_{ad} D_{\text{meas}} = [1 + \alpha_p(T_F - 68)] D_{\text{meas}} \quad (9.50)$$

where D_{meas} is the measured pipe diameter in inches at a reference temperature of 68°F (15.5°C), F_{ad} is the pipe material's thermal expansion correction, and α_p is the coefficient of thermal expansion for the pipe material in in/(in·°F).

Similarly, the bore diameter is corrected for the flowing temperature by

$$d = F_{ad} d_{\text{meas}} = [1 + \alpha_{pE}(T_F - 68)] d_{\text{meas}} \quad (9.51)$$

where d_{meas} is the measured bore diameter in inches at a reference temperature of 68°F (15.5°C), F_{ad} is the thermal expansion correction factor, and α_{pE} is the coefficient of thermal expansion for the primary element material in in/(in·°F).

The SI equations are, for the flowing diameter,

$$D^* = F_{ad}^* D_{\text{meas}}^* = [1 + \alpha_p^*(T^\circ\text{C} - 20)] D_{\text{meas}}^* \quad (9.52)$$

where D_{meas}^* is the measured diameter in millimeters at 20°C, F_{ad}^* is the pipe material thermal expansion factor, and α_p^* is the coefficient of thermal expansion for the pipe material in mm/(mm·°C).

The bore diameter at flowing conditions is computed by

$$d^* = F_{ad}^* d_{\text{meas}}^* = [1 + \alpha_{pE}^*(T^\circ\text{C} - 20)] D_{\text{meas}}^* \quad (9.53)$$

where d_{meas}^* is the measured bore diameter at 20°C in millimeters, F_{ad}^* is the thermal expansion factor of the primary element, and α_{pE}^* is the coefficient of thermal expansion for the primary element material in mm/(mm·°C).

The orifice is manufactured and measured at 68°F; this measured diameter is determined by combining Eqs. (9.50) and (9.52) as

$$d_{\text{meas}} = \frac{d}{F_{ad}} = \frac{\beta D}{F_{ad}} \quad (9.54)$$

where by definition the flowing beta ratio is $\beta = d/D$ (or $d = \beta D$) as substituted in the above.

The Gas Expansion Factor for the Orifice

For convenience, the steady-flow thermodynamic energy equation for gases was rearranged into the form of the liquid equation, which introduced a gas expansion factor to correct for density changes between taps. This factor is defined, based on gas (vapor) test work, as

$$Y = \frac{CY [\text{from gas (vapor) test}]}{C (\text{from liquid test})} \quad (9.55)$$

At small differential pressures, the gas expansion factor approaches 1.

At nozzles, venturis, and other contoured-inlet devices, gas expansion is assumed to be purely axial. For these devices, there is excellent agreement between the adiabatic gas expansion factor [Eq. (9.30)] and laboratory data. Therefore, for contoured devices, the adiabatic gas expansion factor is used to calculate the expansion factor.

At a square-edged orifice, expansion is both axial and radial, and an empirically determined equation is used to calculate the gas expansion factor. Laboratory test work on steam and other compressible fluids was used by Buckingham (1932) to calculate an orifice gas expansion factor. For upstream-tap pressure measurements, Buckingham derived the equation

$$Y_1 = 1 - (0.41 + 0.35\beta^4) \frac{x_1}{k} \quad (9.56)$$

where k is the isentropic exponent, and the downstream tap location is less than $D/2$ from the upstream face of the orifice. This equation may be modified for downstream pressure measurement with Eqs. (9.38), (9.39), and (9.40) to obtain

$$Y_2 = \sqrt{1 + x_2} - (0.41 + 0.35\beta^4) \frac{x_2}{k\sqrt{1 + x_2}} \quad (9.57)$$

Limitations. Normal practice is to limit the ratio of the differential pressure (in inches of water) to flowing pressure to less than 1.0 ($h_w/p_f \leq 1.0$, $\Delta p/p_f \leq 0.04$). This limits, over a 3:1 flow-rate range, the uncorrected error associated with the gas expansion factor. For example, the maximum variation in the gas expansion factor for an upstream pressure tap Y_1 , for a $\beta = 0.75$ orifice, would be ≈ 1.5 percent over the corresponding 9:1 differential-pressure change. For a downstream pressure tap Y_2 , the maximum variation would be ≈ 0.8 percent.

In many installations this uncertainty is acceptable and is included in the overall uncertainty (accuracy) calculation as a directional bias error. For an upstream pressure tap Y_1 , the meter reads high when the differential is above normal design conditions and low when below; for a downstream pressure tap Y_2 , the meter reads low when above and high when below the normal differential, usually 64 in (16 kPa).

The use of a flow computer to continually compute Y_1 or Y_2 eliminates this directional bias error and reduces the uncertainty (accuracy) calculation to the \pm bias error assigned to the gas expansion factor equation.

Cunningham (1951) has shown that Eq. (9.56) is applicable, within his experimental error, up to a critical flow pressure ratio of $p_{f2}/p_{f1} = 0.63$ ($h_w/p_f \leq 11.8$). Marxman and Burlage (1961) concluded that the gas expansion factor equation may also be applied to pipe diameter sizes as low as $\frac{1}{4}$ in. (6.4 mm).

As explained in Chap. 13, a square-edge orifice will not *choke* if the pressure ratio is reduced below the critical pressure ratio. The Cunningham (1951) experimental data correlate the gas expansion factor for low-pressure ratios (Fig. 9.5). For pressure ratios of $p_{f2}/p_{f1} < 0.63$, the following gas expansion factor is suggested for corner, flange, and D and $D/2$ taps:

$$Y_1 = Y_{1,0.63} - 0.35 \left(0.63 - \frac{p_{f2}}{p_{f1}} \right) \quad (9.58)$$

where $Y_{1,0.63}$ is the upstream gas expansion factor computed by Eq. (9.56) at a pressure ratio of 0.63.

For pipe taps or restrictive orifices the relationship is

$$Y_1 = Y_{1,0.77} - 0.0364 \left(0.77 - \frac{p_{f2}}{p_{f1}} \right) \quad (9.59)$$

where $Y_{1,0.77}$ is the upstream gas expansion factor computed by Eq. (9.57) at a pressure ratio of 0.77.

Kinghorn (1986) experimentally demonstrated that the linear relationship between the gas expansion Y_1 and the ratio of $h_w/p_f(\Delta p/p_f)$ is valid only when the

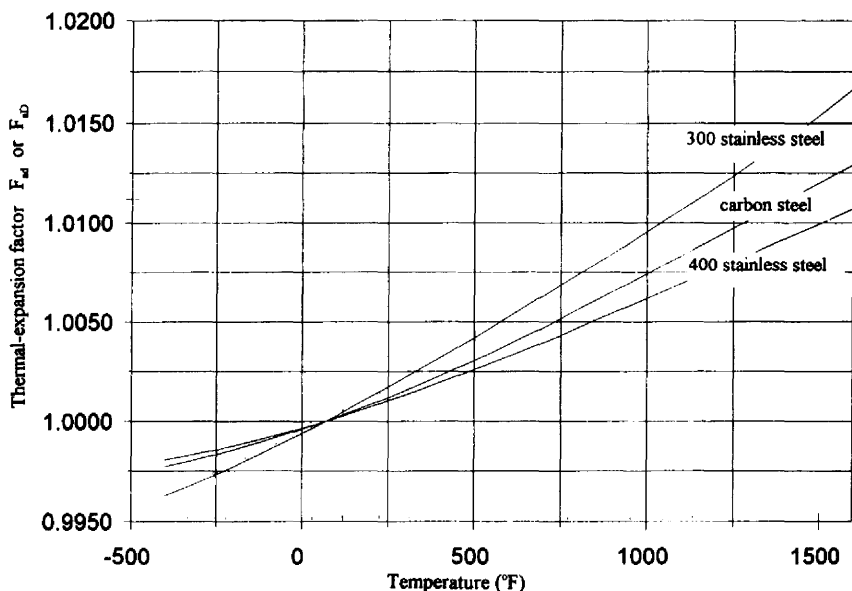


Figure 9.5 Thermal-expansion factor F_{ad} or F_{uD} .

gas expansion factor is less than 0.95 [$Y_1 < 0.95$; ratio of $h_w/p_{f1} < 3.9$ ($\Delta p/p_{f1} < 0.14$)]. Above the ratio of $h_w/p_{f1} = 3.9$ the gas expansion factor change with pressure ratio has pronounced curvature and follows the relationship proposed by von Thibessard (1960) up to the critical flow pressure ratio.

Kinghorn's reported results further indicate that the assigned uncertainty (accuracy) limits specified in ISO 5167 (1991), ANSI/API 2530 (1991), and ASME 3M (1995) should be increased. For a $\beta = 0.66$ orifice, at a pressure ratio of $h_w/p_{f1} = 1.39$ ($\Delta p/p_{f1} = 0.05$), the gas expansion factor equation (9.56) overestimated the gas expansion factor by 0.25 percent.

Fundamental-Unit Liquid and Gas Equation

The *true* mass flow rate equation for both liquids and gases (vapors) is obtained by multiplying the theoretical mass flow equation by the discharge coefficient, the gas expansion factor, and the thermal-expansion factor. The equation for U.S. units is

$$q_{PPS} = 0.09970190 \frac{CY_1 d^2}{\sqrt{1 - \beta^4}} \sqrt{h_w \rho_{f1}} \quad (9.60)$$

The equation for SI units is

$$q_{KPS}^* = 3.512407 \times 10^{-5} \frac{CY_1 d^{*2}}{\sqrt{1 - \beta^4}} \sqrt{\Delta p^* \rho_{f1}^*} \quad (9.61)$$

THE N FACTOR

Derived-Unit Conversion-Factor Equation

The relationships between mass and volumetric flow rate, at both flowing and base conditions, are derived in Chap. 3. From these equations and the pvT density equation, the unit constants for the liquid and gas equations are obtained.

As discussed in Chap. 3, there are three commonly used *liquid* flow-rate units. These are:

1. Mass flow rate (pounds-mass per day, pounds-mass per hour, etc.)
2. Volumetric flow rate at flowing conditions (gallons per minute, gallons per hour, barrels per day, etc.)
3. Volumetric flow rate at a 60°F base volume (barrels per day, gallons per minute, etc.)

A flow equation can be written for each unit to calculate the flow rate from density or specific-gravity values obtained from graphs, from tables, or from measurements. This results in six separate equations; which one is selected depends on the desired flow-rate unit and how density is determined.

In Tables 9.2 and 9.3 are equations that relate the derived flow-rate unit and density-determination equation to the fundamental *liquid* flow-rate-unit equation for both U.S. and SI units. The conversion constant N is subscripted sequentially to

indicate first the flow-rate unit (such as uppercase M for mass flow), and second the method of density determination (G for specific gravity, ρ for density, and pT for the p_vT equation). An uppercase subscript on the flow-rate unit denotes base or fundamental units, such as mass or base volume; a lowercase subscript denotes flowing volume. The conversion constant adjusts the equation both for time base (seconds, minutes, hours) and for the relationship between specific gravity and density.

Four flow-rate units are used in gas (vapor) flows. These are:

1. Mass flow rate (pounds-mass per hour, kilograms per hour, etc.)

TABLE 9.2 Relationship between Fundamental Constant and Derived Flow-Rate Unit for Liquid Flow: U.S. Units

Letter symbol			
Flow rate	Conversion constant	Relationship to fundamental unit equation	Definition
q_M	$N_{M\rho}$	$q_{PPS} = 0.09970190 \frac{q_M}{N_{M\rho}}$	Mass flow rate with density determination Example: $q_M = q_{PPD}$ = pounds-mass per day
q_M	N_{MG}	$q_{PPS} = 0.7873692 \frac{q_M}{N_{MG}}$	Mass flow rate with a specific-gravity determination Example: $q_M = q_{PPM}$ = pounds-mass per minute
q_v	$N_{v\rho}$	$q_{PPS} = 0.09970190[\rho_f] \frac{q_v}{N_{v\rho}}$	Volumetric flow rate at flowing conditions with a density determination Example: $q_v = q_{cfm}$ = cubic feet per minute (flowing)
q_v	N_{vG}	$q_{PPS} = 0.7873692[F_p G_f] \frac{q_v}{N_{vG}}$	Volumetric flow rate at flowing conditions with a specific-gravity determination Example: $q_v = q_{gpm}$ = gallons per minute (flowing)
q_v	$N_{v\rho}$	$q_{PPS} = 0.09970190[\rho_b] \frac{q_v}{N_{v\rho}}$	Volumetric flow rate at base conditions (60°F and 14.696 psia) with a density determination Example: $q_v = q_{GPM}$ = gallons per minute at base conditions
q_v	N_{vG}	$q_{PPS} = 0.7873692[G_b] \left(\frac{q_v}{N_{vG}} \right)$	Volumetric flow rate at base conditions (60°F and 14.69 psia) with a specific-gravity determination Example: $q_v = q_{CFM}$ = cubic feet per minute at base conditions

2. Volumetric flow rate at flowing conditions (flowing cubic feet per minute, flowing cubic meters per hour, etc.)
3. Volumetric flow rate at a standard base pressure and temperature (standard cubic feet per hour, standard cubic feet per day, etc.). ISO Standard 5024 (1976) standardizes on a base of 14.69595 psia (101.325 kPa) and 59°F (15°C)
4. Volumetric flow rate at a selected base pressure and temperature (standard cubic feet per hour at 14.4 psia and 70°F, etc.)

Density may be determined either with a densitometer or by measuring pressure and temperature and calculating the density with the p_vT equations developed in

TABLE 9.3 Relationship between Fundamental Constant and Derived Flow-Rate Unit for Liquid Flow: SI Units

Letter symbol			
Flow rate	Conversion constant	Relationship to fundamental unit equation	Definition
q_M^*	$N_{M_p}^*$	$q_{KPS}^* = 0.00003512407 \frac{q_M^*}{N_{M_p}^*}$	Mass flow rate with density determination Example: $q_{KPD}^* =$ kilograms per day
q_M^*	N_{MG}^*	$q_{KPS}^* = 0.001110172 \frac{q_M^*}{N_{MG}^*}$	Mass flow rate with a specific-gravity determination Example: $q_M^* = q_{KPH}^* =$ kilograms per hour
q_v^*	N_{vp}^*	$q_{KPS}^* = 0.00003512407[\rho_f^*] \frac{q_v^*}{N_{vp}^*}$	Volumetric flow rate at flowing conditions with a density determination Example: $q_v^* = q_{lpm}^* =$ liters per minute (flowing)
q_v^*	N_{vG}^*	$q_{KPS}^* = 0.001110172[F_p G_F] \frac{q_v^*}{N_{vG}^*}$	Volumetric flow rate at flowing conditions with a specific-gravity determination Example: $q_v^* = q_{cmm}^* =$ cubic meters per minute (flowing)
q_v^*	N_{vp}^*	$q_{KPS}^* = 0.00003512407[\rho_b^*] \frac{q_v^*}{N_{vp}^*}$	Volumetric flow rate at base conditions (15.6°C and 101.325 kPa) with a density determination Example: $q_v^* = q_{lpm}^* =$ liters per minute at base conditions
q_v^*	N_{vG}^*	$q_{KPS}^* = 0.001110172[G_b] \left(\frac{q_v^*}{N_{vG}^*} \right)$	Volumetric flow rate at base conditions (15.6°C and 101.325 kPa) with a specific-gravity determination Example: $q_v^* = q_{cmm}^* =$ cubic meters per minute at base conditions

indicate first the flow-rate unit (such as uppercase M for mass flow), and second the method of density determination (G for specific gravity, ρ for density, and pT for the pvT equation). An uppercase subscript on the flow-rate unit denotes base or fundamental units, such as mass or base volume; a lowercase subscript denotes flowing volume. The conversion constant adjusts the equation both for time base (seconds, minutes, hours) and for the relationship between specific gravity and density.

Four flow-rate units are used in gas (vapor) flows. These are:

1. Mass flow rate (pounds-mass per hour, kilograms per hour, etc.)

TABLE 9.2 Relationship between Fundamental Constant and Derived Flow-Rate Unit for Liquid Flow: U.S. Units

Letter symbol			
Flow rate	Conversion constant	Relationship to fundamental unit equation	Definition
q_M	N_{Mp}	$q_{PPS} = 0.09970190 \frac{q_M}{N_{Mp}}$	Mass flow rate with density determination Example: $q_M = q_{PPD}$ = pounds-mass per day
q_M	N_{MG}	$q_{PPS} = 0.7873692 \frac{q_M}{N_{MG}}$	Mass flow rate with a specific-gravity determination Example: $q_M = q_{PPM}$ = pounds-mass per minute
q_v	N_{vp}	$q_{PPS} = 0.09970190[\rho_p] \frac{q_v}{N_{vp}}$	Volumetric flow rate at flowing conditions with a density determination Example: $q_v = q_{cfm}$ = cubic feet per minute (flowing)
q_v	N_{vG}	$q_{PPS} = 0.7873692[F_p G_F] \frac{q_v}{N_{vG}}$	Volumetric flow rate at flowing conditions with a specific-gravity determination Example: $q_v = q_{gpm}$ = gallons per minute (flowing)
q_v	N_{vp}	$q_{PPS} = 0.09970190[\rho_b] \frac{q_v}{N_{vp}}$	Volumetric flow rate at base conditions (60°F and 14.696 psia) with a density determination Example: $q_v = q_{GPM}$ = gallons per minute at base conditions
q_v	N_{vG}	$q_{PPS} = 0.7873692[G_b] \left(\frac{q_v}{N_{vG}} \right)$	Volumetric flow rate at base conditions (60°F and 14.69 psia) with a specific-gravity determination Example: $q_v = q_{CFM}$ = cubic feet per minute at base conditions

2. Volumetric flow rate at flowing conditions (flowing cubic feet per minute, flowing cubic meters per hour, etc.)
3. Volumetric flow rate at a standard base pressure and temperature (standard cubic feet per hour, standard cubic feet per day, etc.). ISO Standard 5024 (1976) standardizes on a base of 14.69595 psia (101.325 kPa) and 59°F (15°C)
4. Volumetric flow rate at a selected base pressure and temperature (standard cubic feet per hour at 14.4 psia and 70°F, etc.)

Density may be determined either with a densitometer or by measuring pressure and temperature and calculating the density with the pvT equations developed in

TABLE 9.3 Relationship between Fundamental Constant and Derived Flow-Rate Unit for Liquid Flow: SI Units

Letter symbol			
Flow rate	Conversion constant	Relationship to fundamental unit equation	Definition
q_M^*	N_{Mp}^*	$q_{KPS}^* = 0.00003512407 \frac{q_M^*}{N_{Mp}^*}$	Mass flow rate with density determination Example: $q_{KPD} =$ kilograms per day
q_M^*	N_{MG}^*	$q_{KPS}^* = 0.001110172 \frac{q_M^*}{N_{MG}^*}$	Mass flow rate with a specific-gravity determination Example: $q_M^* = q_{KPH}^* =$ kilograms per hour
q_v^*	N_{vp}^*	$q_{KPS}^* = 0.00003512407[\rho_f^*] \frac{q_v^*}{N_{vp}^*}$	Volumetric flow rate at flowing conditions with a density determination Example: $q_v^* = q_{LPM}^* =$ liters per minute (flowing)
q_v^*	N_{vG}^*	$q_{KPS}^* = 0.001110172[F_p G_F] \frac{q_v^*}{N_{vG}^*}$	Volumetric flow rate at flowing conditions with a specific-gravity determination Example: $q_v^* = q_{cmm}^* =$ cubic meters per minute (flowing)
q_v^*	N_{vp}^*	$q_{KPS}^* = 0.00003512407[\rho_b^*] \frac{q_v^*}{N_{vp}^*}$	Volumetric flow rate at base conditions (15.6°C and 101.325 kPa) with a density determination Example: $q_v^* = q_{LPM}^* =$ liters per minute at base conditions
q_v^*	N_{vG}^*	$q_{KPS}^* = 0.001110172[G_b] \left(\frac{q_v^*}{N_{vG}^*} \right)$	Volumetric flow rate at base conditions (15.6°C and 101.325 kPa) with a specific-gravity determination Example: $q_v^* = q_{cmm}^* =$ cubic meters per minute at base conditions

Chap. 2. The equations relating these derived units to the fundamental mass flow rate equation are given in Table 9.4 for U.S. units, and in Table 9.5 for SI units.

Gas Factor Equation

In the U.S. natural gas industry a factor equation for the computation of standard cubic feet per hour was derived from the mass flow-rate equation. The equation is derived from

$$(q_{\text{SCFS}})_b = \frac{q_{\text{PPS}}}{\rho_b} \quad (9.62)$$

Substitution of the mass flow-rate Eq. (9.67) and the pvT density relationship of Eqs. (2.10) and (2.14) for flowing and base density computation based on *ideal gravity* yields the flow rate equation for standard cubic feet per hour as follows. The base density is defined by Eq. (2.1) as

$$\rho_b = \frac{2.698825 \ G \ p_b}{Z_b T_b} \quad (9.63)$$

and the flowing density by

$$\rho_{f1} = \frac{2.698825 \ G \ p_{f1}}{Z_f T_f} \quad (9.64)$$

Substituting Eqs. (9.63) and (9.64) into the mass flow-rate Eq. 9.60 yields the flow-rate equation for standard cubic feet per hour as

$$q_{\text{SCFS}} = 218.4834 \frac{Cd^2}{\sqrt{1 - \beta^4}} \frac{Y_1 Z_b T_b \sqrt{p_{f1}}}{p_b \sqrt{G Z_{f1} T_{f1}}} \sqrt{h_w} \quad (9.65)$$

The following factors are then defined:

$$F_{PB} = \frac{14.69595}{p_b} F_{TB} = \frac{T_b}{518.67} F_{TF1} = \sqrt{\frac{518.67}{T_{f1}}} F_{pv1} = \frac{Z_b}{\sqrt{Z_f}} F_G = \frac{1}{\sqrt{G}} \quad (9.66)$$

Rearranging and substituting ($p_b = 14.69595/F_{PB}$, $T_b = 518.67 F_{TB}$, etc.) into Eq. (9.62) gives the *gas factor equation*

$$q_{\text{SCFH}} = 338.5840 \ K d^2 Y_1 F_{PB} F_{TB} F_{TF1} F_{pv1} F_G \sqrt{h_w p_{f1}} \quad (9.67)$$

This equation is cumbersome to implement on computers and care must be used in the proper selection of the constants used in the factors. For example, the constant 338.5840 has a value of 338.178 in AGA literature. This is explained by the use of the inch of water differential pressure unit being selected at 60°F rather than at 68°F, the use of real gravity G_{real} rather than ideal gravity G , and other selected values for the base pressure and temperature. The AGA equation is

$$q_{\text{SCFH}} = 338.178 K d^2 Y_1 F_{pb} F_{tb} F_{f1} F_{pv1, G_r} F_{G_r} \sqrt{h_{w, 60^\circ\text{F}} p_{f1}} \quad (9.68)$$

The factors for this equation are

TABLE 9.4 Relationship between Fundamental Constant and Derived Flow-Rate Unit for Gas Flow: U.S. Units

Letter symbol			
Flow rate	Conversion constant	Relationship to fundamental unit equation	Definition
q_M	N_{M_p}	$q_{PPS} = 0.09970190 \frac{q_M}{N_{M_p}}$	Mass flow rate with a density determination Example: $q_M = q_{PPD}$ = pounds-mass per day
q_M	$N_{M_p T}$	$q_{PPS} = 0.1637908 \frac{q_M}{N_{M_p T}}$	Mass flow rate using the pvT density equation Example: $q_M = q_{PPM}$ = pounds-mass per minute
q_v	N_{vp}	$q_{PPS} = 0.09970190 [\rho_{f1}] \frac{q_v}{N_{vp}}$	Volumetric flow rate at flowing conditions with an upstream tap measurement Example: $q_v = q_{acfm}$ = actual cubic feet per minute
q_v	N_{vpT}	$q_{PPS} = 0.1637908 \left[\frac{Gp_{f1}}{Z_{f1} T_{f1}} \right] \frac{q_v}{N_{vpT}}$	Volumetric flow rate at flowing conditions using the pvT density equation for upstream tap measurements Example: $q_v = q_{acfm}$ = actual cubic feet per minute
q_v	N_{vp}	$q_{PPS} = 0.09970190 [\rho_b] \frac{q_v}{N_{vp}}$	Volumetric flow rate at standard base conditions with a density determination (ρ_b density at 14.696 and 59°F or other selected base values) Example: $q_v = q_{SCFM}$ = standard cubic feet per minute
q_v	N_{vpT}	$q_{PPS} = 0.1637908 \left[\frac{G}{Z_b} \right] \left(\frac{q_v}{N_{vpT}} \right)$	Volumetric flow rate at standard base conditions (14.69595 psia and 59°F) using the pvT density equation (recommended standard base volume) Example: $q_v = q_{SCFH}$ = standard cubic feet per hour
q_{vb}	$(N_{vpT})_b$	$q_{PPS} = 0.1637908 \left[\frac{Gp_b}{Z_b T_b} \right] \frac{q_{vb}}{(N_{vpT})_b}$	Volumetric flow rate at a selected base, other than standard, using the pvT equation Example: $q_{vb} = (q_{SCFD})_{14.4, 70}$ = standard cubic feet per day at 14.4 psia and 70°F

TABLE 9.5 Relationship between Fundamental Constant and Derived Flow-Rate Unit for Gas Flow: SI Units

Letter symbol			
Flow rate	Conversion constant	Relationship to fundamental unit equation	Definition
q_M^*	N_{Mp}^*	$q_{KPS}^* = 0.00003512407 \frac{q_M^*}{N_{Mp}^*}$	Mass flow rate with density determination Example: $q_M^* = q_{KPD}^*$ = kilograms per day
q_M^*	N_{MpT}^*	$q_{KPS}^* = 0.00006555517 \frac{q_M^*}{N_{MpT}^*}$	Mass flow rate using the pvT density equation Example: $q_M^* = q_{KPM}^*$ = kilograms per minute
q_v^*	N_{vp}^*	$q_{KPS}^* = 0.00003512407 [\rho_f^*] \frac{q_v^*}{N_{vp}^*}$	Volumetric flow rate at flowing conditions with an upstream tap density determination Example: $q_v^* = q_{acmm}^*$ = actual cubic meters per minute
q_v^*	N_{vpT}^*	$q_{KPS}^* = 0.00006555517 \left[\frac{Gp_{f1}^*}{Z_{f1} T_{k1}} \right] \frac{q_v^*}{N_{vpT}^*}$	Volumetric flow rate at flowing conditions using the pvT density equation for upstream tap measurements Example: $q_v^* = q_{acmm}^*$ = actual cubic meters per minute
q_v^*	N_{vp}^*	$q_{KPS}^* = 0.00003512407 [\rho_b^*] \frac{q_v^*}{N_{vp}^*}$	Volumetric flow rate at standard or selected base conditions with a density determination Example: $q_v^* = q_{SCMM}^*$ = standard cubic meters per minute
q_v^*	N_{vpT}^*	$q_{KPS}^* = 0.00006555517 \left[\frac{G}{Z_b} \right] \frac{q_v^*}{N_{vpT}^*}$	Volumetric flow rate at standard base conditions (101.325 kPa and 15°C) using the pvT density equation (recommended standard) Example: $q_v^* = q_{SCMH}^*$ = standard cubic meters per hour
q_{vb}^*	$(N_{vpT}^*)_b$	$q_{KPS}^* = 0.00006555517 \left[\frac{Gp_b^*}{Z_b T_{kb}} \right] \frac{q_{vb}^*}{(N_{vpT}^*)_b}$	Volumetric flow rate at a selected base, other than standard, using the pvT equation Example: $q_{vb}^* = (q_{SCMD}^*)_{100,14}$ = standard cubic meters per day at 100 kPa, 14°C

$$K = \frac{C}{\sqrt{1 - \beta_f^4}} \quad F_{tb} = \frac{T_b}{519.67} \quad F_{t1} = \sqrt{\frac{519.67}{T_{f1}}} \\ F_{pv1, Gr} = \sqrt{\frac{Z_b}{Z_{f1}}} \quad F_{Gr} = \sqrt{\frac{1}{G_r}} \quad F_{pb} = \frac{14.73}{p_b} \quad (9.69)$$

The relationships between the fundamental mass flow rate equation and the gas-factor equations are given in Table 9.6 for both U.S. and SI units. The factors may be read from Tables 9.7 through 9.13.

In Tables 9.4 to 9.6, the subscript 1 refers to upstream pressure-tap measurements. For measurements at the downstream tap, these must be changed to the subscript 2, and the expansion-factor equation for a downstream tap location must be used. The compressibility factor and the specific gravity are dimensionless and may be used for both the U.S. and SI system of units. Uppercase subscripts have been given to these factors to indicate that they differ from those used by the natural gas industry, in which similar but lowercase subscripts denote pressure and temperature bases of 14.73 psia and 520°R.

Tables 9.14 through 9.19 contain the N factors for volumetric and mass flow rates in U.S. and SI systems of units.

The Reynolds-Number- N -Factor Relationship

As defined in Chap. 5, the pipe Reynolds number is the basic correlating parameter used to correct for velocity profile. In the English engineering system of units, the Reynolds number at flowing conditions is calculated as

$$R_D = \frac{\rho_f \bar{V}_f D_F}{(\mu_m)_e} \quad (5.1)$$

The mass flow can be calculated as

$$q_{PPS} = \rho_f A_p \bar{V}_f \quad \text{lb}_m/\text{s} \quad (9.12)$$

which can be rearranged as

$$\rho_f \bar{V}_f = \frac{q_{PPS}}{A_p} = \frac{q_{PPS}}{(\pi/4)(D/12)^2} \quad (9.70)$$

Substituting Eq. (9.70) into Eq. (5.1) and converting viscosity to the centipoise unit give the flowing Reynolds number in U.S. units as

$$R_D = 22737.47 \frac{q_{PPS}}{\mu_{cP} D} \quad (9.71)$$

The Reynolds number at flowing conditions for SI units is similarly derived as

$$R_D = 1273239 \frac{q_{KPS}^*}{\mu_{cP} D^*} \quad (9.72)$$

By substituting Eqs. (9.71) and (9.72) into the relationships given in Tables 9.2

TABLE 9.6 Relationship between Fundamental Constant and Derived Flow-Rate Unit for p_vT Gas-Flow Equation Rearranged in Factor Form (F_{PB} , F_{TB} , T_{TF} , F_{pv})

Letter symbol			
Flow rate	Conversion constant	Relationship to fundamental unit equation	Definition
U.S. units			
q_M	N_{Mhp}	$q_{PPS} = 0.007191927 \frac{q_M}{N_{Mhp}}$	Mass flow rate Example: $q_M = q_{PPH}$ = pounds-mass per hour
q_v	N_{vhp}	$q_{PPS} = 0.007191927 \left[\frac{F_{TF}^2 F_{pv}^2 p_{f1}}{F_g^2} \right] \frac{q_v}{N_{vhp}}$	Volumetric flow rate at flowing conditions Example: $q_v = q_{acfs}$ = actual cubic feet per second
q_v	N_{vhp}	$q_{PPS} = 0.007191927 \left[\frac{1}{F_g^2 F_{PB} F_{TB} Z_b} \right] \frac{q_{vb}}{N_{vhp}}$	Volumetric flow rate at standard base or at selected temperature and pressure base Example: $q_v = q_{SCFD}$ = standard cubic feet per day at standard base ($p_b = 14.69595$ psia, $T_b = 518.67^\circ\text{R}$)
SI units			
q_M^*	N_{Mhp}^*	$q_{KPS}^* = 0.000003861870 \frac{q_M^*}{N_{Mhp}^*}$	Mass flow rate Example: $q_M^* = q_{KPM}^*$ = kilograms per minute
q_v^*	N_{vhp}^*	$q_{KPS}^* = 0.000003861870 \left[\frac{F_{TF}^2 F_{pv}^2 p_{f1}^*}{F_g^2} \right] \frac{q_v^*}{N_{vhp}^*}$	Volume flow rate at flowing conditions Example: $q_v^* = q_{acmh}^*$ = actual cubic meters per hour
q_v^*	N_{vhp}^*	$q_{KPS}^* = 0.000003861870 \left[\frac{1}{F_g^2 F_{PB}^* F_{TB}^* Z_b} \right] \frac{q_{vb}^*}{N_{vhp}^*}$	Volume flow rate at standard or selected base pressure and temperature Example: $q_v^* = (q_{SCMH}^*)_{102.16}$ = standard cubic meters per hour at 102 kPa and 16°C

through 9.6, the Reynolds-number equations given in Tables 9.20 through 9.22 are derived in terms of the selected flow-rate unit and the unit conversion factor N .

SIZING VERSUS FLOW-RATE DETERMINATION

There are two distinctly different problems in the use of a differential producer. First, the designer must establish the bore of the primary element to produce a desirable differential pressure at the design flow rate. Second, after the device has been fabricated, the differential pressure and other selected quantities must be measured and then substituted into the flow equation to calculate the flow rate. The designer has the responsibility of selecting which equation variables should be measured (the measured variables) and which can be grouped as unmeasured variables in the meter coefficient factor.

TABLE 9.7 Temperature Base Factor $F_{TB} = T_b/518.67$: U.S. Units

Temperature			Temperature		
°F	°R	F_{TB}	°F	°R	F_{TB}
55	514.67	0.99229	62	521.67	1.00578
56	515.67	0.99422	63	522.67	1.00771
57	516.67	0.99614	64	523.67	1.00964
58	517.67	0.99807	65	524.67	1.01157
59	518.67	1.00000	66	525.67	1.01350
60	519.67	1.00193	67	526.67	1.01542
61	520.67	1.00386	68	526.67	1.01735

TABLE 9.8 Pressure Base Factor $F_{PB} = 14.69595/p_b$: U.S. Units

Pressure base, psia		Pressure base, psia	
	F_{PB}		F_{PB}
14.40	1.02055	15.60	0.94205
14.50	1.01351	15.70	0.93605
14.60	1.00657	15.80	0.93012
14.70	0.99972	15.90	0.92427
14.80	0.99297	16.00	0.91850
14.90	0.98631	16.10	0.91279
15.00	0.97973	16.20	0.90716
15.10	0.97324	16.30	0.90159
15.20	0.96684	16.40	0.89609
15.30	0.96052	16.50	0.89066
15.40	0.95428	16.60	0.88530
15.50	0.94813		

Depending on the sensitivities of the individual variables, the bias error could be small or significant. For example, a $\pm 10^\circ\text{F}$ change in a 90°F (32°C) water flow application causes only a ± 0.1 percent error. But in a 100-psia (700-kPa) flow, a 3:1 flow-rate change results in a 2.5 percent gas-expansion-factor correction. It is important that each variable be investigated and, in particular, that the actual process data be checked against the design information to ensure that no significant differences exist.

To establish the bore, a desired differential pressure is first selected, and the transmitter is then calibrated to that value. Usually the pipe bore is not known initially, and a nominal standard diameter is selected. After the meter run is fabricated, the pipe and primary-element diameters are known, and, although the bore and the range of the differential-pressure transmitter may be exactly as calculated, the beta ratio will be different from the assumed value because the pipe diameter is not the nominal diameter. This means that the dimensional relationships in the flow equation are not the same as those in the sizing equation. This can result in bias errors of 3 to 4 percent in the small line sizes (Fig. 9.6).

The decision as to how accurately the flow rate is to be calculated depends entirely on the design objective. For control purposes, when precision (repeatability) is all that is required, the sizing equation can be used to calculate flow. The added cost of correcting for pressure, temperature, specific gravity, or other process variables may not be warranted. But if accuracy is desired, each of these operating variables and dimensional measurements should be included in the flow equation. It should not be assumed that the accuracy at the single design point applies

TABLE 9.9 Specific-Gravity Factor $F_g = \sqrt{1/G}$: U.S. and SI Units

Specific gravity G	+ .000	+ .001	+ .002	+ .003	+ .004	+ .005	+ .006	+ .007	+ .008	+ .009
.50	1.4142	1.4128	1.4114	1.4100	1.4086	1.4072	1.4058	1.4044	1.4030	1.4017
.51	1.4003	1.3989	1.3975	1.3962	1.3948	1.3935	1.3921	1.3908	1.3894	1.3881
.52	1.3868	1.3854	1.3841	1.3828	1.3814	1.3801	1.3788	1.3775	1.3762	1.3749
.53	1.3736	1.3723	1.3710	1.3697	1.3685	1.3672	1.3659	1.3646	1.3634	1.3621
.54	1.3608	1.3596	1.3583	1.3571	1.3558	1.3546	1.3533	1.3521	1.3509	1.3496
.55	1.3484	1.3472	1.3460	1.3447	1.3435	1.3423	1.3411	1.3399	1.3387	1.3375
.56	1.3363	1.3351	1.3339	1.3327	1.3316	1.3304	1.3292	1.3280	1.3269	1.3257
.57	1.3245	1.3234	1.3222	1.3211	1.3199	1.3188	1.3176	1.3165	1.3153	1.3142
.58	1.3131	1.3119	1.3108	1.3097	1.3086	1.3074	1.3063	1.3052	1.3041	1.3030
.59	1.3019	1.3008	1.2997	1.2986	1.2975	1.2964	1.2953	1.2942	1.2932	1.2921
.60	1.2910	1.2899	1.2888	1.2878	1.2867	1.2856	1.2846	1.2835	1.2825	1.2814
.61	1.2804	1.2793	1.2783	1.2772	1.2762	1.2752	1.2741	1.2731	1.2720	1.2710
.62	1.2700	1.2690	1.2680	1.2669	1.2659	1.2649	1.2639	1.2629	1.2619	1.2609
.63	1.2599	1.2589	1.2579	1.2569	1.2559	1.2549	1.2539	1.2529	1.2520	1.2510
.64	1.2500	1.2490	1.2480	1.2471	1.2461	1.2451	1.2442	1.2432	1.2423	1.2413
.65	1.2403	1.2394	1.2384	1.2375	1.2365	1.2356	1.2347	1.2337	1.2328	1.2318
.66	1.2309	1.2300	1.2290	1.2281	1.2272	1.2263	1.2254	1.2244	1.2235	1.2226
.67	1.2217	1.2208	1.2199	1.2190	1.2181	1.2172	1.2163	1.2154	1.2145	1.2136
.68	1.2127	1.2118	1.2109	1.2100	1.2091	1.2082	1.2074	1.2065	1.2056	1.2047
.69	1.2039	1.2030	1.2021	1.2012	1.2004	1.1995	1.1986	1.1978	1.1969	1.1961

throughout the flow-rate range. The designer should estimate the accuracy over this range, based on expected changes in process conditions.

Sizing or flow-rate computation may be accomplished either graphically or with an iterative process. Graphical solutions are useful for approximate calculations and when the discharge coefficient is not expressed in equation form. Graphical solutions are not as accurate as iterative solutions, and they are not readily accomplished with computer programs.

General Sizing Considerations

The bore is most commonly sized with a chart that directly provides the flow rate. Even when charts are not used, the practice of many companies remains to select the upper-range flow rate and operating flow rate based on prior experience with visually observed circular or strip charts. In Fig. 9.7 are typical square-root flow-rate scale charts. If the maximum design flow rate is selected to be the maximum chart reading except for the decimal point, and the chart is square-root scaled, then a visual chart reading gives the flow rate. If the differential-pressure signal is "square-rooted," then a uniform flow-rate scale is selected (see Fig. 9.8).

The use of a direct-reading chart has the advantage that the rate of flow can be read at a glance. Even if the operating conditions change, this approximate reading is preferred to the use of a multiplying factor. Occasionally, plates are stocked in

TABLE 9.10 Flowing Temperature Factor $F_{TF} = \sqrt{518.67/T_f}$; U.S. Units

Temperature, °F	F_{TF}	Temperature, °F	F_{TF}	Temperature, °F	F_{TF}	Temperature, °F	F_{TF}
20	1.03986	38	1.02088	56	1.00290	74	0.98585
21	1.03878	39	1.01986	57	1.00193	75	0.98492
22	1.03770	40	1.01884	58	1.00097	76	0.98400
23	1.03662	41	1.01782	59	1.00000	77	0.98309
24	1.03555	42	1.01680	60	0.99904	78	0.98217
25	1.03448	43	1.01579	61	0.99808	79	0.98126
26	1.03342	44	1.01478	62	0.99712	80	0.98035
27	1.03235	45	1.01378	63	0.99617	81	0.97944
28	1.03129	46	1.01277	64	0.99521	82	0.97854
29	1.03024	47	1.01177	65	0.99427	83	0.97764
30	1.02919	48	1.01078	66	0.99332	84	0.97674
31	1.02814	49	1.00978	67	0.99238	85	0.97584
32	1.02709	50	1.00879	68	0.99144	86	0.97495
33	1.02605	51	1.00780	69	0.99050	87	0.97405
34	1.02501	52	1.00682	70	0.98956	88	0.97316
35	1.02397	53	1.00583	71	0.98863	89	0.97228
36	1.02294	54	1.00485	72	0.98770	90	0.97139
37	1.02191	55	1.00388	73	0.98677		

TABLE 9.11 Temperature Base Factor $F_{TB}^* = T_{Kb}/288.15$: SI Units

Temperature			Temperature		
°C	K	F_{TB}^*	°C	K	F_{TB}^*
1	274.15	0.95141	21	294.15	1.02032
2	275.15	0.95488	22	295.15	1.02429
3	276.15	0.95835	23	296.15	1.02776
4	277.15	0.96183	24	297.15	1.03123
5	278.15	0.96530	25	298.15	1.03470
6	279.15	0.96877	26	299.15	1.03817
7	280.15	0.97224	27	300.15	1.04164
8	281.15	0.97571	28	301.15	1.04512
9	282.15	0.97918	29	302.15	1.04859
10	283.15	0.98265	30	303.15	1.05206
11	284.15	0.98612	31	304.15	1.05553
12	285.15	0.98959	32	305.15	1.05900
13	286.15	0.99306	33	306.15	1.06247
14	287.15	0.99653	34	307.15	1.06594
15	288.15	1.00000	35	308.15	1.06941
16	289.15	1.00347	36	309.15	1.07288
17	290.15	1.00694	37	310.15	1.07635
18	291.15	1.01041	38	311.15	1.07982
19	292.15	1.01388	39	312.15	1.08329
20	293.15	1.01735	40	313.15	1.08676

TABLE 9.12 Pressure Base Factor $F_{PB}^* = 101.325/p_b^*$: SI Units

Pressure base, kPa	F_{PB}^*	Pressure base, kPa	F_{PB}^*	Pressure base, kPa	F_{PB}^*
95	1.06658	105	0.96500	115	0.88109
96	1.05547	106	0.95590	116	0.87349
97	1.04459	107	0.94696	117	0.86603
98	1.03393	108	0.93819	118	0.85869
99	1.02348	109	0.92959	119	0.85147
100	1.01325	110	0.92114	120	0.84437
101	1.00322	111	0.91284	121	0.83740
102	0.99338	112	0.90469	122	0.83053
103	0.98374	113	0.89668	123	0.82378
104	0.97428	114	0.88882	124	0.81714

TABLE 9.13 Flowing Temperature Factor $F_{TF}^* = \sqrt{288.15/T_K}$; SI Units

Temperature, °C	F_{TF}^*	Temperature, °C	F_{TF}^*	Temperature, °C	F_{TF}^*	Temperature, °C	F_{TF}^*
1.0	1.02522	6.5	1.01508	12.0	1.00525	17.5	0.99569
1.5	1.02428	7.0	1.01418	12.5	1.00437	18.0	0.99483
2.0	1.02335	7.5	1.01327	13.0	1.00349	19.0	0.99313
2.5	1.02242	8.0	1.01237	13.5	1.00261	19.5	0.99228
3.0	1.02150	8.5	1.01147	14.0	1.00174	20.0	0.99144
3.5	1.02057	9.0	1.01058	14.5	1.00087	20.5	0.99059
4.0	1.01965	9.5	1.00968	15.0	1.00000	21.0	0.98975
4.5	1.01873	10.0	1.00879	15.5	0.99913	21.5	0.98891
5.0	1.01782	10.5	1.00790	16.0	0.99827	22.0	0.98807
5.5	1.01690	11.0	1.00701	16.5	0.99741	22.5	0.98723
6.0	1.01599	11.5	1.00613	17.0	0.99655	23.0	0.98640

TABLE 9.14 N Factors for Mass Flow: U.S. Units†

Time	Pound-mass (lb _m)	Kilogram (kg)§	Gram (g)§
N_{Mp} Density equation, <i>liquid and gas</i> (vapor)			
s	0.09970190	0.04522402	45.22402
min	5.982114	2.713441	2713.441
h	358.9268	162.8065	162,806.5
24 h	8614.244	3907.36	3,907,356
N_{MG} Specific-gravity‡ equation, <i>liquid</i>			
s	0.7873692	0.3571447	357.1447
min	47.24215	21.42868	21,428.68
h	2834.529	1285.721	1,285.721
24 h	68,028.70	30,857.30	30,857,300
N_{MeT} p_vT equation, <i>gas</i> (vapor)			
s	0.1637913	0.07429449	74.29449
min	9.827478	4.4576769	4457.669
h	589.6487	267.4602	267,460.2
24 h	14,151.57	6419.044	6,419,044

†The U.S. units are pressure p_i (psia), differential pressure h_w (inches of water at 68°F, 14.696 psia, and standard gravity, 32.17405 ft/s²), temperature T_i (°R), dimensions d and D (in), and density ρ (lb_m/ft³).

‡Specific-gravity base: water at 60°F; pressure = 14.69595 psia.

§For sizing and calculating mass flow in SI units, *but* with measurement in the U.S. units defined above.

$\frac{1}{8}$ -in orifice-bore increments (or other arithmetic progressions) to permit chart standardization and allow flow capacity to be changed through plate selection. If the operating temperature or specific gravity changes from the design conditions, the chart multiplier factor is changed to compute the new conditions.

When this method is used, an orifice plate with a bore that creates a differential near the maximum chart value is chosen. The square-root scale is not direct-reading but, instead, a multiplying factor is used for correction. In selecting the design-condition flow rate, the expected maximum flow rate is rounded either to coincide (except for the decimal point) with the selected upper-range chart value or to a convenient number. Seldom, if ever, is the maximum value selected as 2100 instead of 2000, for example.

Most plants standardize on a single upper-range value for differential-pressure transmitters, for ease in stocking and for interchangeability. Usually, 0 to 100 in H_2O (0 to 25 kPa) is specified for both liquid and gas flows. However, the selection depends on plant experience and preference. It should be noted that as the differential pressure is increased, the overall pressure loss increases, which further increases the pumping cost. But the lower the differential pressure, the higher the beta ratio becomes, and high-beta-ratio primary elements require more upstream pipe and are inherently less accurate.

The 100-in (25-kPa) range is high enough to minimize differences in temperature if long lead lines are used in lieu of close-coupled manifolds. A few applications

TABLE 9.15 N Factors for Mass Flow: SI Units†

Time	Kilogram (kg)	Gram (g)
$N_{M\rho}^*$ Density equation, <i>liquid and gas</i> (vapor)		
s	0.00003512407	0.03512407
min	0.0021074444	2.107444
h	0.1264467	126.4467
24 h	3.034720	3034.720
N_{MG}^* Specific-gravity equation, <i>liquid</i>		
s	0.001110172	1.110172
min	0.06661032	66.61031
h	3.996619	3996.619
24 h	95.91886	95,918.85
N_{MpT}^* p_vT equation, <i>gas</i> (vapor)		
s	0.00006555517	0.06555517
min	0.003933310	3.933310
h	0.2359986	235.9986
24 h	5.663967	5663.967

†The SI units are pressure p_f^* (kPa), differential pressure Δp^* (kPa), temperature T_K ($^{\circ}K$), dimensions d^* and D^* (mm), and density ρ^* (kg/m^3). For differential pressure Δp^* in bars, multiply table values by 10. For pressure p_f^* in bars, multiply by 10. For *both* differential pressure and pressure in bars, multiply by 100. For Reynolds-number calculations (equations from Table 9.21) *do not* change tabular values.

TABLE 9.16 *N* Factors for Volume Flow: U.S. Units†

Time	Cubic foot (ft ³)	Cubic meter (m ³)‡	Liter (L)‡	U.S. gallon (gal)	U.K. liquid (Imp. gal)	Barrel	
						42 gal	50 gal
<i>N_{vp}, N_{vρ}, Density equation, liquid and gas (vapor)</i>							
s	0.09970190	0.002823244	2.823244	0.7458220	0.6210265	0.01775767	0.01491644
min	5.982114	0.1693946	169.3946	44.74932	37.26159	1.065460	0.8949864
h	358.9268	10.16368	10,163.68	2684.959	2235.696	63.92760	53.69919
24 h	8614.244	243.9283	243,928.3	64,439.02	53,656.69	1534.262	1288.780
<i>N_{vG}, N_{VG}, Specific-gravity equation, liquid</i>							
s	0.01262491	0.0003574978	0.3574978	0.09444092	0.07863849	0.002248593	0.001888819
min	0.7574946	0.02144987	21.44987	5.666455	4.718309	0.1349156	0.1133291
h	45.44968	1.286992	1286.992	339.9873	283.0986	8.094936	6.799747
24 h	1090.793	30.88781	30,887.81	8159.696	6794.365	194.2785	163.1939
<i>p<i>v</i>T equation, gas (vapor)</i>							
Time	<i>N_{vp<i>T</i>}, (N_{vρ<i>T</i>})_b</i>			<i>N_{vρ<i>T</i>}§</i>			
	Cubic foot (ft ³)	Cubic meter (m ³)‡	Liter (L)‡	Cubic foot (ft ³)	Cubic meter (m ³)‡	Liter (L)‡	
s	0.0606898	0.001718545	1.718545	2.141951	0.06065330	60.65330	
min	3.641391	0.1031127	103.1127	128.5171	3.639198	3639.198	
h	218.4834	6.186763	6186.763	7711.023	218.3519	218,351.9	
24 h	5243.603	148.4823	148,482.3	185,064.6	5240.445	5,240,445	

†The U.S. units are pressure p_i (psia), differential pressure h_w (inches of water at 68°F, 14.696 psia, and standard gravity, 32.17405 ft/s²), temperature T_i (°R), dimensions d and D (in), and density ρ (lb_m/ft³).

‡For sizing and calculating volume flow in SI units, but with measurements in the U.S. units defined above.

§Standard base volume (ISO 5024): $p_b = 14.69595$ psia; $T_b = 518.67^\circ\text{R}$.

may be found in which the available pressure is insufficient to pass the desired flow through an orifice designed for 100 in (25 kPa). In these cases, lower upper-range values or a Lo-Loss tube is selected; or, both a lower-range differential and a Lo-Loss tube may be used to keep the pressure loss within the design objective. The pressure loss can never exceed the difference between the supply and demand pressures at the operating flow rate, and although recovery may be high, the minimum pressure should be kept above the liquid's vapor pressure to avoid cavitation.

Fixed-bore primary elements, such as flow nozzles, Lo-Loss tubes, and venturis, are seldom replaced to account for changes in flow-rate conditions. Rather, the differential-pressure transmitter is recalibrated to a nonstandard value corresponding to a direct-reading flow chart.

An important early decision is whether accuracy or precision (repeatability) is the design objective. The sizing procedure, fabrication of the meter run, flow-meter-system configuration, and final flow-rate equation can be simple or quite complex, depending on how many of the process variables are assumed to be constant (unmeasured variables) and how many are to be measured (measured variables). For all differential producers, if accuracy is required, it is necessary that dimensional measurements and reference conditions be in accordance with the requirements given in Chap. 8. The accuracy of the installation can be estimated with the procedures outlined in Chap. 4.

TABLE 9.17 N Factors for Volume Flow: SI Units†

N_{vp}^* , N_{vp}^* Density equation, liquid and gas (vapor)			N_{vG}^* , N_{vG}^* Specific-gravity equation, liquid		
Time	Cubic meter (m ³)	Liter (L)	Time	Cubic meter (m ³)	Liter (L)
s	0.00003512407	0.03512407	s	0.000001111270	0.001111270
min	0.002107444	2.107444	min	0.00006667619	0.06667619
h	0.1264467	126.4467	h	0.004000571	4.000571
24 h	3.034720	3034.720	24 h	0.09601371	96.01371
pvT equation, gas (vapor)					
$(N_{vpT}^*$, § $(N_{vpT}^*)_{b^{\ddagger}}$)			N_{vpT}^{\ddagger}		
Time	Cubic meter (m ³)	Liter (L)	Cubic meter (m ³)	Liter (L)	
s	0.00001881927	0.01881927	0.00005351861	0.05351861	
min	0.001129156	1.129156	0.003211117	3.211117	
h	0.06774938	67.74938	0.1926670	192.6670	
24 h	1.625985	1625.985	4.624008	4624.008	

†The SI units are pressure p_f^* (kPa), differential pressure Δp^* (kPa), temperature T_K (K), dimensions d^* and D^* (mm), and density ρ^* (kg/m³). For differential pressure Δp^* in bars, multiply table values by 10. For Reynolds-number calculations (equations from Table 9.21), do not change tabular values.

‡For pressure p_f^* in bars, multiply by 10. For both differential pressure and pressure in bars, multiply by 100.

§For pressure p_f^* in bars, divide by 10. For both differential pressure and pressure in bars, there is no change.

¶Standard base volume (ISO 5024): $p_b^* = 101.325$ kPa; $T_{Kb} = 288.15$ K.

THE S_M -FACTOR EQUATIONS FOR SIZING

The S_M Factor

The fundamental-unit equation [Eq. (9.60) or (9.61)] can be rewritten in a general form for any set of flow-rate units, using the derived-unit conversion factor N , as

$$q = \frac{NCYd^2}{\sqrt{1 - \beta^4}} f(\rho) \sqrt{h_w} \quad (9.73)$$

where the function of density $f(\rho)$ depends on whether the density is determined by densitometer, or by liquid specific gravity or, for gas flows, inferred from the pVT equation. The functional relationships $f(\rho)$ are shown in brackets in Tables 9.2 through 9.6.

Initially, the bore must be determined so as to satisfy a design operating flow rate, pipe size, and desired differential pressure. For bore sizing, the flow-rate equation

TABLE 9.18 N Factors for Gas-Factor Equations (F_{PB} , F_{TB} , F_{TF} , F_{pv}): U.S. Units†

N_{Mhp} Mass-flow equation			
Time	Pound-mass (lb _m)	Kilogram (kg)§	Gram (g)§
s	0.007191927	0.003262203	3.262203
min	0.4315156	0.1957322	195.7322
h	25.89094	11.74393	11,743.93
24 h	621.3825	281.8544	281,854.4
N_{vhp} Volume flow at flowing conditions			
Time	Cubic foot (ft³)	Cubic meter (m³)§	Liter (L)§
s	1.382170	0.03913871	39.13871
min	82.930213	2.348323	2348.323
h	4975.814	140.8994	140,899.4
24 h	119,419.5	3381.585	3,381.585
N_{vhp} Volume flow at selected or standard base‡			
Time	Cubic foot (ft³)	Cubic meter (m³)§	Liter (L)§
s	0.09405112	0.002663231	2.663231
min	5.643067	0.1597939	159.7939
h	338.5840	9.587633	9587.633
24 h	8126.016	230.1032	230,103.2

†The U.S. units are pressure p_i (psia), differential pressure h_w (inches of water at 68°F, 14.696 psia, and standard gravity, 32.17405 ft/s²), dimensions d and D (in), and density ρ (lb_m/ft³).

‡Standard base volume (ISO 5024, 1976): $p_b = 14.69595$ psia; $T_b = 518.67^\circ\text{R}$; $F_{PB} = F_{TB} = 1.0$.

§For sizing and calculating flow in SI units, but with measurements in the U.S. units defined above.

tion is rewritten in terms of these known quantities by introducing a *sizing factor* or S_M factor defined as

$$S_M = \frac{CY\beta^2}{\sqrt{1 - \beta^4}} \quad (9.74)$$

Since $d = \beta D$, Eq. (9.73) can be expressed for both liquids and gases (vapors) as

$$q = NS_M D^2 f(\rho) \sqrt{h_w} \quad (9.75)$$

Rearranging this equation to solve for S_M gives the relationships

TABLE 9.19 N Factors for Gas-Factor Equations
(F_{PB}^* , F_{TB}^* , F_{TF}^* , F_{PV}^*): SI Units†

N_{Mhp}^* Mass-flow equation		
Time	Kilogram (kg)	Gram (g)
s	0.000003861870	0.003861870
min	0.0002317122	0.2317122
h	0.01390273	13.90273
24 h	0.3336656	333.6656
N_{vhp}^* Volume flow at flowing conditions‡		
Time	Cubic meter (m³)	Liter (L)
s	0.0003194568	0.3194568
min	0.01916741	19.16741
h	1.150044	1150.044
24 h	27.60107	27,601.07
N_{vhp}^* Volume flow at selected or standard base§		
Time	Cubic meter (m³)	Liter (L)
s	0.000003152793	0.003152793
min	0.0001891676	0.1891676
h	0.01135006	11.35006
24 h	0.2724013	272.4013

†The SI units are pressure p^* (kPa), differential pressure Δp^* (kPa), temperature T_K (K), and dimensions d^* and D^* (mm). For differential pressure in bars, multiply table values by 10. For Reynolds-number calculations (equations from Table 9.22) *do not* change tabular values.

‡For pressure in bars, divide by 10. For *both* differential pressure and pressure in bars, there is no change.

§Standard base volume (ISO 5024, 1976): $p_B^* = 101.325$ kPa; $T_{Kb} = 218.15$ K (15°C); $F_{PB}^* = 1.0$. For pressure in bars, multiply by 10. For *both* differential pressure and pressure in bars, multiply by 100.

TABLE 9.20 Reynolds Number Related to Derived Flow-Rate Unit: U.S. Units†

Liquid			Gas (vapor)	
Mass flow rate				
Density	$R_D = \left[2266.970 \frac{1}{\mu_{cP} DN_{M\rho}} \right] q_M$	(a)	$R_D = \left[2266.970 \frac{1}{\mu_{cP} DN_{M\rho}} \right] q_M$	(g)
Specific gravity	$R_D = 17,902.78 \frac{1}{\mu_{cP} DN_{MG}} q_m$	(b)		
$p v T$ equation			$R_D = \left[3724.200 \frac{1}{\mu_{cP} DN_{M p T}} \right] q_M$	(h)
Volumetric flow rate at flowing conditions				
Density	$R_D = \left[2266.970 \frac{\rho_f}{\mu_{cP} DN_{v\rho}} \right] q_v$	(c)	$R_D = \left[2266.970 \frac{\rho_{f1}}{\mu_{cP} DN_{v\rho}} \right] q_v$	(i)
Specific gravity	$R_D = \left[17,902.78 \frac{F_p G_F}{\mu_{cP} DN_{vG}} \right] q_v$	(d)		
$p v T$ equation			$R_D = \left[3724.200 \frac{G p_{f1}}{Z_{f1} T_{f1} \mu_{cP} DN_{v p T}} \right] q_v$	(j)
Volumetric flow rate at base conditions				
Density	$R_D = \left[2266.970 \frac{\rho_b}{\mu_{cP} DN_{v\rho}} \right] q_v$	(e)	$R_D = \left[2266.970 \rho_b \frac{1}{\mu_{cP} DN_{v\rho}} \right] q_v$	(k)
Specific gravity	$R_D = \left[17,902.78 \frac{G_b}{\mu_{cP} DN_{vG}} \right] q_v$	(f)		
$p v T$ equation				
Standard base			$R_D = \left[3724.200 \frac{G}{Z_b \mu_{cP} DN_{v p T}} \right] q_v$	(l)
Selected base			$R_D = \left[3724.200 \frac{G p_b}{Z_b T_b \mu_{cP} D(N_{v p T})_b} \right] q_{vb}$	(m)

†*D* in these equations is at flowing conditions: $D = F_{aD} D_{\text{meas}} = [1 + \alpha_p(T_f - 68)]D_{\text{meas}}$, [Eq. (9.50)].

TABLE 9.21 Reynolds Number Related to Derived Flow-Rate Unit: SI Units†

Liquid			Gas (vapor)	
Mass flow rate				
Density	$R_D = \left[44.72136 \frac{1}{\mu_{cP} D^* N_{M\rho}^*} \right] q_M^*$	(a)	$R_D = \left[44.72136 \frac{1}{\mu_{cP} D^* N_{M\rho}^*} \right] q_M^*$	(g)
Specific gravity	$R_D = \left[1413.515 \frac{1}{\mu_{cP} D^* N_{MG}^*} \right] q_M^*$	(b)		
<i>pvT</i> equation			$R_D = \left[83.46744 \frac{1}{\mu_{cP} D^* N_{MpT}^*} \right] q_M^*$	(h)
Volumetric flow rate at flowing conditions				
Density	$R_D = \left[44.72136 \frac{\rho_f^*}{\mu_{cP} D^* N_{vp}^*} \right] q_v^*$	(c)	$R_D = \left[44.72136 \frac{\rho_{f1}^*}{\mu_{cP} D^* N_{vp}^*} \right] q_v^*$	(i)
Specific gravity	$R_D = \left[1413.515 \frac{F_\rho G_F}{\mu_{cP} D^* N_{vG}^*} \right] q_v^*$	(d)		
<i>pvT</i> equation			$R_D = \left[83.46744 \frac{G p_{f1}^*}{Z_{f1} T_{K1}} \frac{1}{\mu_{cP} D^* N_{vpT}^*} \right] q_v^*$	(j)
Volumetric flow rate at base conditions				
Density	$R_D = \left[44.72136 \frac{\rho_b^*}{\mu_{cP} D^* N_{vp}^*} \right] q_v^*$	(e)	$R_D = \left[44.72136 \rho_b^* \frac{1}{\mu_{cP} D^* N_{vp}^*} \right] q_v^*$	(k)
Specific gravity	$R_D = \left[1413.515 \frac{G_b}{\mu_{cP} D^* N_{vG}^*} \right] q_v^*$	(f)		
<i>pvT</i> equation				
Standard base			$R_D = \left[83.46744 \frac{G}{Z_b \mu_{cP} D^* N_{vpT}^*} \right] q_v^*$	(l)
Selected base			$R_D = \left[83.46744 \frac{G p_b^*}{Z_b T_{Kb}} \frac{1}{\mu_{cP} D^* (N_{vpT}^*)_b} \right] q_{vb}^*$	(m)

TABLE 9.22 Reynolds Number Related to Derived Flow-Rate Unit for Gas-Factor Equation: U.S. and SI Units†

pvT equation	U.S. units	SI units
Mass flow rate	$R_D = \left[163.5262 \frac{1}{\mu_{cP} DN_{Mhp}} \right] q_M$ (a)	$R_D = \left[4.917086 \frac{1}{\mu_{cP} D^* N_{Mhp}^*} \right] q_M^*$ (d)
Volumetric flow rate at flowing conditions	$R_D = \left[163.5263 \frac{F_{TF1}^2 F_{pv1}^2 p_{f1}}{Z_b^2 \mu_{cP} DN_{vhp}} \right] q_v$ (b)	$R_D = \left[4.917086 \frac{F_{TF1}^{*2} F_{pv1}^{*2} p_{f1}^{*2}}{Z_b^2 \mu_{cP} D^* N_{vhp}^*} \right] q_v^*$ (e)
Volumetric flow rate at standard or selected base conditions	$R_D = \left[163.5262 \frac{1}{F_g^2 F_{PB} F_{TB} Z_b \mu_{cP} DN_{vhp}} \right] q_{vb}$ (c)	$R_D = \left[4.917086 \frac{1}{F_g^2 F_{PB}^* F_{TB}^* Z_b \mu_{cP} D^* N_{vhp}^*} \right] q_{vb}^*$ (f)

† D and D^* in these equations is at flowing conditions: $D = F_{aD} D_{meas} = [1 + \alpha_p(T_f - 68)]D_{meas}$ [Eq. (9.50)]; $D^* = F_{aD}^* D_{meas}^* = [1 + \alpha_p^*(T_c - 68)]D_{meas}^*$ [Eq. (9.52)].

$$S_M = \frac{CY\beta^2}{\sqrt{1 - \beta^4}} \quad (9.76)$$

$$= \frac{q}{ND^2 f(\rho) \sqrt{h_w}}$$

for U.S. units, and

$$S_M = \frac{CY\beta^2}{\sqrt{1 - \beta^4}} \quad (9.77)$$

$$= \frac{q^*}{N^* D^{*2} f(\rho^*) \sqrt{\Delta p^*}}$$

for SI units.

The value of the S_M factor is *constant* over the flow-rate range. It is calculated by substituting design operating-point data into the right-hand side of Eq. (9.76) or (9.77), in which the β -dependent terms, discharge coefficient, and gas expansion factor are grouped together. Table 9.1 contains the discharge-coefficient equations; Tables 9.23 through 9.25, the S_M factors; and Table 9.26, the gas-expansion-factor equations. Although the thermal-expansion factor F_a is β -dependent for differing pipe and primary-element materials [Eqs. (9.51) and (9.52)], its effect on sizing is negligible.

Since Eq. (9.77) is nonlinear, an iterative solution is required to equate the S_M factor to the β -dependent terms. Equation (9.77) can be rearranged to yield

$$\beta = \frac{1}{[1 + (CY/S_M)^2]^{1/4}} = \left[1 + \left(\frac{CY}{S_M} \right)^2 \right]^{-1/4} \quad (9.78)$$

It can also be expressed as

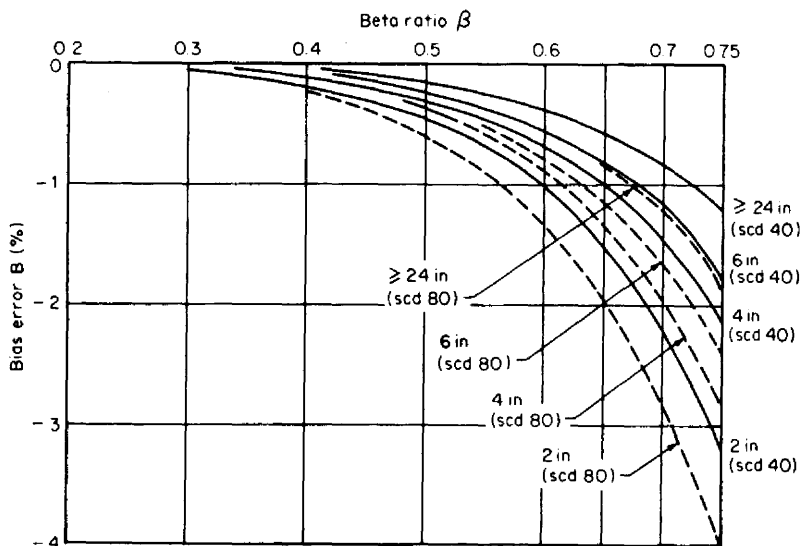


Figure 9.6 Maximum flow-rate bias error for unmeasured pipe diameter.

$$\beta = \sqrt{\frac{S_M}{KY}} \quad (9.79)$$

where K is the flow coefficient defined by Eq. (9.47).

SIZING THE BORE

The β_0 Approximation

The uncertainty of operating data on viscosity, specific gravity, and temperature often precludes accurate measurement; for many plant *control* operations, close measurement tolerances are unnecessary. When precision (repeatability) is of pri-

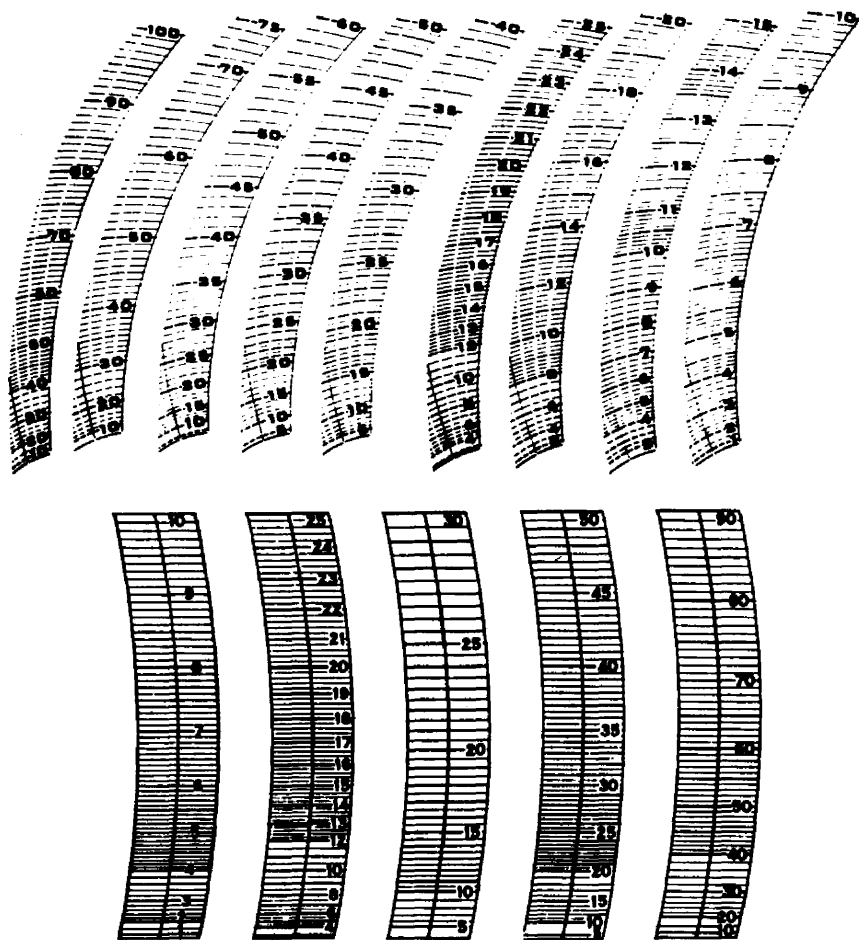


Figure 9.7 Square-roots charts. (Courtesy The Foxboro Co.)

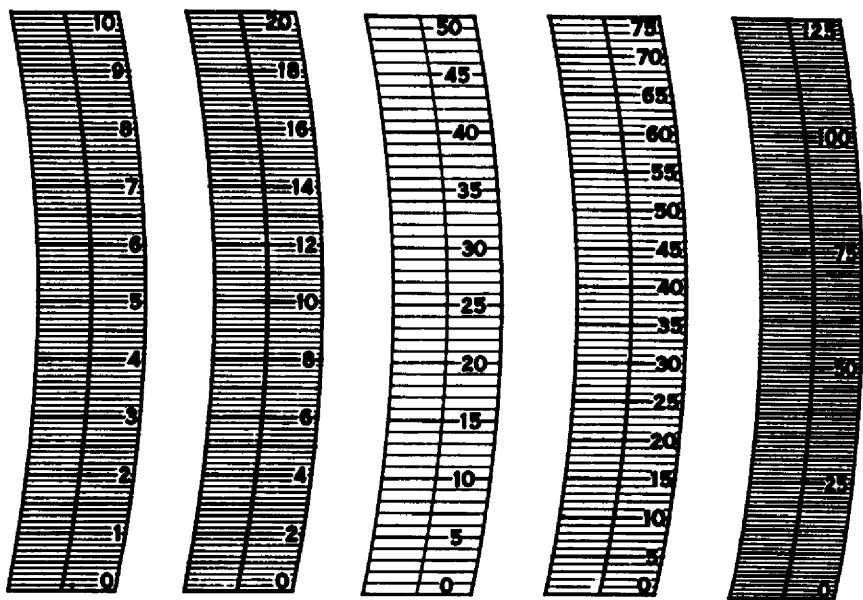
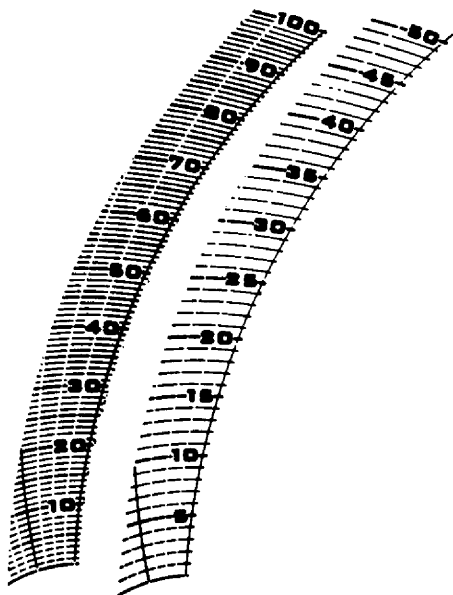


Figure 9.8 Linear charts. (Courtesy The Foxboro Co.)

Liquid		Gas (vapor)
Mass flow rate		
Density	$S_M = \frac{q_M}{N_{Mp} D^2 \sqrt{F_p} \sqrt{\rho_F} \sqrt{h_w}} \quad (a)$	$S_M = \frac{q_M}{N_{Mp} D^2 \sqrt{\rho_{f1}} \sqrt{h_w}} \quad (g)$
Specific gravity	$S_M = \frac{q_M}{N_{MG} F_a D^2 \sqrt{F_p} \sqrt{G_F} \sqrt{h_w}} \quad (b)$	
pvT equation		$S_M = \frac{\sqrt{Z_{f1}} \sqrt{T_{f1}} q_M}{N_{MpT} D^2 \sqrt{G} \sqrt{h_w} p_{f1}} \quad (h)$
Volumetric flow rate at flowing conditions		
Density	$S_M = \frac{\sqrt{F_p} \sqrt{\rho_F} q_v}{N_{vp} D^2 \sqrt{h_w}} \quad (c)$	$S_M = \frac{\sqrt{\rho_{f1}} q_v}{N_{vp} D^2 \sqrt{h_w}} \quad (i)$
Specific gravity	$S_M = \frac{\sqrt{F_p} \sqrt{G_F} q_v}{N_v D^2 \sqrt{h_w}} \quad (d)$	
pvT equation		$S_M = \frac{\sqrt{G} \sqrt{\rho_{f1}} q_v}{N_{vp} \sqrt{Z_{f1}} \sqrt{T_{f1}} D^2 \sqrt{h_w}} \quad (j)$
Volumetric flow rate at base conditions		
Density	$S_M = \frac{\rho_b q_v}{N_{vp} D^2 \sqrt{F_p} \sqrt{\rho_F} \sqrt{h_w}} \quad (e)$	$S_M = \frac{\rho_b q_v}{N_{vp} D^2 \sqrt{\rho_{f1}} \sqrt{h_w}} \quad (k)$
Specific gravity	$S_M = \frac{G_b q_v}{N_{vG} D^2 \sqrt{F_p} \sqrt{G_F} \sqrt{h_w}} \quad (f)$	
pvT equation		
Standard base		$S_M = \frac{\sqrt{Z_{f1}} \sqrt{T_{f1}} \sqrt{G} q_v}{N_{vpT} Z_b D^2 \sqrt{h_w} p_{f1}} \quad (l)$
Selected base		$S_M = \frac{\sqrt{Z_{f1}} \sqrt{T_{f1}} \sqrt{G} p_b q_{vb}}{(N_{vpT})_b Z_b T_b D^2 \sqrt{h_w} p_{f1}} \quad (m)$

Notes: Gas (vapor) equations are written for upstream pressure tap. For downstream pressure tap, change subscript 1 to subscript 2, in ρ_{f2} , p_{f2} , Z_{f2} , etc. D in these equations is at flowing conditions: $D = F_{ad} D_{meas} = [1 + \alpha_p(T_F - 68)] D_{meas}$ [Eq. (9.50)].

TABLE 9.24 Sizing-Factor S_M Equations for SI Flow Units

Liquid		Gas (vapor)
Mass flow rate		
Density	$S_M = \frac{q_M^*}{N_{M\rho}^* D^{*2} \sqrt{F_p} \sqrt{\rho_F^*} \sqrt{\Delta p^*}} \quad (a)$	$S_M = \frac{q_M^*}{N_{M\rho}^* D^{*2} \sqrt{\rho_{f1}^*} \sqrt{\Delta p^*}} \quad (g)$
Specific gravity	$S_M = \frac{q_M^*}{N_{MG}^* F_a^* D^{*2} \sqrt{F_p} \sqrt{G_F} \sqrt{\Delta p^*}} \quad (b)$	
pvT equation		$S_M = \frac{\sqrt{Z_{f1}} \sqrt{T_{K1}} q_M^*}{N_{Mp1}^* D^{*2} \sqrt{G} \sqrt{\Delta p^*} p_{f1}^*} \quad (h)$
Volumetric flow rate at flowing conditions		
Density	$S_M = \frac{\sqrt{F_p} \sqrt{\rho_F^*} q_v^*}{N_{vp}^* D^{*2} \sqrt{\Delta p^*}} \quad (c)$	$S_M = \frac{\sqrt{\rho_{f1}^*} q_v^*}{N_{vp}^* D^{*2} \sqrt{\Delta p^*}} \quad (i)$
Specific gravity	$S_M = \frac{\sqrt{F_p} \sqrt{G_F} q_v^*}{N_{vG}^* D^{*2} \sqrt{\Delta p^*}} \quad (d)$	
pvT equation		$S_M = \frac{\sqrt{G} \sqrt{\rho_{f1}^*} q_v^*}{N_{vpt}^* \sqrt{Z_{f1}} \sqrt{T_{K1}} D^{*2} \sqrt{\Delta p^*}} \quad (j)$
Volumetric flow rate at base conditions		
Density	$S_M = \frac{\rho_b^* q_v^*}{N_{vp}^* D^{*2} \sqrt{F_p} \sqrt{\rho_F^*} \sqrt{\Delta p^*}} \quad (e)$	$S_M = \frac{\rho_b^* q_v^*}{N_{vp}^* D^{*2} \sqrt{\rho_{f1}^*} \sqrt{\Delta p^*}} \quad (k)$
Specific gravity	$S_M = \frac{G_b q_v^*}{N_{vG}^* D^{*2} \sqrt{F_p} \sqrt{G_F} \sqrt{\Delta p^*}} \quad (f)$	
pvT equation		
Standard base		$S_M = \frac{\sqrt{Z_{f1}} \sqrt{T_{K1}} \sqrt{G} q_v^*}{N_{vpT}^* Z_b D^{*2} \sqrt{\Delta p^*} p_{f1}^*} \quad (l)$
Selected base		$S_M = \frac{\sqrt{Z_{f1}} \sqrt{T_{K1}} \sqrt{G} p_b^* q_v^*}{(N_{vpT}^*)_b Z_b T_{Kb} D^{*2} \sqrt{\Delta p^*} p_{f1}^*} \quad (m)$

Notes: Gas (vapor) equations are written for upstream pressure tap. For downstream pressure tap, change subscript 1 to subscript 2, in ρ_{f2} , p_{f2} , Z_{f2} , etc.

TABLE 9.25 Sizing-Factor S_M Equations for Gas Flow Using Gas Factor Equations (F_{PB} , F_{TB} , F_{TF} , F_{pv}): U.S. and SI Units

	U.S. units	SI units
Mass flow rate	$S_M = \frac{Z_b F_g q_M}{N_{Mhp} F_{pv1} F_{TF1} D^2 \sqrt{h_w p_{f1}}} \quad (a)$	$S_M = \frac{Z_b F_g q_M^*}{N_{Mhp}^* F_{pv1} F_{TF1}^* D^{*2} \sqrt{\Delta p^* p_{f1}^*}} \quad (d)$
Volumetric flow rate at flowing conditions	$S_M = \frac{F_{TF1} F_{pv1} \sqrt{p_{f1}} q_v}{N_{vhp} F_g Z_b D^2 \sqrt{h_w}} \quad (b)$	$S_M = \frac{F_{TF1}^* F_{pv1} \sqrt{p_{f1}^*} q_v^*}{N_{vhp}^* F_g Z_b D^{*2} \sqrt{\Delta p^*}} \quad (e)$
Volumetric flow rate at base conditions	$S_M = \frac{q_{vb}}{N_{vhp} F_{PB} F_{TB} F_{TF1} F_{pv1} F_g D^2 \sqrt{h_w p_{f1}}} \quad (c)$	$S_M = \frac{q_{vb}^*}{N_{vhp}^* F_{PB}^* F_{TB}^* F_{TF1}^* F_{pv1} F_g D^{*2} \sqrt{\Delta p^* p_{f1}^*}} \quad (f)$

Notes: Gas (vapor) equations are written for upstream pressure tap. For downstream pressure tap, change subscript 1 to subscript 2 in p_{f2} , p_{f2} , Z_{f2} , etc.
 D and D^* in these equations are at flowing conditions: $D = F_{aD} D_{\text{meas}} = [1 + \alpha_p(T_{\text{F}} - 68)] D_{\text{meas}}$ [Eq. (9.50)]; $D^* = F_{aD}^* D_{\text{meas}}^* = [1 + \alpha_p^*(T_{\text{C}} - 20)] D_{\text{meas}}^*$ [Eq. (9.52)].

TABLE 9.26 Summary of Gas (Vapor) Expansion-Factor Equations

Equation		Pressure relationships	
		U.S. units	SI units
Contoured primary elements (nozzle, venturi, venturi nozzle, Lo-Loss, [†] etc.)			
Upstream measurements	$Y_1 = \left\{ \frac{(1 - \beta^4)[k/(k - 1)](p_{f2}/p_{f1})^{2/k}[1 - (p_{f2}/p_{f1})^{(k-1)/k}]}{[1 - \beta^4(p_{f2}/p_{f1})^{2/k}](1 - p_{f2}/p_{f1})} \right\}^{1/2}$	(a) [‡]	$\frac{p_{f2}}{p_{f1}} = \frac{p_{f2}^*}{p_{f1}^*} = 1 - x_1 \quad (i)$
Downstream measurements	$Y_1 = Y_2 \sqrt{1 + x_2}$	(b) [‡]	$\frac{p_{f2}}{p_{f1}} = \frac{p_{f2}^*}{p_{f1}^*} = \frac{1}{1 + x_2} \quad (j)$
Concentric orifice			
Corner, flange, D and $D/2$ taps			
Upstream measurements	$Y_1 = 1 - (0.41 + 0.35\beta^4) \frac{x_1}{k}$	(c)	
Downstream measurements	$Y_2 = \sqrt{1 + x_2} - (0.41 + 0.35\beta^4) \frac{x_2}{k\sqrt{1 + x_2}}$	(d)	$x_1 = \frac{h_w}{27.73p_{f1}} \quad x_2 = \frac{\Delta p^*}{p_{f1}} \quad (k)$
$2\frac{1}{2}D$ and $8D$			
Upstream measurements	$Y_1 = 1 - [0.333 + 1.145(\beta^2 + 0.7\beta^5 + 12\beta^{13})] \frac{x_1}{k}$	(e)	
Downstream measurements	$Y_2 = \sqrt{1 + x_2} = [0.333 + 1.145(\beta^2 + 0.7\beta^5 + 12\beta^{13})] \frac{x_2}{k\sqrt{1 + x_2}}$	(f)	$x_2 = \frac{h_w}{27.73p_{f2}} \quad x_2 = \frac{\Delta p^*}{p_{f2}^*} \quad (l)$

Eccentric orifice

Upstream measurements	$Y_1 = 1 - (0.1926 + 0.574\beta + 0.9675\beta^2 - 4.24\beta^3 + 3.62\beta^4) \frac{x_1}{k} \quad (g)$	
-----------------------	---	--

Downstream measurements	$Y_2 = \sqrt{1 + x_2} - (0.1926 + 0.574\beta + 0.9675\beta^2 - 4.24\beta^3 + 3.62\beta^4) \frac{x_2}{k\sqrt{1 + x_2}} \quad (h)$	
-------------------------	--	--

Segmental

Upstream measurements	$Y_1 = 1 - (0.6439 - 2.506\beta + 7.05\beta^2 - 8.003\beta^3 + 3.468\beta^4) \frac{x_1}{k}$	
-----------------------	---	--

Downstream measurements	$Y_2 = \sqrt{1 + x_2} - (0.6439 - 2.506\beta + 7.05\beta^2 - 8.003\beta^3 + 3.468\beta^4) \frac{x_2}{k\sqrt{1 + x_2}}$	
-------------------------	--	--

†Registered trademark of Badger Meter, Inc. Manufacturer should be consulted for recommendations.

‡For SI units, substitute $p_{f2}^*/p_{f1}^* = p_{f2}/p_{f1}$ in these equations.

mary interest, the sizing and flow-rate equations can be simplified by approximating the effect of Reynolds number, assuming that the liquid compressibility is negligible, and, in the case of gas flow, assuming that the expansion factor is negligible. The simplified equations have been referred to by Spink (1967) as *plant equations*.

Over normal operating ranges for liquids and gases (vapors), the discharge coefficient does not significantly vary with Reynolds number, and it can be expressed with reasonable accuracy as

$$C = k_1 + k_2 S_M \quad (9.80)$$

where k_1 and k_2 are constants derived by fitting the discharge coefficient at either the infinite Reynolds number (C_∞) or over a selected Reynolds-number range to the value of S_M calculated from Eq. (9.78).

If the gas expansion factor Y is 1.0, the substitution of Eq. (9.80) into Eq. (9.78) gives β_0 , the first approximation to β , as

$$\beta_0 = \left[1 + \left(\frac{k_1 + k_2 S_M}{S_M} \right)^2 \right]^{-1/4} = \left[1 + \left(\frac{k_1}{S_M} + k_2 \right)^2 \right]^{-1/4} \quad (9.81)$$

This simplifying assumption thus allows β_0 to be calculated directly from the S_M factor.

Table 9.27 lists the limits on the variables for approximately 1 to 3 percent accuracy in sizing the bore. In Table 9.28 are the β_0 approximation equations; in Table 9.29, the calculation procedure for liquids; and in Table 9.30, the procedure for gas (vapor) sizing.

Example 9.1. For the gasoline of Example 2.12, determine, by the β_0 method, the bore of a stainless-steel flange-tapped orifice required to measure 100 base gal/min (6.31 L/s) in a 2-in (50-mm) Schedule-80 carbon-steel pipe.

Design information

- Flow rate: $(q_{GPM})_{URV} = 100$ base gal/min
- Differential pressure at URV flow rate: $(h_w)_{URV} = 100$ in
- Flowing pressure: $p_f = 1000$ psia

TABLE 9.27 Limits on β_0 Sizing Method for Approximately 2 Percent Accuracy†

	Liquid	Gas (vapor)
Reynolds number		
Orifice	$R_D \geq 10,000$	$R_D \geq 10,000$
Venturi nozzle	$R_D \geq 100,000$	$R_D \geq 10,000$
Lo-Loss	$R_D \geq 100,000$	$R_D \geq 10,000$
Expansion factor‡	$Y_1 = 1.0$	$\frac{h_w}{p_{f1}} \leq 0.5; \frac{\Delta p^*}{p_{f1}^*} \leq 0.02$
	$Y_2 = 1.0$	$\frac{h_w}{p_{f2}} \leq 1.0; \frac{\Delta p^*}{p_{f2}^*} \leq 0.04$

†Assumes pipe diameter D or D^* is measured.

‡Ratios are based on upper-range differential pressure; operating flow rate is selected as 0.8 of upper-range flow rate, 0.64 of upper-range differential pressure.

- Flowing temperature: $T_F = 80.5^\circ\text{F}$

Scale to normal operating conditions

- Normal flow rate: $(q_{\text{GPM}})_N = 0.8 (q_{\text{GPM}})_{\text{URV}} = 80$ base gal/min
- Normal differential pressure: $(h_w)_N = 0.64 (h_w)_{\text{URV}} = 64$ in

TABLE 9.28 β_0 Approximate Sizing Equations

Type	Equation	
Venturi		
Machined inlet	$\beta_0 = \left[1 + \left(\frac{0.995}{S_M} \right)^2 \right]^{-1/4}$	(a)
Rough-cast inlet	$\beta_0 = \left[1 + \left(\frac{0.984}{S_M} \right)^2 \right]^{-1/4}$	(b)
Rough-welded sheet iron	$\beta_0 = \left[1 + \left(\frac{0.985}{S_M} \right)^2 \right]^{-1/4}$	(c)
Universal Venturi Tube†	$\beta_0 = \left[1 + \left(\frac{0.9797}{S_M} \right)^2 \right]^{-1/4}$	(d)
Lo-Loss tube‡	$\beta_0 = \left[1 + \left(\frac{0.92}{S_M} - 0.31 \right)^2 \right]^{-1/4}$	(e)
Nozzle		
ASME long radius	$\beta_0 = \left[1 + \left(\frac{0.9975}{S_M} \right)^2 \right]^{-1/4}$	(f)
ISA	$\beta_0 = \left[1 + \left(\frac{0.9944}{S_M} - 0.118 \right)^2 \right]^{-1/4}$	(g)
Venturi nozzle (ISA inlet)	$\beta_0 = \left[1 + \left(\frac{0.989}{S_M} - 0.09 \right)^2 \right]^{-1/4}$	(h)
Orifice		
Corner, flange, D -and- $D/2$ taps		
$R_D < 200,000$	$\beta_0 = \left[1 + \left(\frac{0.6}{S_M} + 0.06 \right)^2 \right]^{-1/4}$	(i)
$R_D > 200,000$	$\beta_0 = \left[1 + \left(\frac{0.6}{S_M} \right)^2 \right]^{-1/4}$	(j)
$2\frac{1}{2}D$ and $8D$ taps	$\beta_0 = \left[1 + \left(\frac{0.61}{S_M} + 0.55 \right)^2 \right]^{-1/4}$	(k)
Eccentric, all taps	$\beta_0 = \left[1 + \left(\frac{0.607}{S_M} + 0.088 \right)^2 \right]^{-1/4}$	(l)
Segmental, all taps	$\beta_0 = \left[1 + \left(\frac{0.634}{S_M} - 0.062 \right)^2 \right]^{-1/4}$	(m)
Quadrant ($\beta \leq 0.6$)	$\beta_0 = \left[1 + \left(\frac{0.76}{S_M} + 0.26 \right)^2 \right]^{-1/4}$	(n)
Conic, corner ($\beta \leq 0.3$)	$\beta_0 = \left[1 + \left(\frac{0.734}{S_M} \right)^2 \right]^{-1/4}$	(o)

†From BIF CALC 440/441; the manufacturer should be consulted for exact coefficient information.

‡Derived from Badger Meter, Inc. Lo-Loss flow-tube coefficient curve.

TABLE 9.29 Procedure for β_0 Sizing: Liquids

Procedure	Symbol		Reference
	U.S. units	SI units	
1. Select flow rate, [†] line size differential pressure, and S_M -factor equation			
a. Select the flow-rate value to be at the upper-range chart value, and the minimum far enough out on the chart for the desired readability (the flow unit may be mass or volume).	$(q)_{URV}$	$(q^*)_{URV}$	Figs. 9.7, 9.8
b. Select the S_M -factor equation for liquid for gas based on the flow-rate unit and the method of density determination (ρ_f , G_F).	S_M	S_M	Tables 9.23–9.24
c. Obtain the N factor for the desired flow-rate unit (q_{PPM} , q_{GPM} , q_{cms} , etc.).	N	N^*	Tables 9.14–9.17
d. Select the upper-range differential pressure for the upper-range flow rate. Use $h_w = 100$ in, $\Delta p^* = 25$ kPa if not otherwise specified.	$(h_w)_{URV}$	$(\Delta p^*)_{URV}$	
e. Obtain the nominal pipe diameter from Table B.1. For SI units, $D^* = 25.4D$.	D_{meas}	D^*_{meas}	Table B.1
f. Calculate or graphically obtain the pipe thermal-expansion factor.	F_{aD}	F^*_{aD}	Eq. (9.50) (U.S. units), Eq. (9.52) (SI units), Fig. 9.5, Table B.4
g. Calculate the pipe diameter at flowing conditions.	D	D^*	Eq. (9.50) (U.S. units), Eq. (9.52) (SI units)
h. Calculate or graphically obtain the primary element's thermal-expansion factor.	F_{ad}	F^*_{ad}	Eq. (9.50) (U.S. units), Eq. (9.52) (SI units), Fig. 9.5, Table B.4
2. Scale to normal operating flow rate			
a. Multiply the URV flow rate by 0.8 and use this in all subsequent calculations.	$(q)_N$	$(q^*)_N$	
b. Multiply the upper-range differential pressure by 0.64 and use this in all subsequent calculations.	$(h_w)_N$	$(\Delta p^*)_N$	
3. Obtain fluid properties [‡]			
a. From the selected S_M -factor equation, tabulate the necessary fluid properties to solve for S_M .	S_M	S_M	Tables 9.23–9.24
b. Obtain the necessary density or specific gravity from measurements, tables, graphs, or prediction equations.	ρ , G_F	ρ^* , G_F	App. E

TABLE 9.29 Procedure for β_0 Sizing: Liquids (*Continued*)

Procedure	Symbol		Reference
	U.S. units	SI units	
c. Obtain the fluid viscosity from measurements, tables, or graphs; convert to centipoises if necessary (Table C.2).	μ_{cP}	μ_{cP}	App. F
d. Calculate the pipe Reynolds number to ensure it is above the minimum Reynolds-number range given in Table 9.27.	R_D	R_D	Tables 9.20–9.21, Tables C.4, C.5
4. Calculate S_M factor			
a. Set the liquid compressibility factor F_p to 1.0 if it is unknown or assumed to be negligible.	F_p	F_p	App. E, Eqs. (2.107), (2.110), (2.111)
b. Substitute values into the S_M -factor equation, and solve for S_M .	S_M	S_M	Tables 9.23–9.24
5. Calculate β_0 : For the selected primary device, substitute the value of S_M into the β_0 equation.	β_0	β_0	Table 9.28
6. Calculate the bore of the primary element at 68°F (20°C) as $d_{meas} = \beta D / F_{ad}$	d_{meas}	d_{meas}^*	Eq. (9.54)

†See Chap. 3.

‡See Chap. 2.

• From Table B.4: $\alpha_p = 0.0000067 \text{ in}/(\text{in} \cdot ^\circ\text{F})$ • From Table B.4: $\alpha_{pE} = 0.0000096 \text{ in}/(\text{in} \cdot ^\circ\text{F})$

Calculate S_M factor. For base volume flow with specific-gravity determination, Eq. (f) of Table 9.23 gives

$$S_M = \frac{G_b q_{GPM}}{N_{VG} D^2 \sqrt{F_p} \sqrt{G_F} \sqrt{h_w}}$$

Data for the right-hand side is obtained as follows:

• From Example 2.12: $G_b = 0.7359$ • From Example 2.12: $G_F = 0.7255$ • From Table 9.16: $N_{VG} = 5.6665$ • From Eq. (9.50) $F_{ad} = 1 + \alpha_p (T_F - 68) = 1 + 0.0000067 (80.5 - 68) = 1.00008$ • From Eq. (9.51) $F_{ad} = 1 + \alpha_{pE} (T_F - 68) = 1 + 0.0000096 (80.5 - 68) = 1.00012$ • From Eq. (9.50) $D = F_{ad} D_{meas} = (1.00008)(1.939) = 1.9392$ • From Table B.1: $D_{meas} = 1.939 \text{ in}$ • Liquid compressibility factor: $F_p = 1.0$

Substitution into the S_M -factor equation gives

TABLE 9.30 Procedure for β_0 Sizing: Gases (Vapors)

Procedure	Symbol		Reference
	U.S. units	SI units	
1. Select flow rate† line size, differential pressure, and N factor			
a. Select the upper-range flow-rate value to be at the upper-range chart value, and the minimum far enough out on the chart for the desired readability. The flow unit may be mass or volume; for base volume flow, use 14.69595 psia (101.325 kPa) and 59°F (15°C) as standard, unless contractual or industry standard specifies otherwise.	$(q)_{URV}$	$(q^*)_{URV}$	Figs. 9.7, 9.8
b. Select the N factor for the desired flow-rate unit (p_{PPH} , q_{SCFD} , q_{acms} , etc.) and for the method of determining the density (densitometer, tables, p_vT equation, or gas-factor equation).	N	N^*	Tables 9.14–9.19
c. Select the upper-range differential pressure for maximum flow rate. Use 100 in and $\Delta p^* = 25$ kPa if not otherwise specified.	$(h_w)_{URV}$	$(\Delta p^*)_{URV}$	
d. Limit $h_w/p_f \leq 1.0$ and $\Delta p^*/p_f^* \leq 0.04$; see analytical or graphical-tabular solution procedure for larger ratio calculations.			
e. Obtain the nominal pipe diameter from Table B.1. For SI units, $D^* = 25.4D$.	D_{meas}	D^*_{meas}	Table B.1
f. Calculate or graphically obtain the pipe thermal-expansion factor.	F_{ad}	F^*_{ad}	Eq. (9.50) (U.S. units), Eq. (9.52) (SI units), Fig. 9.5, Table B.4
g. Calculate the pipe diameter at flowing conditions.	D	D^*	Eq. (9.50) (U.S. units), Eq. (9.52) (SI units)
h. Calculate or graphically obtain the primary element's thermal-expansion factor.	F_{ad}	F^*_{ad}	Eq. (9.50) (U.S. units), Eq. (9.52) (SI units), Fig. 9.5, Table B.4
2. Scale to normal operating flow rate			
a. Multiply the selected maximum flow rate by 0.8 and use this in all subsequent calculations.	$(q)_N$	$(q^*)_N$	
b. Multiply the selected upper-range differential pressure by 0.64 and use this in all subsequent calculations.	$(h_w)_N$	$(\Delta p^*)_N$	

TABLE 9.30 Procedure for β_0 Sizing: Gases (Vapors) (*Continued*)

Procedure	Symbol		Reference
	U.S. units	SI units	
3. Obtain fluid properties [‡]			
a. For density determination, obtain the density from tables, graphs, by prediction equation, or from a pvT calculation.	ρ_f	ρ_f^*	Eqs. (2.10), (2.11) Steam (App. G)
b. For pvT equation, select:			
Operating temperature	T_f	T_K	
Specific gravity	G	G	Eq. (2.7) App. D
Compressibility factor	Z_f	Z_f	App. G
c. For the gas-factor equation, calculate or obtain from tables the multiplying factors:			
Temperature base (for standard base, $F_{TB} = F_{TB}^* = 1.0$)	F_{TB}	F_{TB}^*	Eqs. (9.62), (9.67); Tables 9.7, 9.11
Pressure base (for standard base, $F_{PB} = F_{PB}^* = 1.0$)	F_{PB}	F_{PB}^*	Eqs. (9.63), (9.68); Tables 9.8, 9.12
Flowing temperature	F_{TF}	F_{TF}^*	Eqs. (9.66), (9.69); Tables 9.10, 9.13
Specific gravity	F_g	F_g	Eq. (9.64), Table 9.9
Supercompressibility factor	F_{pv}	F_{pv}	Eq. (9.65)
d. Obtain the fluid viscosity from measurements, tables, or graphs; convert to centipoises if necessary (Table C.2).	μ_{cP}	μ_{cP}	App. H, steam (App. G)
e. Calculate the pipe Reynolds number to ensure it is above the minimum Reynolds number given in Table 9.27. For gas (vapor) flows, the Reynolds number is seldom below these limits. Use the normal flow rate for this calculation.	R_D	R_D	Tables 9.20–9.22, Tables C.4, C.5
4. Calculate the S_M factor			
a. Set the base compressibility factor Z_b to 1.0 for most practical applications.	Z_b	Z_b	
b. Substitute values into the S_M -factor equation, and solve for S_M .	S_M	S_M	Tables 9.23–9.25
5. Calculate β_0 : For the selected primary device, substitute the value of S_M into the β_0 equation.	β_0	β_0	Table 9.28
6. Calculate the bore of the primary element at 68°F (20°C) as $d_{meas} = \beta D / F_{ad}$.	d_{meas}	d_{meas}^*	Eq. (9.54)

[†]See Chap. 3.[‡]See Chap. 2.

$$S_M = \frac{(0.7359)(80)}{(5.6665)(1.9392)^2 \sqrt{0.7255} \sqrt{64}} = 0.40547$$

Check Reynolds number. Figure F.13 gives $\nu_{\text{cSt}} = 0.574$. Equation (2.201) is used to convert to centipoise:

$$\mu_{\text{cP}} = \frac{G_f \nu_{\text{cSt}}}{1.001} = \frac{(0.574)(0.7255)}{1.001} = 0.417$$

Then, from Eq. (f) of Table 9.20,

$$(R_D)_N = 17,903 \left[\frac{0.7359}{(0.417)(1.9392)(5.6665)} \right] (80) = 230,023$$

Compute β_0 . Since $(R_D)_N > 200,000$, Eq. (j) of Table 9.28 is used, and

$$\beta_0 = \left[1 + \left(\frac{0.6}{0.40547} \right)^2 \right]^{-1/4} = 0.7483$$

Note: β_0 can be calculated by taking the square root of the bracketed term twice, and then the reciprocal:

$$\begin{aligned} \beta_0 &= \frac{1}{\sqrt{\left[1 + \left(\frac{0.6}{0.40547} \right)^2 \right]^{1/2}}} = \frac{1}{\sqrt{(3.1898)^{1/2}}} \\ &= \frac{1}{\sqrt{1.7860}} = \frac{1}{1.3364} = 0.7483 \end{aligned}$$

Compute bore of orifice at measured temperature with Eq. (9.54):

$$d_{\text{meas}} = \frac{\beta D}{F_{ad}} = \frac{(0.7483)(1.9392)}{1.00012} = 1.451 \text{ in}$$

Example 9.2. Size, by the β_0 method, the bore of an ASME long-radius stainless-steel nozzle and a flange-tapped orifice for a steam flow of 30,000 lb_m/h (13,608 kg/h) in a 6-in (150-mm) Schedule-80S pipe. The pipe is to be of 316 stainless steel.

Design information

- Flow rate: $(q_{\text{PPH}})_{\text{URV}} = 30,000 \text{ lb}_m/\text{h}$
- Differential pressure at URV flow rate: $(h_w)_{\text{URV}} = 100 \text{ in}$
- Flowing upstream pressure: $p_{f1} = 204 \text{ psia}$
- Flowing upstream temperature: $T_F = 460^\circ\text{F}$

Scale to normal operating flow rate.

- Normal flow rate: $(q_{\text{PPH}})_N = 0.8 (q_{\text{PPH}})_{\text{URV}} = 24,000 \text{ lb}_m/\text{h}$
- Normal differential pressure: $(h_w)_N = 0.64 (h_w)_{\text{URV}} = 64 \text{ in}$

Calculate S_M factor. For mass flow with a density determination, Eq. (g) of Table 9.23 is used:

$$S_M = \frac{q_M}{N_{Mp} D^2 \sqrt{\rho_{f1}} \sqrt{h_w}}$$

Data is as follows:

- From Table 9.14: $N_{Mp} = 358.93$
- From Table B.4: $\alpha_{PE} = 0.0000096 \text{ in}/(\text{in} \cdot ^\circ\text{F})$
- From Table B.4: $\alpha_P = 0.0000096 \text{ in}/(\text{in} \cdot ^\circ\text{F})$
- From Eq. (9.50): $F_{ad} = 1 + 0.0000096(460 - 68) = 1.00376$
- From Eq. (9.50): $D = F_{ad} D_{\text{meas.}} = (1.00376)(5.761) = 5.7827$
- From Eq. (9.51): $F_{ad} = 1 + 0.0000096(460 - 68) = 1.00376$
- From Table B.1: $D_{\text{meas.}} = 5.761 \text{ in}$
- From Table G.1: $\rho_{f1} = 0.39524 \text{ lb}_m/\text{ft}^3$; $\mu_{cP} = 0.01747$

Substitution into the S_M -factor equation gives

$$\begin{aligned} S_M &= \frac{24,000}{(358.93)(5.7827)^2 \sqrt{0.39524} \sqrt{64}} \\ &= 0.39759 \end{aligned}$$

Bore of ASME long-radius flow nozzle. The Reynolds number at normal flow rate is, from Eq. (g) of Table 9.20,

$$(R_D)_N = 2267 \left[\frac{1}{(0.01747)(5.7827)(358.93)} \right] (24,000) = 1,500,475$$

Equation (f) of Table 9.28 gives

$$\beta_0 = \left[1 + \left(\frac{0.9975}{0.39759} \right)^2 \right]^{-1/4} = 0.6085$$

and the nozzle bore at 68°F is, by Eq. (9.54),

$$d_{\text{meas}} = \frac{\beta D}{F_{ad}} = \frac{(0.6085)(5.7827)}{1.00376} = 3.506$$

Bore of flange-tapped orifice. Equation (j) of Table 9.28 is used for $R_D > 200,000$:

$$\beta_0 = \left[1 + \left(\frac{0.6}{0.39759} \right)^2 \right]^{-1/4} = 0.7432$$

The orifice bore at 68°F is then, by Eq. (9.54),

$$d_{\text{meas}} = \frac{\beta D}{F_{ad}} = \frac{(0.7432)(5.7827)}{1.00376} = 4.282 \text{ in}$$

Iterative Solution

The solution for β and, hence, for the bore of the primary element is seen via Eq. (9.78) or (9.79) to require iteration, since both the discharge coefficient C and the

gas expansion factor Y are β -dependent. To solve for β , two solution methods are available; both converge rapidly. The first is Newton's method for the solution of numerical equations (Sec. A.1), and the second is simple iteration of Eq. (9.78) or (9.79). Newton's method is the more complex of the two, because of the number of terms contained both in the function and in the derivative of the function. It may be used for computer and programmable-calculator solutions, and it is applied to a sizing example in Sec. A.3. The iteration method is easier to understand, and it rapidly converges with the introduction of β_0 as the initial estimate.

In the iterative method, β_0 is first calculated by following the procedure given in Table 9.29 or 9.30. The substitution of β_0 into the discharge-coefficient equation in the general form of Eq. (9.49) then gives the first estimate of the discharge coefficient as

$$C_0 = (C_x)_0 + \frac{b_0}{R_D^n} \quad (9.82)$$

Substituting the isentropic exponent k and β_0 into the proper gas-expansion-factor equation from Table 9.26 gives the first estimate, $(Y_1)_0$. Then substitution of C_0 and $(Y_1)_0$ into Eq. (9.78) yields the second estimate for β as

$$\beta_1 = \left\{ 1 + \left[\frac{C_0(Y_1)_0}{S_M} \right]^2 \right\}^{-1/4} \quad (9.83)$$

Because β_0 is usually within 1 percent of the actual value of β , and the discharge coefficient for most primary elements is not highly sensitive to β , a single iteration is usually all that is required. Successive iterations can be expressed mathematically as follows:

$$\beta_n = \left\{ 1 + \left[\frac{C_{n-1}(Y_1)_{n-1}}{S_M} \right]^2 \right\}^{-1/4} \quad (9.84)$$

The iteration procedure for liquid sizing is given in Table 9.31, and for gas (vapor) sizing in Table 9.32.

Example 9.3. Correcting for the compressibility of the liquid, determine, by iteration, the orifice bore for the data of Example 9.1.

Recalculate the S_M factor for liquid compressibility. From Example 2.15, $F_p = 1.0088$ for part (a). From Eq. (f) of Table 9.23,

$$S_M = \frac{(0.7359)(80)}{(5.6665)(1.9392)^2 \sqrt{1.0088} \sqrt{0.7255} \sqrt{64}} = 0.40369$$

Iterate for β . From Eq. (j) of Table 9.28,

$$\beta_0 = \left[1 + \left(\frac{0.6}{0.40369} \right)^2 \right]^{-1/4} = 0.74715$$

The discharge-coefficient equation for the initial estimate of beta (β_0) is, from Table 9.1, for $D < 2.3$ in,

$$C_0 = (C_x)_0 + \frac{b_0}{R_D^n} = 0.5959 + 0.0312\beta_0^{2.1} - 0.184\beta_0^2$$

$$+ 0.039 \frac{\beta_0^4}{1 - \beta_0^4} - 0.0337 \frac{\beta_0^3}{D} + \frac{91.71 \beta_0^{2.5}}{(R_D)_N^{0.75}}$$

Substituting $D = 1.939$, $(R_D)_N = 230,040$, and $\beta_0 = 0.74715$ gives

$$C_0 = 0.60957$$

The second estimate for β is then, from Eq. (9.83) with $Y_1 = 1.0$ for liquids,

$$\beta_1 = \left\{ 1 + \left[\frac{0.60957}{0.40369} \right]^2 \right\}^{-1/4} = 0.74308$$

Substitution of β_1 into the flange-tap equation gives the second estimate for the discharge coefficient as $C_1 = 0.60965$. The third estimate for β is then, from Eq. (9.83),

$$\beta_2 = \left[1 + \left(\frac{0.60965}{0.40369} \right)^2 \right]^{-1/4} = 0.74303$$

The fourth estimate is similarly obtained as

TABLE 9.31 Procedure for Iterative Solution: Liquids

Procedure	Symbol		Reference
	U.S. units	SI units	
1. Calculate β_0 : Follow the procedure given in Table 9.29	β_0	β_0	Table 9.28
2. Select the discharge-coefficient equation for the primary device. The general form of the equation is $C = C_\infty + b/R_D^n$.	C	C	Table 9.1
3. Iterate to obtain successive values for β .			
a. Set $Y = 1.0$ for liquids.			
b. Substitute β_0 into the discharge-coefficient equation selected in step 2, and solve for C_0 .	C_0	C_0	
c. Calculate the second estimate for β as	β_1	β_1	Eq. (9.83)
	$\beta_1 = \left[1 + \left(\frac{C_0}{S_M} \right)^2 \right]^{-1/4}$		
d. Repeat from step 3b until $\beta_n - \beta_{n-1} < 0.0001$, where	β_n	β_n	Eq. (9.84)
	$\beta_n = \left[1 + \left(\frac{C_{n-1}}{S_M} \right)^2 \right]^{-1/4}$		
4. Calculate the bore of the primary element at 68°F (20°C) as	d_{meas}	d_{meas}^*	Eq. (9.51) U.S. units, Eq. (9.53) SI units
	$d_{\text{meas}} = \frac{\beta D}{F_{ad}}$		

TABLE 9.32 Procedure for Iterative Solution: Gases (Vapors)

Procedure	Symbol		Reference
	U.S. units	SI units	
1. Calculate β_0 ; Follow the procedure given in Table 9.30	β_0	β_0	Table 9.30
2. Select the discharge-coefficient equation for the primary device. The general form of the equation is $C = C_\infty + b/R_D^n$.	C	C	Table 9.1
3. Iterate to obtain successive values for β .			
a. Substitute β_0 into the discharge-coefficient equation selected in step 2 to obtain an initial estimate.	C_0	C_0	
b. Calculate the initial estimate of the gas expansion factor by substituting β_0 into the expansion-factor equation for the primary device, using the following for the isentropic exponent:			Table 9.26
$k = k_i = \frac{(C_p)_i}{(C_p)_i - 1.986} \text{ for } \frac{h_w}{p_{f1}} \leq 1, \dagger$			
$p_{f1} \leq 0.25 p_c \quad \frac{\Delta p^*}{p_{f1}^*} \leq 0.04$	k_i	k_i	Fig. I.17, Table I.1, Eq. (2.242), Eq. (2.1)
and			Eq. (2.105)
$k = k \text{ (isentropic exponent)} \ddagger \text{ for } \frac{h_w}{p_{f1}} > 1,$			
$p_{f1} > 0.25 p_c \quad \frac{\Delta p^*}{p_{f1}^*} > 0.04,$	k	k	Figs. I.1–I.16 (2.246)
c. Calculate the second estimate for β as	β_1	β_1	Eq. (9.83)
$\beta_1 = \left[1 + \left(\frac{C_0(Y_1)_0}{S_M} \right)^2 \right]^{-1/4}$			
d. Repeat step 3a until $\beta_n - \beta_{n-1} < 0.0001$, where	β_n	β_n	Eq. (9.84)
$\beta_n = \left\{ 1 + \left[\frac{C_{n-1}(Y_1)_{n-1}}{S_M} \right]^2 \right\}^{-1/4}$			
4. Calculate the bore of the primary element at 68°F (20°C) as	d_{meas}	d_{meas}^*	Eq. (9.51) (U.S. units), Eq. (9.53) (SI units)
$d_{\text{meas}} = \frac{\beta D}{F_{ad}}$			

†For maximum bias error of $\pm 0.1\%$ for orifice and $\pm 0.2\%$ for nozzle, venturi, etc.

See Chap. 2 for the calculation and Appendix Sec 1.

$$\beta_3 = \left[1 + \left(\frac{0.60965}{0.40369} \right)^2 \right]^{-1/4} = 0.74303$$

The orifice bore, measured at 68°F, is then, by Eq. (9.54),

$$d_{\text{meas}} = \frac{\beta D}{F_{ad}} = \frac{(0.74303)(1.9392)}{(1.00012)} = 1.4406 \text{ in}$$

Example 9.4. Size, by iteration, the flow-nozzle bore for the conditions of Example 9.2.

Data from Example 9.2 is as follows:

$$(q_{\text{PPH}})_{\text{URV}} = 30,000 \quad (q_{\text{PPH}})_N = 24,000 \quad \beta_0 = 0.6091$$

$$(h_w)_{\text{URV}} = 100 \quad (h_w)_N = 64 \quad S_M = 0.39848$$

$$(R_D)_{\text{URV}} = 1,882,700 \quad p_{f1} = 204 \quad (R_D)_N = 1,502,192$$

The initial estimate of the discharge coefficient, from Table 9.1, is

$$C_0 = 0.9975 - \frac{6.53\beta_0^{0.5}}{(R_{of})_n^{0.5}} = 0.9933$$

The expansion factor is found with Eq. (a) of Table 9.26:

$$(Y_1)_0 = \left\{ \frac{(1 - \beta_0^4)[k_i/(k_i - 1)](p_{f2}/p_{f1})^{2/h_i}[1 - (p_{f2}/p_{f1})^{(h_i-1)/h_i}]}{[1 - \beta_0^4(p_{f2}/p_{f1})^{2/h_i}](1 - p_{f2}/p_{f1})} \right\}^{1/2}$$

From Eq. (i) of Table 9.26,

$$\frac{p_{f2}}{p_{f1}} = 1 - x_1 = 1 - \frac{h_w}{27.73p_{f1}} = 1 - \frac{64}{(27.73)(204)} = 0.9887$$

and, using the ideal-gas isentropic exponent from Eq. (2.275), see Fig. I.16 for real-gas isentropic exponent,

$$k_i = \frac{(C_p)_i}{(C_p)_i - 1.986} = \frac{8.44}{8.44 - 1.986} = 1.308$$

where $(C_p)_i = 8.44 \text{ Btu}/(\text{lb}_m \cdot \text{mol} \cdot ^\circ\text{R})$ is found in Table I.2. Substitution above then gives $(Y_1)_0 = 0.99214$.

The second estimate for β is then, from Eq. (9.83),

$$\begin{aligned} \beta_1 &= \left\{ 1 + \left[\frac{(0.99334)(0.99214)}{0.39848} \right]^2 \right\}^{-1/4} \\ &= 0.6122 \end{aligned}$$

Substitution of β_1 into the expansion-factor and discharge-coefficient equations yields, for second estimates,

$$C_1 = 0.99334 \quad (Y_1)_1 = 0.99210$$

The third estimate for β is then

$$\beta_2 = \left\{ 1 + \left[\frac{(0.99334)(0.99210)}{0.39848} \right]^2 \right\}^{-1/4}$$

$$= 0.61226$$

The primary element bore at 68°F is calculated, by Eq. (9.54), as

$$d_{\text{meas}} = \frac{d}{F_{ad}} = \frac{\beta D}{F_{ad}} = \frac{(0.61167)(5.7827)}{(1.00376)} = 3.523 \text{ in}$$

Example 9.5. Size, by iteration, the flange-tap orifice for the data of Example 9.2, assuming (1) pipe and orifice are stainless steel and (2) the pipe material is carbon steel.

1. Stainless-steel orifice and pipe. From Table 9.1, for $D > 2.3$ in,

$$C = 0.5959 + 0.0312\beta^{2.1} - 0.184\beta^8 + 0.09 \frac{\beta^4}{D(1 - \beta^4)} - 0.0337 \frac{\beta^3}{D}$$

$$+ \frac{91.71\beta^{2.5}}{R_D^{0.75}}$$

The expansion factor is, from Eq. (c) of Table 9.26,

$$Y_1 = 1 - (0.41 + 0.35\beta^4) \frac{x_1}{k}$$

where

$$x_1 = \frac{h_w}{27.73 p_{f1}} = \frac{64}{(27.73)(204)} = 0.01131$$

and

$$k = k_i = 1.308$$

Thus,

$$Y_1 = 1 - 0.008649(0.41 + 0.35\beta^4)$$

The iteration equation for β is Eq. (9.84):

$$\beta_n = \left\{ 1 + \left[\frac{(C_{n-1})(Y_1)_{n-1}}{S_M} \right]^2 \right\}^{-1/4}$$

where $S_M = 0.39759$ and $\beta_0 = 0.74322$ from Example 9.2. The iteration may be tabulated as follows, using six places for calculation accuracy:

	n		
	1	2	3
β_{n-1}	0.7432217	0.743961	0.743989
C_{n-1}	0.600961	0.600893	0.600890
$(Y_1)_{n-1}$	0.995530	0.995526	0.995526
β_n	0.743961	0.743991	0.743992

The primary element bore at 68°F is calculated, by Eq. (9.54), as

$$d_{\text{meas}} = \frac{d}{F_{ad}} = \frac{\beta D}{F_{ad}} = \frac{(0.74399)(5.7827)}{(1.00376)} = 4.286 \text{ in}$$

2. *Stainless-steel orifice plate and carbon-steel pipe.* The carbon-steel pipe diameter at the 460°F flowing temperature is, by Eq. (9.50),

$$\begin{aligned} D &= [1 + \alpha_p(T_F - 68)]D_{\text{meas}} = [1 + 0.0000067(460 - 68)](5.761) \\ &= (1.002627)(5.761) = 5.7761 \text{ in} \end{aligned}$$

where for carbon steel (Table B.4) $\alpha_p = 0.0000067 \text{ in}/(\text{in} \cdot ^\circ\text{F})$.

Substitution into the S_M factor equation yields

$$S_M = \frac{q_{\text{PPH}}}{358.9268 D^2 \sqrt{\rho_{f1} h_w}} = 0.39848$$

Note that the S_M factor is different from the case when the pipe and primary element are of the same material (0.39759 versus 0.39848).

The iteration is tabulated as follows:

n	β_{n-1}	C_{n-1}	Y_{n-1}
1	0.74380	0.60000	0.99553
2	0.74457	0.60091	0.99552
3	0.74460	0.60084	0.99552

The primary element bore at 68°F is calculated, by Eq. (9.54), as

$$d_{\text{meas}} = \frac{d}{F_{ad}} = \frac{\beta D}{F_{ad}} = \frac{(0.74460)(5.776)}{(1.00376)} = 4.285 \text{ in}$$

Example 9.6. A natural gas mixture of 60 percent methane, 20 percent ethane, and 20 percent propane is flowing in an 8-in (200-mm) pipe. The pressure at a downstream pressure tap is 2000 psia (13.8 MPa), and the temperature is 100°F (37.8°C). Size a flange tap orifice to produce 100 in of water (24.85 kPa) when the flow rate is 2,000,000 standard cubic feet per hour at 14.7 psia and 60°F (56,634 SCMH). The pipe has a measured internal diameter of 7.620 in (193.6 mm), and a downstream pressure tap connection is to be installed.

The data for the natural gas mixture at 2000 psia and 100°F is as follows:

Specific gravity	$G = 0.8445$
Flowing compressibility	$Z_{f2} = 0.5688$
Base compressibility	$Z_b = 0.9974$
Viscosity	$\mu\text{cP} = 0.0255 \text{ cP}$
Isentropic exponent	$k = 2.29$

The sizing factor S_M written for standard cubic feet per hour at a selected base, from Table 9.23, Eq. (m), is

$$S_M = \frac{\sqrt{Z_{f2}}\sqrt{T_{f2}}\sqrt{G}p_b q_{SCFH}}{(N_{v_r,T})_b Z_b T_b D^2 \sqrt{h_w p_{f2}}}$$

where $(N_{v_r,T})_b = 218.4834$ from Table 9.16.

The thermal expansion factor for the primary element's bore is, by Eq. (9.51),

$$F_{ad} = 1 + \alpha_{PE}(T_F - 68) = 1 + 0.000096(100 - 68) = 1.00031$$

The pipe diameter of the carbon steel pipe at flowing conditions is obtained by using Eq. (9.50):

$$\begin{aligned} D &= F_{ad} D_{\text{meas}} = 1 + \alpha_p(T_F - 68) = 1 + 0.000067(100 - 68) \\ &= (1.00022)(7.620) = 7.6216 \text{ in} \end{aligned}$$

Substitution yields the sizing factor:

$$S_M = \frac{\sqrt{(0.5688)(100 + 459.67)(0.8445)}(14.7)(2,000,000)}{(218.48)(7.6216)^2(0.9975)(60 + 459.67)0.16336 \sqrt{(100)(2000)}} = 0.16386$$

The initial estimate for beta, by Table 9.28, Eq. (j), is then

$$\beta_0 = \left[1 + \left(\frac{0.6}{S_M} \right)^2 \right]^{-1/4} = \left[1 + \left(\frac{0.6}{0.16386} \right)^2 \right]^{-1/4} = 0.51327$$

The discharge coefficient, from Table 9.1 for $D > 2.3$ is:

$$C = 0.5959 + 0.0312\beta^{2.1} - 0.184\beta^8 + 0.09 \frac{\beta^4}{D(1 - \beta)^4} - 0.0337 \frac{\beta^3}{D} + \frac{91.71\beta^{2.5}}{R_D^{0.75}}$$

where the pipe Reynolds number is calculated from Table 9.20, Eq. (m):

$$R_D = \left[\frac{(3724.2)(0.8445)(14.7)}{(0.9974)(60 + 459.67)(0.0255)(7.62)(218.48)} \right] 2,000,000 = 4,201,225$$

The downstream tap gas expansion factor, from Table 9.26, Eq. (d), is

$$Y_2 = \sqrt{1 + x_2} - (0.41 + 0.35\beta^4) \frac{x_2}{k\sqrt{1 + x_2}}$$

where

$$x_2 = \frac{h_w}{27.73 p_{f2}} = \frac{100}{(27.73)(2000)} = 0.0018$$

and $k = 2.29$.

Thus, $Y_2 = 1.0008996 - 0.00078532(0.41 + 0.35\beta^4)$

The iteration for β then becomes, from Eq. (9.84):

$$\beta_n = \left\{ 1 + \left[\frac{(C_{n-1})(Y_{n-1})}{S_M} \right]^2 \right\}^{-1/4}$$

With $S_M = 0.16386$ and $\beta_0 = 0.51327$, the iteration is as follows:

	<i>n</i>		
	1	2	3
β_{n-1}	0.51327	0.511880	0.511889
C_{n-1}	0.603171	0.603141	0.603141
$(Y_2)_{n-1}$	1.000559	1.000559	1.000559

The primary element bore at 68°F is calculated, by Eq. (9.54), as

$$d_{\text{meas}} = \frac{d}{F_{ad}} = \frac{\beta D}{F_{ad}} = \frac{(0.511889)(7.6216)}{(1.00031)} = 3.900 \text{ in}$$

Example 9.7. Using the gas-factor equation, size by iteration the bore of a corner-tap orifice for a natural gas with a specific gravity of 0.652, flowing at 340 standard m³/h at 100 kPa and 14°C in a 52.50-mm pipe. The following design information is selected for an upstream measurement of pressure and temperature.

Design information:

- Flow rate: $(q_{\text{SCMH}}^*)_{\text{URV}} = 340$ standard m³/h
- Differential pressure at maximum flow rate: $(\Delta p^*)_{\text{URV}} = 10$ kPa
- Upstream flowing pressure: $p_{f*}^* = 184$ kPa
- Upstream absolute temperature: $T_{K1} = 300$ K (26.85°C)
- Plate material: 304 stainless steel
- Pipe material: Carbon steel

Scale to normal operating conditions:

- Normal operating flow rate: $(q_{\text{SCMH}}^*)_N = 0.8(q_{\text{SCMH}}^*)_{\text{URV}} = 272$ standard m³/h
- Normal differential pressure: $(\Delta p^*)_N = 0.64(\Delta p^*)_{\text{URV}} = 6.4$ kPa

Calculate S_M factor. Equation (f) of Table 9.25,

$$S_M = \frac{q_{\text{SCMH}}^*}{N_{Vhp}^* F_{PB}^* F_{TB}^* F_{TF1}^* F_{pv1}^* F_g D^{*2} \sqrt{\Delta p^*} p_{f1}^*}$$

is used here, with q_{SCMH}^* in place of q_{Vb}^* , and the denominator factors may be tabulated as follows:

Factor	Reference	Equation	Value
N_{Vhp}^*	Table 9.19		0.011350
F_{ad}^*	Eq. (9.53)	$F_{ad}^* = 1 + \alpha_{PE}^* (T_c - 20)$	1.00012
	Table B.4	$\alpha_{PE}^* = .000017 \text{ mm}/(\text{mm} \cdot ^\circ\text{C})$	
F_{aD}^*	Eq. (9.52)	$F_{aD}^* = 1 + \alpha_p^* (T_c - 20)$	1.00008
		$\alpha_p^* = .000012 \text{ mm}/(\text{mm} \cdot ^\circ\text{C})$	
F_{PB}^*	Eq. (9.68)	$F_{PB}^* = \frac{101.325}{p_b^*}$	1.0133
F_{TB}^*	Eq. (9.67)	$F_{TB}^* = \frac{T_{Kb}}{288.15}$	0.99653

Factor	Reference	Equation	Value
F_{TF1}^*	Eq. (9.69)	$F_{TF1}^* = \sqrt{\frac{288.15}{T_{K1}}}$	0.98005
F_{pv1}^*	Eq. (2.37)†	$F_{pv1}^* = \sqrt{1 + \frac{4.66p_G 10^{5+1.6G}}{T_{f1}^{3.825}}}$	1.0011
F_g	Eq. (9.64)	$F_g = \sqrt{\frac{1}{G}}$	1.2384

†From Table C.1, $T_{f1} = 1.8T_{K1} = 540^\circ\text{R}$, and $p_G = (184 - 101.325)/6.8948 = 11.991$ psig.

The pipe diameter at flowing conditions is calculated, by Eq. (9.52), as

$$D^* = F_{aD}^* D_{\text{meas}}^* = (1.00008)(52.50) = 52.504 \text{ mm}$$

Substitution into the S_M -factor equation at normal flow rate gives

$$S_M = \frac{272}{(0.011350)(1.0133)(0.99653)(0.98005)(1.0011)(1.2384)(52.504)^2 \sqrt{(6.4)(184)}} = 0.20647$$

Calculate β_0 . From Eq. (f) of Table 9.22,

$$(R_D)_N = 4.9171 \frac{1}{(F_g^2 F_{PB}^* F_{TB}^* Z_b \mu_{cP} D^* N_{Vhp}^*)} (q_{SCMH})_N$$

From Fig. H.16, $\mu_{cP} = 0.0118$, and substitution gives $(R_D)_N = 122,812$. For $R_D < 200,000$, Eq. (i) of Table 9.28 is used to compute

$$\beta_0 = \left[1 + \left(\frac{0.6}{0.20647} + 0.06 \right)^2 \right]^{-1/4} = 0.56523$$

Iterate for β . From Eq. (9.84),

$$\beta_n = \left\{ 1 + \left[\frac{C_{n-1}(Y_1)_{n-1}}{S_M} \right]^2 \right\}^{-1/4}$$

where, from Table 9.1 for corner taps,

$$C_{n-1} = 0.5959 + 0.0312\beta_{n-1}^{2.1} - 0.184\beta_{n-1}^8 + \frac{91.706\beta_{n-1}^{2.5}}{(R_D)_N^{0.75}}$$

Also, from Eq. (c) of Table 9.26,

$$(Y_1)_{n-1} = 1 - (0.41 + 0.35\beta_{n-1}^4) \frac{x_1}{k}$$

where

$$x_1 = \frac{\Delta p^*}{p_{f1}^*} = \frac{6.4}{184} = 0.03478$$

and, from Fig. I.9, $k = 1.27$. The iteration may be tabulated as follows:

	<i>n</i>	
	1	2
β_{n-1}	0.5652	0.5707
C_{n-1}	0.6000	0.6069
$(Y_1)_{n-1}$	0.9878	0.9878
β_n	0.5707	0.5707

The primary element bore at 68°F is calculated, by Eq. (9.54), as

$$d_{\text{meas}}^* = \frac{d^*}{F_{ad}^*} = \frac{\beta D^*}{F_{ad}^*} = \frac{(0.57067)(52.504)}{1.00012} = 29.96 \text{ mm}$$

Graphical Solution

The procedure for graphical sizing is illustrated in Fig. 9.9, and the actual graphs are presented in Chap. 10. In this procedure, the discharge coefficient and gas expansion factor are determined graphically rather than by calculation. The four steps are shown in Fig. 9.9 For Example 9.5 and may be summarized as follows:

- *Step 1 (Fig. 9.9).* Calculate β_0 and the normal operating Reynolds number by following the procedure for liquids in Table 9.29 or that for gases (vapors) in Table 9.30.
- *Step 2 (Fig. 9.9).* Enter the discharge coefficient-Reynolds number curves with the value of β_0 and the normal operating Reynolds number and read the discharge coefficient.
- *Step 3 (Fig. 9.9).* For gases (vapors), enter the appropriate isentropic exponent-primary-element gas expansion factor graph at the normal operating ratio $(h_w)_N/p_f$. Read the gas expansion factor $(Y_1)_0$ from the β line corresponding to β_0 .
- *Step 4 (Fig. 9.9).* Calculate the second estimate of the beta ratio using Eq. (9.84):

$$\beta_1 = \left\{ 1 + \left[\frac{C_0(Y_1)_0}{S_M} \right]^2 \right\}^{-1/4} \quad (9.84)$$

where S_M is the value obtained in the β_0 determination, and C_0 and $(Y_1)_0$ are the graphically obtained discharge coefficient and gas expansion factor. Given the accuracy of the graphs, a third estimate is unwarranted.

SPECIAL CONSIDERATIONS

Several additional multiplying factors may be introduced into the flow equation to compensate for particular measurement situations. These factors are used to correct a moist stream to a dry flow-rate basis, adjust for a nonhomogeneous flow, correct for the manometer-elevation bias, and compensate for a small drain hole through the primary element.

Correction for Steam Quality (Gas-Liquid Flow)

Two-phase flows are nonhomogeneous, and the flow equations do not apply. Several compensating equations have been proposed, to permit the use of the basic equations. Among these are the James (1965–1966) effective-density equation, the Smith-Leang (1974) blockage-factor equation, and Murdock's (1961) modified single-phase pseudo-gas flow-rate equation. The Murdock equation is the easiest to apply if certain simplifying assumptions are made. Murdock reports correlation to within ± 1.5 percent for orifices, and Smith and Leang suggest that the correlation is valid for venturis and nozzles.

Murdock's correlation is derived from 90 test points for steam-water (wet steam), air-water, natural gas-water, natural gas-salt water, and natural gas-distillate combinations and is applicable to both two-phase and two-component liquid-gas flows. The correlation is developed under the assumption that liquid and gas can be treated as if each were flowing *alone*; the total mass flow is the sum of the mass flows of the individual components, and the total flow area equals the sum of the areas occupied by the individual components. If negligible error is introduced when the gas and liquid flow coefficients are assumed equal, then the total mass flow is

Step 1: Calculate β_0

From Eq. (9.81),

$$\beta_0 = \left[1 + \left(\frac{k_1}{S_M} + k_2 \right)^2 \right]^{-1/4}$$

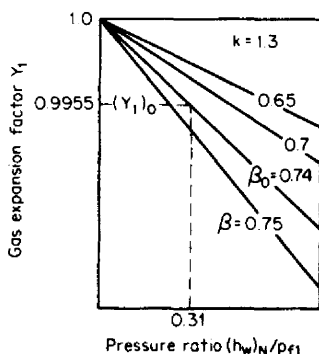
See Table 9.28 for β_0 equations

For Example 9.5,

$$\beta_0 = \left[1 + \left(\frac{0.6}{0.3976} \right)^2 \right]^{-1/4} = 0.7432$$

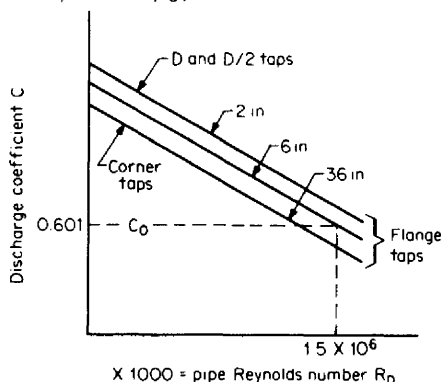
Step 3: Find expansion factor $(Y_1)_0$

[For liquids, $(Y_1)_0 = 1.0$]



Step 2: Find orifice discharge coefficient C_0

For $\beta = 0.74 \approx \beta_0$,



Step 4: Calculate β_1 and d

From Eq. (9.83),

$$\beta_1 = \left[1 + \left(\frac{C_0(Y_1)_0}{S_M} \right)^2 \right]^{-1/4}$$

For Example 9.5,

$$\beta_1 = \left[1 + \left(\frac{(0.601)(0.9955)}{0.3976} \right)^2 \right]^{-1/4} = 0.7440$$

$$d = \beta_1 D = (0.7440)(5.761) = 4.286 \text{ in}$$

Figure 9.9 Steps in graphical sizing; values shown are from Example 9.5. (Graphs are presented in Chap. 10).

$$(q_M)_{TC} = \frac{N_{M\rho} C_g d^2 Y_1 \sqrt{\rho_{g1}} \sqrt{h_w}}{\sqrt{1 - \beta^4} [\mathbf{X} + 1.26(1 - \mathbf{X}) \sqrt{\rho_{g1}/\rho_l}]} \quad (9.85)$$

where the subscript *TC* refers to the two-component flow; *g* to the gas; and *l* to the liquid component. The mixture quality *X*, gas mass flow rate, and liquid mass flow rate are defined by

$$\mathbf{X} = \frac{\text{mass of gas}}{\text{mass of mixture}} \quad (q_M)_g = \mathbf{X}(q_M)_{TC} \quad (q_M)_l = (1 - \mathbf{X})(q_M)_{TC} \quad (9.86)$$

Since the difference between Eq. (9.85) and the mass flow equation (9.60) is the bracketed denominator term in Eq. (9.85), a quality correction factor can be defined as

$$F_x = \frac{1}{\mathbf{X} + 1.26(1 - \mathbf{X}) \sqrt{\rho_{g1}/\rho_l}} \quad (9.87)$$

In calculating the total mass flow, the previously presented mass flow equations are multiplied by this correction factor; the discharge coefficient is calculated at the Reynolds number defined by the dry-gas flow rate [in Eq. (9.86)], and the dry-gas density is used in the mass flow equation. The gas expansion factor is calculated on the basis of the differential pressure produced by the dry gas. If the gas and liquid discharge coefficients are assumed to be approximately equal, the equation given by Murdock simplifies to

$$(h_w)_g = \frac{h_w}{\{1 + [1.26(1 - \mathbf{X})/\mathbf{X}] \sqrt{\rho_{g1}/\rho_l}\}^2} \quad (9.88)$$

In the SI system the mass flow equation is

$$(q_M^*)_{TC} = N_{M\rho}^* \frac{C_g d^{*2}}{\sqrt{1 - \beta^4}} F_x^* Y_1 \sqrt{\rho_{g1}^*} \sqrt{\Delta p^*} \quad (9.89)$$

where F_x^* is defined by

$$F_x^* = \frac{1}{\mathbf{X} + 1.26(1 - \mathbf{X}) \sqrt{\rho_{g1}^*/\rho_l^*}} \quad (9.90)$$

The differential pressure (in kilopascals) of the dry gas is given by

$$(\Delta p^*)_g = \frac{\Delta p^*}{\{1 + [1.26(1 - \mathbf{X})/\mathbf{X}] \sqrt{\rho_{g1}^*/\rho_l^*}\}^2} \quad (9.91)$$

The limits for the Murdock equation are $0.25 \leq \beta \leq 0.5$, $R_D > 100,000$, $Y_1 \geq 0.98$, and $\mathbf{X} \geq 0.9$.

Correction for Saturated Liquids

There are many applications where the liquid at the upstream pressure tap of an orifice is either saturated or contains up to 10 percent by mass saturated vapor.

Vapor is then formed (flashing) as the pressure decreases across the orifice. Experimental evidence indicates that the discharge coefficient C , in the presence of vapor, is about the same as the coefficient for a purely liquid flow, provided the upstream liquid is subcooled or saturated. The experimental work of Romig et al. (1966) shows that the mass flow is underestimated when using a saturated liquid or when liquid containing vapor exists at the upstream tap.

A quality correction factor term F_x is to be inserted in the liquid flow-rate or sizing equation for saturated or vapor-laden liquid upstream of the orifice plate. For saturated liquid ($X = 0$) at the upstream tap, this factor, for both U.S. and SI units, is

$$F_x = F_x^* = 0.968 + 0.112\beta \quad (9.92)$$

If the quality of the fluid at the upstream tap is greater than zero but less than 0.1 ($X \leq 0.1$), the suggested quality correction factor term, for U.S. units, is

$$F_x = 0.94 + 0.2 \frac{\rho_l}{\rho_{TP}} - 0.01 \left(\frac{\rho_l}{\rho_{TP}} \right)^2 \quad (9.93)$$

and for SI units it is

$$F_x^* = 0.94 + 0.2 \frac{\rho_l^*}{\rho_{TP}^*} - 0.01 \left(\frac{\rho_l^*}{\rho_{TP}^*} \right)^2 \quad (9.94)$$

where ρ_l is the density of the saturated liquid and ρ_{TP} is the two-phase density of the vapor-laden liquid at the upstream tap calculated, for U.S. units, by

$$\rho_{TP} = \frac{\rho_l}{1 + X(\rho_l/\rho_g - 1)} \quad (9.95)$$

and, for SI units, by

$$\rho_{TP}^* = \frac{\rho_l^*}{1 + X(\rho_l^*/\rho_g^* - 1)} \quad (9.96)$$

The two-phase upstream pipe Reynolds number is higher than for saturated liquid. The *apparent* viscosity to be used in calculating the pipe Reynolds number may be estimated by

$$\mu_{cP,app} = (1 - X)\mu_{cP,l} \quad (9.97)$$

where $\mu_{cP,l}$ is the viscosity of the saturated liquid phase, in centipoises.

Correction for Drain or Vent Holes

When a wet gas or saturated steam is measured in a horizontal pipe, a pool of liquid may form upstream of the primary element. In liquid flows, small quantities of gas or vapor bubbles tend to collect at the top of the pipe, causing erratic flow measurements. This condition may be alleviated by boring or drilling a small hole nearly flush with the inside diameter of the pipe; the hole is drilled at the bottom (as a drain hole) when condensate is carried in a gas or vapor stream, and at the top (as a vent hole) when a liquid contains entrained gas.

The effect of the hole is to increase the flow by an amount that depends on its area. If the hole diameter is less than one-tenth the bore diameter, the maximum flow through the hole is less than 1 percent of the total flow. The flow equation can be corrected for this added area by introducing a *drain-hole correction factor*. This factor is derived by noting that the total flow is the sum of the main flow and the drain-hole flow, and that the differential pressure is approximately the same for both. The drain-hole (or vent-hole) correction can then be written as

$$F_{DH} = 1 + \sqrt{1 - \beta^2} \frac{C_{DH}}{C} \left(\frac{d_{DH}}{d} \right)^2 \quad (9.98)$$

where C_{DH} is the discharge coefficient of the drain hole, and C is the discharge coefficient of the primary element. If the hole is square-edged, these coefficients are approximately the same, and Eq. (9.98) becomes

$$F_{DH} = 1 + \sqrt{1 - \beta^4} \left(\frac{d_{DH}}{d} \right)^2 \quad (9.99)$$

for orifices, and

$$F_{DH} = 1 + 0.6 \sqrt{1 - \beta^4} \left(\frac{d_{DH}}{d} \right)^2 \quad (9.100)$$

for nozzles and venturis.

If the hole is rounded, C_{DH} approaches the discharge coefficient of a nozzle or venturi, and Eq. (9.98) is approximated by

$$F_{DH} = 1 + 1.66 \sqrt{1 - \beta^4} \left(\frac{d_{DH}}{d} \right)^2 \quad (9.101)$$

for orifices, and

$$F_{DH} = 1 + \sqrt{1 - \beta^4} \left(\frac{d_{DH}}{d} \right)^2 \quad (9.102)$$

for nozzles and venturis.

When the bore is sized, d is initially unknown, and the drain-hole correction factor must be found by iteration. The hole diameter should be kept as small as possible, and the correction factor limited to a value no greater than 1.02 (and preferably less than 1.01). Table 9.33 gives maximum recommended hole diameters.

In small lines the small drain or vent hole may become plugged with dirt or scale. If this is a possibility, the meter run should be located in a vertical pipe, with upward flow to carry entrained gases in liquid streams through the primary element, and downward flow to purge liquids from gas streams.

Correction for Water Vapor

In the chemical and air-reduction industries (and some others), the volume or mass of the dry gas in a moist gas stream may be of interest. To correct to a dry basis, two separate corrections may be necessary. The first is a correction of the dry-gas specific gravity to that of the wet gas. (This correction is necessary only if the specific gravity was calculated from the molecular weights of the dry components,

or if the gas was dried prior to the specific-gravity determination. If the wet-gas specific gravity was measured, this correction is 1.0.) The second correction is a conversion of the measured wet flow rate to a dry-flow basis, using the water-vapor correction-factor equations developed in Chap. 2. These equations, which are multiplying factors for the flow-rate equations, are presented in Table 9.34.

Correction for Indicated Differential

If the differential-pressure measuring element is located substantially below or above the primary element, its reading will not exactly equal the true differential pressure. Corrections for elevation and for the wet-type manometer are developed in Chap. 3 and are summarized in Table 9.35. The differential pressure h_w in the flow equations is replaced with

$$h_w = F_{EL} F_M (h_w)_{ind} \quad (3.34)$$

for U.S. units, and

$$\Delta p^* = F_{EL}^* F_M^* (\Delta p^*)_{ind} \quad (3.35)$$

for SI units.

Example 9.8. Size a D and $D/2$ tap orifice to measure wet steam containing 20 percent liquid at 580 psia (4000 kPa) and $T_f = 483^\circ\text{F}$ (251°C). The 430-stainless-steel plate is to be installed in a carbon-steel pipe with a 2.500-in (63.50-mm) inside diameter. The differential-pressure measuring device has an upper-range value of 500 in H_2O (124.3 kPa), and the total mass flow is 10,320 lb_m/h (4681 kg/h).

TABLE 9.33 Recommended Maximum Drain-Hole (Vent-Hole) Diameters

Primary element bore d , in (mm)	Diameter d_{DH} of vent (drain) hole, in (mm)
1.000–3.500 (25.40–88.90)	$\frac{3}{32}$ (2.38)
3.501–4.125 (88.93–104.78)	$\frac{1}{8}$ (3.18)
4.126–5.000 (104.80–127.00)	$\frac{5}{32}$ (3.96)
5.001–6.000 (127.03–152.40)	$\frac{3}{16}$ (4.76)
6.001–6.750 (152.43–171.45)	$\frac{7}{32}$ (5.56)
6.751–7.500 (171.48–190.50)	$\frac{1}{4}$ (6.35)
7.501–8.375 (190.53–212.73)	$\frac{9}{32}$ (7.14)
8.376–9.250 (212.75–234.95)	$\frac{5}{16}$ (7.94)
9.251–10.000 (234.98–254.00)	$\frac{11}{32}$ (8.73)
10.001–10.875 (254.03–276.23)	$\frac{3}{8}$ (9.53)
10.876–11.625 (276.25–295.28)	$\frac{13}{32}$ (10.32)
11.626–12.500 (295.30–317.50)	$\frac{7}{16}$ (11.11)
12.501–13.250 (317.53–336.55)	$\frac{15}{32}$ (11.91)
> 13.251 (> 336.58)	$\frac{1}{2}$ (12.7)

Determine S_M factor. The S_M -factor equation is Eq. (g) of Table 9.23:

$$S_M = \frac{q_M}{N_{M\rho} D^2 F_x \sqrt{\rho_{g1}} \sqrt{h_w}}$$

The quality factor F_x has already been introduced into this equation, and the density has been replaced with the saturated-vapor density.

TABLE 9.34 Corrections to Flow Equations for Wet Gases

Use	Correction
Specific-gravity correction (mass and volumetric pvT flow-rate equations)	
Dry to wet specific-gravity correction	$G = G_{\text{wet}} = \left[1 + \frac{p_{\text{wv}}}{p_{\text{fl}}} \left(\frac{0.6220}{G_{\text{dry}}} - 1 \right) \right] G_{\text{dry}}$ (a)
Wet specific gravity measured	$G = G_{\text{wet}} = G_{\text{meas}}$
Water-vapor correction factor for volumetric flow-rate equations	
Actual wet flow rate at flowing temperature and pressure, at standard, or at a selected base temperature and pressure	$F_{\text{wv,wet}} = 1.0$ (b)
Saturated flow rate at standard, or at a selected base pressure and temperature	$F_{\text{wv,wet}} = \frac{1 - p_{\text{wv}}/p_{\text{fl}}}{1 - p_{\text{wvb}}/p_b}$ (c)
	$p_b = 14.696$ for standard conditions
	$p_{\text{wv}} =$ saturated vapor pressure at operating temperature
	$p_{\text{wvb}} =$ saturated vapor pressure at base temperature
Dry flow rate at actual flowing pressure and temperature and at standard or at a selected base temperature and pressure	$F_{\text{wv,dry}} = 1 - \frac{p_{\text{wv}}}{p_{\text{fl}}}$ (d)
Mass flow-rate equations	
Dry mass flow rate	$F_{\text{wvm,dry}} = 1 - \frac{0.6220}{G_{\text{wet}}} \frac{Z_{\text{wet}} p_{\text{wv}}}{Z_{\text{wv}} p_{\text{fl}}}$ (e)
	$Z_{\text{wet}} = \left(1 - \frac{p_{\text{wv}}}{p_{\text{fl}}} \right) Z_{\text{dry}} + \frac{p_{\text{wv}}}{p_{\text{fl}}} Z_{\text{wv}}$ (f)

From Table 9.14, $N_{Mp} = 358.93$; and from Table G.1,

$$\rho_{g1} = 1.254 \text{ lb}_m/\text{ft}^3 \quad \rho_l = 49.86 \text{ lb}_m/\text{ft}^3$$

The quality correction factor is then, from Eq. (9.87),

$$F_x = \frac{1}{0.8 + (1.26)(1 - 0.8) \sqrt{1.254/49.86}} = 1.1905$$

Substitution into the S_M -factor equation, with the differential pressure and flow rate scaled to normal operating conditions, gives

TABLE 9.35 Corrections for Differential-Pressure Measurement

Use	Correction
Elevation correction	
Liquid flows and seal fluids for both liquid and gas (vapor) flows (assumes leads at same temperature)	$F_{EL} = 1.0$ (a)
Gas flows†	
U.S. units	$F_{EL} = 1 - 0.01874 \frac{F_L G H_{LL}}{Z_{f1} T_{f1}}$ (b)
SI units	$F_{EL}^* = 1 - 0.03416 \frac{F_L G H_{LL}^*}{Z_{f1} T_{K1}}$ (c)
Manometer factor	
Gas and liquid flows for dry-type secondary devices	$F_M = 1.0$ (d)
Gas flow with no seal fluid in leads‡	
U.S. units	$F_M = 1 - \frac{2.6988 G p_{f1}}{Z_{f1} T_{f1} \rho_m}$ (e)
SI units	$F_M^* = 1 - \frac{3.4834 G p_{f1}^*}{Z_{f1} T_{K1} \rho_m^*}$ (f)
Liquid and gases (vapors) with seal fluid in leads§	
U.S. units	$F_M = 1 - \frac{\rho_{f1}}{\rho_m}$ (g)
SI units	$F_M^* = 1 - \frac{\rho_{f1}^*}{\rho_m^*}$ (h)

†The sign of H_{LL} is + (plus) when located below primary device, and - (minus) when above.

‡If lead-line temperature is not equal to operating temperature, Z and T are to be calculated at lead-line temperature.

§ $\rho_{f1} = \rho_s$ for seal fluid; ρ_m = manometer fluid density.

$$S_M = \frac{8256}{(358.93)(2.5069)^2(1.1905) \sqrt{1.254} \sqrt{320}} \\ = 0.1535$$

The pipe diameter D at flowing conditions is calculated, by Eq. (9.50), as

$$D = F_{aD} D_{\text{meas}} = [1 + 0.0000067(483 - 68)](2.500) = 2.5069 \text{ in}$$

where the thermal expansion factor is, from Table B.4, $\alpha_p = 0.0000067 \text{ in}/(\text{in } ^\circ\text{F})$.

Calculate normal operating Reynolds number for the gas phase. From Table G.1, $\mu_{\text{cp}} = 0.01760$, and from Eq. (9.86),

$$(q_{\text{PPH}})_g = (0.8)(8256) = 6605 \text{ lb}_m/\text{h}$$

Then, from Eq. (g) of Table 9.20 for the gas component (saturated vapor),

$$(R_D)_N = 2266.97 \left[\frac{1}{(0.01760)(2.500)(358.93)} \right] (6605) = 948,104$$

Calculate β_0 . From Eq. (j) of Table 9.28 for $R_D > 200,000$,

$$\beta_0 = \left[1 + \left(\frac{0.6}{0.1535} \right)^2 \right]^{-1/4} = 0.4978$$

Size by iteration. The discharge-coefficient equation for D and $D/2$ taps is, from Table 9.1,

$$C = 0.5959 + 0.0312\beta^{2.1} - 0.184\beta^8 + 0.039 \frac{\beta^4}{1 - \beta^4} \\ - 0.0158\beta^3 + \frac{91.706\beta^{2.5}}{R_D^{0.75}}$$

The gas-expansion-factor equation is Eq. (c) of Table 9.26:

$$Y_1 = 1 - (0.41 + 0.35\beta^4) \frac{x_1}{k}$$

The real-gas isentropic exponent k is read from Fig. I.16, for a quality of 0.8, as $k = 1.063$.

The differential pressure of the gas component at normal conditions is found with Eq. (9.88):

$$(h_w)_g = \frac{320}{\{1 + [1.26(1 - 0.8)/0.8] \sqrt{1.254/49.86}\}^2} = 290.27 \text{ inH}_2\text{O}$$

Then, from Eq. (k) of Table 9.26,

$$x_1 = \frac{290.27}{(27.73)(580)} = 0.01805$$

and the gas expansion factor is, from Eq. (c) of Table 9.26,

$$\begin{aligned}
 Y_1 &= 1 - (0.41 + 0.35 \beta^4) \left(\frac{0.01805}{1.063} \right) \\
 &= 1 - (0.41 + 0.35 \beta^4)(0.01698)
 \end{aligned}$$

Substitution of β_0 into the discharge-coefficient and gas-expansion-factor equations gives

$$C_0 = 0.60355 \quad (Y_1)_0 = 0.99267$$

The second estimate for β is then, by Eq. (9.83),

$$\beta_1 = \left\{ 1 + \left[\frac{(0.60355)(0.99267)}{0.1535} \right]^2 \right\}^{-1/4} = 0.4981$$

A second iteration gives no change in β .

The primary element bore at 68°F is calculated, by Eq. (9.54), as

$$d_{\text{meas}} = \frac{d}{F_{ad}} = \frac{\beta D}{F_{ad}} = \frac{(0.4981)(2.5069)}{1.00398} = 1.244 \text{ in}$$

where the thermal expansion factor for the primary element's bore is, by Eq. (9.51),

$$F_{ad} = 1 + \alpha_{PE}(T_F - 68) = 1 + 0.000096(483 - 68) = 1.00398$$

where, from Table B.4, $\alpha_P = 0.000096 \text{ in}/(\text{in} \cdot ^\circ\text{F})$.

Example 9.9. Size a 303 stainless-steel corner-tap orifice in a 3.970-in (100.8-mm) carbon-steel pipe to measure 24,000 flowing gal/h (90.85 m³/h) of water at 100°F (37.8°C) and 1000 psig (6850 kPa). The differential pressure at the upper-range flow rate is to be 200 in (49.73 kPa), and a density measurement is to be made. The water is aerated, and a 0.25-in (6.4-mm) vent hole is to be drilled through the plate.

The S_M -factor equation, Eq. (c) of Table 9.23, can be written as

$$S_M = \left[\frac{F_{DH} C \beta^2}{\sqrt{1 - \beta^4}} \right] = \frac{\sqrt{F_p} \sqrt{\rho_F} q_{\text{gph}}}{N_{\nu p} D^2 \sqrt{h_w}}$$

where F_{DH} is β -dependent. The bracketed term contains all beta-dependent functions and can be solved iteratively for β as

$$\beta_n = \left\{ 1 + \left[\frac{(F_{DH})_{n-1} C_{n-1}}{S_M} \right]^2 \right\}^{-1/4}$$

where S_M is constant. From Eq. (2.204),

$$F_p = 1 + \frac{p_f}{1000} Z_L = 1 + \frac{1000}{1000} (0.00262) = 1.00262$$

where $Z_L = 0.00262$ is found in Table E.1.

The pipe diameter of the carbon-steel pipe at flowing conditions is obtained by using Eq. (9.50):

$$D = F_{ad} D_{\text{meas}} = 1 + \alpha_p (T_F - 68) = 1 + 0.000067(100 - 68)(3.970) = 3.9709 \text{ in}$$

where $\alpha_p = 0.0000067 \text{ in}/(\text{in} \cdot ^\circ\text{F})$ is from Table B.4.

Now, from Eq. (2.175) or Table E.6, $\rho_F = 61.994 \text{ lb}_m/\text{ft}^3$, and from Table 9.16, $N_{vp} = 2684.96$. Scaling to normal conditions and substitution give

$$S_M = \frac{\sqrt{1.00262} \sqrt{61.994} (19,200)}{(2684.96)(3.9709)^2 \sqrt{128}} = 0.31603$$

The β -dependent terms F_{DH} and C are calculated as follows: For a square-edged vent hole, with $d = \beta D$, Eq. (9.99) is written as

$$F_{DH} = 1 + \sqrt{1 - \beta^4} \left(\frac{d_{DH}}{\beta D} \right)^2$$

where, from Table B.4, $\alpha_{PE} = 0.0000096 \text{ in}/(\text{in} \cdot ^\circ\text{F})$ and $\alpha_p = 0.0000067 \text{ in}/(\text{in} \cdot ^\circ\text{F})$. The discharge coefficient for corner taps is, from Table 9.1,

$$C = 0.5959 + 0.0312\beta^{2.1} - 0.184\beta^8 + \frac{91.706\beta^{2.5}}{R_D^{0.75}}$$

The Reynolds number R_D at normal conditions is calculated from Eq. (c) of Table 9.20 as

$$(R_D)_N = 2266.97 \left(\frac{F_p \rho_F}{\mu_{cp} DN_{vG}} \right) (q_{\text{gph}})_N = 372,509$$

for which Table E.6 gives $\mu_{cp} = 0.6812$, and the substitution $F_p \rho_F = \rho_f$ was used.

With an initial estimate for β from Eq. (j) of Table 9.28,

$$\beta_0 = \left[1 + \left(\frac{0.6}{S_M} \right)^2 \right]^{-1/4} = \left[1 + \left(\frac{0.6}{0.31603} \right)^2 \right]^{-1/4} = 0.68266$$

the iteration may be tabulated as follows:

	<i>n</i>		
	1	2	3
β_{n-1}	0.68266	0.67908	0.67898
$(F_{DH})_{n-1}$	1.00753	1.00763	1.00763
C_{n-1}	0.60000	0.60373	0.60374
β_n	0.67908	0.67898	0.67897

The thermal expansion factor for the primary element's F_{ad} is, by Eq. (9.51),

$$F_{ad} = 1 + \alpha_{PE}(T_F - 68) = 1 + 0.0000096(100 - 68) = 1.00022$$

from Table B.4, $\alpha_{PE} = 0.0000096 \text{ in}/(\text{in} \cdot ^\circ\text{F})$.

The primary element bore at 68°F is calculated, by Eq. (9.54), as

$$d_{\text{meas}} = \frac{d}{F_{ad}} = \frac{\beta D}{F_{ad}} = \frac{(0.67899)(3.9709)}{1.00022} = 2.696 \text{ in}$$

Example 9.10. The natural gas of Example 9.7 is saturated with water vapor. What is the required orifice bore if the flow rate is to be calculated on a dry basis? The S_M -factor equation (f), Table 9.25, including a water-vapor correction, is

$$S_M = \frac{(q_{\text{SCMH}}^*)_{\text{dry}}}{N_{\text{VHP}}^* F_{PB}^* F_{TB}^* F_{TF1}^* F_{\text{pu1}} F_{\text{WV,dry}} F_g D^{*2} \sqrt{\Delta p^* p_f^*}}$$

From Table G.1, the water vapor pressure (saturated) at 184 kPa (26.7 psia) is $p_{\text{WV}} = 0.5119$ psia (3.529 kPa). The water-vapor correction factor for conversion to a dry volume is, from Eq. (d) of Table 9.34,

$$F_{\text{WV,dry}} = 1 - \frac{3.529}{184} = 0.98082$$

The specific gravity is based on the *dry* components and is corrected to a *wet* specific gravity with Eq. (a) of Table 9.34:

$$G_{\text{wet}} = \left[1 + \frac{3.529}{184} \left(\frac{0.6220}{0.652} - 1 \right) \right] (0.652) = 0.6514$$

From Eq. (9.64),

$$F_g = \sqrt{\frac{1}{0.6514}} = 1.2390$$

Substituting $F_{\text{WV,dry}}$, F_g , and values from Example 9.6 into Eq. (f), Table 9.25:

$$\begin{aligned} S_M &= \frac{272}{(0.011350)(1.0133)(0.99653)(0.98005)} \\ &\quad (1.0011)(0.98082)(1.2390)(52.504)^2 \sqrt{(6.4)(184)} \\ &= 0.21043 \end{aligned}$$

Now, recalculation of β_0 for the adjusted S_M factor gives

$$\beta_0 = \left[1 + \left(\frac{0.6}{0.21043} \right)^2 \right]^{-1/4} = 0.5753$$

The iteration of Example 9.6, repeated with $S_M = 0.21040$, gives the following:

	n	
	1	2
β_{n-1}	0.57528	0.5755
C_{n-1}	0.60000	0.60692
$(Y_1)_{n-1}$	0.98772	0.98747
β_n	0.57555	0.57555

The primary element bore at 20°C is calculated, by Eq. (9.54), as

$$d_{\text{meas}}^* = \frac{d^*}{F_{ad}^*} = \frac{\beta D^*}{F_{ad}^*} = \frac{(0.57555)(52.504)}{(1.00011)} = 30.21 \text{ mm}$$

Example 9.11. A wet-type mercury meter is scaled to 100 in (24.86 kPa) and is to be located 50 ft (15.2 m) below an all stainless-steel venturi that is to measure an airflow of 100,000 standard ft³/h (2832 standard m³/h) in a 4-in (100-mm) Schedule-80 pipe. The pressure is 1160 psia (8000 kPa) at a temperature of 80°F (26.7°C). Size the bore if the lead lines are at 60°F (15.6°C). (The venturi is to have a machined inlet.)

Equation (I), Table 9.23, modified for elevation and manometer correction, is

$$S_M = \frac{\sqrt{Z_{f1}} \sqrt{T_{f1}} \sqrt{G} q_v}{N_{vpT} Z_b D^2 \sqrt{F_{EL} F_M (h_w)_{\text{ind}} p_{f1}}}$$

Data are determined as follows:

- From Table G.2: $Z_{f1} = 0.9833$
- From Table 9.16: $N_{vpT} = 7711.02$
- From Table 3.4: $Z_b = 0.99958$
- From Table B.4: $\alpha_{PE} = 0.0000097 \text{ in}/(\text{in} \cdot ^\circ\text{F})$
- For an all stainless-steel venturi: $\alpha_P = \alpha_{PE}$
- From Table B.1: $D = 3.826 \text{ in}$

and from Eq. (b) of Table 9.35, assuming $F_L = 1.0$, the elevation correction factor is

$$F_{EL} = 1 - 0.01874 \left[\frac{(1.0)(1.0)(50)}{(0.9833)(459.67 + 60)} \right] = 0.99817$$

Note: The compressibility factor used in this equation is that for the gas at 60°F; it was obtained by the Redlich-Kwong interpolation method presented in Chap. 2. From Eq. (3.38),

$$\rho_m = \rho_{\text{Hg}} = 846.324[1 - 0.0000101(60 - 60)] = 846.324 \text{ lb}_m/\text{ft}^3$$

Then, from Eq. (e) of Table 9.35, the manometer correction is

$$F_M = 1 - \frac{(2.6988)(1.0)(1160)}{(0.9833)(459.67 + 60)(846.324)} = 0.99276$$

The upper-range flow and differential pressure are scaled to normal operating conditions with

$$(q_{\text{SCFH}})_N = (0.8)(100,000) = 80,000 \quad \text{and} \quad (h_w)_N = (0.64)(100) = 64$$

The pipe diameter of the stainless-steel entrance venturi section at flowing conditions is obtained by using Eq. (9.50):

$$D = F_{aD} D_{\text{meas}} = 1 + \alpha_P (T_F - 68) = 1 + 0.000097(80 - 68) \\ \times (3.826) = 3.8264 \text{ in}$$

Substitution into the S_M -factor equation then gives

$$S_M = \frac{\sqrt{0.9833} \sqrt{459.67 + 80} \sqrt{1.0} (80,000)}{(7711.02)(0.99958)(3.826)^2 \sqrt{(0.99817)(0.99276)(64)(1160)}} \\ = 0.060219$$

Since $(\mu_{cp})_{\text{air}} = 0.021$ from Fig. H.3, the normal operating Reynolds number is, according to Eq. (l) of Table 9.20,

$$(R_D)_N = 3724.20 \frac{1.0}{(0.9996)} \left[\frac{1}{(0.021)(3.826)(7711)} \right] (80,000) \\ = 481,085$$

For a venturi, the discharge coefficient is constant above $R_D = 200,000$, and, from Table 9.1, $C = 0.995$.

From Eq. (a) of Table 9.28, for a machined-inlet venturi,

$$\beta_0 = \left[1 + \left(\frac{0.995}{0.060219} \right)^2 \right]^{-1/4} = 0.2458$$

From Eq. (h) of Table 9.26,

$$x_1 = \frac{F_{EL} F_M (h_w)_{\text{ind}}}{27.73 p_{f1}} = \frac{(0.99817)(0.99276)(64)}{(27.73)(1160)} = 0.001972$$

and from Eq. (g) of the same table,

$$\frac{p_{f2}}{p_{f1}} = 1 - 0.001972 = 0.99803$$

The gas expansion factor at normal operating conditions is, by Eq. (a) of Table 9.26,

$$(Y_1)_N = \left\{ \frac{[1 - (0.2458)^4][1.5/(1.5 - 1)](0.99803)^{2/1.5}[1 - (0.99803)^{(1.5-1)/1.5}]}{[1 - (0.2462)^4(0.99803)^{2/1.5}](1 - 0.99803)} \right\}^{1/2} \\ = 0.99901$$

where the isentropic exponent $k = 1.5$ is found in Fig. I.4.

The second estimate for beta is then, from Eq. (9.83),

$$\beta_1 = \left\{ 1 + \left[\frac{(0.995)(0.99901)}{0.060207} \right]^2 \right\}^{-1/4} = 0.2459$$

The thermal expansion factor for the primary element's F_{ad} is, by Eq. (9.51),

$$F_{ad} = 1 + \alpha_{PE}(T_F - 68) = 1 + 0.0000097(80 - 68) = 1.0012$$

The venturi bore at 68°F is then calculated, by Eq. (9.54), as

$$d_{\text{meas}} = \frac{d}{F_{ad}} = \frac{\beta D}{F_{aD}} = \frac{(0.2459)(3.8264)}{(1.00012)} = 0.9408 \text{ in}$$

Example 9.12. Size a stainless-steel flange tap orifice to meter saturated water flowing in a 2-in Schedule-80 carbon-steel pipe.

Design information

Flow rate: $(q_{\text{PPH}})_{\text{URV}} = 20,000 \text{ lb}_m/\text{h}$

Differential pressure at URV flow rate: $(h_w)_{\text{URV}} = 200$

Flowing pressure: $p_f = 250 \text{ psia}$

Scale to normal conditions

Normal flow: $(q_{\text{PPH}})_N = 0.8(q_{\text{PPH}})_{\text{URV}} = (0.8)(20,000) = 16,000 \text{ lb}_m/\text{h}$

Normal differential: $(h_w)_N = 0.64(h_w)_{\text{URV}} = (0.64)(200) = 128 \text{ in}$

Calculate S_M factor

For mass flow with a density determination, the S_M factor is calculated from Table 9.23, Eq. (a), with $F_p \rho_F = \rho_f$:

$$S_M = \frac{q_M}{N_{Mp} D^2 \sqrt{\rho_f} \sqrt{h_w}}$$

Data for the right-hand side is obtained as follows:

- From Table 9.14: $N_{Mp} = 358.9268$
- From Table B.1: $D_{\text{meas}} = 1.939 \text{ in}$
- From Table G.1: $\rho_f = 53.61499 \text{ lb}_m/\text{ft}^3$
- From Table G.1: $\mu_{cp} = 0.13019$
- From Table G.1: $T_F = 400.97^\circ\text{F}$ (saturation temperature)
- From Table B.4: $\alpha_{PE} = 0.0000096 \text{ in}/(\text{in} \cdot ^\circ\text{F})$
- From Table B.4: $\alpha_P = 0.0000067 \text{ in}/(\text{in} \cdot ^\circ\text{F})$

The pipe diameter of the carbon steel pipe at flowing conditions is obtained by using Eq. (9.50):

$$D = F_{aD} D_{\text{meas}} = 1 + \alpha_P (T_F - 68) = 1 + 0.000067(400.97 - 68) \times (1.939) = 1.94333 \text{ in}$$

Substitution into the S_M factor equation gives

$$S_M = \frac{16,000}{(358.93)(1.939)^2 \sqrt{53.615} \sqrt{128}} = 0.14249$$

The pipe Reynolds number is, by Table 9.20, Eq. (g),

$$R_D = \left[2266.97 \frac{1}{(0.1311)(1.9433)(358.93)} \right] 16,000 = 396,755$$

Substituting the β -dependent F_x factor term into the iterative equation for β [Eq. (9.83)] yields

$$\beta_n = \left\{ 1 + \left[\frac{(F_x)_{n-1} C_{n-1}}{S_M} \right]^2 \right\}^{-1/4}$$

The discharge-coefficient equation, from Table 9.1, for $D < 2.3$ in is

$$C = 0.5959 + 0.0312\beta^{2.1} - 0.184\beta^8 + 0.039 \frac{\beta^4}{(1 - \beta)^4} - 0.0337 \frac{\beta^3}{D} + \frac{91.706\beta^{2.5}}{R_D^{0.75}}$$

and from Eq. (9.92) the quality correction for saturated liquids is

$$F_x = 0.968 + 0.112\beta$$

With an initial estimate for β from Table 9.28, Eq. (j),

$$\beta_0 = \left[1 + \left(\frac{0.6}{S_M} \right)^2 \right]^{-1/4} = \left[1 + \left(\frac{0.6}{0.14249} \right)^2 \right]^{-1/4} = 0.48068$$

The iteration may be tabulated as follows:

	<i>n</i>		
	1	2	3
β_{n-1}	0.48068	0.47485	0.47505
$(F_x)_{n-1}$	1.02184	1.02118	1.02206
C_{n-1}	0.60000	0.60250	0.60234
β_n	0.47485	0.47505	0.47505

The thermal expansion factor for the primary element's F_{ad} is, by Eq. (9.51),

$$F_{ad} = 1 + \alpha_{pE}(T_F - 68) = 1 + 0.0000096(400.97 - 68) = 1.003197$$

The primary element bore at 68°F is calculated by Eq. (9.54) as

$$d_{\text{meas}} = \frac{d}{F_{ad}} = \frac{\beta D}{F_{ad}} = \frac{(0.47505)(1.9433)}{(1.0032)} = 0.9202 \text{ in}$$

FLOW-RATE EQUATIONS

The equations for calculating the flow rates may not be exactly the same as the sizing equations. The discharge coefficient, gas expansion factor, pressure, temperature, dimensional measurements, and, therefore, the actual flow rate may be different from those at design conditions. The number and precision of the corrections made to compensate for these changed variables depends on the accuracy desired. The equations for calculating flow rate are developed in the following sections.

The Basic Flow-Rate Equation

The general form of the flow-rate equation is given by Eq. (9.73) rearranged as

$$q = N \left[\frac{Cd^2}{\sqrt{1 - (d/D)^4}} \right] \left[Yf(\rho) \right] \sqrt{h_w} \quad (9.103)$$

Equation (9.103) shows four separate terms:

1. The N factor, the dimensional constant that relates the measured variables units (d , ρ , and h_w) to the desired flow-rate unit
2. The dimensional and viscosity-dependent terms (C , d , and D)
3. The density-related term, $Yf(\rho)$, where for gases Y is the gas expansion factor and $f(\rho)$ is the function of density selected
4. The measured differential h_w .

Presented in Table 9.36 are complete flow-rate equations for U.S. units, and in Table 9.37 are those for SI units. In Table 9.38 are flow-rate equations for the gas factor equation.

Calculating Flow Rate

Equation (9.103) has two terms that are related to the flow rate, the discharge coefficient C , which is a function of the flow-rate-dependent Reynolds-number term, and, for a gas (vapor), the gas expansion factor Y , which is a function of the measured differential, flowing pressure, beta ratio, and isentropic exponent. The calculation of flow rate then requires an iterative solution, in which an initial estimate is made for the flow rate. This estimate is then used to calculate the Reynolds number and, thereby, a second estimate for the discharge coefficient and hence a second flow-rate estimate. Repeated estimates are made until a suitable closure accuracy is achieved.

Simple Calculation. For the majority of flow measurement installations the assumption that the conditions for which the meter was sized suffices in determining the flow rate. This assumes that all variables at design conditions are true and that changes in the discharge coefficient C and, for a gas (vapor), the gas expansion factor Y are negligible. With these assumptions, Eq. (9.97), for U.S. units, is written as

$$q = N \left[\frac{Cd^2}{\sqrt{1 - (d/D)^4}} \right]_N \left[Yf(\rho) \right]_N \sqrt{h_w} = \left(\frac{q}{\sqrt{h_w}} \right)_N \sqrt{h_w} = F_{MC} \sqrt{h_w} \quad (9.104)$$

and for SI units by

$$\begin{aligned} q^* &= N^* \left[\frac{Cd^{*2}}{\sqrt{1 - (d^*/D^*)^4}} \right]_N \left[Yf(\rho^*) \right]_N \sqrt{\Delta p^*} \\ &= \left(\frac{q^*}{\sqrt{\Delta p^*}} \right)_N \sqrt{\Delta p^*} = F_{MC} \sqrt{\Delta p^*} \end{aligned} \quad (9.105)$$

TABLE 9.36 Flow-Rate Equations, U.S. Units

Liquid		Gas (vapor)		
Mass flow rate				
Density	$q_M = N_{M\rho} \frac{Cd^2}{\sqrt{1 - (d/D)^4}} \sqrt{F_p \rho_F} \sqrt{h_w}$	(a)	$q_M = N_{M\rho} \frac{Cd^2}{\sqrt{1 - (d/D)^4}} Y_1 \sqrt{\rho_{f1}} \sqrt{h_w}$	(g)
Specific gravity	$q_M = N_{MG} \frac{Cd^2}{\sqrt{1 - (d/D)^4}} \sqrt{F_p G_F} \sqrt{h_w}$	(b)		
<i>p</i> <i>v</i> <i>T</i> equation			$q_M = N_{M\rho T} \frac{Cd^2}{\sqrt{1 - (d/D)^4}} \frac{Y_1 \sqrt{G p_{f1}}}{\sqrt{Z_{f1} T_{f1}}} \sqrt{h_w}$	(h)
Volumetric flow rate at flowing conditions				
Density	$q_v = N_{v\rho} \frac{Cd^2}{\sqrt{1 - (d/D)^4}} \frac{1}{\sqrt{F_p \rho_F}} \sqrt{h_w}$	(c)	$q_v = N_{v\rho} \frac{Cd^2}{\sqrt{1 - (d/D)^4}} \frac{Y_1}{\sqrt{\rho_{f1}}} \sqrt{h_w}$	(i)
Specific gravity	$q_v = N_{vG} \frac{Cd^2}{\sqrt{1 - (d/D)^4}} \frac{1}{\sqrt{F_p G_F}} \sqrt{h_w}$	(d)		
<i>p</i> <i>v</i> <i>T</i> equation			$q_v = N_{v\rho T} \frac{Cd^2}{\sqrt{1 - (d/D)^4}} \frac{Y_1 \sqrt{Z_{f1} T_{f1}}}{\sqrt{G p_{f1}}} \sqrt{h_w}$	(j)

Volumetric flow rate at base conditions

Density	$q_v = N_{v\rho} \frac{Cd^2}{\sqrt{1 - (d/D)^4}} \frac{\sqrt{F_p \rho_F}}{\rho_b} \sqrt{h_w}$	(e)	$q_v = N_{v\rho} \frac{Cd^2}{\sqrt{1 - (d/D)^4}} \frac{Y_1 \sqrt{\rho_{f1}}}{\rho_b} \sqrt{h_w}$	(k)
Specific gravity	$q_v = N_{vG} \frac{Cd^2}{\sqrt{1 - (d/D)^4}} \frac{\sqrt{F_p G_F}}{G_b} \sqrt{h_w}$	(f)		
<i>pvT</i> equation				
Standard base			$q_v = N_{v\rho T} \frac{Cd^2}{\sqrt{1 - (d/D)^4}} \frac{Y_1 Z_b \sqrt{p_{f1}}}{\sqrt{G Z_{f1} T_{f1}}} \sqrt{h_w}$	(l)
Selected base			$q_{vb} = (N_{v\rho T})_b \frac{Cd^2}{\sqrt{1 - (d/D)^4}} \frac{Y_1 Z_b T_b \sqrt{p_{f1}}}{p_b \sqrt{G Z_{f1} T_{f1}}} \sqrt{h_w}$	(m)

Notes: Gas (vapor) equations are written for upstream pressure taps. For downstream pressure tap, change subscript 1 to subscript 2 as in ρ_{f2} , P_{f2} , Z_{f2} , etc.
 D and d in these equations are, at flowing conditions, $D = F_{dD} D_{\text{meas}} = [1 + \alpha_P (T_F - 68)] D_{\text{meas}}$ [Eq. (9.51)]; $d = F_{dd} d_{\text{meas}} = [1 + \alpha_{PE} (T_F - 68)] d_{\text{meas}}$ [Eq. (9.50)].

TABLE 9.37 Flow-Rate Equations: SI Units

Liquid		Gas (vapor)		
Mass flow rate				
Density	$q_M^* = N_{Mp}^* \frac{Cd^{*2}}{\sqrt{1 - (d^*/D^*)}} \sqrt{F_p \rho_F^*} \sqrt{\Delta p^*}$	(a)	$q_M^* = N_{Mp}^* \frac{Cd^{*2}}{\sqrt{1 - (d^*/D^*)^4}} Y_1 \sqrt{\rho_{f1}^*} \sqrt{\Delta p^*}$	(g)
Specific gravity	$q_M^* = N_{MG}^* \frac{Cd^{*2}}{\sqrt{1 - (d^*/D^*)^4}} \sqrt{F_p G_F} \sqrt{\Delta p^*}$	(b)		
<i>pvT</i> equation			$q_M^* = N_{MpT}^* \frac{Cd^{*2}}{\sqrt{1 - (d^*/D^*)^4}} \frac{Y_1 \sqrt{G p_{f1}^*}}{\sqrt{Z_{f1} T_{K1}}} \sqrt{\Delta p^*}$	(h)
Volumetric flow rate at flowing conditions				
Density	$q_v^* = N_{vp}^* \frac{Cd^{*2}}{\sqrt{1 - (d^*/D^*)^4}} \frac{1}{\sqrt{F_p \rho_F^*}} \sqrt{\Delta p^*}$	(c)	$q_v^* = N_{vp}^* \frac{Cd^{*2}}{\sqrt{1 - (d^*/D^*)^4}} \frac{Y_1}{\sqrt{\rho_{f1}^*}} \sqrt{\Delta p^*}$	(i)
Specific gravity	$q_v^* = N_{vG}^* \frac{Cd^{*2}}{\sqrt{1 - (d^*/D^*)^4}} \frac{1}{\sqrt{F_p G_F}} \sqrt{\Delta p^*}$	(d)		
<i>pvT</i> equation			$q_v^* = N_{vpT}^* \frac{Cd^{*2}}{\sqrt{1 - (d^*/D^*)^4}} \frac{Y_1 \sqrt{Z_{f1} T_{K1}}}{\sqrt{G p_{f1}^*}} \sqrt{\Delta p^*}$	(j)

TABLE 9.37 Flow-Rate Equations: SI Units

Liquid		Gas (vapor)	
Mass flow rate			
Density	$q_M^* = N_{M\rho}^* \frac{Cd^{*2}}{\sqrt{1 - (d^*/D^*)^4}} \sqrt{F_p \rho_F^*} \sqrt{\Delta p^*}$	(a)	$q_M^* = N_{M\rho}^* \frac{Cd^{*2}}{\sqrt{1 - (d^*/D)^4}} Y_1 \sqrt{\rho_{f1}^*} \sqrt{\Delta p^*}$
Specific gravity	$q_M^* = N_{MG}^* \frac{Cd^{*2}}{\sqrt{1 - (d^*/D^*)^4}} \sqrt{F_p G_F} \sqrt{\Delta p^*}$	(b)	
pvT equation			$q_M^* = N_{M\rho T}^* \frac{Cd^{*2}}{\sqrt{1 - (d^*/D^*)^4}} \frac{Y_1 \sqrt{G p_{f1}^*}}{\sqrt{Z_{f1} T_{K1}}} \sqrt{\Delta p^*}$
Volumetric flow rate at flowing conditions			
Density	$q_v^* = N_{v\rho}^* \frac{Cd^{*2}}{\sqrt{1 - (d^*/D^*)^4}} \frac{1}{\sqrt{F_p \rho_F^*}} \sqrt{\Delta p^*}$	(c)	$q_v^* = N_{v\rho}^* \frac{Cd^{*2}}{\sqrt{1 - (d^*/D^*)^4}} \frac{Y_1}{\sqrt{\rho_{f1}^*}} \sqrt{\Delta p^*}$
Specific gravity	$q_v^* = N_{vG}^* \frac{Cd^{*2}}{\sqrt{1 - (d^*/D^*)^4}} \frac{1}{\sqrt{F_p G_F}} \sqrt{\Delta p^*}$	(d)	
pvT equation			$q_v^* = N_{v\rho T}^* \frac{Cd^{*2}}{\sqrt{1 - (d^*/D^*)^4}} \frac{Y_1 \sqrt{Z_{f1} T_{K1}}}{\sqrt{G p_{f1}^*}} \sqrt{\Delta p^*}$

Volumetric flow rate at base conditions

Density	$q_V^* = N_{V\rho}^* \frac{Cd^{*2}}{\sqrt{1 - (d^*/D^*)^4}} \frac{\sqrt{F_p \rho_F^*}}{\rho_b^*} \sqrt{\Delta p^*} \quad (e)$	$q_V^* = N_{V\rho}^* \frac{Cd^{*2}}{\sqrt{1 - (d^*/D^*)^4}} \frac{Y_1 \sqrt{\rho_{f1}^*}}{\rho_b^*} \sqrt{\Delta p^*} \quad (k)$
Specific gravity	$q_V^* = N_{VG}^* \frac{Cd^{*2}}{\sqrt{1 - (d^*/D^*)^4}} \frac{\sqrt{F_p G_F}}{G_b} \sqrt{\Delta p^*} \quad (f)$	
<i>pvT</i> equation		
Standard base		$q_V^* = N_{V\rho T}^* \frac{Cd^{*2}}{\sqrt{1 - (d^*/D^*)^4}} \frac{Y_1 Z_b \sqrt{p_{f1}^*}}{\sqrt{G Z_{f1} T_{k1}}} \sqrt{\Delta p^*} \quad (l)$
Selected base		$q_{Vb}^* = (N_{V\rho T}^*)_b \frac{Cd^{*2}}{\sqrt{1 - (d^*/D^*)^4}} \frac{Y_1 Z_b T_{kb} \sqrt{p_{f1}^*}}{p_b^* \sqrt{G Z_{f1} T_{k1}}} \sqrt{\Delta p^*} \quad (m)$

Notes: Gas (vapor) equations are written for upstream pressure taps. For downstream pressure tap, change subscript 1 to subscript 2 as in ρ_{f2} , p_{f2} , Z_{f2} , etc. D and d in these equations are, at flowing conditions, $D^* = F_{ad}^* D_{\text{meas}}^* = [1 + \alpha_p(T_c - 20)]D_{\text{meas}}^*$ [Eq. (9.53)]; $d^* = F_{ad}^* d_{\text{meas}}^* = [1 + \alpha_{pk}(T_c - 20)]d_{\text{meas}}^*$ [Eq. (9.52)].

TABLE 9.38 ASME-ISO Flow-Rate Equation Using Factor Equations (F_{PB} , F_{TB} , F_{TF} , F_{pv}): U.S. and SI Units

	U.S. units		SI units	
Mass flow rate	$q_M = N_{Mhp} K d^2 Y_1 F_{pv1} F_{TF1} \frac{\sqrt{h_w p_{f1}}}{F_g Z_b}$	(a)	$q_M^* = N_{Mhp}^* K d^{*2} Y_1 F_{pv1} F_{TF1}^* \frac{\sqrt{\Delta p^* p_{f1}^*}}{F_g Z_b}$	(d)
Volumetric flow rate at flowing conditions	$q_v = N_{vhp} K d^2 Y_1 F_g \frac{Z_b \sqrt{h_w}}{F_{TF1} F_{pv1} \sqrt{p_{f1}}}$	(b)	$q_v^* = N_{vhp}^* K d^{*2} Y_1 F_g \frac{Z_b \sqrt{\Delta p^*}}{F_{TF1}^* F_{pv1} \sqrt{p_{f1}^*}}$	(e)
Volumetric flow rate at base conditions	$q_{vb} = N_{vhp} K d^2 Y_1 F_{PB} F_{TB} F_{TF1} F_{pv1} F_g \sqrt{h_w p_{f1}}$	(c)	$q_{vb}^* = N_{vhp}^* K d^{*2} Y_1 F_{PB}^* F_{TB}^* F_{TF1}^* F_{pv1} F_g \sqrt{\Delta p^* p_{f1}^*}$	(f)

Notes: $K = C / \sqrt{1 - \beta^4}$

d and d^* in these equations are, at flowing conditions: $d = F_{ad} d_{\text{meas}} = [1 + \alpha_{PE}(T_F - 68)] D_{\text{meas}}$ [Eq. (9.51)]; $d^* = F_{ad}^* d_{\text{meas}}^* = [1 + \alpha_{PE}^*(T_{FC} - 20)] D_{\text{meas}}^*$ [Eq. (9.53)].

The subscript N for the bracketed terms denotes that the terms are to be evaluated at normal flowing conditions. The solution for flow rate then reduces to simply the product of a *meter coefficient factor* F_{MC} times the square root of the measured differential h_w (or Δp^*).

Iteration. The exact flow rate is most easily solved for by iteration of the flow-rate equation until a suitable closure accuracy is achieved. The iterative procedure is detailed in Table 9.39 for liquids and in Table 9.40 for gases (vapors).

The procedure can be summarized as five steps:

1. Select the flow-rate equation.
2. Put known quantities into the flow-rate equation.
3. Calculate constants and the first estimate for the flow rate.
4. From the first estimate of the flow rate:

Calculate the pipe Reynolds number.

Calculate the discharge coefficient.

Calculate a second estimate for the flow rate, calculate the Reynolds number based on the flow rate, and repeat until suitable closure is achieved.

5. Display last calculated flow-rate value.

Example 9.13. For the data of Example 9.3, calculate the flow rate for a measured differential of 10 in (1) assuming no Reynolds-number correction and (2) iterating the flow-rate equation for a closure of 0.001 percent.

Data from Example 9.3:

$$\begin{aligned}(q)_N &= 80 & D_{\text{meas}} &= 1.939 \text{ in} & D &= 1.9392 \text{ in} & d_{\text{meas}} &= 1.4407 & d &= 1.4409 \\(h_w)_N &= 64 \text{ in} & N_{VG} &= 5.6665 & G_F &= 0.7359 & F_p &= 1.0088 & G_b &= 0.7359 \\T_F &= 80.5^\circ\text{F} & \mu_{cP} &= 0.417\end{aligned}$$

1. *No Reynolds-number correction.* The flow-rate equation for no Reynolds-number correction is, by Eq. (9.104):

$$q_{\text{GPM}} = F_{MC} \sqrt{h_w} = \frac{(q_{\text{GPM}})_N}{\sqrt{(h_w)_N}} \sqrt{h_w} = \frac{80}{\sqrt{64}} \sqrt{h_w} = 10 \sqrt{h_w}$$

The flow rate, when the meter differential is 10 in, becomes

$$q_{\text{GPM}} = F_{MC} \sqrt{h_w} = 10 \sqrt{10} = 31.623 \text{ base gal/min}$$

2. *Iteration.* The flow-rate equation, from Table 9.36, Eq. (f), is

$$q_v = N_{VG} \frac{Cd^2}{\sqrt{1 - (d/D)^4}} \frac{\sqrt{F_p G_F}}{G_b} \sqrt{h_w}$$

Substituting the constants from Example 9.3 yields

TABLE 9.39 Procedure for Iterative Flow-Rate Solution: Liquids

Procedure	Symbol		Reference
	U.S. units	SI units	
1. Select equations			
a. Flow rate†	q	q^*	Tables 9.36–9.38
b. Obtain N factor for desired flow-rate unit (q_{PPH} , q_{GPM} , etc.)	N	N^*	Tables 9.14–9.19
c. Discharge coefficient	C	C	Table 9.1
d. Pipe Reynolds number	R_D	R_D	Tables 9.20–9.22
2. Obtain values			
a. Measured differential	h_w	Δp^*	
b. Primary element bore at 68°F (20°C)	d_{meas}	d_{meas}^*	From measurement shown on plate
c. Pipe diameter at 68°F (20°C)	D_{meas}	D_{meas}^*	From measurement or Table B.1
d. Measured temperature	T_F	T_C	
<i>If density equation form is selected</i>			
e. Flowing density, uncorrected for pressure	ρ_F	ρ_F^*	App. E or Chap. 2 equations
<i>For base volumes</i>			
f. Base density	ρ_b	ρ_b^*	App. E. or Chap. 2 equations
<i>If specific gravity equation form is selected</i>			
g. Flowing specific gravity, uncorrected for pressure	G_F	G_F	App. E or Chap. 2 equations
<i>For base volumes</i>			
h. Base specific gravity	G_b	G_b	App. E or Chap. 2 equations
i. Liquid compressibility factor; for most fluids, $F_p = 1$	F_p	F_p	App. F or Chap. 2 equations
j. Viscosity	μ_{cP}	μ_{cP}	App. F or Chap. 2 equations
3. Calculate constants and first estimate			
a. Calculate pipe diameter at flowing conditions	D	D^*	Eqs. (9.51)–(9.53)
b. Calculate primary element bore at flowing conditions	d	d^*	Eqs. (9.51)–(9.53)

TABLE 9.39 Procedure for Iterative Flow-Rate Solution: Liquids (*Continued*)

Procedure	Symbol		Reference
	U.S. units	SI units	
c. Calculate first flow rate <i>For square-edged primaries</i> (orifices), let $C = 0.6$ <i>For contoured devices</i> (nozzles, venturis, etc.), let $C = 0.95$	q_{n-1}	q_{n-1}^*	
4. Iterate for the flow rate			
a. Calculate Reynolds number using first estimate for the flow rate, q_{n-1}	R_D	R_D	
b. Calculate discharge coefficient	C	C	
c. Substitute variables into flow-rate equation to obtain next estimate	q_n	q_n^*	
d. Calculate percent difference between last estimate q_n and first estimate q_{n-1} . If >0.001 , <i>return to step (a) and set next</i> <i>estimate = q_n. Exit to step 5 when</i> <i>$\% < 0.001$</i>		$\% = 100 \times (q_{n-1} - q_n)/q_n$	
5. Display flow rate	q	q^*	

†For drain hole or other corrective factors, add the correction factor to the equation as multiplying terms:
 $q = F_{DH} F_{EL} F_M q$.

$$q_{\text{GPM}} = (5.6665) \frac{(C)(1.441)^2}{\sqrt{1 - (1.441/1.939)^4}} \frac{\sqrt{(1.0088)(0.7255)}}{0.7359} \sqrt{h_w}$$

$$= 16.4028 \sqrt{h_w} = 51.870$$

The discharge-coefficient equation, from Table 9.1, is

$$C = 0.5959 + 0.0312\beta^{2.1} - 0.184\beta^8 + 0.039 \frac{\beta^4}{1 - \beta^4} - 0.0337 \frac{\beta^3}{D} + \frac{91.71\beta^{2.5}}{R_D^{0.75}}$$

Substituting $\beta = d/D = 1.4409/1.9392 = 0.7304$ gives

$$C = 0.60549 + 43.65/R_D^{0.75}$$

The pipe Reynolds number is calculated from Table 9.20, Eq. (f), as

$$R_D = \left(17,902.8 \frac{G_b}{\mu_{cP} DN_{VG}} \right) q_v$$

$$= \left[(17,902.8) \frac{(0.7359)}{(0.417)(1.939)(5.6665)} \right] q_{\text{GPM}}$$

$$= 2875.3 q_{\text{GPM}}$$

TABLE 9.40 Procedure for Iterative Flow-Rate Solution: Gases (Vapors)

Procedure	Symbol		Reference
	U.S. units	SI units	
1. Select equations			
a. Flow-rate equation†	$(q)_N$	$(q^*)_N$	Tables 9.36–9.38
b. N factor for the desired flow-rate unit (q_{PPH} , q_{GPM} , etc.)	N	N^*	Tables 9.14–9.19
c. Discharge coefficient	C	C	Table 9.1
d. Gas expansion factor			
Upstream pressure tap	Y_1	Y_1	Table 9.26
Downstream pressure tap	Y_2	Y_2	
e. Pipe Reynolds number	R_D	R_D	Tables 9.20–9.22
2. Obtain			
a. Measured differential	h_w	Δp^*	
b. Primary element bore at 68°F (20°C)	d_{meas}	d_{meas}^*	From measurement shown on plate
c. Pipe diameter at 68°F (20°C)	D_{meas}	D_{meas}^*	From measurement or Table B.1
d. Temperature	T_F	T_C	
e. Flowing pressure			
Upstream pressure tap	P_{f1}	P_{f1}^*	
Downstream pressure tap	P_{f2}	P_{f2}^*	
<i>If density equation is selected</i>			
f. Obtain density			
Upstream pressure tap	ρ_{f1}	ρ_{f1}^*	App. G or Chap. 2 equations
Downstream pressure tap	ρ_{f2}	ρ_{f2}^*	
<i>For standard volumes</i>			
g. Obtain base density			
<i>If p_vT equation is selected</i>			
h. Specific gravity	G	G	Eq. (2.7)
i. Flowing compressibility	Z_f	Z_f	Chap. 2 equations

TABLE 9.40 Procedure for Iterative Flow-Rate Solution: Gases (Vapors) (*Continued*)

Procedure	Symbol		Reference
	U.S. units	SI units	
<i>For standard volumes</i>			
<i>j.</i> Base pressure	p_b	p_b^*	
<i>k.</i> Base temperature	T_b	T_{kb}	
<i>l.</i> Base compressibility	Z_b	Z_b	App. G or Chap. 2 equations
<i>m.</i> Viscosity	μ_{cP}	μ_{cP}	App. F or Chap. 2 equations
<i>n.</i> Isentropic exponent	k	k	App. I or Chap. 2 equations
3. Calculate constants and first estimate for the flow rate			
<i>a.</i> Calculate pipe diameter at flowing conditions	D	D^*	Eqs. (9.51)–(9.53)
<i>b.</i> Calculate primary element bore at flowing conditions	d	d^*	Eqs. (9.51)–(9.53)
<i>c.</i> First flow-rate estimate	q_{n-1}	q_{n-1}^*	
<i>For square-edged primaries (orifices), let $C = 0.6$</i>			
<i>For contoured devices (nozzles, venturis, etc.), let $C = 0.95$</i>			
4. Iterate for the flow rate			
<i>a.</i> Calculate gas expansion			
Upstream pressure tap	Y_1	Y_1	
Downstream pressure tap	Y_2	Y_2	
<i>b.</i> Calculate Reynolds number using first estimate for the flow rate, q_{n-1}	R_D	R_D	
<i>c.</i> Calculate discharge coefficient	C	C	
<i>d.</i> Substitute variables into flow-rate equation to obtain next estimate	q_n	q_n^*	
<i>e.</i> Calculate percent difference between last estimate and first estimate. If >0.001 , return to step (b); if <0.001 , exit to step 5.		$\% = 100 \times (q_{n-1} - q_n)/q_n$	
5. Display flow rate			
	q	q^*	

†For drain hole or other corrective factors, add the correction factor to the equation as multiplying terms:
 $q = F_{DH} F_{EL} F_M q$.

The iterative steps are:

1. Calculate an initial flow rate using a discharge coefficient of $C = 0.6$.
2. Calculate the pipe Reynolds number using the flow rate.
3. From the Reynolds number, calculate the discharge coefficient.
4. Calculate the flow rate using the discharge coefficient of step 3.
5. Calculate the percentage difference. If >0.001 , then return to step 2 and repeat calculation until closure.

The iteration is as follows:

	<i>n</i>		
	1	2	3
$q_{n-1} = 51.870C_{n-1}$	31.122	31.845	31.837
$(R_D)_{n-1} = 2875.3q_{\text{GPM}}$	89,485	91,563	91,541
$C_n = 0.60549 + 43.65/(R_D^{0.75})_{n-1}$	0.61393	0.61379	0.61379
$q_n = 51.870C_n$	31.845	31.837	31.837

Example 9.14. The measured differential is 50 in (12.34 kPa) for the meter sized in accordance with Example 9.6. Calculate the flow rate.

From Table 9.36, the flow-rate equation (m), written for a downstream pressure tap measurement, is

$$q_{vb} = (N_{vPT})_b \frac{Cd^2}{\sqrt{1 - (d/D)^4}} \frac{Y_2 Z_b T_b \sqrt{p_{f2}}}{p_b \sqrt{GZ_{f2} T_{f2}}} \sqrt{h_w}$$

Data from Example 9.6:

$$\begin{aligned} (N_{vPT})_b &= 218.4834 & D_{\text{meas}} &= 7.620 \text{ in} & D &= 7.6215 \text{ in} & d_{\text{meas}} &= 3.9003 \text{ in} \\ & & d &= 3.9015 \text{ in} & & & & \\ p_{f2} &= 2000 \text{ psia} & T_{f2} &= (100 + 459.67) & G &= 0.8445 & Z_{f2} &= 0.5688 \\ Z_b &= 0.9974 & T_f &= 559.67^\circ\text{R} & k &= 2.29 & p_b &= 14.7 \text{ psia} \\ T_b &= (60 + 459.67) & \mu_{\text{cP}} &= 0.0255 & & & & \\ T_b &= 519.67^\circ\text{R} & & & & & & \\ q_{\text{SCFH}} &= 218.43 \frac{C(3.9003)^2 Y_2 (0.9974) (519.67) \sqrt{2000}}{\sqrt{1 - [(3.9003)/(7.620)]^4} (14.7) \sqrt{(0.8445)(0.5688)(559.67)}} \sqrt{h_w} \\ &= 331,412 C Y_2 \sqrt{h_w} \end{aligned}$$

The pipe Reynolds number is calculated from Table 9.20, Eq. (m)

$$R_D = \left[\frac{(3724.2) (0.8445)(14.7)}{(0.9974)(60 + 459.67)(0.0255)(7.62)(218.48)} \right] q_{\text{SCFH}} = 2.101 q_{\text{SCFH}}$$

The discharge-coefficient equation, from Table 9.1, for $D > 2.3$ in is

$$C = 0.5959 + 0.0312\beta^{2.1} - 0.184\beta^8 + 0.09 \frac{\beta^4}{D(1-\beta)^4} - 0.0337 \frac{\beta^3}{D} + \frac{91.706\beta^{2.5}}{R_D^{0.75}}$$

Substituting $\beta = d/D = 0.51190$,

$$C = 0.602956 + 17.193/R_D^{0.75}$$

The downstream pressure tap gas expansion factor from Table 9.26, Eq. (d), is

$$Y_2 = \sqrt{1 + x_2} - (0.41 + 0.35\beta^4) \frac{x_2}{k\sqrt{1 + x_2}}$$

where

$$x_2 = \frac{h_w}{27.73p_{f2}} = \frac{h_w}{(27.73)(2000)} = 0.00001803h_w$$

Substituting, with $k = 2.29$ and $\beta = 0.51184$,

$$Y_2 = \sqrt{1 + 0.00001803h_w} - \frac{0.000003417h_w}{\sqrt{1 + 0.00001803h_w}}$$

The iterative steps are then:

1. Calculate the gas expansion factor.
2. Calculate the flow rate; initially assume $C = 0.6$.
3. Calculate the pipe Reynolds number from the flow rate.
4. Calculate the discharge coefficient.
5. Calculate the flow rate using the discharge coefficient of step 4.
6. Calculate the percentage difference between the flow rate of step 2 and step 5. If >0.001 , then *return* to step 2 until closure.

For $h_w = 50$ in the gas expansion factor $Y_2 = 1.00030$. The flow rate then becomes

$$q_{SCFH} = (331,442)C(1.0003) \sqrt{50} = 2,344,139C$$

The iteration for $h_w = 50$ in is as follows

	<i>n</i>		
	1	2	3
$q_{n-1} = 2,344,139C$	1,406,456	1,413,950	1,413,948
$(R_D)_{n-1} = 2.1010q_{SCFH}$	2,954,472	2,970,215	2,970,211
$C_n = 0.60296 + 17.19/R_D^{0.75}$	0.603197	0.603196	0.603195
$q_n = 2,344,139C_n$	1,413,950	1,413,948	1,413,948

Example 9.15. The internal pipe diameter of Example 9.5 is measured as 5.880 in (149.4 mm) and the bore as 4.289 in (108.9 mm) with other variables remaining constant. Set up the calculation procedure for a single iteration to calculate the flow rate for measured differentials of 20, 40, 60, and 100 in (4.97, 9.97, 14.9, 19.9, and 24.9 kPa).

The mass flow-rate equation from Table 9.36, Eq. (g), is

$$q_M = N_{Mp} \frac{Cd^2}{\sqrt{1 - (d/D)^4}} Y_1 \sqrt{\rho_{f1}} \sqrt{h_w}$$

Data and equations from Example 9.2:

$$\begin{aligned} \alpha_{PE} &= 0.0000096 \text{ in}/(\text{in} \cdot ^\circ\text{F}) & \alpha_P &= 0.0000067 \text{ in}/(\text{in} \cdot ^\circ\text{F}) \\ p_{f1} &= 204 \text{ psia} & T_{f1} &= 460^\circ\text{F} \\ \rho_{f1} &= 0.39524 \text{ lb}_m/\text{ft}^3 & \mu_{cP} &= 0.01747 \\ k &= 1.308 & N_{Mp} &= 358.9268 \end{aligned}$$

The pipe diameter of the carbon-steel pipe at flowing conditions is obtained by using Eq. (9.50):

$$\begin{aligned} D &= F_{aD} D_{\text{meas}} = [1 + \alpha_P(T_F - 68)] D_{\text{meas}} \\ &= [1 + 0.000067(460 - 68)](5.880) = 5.8961 \text{ in} \end{aligned}$$

The primary element bore at the flowing temperature is calculated by Eq. (9.51) as

$$\begin{aligned} d &= F_{ad} d_{\text{meas}} = [1 + \alpha_{PE}(T_F - 68)] d_{\text{meas}} \\ &= [1 + 0.000096(460 - 68)](4.289) = 4.30529 \text{ in} \end{aligned}$$

Substitution then gives

$$q_{PPH} = 358.9268 \frac{C(1.00842)(4.3053)^2}{\sqrt{1 - (4.3053/5.8961)^4}} Y_1 \sqrt{0.39524} \sqrt{h_w} = 4943.92 C Y_1 \sqrt{h_w}$$

The discharge-coefficient equation from Table 9.1, for $D > 2.3$ in, is

$$\begin{aligned} C &= 0.5959 + 0.0312\beta^{2.1} - 0.184\beta^8 + 0.09 \frac{\beta^4}{D(1 - \beta)^4} \\ &\quad - 0.0337 \frac{\beta^3}{D} + \frac{91.706\beta^{2.5}}{R_D^{0.75}} \end{aligned}$$

Substituting $\beta = 0.7302$ gives

$$C = 0.60099 + \frac{41.78}{R_D^{0.75}}$$

The pipe Reynolds number is calculated from Table 9.20, Eq. (g), as

$$R_D = \left[2266.97 \frac{1}{(0.01747)(5.880)(358.93)} \right] q_{PPH} = 61.317 q_{PPH}$$

and the gas (vapor) expansion factor from Table 9.26, Eq. (c), is

$$Y_1 = 1 - (0.41 + 0.35\beta^4) \frac{h_w}{27.73kp_{f1}} = 1 - 0.0000688h_w$$

The steps for a single iteration are:

1. Calculate the gas (vapor) expansion factor.
2. Calculate an initial flow rate assuming $C = 0.6$.
3. Calculate the pipe Reynolds number using the flow rate.
4. From the Reynolds number, calculate the discharge coefficient and the flow rate.

The single iterative values are:

	Differential			
	20	40	60	100
$Y_1 = 1 - 0.0000688h_w$	0.99862	0.99725	0.99587	0.99312
$(q_{PPH})_0 = 0.2966.2Y_1 \sqrt{h_w}$	13,247	18,708	22,881	29,457
$R_D = 61.317(q_{PPH})_0$	814,492	1,150,277	1,406,853	1,811,220
$C = 0.60099 + 41.78/R_D^{0.75}$	0.60253	0.602245	0.602079	0.601903
$q_{PPH} = 4943.92CY_1 \sqrt{h_w}$	13,303	18,778	22,960	29,552

Differential-Pressure Equations

Differential producers are normally used over a 3:1 flow-rate range in order to minimize errors associated with the differential-pressure-measuring device. For example, when the flow rate decreases from 100 to 20 GPM (5:1), the differential will decrease from 100 in (25 kPa) to 4 in (1 kPa), a 25:1 differential-pressure range. A differential-pressure transmitter with a stated accuracy of 0.2 percent of the upper-range differential will then have an actual error of 5 percent at the lower flow rate, an error of 2.5 percent in the flow-rate calculation.

When the 3:1 flow-rate range is exceeded, either the primary element's bore or the range of the differential-pressure-measuring device needs to be changed in order to improve metering accuracy. Today's differential-pressure transmitters may be remotely reranged to reduce (or increase) sensitivity. Although this eliminates removal and recalibration of the transmitter, the accuracy at the reselected range may be degraded.

The equations presented in Table 9.41 for U.S. units or in Table 9.42 for SI units are used to recalculate the differential pressure produced at the rescaled flow rate. Table 9.43 outlines the procedure for liquids and Table 9.44 the procedure for gases (vapors).

Simple Calculation. For many applications the differential-pressure transmitter may simply be scaled from the prior flow-rate value to the new flow-rate value by using the meter coefficient factor F_{MC} as determined from the initial sizing information. This assumes that fluid properties remain unchanged and that directional bias error associated with either the gas expansion factor or the discharge coefficient is acceptable. The simple rescaling equation, with the initial meter coefficient factor $F_{MC,1}$ equal to the new meter factor coefficient $F_{MC,2}$, is

TABLE 9.41 Differential Pressure Equations: U.S. Units

	Liquid		Gas (vapor)	
Density	$h_w = \frac{1 - (d/D)^4}{N_{Mp}^2 C^2 d^4 F_p \rho_F} q_M^2$	(a)	$h_w = \frac{1 - (d/D)^4}{N_{Mp}^2 C^2 d^4 \rho_f Y_1^2} q_M^2$	(g)
Specific gravity	$h_w = \frac{1 - (d/D)^4}{N_{MG}^2 C^2 d^4 F_p G_F} q_M^2$	(b)		
<i>pvT</i> equation			$h_w = \frac{[1 - (d/D)^4] Z_f T_f}{N_{Mpf}^2 C^2 d^4 Y_1^2 G p_f} q_M^2$	(h)
Volumetric flow rate at flowing conditions				
Density	$h_w = \frac{1 - (d/D)^4}{N_{vp}^2 C^2 d^4 F_p \rho_F} q_v^2$	(c)	$h_w = \frac{[1 - (d/D)^4] \rho_f}{N_{vp}^2 C^2 d^4 Y_1^2} q_v^2$	(i)
Specific gravity	$h_w = \frac{1 - (d/D)^4}{N_{vG}^2 C^2 d^4 F_p G_F} q_v^2$	(d)		
<i>pvT</i> equation			$h_w = \frac{[1 - (d/D)^4] G p_f}{N_{vpT}^2 C^2 d^4 Y_1^2 Z_f T_f} q_v^2$	(j)

Volumetric flow rate at base conditions

Density	$h_w = \frac{[1 - (d/D)^4] \rho_b^2}{N_{V\rho}^2 C^2 d^4 F_p \rho_F} q_V^2$	(e)	$h_w = \frac{[1 - (d/D)^4] \rho_b^2}{N_{V\rho}^2 C^2 d^4 Y_1^2 \rho_{f1}} q_V^2$	(k)
Specific gravity	$h_w = \frac{[1 - (d/D)^4] G_b^2}{N_{VG}^2 C^2 d^4 F_p G_F} q_V^2$	(f)		
<i>pvT</i> equation				
Standard base			$h_w = \frac{[1 - (d/D)^4] G Z_{f1} T_{f1}}{N_{VpT}^2 C^2 d^4 Y_1^2 Z_b^2 p_{f1}} q_V^2$	(l)
Selected base			$h_w = \frac{[1 - (d/D)^4] p_b^2 G Z_{f1} T_{f1}}{(N_{VpT})_b^2 C^2 d^4 Y_1^2 Z_b^2 T_b^2 p_{f1}} q_V^2$	(m)

Notes: Gas (vapor) equations are written for upstream pressure tap. For downstream pressure tap change subscript 1 to subscript 2 as in ρ_{f2} , p_{f2} , Z_{f2} , etc.
 D and d in these equations are at flowing conditions: $d = F_{ad} d_{\text{meas}} = [1 + \alpha_{pE}(T_F - 68)] d_{\text{meas}}$ [Eq. (9.50)]; $D = F_{aD} D_{\text{meas}} = [1 + \alpha_p(T_F - 68)] D_{\text{meas}}$ [Eq. (9.51)].

TABLE 9.42 Differential Pressure Equations: SI Units

Liquid		Gas (vapor)		
Mass flow rate				
Density	$\Delta p^* = \frac{1 - (d^*/D^*)^4}{N_{M\rho}^{*2} C^2 d^{*4} F_\rho \rho_F^*} q_M^{*2}$	(a)	$\Delta p^* = \frac{1 - (d^*/D^*)^4}{N_{M\rho}^{*2} C^2 d^{*4} Y_1^2 \rho_{f1}} q_M^*$	(g)
Specific gravity	$\Delta p^* = \frac{1 - (d^*/D^*)^4}{N_{MG}^{*2} C^2 d^{*4} F_\rho G_F} q_M^{*2}$	(b)		
<i>pvt</i> equation			$\Delta p^* = \frac{[1 - (d^*/D^*)^4] Z_{f1} T_{K1}}{N_{M\rho}^{*2} C^2 d^{*4} Y_1^2 G p_{f1}^*} q_M^2$	(h)
Volumetric flow rate at flowing conditions				
Density	$\Delta p^* = \frac{1 - (d^*/D^*)^4}{N_{v\rho}^{*2} C^2 d^{*4} F_\rho \rho_F^*} q_v^{*2}$	(c)	$\Delta p^* = \frac{[1 - (d^*/D^*)^4] \rho_{f1}^*}{N_{v\rho}^{*2} C^2 d^{*4} Y_1^2} q_v^{*2}$	(i)
Specific gravity	$\Delta p^* = \frac{1 - (d^*/D^*)^4}{N_{vG}^{*2} C^2 d^{*4} F_\rho G_F} q_v^{*2}$	(d)		
<i>pvt</i> equation			$\Delta p^* = \frac{[1 - (d^*/D^*)^4] G p_{f1}^*}{N_{v\rho}^{*2} C^2 d^{*4} Y_1^2 Z_{f1} T_{K1}} q_v^2$	(j)

Volumetric flow rate at base conditions

Density	$\Delta p^* = \frac{[1 - (d^*/D^*)^4] \rho_b^2}{N_{V\rho}^{*2} C^2 d^{*4} F_p \rho_F^*} q_V^*$	(e)	$\Delta p^* = \frac{[1 - (d^*/D^*)^4] \rho_b^{*2}}{N_{V\rho}^{*2} C^2 d^{*4} Y_1^2 \rho_{f1}^*} q_V^{*2}$	(k)
Specific gravity	$\Delta p^* = \frac{[1 - (d^*/D^*)^4] G_b^2}{N_{VG}^{*2} C^2 d^{*4} F_p G_F} q_V^{*2}$	(f)		
<i>pvT</i> equation				
Standard base			$\Delta p^* = \frac{[1 - (d^*/D^*)^4] G Z_{f1} T_{K1}}{N_{VpT}^{*2} C^2 d^{*4} Y_1^2 Z_b^2 p_{f1}^*} q_V^{*2}$	(l)
Selected base			$\Delta p^* = \frac{[1 - (d^*/D^*)^4] \rho_b^{*2} G Z_{f1} T_{K1}}{(N_{VpT}^*)_b^2 C^2 d^{*4} Y_1^2 Z_b^2 T_{Kb}^2 p_{f1}^*} q_V^*$	(m)

Notes: Gas (vapor) equations are written for upstream pressure tap. For downstream pressure tap, change subscript 1 to subscript 2 as in ρ_{f2} , p_{f2} , Z_{f2} , etc. D^* and d^* in these equations are at flowing conditions: $d^* = F_{ad}^* d_{\text{meas}}^* = [1 + \alpha_{pF}^* (T_{\text{c}} - 20)] d_{\text{meas}}^*$ [Eq. (9.52)]; $D^* = F_{aD}^* D_{\text{meas}}^* = [1 + \alpha_p (T_{\text{c}} - 20)] D_{\text{meas}}^*$ [Eq. (9.53)].

TABLE 9.43 Procedure for Differential-Pressure Solution: Liquids

Procedure	Symbol		Reference
	U.S. units	SI units	
1. Select equations			
a. Differential pressure†	h_w	Δp^*	Tables 9.42, 9.43
b. Obtain N factor for the desired flow-rate unit (q_{PPH} , q_{GPM} , etc.)	N	N^*	Tables 9.14–9.19
c. Discharge coefficient	C	C	Table 9.1
d. Pipe Reynolds number	R_D	R_D	Tables 9.20–9.22
2. Obtain values for			
a. Flow rate	q	q^*	
b. Primary element bore	d_{meas}	d_{meas}^*	From measurement shown on plate
c. Pipe diameter	D_{meas}	D_{meas}^*	From measurement or Table B.1
d. Temperature	T_F	T_C	
<i>If density form is selected</i>			
e. Flowing density, uncorrected for pressure	ρ_F	ρ_F^*	App. E or Chap. 2 equations
<i>For base volumes</i>			
f. Obtain base density	ρ_b	ρ_b^*	App. E or Chap. 2 equations
<i>If specific gravity equation form is selected</i>			
g. Flowing specific gravity, uncorrected for pressure	G_F	G_F	App. E or Chap. 2 equations
<i>For base volumes</i>			
h. Base specific gravity	G_b	G_b	App. E or Chap. 2 equations
i. Liquid compressibility for most fluids, $F_p = 1.0$	F_p	F_p	App. E or Chap. 2 equations
j. Viscosity	μ_{cP}	μ_{cP}	App. F or Chap. 2 equations
3. Calculate constants			
a. Calculate pipe diameter at flowing conditions	D	D^*	Eqs. (9.51)–(9.53)
b. Calculate primary element bore at flowing conditions	d	d^*	Eqs. (9.51)–(9.53)
c. Reynolds number	R_D	R_D	
d. Discharge coefficient	C	C	Table 9.1

TABLE 9.43 Procedure for Differential-Pressure Solution: Liquids (*Continued*)

Procedure	Symbol		Reference
	U.S. units	SI units	
4. Calculate differential			
a. Substitute variables into differential-pressure equation	h_w	Δp^*	Tables 9.41 and 9.42 equations
5. Display differential	h_w	Δp^*	

†When applicable, add the square of corrective terms to the denominator of the differential equation. For example, for drain holes (vent or weep holes): $h_w = h_u / F_{DH}^2$.

$$h_{w,2} = \left(\frac{q_2}{q_1} \right)^2 h_{w,1} \quad (9.106)$$

where $h_{w,1}$ is the initial differential, $h_{w,2}$ is the new rescaled differential, q_1 is the initial flow rate, and q_2 is the new flow rate.

Iteration. The exact differential must be determined by iteration using the equations presented in Tables 9.41 and 9.42. For liquids the calculation is relatively simple, since no variable in the equation is differential-pressure-dependent. For gases (vapors) the gas expansion factor is dependent on differential pressure, and hence iteration is required. This procedure for liquids is detailed in Table 9.43 for liquids and in Table 9.44 for gases (vapors).

Example 9.16. The flow rate of the gasoline of Example 9.3 has been reduced to 20 base gal/min. Rescale the differential-pressure transmitter for 20 GPM by (1) simple ratio and (2) calculation.

Data from Example 9.3:

$$\begin{aligned} (q)_N &= 80 & D_{\text{meas}} &= 1.939 \text{ in} & D &= 1.9392 \text{ in} & d_{\text{meas}} &= 1.4407 & d &= 1.4409 \\ (h_w)_N &= 64 \text{ in} & N_{VG} &= 5.6665 & G_F &= 0.7359 & F_p &= 1.0088 & G_b &= 0.7359 \\ T_F &= 80.5^\circ\text{F} & \mu_{cP} &= 0.417 \end{aligned}$$

1. **Simple ratio.** The simple ratio, Eq. (9.106), is

$$h_{w,2} = \left(\frac{q_{\text{GPM},2}}{q_{\text{GPM},1}} \right)^2 h_{w,1} = \left(\frac{20}{100} \right)^2 100 = 4 \text{ in}$$

2. **Exact calculation.** The differential-pressure equation from Table 9.41, Eq. (f), is

$$h_w = \frac{[1 - (d/D)^4] G_b^2}{N_{VG}^2 C^2 d^4 F_p G_F} q_{\text{GPM}}^2 = \frac{[1 - (1.441/1.939)^4] (0.7359)^2}{(5.6665)^2 C^2 (1.441)^4 (1.008)(0.7255)} (20)^2$$

The pipe Reynolds number from Example 9.13 is

$$R_D = 2875.3 q_{\text{GPM}} = (2875.3)(20) = 57,506$$

TABLE 9.44 Procedure for Iterative Differential-Pressure Solution: Gases (Vapors)

Procedure	Symbol		Reference
	U.S. units	SI units	
1. Select equations			
a. Differential pressure†	h_w	Δp^*	Tables 9.41, 9.42
b. Obtain N factor for the desired flow-rate unit (q_{PPH} , q_{GPM} , etc.)	N	N^*	Tables 9.14–9.19
c. Discharge coefficient	C	C	Table 9.1
d. Pipe Reynolds number	R_D	R_D	Tables 9.20–9.22
2. Obtain values for			
a. Flow rate	q	q^*	
b. Primary element bore	d_{meas}	d_{meas}^*	From measurement shown on plate
c. Pipe diameter	D_{meas}	D_{meas}^*	From measurement or Table B.1
d. Temperature	T_F	T_C	
e. Measured pressure			
Upstream pressure tap	p_{f1}	p_{f1}^*	
Downstream pressure tap	p_{f2}	p_{f2}^*	
<i>If density equation is selected</i>			
f. Flowing density			
Upstream pressure tap	ρ_{f1}	ρ_{f1}^*	
Downstream pressure tap	ρ_{f2}	ρ_{f2}^*	App. G or Chap. 2 equations
<i>For standard volumes</i>			
g. Base density	ρ_b	ρ_b^*	
<i>If p_vT equation is selected</i>			
h. Specific gravity	G	G	Eq. (2.7)
i. Flowing compressibility			
Upstream pressure tap	Z_{f1}	Z_{f1}	App. G or Chap. 2 equations
Downstream pressure tap	Z_{f2}	Z_{f2}	
<i>For standard volumes</i>			
j. Base pressure	p_b	p_b^*	
k. Base temperature	T_b	T_{kb}	

TABLE 9.44 Procedure for Iterative Differential-Pressure Solution: Gases (Vapors)
(Continued)

Procedure	Symbol		Reference
	U.S. units	SI units	
1. Base compressibility	Z_b	Z_b	App. G or Chap. 2 equations
<i>m.</i> Viscosity	μ_{cP}	μ_{cP}	App. F or Chap. 2 equations
<i>n.</i> Isentropic exponent	k	k	App. I or Chap. 2 equations
3. Calculate constants and first estimate for the differential			
a. Calculate pipe diameter at flowing conditions	D	D^*	Eqs. (9.51)–(9.53)
b. Calculate primary element bore at flowing conditions	d	d^*	Eqs. (9.51)–(9.53)
c. Reynolds number	R_D	R_D	
d. Discharge coefficient	C	C	Table 9.1
e. Calculate the initial differential assuming $Y_{n-1} = 1.0$	$(h_w)_{n-1}$	$(\Delta p^*)_{n-1}$	
4. Iterate for the differential			
a. Calculate the gas expansion factor by using the first estimate of the differential			
Upstream pressure tap	$(Y_1)_{n-1}$	$(Y_1)_{n-1}$	Table 9.26
Downstream pressure tap	$(Y_2)_{n-1}$	$(Y_2)_{n-1}$	
b. Substitute into differential-pressure equation to obtain next estimate.	$(h_w)_n$	$(\Delta p^*)_n$	
c. Calculate percent difference between last estimate and first estimate. If >0.001 , set next estimate equal to last value $(h_w)_n$ or $(\Delta p^*)_n$. Return to step (a) until desired closure is less than 0.001, then exit to step 5.	$\% = 100 \times [(h_w)_{n-1} - (h_w)_n] / (h_w)_n$ $\% = 100 \times (\Delta p^*)_{n-1} - (\Delta p^*)_n / (\Delta p^*)_n$		
5. Display differential	h_w	Δp^*	

†When applicable, add the square of corrective terms to the denominator of the differential equation. For example, for drain holes (vent or weep holes): $h_w = h_w / F_{DH}^2$.

Substitution into the discharge-coefficient equation from Example 9.13 gives

$$C = \frac{0.60549 + 43.66}{R_D^{0.75}} = \frac{0.60549 + 43.66}{57,510^{0.75}} = 0.61725$$

The differential is, by substitution,

$$h_w = \frac{1.48512}{(0.61725)^2} = 3.898 \text{ in}$$

Example 9.17. The flow rate of the natural gas mixture of Example 9.6 is reduced to 1,000,000 (28,317 SCMH). Rescale the differential-pressure transmitter to the new upper range flow rate.

The data from Example 9.6 is as follows:

$$\begin{aligned} D_{\text{meas}} &= 7.620 \text{ in} & D &= 7.6216 \text{ in} & d_{\text{meas}} &= 3.900 & d &= 3.9015 & T_f &= 100^\circ\text{F} \\ P_{f2} &= 2000 \text{ psia} & G &= 0.8445 & Z_{f2} &= 0.5688 & Z_b &= 0.9974 & \mu_{\text{cp}} &= 0.0255 \\ k &= 2.29 & F_a &= 1.0006 & (N_{\text{vpr}})_b &= 218.4834 \end{aligned}$$

From Table 9.41, Eq. (m), the differential-pressure equation is

$$h_w = \frac{(1 - d/D)^4 p_b^2 G Z_{f2} T_{f2}}{(N_{\text{vpr}})_b^2 C^2 d^4 Y_2^2 Z_b^2 T_b^2 P_{f2}} q_{\text{SCFH}}^2$$

Substitution gives

$$\begin{aligned} h_w &= \frac{[1 - (3.900/7.620)^4](14.7)^2(0.8445)(0.5668)(100 + 459.67)}{(218.48)^2 C^2 (3.900)^4 Y_2^2 (0.9974)^2 (60 + 459.67)^2 (2000)} (1,000,000)^2 \\ &= \frac{9.1081}{C^2 Y_2^2} \end{aligned}$$

The pipe Reynolds number is calculated from Table 9.20, Eq. (m):

$$R_D = \left[\frac{(3724.2)(0.8445)(14.7)}{(0.9974)(60 + 459.67)(0.0255)(7.62)(218.48)} \right] 1,000,000 = 2,100,612$$

The discharge-coefficient equation from Table 9.1, for $D > 2.3$ in, is

$$\begin{aligned} C &= 0.5959 + 0.0312\beta^{2.1} - 0.184\beta^8 + 0.09 \frac{\beta^4}{D(1 - \beta)^4} \\ &\quad - 0.0337 \frac{\beta^3}{D} + \frac{91.71\beta^{2.5}}{R_D^{0.75}} \end{aligned}$$

Substituting $\beta = d/D = 0.51190$ and $R_D = 2,100,612$, $C = 0.603226$. Substitution reduces the differential-pressure equation to

$$h_w = \frac{9.10808}{(0.603266)^2 Y_2^2} = \frac{25.027}{Y_2^2}$$

The downstream pressure tap gas expansion factor is a function of h_w , Table 9.26, Eq. (d), and is reduced to the form given in Example 9.14 as

$$Y_2 = \sqrt{1 + 0.00001803h_w} - \frac{0.000003417h_w}{\sqrt{1 + 0.00001803h_w}}$$

Initially assuming the gas expansion factor $Y_2 = 1$, the iterative solution is:

n	$(Y_2)_{n-1}$	$(h_w)_n = 25.027/(Y_2^2)_{n-1}$
1	1.0	25.027
2	1.00014	25.020
3	1.00014	25.020

The differential-pressure transmitter is then rescaled to

$$h_w = 25.020 \text{ in}$$

GENERIC SOLUTION

The sizing, flow-rate, and differential-pressure equations using an N factor as the flow-rate unit conversion constant follow standard U.S. industrial practice. These equations calculate directly standard cubic feet, base or flowing gallons, etc., and are the most suitable for detailing the required input variables.

The generic equations and exact correction terms developed in the following sections substantially reduce the size of a computer program and the resulting programming errors. Additionally, exact constants specified in the various national and international standards are easily changed. This makes them well suited for custody transfer applications using on-site computers. *It should be emphasized that many of the corrections developed in this section are theoretical and that the accuracy of any primary element does not justify applying some of the corrective terms except where the calculation accuracy is of most significance.*

The U.S. Unit Equations

The generic equation from which all flow-rate unit equations were developed is the mass-flow-rate equation:

$$q_{lbm/s} = \frac{\pi}{4} \left[\frac{2g_c(\rho_w)_{T,g0}}{12^5} \right]^{1/2} \frac{CY_1 d_f^2}{\sqrt{1 - (d_f/D)^4}} \sqrt{\rho_{f1}} \sqrt{h_w} \quad (9.107)$$

In Eq. (9.107) the subscript f is used to indicate the terms that are to be calculated at flowing temperature, pressure, and differential pressure.

The constants g_c and $(\rho_w)_{T,g0}$ are exact reference values as presented in the selected standards (ASME, ISO, ANSI, etc.).

Other equation variables are to be exactly calculated based on all known bias errors associated with their determination, or an assumption is made that a correction is unwarranted. The decision not to correct for a particular error should be based on an overall uncertainty (accuracy) analysis of each variable and its effect on the overall computation of the flow rate.

Pipe Diameter Correction. The diameter of the pipe increases with pressures and may increase or decrease in size from the value measured at a reference temperature, usually 68°F (15.5°C). The pipe diameter at flowing conditions is calculated by

$$D_f = F_{ad} F_{Dp} D_{\text{meas}} \quad (9.108)$$

where D_{meas} is in inches and is the measured pipe diameter at a reference temperature.

The thermal expansion term F_{ad} is determined by

$$F_{ad} = 1 + \alpha_p (T_f - T_{D,\text{ref}}) \quad (9.109)$$

where α_p is the pipe material thermal expansion factor, in in/in·°R, T_f is the absolute flowing temperature, in degrees Rankine, and $T_{D,\text{ref}}$ is the absolute temperature at which the pipe diameter is measured.

The pressure correction term F_{Dp} , in Eq. (9.108), is

$$F_{Dp} = 1 + \frac{p_f D_f}{2E_p F_{ad} t_p} \left(1 - \frac{\mu_p}{2} \right) \quad (9.110)$$

where p_f is the flowing pressure, in psia, t_p is the pipe wall thickness, in inches at the reference temperature, E_p is the modulus of elasticity of the pipe material, in psi at the flowing temperature, and μ_p is Poisson's ratio (in/in). *It should be noted that, for flange and corner taps, the pressure taps are in the flange area, making this correction extremely small.*

Bore Diameter Correction. At flowing conditions the bore diameter is a function of both temperature and differential pressure in accordance with the following equation:

$$d_f = F_{ad} F_{\Delta p} d_{\text{meas}} \quad (9.111)$$

The bore diameter d_{meas} , in inches, is the measured bore at a reference temperature and zero differential. The thermal expansion term F_{ad} is calculated by

$$F_{ad} = 1 + \alpha_{PE} (T_f - T_{d,\text{ref}}) \quad (9.112)$$

where α_{PE} is the primary element's thermal expansion factor, T_f is the flowing temperature, and $T_{d,\text{ref}}$ is the temperature at which the bore d_{meas} was measured.

The differential-pressure correction factor for thin orifice plates (Simpson, 1984) is

$$F_{\Delta p} = \left\{ 1 - \frac{h_w}{27.73 E_{PE}} \left[(0.135 \beta_f - 0.1555 \beta_f^2) A^3 + (1.06 \beta_f^{1.3} - 1.17) A^2 \right] \right\}^{-1} \quad (9.113)$$

where h_w is the meter differential, in inches of water, E_{PE} is the modulus of elasticity of the primary element, β_f is the beta ratio at flowing conditions, and A is the ratio of pipe diameter D_f to plate thickness t_{PE} evaluated at flowing temperature and pressure determined by

$$A = \frac{D_f}{F_{ad} t_{PE}} \quad (9.114)$$

where t_{PE} is the thickness of the primary element, in inches. The beta ratio at flowing conditions is then defined by

$$\beta_f = \frac{d_f}{D_f} \quad (9.115)$$

The differential-pressure correction factor for nozzles and venturis, which have cylindrical throats and atmospheric pressure at the outer surfaces, is

$$F_{\Delta p} = 1 + \frac{(p_{f1} - h_w/27.73)d_f}{2E_{PE}F_{ad}t_{PE}} \left(1 - \frac{\mu_{PE}}{2}\right) \quad (9.116)$$

The solution for the pipe diameter and bore of the primary element is iterative and is best determined by computer iteration.

In the above equations negligible error is introduced if the factors $F_{\Delta p}$ and F_{Dp} are calculated using the measured pipe diameter, pipewall thickness, orifice plate thickness, and measured bore diameter. This assumption eliminates the iterative solution for D_f and d_f .

Orifice Pressure Tap Location Correction. For the concentric square-edged orifice the discharge coefficient equations presented in Table 9.1 are based on prescribed pressure tap locations. When the location after installation is measured, the discharge coefficient may be calculated based on measured dimensions (ISO, 1978) by

$$C = 0.5959 + 0.0317\beta_f^{2.1} - 0.1848\beta_f^8 + 0.0909L_1 \frac{\beta_f^4}{1 - \beta_f^4} - 0.0335L_2^2\beta_f^3 + \frac{0.0029\beta_f^{2.5}}{\left(\frac{R_{Df}}{10^6}\right)^{0.75}} \quad (9.117)$$

where L_1 is a dimensionless ratio for the upstream tap and L_2 is the dimensionless ratio for the downstream tap, as measured from the upstream face of the plate. These ratios are given in Table 9.45.

Tap location lengths l_{1f} and l_{2f} may be corrected for thermal effects as follows. For l_{1f} by

$$l_{1f} = 1 + \alpha_p(T_f - T_{D,ref})l_1 = F_{ad}l_1 \quad (9.118)$$

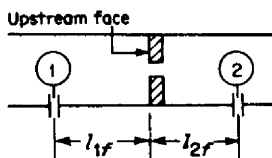
and for l_{2f} by

$$l_{2f} = 1 + \alpha_p(T_f - T_{D,ref})l_2 = F_{ad}l_2 \quad (9.119)$$

where l_1 and l_2 are the measured lengths at the reference temperature when the pipe diameter was measured.

The pipe Reynolds number in Eq. (9.117) is to be calculated by

$$R_{Df} = 22,737.47 \frac{q_{lbm/s}}{\mu_{cP} D_f} \quad (9.120)$$

TABLE 9.45 Dimensionless ratios for Eq. (9.117)

l_{1f} = upstream tap centerline to face of the orifice plate

l_{2f} = upstream face of the orifice plate to downstream tap centerline

$$C = 0.5959 + 0.0317\beta_f^{2.1} - 0.1848\beta_f^8 + 0.0909L_1 \frac{\beta_f^4}{1 - \beta_f^4} - 0.0335L_2\beta_f^3 + \frac{0.0029\beta_f^{2.5}}{(R_{Df}/10^6)^{0.75}}$$

	Ratio	
	L_1	L_2
Corner taps	0.008	0.038
Flange taps		
$L_1 < 0.44$	l_{1f}/D_f	$l_{2f}/D_f + 0.03$
$L_1 \geq 0.44$	0.44	$l_{2f}/D_f + 0.03$
D and $D/2$ (radius taps)	0.44	0.5

The SI Unit Equations

The SI unit generic equation for mass flow is

$$q_{\text{kg/s}} = \frac{\pi}{4} \sqrt{2g_c} \frac{CY_1 d_f^{*2}}{\sqrt{1 - (d_f^*/D_f^*)^4}} \sqrt{\rho_f^*} \sqrt{\Delta P^*} \quad (9.121)$$

where subscript f indicates that the terms are to be calculated at flowing temperature, pressure, and differential pressure. The constant g_c is exactly $1.0 \text{ kg}\cdot\text{m}/(\text{N}\cdot\text{m}^2)$.

Pipe Diameter Correction. The pipe diameter increases with pressure and will increase or decrease with temperature. The pipe diameter at flowing conditions is calculated by

$$D_f^* = F_{aD}^* F_{Dp}^* D_M \quad (9.122)$$

where D_M is the measured diameter, in meters, at a reference temperature, the thermal-expansion term is

$$F_{aD}^* = 1 + \alpha_P^* (T_K - T_{D,\text{ref}}^*) \quad (9.123)$$

where α_P^* is the pipe material's thermal-expansion factor, in $\text{m}/(\text{m}\cdot\text{K})$; T_K is the absolute flowing temperature, in kelvins, and $T_{D,\text{ref}}^*$ is the absolute temperature, in kelvins, at which the pipe diameter is measured.

The pressure correction term F_{Dp} is

$$F_{Dp}^* = 1 + \frac{P_f^* D_f^*}{2E_p^* F_{ad}^* t_p^*} \left(1 - \frac{\mu_p^*}{2}\right) \quad (9.124)$$

where P_f^* is the flowing pressure, in pascals; t_p^* is the pipe wall thickness, in meters, at the reference temperature; E_p^* is the modulus of elasticity of the pipe material, in pascals, at the flowing temperature; and μ_p^* is Poisson's ratio (m/m) of the pipe material. *It should be noted that, for flange and corner taps, the pressure taps are in the flange area, making this correction extremely small.*

Bore Diameter Correction. The bore diameter is a function of both temperature and differential pressure. It is calculated by

$$d_f^* = F_{ad}^* F_{\Delta p}^* d_M \quad (9.125)$$

The bore diameter d_M , in meters, is the measured bore at a reference temperature (and zero differential), and the thermal expansion term is

$$F_{ad}^* = 1 + \alpha_{PE}^* (T_K - T_{d,ref}^*) \quad (9.126)$$

where α_{PE}^* is the primary element's thermal-expansion factor, in m/(m·K) and T_K is the flowing temperature, in kelvins—the temperature at which the bore d_M , in meters, was measured.

The differential-pressure correction factor for thin orifice plates (Simpson, 1984) is

$$F_{\Delta p}^* = \left\{ 1 - \frac{\Delta P^*}{E_{PE}^*} [(0.135 \beta_f - 0.1555 \beta_f^2) A^3 + (1.06 \beta_f^{1.3} - 1.17) A^2] \right\}^{-0.5} \quad (9.127)$$

where ΔP^* is the meter differential, in pascals; E_{PE}^* is the modulus of elasticity of the primary element, in pascals; β_f is the beta ratio at flowing conditions; and A is the ratio of pipe diameter D_f^* to plate thickness t_{PE}^* evaluated at flowing temperature and pressure. The term A is found by

$$A = \frac{D_f^*}{F_{ad}^* t_{PE}^*} \quad (9.128)$$

where t_{PE}^* is the thickness of the primary element, in meters. The beta ratio, at flowing conditions, is

$$\beta_f = \frac{d_f^*}{D_f^*} \quad (9.129)$$

The differential-pressure connection factor for nozzles and venturis, which have cylindrical throats and atmospheric pressure at their outer surfaces, is

$$F_{\Delta p}^* = 1 + \frac{(P_{\beta}^* - \Delta P^*) d_f^*}{2E_{PE}^* F_{ad}^* t_{PE}^*} \left(1 - \frac{\mu_{PE}^*}{2}\right) \quad (9.130)$$

The solution for the pipe diameter and bore of the primary element is iterative and is best determined by computer iteration.

In the above equations, negligible error is introduced if the factors F_{dp}^ and F_{Dp}^* are calculated using the measured pipe diameter, pipe wall thickness, orifice plate thickness, and measured bore diameter. This assumption eliminates the iterative solution for D_f^* and d_f^* .*

Orifice Pressure Tap Location Correction. The discharge coefficient equation (9.117) is based on dimensionless ratios and may be used for SI units for estimating the correction for other than standard tap locations or when tap location measurements are made.

Tap location lengths l_{1f}^* and l_{2f}^* are corrected for temperature as follows. For l_{1f} by

$$l_{1f}^* = 1 + \alpha_p^*(T_K - T_{D,ref}^*)l_1^* = F_{ab}^*l_1^* \quad (9.131)$$

and for l_{2f}^* by

$$l_{2f}^* = 1 + \alpha_p^*(T_K - T_{D,ref}^*)l_2^* = F_{ab}^*l_2^* \quad (9.132)$$

where l_1^* and l_2^* are the tap locations measured from the upstream face of the plate at the reference temperature when the pipe diameter was measured. The dimensionless ratios L_1 and L_2 , defined at flowing conditions, are given in Table 9.45.

The pipe Reynolds number in Eq. (9.117) is to be calculated by

$$R_{Df} = \frac{q_{kg/s}}{(\pi/4)\mu_{Pa,s}D_f^*} \quad (9.133)$$

Computation

The generic flow-rate equation requires that all flow rates first be converted to mass (lb_m/s , kg/s) and that the density be in mass per unit volume (lb_m/ft^3 , kg/m^3). In Table 9.46 are the constants and density equations for U.S. units, and in Table 9.47 are the SI unit equations and constants. These are common to the computational solution flow rate, sizing, and differential pressure.

The generic flow-rate equation may be rearranged to either solve for the bore of the primary element (sizing) or compute the differential pressure. The computational procedure for sizing in U.S. units is presented in Table 9.48 and for SI units in Table 9.49; the generic sizing computations for U.S. and SI units are given in Tables 9.50 and 9.51, respectively. The computation for the differential pressure in U.S. units is given in Table 9.52 and for SI units in Table 9.53.

Example 9.18. Set up the calculation procedure to size the orifice of Example 9.6 using the generic equations. Assume that the thermal effect on tap location and the pressure effect on the pipe bore are negligible. The 316 stainless-steel orifice plate is to be $\frac{1}{8}$ in. (3.18 mm) thick, and the pipe material is carbon steel. *Note:* For calculation accuracy, 10 significant figures are shown.

Data from Example 9.6 is as follows

$$\begin{aligned}(q_{\text{SCFH}})_{\text{URV}} &= 2,000,000 & (h_w)_{\text{URV}} &= 100 \text{ in} & D_{\text{meas}} &= 7.620 \text{ in} & p_{f2} &= 2000 \text{ psia} \\ T_{f2} &= 539.67^\circ\text{R} & G &= 0.8445 & Z_{f2} &= 0.5688 & Z_b &= 0.9974 \\ \mu_{cp} &= 0.0255 & k &= 2.29 & p_b &= 14.7 \text{ psia} & T_b &= 519.67^\circ\text{R}\end{aligned}$$

The generic sizing equation for the S_M factor from Table 9.50 is

$$S_M = \frac{q_{\text{lbm/s}}}{\frac{\pi}{4} \left[\frac{2g_c(\rho_w)_{T_{g0}}}{12^5} \right]^{1/2} D_f^2 \sqrt{\rho_{f2}} \sqrt{h_w}}$$

From Table 9.46 the constants and density conversions are

$$g_c = 32.17405 \text{ lb}_m \cdot \text{ft}/(\text{lb}_f \cdot \text{s}) \quad (\rho_w)_{68, g0} = 62.31572 \text{ lb}_m/\text{ft}^3$$

The flowing density at the downstream tap is then

$$\rho_{f2} = \left(\frac{M_{w, \text{air}}}{R_0} \right) \frac{G p_{f2}}{Z_{f2} T_{f2}}$$

and the density at base conditions ($p_b = 14.7 \text{ psia}$ and $T_b = 519.67^\circ\text{R}$) is

$$\rho_b = \left(\frac{M_{w, \text{air}}}{R_0} \right) \frac{G p_b}{Z_b T_b}$$

Substituting, with $M_{w, \text{air}} = 28.96247/\text{lb}_m/(\text{lb}_m \cdot \text{mol})$ and $R_0 = 10.73151 \text{ psia}/(\text{lb}_m \cdot \text{mol} \cdot ^\circ\text{R})$, the density at flowing conditions is:

$$\rho_{f2} = \left(\frac{M_{w, \text{air}}}{R_0} \right) \frac{G p_{f2}}{Z_{f2} T_{f2}} = \left(\frac{28.96247}{10.73151} \right) \frac{(0.8445)(2000)}{(0.5688)(539.67)} = 14.31900353 \text{ lb}_m/\text{ft}^3$$

and, for the base density,

$$\rho_b = \left(\frac{M_{w, \text{air}}}{R_0} \right) \frac{G p_b}{Z_b T_b} = \left(\frac{28.96247}{10.73151} \right) \frac{(0.8445)(14.7)}{(0.9974)(519.67)} = 0.0646390166 \text{ lb}_m/\text{ft}^3$$

The mass flow rate, from the Table 9.46 conversion equation, is

$$q_{\text{lbm/s}} = \rho_b q_{\text{FT}^3/\text{s}} = (2,000,000/3600)(0.0646390) = 35.91056481$$

The pipe diameter at flowing conditions is calculated from Eq. (9.108):

$$D_f = F_{ad} F_{Dp} D$$

The pipe diameter thermal-expansion correction by Eq. (9.109) is

$$F_{ad} = 1 + \alpha_p (T_f - T_{D, \text{ref}}) = 1 + 0.0000067(539.67 - 527.67) = 1.0002144$$

where the thermal-expansion factor α_p is from Table B.4. The pipe diameter was measured at 60°F ($T_{D, \text{ref}} = 68 + 459.67 = 527.67^\circ\text{R}$).

Assuming the flange thickness negates the pressure correction factor ($F_{Dp} = 1.0$), the corrected pipe diameter becomes

$$D_f = F_{ad} F_{Dp} D = (1.0002144)(1.0)(7.620) = 7.621533728 \text{ in}$$

Substituting the above values into the sizing equation yields

$$S_M = \frac{35.91056}{\frac{\pi}{4} \left[\frac{(2)(32.174)(62.3157)}{12^5} \right]^{1/2} (7.6216)^2 \sqrt{14.3190} \sqrt{100}} = 0.1638574722$$

The initial estimate for beta, from Table 9.28, Eq. (j), is

$$\beta_0 = \left[1 + \left(\frac{0.6}{S_M} \right)^2 \right]^{-1/4} = \left[1 + \left(\frac{0.6}{0.163857} \right)^2 \right]^{-1/4} = 0.5132721$$

Equation (9.84) written for flowing beta is

$$(\beta_f)_n = \left\{ 1 + \left[\frac{C_{n-1}(Y_2)_{n-1}}{S_M} \right]^2 \right\}^{-1/4}$$

The discharge coefficient, also written for flowing beta, from Table 9.1 for $D > 2.3$ in, is

$$C = 0.5959 + 0.0312\beta_f^{2.1} - 0.814\beta_f^8 + 0.09 \frac{\beta_f^4}{D_f(1 - \beta_f^4)} - 0.0337 \frac{\beta_f^3}{D_f} + \frac{91.71\beta_f^{2.5}}{R_{Df}^{0.75}}$$

The pipe Reynolds number, by Eq. (9.120), is

$$R_{Df} = 22,737.47 \frac{q_{lbm/s}}{\mu_{cP} D_f} = 22,737.47 \frac{35.91056}{(0.0255)(7.62116)} = 4,201,226$$

The downstream gas expansion factor is calculated by Table 9.26, Eq. (d),

$$Y_2 = \sqrt{1 + x_2} - (0.41 + 0.35\beta_f^4) \frac{x_2}{k\sqrt{1 + x_2}}$$

where, from Table 9.26, Eq. (i)

$$x_2 = \frac{h_w}{27.73 p_{f2}} = 0.0018031$$

The iteration for the flowing β_f may be tabulated as follows:

	<i>n</i>			
	1	2	3	4
$\beta_{f,n-1}$	0.51322721257	0.5118805093	0.5118928289	0.5118927196
C_{n-1}	0.6031722554	0.6031409585	0.5031412363	0.6031412339
$(Y)_{n-1}$	1.0005595	1.000559706	1.000559704	1.000559704
$\beta_{f,n}$	0.5118805093	0.5118928289	0.5118927196	0.5118927206

The orifice bore diameter at flowing conditions is then

$$d_f = \beta_f D_f = (0.5118927206)(7.621633728) = 3.901458824 \text{ in}$$

The bore is to be machined to a diameter, to be measured at 68°F, of

$$d_{\text{meas}} = \frac{d_f}{F_{ad} F_{\Delta p}}$$

with

$$F_{ad} = 1 + \alpha_{PE}(T_f - T_{d,\text{ref}}) = 1.0 + 0.0000096 (559.67 - 527.67) = 1.0003072$$

where $\alpha_{PE} = 0.0000096 \text{ in}/(\text{in} \cdot ^\circ\text{R})$ from App. B, Table B.4. The differential-pressure correction factor, for a $\frac{1}{8}$ -in-thick orifice plate, with A from Eq. (9.114):

$$A = \frac{D_f}{F_{ad} t_{PE}} = \frac{7.6216}{(1.0003)(0.125)} = 60.9543$$

The differential-pressure correction, using Eq. (9.113) with the modulus of elasticity $E = 30 \times 10^6 \text{ psi}$, is

$$\begin{aligned} F_{\Delta p} &= \left(1 - \frac{100}{(27.73)(30 \times 10^6)} \{ [(0.135)(0.5119) - (0.1555)(0.5119)^2](60.954)^3 \right. \\ &\quad \left. + [(1.06)(0.5119)^{1.3} - 1.17](60.954)^2 \} \right)^{-1/2} \\ &= 1.000224 \end{aligned}$$

Finally, the measured bore diameter at 68°F is calculated as

$$\begin{aligned} d &= \frac{d_f}{F_{ad} F_{\Delta p}} \\ &= \frac{3.90147}{(1.000307)(1.00022)} \\ &= 3.8994 \text{ in} \end{aligned}$$

Example 9.19. Using the generic solution, calculate the flow rate for the flange tap orifice of Example 9.18 if the measured differential is 50 in (12.34 kPa). All other variables remain the same.

Data and calculation results from Examples 9.6 and 9.18 are as follows:

$$\begin{aligned} P_{f2} &= 2000 \text{ psia} & T_{f2} &= 100 + 459.67 & G &= 0.8445 & Z_{f2} &= 0.5688 \\ Z_b &= 0.9974 & &= 559.67^\circ\text{R} & k &= 2.29 & p_b &= 14.7 \text{ psia} \\ \rho_{f2} &= 14.319 \text{ lb}_m/\text{ft}^3 & \mu_{cP} &= 0.0255 & \rho_b &= 0.064639 \text{ lb}_m/\text{ft}^3 & E &= 30 \times 10^6 \text{ psia} \\ D_{\text{meas}} &= 7.62 \text{ in} & D_f &= 7.621634 \text{ in} & d_{\text{meas}} &= 3.8994 \text{ in} & g_c &= 32.17405 \text{ lb}_m \\ (\rho_w)_{T,80} &= 62.31572 \text{ lb}_m/\text{ft}^3 & F_{ad} &= 1.0003072 & T_b &= 519.67^\circ\text{R} & & \cdot \text{ft}/(\text{lb}_f \cdot \text{s}^2) \end{aligned}$$

The generic flow-rate equation (9.107) is

$$q_{lbm/s} = \frac{\pi}{4} \left[\frac{2g_c(\rho_w)_{T,g0}}{12^5} \right]^{1/2} \frac{CY_2 d_f^2}{\sqrt{1 - (d_f/D_f)^4}} \sqrt{\rho_{f2}} \sqrt{h_w}$$

The orifice bore diameter is calculated from Eq. (9.111):

$$d_f = F_{ad} F_{\Delta p} d$$

where, from Eq. (9.113)

$$F_{\Delta p} = \left(1 - \frac{50}{(27.73)(30 \times 10^6)} \{ [(0.135)(0.5119) - (0.1555)(0.5119)^2](60.954)^3 + [(1.06)(0.5119)^{1.3} - 1.17](60.954)^2 \} \right)^{-0.5} \\ = 1.0001119$$

With $F_{ad} = 1.0003072$ from Example 9.18, the flowing bore becomes

$$d_f = (1.0003072)(1.0001119)(3.8994) = 3.901022 \text{ in}$$

Substitution into the generic flow-rate equation yields

$$q_{lbm/s} = \frac{\pi}{4} \left[\frac{(2)(32.17405)(62.31572)}{12^5} \right]^{1/2} \frac{CY_2(3.90102)^2}{\sqrt{1 - (3.9010/7.6216)^4}} \sqrt{14.3190} \sqrt{50} \\ = 42.066927 CY_2$$

The downstream gas expansion factor is calculated for a flowing $\beta_f = d_f/D_f = 3.90102/7.621634 = 0.511835$ from Table 9.26, Eq. (d):

$$Y_2 = \sqrt{1 + x_2} - (0.41 + 0.35\beta_f^4) \frac{x_2}{k \sqrt{1 + x_2}} = 1.0002799$$

where $k = 2.29$ and x_2 is from Table 9.26, Eq. (i):

$$x_2 = \frac{h_w}{27.73 p_{f2}} = 0.00090155$$

The flow-rate equation then becomes

$$q_{lbm/s} = (42.066927)(1.0002799)C = 42.07870C$$

The discharge coefficient, also written for flowing beta, from Table 9.1 for $D > 2.3$ in:

$$C = 0.5959 + 0.0312\beta_f^{2.1} - 0.184\beta_f^8 + 0.09 \frac{\beta_f^4}{D_f(1 - \beta_f^4)} \\ - 0.0337 \frac{\beta_f^3}{D_f} + \frac{91.71\beta_f^{2.5}}{R_{Df}^{0.75}}$$

Substituting $\beta_f = d_f/D_f = 0.5118354$ yields the discharge coefficient

$$C = 0.6029547 + \frac{17.1887}{R_D^{0.75}}$$

The pipe Reynolds number, from Eq. (9.120), is

$$R_{Df} = 22,737.47 \frac{q_{lbm/s}}{\mu_{cp} D_f} = 22,737.47 \frac{q_{lbm/s}}{(0.0255)(7.62116)} = 116,991.4 q_{lbm/s}$$

Thye iteration is as follows. *Note:* Assume initial discharge coefficient $C_{n-1} = C_0 = 0.6$.

	<i>n</i>		
	1	2	3
$q_{n-1} = 42.07870 C_{n-1}$	25.24722	25.381701	25.381662
$(R_D)_{n-1} = 116,991 q_{lbm/s}$	2,953,707	2,969,440	2,969,436
$C_{n-1} = 0.6029547 + 17.1887/R_D^{0.75}$	0.6031960	0.6031950	0.6031950
$q_n = 42.07870 C_{n-1}$	25.381701	25.381661	25.381661

The flow rate converted to standard cubic feet per hour at the selected base pressure and temperature is then

$$q_{SCFH} = q_{FT^3/s} = \frac{3600 q_{lbm/s}}{\rho_b} = \frac{(3600)(25.381661)}{0.06463901} = 1,413,604 \text{ SCFH}$$

ANSI 2530 AND PROPOSED ORIFICE DISCHARGE COEFFICIENT EQUATIONS

The orifice discharge coefficient prediction equation presented in Table 9.1 (ISO 5167, 1991 and ASME 3M, 1995) is based on regression of the data obtained at Ohio State in the 1930s. Throughout the years several prediction equations, which yield similar statistical results, have been used throughout the world.

A significant body of new data has led to the development of three prediction equations (ISO Report, 1994). These equations are:

- The ANSI/APA-2530/AGA-3 (1991)
- The Stolz II equation (1995)
- The NEL/TC28 equation (1995)

The ANSI/API-2530/AGA-3 (1991) is recommended in ANSI 2530. The Stolz II and NEL/TC28 equations are future replacement equations for ANSI 2530 (1991), ISO 5167 (1991), and ASME 3M (1995). Currently ISO/TC 30 has voted to use the NEL/TC28 equation when the ISO 5167 is revised; the other standardizing bodies have yet to decide on a change.

These equations are essentially based on the same data set and, therefore, yield similar statistical results. The Stolz II *rational* equation is of the familiar form C

$= C_\infty + b/R_D^n$ and may be a more practical working equation for general plant and other computations. The ANSI/API 2530 NEL/API equation is considerably more complex and requires more sophisticated on-site computer requirements for a solution.

The ANSI 2530 (1991) discharge coefficient equation is given in Table 9.54 and the proposed NEL/TC 28 and Stolz II equations are in Table 9.55.

The discharge coefficient values computed from the standard equations (ISO-5167, ASME 3M, and ANSI 2530) and the NEL/ISO TC 28 and Stolz II equations are presented in Tables 9.56 through 9.58.

Example 9.20. Using the following orifice equations, size the orifice of Example 9.3: (1) API 2530 (1991), (2) Stolz II (1995), and (3) NEL/TC28 (1995).

Data from Example 9.3 is:

$$(q_{\text{GPM}})_{\text{URV}} = 100 \text{ base gal/min} \quad (h_w)_{\text{URV}} = 100 \text{ in}$$

$$D_{\text{meas}} = 1.939 \text{ in} \quad D = F_{ad} D_{\text{meas}} = 1.9392 \text{ in} \quad S_M = 0.403699$$

$$F_{ad} = 1.00012 \quad R_D = 230,022$$

1. *For the API 2530 (1991) equation.* The API 2530 equation, for a 1.939-in internal pipe diameter, is, from Table 9.54,

$$C_1 = 0.5961 + 0.0291\beta^2 - 0.229\beta^8 + 0.000513(\beta\Gamma)^{0.7} + (0.021 + 0.0049\alpha)\beta^4 \Gamma^{0.35} \\ + (0.0433 + 0.0712e^{-8.5L_1} - 0.1145e^{-6L_1})(1 - 0.23\alpha)\Phi \\ - 0.0116\beta^{1.1}(1 - 4\alpha)(\lambda - 0.52\lambda^{1.3})$$

where

$$\Gamma = \frac{10^6}{R_D} \quad \Phi = \frac{\beta^4}{1 - \beta^4} \quad \alpha = (0.019\beta\Gamma)^{0.8} \quad \lambda = \frac{2L_2}{1 - \beta}$$

for flange taps $L_1 = L_2 = 1/D = 1/1.9392 = 0.5157$ and for a diameter less than 2.8 inch,

$$C = C_1 + 0.003(2.8 - D)(1.0 - \beta)$$

with $\beta_0 = 0.7472$ and $R_D = 230,022$ the iteration is as follows:

n	β_{n-1}	C_n
1	0.74715	0.60957
2	0.74308	0.60965
3	0.74304	0.60965

The orifice bore measured at 68°F is then calculated, by Eq. 9.54, as

$$d_{\text{meas}} = \frac{d}{F_{ad}} = \frac{\beta D}{F_{ad}} = \frac{(0.74304)(1.9392)}{1.00012} = 1.4407 \text{ in}$$

2. *For the Stolz II equation.* The Stolz II equation, for a 1.939-inch pipe, is from Table 9.1 (b)

$$C = C_z + \frac{b}{R_D^{0.5}} = C_{CT,\infty} + C_{\text{tap}} + \frac{2.2\beta^{0.75} + 17.6\beta^6}{R_D^{0.5}}$$

where the corner tap discharge coefficient $C_{CT,\infty}$ at infinite Reynolds number is defined by

$$C_{CT,\infty} = 0.5971 + 0.0262\beta^2 - 0.2172\beta^8$$

and the tap location term C_{tap} is given by

$$C_{\text{tap}} = [0.0377(1 - e^{-0.7L_1}) - 0.0529(e^{-5.2L_1} - e^{-0.7L_1})] \frac{\beta^4}{1 - \beta^4} - [0.0054L_2^{0.35} - 0.0182L_2^{3.8}] \frac{\beta}{1 - \beta}$$

for flange taps $L_1 = L_2 = 1/D = 1/1.93915 = 0.5157$.

With $\beta_0 = 0.7472$ and a flowing Reynolds number $R_{Df} = 230,022$, the iteration is as follows:

n	β_{n-1}	C_{n-1}
1	0.74716	0.61261
2	0.74179	0.61270
3	0.74175	0.61270

The measured bore of the orifice (d_{meas}) measured at 68°F is obtained by Eq. 9.54 as

$$d_{\text{meas}} = \frac{\beta D}{F_{ad}} = \frac{(0.74175)(1.9392)}{1.0012} = 1.4382 \text{ in}$$

3. *For the NEL/TC28 equation.* The discharge coefficient is calculated by

$$C = C_1 + 0.011(0.75 - \beta)(2.8 - D)$$

where the coefficient C_1 is

$$C_1 = 0.5961 + 0.0261\beta^2 - 0.216\beta^8 + 0.000521(\beta\Gamma)^{0.7} + (0.0188 + 0.0063\alpha)\beta^{3.5}\Gamma^{0.3} + (0.043 + 0.080e^{-10L_1} - 0.123e^{-7L_1})(1 - 0.11\alpha)\Phi - 0.031(\lambda - 0.8\lambda^{1.1})\beta^{1.3}$$

with

$$\Gamma = \frac{10^6}{R_D} \quad \Phi = \frac{\beta^4}{1 - \beta^4} \quad \alpha = (0.019\beta\Gamma)^{0.8} \quad \lambda = \frac{2L_2}{1 - \beta}$$

for flange taps $L_1 = L_2 = 1/D = 1/1.93915 = 0.5157$.

The iteration is as follows:

n	β_{n-1}	C_{n-1}
1	0.74716	0.61292
2	0.74166	0.61297
3	0.74164	0.61297

The orifice bore at room or reference temperature is then, by Eq. 9.54,

$$d_{\text{meas}} = \frac{d}{F_{ad}} = \frac{\beta D}{F_{ad}} = \frac{(0.74164)(1.9392)}{1.00012} = 1.4380 \text{ in}$$

Example 9.21. Using the Stolz II and NEL/TC28 orifice discharge coefficient equations and the thermal expansion coefficient equations, resize the orifice bore for Example 9.6 using (1) the Stolz II (1995) and (2) the NEL/TC 28 equation.

Data from Example 9.6 are as follows:

$$(q_{\text{SCFH}})_{\text{URV}} = 2,000,000 \text{ SCFH} \quad (h_w)_{\text{URV}} = 100 \text{ in} \quad G = 0.8445 \quad Z_{f2} = 0.5688$$

$$Z_b = 0.9974 \quad \mu_{\text{cP}} = 0.0255 \text{ cP} \quad k = 2.29 \quad D_{\text{meas}} = 7.620 \text{ in}$$

From Table B.4 the thermal expansion coefficient for the carbon-steel pipe is

$$\alpha_p = 5.877 \times 10^{-6} + 2.538 \times 10^{-9} T_F - 2.575 \times 10^{-13} T_F^2 - 2.042 \times 10^{-16} T_F^3 = 0.00000613$$

The pipe diameter at flow condition is calculated, by Eq. 9.50, as

$$D = F_{ad} D_{\text{meas}} = [1 + \alpha_p (T_F - 68)] D = [1 + 0.00000613(100 - 68)](6.065) = (1.0002)(7.620) = 7.6215 \text{ in}$$

Substitution into the S_M -factor equation from Table C.6 gives

$$S_M = \frac{p_b \sqrt{Z_{f2} T_{f2} G} (q_{\text{SCFH}})_b}{218.4834 Z_b T_b D^2 \sqrt{h_w p_{f2}}} = 0.16386$$

The Reynolds number at flowing conditions is, by the equation of Table C.6,

$$R_D = \frac{17.04569 G p_b (q_{\text{SCFH}})_b}{Z_b T_b \mu_{\text{cP}} D} = 3,361,043$$

The initial estimate for beta β_0 is then, from Table 9.20, Eq. (j),

$$\beta_0 = \left[1 + \left(\frac{0.6}{S_M} \right)^2 \right]^{-1/4} = \left[1 + \left(\frac{0.6}{0.16386} \right)^2 \right]^{-1/4} = 0.51328$$

1. For the Stolz II equation. The Stolz II equation, for a 7.6215-in pipe, is, from Table 9.55,

$$C = C_x + \frac{b}{R_D^{0.5}} = C_{CT,x} + C_{\text{tap}} + \frac{2.2\beta^{0.75} + 17.6\beta^6}{R_D^{0.5}}$$

where the corner tap discharge coefficient $C_{CT,\infty}$ at infinite Reynolds number is defined by

$$C_{CT,\infty} = 0.5949 + 0.033\beta^2 - 0.2233\beta^8$$

and the tap location term C_{tap} is given by

$$C_{\text{tap}} = [0.0377(1 - e^{-0.7L_1}) - 0.0529(e^{-5.2L_1} - e^{-0.7L_1})] \frac{\beta^4}{1 - \beta^4} - [0.0054L_2^{0.35} - 0.0182L_2^{3.8}] \frac{\beta}{1 - \beta}$$

for flange taps $L_1 = L_2 = 1/D_f = 1/ = 0.1312$.

With $\beta_0 = 0.51328$ and a flowing Reynolds number $R_D = 3,361,043$ the iteration is as follows:

n	β_{n-1}	C_n	$Y_{2,n}$
1	0.51328	0.60248	1.000358
2	0.51221	0.60246	1.000358
3	0.51222	0.60246	1.000358

The bore of the orifice measure at 68°F is obtained by combining Eq. 9.54 as

$$d_{\text{meas}} = \frac{\beta D}{F_{ad}} = \frac{(0.51222)(7.6215)}{1.00029} = 3.9027 \text{ in}$$

where F_{ad} is computed from the stainless-steel thermal expansion factor of Table B.4 as

$$\alpha_{PE} = 8.949 \times 10^{-6} + 2.009 \times 10^{-9}T_F - 1.043 \times 10^{-12}T_F^2 + 3.381 \times 10^{-16}T_F^3 = 0.00000914 \text{ in}/(\text{in} \cdot ^\circ\text{F})$$

Then by Eq. 9.51

$$F_{ad} = 1 + \alpha_{PE}(T_F - 68) = 1 + 0.00000914(100 - 68) = 1.00029$$

2. For the NEL/TC 28 equation. The NEL/TC 28 (1995) equation for the discharge coefficient for $D_f > 2.8$ in Table 9.55 is

$$C = 0.5961 + 0.0261\beta^2 - 0.216\beta^8 + 0.000521(\beta\Gamma)^{0.7} + (0.0188 + 0.0063\alpha)\beta^{3.5}\Gamma^{0.3} + (0.043 + 0.080e^{-10L_1} - 0.123e^{-7L_1})(1 - 0.11\alpha)\Phi - 0.031(\lambda - 0.8\lambda^{1.1})\beta^{1.3}$$

for flange taps $L_1 = L_2 = 1/D_f = 0.1312$, and from Table 9.1 (b)

$$\Gamma = \frac{10^6}{R_D} \quad \Phi = \frac{\beta^4}{1 - \beta^4} \quad \alpha = (0.019\beta\Gamma)^{0.8} \quad \lambda = \frac{2L_2}{1 - \beta}$$

The iteration is as follows:

n	β_{n-1}	C_n	$Y_{2,n}$
1	0.51328	0.60276	1.000358
2	0.51210	0.60273	1.000358
3	0.51211	0.60273	1.000358

The orifice bore at room or reference temperature of 68°F is then, by Eq. 9.54,

$$d_{\text{meas}} = \frac{\beta D}{F_{ad}} = \frac{(0.51211)(7.6215)}{1.00029} = 3.9022 \text{ in}$$

Example 9.22. For the data of Example 9.3, calculate the flow rate for a measured differential of 10 in iterating for the flow-rate using (1) the Stolz II (1995) equation and (2) the NEL/TC 28 (1995) equation.

Data from Example 9.3 are as follows:

$$(q)_N = 80 \quad (h_w)_N = 64 \text{ in} \quad N_{VG} = 5.6665 \quad D_{\text{meas}} = 1.939 \quad D = 1.9392$$

$$d = 1.4832 \text{ in} \quad d_f = 1.4384 \quad G_F = 0.7255 \quad G_b = 0.7359 \quad F_p = 1.0088$$

$$F_{ad} = 1.0012$$

$$F_{aD} = 1.00008 \quad T_F = 80.5^\circ\text{F} \quad \mu_{cP} = 0.417 \text{ cP} \quad R_D = 2875.3 q_{\text{gpm}}$$

The flow-rate equation from Table 9.36 (b), Eq. (f), is

$$q_V = N_{VG} \frac{C d^2}{\sqrt{1 - (d/D)^4}} \frac{\sqrt{F_p} G_F}{G_b} \sqrt{h_w}$$

Substituting from Example 9.3 yields

$$\begin{aligned} q_{\text{GPM}} &= (5.6665) \frac{C(1.43837)^2}{\sqrt{1 - (1.43847/1.9392)^4}} \frac{\sqrt{(1.0088)(0.7255)}}{0.7359} \sqrt{h_w} \\ &= 16.321C \sqrt{h_w} \end{aligned}$$

1. The Stolz II equation. For $L_1 = L_2 = 1/1.9392$ and $\beta_f = 1.4384/1.9392 = 0.7418$ from Table 9.55

$$C = C_x + \frac{b}{R_D^{0.5}} = C_{CT,x} + C_{\text{tap}} + \frac{2.2\beta^{0.75} + 17.6\beta^6}{R_D^{0.5}}$$

where the corner tap discharge coefficient $C_{CT,x}$ at infinite Reynolds number is

$$C_{CT,x} = 0.5971 + 0.0262\beta^2 - 0.2172\beta^8 = 0.59161$$

and the tap location term C_{tap} is given by

$$\begin{aligned} C_{\text{tap}} &= [0.0377(1 - e^{-0.7L_1}) - 0.0529(e^{-5.2L_1} - e^{-0.7L_1})] \frac{\beta^4}{1 - \beta^4} \\ &\quad - [0.0054L_2^{0.35} - 0.0182L_2^{3.8}] \frac{\beta}{1 - \beta} = 0.0113 \end{aligned}$$

then

$$C = 0.59161 + 0.0113 + \frac{4.689}{R_{Df}^{0.5}} = 0.60293 + \frac{4.689}{R_{Df}^{0.5}}$$

The iteration is as follows:

n	C_{n-1}	q_{n-1}	$R_{D,n-1}$
1	0.60000	30.967	89039
2	0.61864	31.929	91806
3	0.61841	31.917	91771

2. *Iteration with the NEL/TC28 equation.* The discharge coefficient is calculated by

$$C = C_1 + 0.011(0.75 - \beta)(2.8 - D)$$

where the coefficient C_1 is

$$C_1 = 0.5961 + 0.0261\beta^2 - 0.216\beta^8 + 0.000521(\beta\Gamma)^{0.7} + (0.0188 + 0.0063\alpha)\beta^{3.5}\Gamma^{0.3} + (0.043 + 0.080e^{-10L_1} - 0.123e^{-7L_1})(1 - 0.11\alpha)\Phi - 0.031(\lambda - 0.8\lambda^{1.1})\beta^{1.3}$$

$$\text{with } \Gamma = \frac{10^6}{R_D} \quad \Phi = \frac{\beta^4}{1 - \beta^4} \quad \alpha = (0.019\beta\Gamma)^{0.8} \quad \lambda = \frac{2L_2}{1 - \beta}$$

The iteration is as follows:

n	C_{n-1}	q_{n-1}	$R_{D,n-1}$
1	0.60000	30.967	89,039
2	0.61791	31.891	91,697
3	0.61772	31.882	91,669

Example 9.23. The measured differential is 50 in (12.34 kPa) for the meter sized by the Stolz II discharge coefficient of Example 9.21. Calculate the flow-rate using (1) the Stolz II (1995) equation, (2) the NEL/TC28 (1995), and (3) the bias error between the computations.

Assuming the meter is fabricated and installed to the sizing data, the flowing diameters and beta ratio are

$$D = 7.6215 \text{ in} \quad d = 3.9038 \text{ in} \quad \beta = 0.51222$$

The data from Example 9.21 are:

$$p_{f2} = 2000 \text{ psia} \quad T_{f2} = 559.67 \quad G = 0.8445 \quad Z_{f2} = 0.5688 \quad Z_b = 0.9974$$

$$T_b = 519.67^\circ\text{R} \quad p_b = 14.7 \text{ psia} \quad \mu_{cp} = 0.255 \quad k = 2.29$$

Substitution into the flow-rate equation (Table C.8) gives

$$(q_{\text{SCFH}})_b = 218.4834 \frac{Cd^2}{\sqrt{1 - (d/D)^4}} \frac{Y_2 Z_b T_b \sqrt{p_{f2}}}{p_b \sqrt{G Z_{f2} T_{f1}}} \sqrt{h_w} = 331,854 C Y_2 \sqrt{h_w}$$

The downstream gas expansion factor Y_2 from Table 9.26, Eq. (d), is

$$Y_2 = \sqrt{1 + x_2} - (0.41 + 0.35\beta^4) \frac{x_2}{k \sqrt{1 + x_2}} = 1.00028$$

where

$$x_2 = \frac{h_w}{27.73 p_{f2}} = \frac{h_w}{(27.73)(2000)} = 0.00001803 h_w = 0.0009015$$

1. *Stolz II (1995)*. With $L_1 = L_2 = 1/7.62149$ and $\beta_f = 3.9039/7.6215 = 0.51222$, from Table 9.1(b)

$$C = C_\infty + \frac{b}{R_D^{0.5}} = C_{CT,\infty} + C_{\text{tap}} + \frac{2.2\beta^{0.75} + 17.6\beta^6}{R_D^{0.5}}$$

where the corner tap discharge coefficient $C_{CT,\infty}$ at infinite Reynolds number is

$$C_{CT,\infty} = 0.5949 + 0.033\beta^2 - 0.2233\beta^8 = 0.60250$$

and the tap location term C_{tap} is given by

$$C_{\text{tap}} = [0.0377(1 - e^{-0.7L_1}) - 0.0529(e^{-5.2L_1} - e^{-0.7L_1})] \frac{\beta^4}{1 - \beta^4} \\ - [0.0054L_2^{0.35} - 0.0182L_2^{3.8}] \frac{\beta}{1 - \beta} = -0.00094$$

Then

$$C = 0.60250 - 0.00094 + \frac{4.689}{R_D^{0.5}} = 0.60156 + \frac{1.6496}{R_D^{0.5}}$$

The iteration is as follows:

n	C_{n-1}	q_{n-1}	$R_{D,n-1}$
1	0.600000	1,408,333	2,958,417
2	0.602518	1,414,243	2,970,831
3	0.602516	1,414,238	2,970,821

2. *The NELTC28 (1995) equation*. The discharge coefficient is calculated by

$$C = C_1 + 0.011(0.75 - \beta)2.8 - D)$$

where the coefficient C_1 is

$$C_1 = 0.5961 + 0.0261\beta^2 - 0.216\beta^8 + 0.000521(\beta\Gamma)^{0.7} \\ + (0.0188 + 0.0063\alpha)\beta^{3.5}\Gamma^{0.3} + (0.043 + 0.080e^{-10L_1} \\ - 0.123e^{-7L_1})(1 - 0.11\alpha)\Phi - 0.031(\lambda - 0.8\lambda^{1.1})\beta^{1.3}$$

with

$$\Gamma = \frac{10^6}{R_D} \quad \Phi = \frac{\beta^4}{1 - \beta^4} \quad \alpha = (0.019\beta \Gamma)^{0.8} \quad \lambda = \frac{2L_2}{1 - \beta}$$

The iteration is as follows:

n	C_{n-1}	q_{n-1}	$R_{D,n-1}$
1	0.600000	1,408,333	2,958,417
2	0.602794	1,414,891	2,972,194
3	0.602792	1,414,886	2,972,183

3. *Bias error.* By Equation (4.5)

$$\begin{aligned} \pm B &= \pm \frac{q_{\text{StolzII}} - \bar{q}}{\bar{q}} 100 = \pm \frac{q_{\text{NEL/TC28}} - \bar{q}}{\bar{q}} 100 \\ &= \pm \frac{1,414,238 - 1,414,562}{1,414,562} 100 = \pm 0.02\% \end{aligned}$$

where the true value I , is assumed to be the value calculated by the average value \bar{I} of both equations $\bar{q} = (1,414,886 + 1,414,238)/2 = 1,414,562$.

ACCURACY

In Chap. 4, accuracy and bias-error equations were developed using sensitivity coefficients, and these can be extended to include each variable in the selected flow-rate equation. Since the accuracy that is finally achieved depends on the selection of the variables to be measured, the decision as to the degree of accuracy can be made only by the designer, who knows the process. Equations can only assist the designer in estimating which variables may be considered negligible and which must be measured. It is obvious that the best accuracy can be achieved only if all variables are measured and accounted for, and that the recommendations of Chap. 8 should be followed.

In Table 9.59 are the recommended coefficient accuracy and restrictions on Reynolds number and line size for the discharge-coefficient equations of Table 9.1; in Table 9.60 are accuracy values for the gas expansion factor; and in Table 9.61 are the sensitivity-coefficient equations. The sensitivity coefficients for both bore and pipe diameters are presented in Fig. 9.10.

Example 9.24. Given the accuracy of each variable (as tabulated below), estimate the flow-rate accuracy for the gasoline flow of Example 9.13 if the measured differential pressure is 72 in (17.9 kPa).

From Eq. (4.35), the accuracy is calculated as

$$\begin{aligned} (\text{Acc})_{\text{GPM}} &= \pm \{ [X_{h_w}(\text{Acc})_{h_w}]^2 + [X_D(\text{Acc})_D]^2 + [X_d(\text{Acc})_d]^2 \\ &\quad + [X_{G_f}(\text{Acc})_{G_f}]^2 + [X_{G_b}(\text{Acc})_{G_b}]^2 + [X_C(\text{Acc})_C]^2 \}^{1/2} \end{aligned}$$

The calculation may be tabulated as follows:

Property	Acc, %	Sensitivity coefficient X (Table 9.44)	$[X(\text{Acc})]^2$
Differential pressure h_w			
Transducer, $\pm 0.2\%$ URV	$(\text{Acc})_{h_w} = \pm \frac{100}{72} 0.2 = \pm 0.278$	$X_{h_w} = \frac{1}{2}$	0.0193
Recorder, $\pm 0.5\%$ URV	$(\text{Acc})_{h_w} = \frac{100}{72} 0.5 = \pm 0.694$	$X_{h_w} = \frac{1}{2}$	0.1204
Pipe diameter D			
1.939 ± 0.005 in	$(\text{Acc})_D = \pm \frac{0.005}{1.939} 100 = \pm 0.258$	$X_D = \frac{2\beta^4}{1 - \beta^4} = -0.88$	0.0515
Orifice bore d			
1.441 ± 0.001 in	$(\text{Acc})_d = \pm \frac{0.001}{1.441} 100 = \pm 0.0694$	$X_d = \frac{2}{1 - \beta^4} = 2.88$	0.0399
Flowing specific gravity $G_f = F_p G_F$			
G_F	$(\text{Acc})_{G_f} = \pm 0.1$	$X_{G_f} = \frac{1}{2}$	0.0025
F_p	$(\text{Acc})_{G_f} = \pm 0.2$	$X_{G_f} = \frac{1}{2}$	0.0100
Base specific gravity G_b	$(\text{Acc})_{G_b} = \pm 0.1$	$X_{G_b} = -1$	0.0100
Discharge coefficient C (Table 9.59)	$(\text{Acc})_C = \pm \beta = \pm 0.743$	$X_C = 1$	<u>0.5521</u> 0.8057

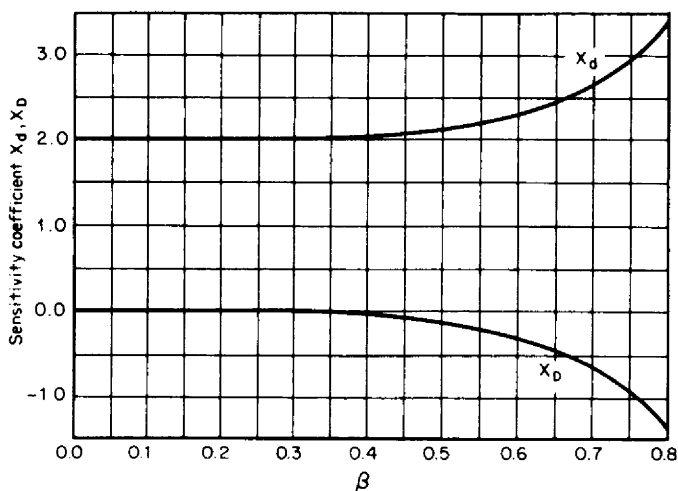


Figure 9.10 Bore and pipe-diameter sensitivity coefficient.

Then

$$(\text{Acc})_{\text{GPM}} = \pm \{\Sigma[X(\text{Acc})]^2\}^{1/2} = \pm (0.8057)^{1/2} = \pm 0.9 \text{ percent}$$

Example 9.25. Estimate the flow-rate accuracy for Example 9.15 if the measured differential pressure is 100 in (24.9 kPa).

By Eq. (4.35), the accuracy equation is written

$$(\text{Acc})_{\text{PPH}} = \pm \{[X_{h_w}(\text{Acc})_{h_w}]^2 + [X_d(\text{Acc})_d]^2 + [X_D(\text{Acc})_D]^2 + [X_C(\text{Acc})_C]^2 + [X_p(\text{Acc})_p]^2 + [X_Y(\text{Acc})_Y]^2\}^{1/2}$$

From Example 9.15, $D = 5.880$ in, $d = 4.289$ in, and $\beta = 0.7294$. Then the calculation is tabulated as follows:

Property	Acc	X (Table 9.56)	$[X(\text{Acc})]^2$
h_w	$\pm 0.5\%$	$\frac{1}{2}$	0.0625
d	± 0.002 in; $\pm 0.047\%$	$\frac{2}{1 - \beta^4} = 2.79$	0.0172
D	± 0.004 in; $\pm 0.068\%$	$-\frac{2\beta^4}{1 - \beta^4} = -0.79$	0.0029
C	$\pm \beta = \pm 0.729\%$ (Table 9.55)	1.0	0.5314
Y	$\pm 0.144 \frac{h_w}{p_f} = \pm 0.071\%$ (Table 9.60)	1.0	0.0050
p_f	$\pm 0.2\%$	$\frac{1}{2}$	0.0100
			0.6290

The flow-rate accuracy is then

$$(\text{Acc})_{\text{PPH}} = \{\Sigma[X(\text{Acc})]^2\}^{1/2} = \pm 0.8 \text{ percent}$$

Wide-Range Metering

The square-root relationship between flow rate and differential pressure limits the practical flow-rate range to 4:1. However, primary elements are capable of operating over wider ranges; they are limited on the high side by permissible pressure loss and structural considerations (plate bending), and on the low side by minimum differential and low-Reynolds-number effects on coefficients. Typically, an orifice which develops 100 in (25 kPa) at 100 percent flow develops only 1 in at 10 percent of the upper-range flow rate. Accurate reading of flow variations at the 10 percent level is impractical on the normal meter scale, which is calibrated uniformly in differential pressure.

The square root of the differential pressure may be taken to obtain a linear response in terms of flow. This increases the readability significantly at flows of less than 50 percent of the upper-range value. Accuracy is, however, not improved, since the same error in differential pressure causes the same error in flow determination.

Several approaches to wide-range flow measurement are available. Where major variations are infrequent and predictable, as with seasonal loads, a simple procedure is to change orifice plates, using a size to match the anticipated upper-range flow rates. Orifice fittings that permit orifice-plate changes are available (Fig. 9.11).

For flows that vary frequently and unpredictably, two or more parallel orifice meter runs are commonly used. Meter runs are sequenced in and out by valves, so that the operating meter or meters are kept in the upper portion of their ranges. A number of versions of this approach are employed, including some that can shift from manual to completely automated operation using computers for sequencing.

An alternative procedure is to connect two differential-pressure transmitters across a single orifice. A typical combination consists of 180- and 20-in (45- and 5-kPa) URV transmitters. For flows about 33 percent of the URV, the measurement is made with the 180-in (45-kPa) transmitter, while the 20-in (5-kPa) transmitter remains inactive. For flows between 10 and 33 percent [differential pressure between 1.8 and 20 in (0.45 and 5 kPa)], the 20-in (5-kPa) transmitter operates. A two-pen recorder can be used to continuously record the output of both transmitters. More complex systems with pneumatic, electronic, and analog computers or with microprocessors are available (see Chap. 11); these have a single output signal for indicating, recording, controlling, and totalizing.

Sensitivity coefficients and Reynolds-number correction factors F_{RD} are used to estimate accuracy over the metering range. Example 9.26 is a sample calculation, with the results shown in Fig. 9.12. In this particular case the low-Reynolds-number

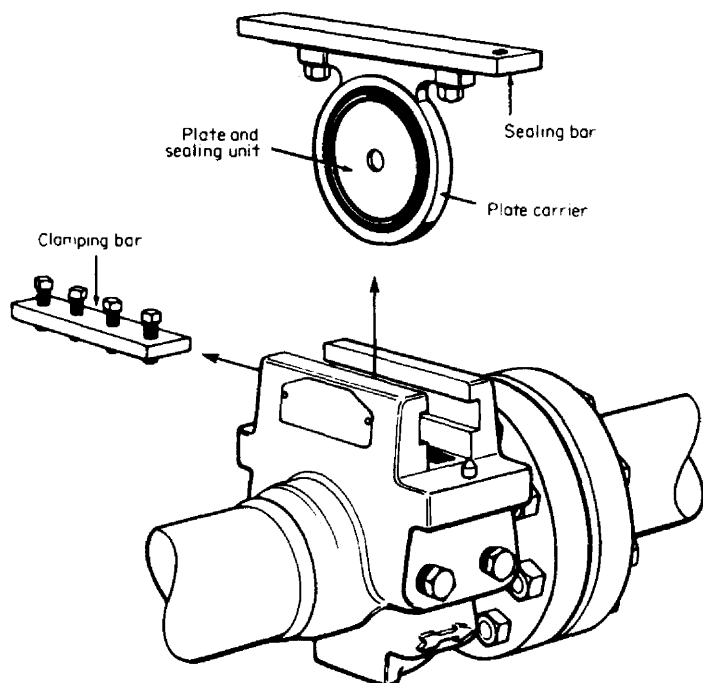


Figure 9.11 Orifice fitting. (Courtesy Daniel Industries, Inc.) To change the orifice plate, only five steps are required.

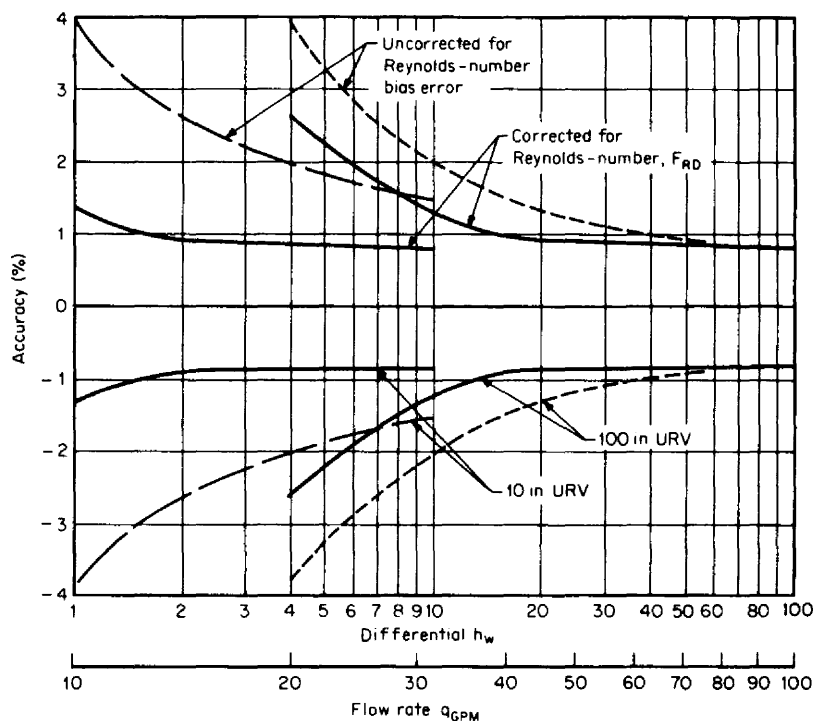


Figure 9.12 Wide-range-metering accuracy envelopes for Example 9.23.

influence on the coefficient can result in significant errors (2.7 percent). An analysis of this type is suggested for all wide metering applications.

Example 9.26. Calculate the accuracy of the natural gas measurement in Example 9.6 if the differential pressure is 3 kPa.

For the flow-rate equation, the accuracy equation is written as

$$(\text{Acc})_{\text{SCMH}} = \pm \{ [X_{\Delta p^*}(\text{Acc})_{\Delta p^*}]^2 + [X_{d^*}(\text{Acc})_{d^*}]^2 + [X_{D^*}(\text{Acc})_{D^*}]^2 + [X_C(\text{Acc})_C]^2 + [X_p(\text{Acc})_p]^2 + [X_T(\text{Acc})_T]^2 + [X_G(\text{Acc})_G]^2 + [X_Z(\text{Acc})_Z]^2 + [X_Y(\text{Acc})_Y]^2 \}^{1/2}$$

In this equation, Z replaces F_{pv} and G replaces F_g of the flow equation.

From Example 9.6, $D^* = 52.50$ mm, $d^* = 29.96$ mm, and $\beta = 0.5707$. The calculation of the accuracy may then be tabulated as:

Property	Acc	X (Table 9.56)	$[X(\text{Acc})]^2$
Δp^*	$\pm 0.6\%$	$+\frac{1}{2}$	0.0900
d^*	± 0.02 mm $\pm 0.067\%$	$+\frac{2}{1 - \beta^4} = 2.24$	0.0225
D^*	± 0.10 mm $\pm 0.191\%$	$-\frac{2\beta^4}{1 - \beta^4} = -0.24$	0.0021

Property	Acc	X (Table 9.56)	$[X(\text{Acc})]^2$
C	$\pm 0.6\%$ (Table 9.54)	1.0	0.3600
p_{f1}^*	$\pm 0.5\%$ (Absolute)	$\frac{1}{2}$	0.0625
T_{K1}	$\pm 0.25\%$ (Absolute)	$-\frac{1}{2}$	0.0156
G	$\pm 0.15\%$	$-\frac{1}{2}$	0.0056
Z_f	$\pm 0.2\%$	$-\frac{1}{2}$	0.0100
Y	$\pm 4 \frac{\Delta p^*}{p_{f1}^*} = 0.065\%$	1.0	<u>0.0042</u>
	Table (9.60)		0.5725

The accuracy is then

$$(\text{Acc})_{\text{SCMH}} = \pm \{\sum [X(\text{Acc})]^2\}^{1/2} = \pm 0.76 \text{ percent}$$

Example 9.27. In Example 9.26, 10-in (2.5-kPa) and 100-in (25-kPa) URV differential-pressure transmitters are to be used to measure over a 10:1 flow-rate range. Assuming the flow-rate calculation is performed with a single iteration, determine the accuracy with (1) no Reynolds-number correction and (2) a Reynolds-number correction. Assume the Reynolds-number bias error can be either positive or negative to obtain a \pm percent accuracy envelope; calculate the accuracy for the low-range transmitter at $h_w = 1, 2.5, 5, 7.5$, and 10 in, and for the high-range transmitter at $h_w = 11, 25, 50, 75$, and 100 in.

If the Reynolds-number bias error is treated as a bias range (\pm), the accuracy equation becomes, from Eq. (4.9),

$$\text{Acc} = \pm B_q \pm (\text{Acc})_q$$

The Reynolds-number bias error can be written as

$$\pm B_q = \pm \frac{C_N}{C} - 1$$

where C_N is the discharge coefficient at the normal operating Reynolds number ($C_N = 0.6097$) and C is calculated by the Example 9.13 equation

$$C = 0.60549 + \frac{43.66}{R_D^{0.75}}$$

The pipe Reynolds number may be determined by the equation developed in part (2) of Example 9.13; and for a single iteration it becomes:

$$R_D = 2875.5 q_{\text{GPM}} = (2875.5)(10 \sqrt{hw}) = 28,755 \sqrt{hw}$$

where the first estimate at the flow rate q_{GPM} is from part 1.

If the discharge coefficient is not corrected for Reynolds number in Example 9.24, the accuracy of the flow-rate determination is

$$(\text{Acc})_{\text{GPM}} = \pm \{ [X_{h_w}(\text{Acc})_{h_w}]^2 + 0.0515 + 0.0399 + 0.0025 + 0.010 + 0.010 + 0.5521 \}^{1/2} = \pm \{ [(X_{h_w})(\text{Acc})_{h_w}]^2 + 0.666 \}^{1/2}$$

with

$$X_{h_w}(\text{Acc})_{h_w} = \frac{1}{2} \frac{(h_w)_{\text{URV}}}{h_w} 0.2 = 0.1 \frac{(h_w)_{\text{URV}}}{h_w}$$

where $(h_w)_{\text{URV}}$ is the upper-range value of the differential-pressure transmitter, and h_w is the measured differential. Then

$$\text{Acc} = \pm (\text{Bq}) 100 \pm \left\{ \left[0.1 \frac{(h_w)_{\text{URV}}}{h_w} \right]^2 + 0.666 \right\}^{1/2}$$

The calculation is tabulated as follows (see Fig. 9.12 for envelopes):

h_w	$\frac{C_N}{C} - 1$	$B_q, \%$	Acc, % (corrected) [†]	Acc, % (uncorrected) [‡]
Low range				
1	1.0249	± 2.43	± 1.3	± 3.7
2.5	1.0158	± 1.56	± 0.9	± 2.4
5	1.0107	± 1.06	± 0.8	± 1.9
7.5	1.0082	± 0.82	± 0.8	± 1.6
10	1.0067	± 0.67	± 0.8	± 1.5
High range				
11	1.0062	± 0.62	± 1.2	± 1.8
25	1.0028	± 0.28	± 0.9	± 1.2
50	1.0006	± 0.06	± 0.8	± 0.9
75	0.9995	± 0.05	± 0.8	± 0.9
100	0.9989	± 0.11	± 0.8	± 0.9

[†]Accuracy corrected for Reynolds number.

[‡]Accuracy uncorrected for Reynolds number.

Example 9.28. For the data given in Example 9.3, use sensitivity coefficients to estimate the bias error and to correct the flow rate for a 10-in (2.5-kPa) differential measurement (1) for Reynolds number and (2) if $G_F = 0.7220$ and $G_b = 0.7300$. (See Example 9.13 for the exact calculation.)

1. Bias error and Reynolds-number correction. The flow rate for a 10-in differential, based on normal conditions, is derived in Example 9.13 as

$$(q_{\text{GPM}})_N = 10.00 \sqrt{h_w} = 10.00 \sqrt{10} = 31.623 \text{ base gal/min}$$

The Reynolds number at flowing conditions is calculated from the equation given in Example 9.2 as

$$R_D = 17,903 \frac{G_b}{\mu_{cp} DN_{VG}} q_{GPM} = 17,903 \left[\frac{0.7300}{(0.417)(1.939)(5.6665)} \right] \quad (31.623)$$

$$= 90,203$$

The coefficient indicating the sensitivity of the discharge coefficient to Reynolds number is given in Table 9.61 as

$$X_{RD} = - \frac{69 \beta^{2.5}}{C R_D^{0.75}} = - \frac{(69)(0.7430)^{2.5}}{(0.6097)(230,040)^{0.75}} = -0.00513$$

where $C = C_N = 0.6097$ from Example 9.13, and $(R_D)_N = 230,040$ and $\beta = 0.7430$ from Example 9.3.

Since the indicated flow rate is based on normal conditions, the bias error in the Reynolds number is, by Eq. (4.5),

$$B_{RD} = \frac{\bar{I} - I_t}{I_t} (100) = \frac{230,040 - 90,203}{90,203} (100) = +155 \text{ percent}$$

where the true value of the Reynolds number I_t is 90,203. The bias error in the flow rate is then estimated with Eq. (4.34) as

$$B_{GPM} = X_{RD} B_{RD} = (-0.00513)(155) = -0.79 \text{ percent}$$

The Reynolds-number correction, from Eq. (4.6), is then

$$F_{B,RD} = \left(1 + \frac{B_{GPM}}{100} \right)^{-1} = \left(1 + \frac{-0.79}{100} \right)^{-1} = 1.008$$

and the corrected flow rate is

$$q_{GPM} = F_{B,RD}(q_{GPM})_N = (1.008)(31.623) = 31.88 \text{ base gal/min}$$

This compares to 31.83 base gal/min as calculated in Example 9.13. The difference is attributable to the nonlinearity of the sensitivity coefficient with Reynolds number and the change in discharge coefficient with Reynolds number.

2. Bias error and correction for base and flowing specific-gravity differences.

The sensitivity coefficient for base specific gravity is, from Table 9.61, $X_{Gb} = -1$; for specific gravity at flowing conditions, it is $X_{Gf} = +\frac{1}{2}$. The bias error for a base specific gravity of 0.7300 is, by Eq. (4.5),

$$B_{Gb} = \frac{\bar{I} - I_t}{I_t} (100) = \frac{0.7359 - 0.7300}{0.7300} (100) = +0.81 \text{ percent}$$

The flow-rate bias error is calculated with Eq. (4.34) as

$$B_{GPM} = X_{Gb} B_{Gb} = (-1)(0.81) = -0.81 \text{ percent}$$

and the correction is, from Eq. (4.6),

$$F_{B,Gb} = \left(1 + \frac{B_{GPM}}{100} \right)^{-1} = \left(1 + \frac{-0.81}{100} \right)^{-1} = 1.008$$

The bias error for a flowing specific gravity of 0.7220 is, by Eq. (4.5),

$$B_{GF} = \frac{\bar{I} - I_t}{I_t} (100) = \frac{0.7255 - 0.7220}{0.7220} (100) = +0.49 \text{ percent}$$

The flow-rate bias error is then, by Eq. (4.26),

$$B_{GPM} = X_{GF} B_{GF} = (+\frac{1}{2})(+0.49) = +0.24 \text{ percent}$$

and, with Eq. (4.6), the correction becomes

$$F_{B,GF} = \left(1 + \frac{B_{GPM}}{100}\right)^{-1} = \left(1 + \frac{+0.24}{100}\right)^{-1} = 0.9976$$

The flow rate, corrected for Reynolds number and for differences in base specific gravity and flowing specific gravity from normal conditions, is then

$$\begin{aligned} q_{GPM} &= F_{B,RD} F_{B,Gb} F_{B,GF} (q_{GPM})_N = (1.008)(1.008)(0.9976)(31.623) \\ &= 32.05 \text{ base gal/min} \end{aligned}$$

TABLE 9.46 Constants, Density Flow-Rate Conversion Equations: U.S. Units

Constants			
Dimensionless conversion constant	$g_c = 32.17405 \text{ lb}_m \cdot \text{ft}/(\text{lb}_f \cdot \text{s}^2)$		
Reference water density, Eq. (2.75)	$(\rho_w)_{68, g_0} = 62.31572 \text{ lb}_m/\text{ft}^3$ $(\rho_w)_{68, g_0} = 62.36630 \text{ lb}_m/\text{ft}^3$		
Universal gas constant	$R_0 = 10.73151 \text{ psia}/(\text{lb}_m \cdot \text{mol} \cdot ^\circ\text{R})$		
Molecular weight of air	$M_{w, \text{air}} = 28.96247 \text{ lb}_m/(\text{lb}_m \cdot \text{mol})$, Table 2.2		
Cubic feet to gallons	1 gal = 0.13368056 ft ³		
Density equations			
	Liquid	Gas (vapor)	
Equation†	$\rho_f = f(p_f, T_f)$ Liquid (specific gravity)	$\rho_g = f(p_g, T_g, M_w)$ Gas ($p_v T$ equation)	
Flowing‡, §	$\rho_f = [(\rho_w)_{60, g_0}] F_p G_F$	$\rho_g = \left(\frac{M_{w, \text{air}}}{R_0} \right) \frac{G p_g}{Z_g T_g}$	
Base‡, §	$\rho_b = [(\rho_w)_{60, g_0}] G_b$ [] = 62.36630 lb _m /ft ³	$\rho_b = \left(\frac{M_{w, \text{air}}}{R_0} \right) \frac{G p_b}{Z_b T_b}$ () = 2.698825 lb _m ·°R/(psia·ft ³)	
Flow-rate conversion equations¶			
Conversion to rate/s	$q_{PPS} = q_{PPH}/3600$	$q_{gps} = q_{gpm}/60$ $q_{acfs} = q_{acfh}/3600$ $q_{lbm/s} = q_{PPS}$	$q_{GPS} = q_{GPM}/60$ $q_{SCFS} = q_{SCFH}/3600$
Mass flow			
Volumetric			
Flowing			
Cubic feet	$q_{lbm/s} = \rho_f (q_{ft^3/s})$		
Gallons	$q_{lbm/s} = \rho_f (q_{ft^3/s}) = \rho_f (0.13368056 q_{gps})$		
Barrels (42 gal/bbl)	$q_{lbm/s} = \rho_f (q_{ft^3/s}) = \rho_f (0.13368056/42 q_{bps})$		
Base/standard			
Cubic feet	$q_{lbm/s} = \rho_b (q_{FT^3/s})$		
Gallons	$q_{lbm/s} = \rho_b (q_{FT^3/s}) = \rho_b (0.13368056 q_{GPS})$		
Barrels (42 gal/bbl)	$q_{lbm/s} = \rho_b (q_{FT^3/s}) = \rho_b (0.13368056/42 q_{BPS})$		

†For downstream pressure measurement, change subscript 1 to 2 as in p_2 , T_2 , Z_2 , etc.‡Pressure p_f and p_b in psia. Normally, liquid specific gravity G_b and G_F are based on 60°F water and the inch of water pressure unit on either 68°F (ASME 3M), or 60°F (ANSI 2530) water density.

¶Capitals on subscripts or in type denote base or standard volumes.

TABLE 9.47 Constants, Density Flow-Rate Conversion Equations: SI Units

Constants			
Dimensionless conversion constant	$g_c = 1 \text{ kg}\cdot\text{m}/(\text{N}\cdot\text{s}^2)$		
Reference water density	$(\rho_w^*)_{20,80} = 998.2019 \text{ kg}/\text{m}^3$ [(Eq. (2.137))] $(\rho_w^*)_{15.6,80} = 999.0121 \text{ kg}/\text{m}^3$		
Universal gas constant	$R_{0E}^* = 8314.41 \text{ J}/(\text{kg}\cdot\text{mol}\cdot\text{K})$		
Molecular weight of air	$M_{w,\text{air}} = 28.96247 \text{ kg}/(\text{kg}\cdot\text{mol})$, Table 2.8		
Density equations			
	Liquid	Gas (vapor)	
Equation†	$\rho_f^* = f(P_f^*, T_K)$ Liquid (specific gravity)	$\rho_f = (P_f^*, T_K, M_w)$ Gas (p_vT equation)	
Flowing‡,§	$\rho_f^* = [(\rho_w^*)_{15.6,80}]F_p G_F$ [] = 999.0121 kg/m³	$\rho_f^* = \left(\frac{M_{w,\text{air}}}{R_{0E}^*}\right) \frac{GP_f^*}{Z_f T_{K1}}$ () = 0.003483407 kg·K/J	
Base‡,§	$\rho_b = [(\rho_w^*)_{15.6,80}]G_b$	$\rho_b^* = \left(\frac{M_{w,\text{air}}}{R_{0E}^*}\right) \frac{GP_b^*}{Z_b T_{Kb}}$	
Flow-rate conversion equations¶			
Conversion to rate/s	$q_{\text{kg}/s} = q_{\text{KPM}}/60$	$q_{\text{m}^3/s} = q_{\text{acmm}}/60$	$q_{\text{M}^3/s} = q_{\text{SCMM}}/60$
		$q_{\text{l}/s} = q_{\text{lpm}}/60$	$q_{\text{L}/s} = q_{\text{LPM}}/60$
	$q_{\text{kg}/s} = q_{\text{KPH}}/3600$	$q_{\text{m}^3/s} = q_{\text{acmh}}/3600$	$q_{\text{M}^3/s} = q_{\text{SCMH}}/3600$
		$q_{\text{l}/s} = q_{\text{lph}}/3600$	$q_{\text{L}/s} = q_{\text{LPH}}/3600$
		$q_{\text{kg}/s} = q_{\text{kg}/s}$	
Mass flow			
Volumetric			
Flowing¶			
Meters	$q_{\text{kg}/s} = \rho_f^*(q_{\text{m}^3/s})$		
Liters	$q_{\text{kg}/s} = \rho_f^*(q_{\text{m}^3/s}) = \rho_f^*(q_{\text{lps}}/1000)$		
Base/standard¶			
Meters	$q_{\text{kg}/s} = \rho_b^*(q_{\text{M}^3/s})$		
Liters	$q_{\text{kg}/s} = \rho_b^*(q_{\text{M}^3/s}) = \rho_b^*(q_{\text{LPS}}/1000)$		

†For downstream pressure measurement change subscript 1 to 2, as in P_2^* , T_{K2} , Z_{f2} , etc.‡Pressures P_f^* and P_b^* are in pascals. Normally, liquid specific gravity G_b and G_F are based on 15.6°C water.

¶Capitals on subscripts and in text denote base or standard volumes.

TABLE 9.48 Generic Flow-Rate Computation: U.S. Units†

Input Table 9.46 constants and equations		
Constants	$(\rho_w)_{68, g_0}, (\rho_w)_{60, g_0}, g_c, R_0, M_{w, air}$	Table 9.46
Equations	Density equations	Table 9.46
Input variables		
Dimensions	Pipe diameter D_{meas} , bore diameter d_{meas}	
Measurements	Pressure P_f , temperature T_f , differential h_w	
Fluid properties		
<i>For measured values or equations, enter or calculate flowing density ρ_f, viscosity μ_{cP}, isentropic exponent (gas/vapor) k, and base density ρ_b</i>		
<i>For liquid specific gravity, enter F_p, G_F, G_b, μ_{cP} and calculate ρ_f, ρ_b</i>		
<i>For gas pVT equation, enter $G, Z_f, p_b, T_b, Z_b, \mu_{cP}, k$ and calculate ρ_f, ρ_b</i>		
Correct dimensions to flowing conditions		
Pipe diameter	$D_f = F_{ad} F_{Dp} D_{meas}$	Eqs. (9.108)–(9.110)
Bore diameter	$d_f = F_{ad} F_{\Delta p} d_{meas}$	Eqs. (9.111)–(9.114)
Beta	$\beta_f = d_f / D_f$	Eq. (9.115)
Iterate for mass flow rate		
a. Calculate gas expansion factor		
	$Y_1 = f(\beta_f, h_w, p_f, k)$	Table 9.26
For liquids $Y_1 = 1.0$		
b. Calculate mass flow rate†,‡: Initially assume $C = 0.6$ for orifice, all others $C = 0.95$		
	$q_{lbm/s} = \frac{\pi}{4} \left[\frac{2g_c(\rho_w)_{T, g_0}}{12^5} \right]^{1/2} \frac{CY_1 d_f^2}{\sqrt{1 - (d_f/D_f)^4}} \sqrt{\rho_f} \sqrt{h_w}$	Eq. (9.107)
{ } = 0.09970190 for inch of water h_w at 68°F: ASME MFC 3M		
{ } = 0.09974236 for inch of water h_w at 60°F: AGA 3, ANSI 2530		
c. Calculate discharge coefficient		
	$R_{Df} = 22737.47 q_{lbm/s} / (\mu_{cP} D_f)$	Eq. (9.120)
	$C = C_x + b / R_{Df}^n$	Eq. (9.49)
	$C_x = f(\beta_f)$ or $f(\beta_f, D_f)$	Table 9.1
	$b = f(\beta_f)$ or $f(\beta_f, D_f)$	Table 9.1
	n	Table 9.1
d. Return to the equation in (b) and repeat until suitable closure, then exit		

TABLE 9.48 Generic Flow-Rate Computation: U.S. Units† (*Continued*)

Volumetric flow rate at flowing conditions

Flowing cubic feet	$q_{ft^3/s} = \frac{q_{lbm/s}}{\rho_f}$
Flowing gallons (liquid)	$q_{gal/s} = \frac{q_{ft^3/s}}{0.13368056}$

Volumetric flow rate at base conditions

Base/standard cubic feet (liquid, gas)	$q_{FT^3/s} = \frac{q_{LBm/s}}{\rho_b}$
Base gallons (liquid)	$q_{GAL/s} = \frac{q_{FT^3/s}}{0.13368056}$

Time conversion

$q_{PPS} = q_{lbm/s}$	$q_{PPM} = 60q_{lbm/s}$	$q_{PPH} = 3600q_{lbm/s}$	$q_{PPD} = 86400q_{lbm/s}$
$q_{acfs} = q_{ft^3/s}$	$q_{acfm} = 60q_{ft^3/s}$	$q_{acfh} = 3600q_{ft^3/s}$	$q_{acfd} = 86400q_{ft^3/s}$
$q_{SCFS} = q_{FT^3/s}$	$q_{SCFM} = 60q_{FT^3/s}$	$q_{SCFH} = 3600q_{FT^3/s}$	$q_{SCFD} = 86400q_{FT^3/s}$
$q_{gps} = q_{gal/s}$	$q_{gpm} = 60q_{gal/s}$	$q_{gph} = 3600q_{gal/s}$	$q_{gpd} = 86400q_{gal/s}$
$q_{GPS} = q_{GAL/s}$	$q_{GPM} = 60q_{GAL/s}$	$q_{GPH} = 3600q_{GAL/s}$	$q_{GPD} = 86400q_{GAL/s}$

†Dimensions: D_f and d_f (inches), pressure p_f (psia), differential h_w (inches of water at reference temperature), temperature T_f (°R), and density ρ_f (lb_m/ft³).

‡For downstream pressure tap change subscript 1 to 2 as in p_{f2} , Z_{f2} , and T_{p2} . h_w is in inches of water at selected water density (ρ_w) _{T, g_0} [60 or 68°F; ASME 3M uses 68°F, and ANSI 2530 (AGA 3) uses 60°F].

¶For drain hole or other corrective factors, add to equation as multiplying terms: $q_{lbm/s} = F_{DH} F_{EL} F_M$

$q_{lbm/s} :$

TABLE 9.49 Generic Flow-Rate Computation: SI Units†

Input Table 9.47 constants and equations		
Constants	$(\rho_w^*)_{20, g_0}$, $(\rho_w^*)_{15.6, g_0}$, R_{OE}^* , $M_{w, air}$	Table 9.47
Equations	Density equations	Table 9.47
Input variables		
Dimensions	Pipe diameter D_M , bore diameter d_M	
Measurements	Differential ΔP^* , pressure P_f^* , temperature T_K	
Fluid properties		
<i>For measured values or equations</i> , enter or calculate flowing density ρ_f^* , viscosity μ_{pas} , isentropic exponent (gas/vapor) k , and base density ρ_b^*		
<i>For liquid specific gravity</i> , enter F_p , G_F , G_b , μ_{pas} and calculate ρ_f^* , ρ_b^*		
<i>For pVT equation</i> , enter G , Z_f , P_b^* , T_{Kb} , μ_{pas} , k and calculate ρ_f , ρ_b		
Correct dimensions to flowing conditions		
Pipe diameter	$D_f^* = F_{ad}^* F_{Dp}^* D_M$	Eqs. (9.122)–(9.124)
Bore diameter	$d_f^* = F_{ad}^* F_{\Delta p}^* d_M$	Eqs. (9.125)–(9.128)
Beta	$\beta_f = d_f^*/D_f^*$	Eq. (9.129)
Iterate for mass flow rate		
a. Calculate gas expansion factor		
	$Y_1 = f(\beta_f, \Delta P^*, P_{f1}^*, k)$	Table 9.26
For liquids $Y_1 = 1.0$		
b. Calculate mass flow rate:†,‡: Initially assume $C = 0.6$ for orifice, all others $C = 0.95$		
	$q_{kg/s} = \left(\frac{\pi}{4} \sqrt{2} \right) \frac{CY_1 d_f^{*2}}{\sqrt{1 - (d_f^*/D_f^*)^4}} \sqrt{\rho_{f1}^*} \sqrt{\Delta P^*}$	Eq. (9.121)
$() = 1.110720735$		
c. Calculate discharge coefficient		
	$R_{Df} = q_{kg/s} / (\pi/4 \mu_{pas} D_f^*)$	Eq. (9.133)
	$C = C_\infty + b/R_{Df}^n$	Eq. (9.49)
	$C_\infty = f(\beta_f)$ or $f(\beta_f, D_f)$	Table 9.1
	$b = f(\beta_f)$ or $f(\beta_f, D_f)$	Table 9.1
	n	Table 9.1
d. Return to the equation in (b) and repeat until suitable closure, then exit		

TABLE 9.49 Generic Flow-Rate Computation: SI Units† (*Continued*)

Volumetric flow rate at flowing conditions				
Flowing cubic meters	$q_{m^3/s} = \frac{q_{kg/s}}{\rho_{fl}^*}$			
Volumetric flow rate at base conditions				
Base/standard cubic meters (liquid, gas)	$q_{M^3/s} = \frac{q_{kg/s}}{\rho_b^*}$			
Time conversion				
$q_{KGS}^* = q_{kg/s}^*$	$q_{KGM}^* = 60q_{kg/s}^*$	$q_{KPH}^* = 3600q_{kg/s}^*$	$q_{KPD}^* = 86,400q_{kg/s}^*$	
$q_{a\ cms}^* = q_{m^3/s}^*$	$q_{a\ cmm}^* = 60q_{m^3/s}^*$	$q_{a\ cmh}^* = 3600q_{m^3/s}^*$	$q_{a\ cmd}^* = 86,400q_{m^3/s}^*$	
$q_{SCMS}^* = q_{M^3/s}^*$	$q_{SCMM}^* = 60q_{M^3/s}^*$	$q_{SCMH}^* = 3600q_{M^3/s}^*$	$q_{SCMD}^* = 86,400q_{M^3/s}^*$	

†Dimensions: D_f^* and d_f^* are in meters; pressure P_f^* and differential ΔP^* are in pascals; temperatures T_K and T_{Kb} are in kelvins; and density ρ_f^* is in kg/m^3 .

‡For downstream pressure tap change subscript 1 to subscript 2.

¶For drain hole or other corrective factors, add to equation as multiplying terms: $q_{kg/s} = F_{DH}^* F_{EL} F_M$ kg/s .

TABLE 9.50 Generic Sizing Computation: U.S. Units

Input Table 9.46 constants and equations		
Constants	$(\rho_w)_{68, g_0}, (\rho_w)_{60, g_0}, g_c, R_0, M_{w, air}$	Table 9.46
Equations	Density equations	Table 9.46
Input design conditions at normal flow rate		
Flow rate	$(q_{PPH})_N, (q_{GPM})_N, (q_{gpm})_N, (q_{SCFH})_N$, etc.	
Dimension†	Pipe diameter D_{meas} (measured at a reference temperature)	
Design conditions†,‡	Differential $(h_w)_N$, pressure p_f , temperature T_f	
Fluid properties‡		
<i>For measured values or equations, enter or calculate flowing density ρ_f, viscosity μ_{cP}, isentropic exponent (gas/vapor) k, and base density ρ_b</i>		
<i>For liquid specific gravity, enter F_p, G_F, G_b, μ_{cP} and calculate ρ_f, ρ_b</i>		
<i>For gas pvT equation, enter $G, Z_f, p_b, T_b, Z_b, \mu_{cP}, k$ and calculate ρ_f, ρ_b</i>		
Correct pipe diameter to flowing conditions		
Pipe diameter	$D_f = F_{aD} F_{Dp} D_{meas}$	Eqs. (9.108)–(9.110)
Convert flow rate to mass flow rate		
First convert flow rate to a per-second basis: $q_{lbm/s} = q_{PPH}/3600, q_{GPM} = q_{GPM}/60, q_{SCFS} = q_{SCFS}/3600$, etc.		Table 9.46
Then calculate mass flow rate $(lb_m/s)_N$		Table 9.46
Calculate sizing factor†,‡,¶		

$$S_M = \frac{(q_{lbm/s})_N}{\left\{ \frac{\pi}{4} \left[\frac{2g_c(\rho_w)_{T, g_0}}{12^5} \right]^{1/2} \right\} D_f^2 \sqrt{\rho_f} \sqrt{(h_w)_N}}$$

{ } = 0.09970190 for inches of water at 68°F; ASME MFC-3M

{ } = 0.09974236 for inches of water at 60°F; AGA 3, ANSI 2530

TABLE 9.50 Generic Sizing Computation: U.S. Units† (*Continued*)

Iterate for flowing beta	
a. Calculate the pipe Reynolds number	
$R_D = 22737.47 (q_{lbm/s})_N / (\mu_{cp} D_f)$	Eq. (9.120)
b. Calculate flowing beta ratio. Initially assume $Y_1 = 1.0$, $C = 0.6$ for orifices; all others $C = 0.95$.	
$\beta_f = \left[1 + \left(\frac{CY_1}{S_M} \right)^2 \right]^{-1/4}$	
c. Calculate discharge coefficient	
$C = C_\infty + b/R_{Df}^n$	Eq. (9.49)
$C_\infty = f(\beta_f)$ or $f(\beta_f, D_f)$	Table 9.1
$b = f(\beta_f)$ or $f(\beta_f, D_f)$	Table 9.1
$n = f(\beta_f)$ or $f(\beta_f, D_f)$	Table 9.1
d. Calculate the gas expansion factor. <i>For liquids</i> , $Y_1 = 1.0$.	
$Y_1 = f[\beta_f, (h_w)_N, p_{f1}, k]$	Table 9.26
e. Return to the equation in (b) and substitute C and Y_1 and calculate the next estimate for β_f . Repeat until suitable closure, then <i>exit</i> .	
Compute measured primary-element bore	
$d_{meas} = \frac{\beta_f D_f}{F_{ad} F_{\Delta p}}$	Eqs. (9.108)–(9.115)
†Dimensions: D , D_f , and d_f (inches), pressure p_f (psia), differential h_w (inches of water at reference temperature), temperature T_f (°R), and density ρ_f (lb _m /ft ³).	
‡For downstream pressure tap change subscript 1 to 2 as in ρ_2 , p_2 , Z_2 , and T_2 . h_w is in inches of water at selected water density (ρ_w) _{T_{s0}} [60 or 68°F; ASME 3M uses 68°F, and ANSI 2530 (AGA 3) uses 60°F].	
¶When applicable, insert β -dependent factor terms in numerator as $\beta_f = [1 + (CF_{DH} Y/S_M)^2]^{-1/4}$.	

TABLE 9.51 Generic Sizing Computation: SI Units

Input Table 9.47 constants and equations		
Constants	$(\rho_w^*)_{20, g_0}, (\rho_w^*)_{15.6, g_0}, R_{0E}^*, M_{w, air}$	Table 9.47
Equations	Density equations	Table 9.47
Input design conditions at normal flow rate		
Flow rate	$(q_{KPH})_N, (q_{LPM})_N, (q_{SCMH})_N$, etc.	
Dimension†	Pipe diameter D_M (measured at a reference temperature)	
Design conditions‡,§	Differential $(\Delta P^*)_N$, pressure P_f , temperature T_K	
Fluid properties†		
<i>For measured values or equations, enter or calculate flowing density ρ_f^*, viscosity $\mu_{Pa\cdot s}$, isentropic exponent (gas/vapor) k, and base density ρ_b^*</i>		
<i>For liquid specific gravity, enter $F_p, G_F, G_b, \mu_{Pa\cdot s}$ and calculate ρ_f^*, ρ_b^*</i>		
<i>For gas pvT equation, enter $G, Z_f, p_b, T_b, Z_b, \mu_{Pa\cdot s}, k$ and calculate ρ_f, ρ_b</i>		
Correct pipe diameter to flowing conditions		
Pipe diameter†	$D_f^* = F_{aD}^* F_{Dp}^* D_M$	Eqs. (9.108)–(9.110) (9.110)
Convert flow rate to mass flow rate		
First convert flow rate to a per second basis: $q_{kg/s} = q_{KPH}/3600, q_{LPS} = q_{LPM}/60, q_{SCMS} = q_{SCMH}/3600$, etc.		Table 9.47
Then calculate mass flow $(q_{kg/s})_N$		Table 9.47
Calculate sizing factor‡,§,¶		

$$S_M = \frac{(q_{kg/s})_N}{\left(\frac{\pi}{4} \sqrt{2}\right) D_f^* \sqrt{\rho_f^*} \sqrt{(\Delta P^*)_N}}$$

$$(\quad) = 1.110720735$$

TABLE 9.51 Generic Sizing Computation: SI Units† (*Continued*)

Iterate for flowing beta	
a. Calculate the pipe Reynolds number $R_D = (q_{kg/s})_N / \left(\frac{\pi}{4} \mu_{Pa's} D_f^* \right)$	Eq. (9.133)
b. Calculate flowing beta ratio. Initially assume $Y_1 = 1$, $C = 0.6$ for orifices and $C = 0.95$ for all others.	
$\beta_f = \left[1 + \left(\frac{CY_1}{S_M} \right)^2 \right]^{-1/4}$	
c. Calculate discharge coefficient	
$C = C_\infty + \frac{b}{R_{Df}^n}$	
$C_\infty = f(\beta_f)$ or $f(\beta_f, D_f^*)$	Table 9.1
$b = f(\beta_f)$ or $f(\beta_f, D_f^*)$	Table 9.1
$n = f(\beta_f)$ or $f(\beta_f, D_f^*)$	Table 9.1
d. Calculate the gas expansion factor. <i>For liquids</i> , $Y_1 = 1.0$.	
$Y_1 = f(\beta_f, (\Delta P^*)_N, P_{f1}^*, k)$	Table 9.26
e. Return to the equation in (b) and substitute C and Y_1 and calculate the next estimate for β_f . Repeat until suitable closure, then <i>exit</i> .	

 Compute measured primary-element bore

$$d_M = \frac{\beta_f D_f^*}{F_{ad}^* F_{\Delta p}^*} \text{ Eqs. (9.126)–(9.130)}$$

†Dimensions D_M , D_f^* , d_M , and d_f^* are in meters, pressure P^* and differential pressure ΔP^* are in pascals (N/m²), temperature T_K is in kelvins, and density ρ_f^* is in kg/m³.

‡For downstream pressure tap, change subscript 1 to 2 as in P_{f2}^* , ρ_{f2}^* , Z_{f2} , and T_{K2} .

¶When applicable, insert β -dependent factor terms in numerator as $\beta_f = [1 + (CF_{DH} Y/S_M)^2]^{-1/4}$.

TABLE 9.52 Generic Differential-Pressure Computation: U.S. Units

Input Table 9.46 constants and equations		
Constants	$(\rho_w)_{68,g_0}, (\rho_w)_{60,g_0}, g_c, R_0, M_{w,air}$	Table 9.46
Equations	Density equations	Table 9.46
Input design conditions at selected flow rate		
Flow rate	$q_{PPH}, q_{GPM}, q_{gpm}, q_{SCFH}, \text{etc.}$	
Dimension†	Pipe diameter D_{meas} , primary-element bore d	
Design conditions‡,§	Pressure p_{f1} , temperature T_{f1}	
Fluid properties†		
<i>For measured values or equations, enter or calculate flowing density ρ_f, viscosity μ_{cP}, isentropic exponent (gas/vapor) k, and base density ρ_b</i>		
<i>For liquid specific gravity, enter F_p, G_F, G_b, μ_{cP} and calculate ρ_f, ρ_b</i>		
<i>For gas pvT equation, enter $G, Z_f, p_b, T_b, Z_b, \mu_{cP}, k$ and calculate ρ_f, ρ_b</i>		
Correct dimensions to flowing conditions		
Pipe diameter	$D_f = F_{ad} F_{Dp} D_{meas}$	Eqs. (9.108)–(9.110)
Bore diameter	$d_f = F_{ad} F_{\Delta P} d_{meas}$	Eqs. (9.111)–(9.114)
Convert flow rate to mass flow rate		
First convert flow rate to a per-second basis: $q_{lb_m/s} = q_{PPH}/3600$ $q_{GPS} = q_{GPM}/60, q_{SCFS} = q_{SCFH}/3600, \text{etc.}$		Table 9.46
Then calculate mass flow rate $(lb_m/s)_N$		Table 9.46

TABLE 9.52 Generic Differential-Pressure Computation: U.S. Units† (*Continued*)

Iterate for the differential†,‡

a. Calculate discharge coefficient

$$C = C_z + \frac{b}{R_{Df}^n} \quad \text{Eq. (9.49)}$$

$$C_z = f(\beta_f) \quad \text{or} \quad f(\beta_f, D_f) \quad \text{Table 9.1}$$

$$b = f(\beta_f) \quad \text{or} \quad f(\beta_f, D_f) \quad \text{Table 9.1}$$

$$n = f(\beta_f) \quad \text{or} \quad f(\beta_f, D_f) \quad \text{Table 9.1}$$

$$R_d = 22737.47 q_{\text{lbm/s}} / (\mu_{\text{cP}} D_f) \quad \text{Eq. (9.120)}$$

Initially assume $Y_1 = 1.0$; for liquids, $Y_1 = Y_2 = 1.0$.

b. Calculate the differential¶

$$h_w = \frac{[1 - (d_f/D_f)^4] q_{\text{lbm/s}}^2}{\left\{ \frac{\pi}{4} \left(\frac{2g_c(\rho_w)_{T_{B0}}}{12^5} \right)^{1/2} \right\}^2 d_f^4 C^2 Y_1^2 \rho_f}$$

{ } = 0.09970190 for h_w at 68°F; ASME MFC 3M{ } = 0.09974236 for h_w at 60°F; AGA 3, ANSI 2530c. Calculate the gas expansion factor. For liquids, $Y_1 = 1.0$.

$$Y_1 = f(\beta_f, h_w, p_f, k) \quad \text{Table 9.26}$$

d. Return to the equation in (b); substitute Y_1 ; and calculate the next estimate for h_w . Repeat until suitable closure, then exit.†Dimensions: D , D_f , d , and d_f (inches), pressure p_f (psia), differential h_w (inches of water at reference temperature), temperature T_f (°R), and density ρ_f (lb_m/ft³).‡For downstream pressure tap change subscript 1 to 2 as in ρ_{f2} , p_{f2} , Z_{f2} , and T_{f2} . h_w is in inches of water at selected water density $(\rho_w)_{T_{B0}}$ [60 or 68°F; ASME 3M uses 68°F, and ANSI 2530 (AGA 3) uses 60°F].¶When applicable, add the square of corrective terms to the denominator of the differential equation. For example, for drain holes (vent or weep holes): $h_w = h_w / F_{DH}^2$.

TABLE 9.53 Generic Differential Pressure Computation: SI Units

Input Table 9.46 constants and equations		
Constants	$(\rho_w^*)_{20,g_0}, (\rho_w^*)_{15.6,g_0}, R_{0E}^*, M_{w,air}$	Table 9.46
Equations	Density equations	Table 9.46
Input design conditions at normal flow rate		
Flow rate	$q_{KPH}, q_{LPM}, q_{gpm}, q_{SCMH}, \text{etc.}$	
Dimension†	Pipe diameter D_M , primary-element bore d_M	
Design conditions‡,§	Pressure P_1^* , temperature T_{K1}	
Fluid properties†		
<i>For measured values or equations, enter or calculate flowing density ρ_f^*, viscosity μ_{pas}, isentropic exponent (gas/vapor) k, and base density ρ_b^*</i>		
<i>For liquid specific gravity, enter F_p, G_F, G_b, μ_{pas} and calculate ρ_f^*, ρ_b^*</i>		
<i>For gas pvT equation, enter $G, Z_f, P_b^*, T_{kb}, \mu_{pas}, k$ and calculate ρ_f^*, ρ_b^*</i>		
Correct dimensions to flowing conditions		
Pipe diameter†	$D_f^* = F_{ad}^* F_{Dp}^* D_M$	Eqs. (9.108)–(9.110)
Bore diameter	$d_f^* = F_{ad}^* F_{\Delta P}^* d_M$	Eqs. (9.125)–(9.130)
Convert flow rate to mass flow rate		
First convert flow rate to a per-second basis: $q_{kg/s} = q_{KPH}/3600$ $q_{LPS} = q_{LPM}/60, q_{SCMS} = q_{SCMH}/3600, \text{etc.}$		Table 9.46
Then calculate mass flow rate $q_{kg/s}$		Table 9.46

TABLE 9.53 Generic Differential Pressure Computation: SI Units† (*Continued*)

Iterate for the differential‡,§	
a. Calculate discharge coefficient	
$C = C_\infty + \frac{b}{R_{df}''}$	Eq. (9.49a)
$C_\infty = f(\beta_f) \quad \text{or} \quad f(\beta_f, D_f^*)$	Table 9.1
$b = f(\beta_f) \quad \text{or} \quad f(\beta_f, D_f^*)$	Table 9.1
$n = f(\beta_f) \quad \text{or} \quad f(\beta_f, D_f^*)$	Eq. (9.133)
$R_D = q_{kg/s} / (\pi/4 \mu_{Pa-s} D_f^*)$	
b. Calculate the differential: Initially assume $Y_1 = 1.0$; for liquids $Y_1 = 1.0$	
$\Delta P^* = \frac{[1 - (d_f^*/D_f^*)^4] q_{kg/s}}{\left(\frac{\pi}{4} \sqrt{2}\right)^2 d_f^{*4} C^2 Y_1^2 \rho_f^*}$	
c. Calculate the gas expansion factor. For liquids, $Y_1 = 1.0$.	
$Y_1 = f(\beta_f, \Delta P^*, P_f, k)$	Table 9.26
d. Return to the equation in (b); substitute Y_1; and calculate the next estimate for ΔP^*. Repeat until suitable closure, then exit.	

†Dimensions: D_M , D_f^* , d_M , and d_f^* in meters; pressure P_f^* and differential pressure ΔP^* , in pascals (N/m²); temperature T_K , in kelvins, and density ρ_f^* , in kg/m³.

‡For downstream pressure tap change subscript 1 to 2 as in ρ_{f2}^* , P_{f2}^* , Z_{f2} , and T_{K2} .

§When applicable, add the square of corrective terms to the denominator of the differential equation. For example, for drain holes (vent or weep holes): $\Delta P^* = \Delta P^* / F_{DH}^{*2}$.

TABLE 9.54 ANSI 2530 Orifice Discharge Coefficient Equation

U.S.	SI			U.S.	SI
d	d^*	Orifice bore diameter at flowing conditions	$d = [1 + \alpha_{PE} T_F - 68] d_{\text{meas}}$	in	mm
D	D^*	Pipe diameter at flowing conditions	$D = [1 + \alpha_P (T_F - 68)] D_{\text{meas}}$	in	mm
R_D		Pipe Reynolds number at flowing conditions			
L_1		Upstream tap term			
L_2		Downstream tap term			
β		Beta ratio at flowing conditions	$\beta = d/D$		
		Corner	Flange	$D \text{ \& } D/2$	
		U.S.	SI	U.S.	SI
L_1		0	0	1.0	1.0
L_2		0	0	0.47	0.47

$$C_1 = 0.5961 + 0.0291\beta^2 - 0.229\beta^8 + 0.000513(\beta\Gamma)^{0.7} + (0.021 + 0.0049\alpha)\beta^4\Gamma^{0.35} \\ + (0.0433 + 0.0712e^{-8.5L_1} - 0.1145e^{-6L_1})(1 - 0.23\alpha)\Phi - 0.0116\beta^{1.1}(1 - 4\alpha)(\lambda - 0.52\lambda^{1.3})$$

$$\Gamma = \frac{10^6}{R_D} \quad \Phi = \frac{\beta^4}{1 - \beta^4} \quad \alpha = (0.019\beta_f\Gamma)^{0.8} \quad \lambda = \frac{2L_2}{1 - \beta}$$

$$D > 2.8 \text{ in (71.12 mm)} \quad C = C_1$$

$$D < 2.8 \text{ in} \quad C = C_1 + 0.003(2.8 - D)(1.0 - \beta)$$

$$D^* < 71.12 \text{ mm} \quad C = C_1 + 0.003 \left(2.8 - \frac{D^*}{25.4} \right) (1.0 - \beta)$$

Note: Constant 0.003 has units of in^{-1} .

Accuracy (uncertainty)

$$\text{For } \beta \leq 0.175 \text{ (Acc)}_c = \left[1 + 0.7895 \left(\frac{4000}{R_D} \right)^{0.8} \right] (0.7 - 1.055\beta)$$

$$\text{For } \beta > 0.175 \text{ (Acc)}_c = \left[1 + 0.7895 \left(\frac{4000}{R_D} \right)^{0.8} \right] (0.56 - 0.255\beta + 1.9316\beta^8)$$

$$\text{For } d < 0.45 \text{ in (11.4 mm) (Acc)}_c = \pm 3\%$$

TABLE 9.55 Proposed NEL/TC 28 and Stolz II Orifice Discharge Equations

U.S.	SI			U.S.	SI	
d	d^*	Orifice bore diameter at flowing conditions,	$D = [1 + \alpha_{PE} T_F - 68] D_{\text{meas}}$	in	mm	
D	D^*	Pipe diameter at flowing conditions,	$D = [1 + \alpha_P^*(T_{\text{c}} - 20)] D_{\text{meas}}^*$	in	mm	
R_D		Pipe Reynolds number at flowing conditions		Dimensionless		
L_1		Upstream tap dimensionless location		Dimensionless		
L_2		Downstream tap dimensionless location		Dimensionless		
β		Beta ratio at flowing conditions,	$\beta = d/D$ or d^*/D^*	Dimensionless		
	Corner		Flange		D D/2	
	U.S.	SI	U.S.	SI	U.S.	SI
L_1	0	0	$1/D$	$25.4/D^*$	1.0	1.0
L_2	0	0	$1/D_f$	$25.4/D^*$	0.47	0.47

$$C_1 = 0.5961 + 0.0261\beta^2 - 0.216\beta^8 + 0.000521(\beta\Gamma)^{0.7} + (0.0188 + 0.0063\alpha)\beta^{3.5}\Gamma^{0.3} \\ + (0.043 + 0.080e^{-10L_1} - 0.123e^{-7L_1})(1 - 0.11\alpha)\Phi - 0.031(\lambda - 0.8\lambda^{1.1})\beta^{1.3}$$

$$\Gamma = \frac{10^6}{R_D} \quad \Phi = \frac{\beta^4}{1 - \beta^4} \quad \alpha = (0.019\beta)^{0.8} \quad \lambda = \frac{2L_2}{1 - \beta}$$

$$D_f \geq 2.8 \text{ in (71.12 mm)} \quad C = C_1$$

$$D_f < 2.8 \text{ in} \quad C = C_1 + 0.011(0.75 - \beta)(2.8 - D)$$

$$D_f^* < 71.12 \text{ mm} \quad C = C_1 + 0.011(0.75 - \beta) \left(2.8 - \frac{D^*}{25.4} \right)$$

Note: Constant 0.011 has units of in^{-1} .

Stolz II

$$C = C_x + \frac{b}{R_D^{0.5}}$$

$$C_x = C_{CT,x} + C_{\text{tap}} \quad b = 2.2\beta^{0.75} + 17.6\beta^6$$

$$D \geq 2.8 \text{ in (71.12 mm)} \quad C_{CT,x} = 0.5949 + 0.033\beta^2 - 0.2233\beta^8$$

$$D < 2.8 \text{ in (71.12 mm)} \quad C_{CT,x} = 0.5971 + 0.0262\beta^2 - 0.2172\beta^8$$

$$C_{\text{tap}} = [0.0377(1 - e^{-0.7L_1}) - 0.0529(e^{-5.2L_1} - e^{-0.7L_1})] \frac{\beta^4}{1 - \beta^4} - [0.0054L_2^{0.35} - 0.0182L_2^{3.8}] \frac{\beta}{1 - \beta}$$

Note: For corner taps, $L_1 = L_2 = 0$; therefore, $C_{\text{tap}} = 0$ and $C_x = C_{CT,x}$ (Stolz II only).

TABLE 9.56 Standard and Proposed Flange Tap Discharge Coefficients

Pipe diameter				Standard		Proposed equations		Pipe diameter				Standard		Proposed equations	
in	mm	Beta	R_D	ISO 5167 ASME 3M	ANSI/API AGA/2530	Stolz II	NEL/TC28	in	mm	Beta	R_D	ISO 5167 ASME 3M	ANSI/API AGA/2530	Stolz II	NEL/TC28
2.00	50.80	0.25	5,000	0.60230	0.60711	0.60899	0.61007	6.00	152.40	0.25	5,000	0.60239	0.60594	0.60718	0.60621
			10,000	0.60035	0.60383	0.60575	0.60672				10,000	0.60043	0.60269	0.60394	0.60286
			100,000	0.59799	0.59958	0.60041	0.60237				100,000	0.59808	0.59849	0.59859	0.59850
			1,000,000	0.59758	0.59869	0.59871	0.60142				1,000,000	0.59766	0.59760	0.59690	0.59755
			10,000,000	0.59750	0.59848	0.59818	0.60119				10,000,000	0.59758	0.59740	0.59637	0.59732
		0.50	5,000	0.63022	0.62677	0.62523	0.62835			0.50	5,000	0.63002	0.62624	0.62374	0.62671
			10,000	0.61916	0.61827	0.61867	0.61956				10,000	0.61897	0.61771	0.61718	0.61782
			100,000	0.60584	0.60697	0.60784	0.60809				100,000	0.60564	0.60638	0.60635	0.60623
			1,000,000	0.60347	0.60399	0.60442	0.60503				1,000,000	0.60327	0.60340	0.60293	0.60315
			10,000,000	0.60304	0.60301	0.60334	0.60394				10,000,000	0.60285	0.60241	0.60185	0.60205
		0.75	5,000	0.68061	0.67065	0.67127	0.67311			0.75	5,000	0.67424	0.67262	0.66531	0.66809
			10,000	0.65015	0.65084	0.65095	0.64819				10,000	0.64378	0.64561	0.64499	0.64217
			100,000	0.61342	0.61790	0.61740	0.61706				100,000	0.60705	0.61063	0.61145	0.60990
			1,000,000	0.60689	0.60786	0.60680	0.60798				1,000,000	0.60052	0.60027	0.60084	0.60064
			10,000,000	0.60573	0.60389	0.60344	0.60420				10,000,000	0.59936	0.59625	0.59748	0.59683

3.00	76.20	0.25	5,000	0.60236	0.60559	0.60705	0.60590	12.00	304.80	0.25	5,000	0.60240	0.60616	0.60734	0.60641
			10,000	0.60040	0.60232	0.60381	0.60255				10,000	0.60045	0.60293	0.60410	0.60306
			100,000	0.59805	0.59809	0.59846	0.59820				100,000	0.59809	0.59874	0.59875	0.59870
			1,000,000	0.59763	0.59720	0.59677	0.59725				1,000,000	0.59767	0.59785	0.59706	0.59775
			10,000,000	0.59755	0.59700	0.59623	0.59702				10,000,000	0.59760	0.59765	0.59652	0.59752
		0.5	5,000	0.63032	0.62589	0.62396	0.62645			0.50	5,000	0.62987	0.62647	0.62359	0.62688
			10,000	0.61927	0.61739	0.61741	0.61764				10,000	0.61882	0.61792	0.61703	0.61794
			100,000	0.60594	0.60610	0.60658	0.60613				100,000	0.60549	0.60657	0.60621	0.60628
			1,000,000	0.60357	0.60312	0.60316	0.60307				1,000,000	0.60312	0.60358	0.60278	0.60320
			10,000,000	0.60315	0.60213	0.60207	0.60197				10,000,000	0.60270	0.60260	0.60170	0.60210
		0.75	5,000	0.67881	0.67426	0.66899	0.67130			0.75	5,000	0.67195	0.67180	0.66191	0.66614
			10,000	0.64835	0.64840	0.64867	0.64609				10,000	0.64149	0.64405	0.64159	0.63968
			100,000	0.61162	0.61472	0.61513	0.61462				100,000	0.60476	0.60822	0.60805	0.60680
			1,000,000	0.60509	0.60457	0.60452	0.60549				1,000,000	0.59823	0.59773	0.59744	0.59744
			10,000,000	0.60393	0.60058	0.60116	0.60170				10,000,000	0.59707	0.59368	0.59409	0.59362

TABLE 9.56 Standard and Proposed Flange Tap Discharge Coefficients (*Continued*)

Pipe diameter				Standard		Proposed equations		Pipe diameter				Standard		Proposed equations	
in	mm	Beta	R_D	ISO 5167 ASME 3M	ANSI/API AGA/2530	Stolz II	NEL/TC28	in	mm	Beta	R_D	ISO 5167 ASME 3M	ANSI/API AGA/2530	Stolz II	NEL/TC28
4.00	101.60	0.25	5,000	0.60237	0.60575	0.60708	0.60604	24.00	609.60	0.25	5,000	0.60241	0.60629	0.60747	0.60655
			10,000	0.60042	0.60250	0.60384	0.60269				10,000	0.60045	0.60307	0.60423	0.60319
			100,000	0.59806	0.59828	0.59850	0.59834				100,000	0.59810	0.59889	0.59888	0.59883
			1,000,000	0.59764	0.59739	0.59681	0.59739				1,000,000	0.59768	0.59800	0.59719	0.59788
			10,000,000	0.59757	0.59719	0.59627	0.59716				10,000,000	0.59760	0.59780	0.59665	0.59765
		0.50	5,000	0.63017	0.62606	0.62384	0.62659			0.5	5,000	0.62980	0.62666	0.62355	0.62709
			10,000	0.61912	0.61755	0.61728	0.61774				10,000	0.61875	0.61810	0.61699	0.61812
			100,000	0.60579	0.60625	0.60646	0.60620				100,000	0.60542	0.60675	0.60617	0.60643
			1,000,000	0.60342	0.60327	0.60303	0.60313				1,000,000	0.60305	0.60376	0.60274	0.60334
			10,000,000	0.60300	0.60228	0.60195	0.60204				10,000,000	0.60262	0.60278	0.60166	0.60224
		0.75	5,000	0.67652	0.67351	0.66747	0.66993			0.75	5,000	0.67081	0.67162	0.65972	0.66560
			10,000	0.64607	0.64714	0.64715	0.64443				10,000	0.64035	0.64353	0.63940	0.63888
			100,000	0.60934	0.61290	0.61361	0.61263				100,000	0.60362	0.60733	0.60586	0.60569
			1,000,000	0.60280	0.60266	0.60300	0.60345				1,000,000	0.59709	0.59678	0.59525	0.59629
			10,000,000	0.60164	0.59866	0.59965	0.59965				10,000,000	0.59593	0.59273	0.59190	0.59246

TABLE 9.57 Standard and Proposed Corner Tap Discharge Coefficients

Pipe diameter		Beta	R_D	Standard†		Proposed equations†	
in	mm			ISO 5167 ASME 3M	ANSI/API AGA/2530	Stolz II	NEL/TC 28
<2.8	<71.12						
2.00	50.80	0.25	5,000	0.60241	0.60826	0.60980	0.61114
2.00	50.80	0.25	10,000	0.60046	0.60504	0.60656	0.60778
2.00	50.80	0.25	100,000	0.59810	0.60087	0.60121	0.60342
2.00	50.80	0.25	1,000,000	0.59769	0.59999	0.59952	0.60247
2.00	50.80	0.25	10,000,000	0.59761	0.59979	0.59898	0.60224
2.00	50.80	0.50	5,000	0.62972	0.62817	0.62519	0.62977
2.00	50.80	0.50	10,000	0.61867	0.61963	0.61863	0.62078
2.00	50.80	0.50	100,000	0.60534	0.60830	0.60781	0.60907
2.00	50.80	0.50	1,000,000	0.60297	0.60531	0.60438	0.60598
2.00	50.80	0.50	10,000,000	0.60255	0.60433	0.60330	0.60488
2.00	50.80	0.75	5,000	0.66966	0.67253	0.65947	0.66628
2.00	50.80	0.75	10,000	0.63921	0.64425	0.63915	0.63937
2.00	50.80	0.75	100,000	0.60248	0.60784	0.60561	0.60596
2.00	50.80	0.75	1,000,000	0.59594	0.59726	0.59500	0.59653
2.00	50.80	0.75	10,000,000	0.59478	0.59320	0.59164	0.59269
>=2.8	>=71.12	0.25	5,000	0.60241	0.60646	0.60802	0.60674
		0.25	10,000	0.60046	0.60324	0.60478	0.60338
		0.25	100,000	0.59810	0.59907	0.59943	0.59902
		0.25	1,000,000	0.59769	0.59819	0.59774	0.59807
		0.25	10,000,000	0.59761	0.59799	0.59721	0.59784
		0.50	5,000	0.62972	0.62697	0.62467	0.62757
		0.50	10,000	0.61867	0.61843	0.61811	0.61858
		0.50	100,000	0.60534	0.60710	0.60728	0.60687
		0.50	1,000,000	0.60297	0.60411	0.60386	0.60378
		0.50	10,000,000	0.60255	0.60313	0.60278	0.60268
		0.75	5,000	0.66966	0.67193	0.66048	0.66628
		0.75	10,000	0.63921	0.64365	0.64016	0.63937
		0.75	100,000	0.60248	0.60724	0.60662	0.60596
		0.75	1,000,000	0.59594	0.59666	0.59601	0.59653
		0.75	10,000,000	0.59478	0.59260	0.59266	0.59269

†The ANSI 2530 and proposed NEL/TC 28 equations are line-size-dependent for $D < 2.8$ in (71.12 mm).

TABLE 9.58 Standard and Proposed D & $D/2$ Tap Discharge Coefficients

Pipe diameter		Beta	R_D	Standard [†]		Proposed equations [†]	
in	mm			ISO 5167 ASME 3M	ANSI/API AGA/2530	Stolz II	NEL/TC 28
<2.8 2.00	<71.12 50.80	0.25	5,000	0.60232	0.60717	0.60893	0.61012
			10,000	0.60037	0.60390	0.60569	0.60677
			100,000	0.59801	0.59965	0.60035	0.60242
			1,000,000	0.59759	0.59876	0.59866	0.60148
			10,000,000	0.59752	0.59856	0.59812	0.60124
		0.50	5,000	0.63034	0.62704	0.62507	0.62861
			10,000	0.61929	0.61860	0.61852	0.61984
			100,000	0.60596	0.60737	0.60769	0.60838
			1,000,000	0.60359	0.60440	0.60427	0.60533
			10,000,000	0.60317	0.60342	0.60319	0.60424
		0.75	5,000	0.68103	0.67699	0.67094	0.67413
			10,000	0.65057	0.65223	0.65062	0.64937
			100,000	0.61384	0.61981	0.61707	0.61840
			1,000,000	0.60731	0.60986	0.60647	0.60935
			10,000,000	0.60615	0.60590	0.60311	0.60558
>=2.8 =>71.12	>=71.12	0.25	5,000	0.60232	0.60537	0.60716	0.60572
			10,000	0.60037	0.60210	0.60392	0.60237
			100,000	0.59801	0.59785	0.59857	0.59802
			1,000,000	0.59759	0.59696	0.59688	0.59708
			10,000,000	0.59752	0.59676	0.59635	0.59684
		0.50	5,000	0.63034	0.62584	0.62455	0.62641
			10,000	0.61929	0.61740	0.61799	0.61764
			100,000	0.60596	0.60617	0.60717	0.60618
			1,000,000	0.60359	0.60320	0.60374	0.60313
			10,000,000	0.60317	0.60222	0.60266	0.60204
		0.75	5,000	0.68103	0.67639	0.67195	0.67413
			10,000	0.65057	0.65163	0.65163	0.64937
			100,000	0.61384	0.61921	0.61809	0.61840
			1,000,000	0.60731	0.60926	0.60748	0.60935
			10,000,000	0.60615	0.60530	0.60413	0.60558

[†]The ANSI 2530 and Proposed NEL/TC 28 equations are line-size-dependent for $D < 2.8$ in (71.12 mm)

TABLE 9.59 Recommended Accuracy and Restrictions for Equations of Table 9.1†

Primary device	Nominal pipe diameter D , in (mm)	Beta ratio β	Pipe Reynolds-number R_D range	Coefficient accuracy, %
Venturi				
Machined inlet	2–10 (50–250)	0.4–0.75	2×10^5 to 10^6	± 1
Rough cast	4–32 (100–800)	0.3–0.75	2×10^5 to 10^6	± 0.7
Rough-welded sheet-iron inlet	8–48 (200–1500)	0.4–0.7	2×10^5 to 10^6	± 1.5
Universal Venturi Tube‡	≥ 3 (≥ 75)	0.2–0.75	$> 7.5 \times 10^4$	± 0.5
Lo-Loss‡	3–120 (75–3000)	0.35–0.85	1.25×10^5 to 3.5×10^6	± 1
Nozzle				
ASME	2–16 (50–400)	0.25–0.75	10^4 to 10^7	± 2.0
ISA	2–20 (50–500)	0.3–0.6	10^5 to 10^6	± 0.8
		0.6–0.75	2×10^5 to 10^7	$2\beta - 0.4$

TABLE 9.59 Recommended Accuracy and Restrictions for Equations of Table 9.1† (*Continued*)

Primary device	Nominal pipe diameter D , in (mm)	Beta ratio β	Pipe Reynolds-number R_D range	Coefficient accuracy, %
Venturi nozzle	3–20 (75–500)	0.3–0.75	2×10^5 to 2×10^6	$\pm 1.2 \pm 1.5 \beta^4$
Orifice				
Corner flange, D and $D/2$	2–36 (50–900)¶	0.2–0.6	10^4 to 10^7	± 0.6
		0.6–0.75	10^4 to 10^7	$\pm \beta$
		0.2–0.75	2×10^3 to 10^4	$\pm 0.6 \pm \beta$
$2\frac{1}{2}D$ and $8D$ (Pipetaps)	2–36 (50–900)	0.2–0.5	10^4 to 10^7	± 0.8 ± 1.6
		0.51–0.7		
Quadrant-edged	1–30 (25–750)	0.24–0.6	$R_{D,\min} < R_d < 10^5 \beta$	± 2
Flanged and corner			$R_{D,\min} = 1000 \beta + 9.4(\beta - 0.24)^8$	
Conical entrance	>1 (25)	0.1–0.316	$250 \beta \leq R_D \leq 5000 \beta$ for $C = 0.730$	± 2
Corner			$5000 \beta \leq R_D \leq 2 \times 10^5 \beta$ for $C = 0.734$	± 2

Honed meter runs	$\frac{1}{2}$ – $1\frac{1}{2}$ (12–40)	0.1–0.8	>1000	± 0.75
Flange, corner				
Integral flow orifice assembly (IFOA) (Foxboro)		Std sizes	$1500/\beta \leq R_D/\beta$	± 0.75
IFOA (Foxboro)				
Eccentric§				
Flange and vena contracta	4(100) 6–14 (150–350)	0.3–0.75 0.3–0.75	10^4 to 10^6 10^4 to 10^6	± 2 ± 1.5
Segmental§				
Flange and vena contracta	4–14 (150–350)	0.35–0.75	10^4 to 10^6	± 2

†ISO 5167 (1991) and ASME *Fluid Meters* (1971) show slightly different values for some devices.

‡The manufacturer should be consulted for recommendations.

¶For $\frac{1}{2} \leq D \leq 1\frac{1}{2}$ in ($12 \leq D^* 40$ mm) use honed-orifice meter run or Foxboro IFOA.

TABLE 9.60 Accuracy of Gas-Expansion-Factor Equations in Table 9.26

Device	Accuracy, %	
	U.S. units	SI units
Contoured		
Venturi, venturi nozzle, Universal Venturi Tube,† Lo-Loss tube†	$\pm (0.144 + 3.61 \beta^8) \frac{h_w}{p_{f1}}$	$\pm (4 + 100 \beta^8) \frac{\Delta p^*}{p_{f1}^*}$
Nozzle (ASME, ISA)	$\pm 0.072 \frac{h_w}{p_{f1}}$	$\pm 2 \frac{\Delta p^*}{p_{f1}^*}$
Orifice		
Corner, flange, D and $D/2$	$\pm 0.144 \frac{h_w}{p_{f1}}$	$\pm 4 \frac{\Delta p^*}{p_{f1}^*}$
$2\frac{1}{2}D$ and $8D$, eccentric, segmental‡	$\pm 0.3 \frac{h_w}{p_{f1}}$	$\pm 8 \frac{\Delta p^*}{p_{f1}^*}$

†Manufacturers should be consulted for recommendations.

‡Gas-expansion-factor curves are given in Chap. 10.

Source: ISO 5167 (1991).

TABLE 9.61 Sensitivity Coefficients

	Coefficient sign					Sensitivity coefficient	Reference
	Symbol		Volume		Mass		
	U.S.	SI	Flowing	Base			
Discharge coefficient†	C	C	+	+	+	$X_C = +1.0$	Tables 9.1, 9.42
Reynolds-number influence						$X_{RD} = 1.0$	
Venturi (all)							
Nozzle							
ASME long radius						$X_{RD} = +\frac{+3.27\beta^{0.5}}{CR_D^{0.5}}$	
ISA						$\frac{(0.002\beta^2 - 0.0038\beta^{4.15})10^{6.9}}{CR_D^{1.15}}$	
Orifice (all taps)						$X_{RD} = -\frac{69\beta^{2.5}}{CR_D^{0.75}}$	
Gas expansion factor‡	Y	Y	+	+	+	$X_Y = 1.0$	Tables 9.26, 9.43
Pipe diameter	D	D^*	−	−	−	$X_D = -\frac{2\beta^4}{1 - \beta^4}$	Fig. 9.10
Bore diameter	d	d^*	+	+	+	$X_d = +\frac{2}{1 - \beta^4}$	Fig. 9.10
Differential pressure	h_w	Δp^*	+	+	+	$X_{h_w} = \frac{1}{2}$	

TABLE 9.61 Sensitivity Coefficients (*Continued*)

	Symbol		Coefficient sign			Sensitivity coefficient	Reference
			Volume		Mass		
	U.S.	SI	Flowing	Base			
Density							
Liquids, gases (vapors)	ρ_f	ρ_f^*	—	+	+	$X_\rho = \frac{1}{2}$	
Liquids	G_f	G_f	—	+	+	$X_{G_f} = \frac{1}{2}$	
	ρ_b	ρ_b^*	NA	—	NA	$X_{\rho_b} = -1$	
	G_b	G_b	NA	—	NA	$X_{G_b} = -1$	
<i>pvT</i> equation							
Pressure							
Gauge	p_G	p_G^*	—	+	+	$X_{pG} = \frac{1}{2} \frac{p_G}{p_G + 14.7}$ for $p_G > 1$ psig (7 kPa)	
Absolute	p_{f1}	p_{f1}^*	—	+	+	$X_p = \frac{1}{2}$	
Temperature							
Fahrenheit (Celsius)	T_F	$T_{\text{°C}}$	+	—	—	$X_{TF} = \frac{1}{2} \frac{ T_F }{460 + T_F}$ for $T_F > 1^{\circ}\text{F}$ and $T_F < -1^{\circ}\text{F}$	
Absolute	T_{f1}	T_{K1}	+	—	—	$X_T = \frac{1}{2}$	
Specific gravity	G	G	—	—	+	$X_G = \frac{1}{2}$	
Compressibility	Z_{f1}	Z_{f1}	+	—	—	$X_Z = \frac{1}{2}$	

†The influence of a change in d , d^* and D , and D^* in the discharge-coefficient equations are considered negligible.

‡The influences of a change in h_w , Δp^* , p_{f1} , p_{f1}^* , k , d , d^* , D , and D^* in the gas-expansion-factor equation are considered negligible.

REFERENCES

- ANSI/2530 (AGA3) *Chap. 14, Sec. 3, Part 1—General Equations and Uncertainty Guideline*, ANSI, New York, 1991.
- ASME MFC-14M, *Measurement of Fluid Flow Using Small Bore Precision Orifice Meters*, ASME, New York, 1995.
- ASME 3M: *Differential Producers Used for the Measurement of Fluid Flow in Pipes (Orifice, Nozzle, Nozzle Venturi, Venturi)*, ASME, New York, 1995.
- ASME: *Fluid Meters*, 6th ed., ASME, New York, 1971.
- Buckingham, E.: "Notes on the Orifice Meter; the Expansion Factor for Gases," *J. Res. Nat. Bur. Stand.*, vol. 9, p. 61, 1932.
- Cunningham, R. G.: "Orifice Meters with Supercritical Flow," *Trans. ASME*, vol. 73, pp. 625–630, 1951.
- Freeman, M.: *Segmental, Eccentric, and Quadrant Edge Coefficients and Gas Expansion Factors*, private communication, 1988.
- ISO/TC 30/SC2, *Interim Report on the Conversion of the Universal Equation to the Upstream Edge Reference*, ISO/TC30/SC2(France 25)103E, October 1978.
- ISO Report, *Report from the Joint ISO-TC30/SC2, ISO-TC-28/SC5 Working Group for a New Discharge Coefficient for Orifice Plates*, (rev. 1 of 7), July 1994.
- ISO Standard 5024, *Petroleum Liquids and Gases—Measurement—Standard Reference Conditions*, ISO 5024-1976(E), Geneva, 1976.
- ISO Standard 5167, *Measurement of Fluid Flow by Means of Orifice Plates, Nozzles, and Venturi Tubes in Circular Cross-Section Conduits Running Full*, ISO 5167-1991(E) 1991.
- James, R.: "Metering of Steam/Water Two-Phase Flow by Sharp Edged Orifices," *Proc. Inst. Mech. Eng.*, vol. 180, pt. 1, no. 23, pp. 549–572, 1965–1966.
- Kinghorn, F. C.: "The Expansibility Correction for Orifice Plates: EEC Data," *Int. Conf. Flow Meas. in Mid-80's*, paper 5.2, East Kilbride, Scotland, pub. NEL, 1986.
- Marxman, R. A., and H. Burlage: "Expansion Coefficients for Orifice Meters in Pipes Less Than One Inch in Diameter," *J. Basic Eng.*, pp. 289–298, June 1961.
- Murdock, J. W.: "Two-Phase Flow Measurement with Orifice," ASME Paper 61-WA-27, 1961.
- Romig, R. P., R. R. Rothfus, and R. I. Kermode: "Partial Vaporization in Orifices and Valves," *I&EC Proc. Design Dev.*, vol. 5, no. 3, July 1966.
- Simpson, R. J.: "Flexible Orifice Plates," *Meas. and Control*, vol. 17, pp. 249–253, July/August 1984.
- Smith, R. V., and J. T. Leang: "Evaluations of Correlations for Two-Phase Flowmeters—Three Current—One New," ASME Paper 74-WA-FM-5, 1974.
- Spink, L. K.: *Principles and Practice of Flowmeter Engineering*, 9th ed., The Foxboro Company, Foxboro, Mass., 1967.
- von Thibessard, G.: "Über die Expansionszahl bei der Durchflugmessung mit Normblenden," *Sonderdruck aus Brennstoff-Wärme-Kraft (BWK) Bd. 12, Nr. 3S97/101*, pp. 97–101, 1960.

DIFFERENTIAL PRODUCERS: DESIGN INFORMATION

Measured differential pressures depend on both fluid characteristics and primary-element geometry. The proper use of differential producers requires adherence to the installation requirements given in Chap. 8 and the details presented in this chapter.

This chapter is concerned with differential producers that are usually sized to produce a selected differential at a design flow rate. In Chap. 11, design information is presented for fixed-geometry devices, for which the differential (or, for a target flowmeter, the force on the target) must be determined for the design flow rate. The graphs presented for discharge coefficients and gas expansion factors were developed from the equations of Chap. 9 when applicable. Others are based on recommendations given in the technical literature.

ORIFICES

Concentric Square-Edged Orifice

Shown in Fig. 10.1 is the pressure profile along a meter run containing a concentric square-edged orifice. The pressure first increases, beginning at approximately $0.5D$ upstream, and then decreases to a minimum at the vena contracta. From this point, the pressure recovers to the initial upstream pressure (less pressure losses due to friction and energy losses). The specific tap location discharge-coefficient equation presented in Table 9.1 and the generalized tap location equation (9.117) were developed by Stolz from empirical discharge-coefficient data and this type of pressure-gradient data.

Pressure-tap spacing requirements for flange, D and $D/2$, and $2\frac{1}{2}D$ and $8D$ taps are given in Fig. 10.2. Individual and annular-slot corner-tap design requirements are presented in Fig. 10.3.

Illustrated in Fig. 10.4a are the two most commonly used orifice plates types. The paddle design is the most common and is easily installed between orifice flanges. The *universal* circular design is for installation in either a single- or dual-chamber orifice fitting or in a plate holder ring-type joint for mounting between grooved flanges (Fig. 10.4b). The outside diameter of the paddle type varies with the pipe schedule size to assure concentricity when installed between the flange bolts.

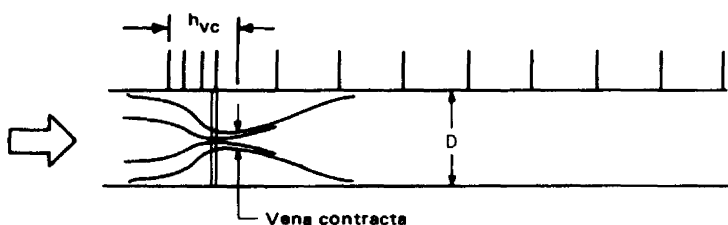
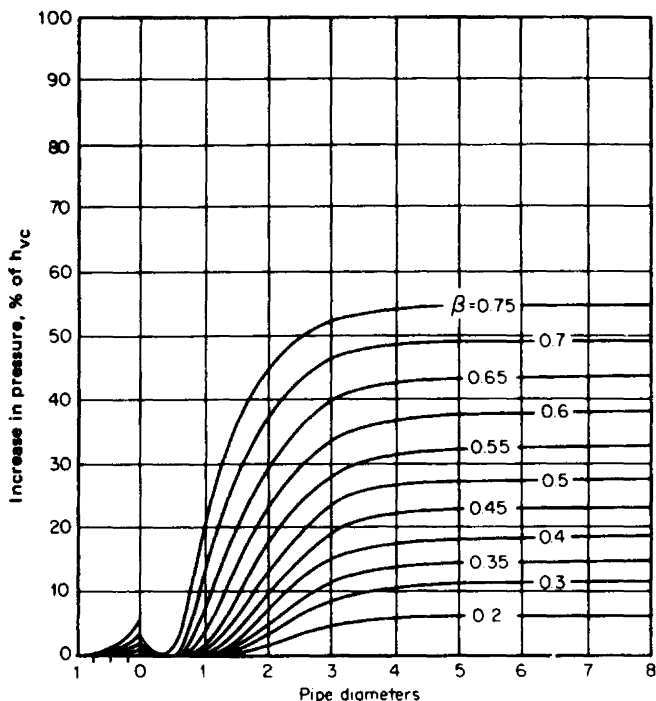


Figure 10.1 Concentric square-edged orifice: pressure profile.

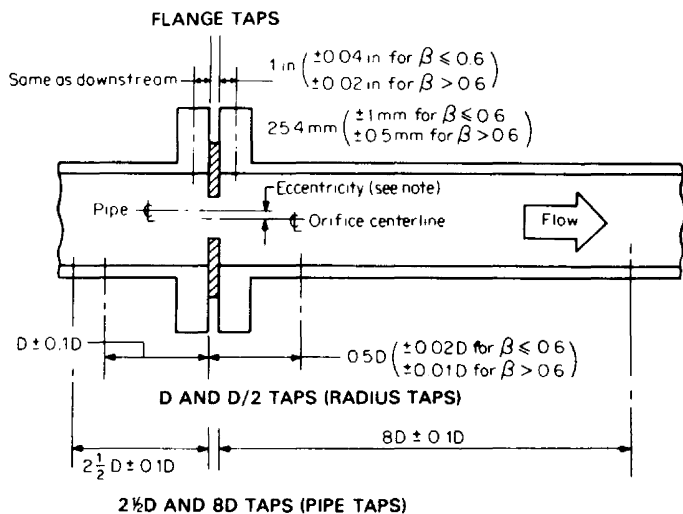
The least expensive and most common installation is to install the plate between gasketed raised-faced flanges. In the flange tap meter the gasket must be compatible with the fluid, must not produce into the pipe, and must not exceed 1/16 in (1.6 mm) in thickness. The orifice flanges have tap holes located 1 in (25.4 mm) from the face of each orifice when a 1/16-in (1.6-mm) gasket is inserted. Flanges are spread apart for inserting the plate by a jackscrew. For high-pressure service, 900-psi (6000-kPa) ANSI or higher service, the ring-type flange seal is commonly used. These flanges have a groove in the face of each flange that the ring fits into and seals (Fig. 10.4b).

Either a least-expensive-type single-chamber or two-chamber orifice fitting is selected when orifice changing is frequently done. The single-chamber design requires depressurization of the flow line prior to removal of the plate from the fitting. The dual-chamber design allows for removal of the plate under pressure after the plate has been pressure-isolated by moving the plate from the first to the second chamber. A pressure seal between chambers then allows for venting the second

TABLE 10.1 Minimum Plate Thickness

Pipe diameter	Minimum plate thickness, in (mm), for differential pressure h_w and Δp^*		
	$h_w = 100$ in $\Delta p^* = 24.9$ kPa	100–200 in 25 to 49.9 kPa	201–1000 in 50.0 to 250 kPa
$D \leq 6$ in ($D^* \leq 150$ mm)			
$0.2 \leq \beta \leq 0.75$	0.125 (3.18)	0.125 (3.18)	0.125 (3.18)
$8 \leq D \leq 10$ in ($200 \leq D^* \leq 250$ mm)			
$0.2 \leq \beta \leq 0.75$	0.125 (3.18)	0.125 (3.18)	0.188 (4.78)
$12 \leq D \leq 20$ in ($300 \leq D^* \leq 500$ mm)			
$\beta \leq 0.5$	0.250 (6.35)	0.250 (6.35)	0.375 (9.53)
$\beta \geq 0.5$	0.188 (4.76)	0.188 (4.76)	0.375 (9.53)
$24 \leq D \leq 36$ in ($600 \leq D^* \leq 900$ mm)			
$\beta \leq 0.5$	0.375 (9.53)	0.375 (9.53)	0.500 (12.7)
$\beta \geq 0.5$	0.250 (6.35)	0.375 (9.53)	0.500 (12.7)

Source: ASME (1971).



Note: Maximum eccentricity is $\pm 0.0025D/(0.1 + 2.3 \beta^4)$

Figure 10.2 Pressure-tap spacing.

chamber before plate removal. Care in selecting the correct material and sealing design is important for high-temperature and high-pressure applications. The stainless or cadmium-plated carbon steel clip ring is usually used for high-pressure applications or for temperatures up to 1200°F (649°C). Cadmium-plated carbon steel units are recommended for service up to 600°F (315°C), and stainless steel unit for temperatures up to 1000°F (520°C) with Inconel being used for higher temperatures.

In the design of the orifice, it is important that the recommendations of Fig. 10.4c and Table 10.1 (for plate thickness) be followed. Edge sharpness, concentricity, plate bending, surface finish, etc., will alter the discharge coefficient and

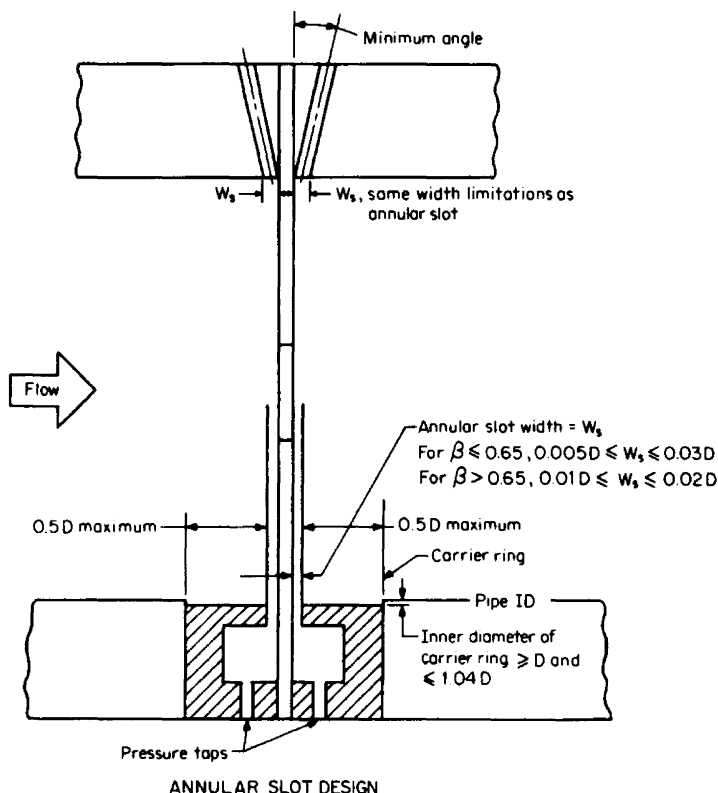


Figure 10.3 Corner taps.

degrade the accuracy of the installation. If the orifice is intended for measuring reverse flows, the plate should not be beveled, and its thickness should be between $0.005D$ and $0.02D$. In these cases, the differential should be as low as practicable consistent with the desired accuracy.

Usually, standard plate sizes are selected from Table 10.1 to minimize bore changes with the impressed differential; refer to Eq. (9.113) or (9.127) for error estimate with differential. However, in some installations high differential may be desired for restricting the flow rate or for other purposes. In these cases the minimum plate thickness may be of more importance than metering accuracy. Assuming support of the plate is at the pipe diameter, the minimum plate thickness to prevent yielding (Simpson, 1984) is

$$t_{\min} \geq \left[\frac{(0.681 - 0.651\beta)h_w}{27.73\sigma_y} \right]^{1/2} D \quad (10.1)$$

where t_{\min} is the minimum plate thickness, in inches, D is the pipe diameter, in inches, h_w is the differential pressure, in inches of water, and σ_y is the yield stress of the plate material, in lb_f/in^2 .

The SI unit equation is

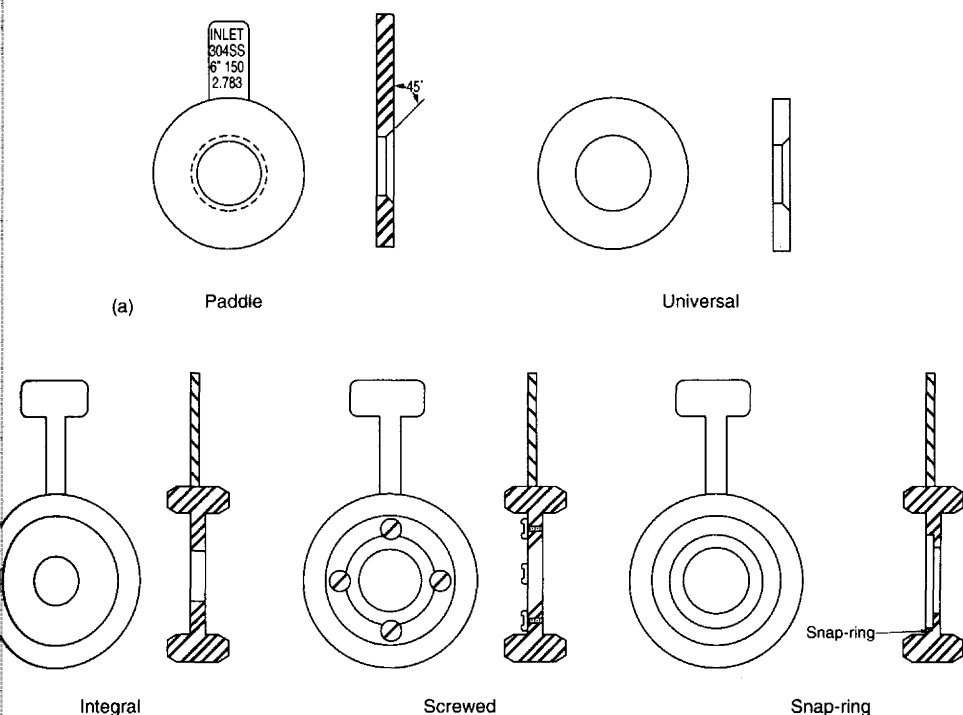


Figure 10.4 Concentric square-edged orifice.

$$t_{\min}^* \geq \left[\frac{(0.681 - 0.651 \beta) \Delta P^*}{\sigma_y^*} \right]^{1/2} D_M \quad (10.2)$$

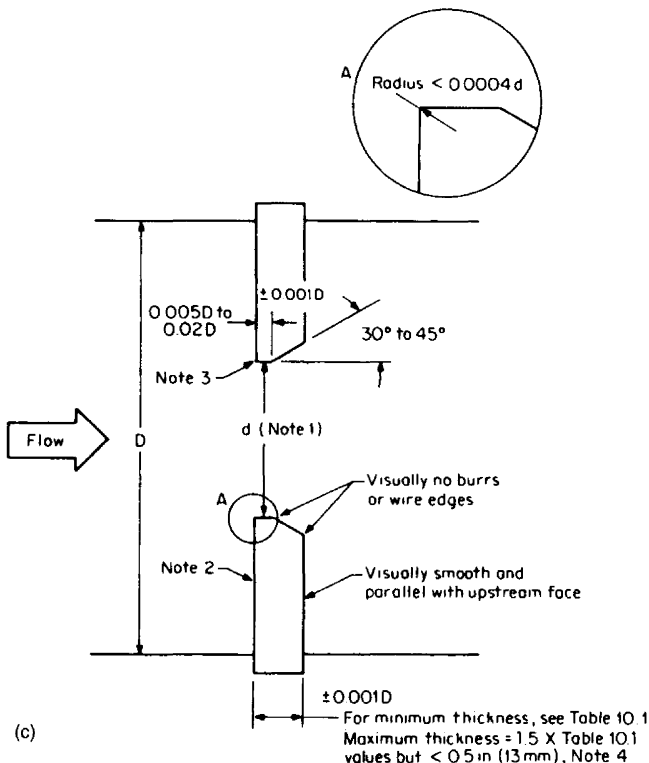
where t_{\min}^* and D_M are in meters and ΔP^* and σ_y^* are in pascals.

In Figs. 10.5 through 10.22 are graphs of the discharge coefficient developed from equations given in Table 9.1. The minimum Reynolds number is limited to 10,000 for 2-in (50-mm) pipe. For lower values, the coefficient curves of Fig. 10.22 should be used. The equations of Table 9.1 will, however, predict coefficients to within $\pm 0.6 \pm \beta$ percent for Reynolds numbers from 2000 to 10,000, which is the estimated accuracy of the data used to develop the curves in Fig. 10.22. It should be noted that the Reynolds-number axis in Fig. 10.22 is scaled for *bore* Reynolds number, or pipe Reynolds number divided by β .

In Figs. 10.23 through 10.34 are the expansion-factor curves for upstream and downstream pressure measurements. These were developed from equations given in Table 9.26, and the accuracies given in Table 9.43 apply.

Small-Bore Meter Runs

The orifice discharge-coefficient prediction equations given in the standards were developed from test data where the smallest pipe diameter was 2.039 in (51.8 mm). These equations are generally acceptable for pipe diameters of 1.8 in (45 mm) and larger. For smaller line sizes, the effects of plate eccentricity, pipe roughness, and



Notes: (1) Mean of four diameters, no diameter $> 0.05\%$ of mean diameter. (2) Maximum slope less than 1% from perpendicular; relative roughness $< 10^{-4}d$ over a circle not less than $1.5d$. (3) Visually does not reflect a beam of light, finish with a fine radial cut from center outward.

(4) ANSI/ASME MFC 3M 1985

Figure 10.4 (Continued)

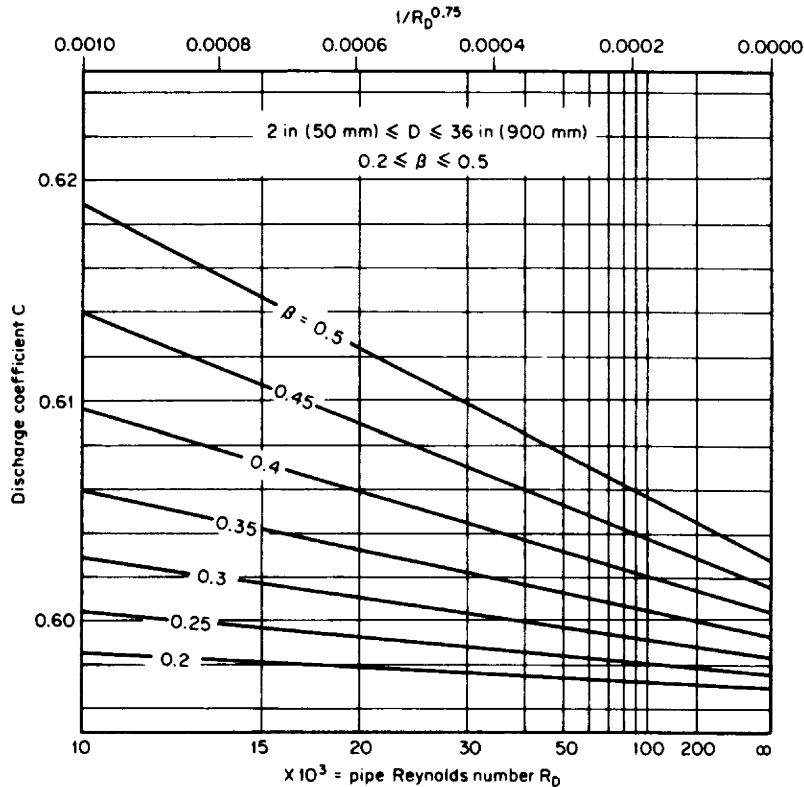


Figure 10.5 C versus R_D for concentric square-edged orifice; corner, flange, D and $D/2$ taps.

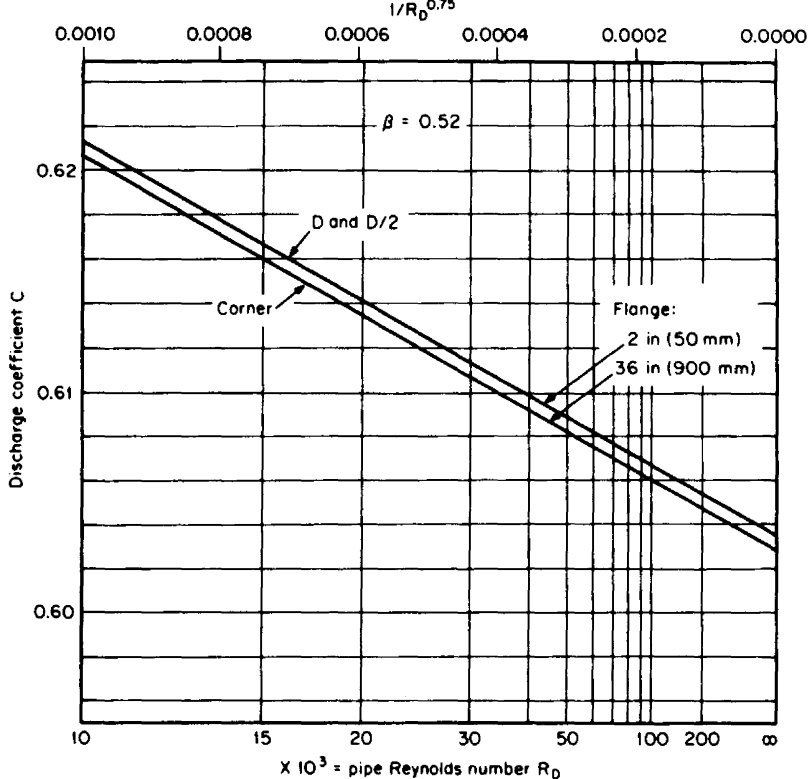


Figure 10.6 C versus R_D for concentric square-edged orifice; corner, flange, D and $D/2$ taps.

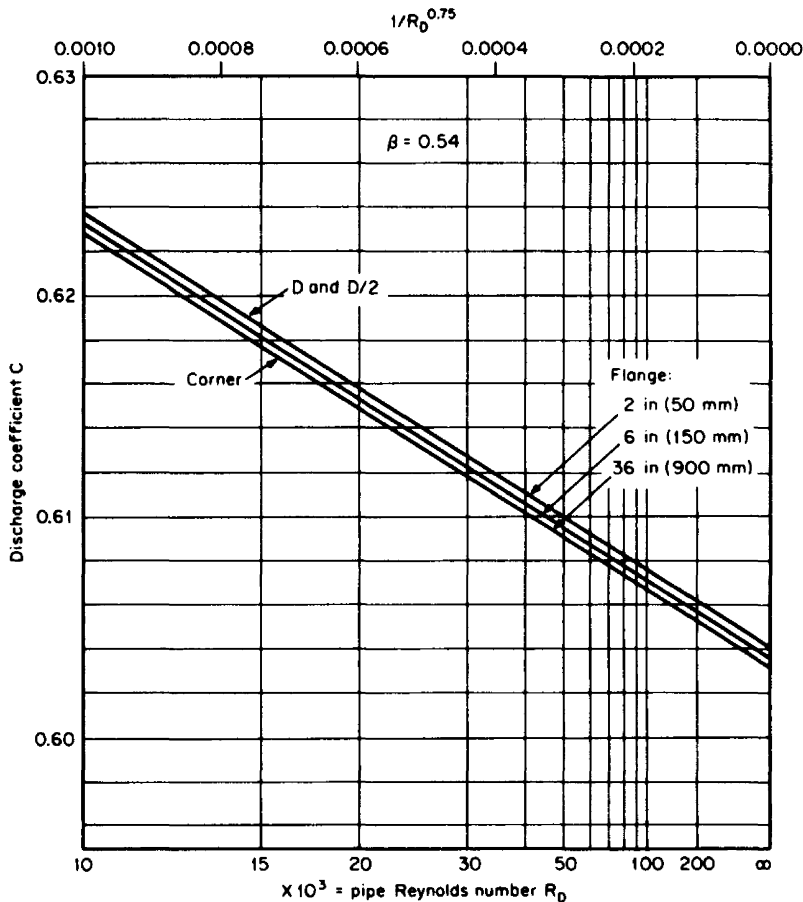


Figure 10.7 C versus R_D for concentric square-edged orifice; corner, flange, D and $D/2$ taps.

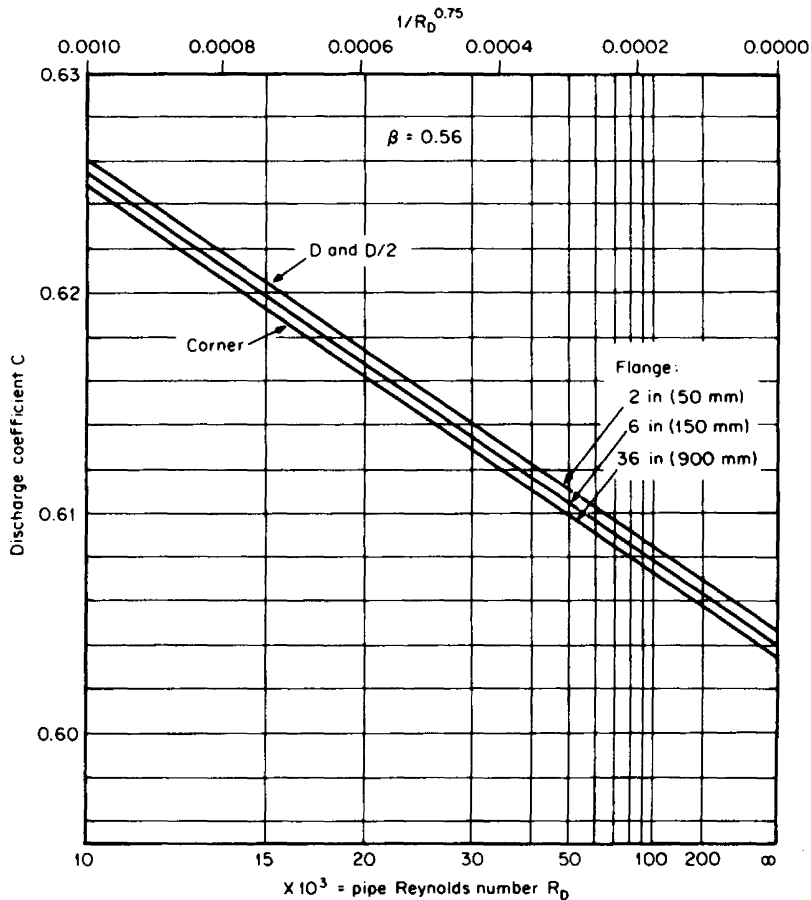


Figure 10.8 C versus R_D for concentric square-edged orifice; corner, flange, D and $D/2$ taps.

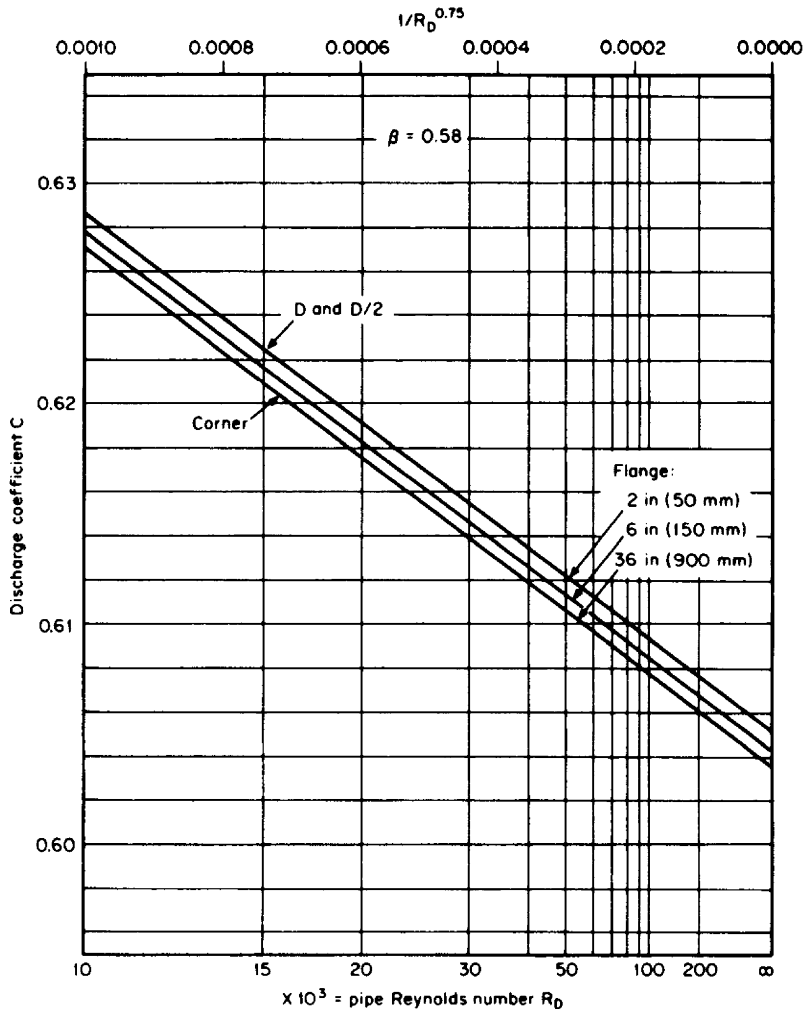


Figure 10.9 C versus R_D for concentric square-edged orifice; corner, flange, D and $D/2$ taps.

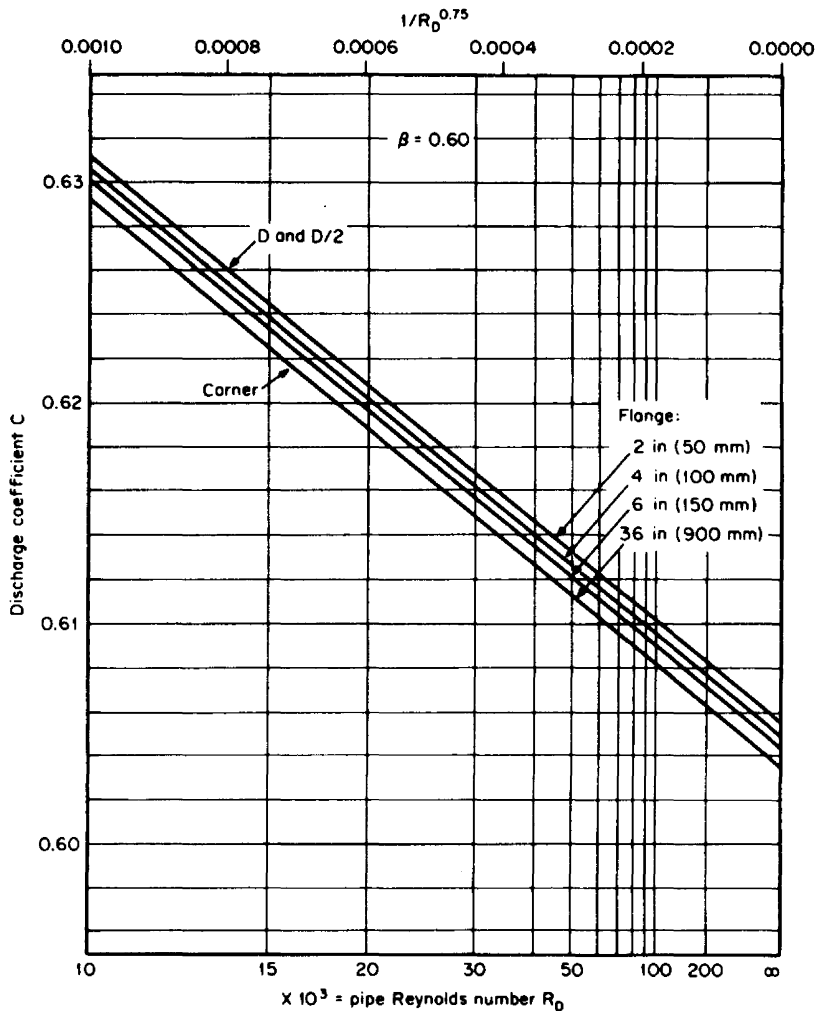


Figure 10.10 C versus R_D for concentric square-edged orifice; corner, flange, D and $D/2$ taps.

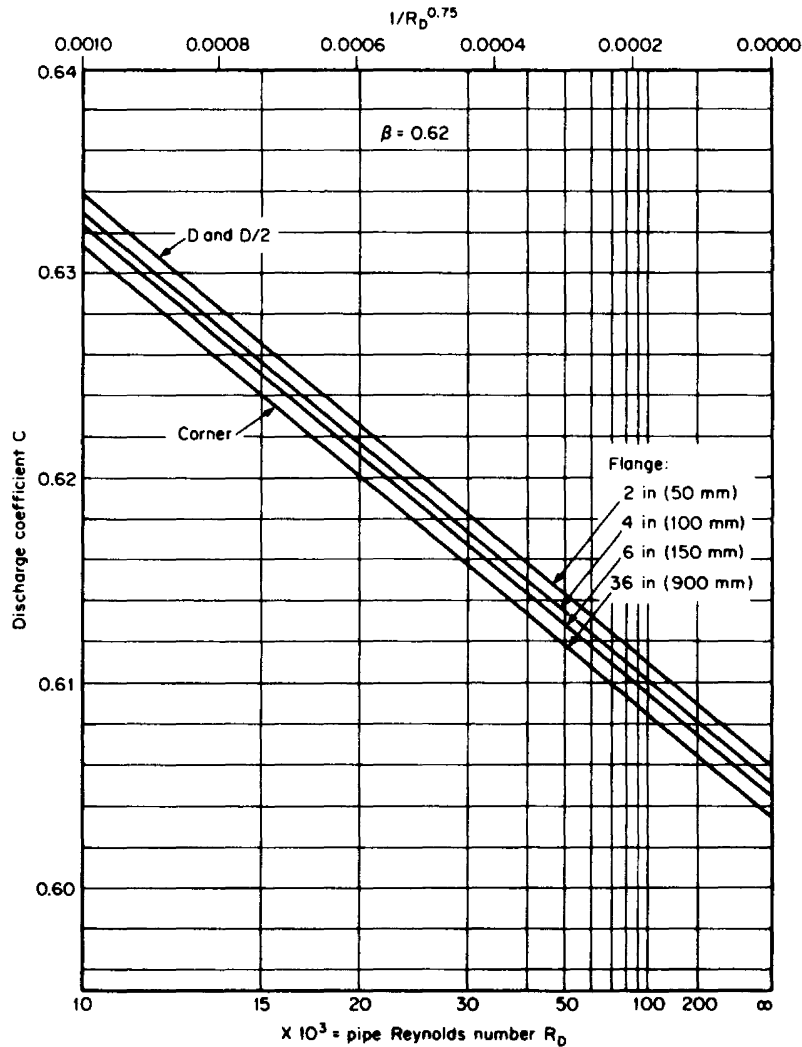


Figure 10.11 C versus R_D for concentric square-edged orifice; corner, flange, D and $D/2$ taps.

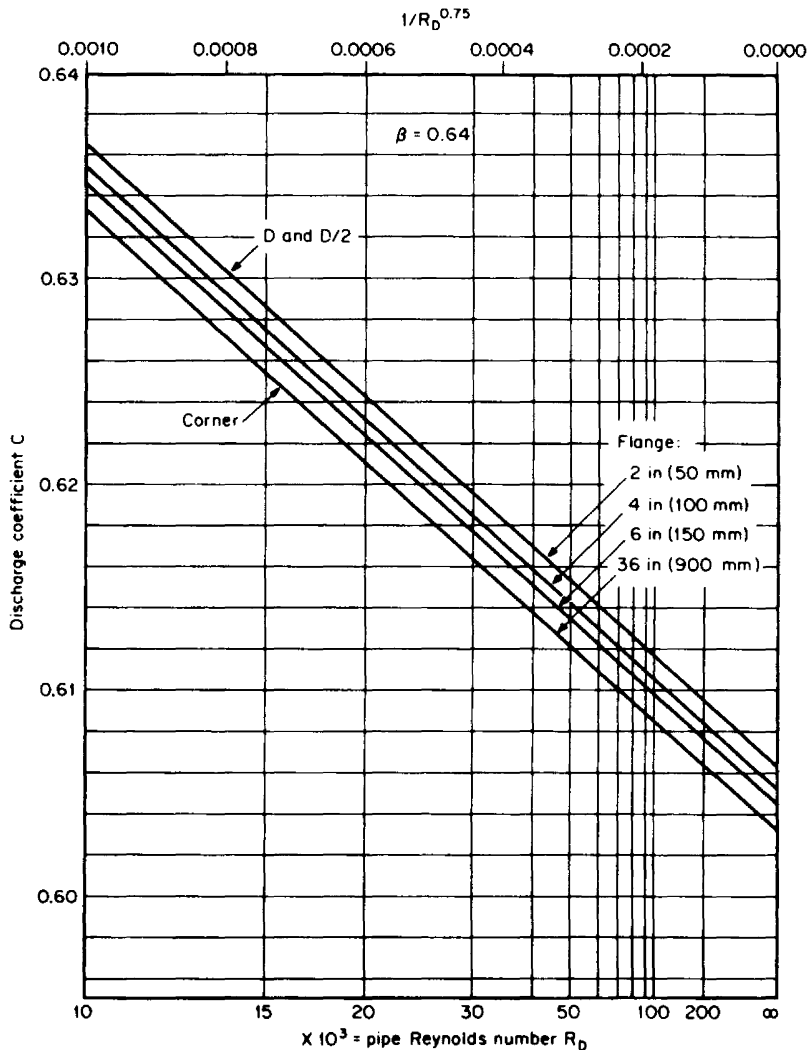


Figure 10.12 C versus R_D for concentric square-edged orifice; corner, flange, D and $D/2$ taps.

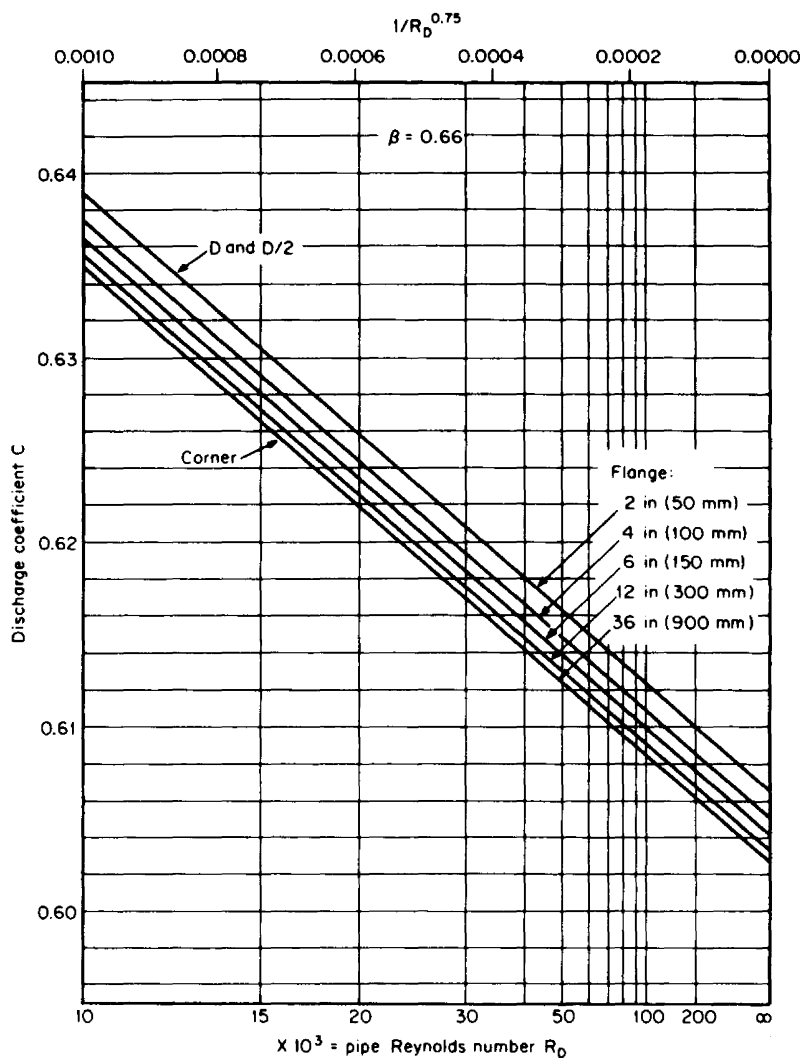


Figure 10.13 C versus R_D for concentric square-edged orifice; corner, flange, D and $D/2$ taps.

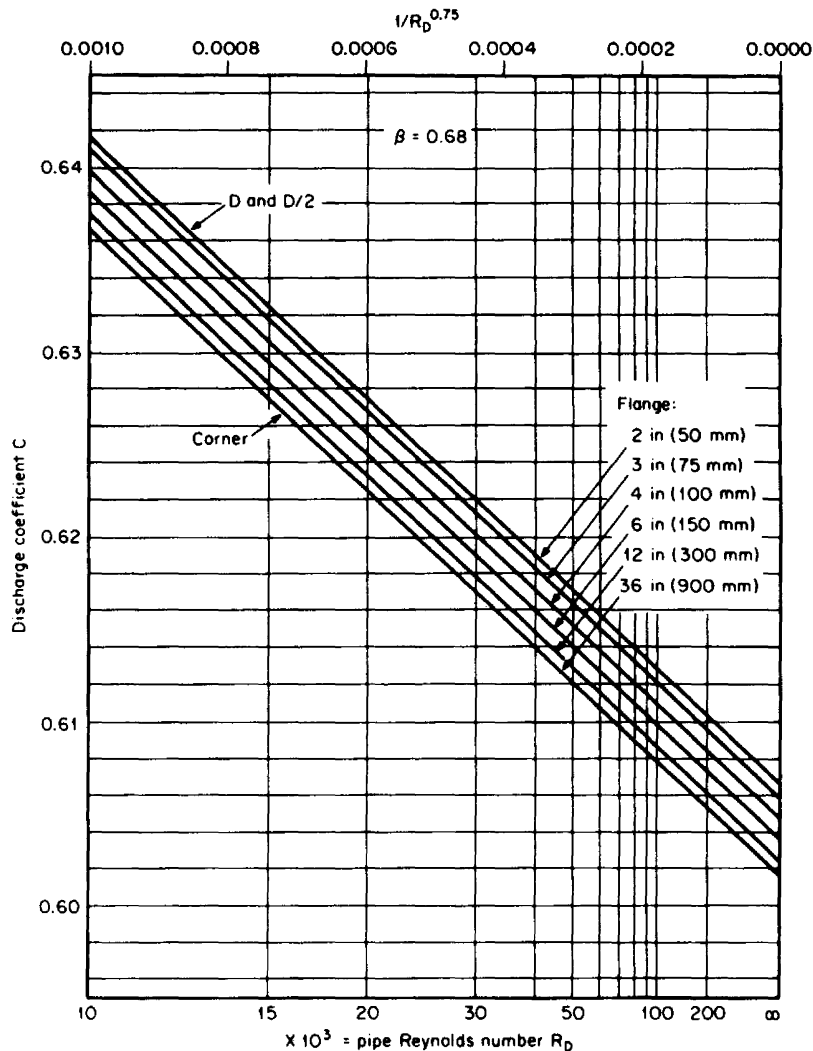


Figure 10.14 C versus R_D for concentric square-edged orifice; corner, flange, D and $D/2$ taps.

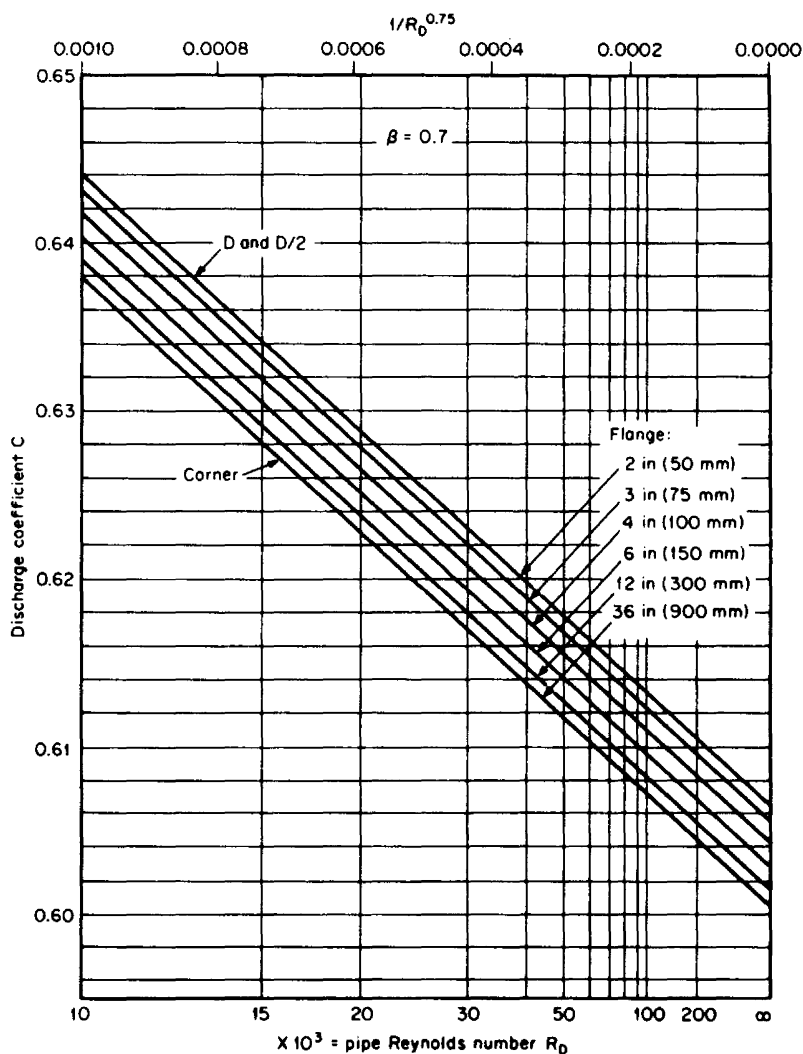


Figure 10.15 C versus R_D for concentric square-edged orifice; corner, flange, D and $D/2$ taps.

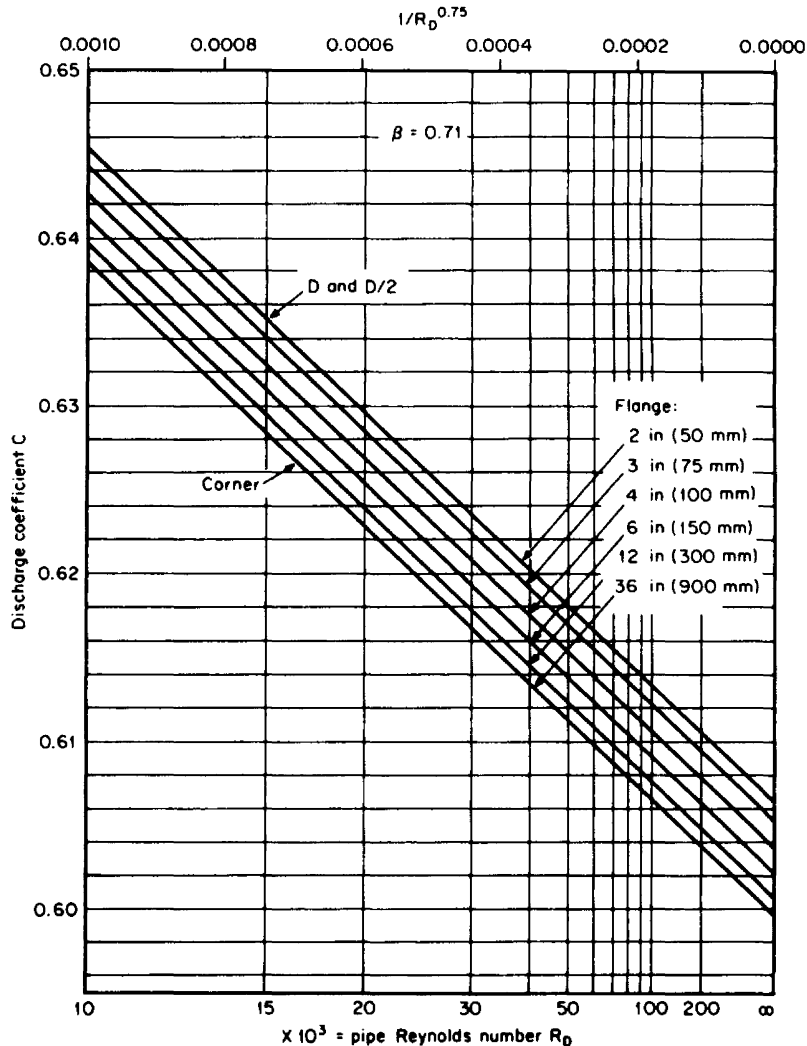


Figure 10.16 C versus R_D for concentric square-edged orifice; corner, flange, D and $D/2$ taps.

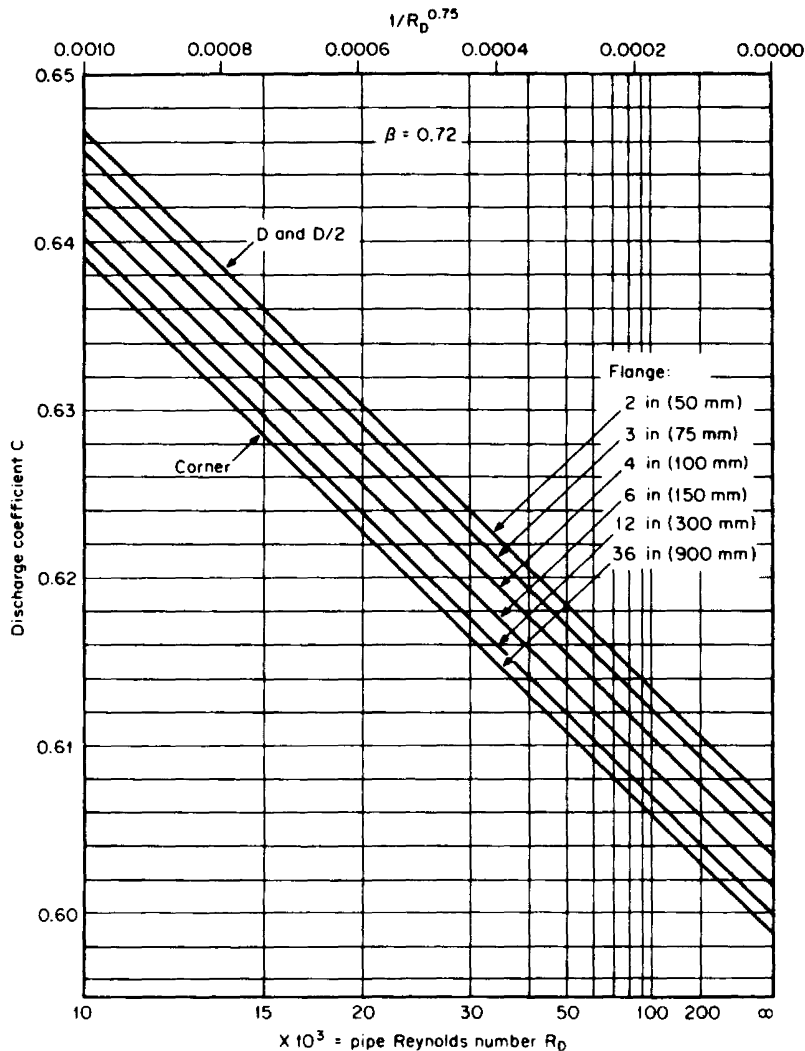


Figure 10.17 C versus R_D for concentric square-edged orifice; corner, flange, D and $D/2$ taps.

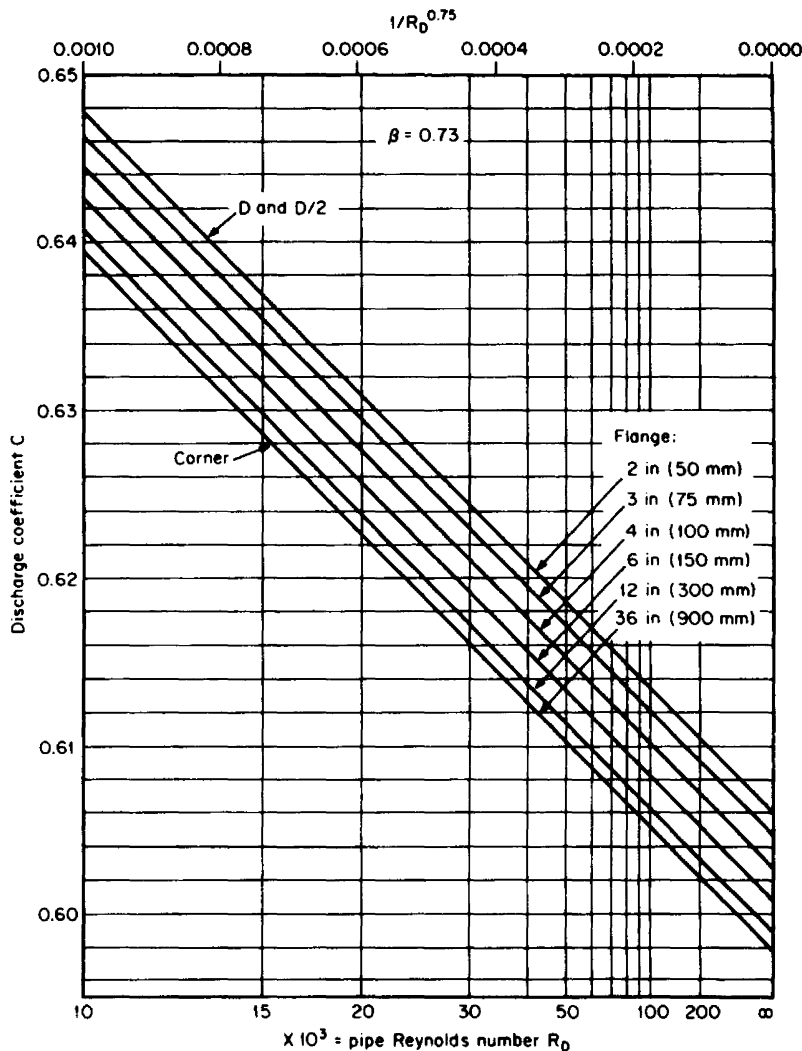


Figure 10.18 C versus R_D for concentric square-edged orifice; corner, flange, D and $D/2$ taps.

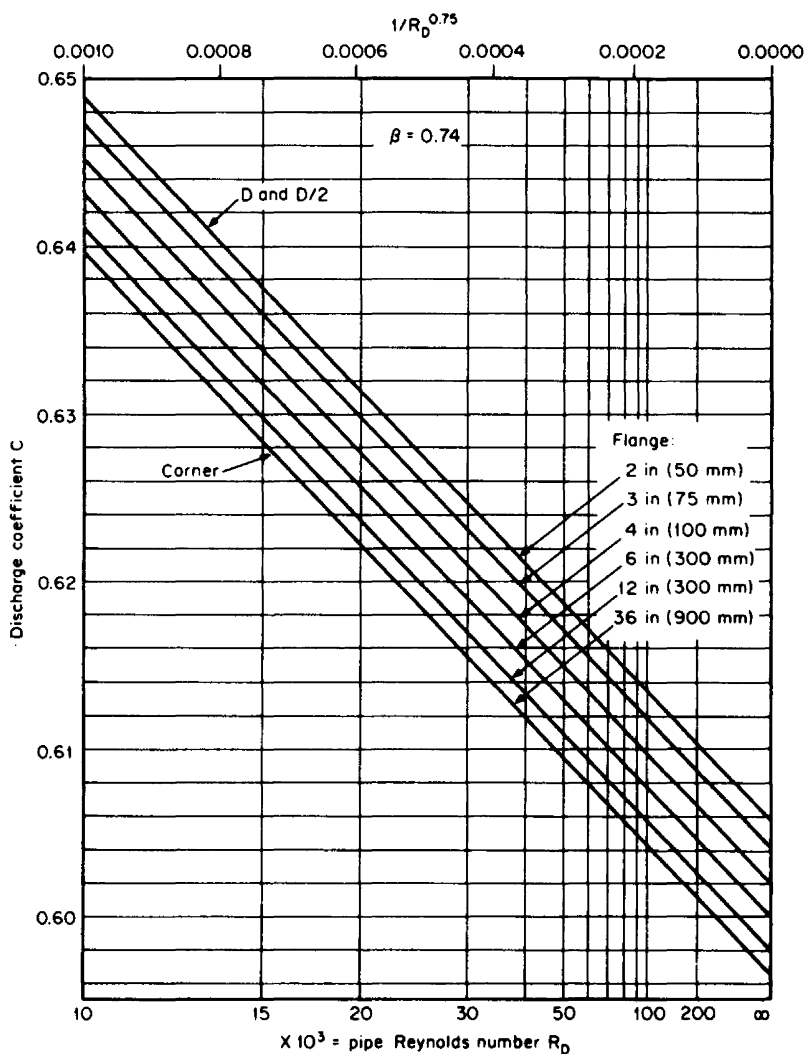


Figure 10.19 C versus R_D for concentric square-edged orifice; corner, flange, D and $D/2$ taps.

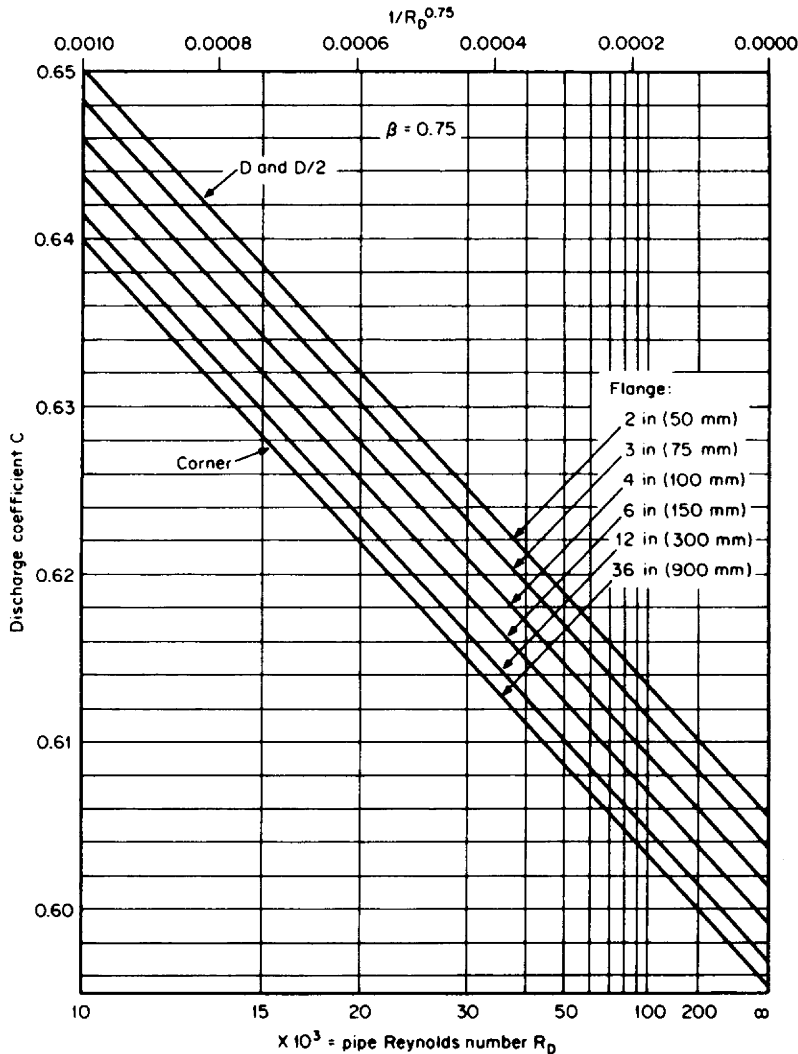


Figure 10.20 C versus R_D for concentric square-edged orifice; corner, flange, D and $D/2$ taps.

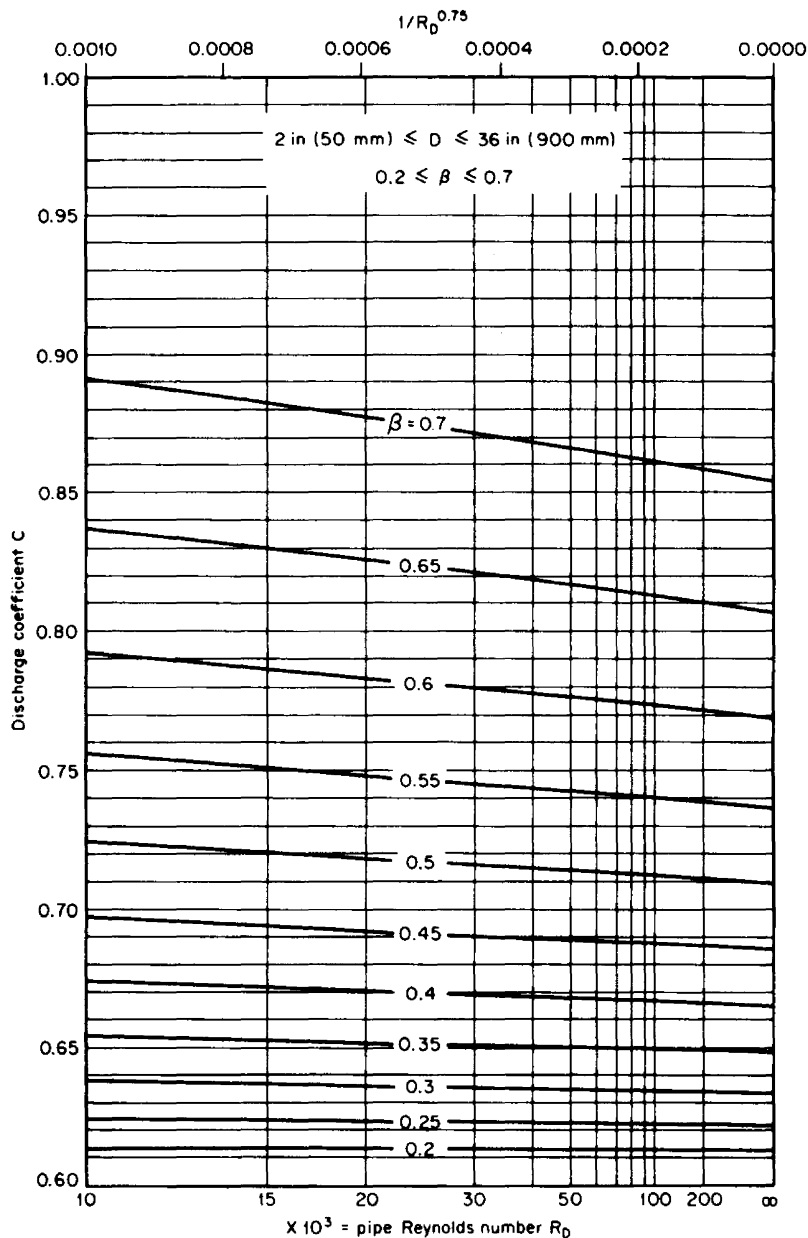


Figure 10.21 C versus R_D for concentric square-edged orifice; $2\frac{1}{2}D$ and $8D$ taps (pipe taps).

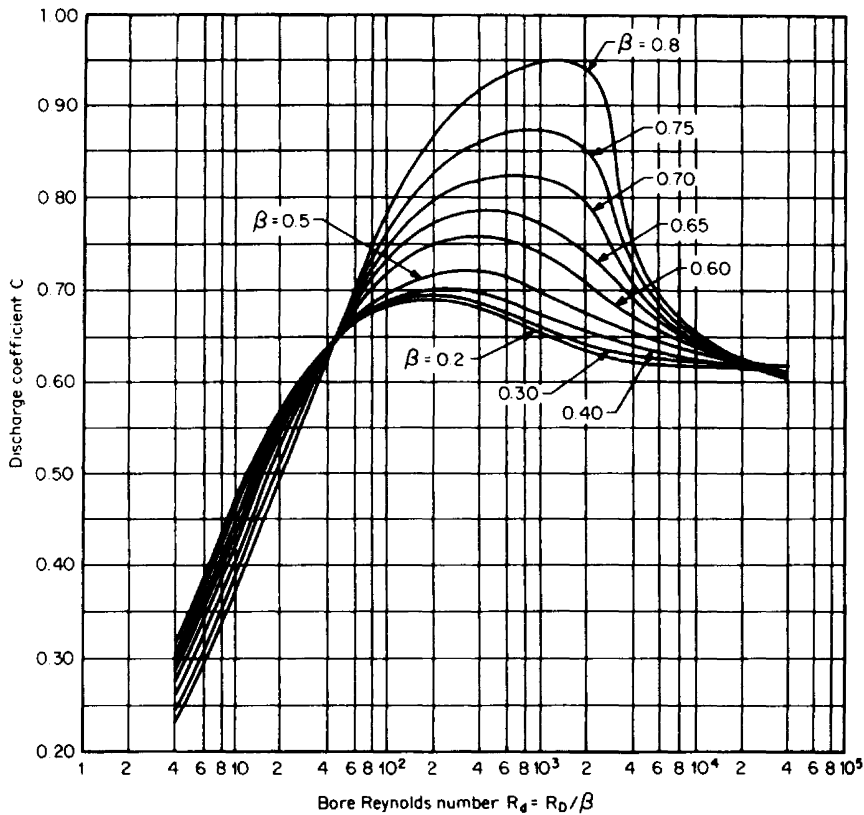


Figure 10.22 C versus R_d for concentric square-edged orifice; corner, flange, D and $D/2$ taps.

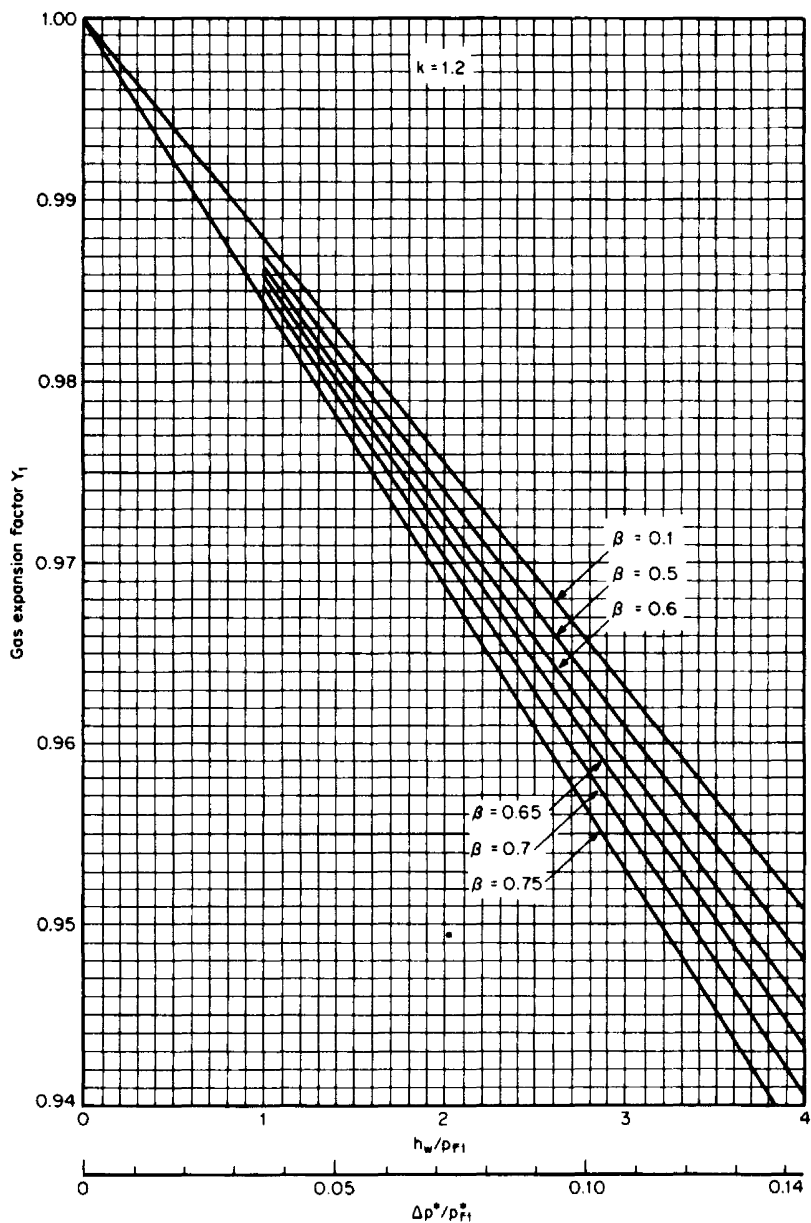


Figure 10.23 Gas expansion factor Y_1 for concentric square-edged orifice; corner, flange, D and $D/2$ taps.

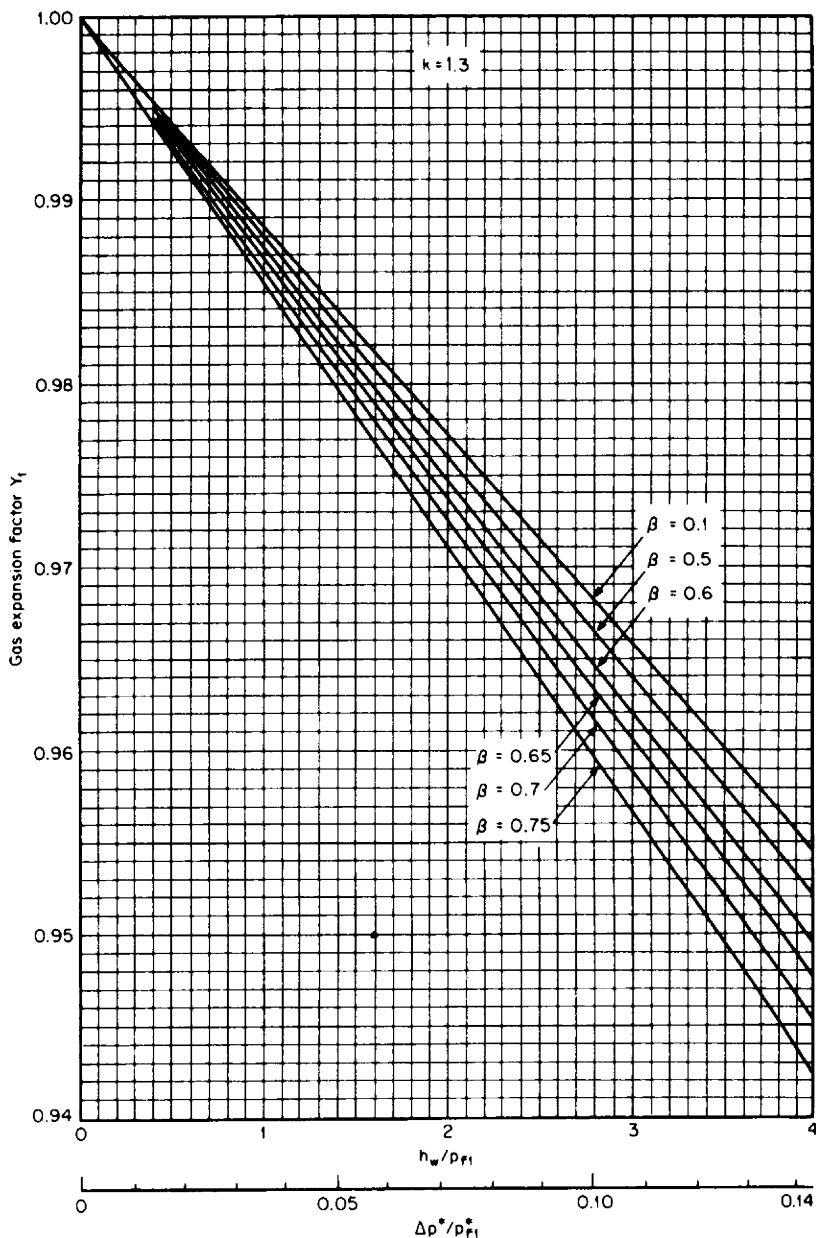


Figure 10.24 Gas expansion factor Y_1 for concentric square-edged orifice; corner, flange, D and $D/2$ taps.

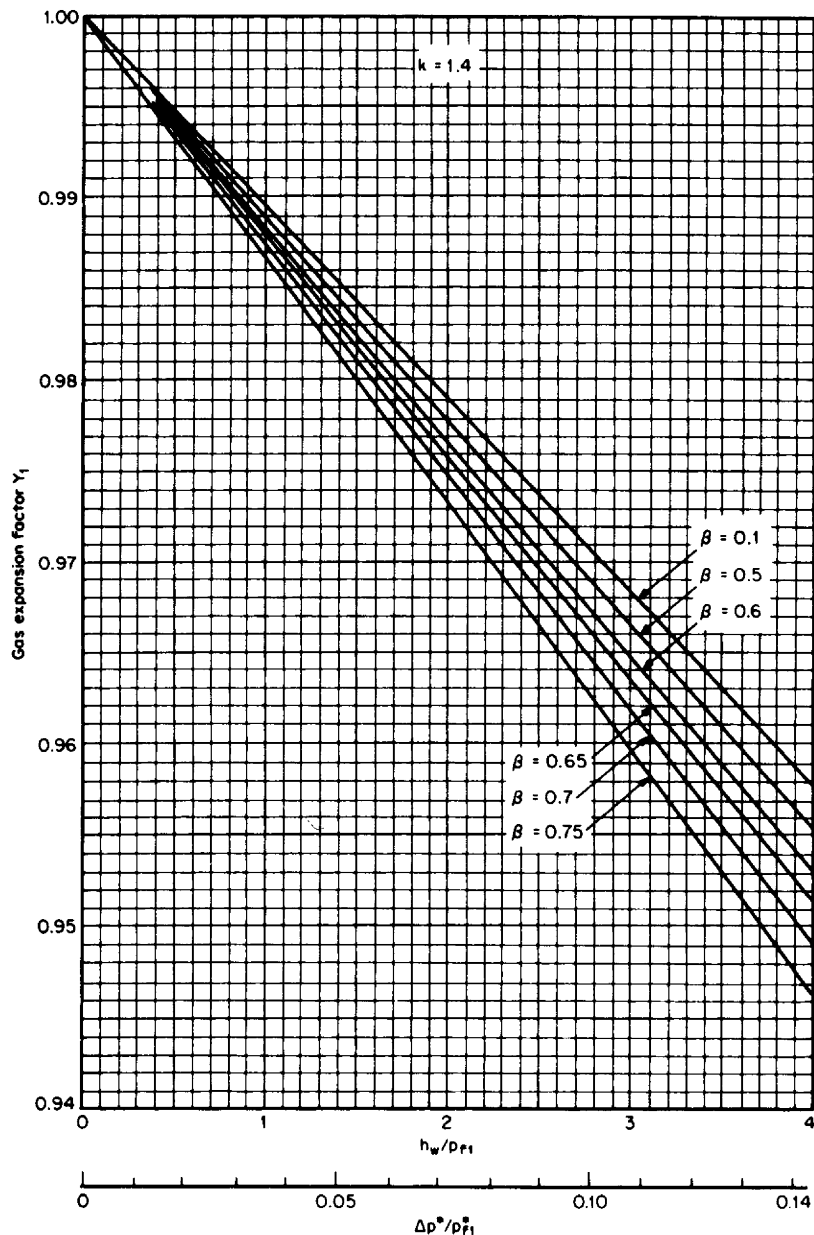


Figure 10.25 Gas expansion factor Y_1 for concentric square-edged orifice; corner, flange, D and $D/2$ taps.

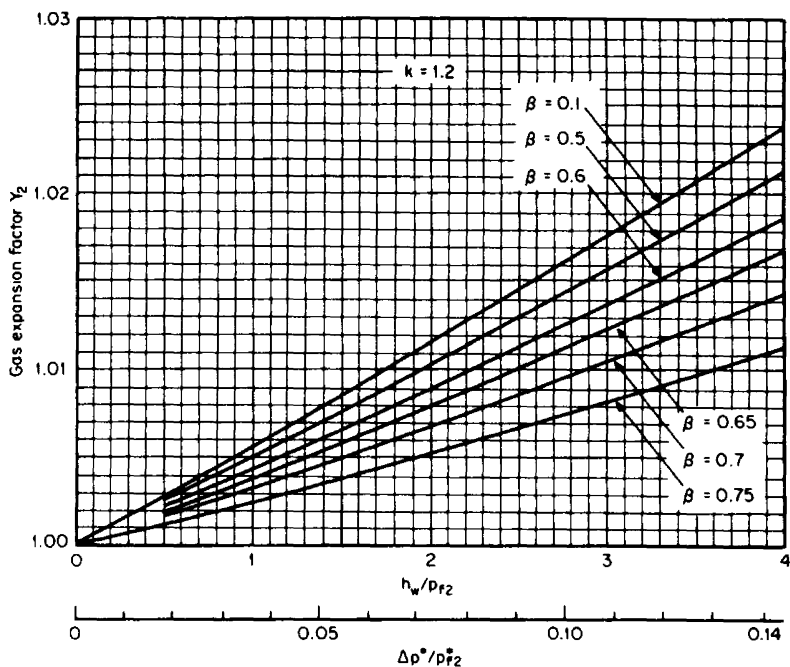


Figure 10.26 Gas expansion factor Y_2 for concentric square-edged orifice; corner, flange, D and $D/2$ taps.

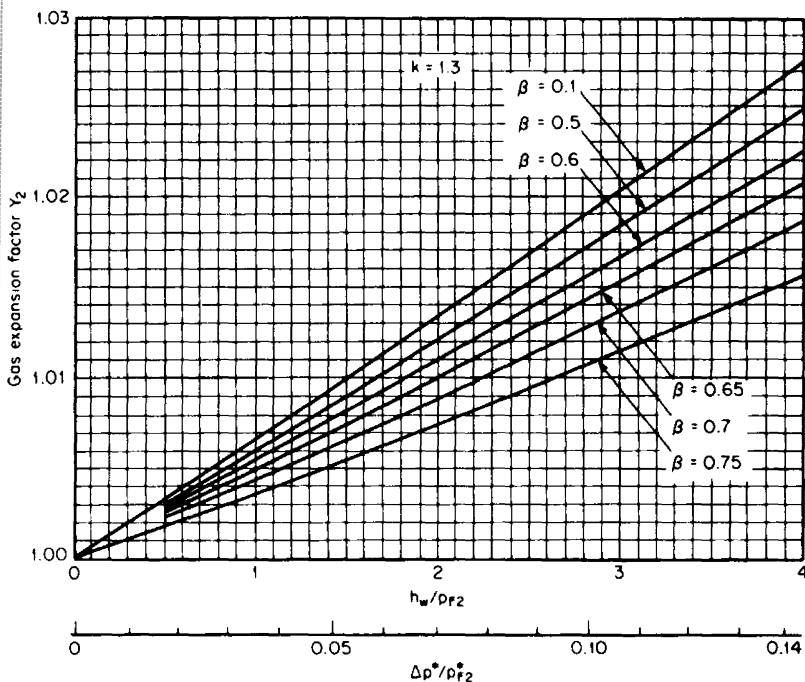


Figure 10.27 Gas expansion factor Y_2 for concentric square-edged orifice; corner, flange, D and $D/2$ taps.

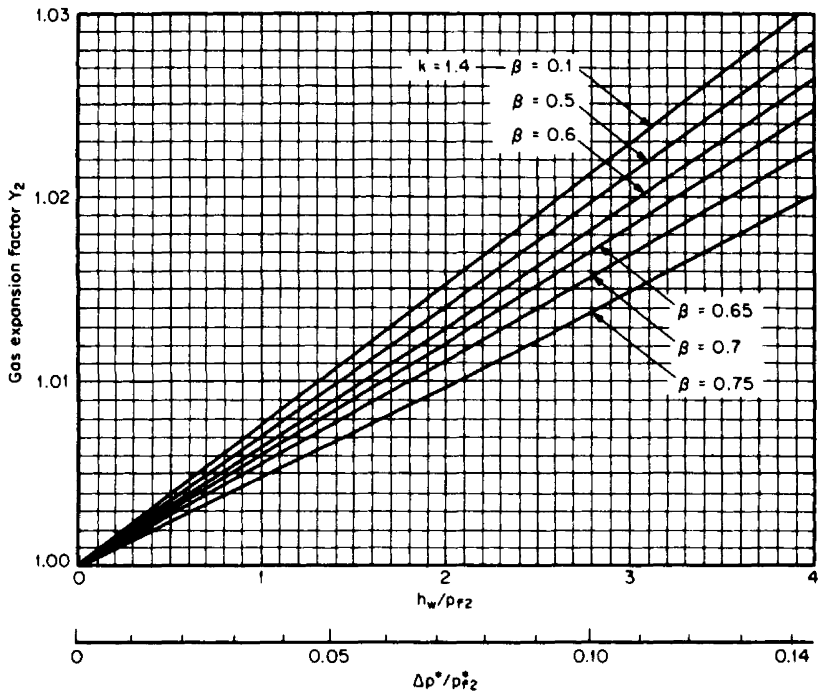


Figure 10.28 Gas expansion factor Y_2 for concentric square-edged orifice; corner, flange, D and $D/2$ taps.

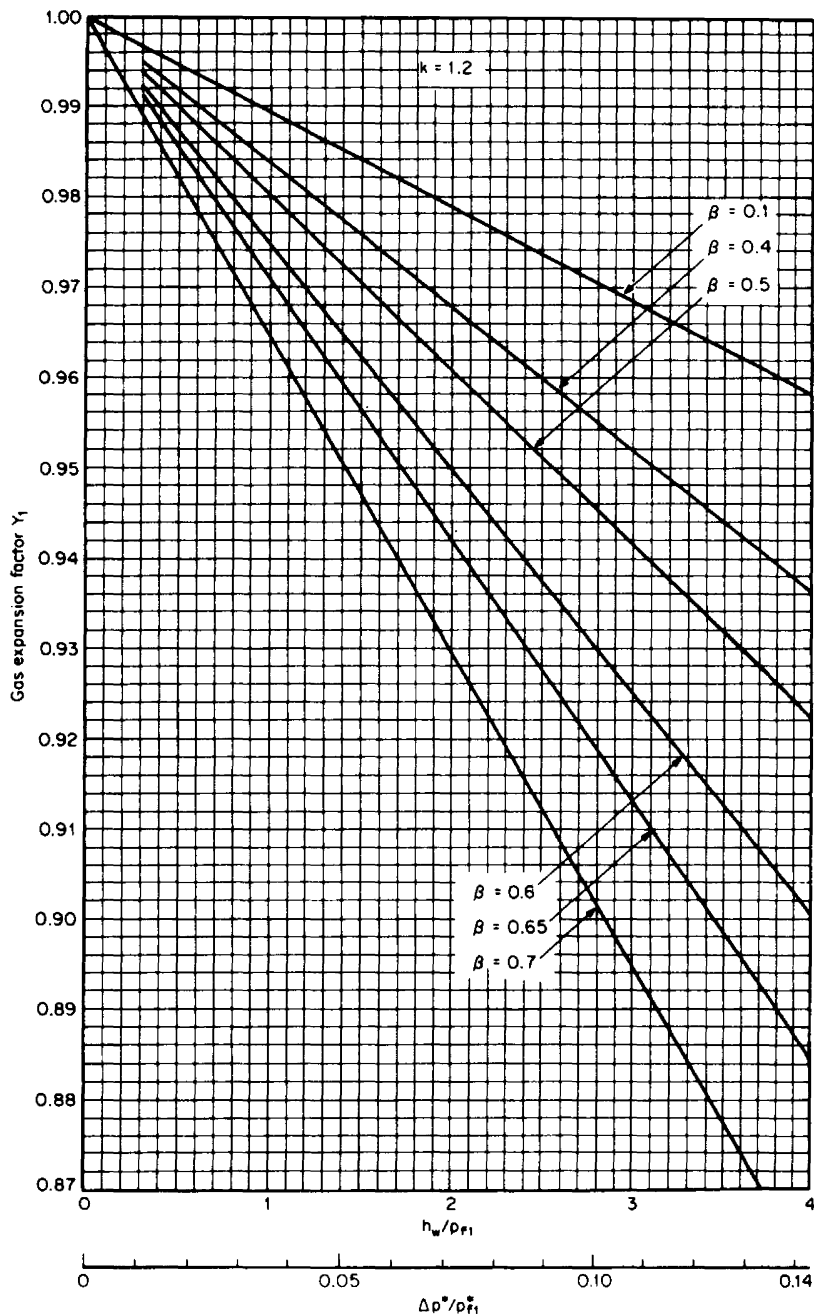


Figure 10.29 Gas expansion factor Y_1 for concentric square-edged orifice; $2\frac{1}{2}D$ and $8D$ taps.

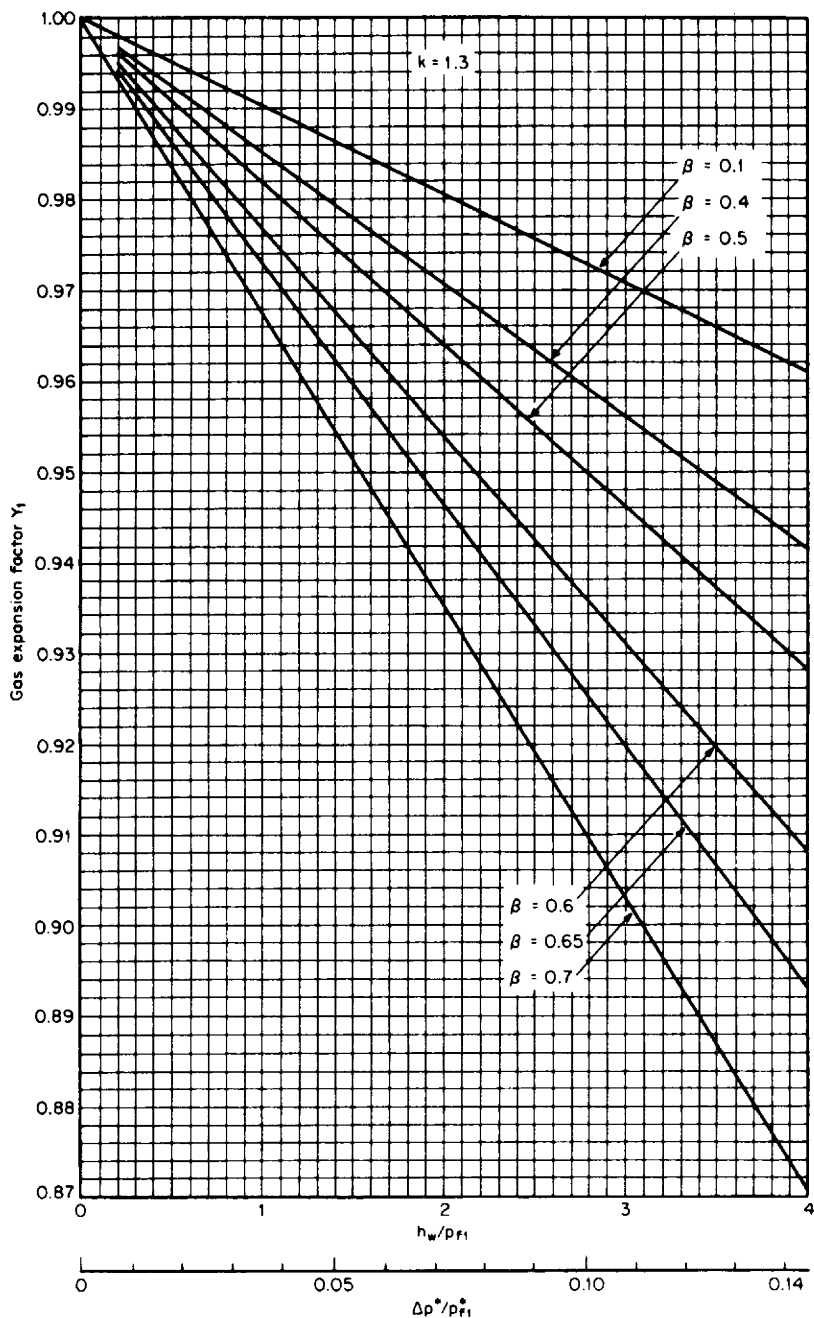


Figure 10.30 Gas expansion factor Y_1 for concentric square-edged orifice; $2\frac{1}{2}D$ and $8D$ taps.

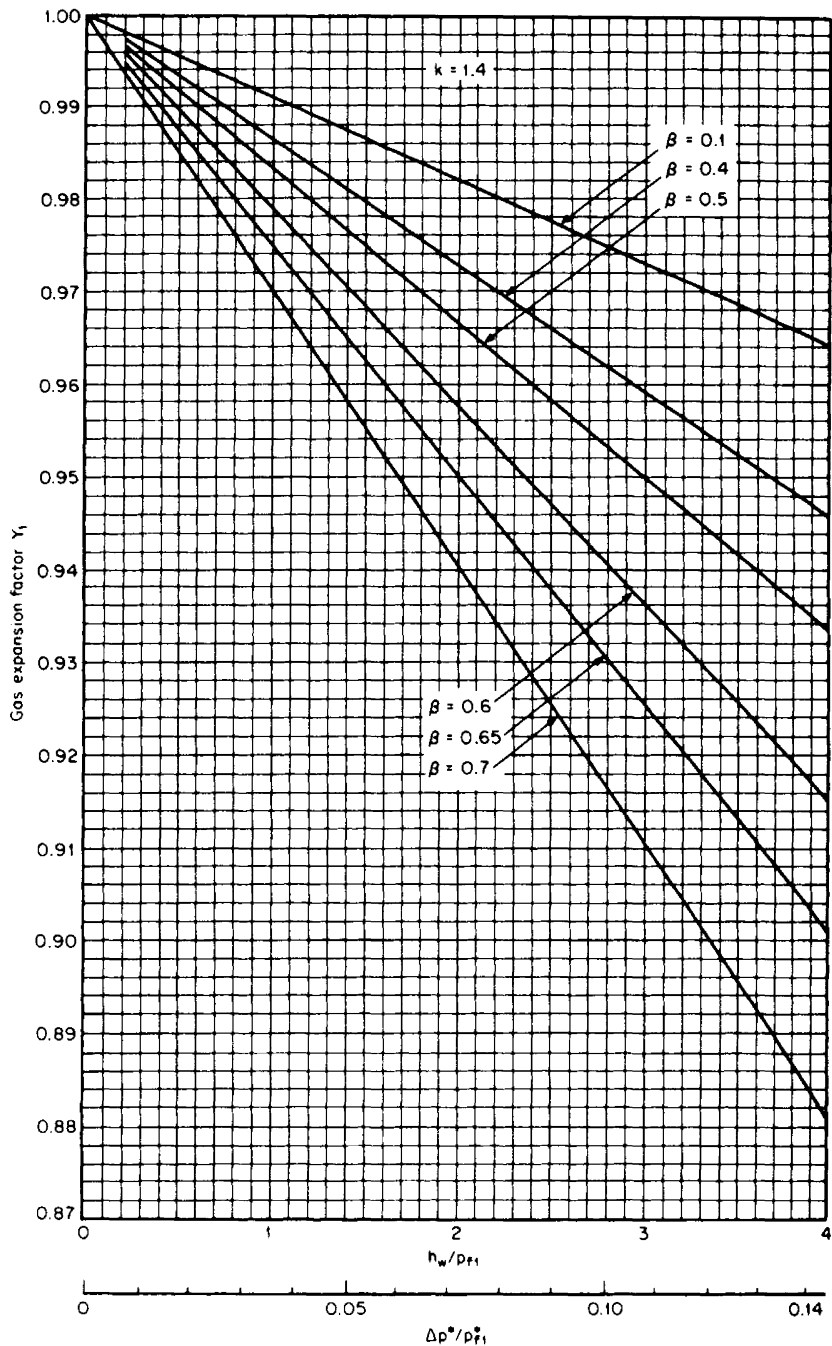


Figure 10.31 Gas expansion factor Y_1 for concentric square-edged orifice; $2\frac{1}{2}D$ and $8D$ taps.

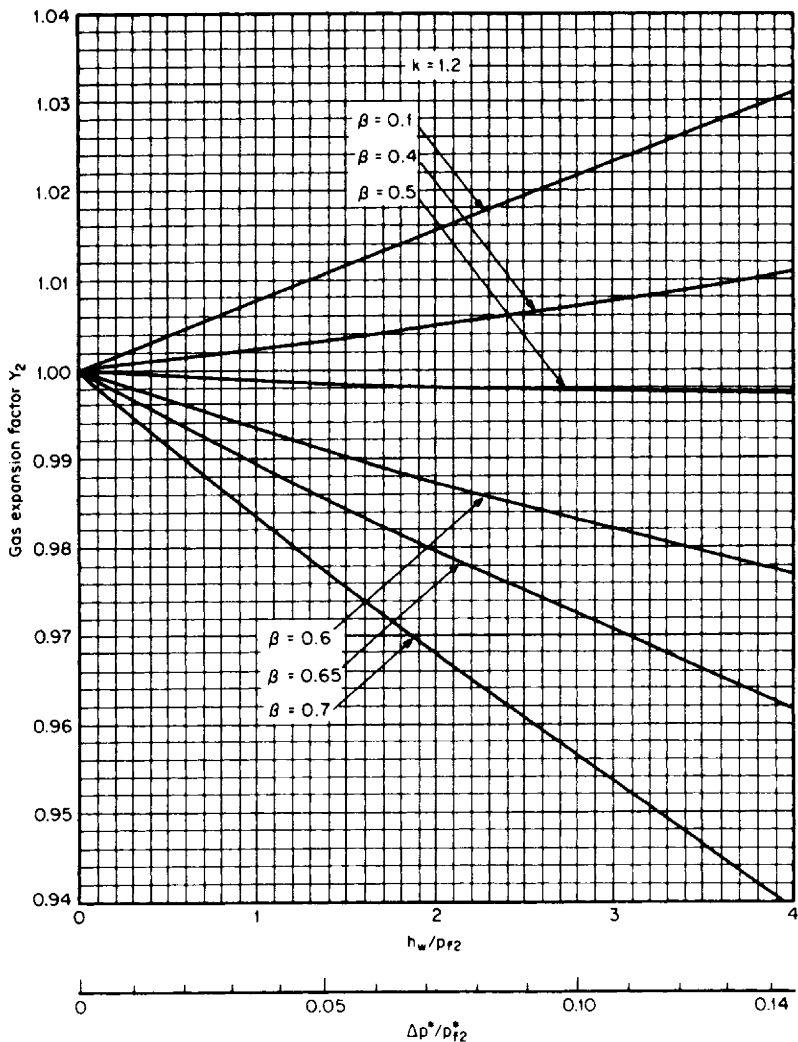


Figure 10.32 Gas expansion factor Y_1 for concentric square-edged orifice; $2\frac{1}{2}D$ and $8D$ taps.

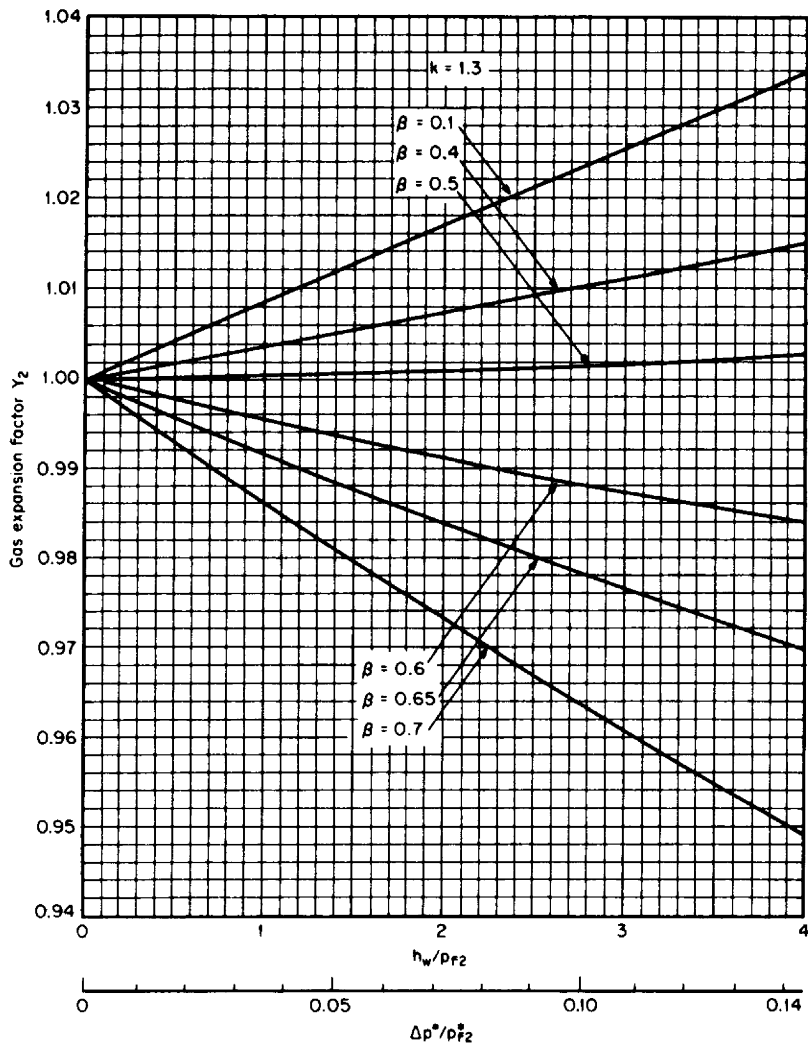


Figure 10.33 Gas expansion factor Y_2 for concentric square-edged orifice; $2\frac{1}{2}D$ and $8D$ taps.

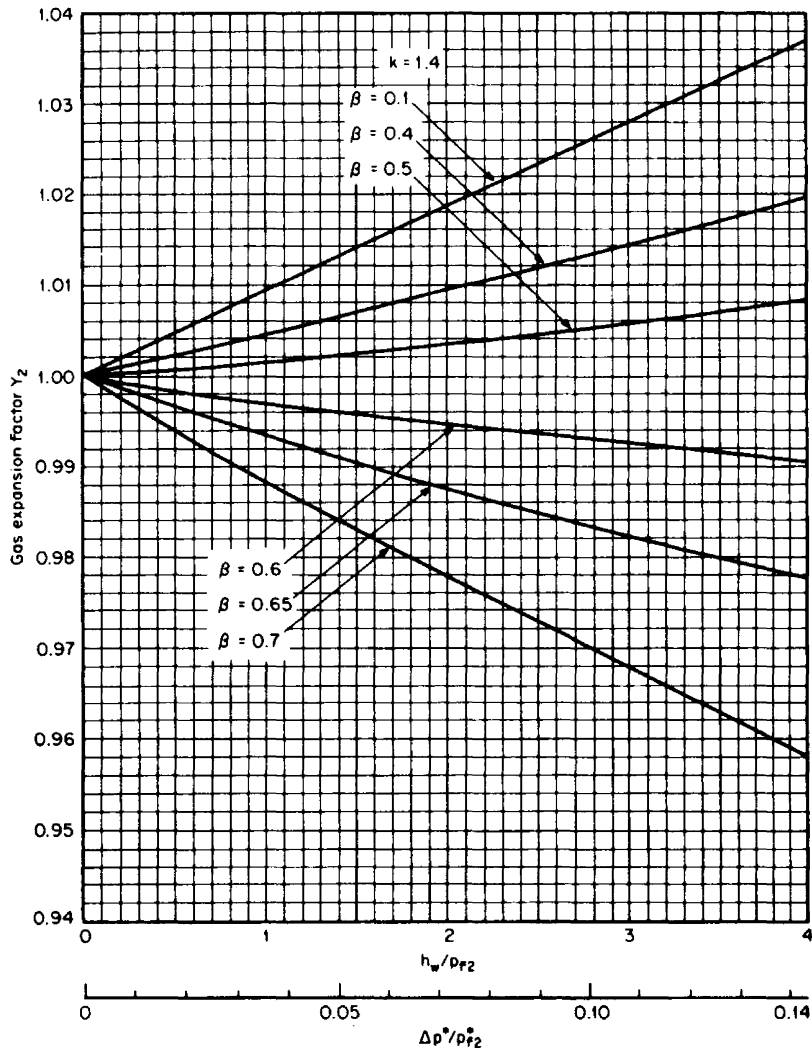
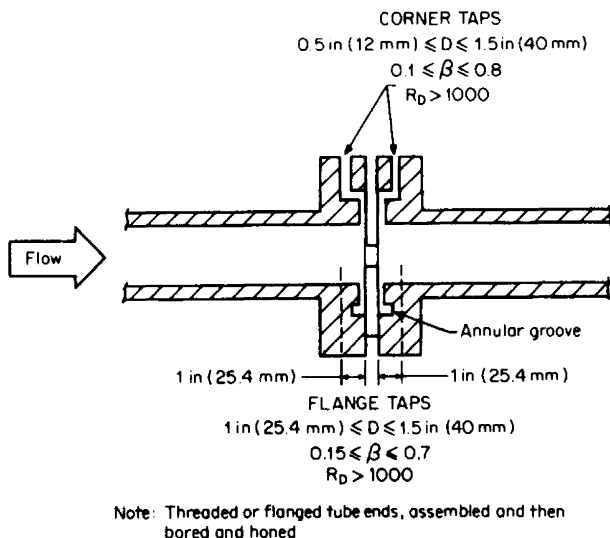


Figure 10.34 Gas expansion factor Y_2 for $2\frac{1}{2}D$ and $8D$ taps.



Note: Threaded or flanged tube ends, assembled and then bored and honed

Figure 10.35 Honed-orifice meter run.

pressure-tap geometry are magnified and meters are specifically designed to minimize these effects.

The Foxboro Integral Orifice Flow Meter Assembly (IFOA) and the honed-orifice meter run, shown in Fig. 10.35, are widely used in line sizes of $\frac{1}{2}$ to $1\frac{1}{2}$ in (12.5 to 49 mm). They have corner taps, since flange or D and $D/2$ taps would be located in regions where pipe friction would influence the differential.

The discharge-coefficient equations for the IFOA corner and honed-orifice meter runs with corner and flange taps are given in Table 9.1. The gas expansion factors shown in Figs. 10.23 through 10.28 should be used for the corner tap design, and the gas expansion factors shown in Figs. 10.29 through 10.34 may be used to approximate the flange tap values.

Low-Reynolds-Number Orifices

For Reynolds numbers below 10,000, the discharge coefficient of a square-edged orifice changes appreciably with either flow rate or viscosity (see Fig. 10.22). For this reason, either a quadrant- or conical-edged inlet is used. Both geometries have an essentially constant coefficient in the laminar flow regime. These geometries are covered in BSI Standard 1042 (1964), but no U.S. or international standard is available.

Eujen (1977) and others have reported that upstream pipe length alters the coefficient for both designs by from ± 1.5 to ± 2 percent. The laminar parabolic profile is not fully developed for short pipe lengths, and the coefficient rises when the upstream length is increased. This is practically eliminated by installing upstream diffuser plates, similar to the Sprengle plates discussed in Chap. 5.

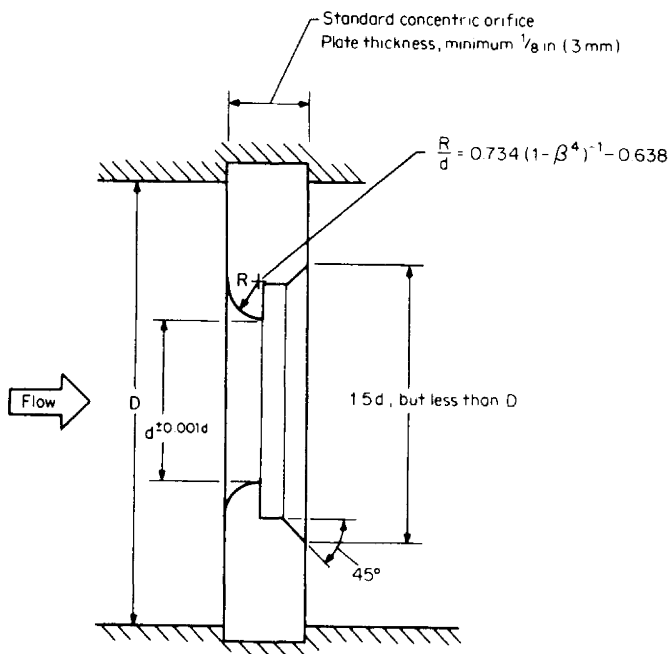


Figure 10.36 Quadrant (quarter-circle) concentric orifice.

Quadrant-Edged Orifice. The quadrant, or quarter-circle orifice, is shown in Fig. 10.36. It is readily manufactured from standard orifice-plate blanks with a high degree of conformity. It is relatively immune to the effects of corrosion, erosion, and the deposit of solids at the surface of the orifice.

The Reynolds-number range over which the coefficient is constant is shown in Fig. 10.37. In Fig. 10.38, the discharge is plotted versus β . Since the effect of upstream length is greatest for large β , it is recommended that β be sized as small as practicable. The beta ratio is sized graphically by the procedure given in Chap. 9; the β_0 equation is given in Table 9.28.

Conical-Entrance Orifice. In the conical-entrance orifice the quarter-circle of the quadrant is replaced by a conical inlet, as shown in Fig. 10.39. This inlet geometry provides for a lower Reynolds-number limit. The plate is considered by some to be more difficult to manufacture than the quadrant-edged orifice plate, because the bore-section land is difficult to reproduce accurately in some sizes.

Depending on the Reynolds-number range, the discharge coefficient is assigned two different values. These are shown in Fig. 10.40 (and in Fig. 10.38). Substitution of the discharge coefficient for the selected Reynolds-number range into Eq. (9.83) will exactly size the bore, since the coefficient is assumed constant over each range.

Eccentric and Segmental Orifices These orifices were developed to meter both liquids containing sediment and gases entrained within liquids. Their construction materials, plate thickness, edge sharpness, etc., are identical to those for the square-edged concentric orifice. Also, their sizing and flow equations are the same as for other differential producers.

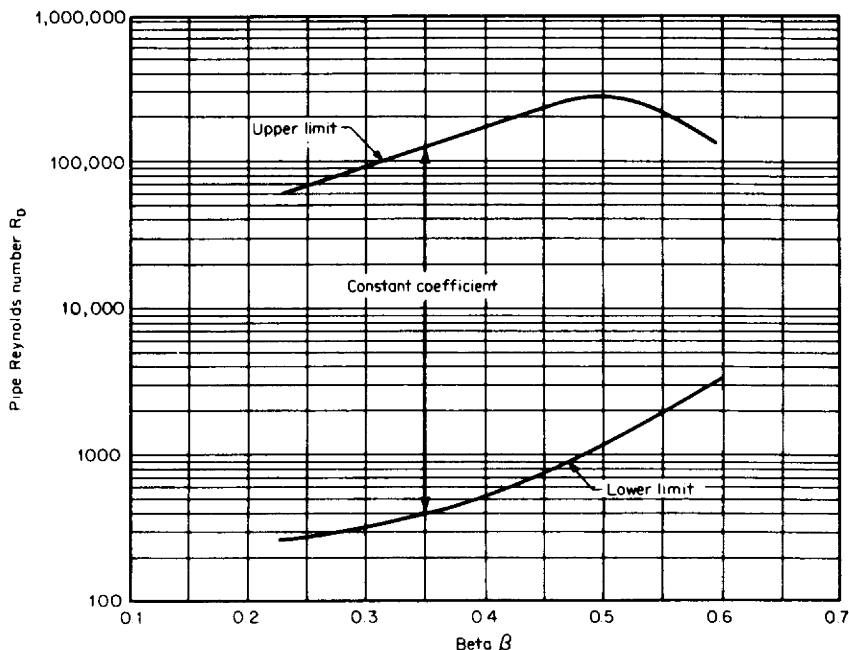


Figure 10.37 Quadrant-orifice Reynolds-number range.

The discharge coefficient curves and prediction equations presented in Table 9.1 were developed from data obtained in an ASME test program. The initial 4-in (100-mm) and 6-in (150-mm) calibration results were reported by Beitler and Masson (1949). A later ASME fluid meters committee report extending line sizes to 10 and 14 in (250 and 350 mm) was prepared by Lindahl and Beitler (1954). The test data was for both flange and vena contracta taps, with the flange taps located at the conventional 1-in (25-mm) spacing. The location of the vena contracta, which was determined experimentally, is shown in Fig. 10.41.

Segmental Orifice. The segmental orifice is shown in Fig. 10.42. The opening is a segment of a circle having a diameter of 98 percent of the pipe diameter. The circular section of the opening should be concentric with the pipe and accurately centered, to ensure that the opening is not covered by the inlet pipe or gaskets or because of the pipe eccentricity.

For segmental orifices, an equivalent value β_c is used for the diameter ratio; it is equal to the diameter ratio of a circular orifice which has an aperture equal in area to the area of the segment. The relationship between the sized beta ratio and the segment geometry is

$$\beta_c = \frac{d}{D_c} = \frac{\beta}{0.98} = \left(\frac{1}{\pi} \left\{ \arccos \left(1 - \frac{2H_s}{D_c} \right) - 2 \left(1 - \frac{2H_s}{D_c} \right) \left[\frac{H_s}{D_c} - \left(\frac{H_s}{D_c} \right)^2 \right]^{1/2} \right\} \right)^{1/2} \quad (10.3)$$

An iterative solution is required to obtain the segment height H_s . Table 10.2 presents

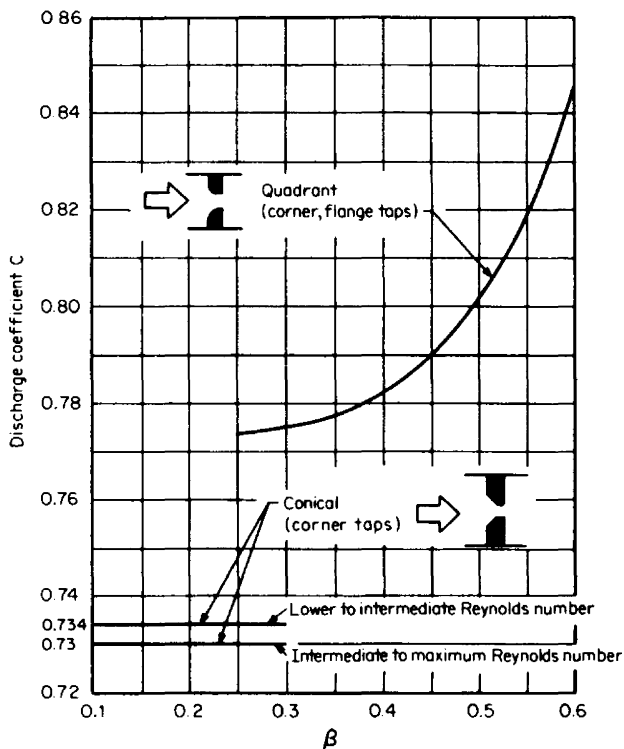


Figure 10.38 Discharge coefficient for quadrant and conical orifices.

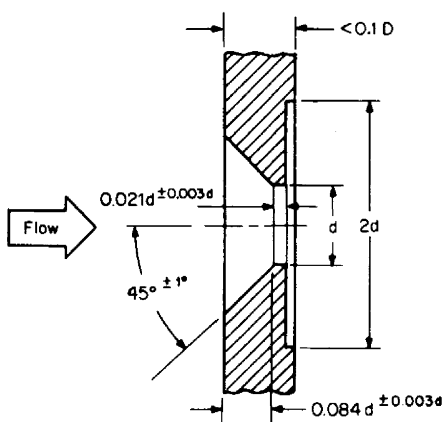


Figure 10.39 Conical-entrance orifice.

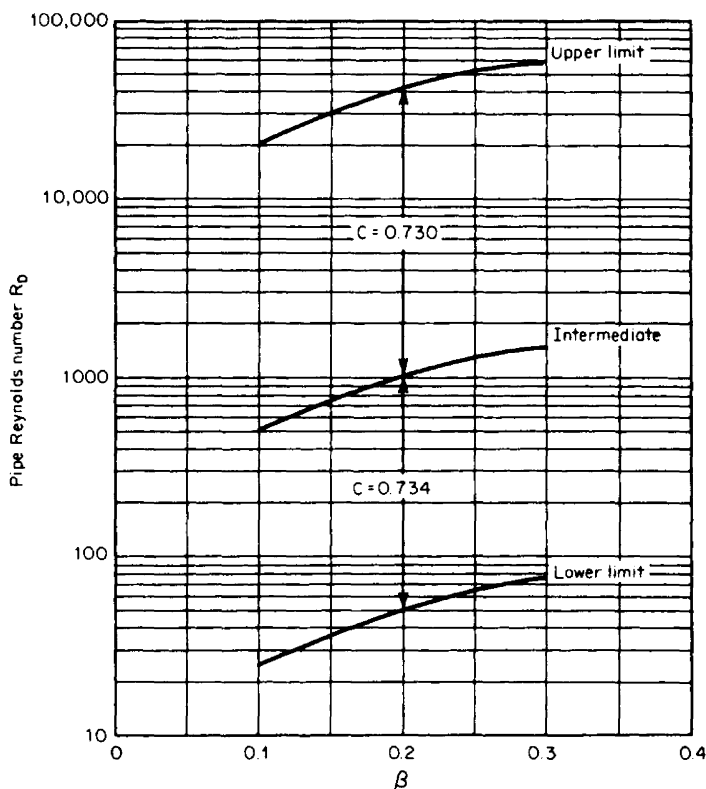


Figure 10.40 Conical-orifice Reynolds-number ranges.

the dimensional relationship given by Eq. (10.3) for a concentric orifice and a segmental orifice.

The segmental orifice has one characteristic that makes it useful for special service; it eliminates damming of foreign material at the side of the pipe on which the opening is located. This characteristic makes it useful for measuring wet steam, liquids containing granular solids, and oils containing water when the measurement must be made in a horizontal pipe. When the orifice may be located in a vertical run with the flow in a *downward* direction, the concentric orifice is preferred because of its better discharge-coefficient accuracy.

When liquids containing gas or vapor must be measured in a horizontal pipe, the segmental orifice may be used with the opening at the top of the pipe. However, for these fluids, the concentric orifice in a vertical pipe, with the flow in an *upward* direction, is preferred for greater accuracy—if a suitable location is available. Segmental orifice plates should not be used to measure liquids containing sticky solids or solids having a density near that of the flowing liquid. It is affected in the same way as the concentric orifice by deposits on the face or edge of the orifice.

Coefficient data are presented in Fig. 10.43 for both flange and vena contracta taps, and in Figs. 10.44 through 10.46 are graphs of the gas expansion factor. These apply only where taps are located at points in line with the midpoint of the solid segment of the orifice plate. This restriction often makes application to liquids

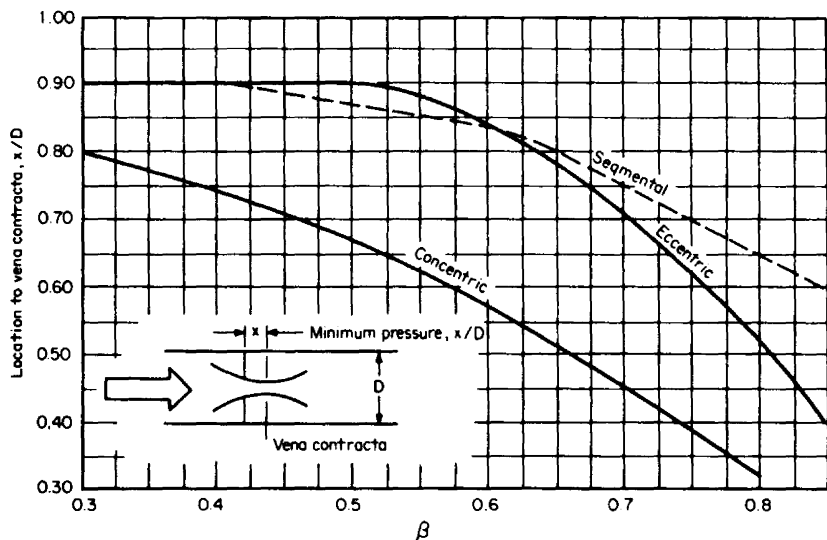


Figure 10.41 Location of minimum pressure (vena contracta).

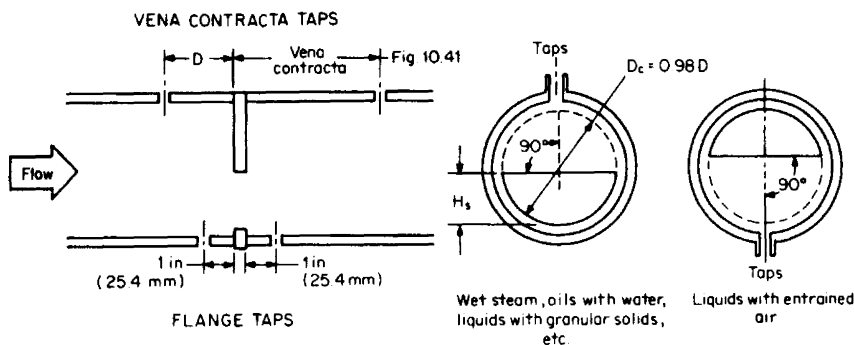
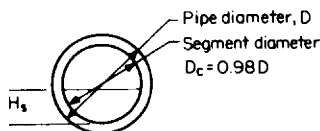


Figure 10.42 Segmental orifice.

containing both vapors and solids undesirable, because it necessitates bringing the taps out above the horizontal line at an angle such that excessive maintenance results, due to the accumulation of air or vapor. Data for eccentric orifices with taps at 90° from the point of tangency are available; hence eccentric orifices are preferable for such applications.

The spread of segmental-orifice data points was so great that any effect of Reynolds number on the discharge coefficient was obscured. Twice the standard deviation of the test data is ± 2.2 percent for vena contracta taps, and ± 1.9 percent for flange taps.

Eccentric Orifice. The eccentric orifice is shown in Fig. 10.47, with two tap arrangements. The orifice bore is tangent to a circle with a diameter equal to 98 percent of that of the pipe and concentric with the pipe. When the plate is installed,

TABLE 10.2 Segmental Orifice Dimensional Table

$$\beta_c = \frac{d}{D_c} = \frac{\beta}{0.98} = \left(\frac{1}{\pi} \left[\arccos \left(1 - \frac{2H_s}{D_c} \right) - 2 \left(1 - \frac{2H_s}{D_c} \right) \left[\frac{H_s}{D_c} - \left(\frac{H_s}{D_c} \right)^2 \right]^{1/2} \right] \right)^{1/2}$$

d/D_c	H_s/D_c	d/D_c	H_s/D_c	d/D_c	H_s/D_c
0.250	0.11331	0.380	0.20198	0.510	0.30665
0.255	0.11641	0.385	0.20571	0.515	0.31101
0.260	0.11955	0.390	0.20946	0.520	0.31539
0.265	0.12271	0.395	0.21324	0.525	0.31980
0.270	0.12589	0.400	0.21704	0.530	0.32423
0.275	0.12910	0.405	0.22086	0.535	0.32869
0.280	0.13233	0.410	0.22470	0.540	0.33317
0.285	0.13559	0.415	0.22857	0.545	0.33769
0.290	0.13887	0.420	0.23247	0.550	0.34222
0.295	0.14218	0.425	0.23638	0.555	0.34679
0.300	0.14551	0.430	0.24032	0.560	0.35138
0.305	0.14886	0.435	0.24429	0.565	0.35600
0.310	0.15224	0.440	0.24827	0.570	0.36065
0.315	0.15564	0.445	0.25229	0.575	0.36533
0.320	0.15906	0.450	0.25632	0.580	0.37003
0.325	0.16251	0.455	0.26038	0.585	0.37476
0.330	0.16598	0.460	0.26446	0.590	0.37952
0.335	0.16947	0.465	0.26857	0.595	0.38431
0.340	0.17299	0.470	0.27270	0.600	0.38913
0.345	0.17653	0.475	0.27686	0.605	0.39398
0.350	0.18010	0.480	0.28104	0.610	0.39885
0.355	0.18369	0.485	0.28525	0.615	0.40376
0.360	0.18730	0.490	0.28948	0.620	0.40870
0.365	0.19094	0.495	0.29373	0.625	0.41367
0.370	0.19459	0.500	0.29801	0.630	0.41867
0.375	0.19828	0.505	0.30232	0.635	0.42370

no portion of the hole must be covered by the flange or gasket. The orifice bore is calculated in exactly the same way as the bore of a square-edged orifice.

The eccentric orifice has the advantages of the segmental orifice, but it does not allow free drainage over as much of the pipe circumference. In all other respects, the eccentric orifice is superior to the segmental.

Discharge coefficients are presented in Fig. 10.48 for diametrically opposite flange taps, and in Fig. 10.49 for side, or 90°, taps. In Figs. 10.50 and 10.51 are discharge coefficients for diametrically opposite and 90° vena contracta taps. Figures 10.52 through 10.54 contain the gas-expansion-factor curves.

The discharge-coefficient curves are presented at pipe Reynolds numbers of 10,000 and 1,000,000. The general form of the equation for coefficient interpolation using a graphical method is

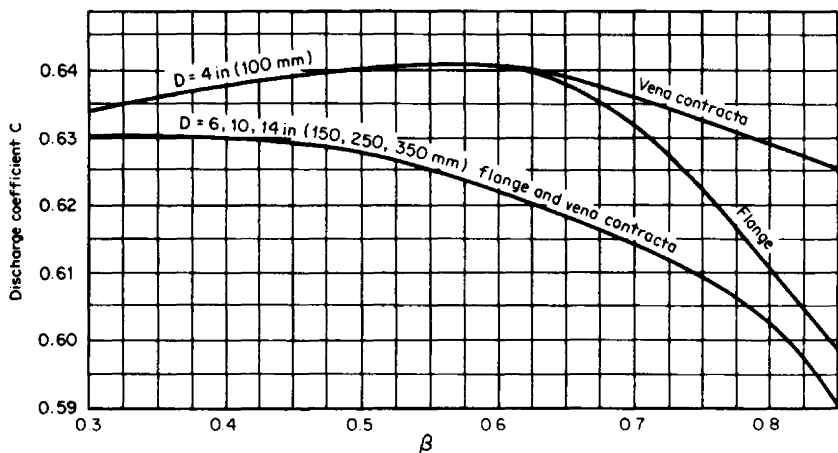
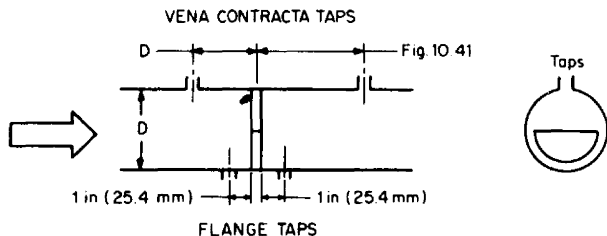


Figure 10.43 Discharge coefficient for segmental orifice; flange and vena contracta taps.

$$C = k_1 + \frac{k_2}{R_D^{0.5}} \quad (10.4)$$

where the constants k_1 and k_2 are derived from the graphically determined coefficients at the value of β_0 as

$$k_1 = C_{\max} - 1.11111(C_{\max} - C_{\min}) \quad (10.5)$$

and

$$k_2 = 111.111(C_{\max} - C_{\min}) \quad (10.6)$$

The subscripts max and min refer to the maximum and minimum discharge coefficients at pipe Reynolds numbers of 10,000 and 1,000,000.

Example 10.1. For liquid flow in a 4.000-in (101.6-mm) pipe, the S_M factor is calculated as 0.2500. Size a segmental and an eccentric orifice for a pipe Reynolds number of 250,000. Both are to have diametrically opposite flange taps.

Segmental orifice. From Eq. (m) of Table 9.28, the initial estimate for β is

$$\beta_0 = \left[1 + \left(\frac{0.634}{S_M} - 0.062 \right)^2 \right]^{-1/4} = \left[1 + \left(\frac{0.634}{0.2500} - 0.062 \right)^2 \right]^{-1/4} = 0.6122$$

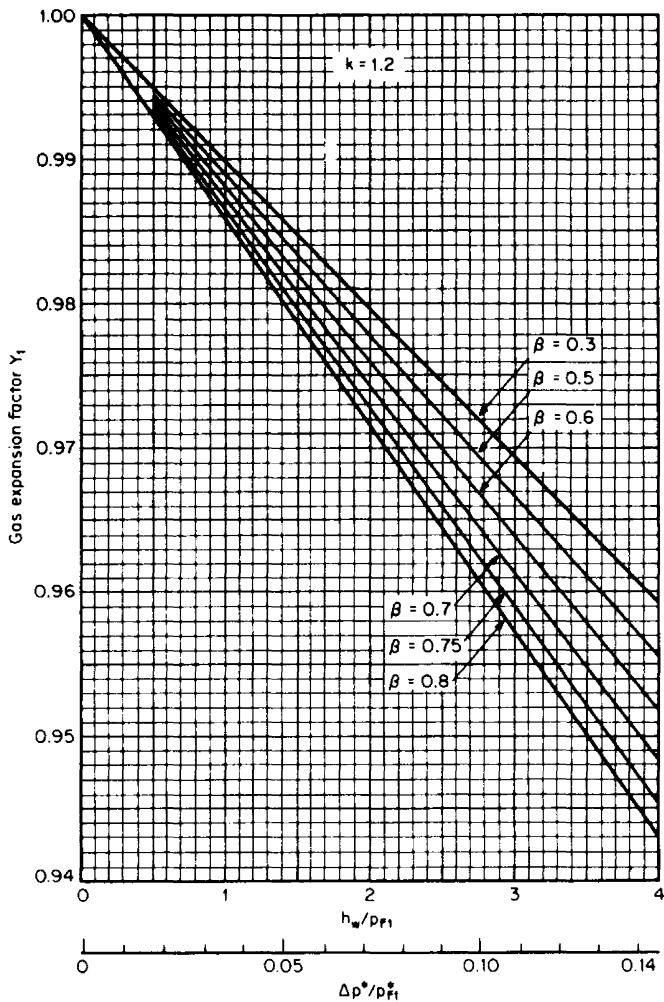


Figure 10.44 Gas expansion factor Y_1 for segmental orifice.

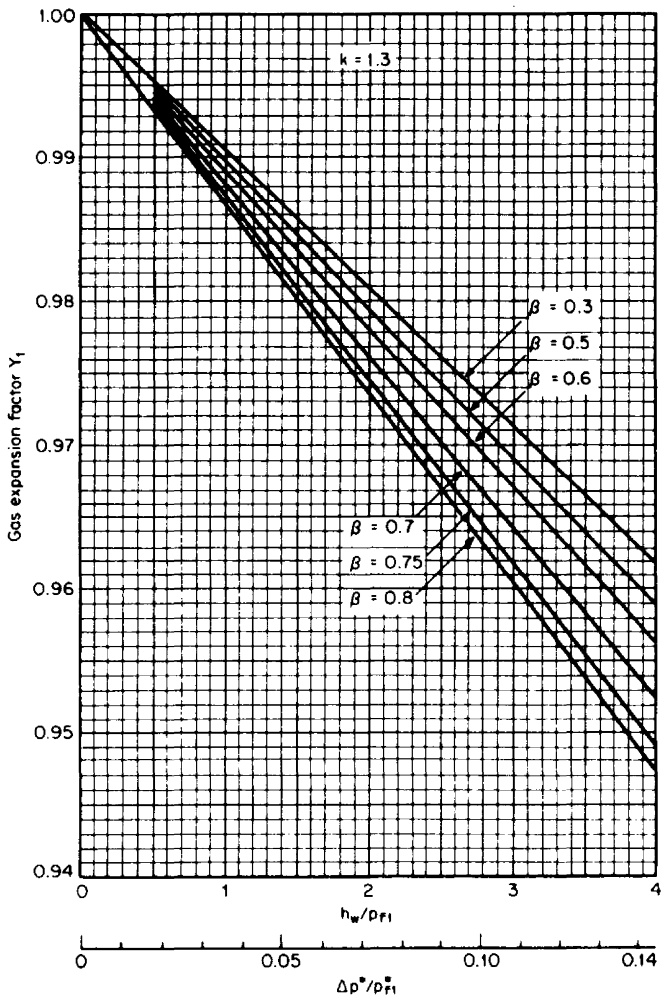


Figure 10.45 Gas expansion factor Y_1 for segmental orifice.

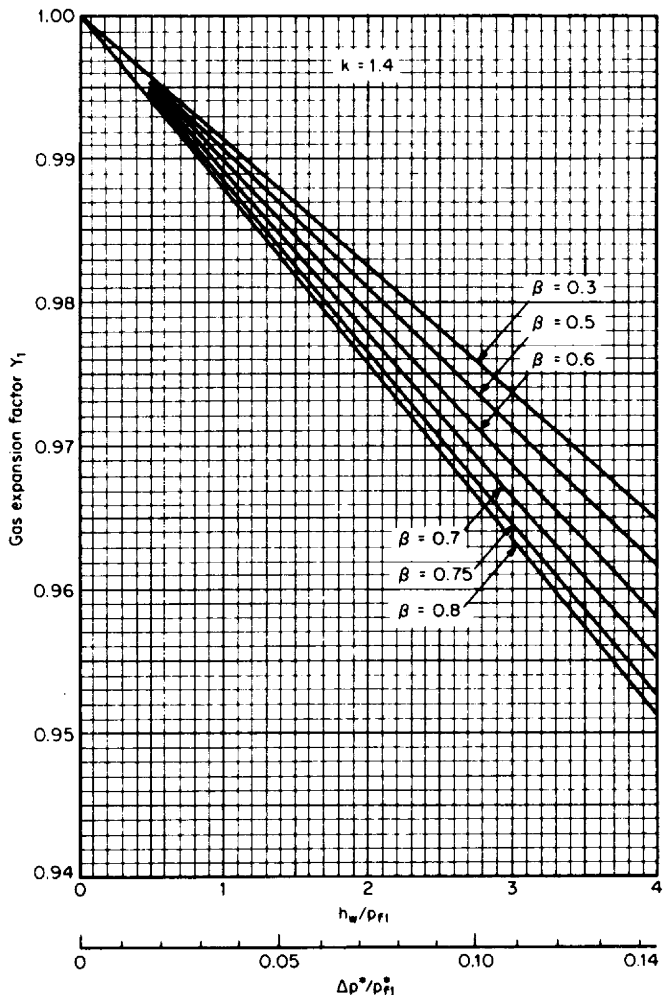
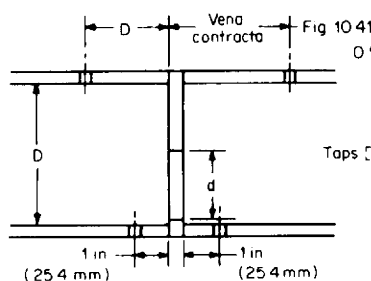


Figure 10.46 Gas expansion factor Y_1 for segmental orifice.

VENA CONTRACTA TAPS



FLANGE TAPS

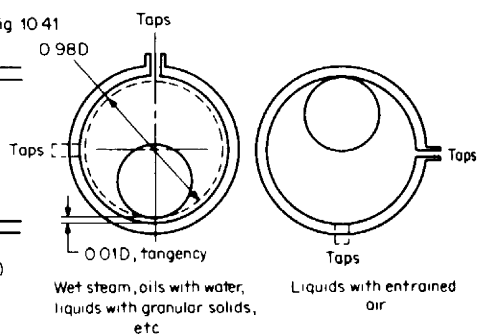


Figure 10.47 Eccentric orifice.

1 in (25.4 mm) 1 in (25.4 mm)

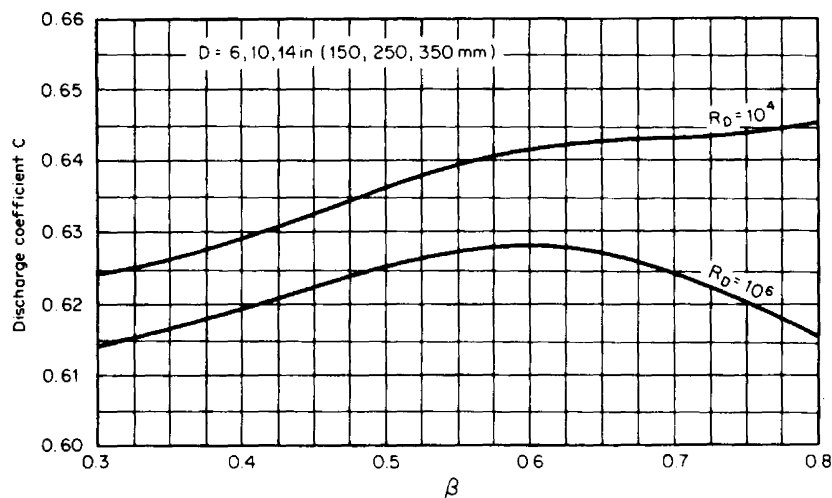
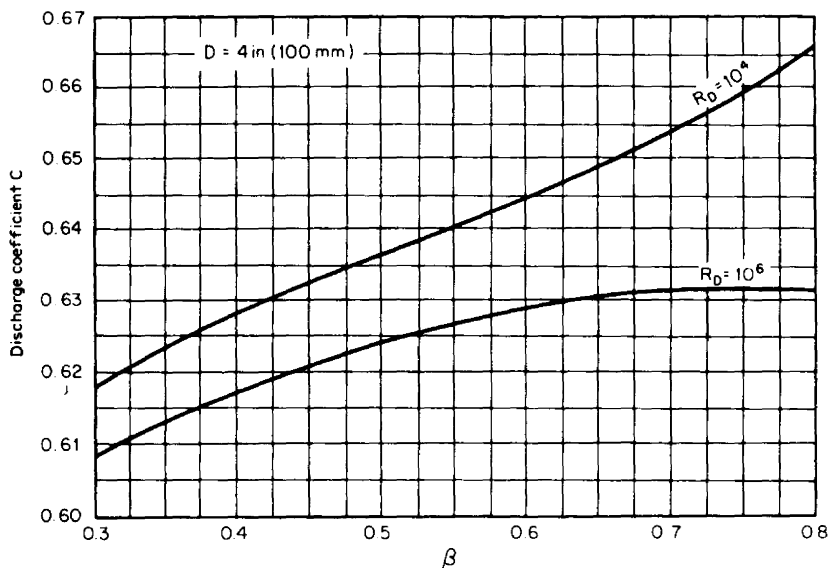
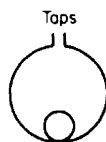
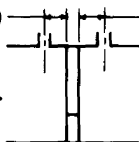


Figure 10.48 Discharge coefficient for eccentric orifice; flange taps.

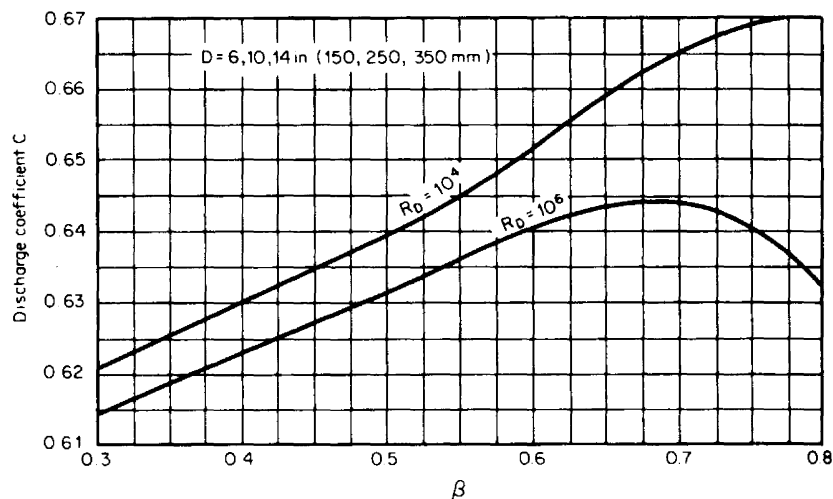
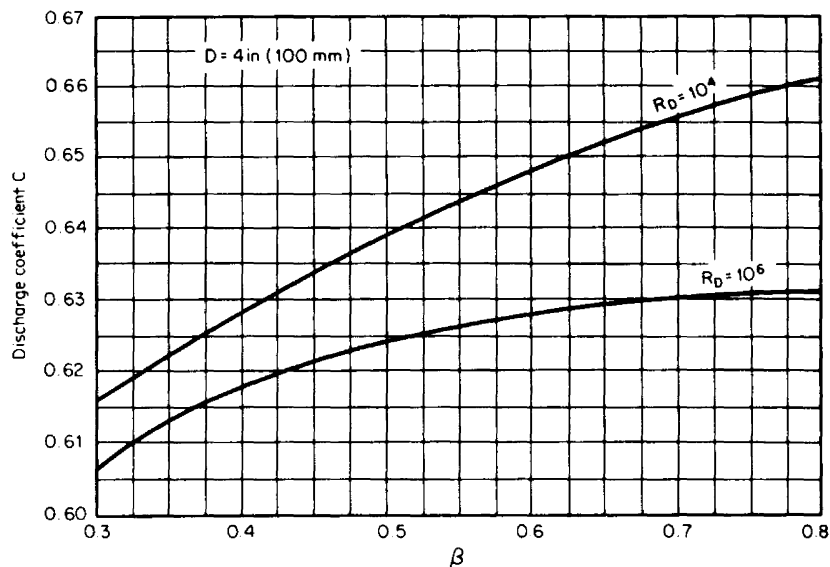
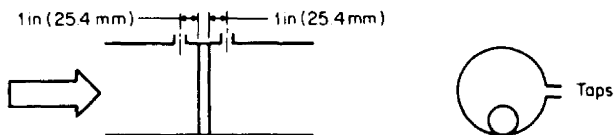


Figure 10.49 Discharge coefficient for eccentric orifice; flange taps.

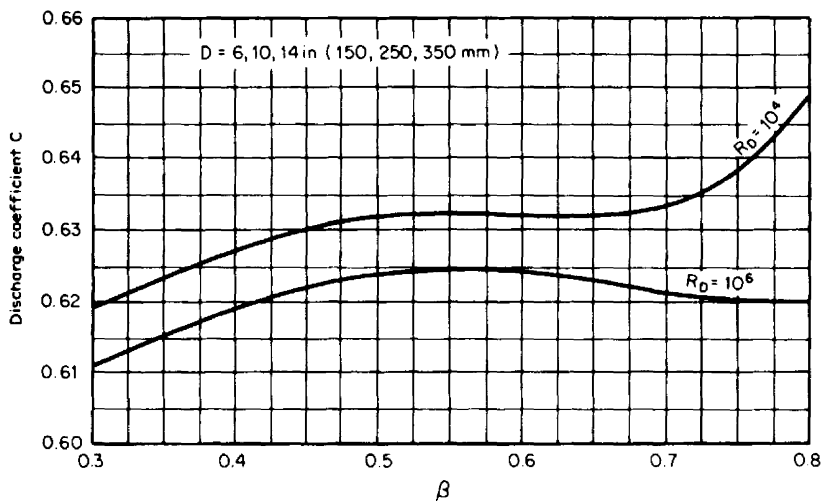
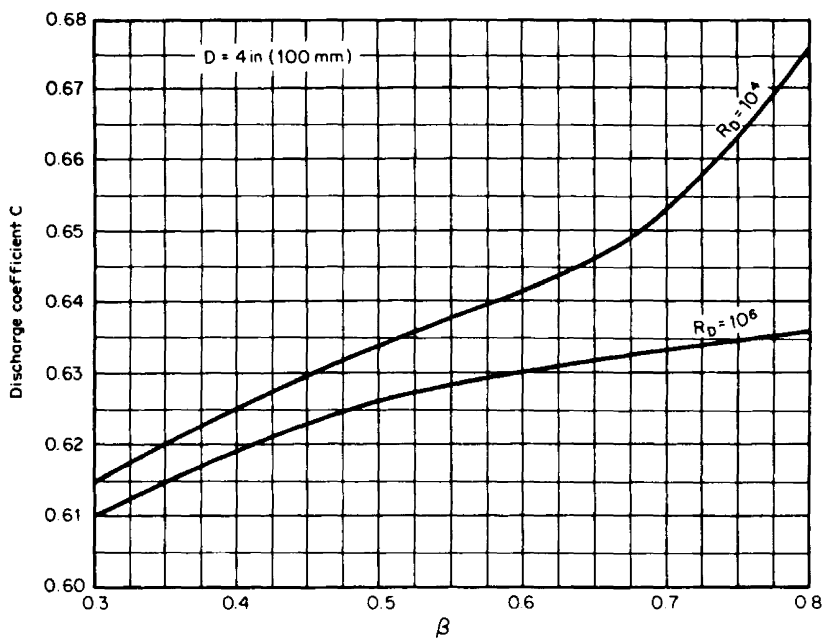
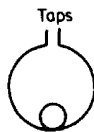
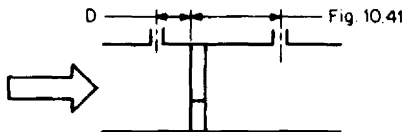


Figure 10.50 Discharge coefficient for eccentric orifice; vena contracta taps.

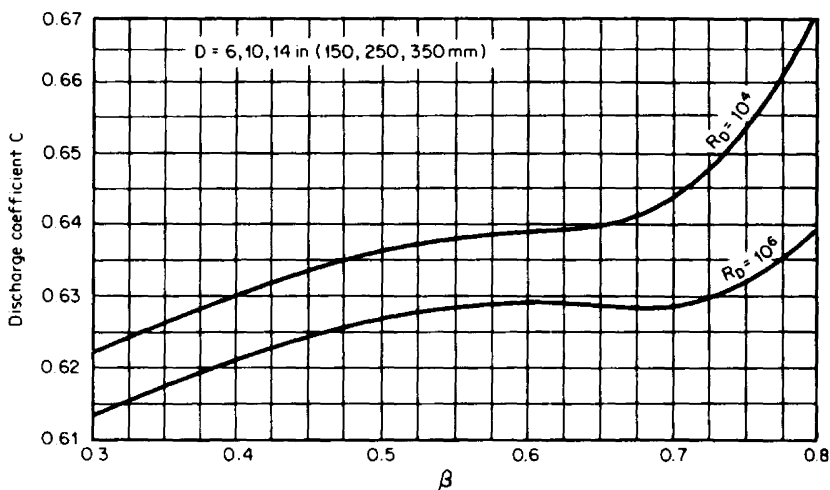
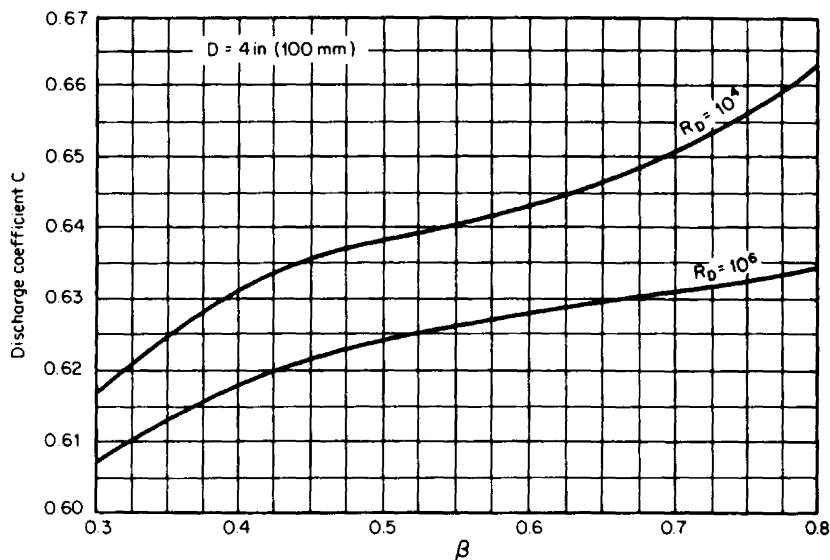
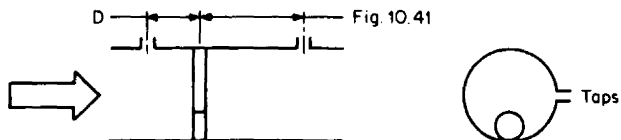


Figure 10.51 Discharge coefficient for eccentric orifice; vena contracta taps.

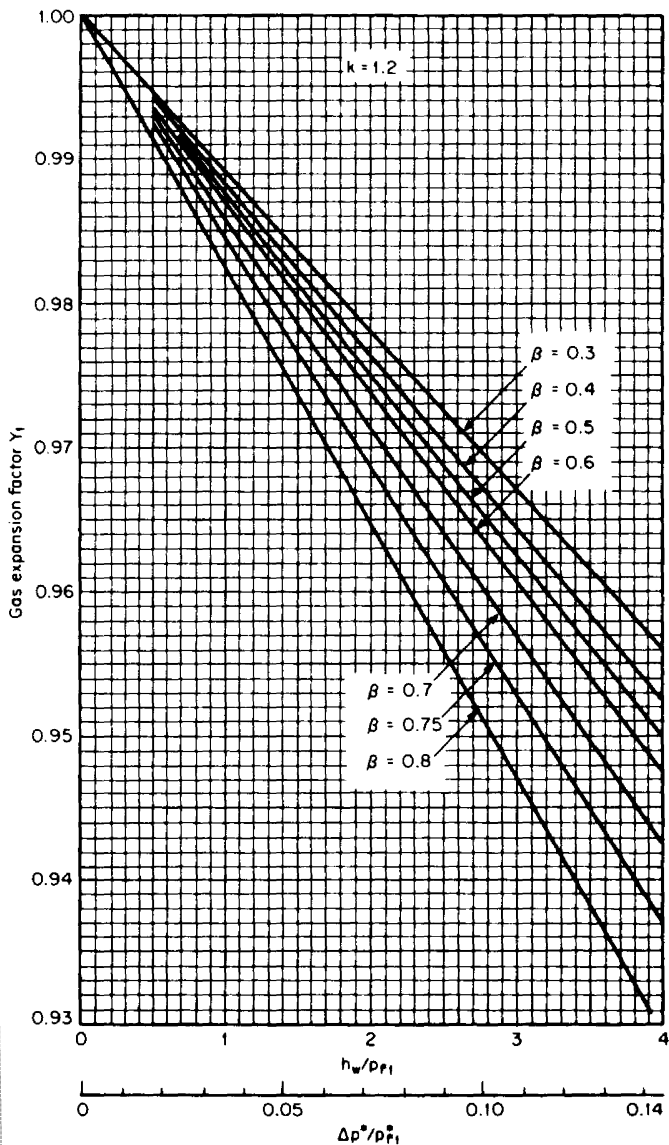


Figure 10.52 Gas expansion factor for eccentric orifice.

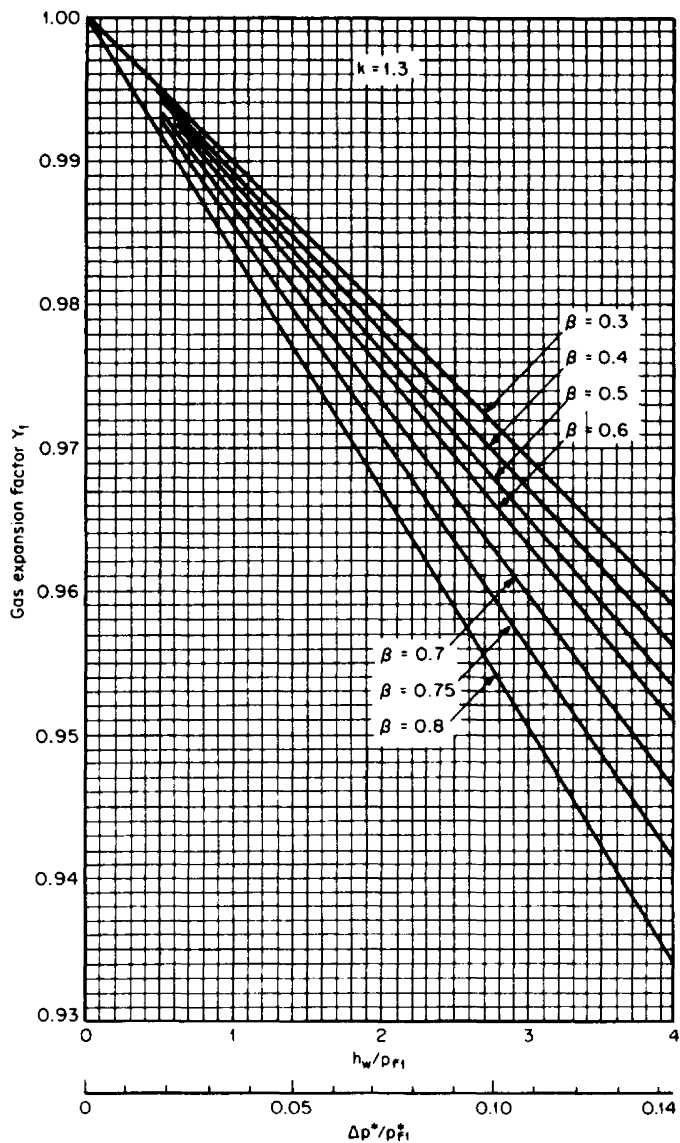


Figure 10.53 Gas expansion factor for eccentric orifice.

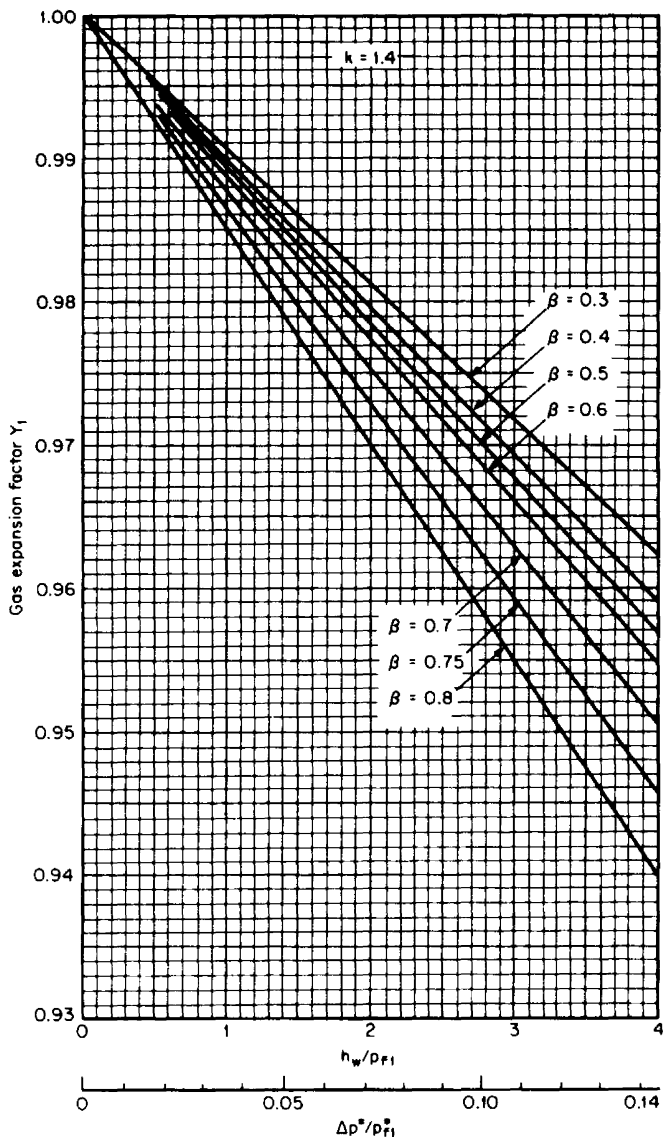


Figure 10.54 Gas expansion factor for eccentric orifice.

By entering Fig. 10.43 at this value, the discharge coefficient is read as $C = 0.641$. Substitution into Eq. (9.83), with $(Y_1)_0 = 1.0$ for liquids, gives

$$\beta_1 = \left\{ 1 + \left[\frac{C_0(Y_1)_0}{S_M} \right]^2 \right\}^{-1/4} = \left\{ 1 + \left[\frac{(0.641)(1.0)}{0.2500} \right]^2 \right\}^{-1/4} = 0.6028$$

A third estimate is unnecessary, since the discharge coefficient remains the same.

The diameter of the segment is

$$D_c = 0.980D = (0.98)(4.00) = 3.92 \text{ in}$$

and

$$\beta_c = \frac{\beta}{0.98} = \frac{0.6028}{0.98} = 0.6151$$

Either from Eq. (10.3) or by interpolation in Table 10.2,

$$\frac{H_s}{D_c} = 0.4038 + \left(\frac{0.4040 - 0.4038}{(0.61524 - 0.61503)} \right) (0.6151 - 0.61503) = 0.4039$$

and

$$H_s = 0.4039D_c = (0.4039)(3.92) = 1.583 \text{ in}$$

Eccentric orifice. From Eq. (1) of Table 9.28, the initial estimate for β is

$$\beta_0 = \left[1 + \left(\frac{0.607}{S_M} + 0.088 \right)^2 \right]^{-1/4} = \left[1 + \left(\frac{0.607}{0.2500} + 0.088 \right)^2 \right]^{-1/4} = 0.6077$$

From Figure 10.48 for flange taps and with this estimate of β ,

$$C_{\max} = 0.6442 \quad R_D = 10,000$$

$$C_{\min} = 0.6285 \quad R_D = 1,000,000$$

The equation constants are then, by Eqs. (10.5) and (10.6),

$$k_1 = 0.6442 - 1.11111(0.6442 - 0.6285) = 0.6268$$

$$k_2 = 111.111(0.6442 - 0.6285) = 1.744$$

The discharge coefficient at $R_D = 250,000$ is then, by Eq. (10.4),

$$C = k_1 + \frac{k_2}{R_D^{0.5}} = 0.6268 + \frac{1.744}{(250,000)^{0.5}} = 0.6303$$

The second estimate for β is, by Eq. (9.83) with $Y_1 = 1.0$ for liquids,

$$\beta_1 = \left\{ 1 + \left| \frac{C_0(Y_1)_0}{S_M} \right|^2 \right\}^{-1/4} = \left\{ 1 + \left| \frac{(0.6303)(1.0)}{0.2500} \right|^2 \right\}^{-1/4} = 0.6072$$

A third estimate is unwarranted, and the orifice bore is

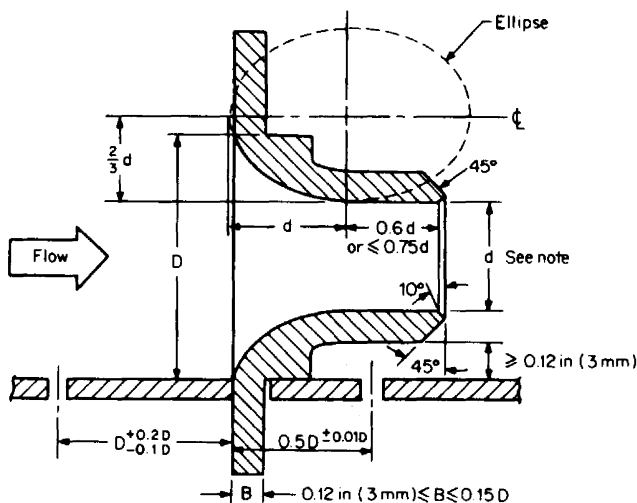
$$d = \beta D = (0.6072)(4.000) = 2.429 \text{ in}$$

CONTOURED DEVICES

Contoured inlet devices have the advantage of sweeping solids through the throat, and, with an attached divergent cone, of reducing permanent pressure loss. Usually these devices are of more rugged construction than orifices and, therefore, are more suitable for steam or other high-velocity applications.

Flow Nozzles

Several flow-nozzle contours are available. The ASME wall-tap flow nozzle (either low- or high- β series) is preferred in the United States, while in Europe the ISA 1932 design is widely used. In the United States, the ASME low- β -series nozzle is sometimes modified to have throat taps, and this has become the accepted standard for testing steam-turbine performance.



Note. For throat diameter, no measurement more than 0.05% from average of at least four measurements.

Figure 10.55 ASME long-radius nozzle, $0.2 \leq \beta \leq 0.5$ (low-beta).

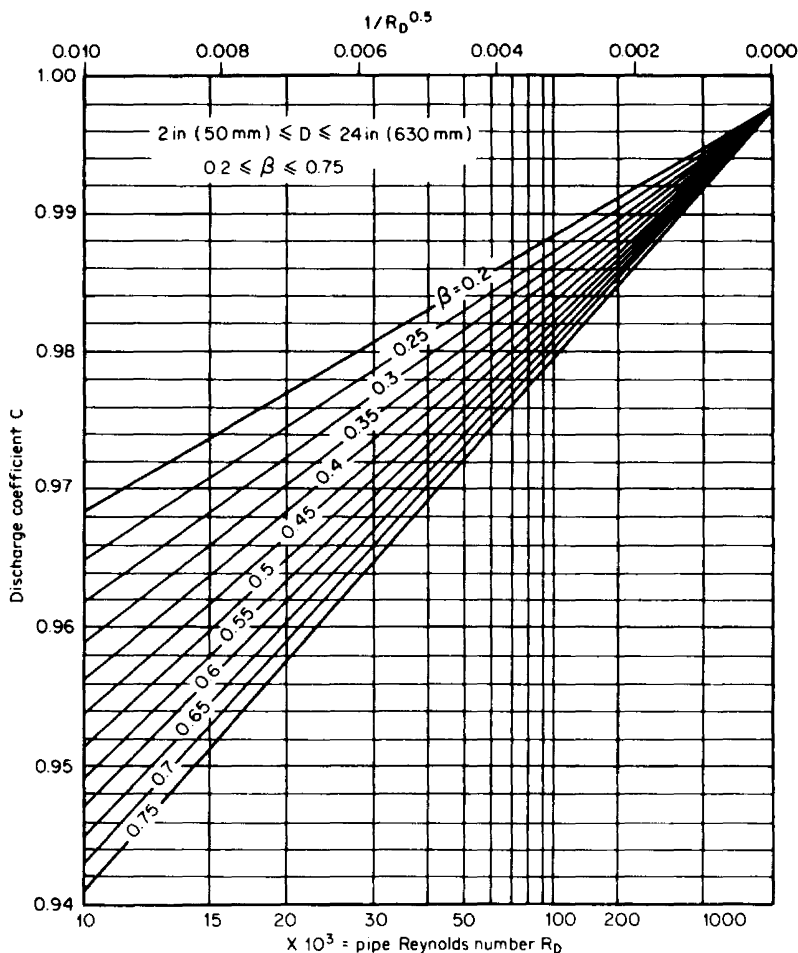


Figure 10.57 Discharge coefficient for ASME flow nozzle.

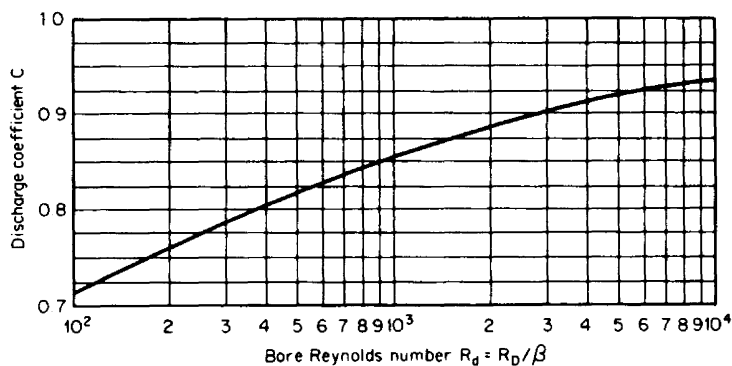
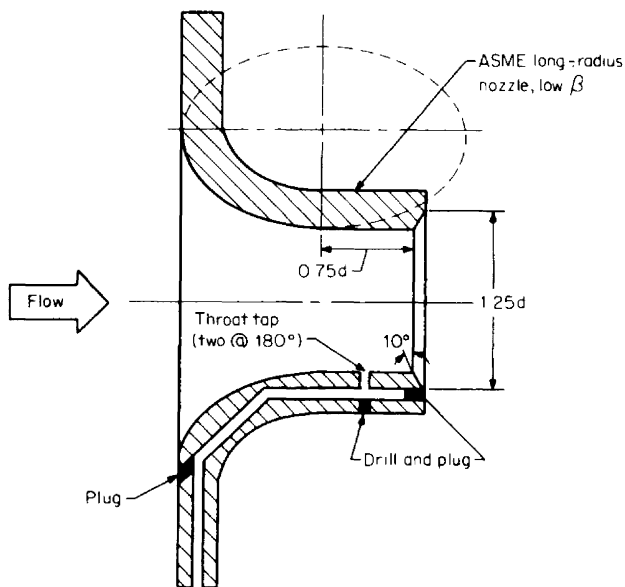
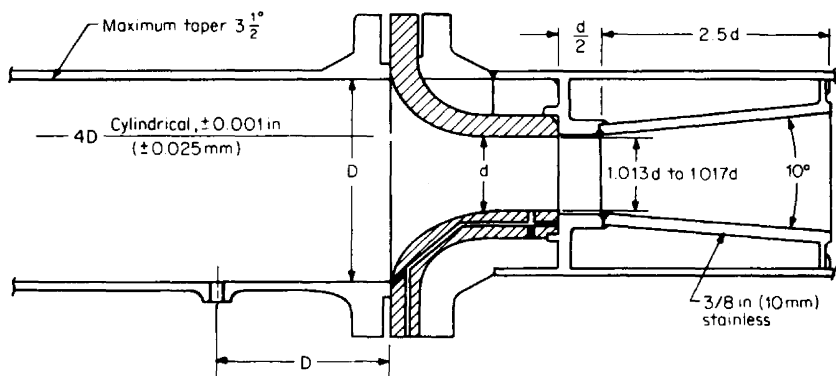


Figure 10.58 Discharge coefficient for ASME long-radius nozzle.

ASME Throat-Tap Nozzle (PTC-6 Nozzle). In the testing of steam turbines, a high degree of accuracy is required. Extensive test work on an ASME long-radius nozzle with diametric throat taps has led to standardization on the ANSI/ASME PTC-6 (1995) nozzle for these performance tests. The nozzle design is shown in Fig. 10.59.



(a)



(b)

Figure 10.59 ASME PTC-6 throat-tap nozzle. (a) Throat-tap nozzle. (b) With diffuser cone.

It is required that the nozzle be water-calibrated to the highest obtainable Reynolds number, and that the discharge-coefficient curve be within ± 0.25 percent of the curve shown in Fig. 10.60. The beta ratio is limited to 0.25 to 0.5. For beta ratios other than 0.43, the discharge coefficient-versus-bore Reynolds number curve must fit, within ± 0.25 percent, the equation shown in Fig. 10.60.

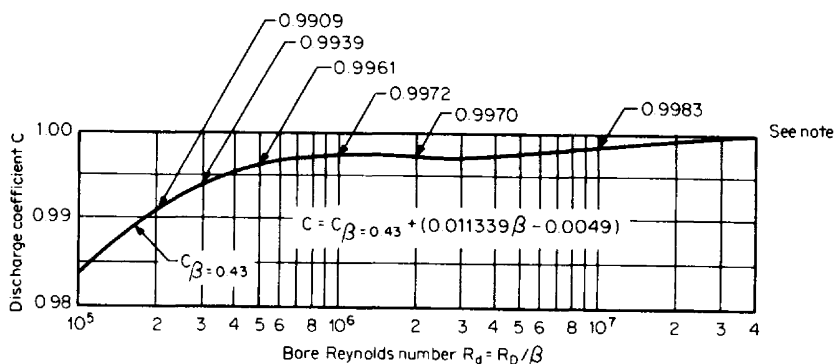


Figure 10.60 Discharge coefficient for ASME PTC-6 throat-tap nozzle, $0.25 \leq \beta \leq 0.5$.

For general applications, where performance testing is not required, the PTC-6 nozzle has a ± 0.5 percent uncalibrated accuracy. This compares to ± 2 percent for the wall-tap nozzle, and the added expense of tap drilling may be warranted if accuracy is desired.

ISA 1932 Nozzle. The ISA 1932 nozzle shown in Fig. 10.61 has a double-radius-contoured inlet with corner tapping. It is used extensively in Europe but seldom in the United States. The nozzle's discharge-coefficient equation is shown in Table 9.1 and graphed in Fig. 10.62.

Venturi Nozzle. The ISA 1932 nozzle, fitted with a venturi divergent downstream section, reduces the overall pressure loss. This nozzle, too, is widely used in Europe but seldom in the United States. The included angle may be from 10° to 30° , as shown in Fig. 10.63. The length of the divergent section has practically no influence on the discharge coefficient, but the truncated version, which has the maximum included angle, has a slightly higher pressure loss.

Classical Venturi Tube

The design of the classical, or Herschel, venturis is shown in Fig. 10.64. Depending on the manufacturing method, these are conveniently grouped as:

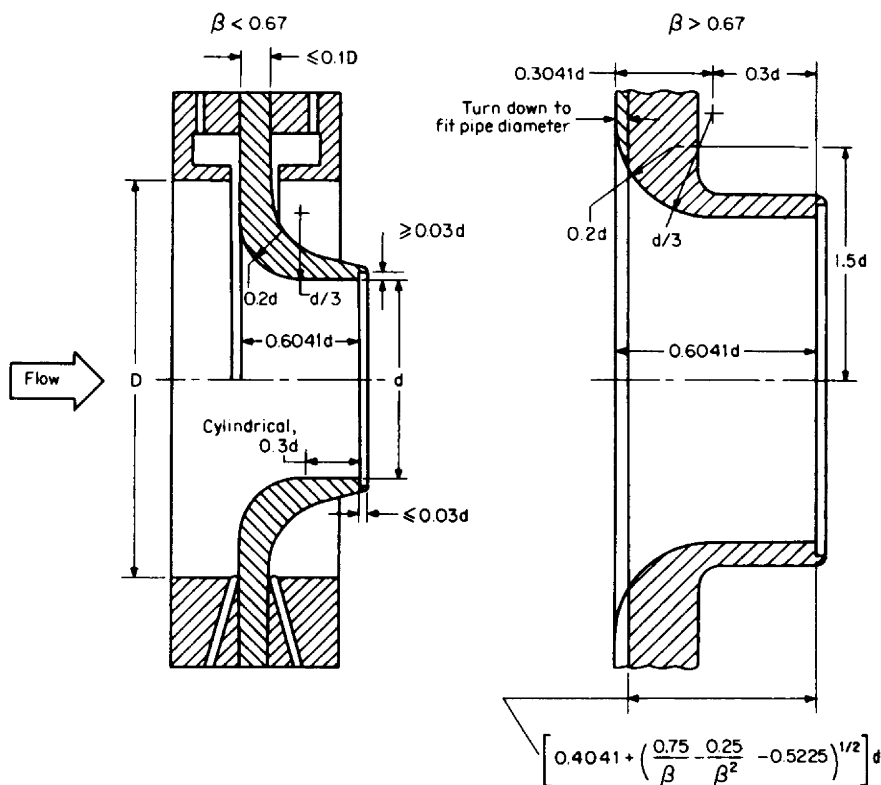


Figure 10.61 ISA nozzle.

1. Classical venturi with rough-cast inlet, recommended for line sizes of 4 to 32 in (100 to 800 mm)
2. Classical venturi with machined inlet, recommended for line sizes of 2 to 10 in (50 to 250 mm)
3. Classical venturi with rough-welded sheet-iron inlet, for line sizes of 8 to 48 in (200 to 1200 mm)

Venturis in the first two groups are cast in a sand mold, and the inlet may be left as cast (group 1) or machined (group 2). Although standards limit the maximum line size to 48 in (1200 mm), classical venturis have been fabricated for use in 120-in (3000-mm) lines. In the United States, the rough-cast inlet is almost always used, while in Europe all three groups are commonly used.

The exit cone (recovery cone) may have an included angle between 7° and 15°, with 7° being preferred for minimum permanent pressure loss. The 7° cone may be shortened to reduce lay-in length without significantly altering recovery.

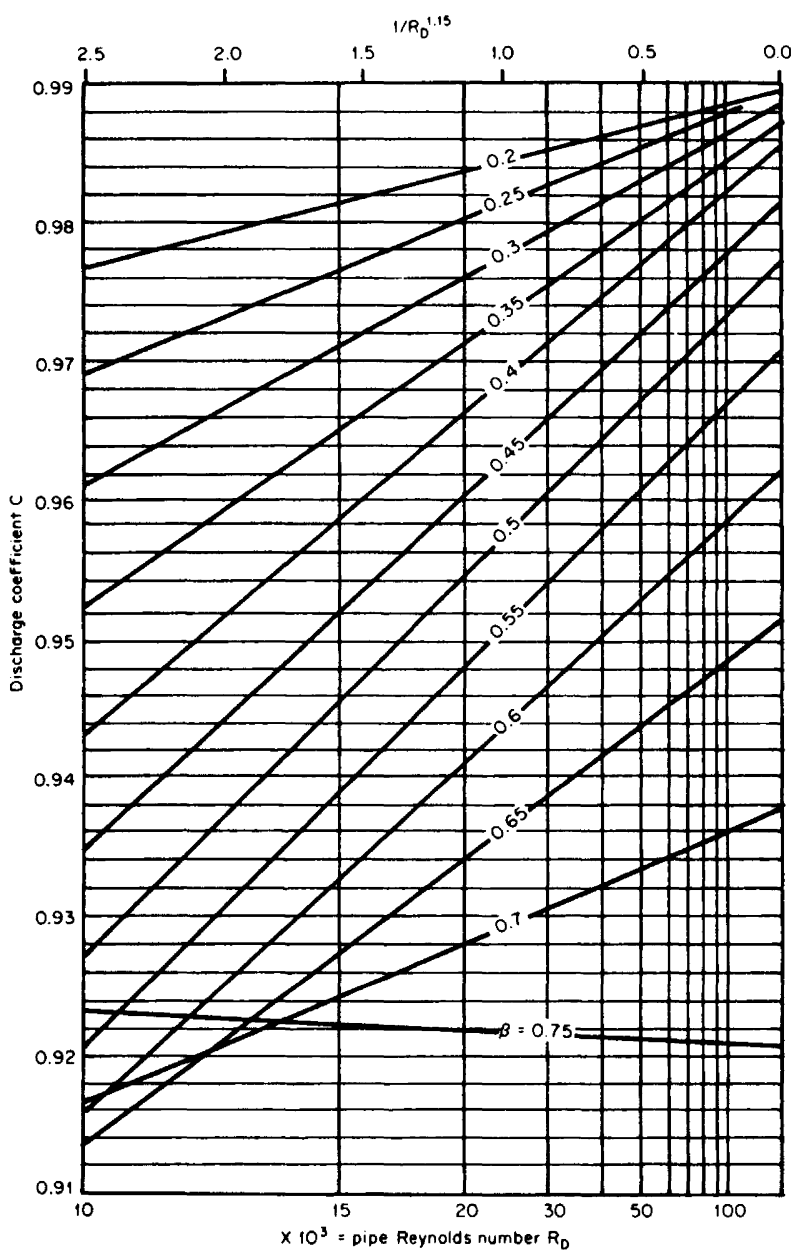


Figure 10.62 Discharge coefficient for ISA flow nozzle.

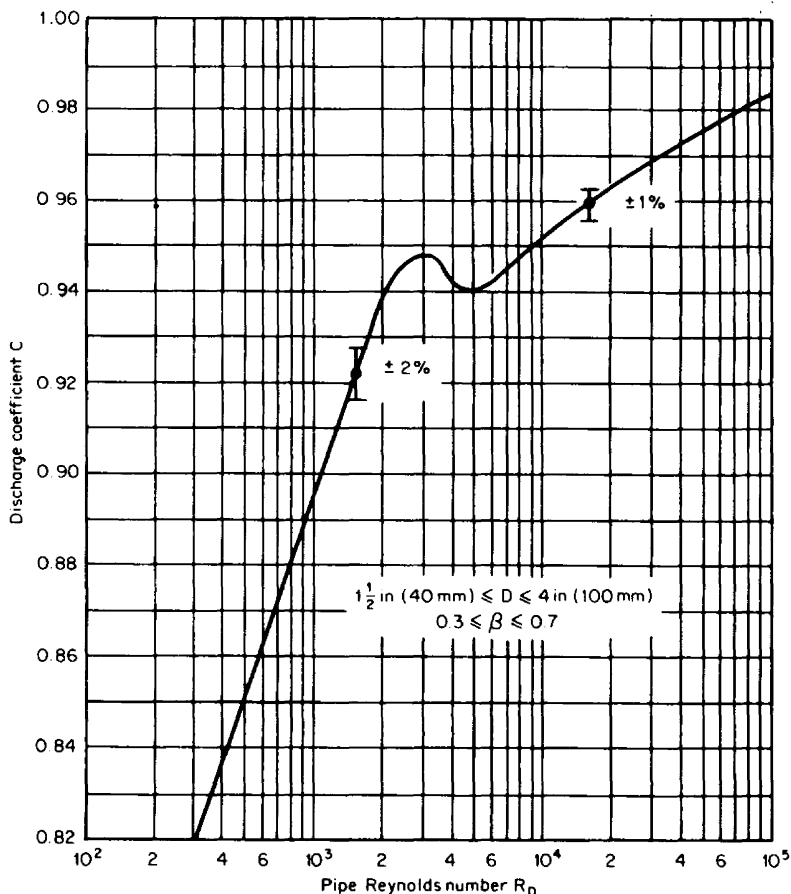


Figure 10.65 Discharge coefficient for venturi. (Fluidic Techniques, Inc., data, obtained in Foxboro Co. hydraulic laboratory; used with permission.)

Universal Venturi Tube

This proprietary device was designed to reduce overall lay-in length but retain the pressure recovery and coefficient constancy of the classical venturi. The *hydraulic shape* is shown in Fig. 10.66.

The manufacturer claims ± 0.5 percent discharge-coefficient accuracy with uncalibrated tubes for pipe Reynolds numbers greater than 75,000. Figure 10.67 gives the percent variation in discharge coefficient for Reynolds numbers down to approximately 7000. Several ASME papers by Halmi (1974) detail the hydraulic shape and discharge coefficient as well as the installation requirements, head loss, and compressible-flow characteristics. Inoue (1982) presents a generalized solution for the discharge coefficient of short laying length venturis. The manufacturer should

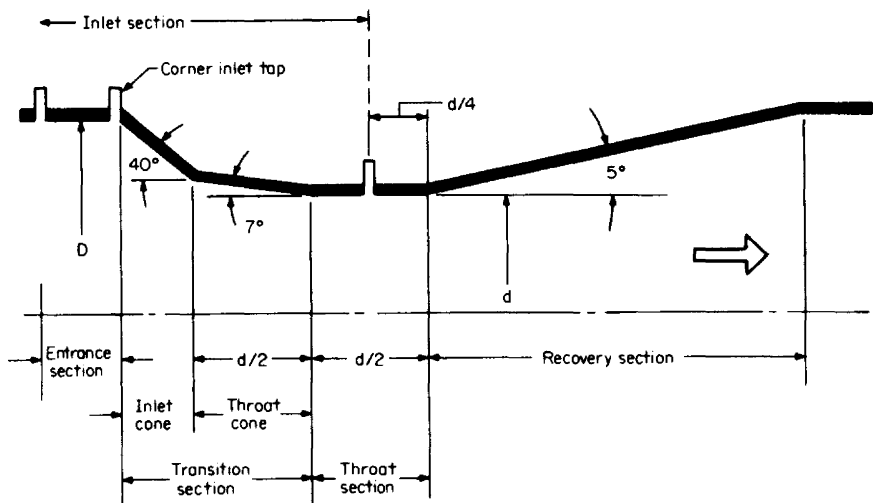


Figure 10.66 Hydraulic shape of the UVT. (Courtesy BIF.)

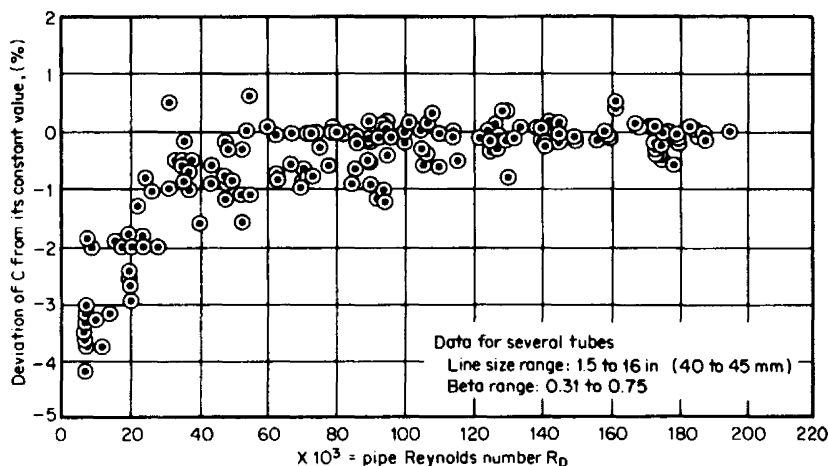


Figure 10.67 Discharge coefficient for Universal Venturi Tube. (Compiled by BIF.)

be consulted for exact sizing information, accuracy specifications, and installation recommendations.

Lo-Loss Flow Tube

Several proprietary primary devices are available which have low overall pressure loss relative to the produced differential. These include the Lo-Loss flow tube, the

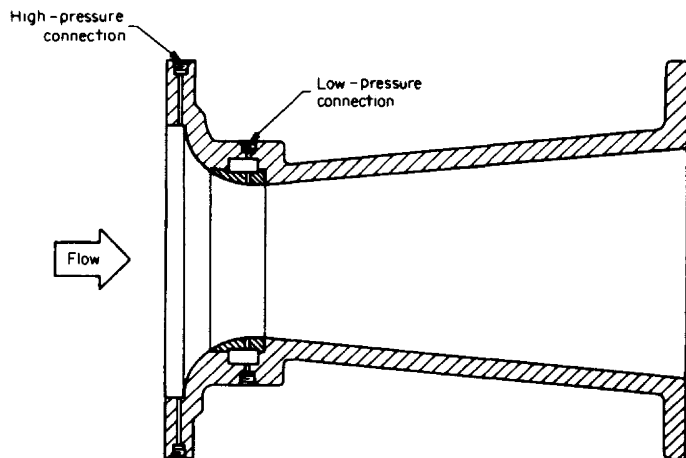


Figure 10.68 Lo-Loss flow tube. (Courtesy Badger Meter, Inc.)

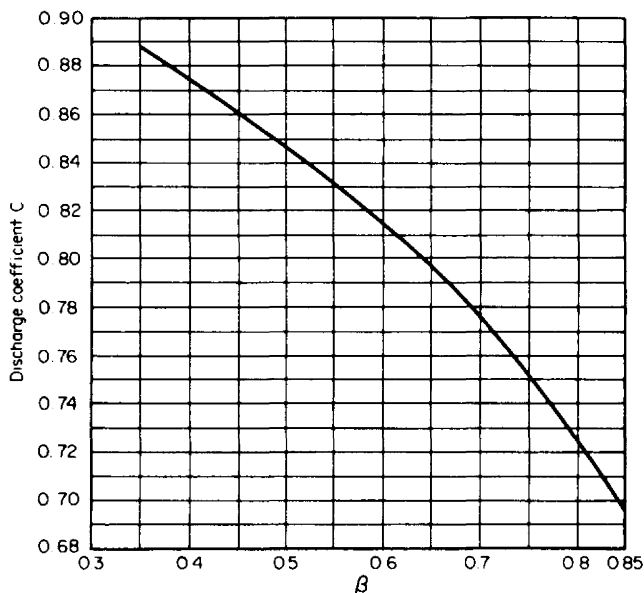


Figure 10.69 Discharge coefficient for Lo-Loss flow tube. (Courtesy Badger Meter, Inc.)

Dall Tube, the Foster flow tube (Gentile Tube), and the Twin Throat venturi tube.

In the Lo-Loss flow tube (Fig. 10.68), the upstream tap is located in the corner, and the downstream tap at or very close to the minimum throat diameter. This gives a higher differential than other tap locations, and the exit recovery cone reduces overall pressure loss.

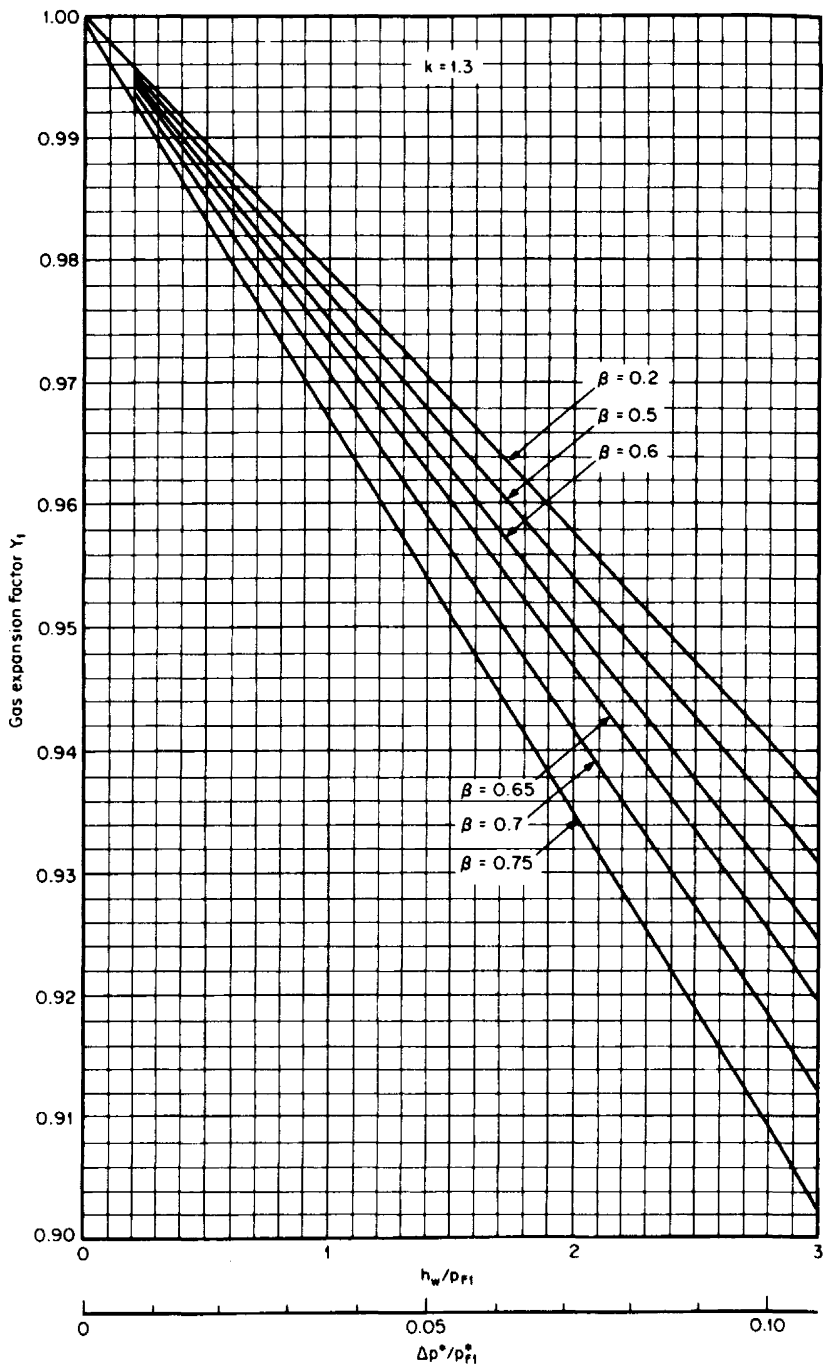


Figure 10.70 Gas expansion factor Y_1 for contoured-inlet primaries.

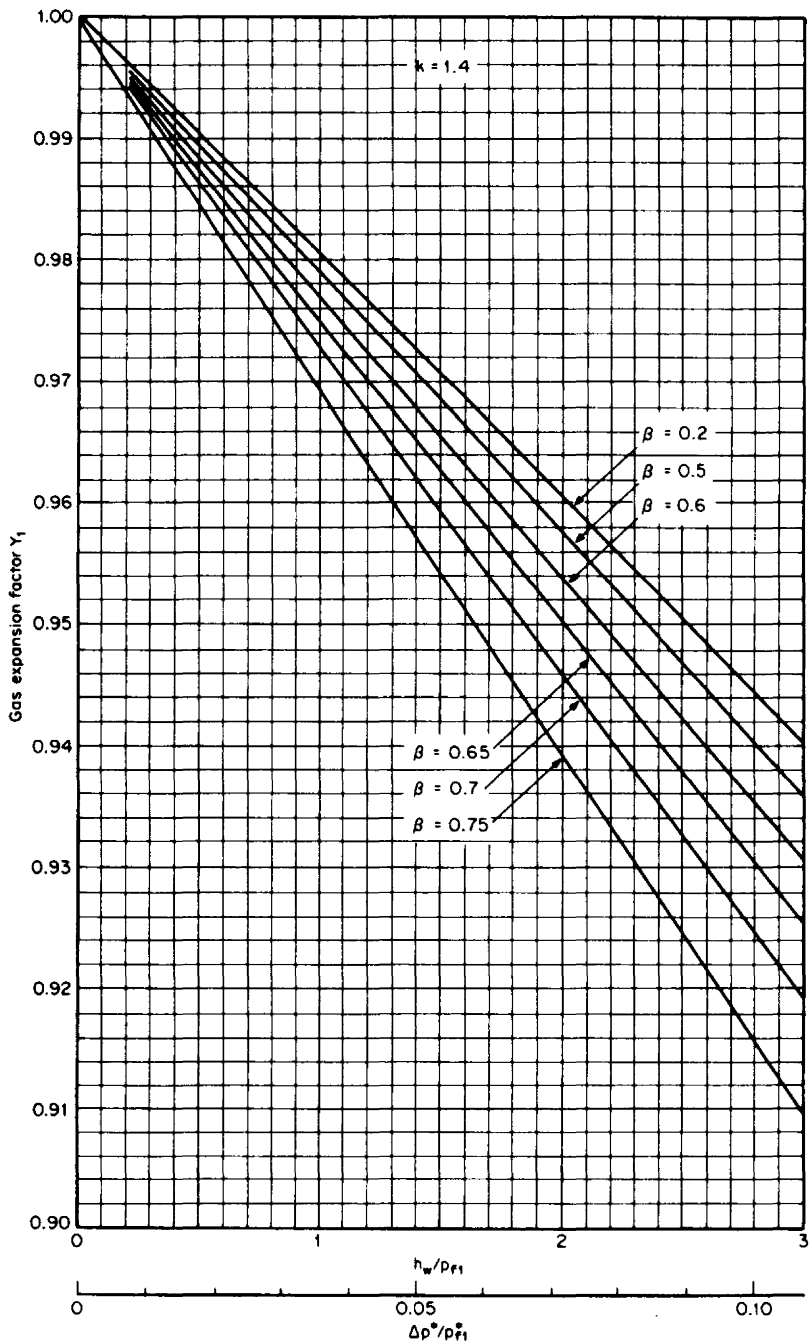


Figure 10.71 Gas expansion factor Y_1 for contoured-inlet primaries.

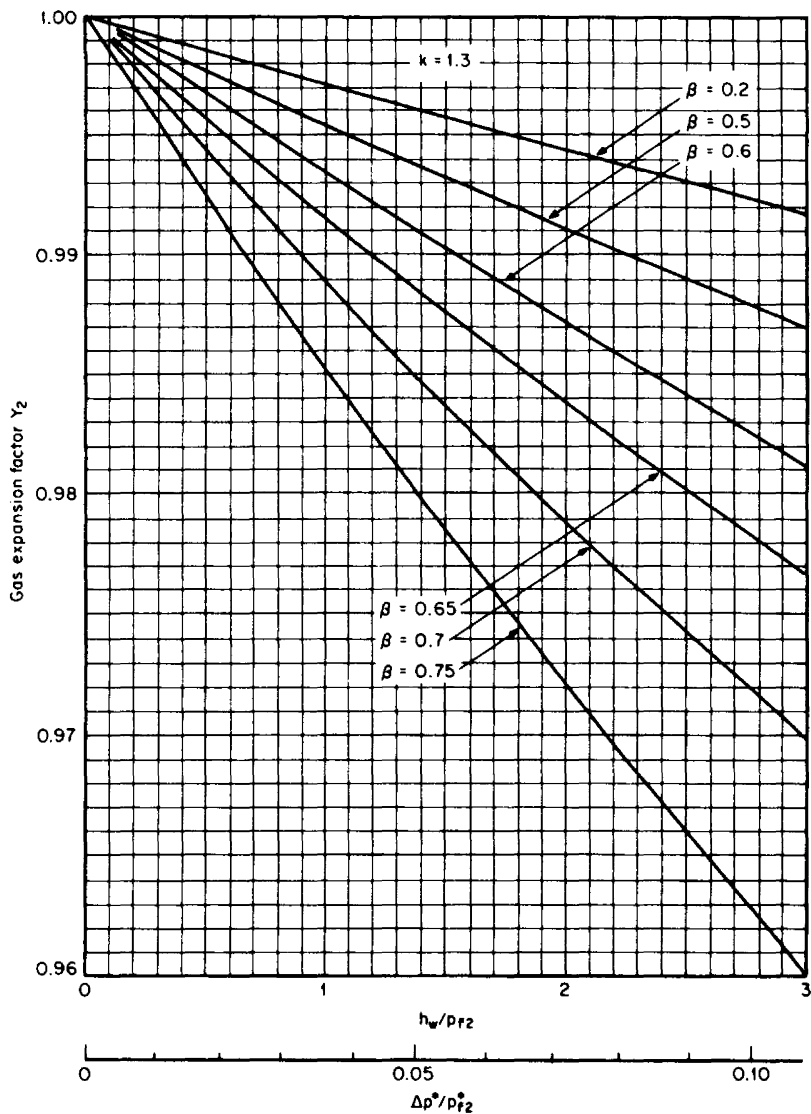


Figure 10.72 Gas expansion factor Y_2 for contoured inlet primaries.

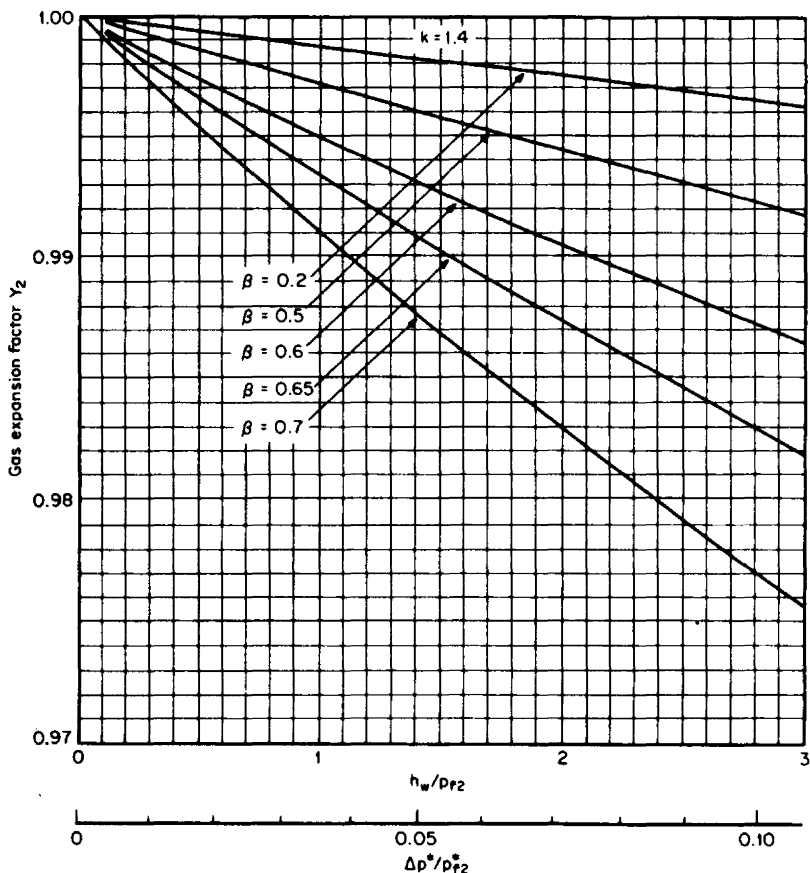


Figure 10.73 Gas expansion factor Y_2 for contoured inlet primaries.

The discharge coefficient is a function of β and is usually constant for pipe Reynolds numbers above 100,000. Its Reynolds-number range depends, however, on the manufacturer's recommendations and available test data. A graph of discharge coefficient versus β for a Lo-Loss flow tube is shown in Fig. 10.69. Similar curves are available from the manufacturers of the other designs.

GAS-EXPANSION-FACTOR CURVES

The gas expansion factor for contoured-inlet devices was derived in Chap. 9 and is expressed by Eq. (9.30). Curves of this equation are given in Figs. 10.70 through 10.73 for two different isentropic exponents and for upstream and downstream pressure measurements.

REFERENCES

- ANSI/ASME PTC-6, *Steam Turbines* (performance test code), ASME, New York, 1995.
- ASME MFC 3M: *Differential Producers Used for the Measurement of Fluid Flow in Pipes (Orifice, Nozzle, Nozzle Venturi, Venturi)*, ASME, New York, 1995.
- ASME: *Fluid Meters*, pp. 214–215, ASME, New York, 1971.
- Beitler, S. R., and D. J. Masson: "Calibration of Eccentric and Segmental Orifices in 4- and 6-in. Pipe Lines," *Trans. ASME*, vol. 71, p. 751, 1949.
- Benedict, R. P.: "Most Probable Discharge Coefficients for ASME Flow Nozzles," *J. Basic Eng.*, vol. 88, p. 734, 1966.
- BSI Standard 1042, *Methods for the Measurement of Fluid Flow in Pipes*, pt. 1, *Orifice Plates, Nozzles and Venturi Tubes*, UDC 53254.08, British Standards Institution, London, 1964.
- Eujen, E.: *Comparison Measurements between Two Different Primary Elements in the Range of Laminar Flow*, ISO/TC/30 (Germany 5) 83, International Standards Organization, Paris, 1977.
- Halmi, D.: "Metering Performance Investigation and Substantiation of the Universal Venturi Tube," pts. 1 and 2, *Fluids Eng.*, vol. 96, no. 2, pp. 124–138, 1974.
- Inoue, Masahiro: "Discharge Coefficient for Venturi Flowmeter with Short Laying Length," *J. Fluids Eng.*, ASME, vol. 104, no. 4, pp. 463–468, 1982.
- Lindahl, E. J., and S. R. Beitler: *Coefficients of Discharge for Eccentric and Segmental Orifices in 4-in., 6-in., 10-in., and 14-in. Pipe*, ASME Fluid Meters Research Report, 1954.
- Simpson, R. J.: "Flexible Orifice Plates," *Meas. and Control*, vol. 17, July/August 1984.
- Stolz, J.: "A Universal Equation for the Calculation of Discharge Coefficients of Orifice Plates," ISO 5167, *Flomeko 1978, IMEKO Conference on Flow Measurement of Fluids*, Groningen, North-Holland, Amsterdam, 1978.
- Teyssandier, R. G.: "Discharge Coefficients for Small (<100 mm) ASME Long Radius Nozzles," *ASME paper 86-WA/FM-2*, December 1986.

DIFFERENTIAL PRODUCERS: FIXED-GEOMETRY DEVICES

Chapter 9 covers differential producers that are sized by determining primary-element dimensions that will produce a chosen differential at a design flow rate. An alternative is to select a fixed-geometry primary device. These have limited dimensional selectivity; therefore, the differential pressure or target force, rather than the flowmeter dimensions, must be calculated to match the design flow rate.

Arithmetic-progression orifices, annular orifices, target flowmeters, integral orifices, Annubars, and elbow flowmeters are covered in this chapter. The flow-rate equations developed in Chap. 9 (Tables 9.36 through 9.38) apply to these devices. However, several of the symbols may be changed, grouped, or set equal to 1, depending on the device, how the geometry affects the differential pressure or target force, and whether an expansion factor is required. Table 11.1 presents the necessary modifications to these equations. The necessary graphs and equations and examples of the calculation procedure are given in the remainder of this chapter.

ARITHMETIC-PROGRESSION ORIFICES (EVEN-SIZED ORIFICES)

To change flow capacity, many plants stock a series of orifice plates with fixed-increment (arithmetic-progression) bore increases. Measurement equipment, pipe diameter, and fluid properties remain constant, and it becomes necessary to determine flow rates for fixed-range differential-pressure transmitters (50 in, 100 in, etc.). The general form of the flow-rate equation is given by Eq. (9.103) as

$$q = N \frac{CY\beta^2}{\sqrt{1 - \beta^4}} D^2 f(\rho) \sqrt{h_w} \quad (9.103)$$

where $d^2 = \beta^2 D^2$ has been substituted. With constant fluid properties, design URV differential, and pipe size, the variables are conveniently grouped as

$$q = \frac{CY\beta^2}{\sqrt{1 - \beta^4}} [ND^2 f(\rho) \sqrt{h_w}] \quad (11.1)$$

where the bracketed term remains constant for a given differential, and the β -dependent quantities change with bore increment and Reynolds number. Equation

TABLE 11.1 Substitution of Variables in the Flow-Rate Equations of Tables 9.36 through 9.38

Primary element	$\frac{C}{\sqrt{1 - (d/D)^4}}$	Y_1	F_α	Geometry factor d^2		Differential pressure	
				U.S. units	SI units	U.S. (h_w)	SI (Δp^*)
Arithmetic progression orifice (even-sized)	$\frac{C}{\sqrt{1 - \beta^4}}$	Y_1 (Table 9.26)	F_α, F_α^* [Eqs. (9.52), (9.54)]	$\beta^2 D^2$	$\beta^2 D^{*2}$	h_w	Δp^*
Annular orifice	K (Fig. 11.2)	1.0	F_α, F_α^* [Eqs. (11.6), (11.7)]	$(1 - \beta_T^2)D^2$	$(1 - \beta_T^2)D^{*2}$	h_w	Δp^*
Target flowmeter (Foxboro)	K (Figs. 11.4–11.11, Table 11.3)	1.0	F_α, F_α^* [Eqs. (11.6), (11.7)]	$5.941939 \frac{1 - \beta_T^2}{\beta_T} D$ (D = meter bore)†	$35.68248 \left(\frac{1 - \beta_T^2}{\beta_T} \right) D^*$ (D^* = meter bore)†	F_T	F_T^*
Integral orifice	K (Foxboro, Table 11.4, Figs. 11.17–11.22; Taylor, Table 11.4)	1.0	F_α, F_α^* [Eqs. (9.52), (9.54)]	d^2	d^{*2}	h_w	Δp^*
Annubar† (Dieterich Standard Corp.)	$F_K K_{\text{ref}}$ (Tables 11.6, 11.7)	Y_1 (Table 11.8)	F_α, F_α^* [Eqs. (9.52), (9.54)]	D^2	D^{*2}	h_w	Δp^*
Diamond II	K (Table 11.9)						
Elbow	K [Table 11.8, Eq. (11.8)]	1.0	F_α, F_α^* [Eqs. (9.52), (9.54)]	D^2	D^{*2}	h_w	Δp^*

†See Table 11.2.

‡Dieterich Standard Corp.

(11.1) is nonlinear and therefore must be solved by iteration to calculate the flow rate.

The solution rapidly converges if an initial discharge coefficient of 0.6 is assumed. The first estimate for the flow rate then is

$$q_0 = \frac{0.6Y\beta^2}{\sqrt{1-\beta^4}} ND^2 f(\rho) \sqrt{h_w} \quad (11.2)$$

With this estimate, the Reynolds number is calculated by using the equations of Tables 9.20 through 9.22, and the discharge coefficient is either calculated with the equations of Table 9.1 or obtained from the curves presented in Chap. 10. The second flow-rate estimate is then

$$q_1 = \frac{C_1 Y \beta^2}{\sqrt{1-\beta^4}} ND^2 f(\rho) \sqrt{h_w} \quad (11.3)$$

Depending on the desired accuracy, the procedure may be repeated by recalculating the Reynolds number, recalculating the discharge coefficient, and then substituting into Eq. (11.3).

INTEGRAL ORIFICE

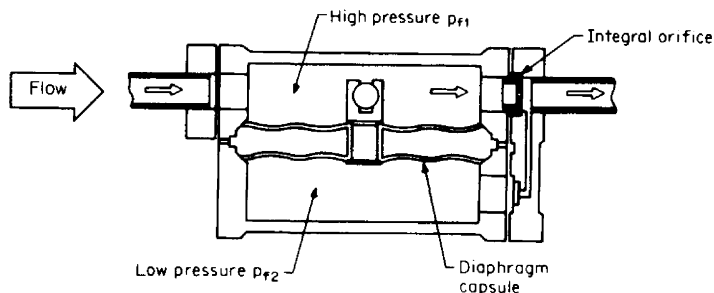
Several manufacturers install fixed-bore orifices in manifolds that are an *integral* part of the differential-pressure transmitter. These not only provide a compact installation but also extend differential producers to very low flow-rate capabilities—for liquids down to 0.04 gal/min (0.015 L/min), and for gases as low as 0.9 standard ft³/h (25 standard L/h).

The wide range of today's differential-pressure transmitters [5 to 850 in (1.3 to 210 kPa)], combined with available bore sizes, provides a wide flow-rate capability. Accuracies of 1½ to 3 percent are claimed for uncalibrated units over selected Reynolds-number ranges. Felton (1972) presents calibration data collected over a 4-year period that demonstrates a precision of ±0.25 percent.

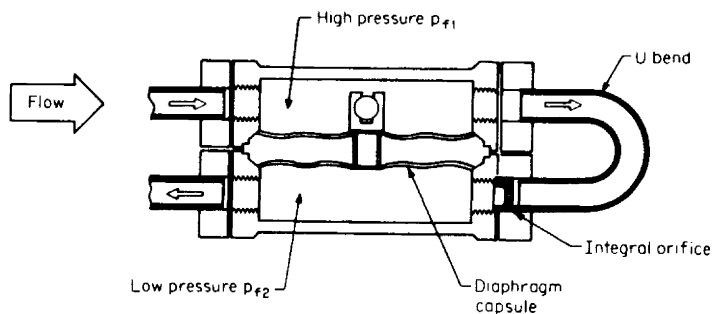
Foxboro offers two integral-orifice flow assemblies, the in-line type and the U-bend type. The in-line type, illustrated in Fig. 11.1a, is designed for the process fluid to pass through the high-pressure side of the transmitter and the orifice only. A cross-port in the manifold, just downstream of the orifice, allows the lower downstream pressure to be sensed by the low-pressure side of the transmitter. In the 180° U-bend type, shown in Fig. 11.1b, process fluid enters the transmitter's high-pressure side, passes through a U bend which contains the orifice, and then exits through the low-pressure side. This design virtually eliminates cavities and dead-end passageways, making it ideal for fluids which may precipitate solids, congeal, or polymerize and for vapors that tend to condense. Both process connections are on the same end of the transmitter body.

The Taylor integral orifice is an in-line flow-element assembly (Fig. 11.2a), close-coupled to the differential-pressure transmitter (Fig. 11.2b). Inlet piping is either 1-in NPT (25 mm) or 1½-in NPT (40 mm). Liquids, gases, and steam can be measured.

For both Foxboro and Taylor integral orifices, the flow equation is modified by replacing $C/\sqrt{1-(d/D)^4}$ with the flow coefficient K and Y_1 with 1.0.



(a)



(b)

Figure 11.1 Foxboro in-line and U-bend integral orifices. (a) In-line. (b) U-bend.

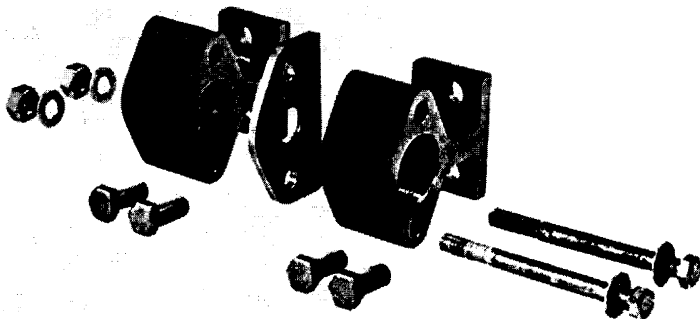
Available orifice bores, uncalibrated accuracy, Reynolds-number ranges, and flow coefficients are given in Tables 11.2 and 11.3. In Figs. 11.3 through 11.8 are curves of flow coefficient versus bore Reynolds number for the Foxboro orifices. Because of the tap locations, the permanent pressure loss equals the operating differential pressure. For gas (vapor) flows, no gas expansion factor has been determined. It is recommended that pressure ratios be limited to

$$\frac{h_w}{p_{f1}} \leq 1.5 \quad \text{and} \quad \frac{\Delta p^*}{p_{f1}^*} \leq 0.054$$

Example 11.1. A 0.020-in (0.508-mm) Foxboro stainless-steel integral orifice is to measure the flow rate of the gasoline of Example 2.12. The maximum flow rate is 0.025 flowing gal/min (0.095 flowing L/min). Determine (1) the upper-range value for the differential-pressure transmitter and (2) the flow rate when the differential pressure is 20 percent of the URV.

The flow-rate equation for flowing gallons per minute is, from Eq. (d) of Table 9.36,

$$q_{\text{gpm}} = N_{vG} \frac{Cd^2}{\sqrt{1 - (d/D)^4}} \frac{1}{\sqrt{F_p G_F}} \sqrt{h_w}$$



(a)



(b)

Figure 11.2 Taylor in-line integral orifice. (a) Orifice assembly. (b) Installed with transmitter.
(Courtesy ABB-Kent Taylor.)

TABLE 11.2 Integral-Orifice Bores and Flow Coefficients (Foxboro, Taylor)

Orifice bore, d , in (mm)	Accuracy (uncalibrated flow coefficient), %	Reynolds-number limits†	Flow coefficients K	
			In line	U bend
Foxboro				
0.0200 (0.508)	± 3	$R_d \geq 3,000$ $R_d < 3,000$	0.868 See Fig. 11.3	0.921
0.0340 (0.8636)	± 3	$R_d \geq 10,000$ $R_d < 10,000$	0.906 See Fig. 11.4	0.930
0.0595 (1.5113)	± 3	$R_d \geq 2,000$ $R_d < 2,000$	0.882 See Fig. 11.5	0.890
0.0995 (2.5273)	± 3	$R_d \geq 1,500$ $R_d < 1,500$	0.806 See Fig. 11.6	0.850
0.1590 (4.0386)	± 3	$R_d \geq 1,000$ $R_d < 1,000$	0.772 See Fig. 11.7	0.821
0.250 (6.350)	± 3	$R_d \geq 2,000$ $R_d < 2,000$	0.855 See Fig. 11.8	0.911
Taylor				
0.020 (0.508)	± 5	$R_D \geq 5,000$ $D = 1$ in $D^* = 25$ mm	0.645	
0.035 (0.888)	± 5		0.635	
0.065 (1.651)	± 4		0.620	
0.113 (2.870)	± 2		0.605	
0.196 (4.9784)	± 2	$R_D \geq 5,000$ $D = 1.5$ in $D^* = 40$ mm	0.603	
0.340 (8.636)	± 2		0.605	
0.500 (12.700)	± 2		0.630	
0.735 (18.669)	± 2		0.715	
0.500 (12.700)	± 1.5	$R_D \geq 5,000$ $D = 1.5$ in $D^* = 40$ mm	0.611	
0.612 (15.545)	± 1.5		0.614	
0.750 (19.05)	± 1.5		0.623	
0.917 (23.292)	± 1.5		0.650	
1.127 (28.626)	± 1.5		0.714	

† R_d = bore Reynolds number; R_D = pipe Reynolds number.

TABLE 11.3 Integral and Annular Orifice Flow-Coefficient Equations

Orifice bore d , in (mm)	R_d	Flow coefficient K
Integral orifice		
0.0200 (0.508)	$\geq 3,000$	0.868
	$< 3,000$	$2.194 - 0.906 \ln (R_d) + 0.165[\ln (R_d)]^2 - 0.0091[\ln (R_d)]^3$
0.034 (0.8636)	$\geq 10,000$	0.906
	$< 10,000$	$0.2025 + 0.0834 \ln (R_d) + 0.0067[\ln (R_d)]^2 - 0.00082[\ln (R_d)]^3$
0.0595 (1.5113)	$\geq 2,000$	0.889
	$< 2,000$	$-0.5395 + 0.4548 \ln (R_d) - 0.0505[\ln (R_d)]^2 + 0.00201[\ln (R_d)]^3$
0.0995 (2.5273)	$\geq 1,500$	0.806
	$< 1,500$	$0.2015 + 0.1031 \ln (R_d) + 0.0051[\ln (R_d)]^2 - 0.001076[\ln (R_d)]^3$
0.1590 (4.0386)	$\geq 1,000$	0.772
	$< 1,000$	$-0.5271 + 0.4704 \ln (R_d) - 0.0542[\ln (R_d)]^2 + 0.00193[\ln (R_d)]^3$
0.250 (6.350)	$\geq 2,000$	0.855
	$< 2,000$	$-1.3115 + 0.7769 \ln (R_d) - 0.0962[\ln (R_d)]^2 + 0.00414[\ln (R_d)]^3$
Annular orifice		
$0.6684 + 1.376 \beta_T - 3.266 \beta_T^2 + 1.911 \beta_T^3$		

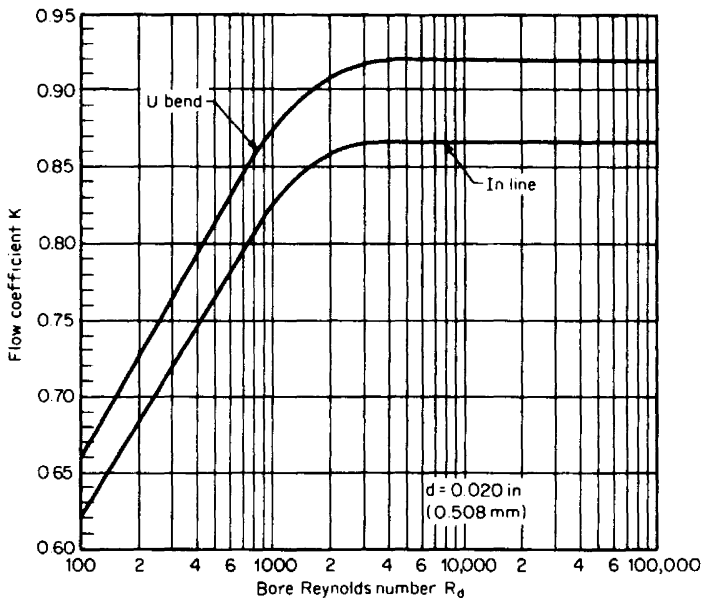


Figure 11.3 Integral-orifice flow coefficient K : $d = 0.020$ in (0.508 mm). (Courtesy The Foxboro Co.)

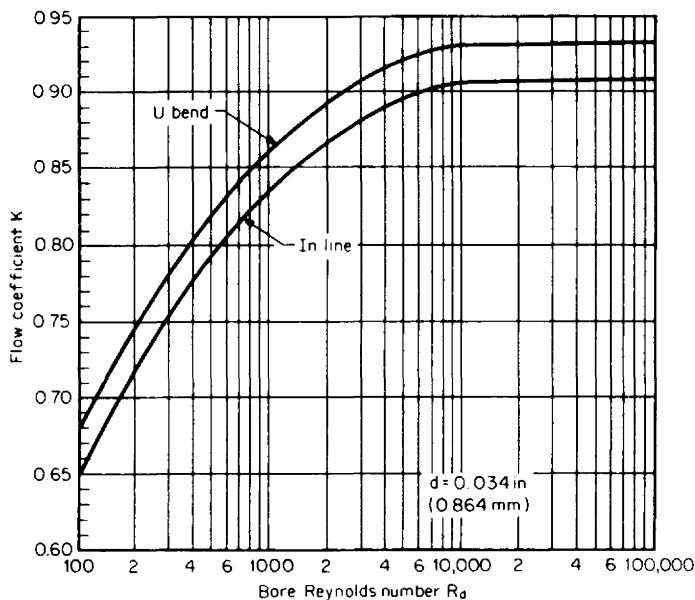


Figure 11.4 Integral-orifice flow coefficient K : $d = 0.034 \text{ in}$ (0.864 mm). (Courtesy The Foxboro Co.)

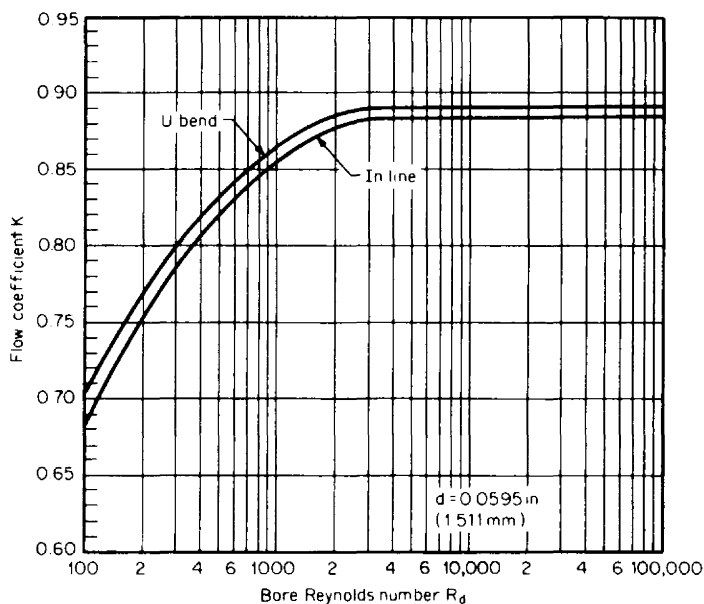


Figure 11.5 Integral-orifice flow coefficient K : $d = 0.0595 \text{ in}$ (1.511 mm). (Courtesy The Foxboro Co.)

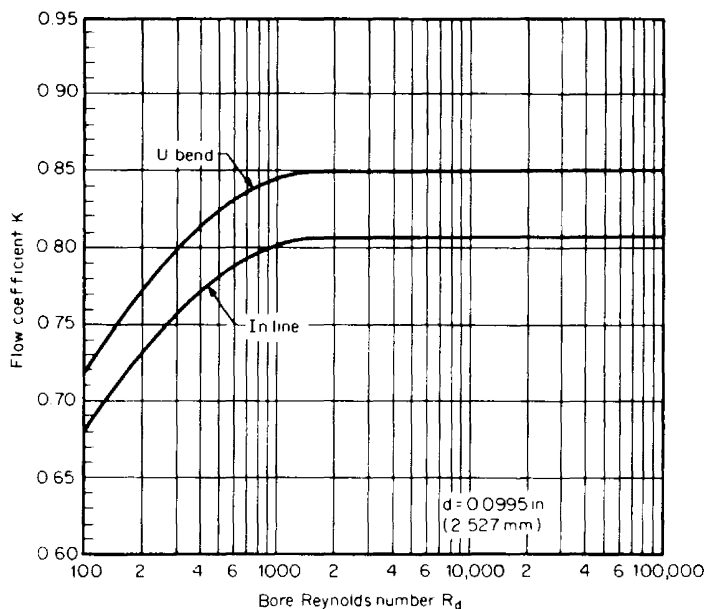


Figure 11.6 Integral-orifice flow coefficient K : $d = 0.0995 \text{ in}$ (2.527 mm). (Courtesy The Foxboro Co.)

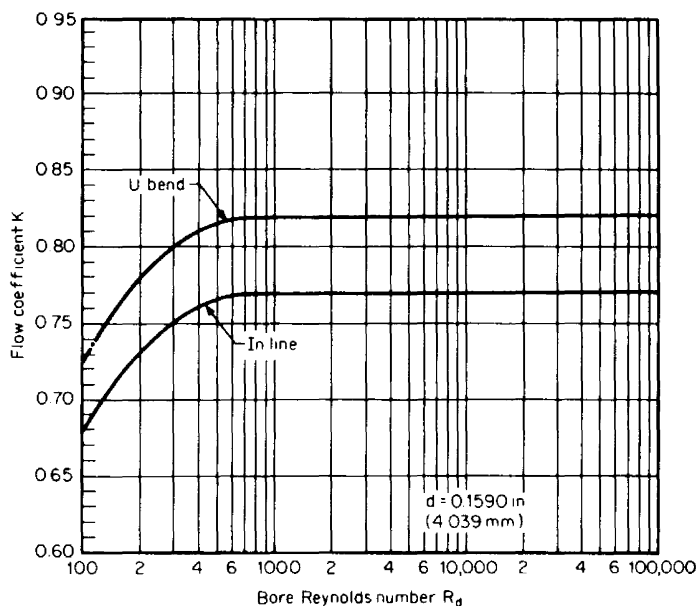


Figure 11.7 Integral-orifice flow coefficient K : $d = 0.1590 \text{ in}$ (4.039 mm). (Courtesy The Foxboro Co.)

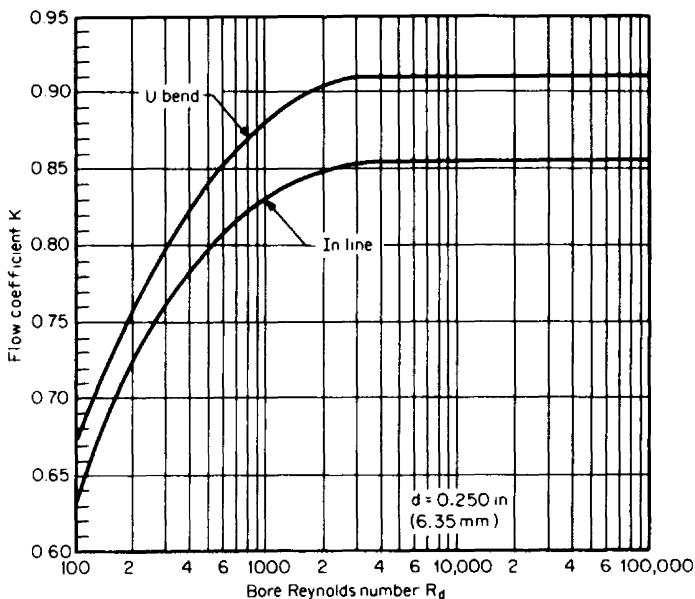


Figure 11.8 Integral-orifice flow coefficient K : $d = 0.250$ in (6.35 mm). (Courtesy The Foxboro Co.)

Substitution of variables from Table 11.1 gives the integral-orifice flow-rate equation as

$$q_{\text{gpm}} = N_{vG} K d^2 \frac{\sqrt{h_w}}{\sqrt{F_p} \sqrt{G_F}}$$

The design information is as follows:

- From Table 9.16: $N_{vG} = 5.6665$
- From Example 9.1: $F_{ad} = 1 + (0.0000096)(80.5 - 68) = 1.0001$
- From Example 2.15: $F_p = 1.0088$
- From Example 2.12: $G_F = 0.7255$

The bore of the integral orifice at 80.5°F is, by Eq. (9.51),

$$d = F_{ad} d_{\text{meas}} = (1.0001)(0.020) = 0.020$$

Scaling the flow rate to normal operating conditions and rearranging the flow-rate equation to solve for the differential give

$$\begin{aligned} h_w &= \left(\frac{\sqrt{F_p} \sqrt{G_F} q_{\text{gpm}}}{N_{vG} K d^2} \right)^2 = \left[\frac{\sqrt{1.0088} \sqrt{0.7255} (0.025)(0.8)}{(5.6665)(K)(0.020)^2} \right]^2 \\ &= \frac{59.96}{K^2} \end{aligned}$$

The bore Reynolds number at normal conditions is calculated from Eq. (d) of Table 9.20 with bore diameter substituted for pipe diameter:

$$R_d = 17,903 \frac{F_p G_F}{\mu_{cp} d N_{vG}} q_{\text{gpm}} = 17,903 \frac{(1.0088)(0.7255)}{(0.417)(0.020)(5.6665)}$$

$$q_{\text{gpm}} = 277,260 q_{\text{gpm}}$$

$$(R_d)_N = (277,260)(0.025)(0.8) = 5,545$$

where $\mu_{cp} = 0.417$ from Example 9.3. The flow coefficient $K = 0.868$ is constant for $R_d > 3000$.

1. Substitution gives the differential at normal operating conditions as

$$(h_w)_N = \frac{56.96}{K^2} = \frac{56.96}{(0.868)^2} = 75.60 \text{ in}$$

The differential at URV flow is then

$$(h_w)_{\text{URV}} = 75.60 \frac{1}{0.64} = 118.1 \text{ in}$$

2. Assuming the flow coefficient is constant, the flow-rate equation gives

$$\begin{aligned} q_{\text{gpm}} &= N_{vG} K F_a d^2 \frac{\sqrt{h_w}}{\sqrt{F_p} \sqrt{G_F}} = (5.6665)(0.868)(0.020)^2 \frac{\sqrt{h_w}}{\sqrt{1.0088} \sqrt{0.7255}} \\ &= F_{MC} \sqrt{h_w} = 0.00230 \sqrt{h_w} \end{aligned}$$

where the meter-coefficient factor $F_{MC} = 0.00230$. The flow rate at 20 percent URV is then

$$q_{\text{gpm}} = F_{MC} \sqrt{h_w} = 0.00230 \sqrt{(0.20)(118.1)} = 0.0112 \text{ gal/min}$$

Example 11.2. For a maximum differential pressure of 50 kPa, select the bore and determine the URV for a differential-pressure transmitter for (1) Foxboro and (2) Taylor stainless-steel integral orifices to measure an airflow of 50 standard L/min (ISO Standard 5024 base). The air is flowing at a temperature of 27°C and an absolute pressure of 1000 kPa.

The flow-rate equation, from Eq. (1) of Table 9.37, is

$$q_{\text{SLPM}}^* = N_{vPT}^* \frac{Cd^{*2}}{\sqrt{1 - (d^*/D^*)^4}} \frac{Y_1 Z_b \sqrt{p_{f1}^*}}{\sqrt{G Z_{f1}} T_{K1}} \sqrt{\Delta p^*}$$

Substitution of variables from Table 11.1 gives the integral-orifice flow-rate equation as

$$q_{\text{SLPM}}^* = N_{vPT}^* K F_a^* Z_b d^{*2} \frac{\sqrt{\Delta p^*} p_{f1}^*}{\sqrt{Z_{f1}} \sqrt{T_{K1}} \sqrt{G}}$$

From Table 9.17, $N_{vPT}^* = 3.2111$, and from Eq. (9.54) and Table B.4,

$$F_a^* d = 1 + \alpha_{PE}^* (T_c - 20) = 1 + (0.0000173)(27 - 20) = 1.0001$$

From Table G.2, $Z_{f1} = 0.9974$, and from Eq. (3.39),

$$T_{K1} = 273.17 + 27 = 300.15 \text{ K}$$

For air, $G = 1.0$, and Z_b is assumed equal to 1.0. Then, rearranging the flow-rate equation to solve for the differential pressure gives

$$\begin{aligned} \Delta p^* &= \left(\frac{\sqrt{Z_{f1}} \sqrt{T_{K1}} \sqrt{G} q_{\text{SLPM}}^*}{N_{\text{vPT}}^* K Z_b d^{*2} \sqrt{p_{f1}^*}} \right)^2 = \left[\frac{\sqrt{0.9974} \sqrt{300.15} \sqrt{1.0} (50)}{(3.2111) K d^{*2} \sqrt{1000}} \right]^2 \\ &= \frac{72.549}{K^2 d^{*4}} \end{aligned}$$

and

$$d^* = \left(\frac{72.549}{K^2 \Delta p^*} \right)^{1/4}$$

1. *Foxboro integral orifice.* Assuming $K = 0.9$, the bore diameter for $\Delta p^* = 50$ kPa is

$$d^* = \left[\frac{72.549}{(0.9)^2 (50)} \right]^{1/4} = 1.157 \text{ mm}$$

The bore at room temperature is then, by Eq. (9.51),

$$d_{\text{meas}} = \frac{d_f}{F_a^* d} = \frac{1.157}{1.0001} = 1.157$$

A bore equal to or greater than 1.157 mm must be selected so as *not* to produce a differential greater than 50 kPa.

Now, from Table 11.2, $d^* = 1.5113$ mm. The bore Reynolds number is calculated from Eq. (1) of Table 9.21 by replacing D^* with d^* :

$$\begin{aligned} R_d &= 83.467 \frac{G}{Z_b \mu_{\text{cP}} d^* N_{\text{vPT}}^*} q_{\text{SLPM}}^* \\ &= 83.467 \frac{1.0}{1.0 (0.018)(1.5113)(3.2111)} q_{\text{SLPM}}^* = 955.5 q_{\text{SLPM}}^* \end{aligned}$$

where $\mu_{\text{cP}} = 0.018$ from Fig. H.1. At normal operating conditions the flow rate is $(q_{\text{SLPM}}^*)_N = (0.8)(50) = 40$, and the bore Reynolds number is $(R_d)_N = (955.5)(40) = 38,220$. From Table 11.3 or Fig. 11.5, the flow coefficient is $K = 0.882$. Since K is constant for $R_d > 2000$, the URV of the differential-pressure transmitter is

$$\Delta p^* = \frac{72.549}{K^2 d^{*4}} = \frac{72.549}{(0.882)^2 (1.5113)^4} = 17.88 \text{ kPa}$$

2. *Taylor integral orifice.* Assuming $K = 0.6$ (see Table 11.2), the bore for $\Delta p^* = 50$ kPa is

$$d^* = \left[\frac{72.549}{(0.6)(50)} \right]^{1/4} = 1.247 \text{ mm}$$

The next largest bore from Table 11.2 is $d^* = 1.651 \text{ mm}$, and $K = 0.620$. The URV of the differential-pressure transmitter is then

$$\Delta p^* = \frac{72.549}{(0.620)^2(1.651)^4} = 25.401 \text{ kPa}$$

ANNULAR METERS

There are several differential producers, or meters that produce a force, that are of an *annular* design. In these designs the flow is diverted to the outside of the meter body (or pipe wall) by a central disk, cone, or target rather than converging into a restricted area to produce the differential (or force). These meters are discussed below. These meters are proprietary, and the accuracy specifications, features, and installation requirements should be confirmed with the manufacturer.

Annular Orifice

The annular orifice is shown in Fig. 11.9. It consists of a disk supported concentrically in a pipe section by supporting spiders. Upstream and downstream pressures are transmitted through the central shaft to the differential-pressure transmitter. The earliest experimental test work on this device was done by Howell (1939), using air and diameter ratios from 0.7 to 0.9. Bell and Bergelin (1957, 1962) experimentally tested 21 annular orifices with beta ratios between 0.95 and 0.996, and they reported good agreement with other published results. Although limited low-Reynolds-number data are available for β_T in the range of 0.7 to 0.9, the flow coefficient appears to be constant above a pipe Reynolds number of 10,000.

The annular orifice has the advantages of providing free drainage for heavy materials at the bottom of the pipe while, at the same time, allowing gas or vapor to pass along the top of the pipe. Its major disadvantages are the lack of extensive data and the dependence on pipe dimension to define flow area; the latter becomes more serious as β_T approaches 0.9.

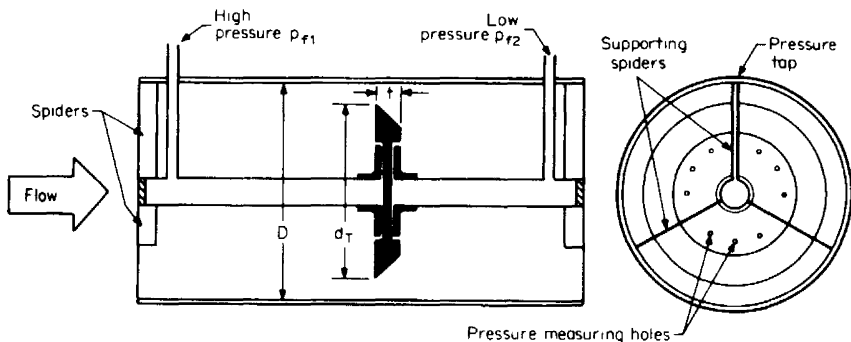


Figure 11.9 Annular orifice.

The flow coefficient K as determined by Howell (1939) is presented in Fig. 11.10 and a fitted equation in Table 11.3. For gas (vapor) flows, no gas expansion factor has been determined. The thermal-expansion-factor correction is the same as for other differential producers. The overall pressure loss is approximately the same as that of the target flowmeter for the same beta ratio.

Example 11.3. An annular orifice with $\beta_T = 0.75$ is to measure the steam flow of Example 9.2. Calculate the upper-range value for the differential-pressure transmitter and the flow rate if the differential pressure is 100 in (24.9 kPa).

The flow-rate equation is, from Eq. (g) of Table 9.36,

$$q_{PPH} = N_{M\rho} \frac{CY_1 d^2}{\sqrt{1 - (d/D)^4}} \sqrt{\rho_{f1}} \sqrt{h_w}$$

Substituting variables from Table 11.1 gives the equation for an annular orifice as

$$q_{PPH} = N_{M\rho} K (1 - \beta_T^2) D^2 \sqrt{\rho_{f1}} \sqrt{h_w}$$

From Example 9.2,

$$(q_{PPH})_{URV} = 30,000 \text{ lb}_m/\text{h} \quad N_{M\rho} = 358.93$$

$$\beta_T = 0.75 \quad D = 5.761 \text{ in} \quad \rho_{f1} = 0.39524 \text{ lb}_m/\text{ft}^3$$

and from Fig. 11.10, $K = 0.669$. Substitution and rearrangement then give

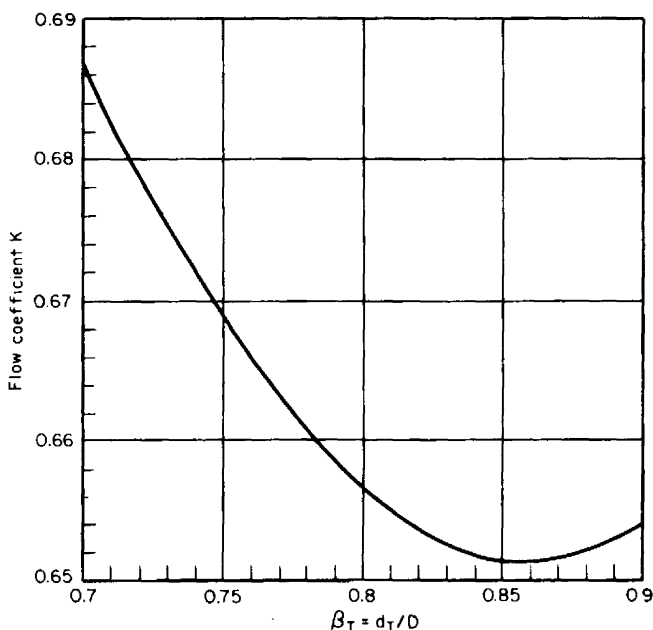


Figure 11.10 Annular-orifice flow coefficient.

$$(h_w)_{URV} = \left\{ \frac{30,000}{(358.93)(0.669)[1 - (0.75)^2](5.761)^2 \sqrt{0.39524}} \right\}^2 = 184.53 \text{ in}$$

At $h_w = 100$, the flow rate is calculated as

$$q_{PPH} = (358.93)(0.669)(1.0075)[1 - (0.75)^2](5.761)^2 \sqrt{0.39524} \sqrt{h_w}$$

$$= F_{MC} \sqrt{h_w} = 2208.4 \sqrt{h_w} = 2208.4 \sqrt{100} = 22,084 \text{ lb}_m/\text{h}$$

Target Flowmeter

The acceleration of fluid into the annular space around a concentric target (disk) creates a reduced pressure at the target's rear surface (Fig. 11.11a). The force on the target is the difference between the upstream and downstream surface pressures,

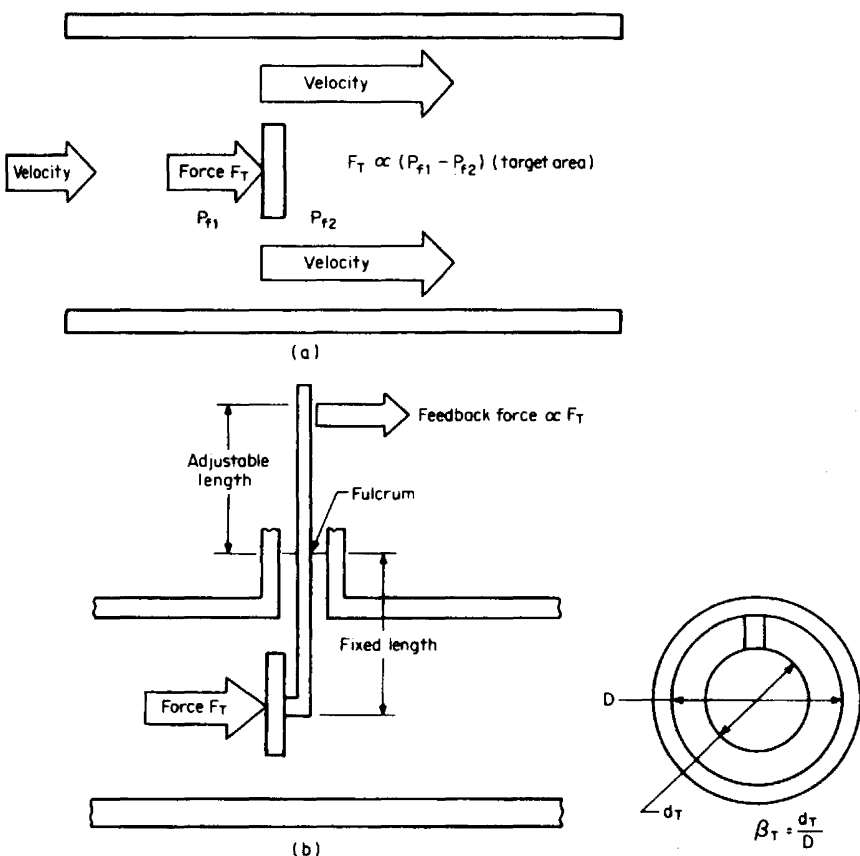


Figure 11.11 Target flowmeter. (a) Basic principle. (b) Foxboro force-balance target flowmeter. (Courtesy The Foxboro Co.)

integrated over the target area. By Bernoulli's equation, the square root of this force is proportional to the flow rate.

Foxboro. Foxboro's target flowmeter balances the target force with a feedback force applied above a fulcrum (Fig. 11.11b). The moment arm to the target force is constant, and a variable range is achieved by adjusting the position of the fulcrum. The output is a standardized 3- to 15-lb/in² (20- to 100-kPa) or 4- to 20-mA signal proportional to target force. Flowmeters are calibrated by suspending weights from the target centerline and adjusting the variable moment arm to the desired upper-range value.

The flow-rate equations given in Tables 9.36 through 9.38 are modified by substituting the geometry factor for d^2 and the flow coefficient K for $C/\sqrt{1 - (d/D)^4}$ to obtain the flow-rate equation for the target flowmeter. The gas-expansion factor is set equal to 1.0. Geometry factors and allowable force limits for available fixed-geometry flowmeters are given in Table 11.4. Recommended installation lengths are based on equivalent orifice beta ratios; these are also given in Table 11.4.

Curran (1981) gives the flow-coefficient equations and pipe-Reynolds-number curves for Foxboro's fixed-geometry targets in $\frac{1}{2}$ -in (15-mm) through 4-in (100-mm) meter sizes. These are presented in Table 11.5 and Figs. 11.12 through 11.19. Test work on natural gas by Reinecke et al. (1966) with similar calibrated flowmeters showed no gas-expansion-factor error and flow performance equivalent to that of a series-installed orifice.

The permanent pressure loss in pounds-force per square inch can be calculated as

$$\Delta p_L = \frac{0.199K^2(1 - \beta_T^2)^2}{D^2\beta_T^2(1 - \beta_T)^{2.75}} F_T = K_{LT}F_T \quad (11.4)$$

and in kilopascals as

$$\Delta p_L^* = \frac{198.2K^2(1 - \beta_T^2)^2}{D^{*2}\beta_T^2(1 - \beta_T)^{2.75}} F_T^* = K_{LT}^*F_T^* \quad (11.5)$$

Values of the loss coefficients K_{LT} and K_{LT}^* at $R_D = 100,000$ for fixed-geometry targets are given in Table 11.4.

The thermal-expansion-factor correction for target flowmeters is

$$F_\alpha = 1 + \alpha_{PE}(T_F - 68) \quad (11.6)$$

for U.S. units, and

$$F_\alpha = 1 + \alpha_{PE}^*(T_{cC} - 20) \quad (11.7)$$

for SI units.

Ramapo. The Ramapo target flowmeter (Fig. 11.20) uses bonded strain gauges in a bridge circuit to measure target force. These gauges are outside the fluid and translate the force into an electrical output proportional to the flow rate squared. Two of the four strain gauges are bonded to the sensing tube on the forward side and two are located on the reverse side (Fig. 11.21). These are interconnected to produce an active four-arm strain gauge bridge circuit. At zero force (no flow) the bridge is balanced and the circuit output is zero. Under flowing conditions the target

TABLE 11.4 Geometry Constants for Target Flowmeters (Foxboro)

Nominal line size, in (mm)	Meter bore D , in (mm)	Target diameter d_T , in (mm)	β_T $\left(\frac{d_T}{D}\right)$	Pressure-loss coefficient		Force limits		Geometry factor		Installation (equivalent orifice beta ratio)
				U.S. units (K_{LT}^\dagger)	SI units ($K_{LT}^{*\ddagger}$)	U.S. units (lb_f)	SI units (N)	U.S. units§	SI units¶	
0.5 (15)	0.546 (13.87)	0.4368 (11.09)	0.8	5.41	8.35	$1.5 \leq F_T$ ≤ 15.3	$6.67 \leq F_T^*$ ≤ 68.1	1.459934	222.6865	0.6
1 (25)	0.957 (24.31)	0.7656 (19.45)	0.8	1.82	2.81	$1.3 \leq F_T$ ≤ 13.1	$5.78 \leq F_T^*$ ≤ 58.3	2.558896	390.2132	0.6
2 (50)	2.067 (52.50)	1.3610 (34.57)	0.6584	0.322	0.497	$1.9 \leq F_T$ ≤ 19.2	$8.5 \leq F_T^*$ ≤ 85.4	10.56612	1611.670	0.75
2 (50)	2.067 (52.50)	1.6679 (42.37)	0.8069	0.330	0.509	$1.9 \leq F_T$ ≤ 19.2	$8.5 \leq F_T^*$ ≤ 85.4	5.310298	809.9895	0.6
3 (75)	3.068 (77.93)	1.604 (40.74)	0.5228	0.126	0.195	$1.6 \leq F_T$ ≤ 16.2	$7.12 \leq F_T^*$ ≤ 72.1	25.33773	3864.811	0.8
3 (75)	3.068 (77.93)	2.301 (58.45)	0.75	0.133	0.205	$1.6 \leq F_T$ ≤ 16.2	$7.12 \leq F_T^*$ ≤ 72.1	10.63409	1622.038	0.65
4 (100)	4.026 (102.26)	1.6679 (42.37)	0.4143	0.093	0.144	$1.4 \leq F_T$ ≤ 13.7	$6.23 \leq F_T^*$ ≤ 60.9	47.83329	7296.099	0.75
4 (100)	4.026 (102.26)	2.678 (68.02)	0.6652	0.072	0.111	$1.4 \leq F_T$ ≤ 13.7	$6.23 \leq F_T^*$ ≤ 60.9	20.05125	3058.455	0.75

$^\dagger K_{LT} = (0.199/D^2)K^2[(1 - \beta_T^2)/\beta_T]^2[1/(1 - \beta_T)^{2.75}]$.

$^\ddagger K_{LT}^* = (198.2/D^{*2})K^2[(1 - \beta_T^2)/\beta_T]^2[1/(1 - \beta_T)^{2.75}]$, where K is the flow coefficient at $R_D = 100,000$.

§ Equal to $5.941939[(1 - \beta_T^2)/\beta_T]D$.

¶ Equal to $35.68248[(1 - \beta_T^2)/\beta_T]D^*$.

TABLE 11.5 Target-Flowmeter Flow-Coefficient Equations (Foxboro)

Nominal line size, in (mm)	β_T	Reynolds-number range	Accuracy (uncalibrated), %	Flow coefficient K
0.5 (15)	0.8	$111 \leq R_D \leq 4000$	± 2	$K = -15.8447766 + 23.0693751 \log R_D - 11.958139(\log R_D)^2 + 2.7183724(\log R_D)^3 - 0.2283791(\log R_D)^4$
0.5 (15)	0.8	$R_D > 4000$	± 2.7	$K = 0.69163$
1 (25)	0.8	$44 \leq R_D \leq 4000$	± 2.5	$K = 27.7292586 - 57.2484112 \log R_D + 46.3134298(\log R_D)^2 - 18.1122003(\log R_D)^3 + 3.4484014(\log R_D)^4 - 0.2568661(\log R_D)^5$
1 (25)	0.8	$R_D > 4000$	± 1.8	$K = 0.70365$
2 (50)	0.658	$167 \leq R_D \leq 4000$	± 1.9	$K = -9.3752781 + 13.5112009 \log R_D - 6.8267566(\log R_D)^2 + 1.5191852(\log R_D)^3 - 0.1253178(\log R_D)^4$
2 (50)	0.658	$R_D > 4000$	± 1.0	$K = 0.57553 + 0.012744 \log R_D$
2 (50)	0.807	$129 \leq R_D \leq 4000$	± 2.7	$K = -10.8240856 + 14.7439321 \log R_D - 6.9467876(\log R_D)^2 + 1.4199689(\log R_D)^3 - 0.1061497(\log R_D)^4$
2 (50)	0.807	$R_D > 4000$	± 1.1	$K = 0.61852 + 0.0045082 \log R_D$
3 (80)	0.523	$319 \leq R_D \leq 4000$	± 6.3	$K = -18.0866104 + 24.5119444 \log R_D - 11.9261559(\log R_D)^2 + 2.5315746(\log R_D)^3 - 0.1969396(\log R_D)^4$
3 (80)	0.523	$R_D > 4000$	± 2.0	$K = 0.57810 + 0.011170 \log R_D$
3 (80)	0.750	$178 \leq R_D \leq 4000$	± 2.3	$K = -2.5116530 + 3.3406322 \log R_D - 1.1874923(\log R_D)^2 + 0.1393851(\log R_D)^3$
3 (80)	0.750	$R_D > 4000$	± 1.7	$K = 0.59294 + 0.0090958 \log R_D$
4 (100)	0.414	$530 \leq R_D \leq 4000$	± 1.4	$K = -66.9527450 + 86.3212859 \log R_D - 41.0847774(\log R_D)^2 + 8.6108367(\log R_D)^3 - 0.6694608(\log R_D)^4$
4 (100)	0.414	$R_D > 4000$	± 0.7	$K = 0.587071 + 0.014652 \log R_D$
4 (100)	0.665	$240 \leq R_D \leq 4000$	± 2.1	$K = -18.7909023 + 26.1845236 \log R_D - 13.0980936(\log R_D)^2 + 2.8696266(\log R_D)^3 - 0.2319703(\log R_D)^4$

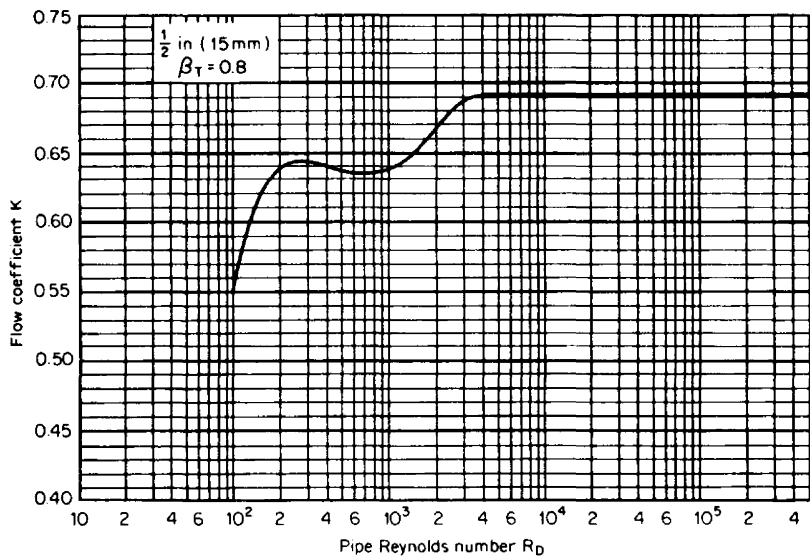


Figure 11.12 Target-flowmeter flow coefficient: $\frac{1}{2}$ -in (15-mm) bore, $\beta_T = 0.8$.

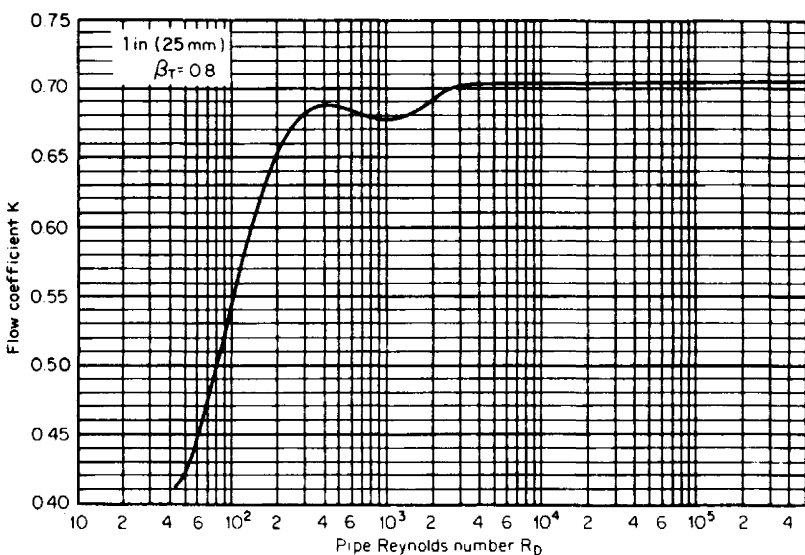


Figure 11.13 Target-flowmeter flow coefficient, 1-in (25-mm) bore, $\beta_T = 0.8$.

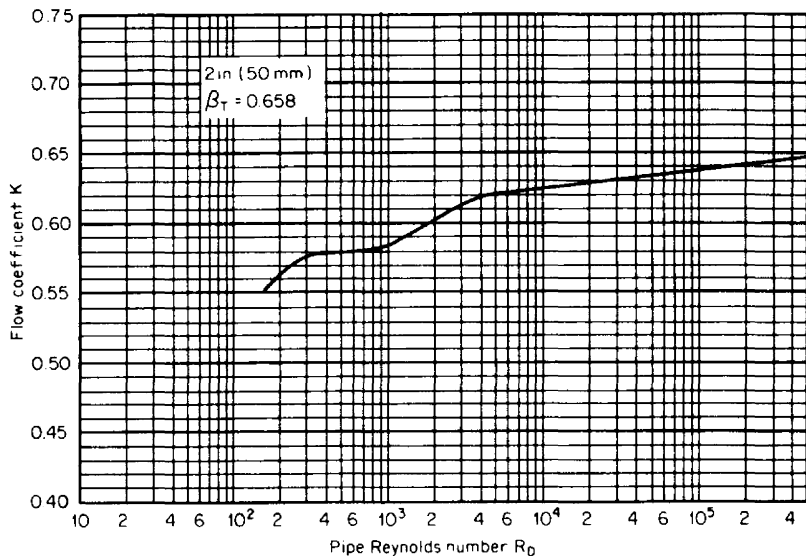


Figure 11.14 Target-flowmeter flow coefficient, 2-in (50-mm) bore, $\beta_T = 0.658$.

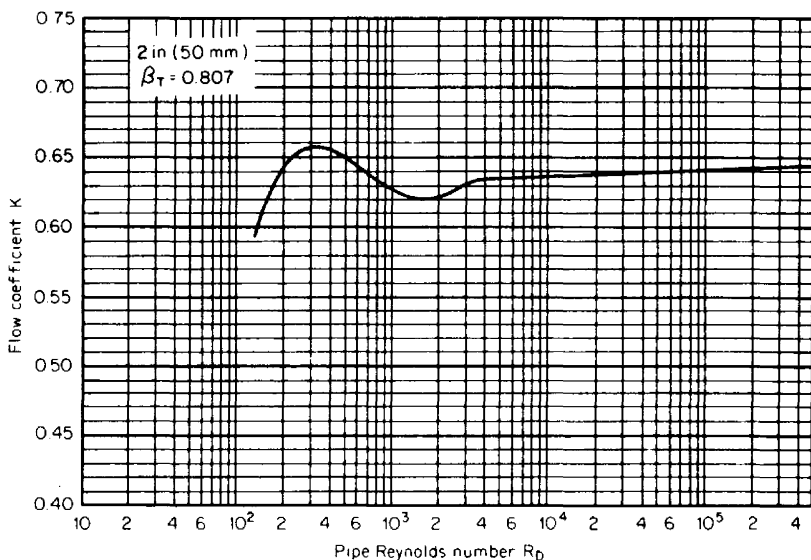


Figure 11.15 Target-flowmeter flow coefficient, 2-in (50-mm) bore, $\beta_T = 0.807$.

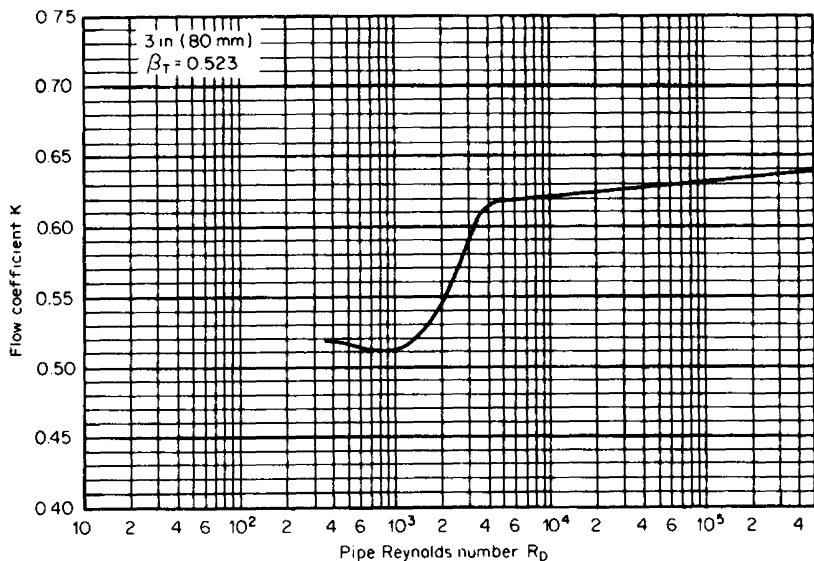


Figure 11.16 Target-flowmeter flow coefficient, 3-in (75-mm) bore, $\beta_T = 0.523$.

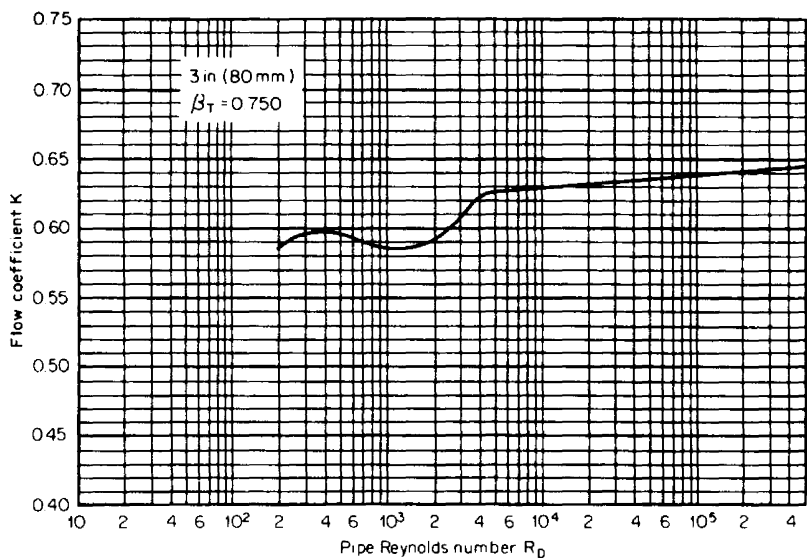


Figure 11.17 Target-flowmeter flow coefficient, 3-in (75-mm) bore, $\beta_T = 0.750$.

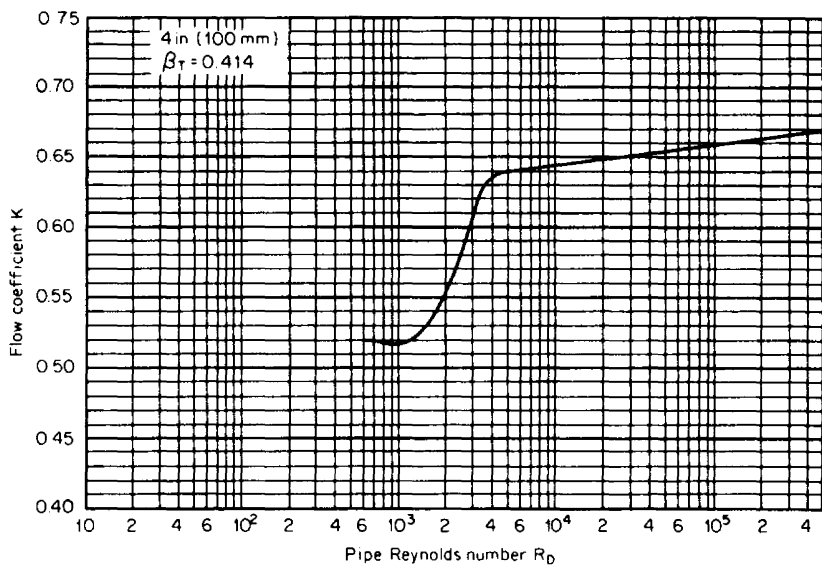


Figure 11.18 Target-flowmeter flow coefficient, 4-in (100-mm) bore, $\beta_T = 0.414$.

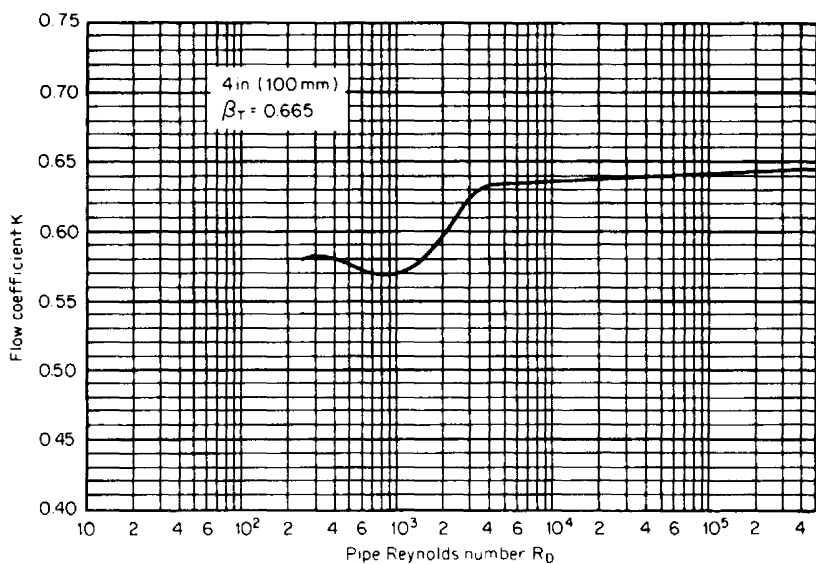


Figure 11.19 Target-flowmeter flow coefficient, 4-in (100-mm) bore, $\beta_T = 0.656$.

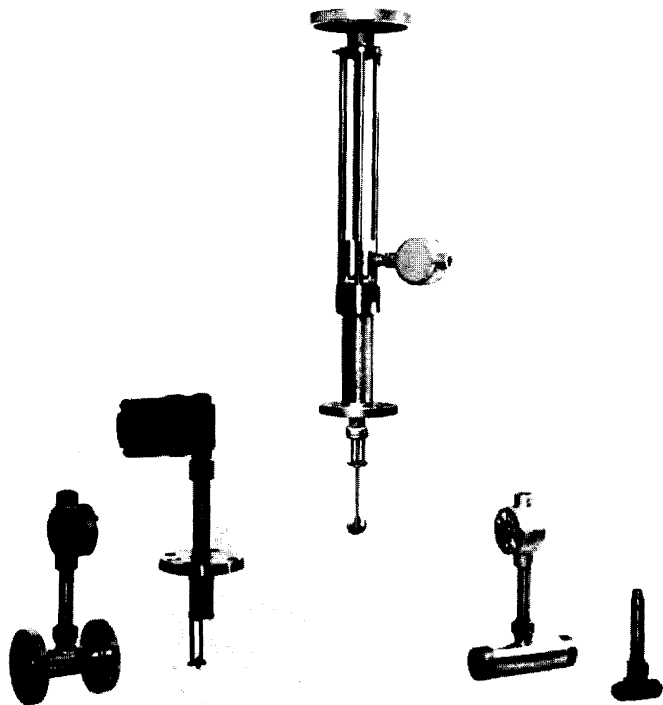


Figure 11.20 Ramapo Target Flowmeters. (Courtesy Hersey Measurement Co.)

force acting on the *sensing tube* compresses two of the gauges and places the other two in tension, which unbalances the bridge circuit. The standard output is 2.0 mV/V full scale with lower output signals available for specific applications.

In lines size of 1/2- to 6-in (12.5- to 150-mm) wafer bodies, spool piece flanged meters, 37° flare inlet, or pipe thread bodies are available. The fixed insertion or retractable design is used in 2- to 60-in (50- to 1500-mm) existing pipe sizes. Meter designs are available to meter liquid, gas, and steam. Some designs can handle pressures up to 10,000 psi (70 MPa) with rangeability up to 15:1 being offered.

The literature (Clark, 1986) lists some of the following features:

- Lines size 3/8 in (10 mm) and larger with some applications in pipe sizes to 96 in (2500 mm) and ducts to 10 ft²
- Typically, 10:1 rangeability with 15:1 range available
- Bidirectional flow with the flow direction being indicated by the polarity change in the electrical output
- Low overall pressure loss that ranges from 2 psi (14 kPa) at maximum flow for a 1-in (25-mm) meter to several inches of water for lines sizes 8 in (200 mm)
- Pressure rating up to 10,000 psi (70 MPa)

4-WIRE BRIDGE
RD OUTPUT =
VOLTS PER
EXCITATION

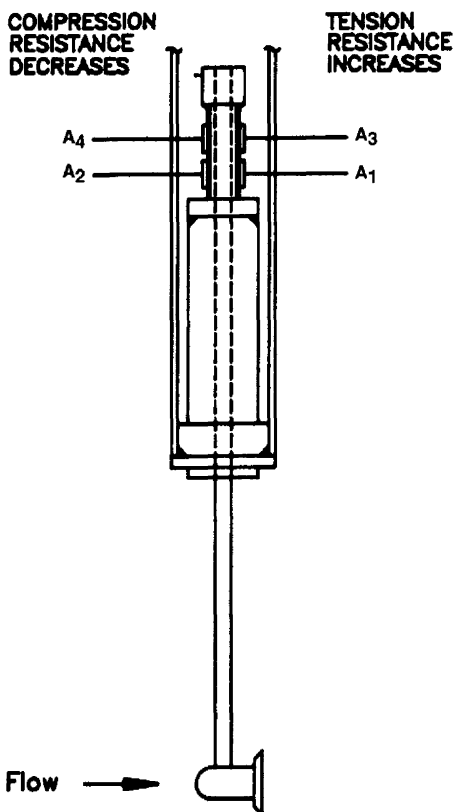
TERMINAL 1 OR A
EXCITATION +
GRN WIRE

TERMINAL 2 OR B
SIGNAL +
WHT WIRE

TERMINAL 4 OR D
EXCITATION -
BLK WIRE

TERMINAL 3 OR C
SIGNAL -
RED WIRE

mV



Measurement Co.)

- Temperature ranges of -320°F to 500°F (-212°C to 260°C)
- Long-term reliability based on independent life test of 100E6 forward and reverse cycles with no significant change in measured variable properties
- Field calibration by checking the target diameter and force factor (sensitivity factor) to the original specifications provided with the meter

Meters are sized by the *equivalent water flow method*. In this method the equivalent water flow rate is computed that corresponds to the target force. The *equivalent water flow* equations are presented in Table 11.6 for U.S. units and in Table 11.7 for SI units. The flowing gallons per minute q_{gpm} for the Ramapo meters are given in Table 11.6.

The design considerations are:

- The pipe Reynolds number must be above 1000.
- Calculate the equivalent *full-scale* water flow rate using the equation given in Table 11.8.
- If this *full-scale* rate falls between A and B of the values of Table 11.8, a 15:1 range is obtained.
- For lower full-scale pressure loss, meters, within the same line size, may be operated at 1 mV/V. Multiply the pressure loss by 0.5.
- For a turndown of 10:1 multiply the flow rate range by 0.707.
- For higher-flow-rate ranges within a given line size, meters are manufactured with a 5000-psi (35-MPa) element. Multiply the flow rate B by 1.4. The full-scale pressure loss will be twice the listed loss.

Gilflow

The Gilflo meter was designed to meter liquids, gases, and vapor flows. It is a spring-load variable annular area differential producer. As the flow rate increases (Fig. 11.22), the shaped plug moves downstream against a spring force. By shaping the plug, the produced differential pressure is linear with the flow rate.

Meters are selected by the *equivalent flow rate of water* method. These U.S. unit equations are presented in Table 11.6 and the SI unit equations in Table 11.7. The equivalent water flow rate ranges are given in Table 11.9 for the "spool" and "G" designs. The manufacturer should be consulted for the exact sizing information and the differential that will be produced.

The following are some of the features listed in the literature (manufacturer should be consulted for any changes or additions):

- Linear differential pressure output is over a 100:1 range.
- Meters are calibrated with water in a laboratory.
- Minimum upstream pipe is 6 pipe diameters.
- Suitable for most industrial fluids.
- Sizes 2 to 16 in (50 to 400 mm).
- Pressure to 3000 psig (200 bar, gauge).
- Temperatures to 840°F (450°C).

TABLE 11.6 Equivalent Water Flow-Rate Equations, U.S. Units

Liquid		Gas (vapor)
Mass flow		
Density	$q_{\text{gpm,equiv}} = \frac{5.66645 q_M}{N_{M\rho} \sqrt{F_p} \rho_F}$	$q_{\text{gpm,equiv}} = \frac{5.66645 q_M}{N_{M\rho} \sqrt{\rho_f}}$
Specific gravity	$q_{\text{gpm,equiv}} = \frac{5.66645 q_M}{N_{MG} \sqrt{F_p} G_F}$	
$p_v T$ equation		$q_{\text{gpm,equiv}} = \frac{5.66645 \sqrt{Z_{f1} T_{f1}} q_M}{N_{MpT} \sqrt{G p_{f1}}}$
Volumetric flow rate at flowing conditions		
Density	$q_{\text{gpm,equiv}} = \frac{5.66645 \sqrt{F_p} \rho_F q_v}{N_{v\rho}}$	$q_{\text{gpm,equiv}} = \frac{5.66645 \sqrt{\rho_{f1}} q_v}{N_{v\rho}}$
Specific gravity	$q_{\text{gpm,equiv}} = \frac{5.66645 \sqrt{F_p} G_F q_v}{N_{vG}}$	
$p_v T$ equation		$q_{\text{gpm,equiv}} = \frac{5.66645 \sqrt{G p_{f1}} q_v}{N_{vpT} \sqrt{Z_{f1} T_{f1}}}$
Volumetric flow rate at base conditions		
Density	$q_{\text{gpm,equiv}} = \frac{5.66645 \rho_b q_v}{N_{v\rho} \sqrt{F_p} \rho_F}$	
Specific gravity	$q_{\text{gpm,equiv}} = \frac{5.66645 G_b q_v}{N_{vG} \sqrt{F_p} G_F}$	
$p_v T$ equation		$q_{\text{gpm,equiv}} = \frac{5.66645 \sqrt{Z_{f1} G T_{f1}} \rho_b q_{vb}}{(N_{vpT})_b Z_b T_b \sqrt{p_{f1}}}$

TABLE 11.7 Equivalent Water Flow-Rate Equations, SI Units

Liquid		Gas (vapor)
Mass flow		
Density	$q_{\text{gpm,equiv}} = \frac{5.66645 q_M^*}{N_{M\rho}^* \sqrt{F_p} \rho_F^*}$	$q_{\text{gpm,equiv}} = \frac{5.66645 q_M^*}{N_{M\rho}^* \sqrt{\rho_f^*}}$
Specific gravity	$q_{\text{gpm,equiv}} = \frac{5.66645 q_M^*}{N_{MG}^* \sqrt{F_p} G_F}$	
<i>pvT</i> equation		$q_{\text{gpm,equiv}} = \frac{5.66645 \sqrt{Z_{f1} T_{K1}} q_M^*}{N_{MpT}^* \sqrt{G p_{f1}^*}}$
Volumetric flow rate at flowing conditions		
Density	$q_{\text{gpm,equiv}} = \frac{5.66645 \sqrt{F_p} \rho_F^* q_v^*}{N_{v\rho}^*}$	$q_{\text{gpm,equiv}} = \frac{5.66645 \sqrt{\rho_{f1}^*} q_v^*}{N_{v\rho}^*}$
Specific gravity	$q_{\text{gpm,equiv}} = \frac{5.66645 \sqrt{F_p} G_F q_v^*}{N_{vG}^*}$	
<i>pvT</i> equation		$q_{\text{gpm,equiv}} = \frac{5.66645 \sqrt{G p_{f1}^*} q_v^*}{N_{vpT}^* \sqrt{Z_{f1} T_{K1}}}$
Volumetric flow rate at base conditions		
Density	$q_{\text{gpm,equiv}} = \frac{5.66645 \rho_b^* q_v^*}{N_{v\rho}^* \sqrt{F_p} \rho_F^*}$	
Specific gravity	$q_{\text{gpm,equiv}} = \frac{5.66645 G_b q_v^*}{N_{vG}^* \sqrt{F_p} G_F}$	
<i>pvT</i> equation		$q_{\text{gpm,equiv}} = \frac{5.66645 \sqrt{Z_{f1} G T_{K1}} \rho_b^* q_v^*}{(N_{vpT}^*)_b Z_b T_{Kb} \sqrt{p_{f1}^*}}$

TABLE 11.8 Equivalent Water Flow Rates for Ramapo Target Flowmeter, q_{gpm}

37 flare tube meter							Wafer, MNPT, and flanged pipe meters						
Tube† size	Bore ID	App. gpm min. range		App. gpm max. range		App. FS psi drop	Pipe size	Pipe ID	App. gpm min. range		App. gpm max. range		App. FS psi drop
		A		B					A		B		
0.5	0.391	0.13	2.0	0.67	10.0	35.0	0.5	0.622	0.2	3.0	2.0	30.0	14.0
0.75	0.609	0.20	3.0	2.00	30.0	14.0	0.75	0.824	0.7	10.0	4.0	60.0	8.0
1.0	0.844	0.67	10.0	4.67	70.0	8.0	1.0	1.049	1.0	15.0	5.3	80.0	5.0
1.25	1.078	2.00	30.0	6.67	100.0	4.0			1.7	25.0	6.7	100.0	3.5
							1.25	1.380					
1.5	1.312	2.67	40.0	10.00	150.0	2.0	1.5	1.610	2.0	30.0	8.0	120.0	2.5
2.0	1.781	3.33	50.0	13.33	200.0	1.0	2.0	2.067	2.7	40.0	13.3	200.0	1.0
							2.5	2.469	3.3	50.0	16.7	250.0	0.8
							3.0	3.068	4.7	70.0	23.3	350.0	0.6
							4.0‡	4.020	6.7	100.0	40.0	600.0	0.4
							5.0‡	5.047	10.0	150.0	66.7	1000.0	0.3
							6.0‡	6.065	13.3	200.0	93.3	1400.0	0.2

Probe (2-in MTG)						Probe (4-in MTG)				
Line size (ln)	ID (ln)	Min. Range		Max. Range		Min. Range		Max. Range		FS psi drop
		A		B		A		B		
4	4.026	20	294	30	457	10	143	30	457	0.1452
5	5.047	31	462	48	718	15	225	48	718	0.0924
6	6.065	44	667	69	1036	22	324	69	1036	0.0640
8	7.981	77	1155	120	1795	37	562	120	1795	0.0369
10	10.020	121	1820	189	2829	59	886	189	2829	0.0234
12	11.938	172	2584	268	4015	84	1257	268	4015	0.0165
14	13.250	212	3183	330	4946	103	1548	330	4946	0.0134
16	15.250	281	4216	437	6552	137	2051	437	6552	0.0101
18	17.250	360	5395	559	8384	175	2625	559	8384	0.0079
20	19.250	448	6718	696	10441	218	3268	696	10441	0.0064
22	21.250	546	8187	848	12723	266	3983	848	12723	0.0052
24	23.250	653	9800	1015	15230	318	4768	1015	15230	0.0044
26	25.250	771	11559	1198	17963	375	5623	1198	17963	0.0037
28	27.250	898	13463	1395	20922	437	6549	1395	20922	0.0032
30	29.250	1034	15511	1607	24105	503	7546	1607	24105	0.0028
32	31.250	1180	17705	1834	27515	574	8613	1834	27515	0.0024
34	33.250	1336	20044	2077	31149	650	9751	2077	31149	0.0021
36	35.250	1502	22528	2334	35009	731	10959	2334	35009	0.0019
38	37.250	1677	25157	2606	39095	816	12238	2606	39095	0.0017
40	39.250	1862	27930	2894	43405	906	13588	2894	43405	0.0015
42	41.250	2057	30849	3196	47942	1001	15008	3196	47942	0.0014
44	43.250	2261	33913	3514	52703	1100	16498	3514	52703	0.0013

TABLE 11.8 Equivalent Water Flow Rates for Ramapo Target Flowmeter, q_{gpm} (Continued)

Probe (2-in MTG)						Probe (4-in MTG)				FS psi drop
Line size (ln)	ID (ln)	Min. Range		Max. Range		Min. Range		Max. Range		
		A	B	A	B	A	B			
46	45.250	2475	37122	3846	57690	1204	18060	3846	57690	0.0011
48	47.250	2698	40476	4193	62902	1313	19691	4193	62902	0.0011
50	49.250	2932	43975	4556	68340	1426	21393	4556	68340	0.0010
52	51.250	3175	47620	4934	74003	1544	23166	4934	74003	0.0009
54	53.250	3427	51409	5326	79892	1667	25010	5326	79892	0.0008
56	55.250	3690	55343	5734	86006	1795	26924	5734	86006	0.0008
58	57.250	3961	59422	6156	92345	1927	28908	6156	92345	0.0007
60	59.250	4243	63646	6594	98910	2064	30963	6594	98910	0.0007

†Based on copper tubing.

‡Wafer and flanged meters only.

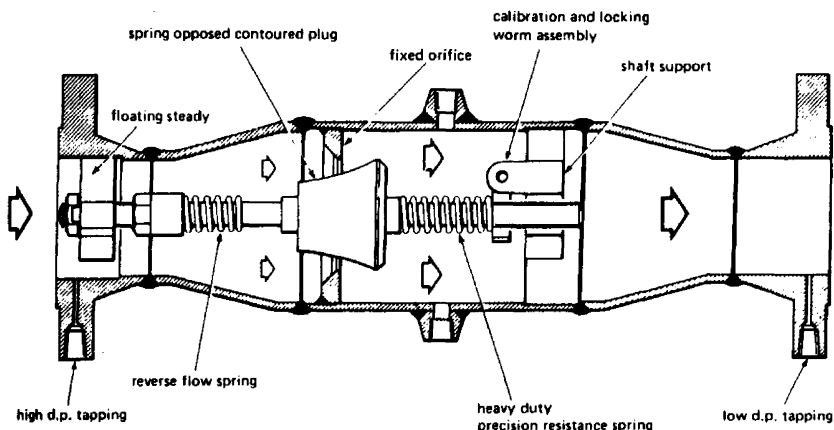


Figure 11.22 Gilflo meter. (Courtesy Gilflo, Spirax/Sarco Engineering Group.)

TABLE 11.9 Equivalent Water Flow Rate for Gilflo Meter,

q_{gpm}

Size in (mm)	Type	Minimum	Maximum Range
2 (50)	Spool	0	6.1 to 27.7
	B	0	21 to 104
3 (75)	Spool	0	21 to 104
	B	0	61.3 to 264
4 (100)	Spool	0	61.3 to 264
	B	0	181 to 554
6 (150)	Spool	0	181 to 554
	B	0	403 to 1109
8 (200)	Spool	0	403 to 1109
	B	0	1057 to 2113
10 (250)	B	0	1057 to 2905
12 (300)	Spool	0	687 to 1928
	B	0	1585 to 5045
16 (400)	Spool	0	871 to 2423
	B	0	3853 to 8195

Example 11.4. Size a Gilflo G-series meter-to-meter 140 psia (965 kPa) saturated steam. The maximum flow rate is 40,000 lb/h (18,143 kg/h).

The equivalent water flow-rate equation is selected from Table 11.6:

$$q_{\text{gpm,equiv}} = \frac{5.66645 q_{\text{PPH}}}{N_{M\rho} \sqrt{\rho_f}}$$

From Table 9.14, $N_{M\rho} = 358.9268$ and from App. G, Table G.1, $\rho_f = 0.31066 \text{ lb}_m/\text{ft}^3$. Substitution yields the equivalent water flow rate as

$$q_{\text{gpm,equiv}} = \frac{(5.66645)(40,000)}{358.9268 \sqrt{0.311066}} = 1133 \text{ gpm}$$

From Table 11.9 the equivalent water flow rate falls within the range of 1057 to 2113 and 1057 to 2905 of an 8-in B type or a 10-in B-type G series. Either can be used for this application.

V-Cone

The V-cone (Fig. 11.23) produces a differential across a centered cone in a precision meter tube. The differential pressure is the difference in pressure between the static line pressure p_{f1} measured at the upstream tap and the pressure from a tap located at the forward section of the cone p_{f2} . An equivalent beta is substituted into the

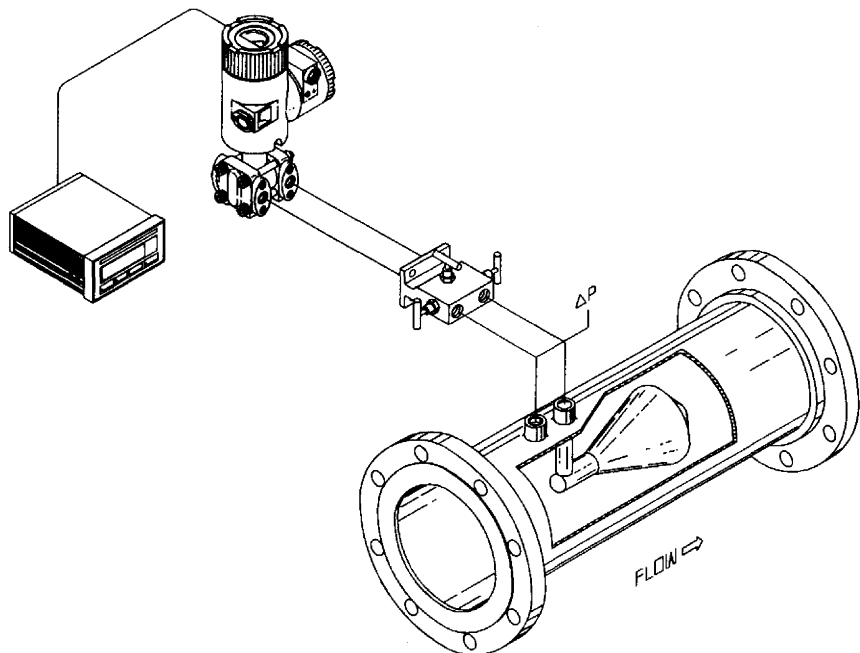


Figure 11.23 V-Cone. (Courtesy McCrometer Div. of Ketema.)

flow rate or differential pressure equations presented in Chap. 9. This flowing beta is

$$\beta_{f,V\text{-cone}} = \frac{\sqrt{D^2 - d_{f,\text{cone}}^2}}{D} \quad (11.8)$$

where D is the meter bore at flowing temperature and $d_{f,\text{cone}}$ is the cone diameter at flowing temperature.

The equivalent bore diameter being defined by

$$d = \beta_{f,V\text{-cone}} D \quad (11.9)$$

Each V-cone is flow-calibrated to obtain the discharge coefficient C that is to be used in the flow-rate equation. The typical range of C is from 0.75 to 0.85. The adiabatic gas expansion factor is to be used for gas (vapor) flow provided $Y_1 < 0.96$. Otherwise an expansion factor is derived from calibration data on a compressible fluid (air, etc.).

The literature lists some of the following features:

- Two designs: 1/2 to 36 in (25 to 900 mm) in the precision bore version and 6 to 72 in (150 to 1800 mm) insertion type.
- Standard betas in precision bore tubing $\beta_{V\text{-cone}} = 0.45, 0.55, 0.65, 0.75$, and 0.85 .
- Reduced downstream laying lengths (see Fig. 11.24).
- An accuracy of ± 0.5 percent in the majority of applications.
- A repeatability of ± 0.1 percent.
- A typical range of 15:1.
- Minimum Reynolds number of 8000; for lower Reynolds number a fitted expression is used.
- A swept-through design that eliminates gaseous or solid entrapment.
- Standard size cones available to minimize overall pressure loss or to increase rangeability.
- 600 psi (40 bar) pressure.
- 700°F (370°C) temperature.
- Used for static mixing by vortex mixing downstream of the cone.

Example 11.5. For a V-cone meter write the equation to compute a liquid base gallon per minute q_{GPM} flow rate using the specific gravity equation.

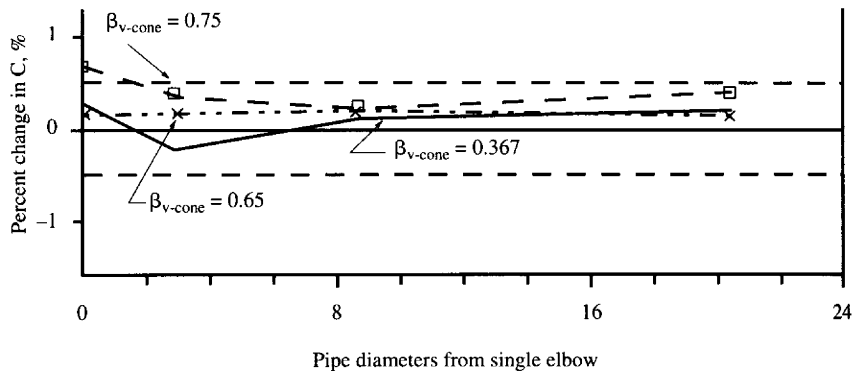
The differential producer flow rate equation is, from Table 9.36, written as

$$q_{\text{GPM}} = N_{\text{VG}} \frac{C d^2}{\sqrt{1 - (d/D)^4}} \frac{\sqrt{F_p G_F}}{G_b} \sqrt{h_w} = 5.66645 \frac{C \beta_{f,V\text{-cone}}^2 D^2}{\sqrt{1 - \beta_{f,V\text{-cone}}^4}} \frac{\sqrt{F_p G_F}}{G_b} \sqrt{h_w}$$

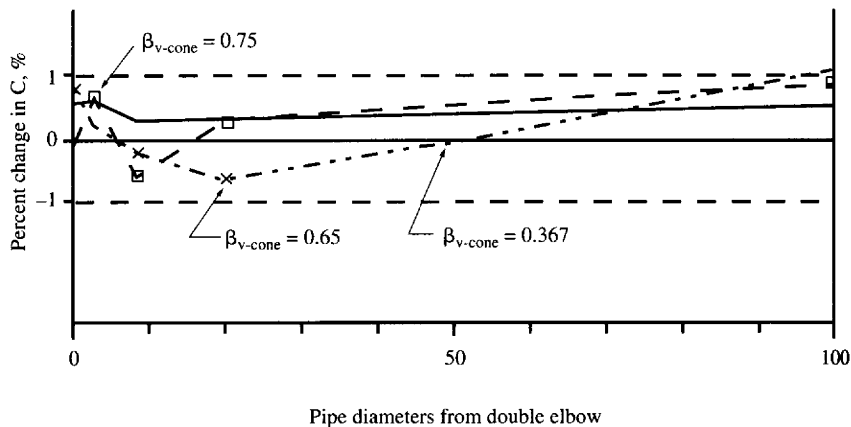
where the following relationship from Eq. 11.8 and $N_{\text{VG}} = 5.666455$ from Table 9.16 have been substituted:

$$\beta = \frac{d}{D} = \beta_{f,V\text{-cone}} = \frac{\sqrt{D^2 - d_{f,V\text{-cone}}^2}}{D}$$

and from Eq. 11.9



(a)



(b)

Figure 11.24 V-Cone. (a) Downstream of a single elbow. (b) Downstream of double out of plane elbows. (Courtesy McCrometer Div. of Ketema.)

$$d^2 = \beta_{f,V\text{-cone}}^2 D^2$$

WEDGE-TYPE RESTRICTIONS

There are several types of apertures through which the flow is constricted to produce a differential. The most common geometry is circular. Others include the annular and the *wedge* or segmental shape. In these geometries the streamlines are not concentric but are forced to the outside. The entering velocity profile will then have a differing effect on the produced differential and resulting discharge coefficient variations with Reynolds number. The segmental orifice is discussed in Chap. 10 and the annular devices, in this chapter; the Taylor wedge meter is discussed below.

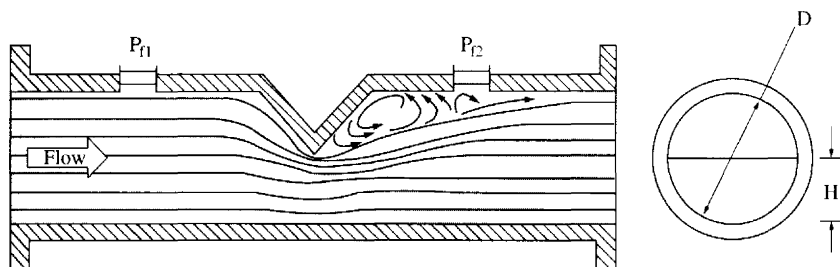
Taylor Wedge Meter Geometry

Shown in Fig. 11.25 is the basic geometry of a *wedge* flowmeter. The fluid is diverted downward in similar fashion to a segmental orifice but along a sloping wedge shape as opposed to a sharp edge. Pressure taps are located approximately one diameter upstream and downstream. This geometry and the use of remote seals makes these meters suitable for air-entrained liquids, slurry flow, water-laden gases, and, in general, any difficult-to-meter fluid.

Test results have shown that the effect of multiple or single elbows upstream and other disturbances are negligible at 10 to 20 pipe diameters and that the coefficient is essentially constant over a wide Reynolds number range. Some of the features are:

- Pipe sizes from 1/2 to 24 in (12.5 to 600 mm)
- Constant coefficient over a wide Reynolds number range
- Low overall pressure loss
- Suitable for slurry, corrosive, abrasive, or clean liquid, gas, or vapor flows

The product differential is a function of the ratio of segment height H to the meter body diameter D (Fig. 11.25). The equivalent beta ratio is



$$\beta_{\text{Wedge}} = \frac{d}{D} = \left(\frac{1}{\pi} \left\{ \arccos \left(1 - \frac{2H}{D} \right) - 2 \left(1 - \frac{2H}{D} \right) \left[\frac{H}{D} - \left(\frac{H}{D} \right)^2 \right]^{1/2} \right\} \right)^{1/2}$$

Figure 11.25 Wedge Flowmeter. (Courtesy ABB-Kent Taylor.)

$$\beta_{\text{wedge}} = \frac{d_f}{D_f} = \left(\frac{1}{\pi} \left[\arccos \left(1 - \frac{2H}{D} \right) - 2 \left(1 - \frac{2H}{D} \right) \left[\frac{H}{D} - \left(\frac{H}{D} \right)^2 \right]^{1/2} \right] \right)^{1/2} \quad (11.10)$$

where H is the segment height and D is the meter diameter.

The flow rate and differential equations given in Chap. 9 are used with the substitution for the flowing bore diameter d

$$d = \beta_{\text{wedge}} D \quad (11.11)$$

where D is defined by

$$D = F_{ad} D_{\text{meas}} = [1 + \alpha_p (T_F - 68)] D \quad (11.12)$$

The following yield ± 2 percent results for the discharge coefficient as defined in Chap. 9:

$$\text{For } D = 0.5 \text{ in (12.5 mm)} \quad C = 0.7883 + 0.107(1 - \beta_{\text{wedge}}^2) \quad (11.13)$$

$$\text{for } D = 1 \text{ to } 1.5 \text{ in (25 to 75 mm)} \quad C = 0.6143 + 0.718(1 - \beta_{\text{wedge}}^2) \quad (11.14)$$

$$\text{and, for } D > 1.5 \text{ in (75 mm)} \quad C = 0.5433 + 0.2453(1 - \beta_{\text{wedge}}^2) \quad (11.15)$$

Table 11.10 presents the Kd^2 values for the Taylor wedge. These values are substituted into the flow or differential pressure equations as

$$\frac{Cd^2}{\sqrt{1 - (d/D)^4}} = Kd^2 \quad (11.16)$$

where d is the flowing equivalent diameter defined by

$$d = F_{ad} d_{\text{meas}} = [1 + \alpha_{pE} (T_F - 68)] d_{\text{meas}} \quad (11.17)$$

For gas (vapor) flows the orifice gas expansion factor is selected. This equation is, for U.S. units,

$$Y_1 = 1 - (0.41 - 0.35\beta^4) \frac{h_w}{27.73 \text{ } kp_{f1}} \quad (11.18)$$

and, for SI units,

$$Y_1 = 1 - (0.41 + 0.35\beta^4) \frac{\Delta p}{kp_{f1}^*} \quad (11.19)$$

Example 11.6. A 1.02 specific gravity slurry is flowing through a 6-in (150-mm) wedge flowmeter that has an equivalent beta of 0.502. If the recorded differential is 85 in of water (21.2 kPa), what is the flowing gallons per minute using (1) the standard Kd^2 values and (2) the general discharge coefficient equation?

1. The flow-rate equation is obtained by substitution of Eq. (11.16) into the flow-rate equation from Table 9.36a:

$$q_{\text{gpm}} = 5.66645 \frac{Cd^2}{\sqrt{1 - (d/D)^4}} \sqrt{F_p G_F} \sqrt{h_w} = 5.66645 Kd^2 \sqrt{F_p G_F} \sqrt{h_w}$$

Table 11.10 Wedge Flowmeter Coefficients Kd^2

<i>D</i>					<i>D</i>				
in	mm	<i>H/D</i>	β_{wedge}	Kd^2	in	mm	<i>H/D</i>	β_{wedge}	Kd^2
0.5	13.	0.200	0.377	0.048	3.0	75.	0.400	0.611	2.620
1.0	25.	0.200	0.377	0.120	4.0	100.	0.400	0.611	4.600
1.5	40.	0.200	0.377	0.271	6.0	150.	0.400	0.611	10.340
2.0	50.	0.200	0.377	0.471	8.0	200.	0.400	0.611	17.700
3.0	75.	0.200	0.377	1.010	10.0	250.	0.400	0.611	28.200
4.0	100.	0.200	0.377	1.760	12.0	300.	0.400	0.611	40.200
0.5	13.	0.300	0.502	0.089	14.0	350.	0.400	0.611	49.000
1.0	25.	0.300	0.502	0.215	16.0	400.	0.400	0.611	63.000
1.5	40.	0.300	0.502	0.468	18.0	450.	0.400	0.611	80.000
2.0	50.	0.300	0.502	0.805	20.0	500.	0.400	0.611	100.000
3.0	75.	0.300	0.502	1.760	24.0	600.	0.400	0.611	145.000
4.0	100.	0.300	0.502	3.100	0.5	13.	0.500	0.707	0.185
6.0	150.	0.300	0.502	6.840	1.0	25.	0.500	0.707	0.430
8.0	200.	0.300	0.502	11.900	1.5	40.	0.500	0.707	1.056
10.0	250.	0.300	0.052	19.300	2.0	50.	0.500	0.707	1.670
12.0	300.	0.300	0.502	27.000	3.0	75.	0.500	0.707	3.650
14.0	350.	0.300	0.502	32.600	4.0	100.	0.500	0.707	6.300
16.0	400.	0.300	0.502	42.300	6.0	150.	0.500	0.707	14.130
18.0	450.	0.300	0.502	54.000	8.0	200.	0.500	0.707	24.200
20.0	500.	0.300	0.502	67.000	10.0	250.	0.500	0.707	38.100
24.0	600.	0.300	0.502	97.000	12.0	300.	0.500	0.707	56.800
0.5	13.	0.400	0.600	0.130	14.0	350.	0.500	0.707	67.000
1.0	25.	0.400	0.611	0.317	16.0	400.	0.500	0.707	85.000
1.5	40.	0.400	0.611	0.732	18.0	450.	0.500	0.707	109.000
2.0	50.	0.400	0.611	1.200	20.0	500.	0.500	0.707	133.000
					24.0	600.	0.500	0.707	194.000

Assuming no liquid compressibility ($F_p = 1.0$) and negligible thermal expansion ($F_{ad} = 1.0$), the flow rate is then computed as

$$q_{\text{gpm}} = (5.66645)(6.840) \sqrt{(1.0)(1.02)} \sqrt{85} \\ = 361 \text{ gpm (flowing gallons per minute)}$$

where $Kd^2 = 6.840$ from Table 11.10.

2. The general discharge coefficient by Eq. (11.15) is

$$C = 0.5433 + 0.2453(1 - \beta_{\text{wedge}}^2) = 0.5433 + 0.2453(1 - 0.502^2) = 0.7267$$

with the equivalent bore being, from Eq. (9.51),

$$d = \beta D = \beta F_{ad} D = (0.502)(1.0)(6.065) = 3.0446$$

where the meter diameter D is assumed to be that of a 6-in schedule 40 diameter (Table B.1):

$$q_{\text{gpm}} = 5.66645 \frac{Cd^2}{\sqrt{1 - (d/D)^4}} \sqrt{F_p G_F} \sqrt{h_w} \\ = (5.66645) \frac{(0.7267)(3.0446)^2}{\sqrt{1 - (3.0446/6.065)^4}} \sqrt{(1.0)(1.02)} \sqrt{85} = 355_{\text{gpm}}$$

where $D_f = F_{ad} D_{\text{meas}} = D_{\text{meas}} = 6.065$ in for negligible thermal expansion ($F_{ad} = 1.0$).

DYNAMIC PRESSURE DEVICES

Total, or stagnation, pressure measurements are commonly used to establish overall pressure loss, local velocity, and flow rates. A total (stagnation) pressure (Fig. 11.26a) is measured by inserting a bent tube into the flow and measuring the pressure. The total pressure is the sum of the fluid's static pressure and the dynamic pressure and is defined as

$$P_T = P_f + \frac{\rho_f V_p^2}{2g_c} \quad (11.20)$$

where P_T is the total, or stagnation, (lb_f/ft^2 , Pa) pressure, P_f is the static pressure (lb_f/ft^2 , Pa) at the measured point, V_p is the velocity (ft/s , m/s) of the fluid at the location of the probe tip, and ρ_f is the fluid density (lb_m/ft^3 , kg/m^3).

Equation 11.20 can be rearranged to an equation for calculating the point velocity as

$$V_p = \sqrt{\frac{2g_c(P_T - P_f)}{\rho_f}} \quad (11.21)$$

For a gas (vapor) flow the fluid is assumed to be isentropically compressed at the impact point, and a gas compression factor can be derived as, for U.S. units,

$$\Gamma_{\text{Pitot}} = \sqrt{1 - \frac{1}{2k} \frac{h_w}{27.73p_f} + \frac{k-1}{6k^2} \left(\frac{h_w}{27.73p_f} \right)^2} \quad (11.22)$$

and, for SI units,

$$\Gamma_{\text{Pitot}} = \sqrt{1 - \frac{1}{2k} \frac{\Delta p^*}{p_f^*} + \frac{k-1}{6k^2} \left(\frac{\Delta p^*}{p_f^*} \right)^2} \quad (11.23)$$

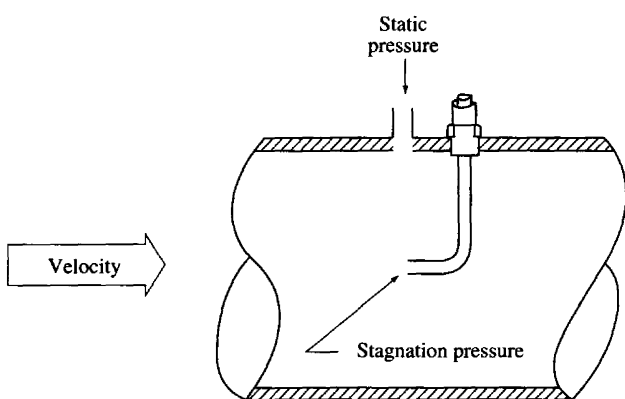
where k is the isentropic exponent.

Pitot Tube

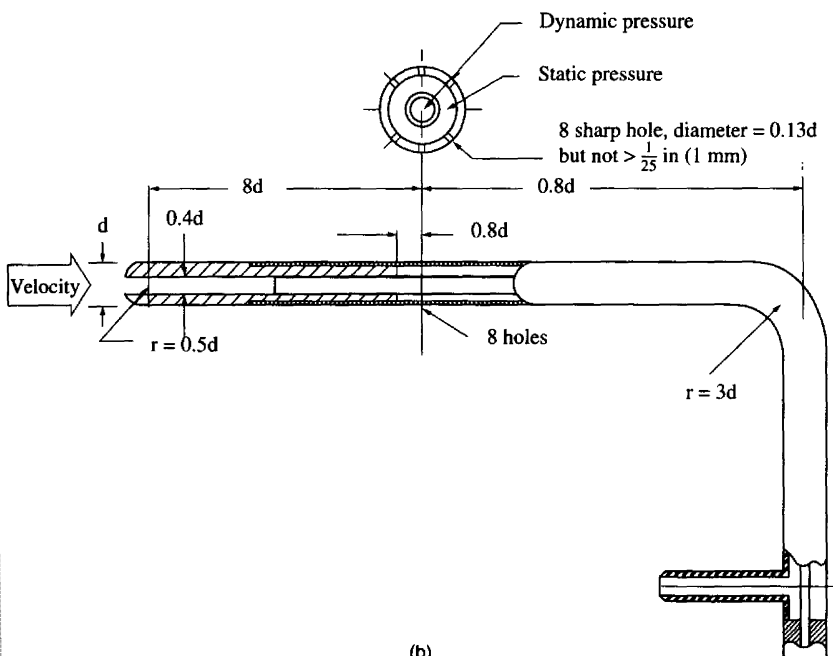
A pitot tube consists of an impact tube bent at 90° to the flow with static pressure openings located downstream of the stagnation measuring point (Fig. 11.26b and c). The two pressure lines are coaxial such that the inner tube transmits the total (stagnation) pressure and the outer tube the static pressure. A differential pressure transmitter connected to the impact pressure port and the static pressure port will measure the difference in pressure. The equation for point velocity is then, for U.S. units (ft/s),

$$V_p = 18.27999 K_{\text{Pitot}} \Gamma_{\text{Pitot}} \sqrt{\frac{h_w}{\rho_f}} \quad (11.24)$$

and, for SI units (m/s),

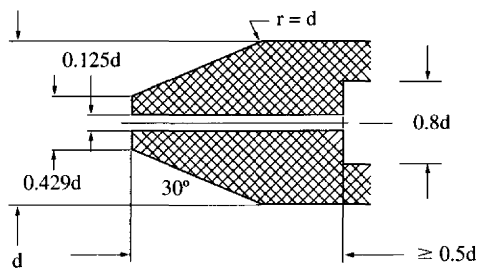
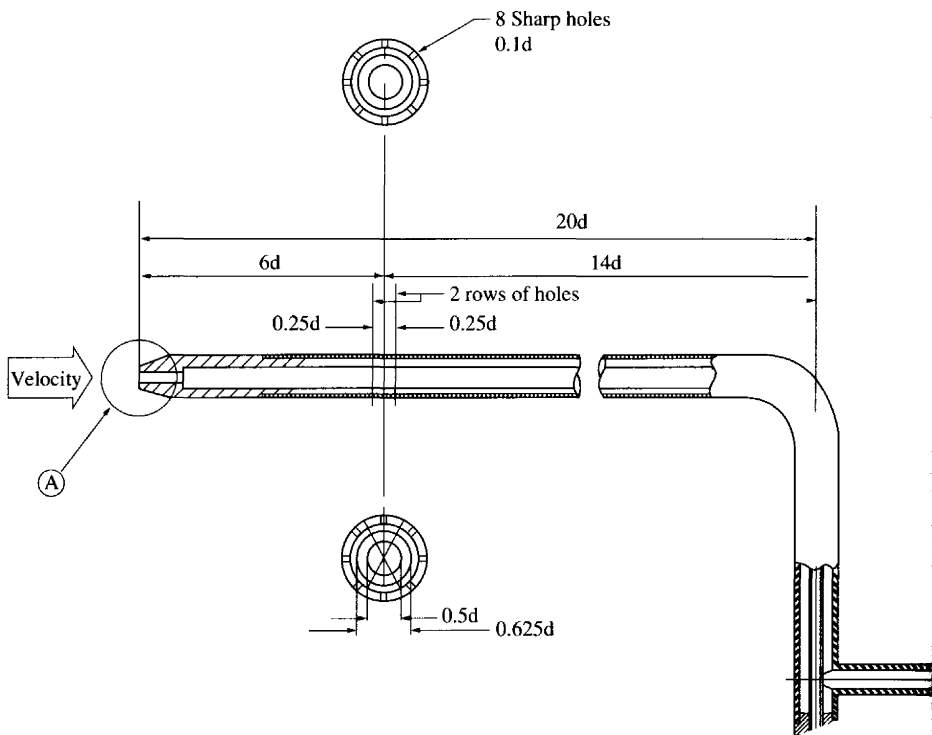


(a)



(b)

Figure 11.26 Pitot tubes. (a) Basic pitot. (b) ISO rounded nose. (c) ISO tapered nose.



(c)

Figure 11.26 (Continued)

$$V_p^* = 44.72136 K_{\text{Pitot}} \Gamma_{\text{Pitot}} \sqrt{\frac{\Delta p^*}{\rho_f^*}} \quad (11.25)$$

In Eqs. 11.24 and 11.25 K_{Pitot} is pitot coefficient and Γ_{Pitot} is the gas (vapor) compression factor, the gas expansion factor Γ_{Pitot} being equal to 1.0 for a liquid. For standardized pitots (ISO 3966, 1977) the pitot coefficient K_{Pitot} is 1.0.

There are numerous pitot-tube-type designs, and the coefficient may range from 0.8 to 1.0 depending upon design. For these cases a calibrated coefficient is used or an average valve for the design is provided by the manufacturer.

The flow rate is calculated by traversing the circular section to establish a mean velocity location. The pitot is then placed at that point. Table 11.11 shows traverse positions for several methods used for establishing this average location. Note that the average volumetric flow rate is then

$$q_{\text{cfs}} = A \bar{V}_f \quad (11.26)$$

where A is the area of the pipe (ft^2) and \bar{V}_f is the average pipe line velocity. This velocity is the calculated velocity for a pitot located at a point in the pipe corresponding to average velocity as determined by a velocity traverse.

The substitution of variables for the flow rate equations of Tables 9.36 through 9.38 is then

$$K_{\text{Pitot}} \Gamma_{\text{Pitot}} D^2 = \frac{C Y_1 d^2}{\sqrt{1 - (d/D)^4}} \quad (11.27)$$

Precautions. Pitot tubes are primarily used to measure velocity at a point. If the flow is distorted or the pitot is located at a fixed position, the effect of profile changes with Reynolds number will not be measured, and an error is introduced. ISO 3966 estimates that an accuracy of ± 2 percent is possible for a traversed pipe with an axisymmetric velocity profile. To achieve this accuracy, other corrections may need to be made. The following possible bias errors are listed:

- Pitot tube coefficient (K_{Pitot})
- Stem blockage
- Local velocity correction
- Reynolds number correction
- Traverse velocity gradients
- Turbulence correction for static pressure location aft of the total pressure plane
- Inclination of pitot tube with respect to the flow direction

Example 11.7. A pitot tube is to be used to measure 80°F (27°C) water flowing in a 24-in schedule 40 pipe. Assuming that sufficient upstream pipe is available to establish a turbulent profile, what is (1) the location for the pitot if the relative pipe roughness is $\varepsilon/D = 0.001$, (2) the flow rate in flowing gallons per minute q_{gpm} if the differential is 10 in of water using the basic pitot equation, and (3) using the equations of Chap. 9?

Data are determined as follows:

- From Table 9.16, $N_{vp} = 44.7493$
- From Table B.1, $D_{\text{meas}} = 22.624$ in
- From Table B.4, $\alpha_p = 0.0000067$ in/(in $\cdot^\circ\text{F}$)
- From Table E.4, $\rho_f = 62.216$ lb $_m$ /ft 3

TABLE 11.11 Location for Averaging with a Pitot Tube

Locations		Centroid of equal area		Newton-Cotes		Tchebyshef		Gauss	
		Radius	Weight	Radius	Weight	Radius	Weight	Radius	Weight
2	1	0.500	1/2	0	1/2	0.4597	1/2	0.4597	1/2
	2	0.866	1/2	1	1/2	0.8881	1/2	0.8881	1/2
3	1	0.4082	1/3	0	0.1667	0.3754	1/3	0.3357	0.2778
	2	0.7071	1/3	0.7071	0.6667	0.7252	1/3	0.7071	0.4444
	3	0.9129	1/3	1.0	0.1667	0.9358	1/3	0.9420	0.2778
4	1	0.3536	1/4	0	0.1250	0.3314	1/4	0.2635	0.1739
	2	0.6124	1/4	0.5774	0.3750	0.6124	1/4	0.5745	0.3261
	3	0.7906	1/4	0.8165	0.3750	0.8000	1/4	0.8185	0.3261
	4	0.9354	1/4	1	0.1250	0.9524	1/4	0.9647	0.1739
5	1	0.3162	1/5	0	0.0778	0.2866	1/5	0.2166	0.1185
	2	0.5477	1/5	0.5000	0.3556	0.5700	1/5	0.4804	0.2393
	3	0.7071	1/5	0.7071	0.1333	0.6892	1/5	0.7071	0.2844
	4	0.8367	1/5	0.8660	0.3556	0.8472	1/5	0.8771	0.2393
	5	0.9487	1/5	1	0.0778	0.9622	1/5	0.9763	0.1185

1. The location of the pitot can be determined from Fig. 5.4 by initially assuming that the pipe Reynolds number is 1,000,000. From Fig. 5.4 for a relative roughness of $\epsilon/D = 0.001$, the location from the pipe wall is

$$\frac{\bar{y}}{r_p} = 0.29$$

The pipe diameter corrected for thermal expansion is

$$\begin{aligned} D &= [1 + \alpha_p(T_F - 68)]D_{\text{meas}} \\ &= [1 + 0.0000067(80 - 68)] 22.624 = 22.626 \text{ in} \end{aligned}$$

and the pitot would then be located from the pipe wall by

$$\bar{y} = 0.29 \frac{D}{2} = 0.29 \frac{22.626}{2} = 3.28 \text{ in}$$

The velocity at this average point is, by Eq. 11.24,

$$\bar{V}_f = 18.28 K_{\text{Pitot}} \Gamma_{\text{Pitot}} \sqrt{\frac{h_w}{\rho_f}} = (18.28)(1.0)(1.0) \sqrt{\frac{10}{62.216}} = 7.329 \text{ ft/s}$$

where for a pitot $K_{\text{Pitot}} = 1.0$ and for a liquid $\Gamma_{\text{Pitot}} = 1.0$.

The volumetric flow rate is then, by Eq. 11.26,

$$q_{\text{cfs}} = A \bar{V}_f = \left[\frac{\pi \left(\frac{D}{12} \right)^2}{4} \right] \bar{V}_f = \left[\frac{\pi \left(\frac{22.626}{12} \right)^2}{4} \right] 7.329 = 20.463 \text{ ft}^3/\text{s}$$

and by Eq. 3.57 the flowing gallons per minute is

$$q_{\text{gpm}} = 448.8312 q_{\text{cfs}} = (448.8312)(20.463) = 9184 \text{ gpm}$$

2. From Table 9.36 the flow-rate equation is

$$q_v = q_{\text{gpm}} = N_{vp} \frac{Cd^2}{\sqrt{1 - (d/D)^4}} \frac{1}{\sqrt{F_p \rho_F}} \sqrt{h_w} = 44.74932 K_{\text{Pitot}} D^2 \frac{1}{\sqrt{F_p \rho_F}} \sqrt{h_w}$$

where Eq. (11.27) has been substituted, $K_{\text{Pitot}} D^2 = Cd^2 / \sqrt{1 - (d/D)^4}$ for a liquid $\Gamma_{\text{Pitot}} = Y_1 = 1.0$

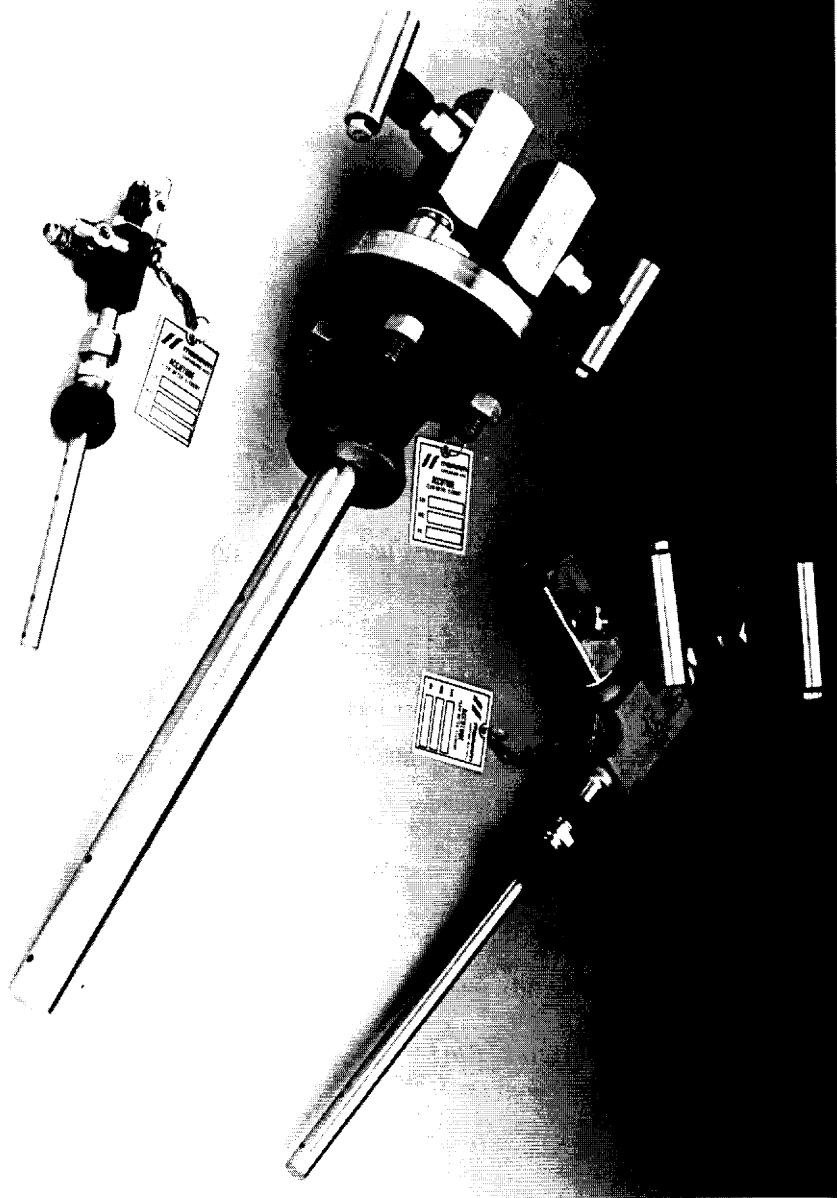
Substitution yields the flow rate as

$$q_{\text{gpm}} = (44.749)(1.0)(22.626)^2 \frac{1}{\sqrt{(1.0)(62.216)}} \sqrt{10} = 9184 \text{ gpm}$$

Area Averaging

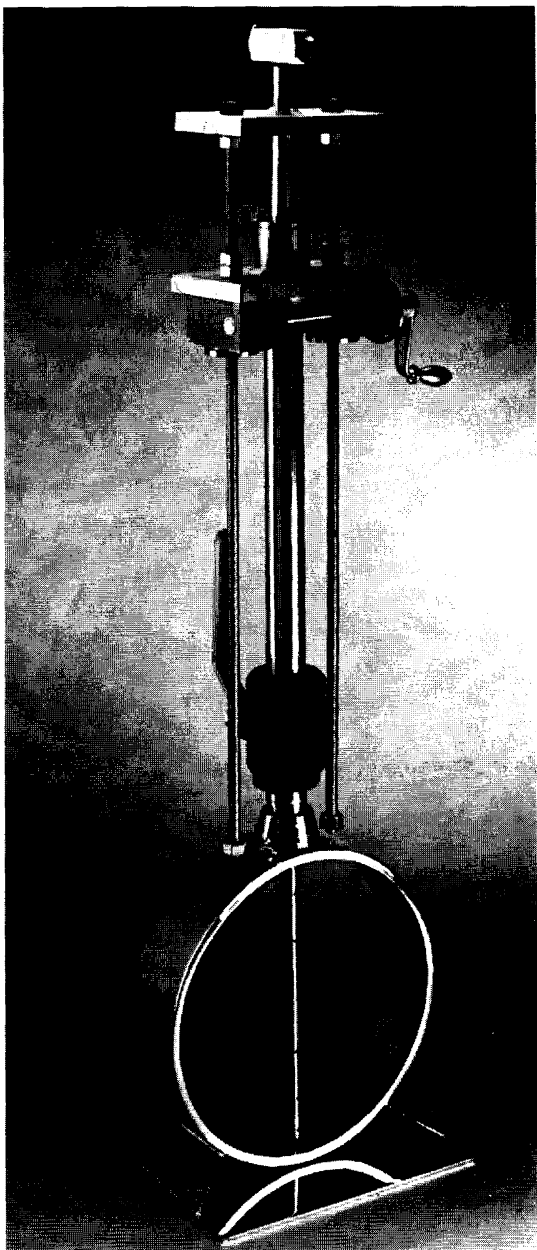
Pitot tubes are seldom used in industrial applications because of vibration, lack of ruggedness, and the need for a velocity traverse to obtain measurements within approximately ± 2 percent. Multiport elements based on the pitot principle are, however, widely used in many applications.

There are several basic design geometries for multiport averaging pitot-primary meters (ASME MFC-SC17, 1988). The strut may be round (Fig. 11.27a), diamond



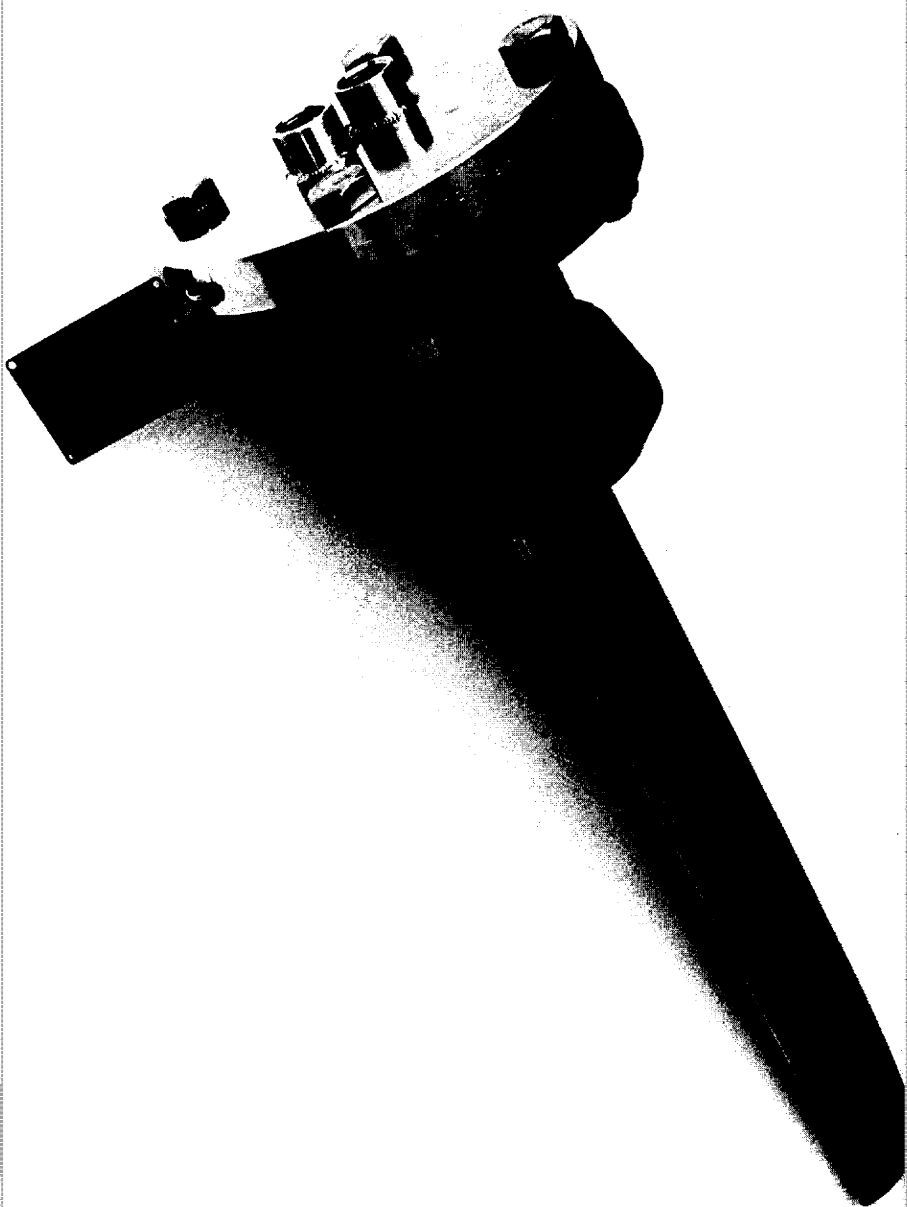
(a)

Figure 11.27 Area averaging meters. (a) Accutube. (Courtesy Meriam Instrument.) (b) Annubar. (Courtesy Dieterich Standard Corp.) (c) Ellipse. (Courtesy PRESSO Meter Corporation.)



(b)

Figure 11.27 *(Continued)*



(c)

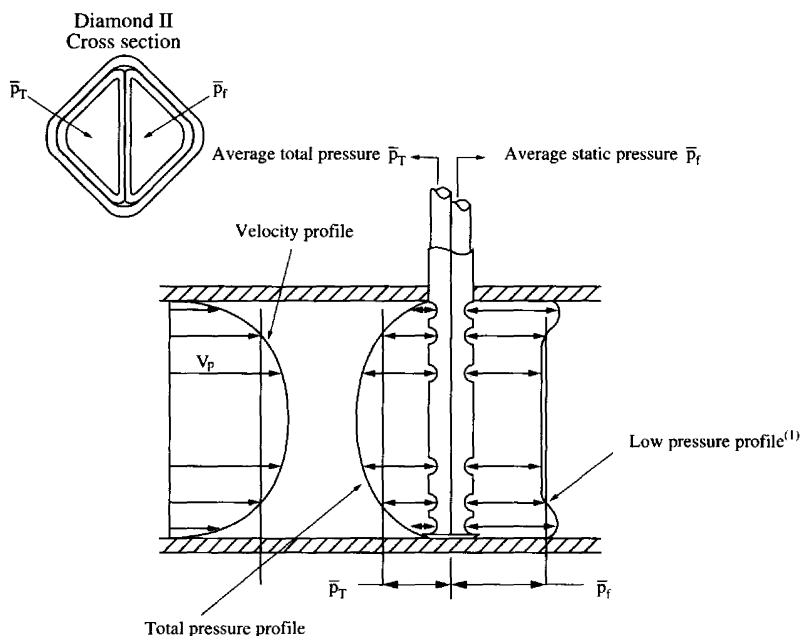
Figure 11.27 *(Continued)*

(Fig. 11.27b), or elliptical (Fig. 11.27c). The basic principle (Fig. 11.28) is to locate upstream total pressure ports along a strut that spans the pipe. These total pressure measuring points are positioned at the defining *area averaging* location for the averaging method selected, such as Tchebyshef, centroid of area, Gauss, etc. The measuring *static pressure* ports are positioned downstream at a location selected by the manufacturer to give the optimum performance. The measured *static pressure* is normally lower than the true fluid static pressure because of a *suction* effect at these locations. This pressure is generally referred to as the *low pressure*.

The upstream velocity profile produces the total pressure profile and the low-pressure profile shown in Fig. 11.28. The averaged total pressure \bar{p}_T and flowing low pressure \bar{p}_f are transmitted to a differential pressure transmitter through the channel sections, the pressure tap locations being placed in accordance with the averaging method.

The performance of uncalibrated Diamond II annubar is based on extensive data used to develop a flow coefficient equation. The annubar uses the ratio of projected sensor area to pipe area as the correlating parameter (Fig. 11.29). The dimensional similarity of the annubar's geometry and the statistical correlation of various line-size data have demonstrated that this correlation yields a prediction equation within the manufacturer's uncertainty limits. The ratio of areas can be expressed, in terms of an effective beta, as

$$\beta_{f,ann} = \sqrt{\frac{\text{projected area}}{\text{pipe area}}} = \sqrt{\frac{d_{f,ann} D}{\pi/4 D^2}} = \sqrt{\frac{4}{\pi} \frac{d_{ann}}{D}} \quad (11.28)$$



⁽¹⁾This pressure is normally less than the true fluid static pressure

Figure 11.28 Diamond II Annubar principle of operation.

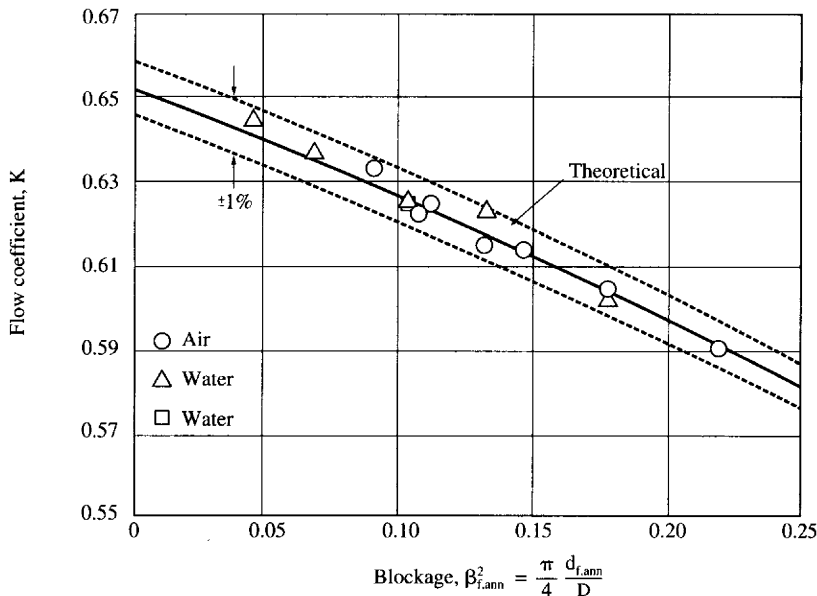


Figure 11.29 Blockage effect of flow coefficient. (Courtesy Dieterich Standard Corp.)

where $d_{f,ann}$ is the width of the annubar, and D is the pipe diameter, both at flowing conditions.

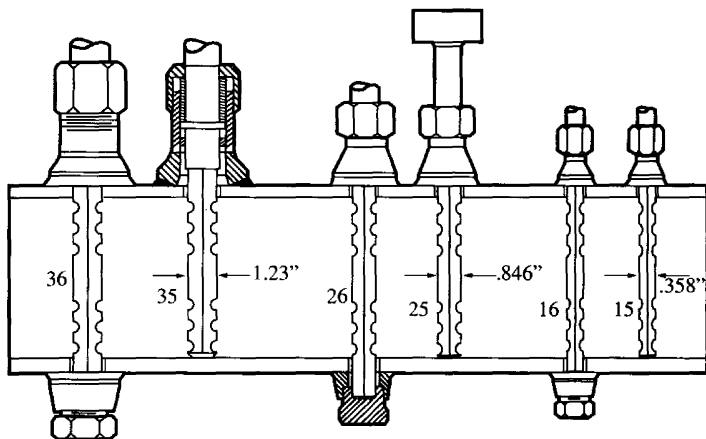
This *blockage* relationship (Wyler 1975) provides an experimental and theoretical basis for the equation. As blockage $\beta_{f,ann}$ increases when a similar probe is inserted in a smaller pipe, the confining wall causes the local velocity to increase at the sensor, developing a higher total pressure. This results in a lower flow coefficient, as seen in Fig. 11.29.

The Diamond II annubar flow coefficient was derived based on two assumptions:

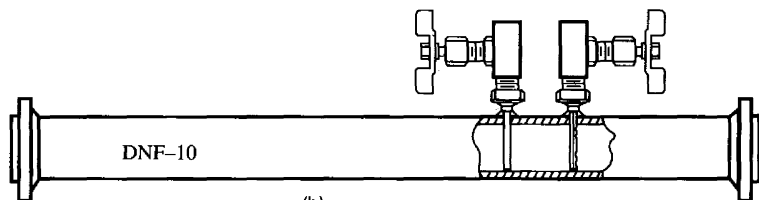
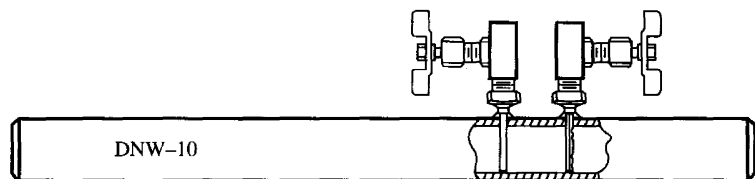
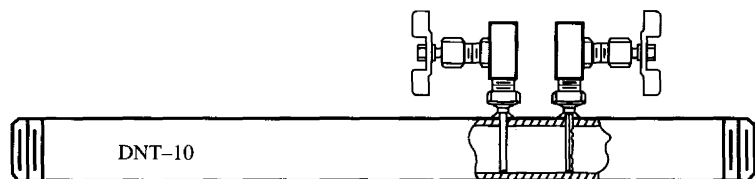
1. The measured low pressure is lower than the line *static pressure* because of flow separation. This results in a *suction* effect that provides a differential approximately twice that of a traditional pitot tube.
2. The blockage effect results in a slightly higher differential.

Meters are designed to either be supported at both ends or supported at one end only (Fig. 11.30). Insert meters are widely used and *hot tapping* is easily accomplished. Since the primary element spans the pipe vortex, shedding or other fluid-induced forces will act on the structure. This requires that structural integrity under operating conditions be checked. The manufacturer's literature or sizing/flow PC software usually provides checks for these conditions.

Overall pressure loss depends on geometry and blockage ratio. For large pipe sizes overall pressure loss is negligible; manufacturers should be consulted for overall pressure loss estimates. Accuracy claims range from $\pm 3/4$ to 3 percent depending on design and installation conditions. The upstream straight lengths of pipe are specified by the manufacturer. The differential pressure lead line connections are important, and the manufacturer's instructions should be carefully followed.



(a)



(b)

Figure 11.30 Diamond II Annubar models. (a) Regular. (b) Inline. (Courtesy Dieterich Standard Corp.)

The flow rate and differential pressure equations of Chap. 9 are used with the substitution of, for U.S. units,

$$KYD_f^2 = \frac{CY_1 d^2}{\sqrt{1 - (d/D)^4}} \quad (11.29)$$

and, for SI units,

$$KYD_f^{*2} = \frac{CY_1 d^{*2}}{\sqrt{1 - (d^*/D^*)^4}} \quad (11.30)$$

For liquids $Y = 1.0$.

Table 11.12 gives the flow coefficient values K , gas expansion factor Y for the cylindrical Diamond II annubar, and the PRESSO ellipse geometries. Table 11.13 are the U.S./SI differential pressure equations, and in Table 11.14 are the U.S./SI flow rate equations.

Example 11.8. An area-averaging meter is to be used to measure the 80°F (27°C) water of Example 11.7. Determine the differential for (1) a Meriam accutube (2) a 1 1/4-in (31.8-mm) Ellipse meter, and (3) a type 35 Diamond II annubar.

Data are determined as follows

- From Table 9.16, $N_{vp} = 44.7493$
- From Table B.1, $D_{meas} = 22.626$ in
- From Table B.4, $\alpha_p = 0.0000067$ in/(in·°F)
- From Table B.4, $\alpha_{pE} = 0.0000097$ in/(in·°F)
- From Table E.4, $\rho_F = 62.216$ lb_m/ft³

The differential pressure equation from Table 9.41(c) is

$$h_w = \frac{1 - (d_f/D_f)^4 F_p \rho_F}{N_{vp}^2 C^2 d^4} q_v^2 = \frac{q_{gpm}^2 F_p \rho_F}{(44.7493)^2 K^2 D^4} = \frac{(9184)^2 (1.0) (62.216)}{(44.7493)^2 K^2 (22.626)^4} = \frac{10}{K^2}$$

where the substitution of variables from Eq. 11.29 has been made with $Y = 1.0$ for a liquid, and the flow rate and corrected diameter are from Example 11.7.

1. For a 1 in (25-mm) Accutube cylinder with the flow coefficient from Table 11.12,

$$h_w = \frac{10}{K^2} = \frac{10}{(0.708)^2} = 19.9 \text{ in}$$

where $K = 0.708$ is from Table 11.12.

2. For a 1 1/4 in ellipse geometry,

$$h_w = \frac{10}{(0.7050)^2} = 20.1 \text{ in}$$

where $K = 0.7050$ is from Table 11.12.

3. For a Diamond II Annubar, the blockage for a Type 35 Annubar is calculated by

$$d_{f,ann} = [1 + \alpha_{pE}(T_F - 68)]d_{ann} = [1 + 0.0000095(80 - 68)]1.23 = 1.2301$$

TABLE 11.12 Flow Coefficients K and Expansion Factors for Area Averaging Flow Meters†

Annubar Diamond II geometry					
Flow coefficient					
$K = \frac{1 - a \beta_{\text{ann}}^2}{\sqrt{1 + b(1 - a \beta_{\text{ann}}^2)^2}}$					
Types 15, 16, 25, 26, 35, 36, 45, 46	$a = 0.8468$	$b = 1.34966$			
Type 10	$a = 1.38155$	$b = 1.20107$			
$\beta_{\text{ann}} = \sqrt{\frac{4}{\pi} \frac{d_{f,\text{ann}}}{D}} \quad d_{f,\text{ann}} = [1 + \alpha_{\text{ann}}(T_F - 68)]d_{\text{ann}} \quad D = [1 + \alpha_P(T_F - 68)]D_{\text{meas}}$					
Type	10	15/16	25/26	35/36	45/46
d_{ann} in (mm)	0.1830 (4.6482)	0.3576 (9.0830)	0.8460 (21.4884)	1.2300 (31.242)	1.980 (50.292)
Expansion factor					
U.S. units	$Y = 1 - [0.31424 - (1 - \beta_{\text{ann}})^2 - 0.09484] \frac{h_w}{27.73kp_f}$				
SI units	$Y = 1 - [0.31424 - (1 - \beta_{\text{ann}})^2 - 0.09484] \frac{\Delta p^*}{p_f}$				

TABLE 11.12 Flow Coefficients K and Expansion Factors for Area Averaging Flow Meters† (*Continued*)

Pipe size scd. 40	Ellipse PRESSO Ellipse Geometry				Cylinder Meriam Accutube			
	$\frac{7}{8}$ in 22.2 mm	$1\frac{1}{4}$ in 31.75 mm	$2\frac{1}{4}$ in 57.15 mm	$\frac{3}{8}$ in 10 mm	$\frac{1}{2}$ in 12.5 mm	$\frac{3}{4}$ in 20 mm	1 25 mm	$2\frac{3}{8}$ in 60 mm
	Flow coefficient							
2	0.6295			0.638	0.557			
$2\frac{1}{2}$	0.6364			0.617	0.598			
3	0.6523			0.665	0.645			
$3\frac{1}{2}$	0.6528			0.661	0.630			
4	0.7180			0.672	0.656			
5	0.7288			0.671	0.656			
6	0.7377			0.706	0.662	0.706	0.647	
8	0.8088	0.7633		0.665	0.673	0.686	0.678	
10	0.7829	0.7515		0.696	0.682	0.676	0.657	
12	0.7446	0.7375				0.683	0.677	
14	0.7333	0.7457	0.7212			0.698	0.665	0.603
16	0.7281	0.7144	0.7133			0.688	0.691	0.618
18	0.7201	0.7125	0.7115			0.689	0.678	0.628
20	0.7196	0.7105	0.7100			0.686	0.705	0.634
24	0.7187	0.7050	0.6655			0.789	0.708	0.645
30	0.7155	0.7025	0.7015			0.720	0.664	0.671
36	0.7111	0.7017	0.6985			0.757	0.663	0.652
42	0.7100	0.6995	0.6979			0.697	0.672	0.733
	Expansion factor							

TABLE 11.13 U.S./SI Unit Differential Pressure Equations for Elbow and Area Averaging Meters

	U.S.	SI
	Mass flow rate (Liquid/gas/vapor)	
Density	$h_w = \frac{1}{(358.9268KD^2 Y) \rho_{f1}^2} q_{PPH}^2$	$\Delta p^* = \frac{1}{(0.126447KD^{*2} Y) \rho_{f1}^{*2}} q_{KPH}^2$
	Volumetric at flowing conditions (Liquid)	
Specific gravity	$h_w = \frac{F_p G_F}{(5.666455KD^2)^2} q_{GPM}^2$	$\Delta p^* = \frac{F_p G_F}{(0.06667619KD^{*2})^2} q_{lpm}^2$
	Volumetric at base conditions (Liquid)	
Specific gravity	$h_w = \frac{G_b^2}{(5.666455KD^2)^2 F_p G_F} q_{GPM}^2$	$\Delta p^* = \frac{G_b^2}{(0.06667619KD^{*2})^2 F_p G_F} q_{LPM}^2$
	Volumetric at base conditions (Gas)	
<i>pvT</i> equation	$h_w = \frac{p_b^2 G Z_{f1} T_{f1}}{(218.4834KD^2 Y Z_b T_b)^2 p_{f1}} (q_{SCFH})_b^2$	$\Delta p^* = \frac{p_b^2 G Z_{f1} T_{K1}}{(0.06774938KD^{*2} Y Z_b T_{Kb})^2 p_{f1}} (q_{SCMH})_b^2$

Note: For liquids $Y = 1.0$.

TABLE 11.14 U.S./SI Unit Flow Rate Equations for Elbow and Area Averaging Meters

Mass flow rate (Vapor)		
Density	$q_{PPH} = 358.9268 KYD^2 \sqrt{h_w \rho_{f1}}$ $R_{Df} = \frac{6.31597 q_{PPH}}{\mu_{cP} D}$	$q_{KPH} = 0.126447 KYD^{*2} \sqrt{\Delta p^* \rho_{f1}^*}$ $R_{Df} = \frac{353.676 q_{KPH}}{\mu_{cP} D^*}$
Volumetric flow rate at flowing conditions (Liquid)		
Specific gravity	$q_{gpm} = 5.666455 KDd^2 \sqrt{F_p G_F} \sqrt{h_w}$ $R_{Df} = \frac{3159.432 F_p G_F q_{gpm}}{\mu_{cP} D}$	$q_{lpm} = 0.06667619 KDd^{*2} \sqrt{F_p G_F} \sqrt{\Delta p^*}$ $R_{Df} = \frac{21199.697 F_p G_F q_{lpm}}{\mu_{cP} D_f^*}$
Volumetric flow rate at base conditions (Liquid)		
Specific gravity	$q_{GPM} = 5.666455 KD^2 \frac{\sqrt{F_p G_F}}{G_b} \sqrt{h_w}$ $R_{Df} = \frac{3159.432 G_b q_{GPM}}{\mu_{cP} D}$	$q_{LPM} = 0.06667619 KD^{*2} \frac{\sqrt{F_p}}{G_b} \sqrt{\Delta p^*}$ $R_{Df} = \frac{21199.697 G_b q_{LPM}}{\mu_{cP} D^*}$
(Gas)		
PVT equation	$(q_{SCFH})_b = 218.4834 KD^2 \frac{Y Z_b T_b \sqrt{p_{f1}}}{p_b \sqrt{G Z_{f1} T_{f1}}} \sqrt{h_w}$ $R_{Df} = \frac{17.04569 G p_b (q_{SCFH})_b}{Z_b T_b \mu_{cP} D}$	$(q_{SCMH})_b = 0.06774938 KD^{*2} \frac{Y_1 Z_b T_{kb} \sqrt{p_{f1}^*}}{p_b^* \sqrt{G Z_{f1} T_{K1}}} \sqrt{\Delta p^*}$ $R_{Df} = \frac{1232.003 G p_b (q_{SCMH})_b}{Z_b T_b \mu_{cP} D^*}$

then, by Eq. 11.26,

$$\beta_{f,ann} = \sqrt{\frac{4}{\pi} \frac{d_{f,ann}}{D}} = \sqrt{\frac{4}{\pi} \frac{1.2301}{22.626}} = 0.2631$$

Substitution into the flow coefficient equation of Table 11.12 yields

$$K = \frac{1 - 0.8468 \beta_{f,ann}^2}{\sqrt{1 + 1.34966(1 - 0.8468 \beta_{f,ann}^2)^2}} = 0.63525$$

the produced differential is then

$$h_w = \frac{10}{(0.63525)^2} = 24.8 \text{ in}$$

Example 11.9. A 15-mm target flowmeter is to measure the flow rate of the gasoline of Example 2.12. The maximum flow rate is 50 L/min. Determine (1) the upper-range force value F_{URV} , (2) the flow rate when the reading is 20 percent of the URV, and (3) the overall pressure loss at maximum flow. (The flow rate is to be measured in base volume units.)

The flow-rate equation [Eq. (f) of Table 9.37] is

$$q_{LPM}^* = N_{VG}^* \frac{Cd^*}{\sqrt{1 - (d^*/D^*)^4}} \frac{\sqrt{F_p} \sqrt{G_F}}{G_b} \sqrt{\Delta p^*}$$

Substitution of variables from Table 11.1 gives the flow-rate equation for a target flowmeter as

$$q_{LPM}^* = N_{VG}^* K (35.68248) \frac{1 - \beta_T^2}{\beta_T} D^* \sqrt{F_p} \sqrt{G_F} \frac{\sqrt{F_T^*}}{G_b}$$

Data is determined as follows: From Table 9.17, $N_{VG}^* = 0.0666762$. From Eq. (11.7),

$$F_a^* = 1 + \alpha_{PE}^* (T_{cC} - 20) = 1 + 0.0000173(26.9 - 20) = 1.00012$$

where, from Table B.4, $\alpha_{PE}^* = 0.0000173 \text{ mm}/(\text{mm} \cdot ^\circ\text{C})$. The geometry factor is, from Table 11.4,

$$35.68248 \frac{1 - \beta_T^2}{\beta_T} D^* = 222.6825$$

From Example 2.16, $F_p = 1.0088$; from Example 2.12, $G_F = 0.7255$ and $G_b = 0.7359$; and, from Example 9.1, $\mu_{cP} = 0.417$.

Substitution now gives

$$\begin{aligned} q_{LPM}^* &= (0.0666762)(K)(1.00012)(222.6865) \sqrt{1.0088} \sqrt{0.7255} \frac{\sqrt{F_T^*}}{0.7359} \\ &= 17.263K \sqrt{F_T^*} \end{aligned}$$

The pipe Reynolds number is, by Eq. (f) of Table 9.21,

$$R_D = 1413.5 \frac{G_b}{\mu_{cP} D^* N_{VG}^*} q_V^* = 1413.5 \frac{0.7359}{(0.417)(13.87)(0.06667)} q_{LPM}^*$$

$$= 2698 q_{LPM}^*$$

Scaling to normal operating conditions gives

$$(q_{LPM}^*)_N = 0.8(q_{LPM}^*)_{URV} = 40$$

The Reynolds number is then

$$(R_D)_N = (2698)(40) = 107,920$$

From Table 11.5 or Fig. 11.12, the flow coefficient is $K = 0.69163$. Rearranging the flow-rate equation to solve for target force yields

$$(F_T^*)_N = \left(\frac{q_{LPM}^*}{17.263K} \right)_N^2 = \left[\frac{40}{(17.263)(0.69163)} \right]^2 = 11.224 \text{ N}$$

1. The upper-range force value is then

$$(F_T^*)_{URV} = 11.224 \left(\frac{50}{40} \right)^2 = 17.54 \text{ N}$$

2. The flow rate at 20 percent of URV is

$$q_{LPM}^* = 17.263K \sqrt{F_T^*} = (17.263)(0.69163) \sqrt{F_T^*}$$

$$= F_{MC} \sqrt{F_T^*} = 11.940 \sqrt{(0.2)(17.54)}$$

$$= 22.36 \text{ L/min}$$

(Note: The flow coefficient is constant for $R_D > 4000$.)

3. The overall pressure loss at URV flow is, from Eq. (11.1) and Table 11.4 for the loss coefficient,

$$\Delta p_L^* = K_{LT}^* F_T^* = (8.35)(17.54) = 146 \text{ kPa}$$

Example 11.10. A 3-in (75-mm) target flowmeter with $\beta_T = 0.523$ is to measure the flow rate of ammonia vapor. The URV flow rate is 12,500 lb_m/h (5670 kg/h). Determine (1) the upper-range force value $(F_T^*)_{URV}$, (2) the maximum permanent pressure loss, and (3) the flow rate at 25 percent of URV target force.

The process conditions are

$$T_F = 100^\circ\text{F} \quad p_G = 165 \text{ psig} \quad \mu_{cP} = 0.0105 \quad \rho_f = 0.5797 \text{ lb}_m/\text{ft}^3$$

From Eq. (g) of Table 9.36, the flow-rate equation is

$$q_{PPH} = N_{MP} \frac{Cd^2}{\sqrt{1 - (d/D)^4}} Y_1 \sqrt{\rho_{f1}} \sqrt{h_w}$$

Substitution of variables from Table 11.1 gives the target-flowmeter flow-rate equation as

$$q_{\text{PPH}} = N_{M\rho} K F_a (5.941939) \frac{1 - \beta_T^2}{\beta_T} D \sqrt{\rho_f} \sqrt{F_T}$$

From Table 9.14, $N_{M\rho} = 358.9268$, and from Eq. (11.6),

$$F_a = 1 + \alpha_{PE}(T_F - 68) = 1 + (0.0000096)(100 - 68) = 1.00031$$

where, from Table B.4, $\alpha_{PE} = 0.0000096 \text{ in}/(\text{in} \cdot ^\circ\text{F})$. The geometry factor, from Table 11.4 is,

$$5.941939 \frac{1 - \beta_T^2}{\beta_T} D = 25.33773$$

Substitution now gives

$$\begin{aligned} q_{\text{PPH}} &= (358.9268)(K)(1.00031)(25.33773) \sqrt{0.5797} \sqrt{F_T} \\ &= 6926.4K \sqrt{F_T} \end{aligned}$$

The pipe Reynolds number is, from Eq. (g) of Table 9.20,

$$\begin{aligned} R_D &= 2266.97 \frac{1}{\mu_{cP} DN_{M\rho}} q_{\text{PPH}} = 2266.97 \frac{1}{(0.0105)(3.068)(358.93)} q_{\text{PPH}} \\ &= 196.1 q_{\text{PPH}} \end{aligned}$$

Scaled to normal operating conditions, the flow rate is

$$(q_{\text{PPH}})_N = 0.8(q_{\text{PPH}})_{\text{URV}} = (0.8)(12,500) = 10,000$$

The Reynolds number at normal conditions is then

$$(R_D)_N = (196.1)(10,000) = 1,961,000$$

From Table 11.5, for a target flowmeter with $\beta = 0.523$,

$$\begin{aligned} K &= 0.57810 + 0.011170 \log R_D = 0.57810 + 0.011170 \log 1,961,000 \\ &= 0.64839 \end{aligned}$$

The target force at normal conditions is then

$$(F_T)_N = \left(\frac{q_{\text{PPH}}}{6926.4K} \right)^2 = \left[\frac{10,000}{(6926.4)(0.64839)} \right]^2 = 4.958 \text{ lb}_f$$

1. The upper-range force is then

$$(F_T)_{\text{URV}} = 4.958 \left(\frac{12,500}{10,000} \right)^2 = 7.747 \text{ lb}_f$$

2. The maximum permanent pressure loss is, from Eq. (11.4), with the loss coefficient from Table 11.4,

$$\Delta p_L = K_{LT} F_T = (0.126)(7.747) = 0.98 \text{ lb/in}^2$$

3. The flow rate at 25 percent URV target force is

$$q_{PPH} = 6926.4K \sqrt{F_T} = 6926.4K \sqrt{(0.25)(7.747)} = 9639.3K$$

For an initial estimate $K_0 = 0.64839$, the Reynolds number is

$$R_D = 196.1q_{PPH} = (196.1)(9639.3)(0.64839) = 1,225,600$$

which, when substituted into the flow-coefficient equation, gives the second estimate for K as

$$K_1 = 0.57810 + 0.011170 \log R_D = 0.64611$$

A third estimate gives

$$(q_{PPH})_2 = 9639.3K_1 = 6228.0 \quad R_D = 1,221,300$$

and

$$K_2 = 0.64609$$

The flow rate is then

$$q_{PPH} = 9639.3K_2 = (9639.3)(0.64609) = 6227.9 \text{ lb}_m/\text{h}$$

Without iteration the flow rate would be calculated as

$$q_{PPH} = F_{MC} \sqrt{F_T} = (6926.4)(0.64839) \sqrt{F_T} = 4491 \sqrt{F_T} = 6250 \text{ lb}_m/\text{h}$$

ELBOW FLOWMETER

When fluid moves around the curved path of an elbow, it is subjected to an angular acceleration. The resulting centrifugal force creates a differential pressure between the inner and outer radii. The square root of this differential is proportional to the flow rate and is the basis of the operation of the elbow flowmeter.

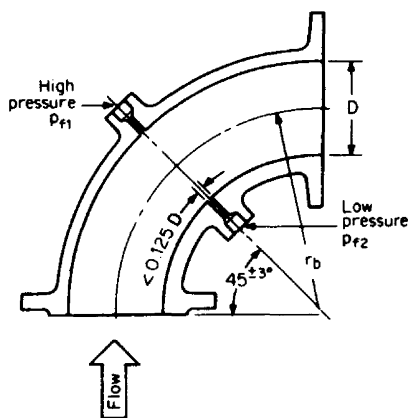


Figure 11.31 Elbow flowmeter.

The elbow flowmeter is shown in Fig. 11.31. Pressure taps are located at 45° and are of the same construction as orifice taps. Special care must be used to align the tap holes in both planes; the alignment should be checked by sliding a rod through the taps. The inside of the elbow should be commercially smooth, and the mean diameter D must be taken as the average of four measurements made at the entrance and exit elbow plane. The bend radius r_b is the mean of the inside and outside radii.

Murdock (1963) correlated available elbow-tap data with the Lansford (1936) flow-coefficient equation to within ± 4 percent, provided normal upstream straight-pipe requirements for high-

β orifices are followed. The Lansford flow-coefficient equation is, with the addition of the recommended ASME (1971) Reynolds-number correction term,

$$K = \sqrt{\frac{r_b}{2D}} + \frac{6.5 \sqrt{r_b/2D}}{R_D^{0.5}} \quad (11.31)$$

where $R_D > 10^4$ and $r_b/D > 1.25$. For these limits, Eq. (11.31) provides the flow coefficient to within ± 4 percent. Values of $\sqrt{r_b/2D}$ for standard elbows are listed in Table 11.15. Precision is comparable with that of an orifice with a calibrated elbow.

Some tests have indicated that the differential measured at $22\frac{1}{2}^\circ$ rather than at 45° is more stable, reliable, and less affected by approach conditions. The equation for $22\frac{1}{2}^\circ$ taps is

$$K = \frac{[(2r_b/D)^2 - 1]\{\ln[(2r_b/D + 1)/(2r_b/D - 1)]\}}{4 \sqrt{2r_b/D}} \quad (11.32)$$

The flow-rate and differential-pressure equations of Chap. 9 are used with the substitution of, for U.S. units,

$$\frac{CY_1 d^2}{\sqrt{1 - (d/D)^4}} = KYD^2 \quad (11.33)$$

and, for SI units,

$$\frac{CY_1 d^{*2}}{\sqrt{1 - (d^*/D^*)^4}} = KYD^{*2} \quad (11.34)$$

Listed in Table 11.13 are the differential pressure equations and in Table 11.14 are the flow-rate equation for elbow flowmeters.

The gas expansion factor has not been experimentally determined for all fluids. A single test by Reimer (1983), using air as the flowing medium, yielded a gas expansion factor expressed, for U.S. units, as

TABLE 11.15 Values of $\sqrt{r_b/2D}$ for Welding-End Elbows

Nominal line size D , in (mm)	$\sqrt{r_b/2D}$			
	Short radius		Long radius	
	Schedule 40	Schedule 80	Schedule 40	Schedule 80
2(50)	0.696	0.718	0.852	0.880
3(75)	0.699	0.719	0.856	0.881
4(100)	0.705	0.723	0.863	0.885
6(150)	0.703	0.721	0.861	0.884
8(200)	0.708	0.724	0.867	0.887
10(250)	0.706	0.716	0.865	0.877
12(300)	0.707	0.715	0.866	0.875

$$Y_1 = 1 + 1.3 \left(\frac{h_w}{27.73 p_{f1}} \right)^{1/2} \quad (11.35)$$

and, for SI units, by

$$Y_1 = 1 + 1.3 \left(\frac{\Delta p^*}{p_{f1}^*} \right) \quad (11.36)$$

In the flow-rate and differential equations, K replaces the term $C/\sqrt{1 - (d/D)^4}$ and D^2 replaces d^2 . Upstream piping should be in accordance with an orifice for which $\beta = 0.75$, with a minimum of 10 pipe diameters of straight pipe.

Example 11.11. For the gas flow data presented below, calculate the upper-range value for a differential-pressure transmitter to be used with a Schedule-80 long-radius elbow; also calculate the flow rate when the differential is 50 percent of the URV.

For a selected base, the flow-rate equation [Eq. (m) of Table 9.37] is

$$q_{SCMH}^* = (N_{vPT}^*)_b \frac{Cd^2}{\sqrt{1 - (d^*/D^*)^4}} \frac{Y_1 Z_b T_{kb} \sqrt{p_{f1}^*}}{p_b^* \sqrt{G Z_{f1} T_{k1}}} \sqrt{\Delta p^*}$$

Substituting the variables from Table 11.1 gives the elbow-flowmeter flow-rate equation as

$$q_{SCMH}^* = (N_{vPT}^*)_b K Z_b T_{kb} D^{*2} \frac{\sqrt{\Delta p^*} p_{f1}^*}{\sqrt{Z_{f1}} \sqrt{T_{k1}} \sqrt{G} p_b^*}$$

Flow data is

$$(N_{vPT}^*)_b = 0.067749 \quad D_{meas}^* = 300 \text{ mm} \quad G = 0.63$$

$$Z_b = 1.0 \quad p_{f1}^* = 8700 \text{ kPa} \quad p_b^* = 103 \text{ kPa}$$

$$T_{kb} = 288.15 \text{ K} \quad Z_{f1} = 0.8840 \quad F_{aD}^* = 1.0003$$

$$T_{k1} = 323.15 \text{ K}$$

Scaling to normal operating conditions and substituting gives

$$(0.8)(170,000) = (0.067749)(1.0)(288.15)(300.09)^2 K_N$$

$$\times \frac{\sqrt{\Delta p^*}_N \sqrt{8700}}{\sqrt{0.8840} \sqrt{323.15} \sqrt{0.63} (103)}$$

$$(0.8)(170,000) = 118,684 K_N \sqrt{(\Delta p^*)_N}$$

$$K_N \sqrt{(\Delta p^*)_N} = 1.1459$$

where $D^* = F_{aD}^* D_{meas} = (1.0003)(300) = 300.09 \text{ mm}$.

The flow coefficient K is given by Eq. (11.35) in SI units as

$$K = \sqrt{\frac{r_b^*}{2D^*}} + \frac{6.5 \sqrt{r_b^*/2D^*}}{R_D^{0.5}}$$

For a long-radius bend, $r_b^*/D^* = r_b/D$, and, from Table 11.10, $\sqrt{r_b/2D} = 0.875$. At normal operating conditions, the Reynolds number from Example 11.7 is $(R_D)_N = 8,674,000$. Substitution into Eq. (11.34) gives

$$K_N = 0.875 + \frac{(6.5)(0.875)}{(8,674,000)^{0.5}} = 0.8769$$

The differential pressure at normal conditions is then

$$(\Delta p^*)_N = \left(\frac{1.1459}{K_N} \right)^2 = \left(\frac{1.1459}{0.8769} \right)^2 = 1.708 \text{ kPa}$$

and the differential at the URV is

$$(\Delta p^*)_{URV} = 1.708 \frac{1}{0.64} = 2.668 \text{ kPa}$$

The initial estimate of the flow rate at 20 percent of the URV is

$$q_{SCMH}^* = 118,684K \sqrt{\Delta p^*} = (118,684)(0.8769) \sqrt{(0.2)(2.668)} = 76,024$$

Example 11.12. For the gasoline of Example 9.3, calculate the flow rate in base gallons per minute if the differential pressure across a short radius 45° elbow tap meter is 4 in (1 kPa) of water.

Data from Example 9.3 is:

$$G_F = 0.7255 \quad G_b = 0.7395 \quad F_p = 1.0088 \quad \alpha_p = 0.0000096 \text{ in}/(\text{in} \cdot ^\circ\text{F})$$

$$\mu_{cp} = 0.417 \quad T_F = 80.5^\circ\text{F} \quad D_{meas} = 1.939 \text{ in}$$

The flow coefficient equation is written from Eq. (11.11) as

$$K = \sqrt{\frac{r_b}{2D}} + \frac{6.5 \sqrt{r_b/D}}{R_D^{0.5}} = 0.696 + \frac{(6.5)(0.696)}{R_D^{0.5}} = 0.696 + \frac{4.524}{R_D^{0.5}}$$

The corrected pipe diameter is, from Equation 9.50,

$$D = [1 + \alpha_p(T_F - 68)]D_{meas} = [1 + 0.0000096(80.5 - 68)](1.939) = 1.9392 \text{ in}$$

The flow rate equation, from Table 11.14 is

$$\begin{aligned} q_{GPM} &= 5.66645KD^2 \frac{\sqrt{F_p G_F}}{G_b} \sqrt{h_w} \\ &= (5.666)(K)(1.9392)^2 \frac{\sqrt{(1.0088)(0.7255)}}{(0.7359)} \sqrt{h_w} = 24.77K \sqrt{h_w} \end{aligned}$$

The flowing Reynolds is, from Table 11.14,

$$R_{Df} = \frac{3159 G_b q_{GPM}}{\mu_{cp} D} = \frac{(3159)(0.7359)q_{GPM}}{(0.417)(1.9392)} = 2874q_{gpm}$$

The iteration for flow rate is then

	<i>n</i>		
	1	2	3
$q_{n-1} = 24.77 K_{n-1} \sqrt{h_w}$	34.478	35.192	35.184
$(R_D)_{n-1} = 2874 q_{n-1}$	99,095	101,141	101,118
$K_n = 0.696 + \frac{4.524}{(R_D^{0.5})_{n-1}}$	0.7104	0.7102	0.7102
$q_n = 24.77 K_n \sqrt{h_w}$	35.192	35.184	35.184

The Reynolds number is calculated as, from Eq. (m) of Table 9.21,

$$R_D = 83.467 \frac{G p_b^*}{Z_b T_{Kb} \mu_{cP} D^* (N_{vPT}^*)_b} q_{SCMH}^*$$

From Fig. H.6, $\mu_{cP} = 0.0145$, and, assuming $Z_b = 1.0$,

$$R_D = 83.467 \frac{(0.63)(103)}{(1.0)(288.15)} \frac{1}{(0.0145)(300)(0.06775)} q_{SCMH}^*$$

$$R_D = (63.780)(76,024) = 4,849,000$$

and the flow coefficient K becomes

$$K = 0.875 + \frac{(6.5)(0.875)}{(4,849,000)^{0.5}} = 0.8776$$

The flow rate is then

$$q_{SCMH}^* = (118,684)(0.8776) \sqrt{(0.2)(2.668)} = 76,085 \text{ standard m}^3/\text{h}$$

Without a Reynolds-number correction, the flow-rate equation is written as

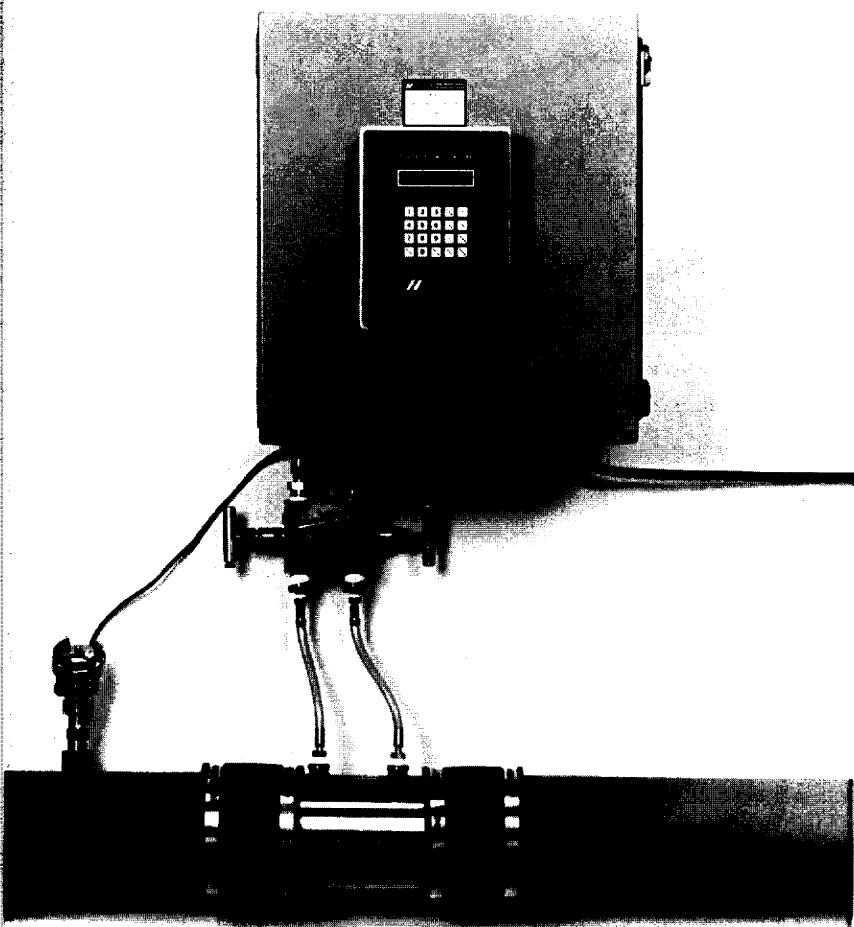
$$q_{SCMH}^* = 118,684 K_N \sqrt{\Delta p^*} = 104,074 \sqrt{\Delta p^*} = F_{MC} \sqrt{\Delta p^*}$$

where F_{MC} , the meter-coefficient factor, is 104,074. The uncorrected flow rate at 20 percent of the URV is then

$$q_{SCMH}^* = F_{MC} \sqrt{\Delta p^*} = 104,074 \sqrt{(0.2)(2.668)} = 76,024 \text{ standard m}^3/\text{h}$$

LAMINAR FLOW ELEMENT

Laminar flow occurs when the Reynolds number is below 2000. In this flow regime the pressure loss across a length of pipe is inversely proportional to the Reynolds number. Shown in Fig. 11.32a is a laminar flowmeter that consists of a large number of small-diameter channels (Fig. 11.32b). The flow through these parallel ducts is essentially the entering pipeline velocity. If dimensions are reduced, laminar flow will occur within each duct section. The differential across the *laminar* element is then proportional to the flow rate (velocity) in accordance with the Hagan-Poiseuille law for laminar flow pressure drop. The flow rate for laminar meters can then be expressed as



(a)

Figure 11.32 Laminar flowmeter. (a) Meriam Model 50MH10. (b) Meriam matrix. (Courtesy Meriam Instrument.)

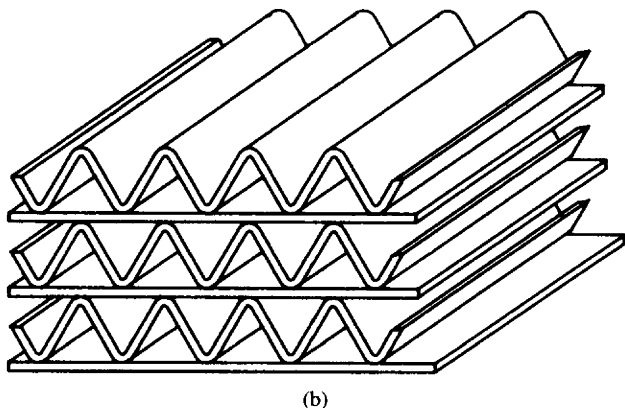


Figure 11.32 (Continued)

$$q = \frac{k_1 \Delta P}{\mu} \quad (11.37)$$

where k_1 is a constant based on meter design, q is the volumetric flow rate, and μ is the absolute viscosity.

The overall pressure loss is the same as the produced differential, approximately 8 in (2.5 kPa) of water. Meters are normally used on gas flows, but the principle applies to liquids. Meters are calibrated to establish the k_1 factor to within ± 0.5 percent. The lower limit of the linear flow-rate range is limited to the acceptable accuracy of the differential pressure measurement device. Since laminar flow is achieved by small passage areas, as small as 0.009 in (0.228 mm) in some meter sizes, the metered fluid must be clean. Accuracy of ± 0.25 percent is attainable with a precision of ± 0.1 percent (Weigand and Lombardo, 1989).

The laminar flow element is often used in pulsative flow applications because of its linear relationship, and the element itself introduces a damping action on the system. To minimize the error in the measurement of differential when large pulsative amplitudes are encountered, it is recommended that porous plugs (or linear damping devices) be inserted in the differential pressure tap lead lines.

Laminar flow elements are widely used to meter the flow of clean low-pressure gases and are commonly used to measure air flow to internal combustion engines, where severe pulsative flow conditions occur. Other examples are air flow for fans, air motors, valves, and filters. The measurements of leakage rates from airplane cabins, home windows, and storm windows are other applications.

Figure 11.33 and Table 11.16 list the capacities of the Meriam laminar flow-meter. The capacity shown for each meter is in standard cubic feet per minute of air at a pressure base of 29.92 in Hg (14.695 psia, 101.32 kPa) and at a base temperature of 70°F (21.1°C). The listed values are to be used for sizing purposes only. The flow-rate equation to be used for a particular application will depend on additional correction factors depending on the flow-rate units desired. The manufacturer should be consulted for any specific application factors. The flow rate of gases other than air are determined, for sizing purpose, by

$$q_{\text{SCFM, gas}} = \left(\frac{14.695}{p_f} \right) \left(\frac{T_f}{530} \right) \left(\frac{\mu_{\text{cP, gas}}}{0.018187} \right) q_{\text{SCFM, air}} \quad (11.38)$$

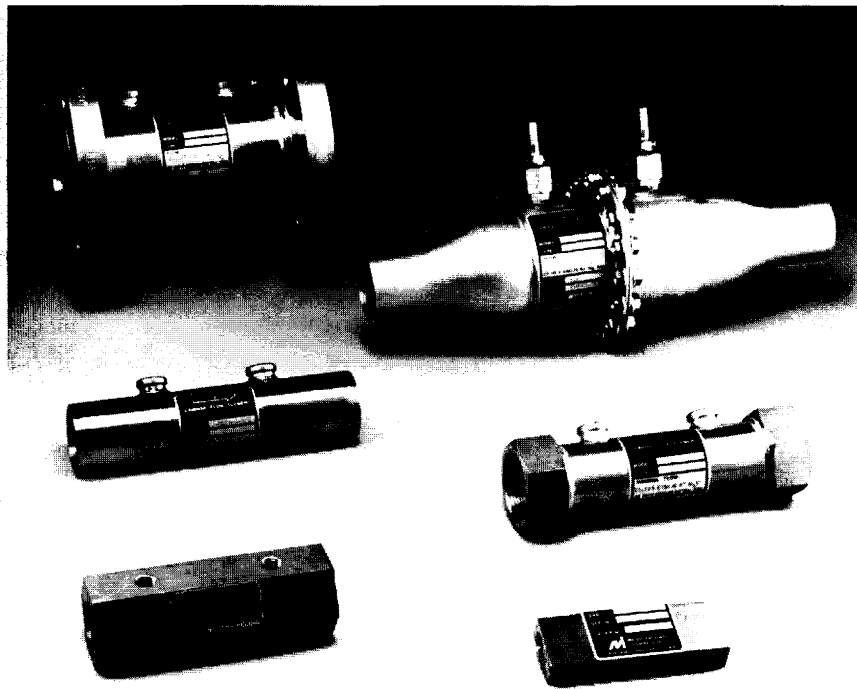


Figure 11.33 Meriam laminar flowmeter models. Row 1 Model 50MY15 Model 50MC2. Row 2 Model 50MH10 Model 50MW20. Row 3 Model 50MJ10 Model 50MK10. (Courtesy Meriam Instrument.)

To maintain *laminar* flow with linearity, the meter must be within the operating Reynolds number range. The Meriam laminar flowmeters will produce linear flow characteristics when the Reynolds number is 150 in (101.6 mm) of water and is 300 at 8-in (203.2-mm) differential. The maximum Reynolds number is calculated by

$$R_{D,\max} = \frac{0.0464 G p_f h_{w,\text{gas}}}{\mu_{cp}} \quad (11.39)$$

The differential for the gas is determined by the ratio equation at maximum flow,

$$h_w = \frac{q_{\text{SCFM,gas}}}{q_{\text{SCFM,air}}} h_{w,\text{air}} \quad (11.40)$$

Example 11.13. Select a Meriam laminar flowmeter for an argon flow rate of 0.9 SCFM at a pressure of 34.695 psia (239 kPa) and a temperature of 60°F (15.6°C). The properties of helium are:

- Viscosity, $\mu_{cp} = 0.02225$ cP
- Specific gravity, $G = 0.138$

The equivalent air flow rate by Eq. (11.38) is

TABLE 11.16 Meriam Laminar Flow Elements*

Size in	mm	Model	q_{SCFM}^{\dagger}	$q_{cc/min}^{\dagger}$	$q_{litres/min}^{\dagger}$	h_w	Differential (max) mmH ₂ O
1/4	6	50MK10-8	0.00019	5.38		4	101.6
		7	0.00062	17.70		4	101.6
		6	0.00124	35.10		4	101.6
		5	0.00250	70.80		4	101.6
		4	0.00460	130.00		4	101.6
		3	0.00180	229.00		4	101.6
		2	0.01490	422.00		4	101.6
		1	0.04600	1300.00		4	101.6
1/2	13	50MJ10-14	0.10		2.83	8	203.2
		13	0.18		5.10	8	203.2
		12	0.38		10.80	8	203.2
		11	0.70		19.80	8	203.2
		10	1.60		45.30	8	203.2
		9	3.00		85.00	8	203.2
1	25	50Mw20-1	7.7		212	8	203.2
1 1/4	32	1 1/4	22		633	8	203.2
1 1/2	38	1 1/2	40		1130	8	203.2
1	25	50MH10-1	8		212	8	203.2
1 1/4	32	1 1/4	16		453	8	203.2
1 1/2	38	1 1/2	23		651	8	203.2
2	51	2	40		1130	8	203.2
3	76	3	90		2550	8	203.2
4	76	4	160		4530	8	203.2
	102	5	250		7080	8	203.2
5							
6	127	6	360		10200	8	203.2
8	152	8	640		18100	8	203.2
10	203	10	1000		28300	8	203.2
12	254	12	1440		40800	8	203.2
16	305	16	2250		63700	8	203.2
2 1/2	64	50MY-2 1/2	60		1700	8	203.2
3	76	3	90		2550	8	203.2
4	102	4	160		4530	8	203.2
5	127	5	250		7080	8	203.2
6	152	6	360		10200	8	203.2
8	203	8	640		18100	8	203.2
10	254	10	1000		28300	8	203.2
12	305	12	1440		40800	8	203.2
16	406	16	2250		63700	8	203.2
Hose Size							
2" I.D.	50	50MC2-2	100		28300	8	203.2
4" I.D.	100	4	400		11300	8	203.2
6" I.D.	150	6	1000		28300	8	203.2
8" I.D.	200	8	2250		63700	8	203.2

*Manufacturer should be consulted for latest information: rated flow for standard units is 30 psig (207 kPa) and 150°F (65.6°C)

[†]Base gas air: p_b = at 14.695 psia (101.32 kPa), T_b = 529.67°R (294.26 K), μ_{cp} = 0.01817 $R_{D,base}$ = 300 at h_w = 8 in, or at h_w = 4 in $R_{D,base}$ = 150

$$q_{\text{SCFM,gas}} = \left(\frac{14.695}{p_f} \right) \left(\frac{T_f}{529.67} \right) \left(\frac{\mu_{\text{cP,gas}}}{0.018187} \right) \\ = \left(\frac{14.695}{34.695} \right) \left(\frac{459.67 + 60}{529.67} \right) \left(\frac{0.022251}{0.018187} \right) (0.9) = 4.58 \text{ SCFM}$$

From Table 11.16 the Model 50MJ10-11 has a 0.7 rating at $h_w = 8$ in. The differential, by Eq. (11.34), is

$$h_w = (8) \left(\frac{0.458}{0.7} \right) = 5.23 \text{ in}$$

The Reynolds number is then, by Eq. (11.39),

$$R_{D,\text{max}} = \frac{0.0464 G p_f h_{w,\text{gas}}}{\mu_{\text{cP}}} = \frac{(0.0464)(0.138)(34.695)(5.23)}{(0.02225)} = 522$$

This Reynolds number is greater than 300 and a larger size needs to be selected. A Model 50MJ Type 10 will produce

$$h_{w,\text{gas}} = 2.29 \text{ and } R_{D,\text{max}} = 228$$

REFERENCES

- ASME: *Fluid Meters*, 6th ed., ASME, New York, 1971.
- ASME MFC-SC17, *Measurement of Fluid Flow in Closed Conduits using Multiport Averaging Pitot-Primary Meters* (draft), ASME MFC-SC-17, 1988.
- Bell, K. J., and O. D. Bergelin: "Flow through Annular Orifices," *Trans. ASME*, vol. 79, pp. 593-601, 1957.
- and —: "Laminar and Transition Flow in Annular Orifices of Fine Clearance," *Flow Measurement in Closed Conduits* (symp. proc.), Her Majesty's Stationery Office, Edinburgh, 1962.
- Clark, T. W.: "Design and Operation of Target Flowmeters," *Encyclopedia of Fluid Mechanics*, Gulf Pub. Co., Houston, TX, 1986.
- Curran, D. E.: "Laboratory Determination of Flow Coefficient Values for the Target Type Flowmeter at Low Reynolds Number Flows," in *Flow, Its Measurement and Control in Science and Industry*, vol. 2, ISA, Research Triangle Park, N.C., 1981.
- Felton, G. L.: "Low Flow Measurement with the Integral Orifice," *Chem. Eng. Proc.*, vol. 68, no. 1, 1972.
- Howell, A. R.: *Annular Airflow Orifice*, Report 1934, Ministry of Aircraft, London, 1939.
- ISO 3966, *Measurement of Fluid Flow in Closed Conduits—Velocity Area Method Using Pitot Static Tubes*, International Standards Organization, Geneva, 1977.
- Lansford, W. M.: *The Use of an Elbow in a Pipe Line for Determining the Rate of Flow in a Pipe*, University of Illinois Engineering Experimental Station Bulletin 289, 1936.
- Murdock, J. W., C. J. Foltz, and C. Gregory: "Performance Characteristics of Elbow Flowmeters," ASME WAM Paper 63-WA-17, 1963.
- Reimer, R. M.: "Elbow Meter Measurement of Air Flow at High Pressure Ratio," ASME paper 83-WA/FM-1, 1983.

Reinecke, M. E., W. G. Ragains, W. G. Fox, and R. W. Miller: "An Experimental Study of the Capability of Measuring Gas Mass Flow," *Pittsburgh Flow Measurement Symposium*, vol. 1, ASME, New York, 1966.

Weigand, J., and L. Lombardo: "The Use of Laminar Flow Element in Computerized Flow Measurement," ISA paper 89-002, ISA, 1989.

Wyler, J. S.: "Probe Blockage Effect in Free Jets and Closed Tunnels," *Trans. ASME, J. Eng. Power*, p. 509, October 1975.

DIFFERENTIAL PRODUCERS: COMPUTATIONS

Depending on the desired accuracy, flow-rate determination may require only a simple visual observation of differential pressure on a square-root chart, or it may involve the use of a dedicated microprocessor that receives several measurement signals and calculates the flow rate. Compensation for pressure and/or temperature variations on chart indications may mean using pneumatic or electronic analog computers. Total flow, rather than flow rate, can be computed or determined by chart integration. The choice of measurement equipment, calculation procedure, computation means, and data-transmission means is extensive. This chapter presents some of the commonly used equipment and calculations for chart integration.

GENERAL PRINCIPLES

Measured and Unmeasured Variables

The flow-rate calculation can be viewed as the product of three terms: an unmeasured-variable term, a measured-variable term, and differential pressure. Differential pressure is always measured. The unmeasured-variables term includes a unit conversion factor and all factors assumed to be constant; the measured variables are quantities that must be measured for the desired accuracy (see Chap. 4). The unmeasured variables are combined into a meter-coefficient factor F_{MC} which commonly includes pipe and primary-element bore dimensions and the discharge coefficient. Measured variables are usually density-related (such as pressure and temperature) or are derived from other measurements (such as the Reynolds-number correction, which is derived from the flow rate, and the gas expansion factor, which is derived from differential- and absolute-pressure measurements). Depending on process variations, the designer determines which variables must be measured and which can be assumed constant.

As an example, the mass flow equation for liquids may be written as

$$q_{PPH} = [N_{MP} K d^2 \sqrt{F_p}]_{UMV} [G_F]_{MV} \sqrt{h_w} \quad (12.1)$$

The first bracketed term contains the unmeasured variables; that is, after the pipe and bore diameter are measured and the thermal-expansion factor, liquid-compressibility factor, and discharge coefficient are calculated, the designer con-

siders their product constant. The flow coefficient K appears within the brackets, which implies that this Reynolds-number factor is also assumed constant. The second bracketed term is the measured variable, specific gravity. The equation thus reduces to

$$q_{PPH} = [F_{MC}]_{UMV} [\sqrt{G_F}]_{MV} \sqrt{h_w} \quad (12.2)$$

If the specific gravity were assumed constant, it would be included as an unmeasured variable, and the equation would be simplified to

$$q_{PPH} = [F_{MC}]_{UMV} \sqrt{h_w} \quad (12.3)$$

Similar simplified equations can be written for the equations given in Tables 9.36 through 9.38, and for the fixed-geometry devices discussed in Chap. 11. For many flow measurements, particularly when differential producers have been sized at normal flow-rate conditions, Eq. (12.3) is acceptable. However, for range and when temperature and pressure vary significantly, the designer must decide whether the added cost of including additional *measured* variables is warranted. *It is worth noting that initially selected design conditions may be different from process conditions. Significant errors can result if the values of the unmeasured variables are not checked. Using computers for more accurate calculation when unmeasured variables are inaccurate would be of little value.*

Analog Computers

Many manufacturers supply analog computers that receive two or three standardized 3- to 15-lb/in² (20- to 100-kPa), 4- to 20-mA, or 0- to 5-V input signals proportional to measured variables—for example, differential pressure, temperature, and absolute pressure. Pneumatic computers receive scaled inputs and *mechanically* perform the calculation, whereas electronic computers use passive circuits to ratio and scale. Both output a standardized signal proportional to:

1. The product of two or more inputs
2. The quotient of two or more inputs
3. The square root of a single input or the square root of the product of two inputs

Figure 12.1 shows an analog computer that receives three 4- to 20-mA signals, and in Fig. 12.2 is a pneumatic analog computer that receives scaled 3- to 15-lb/in² (20- to 100-kPa) inputs. Provided the inputs are properly scaled, the computer will correct for pressure, temperature, and specific-gravity changes for a gas-flow application, or for any combination of selected variables. The output is then a corrected standardized signal suitable for use with chart recorders, indicators, controllers, etc. Figure 12.3 shows a typical pneumatic-computer arrangement for pressure and temperature computation for a gas flow.

Modern analog circuits have excellent computational accuracy, along with stability. Analog units are small in size, have a good price-to-performance ratio, and are widely used when process variables change significantly.

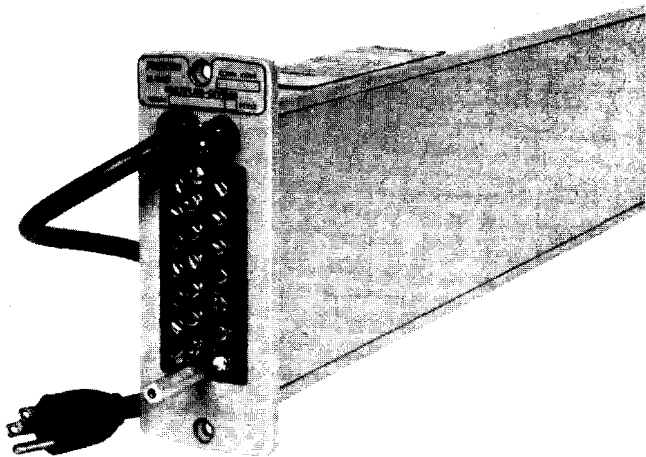


Figure 12.1 Three-input electronic analog computer. (Courtesy The Foxboro Co.)

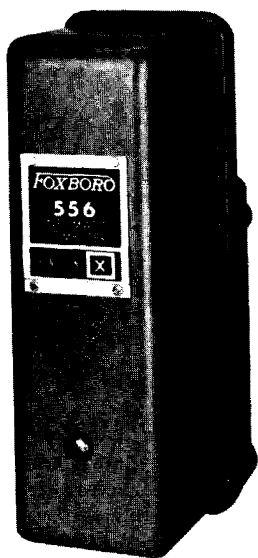


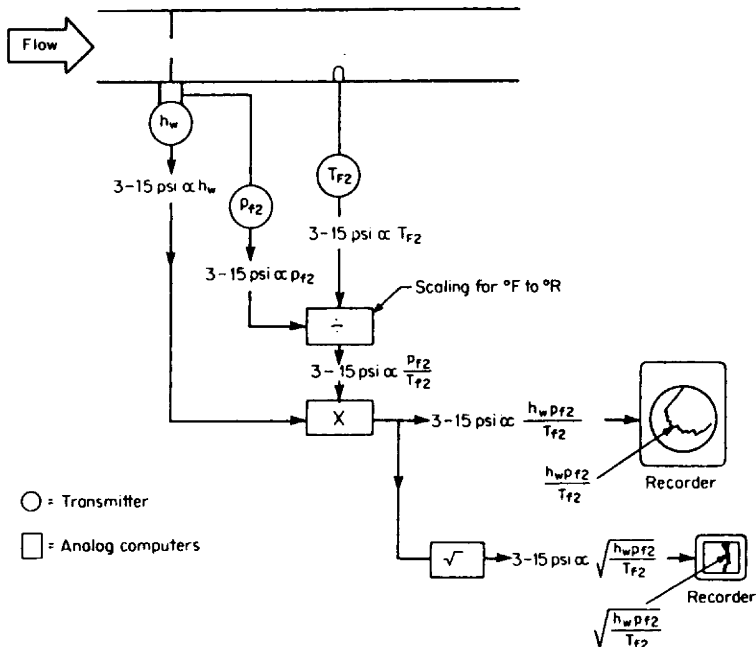
Figure 12.2 Pneumatic analog computer. (Courtesy The Foxboro Co.)

Digital Flow Computers

The need for improved calculation accuracy led to the development of dedicated on-site digital computers. Receiving inputs from transmitters (Fig. 12.4), these computers can be programmed to correct for Reynolds number, gas expansion factor, temperature, pressure, and gas compressibility, and to display either flow rate or total volume (Fig. 12.5). Also, meter runs and differential-pressure transmitters with different upper-range values may be computer-selected for wide-range metering.

Many gas pipeline companies (Datta-Barua, 1984) have adopted a systems approach to flow computation, where individual field flow computers are linked via microwave or serial telephone line to the host computer. These battery backed up field computers receive instructions from the host but perform all necessary flow calculations onsite.

In the process industries, digital instrumentation and microprocessors are causing a fundamental change in orifice flow measurement methods. The use of either central or dedicated on-site computers to perform calculations is becoming commonplace. Many of the process variables previously grouped as unmeasured are now measured and accounted for in calculations. In addition, instrument bias error is now being continuously corrected by computers, via stored calibration data. Trans-



Flow-rate equation:

$$q_v = \left(N_{v0T} K F_0 Y_2 \frac{Z_b}{\sqrt{G}} \frac{d^2}{\sqrt{Z_{f2}}} \right)_{UMV} \left(\frac{\sqrt{p_{f2}}}{\sqrt{T_{f2}}} \right)_{MV} \sqrt{h_w} = F_{MC} \sqrt{\frac{h_w p_{f2}}{T_{f2}}}$$

Figure 12.3 Computing gas flows with pneumatic analog computers.

mitter zeroing and changes of differential-pressure transmitters for wide-range meters are now also computer-controlled.

Integrated Flow

When the flow-rate equation is used, it is written for a particular item unit, as in gallons per minute or gallons per day. However, the differential pressure and measured variables change continually within any unit of time. The total quantity to be measured over a selected time interval then must be the *integrated* total over this interval for these changing conditions. The total flow over any time interval is then

$$Q = \int_0^t q \, dt \quad (12.4)$$

For example, for Eq. (12.3) the integrated flow on a daily basis would be written as

$$Q_{PPD} = \int q_{PPH} \, dt = F_{MC} \int_0^t \sqrt{h_w} \, dt \quad (12.5)$$

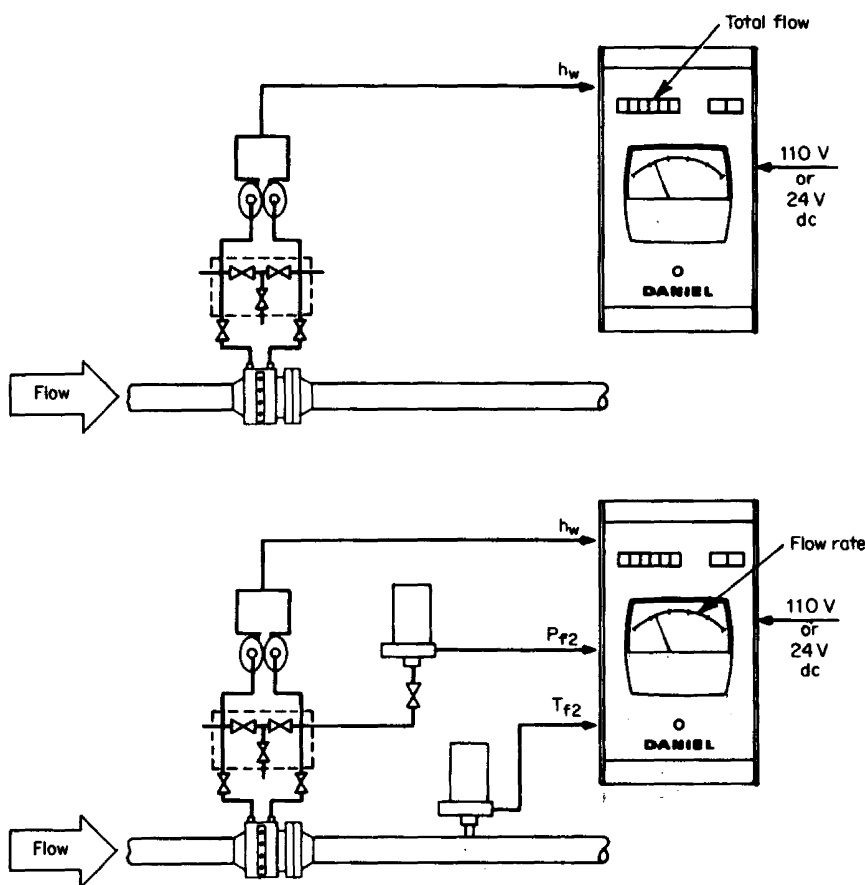


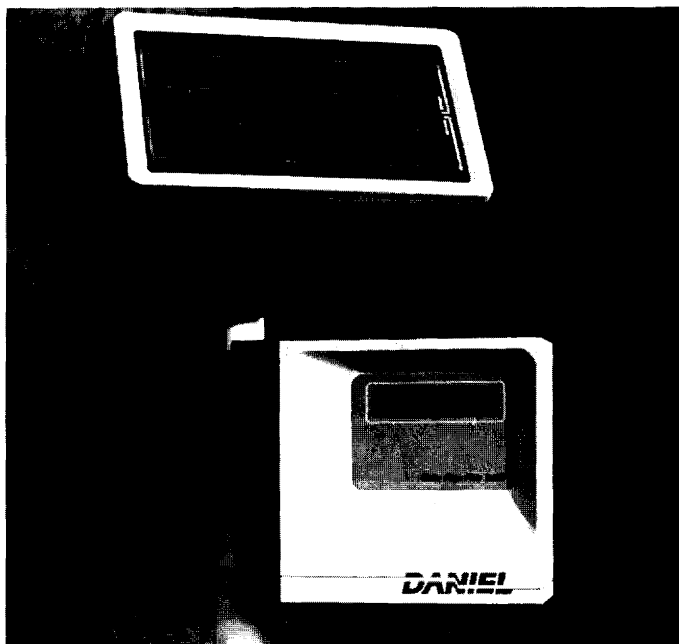
Figure 12.4 Digital on-site flow computer. (Courtesy Daniel Industries, Inc.)

where the integral is evaluated by chart integration, computer summation, or visual observation of chart records. If the flow-rate unit is gallons per minute and total gallons per day are required, Eq. (12.4) would be written as

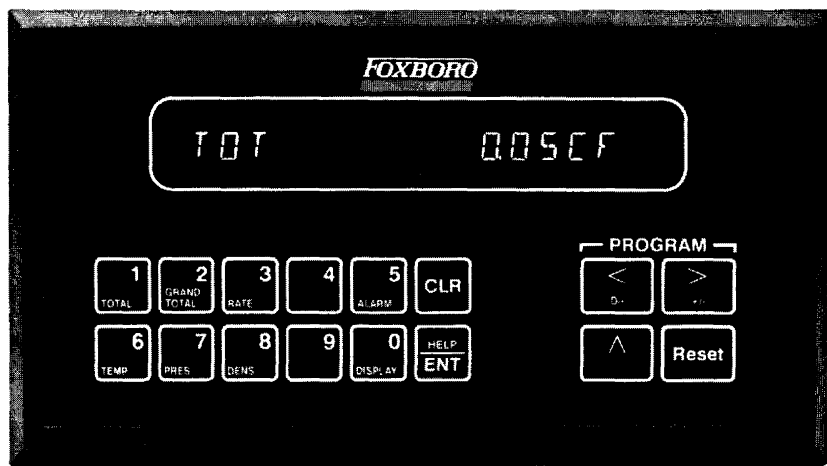
$$Q_{\text{GPD}} = \int q_{\text{GPM}} dt = F_{\text{MC}} \int_0^t \sqrt{h_w} dt \quad (12.6)$$

where the integration limits in Eqs. (12.5) and (12.6) define the period of interest. The general expression for total flow is then, by Eq. (12.1),

$$Q = \int_0^t q dt = []_{\text{UMV}} \int_0^t []_{\text{MV}} \sqrt{h_w} dt \quad (12.7)$$



(a)



(b)

Figure 12.5 On-site flow computers. (a) Solar powered. (Courtesy Daniels Industries.) (b) General Purpose. (Courtesy The Foxboro Co.)

Distributive Control System

The certification of companies to the ISO 9000 standards has resulted in a management set of quality standards. These ISO standards are increasingly being used by many companies in documentation and preventive maintenance and for statistical quality control. Greater importance (Sperber, 1995) has been placed on these items in ISO 9001, the most detailed of the ISO 9000 series. The importance of documentation has subsequently led to increased importance of the computer system for logging and computing flow data and to provide the necessary information for any quality program. This documentation is now being achieved by the Distributive Control System (DCS).

The DCS allows for the storage and retrieval of data and the appropriate flow-rate computations for numerous streams. In combination with the computer-aided calibration calibrators (see Fig. 12.6) (Shook 1995), the associated flow measurement instrumentation can be verified and the calibration data made readily available.

PLANIMETERING

Many industries retain charts as permanent records for accounting purposes. It is also common practice to use chart recorders (Fig. 12.7) for visual observation of flow rate and flow-rate trends, and for daily or weekly accounting of feedstocks and steam usage. Total flow is obtained by *planimetering* either a circular- or strip-chart recording. A single-pen recording of differential pressure or a three-pen re-



(a)



(b)

Figure 12.6 CAC system. (a) Calibrator. (Courtesy FLUKE, Corporation). (b) System. (Courtesy Honeywell Loveland Company.)



Figure 12.7 Recorder. (Courtesy The Foxboro Co.).

recording of pressure, temperature, and differential pressure is available, with selection depending on the number of measured variables.

The integration device can be a manually operated desktop integrator for circular charts (Fig. 12.8), a strip-chart integrator (Fig. 12.9), or a computer-based chart integrator (Fig. 12.10).

Uniform Circular Charts

Uniform charts are divided into equal segments between an inner radius r_i and an outer radius r_o . Along an arc over which the pen travels, charts may be marked in either percentage of span (URV to LRV) or in units of the measured variables ($^{\circ}\text{F}$, psia, q).

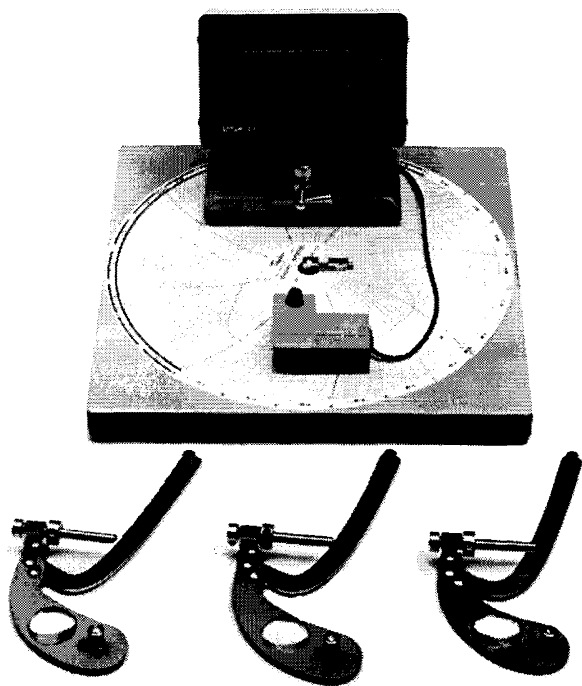


Figure 12.8 Square-root planimeter. (*Courtesy Lasico.*)

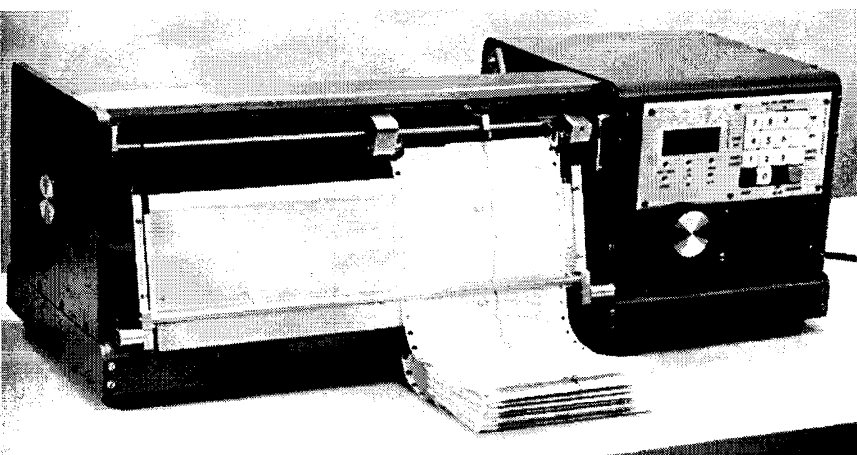


Figure 12.9 Strip-chart planimeter. (*Courtesy Flow Measurement, Inc., Tulsa, OK*)

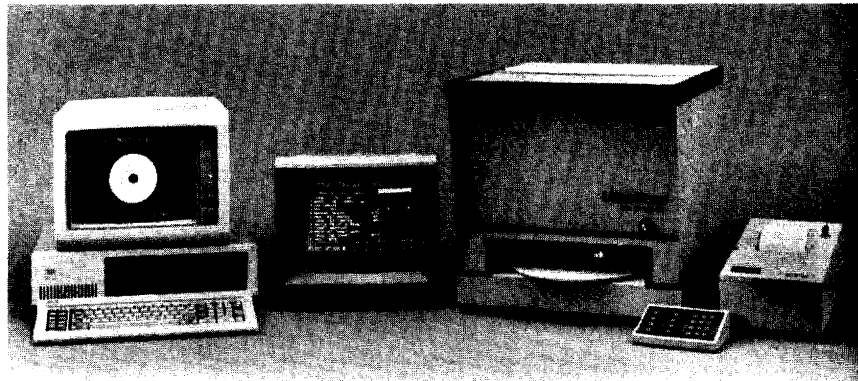


Figure 12.10 Computer-based chart integrator. (Courtesy UGC Industries Inc.)

Shown in Fig. 12.11a is the nomenclature for a uniform circular chart. For a planimeter that integrates radially, the average value of the measured variable is calculated by substituting the planimeter reading $(P_{rdg})_{MV}$ into the equation

$$(MV)_{av} = [(MV)_{URV} - (MV)_{LRV}] \left(\frac{r_i}{r_o - r_i} \right) \left[\frac{F_{ARC} N_t (P_{rdg})_{MV}}{(P_{rdg})_0} - 1 \right] + (MV)_{URV} \quad (12.8)$$

where N_t is calculated as

$$N_t = \frac{\text{number of hours represented by } 360^\circ \text{ chart rotation}}{\text{number of hours planimtered}} \quad (12.9)$$

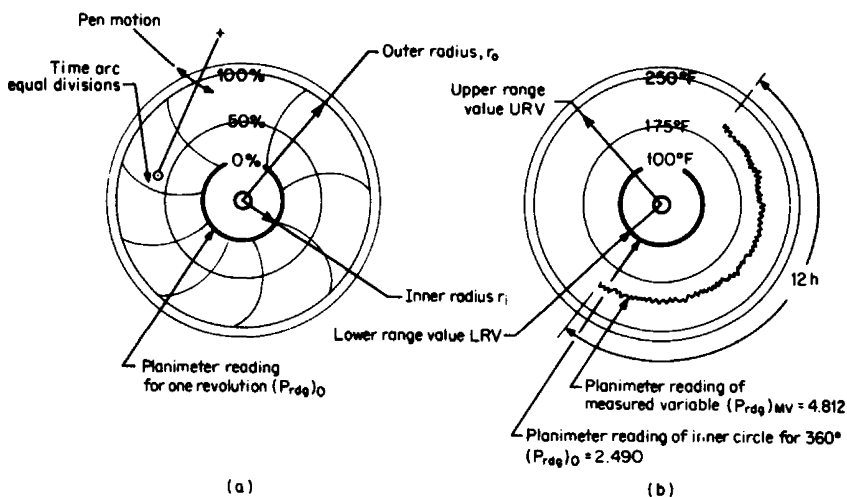


Figure 12.11 Uniform chart. (a) Chart nomenclature. (b) Radial-planimeter nomenclature (values from Example 12.1).

The total quantity of the measured variable over the integration period is then

$$(MV)_t = t(MV)_{av} \quad (12.10)$$

where t is the number of hours planimetered.

The arc correction factor F_{ARC} is read from Fig. 12.12 for the product of $N_t(P_{rdg})_{MV}$. This correction is required because radial planimeters average radial distances and, hence, are accurate only with a chart employing equal radial divisions, whereas uniform charts employ equal increments along an arc (see Fig. 12.11).

Unless the differential and static pressures remain essentially constant (Fig. 12.13) or a square-root signal inputs the recorder, radial planimeters should *not* be used to average differential-pressure or static-pressure charts. For example, in Fig. 12.14, the average for the high period is approximately 75, and for the low period approximately 35.6. If the entire record were averaged at one operation by a radial planimeter, the result would be 55.3, and the square root of 55.3 is 7.4364. If, however, the periods were averaged separately and the average square root determined, the result would be one-half the sum of the square root of 75 (8.6603) and the square root of 35.6 (5.9666), or 7.3135. The error in this particular case is not very large, but it would increase rapidly as the difference between the averages for the high and low periods increased. For example, if the high period averaged approximately 90.6 and the low period 20, the average for the entire record would still be 55.3, and its square root 7.4364. But the average of the square root of 90.6 (9.5184) and the square root of 20 (4.4721) would be 6.9955. It is obvious that the desired result is the average square root, and not the square root of the average.

Example 12.1. A temperature measurement is recorded on a 24-h, 12-in (300-mm) uniform Foxboro circular chart (Fig. 12.11*b*). The chart range is 100 to 250°F (37.8 to 121°C). Planimetering the chart for 12 h with a radial planimeter gives a reading of 4.812. Determine the average temperature.

For a Foxboro chart,

$$r_i = 0.996 \text{ in} \quad r_o = 4.96 \text{ in}$$

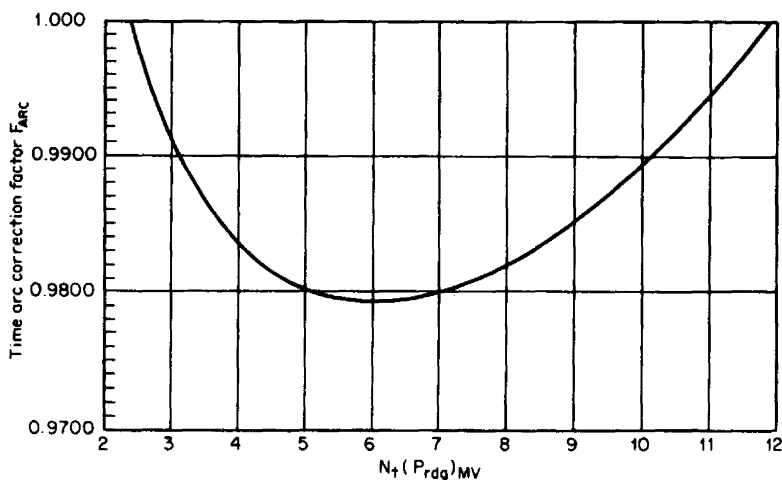


Figure 12.12 Radial-planimeter time-arc correction.

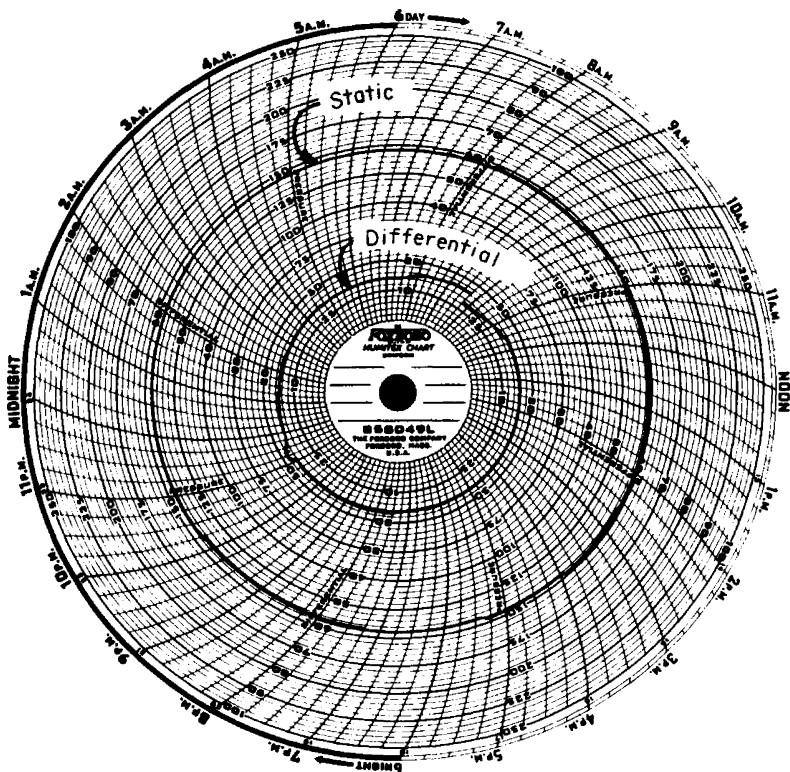


Figure 12.13 Chart that can be averaged by observation or by a radial planimeter.

Planimetry of the inner circle for 360° gives

$$(P_{rdg})_0 = 2.490$$

The time factor is, by Eq. (12.9),

$$N_t = \frac{24}{12} = 2$$

From Fig. 12.12, the time-arc correction factor for

$$N_t(P_{rdg})_{MV} = (2)(4.812) = 9.624$$

is $F_{ARC} = 0.9876$. From Eq. (12.8), the average temperature is

$$(MV)_{av} = [(MV)_{URV} - (MV)_{LRV}] \frac{r_i}{r_o - r_i} \left[\frac{F_{ARC} N_t (P_{rdg})_{MV}}{(P_{rdg})_0} - 1 \right] + (MV)_{LRV}$$

Substitution gives

$$(T_F)_{av} = (250 - 100)(0.2513) \left[\frac{(0.9876)(2)(4.812)}{2.490} - 1 \right] + 100 = 206.2^\circ F$$

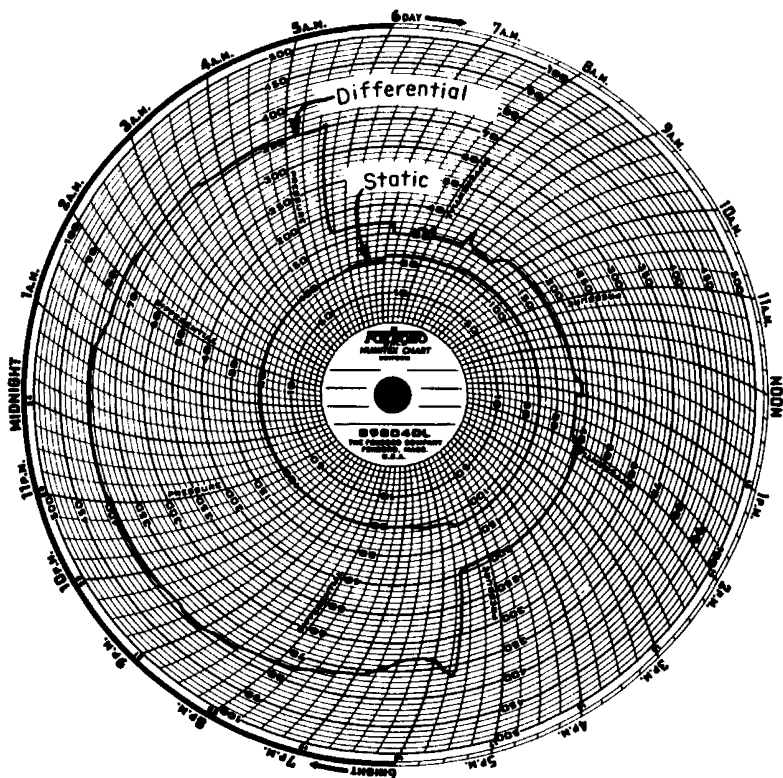


Figure 12.14 Chart which should not be averaged by a radial planimeter.

Example 12.2. For Example 9.13, an analog computer transmits the square root of the differential-pressure-transmitter signal to a chart recorder. A planimeter reading of 4.812 is obtained for a 12-h integration of a 12-in, 24-h Foxboro 0- to 100-in (24.9-kPa) uniform circular chart. What is the total flow, in gallons, for the 12-h period?

From Example 9.13, the flow rate is calculated as

$$q_{\text{GPM}} = F_{\text{MC}} \sqrt{h_w} = 10.00 \sqrt{h_w}$$

The upper-range value of the flow rate on an hourly basis is

$$(q_{\text{GPH}})_{\text{URV}} = (10.00)(60) \sqrt{(h_w)_{\text{URV}}} = (10.00)(60) \sqrt{100} = 6000 \text{ base gal/h}$$

where $(h_w)_{\text{URV}} = 100$, and the lower-range value $(h_w)_{\text{LRV}}$ is 0. For the values of Example 12.1, the average of the measured variable is, by Eq. (12.8),

$$\begin{aligned} (\text{MV})_{\text{av}} &= (q_{\text{GPH}})_{\text{av}} = 0.2513 [(\text{MV})_{\text{URV}} - (\text{MV})_{\text{LRV}}] \left[\frac{F_{\text{ARC}} N_f (P_{\text{rdg}})_{\text{MV}}}{2.490} - 1 \right] \\ &+ (\text{MV})_{\text{LRV}} = (0.2513)(6000) \left[\frac{(0.9876)(2)(4.812)}{2.490} - 1 \right] + 0 = 4248 \end{aligned}$$

Then, from Eq. (12.10),

$$Q_{\text{GAL}} = t(\text{MV})_{\text{av}} = (12)(4248) = 50,970 \text{ base gal}$$

Strip Charts

A strip-chart planimeter is shown in Fig. 12.9. Standard strip charts are 4 in (100 mm) wide, with a recorder speed of 0.75 in/h (19 mm/h). Chart widths of 1 to 12 in (25 to 300 mm) and varying chart speeds are available. The planimeter is calibrated to an upper-range reading corresponding to the upper-range value of the measured variable; at a zero chart reading, the planimeter registers zero. Total integrated flow is then calculated as

$$Q_t = P_{\text{rdg}} \left[\frac{q}{P_{\text{rdg}}} \right]_{\text{URV}} \quad (12.11)$$

where the bracketed values are to be taken at the upper-range value for the flow rate and planimetered over the time period specified for the planimeter.

Example 12.3. For Example 9.13, a pneumatic analog computer transmits the square root of the differential-pressure-transmitter signal to a strip-chart recorder. A linear strip-chart planimeter records 860 when the record is traced for 24 h. If the planimeter's upper-range value is 1000 counts for a 24-h trace, what is the total flow?

The upper-range value of the flow rate for 24 h is, from Example 9.13,

$$\begin{aligned} q_{\text{GPD}} &= (24)(60)q_{\text{GPM}} = (24)(60)(10.00)\sqrt{(h_w)_{\text{URV}}} = 14,400\sqrt{100} \\ &= 144,000 \text{ base gal/24 h} \end{aligned}$$

The total flow for 24 h is then

$$Q_{\text{GAL}} = (P_{\text{rdg}})_{\text{MV}} \left(\frac{q}{P_{\text{rdg}}} \right)_{\text{URV}} = 860 \frac{144,000}{1000} = 123,840 \text{ base gal}$$

Example 12.4. For the gasoline flow of Example 9.13, the differential pressure is recorded on a 12-in (300-mm), 24-h circular chart. The record is planimetered over a 24-h period, and a reading of 4.720 is obtained. Determine the total flow over the planimetered period if the planimeter reads 5.00 when tracing the 100-in (25-kPa) upper-range differential-pressure value for 24 h.

The upper-range value of the flow rate over the chart's time period (24 h) is, from Example 9.13,

$$q_{\text{GPD}} = (24)(60)(q_{\text{GPM}})_{\text{URV}} = (24)(60)(10)\sqrt{100} = 144,000 \text{ base gal/24 h}$$

The total flow for 24 h is then, from Eq. (12.12),

$$Q_{\text{GAL}} = (P_{\text{rdg}})_{h_w} \left(\frac{q}{P_{\text{rdg}}} \right)_{\text{URV}} = (4.720) \frac{144,000}{5} = 136,000 \text{ base gal}$$

Square-Root Planimeters

Square-root planimeters instantaneously average the square root of the measured variable as the chart record (differential- or static-pressure recording) is traced. Integration is along the arc, and the record may be mechanically averaged or computer calculated (Fig. 12.10). For gas flows, the square root of the product of the differential and absolute pressures is required; this may be calculated from two planimeter readings or by a computer-based integrator that displays a single value.

When only the differential pressure is recorded, the total flow over a specified time period is calculated as

$$Q_t = (P_{rdg})_{h_w} \left[\frac{q}{(P_{rdg})_{h_w}} \right]_{URV} \quad (12.12)$$

where the quantities within the brackets are to be taken at the upper-range value for both flow rate and planimeter for 360° chart rotation. In gas (vapor) flows, both the differential and static pressures are usually planimetered. In this case, the total flow over a specified time period is calculated as

$$Q_t = (P_{rdg})_{h_w} (P_{rdg})_{pf1} \left[\frac{q}{(P_{rdg})_{h_w} (P_{rdg})_{pf1}} \right]_{URV} \quad (12.13)$$

Example 12.5. For the natural gas flow of Example 9.7, the differential and absolute static pressure are recorded for 12 h on a 12-in (300-mm), 24-h circular chart. The planimetered reading of the differential-pressure record is 2.415, and that of the static-pressure record is 2.250. Determine the total flow in standard cubic meters over the 12-h planimetered period. (The planimeter reads 5.00 when tracing the upper-range values.)

From Eq. (f) of Table 9.38, the flow-rate equation can be written in terms of measured and unmeasured variables as

$$q_{vb}^* = (N_{vhp}^* K F_a^* Y F_{PB}^* F_{TF1}^* F_{pv1} Z_b F_g d^{*2})_{UMV} (\sqrt{p_{f1}^*})_{MV} \sqrt{\Delta p^*}$$

Substituting the values given in Example 9.7 yields

$$q_{SCMH}^* = F_{MC} \sqrt{p_{f1}^*} \sqrt{\Delta p_{f1}^*} = 7.9264 \sqrt{p_{f1}^*} \sqrt{\Delta p_{f1}^*}$$

The upper-range value for 24 h is

$$\begin{aligned} q_{SCMD}^* &= 24 F_{MC} \sqrt{(p_{f1}^*)_{URV}} \sqrt{(\Delta p^*)_{URV}} = (24)(7.9264) \sqrt{184} \sqrt{10} \\ &= 8160 \text{ standard m}^3/24 \text{ h} \end{aligned}$$

The planimetered time factor is, by Eq. (12.9), $N_t = 24/12 = 2$. The total flow for 12 h is then, by Eq. (12.13),

$$\begin{aligned} Q_{SCM}^* &= (P_{rdg})_{\Delta p^*} (P_{rdg})_{pf1} \left[\frac{q^*}{(P_{rdg})_{\Delta p^*} (P_{rdg})_{pf1}} \right]_{URV} \\ &= (2)(2.415)(2.250) \frac{8160}{(5)(5)} = 3547 \text{ standard m}^3 \end{aligned}$$

REFERENCES

- Datta-Barua, Lohit: "Systems Approach to Electronic Measurement Taken for Gas Custody Transfer," *Technology, Oil Gas J.*, pp. 79–83, September 24, 1984.
- Shook, P.: "From Field Calibrators to Instrument Management Systems," *Control*, January 1995.
- Sperber, R.: "Revised ISO Shouldn't Hurt . . . Much," *Control Magazine*, January 1995.

CRITICAL FLOW

When a gas accelerates through a restriction, its density decreases and its velocity increases. Since the mass flow per unit area (mass flux) is a function of both density and velocity, a critical area exists at which the mass flux is at a maximum. In this area, the velocity is sonic, and further decreasing the downstream pressure will not increase the mass flow. This is referred to as *choked* or *critical flow*. For liquids, if the pressure at the minimum area is reduced to the liquid's vapor pressure, a cavitation zone is formed which restricts the flow. Further decreases in pressure will not increase the flow rate. In both cases, mass flow can only be increased by increasing the upstream pressure.

Critical flow nozzles are widely used as secondary standards to test air compressors, steam generators, and natural gas flowmeters. Over the last 20 years the aerospace industry has developed a critical nozzle with a downstream diffuser (venturi) recovery section that gives minimum overall pressure loss to maintain critical flow. Cavitating venturis or restrictive orifices are used as flow limiters in the event of a downstream system failure.

GASES

Basic Principles

Figure 13.1 shows the pressure-velocity relationship for a convergent-divergent passage through which a compressible fluid accelerates. As the downstream pressure p_{f3} decreases, the throat velocity V_t increases until a *critical pressure ratio*[†] is reached at which the throat velocity is sonic. Further decreases in the downstream pressure will not increase the mass flow rate. The flow is referred to as *subsonic* down to the critical pressure ratio, and *critical* below this ratio. In critical flow the throat velocity is always sonic, but the velocity increases in the diffuser section, where a normal shock front occurs. Depending on the downstream pressure, four flow conditions are possible:

1. For pressure ratios greater than critical, the flow remains subsonic and may be calculated with the relationships given in Chap. 9.
2. When p_{f3} is reduced to the value at which sonic throat velocity first occurred, the flow decelerates in the divergent section to a subsonic velocity; the gas

[†]The critical (or choking) pressure ratio is discussed in detail later in this chapter.

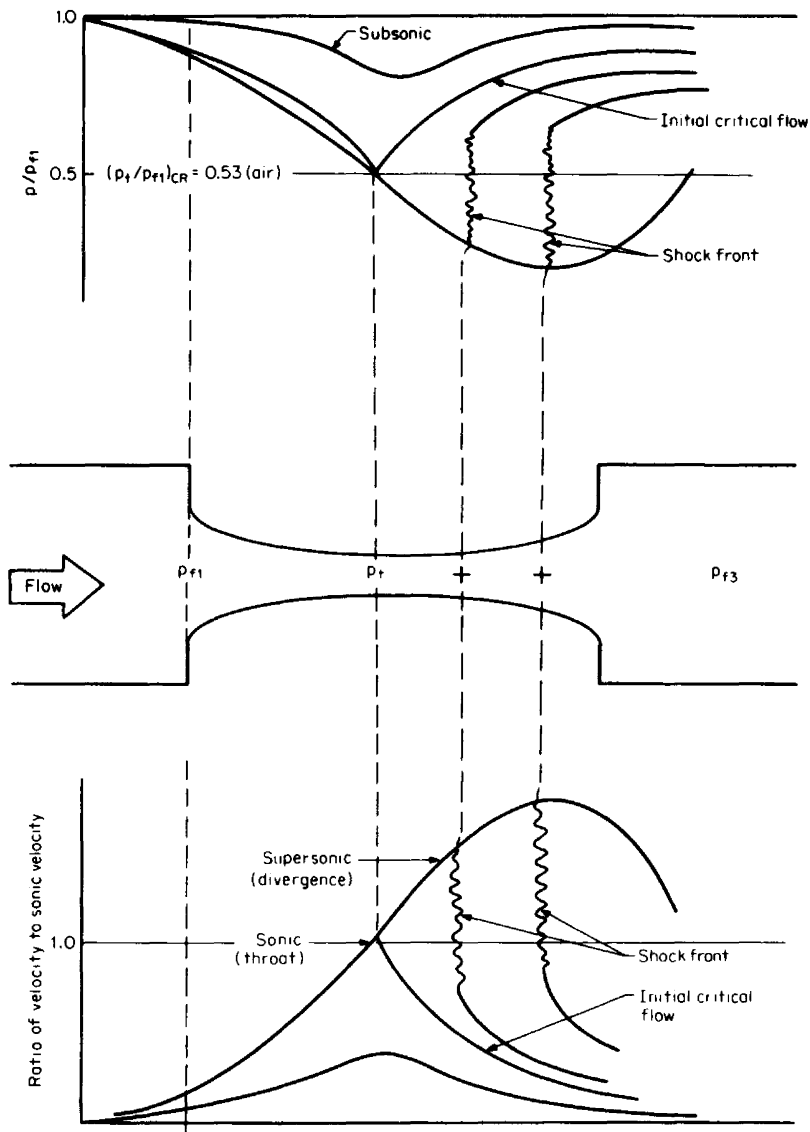


Figure 13.1 Pressure and velocity relationships for a venturi nozzle.

expands isentropically to throat pressure and then returns to the higher downstream pressure.

3. Reducing the downstream pressure further will not alter the critical pressure ratio between the upstream and throat pressures, but the velocity increases up to a normal shock wave in the divergent section. The flow across the shock is not isentropic, and the velocity abruptly changes from a supersonic speed to a subsonic speed.

4. The shock-front location moves progressively downstream with further pressure reductions, until it no longer occurs within the divergent section. The flow then accelerates steadily throughout the nozzle and is subsonic in the convergent passage, sonic at the throat, and supersonic within the divergent section.

The minimum downstream pressure at which critical flow begins is dependent on the geometry and the isentropic exponent of the gas. With a divergent section the choking pressure ratio is approximately 5 to 10 percent of the upstream pressure, but with no divergent section it is approximately 50 percent of the upstream pressure.

Engineering Equations

The mass flow-rate equation is derived from mass flow continuity between upstream and throat sections as

$$(q_{PPS})_1 = A_t \rho_{ft} \bar{V}_t \quad (13.1)$$

where the subscript t refers to throat conditions. Sonic velocity is the speed at which small pressure changes propagate as waves through a compressible fluid. A one-dimensional isentropic model gives the sonic velocity as the square root of the ratio of pressure to density change; that is,

$$\bar{V}_t = \bar{V}_{son} = \sqrt{\left(\frac{dP}{d\rho}\right)_s} \quad (13.2)$$

where the subscript s refers to an isentropic expansion from inlet to throat. Substitution of Eq. (9.27) into Eq. (13.2) yields the sonic throat velocity as

$$\bar{V}_t = \bar{V}_{son} = \sqrt{\frac{kg_c P_t}{\rho_{ft}}} \quad (13.3)$$

where k is the isentropic exponent (see Chap. 2). Substituting Eq. (13.3) into Eq. (13.1) gives the mass flow equation in U.S. units as

$$q_{PPS} = CA_t \sqrt{kg_c P_t \rho_{ft}} \quad (13.4)$$

where C is the coefficient of discharge relating the actual flow rate to a one-dimensional nonviscous (ideal) flow rate.

In practice, static pressures and temperatures are measured at an upstream location, and equations are developed using total (stagnation) pressure and temperature (see Chap. 3). For isentropic expansion, the mass flow-rate equation for a density determination can be developed from the isentropic relationships given by

$$\begin{aligned} \left(\frac{P_t}{P_{f1}}\right)_T &= \left(\frac{2}{k+1}\right)^{k/(k-1)} & \left(\frac{\rho_t}{\rho_{f1}}\right)_T &= \left(\frac{2}{k+1}\right)^{1/(k-1)} \\ \left(\frac{T_t}{T_{f1}}\right)_T &= \frac{2}{k+1} \end{aligned} \quad (13.5)$$

where the subscript T refers to total, or stagnation, upstream conditions. Substituting Eq. (13.5) into Eq. (13.4) yields the fundamental mass flow-rate equation

$$q_{PPS} = CA_t \left[k \left(\frac{2}{k+1} \right)^{(k+1)/(k-1)} \right]^{1/2} \sqrt{g_c(P_{f1}\rho_{f1})_T} \quad (13.6)$$

for U.S. units (pounds-force, pounds-mass, feet, seconds), and

$$q_{KPS}^* = CA_t^* \left[k \left(\frac{2}{k+1} \right)^{(k+1)/(k-1)} \right]^{1/2} \sqrt{(P_{f1}^*\rho_{f1}^*)_T} \quad (13.7)$$

for SI units (kilograms, newtons, seconds).

In practice, wall pressure taps are used to measure pressure; the total pressure is seldom measured with impact or simple pitot tubes that might disrupt the flow. The relationship between the total and static pressures for any value of β is

$$\left[\frac{P_{f1}}{(P_{f1})_T} \right]^{2/k} - \left[\frac{P_{f1}}{(P_{f1})_T} \right]^{(k+1)/k} = \beta^4 \frac{k-1}{2} \left(\frac{2}{k+1} \right)^{(k+1)/(k-1)} \quad (13.8)$$

For $\beta < 0.5$ the equation relating total to measured static pressure is well approximated by

$$(p_{f1})_T = \left[1 - \frac{k}{2} \left(\frac{2}{k+1} \right)^{(k+1)/(k-1)} \beta^4 \right]^{-1} p_{f1} = F_{TP} p_{f1} \quad (13.9)$$

As noted in Chap. 3, a thermal well needs no correction for stagnation conditions since, in general, the total temperature is measured. The upstream density ρ_{f1} may be calculated from the pvT equations rather than found by measurement. Substituting Eqs. (2.10) and (2.11) into Eqs. (13.6) and (13.7) and using U.S. and SI engineering pressure units (pounds per square inch absolute, kilopascals) give the engineering equations for density and for pvT density determination for a wall pressure tap:

$$q_{PPS} = 0.3712458Cd^2\sqrt{Z_{f1}} Y_{CR} \sqrt{\rho_{f1}} \sqrt{F_{TP}} \sqrt{p_{f1}} \quad (13.10)$$

$$q_{PPS} = 0.6098863Cd^2Y_{CR} \sqrt{\frac{G}{T_{f1}}} F_{TP} p_{f1} \quad (13.11)$$

for U.S. units, and

$$q_{KPS}^* = 0.00002483647Cd^{*2}\sqrt{Z_{f1}} Y_{CR} \sqrt{\rho_{f1}^*} \sqrt{F_{TP}p_{f1}^*} \quad (13.12)$$

$$q_{KPS}^* = 0.00004635451Cd^{*2}Y_{CR} \sqrt{\frac{G}{T_{K1}}} F_{TP} p_{f1}^* \quad (13.13)$$

for SI units. In these equations Y_{CR} is the critical flow function, defined as

$$Y_{CR} = \left[\frac{k}{Z_{f1}} \left(\frac{2}{k+1} \right)^{(k+1)/(k-1)} \right]^{1/2} \quad (13.14)$$

Table 13.1 presents the U.S.- and SI-unit equations for mass and volumetric flow-rate calculations on an hourly basis.

Shen et al. (1989) have shown good agreement between the sonic nozzle metering natural gas and a turbine meter, while an orifice calibration accuracy is size-dependent. Deviations between the test meters and the sonic nozzles are generally

TABLE 13.1 Mass and Volumetric Flow-Rate Equations for Critical Flowmeters: U.S. and SI Units

U.S. units		SI units		
Mass flow rate				
Density	$q_{PPH} = 1336.485Cd^2\sqrt{Z_{f1}} Y_{CR} \sqrt{\rho_{f1}} \sqrt{F_{TP}} \sqrt{p_{f1}}$	(a)	$q_{KPH}^* = 0.08941130Cd^{*2}\sqrt{Z_{f1}} Y_{CR} \sqrt{\rho_{f1}^*} \sqrt{F_{TP}} \sqrt{p_{f1}^*}$	(h)
<i>p</i> <i>v</i> <i>T</i> equation	$q_{PPH} = 2195.591Cd^2Y_{CR} \sqrt{\frac{G}{T_{f1}}} F_{TP}p_{f1}$	(b)	$q_{KPH}^* = 0.1668762Cd^{*2}Y_{CR} \sqrt{\frac{G}{T_{k1}}} F_{TP}p_{f1}^*$	(i)
Volumetric flow rate at flowing conditions				
Density	$q_{acfh} = 1336.485Cd^2 \sqrt{Z_{f1}} Y_{CR} \frac{\sqrt{F_{TP}}}{\sqrt{\rho_{f1}}} \sqrt{p_{f1}}$	(c)	$q_{acmh}^* = 0.08941130Cd^{*2} \sqrt{Z_{f1}} Y_{CR} \frac{\sqrt{F_{TP}}}{\sqrt{\rho_{f1}^*}} \sqrt{p_{f1}^*}$	(j)
<i>p</i> <i>v</i> <i>T</i> equation	$q_{acfh} = 813.5358Cd^2Z_{f1}Y_{CR} \sqrt{\frac{T_{f1}}{G}}$	(d)	$q_{acmh}^* = 0.04790604Cd^{*2}Z_{f1}Y_{CR} \sqrt{\frac{T_{K1}}{G_1}}$	(k)
Volumetric flow rate at base conditions				
Density	$(q_{SCFH})_b = 1336.485Cd^2\sqrt{Z_{f1}} Y_{CR} \frac{\sqrt{\rho_{f1}}}{\rho_b} \sqrt{F_{TP}} \sqrt{p_{f1}}$	(e)	$(q_{SCMH}^*)_b = 0.08941130Cd^{*2}\sqrt{Z_{f1}} Y_{CR} \frac{\sqrt{\rho_{f1}^*}}{\rho_b^*} \sqrt{F_{TP}} \sqrt{p_{f1}^*}$	(l)
<i>p</i> <i>v</i> <i>T</i> equation (standard or selected base)	$q_{SCFH} = 28712.44Cd^2Z_b Y_{CR} \sqrt{\frac{1}{T_{f1}G}} F_{TP}p_{f1}$	(f)	$q_{SCMH}^* = 0.1362361Cd^{*2}Z_b Y_{CR} \frac{1}{T_{K1}G} F_{TP}p_{f1}^*$	(m)
	$(q_{SCFH})_b = 813.5358Cd^2 \frac{Z_bT_b}{p_b} Y_{CR} \sqrt{\frac{1}{T_{f1}G}} F_{TP}p_{f1}$	(g)	$(q_{SCMH}^*)_b = 0.04790604Cd^{*2} \frac{Z_bT_{kb}}{p_b^*} Y_{CR} \sqrt{\frac{1}{T_{K1}G}} F_{TP}p_{f1}^*$	(n)

higher for unprocessed gas streams. Savidge and Shen (1989) developed an improved prediction equation for natural gas using the AGA 8 equation of state model. The computed values using the Johnson method based on Vennix Kobayashi state equation would predict the speed of sound in most natural gas pipelines to within ± 0.1 percent.

Critical Flow Function

The critical flow function Y_{CR} is defined as the normalized mass flux at sonic conditions for the steady isentropic flow of an inviscid, one-dimensional fluid dynamic model. The calculation procedure requires both entropy and enthalpy functions be derived from the equation of state for the fluid being metered. A complete derivation is beyond the scope of this book, and the reader is referred to ASME/ANSI MFC-7M (1987) or ISO9300 (1990) for a detailed computational treatment and a list of appropriate references.

The critical flow functions listed below are widely used for general-type flow measurement calculations. The function may be calculated with the isentropic exponent curves presented in App. I, found by the graphical or Redlich-Kwong method presented in Chap. 2, or obtained from tables.

Sullivan Tables. Presented in Tables 13.2 through 13.7 are the critical flow functions for air, argon, carbon dioxide, methane, nitrogen, and oxygen provided by D. A. Sullivan (1981). These tables are incorporated in an ISO Standard and are based on the Bender (1970) thermal equations of state.

Murdock-Bauman Tables (Superheated Steam). Table 13.8 lists the critical flow function for superheated steam, as developed by Murdock and Bauman (1963). The original table was developed using Arnberg's critical flow function (1962), which included both the specific gas constant R and the gravitational constant g_c . The relationship between Arnberg's critical flow function and Eq. (13.14) is

$$Y_{CR} = \sqrt{\frac{144R_0}{(M_w)_{H_2O}g_c}} Y_{Arn} = 1.632819Y_{Arn} \quad (13.15)$$

In Table 13.8 the Murdock-Bauman tabular values are modified by Eq. (13.15).

Johnson Tables (Methane and Natural Gas). In the natural gas industry, the Johnson (1970, 1971) methane and natural gas critical-flow-function tables are widely used. These were calculated using the state equation of Benedict et al. (1940) and are based on 19 natural gas mixtures in the pressure range 0 to 1000 psia (0 to 7000 kPa) and temperature range 450 to 700°R (250 to 390 K).

Johnson reduced the critical flow function to two empirical linear equations for components of no more than four carbon atoms. First a composition factor is determined as

$$f = x_{C_2H_6} + x_{CO_2} - \frac{1}{2}x_{N_2} + 2x_{C_3H_8} + 3x_{C_4H_{10}} \quad (13.16)$$

[In Table 13.9 are the mole-fraction composition limits for Eq. (13.16). Sullivan (1981) suggests that Eq. (13.16) *not* be extrapolated outside these values and that f be limited to the range 0 to 0.2.] Next, from the composition factor f , the isentropic-exponent relationship of Eq. (13.14) is calculated as

TABLE 13.2 Critical Flow Function Y_{CR} for Air

Temperature		Pressure $F_{TP}p_{f1}$, psia (kPa)										
°F	°C	0 (0)	145 (1000)	290 (2000)	435 (3000)	580 (4000)	725 (5000)	870 (6000)	1015 (7000)	1160 (8000)	1305 (9000)	1450 (10,000)
—	—											
58	−50	0.6850	0.6945	0.6994	0.7069	0.7148	0.7230	0.7316	0.7407	0.7497	0.7588	0.7675
—	—											
13	−25	0.6850	0.6900	0.6952	0.7004	0.7059	0.7113	0.7168	0.7224	0.7281	0.7336	0.7391
32	0	0.6887	0.6887	0.6925	0.6962	0.7000	0.7038	0.7076	0.7113	0.7150	0.7187	0.7224
77	25	0.6850	0.6876	0.6904	0.6927	0.6958	0.6982	0.7011	0.7037	0.7062	0.7087	0.7111
122	50	0.6849	0.6870	0.6889	0.6910	0.6930	0.6949	0.6968	0.6987	0.7005	0.7022	0.7039
167	75	0.6848	0.6863	0.6878	0.6893	0.6907	0.6921	0.6935	0.6949	0.6961	0.6974	0.6985
212	100	0.6847	0.6858	0.6869	0.6880	0.6890	0.6900	0.6910	0.6920	0.6928	0.6937	0.6946

Source: Sullivan (1981).

TABLE 13.3 Critical Flow Function Y_{CR} for Argon

Temperature		Total pressure $F_{TP}p_{f1}$, psia (kPa)											
°F	°C	0 (0)	72.5 (500)	145 (1000)	290 (2000)	435 (3000)	580 (4000)	725 (5000)	870 (6000)	1015 (7000)	1160 (8000)	1305 (9000)	1450 (10,000)
-58	-50	0.7262	0.7310	0.7358	0.7460	0.7567	0.7679	0.7797	0.7922	0.8053	0.8191	0.8335	0.8484
-13	-25	0.7262	0.7297	0.7333	0.7407	0.7482	0.7560	0.7639	0.7720	0.7803	0.7888	0.7975	0.8602
32	0	0.7262	0.7289	0.7316	0.7372	0.7427	0.7484	0.7540	0.7598	0.7655	0.7713	0.7772	0.7830
77	25	0.7262	0.7283	0.7304	0.7347	0.7389	0.7432	0.7474	0.7517	0.7559	0.7601	0.7643	0.7684
122	50	0.7262	0.7279	0.7295	0.7329	0.7362	0.7395	0.7427	0.7460	0.7492	0.7523	0.7555	0.7585
167	75	0.7262	0.7275	0.7289	0.7315	0.7342	0.7367	0.7393	0.7418	0.7443	0.7467	0.7491	0.7515
212	100	0.7262	0.7273	0.7284	0.7305	0.7326	0.7347	0.7367	0.7387	0.7406	0.7426	0.7444	0.7463

Source: Sullivan (1981).

TABLE 13.4 Critical Flow Function Y_{CR} for Carbon Dioxide

Temperature		Total pressure $F_{TP}p_{f1}$, psia (kPa)											
°F	°C	0 (0)	72.5 (500)	145 (1000)	290 (2000)	435 (3000)	580 (4000)	725 (5000)	870 (6000)	1015 (7000)	1160 (8000)	1305 (9000)	1450 (10,000)
-58	-50	0.6739	—	—	—	—	—	—	—	—	—	—	—
-13	-25	0.6713	0.6864	—	—	—	—	—	—	—	—	—	—
32	0	0.6689	0.6797	0.6918	—	—	—	—	—	—	—	—	—
77	25	0.6668	0.6748	0.6834	0.7032	0.7277	—	—	—	—	—	—	—
122	50	0.6649	0.6709	0.6774	0.6915	0.7077	0.7267	0.7497	0.7783	0.8162	—	—	—
167	75	0.6632	0.6679	0.6728	0.6833	0.6949	0.7078	0.7222	0.7386	0.7575	0.7795	0.8056	0.8369
212	100	0.6616	0.6653	0.6692	0.6772	0.6859	0.6952	0.7053	0.7163	0.7282	0.7412	0.7555	0.7713

Source: Sullivan (1981).

TABLE 13.5 Critical Flow Function Y_{CR} for Methane

Temperature		Total pressure $F_{TP}p_{f1}$, psia (kPa)											
°F	°C	0 (0)	72.5 (500)	145 (1000)	290 (2000)	435 (3000)	580 (4000)	725 (5000)	870 (6000)	1015 (7000)	1160 (8000)	1305 (9000)	1450 (10,000)
-58	-50	0.6726	0.6798	0.6875	0.7048	0.7254	0.7506	0.7827	0.8249	0.8824			
-13	-25	0.6719	0.6771	0.6825	0.6943	0.7075	0.7223	0.7390	0.7581	0.7799	0.8047	0.8324	0.8623
32	0	0.6708	0.6747	0.6787	0.6872	0.6963	0.7061	0.7167	0.7281	0.7404	0.7536	0.7676	0.7823
77	25	0.6694	0.6724	0.6754	0.6817	0.6884	0.6953	0.7026	0.7102	0.7182	0.7266	0.7352	0.7441
122	50	0.6678	0.6701	0.6724	0.6772	0.6822	0.6873	0.6925	0.6980	0.7036	0.7093	0.7151	0.7211
167	75	0.6659	0.6677	0.6695	0.6732	0.6770	0.6808	0.6848	0.6888	0.6929	0.6970	0.7012	0.7054
212	100	0.6639	0.6653	0.6667	0.6696	0.6725	0.6755	0.6784	0.6815	0.6845	0.6876	0.6907	0.6938

Source: Sullivan (1981).

TABLE 13.6 Critical Flow Function Y_{CR} for Nitrogen

Temperature		Total pressure $F_{TP}p_{f1}$, psia (kPa)											
°F	°C	0 (0)	72.5 (500)	145 (1000)	290 (2000)	435 (3000)	580 (4000)	725 (5000)	870 (6000)	1015 (7000)	1160 (8000)	1305 (9000)	1450 (10,000)
-58	-50	0.6848	0.6878	0.6908	0.6970	0.7035	0.7102	0.7171	0.7243	0.7315	0.7389	0.7462	0.7536
-13	-25	0.6848	0.6869	0.6891	0.6934	0.6978	0.7023	0.7069	0.7115	0.7161	0.7208	0.7254	0.7299
32	0	0.6848	0.6863	0.6879	0.6910	0.6941	0.6972	0.7004	0.7035	0.7067	0.7097	0.7128	0.7158
77	25	0.6848	0.6859	0.6870	0.6893	0.6915	0.6938	0.6960	0.6982	0.7004	0.7025	0.7046	0.7066
122	50	0.6847	0.6855	0.6864	0.6880	0.6896	0.6913	0.6928	0.6944	0.6959	0.6974	0.6989	0.7003
167	75	0.6846	0.6853	0.6859	0.6871	0.6882	0.6894	0.6905	0.6916	0.6927	0.6938	0.6948	0.6958
212	100	0.6845	0.6850	0.6854	0.6863	0.6871	0.6880	0.6888	0.6895	0.6903	0.6910	0.6917	0.6924

Source: Sullivan (1981).

TABLE 13.7 Critical Flow Function Y_{CR} for Oxygen

Temperature		Total pressure $F_{TP}p_{f1}$, psia (kPa)											
°F	°C	0 (0)	72.5 (500)	145 (1000)	290 (2000)	435 (3000)	580 (4000)	725 (5000)	870 (6000)	1015 (7000)	1160 (8000)	1305 (9000)	1450 (10,000)
-58	-50	0.6846	0.6886	0.6927	0.7013	0.7104	0.7201	0.7304	0.7413	0.7528	0.7650	0.7779	0.7914
-13	-25	0.6845	0.6875	0.6905	0.6966	0.7030	0.7096	0.7164	0.7234	0.7307	0.7381	0.7457	0.7535
32	0	0.6844	0.6866	0.6889	0.6934	0.6981	0.7028	0.7076	0.7125	0.7175	0.7225	0.7276	0.7326
77	25	0.6842	0.6859	0.6876	0.6911	0.6946	0.6981	0.7016	0.7052	0.7087	0.7123	0.7159	0.7194
122	50	0.6839	0.6852	0.6865	0.6892	0.6919	0.6945	0.6972	0.6999	0.7025	0.7051	0.7078	0.7103
167	75	0.6835	0.6845	0.6855	0.6876	0.6897	0.6917	0.6938	0.6958	0.6978	0.6998	0.7017	0.7037
212	100	0.6829	0.6837	0.6845	0.6861	0.6877	0.6893	0.6909	0.6925	0.6940	0.6955	0.6970	0.6984

Source: Sullivan (1981).

TABLE 13.8 Critical Flow Function Y_{CR} for Superheated Steam

Temperature		Total pressure $F_{TP} p_{f1}$, psia (kPa)								
°C	°F	0 (0)	1 (7)	100 (700)	500 (3450)	1000 (6900)	2000 (13,800)	3000 (20,700)	4000 (27,600)	5000 (34,500)
93		0.6724	0.6727							
104	220	0.6722	0.6726							
116	240	0.6719	0.6724							
127	260	0.6719	0.6722							
138	280	0.6716	0.6721							
149	300	0.6714	0.6717							
160	320	0.6713	0.6716							
171	340	0.6711	0.6714							
182	360	0.6711	0.6711							
193	380	0.6708	0.6709							
204	400	0.6706	0.6708							
216	420	0.6703	0.6704	0.6802						
227	440	0.6701	0.6703	0.6791						
238	460	0.6699	0.6699	0.6781						
249	480	0.6698	0.6698	0.6673						
260	500	0.6695	0.6696	0.6765						
271	520	0.6693	0.6695	0.6757						
282	540	0.6690	0.6693	0.6750	0.7041					
293	560	0.6688	0.6690	0.6744	0.7011					
304	580	0.6686	0.6688	0.6739	0.6985					
316	600	0.6683	0.6685	0.6732	0.6957					
327	620	0.6680	0.6683	0.6727	0.6935	0.7274				
338	640	0.6678	0.6680	0.6722	0.6912	0.7201				
349	660	0.6675	0.6680	0.6717	0.6890	0.7150				
360	680	0.6673	0.6677	0.6713	0.6871	0.7111				

TABLE 13.8 Critical Flow Function Y_{CR} for Superheated Steam (Continued)

Temperature		Total pressure $F_{TP} p_{f1}$, psia (kPa)								
°C	°F	0 (0)	1 (7)	100 (700)	500 (3450)	1000 (6900)	2000 (13,800)	3000 (20,700)	4000 (27,600)	5000 (34,500)
371	700	0.6670	0.6675	0.6708	0.6855	0.7075	0.7772			
382	720	0.6667	0.6672	0.6703	0.6838	0.7044	0.7632			
393	740	0.6665	0.6670	0.6698	0.6824	0.7011	0.7534			
404	760	0.6662	0.6668	0.6693	0.6812	0.6984	0.7455	0.8262		
416	780	0.6660	0.6665	0.6688	0.6801	0.6961	0.7385	0.8071		
427	800	0.6657	0.6664	0.6685	0.6789	0.6938	0.7316	0.8803	0.8803	
438	820	0.6654	0.6662	0.6680	0.6780	0.6918	0.7261	0.7746	0.8461	0.9879
449	840	0.6652	0.6659	0.6673	0.6770	0.6899	0.7212	0.7638	0.8252	0.9418
460	860	0.6650	0.6657	0.6670	0.6760	0.6981	0.7171	0.7549	0.8060	0.8853
471	880	0.6649	0.6655	0.6667	0.6750	0.6864	0.7132	0.7473	0.7900	0.8562
482	900	0.6646	0.6652	0.6664	0.6742	0.6848	0.7098	0.7406	0.7778	0.8839
493	920	0.6642	0.6650	0.6660	0.6734	0.6833	0.7065	0.7349	0.7679	0.8159
504	940	0.6641	0.6647	0.6657	0.6727	0.6820	0.7037	0.7300	0.7589	0.8014
516	960	0.6637	0.6646	0.6654	0.6721	0.6807	0.7011	0.7255	0.7513	0.7885
527	980	0.6636	0.6644	0.6650	0.6714	0.6780	0.6988	0.7212	0.7452	0.7775
538	1000	0.6633	0.6641	0.6649	0.6708	0.6788	0.6962	0.7168	0.7406	0.7691
566	1050	0.6626	0.6636	0.6641	0.6695	0.6765	0.6915	0.7088	0.7304	0.7503
593	1110	0.6621	0.6629	0.6639	0.6685	0.6745	0.6876	0.7023	0.7180	0.7399
621	1150	0.6615	0.6624	0.6633	0.6675	0.6729	0.6843	0.6971	0.7126	0.7266
649	1200	0.6608	0.6618	0.6628	0.6665	0.6714	0.6815	0.6925	0.7047	0.7171
677	1250	0.6601	0.6611	0.6623	0.6657	0.6698	0.6789	0.6889	0.6990	0.7098
704	1300	0.6597	0.6605	0.6616	0.6647	0.6683	0.6765	0.6855	0.6946	0.7041
732	1350	0.6592	0.6598	0.6608	0.6637	0.6668	0.6742	0.6820	0.6904	0.6990
760	1400	0.6587	0.6592	0.6600	0.6626	0.6655	0.6719	0.6791	0.6866	0.6944
788	1450	0.6582	0.6585	0.6592	0.6616	0.6641	0.6698	0.6760	0.6832	0.6904
816	1500	0.6577	0.6579	0.6582	0.6605	0.6628	0.6677	0.6745	0.6797	0.6868
843	1550	0.6572	0.6570	0.6572	0.6593	0.6613	0.6657	0.6732	0.6765	0.6830
		0.6567	0.6564	0.6564	0.6582	0.6602	0.6637	0.6678	0.6734	0.6794

TABLE 13.9 Permissible Mole Fractions for Johnson's Methane-Natural Gas Mixtures

Substance	Mole fraction x
Methane (CH ₄)	0.840–1.000
Ethane (C ₂ H ₆)	0–0.11
Propane (C ₃ H ₈)	0–0.020
2-Methyl propane (C ₃ H ₈)	0–0.004
Butane (C ₄ H ₁₀)	0–0.004
Nitrogen (N ₂)	0–0.023
Carbon dioxide (CO ₂)	0–0.017

Source: Sullivan (1981).

$$\sqrt{Z_{f1}} Y_{CR} \left[k \left(\frac{2}{k+1} \right)^{(k+1)/(k-1)} \right]^{1/2} = a_c f + b_c \quad (13.17)$$

where a_c and b_c are functions of total pressure and temperature. Values are listed in Table 13.10. [In Eq. (13.17), b_c represents the contribution of methane, and $a_c f$ the contribution of other components.] The square root of the compressibility factor in Eq. (13.17) is determined as

$$\sqrt{Z_{f1}} = a_z f + b_z \quad (13.18)$$

where a_z and b_z are functions of total pressure and temperature. These are listed in Table 13.11. Finally, substitution of Eq. (13.18) into Eq. (13.17) and rearranging give the critical flow function as

$$Y_{CR} = \frac{a_c f + b_c}{a_z f + b_z} \quad (13.19)$$

Sullivan, in a private communication, proposed the following accuracy formula for Eq. (13.19):

$$(\text{ACC})_{Y_{CR}} = 0.04 + 0.00021 F_{TP} p_{f1} + f \quad (13.20)$$

for U.S. units, and

$$(\text{ACC})_{Y_{CR}} = 0.04 + 0.00003 F_{TP} p_{f1}^* + f \quad (13.21)$$

for SI units. Equations (13.20) and (13.21) yield an accuracy of ± 0.25 percent at 1000 psia (7000 kPa) for methane ($f = 0$) and, for a maximum composition factor of 0.2, yield the value ± 0.45 percent.

Discharge Coefficient

The venturi nozzle, ASME long-radius nozzle, and square-edged orifice are commonly used critical flowmeters; the accepted standard is the venturi nozzle. The discharge coefficient depends on the inlet contour (sharp or contoured), throat length, and bore Reynolds number (Fig. 13.2).

An advantage of the linear relationship between mass flow rate and the upstream pressure is that no error occurs when a time-averaged signal is used to compute

TABLE 13.10 Values of a_c and b_c for Methane and Natural Gas

Temperature		Total pressure $F_{TP}p_{f1}$										
K	°R	0 (0)	100 (690)	200 (1380)	300 (2070)	400 (2760)	500 (3450)	600 (4140)	700 (4825)	800 (5120)	900 (6200)	1000 (6900)
Values of a_c												
250	450	-0.0265	-0.0297	-0.0330	-0.0365	-0.0399	-0.0430	-0.0452	-0.0458	-0.0435	-0.0361	-0.0206
256	460	-0.0272	-0.0302	-0.0334	-0.0366	-0.0398	-0.0426	-0.0448	-0.0457	-0.0443	-0.0394	-0.0290
261	470	-0.0279	-0.0308	-0.0338	-0.0368	-0.0398	-0.0424	-0.0445	-0.0455	-0.0448	-0.0414	-0.0343
267	480	-0.0285	-0.0313	-0.0342	-0.0371	-0.0398	-0.0423	-0.0442	-0.0453	-0.0451	-0.0428	-0.0376
272	490	-0.0292	-0.0318	-0.0346	-0.0373	-0.0399	-0.0422	-0.0441	-0.0452	-0.0452	-0.0437	-0.0399
278	500	-0.0298	-0.0324	-0.0350	-0.0375	-0.0400	-0.0422	-0.0440	-0.0451	-0.0454	-0.0443	-0.0416
283	510	-0.0304	-0.0329	-0.0353	-0.0378	-0.0401	-0.0422	-0.0439	-0.0451	-0.0455	-0.0448	-0.0427
289	520	-0.0310	-0.0333	-0.0357	-0.0380	-0.0402	-0.0422	-0.0439	-0.0450	-0.0455	-0.0451	-0.0436
294	530	-0.0315	-0.0338	-0.0361	-0.0383	-0.0404	-0.0423	-0.0439	-0.0450	-0.0456	-0.0454	-0.0443
300	540	-0.0321	-0.0343	-0.0365	-0.0386	-0.0406	-0.0424	-0.0439	-0.0450	-0.0456	-0.0456	-0.0448
306	550	-0.0326	-0.0347	-0.0368	-0.0388	-0.0407	-0.0425	-0.0439	-0.0450	-0.0457	-0.0458	-0.0452
311	560	-0.0331	-0.0351	-0.0371	-0.0391	-0.0409	-0.0426	-0.0440	-0.0451	-0.0458	-0.0459	-0.0455
317	570	-0.0335	-0.0355	-0.0375	-0.0393	-0.0411	-0.0427	-0.0440	-0.0451	-0.0458	-0.0461	-0.0458
322	580	-0.0340	-0.0359	-0.0378	-0.0396	-0.0412	-0.0428	-0.0441	-0.0451	-0.0458	-0.0462	-0.0460
328	590	-0.0344	-0.0362	-0.0380	-0.0398	-0.0414	-0.0428	-0.0441	-0.0451	-0.0459	-0.0462	-0.0462
333	600	-0.0348	-0.0366	-0.0383	-0.0400	-0.0415	-0.0429	-0.0441	-0.0451	-0.0459	-0.0463	-0.0463
338	610	-0.0351	-0.0368	-0.0385	-0.0401	-0.0416	-0.0430	-0.0442	-0.0451	-0.0459	-0.0463	-0.0464
344	620	-0.0354	-0.0371	-0.0387	-0.0403	-0.0417	-0.0430	-0.0442	-0.0451	-0.0458	-0.0463	-0.0464
350	630	-0.0357	-0.0373	-0.0389	-0.0404	-0.0418	-0.0430	-0.0442	-0.0451	-0.0458	-0.0462	-0.0464
356	640	-0.0360	-0.0375	-0.0390	-0.0405	-0.0418	-0.0430	-0.0441	-0.0450	-0.0457	-0.0462	-0.0464
361	650	-0.0362	-0.0377	-0.0392	-0.0406	-0.0418	-0.0430	-0.0441	-0.0449	-0.0456	-0.0461	-0.0463
367	660	-0.0363	-0.0378	-0.0392	-0.0406	-0.0418	-0.0430	-0.0440	-0.0448	-0.0455	-0.0460	-0.0462
372	670	-0.0365	-0.0379	-0.0393	-0.0406	-0.0418	-0.0429	-0.0439	-0.0447	-0.0453	-0.0458	-0.0461
378	680	-0.0366	-0.0380	-0.0393	-0.0406	-0.0417	-0.0428	-0.0437	-0.0445	-0.0452	-0.0456	-0.0459
383	690	-0.0367	-0.0380	-0.0393	-0.0405	-0.0416	-0.0427	-0.0436	-0.0443	-0.0450	-0.0454	-0.0457
389	700	-0.0367	-0.0380	-0.0392	-0.0404	-0.0415	-0.0425	-0.0434	-0.0441	-0.0447	-0.0452	-0.0455

Values of b_c

250	450	0.6719	0.6715	0.6713	0.6712	0.6713	0.6717	0.6723	0.6733	0.6747	0.6767	0.6791
256	460	0.6717	0.6714	0.6712	0.6712	0.6713	0.6717	0.6724	0.6734	0.6748	0.6766	0.6789
261	470	0.6714	0.6712	0.6711	0.6711	0.6714	0.6718	0.6725	0.6734	0.6747	0.6764	0.6786
267	480	0.6712	0.6710	0.6710	0.6711	0.6713	0.6718	0.6725	0.6734	0.6747	0.6763	0.6783
272	490	0.6709	0.6708	0.6708	0.6709	0.6712	0.6717	0.6724	0.6734	0.6746	0.6761	0.6780
278	500	0.6707	0.6706	0.6706	0.6708	0.6711	0.6716	0.6723	0.6733	0.6745	0.6759	0.6777
283	510	0.6704	0.6703	0.6704	0.6706	0.6710	0.6715	0.6722	0.6731	0.6743	0.6757	0.6774
289	520	0.6701	0.6701	0.6702	0.6704	0.6708	0.6714	0.6721	0.6730	0.6741	0.6755	0.6771
294	530	0.6698	0.6698	0.6699	0.6702	0.6706	0.6712	0.6719	0.6728	0.6739	0.6752	0.6767
300	540	0.6694	0.6695	0.6697	0.6700	0.6704	0.6709	0.6717	0.6726	0.6736	0.6749	0.6764
306	550	0.6691	0.6692	0.6694	0.6697	0.6701	0.6707	0.6714	0.6723	0.6734	0.6746	0.6760
311	560	0.6687	0.6689	0.6691	0.6694	0.6699	0.6704	0.6712	0.6720	0.6731	0.6743	0.6756
317	570	0.6684	0.6685	0.6687	0.6691	0.6696	0.6701	0.6709	0.6717	0.6727	0.6739	0.6753
322	580	0.6680	0.6681	0.6684	0.6688	0.6692	0.6698	0.6706	0.6714	0.6724	0.6735	0.6748
328	590	0.6676	0.6678	0.6680	0.6684	0.6689	0.6695	0.6702	0.6711	0.6720	0.6732	0.6744
333	600	0.6672	0.6674	0.6677	0.6681	0.6686	0.6692	0.6699	0.6707	0.6717	0.6728	0.6740
338	610	0.6668	0.6670	0.6673	0.6677	0.6682	0.6688	0.6695	0.6703	0.6713	0.6723	0.6735
344	620	0.6663	0.6666	0.6669	0.6673	0.6678	0.6684	0.6691	0.6699	0.6709	0.6719	0.6731
350	630	0.6659	0.6662	0.6665	0.6669	0.6674	0.6680	0.6687	0.6695	0.6705	0.6715	0.6726
356	640	0.6655	0.6657	0.6661	0.6665	0.6670	0.6676	0.6683	0.6691	0.6700	0.6710	0.6721
361	650	0.6650	0.6653	0.6656	0.6661	0.6666	0.6672	0.6679	0.6687	0.6696	0.6706	0.6717
367	660	0.6646	0.6649	0.6652	0.6657	0.6662	0.6668	0.6675	0.6683	0.6691	0.6701	0.6712
372	670	0.6641	0.6644	0.6648	0.6652	0.6658	0.6664	0.6671	0.6678	0.6687	0.6696	0.6707
378	680	0.6637	0.6640	0.6643	0.6648	0.6653	0.6659	0.6666	0.6674	0.6682	0.6692	0.6702
383	690	0.6632	0.6635	0.6639	0.6644	0.6649	0.6655	0.6662	0.6669	0.6678	0.6687	0.6697
389	700	0.6627	0.6631	0.6635	0.6639	0.6644	0.6651	0.6657	0.6665	0.6673	0.6682	0.6692

TABLE 13.11 Values of a_z and b_z for Methane and Natural Gas

Temperature		Total pressure $F_{TP} p_{f1}$, psia (kPa)										
K	°R	0 (0)	100 (690)	200 (1380)	300 (2070)	400 (2760)	500 (3450)	600 (4140)	700 (4825)	800 (5120)	900 (6200)	1000 (6900)
Values of a_z												
250	450	0	-0.0252	-0.0530	-0.0837	-0.1179	-0.1561	-0.1988	-0.2464	-0.2991	-0.3564	-0.4162
256	460	0	-0.0234	-0.0490	-0.0770	-0.1078	-0.1417	-0.1790	-0.2199	-0.2644	-0.3118	-0.3610
261	470	0	-0.0218	-0.0454	-0.0710	-0.0989	-0.1293	-0.1622	-0.1978	-0.2360	-0.2762	-0.3175
267	480	0	-0.0203	-0.0422	-0.0657	-0.0911	-0.1184	-0.1478	-0.1791	-0.2123	-0.2469	-0.2823
272	490	0	-0.0190	-0.0393	-0.0610	-0.0842	-0.1089	-0.1353	-0.1631	-0.1923	-0.2225	-0.2532
278	500	0	-0.0178	-0.0366	-0.0567	-0.0780	-0.1005	-0.1243	-0.1493	-0.1752	-0.2018	-0.2288
283	510	0	-0.0166	-0.0342	-0.0528	-0.0724	-0.0931	-0.1147	-0.1371	-0.1604	-0.1841	-0.2079
289	520	0	-0.0156	-0.0321	-0.0493	-0.0675	-0.0864	-0.1061	-0.1265	-0.1474	-0.1687	-0.1900
294	530	0	-0.0147	-0.0301	-0.0462	-0.0630	-0.0804	-0.0984	-0.1170	-0.1360	-0.1552	-0.1743
300	540	0	-0.0138	-0.0283	-0.0433	-0.0589	-0.0750	-0.0916	-0.1086	-0.1259	-0.1433	-0.1606
306	550	0	-0.0130	-0.0266	-0.0406	-0.0551	-0.0701	-0.0854	-0.1010	-0.1169	-0.1327	-0.1485
311	560	0	-0.0123	-0.0251	-0.0382	-0.0518	-0.0656	-0.0798	-0.0942	-0.1088	-0.1233	-0.1377
317	570	0	-0.0116	-0.0236	-0.0360	-0.0487	-0.0616	-0.0748	-0.0881	-0.1015	-0.1149	-0.1281
322	580	0	-0.0110	-0.0223	-0.0339	-0.0458	-0.0579	-0.0701	-0.0825	-0.0949	-0.1072	-0.1194
328	590	0	-0.0104	-0.0211	-0.0320	-0.0432	-0.0545	-0.0659	-0.0774	-0.0889	-0.1003	-0.1116
333	600	0	-0.0099	-0.0200	-0.0303	-0.0408	-0.0514	-0.0441	-0.0451	-0.0459	-0.0463	-0.0463
338	610	0	-0.0094	-0.0190	-0.0287	-0.0385	-0.0485	-0.0585	-0.0685	-0.0785	-0.0463	-0.0464
344	620	0	-0.0089	-0.0180	-0.0272	-0.0365	-0.0458	-0.0552	-0.0646	-0.0739	-0.0831	-0.0921
350	630	0	-0.0085	-0.0171	-0.0258	-0.0346	-0.0434	-0.0522	-0.0610	-0.0697	-0.0783	-0.0867
356	640	0	-0.0081	-0.0162	-0.0245	-0.0328	-0.0411	-0.0494	-0.0577	-0.0658	-0.0739	-0.0818
361	650	0	-0.0077	-0.0154	-0.0233	-0.0311	-0.0390	-0.0468	-0.0546	-0.0623	-0.0698	-0.0772
367	660	0	-0.0073	-0.0147	-0.0221	-0.0296	-0.0370	-0.0444	-0.0517	-0.0589	-0.0660	-0.0730
372	670	0	-0.0070	-0.0140	-0.0211	-0.0281	-0.0352	-0.0422	-0.0491	-0.0559	-0.0625	-0.0691
378	680	0	-0.0067	-0.0134	-0.0201	-0.0268	-0.0334	-0.0401	-0.0466	-0.0530	-0.0593	-0.0654
383	690	0	-0.0064	-0.0128	-0.0192	-0.0255	-0.0318	-0.0381	-0.0443	-0.0503	-0.0563	-0.0621
389	700	0	-0.0061	-0.0122	-0.0183	-0.0243	-0.0303	-0.0363	-0.0421	-0.0479	-0.0535	-0.0589

Values of b_{cz}

250	450	1.0000	0.9891	0.9880	0.9667	0.9552	0.9434	0.9315	0.9195	0.9075	0.8955	0.8837
256	460	1.0000	0.9899	0.9796	0.9692	0.9585	0.9478	0.9370	0.9261	0.9152	0.9044	0.8938
261	470	1.0000	0.9906	0.9810	0.9714	0.9616	0.9518	0.9419	0.9320	0.9221	0.9124	0.9028
267	480	1.0000	0.9912	0.9824	0.9734	0.9644	0.9553	0.9463	0.9373	0.9283	0.9195	0.9109
272	490	1.0000	0.9918	0.9836	0.9753	0.9659	0.9586	0.9503	0.9420	0.9339	0.9259	0.9181
278	500	1.0000	0.9924	0.9847	0.9770	0.9693	0.9616	0.9539	0.9464	0.9389	0.9316	0.9245
283	510	1.0000	0.9929	0.9857	0.9785	0.9714	0.9643	0.9573	0.9503	0.9435	0.9369	0.9304
289	520	1.0000	0.9933	0.9866	0.9800	0.9734	0.9668	0.9603	0.9539	0.9477	0.9416	0.9357
294	530	1.0000	0.9937	0.9875	0.9813	0.9752	0.9691	0.9631	0.9572	0.9515	0.9459	0.9406
300	540	1.0000	0.9941	0.9883	0.9826	0.9768	0.9712	0.9657	0.9603	0.9550	0.9499	0.9450
306	550	1.0000	0.9945	0.9891	0.9837	0.9784	0.9732	0.9681	0.9631	0.9582	0.9535	0.9490
311	560	1.0000	0.9949	0.9898	0.9848	0.9798	0.9750	0.9702	0.9656	0.9612	0.9569	0.9527
317	570	1.0000	0.9952	0.9904	0.9857	0.9811	0.9766	0.9723	0.9680	0.9639	0.9599	0.9562
322	580	1.0000	0.9955	0.9910	0.9866	0.9824	0.9782	0.9741	0.9702	0.9664	0.9628	0.9593
328	590	1.0000	0.9958	0.9916	0.9875	0.9835	0.9797	0.9759	0.9723	0.9688	0.9654	0.9622
333	600	1.0000	0.9960	0.9921	0.9883	0.9846	0.9810	0.9775	0.9741	0.9709	0.9678	0.9649
338	610	1.0000	0.9963	0.9926	0.9891	0.9856	0.9823	0.9790	0.9759	0.9729	0.9701	0.9674
344	620	1.0000	0.9965	0.9931	0.9898	0.9865	0.9834	0.9804	0.9776	0.9748	0.9722	0.9698
350	630	1.0000	0.9967	0.9935	0.9904	0.9874	0.9845	0.9817	0.9791	0.9766	0.9742	0.9719
356	640	1.0000	0.9969	0.9939	0.9910	0.9882	0.9856	0.9830	0.9805	0.9782	0.9760	0.9740
361	650	1.0000	0.9971	0.9943	0.9916	0.9890	0.9865	0.9841	0.9819	0.9797	0.9777	0.9758
367	660	1.0000	0.9973	0.9947	0.9922	0.9897	0.9874	0.9852	0.9831	0.9812	0.9793	0.9776
372	670	1.0000	0.9975	0.9950	0.9927	0.9904	0.9883	0.9862	0.9843	0.9825	0.9808	0.9793
378	680	1.0000	0.9976	0.9953	0.9931	0.9911	0.9891	0.9872	0.9854	0.9838	0.9822	0.9808
383	690	1.0000	0.9978	0.9956	0.9936	0.9917	0.9898	0.9881	0.9865	0.9849	0.9835	0.9823
389	700	1.0000	0.9979	0.9959	0.9940	0.9922	0.9905	0.9889	0.9874	0.9861	0.9848	0.9836

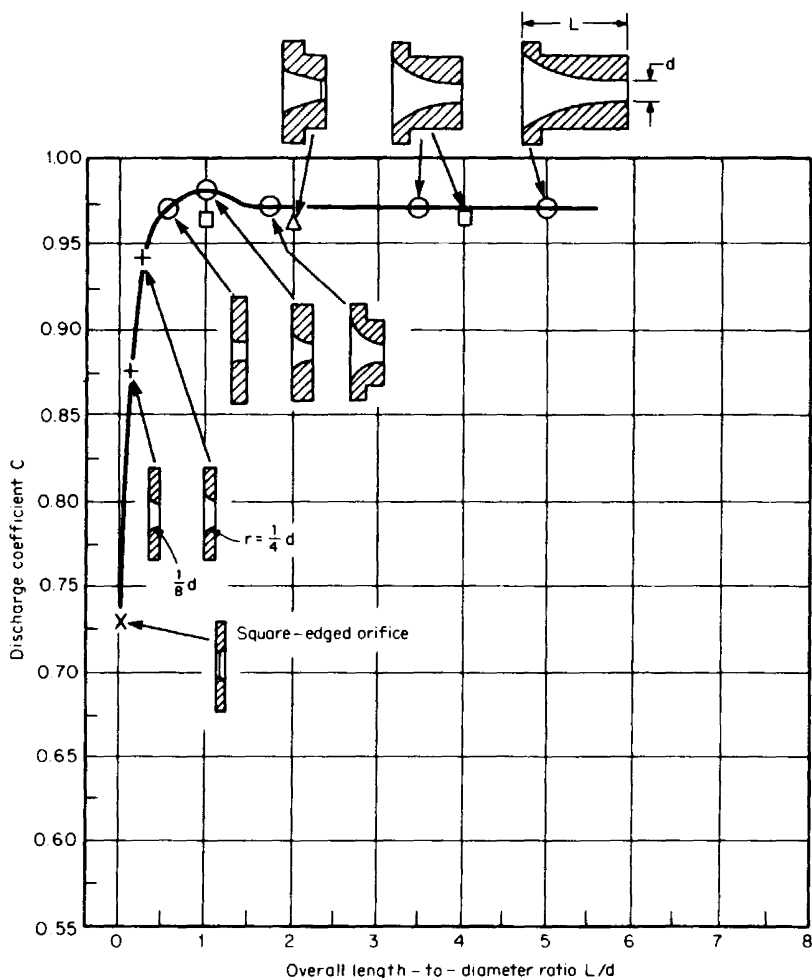


Figure 13.2 Discharge coefficient versus nozzle length-to-bore ratio.

the mean flow rate of a pulsating flow. Kaster et al. (1964) tested quadrant and cylindrical nozzles to measure the pulsating flow of two reciprocating and one rotary positive displacement air compressor and found no significant effect on the discharge coefficient with that obtained under steady flow conditions.

Amini and Owen (1995) and Owen and Hussein (1991) investigated the use of critical nozzles for the measurement of wet (quality) and dry saturated steam. The discharge coefficient presented in Table 13.4 was found to apply, and for wet steam the correction factor of Eq. (9.87) was determined to be the best correlation. The measurement accuracy being estimated as ± 2 to 3 percent.

ISO Critical Venturi Nozzle. Toroidal and cylindrical-throat ISO (1990) critical venturi nozzles are shown in Fig. 13.3. In Fig. 13.4 are the available data on these nozzles (Hillbrath, 1981), plotted against throat Reynolds number R_d . This data is

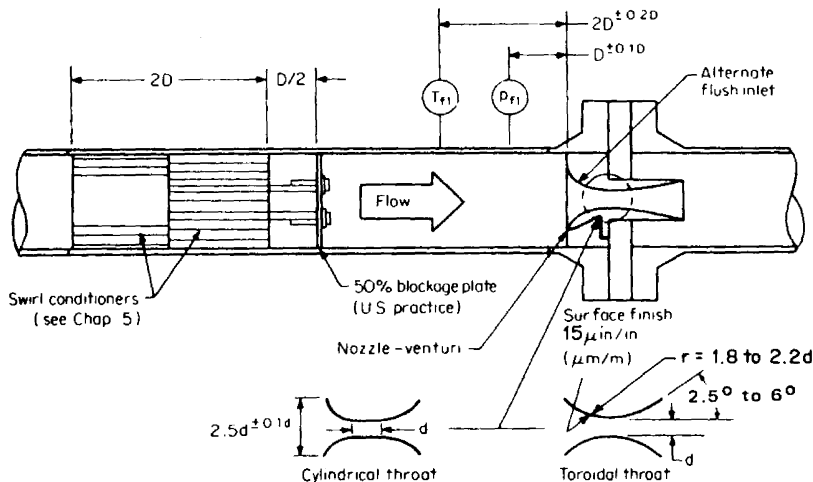


Figure 13.3 ASME/ISO critical venturi nozzle.

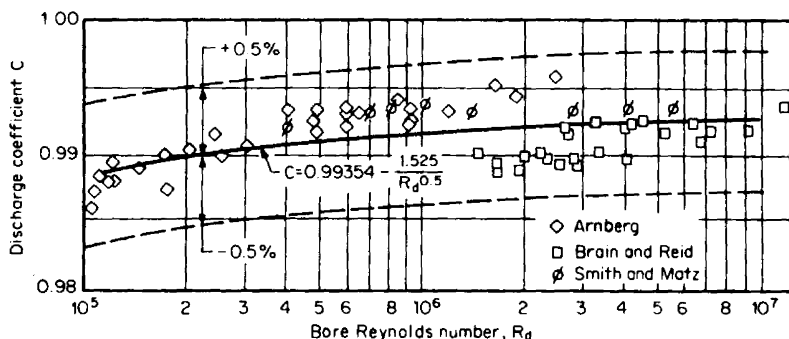


Figure 13.4 Discharge coefficient for venturi nozzle.

from the work of Smith and Matz (1973), Arnberg (1962), and Brain and Macdonald (1977). The general form of the prediction equation is

$$C = C_{\infty} - \frac{b}{R_d^n} \quad (13.22)$$

Constants for this equation and uncalibrated accuracy values are given in Table 13.12.

ASME Long-Radius Nozzle. The discharge-coefficient data for the ASME long-radius nozzle presented by Szanislo (1975) is within the accuracy envelope for the ISO cylindrical-throat venturi nozzle. Although only a single value of β (0.18) was tested, other investigators have found agreement within the accuracy specified for the subsonic flow-coefficient equation given in Table 9.1. While no standard exists for this nozzle, it is suggested that the ISO prediction equation be used with the accuracy increased to ± 0.75 percent.

TABLE 13.12 Discharge-Coefficient-Equation Constants for Critical Flowmeters

Device	Constants†			Uncalibrated accuracy, %
	<i>a</i>	<i>b</i>	<i>n</i>	
ASME-ISO toroidal throat ($\beta < 0.25$) $10^5 < R_d < 10^7$	0.99354	1.525	± 0.5	0.5
ASME-ISO cylindrical throat and ASME long-radius nozzle‡ ($\beta < 0.25$)				
$10^4 < R_d < 3.5 \times 10^5$	1.0000	7.21	0.5	± 0.5
$3.5 \times 10^5 < R_d < 2.5 \times 10^6$	0.9887	0	0	± 0.5
$2.5 \times 10^6 < R_d < 2 \times 10^7$	1.000	0.222	0.2	± 0.5
Square-edged orifice ($\beta < 0.5$; plate thickness, <i>d</i> to <i>6d</i>) $R_d > 10^5$	0.83932	0	0	± 1.6

† $C = a - b/R_d^n$.‡Add ± 0.25 percent to uncalibrated accuracy.

Square-Edged Orifice. Cunningham (1951 first drew attention to the fact that choked flow will not occur across a standard, thin, square-edged orifice. Recently Ward-Smith (1979) showed theoretically that, for choking to occur, the discharge coefficient must approach unity. His highest measured value was approximately 0.9, and during his work the orifice remained unchoked down to a choking pressure ratio of 0.2. However, choked flow is achieved by increasing the plate thickness. For a sharp edge and for ratios of plate thickness to bore diameter between 1 and 6, the discharge coefficient is

$$C = 0.83932 \quad (13.23)$$

This value, the average of the data given in the Ward-Smith paper, has an estimated accuracy of ± 1.6 percent.

Choking Pressure Ratio

The downstream pressure p_{f3} at which choked flow first occurs depends on the exit conditions. For flow without a diffuser, the choking pressure ratio is developed on the assumption of steady isentropic flow as

$$\frac{p_{f3}}{F_{TP}p_{f1}} \leq \left(\frac{2}{k_i + 1} \right)^{k_i/(k_i - 1)} \quad (13.24)$$

where k_i is the isentropic exponent of an ideal gas (see Chap. 2). This equation applies to ASME long-radius nozzles and to *thick* square-edged orifices.

For a venturi nozzle, Hillbrath et al. (1975) have shown that the choking pressure ratio may vary from 0.8 to 0.95, depending on the diffuser area ratio. A diffuser that is four throat diameters in length with a divergence half-angle of 4° (included angle of 8°) produces a choking pressure ratio of approximately 0.9; the ratio is 0.8 for a one-diameter length. For longer diffuser lengths, critical flow can be produced at a ratio of 0.95.

Example 13.1. A toroidal-throat critical venturi nozzle is to be used to measure natural gas flowing at 7,500,000 standard ft³/h (212,380 standard m³/h) in a 12-in [$D = 11.370$ in (290 mm)] line. For a design pressure of 740 psia (5100 kPa) and temperature of 75°F (24°C), what is the nozzle bore if pressure and temperature measurements are made?

The gas composition is as follows:

Substance	Mole fraction x_i	Molecular weight M_{wi} †	$x_i M_{wi}$
Methane	0.9150	16.043	14.6793
Ethane	0.0370	30.070	1.1126
Propane	0.0090	44.097	0.3969
Butane	0.0010	58.124	0.0581
Nitrogen	0.0110	28.013	0.3081
Carbon dioxide	0.0270	44.010	1.1883
			17.7433

†From Table D.1.

From Eq. (2.90),

$$(M_w)_{\text{mix}} = \sum x_i M_{wi} = 17.7433$$

The mixture's specific gravity is, by Eq. (2.7),

$$G = \frac{(M_w)_{\text{mix}}}{(M_w)_{\text{air}}} = \frac{17.7433}{28.9625} = 0.61263$$

The flow-rate equation for pressure and temperature measurements (pvT equation) is, from Eq. (f) of Table 13.1,

$$q_{\text{SCFH}} = 28,712.44 C d^2 Z_b Y_{\text{CR}} \sqrt{\frac{1}{T_{f1} G}} F_{TP} p_{f1}$$

Rearrangement to solve for bore yields

$$d = \left(\frac{q_{\text{SCFH}} \sqrt{T_{f1} G}}{28,712.44 C Z_b Y_{\text{CR}} F_{TP} p_{f1}} \right)^{1/2}$$

From Eq. (13.18), $Z_b = (a_z f + b_z)^2$. At base conditions (Table 13.11), for $T_b = 518.67^\circ\text{R}$ and $p_b = 14.69595$ psia,

$$a_z = -0.00231 \quad b_z = 0.99901$$

and, by Eq. (13.16),

$$\begin{aligned} f &= x_{\text{C}_2\text{H}_6} + x_{\text{CO}_2} - \frac{1}{2} x_{\text{N}_2} + 2x_{\text{C}_3\text{H}_8} + 3x_{\text{C}_4\text{H}_{10}} \\ &= 0.0370 + 0.0270 - \left(\frac{1}{2}\right)(0.0110) + (2)(0.0090) + (3)(0.0010) = 0.0795 \end{aligned}$$

Then

$$Z_b = [(-0.00231)(0.0795) + 0.99901]^2 = 0.99765$$

From Tables 13.10 and 13.11, for $p_{f1} = 740$ psia and $T_{f1} = 459.67 + 75 = 534.67^\circ\text{R}$

$$\begin{aligned}a_c &= -0.0452 & b_c &= 0.6731 \\a_z &= -0.1201 & b_z &= 0.95655\end{aligned}$$

The critical flow function Y_{CR} is then, by Eq. (13.19),

$$Y_{\text{CR}} = \frac{a_c f + b_c}{a_z f + b_z} = \frac{(-0.0452)(0.0795) + 0.6731}{(-0.1201)(0.0795) + 0.95655} = 0.70697$$

Substitution into the diameter equation yields

$$d = \left[\frac{7,500,000 \sqrt{(534.67)(0.61263)}}{(28,712.44)(0.99765)(0.70697)(740)} \right]^{1/2} \left(\frac{1}{CF_{TP}} \right)^{1/2} = 3.0096 \left(\frac{1}{CF_{TP}} \right)^{1/2}$$

The initial assumptions for the values of the discharge coefficient and the total-pressure correction are $C_0 = 0.99354$ and $F_{TP} = 1.0$. Then

$$d = 3.0096 \left[\frac{1}{(0.99354)(1.0)} \right]^{1/2} = 3.0194 \text{ in}$$

The discharge coefficient is given by Eq. (13.22) and Table 13.12 as

$$C = 0.99354 - \frac{1.525}{R_d^{0.5}}$$

From Table C.4 with $d = D$, the bore Reynolds number is

$$R_d = \frac{0.4830 G q_{\text{SCFH}}}{Z_b d \mu_{\text{cP}}} = \frac{(0.4830)(0.6126)(7,500,000)}{(0.9977)(3.019)(0.0142)} = 51,884,000$$

where, from Fig. H.16, $\mu_{\text{cP}} = 0.0142$. Substitution then gives

$$C = 0.99354 - \frac{1.525}{(51,884,000)^{0.5}} = 0.99333$$

The total-pressure correction for $\beta = d/D = 3.0194/11.370 = 0.2655$ is, by Eq. (13.9),

$$\begin{aligned}F_{TP} &= \left[1 - \frac{k_i}{2} \left(\frac{2}{k_i + 1} \right)^{(k_i+1)/(k_i-1)} \beta^4 \right]^{-1} \\&= \left[1 - \frac{1.32}{2} \left(\frac{2}{1.32 + 1} \right)^{(1.32+1)/(1.32-1)} (0.2655)^4 \right]^{-1} = 1.0011\end{aligned}$$

where, from Fig. I.9, $k = 1.32$.

Substitution into the bore equation now gives

$$d = 3.0096 \left(\frac{1}{CF_{TP}} \right)^{1/2} = 3.0096 \left[\frac{1}{(0.99333)(1.0011)} \right]^{1/2} = 3.018 \text{ in}$$

Further iterations are unwarranted, since neither F_{TP} nor C is highly sensitive to bore changes.

Example 13.2. Superheated steam at 500 psia (3450 kPa) and 660°F (350°C) is flowing in a 4-in (100-mm) schedule-80 pipe through a 2-in (50-mm) thick square-edged orifice that has a 1.000-in (25-mm) bore. If the downstream pressure is 200 psia (1380 kPa), what is the mass flow?

For a thick orifice the choking pressure ratio is given by Eq. (13.24) as

$$\frac{p_{f3}}{F_{TP}p_{f1}} \leq \left(\frac{2}{k_i + 1} \right)^{k_i/(k_i-1)}$$

From Eq. (2.241), with $(C_p)_i = 8.73$ from Table I.2,

$$k_i = \frac{(C_p)_i}{(C_p)_i - 1.986} = \frac{8.73}{8.73 - 1.986} = 1.295$$

Then, by Eq. (13.9), with $\beta = d/D = 1.000/3.826 = 0.2614$ (where D was found from Table B.1),

$$\begin{aligned} F_{TP} &= \left[1 - \frac{k_i}{2} \left(\frac{2}{k_i + 1} \right)^{(k_i+1)/(k_i-1)} \beta^4 \right]^{-1} \\ &= \left[1 - \frac{1.295}{2} \left(\frac{2}{1.295 + 1} \right)^{(1.295+1)/(1.295-1)} (0.2614)^4 \right]^{-1} = 1.0010 \end{aligned}$$

and

$$\begin{aligned} p_{f3} &\leq \left(\frac{2}{k_i + 1} \right)^{k_i/(k_i-1)} F_{TP}p_{f1} \\ &= \left(\frac{2}{1.295 + 1} \right)^{1.295/(1.295-1)} (1.0010)(500) = 274 \text{ psia} \end{aligned}$$

Since $p_{f3} = 200 \leq 274$, the orifice is choked.

The mass flow-rate equation, from Eq. (b) of Table 13.1, is

$$q_{PPH} = 2195.591 C d^2 Y_{CR} \sqrt{\frac{G}{T_{f1}}} F_{TP} p_{f1}$$

For a thick square-edged orifice, the discharge coefficient is, by Eq. (13.23), $C = 0.83932$. Other required data are as follows: From Table 13.8, $Y_{CR} = 0.6890$. From Eq. (2.7),

$$G = \frac{(M_w)_{H_2O}}{M_{w,air}} = \frac{18.0153}{28.9625} = 0.6220$$

where, from Table D.1, $(M_w)_{H_2O} = 18.0153$ and $M_{w,air} = 28.9625$. Finally, from Eq. (3.38),

$$T_{f1} = T_F + 459.67 = 660 + 459.67 = 1119.67^\circ\text{R}$$

and substitution into the mass flow equation yields

$$q_{\text{PPH}} = (2195.591)(0.83932)(1.0)^2(0.6890) \sqrt{\frac{0.6220}{1119.67}} (1.0010)(500)$$

$$= 14,978 \text{ lb}_m/\text{h}$$

LIQUIDS

In some applications it is important to limit the flow rate to a maximum value if a valve, pipe, or other system component fails downstream. Liquid *choked* flow occurs if a cavitation barrier exists within the flowmeter. Downstream pressure changes cannot be transmitted through the barrier, and only an upstream pressure change can increase the flow rate.

As shown in Chap. 5, the cavitation zone is more clearly defined in a venturi, whereas for an orifice the location may change. For these reasons, *cavitating* choked venturis are usually selected for flow-limiting use. Choked, thin, sharp-edged orifices may be used, but they are less accurate and not as structurally suited should cavitation persist for long periods. A square-edged or slightly rounded, *thick* inlet orifice is suggested as an inexpensive alternative.

Engineering Equations

The sizing and flow-rate equations developed in Chap. 9 may be used after substitution, for the differential pressure, of

$$h_w = 27.72976(p_{f1} - p_v) \quad (13.25)$$

for U.S. units, and

$$\Delta p^* = p_{f1}^* - p_v^* \quad (13.26)$$

for SI units, where p_{f1} , p_{f1}^* , p_v , and p_v^* are in absolute pressure units. With these substitutions, sizing and flow-rate calculations are performed in the manner outlined in Chap. 9. Table 13.13 gives the recommended design and discharge coefficients to be used in the equations.

Example 13.3. Water at 20 psig (1380 kPa) is flowing at 100°F (37.8°C) in a 2-in (50-mm) schedule-80 pipe. Size a machined-inlet stainless-steel venturi to limit the flow rate to 100 gal/min (378.5 L/min). (Assume the barometric pressure is 14.47 psia.)

From Eq. (c) of Table 9.23, the sizing equation for gallons per minute at flowing conditions is

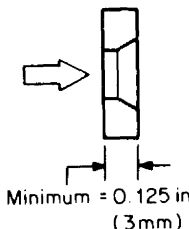
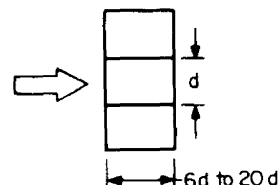
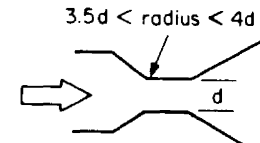
$$S_M = \frac{\sqrt{F} \sqrt{\rho_F} q_v}{N_{v\rho} F_a D^2 \sqrt{h_w}}$$

Substitution of variables from Eq. (13.25),

$$h_w = 27.72976(p_{f1} - p_v)$$

yields

TABLE 13.13 Recommended Designs and Coefficients for Liquid Choked Flowmeters

Device		Discharge coefficient C	Source
Square-edged orifice (refer to Fig. 10.4 for additional details)		0.6	Numachi et al. (1960)
Thick square-edged orifice (refer to Fig. 10.4 for additional details)		0.899	Nurick (1976)
Venturi (refer to Fig. 10.64 for additional details)		0.985	Bonnington (1961)

$$S_M = \frac{\sqrt{F_p} \sqrt{\rho_F} q_v}{N_{vp} F_a D^2 \sqrt{27.72976} \sqrt{p_{f1} - p_v}} = \frac{\sqrt{F_p} \sqrt{\rho_F} q_{\text{gpm}}}{5.2659 N_{vp} F_a D^2 \sqrt{p_{f1} - p_v}}$$

From Table 9.16, $N_{vp} = 44.749$, and from Eq. (9.52),

$$F_a = 1 + 2\alpha_{pE}(T_F - 68) = 1 + 2(0.0000096)(100 - 68) = 1.0006$$

where, from Table B.4, $\alpha_{pE} = 0.0000096 \text{ in}/(\text{in} \cdot ^\circ\text{F})$. In addition,

From Table B.1: $D = 1.939 \text{ in}$

By Eq. (3.15): $p_{f1} = p_G + p_B = 200 + 14.47 = 214.47 \text{ psia}$

From Fig. D.5: $p_v = 0.95 \text{ psia}$ at 100°F

From Eq. (2.137) or Table E.6: $\rho_F = 61.994 \text{ lb}_m/\text{ft}^3$

For negligible liquid compressibility, $F_p = 1.0$, and substitution gives

$$S_M = \frac{\sqrt{1.0} \sqrt{61.994} 100}{(5.2659)(44.759)(1.0006)(1.939)^2 \sqrt{214.47 - 0.95}} = 0.06077$$

The beta ratio is calculated from Eq. (9.78), with $Y_1 = 1.0$ for liquids and (from Table 9.1) $C = 0.995$ for a venturi, as

$$\beta = \left[1 + \left(\frac{CY_1}{S_M} \right)^2 \right]^{-1/4} = \left\{ 1 + \left[\frac{(0.995)(1.0)}{0.06077} \right]^2 \right\}^{-1/4} = 0.2469$$

The venturi bore is then

$$d = \beta D = (0.2469)(1.939) = 0.4788 \text{ in}$$

Example 13.4. In Example 13.3 the pressure increases to 220 psig (1520 kPa). Determine the flow rate if the temperature remains at 100°F (37.8°C).

From Eq. (c) of Table 9.36, the flow-rate equation is

$$q_{\text{gpm}} = N_{\nu\rho} S_M D^2 \frac{\sqrt{h_w}}{\sqrt{F_p} \sqrt{\rho_F}}$$

Substitution of the values given in Example 13.3 with $F_{RD} = 1.0$ and $F_p = 1.0$ yields

$$\begin{aligned} q_{\text{gpm}} &= (5.2659)(44.749)(0.06078)(1.939)^2 \frac{\sqrt{p_{f1} - 0.95}}{\sqrt{61.995}} \\ &= 6.843 \sqrt{p_{f1} - 0.95} = 6.843 \sqrt{(220 + 14.47) - 0.95} = 104.6 \text{ gal/min} \end{aligned}$$

REFERENCES

- Amini A., and I. Owen: "The Use of Critical Flow Venturi Nozzles with Saturated Wet Steam," *Flow Measurement and Instrumentation*, vol. 6, no. 1, pp. 41–47, 1995.
- Amberg, B. T.: "Review of Critical Flow Meters for Gas Flow Measurements," *J. Basic Eng.*, ser. D, vol. 84, pp. 447–460, 1962.
- ASME/ANSI MFC-7M, *Measurement of Gas Flow by Means of Critical Flow Venturi Nozzle*, ASME, New York, 1987.
- Bender, E.: "Equations of State Exactly Representing the Phase Behavior of Pure Substances," *Proc. of the 5th Symp. on Thermodynamic Properties*, pp. 227–235, ASME, New York, 1970.
- Benedict, M., G. B. Webb, and L. C. Rubin: "An Empirical Equation for Thermodynamic Properties of Light Hydrocarbons and Their Mixtures," *J. Chem. Phys.*, vol. 8, no. 4, pp. 334–345, 1940.
- Bonnington, S. T.: *The Influence of Cavitation on the Performance of Standard Flowmeters*, BHRA Report RR701, Bedford, U.K., 1961.
- Brain, T. J. S., and L. M. Macdonald: "Evaluation of the Performance of Small-Scale Critical Flow Venturis Using the NEL Gravimetric Gas Flow Standard Test Facility," *Fluid Flow Measurement in the Mid 1970's*, pp. 103–125, Her Majesty's Stationery Office, Edinburgh, 1977.
- Cunningham, R. G.: "Orifice Meters with Supercritical Flow," *Trans. ASME*, vol. 73, pp. 625–630, 1951.
- Hillbrath, H. S.: "The Critical Flow Venturi—An Update," in *Flow, Its Measurement and Control in Science and Industry*, vol. 2, pp. 407–420, ISA, Research Triangle Park, N.C., 1981.
- , W. P. Dill, and W. A. Wacker: "The Choking Pressure Ratio of a Critical Flow Venturi," *J. Eng. Ind.*, ser. B, vol. 97, no. 4, pp. 1251–1256, 1975.
- ISO Standard 9300, *Measurement of Gas Flow by Means of Critical Flow Venturi Nozzles* ISO, Geneva, 1990.

- Johnson, R. C.: "Calculations of the Flow of Natural Gas through Critical Flowmeters," *J. Basic Eng.*, ser. D, vol. 92, no. 3, pp. 580-589, 1970.
- : *A Set of Fortran IV Routines Used to Calculate the Mass Flow Rate of Natural Gas through Nozzles*, NASA TM X-2240, 1971.
- : *Tables of Critical Flow Functions and Thermodynamic Properties for Methane and Computational Procedures for both Methane and Natural Gas*, NASA SP-3074, 1972.
- Kastner, L. T., T. I. Williams, and E. A. Snowden: "Critical Flow Nozzle Meter and Its Application to the Measurement of Mass Flow Rate in Steady and Pulsating Streams of Gas," *J. Mech. Eng. Sci.*, vol. 6, no. 1, 1964.
- Murdock, J. W., and J. M. Bauman: "The Critical Flow Function for Superheated Steam," *ASME Winter Annual Meeting*, Paper 63-WA-19, New York, 1963.
- Numachi, F., M. Yamabe, and R. Oba: "Cavitation Effect on the Discharge Coefficient of the Sharp-Edged Orifice Plate," *J. Basic Eng.*, vol. 82, pp. 1-11, 1960.
- Nurick, W. H.: "Orifice Cavitation and Its Effect on Spray Mixing," *J. Fluids Eng.*, vol. 98, pp. 681-687, 1976.
- Owen, I., and I. B. Hussein: "Calibration of Flowmeters in Superheated and Wet Steam," *Flow Measurement and Instrumentation*, vol. 2, no. 4, pp. 209-215, 1991.
- Savidge, J. L., and J. J. S. Shen: "Evaluation of Critical Flow Factor and Speed of Sound Methods for Gas Measurements," Int. Gas Research Committee, Tokyo, November 6-9, 1989.
- Shen, J. J. S., V. C. Ting, and E. H. Jones, "Application of Sonic Nozzles in Field Calibration of Natural Gas Flows," *Energy Resources and Tech.*, vol. III, pp. 205-213, December 1989.
- Smith, R. E., and R. J. Matz: "Performance Characteristics of an 8-Inch-Diameter ASME Nozzle Operating at Compressible and Incompressible Conditions," *J. Basic Eng.*, vol. 95, no. 4, 1973.
- Sullivan, D. A.: "Historical Review of Real-Fluid Isentropic Flow Models," *ASME Winter Annual Meeting*, Paper 79-WA/FM-1, New York, 1981.
- : private communication concerning real-fluid isentropic models, 1981.
- Szanişzlo, F. C.: "Experimental and Analytical Sonic Nozzle Discharge Coefficients for Reynolds Numbers up to 8×10^6 ," *J. Eng. Power*, vol. 97, pp. 521-526, 1975.
- Ward-Smith, A. J.: "Critical Flowmetering: The Characteristics of Cylindrical Nozzles with Sharp Upstream Edges," *Int. J. Heat Fluid Flow*, vol. 1, no. 3, pp. 123-132, 1979.

LINEAR FLOWMETERS

In general, flowmeters whose output is not proportional to the square of the flow rate divided by the fluid density are *linear* flowmeters. Either the operating principle yields a direct linear output or, through electronics, the output is linearized to volumetric or mass flow units. These meters can be grouped into two classes: pulse-frequency types and linear-scale flowmeters. Both are discussed in this chapter.

PULSE-FREQUENCY TYPE

Turbine and vortex flowmeters produce a frequency (pulse train) proportional to the pipeline velocity, and positive-displacement meters produce one pulse per unit volume. Although based on different operating principles, these *pulse-type* meters respond to flowing conditions and, therefore, the pertinent engineering equations for flowing and base volumes and for mass flow are the same. With turbine and vortex flowmeters, flow rate is commonly measured by frequency or by frequency-to-analog conversion, but this is seldom the case for the low-resolution positive-displacement meters.

The signature curves for vortex and turbine flowmeters, although different in shape, are linear over 20:1 or 30:1 flow-rate ranges, and, hence a mean meter coefficient (K factor) is given. Positive-displacement flowmeters are usually calibrated in the desired volumetric units and, through suitable internal gearing, directly display the total volume. For turbine and vortex flowmeters, the integrated count is electronically scaled, using the K factor, to display the total volume. Through suitable electronics and computer or mechanical computations, base volume or mass flow is also displayed.

Engineering Equations

K Factor. The K factor defines the relationship between flow rate and frequency for vortex and turbine flowmeters. For liquid turbine meters, this factor is obtained by water calibration; for gas meters, by a low-pressure bell prover test. The K factor (in any volume units) is defined as

$$K_{F,v} = \frac{f_{Hz}}{q_v} = \frac{\text{pulses}}{\text{unit volume}} \quad (14.1)$$

where q_v denotes the volume flow rate (in gallons, cubic meters, etc., per second), and f_{Hz} is the frequency in pulses per second. The K factor then has the units of pulses per unit volume. For both liquids and gases (vapors), the K factor is obtained over a flow-rate range and plotted versus flow rate. Shown in Fig. 14.1a is a typical signature curve for a turbine flowmeter.

Depending on the flow-rate range, which is usually specified as 20:1, 25:1, or 30:1, a *linearity* envelope is specified, such as ± 0.5 percent, ± 0.75 percent, or ± 1 percent. Since signature curves vary with design, manufacturers' designated linear ranges are different. Usually, the percentage assigned to the linearity envelope is acceptable, and the *true* K factor [Eq. (14.1)] is seldom corrected. A *mean* K factor, defined as the mean of the maximum and minimum K factors over the designated range,

$$\bar{K}_{F,v} = \frac{(K_{F,v})_{\max} + (K_{F,v})_{\min}}{2} \quad (14.2)$$

is also used.

Several influence quantities bias or alter the signature curve. Viscosity, meter-body expansion with pressure and temperature, and (for gas turbine flowmeters) the influence of flowing pressure (density) are sometimes considered. Manufacturers specify, based on test data, a limiting viscosity or Reynolds number to maintain linearity. For liquids, the effects of both pressure and temperature are small (≤ 0.01 percent) and usually considered negligible. However, for high-accuracy custody-transfer measurements API Chap. 11.2.1 (1987), corrections are applied and sometimes calibration curves are programmed for computer corrections.

Meter Factor. In some applications, the reciprocal of the K factor is used. This is referred to as the *meter factor* and defined as

$$K_{MF,v} = \frac{1}{K_{F,v}} = \frac{q_v}{f_{Hz}} \quad (14.3)$$

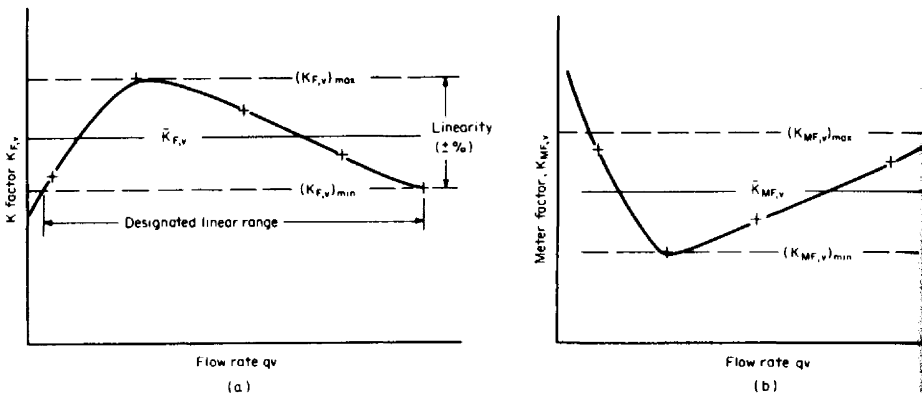


Figure 14.1 K -factor and meter-factor signature curves. (a) K Factor. (b) Meter factor.

TABLE 14.1 Liquid Flow Rate Equations: U.S. and SI Units

	U.S. units ($\bar{K}_{F,v}$ pulses/gal)†		SI units ($\bar{K}_{F,v}^*$ pulses/l)‡	
Mass flow rate				
Density	$q_{PPH} = 481.2500 \frac{\rho_f f_{Hz}}{\bar{K}_{F,gal}}$	(a)	$q_{KPH}^* = 3.6 \frac{\rho_f^* f_{Hz}}{\bar{K}_{F,l}^*}$	(f)
Specific gravity	$q_{PPH} = 30,013.780 \frac{F_p G_F f_{Hz}}{\bar{K}_{F,gal}}$	(b)	$q_{KPH}^* = 3596.443 \frac{F_p G_F f_{Hz}}{\bar{K}_{F,l}^*}$	(g)
Volumetric flow rate at flowing conditions				
	$q_{gpm} = 60 \frac{f_{Hz}}{\bar{K}_{F,gal}}$	(c)	$q_{LPM}^* = 60 \frac{F_p G_F f_{Hz}}{G_b \bar{K}_{F,l}^*}$	(h)
Volumetric flow rate at base conditions				
Density	$q_{GPM} = 60 \frac{\rho_f}{\rho_b} \frac{f_{Hz}}{\bar{K}_{F,gal}}$	(d)	$q_{LPM}^* = 60 \frac{\rho_f^* f_{Hz}}{\rho_b^* \bar{K}_{F,l}^*}$	(i)
Specific gravity	$q_{GPM} = 60 \frac{F_p G_F f_{Hz}}{G_b \bar{K}_{F,gal}}$	(e)	$q_{LPM}^* = 60 \frac{F_p G_F f_{Hz}}{G_b \bar{K}_{F,l}^*}$	(j)

† Substitute $K_{F,v}$ for $\bar{K}_{F,v}$ if signature curve or an equation is used.

‡ Subscript l refers to flowing liters.

The meter factor has the units of unit volume per pulse. † The *mean* meter factor is defined as

$$\bar{K}_{MF,v} = \frac{1}{\bar{K}_{F,v}} = \frac{(K_{MF,v})_{\max} + (K_{MF,v})_{\min}}{2} \quad (14.4)$$

When the meter factor is given, flow rate or total volume is calculated by multiplication rather than division. As shown in Fig. 14.1b, the meter-factor signature curve is the mirror image of the *K*-factor curve.

Flow Rate and Total Volume. The *K* factor has the units of pulses per unit volume—that is, pulses per gallon, per barrel, per cubic meter, etc. Since the frequency is directly proportional to the volumetric flow rate, conversion to base volume or to mass is by the equations developed in Chap. 3. Tables 14.1 through 14.4 list the commonly used U.S.- and SI-unit flow-rate and total-volume equations for mass flow and volumetric flow rate at both flowing and base conditions.

Two-Phase Flows. Vortex and specially designed turbine flowmeters are used to meter quality (wet) steam and other two-phase fluids, such as ammonia, where both liquid and gas (vapor) are present. In these nonhomogeneous applications, mass flow is calculated, and an *effective density* must be used in the equation. Some

† ANSI/API MPMS 12.2F (1981) defines meter factor as prover volume divided by registered volume. In the metering of liquid hydrocarbons, the requirements of this manual must be strictly adhered to.

TABLE 14.2 Liquid Total-Flow Equations: U.S. and SI Units†

		U.S. units ($\bar{K}_{F,v}$ pulses/gal)†		SI units ($\bar{K}_{F,v}^*$ pulses/L)†‡
Mass flow				
Density	$Q_{lbm} = 0.1336806 \rho_f \frac{\text{pulses}}{\bar{K}_{F,gal}}$	(a)	$Q_{kg}^* = \frac{\rho_f^*}{1000} \frac{\text{pulses}}{\bar{K}_{F,l}^*}$	(f)
Specific gravity	$Q_{lbm} = 8.337161 F_p G_F \frac{\text{pulses}}{\bar{K}_{F,gal}}$	(b)	$Q_{kg}^* = 0.999012 F_p G_F \frac{\text{pulses}}{\bar{K}_{F,l}^*}$	(g)
Volumetric flow at flowing conditions				
	$Q_{gal} = \frac{\text{pulses}}{\bar{K}_{F,gal}}$	(c)	$Q_l^* = \frac{\text{pulses}}{\bar{K}_{F,l}^*}$	(h)
Volumetric flow at base conditions				
Density	$Q_{GAL} = \frac{\rho_f}{\rho_b} \frac{\text{pulses}}{\bar{K}_{F,gal}}$	(d)	$Q_L^* = \frac{\rho_f^*}{\rho_b^*} \frac{\text{pulses}}{\bar{K}_{F,l}^*}$	(i)
Specific gravity	$Q_{GAL} = \frac{F_p G_F}{G_b} \frac{\text{pulses}}{\bar{K}_{F,gal}}$	(e)	$Q_L^* = \frac{F_p G_F}{G_b} \frac{\text{pulses}}{\bar{K}_{F,l}^*}$	(j)

†Substitute $K_{F,v}$ for $\bar{K}_{F,v}$ if signature curve or an equation is used.‡Subscript l refers to flowing liters, and L to base liters.

manufacturers recommend dividing the gas-phase density by the mixture's quality to yield a higher density value, under the assumption that the liquid is a mist homogeneously mixed with the gas. This approach was suggested by Spink (1967) for differential producers and has been widely used. However, the work of Hussein and Owen (1991) suggest that the following effective two-phase density equation would correlate the data in the range of $0.82 < X \leq 1.0$:

$$\rho_{TP} = \left\{ \frac{1}{X + [1.26(1 - X) \sqrt{\rho_g / \rho_l}]} \right\}^{1/2} \rho_g \quad (14.5)$$

It is important that the density of either a single- or two-phase vapor mixture be calculated or measured at the location recommended by the manufacturer.

Kegel (1988) performed tests to characterize the performance of vortex-shedding flowmeters under two-phase and two-component (gas-liquid) flow conditions. Data was taken in 2- and 3-in (50- and 75-mm) horizontal lines with both wet steam and an air-water mixture. Based on these tests, two conclusions were drawn. First, in a flow consisting of a homogeneous vapor-droplet mixture the vortex-shedding frequency is proportional to the mixture's average velocity. This was observed over a quality range of 20 to 100 percent, where quality is defined as the portion of the mass flow rate that is in the vapor phase. The second conclusion was that, when a liquid film is present, a pool of liquid runs along the bottom of the pipe and the strut must be parallel or nominally horizontal. A highly erratic signal was observed when the strut was installed vertically.

Kegel further observed that care must be taken in the interpretation of the meter signal, since the lower liquid velocity phase acts to reduce the flow area through which the higher-velocity gas (vapor) phase is flowing. The apparent mixture ve-

TABLE 14.3 Gas (Vapor) Flow-Rate Equations: U.S. and SI Units

	U.S. units ($\bar{K}_{F,v}$ pulses/ft ³)†		SI units ($\bar{K}_{F,v}^*$ pulses/m ³)†	
Mass flow rate				
Density	$q_{PPH} = 3600 \rho_f \frac{f_{Hz}}{\bar{K}_{F,\text{ft}^3}}$	(a)	$q_{KPH}^* = 3600 \rho_f^* \frac{f_{Hz}}{\bar{K}_{F,\text{m}^3}^*}$	(g)
<i>pvT</i> equation	$q_{PPH} = 9715.77 \frac{G p_f}{Z_f T_f} \frac{f_{Hz}}{\bar{K}_{F,\text{ft}^3}}$	(b)	$q_{KPH}^* = 12,540.27 \frac{G p_f^*}{Z_f T_K} \frac{f_{Hz}}{\bar{K}_{F,\text{m}^3}^*}$	(h)
Volumetric flow rate at flowing conditions				
	$q_{acfh} = 3600 \frac{f_{Hz}}{\bar{K}_{F,\text{ft}^3}}$	(c)	$q_{a\text{ cmh}}^* = 3600 \frac{f_{Hz}}{\bar{K}_{F,\text{m}^3}^*}$	(i)
Volumetric flow rate at base conditions				
Density	$q_{SCFH} = 3600 \frac{\rho_f}{\rho_b} \frac{f_{Hz}}{\bar{K}_{F,\text{ft}^3}}$	(d)	$q_{SCMH}^* = 3600 \frac{\rho_f^*}{\bar{K}_{F,\text{m}}^*} \frac{f_{Hz}}{\bar{K}_{F,\text{m}^3}^*}$	(j)
<i>pvT</i> equation				
Standard base	$q_{SCFH} = 127,056.24 \frac{Z_b p_f}{Z_f T_f} \frac{f_{Hz}}{\bar{K}_{F,\text{ft}^3}}$	(e)	$q_{SCMH}^* = 10,237.75 \frac{Z_b p_f^*}{Z_f T_K} \frac{f_{Hz}}{\bar{K}_{F,\text{m}^3}^*}$	(k)
Selected base	$q_{SCFH} = 3600 \frac{Z_b T_b p_f}{Z_f T_f \rho_b} \frac{f_{Hz}}{\bar{K}_{F,\text{ft}^3}}$	(f)	$q_{SCMH}^* = 3600 \frac{Z_b T_{Kb} p_f^*}{Z_f T_K \rho_b^*} \frac{f_{Hz}}{\bar{K}_{F,\text{m}^3}^*}$	(l)

†Substitute $K_{F,v}$ for $\bar{K}_{F,v}$ if signature curve or an equation is used.

TABLE 14.4 Gas (Vapor) Total-Flow Equations: U.S. and SI Units

U.S. units ($\bar{K}_{F,v}$ pulses/ft ³) [†]		SI units ($\bar{K}_{F,v}^*$ = pulses/m ³) ^{d ‡}		
Mass flow				
Density	$Q_{lbm} = \rho_f \frac{\text{pulses}}{\bar{K}_{F,ft^3}}$	(a)	$Q_{kg}^* = \rho_f^* \frac{\text{pulses}}{\bar{K}_{F,m^3}^*}$	(g)
<i>p</i> <i>v</i> <i>T</i> equation	$Q_{lbm} = 2.698825 \frac{p_f G}{Z_f T_f} \frac{\text{pulses}}{\bar{K}_{F,ft^3}}$	(b)	$Q_{kg}^* = 3.483407 \frac{p_f^* G}{Z_f T_K} \frac{\text{pulses}}{\bar{K}_{F,m^3}^*}$	(h)
Volumetric flow at flowing conditions				
	$Q_{acf} = \frac{\text{pulses}}{\bar{K}_{F,ft^3}}$	(c)	$Q_{a\ cm}^* = \frac{\text{pulses}}{\bar{K}_{F,m^3}^*}$	(i)
Volumetric flow at base conditions				
Density	$Q_{SCF} = \frac{\rho_f}{\rho_b} \frac{\text{pulses}}{\bar{K}_{F,ft^3}}$	(d)	$Q_{SCM}^* = \frac{\rho_f^*}{\rho_b^*} \frac{\text{pulses}}{\bar{K}_{F,m^3}^*}$	(j)
<i>p</i> <i>v</i> <i>T</i> equation				
Standard base	$Q_{SCF} = 35.29340 \frac{Z_b}{Z_f} \frac{p_f}{T_f} \frac{\text{pulses}}{\bar{K}_{F,ft^3}}$	(e)	$Q_{SCM}^* = 2.843819 \frac{Z_b}{Z_f} \frac{p_f^*}{T_K} \frac{\text{pulses}}{\bar{K}_{F,m^3}^*}$	(k)
Selected base	$Q_{SCF} = \frac{Z_b}{Z_f} \frac{T_b}{T_f} \frac{p_f}{p_b} \frac{\text{pulses}}{\bar{K}_{F,ft^3}}$	(f)	$Q_{SCM}^* = \frac{Z_b}{Z_f} \frac{T_{Kb}}{T_K} \frac{p_f^*}{p_b^*} \frac{\text{pulses}}{\bar{K}_{F,m^3}^*}$	(l)

[†]Substitute $K_{F,v}$ for $\bar{K}_{F,v}$ if signature curve or an equation is used.[‡]Subscripts acm and SCM refer to flowing and base or standard cubic meters, respectively.

locity is, therefore, increased and a higher shedding frequency is observed than when no liquid is present.

Accuracy. For an estimate of measurement accuracy, the accuracy of the K factor (or meter factor) must be estimated and then combined with the accuracy of each measured quantity (see Chap. 4) by the root-sum-squared method. The sensitivity coefficients for the variables in Tables 14.1 to 14.4 are all 1.0, with the sign either positive for a numerator value or negative for a denominator value.

The accuracy of the K factor (or meter factor) should be obtained from the manufacturer, but it may be conservatively estimated as

$$(\text{Acc})_{K_{F,w}} = \pm (\text{Acc})_{\text{LAB}} \pm \sqrt{L^2 \pm 4\sigma_p^2} \quad (14.6)$$

where $(\text{Acc})_{\text{LAB}}$ is the laboratory accuracy, and σ_p is the precision of the two data points used to define the linearity envelope.

Turbine Flowmeter

Principle of Operation. Figure 14.2a shows the velocity vector diagram for an *ideal* helical-bladed turbine flowmeter. The velocity of the entering fluid displaces the blades, and the vector sum of the fluid velocity with respect to the blade $\mathbf{V}_{f/B}$ and the blade rotational velocity \mathbf{V}_B equals the entering axial velocity vector \mathbf{V}_f . In this ideal case, the velocity leaving the blades is, therefore, not displaced with respect to the entering velocity vector. In the real case, retarding torques from blade fluid friction, bearing friction, tip clearing (windage), etc., are present and cause the exit velocity to be displaced from the entering vector; the blades therefore rotate at a speed below the theoretically predicted speed. This decrease in rotational velocity, referred to as *slip*, results in an exit swirl velocity component that changes with retarding torque. This velocity component provides the kinetic energy to balance the retarding torques.

Assuming a flat (rectilinear) entering velocity profile, Rubin et al. (1965) considered both momentum and airfoil approaches to explain the relationship between driving and retarding torques. The data was presented in terms of a slip parameter, which is the ratio of the tangent of the effective angle of attack to the blade angle. Thompson and Grey (1970) extended this analysis to include a variable lift coef-

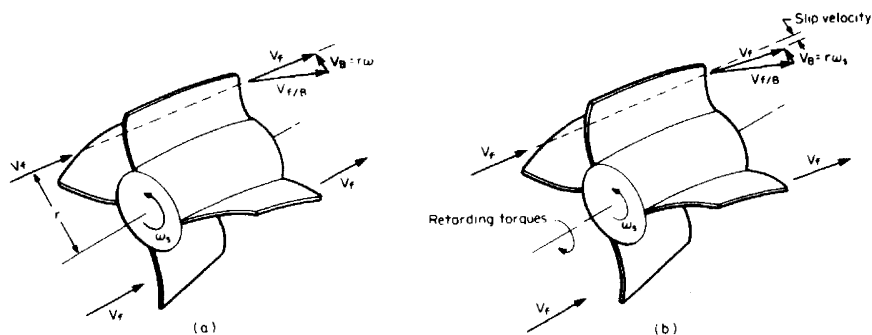


Figure 14.2 Fluid-velocity vector diagram for a turbine flowmeter. (a) Ideal. (b) With retarding torque.

ficient and annular velocity profile. Furness (1987) has recently developed a detailed 47-parameter computer model that considers all known influences. This study indicates that, for constant-blade-angle meters, gas turbine meter blades should have significantly different blade aspect ratios than are commonly used in gas turbine meters. This analysis has led to a better understanding of the relationship among the numerous parameters affecting meter performance.

Liquid Flowmeters. Liquid turbine flowmeters are available with straight, helical, and T-shaped blades (Fig. 14.3). A multiholed shroud ring (Fig. 14.3a) is also widely used to increase the frequency for the same number of blades. Depending on line size, flow-rate range, and metered fluid, either ball or journal bearings (Fig. 14.3b) are selected. Except for very clean lubricating-type liquids, journal bearings with a thrust ball (Fig. 14.3c) are usually chosen. Bearing wear (in both ball and journal types) increases the retarding torques, which, in turn, alter the K factor at lower flow rates.

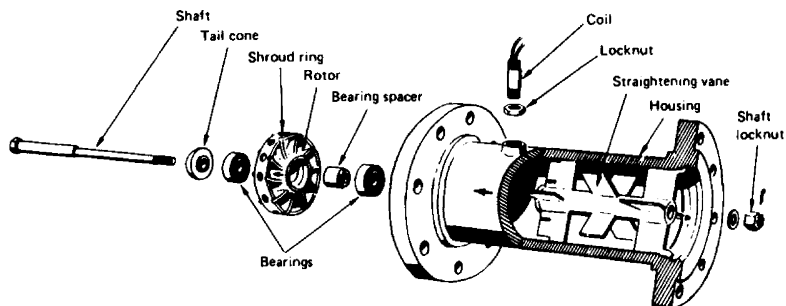
Two basic types of detection devices are available: magnetic and modulated-carrier. In the magnetic type, the magnetic pick-off may be in the external coil assembly (reluctance pick-off). Less drag is associated with the inductive pick-off, and, due to the reduced retarding torques, linearity is slightly improved (Fig. 14.4b). The modulated-carrier pick-off detector operates through the modulation of a 45-kHz carrier frequency by the passage of the turbine blade. Since retarding torques are minimal, this detector can improve low-velocity (or low-density-flow) performance. The magnetic-reluctance pick-off is the most widely used for reasons of economics, but the other detection methods may be selected for better low-range performance.

The effect of fluid viscosity is illustrated in Fig. 14.4c. In general, blade friction increases with viscosity, resulting in a decrease in speed for the same flow rate. The effect of viscosity is, however, difficult to predict, because bearing friction, tip clearance, drag, velocity profile, and blade friction are also viscosity-dependent.

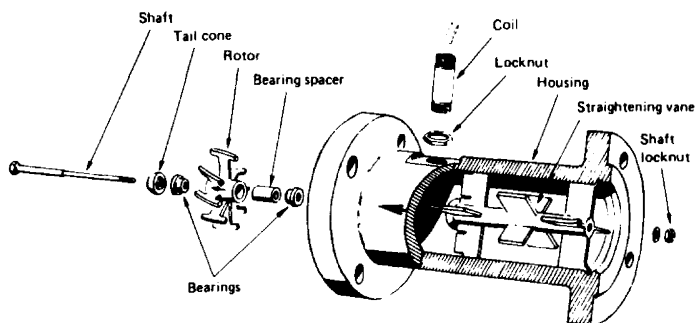
Turbine meters are sometimes checked by a *spin* test in which the rotor is spun by a jet of air. The time for the rotor to stop after removal of the jet is checked against prior spin-test times to detect increased torques. Although no specific value for the change in K factor can be determined, a decreased time usually indicates that recalibration or new bearings are required. Additionally, a spin test is an excellent check on overall system circuitry. Extreme care should be exercised, however, so as not to overspeed the rotor during the spin test. Figure 14.4a illustrates the change in K factor with increasing bearing friction.

Industrial liquid turbine flowmeters are water-calibrated to obtain the K -factor signature curve. For fluids with other viscosities, any of five correction methods may be used; the method selected depends on the manufacturer and the desired accuracy. The five methods are as follows:

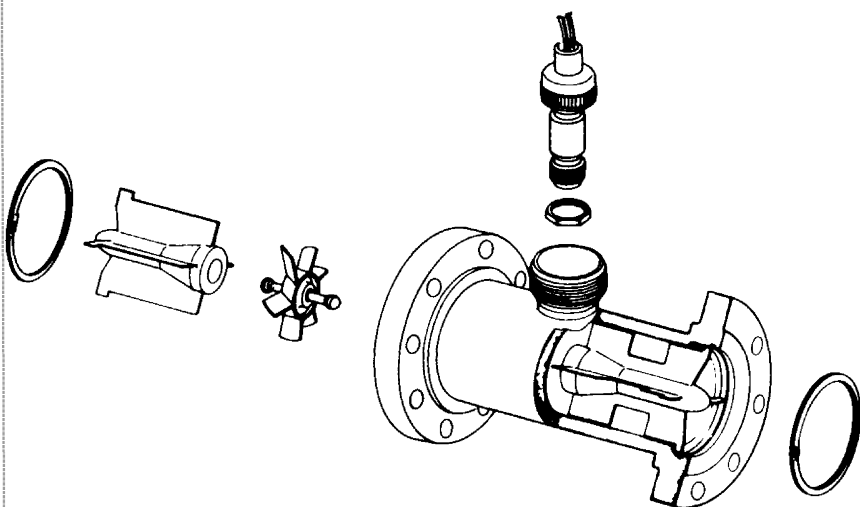
1. A type test is conducted for each meter size, and a bias error curve is given (Fig. 14.5a).
2. The flowmeter is calibrated using the fluid to be metered, and a calibration curve is used for correction; alternatively, a fluid with similar viscosity and density may be used.
3. The flow rate or frequency is divided by the kinematic viscosity, usually in centistokes, and a universal K -factor curve is presented (Jennings, 1977). Shown in Fig. 14.5b is a typical universal viscosity curve that some manufacturers use to represent the viscosity effect on a single plot. This curve is then used to calculate flow rates by iteration from known frequency and viscosity values.



(a)



(b)



(c)

Figure 14.3 Turbine-flowmeter blade and bearing designs. (Courtesy The Foxboro Co.) (a) Helical blades with ball bearings. (b) Helical T blades with ball bearings. (c) Straight blades with journal bearing and thrust ball.

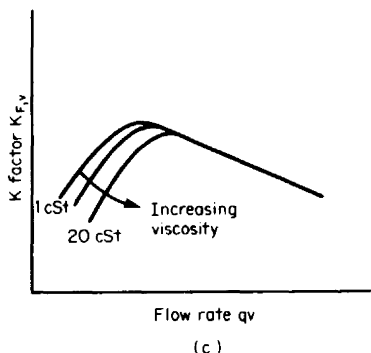
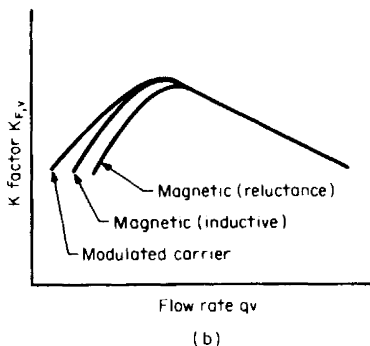
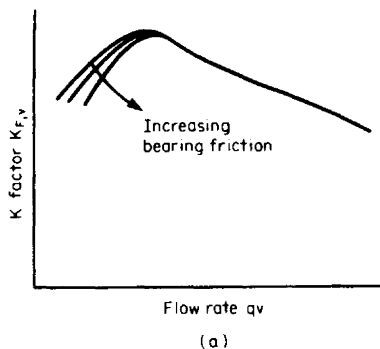


Figure 14.4 Effects of retarding torques. (a) Bearing friction. (b) Pick-off method. (c) Viscosity.

4. Numerous data points are obtained at different viscosities, for the fluid to be metered. This data is then fitted to two polynomial series-expansion equations (Fig. 14.4c). The true flow rate is then computer-calculated from viscosity and frequency values (Ball, 1977; Jones, 1985).
5. The meter is calibrated in situ with a ball prover. This method is used for the custody transfer of liquid hydrocarbons; API 2101 should be consulted for calculation procedures.

Turbine flowmeters are usually calibrated at moderate pressures [<100 psia (700 kPa)] and with ambient-temperature fluids. Except for the custody transfer of petroleum liquids, small geometry changes with pressure are not normally considered. API 2101 should be consulted for the combined correction for pressure and temperature. ANSI (ISA RP) 31.1 (1977) recommends a temperature correction for accurate measurement. This correction is

$$(K_{F,v})_{\text{flow}} = \frac{(K_{F,v})_{\text{calib}}}{1 + 3\alpha_{\text{HO}}(T_F - T_{F,\text{calib}})} \quad (14.7)$$

for U.S. units, and

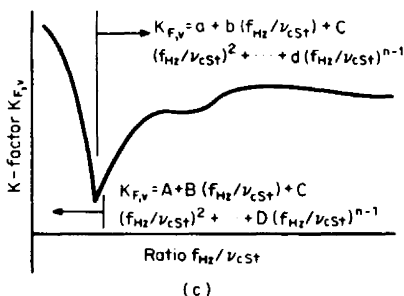
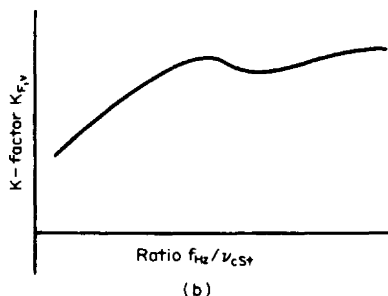
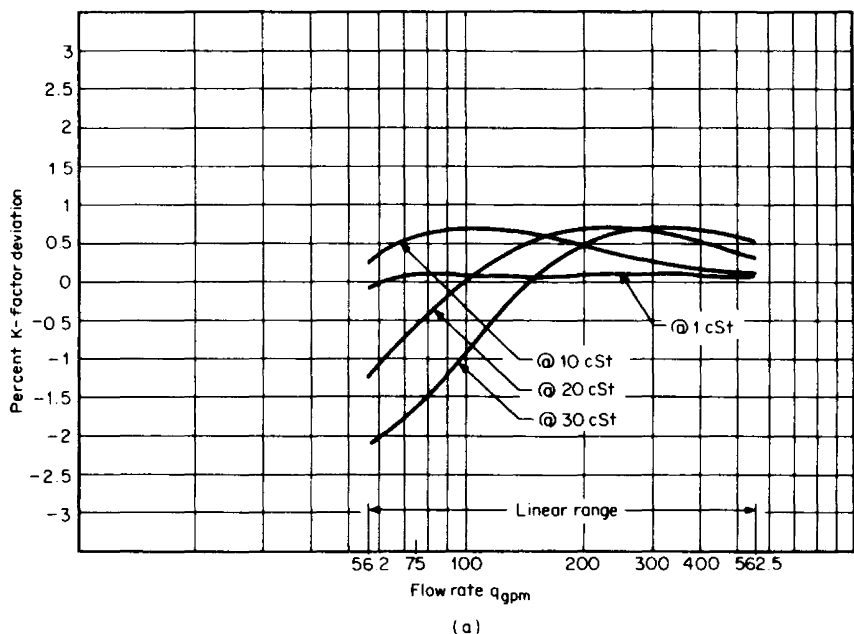


Figure 14.5 Viscosity corrections. (a) Type testing. (b) Universal viscosity curve. (c) Polynomial fitted curves for a single fluid.

$$(K_{F,v})_{\text{flow}} = \frac{(K_{F,v})_{\text{calib}}}{1 + 3\alpha_{HO}^*(T_c - T_{c,\text{calib}})} \quad (14.8)$$

for SI units, where α_{HO} and α_{HO}^* are the thermal-expansion coefficients of the meter housing, and the subscripts flow and calib refer to flowing and calibration conditions.

Since blade and bearing designs vary widely among manufacturers, it is important that each meter be installed in accordance with the manufacturer's recommendations. Precautions such as overspeeding protection and the installation of upstream strainers must be strictly followed for reliable performance. Typically, 10

TABLE 14.5 Typical Mesh Numbers for Upstream Strainers

Flowmeter size, in (mm)	Mesh number	Hole size, in (mm)
$\frac{1}{2}$, $\frac{3}{4}$ (12, 20)	100	0.0059 (0.15)
1, 2, 3 (25, 50, 75)	80	0.0070 (0.18)
4, 6 (100, 150)	60	0.0098 (0.25)
8, 10, 12 (200, 250, 300)	40	0.0165 (0.42)

diameters of upstream pipe and 5 diameters of downstream pipe are required. The strainer mesh numbers shown in Table 14.5 are usually suggested.

Gas Flowmeters. Figure 14.6a illustrates a single-rotor gas turbine flowmeter. As the gas enters, it is constricted into an annular space that is approximately one-third the area of the housing. The area reduction increases the gas velocity, providing more driving torque and thereby improving low-flow-rate performance. The rotor is usually of high-strength plastic, molded to the desired angle of attack. The rotor is supported by ball bearings that are either permanently lubricated or lubricated through a wet-wicking system. For protection, the bearings are enclosed in the central housing. Integral gearing and electronic pick-off are available.

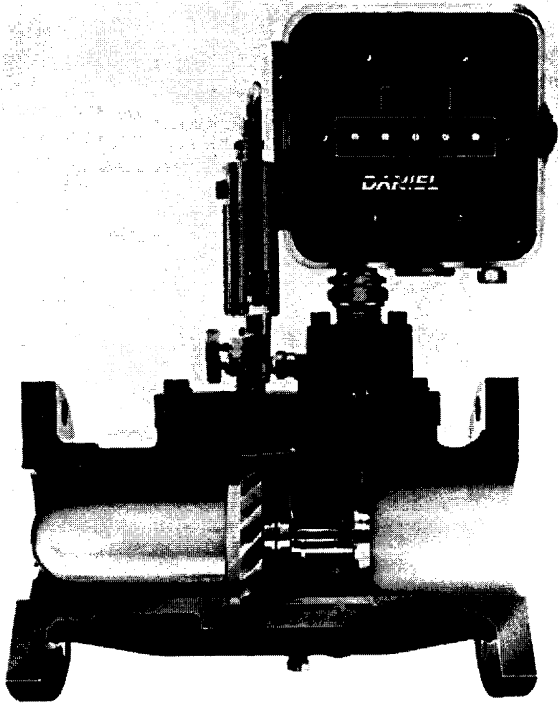
In the Equimeter Auto-Adjust Turbo-Meter (Fig. 14.6b), a sensor rotor, placed downstream from the main rotor, responds to changes in the exit angle of the fluid leaving the main rotor (Lee, 1982, 1987). The pulse output of this sensor rotor is electronically subtracted from the pulse output of the main rotor to produce an adjusted output which automatically and continuously corrects to the original meter calibration accuracy. This adjustment occurs despite differences in retarding torques, bearing wear and contamination, or upstream flow between field conditions and calibration conditions. The ratio of sensor-rotor output to main-rotor output at flowing conditions is also automatically and continuously compared with that at calibration conditions. This provides a self-check of the device's own mechanical and electrical operation as well as the upstream flow conditions; it also gives an indication of the deviation from original calibration conditions that is being corrected for by the sensor rotor.

In the mechanical gear-train type pick-off, blade rotation is transmitted through a magnetic coupling to an index counter. Through suitable gear ratios, the index reads in flowing volume units. The mechanical gearing increases the retarding torque, and, therefore, its low-flow-rate performance is not as good as that of the magnetic-pick-off types.

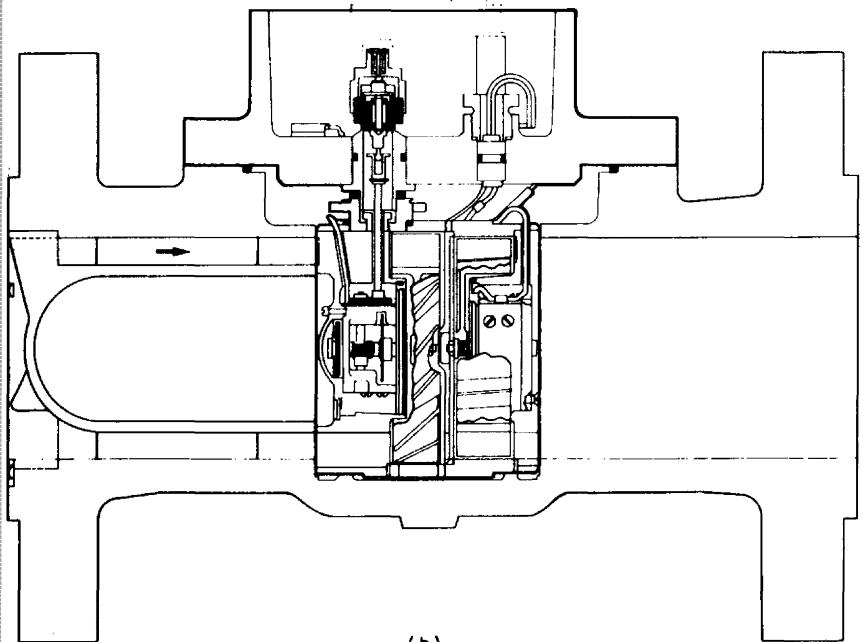
The measuring unit, consisting of rotor, shaft, and bearing assembly, is removable through the side or top of the meter housing. For electrical pulse meters, the detector system and associated electronics are outside the body.

AGA Report 7, ANSI/ASME MFC-4M (1986), and ISO 9951 (1992) give the performance of gas turbine metering as ± 1 percent of flowing volume, with a precision of ± 0.1 percent. The designated linearity range is a function of velocity profile, fluid drag, and nonfluid drag effects. The effects of these quantities on rotor speed are summarized in Fig. 14.7 for pipe Reynolds numbers below 100,000. Lee (1987) has demonstrated that, except for low-pressure air test, the meter factor obtained on air is the same as that obtained on natural gas.

To achieve the desired accuracy, the flowmeter should be installed according to the manufacturer's recommendations. Shown in Fig. 14.8 are the straight-length requirements given in AGA Report 7 (1981). Rotor overspeeding resulting from



(a)



(b)

Figure 14.6 Gas turbine flowmeter. (a) Single rotor. (Courtesy Daniel Industries.) (b) Auto-Adjust. (Courtesy Equimeter, Inc.)

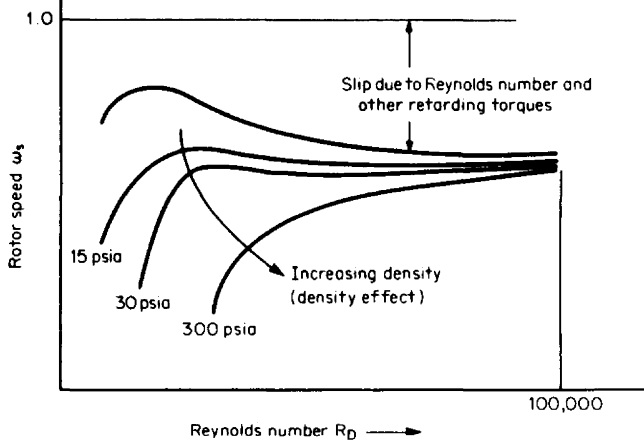


Figure 14.7 Gas-turbine-flowmeter performance at low Reynolds numbers.

pressuring, purging, venting, or operating the meter in reverse can damage the meter. Usually the manufacturer limits overspeed to 150 percent of the rated capacity, and that only for short time periods. AGA Report 7 suggests that blow-down valves be less than one-sixth the meter size, or, for high-pressure installations, that critical flow nozzles (see Chap. 13) be installed to limit the flow to 120 percent of rated capacity.

Vortex Flowmeters

Principle of Operation. Vortex shedding is a common flow phenomenon in which rotating zones of fluid are shed downstream of a barrier placed in a moving stream. This *roll-up* of fluid, first from one side of the barrier and then the other, is responsible for the waving of flags and the singing (aeolian tones) of telephone wires. The subject of vortex shedding is treated in most fluid dynamics texts and in numerous technical papers. To date, however, no complete theoretical explanation of the fundamental nature of vortex formation and the resulting alternate shedding pattern has been advanced.

Figure 14.9 shows the basic vortex-shedding principle (Corpron et al., 1978) and in Fig. 14.10 are sequential photographs of vortex shedding. As the flow is split into two streams, the instability of the shear layer causes the fluid to roll up into a well-defined vortex, the time for complete vortex formation depending on vortex-element (barrier) geometry. After it is formed, the vortex sheds, and a second vortex begins to form on the opposite side of the element. If the vortex shedding is stable, the time for complete formation of the second vortex is the same as that for the first vortex, with the formation time proportional to velocity. The pattern is then repeated alternately from side to side, resulting in the familiar downstream *von Karman* (1912) *vortex street*. The vortex shedding results in pressure and velocity changes around and downstream of the vortex element. By placing pressure, ther-

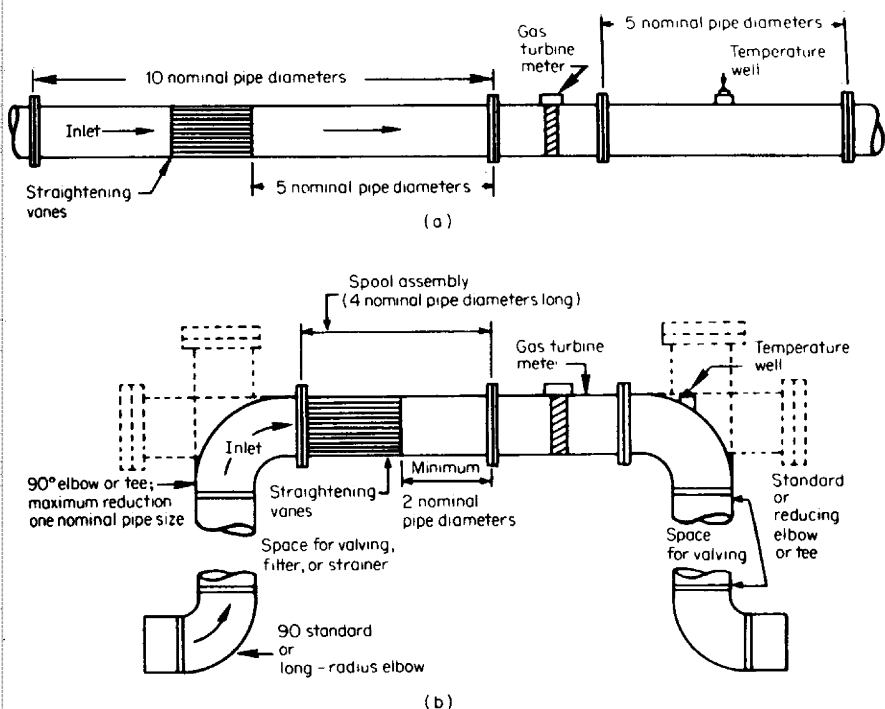


Figure 14.8 Recommended minimum lengths for gas turbine flowmeter. (From AGA Report No. 7.) (a) Straight-through recommended design. (b) Optional design for close coupling. (c) Optional design for close coupling with integral flow conditioners. (d) Recommended for angle-body design.

mal, or ultrasonic detectors in a location where the signal is high, the vortex-shedding frequency may be measured.

Strouhal (1878) made the first experimental observation of the shedding phenomenon. He showed that the shedding frequency of a vibrating wire in the wind was related to the wind velocity and wire diameter. The *Strouhal number* is still widely used as the basic vortex-shedding correlation; it is computed as

$$S = \frac{f_{Hz} h_F}{V_{free}} \quad (14.9)$$

where S is the Strouhal number, h_F the barrier width in feet, and V_{free} the free-stream velocity.

Experimental evidence indicates that the Strouhal number is essentially constant over wide velocity ranges and is independent of fluid density. Data obtained with industrial meters on liquids (Inkley et al., 1980), steam, natural gas (Miller et al., 1984), and air (White et al., 1974) substantiates this density independence. The pipeline velocity profile does, however, influence the constancy of the Strouhal number.

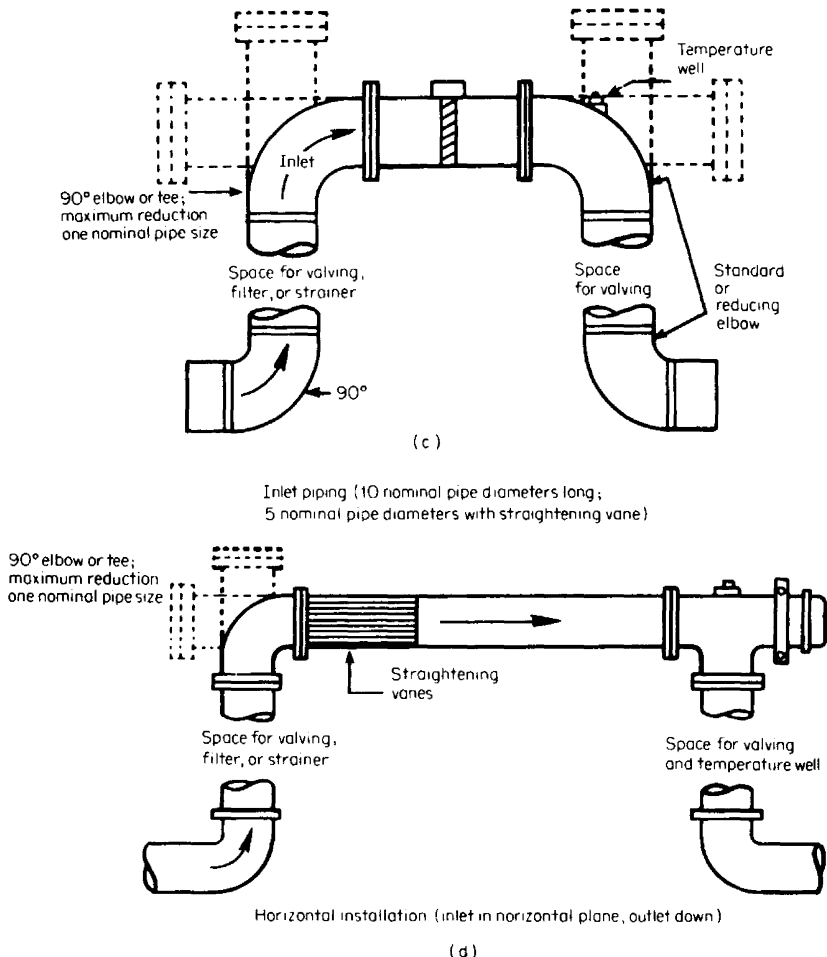


Figure 14.8 (Continued)

Industrial Flowmeters. Generally, vortex flowmeters are made up of three parts: a vortex-generating element fully spanning the pipe, a sensor to convert shedding energy into an electrical pulse signal, and a transmitter for amplification and conditioning. The significant differences among vortex-flowmeter designs are in the element shape and the sensor. Shown in Fig. 14.11 are the geometries of some vortex-generating elements.

The shedding frequency is a function of barrier width, barrier length, and the ratio of barrier width to meter bore. The relationship between frequency and geometry is empirically determined, since even for free-stream flows the theoretical relationship between near and far wake has not been developed.

The signature curves for vortex flowmeters generally have two distinct shapes, depending on element design, as shown in Fig. 14.12. Linearity ranges from 0.5 percent of rate to ± 1 percent of the upper-range flow rate over a 20:1 range. The

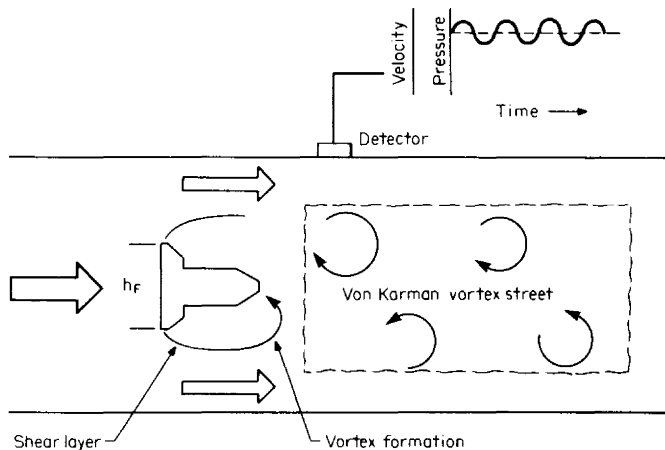


Figure 14.9 Vortex shedding from a bluff body.

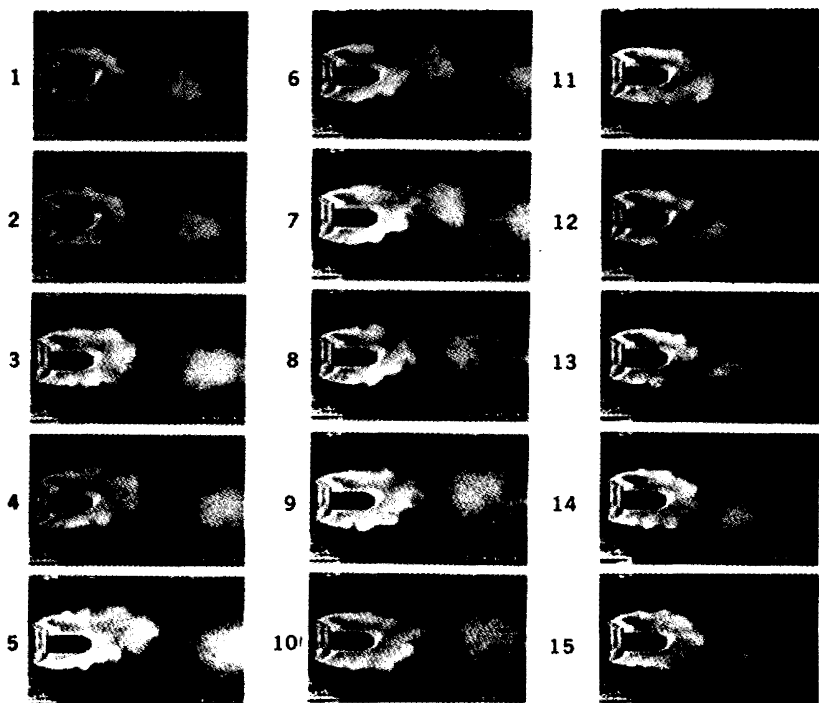


Figure 14.10 Sequential photographs of vortex shedding showing one cycle of shedding from a t-cross-section cylinder in a pipe at 0.04 s/frame. (From Corpron et al., 1978.)

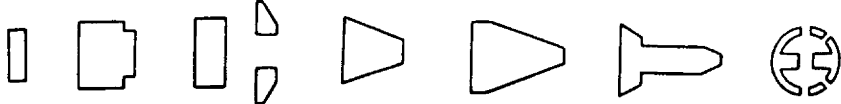


Figure 14.11 Vortex-element geometries.

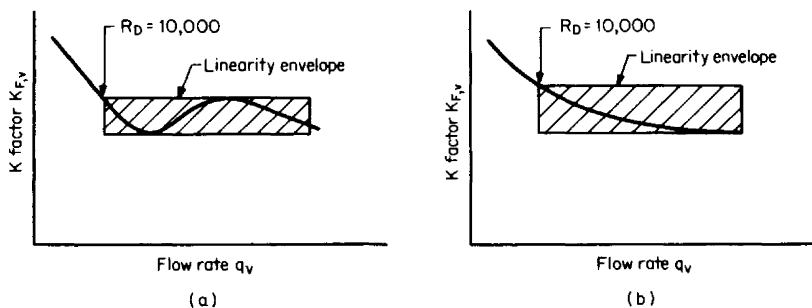


Figure 14.12 Typical vortex-flowmeter signature curves. (a) S shape. (b) C Shape.

lower-limit Reynolds number is usually specified as 10,000; no upper limit has been experimentally determined.

The minimum velocity that can be measured depends on the detector type. For liquids, where density variations are small, the lower limit is generally 1 to 2 ft/s (0.3 to 0.6 m/s). For gases (vapors), the minimum velocity may depend on the fluid density, which is a function of process pressure, temperature, and specific gravity. Manufacturers should be consulted for lower-limit values.

Presently, vortex flowmeters are individually water-calibrated to determine the mean K factor. Miller et al. (1977) present data on 167 meters that indicate a ± 0.3 percent agreement in mean K factors. This suggests that, in the future, meters may be assigned K factors and not individually calibrated.

ASME/ANSI MFC-6M (1987) covers vortex flowmeters. The flow rate and total flow are given in Tables 14.1 through 14.4. The actual and mean K -factors are given by Eqs. (14.1) and (14.2), respectively, and the correction for thermal changes by Eqs. (14.7) and (14.8).

Positive-Displacement Flowmeters

Principle of Operation. Positive-displacement meters measure total flowing volumes by repeatedly filling and discharging fixed volumes. Many different designs are available for both liquid and gas flows, ranging from household water meters to large-volume natural gas meters (see Chap. 6). *Fluid Meters* (ASME, 1971) divides positive-displacement meters into three broad classes. In the first are meters in which one wall is of a flexible material that moves to displace the volume with no leakage into another chamber. In the second are meters in which a mechanical seal is used between movable and stationary walls. The third class of meters employs a capillary or film seal between the moving and stationary elements.

The permanent pressure loss (pressure drop) provides the energy to drive the mechanical system and moving compartments. This is usually lowest for the film-seal class and highest for meters with reciprocating pistons.

Positive-displacement meters are widely used as *cash* (cash transaction) register meters, and for this reason are invariably calibrated and adjusted to state or national regulatory standards. In the United States, for gases (vapors), standards prepared by AGA (ANSI B109.2, 1980; ANSI B109.3, 1980) and AGA Report 6 (1975) are followed; for liquid petroleum products, ANSI Z11.170 (1960) is followed.

These standards specify a ± 1 percent accuracy between the register reading and the *true* flow as defined by certified volume cans, weigh-tank readings, bell prover tests, or a critical-flow prover (critical nozzle). Mechanical adjustments within the meter are usually provided to correct register readings to the referenced volume.

Because of the many available designs, no single signature curve can be established. However, the curve shown in Fig. 14.13 can be used qualitatively to represent the characteristics of positive-displacement meters. The horizontal line represents the calculated dimensional volume displacements, which are theoretically unaffected by flow rate. The C-shaped curve is the true meter factor (unit volume per pulse count); because of leakage (slip), the curve is above the calculated volume line. The meter is calibrated, or *proofed*, by adjusting the register reading to within ± 1 percent of the true volume over the rated flow-rate range.

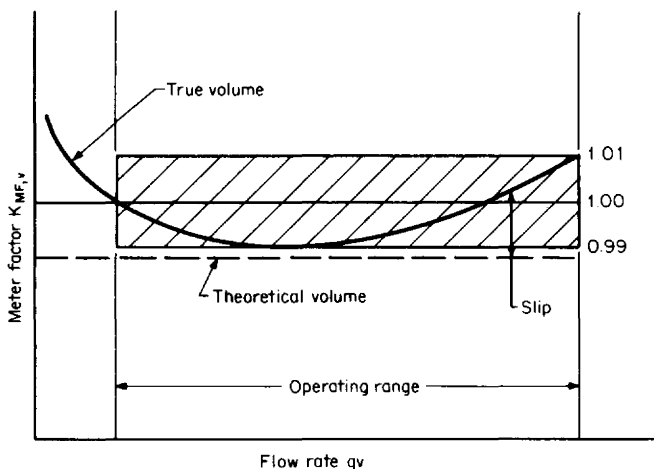


Figure 14.13 Representative positive-displacement signature curve.

Liquid Flowmeters. Liquid meters range from household water meters to those used to measure liquefied petroleum gas (LPG). Corrections for liquid compressibility and temperature may be required, depending on the desired accuracy. Regarding meters (or auxiliary equipment) for high-accuracy applications, ANSI Z11.170 suggests the following considerations:

1. Range of operating flow rate and whether the flow is continuous or intermittent
2. Maximum flowing pressure and allowable permanent pressure loss
3. Type of liquid (or liquids) the meter will measure, including viscosity and corrosivity
4. Temperature range and whether automatic temperature compensation is applicable
5. Type of register or ticket printer required
6. Required accuracy and ease of meter-registration adjustment
7. Type and method of meter proving (volume cans, weighing, etc.)
8. Maintenance cost
9. Quantity and size of foreign matter
10. Space availability

Certain precautions are necessary to prevent the passage of vapor or air, including the installation of air eliminators and eliminating leaky valves and pump seals. Further, it is important that system design ensure that vapor from liquids is not released and that strainers are installed to remove sediment.

Gas Flowmeters. The rated capacity of a natural gas positive-displacement meter is the maximum flow rate at which the meter may be operated; it is specified in flowing cubic feet (flowing cubic meters), or standard cubic feet (standard cubic meters). In the United States, standard volumes are calculated at 14.73 psia (101.56 kPa) and 60°F (15.6°C) (ANSI/API 2562, 1969) or at other selected (contract) base pressures and temperatures.

In many designs, mechanical temperature and pressure compensations are available to adjust the register reading to standard volume units. ANSI/API 2562 (1969) requires that the index dial of a temperature-compensated meter with pressure compensation indicate in contrasting colors that the meter is temperature-compensated to a given base. For example, such a dial indication is "Cubic feet, pressure-compensated to 10 psig (69 kPa) nominal and temperature-compensated to 60°F (15.6°C)."

The measuring compartment of the rotary-type gas meter is located between a stationary case and rotating elements. Rotation is usually transmitted mechanically to an index which registers the flowing volume. Because of the close clearances between mating elements, wear can degrade performance. ANSI B109.3 (1980) requires that meters be given a 4000-h, 50-psig (344.7-kPa) life test during which the meter factor must remain within 1 percent of rated capacity over a 10:1 range. The permanent pressure loss is used as an indication of meter condition, to detect wear. A maximum differential pressure of 0.1 in (0.025 kPa) is specified when air is used to start rotation. When the differential exceeds 50 percent of the original value, the meter should be opened and inspected for wear.

Diaphragm-type gas displacement meters are classified via the flowing volume of a 0.6-specific-gravity gas at 0.5 in (0.125 kPa) differential pressure across the meter (ANSI B109.2, 1980). Meter classes are shown in Table 14.6. These classes are determined with a bell prover, using air, with test data referred to standard conditions of 60°F (15.6°C) and 14.73 psia (101.6 kPa).

Example 14.1. A turbine meter with a stainless-steel body and a mean K factor of 50.00 pulses/gal, determined with 68°F (20°C) water, is metering the gasoline of Example 2.16. Assuming no correction for viscosity, what is the base flow rate if the pulse frequency is 200 Hz?

TABLE 14.6 Classes of Diaphragm-Type Gas Displacement Meters

Class		
U.S.	OIML†	Range, ft ³ /h (m ³ /h)
500	16	500–899 (14.2–25.5)
900	25	900–1399 (25.5–39.6)
1400	40	1400–2299 (39.6–65.1)
2300	65	2300–3499 (65.1–99.1)
3500	100	3500–5599 (99.1–158.5)

†International Organization of Legal Metrology, approximate ratings.

Source: ANSI B109.2 (1980).

The flow rate in base gallons per minute is calculated from Eq. (e) of Table 14.1:

$$q_{\text{GPM}} = 60 \frac{F_p G_F f_{\text{Hz}}}{G_b \bar{K}_{F,\text{gal}}}$$

Data is as follows:

- From Example 2.16: $F_p = 1.0088$
- From Example 2.12: $G_F = 0.7255$ and $G_b = 0.7359$ at $T_F = 80.5^\circ\text{F}$

Assuming minimum and maximum data points are equally biased by temperature, the mean K factor is, from Eq. (14.7),

$$\begin{aligned} (\bar{K}_{F,\text{gal}})_{\text{flow}} &= \frac{(\bar{K}_{F,\text{gal}})_{\text{calib}}}{1 + 3\alpha_{\text{HO}}(T_F - T_{F,\text{calib}})} = \frac{50.00}{1 + (3)(0.0000096)(80.5 - 68)} \\ &= 49.982 \end{aligned}$$

where, from Table B.4, $\alpha_{\text{HO}} = 0.0000096 \text{ in}/(\text{in} \cdot ^\circ\text{F})$. Substitution then gives the base volumetric flow rate as

$$q_{\text{GPM}} = 60 \frac{(1.0088)(0.7255)(200)}{(0.7359)(49.982)} = 238.8 \text{ base gal/min}$$

Example 14.2. Estimate the measurement accuracy for the gasoline flow of Example 14.1 given the following accuracy estimates:

Manufacturer's data

- Linearity: $\bar{L} = \pm 0.5$ percent
- Laboratory accuracy: $(\text{ACC})_{\text{LAB}} = \pm 0.15$ percent
- Data-point precision: $\sigma_p = \pm 0.05$ percent

Fluid-property estimates

- Flowing specific gravity: $(\text{ACC})_{G_F} = \pm 0.1$ percent

- Base specific gravity: $(ACC)_{Gb} = \pm 0.1$ percent
- Compressibility factor: $(ACC)_{Fp} = \pm 0.2$ percent

Since *all* sensitivity coefficients are 1.0, the flow-rate accuracy is estimated with Eq. (4.32):

$$(ACC)_{GPM} = \pm [(ACC)_{KF,gal}^2 + (ACC)_{GF}^2 + (ACC)_{Fp}^2 + (ACC)_{Gb}^2]^{1/2}$$

The estimated accuracy of the mean K factor is, by Eq. (14.6),

$$(ACC)_{KF,gal} = \pm (ACC)_{LAB} \pm \sqrt{L^2 + 4\sigma_p^2} = \pm 0.15 \\ \pm \sqrt{(0.5)^2 + 4(0.05)^2} = \pm 0.66 \text{ percent}$$

The accuracy is then estimated as

$$(ACC)_{GPM} = \pm [(0.66)^2 + (0.1)^2 + (0.1)^2 + (0.2)^2]^{1/2} = \pm 0.7 \text{ percent}$$

Example 14.3. A vortex flowmeter is metering 140-psia (965-kPa) 95 percent quality steam. If the mean K factor is 64 pulses/ft³ (2295 pulses/m³), what is the (1) total mass flow if the counter registers 100,000, and (2) the mass of saturated vapor (steam)?

For a two-phase flow, total flow is calculated from Eq. (a) of Table 14.4 by substituting $\rho_{TP} = \rho_f$:

$$Q_{lbm} = \rho_{TP} \frac{\text{pulses}}{\bar{K}_{FT^3}}$$

The effective two-phase density is, by Eq. (14.5),

$$\rho_{TP} = \frac{\rho_g}{X^{1.53} + (1 - X)^{1.53}} \rho_g / \rho_l = \frac{0.31066}{(0.95)^{1.53} + [1 - (0.95)^{1.53}](0.31066/55.476)} \\ = 0.33587 \text{ lb}_m/\text{ft}^3$$

where, from Table G.1, $\rho_g = 0.31066 \text{ lb}_m/\text{ft}^3$ and $\rho_l = 55.476 \text{ lb}_m/\text{ft}^3$.

1. The total mass flow is then

$$Q_{lbm} = 0.33587 \frac{100,000}{65} = 516.7 \text{ lb}_m$$

2. The mass of saturated vapor is, by Eq. (9.86),

$$(Q_{lbm})_g = X(Q_{lbm})_{TC} = (0.95)(516.7) = 490.9 \text{ lb}_m$$

Example 14.4. A vortex flowmeter is measuring the water-vapor-saturated natural gas of Example 9.10. The mean K factor is 6600 pulses/m³. For 100,000 pulses, what is the total dry volume (ISO Standard 5024 base), and what are the wet and dry flow rates if the pulse frequency is 285 Hz?

Since pulse-type meters measure at flowing conditions, the standard volume of wet natural gas is calculated from Eq. (k) of Table 14.4 as

$$(Q_{SCM}^*)_{wet} = 2.843819 \frac{Z_b p_f^*}{Z_f T_K} \frac{\text{pulses}}{\bar{K}_{F,m^3}}$$

Data from Examples 9.10 and 9.7 is

$$Z_b = 0.99743 \quad F_{pv} = 1.0011 \quad p_f^* = 184 \text{ kPa} \quad T_K = 300 \text{ K}$$

and, from Eq. (9.65),

$$Z_f = \frac{Z_b}{F_{pv}^2} = \frac{0.99743}{(1.0011)^2} = 0.9952$$

Substitution gives

$$(Q_{SCM}^*)_{\text{wet}} = 2.843819 \frac{0.99743}{0.9952} \frac{184}{300} \frac{100,000}{6600} = 26.486 \text{ standard m}^3 \text{ (wet)}$$

The dry volume is calculated, using Eq. (2.66), as

$$F_{wv,\text{dry}} = \frac{V_{\text{dry}}}{V_{\text{wet}}} = \frac{(Q_{SCM})_{\text{dry}}}{(Q_{SCM})_{\text{wet}}}$$

Then, with $F_{wv,\text{dry}} = 0.98082$ from Example 9.10,

$$(Q_{SCM}^*)_{\text{dry}} = (0.98082)(26.486) = 25.978 \text{ standard m}^3 \text{ (dry)}$$

The wet flow rate is calculated with Eq. (k) of Table 14.3:

$$\begin{aligned} (q_{SCMH}^*)_{\text{wet}} &= 10,237.75 \frac{Z_b}{Z_f} \frac{p_f^*}{T_K} \frac{f_{Hz}}{\bar{K}_{F,m^3}} = 10,237.75 \frac{0.99743}{0.9952} \frac{184}{300} \frac{285}{6600} \\ &= 21.75 \text{ standard m}^3/\text{h (wet)} \end{aligned}$$

The dry flow rate is

$$\begin{aligned} (q_{SCMH}^*)_{\text{dry}} &= (F_{wv,\text{dry}})(q_{SCMH}^*)_{\text{wet}} = (0.98082)(21.75) \\ &= 21.43 \text{ standard m}^3/\text{h (dry)} \end{aligned}$$

LINEAR-OUTPUT FLOWMETERS

Magnetic Flowmeter

Principle of Operation. The electromagnetic flowmeter is based on Faraday's (1892) law of magnetic induction. When a conductive fluid passes through a magnetic field (Fig. 14.14), a voltage is generated at right angles to the velocity and magnetic-field vectors. This signal voltage e_s is a summation of individual voltages generated by differential volumes moving at differing velocities across the pipe section. Shercliff (1961) mathematically demonstrated, by introducing a *weightlifting function*, that the signal voltage represents the average velocity for axisymmetric profiles. The signal voltage can then be simply expressed as

$$e_s = kDB_f\bar{V}_f \quad (14.10)$$

where k is constant, D is the distance between electrodes, B_f is the magnetic flux density, and \bar{V}_f is the average velocity. For a circular pipe the volumetric flow rate then is

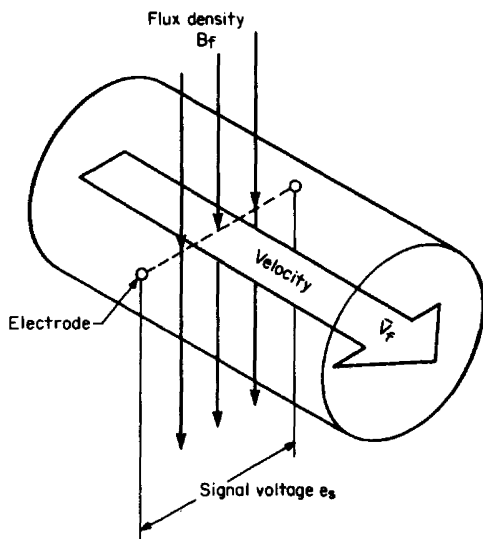


Figure 14.14 Principle of operation of the magnetic flowmeter.

$$q_{ve} = \frac{\pi}{4} k_1 D \frac{e_s}{B_f} \quad (14.11)$$

where k_1 is a constant determined by calibration.

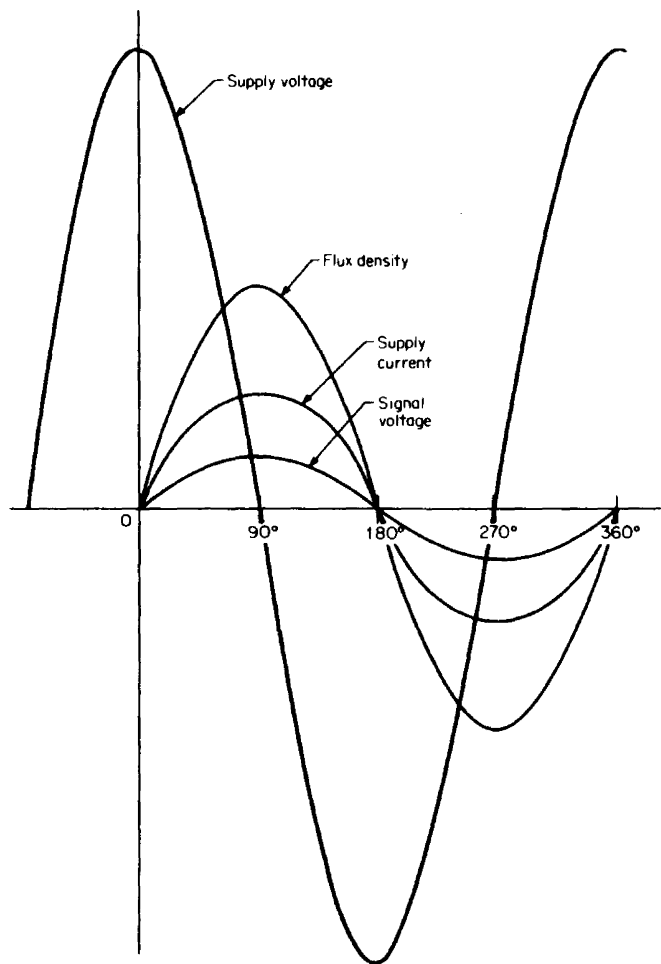
The three principal methods of producing flux density B_f are

1. Permanent-magnet or dc excitation
2. Normal 50- or 60-Hz ac power-line sinusoidal excitation
3. Pulsed excitation of any frequency

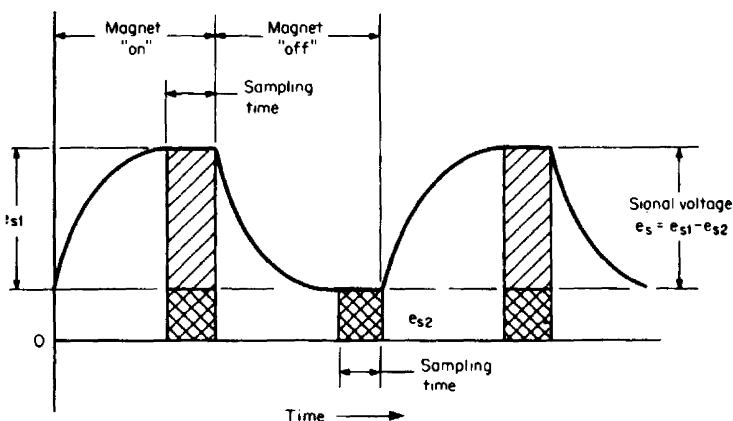
The dc magnetic flowmeter is well suited to pulsating flows and for measuring very high conductivity fluids, such as molten metals and mercury. However, for lower-conductivity, ion-conducting fluids, time-variant polarization occurs at the electrode, and for this reason dc excitation is not used. Since polarization potentials are eliminated by sinusoidal excitation, ac or short-duration pulsed-dc systems are most commonly used for these fluids.

Figure 14.15 presents the relationship between signal voltage, excitation voltage, and current for ac and dc systems. In ac systems (Fig. 14.15a), the signal voltage is in phase with the supply current and approximately 90° out of phase with the supply voltage. Since a change in voltage or current results in a signal-voltage change, a reference signal is used, and the ratio of e_s/B_f is measured by the secondary [Eq. (14.11)]. This reference signal may be derived as a constant signal by regulating the coil current, derived from the supply voltage or current, or derived by measuring flux density in the laminated core or within the air gap.

In pulsed-dc systems, a low-frequency on-off (or plus-minus) square-wave current powers the electromagnet, producing the signal voltage shown in Fig. 14.15b. When the field is *on*, the secondary device measures and stores this signal voltage,



(a)



(b)

Figure 14.15 Magnetic-flowmeter systems. (a) AC system. (b) Pulsed-dc system. (Courtesy Fischer & Porter.) (c) YEW dual frequency excitation.

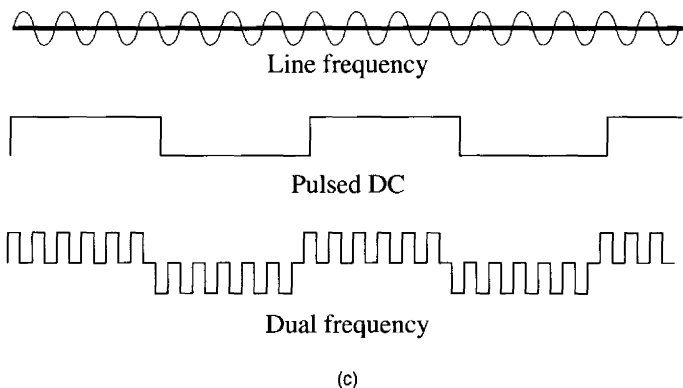


Figure 14.15 (Continued)

which is a composite of the flow signal plus non-flow-related voltages. During the period when the field is turned *off*, the secondary measures the non-flow-related voltages. The flow-rate signal is obtained by subtraction.

The YEW dual-frequency excitation design (Kuromori et al., 1989) offers the combined features of low- and high-frequency field excitation (Fig. 14.15c). Zero stability is improved by the lower frequency, and the response speed is increased by the higher frequency. This is accomplished by powering the coils with a two-component current system, one being higher than the line frequency. This frequency provides a measurement signal that is insensitive to the low-frequency noise generated at the electrode-fluid interface. The other component is a lower than the line frequency rectangular wave form. This component provides the improved zero stability.

The Hersey Measurement Balanced Electrode Plane (B.E.P.) meter (Scarpa, 1993) takes advantage of the fact that no flow-induced potentials exist in the same plane as the sensing electrodes, along a parallel axis to the induced magnetic field, and rotated 90° from the sensing electrode. By installing ground electrodes at these locations, an averaging of the velocity profile will occur within the plane of the balancing electrodes. This feature will theoretically vector sum all out-of-phase flow-induced vectors for improved averaging of axisymmetric or skewed velocity vectors.

Whether ac- or dc-powered, the flow signal varies with the field intensity, is in the millivolt range, and contains non-flow-related voltages. These are compensated for by continuously forming a ratio of the signal to a reference signal. It is this ratio that is scaled by water calibration to obtain an overall meter factor in the desired flowing volumetric flow-rate unit.

It is important to recognize that magnetic flowmeters are designed as total flow-metering systems consisting of primary and secondary devices. The function of the primary device is to produce the signal; the secondary device corrects for changes in phase relationships and in the supply voltage (or current) and minimizes non-flow-related voltages associated with the primary and the connecting cables.

Industrial Flowmeters. ISO 6817 (1992) and ASME-MF6-16M (1995) defines the electromagnetic flowmeter as follows:

The electromagnetic flowmeter is an assembly of a primary device through which the process fluid flows, and of a secondary device which converts the low level signal

generated by the primary device into a suitable standardized signal for acceptance by industrial instrumentation. The system produces an output signal proportional to volumetric flowrate (or average velocity). Its application is generally limited only by the requirement that the metered fluid shall be conductive and nonmagnetic.

Shown in Fig. 14.16 is an exploded view of one design of primary device. The primary consists of (1) a tube, (2) two coils, (3) electrodes, (4) a laminated iron core, (5) a cover, and (6) end connections. The tube provides support for the assembly and may be of nonmagnetic stainless steel or fiberglass-reinforced plastic. Stainless-steel tubes are lined with a suitable insulating material, such as ptfe, polyurethane, or rubber, to prevent short-circuiting of the generated voltage. The sad-

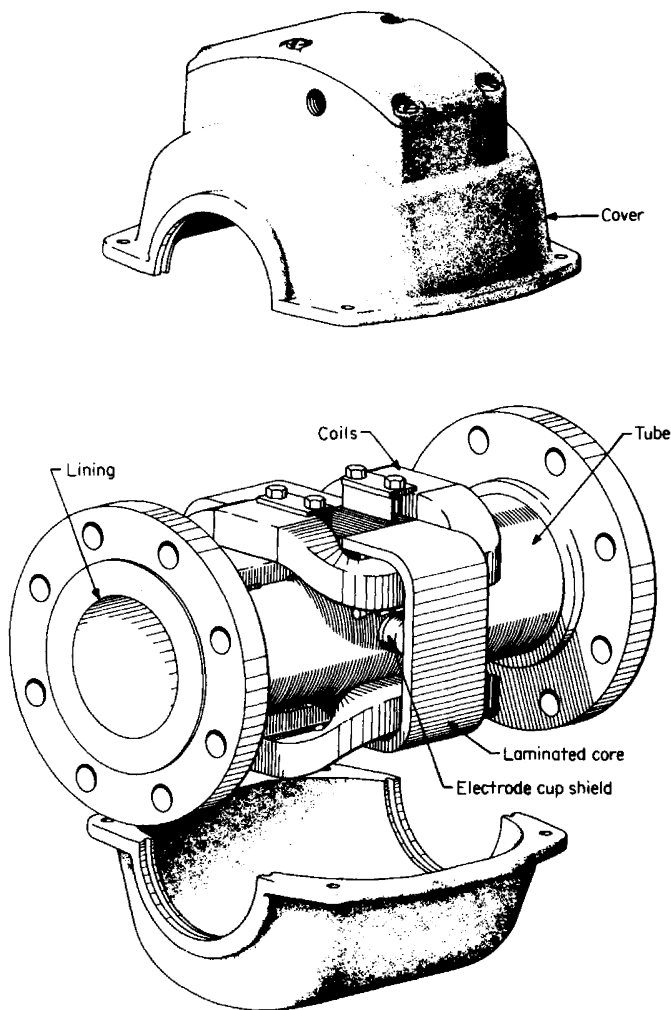


Figure 14.16 Basic construction of the primary device of a magnetic flowmeter. (Courtesy The Foxboro Co.)

de-shaped coils of copper wire produce the magnetic field, which is focused at right angles into the process fluid by the laminated iron core. The generated voltage is detected by two small diametrically opposed electrodes.

The meter size and liner and electrode materials depend largely on the fluid to be metered. Table 14.7 lists the upper-range-value flow rates given by one manufacturer. In general, six basic tube types are used:

1. *Unlined resin tubes.* These are unlined glass-fiber-reinforced tubes with epoxy or polyester resin as the glass bonding agent. The nonconductive, nonpermeable tubes of this type require no liner and are free from the eddy-current problems associated with lined metal tubes. They are used for applications with limited temperature, pressure, and corrosive severity. Reinforced resin flow tubes are lower in price than corresponding sizes of lined metal units and are suitable for a wide variety of applications.
2. *ptfe-lined tubes.* Because of its high temperature rating and its inertness to a wide variety of acids and bases, ptfe is the most commonly used flow-tube lining material. A preformed "tube" of ptfe is mechanically fitted into an AISI type-304 nonmagnetic stainless steel tube, and the ptfe ends are flared out over the tube end connections to effectively isolate the process liquid from the steel. The recommended maximum process temperature for this type of tube is 350°F (175°C).
3. *Polyurethane-lined tubes.* For some applications, a ptfe flow-tube lining does not have adequate abrasion resistance. Where extreme resistance to wear or erosion by solid particles in the process stream is required, polyurethane lining is often the best choice. The polyurethane liner extends over the raised face of the flange. Polyurethane is resilient and abrasion resistant, but it cannot be used at very high temperatures or with strong acids or bases.
4. *Neoprene-lined tubes.* Neoprene-lined flow tubes have greater abrasion resistance than ptfe-lined tubes and are moderately resistant to chemical attack. They can be used at higher temperatures than polyurethane-lined tubes and are considered a good general-purpose flow tube.
5. *Sanitary lined tube.* A ptfe-lined flow tube with quick-disconnect sanitary end connections is used in consumable-product processes. These sanitary flow tubes are ideally suited for use with dairy products, beer, soft drinks, coffee, molasses, and corn syrup. Processed products, such as catsup and other viscous, sticky, or otherwise difficult-to-measure liquids, are also easily measured.
6. *Ceramic.* Ceramic liners allow for higher temperatures and usually higher fluid velocities than other liners, and the meter diameter is least affected by either pressure or temperature. In general, a ceramic liner is suitable for all fluid applications and has excellent wear properties for abrasive or slurry applications. Thermal and mechanical shock are to be avoided, since the meter is more fragile.

The electrodes are made of a nonmagnetic material such as AISI type-316L stainless steel, platinum-10 percent iridium, hastelloy C, titanium, or tantalum. Conical electrodes, electrode boil-off, and ultrasonic electrode cleaning are sometimes available as optional features for removing contamination from the electrodes.

Application. Magnetic flowmeters are suitable for use with liquids that have electrical conductivities of 1 $\mu\text{S}/\text{cm}$ or larger. For clean liquids, the minimum upper-range velocity is approximately 1 ft/s (0.3 m/s), and a 10:1 range is usually given. When liquid-bearing solids, abrasive slurries, sludges, and immiscible liquids are

TABLE 14.7 Flow-Rate Ranges for Selected Liner Materials†

Nominal upper-range value flow rates, L/s (gal/min)													
										Unlined glass-fiber-reinforced resin flow tube			
Nominal flow-tube size		ptfe-lined sanitary flow tube		ptfe-lined flow tube		Polyurethane-lined flow tube				Epoxy resin		Polyester resin	
mm	in	Mini-mum	Maxi-mum	Mini-mum	Maxi-mum	Mini-mum	Maxi-mum	Mini-mum	Maxi-mum	Mini-mum	Maxi-mum	Mini-mum	Maxi-mum
15	$\frac{1}{2}$	0.145 (2.3)	0.75 (12.0)	0.145 (2.3)	0.75 (12.0)								
25	1	0.505 (8.0)	3.03 (48.0)	0.505 (8.0)	3.03 (48.0)								
40	$1\frac{1}{2}$	1.26 (20.0)	75.7 (120)	1.26 (20.0)	75.7 (120)								
50	2	2.14 (34.0)	12.8 (203)	2.14 (34.0)	12.8 (203)	1.45 (23.0)	7.70 (122)			1.8 (29)	9.7 (154)		
80	3	4.67 (74.0)	29.6 (469)	4.67 (74.0)	29.6 (469)	3.91 (62.0)	24.4 (387)			4.6 (72)	25 (400)		
100	4			8.45 (134)	51.7 (820)	6.75 (107)	41.1 (652)			8.1 (129)	47 (752)		
150	6			18.9 (300)	114 (1815)	16.5 (262)	111 (1760)			19 (295)	111 (1765)		
200	8			33.1 (524)	198 (3130)	30.2 (478)	208 (3300)			34 (527)	195 (3121)		
250	10			52.1 (826)	315 (5000)	48.6 (770)	343 (5430)					54 (834)	309 (4895)
300	12			74.4 (1180)	451 (7150)	70.4 (1116)	500 (7920)					75 (1177)	445 (7050)
350	14					96 (1516)	676 (10,744)	96 (1516)	553 (8758)			96 (1516)	532 (8434)

TABLE 14.7 Flow-Rate Ranges for Selected Liner Materials† (*Continued*)

Nominal upper-range value flow rates, L/s (gal/min)													
Nominal flow-tube size		ptfe-lined sanitary flow tube		ptfe-lined flow tube		Polyurethane-lined flow tube		Unlined glass-fiber-reinforced resin flow tube					
								Epoxy resin		Polyester resin			
mm	in	Mini-mum	Maxi-mum	Mini-mum	Maxi-mum	Mini-mum	Maxi-mum	Mini-mum	Maxi-mum	Mini-mum	Maxi-mum	Mini-mum	Maxi-mum
350	14					(1819) 127	(10,744) 895	(8758) 127	(8758) 730			(1786) 124	(8434) 695
400	16					(2000) 151	(14,232) 895	(2000) 151	(11,573) 730			(1961) 147	(11,015) 695
400	16					(2381) 158	(14,232) 1145	(2381) 158	(11,573) 933			(2326) 158	(11,015) 880
450	18					(2500) 191	(18,210) 1145	(2500) 191	(14,780) 933			(2500) 186	(13,942) 880
450	18					(3031) 198	(18,210) 1427	(3031) 198	(14,780) 1160			(2942) 192	(13,942) 1093
500	20					(3125) 234	(22,678) 1427	(3125) 234	(18,378) 1160			(3031) 235	(17,326) 1093
500	20					(3704) 287	(22,678) 2037	(3704) 287	(18,378) 1689			(3704) 281	(17,326) 1582
600	24					(4546) 351	(32,374) 2037	(4546) 351	(26,751) 1689			(4445) 334	(25,061) 1582
600	24					(5556) 454	(32,374) 3239	(5556) 454	(26,751) 2673			(5291) 445	(25,061) 2577
750	30					(7195) 544	(51,458) 3239	(7195) 544	(42,246) 2673			(7043) 535	(40,820) 2577
750	30					(8621) 658	(51,468) 4718	(8621) 658	(42,246) 3868			(8475) 646	(40,820) 3732
900	36					(10,417) 789	(74,969) 4718	(10,417) 789	(61,627) 3868			(10,205) 776	(59,121) 3732
						(12,500)	(74,969)	(12,500)	(61,267)			(12,196)	(59,121)

metered, a minimum or maximum velocity is suggested by manufacturers to reduce coating, liner wear, and maintenance cost.

The energy dissipated by the coils causes local heating in the flow tube. At no-flow condition, with the coils energized, the temperature rise is approximately 30°F for an unfilled tube and 20°F for a filled tube. Depending on whether the coils are series- or parallel-connected, the temperature rise can be as high as 100°F (parallel) for an unfilled tube. For this reason, manufacturers suggest that the primary always be kept filled with liquid, to prevent liner damage and to minimize baking of solids into the liner and/or electrodes.

In general, settleable solids require a minimum velocity of 5 ft/s (1.5 m/s) to minimize coating. The primary should be installed vertically, with the flow upward, and at no-flow condition the tube should remain full to prevent excessive temperature rise. For abrasive slurries, rubber or some other abrasion-resistant material should be selected for the liner. An upstream projection ring, similar to a high-beta-ratio orifice, is sometimes installed to protect the leading edge of the flowmeter. The velocity should not exceed 10 ft/s (3 m/s).

Performance. Magnetic flowmeters are water-calibrated, and a standardized output signal is scaled to suitable volumetric flow-rate units. Performance specifications are given at reference conditions based on type testing for ranges of influence quantities, such as supply voltage, frequency, temperature, and fluid conductivity. These are specified by the manufacturer.

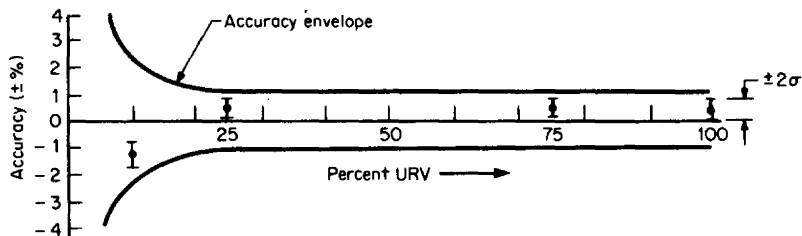
Reference accuracy envelopes are specified, within which bias error and data-point precision are included. Figure 14.17 presents typical reference-condition accuracy envelopes, and Table 14.8 contains reference conditions specified in ISO 6817 (1992) for flow conditions and for the primary and secondary device and ISO DP-9104 (1991) for evaluating the performance of electromagnetic flowmeters. Table 14.9 gives the test results reported by Tsuchida (1982) for the minimum-required upstream lengths for several magnetic flowmeters.

The magnetic flowmeter's signature curve shows little, if any, change over the laminar-to-turbulent profile transition regime, and Reynolds-number corrections are not applied. Except for a minimum conductivity level, the effects of fluid properties on performance are minimal. However, magnetic-flowmeter system designs vary widely among manufacturers, and it is important that the manufacturer's recommendations as to conductivity limits, cable lengths, installation procedure, etc., be followed for reliable performance ASME 16M (1995).

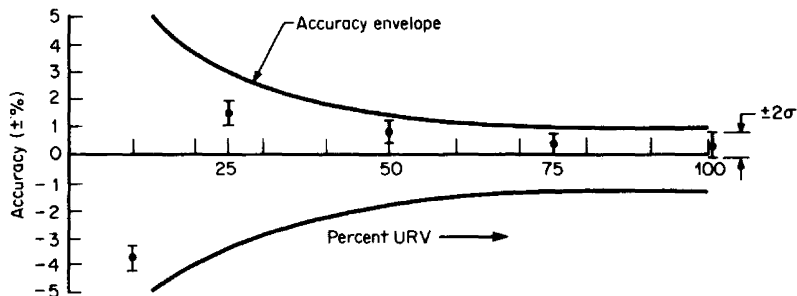
Ultrasonic Flowmeters

Lynnworth (1979) lists eight different types of ultrasonic flowmeters, but two basic types are most commonly used in industry: counterpropagating (time-of-flight) and reflection (Doppler). Both are used for liquids—counterpropagating meters for clean liquids, and the Doppler type for flows that contain the particulate matter required for signal reflection.

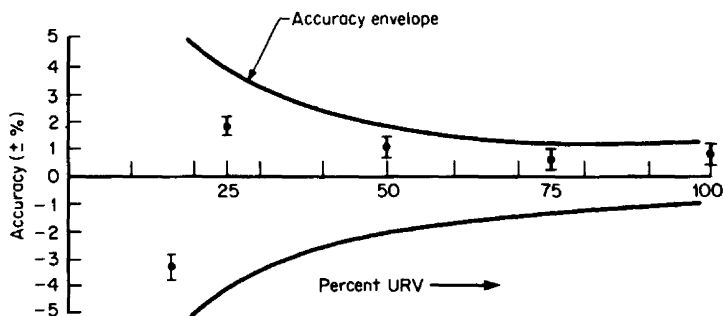
Counterpropagating Flowmeter. The operation of the counterpropagating flowmeter is based on the fact that the speed of an acoustic pressure wave increases in the direction of flow and decreases when directed against the flow, which causes differing transit times. By measuring these two times, or by measuring frequency differences, the pipeline velocity is inferred. In practice, up to four acoustic paths are used to better estimate the average velocity and, hence, the average volumetric flow rate.



(a)



(b)



(c)

Figure 14.17 Reference-condition accuracy envelopes. (a) 1 percent of rate or 0.2 percent of URV, whichever is greatest. (b) 1 percent of URV flow rate. (c) 0.5 percent URV 0.5 percent of rate.

Figure 14.18 shows the velocity vector diagrams that describe the relationships used to develop the flow equations for counterpropagating flowmeters. An upstream piezoelectric transmitter provides a pulse that travels at the speed of sound through the liquid, along path length L_p and at path angle θ . This pulse is detected by the downstream piezoelectric receiver. The upstream transmitter and downstream receiver (transducers) are actually used alternately as transmitter and receiver, first to direct a pulse downstream, parallel to the velocity vector (Fig. 14.18b), and then upstream, in opposition to the velocity vector (Fig. 14.18c). The apparent velocity

TABLE 14.8 Magnetic-Flowmeter Reference Conditions

	Flow (water)	Primary device	Secondary device
Temperature	40–100°F (4–40°C)	32–86°F (0–30°C)	50–86°F (10–30°C)
Pressure	<75 psig (<500 kPa)	<75 psig (<500 kPa)	
Conductivity	50–5000 Σ S/cm†		
Power supply			Rated voltage $\pm 2\%$
Voltage			Nominal frequency $\pm 0.5\%$
Frequency			$\leq 0.05\%$ (IEC Publication 359)
Distortion			
Piping	Minimum: 5 pipe diameters		
Signal output			See IEC publication 381A

†Microsiemens per centimeter.

Source: ISO 6817 (1992).

TABLE 14.9 Minimum Upstream Lengths for Magnetic Flowmeters

Pipe fitting	Minimum length PD
Elbows	
Single	10
Two in perpendicular planes	10
Expander	5
Reducer	3
Valves	
Ball	5
Butterfly	15
Gate	10

Source: Tsuchida (1982).

of the downstream pulses is higher than sonic velocity, and that of the upstream pulses is lower.

The downstream transit time is

$$t_{DN} = \frac{L_p}{V_{SO} + \bar{V}_f \cos \theta} \quad (14.12)$$

and the upstream time is

$$t_{UP} = \frac{L_p}{V_{SO} - \bar{V}_f \cos \theta} \quad (14.13)$$

From these time equations the following relationships are derived:

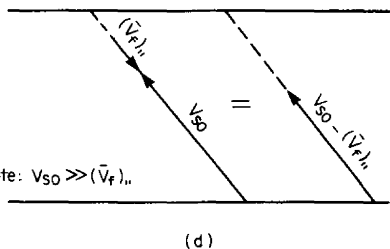
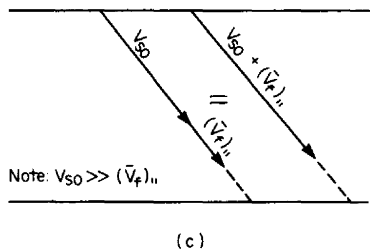
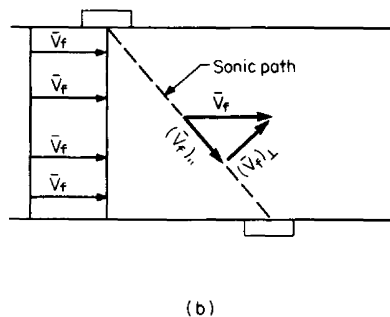
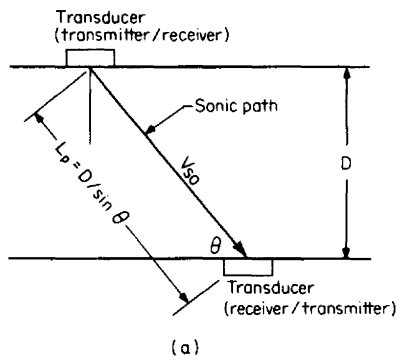


Figure 14.18 Vector diagrams for counterpropagating ultrasonic flowmeters. (a) No flow. (b) Velocity vector parallel to sonic path. (c) Upstream apparent velocity. (d) Downstream apparent velocity.

$$\frac{1}{t_{DN}} - \frac{1}{t_{UP}} = \frac{t_{UP} - t_{DN}}{t_{DN}t_{UP}} = \frac{2 \cos \theta}{L_p} \bar{V}_f \quad (14.14)$$

The average volumetric flow rate for a circular pipe then is

$$q_{cfs} = K_{UF} \left[\frac{\pi D_F^3}{4 \sin 2\theta} \right] \frac{t_{UP} - t_{DN}}{t_{UP}t_{DN}} \quad (14.15)$$

for U.S. units, and

$$q_{c\ ms}^* = K_{UF} \left[\frac{\pi D_M^3}{4 \sin 2\theta} \right] \frac{t_{UP} - t_{DN}}{t_{UP}t_{DN}} \quad (14.16)$$

for SI units, where the flow coefficient K_{UF} is introduced as a Reynolds-number correction for velocity profile. The bracketed quantities are usually assumed constant, and the flow coefficient and time term are computer-calculated to provide the flow rate.

In another approach, called the *frequency-difference* or (sing-around) approach, reception of the acoustical signal at the receiver initiates transmission of the subsequent signal. Upstream and downstream frequencies are generated proportional to their respective transit times, so that

$$(f_{Hz})_{UP} = \frac{1}{t_{UP}} \quad (f_{Hz})_{DN} = \frac{1}{t_{DN}} \quad (14.17)$$

Substitution into Eq. (14.15) and (14.16) yields

$$q_{cfs} = K_{UF} \left[\frac{\pi D_F^3}{4 \sin 2\theta} \right] \{ (f_{Hz})_{DN} - (f_{Hz})_{UP} \} \quad (14.18)$$

for U.S. units, and

$$q_{c\ ms}^* = K_{UF} \left[\frac{\pi D_M^3}{4 \sin 2\theta} \right] \{ (f_{Hz})_{DN} - (f_{Hz})_{UP} \} \quad (14.19)$$

for SI units.

Equations (14.12) through (14.19) are based on the assumption that the transducers are in direct contact with the fluid. If a protecting intervening material or a clamp-on transducer is used, the transit times and entering path angle are altered. These effects are mathematically modeled and corrected for by the secondary device.

The flow coefficient K_{UF} for a multipath ultrasonic flowmeter is defined in ANSI/ASME MFC-5M (1994) as

$$K_{UF} = \frac{q_v}{A_p \sum_{i=1}^n W_i \bar{V}_i} \quad (14.20)$$

where A_p is the pipe area (in square feet or square meters), W_i is a weighting function for each path, \bar{V}_i is the axial velocity along each path, and n is the number of paths. The reciprocal of the flow coefficient-pipe Reynolds number signature curve shown in Fig. 14.19 was derived by Vignos (1981) in the turbulent flow regime for a single-path flowmeter with transducers mounted along the pipe axis. The Vignos equation for the flowmeter with a single path along the pipe axis is

$$K_{UF} = \left[1 + \frac{5}{4} \sqrt{\frac{f}{8}} \right]^{-1} \quad (14.21)$$

where f is the pipe friction factor defined by Eq. (5.9).

The flow-coefficient variation from laminar to turbulent flow (approximately 30 percent) and variations within the turbulent regime can be reduced by locating the transducers off the pipe axis or by increasing the number of paths.

Secondary flows caused by upstream fittings (see Chap. 5) can significantly alter the flow coefficient. The magnitude of this effect depends on the number of transducers and their orientation with respect to the nonaxial velocity components. Long, straight runs of pipe, the use of flow conditioners, and multipath flowmeters are suggested (ANSI/ASME MFC-5M, 1995) to obtain desired accuracy.

Doppler Flowmeter. Doppler ultrasonic flowmeters operate by the reflection of sonic energy from scatterers (particulate matter) in the fluid, back to a receiver. If the scatterers are moving at the velocity of the fluid, the Doppler frequency shift is proportional to the volumetric flow rate. The receiver may be the same transducer as the transmitter or a separate transducer. A typical meter consists of two piezo-

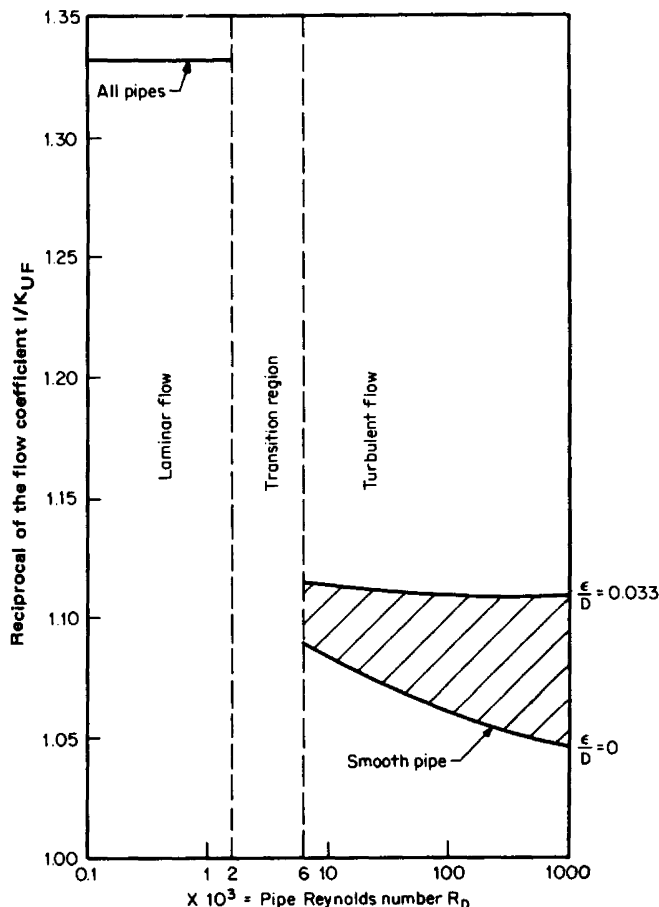


Figure 14.19 Ultrasonic-flowmeter signature curve for single path along pipe axis.

electric transducers (Fig. 14.20) clamped to the pipe or contained within a housing. The transmitter projects a continuous beam into the fluid, at a frequency of from 0.5 to 10 MHz. The receiver measures the frequency of the reflections from particles in the fluid. This frequency is Doppler-shifted by the velocity of the particles. The volumetric flow rate is then calculated as

$$q_{\text{cfs}} = \left[\frac{\pi}{4} D_F^2 \frac{V_{SO}}{\sin \theta} \right] \frac{\Delta f_{\text{Hz}}}{(f_{\text{Hz}})_{\text{CW}}} \quad (14.22)$$

for U.S. units, and

$$q_{\text{c ms}}^* = \left[\frac{\pi}{4} D_M^2 \frac{V_{SO}^*}{\sin \theta} \right] \frac{\Delta f_{\text{Hz}}}{(f_{\text{Hz}})_{\text{CW}}} \quad (14.23)$$

for SI units, where Δf_{Hz} is the Doppler frequency shift, θ the beam angle, and $(f_{Hz})_{CW}$ the transmitter's fixed frequency.

Industrial Flowmeters. Industrial ultrasonic flowmeters are designed as total systems. The primary device consists of two or more transducers which are either permanently attached to a spool piece (Fig. 14.21a) or clamped onto existing pipe (Fig. 14.21b). However, transducer designs vary widely among manufacturers, ranging from clamp-on types to those in recessed pockets in the pipe wall (Fig. 14.22). Single or multiacoustic paths may be used, and they may traverse the pipe along a

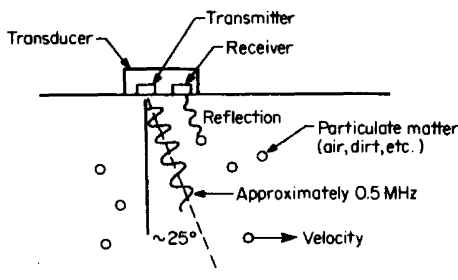
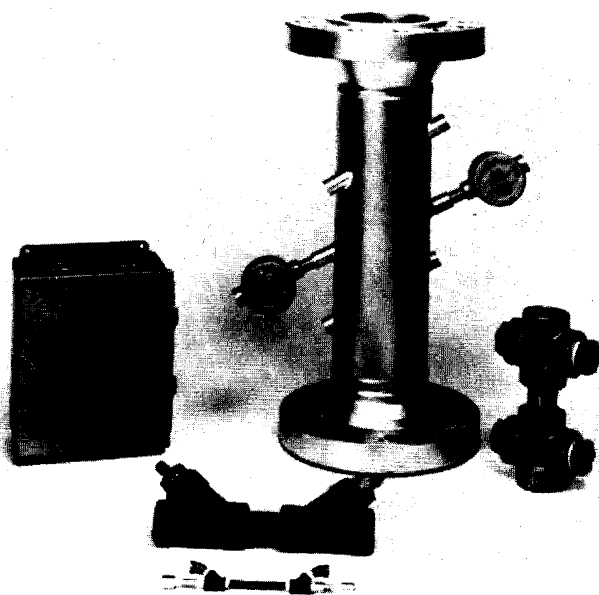
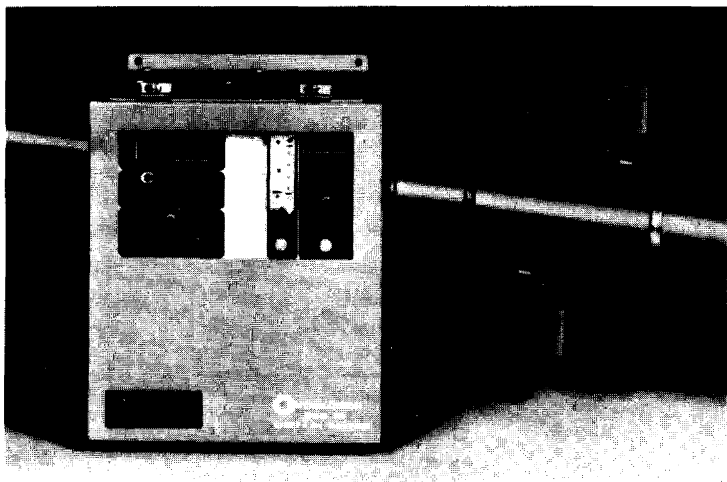


Figure 14.20 Doppler flowmeter.

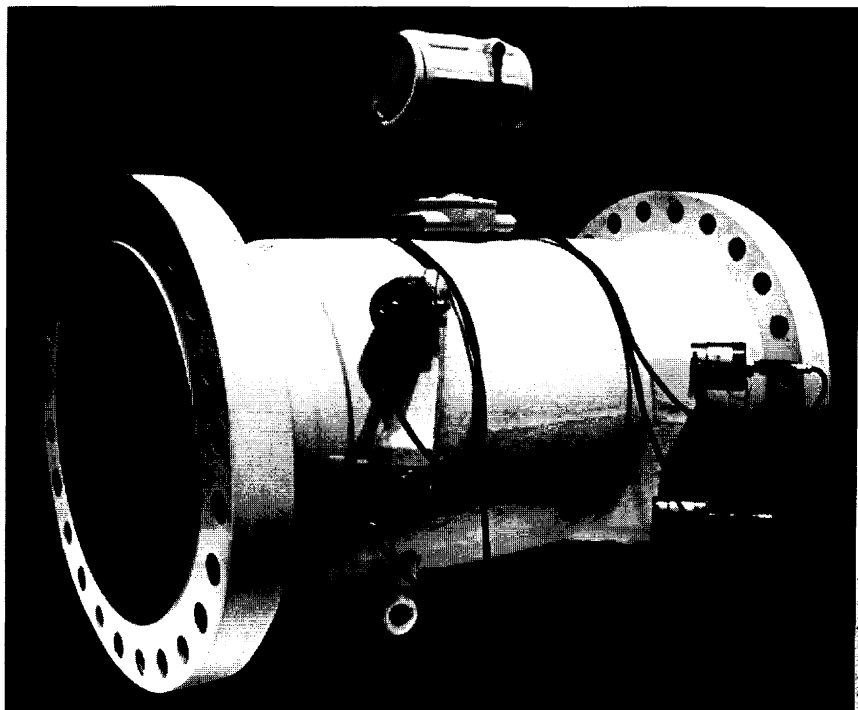


(a)

Figure 14.21 Industrial ultrasonic flowmeter. (a) Spool-piece meter. (Courtesy Panametrics.) (b) Clamp-on meter. (Courtesy Controlotron.) (c) Four path gas ultrasonic flowmeter. (Courtesy Daniel Industries.)



(b)



(c)

Figure 14.21 (Continued)

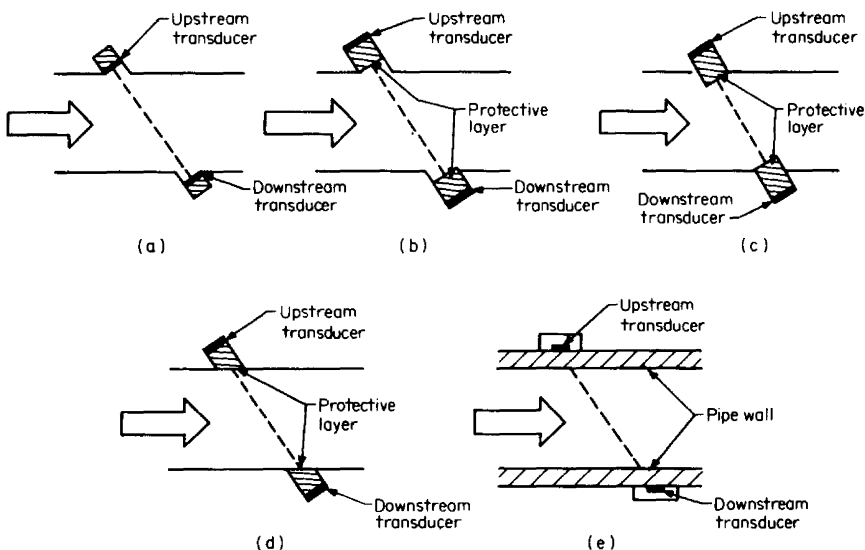


Figure 14.22 Transducer designs. (a) Recessed process exposed. (b) Recessed process protected. (c) Protruding process protected. (d) Flush process protected. (e) Clamp-on.

diameter, along a chord, or along the pipe axis (Fig. 14.23). The function of the secondary device is to make the measurements (of time or frequency), process the data, perform computations for Reynolds-number and other corrections, and output a standardized signal.

Ultrasonic flowmeters have been successfully used for many fluids, ranging from crude oil to sludge flows. However, the applicability of a particular type of meter is very much a function of the experience of its manufacturer. For this reason, the performance and application specifications of the various manufacturers can differ widely. Schmidt (1980), reporting on Doppler and counterpropagating industrial flowmeters, notes that meters *appear* to be ± 0.5 percent repeatable, and ± 1 percent repeatable among different but related fluids. However, he indicates that the as-received calibration factor may vary considerably and suggests that meters be field calibrated.

Presently, no single design can be considered a multipurpose flowmeter; each manufacturer tends to choose certain desirable features for a particular design. Many proprietary (and unpublished) laboratory flow tests have been conducted on the various designs, but little independent data is available to indicate performance under laboratory or industrial conditions. Usually, the manufacturer and user work closely together to verify applicability. Lynnworth (1989) has prepared an excellent

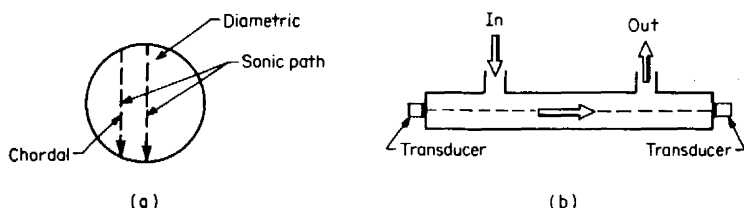


Figure 14.23 Acoustic paths. (a) Chordal and diametric. (b) Axial.

reference book on ultrasonic flow measurement and other uses of ultrasonics for process measurements.

Clamp-on meters are now widely used because they provide a useful portable survey tool. Provided the limitations are known and recognized, Cairnery (1991) estimates that with care ± 5 percent of reading accuracy can be achieved. However, he states:

It is not like some kind of flow multimeter that can be taken out and used by inexperienced personnel; its suitability for each different flow measurement situation must be carefully assessed and when in use nothing should be taken for granted, particularly 'black box' electronics.

Ultrasonic flowmeters that measure gas flows (Fig. 14.21c) are available; similar meter designs are also used on flare gas mass flow applications. The four paths for this ultrasonic flowmeter are chosen to minimize upstream profile effects, with each path having two transducers that act alternately as transmitter and receiver. The accurate measurement of the transducer locations allows for the meter factor to be determined without a flow calibration.

These gas meters may be multipath or of the reflective type. There is no overall pressure loss. (Obstructionless, fast response times, wide operating ranges, and relative insensitivity to upstream fitting are claimed features. The response time for some designs is sufficient to meter pulsating flows over a 50:1 turndown in lines sizes 6 to 48 in, 150 to 1200 mm.)

Variable-Area Flowmeters

Principle of Operation. In differential producers the restricted flow area is fixed, and the differential pressure varies and is used to infer flow rate. In the most common variable-area flowmeters (Fig. 14.24a), a float, moving vertically within a linearly tapered tube, exposes a variable area to the flow. At design conditions the differential pressure remains constant across the float, because buoyant and weight forces are constant and the float height changes to expose the area that satisfies Bernoulli's equation. The flow area between tube and float is then an indication of the flow rate. Since the float height is a linear function of the flow area, visual observation or some other detection means allows the flow rate to be observed.

Several design variations are used to provide an area that varies with flow rate. These include an orifice and plug (Fig. 14.24b), a slotted cylinder and piston (Fig. 14.24c), and a piston (Fig. 14.24d). The basic operating principle remains the same in all cases: to alter the flow area by maintaining a constant pressure drop across a variable area, and then to infer the flow rate from position.

The basic geometry of a tapered-tube variable-area meter is shown in Fig. 14.25. The fluid enters at the bottom, flows upward through the tapered tube, accelerates to a higher velocity through the annular area around the float, and leaves at the top. Bernoulli's general energy equation (9.10) for a liquid, written between entering area and annular area (Fig. 14.25a), yields, in the English engineering system of units (pounds-force, pounds-mass, feet, seconds),

$$\frac{P_f}{\rho_f} + \frac{\bar{V}_f^2}{2g_c} + H_{EL1} = \frac{P_f}{\rho_f} + \frac{\bar{V}_f^2}{2g_c} + H_{EL2} \quad (14.24)$$

Neglecting elevation difference gives

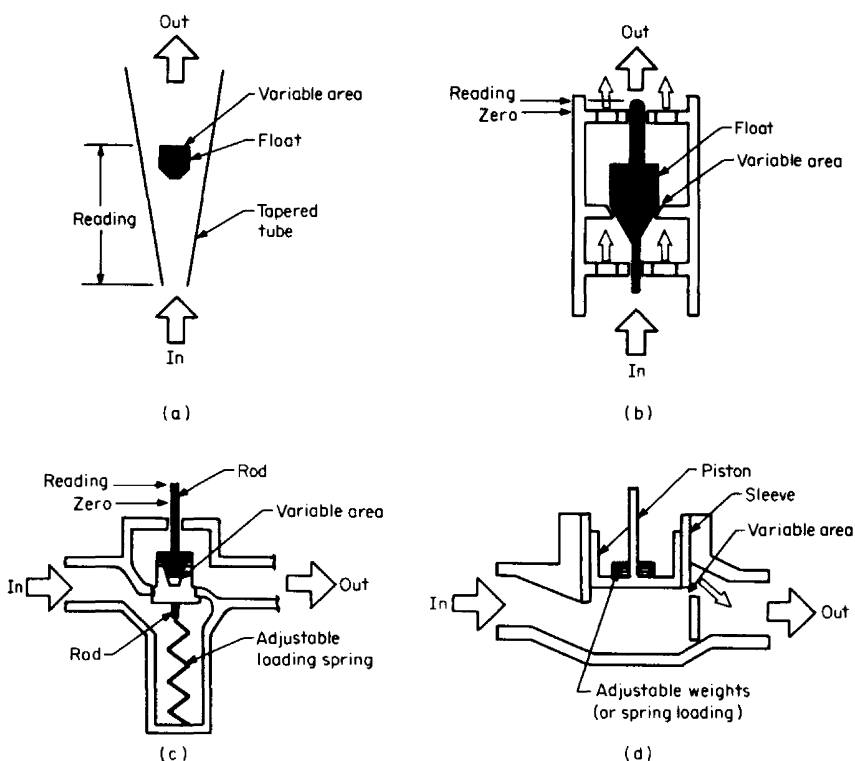


Figure 14.24 Types of variable flowmeter. (a) Tapered tube. (b) Orifice and plug. (c) Slotted cylinder. (d) Piston.

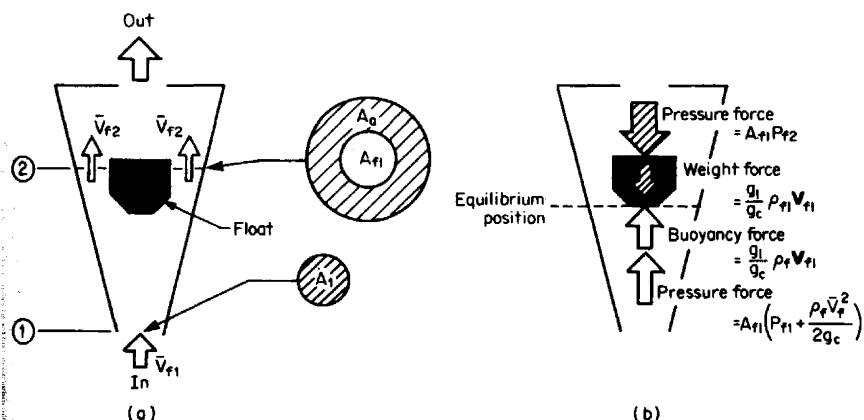


Figure 14.25 Variable-area flowmeter. (a) Area and velocity relationships. (b) Force diagram.

$$P_{f1} - P_{f2} = \frac{\rho_f}{2g_c} (\bar{V}_{f2}^2 - \bar{V}_{f1}^2) \quad (14.25)$$

If it is assumed for simplicity that the downward pressure acting on the float is the static pressure at section 2, and that the upward pressure is the total pressure [Eq. (9.7)], then for static equilibrium (Fig. 14.25b) at any float position the sum of the forces becomes

$$A_{f1} \left(P_{f1} + \frac{\rho_f \bar{V}_{f1}^2}{2g_c} \right) + \frac{g_l}{g_c} \rho_f V_{f1} = \frac{g_l}{g_c} \rho_f V_{f1} + A_{f1} P_{f2} \quad (14.26)$$

where A_{f1} is the effective area of the float, V_{f1} the float volume, P_{f1} and P_{f2} the upstream and downstream pressures at sections 1 and 2, and \bar{V}_{f1} and \bar{V}_{f2} the upstream and downstream velocities at sections 1 and 2. Mass flow continuity between sections 1 and 2 for a constant-density fluid (liquid) gives

$$A_a \bar{V}_{f2} = A_1 \bar{V}_{f1} \quad (14.27)$$

where A_a is the annular area between float and tube wall. Introducing a flow coefficient K_{VA} to correct for factors not included in the analysis and combining Eqs. (14.25) to (14.27) give the basic liquid equation for variable-area meters in U.S. units as

$$q_{cfs} = \left[K_{VA} \sqrt{\frac{2g_l V_{f1}}{A_{f1}}} \right] \sqrt{\frac{\rho_{f1}}{\rho_f} - 1} A_a \quad (14.28)$$

By a similar derivation the SI-unit equation becomes

$$q_{c^*ms} = \left[K_{VA} \sqrt{\frac{2g_l^* V_{f1}^*}{A_{f1}^*}} \right] \sqrt{\frac{\rho_{f1}^*}{\rho_f^*} - 1} A_a^* \quad (14.29)$$

For a given flowmeter the quantity in brackets is assumed constant, and the annular area A_a is directly proportional to the float height. For compressible fluids, *Fluid Meters* (ASME, 1971) introduces an expansion factor to correct for density variation across the float. This correction is usually negligible and, by calibration, is included in the flow coefficient. Equations (14.28) and (14.29) are used as the basic correlation equations for liquids and gases, for selecting float materials, and predicting changes in fluid density.

Engineering Equations. Variable-area flowmeters are usually calibrated for a specific fluid, and a correction factor is applied if a meter is to be used for a fluid of different density or viscosity. Viscosity corrections are, however, difficult to calculate, and for this reason special float designs (Fig. 14.26) are used or the meter is calibrated with the new fluid. A *viscosity immunity ceiling*, below which no viscosity correction is required, is sometimes given for a float design. Viscosity effects are also reduced by using cylinder-and-plug type variable-area meters for measuring high-viscosity fluids (bunker C, tar, liquid chemicals). The manufacturer should be consulted for the viscosity limit for a given design.

When the fluid is at design (or calibration) conditions, the meter reads correctly in the desired volume or mass flow-rate units. However, if conditions change or the meter is used for some other fluid, a correction factor is necessary to obtain the true flow rate. This factor is derived as the ratio of Eq. (14.28) or Eq. (14.29) at

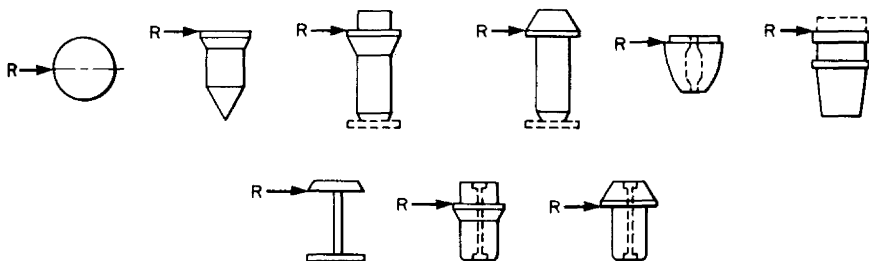


Figure 14.26 Float designs. R = reading edge of float. All floats are shown in the correct metering position. (Courtesy Fisher and Porter.)

flowing conditions to the same equation at design conditions. The corrected flow rate is then calculated with

$$F_{VA} = \frac{q_v}{(q_v)_{des}} \quad F_{VA} = \frac{q_v}{(q_v)_{des}} \quad F_{VA} = \frac{q_M}{(q_M)_{des}} \quad (14.30)$$

where F_{VA} is the correction factor for the variable-area flowmeter reading.

Table 14.10 gives the specific gravities of some float materials, and Table 14.11 presents the U.S.-unit liquid and gas correction factors for mass, flowing-volume, and base-volume flow rates. Table 14.12 presents the correction factors for SI units, and Table 14.13 presents typical ratings for glass variable-area flowmeters. For gas (vapor) flows the buoyancy of the float is normally assumed negligible. The manufacturer should be consulted for the engineering equations for spring-loaded variable flowmeters. An improved variable area correlation (Gilmont, 1991) has been proposed to correlate experimental data using the Archimedes number that is commonly used in fluidized bed analysis. Additional investigations by Bückle et al. (1992, 1995), using laser Doppler anemometry, has also improved the design information available for these meters.

TABLE 14.10 Specific Gravities G_f † of Float Materials

Float material	Specific gravity G_f	Float material	Specific gravity G_f
Dowmetal ^a	1.80	Everdur ^c	8.54
Porcelain	2.41	Monel	8.80
Glass	2.54	Bronze	8.80
Aluminum	2.79	Nickel	8.85
Titanium	4.50	Hastelloy C ^d	8.94
Steel (carbon)	7.80	Hastelloy B ^c	9.24
Durimet ^b	8.02	Lead (10% antimony)	10.67
Stainless steel (316)	8.02	Tantalum	16.6
Brass	8.46		

† $G_f = \rho_f/62.37$.

^aTrademark of Dow Chemical Co.

^bTrademark of Duriron Co.

^cTrademark of Anaconda American Brass Co.

^dTrademark of Union Carbide Corp.

^eTrademark of Huntington Alloy Products Division, International Nickel Co.

TABLE 14.11 Correction Factor F_{VA} for Variable-Area Flowmeters: U.S. Units

Liquid		Gas (vapor)	
Mass flow rate			
Density	$F_{VA} = \sqrt{\frac{(\rho_{fl} - \rho_f)\rho_f}{[(\rho_{fl} - \rho_f)\rho_f]_{des}}}$	(a)	$F_{VA} = \sqrt{\frac{\rho_f}{(\rho_f)_{des}}}$ (g)
Specific gravity	$F_{VA} = \sqrt{\frac{(G_{fl} - F_p G_F)F_p G_F}{[(G_{fl} - F_p G_F)F_p G_F]_{des}}}$	(b)	
pvT equation			$F_{VA} = \sqrt{\left(\frac{Z_f T_f}{G p_f}\right)_{des} \frac{G p_f}{Z_f T_f}}$ (h)
Volumetric flow rate at flowing conditions			
Density	$F_{VA} = \sqrt{\left(\frac{(\rho_f)}{\rho_{fl} - \rho_f}\right)_{des} \frac{\rho_{fl} - \rho_f}{\rho_f}}$	(c)	$F_{VA} = \sqrt{\frac{(\rho_f)_{des}}{\rho_f}}$ (i)
Specific gravity	$F_{VA} = \sqrt{\left(\frac{F_p G_F}{G_{fl} - F_p G_F}\right)_{des} \frac{G_{fl} - F_p G_F}{F_p G_F}}$	(d)	
pvT equation			$F_{VA} = \sqrt{\left(\frac{G p_f}{Z_f T_f}\right)_{des} \frac{Z_f T_f}{G p_f}}$ (j)

Density	$F_{VA} = \frac{(\rho_b)_{des}}{\rho_b} \sqrt{\frac{(\rho_{fl} - \rho_f)\rho_f}{[(\rho_{fl} - \rho_f)\rho_f]_{des}}}$	(e)	$F_{VA} = \frac{(\rho_b)_{des}}{\rho_b} \sqrt{\frac{\rho_f}{(\rho_f)_{des}}}$	(k)
Specific gravity	$F_{VA} = \frac{(G_b)_{des}}{G_b} \sqrt{\frac{(G_{fl} - F_P G_b)F_P G_F}{[(G_{fl} - F_P G_F)F_P G_F]_{des}}}$	(f)		
<i>pvT</i> equation				
Standard base			$F_{VA} = \left(\frac{G}{Z_b}\right)_{des} \frac{Z_b}{G} \sqrt{\left(\frac{Z_f T_f}{G p_f}\right)_{des} \frac{G p_f}{Z_f T_f}}$	(l)
Selected base			$F_{VA} = \left(\frac{G p_b}{Z_b T_b}\right)_{des} \frac{Z_b T_b}{G p_b} \sqrt{\left(\frac{Z_f T_f}{G p_f}\right)_{des} \frac{G p_f}{Z_f T_f}}$	(m)

TABLE 14.12 Correction Factor F_{VA} for Variable-Area Flowmeters: SI Units

Liquid		Gas (vapor)	
Mass flow rate			
Density	$F_{VA} = \sqrt{\frac{(\rho_{fl}^* - \rho_f^*)\rho_f^*}{[(\rho_{fl}^* - \rho_f^*)\rho_f]_{des}}}$	(a)	$F_{VA} = \sqrt{\frac{\rho_f^*}{(\rho_f^*)_{des}}}$ (g)
Specific gravity	$F_{VA} = \sqrt{\frac{(G_{fl} - F_p G_F)F_p G_F}{[(G_{fl} - F_p G_F)F_p G_F]_{des}}}$	(b)	
$p_v T$ equation			$F_{VA} = \sqrt{\left(\frac{Z_f T_K}{G p_f^*}\right)_{des} \frac{G p_f^*}{Z_f T_K}}$ (h)
Volumetric flow rate at flowing conditions			
Density	$F_{VA} = \sqrt{\left(\frac{\rho_f^*}{\rho_{fl}^* - \rho_f^*}\right)_{des} \frac{\rho_{fl}^* - \rho_f^*}{\rho_f^*}}$	(c)	$F_{VA} = \sqrt{\frac{(\rho_f^*)_{des}}{\rho_f^*}}$ (i)
Specific gravity	$F_{VA} = \sqrt{\left(\frac{F_p G_F}{G_{fl} - F_p G_F}\right)_{des} \frac{G_{fl} - F_p G_F}{F_p G_F}}$	(d)	
$p_v T$ equation			$F_{VA} = \sqrt{\left(\frac{G p_f^*}{Z_f T_K}\right)_{des} \frac{Z_f T_K}{G p_f^*}}$ (j)

Volumetric flow rate at base conditions

Density	$F_{VA} = \frac{(\rho_b^*)_{des}}{\rho_b^*} \sqrt{\frac{(\rho_{fl}^* - \rho_f^*)\rho_f^*}{[(\rho_f^* - \rho_f^*)\rho_f^*]_{des}}}$	(e)	$F_{VA} = \frac{(\rho_b^*)_{des}}{\rho_b^*} \sqrt{\frac{\rho_f^*}{(\rho_f^*)_{des}}}$	(k)
Specific gravity	$F_{VA} = \frac{(G_b)_{des}}{G_b} \sqrt{\frac{(G_{fl} - F_P G_b)F_P G_F}{[(G_{fl} - F_P G_F)F_P G_F]_{des}}}$	(f)		
<i>pvt</i> equation				
Standard base			$F_{VA} = \left(\frac{G}{Z_b}\right)_{des} \frac{Z_b}{G} \sqrt{\left(\frac{Z_f T_f}{G p_f^*}\right)_{des} \left(\frac{G p_f^*}{Z_f T_K}\right)}$	(l)
Selected base			$F_{VA} = \left(\frac{G p_b^*}{Z_b T_{Kb}}\right)_{des} \left(\frac{Z_b T_{Kb}}{G p_b^*}\right) \sqrt{\left(\frac{Z_f T_K}{G p_f^*}\right)_{calib} \left(\frac{G p_f^*}{Z_f T_K}\right)}$	(m)

TABLE 14.13 Typical Ratings for Glass Variable-Area Flowmeters

Tube diameters, in (mm)	Safe working pressure, psig (kPa)	Temperature, °F (°C)	Capacity		Overall pressure loss (water), psid (kPa)
			Air†, SCFM (L/s)	Water‡, gal/min (L/s)	
$\frac{1}{4}$ (6.3)	450 (3100)	200 (90)	0.15–1.8 (0.07–0.85)	0.025–0.5 (0.002–0.03)	0.04–0.37 (0.3–2.5)
$\frac{1}{2}$ (12.5)	300 (2070)	180 (80)	1–20 (0.5–10)	0.25–5 (0.02–0.3)	0.04–1.2 (0.3–8)
1 (25)	180 (1240)	160 (70)	18–122 (8.5–58)	4–30 (0.25–1.9)	0.3–0.4 (2–3)
$1\frac{1}{2}$ (40)	130 (900)	150 (65)	48–226 (23–107)	13–54 (0.8–3.4)	0.3–3.6 (2–25)
2 (50)	100 (700)	140 (60)	73–384 (37–180)	20–90 (1.3–5.7)	0.4–4 (3–28)
3 (75)	60 (414)	130 (55)	205–500 (100–236)	60–120 (3.8–7.6)	0.7–1.4 (5–10)

†Air at standard conditions: $p_b = 14.696$ psia ($p_b^* = 101.325$ kPa); $T_b = 518.67^\circ\text{R}$ ($T_{kb} = 288.15$ K).

‡Water at 60°F (15.6°C) and 14.696 psia (101.325 kPa).

Source: Adapted from Fees (1974).

Industrial Flowmeters. Industrial variable-area flowmeters range from a simple ball floating in a glass tube to high-pressure piston-type meters in 600-lb (4000-kPa) valve bodies. Several flowmeters are illustrated in Chap. 6. Readings may be obtained visually or through a magnetic coupling, a dial reading, or some standardized output. Variable-area meters have advantages in that the overall pressure loss is nearly constant, the meters are small in size, and almost any corrosive fluid can be metered. Their accuracy ranges from ± 0.5 to ± 2 percent of the URV flow rate, depending on design.

The simple direct-viewing glass-tube meter is the most popular for reasons of economics, and armored-tube meters extend applications to high-pressure service. Orifice and tapered-plug meters (Fig. 14.25*b*) are low-cost, compact variable-area flowmeters. Because of their small size and low cost, these meters are frequently selected for purge-water flows where accuracy is not required.

Piston-type meters are made of steel, cast iron, and other metals and are installed in a valve body in line sizes up to 4 in (100 mm). These meters are suitable for high-pressure liquids and gas (vapor) applications. Their range is adjustable by varying a spring force or changing weights. Since these meters are relatively less sensitive to vertical installation (at least within $\pm 5^\circ$ of vertical), they are preferred for mobile or marine installations. They are quite rugged and are commonly used in gasoline, kerosene, and tar applications. However, the fluid must be clean, and a strainer may be necessary.

Periodic cleaning and an upstream strainer are usually recommended for dirty flows. A leak-type bypass manifold (Fig. 14.27) is suggested for applications where shutdown is undesirable. The upstream and downstream piping configurations have little effect on meter performance, and no straight lengths are given.

Example 14.5. A variable-area flowmeter with a stainless-steel float was calibrated to measure the gasoline of Example 2.12 in base gallons per minute at a line pressure of 100 psig (690 kPa). If the flowing temperature is 100°F (37.8°C) and the pressure is 300 psig (2070 kPa), what is the flow rate for a meter reading of 10 gal/min (0.631 L/s)?

The flow rate is calculated with Eq. (14.30)

$$q_{\text{GPM}} = F_{VA}(q_{\text{GPM}})_{\text{des}}$$

where the correction factor F_{VA} is, from Eq. (f) of Table 14.11,

$$F_{VA} = \frac{(G_b)_{\text{des}}}{G_b} \sqrt{\frac{(G_f - F_P G_F) F_P G_F}{[(G_f - F_P G_F) F_P G_F]_{\text{des}}}}$$

Required data at design (calibrated) conditions is:

- From Example 2.12: $(G_b)_{\text{des}} = 0.7359$
- From Example 2.12: $(G_F)_{\text{des}} = 0.7255$
- From Table 14.10: $G_f = 8.02$

The liquid compressibility factor is, from Eq. (2.213),

$$(F_P)_{\text{des}} = 1 + Z_L \frac{P_f}{1000} = 1 + 0.0088 \frac{114.7}{1000} = 1.0010$$

where $Z_L = 0.0088$ from Fig. E.22.

The density at flowing conditions (uncorrected for pressure) is, from Eq. (2.189),

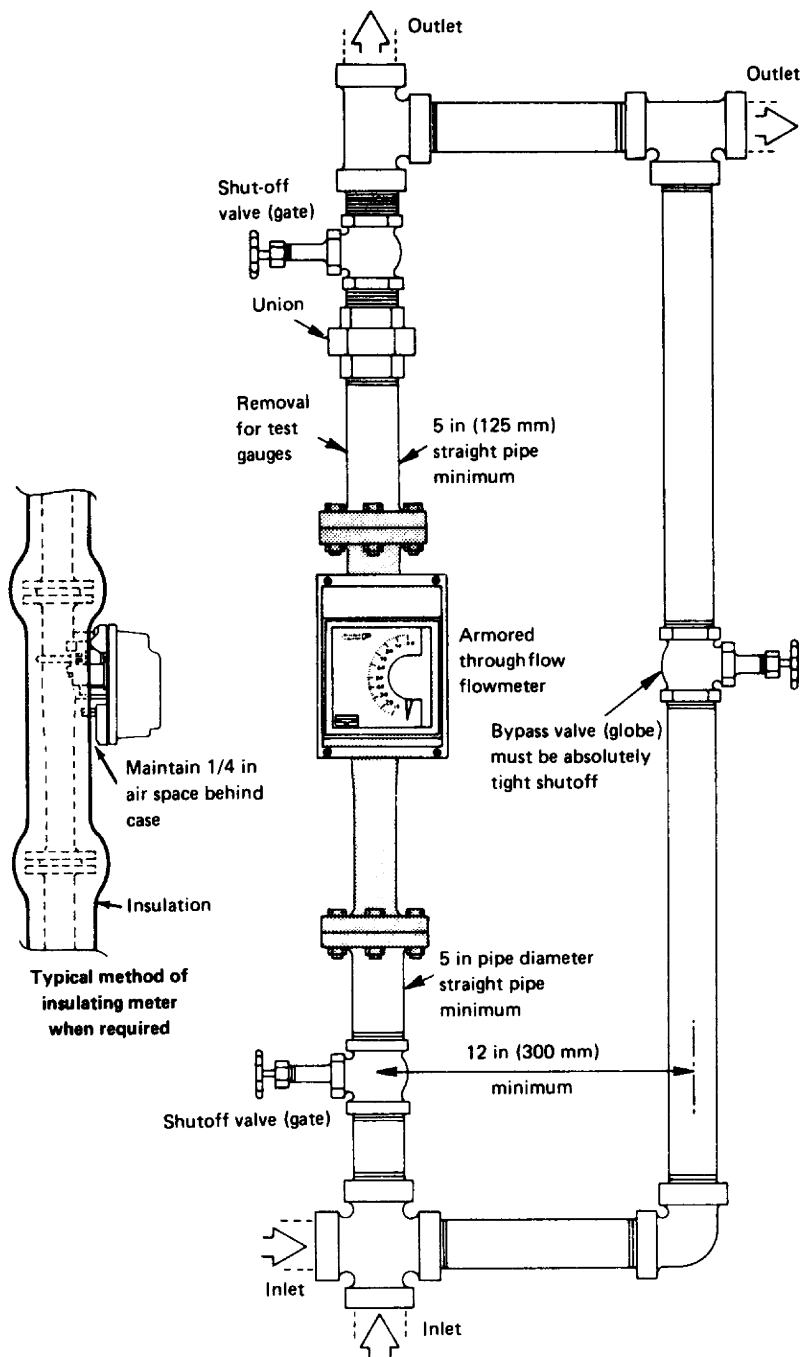


Figure 14.27 Typical variable-area-flowmeter installation with bypass manifold.
(Courtesy Fischer & Porter.)

$$\rho_F^* = \rho_b^* \exp[-\alpha_b \Delta T_F (1 + 0.8 \alpha_b \Delta T_F)]$$

where, from Example 2.12, $\rho_b^* = 735.14 \text{ kg/m}^3$, and, from Eq. (2.188),

$$\alpha_b = \frac{K_0}{\rho_b^{*2}} + \frac{K_1}{\rho_b^*} = \frac{192.4511}{(735.14)^2} + \frac{0.2438}{735.14} = 0.0006878$$

Since $\Delta T_F = 100 - 60 = 40^\circ\text{F}$,

$$\rho_F^* = 735.14 \exp \{(-0.0006878)(40)[1 + (0.8)(0.0006878)(40)]\} = 714.76 \text{ kg/m}^3$$

The specific gravity at flowing conditions is then, by Eq. (2.174),

$$G_F = \frac{\rho_F^*}{999.012} = \frac{714.76}{999.012} = 0.7155$$

The liquid compressibility factor at flowing conditions is, from Eq. (2.213),

$$F_p = 1 + Z_L \frac{p_f}{1000} = 1 + 0.009 \frac{314.7}{1000} = 1.0028$$

where $Z_L = 0.009$ from Fig. E.22. Because $(G_b)_{\text{des}} = G_b$ and $(G_f)_{\text{des}} = G_f$,

$$F_{VA} = \frac{0.7359}{0.7359} \sqrt{\frac{[(8.02 - (1.0028)(0.7155))(1.0028)(0.7155)]}{[(8.02 - (1.0010)(0.7255))(1.0010)(0.7255)]}} = 0.9946$$

The flow rate is then

$$q_{\text{GPM}} = (0.9946)(10) = 9.946 \text{ base gal/min}$$

Example 14.6. The variable-area flowmeter of Example 14.5 is being used to meter water at 100°F (37.8°C) and 14.7 psia (101 kPa). If the reading is 10 gal/min (37.9 L/min), what is the flow rate?

The water flow rate is calculated by Eq. (14.30):

$$(q_{\text{GPM}})_{\text{water}} = F_{VA} (q_{\text{GPM}})_{\text{gasoline}}$$

The correction factor is, from Eq. (f) of Table 14.11,

$$F_{VA} = \frac{(G_b)_{\text{des}}}{G_b} \sqrt{\frac{(G_f - F_p G_F) F_p G_F}{[(G_f - F_p G_F) F_p G_F]_{\text{des}}}}$$

Design data, from Example 14.5, is:

$$(G_f)_{\text{des}} = 8.02 \quad (F_p)_{\text{des}} = 1.0010 \quad (G_F)_{\text{des}} = 0.7255 \quad (G_b)_{\text{des}} = 0.7359$$

For flowing conditions, $G_f = 8.02$. From Table E.6, $\rho_F = 61.994 \text{ lb}_m/\text{ft}^3$, and, by Eq. (2.175), $G_F = 61.994/62.3663 = 0.99402$. It is assumed that $F_p = 1.0$, and, for water, $G_b = 1.0$. Then substitution gives

$$F_{VA} = \frac{0.7359}{1.0} \sqrt{\frac{[(8.02) - (1.0)(0.99402)](1.0)(0.99402)}{[(8.02 - (1.0010)(0.7255))(1.0010)(0.7255)]}} = 0.8450$$

The flow rate is then

$$q_{\text{GPM}} = (0.8450)(10) = 8.45 \text{ base gal/min}$$

Example 14.7. A variable-area flowmeter was calibrated on air at 101.325 kPa and 15°C to read standard cubic meters per hour. The meter is being used to measure the water-vapor-saturated natural gas of Example 9.10. For a reading of 10 standard m³/h, what is the dry natural gas flow rate?

The dry-gas flow rate is calculated by combining Eqs. (14.30) and (2.112) as

$$(q_{\text{SCMH}})_{\text{dry}} = F_{\text{WV,dry}}(q_{\text{SCMH}})_{\text{wet}} = F_{\text{WV,dry}} F_{\text{VA}}(q_{\text{SCMH}})_{\text{air}}$$

From Example 9.10, $F_{\text{WV,dry}} = 0.98082$. From Eq. (1) of Table 14.12, the correction factor F_{VA} is

$$F_{\text{VA}} = \left(\frac{G}{Z_b}\right)_{\text{des}} \left(\frac{Z_b}{G_{\text{wet}}}\right) \sqrt{\left(\frac{Z_f T_K}{G p_f^*}\right)_{\text{des}} \frac{G_{\text{wet}} p_f^*}{Z_f T_k}}$$

where G_{wet} replaces G because the meter is measuring wet gas.

At design (calibrated) conditions,

$$G_{\text{des}} = 1.0 \quad \text{for air}$$

$$(Z_b)_{\text{des}} = (Z_f)_{\text{des}} = 0.99743$$

$$(T_K)_{\text{des}} = 288.15 \text{ K}$$

$$(p_b^*)_{\text{des}} = (p_f^*)_{\text{des}} = 101.325 \text{ kPa}$$

and at flowing conditions,

$$G_{\text{wet}} = 0.6514 \quad T_K = 300 \text{ K}$$

from Example 9.10;

$$Z_f = \frac{Z_b}{F_{\text{pv}}^2} = 0.9952$$

from Eq. (9.65); and

$$Z_b = 1.0 \quad p_f^* = 184 \text{ kPa}$$

Substitution then gives

$$F_{\text{VA}} = \frac{1.0}{1.0} \frac{0.9974}{0.6514} \sqrt{\frac{(1.0)(288.15)}{(1.0)(101.325)} \frac{(0.6514)(184)}{(0.9952)(300)}} = 1.636$$

and the dry-volume flow rate is

$$(q_{\text{SCMH}})_{\text{dry}} = (0.98082)(1.636)(10) = 16.05 \text{ standard m}^3/\text{h}$$

Coriolis Mass Flowmeter

An element of fluid moving at constant velocity along a straight length of pipe possesses no components of acceleration (Fig. 14.28a). If, however, the pipe is rotated at the same instant, then a *complementary-acceleration* or *Coriolis accel-*

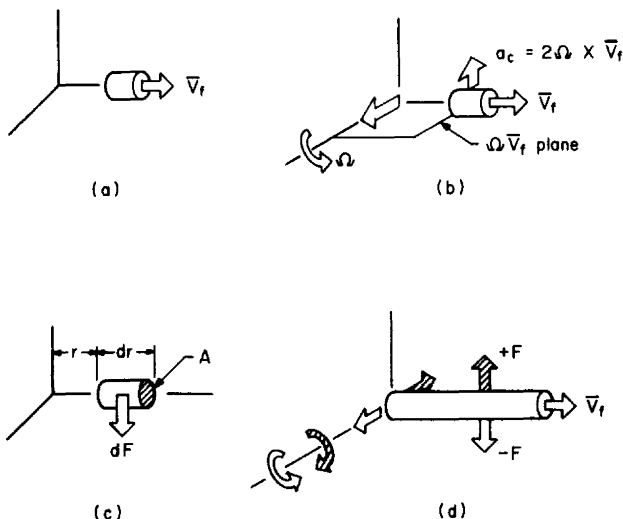


Figure 14.28 Coriolis mass flowmeter components. (a) Velocity. (b) Coriolis acceleration. (c) Elemental force. (d) Vibratory forces.

eration, after the French mathematician De Coriolis, is produced on the fluid element. It is this component of acceleration that produces an inertial force on the pipe proportional to the mass flow rate. The Coriolis force is the fundamental operational principle behind the Coriolis mass flowmeters.

The Coriolis acceleration for a particle of mass dm moving along a rotating straight pipe (Fig. 14.28b) is

$$a_c = 2\Omega \times \bar{V}_f \quad (14.31)$$

The \times in this *vector* equation indicates that the acceleration vector is the cross product of the rotational and axial fluid velocity vector. That is, the Coriolis acceleration vector is perpendicular to the plane containing the fluid velocity and rotational vector.

By Newton's second law ($F = ma$), the incremental inertial force on the pipe wall, produced by the Coriolis acceleration component (Fig. 14.18c), is

$$dF = (dm)(a_c) = (\rho_f A dr)(2\Omega \bar{V}_f) = (2\Omega)(\rho_f A \bar{V}_f) dr = 2\Omega q_m dr \quad (14.32)$$

where the elemental force dF is perpendicular to the plane of the velocity and rotational vector. It acts in a direction perpendicular to the pipe and opposes the rotational motion.

The total inertial force on the pipe wall is obtained by integration along the length of pipe as

$$F = 2\Omega q_M \int_0^l dr = 2l\Omega q_M \quad (14.33)$$

The mass flow rate q_M is then, by rearranging Eq. (14.33),

$$q_M = \frac{F}{2l\Omega} \quad (14.34)$$

In practice, the pipe is not rotated but oscillated, usually by electromagnetic driving coils, at the natural frequency of the structure. The rotational velocity vector Ω , in Eq. (14.34), is then time-dependent, as are the produced oscillating Coriolis forces (Fig. 14.28d).

By applying an oscillatory motion, it is possible to rigidly support the pipe and eliminate bearings. Since the pipe is now *grounded*, the system stiffness is greatly increased, limiting the motion that can be safely withstood without failure. To decrease stiffness, long tubes are used which may take on various shapes in order to minimize the overall laying length (Fig. 14.29). These shapes, however, increase the overall pressure loss.

Coriolis meters are dynamic systems (Mattar, 1988) in which the drive angular velocity Ω_d is in phase with produced Coriolis acceleration and, hence, 180° out of phase with the Coriolis force of the fluid on the pipe. Figure 14.30a and b illustrates the time histogram for the angular velocity, Ω_d , produced Coriolis forces, and resulting displacements. There are two distinctly different modes of vibration, a vibration of the electromagnetically driven piping circuit (at its natural frequency) and the vibratory mode produced by Coriolis forces driving the pipe at a frequency corresponding to the natural frequency of the first mode.

The deflections produced in the driven portion δ_d (at the resonant frequency) and the deflection δ_f resulting from the driving Coriolis force are illustrated in Fig.

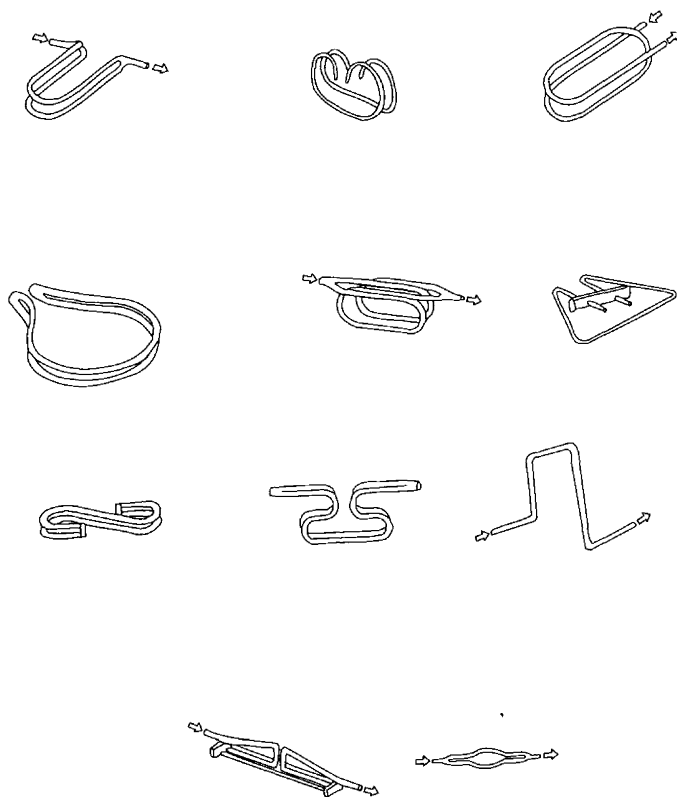


Figure 14.29 Shapes used for Coriolis mass flowmeter.

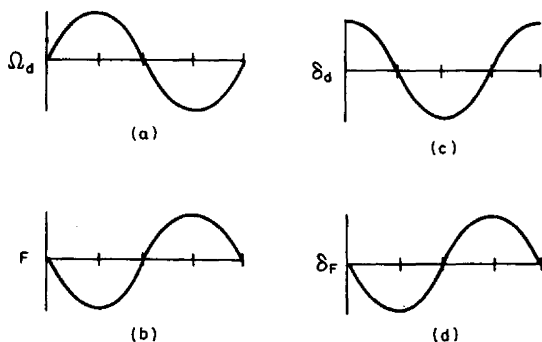


Figure 14.30 Coriolis frequency and displacement relationships. (a) Angular frequency. (b) Force. (c) Drive displacement mode. (d) Force displacement mode.

14.30c and d. It should be noted that, when the drive deflection δ_d goes through zero, the deflection δ_F produced by the Coriolis force is at a maximum. This quadrature difference between the two modes allows for (1) amplitude detection of the two modes, (2) phase difference, or (3) zero crossing detection to determine the mass flow rate.

Dual pipes are common, since they serve to decrease power requirements. This results in a *balanced tuning fork* system that minimizes the energy leaving or entering the system from external sources. The fluid may be routed serially or in parallel depending on the manufacturer.

The drive and Coriolis deflection modes are unique to each manufacturer, as is the method of detecting and relating the measured amplitude (Coriolis) to the mass flow rate. Flow calibration is required to determine the meter constant. For a statically loaded spring, a simple liquid calibration, using a single-density fluid, would be sufficient to establish the meter factor for all densities, provided the systems stiffness (spring constant) were corrected for thermal changes. However, the loads are not statically applied but are instead applied at the drive frequency. A mechanical transfer function is therefore introduced in addition to the static function.

Figure 14.31 illustrates the two-modal vibratory system and shows that small mass changes, due to density variations from the calibration value, in either vibratory mode must be considered in order to minimize density effects. Manufacturers should be consulted for the density range over which their meter will perform within specifications.

Meter Designs Considerations

Early meters were of a single U-tube design, but these have almost been totally replaced by dual-tube designs in which the fluid is split into two approximately equal streams. Currently dual tubes predominate, but single-tube designs are being reintroduced (Baker, 1994). In dual-tube meters the deflection is measured between two countervibrating tubes in order to minimize or eliminate external vibration effects.

Cyclic stresses can cause corrosive fatigue of the thin vibrating tube, and early meters occasionally experienced leakage problems that were the result of fluid aggressiveness on the joint welds. The proper selection of tube material, knowledge

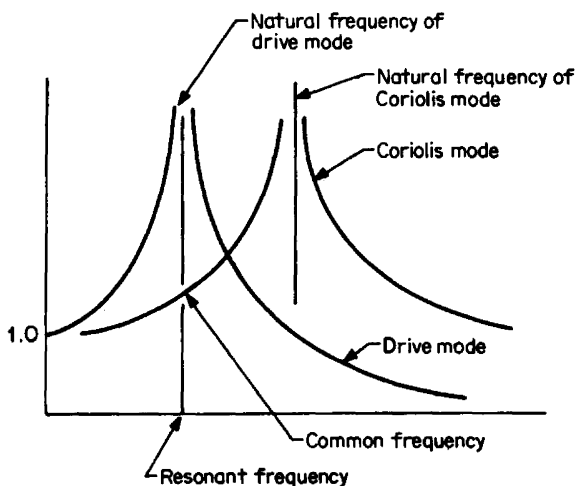


Figure 14.31 Coriolis and drive mode frequency relationships.

of process variables, familiarity with the various meter designs, and newer designs have essentially solved this problem. However, some manufacturers offer a secondary containment vessel in the event of a failure.

Tubes are vibrated at their natural frequency by magnetic drives with the Coriolis forces twisting the tubes by approximately 4° (Wagner, 1988). This allows the sensors, mounted on the tubes, to pass through a common plane at differing times. The relative velocity of the tubes is motion-detected to provide two discrete signals that have essentially a zero phase difference at no flow. The phase difference increases in proportion to the mass flow rate. Other electronic designs measure the time difference by gating a signal from a high-frequency *clock*. The time difference is proportional to mass flow rate.

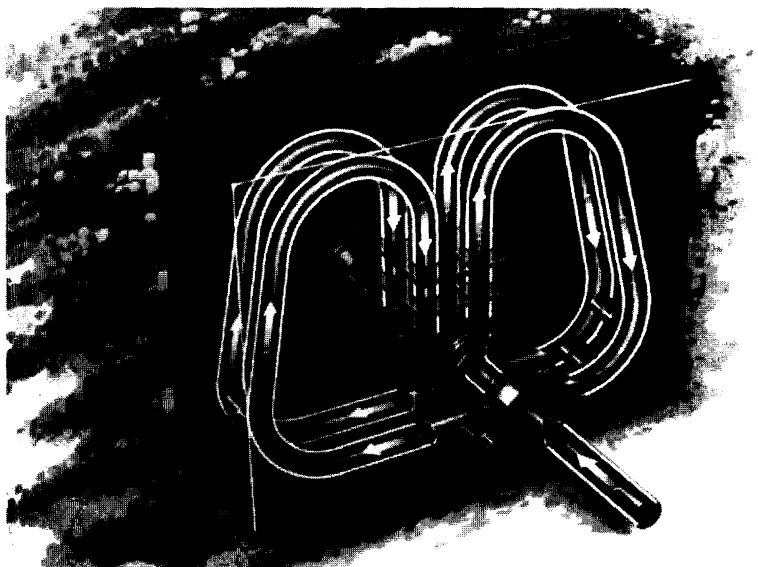
The vibration frequency is proportional to flowing density. This measurement and display of density have become common features offered by many manufacturers.

The MicroMotion secondary integrates the sensed velocity to obtain location (position) integration, also removing white noise. The Foxboro mass flowmeter (Fig. 14.32) uses an antiphase measurement system and a double-drive method in order to produce rotation at the straight tube section. This design feature significantly reduces vibratory stresses and possible joint failures.

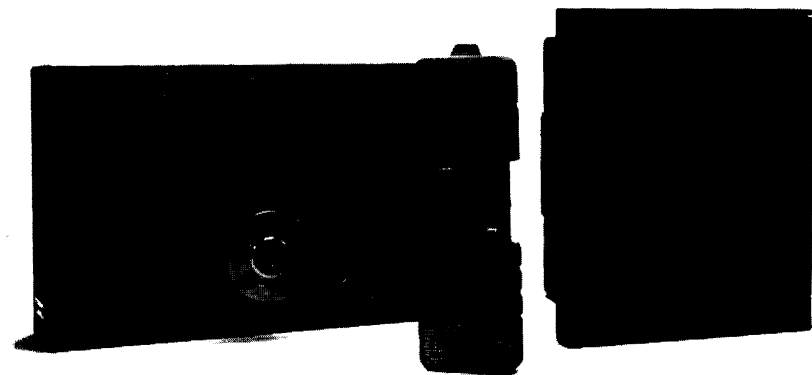
Other meter manufacturers also offer similar low-joint-stress designs. The design of the tubing circuit varies between manufacturers, with the selected geometry depending on the design objective. Wagner (1988) and Baker (1994) list the following tube design considerations:

- A long tube increases weight and overall pressure but also increases the Coriolis forces and the twist between tubes.
- A tube diameter increase, for the same bore, will not effect the Coriolis forces but will increase stresses, meter weight, and twist angle.

These features combined with operating conditions and fluid compatibility (Table 14.14), with the selected tube material are important when selecting the meter. For



(a)



(b)

Figure 14.32 Foxboro Coriolis mass flowmeter. (a) Fluid path. (b) Flowmeter. (Courtesy The Foxboro Co.)

TABLE 14.14 Fluid Compatibility with 316-L Stainless Steel

Compatible fluids	Incompatible fluids
Acids (fatty)	Acetic acid at high temperatures and concentrations
Adhesives	Ammonium chloride
Asphalt	Bromine
Beer	Calcium chloride
CNG	Dyes
Crude oil (sour)	Fluids containing halogen ions
Ethylene oxide	Iodine (except for 100% dry)
Fruit juices	Ink
Fuel oils	Mustard
Isopropanol	Sea water
Lime slurries	
Liquefied N ₂ , O ₂ , LPG	
Magnetic slurries	
Milk cream	
Nitric acid	
Olephins	
Paint	
Peanut butter	
Phosphoric acid	
Pie fillings	
Polymers	
Polypropylene	
Sodium hydroxide	
Sulfur (molten)	
Tar sands	
Urethane	

some particularly aggressive fluids a secondary containment may be required to protect against a tube failure caused by cyclic stresses. Some manufacturers offer a secondary containment vessel for use with particularly hazardous and aggressive fluids.

Coriolis mass flowmeters are increasingly being used in many applications because of their wide rangeability, accuracy, and demonstrated reliability over a long period of time. Currently meters are offered by many manufacturers with somewhat different specifications. ASME MFC-11M (1994), ISO 10790 (1994), and OIML R 105 (1993) standards cover Coriolis mass flowmeters for liquid applications. General specifications are summarized as shown in Table 14.15.

Pulsation. Vetter and Notzon (1994) conducted several test on a U-tube design flowmeter and concuded that if the flowmeter is operated in a monofrequent pulsation range of 10 to 200 Hz, a small relative error of <25 percent may be present.

TABLE 14.15 Typical Coriolis Mass Flowmeter Specifications

Line size	0.2 to 24 in (5 to 600 mm)
Mass flow rate	Low range 0 to 7 lb _m /h (0 to 3 kg/h) High range 0 to 150,000 lb _m /h (0 to 680,000 kg/h)
Accuracy (uncertainty)	±0.25%, ± zero stability
Zero stability	±0.02% URV
Precision	±0.10%
Density measurement	0 to 190 lb _m /ft ³ (0 to 3,000 kg/m ³)
Accuracy (uncertainty)	±0.0002 g/cm ³ to ±0.01 g/cm ³
Pressure	Up to 5700 psig (393 bar, gauge) Minimum: May apply; check with manufacturer
Pressure loss (overall pressure loss)	Refer to manufacturer
Rangeability	20:1 to 100:1 depending on accuracy requirements (see accuracy)
Temperature	−420 to 380°F (−200 to 190°C)

Source: Baker (1994).

However, at the torsional frequency an abrupt measurement error occurs that can exceed 100 percent. They stated:

This extreme excursion signifying a resonance condition, which for large amplitudes of the pulsation is also audibly recognizable by the sudden appearance of knocking noises.

Leak Detection. Mutual interference (Kiel, 1991) will occur when Coriolis meters are installed in series for leak detection or monitoring separation processes or when the difference or summation of two or more streams is important. The specific features of the measurement transducers result in reduced precision and overall accuracy (uncertainty). The successful matching of the mechanical transfer functions of the measurement transducers will determine the resulting error. These coupling effects are reduced by the decoupling methods shown in Fig. 14.33 or by tuning the dynamic characteristic of the transducers by simply shifting the compliance modal mass of one of the transducers.

Fuel Measurement. The Coriolis mass flowmeter's wide-range accuracy and negligible sensitivity to viscosity and density reduce the risk of error in the field testing of liquid fuel measurements for gas turbine testing. MacLeod and Grabe (1995) report good agreement between the accepted turbine meter test procedure and the test results from a Coriolis mass flowmeter. However, they caution that the electronics required frequent adjustments to ensure that large undetected errors could not occur.

Installation. Meter are usually considered to be insensitive to upstream disturbance but may be sensitive to orientation and external vibratory influences. It is usually suggested that the meter be mounted vertically to self-purge any system gas or vapor. Horizontal installations should consider a planar arrangement of the dual tubes in order to equalize any gas bubbles; these can lead to large zero errors.

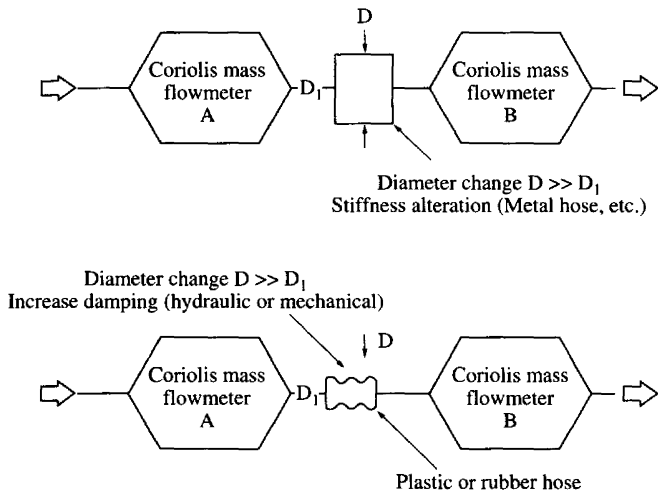


Figure 14.33 Decoupling techniques. (a) Dynamic mismatching the characteristics. (b) Simple damping.

The high-pressure loss of some designs may lead to cavitation, or flashing which should be avoided. For multicomponent flows with abrasive particles the maximum velocity through the tubes should be 6 ft/s (2 m/s).

REFERENCES

- AGA Report 6, *Methods of Testing Large Capacity Displacement Meters*, American Gas Association, Arlington, Va., 1975.
- AGA Report 7, *Measurement of Fuel Gas by Turbine Meters*, catalog no. XQ0580, American Gas Association, Arlington, Va., 1981.
- ANSI (ISA RP) 31.1, *Specifications, Installation, and Calibration of Turbine Flowmeters*, ANSI, New York, 1977.
- ANSI B109.2, *Gas Capacity at 0.5 Inches of Water (0.125 kPa) Differential for a 0.6 Specific Gravity Gas Referred to 60°F (15.6°C) and 14.73 psia (101.6 kPa)*, ANSI, New York, 1980.
- ANSI B109.3, *Rotary Type Gas Displacement Meters*, ANSI, New York, 1980.
- ANSI Z11.170, *Measurement of Petroleum Liquid Hydrocarbon by Positive Displacement Meter (API Standard 1101)*, ANSI, New York, 1960.
- ANSI/API MPMS 12.2F, *Instructions for Calculating Liquid Petroleum Quantities Measured by Turbine or Displacement Meters*, 1st ed., ANSI, New York, 1981.
- ANSI/API 2562, *Natural Gas*, ANSI, New York, 1969.
- ANSI/ASME MFC-5M, *Measurement of Liquid Flow in Closed Conduits Using Transit-Time Ultrasonic Flowmeters* (draft standard), ASME, New York, 1994.
- API Chap. 11.2.1, *Compressibility Factors for Hydrocarbons*, 1st ed., American Petroleum Institute, Washington, D.C., 1987.
- ASME: *Fluid Meters, Their Theory and Application*, 6th ed., ASME, New York, 1971.
- ASME MFC-16M, *Measurement of Fluid Flow in Closed Conduits by Means of Electromagnetic Flowmeters*, ASME, New York, 1995.

- Baker, R. C.: "Coriolis Flowmeters: Industrial Practice and Published Information," *Flow Measurement and Instrumentation*, vol. 5, no. 4, pp. 229-246, 1994.
- Ball, J. M.: "Viscosity Effects of the Turbine Flowmeter," *Proc. of the Symp. on Flow*, NBS publication 484, pp. 847-869, U.S. Government Printing Office, Washington, D.C., 1977.
- Bückle, U., F. Durst, B. Howe, and A. Melling: "Investigations of a Floating Element Flowmeter," *Flow Measurement and Instrumentation*, vol. 3, no. 4, pp. 215-225, 1992.
- , ———, and ———: "Further Investigation of a Floating Element Flowmeter," *Flow Measurement and Instrumentation*, vol. 6, no. 1, pp. 75-78, 1995.
- Cairney, W. D.: "Typical Flow Measurement Problems and Their Solution in the Electricity Supply Industry," *Flow Measurement and Instrumentation*, vol. 2, no. 4, pp. 217-223, 1991.
- Corpron, G. P., W. M. Mattar, D. A. Richardson, and G. E. Sgourakes: "Fluctuating Pressure Profile and Sensor Design for a Vortex Flowmeter," ASME WAM Paper 78-WA/FM-3, 1978.
- Faraday, M.: *Philos. Trans. R. Soc. London Ser. A*, p. 125, 1892.
- Fees, Charles E.: *Process Instruments and Control Handbook*, chap. 4, McGraw-Hill, New York, 1974.
- Furness, R. A.: "Use of Turbine Meter for High Accuracy Gas Flow-Rate Measurements," *Proc. Symp. Meas.*, Transtech, Montreal, November 1987.
- Gilmont, R.: "Rotameters/Variable Area Flowmeters," *Comments, Measurement & Control*, September 1991.
- Hussein, I. B., and I. Owen: "Calibration of Flowmeters in Superheated and Wet Steam," *Flow Measurement and Instrumentation*, vol. 2, no. 4, pp. 209-215, 1991.
- IEC Publication 381A, International Electrical Commission, Geneva.
- Inkley, F. A., D. C. Walden, and D. J. Scott: "Flow Characteristics of Vortex Flowmeters," *Meas. Control*, vol. 13, pp. 166-169, 1980.
- ISO Standard 5024, *Petroleum Liquids and Gases—Measurement—Standard Reference Conditions*, ISO 5024-1976(E), Geneva, 1976.
- ISO 6817, *Measurement of Conductive Fluid Fluoride in Closed Conduits—Methods Using Electromagnetic Flowmeters*, ISO, 1992.
- ISO DP9104, *Methods of Evaluating the Performance of Electromagnetic Flowmeters for Incompressible Liquids in Closed Conduits* (draft), ISO Int. Std., ISO TC30 SC5, Geneva, 1991.
- ISO Standard 9951, *Measurement of Gas Flow in Closed Conduits—Turbine Meters*, ISO, Geneva, 1992.
- ISO Standard 10790, *Measurement of Fluid Flow in Closed Conduits—Coriolis Mass Flowmeters*, ISO, Geneva, 1994.
- Jennings, R.: "Digital Compensation Techniques for Positive Displacement and Turbine Flowmeters," *Proc. of the Symp. on Flow*, NBS publication 484, pp. 821-846, 1977.
- Jones, F. E.: "Algorithm for Ascertaining Linear Range of Turbine Flow Meters," *Rev. Sci. Instrum.*, **56**(9), September 1985.
- Kegel, T.: *Two-Phase and Multi-component Flows Using a Vortex Flowmeter*, Foxboro Co. Research Note, private communication, 1988.
- Kiehl, L.: "Difference Measurement Using Coriolis Mass Flowmeters," *Flow Measurement and Instrumentation*, vol. 2, no. 2, pp. 135-138, 1991.
- Kuromori, K., Sh. Goto, and Y. Matsunaga: "Advanced Magnetic Flowmeters with Dual Frequency Excitation," *Proc. 5th Int. IMEKO Conference on Flow Measurement*, pp. 135-142, VDI Verlag, 1989.
- Lee, W. F. Z., D. C. Blakeslee, and R. V. White: "A Self-Correcting and Self-Checking Gas Turbine Meter," *J. Fluid Eng.*, vol. 104, no. 2, pp. 143-149, 1982.
- Lee, W. L.: "Turbine Meter Accuracy in Air vs. Natural Gas," *Proc. AGA Dist. and Trans. Conf.*, May 4-6, 1987.
- Lynnworth, L. C.: "Ultrasonic Flowmeters," p. 407-525 in W. P. Mason and R. N. Thurston (eds.), *Physical Acoustics*, vol. 14, Academic, New York, 1979.

- Lynnworth, L. C.: *Ultrasonic Measurements for Process Control*, Academic Press, New York, 1989.
- MacLeod, J. D., and W. Grabe: "Comparison of Coriolis and Turbine-Type Flowmeters for Fuel Measurement in Gas Turbine Testing," *J. of Engr. for Gas Turbines and Power*, ASME, vol. 117, 1995.
- Mattar, W.: "Coriolis Mass Flowmetering," private communication, 1988.
- Miller, R. W., J. P. DeCarlo, and J. T. Cullen: "A Vortex Flowmeter—Calibration Results and Application Experiences," *Proc. of the Symp. on Flow*, NBS publication 484, pp. 549–570, 1977.
- Miller, R. W., C. Wilkes, and E. Jones: "Vortex and Orifice Metering of Natural Gas," *Mass Flow Meas.*, pp. 1–7, ASME WAM, FED, vol. 17, ASME, 1984.
- OIML R 105, *Direct Mass Flow Measuring System for Quantities of Liquids*, OIML, Geneva, 1993.
- Rubin, M., R. W. Miller, and W. G. Fox: "Driving Torques in a Theoretical Model of a Turbine Meter," *J. Basic Eng.*, ser. D, vol. 87, no. 2, pp. 413–420, 1965.
- Scarpa, T.: "Magmeter Spotlights New Technology," *INTECH Industry*, pp. 53–55, April 1993.
- Schmidt, T. R.: "Clamp-on Ultrasonic Flowmeters," *Trans. ISA*, vol. 4, pp. 111–126, 1980.
- Shercliff, J. A.: *The Theory of Electromagnetic Flow Measurement*, Cambridge University Press, Cambridge, England, 1961.
- Spink, L. K.: *Principles and Practice of Flowmeter Engineering*, 9th ed., The Foxboro Company, Foxboro, Mass., 1967.
- Strouhal, F.: "Über eine besondere Art der Tonerregung," *Ann. Phys. Chem.*, vol. 5, p. 216, 1878.
- Thompson, R. E., and J. Grey: "Turbine Flowmeter Performance Model," *J. Basic Eng.*, ser. D, vol. 92, no. 4, pp. 712–723, 1970.
- Tsuchida, T., Y. Terashima, and T. Machiyama: "The Effects of Flow Velocity Profile on the Electromagnetic Flowmeters," *Report of Research*, Nippon Inst. of Tech., 1982.
- Vetter, G., and S. Notzon: "Effect of Pulsating Flow on Coriolis Mass Flowmeters," *Flow Measurement and Instrumentation*, vol. 5, no. 4, pp. 263–273, 1994.
- Vignos, J. H.: "Effect of Velocity Profile on Flow Measurement in the Turbulent Regime," private communication, 1981.
- von Karman, T., and H. Rubach: "Über den Mechanismus des Flüssigkeits und Luftwiderstanders" ("On the Mechanism of Fluid Resistance"), *Phys. Z.*, vol. 13, p. 49, 1912.
- Wagner, J. J.: "Effects of Sensor Design and Application Data on Coriolis Mass Meter Performance: An Overview," *Int. Conf. on Flow Measurement*, London, UK, 1988.
- White, D. F., A. E. Rodely, and C. L. McMurtie: "The Vortex Shedding Flowmeter," *Flow, Its Measurement and Control in Science and Industry*, vol. 1, pt. 2, pp. 967–974, ISA, Research Triangle Park, N.C., 1974.

METER INFLUENCE QUANTITIES

The proper use of any flowmeter assumes that the appropriate ISO, ASME, ANSI, AGA, API, etc., standards and recommendations of the manufacturer have been adhered to in order to achieve reference accuracy (overall uncertainty) conditions. This chapter presents the available information on the effects of departure from these conditions. These are referred to as *influence quantities* and may be related to the primary element, secondary element, the flowmeter, or any internal or external factors associated with the in-situ conditions.

Coriolis mass, magnetic, turbine, positive displacement, ultrasonic, and vortex flowmeters are considered proprietary designs and, in general, the performance between differing designs will not be the same. The information presented is available in the literature and the reader should use the information in this chapter primarily for assisting in locating possible metering errors. In all cases the manufacturer should be consulted for the latest information on a particular design.

Information about each of the following meters is presented in tabular form with a brief description of some *influences* and a referenced figure number.

Coriolis mass flowmeter. Table 15.1 and Figs. 15.1 to 15.7 give some of the reported influence quantities for the Coriolis mass flowmeters.

Differential producers (orifice, nozzle, and venturi). Tables 15.2 and 15.3 and Figs. 15.8 to 15.23 give the reported influence quantities for the orifice, flow nozzle, and venturi flowmeters.

Magnetic flowmeter. Table 15.4 and Figs. 15.24 to 15.34 present reported influence quantities for magnetic flowmeters.

Positive-displacement meters. Table 15.5 and Fig. 15.35 give some of the reported influence quantities for positive-displacement meters.

Turbine flowmeter. Table 15.6 and Figs. 15.36 to 15.44 present some of the reported influence quantities for turbine flowmeters.

Ultrasonic flowmeter. Table 15.7 and Figs. 15.45 to 15.52 present some of the reported influence quantities for turbine flowmeters.

Vortex flowmeter. Table 15.8 and Figs. 15.52 to 15.64 give some of the reported influence quantities for turbine flowmeters.

TABLE 15.1 Influence Quantities on Coriolis Mass Flowmeters

Fatigue

Stress corrosion cracking, pitting, and intergranular stress corrosion may occur in some designs, particularly if free halogens are present.

Fluid properties

Density/viscosity sensitivity (Fig. 15.1)

Multicomponent flows, with abrasive particles; maximum velocity through the tubes should be 6 ft/s (2m/s).

Void fraction effect (Fig. 15.2)

Bubbly flow effect (Fig. 15.3)

Installation

Vertical installation preferred in order to self-purge gas (vapor) for horizontal equalize potential gas (vapor) bubbles by installation.

Some meters' high-pressure loss may lead to cavitation.

Mutual interference

Meters installed in series may experience mutual interference resulting in error. Reduce this effect by decoupling methods shown in Fig. 14.32a, b or by tuning the dynamic characteristic of the transducers by simply shifting the compliance modal mass of one of the transducers.

Pulsation

Significant errors will occur if pulsation frequency at vibratory frequency is characterized by audible knocking noises.

Typical effects (Fig. 15.4)

Vibration sensitivity

Sensitive to inadequate supporting which has a natural frequency within 20% of the operating frequency.

Zero stability

Effect of zero (Fig. 15.5)

Pressure effect general + zero error (Fig. 15.6)

Temperature increase - zero effect (Fig. 15.7)

Sources: Baker (1994), Birker (1989), Frankvoort (1989), Grumski et al. (1984), Hemp et al. (1989), ISO 10790 (1994), Kiel (1991), Wagner (1988).

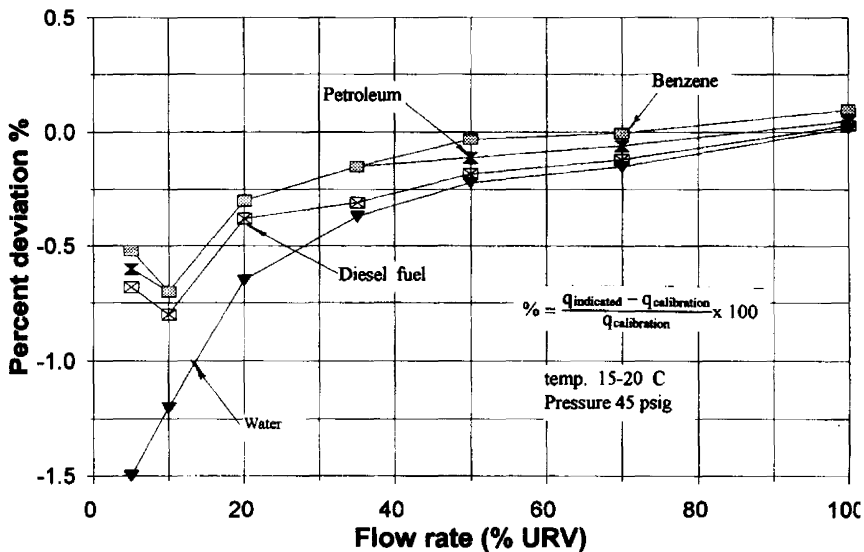
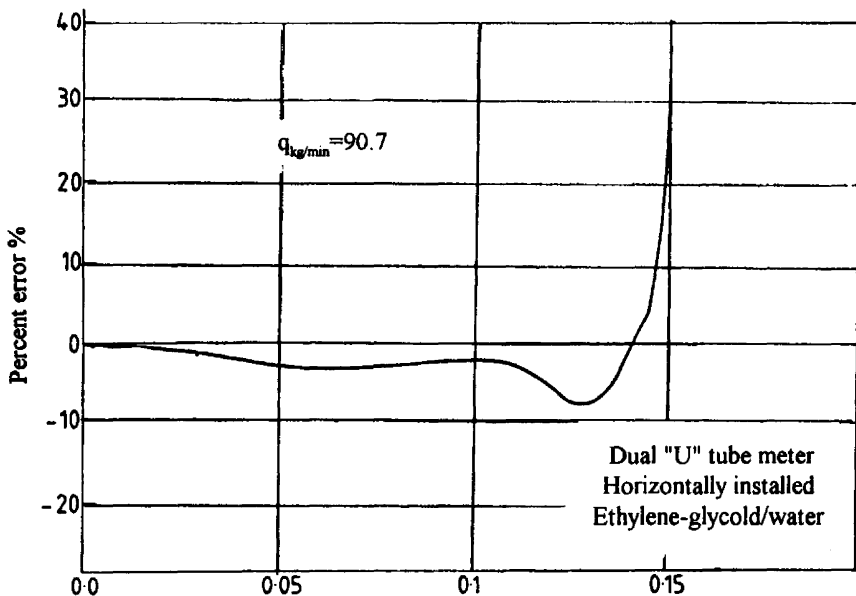


Figure 15.1 Effect of density/viscosity on a Coriolis mass flowmeter.



$$\text{Void fraction} = \frac{\text{air volumetric flow rate}}{\text{liquid volumetric flow rate} + \text{air volumetric flow rate}}$$

Figure 15.2 Effect of two-component flow on a Coriolis mass flowmeter.

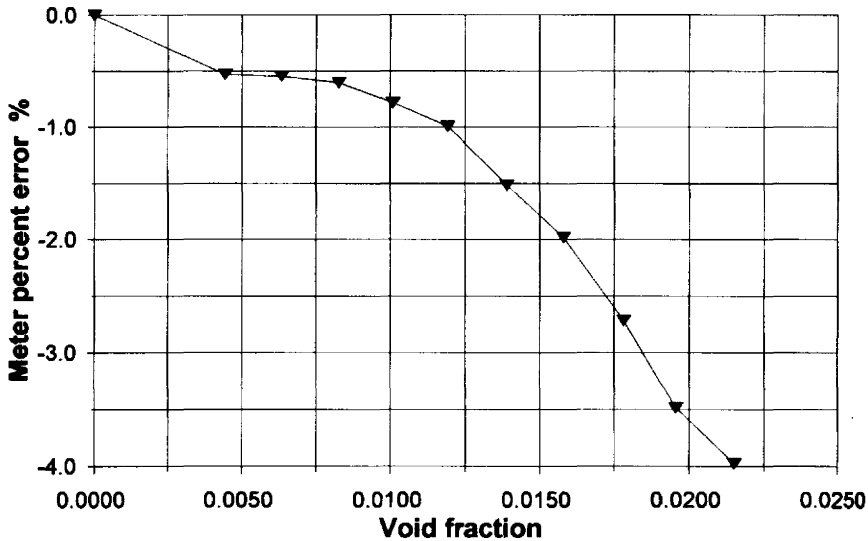
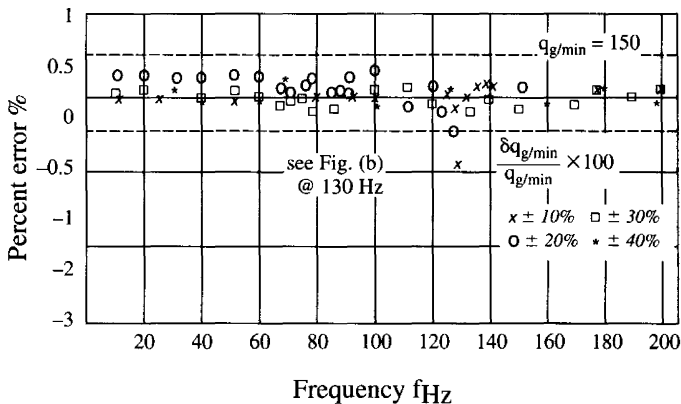
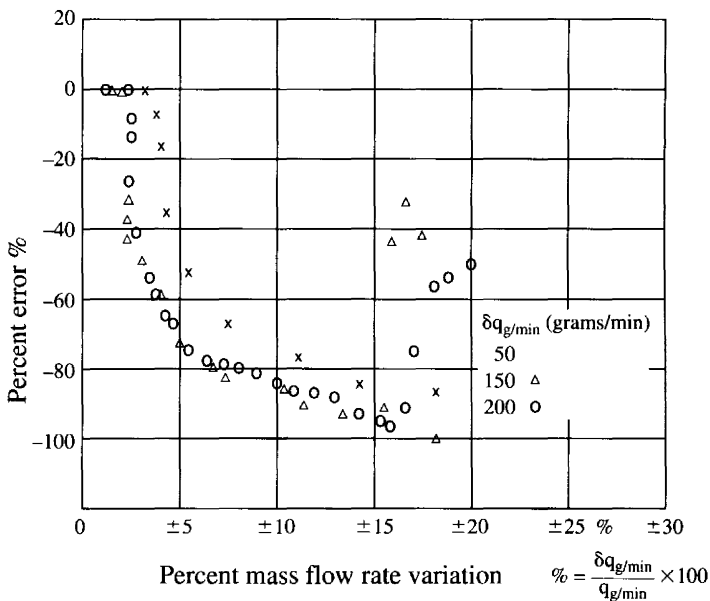


Figure 15.3 Effect of bubbly flow on a Coriolis mass flowmeter.



(a)



(b)

Figure 15.4 Pulsating flow effect on a “U” tube Coriolis mass flowmeter. (a) Normal. (b) At 130 Hz.

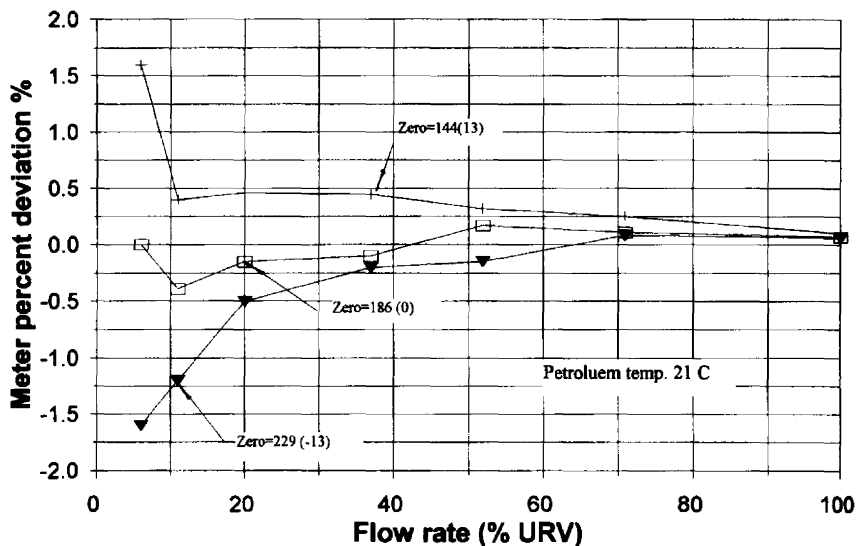


Figure 15.5 Effect of zero on the calibration curve for a Coriolis mass flowmeter.

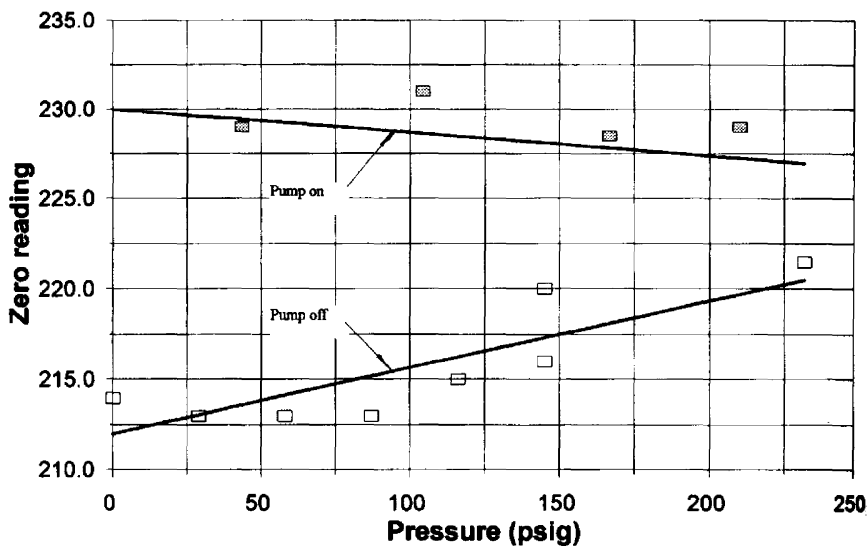


Figure 15.6 Effect of pressure of the zero of a Coriolis mass flowmeter.

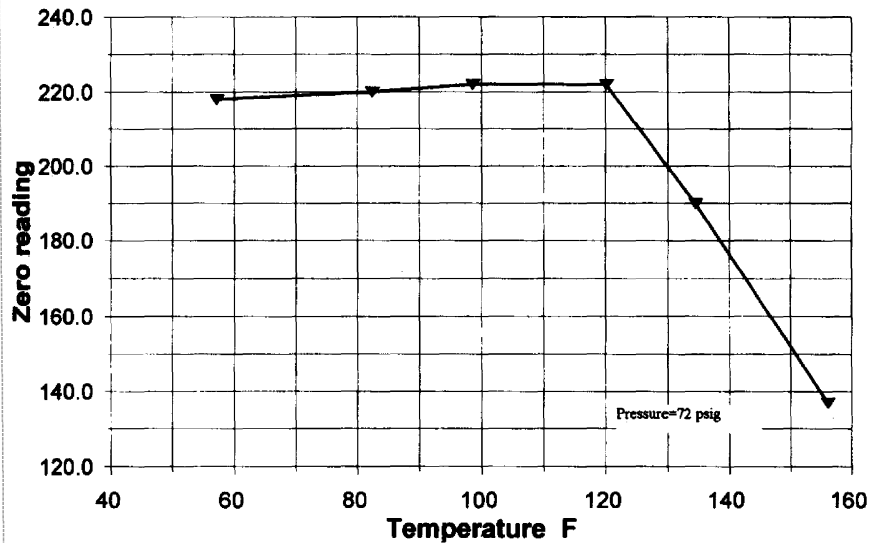


Figure 15.7 Effect of temperature on the zero of a Coriolis mass flowmeter.

TABLE 15.2 Influence Quantities for an Orifice Flowmeter

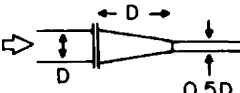
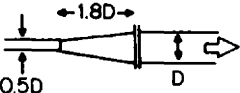
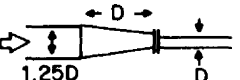
	β	R_D or F_C	Bias†
Piping			
Upstream			
Carrier ring too small			Fig. 15.8a
Roughness (pipe)			
$\epsilon/D = 0.00008$ (80 μin)	$\beta = 0.5$	$R_D = 20,000$	-3
$\epsilon/D = 0.00062$ (620 μin)		$R_D = 20,000$	-2
	$\beta = 0.73$	$R_D > 100,000$	Fig. 15.9
Disturbances‡			
Single elbow			Fig. 15.10
Two or more elbows in same plane			Fig. 15.11
Two elbows in perpendicular planes			Fig. 15.12
With 5-11 PD spacer			Fig. 15.13
Three elbows in successive perpendicular planes			Fig. 15.14
Globe valve and regulator			Fig. 15.15
Tapered sections			
Convergence			
	$\beta = 0.4$	$F_C = 1 \pm 0.005$	± 0.5
	$\beta = 0.7$	$F_C = 0.98$	+2
Divergent			
	$\beta = 0.4$	$F_C = 1.11$	-11
	$\beta = 0.7$	$F_C = 2.0$	-200
Conditioner (upstream)			
Tube bundle (see Fig. 5.33)	$\beta = 0.57$		$6D$ $20D$ $45D$
	$\beta = 0.66$		+0.2 -0.4 -0.1
	$\beta = 0.75$		+1.0 -0.25
			+0.5 -0.75 -0.25
			Fig. 15.16a, b
Zanker (see Fig. 5.33)	$\beta = 0.57$		-0.5 -0.2 0
	$\beta = 0.75$		-0.75 -0.2 0
	$\beta = 0.57$		-0.2 -0.2 0
Sprenkle			
Thermowell (<15 PD upstream and diam. > 0.04D)			+2
Downstream			
Roughness	$\epsilon/D > 0.0003$ (300 μin)		<0.3
Convergence taper			
	$\beta = 0.4$	$F_C = 1 \pm 0.005$	± 0.5
	$\beta = 0.7$	$F_C = 0.98$	+2

TABLE 15.2 Influence Quantities for an Orifice Flowmeter (*Continued*)

	β	R_D or F_C	Bias†
Pressure taps			
Location			Eq. (9.113)
Size			+ bias
Burrs			-30 to +30
Orifice plate			
Edge roundness (r_e = edge radius)			Fig. 15.17
Maximum reported value after service			-2.5
Upstream surface finish $\epsilon/d > 0.001$ (1000 μin)			-3.5
Deformed plate			
1/4 in (6 mm) concave, using unbent diameter d			-10
Fully bent $>1/4$ in (>6 mm), using unbent diameter d			-18
Correcting for diameter d_{bent}			-4
Beveled plate installed backwards (use conic $C = 0.73$)			-18
Thick orifice ($2 \times$ correct thickness)	$\beta = 0.2$		-1
	$\beta < 0.7$		+1
Bore eccentric to pipe bore (3% D)			Fig. 15.18
Max. error eccentricity toward taps	$\beta = 0.42$		< -0.25
	$\beta = 0.52$		-0.5
	$\beta = 0.63$		-0.75
	$\beta = 0.73$		-1.5
Deposits upstream			To -50
Vibration (60 Hz)			+20 to +250
Noise. Acoustic noise test on a $D = 600$ -mm orifice meter in natural gas at 50 bar			
170 dBA reduces C by 0.5% ($\beta = 0.4$)($D + D/2$) and -0.4 for flange taps			
if dBA < 145 , max. variation $\pm 0.15\%$			

†Positive bias indicates meter is reading high, discharge coefficient is lower than with described condition: $B_C = 100(C - C_{\text{cond}})/C_{\text{cond}}$, C = reference coefficient, C_{cond} = coefficient with described condition.

‡ F_C shown in figures is a flow-rate multiplying factor. $q_{\text{true}} = C_{\text{cond}}/C(q_{\text{ind}}) = F_C(q_{\text{ind}})$ $B_C = 1/F_C - 1 \approx 1 - F_C$

Sources: Starrett (1965), Mottram and Spencer (1983), Miller (1988), Shell (1985), Norman et al. (1995).

TABLE 15.3 Influence Quantities for Nozzles and Venturis

	Bias B_C †	
	Venturi	Nozzle
Piping		
Upstream		
Carrier ring to small (step less than $0.1D$)	NA	Fig. 15.8b
Eccentric or small gasket between ring and flange	NA	-60 to +60
Disturbances‡		
Single elbow	Fig. 15.19	
Two elbows in perpendicular planes	Fig. 15.20a, b	
Reducer	Fig. 15.21a	
Enlargement	Fig. 15.21b	
Roughness	To +4	To +4
Downstream		
Roughness	-Bias	Negligible
Meter		
Radius of cone to cylindrical throat incorrect	To +2%	NA
Piezometer irregular and corroded	+1	NA
Entrance surface rusty	To +2	To +2
Oil coating	Fig. 15.22	
Surface finish	Fig. 15.23	
Cylindrical throat lightly coated	To +0.5	To +0.5
Step in cylindrical throat ($<0.003d$)	To -1	To -1
Slight outward downstream taper in throat	To -1	To -1
Pressure taps		
Size	+Bias	+Bias
Burrs	-30 to +30	-30 to +30

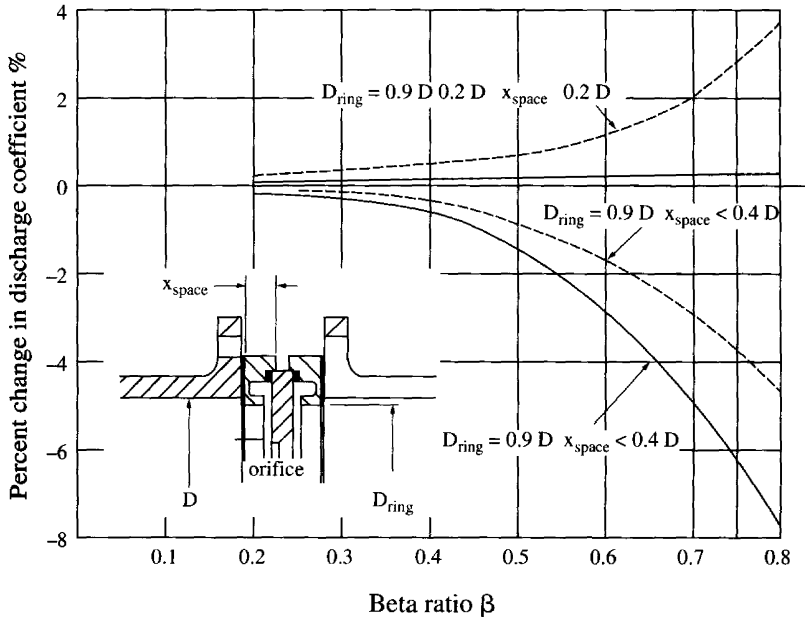
†Positive bias indicates meter is reading high, discharge coefficient is lower than with described condition. $B_C = 100(C - C_{\text{cond}})/C_{\text{cond}}$, C = reference coefficient, C_{cond} = coefficient with described condition.

‡ F_c shown in figures is a flow-rate multiplying factor.

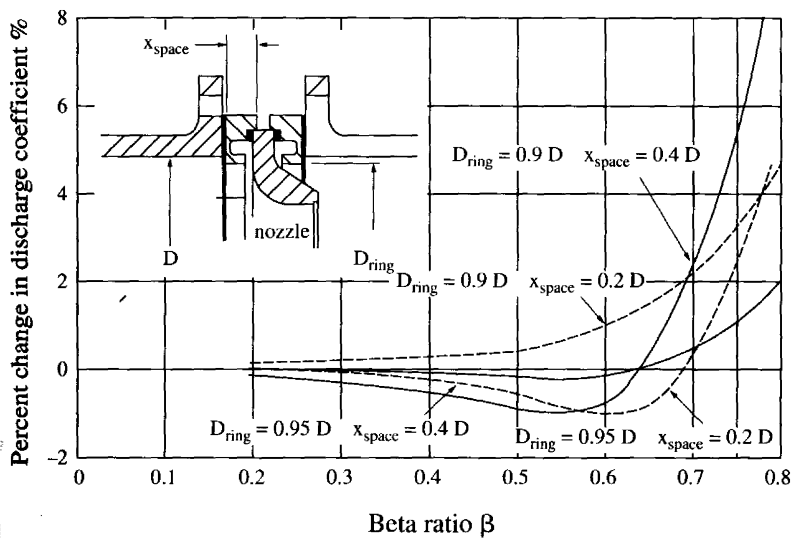
$$q_{\text{true}} = C_{\text{cond}}/C(q_{\text{ind}}) = F_c(q_{\text{ind}}) \quad B_c = 1/F_c - 1 \approx 1 - F_c$$

$$q_{\text{true}} = C_{\text{cond}}/C(q_{\text{ind}}) = F_c(q_{\text{ind}}) \quad B_c = 1/F_c - 1 \approx 1 - F_c$$

Sources: Jorissen (1950), Starrett (1965), Miller (1988), Shell (1985), Hobbs and Humphreys (1990), Hutton (1954, 1974).



(a)



(b)

Figure 15.8 Effect of carrier ring. (a) Orifice. (b) nozzle.

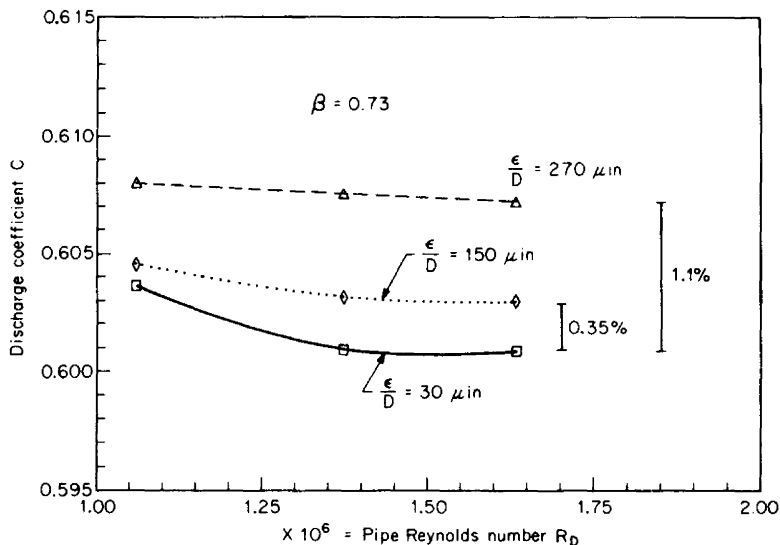


Figure 15.9 Effect of pipe roughness on an orifice flowmeter. (Source GRI 1987.)

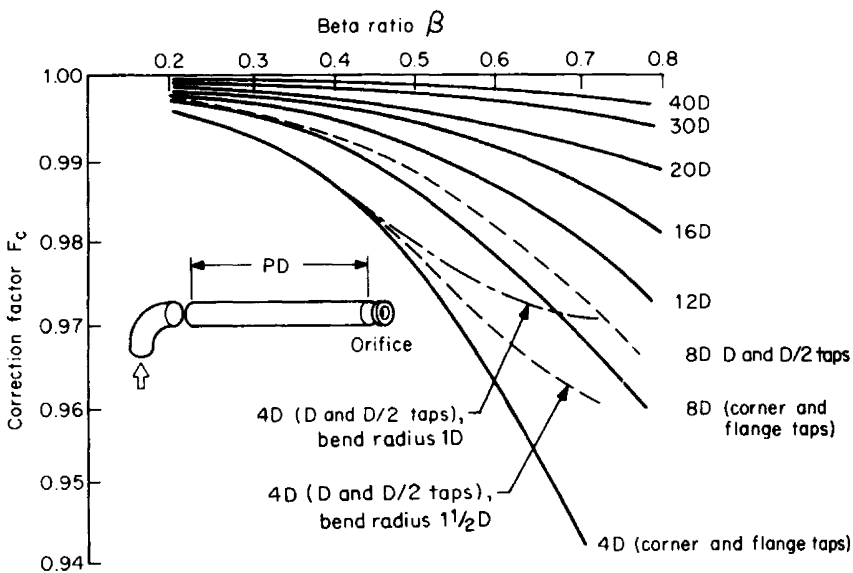


Figure 15.10 Single elbow upstream of an orifice flowmeter.

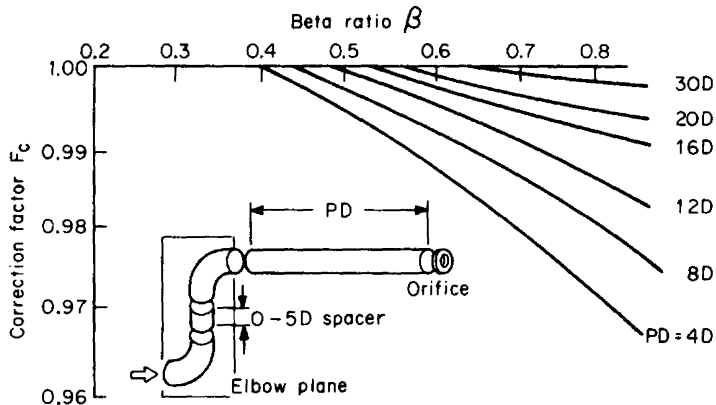
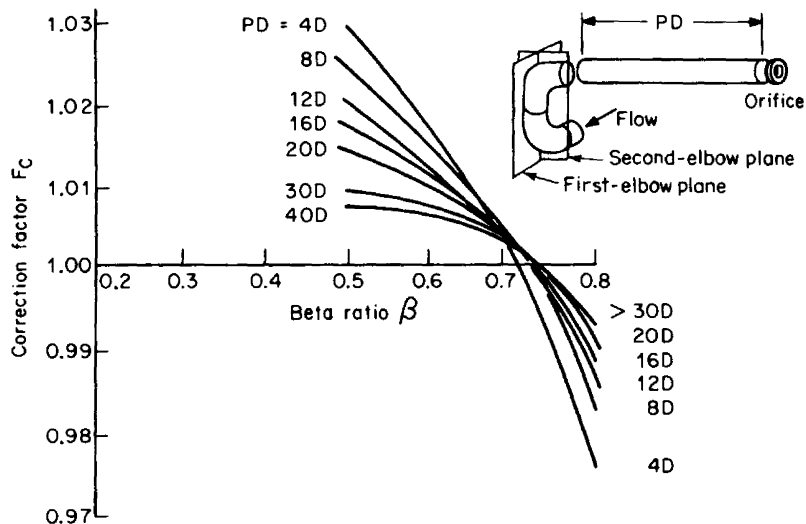
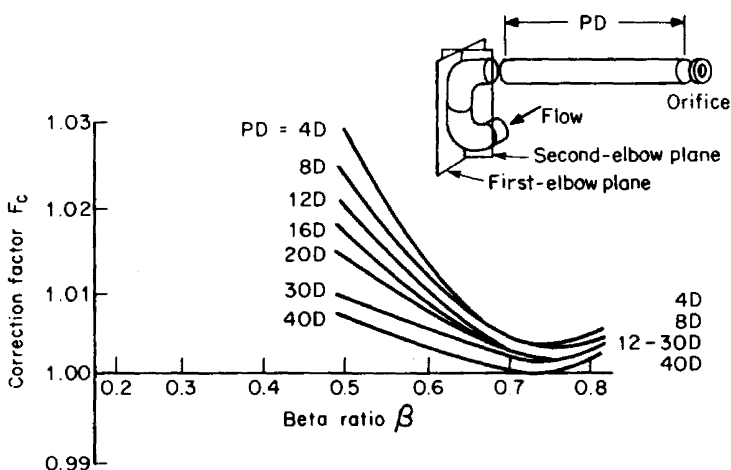


Figure 15.11 Two elbows in the same plane upstream of an orifice flowmeter.



(a)



(b)

Figure 15.12 Two elbows in mutually perpendicular planes upstream of an orifice flowmeter. (a) Flange and corner taps. (b) D and D/2 taps.

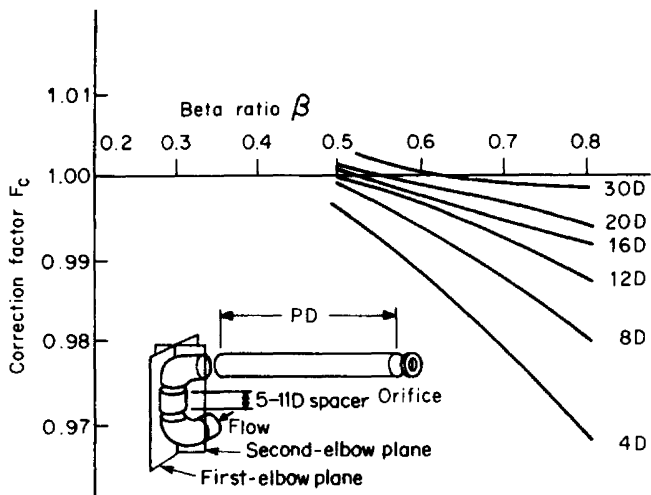


Figure 15.13 Two elbows in mutually perpendicular planes with a 5- to 11-PD spacer upstream of an orifice flowmeter.

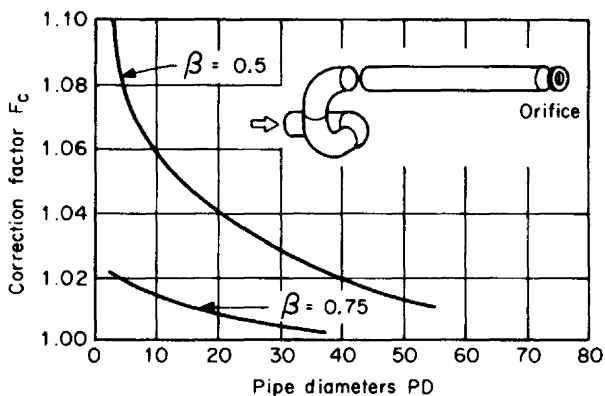


Figure 15.14 Three elbows in successive perpendicular planes upstream of an orifice flowmeter.

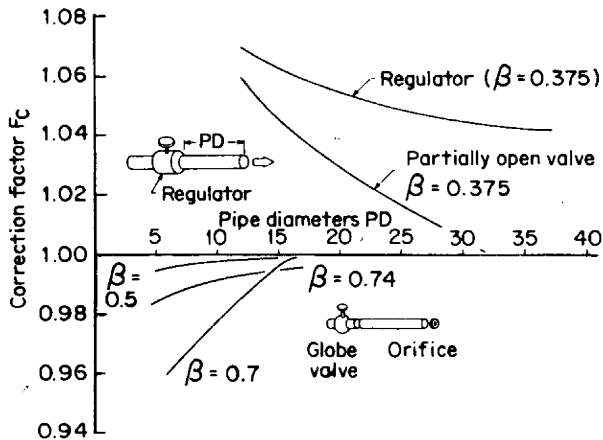
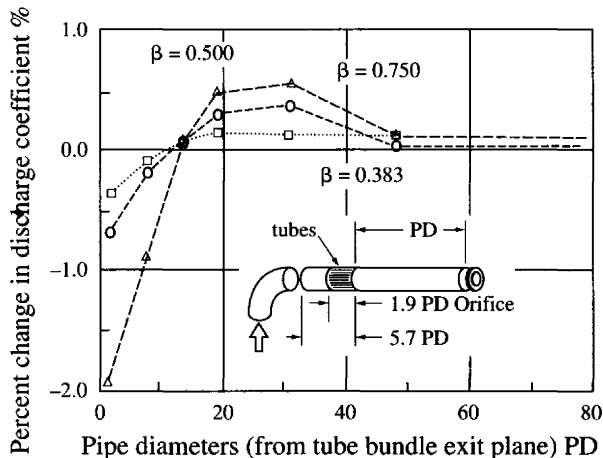
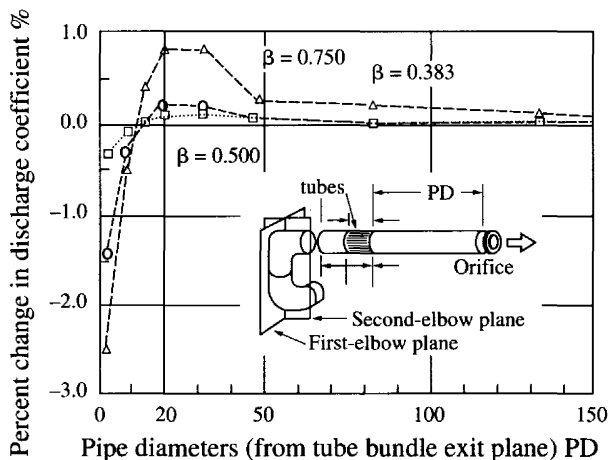


Figure 15.15 Globe valve and regulator upstream of an orifice flowmeter.



(a)



(b)

Figure 15.16 Effect of flow straighteners on an orifice flowmeter. (a) Single elbow. (b) Multiple elbows in different planes.

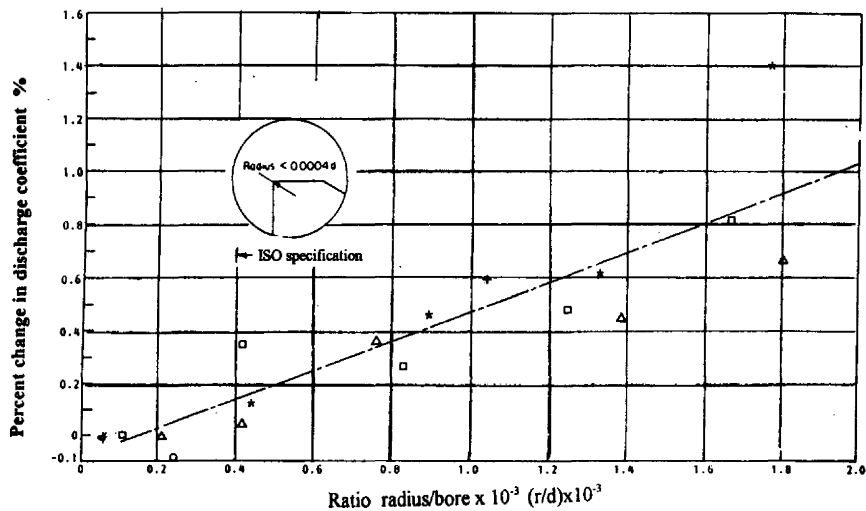


Figure 15.17 Effect of edge sharpness on the discharge coefficient.

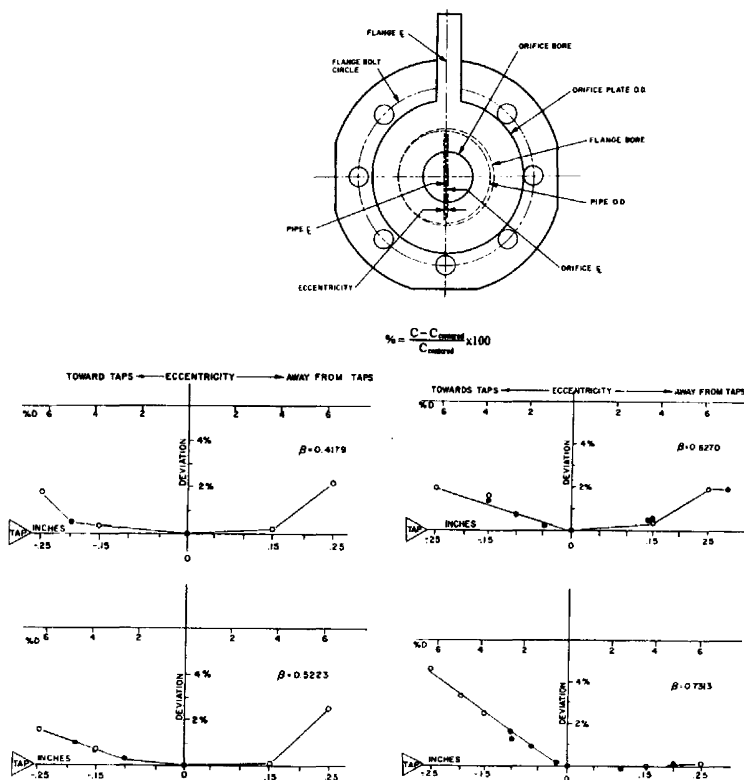


Figure 15.18 Eccentricity effect on the orifice discharge coefficient.

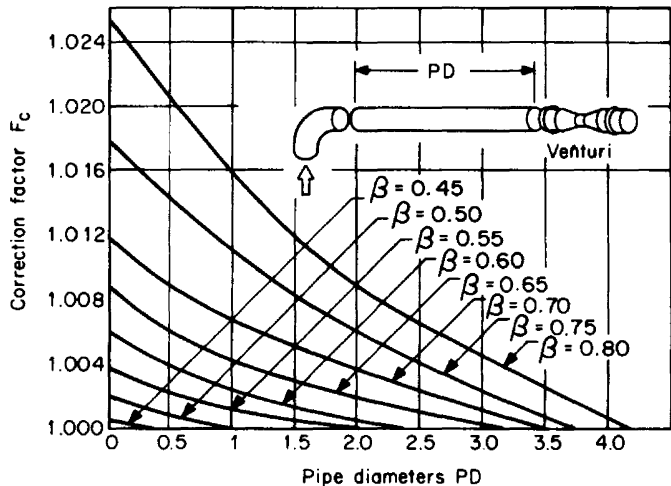


Figure 15.19 Single elbow upstream of a venturi flowmeter.

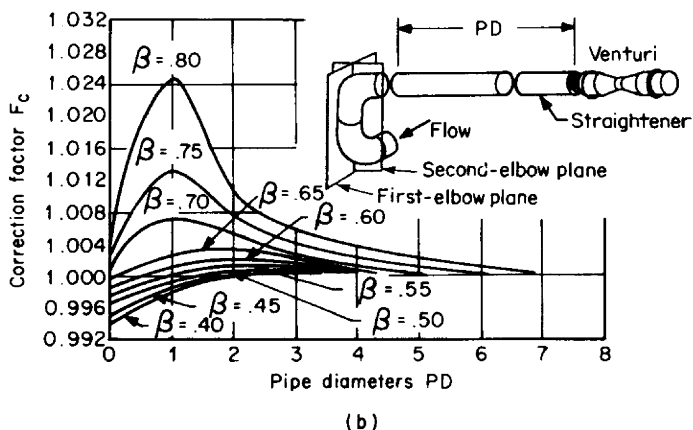
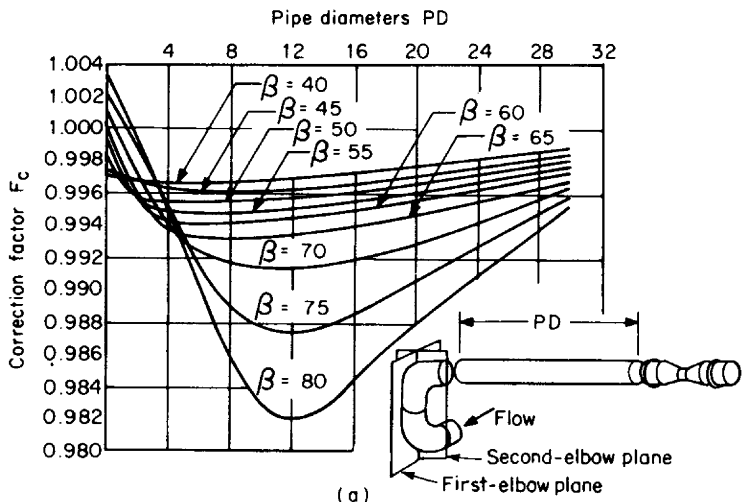


Figure 15.20 Two elbows in perpendicular planes upstream of a venturi flowmeter. (a) Without straightener. (b) With straightener.

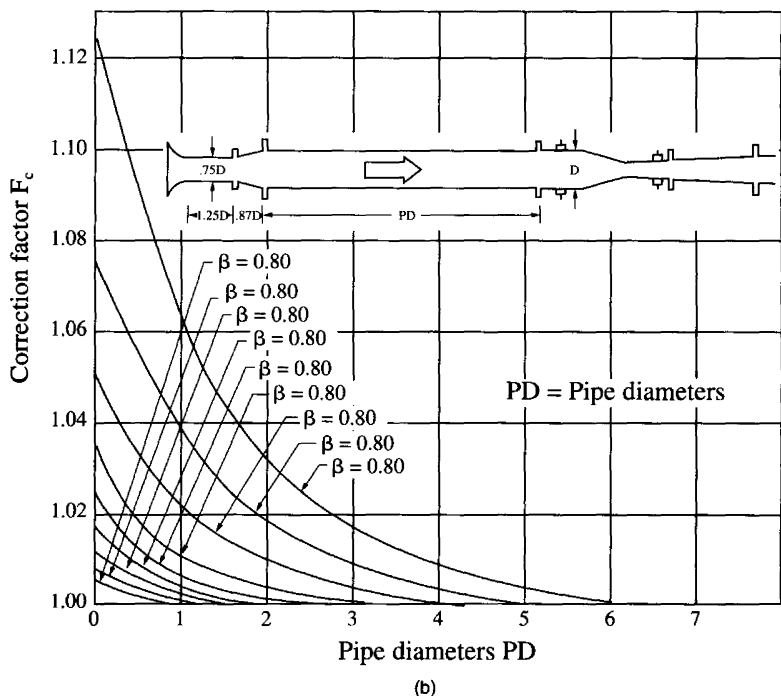
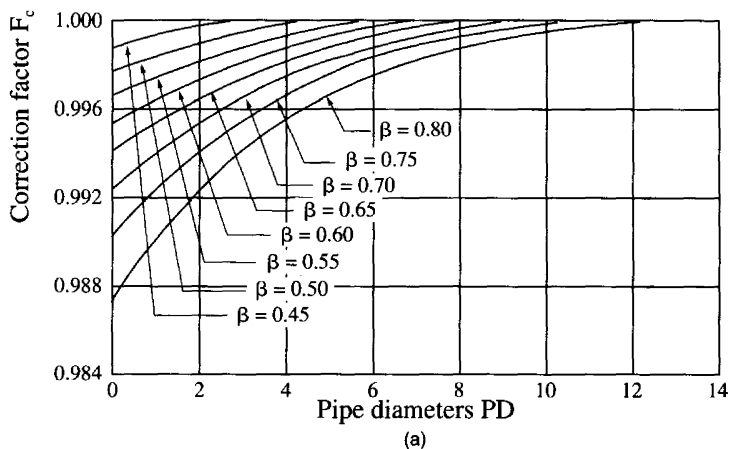
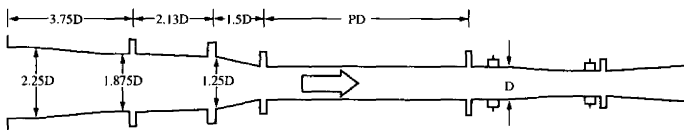


Figure 15.21 Upstream piping effect on venturi. (a) Reducer. (b) Enlargement.

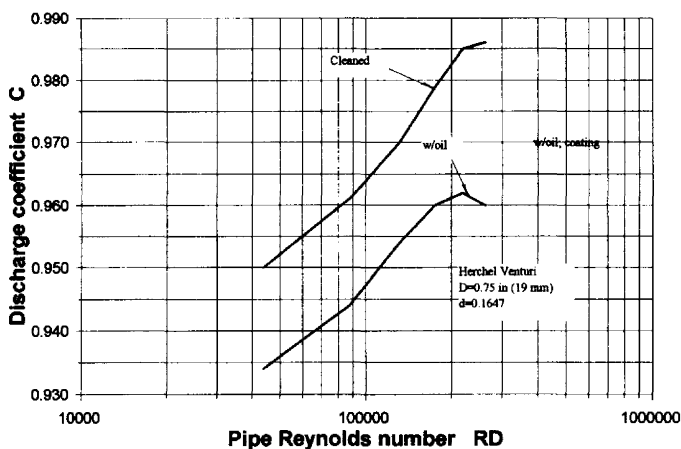


Figure 15.22 Venturi coefficient change with usage. (a) 36 in. (b) 12 in.

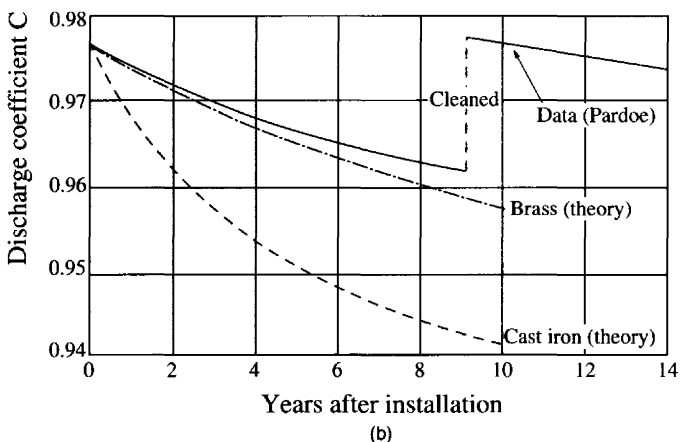
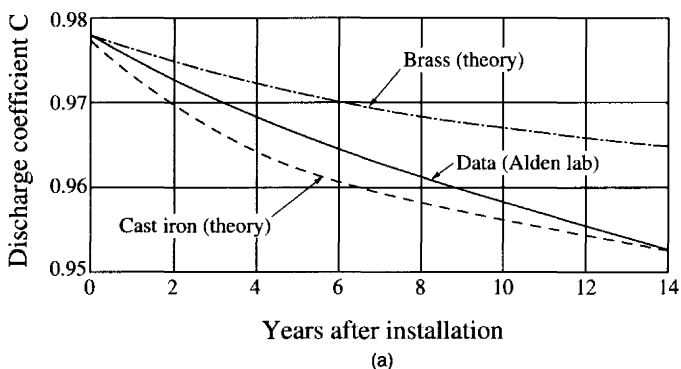


Figure 15.23 Effect of oil coating on a venturi.

TABLE 15.4 Influence Quantities on Magnetic Flowmeters**Deposits**

- Conductive or magnetic properties (rust) or other fluid-born impurities can coat flowtube and change meter sensitivity and meter zero; generally meters read low.

Installation

Single elbow	Fig. 15.24
Two elbows in reverse flow—no spacer	Fig. 15.25
Two elbows, same plane, reverse flow—5D spacer	Fig. 15.26
Two elbows, same plane—no spacer	Fig. 15.27
Two elbows, same plane—5D spacer	Fig. 15.28
Two elbows, perpendicular planes—no spacer	Fig. 15.29
Two elbows, perpendicular planes—5D spacer	Fig. 15.30
Two elbows, perpendicular planes—no spacer	Fig. 15.31
Two elbows, perpendicular planes—5D spacer	Fig. 15.32
Reducer and an enlarger	Fig. 15.33

Multicomponent flows

- Install vertically to minimize nonhomogeneous mixing of components

Air/water mixture

Oil/water Reads low

Magnetic slurries Reads high

Fig. 15.34
<6.5%**Potential bias conditions (generally negligible)**

Cable length from primary to secondary

Thermal expansion

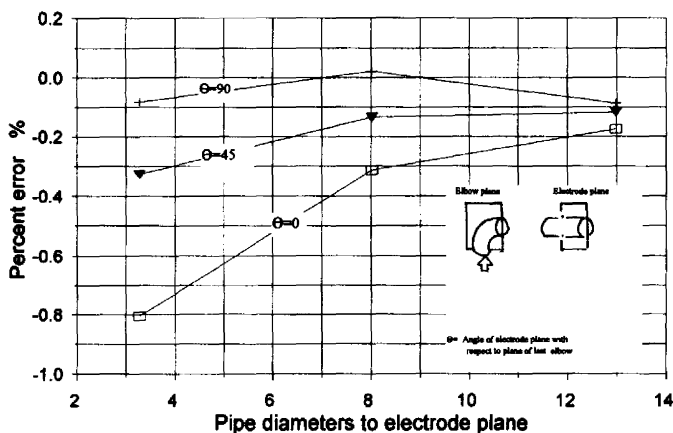
Conductivity

Power supply condition (harmonic, voltage variations, etc.)

Pipe protection (cathodic)

Vibration

Sources: Baker and Deacon (1983), Haltunen (1990), Mattingly et al. (1987), Mattingly and Yeh (1991), Tsuchida et al. (1982).

**Figure 15.24** Effect of single elbow on a magnetic flowmeter.

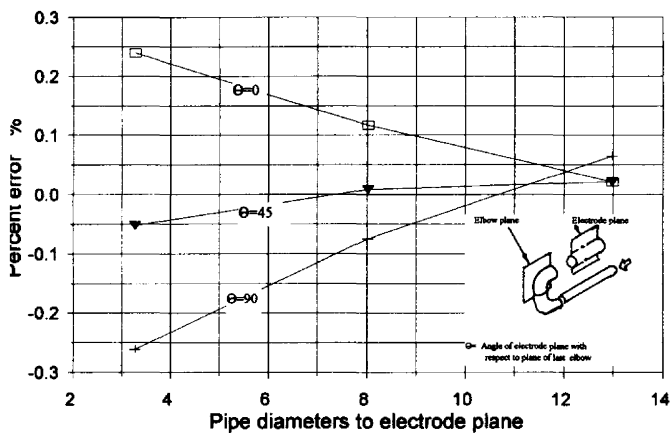


Figure 15.25 Effect of two elbows in same plane in a reverse flow on a magnetic flowmeter-no spacer.

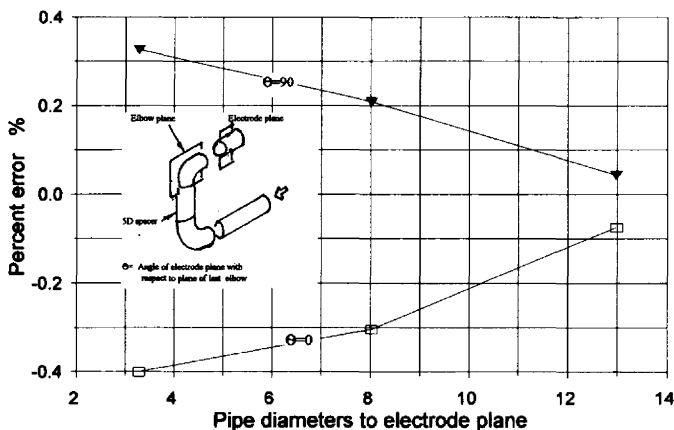


Figure 15.26 Effect of two elbows in same plane in a reverse flow on a magnetic flowmeter-5D spacer.

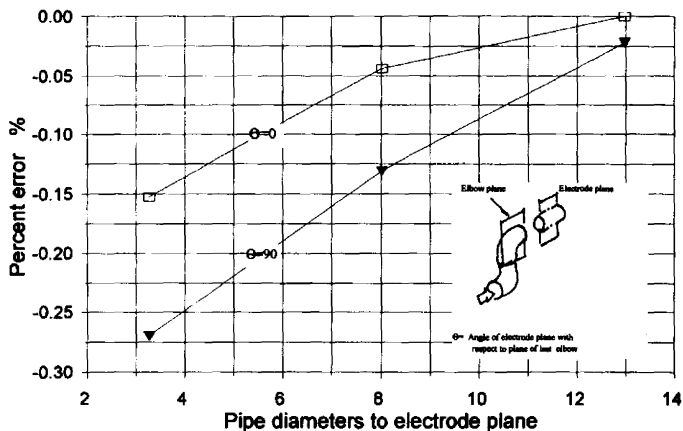


Figure 15.27 Effect of two elbows in same plane flow on a magnetic flowmeter-no spacer.

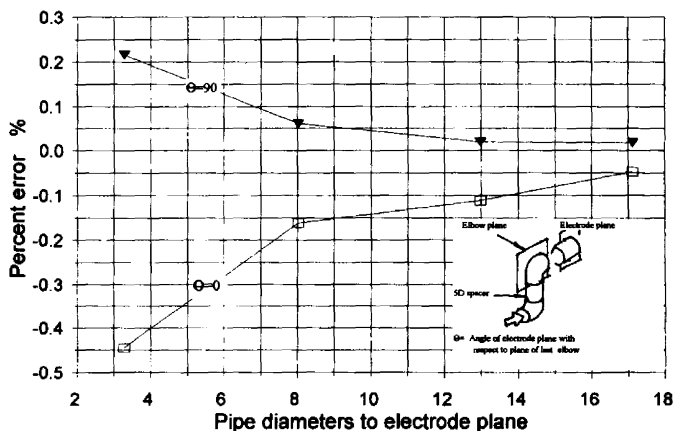


Figure 15.28 Effect of two elbows in same plane on a magnetic flowmeter-5D spacer.

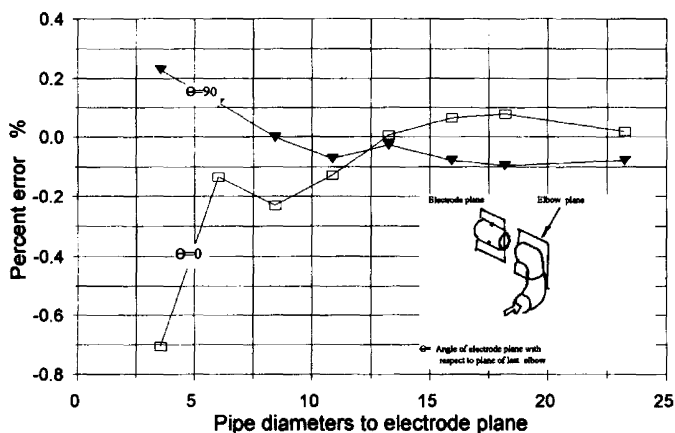


Figure 15.29 Effect of two elbows in perpendicular planes on a magnetic flowmeter-no spacer.

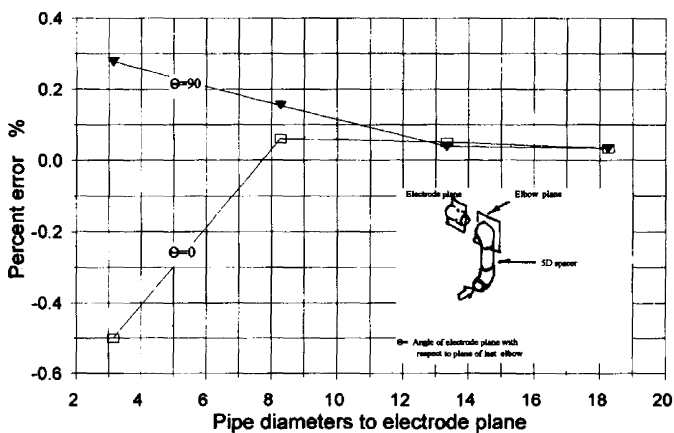


Figure 15.30 Effect of two elbows in perpendicular planes on a magnetic flowmeter-5D spacer.

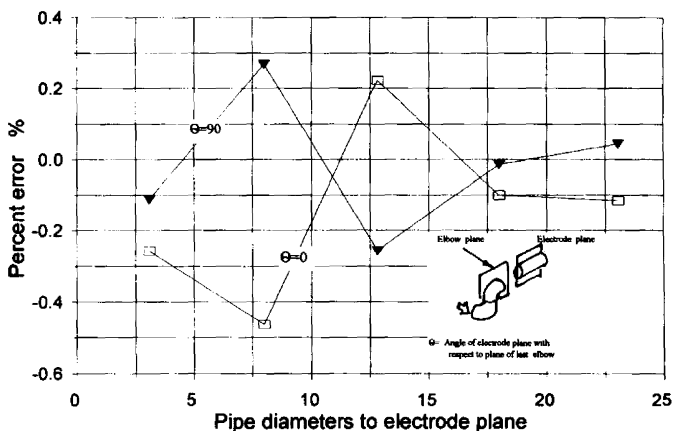


Figure 15.31 Effect of two elbows in perpendicular planes on a magnetic flowmeter-no spacer.

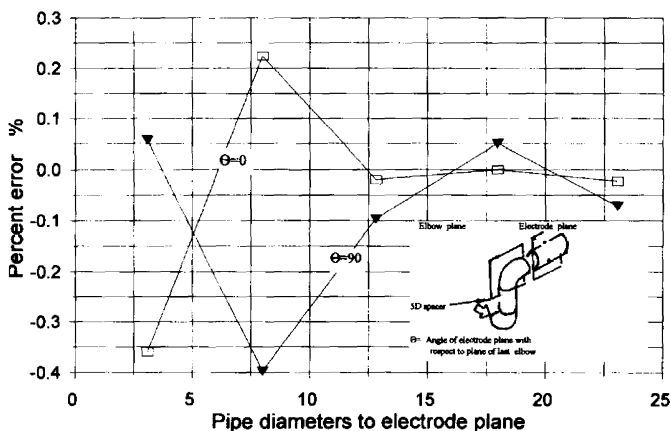


Figure 15.32 Effect of two elbows in perpendicular planes on a magnetic flowmeter-5D spacer.

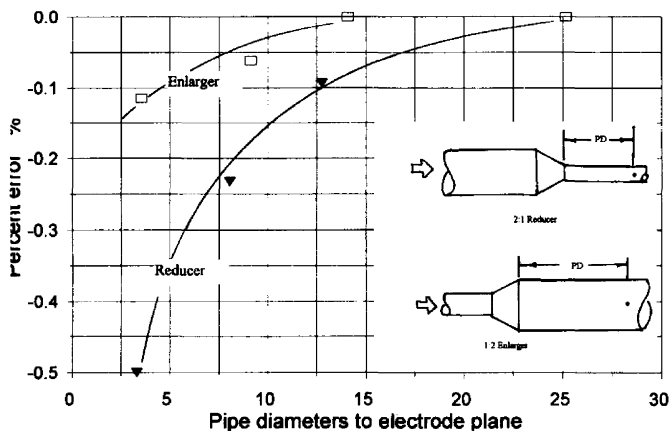


Figure 15.33 Effect of a reducer and an enlarger on a magnetic flowmeter.

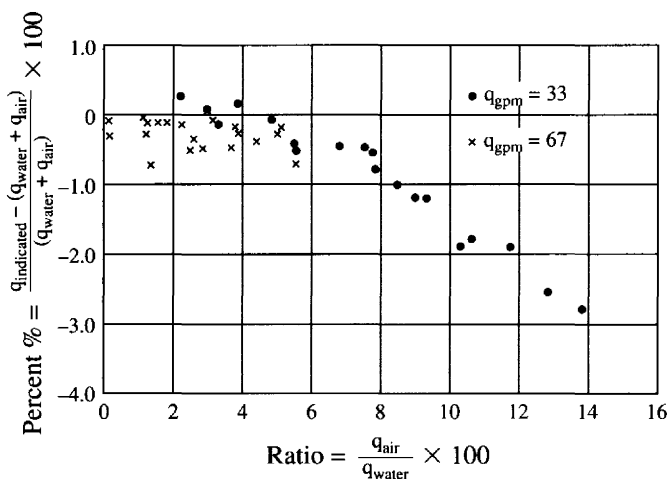


Figure 15.34 Air/water mixture effect on a 2-inch magnetic flowmeter.

TABLE 15.5 Influence Quantities on a Positive-Displacement Flowmeter

Precautions

Filter fluid if necessary; susceptible to entrained particles with differential pressure measurement across filter as check.

Pipeline stress can damage meter.

Sufficient flow to prevent starving meter at maximum flow.

Irreparable damage caused by overspeeding due to steam cleaning.

Provide flow controller to avoid overspeeding.

Install meters at pump discharge.

Wear results in underregistration.

Pumping

Pressure

Meter will be irreparable due to overspeeding on gas flow applications.

Pulsating flow

Pulsating gas flow can damage meter. Fig. 15.35

Pressure source ideally centrifugal or head tank.

Bias errors

Liquid flows will overregister due to gas bubbles.

Viscosity (fuel oil/gasoline/propane) 1 to 100 cP + 1.2%.

Sources: Jeannon (1975), Baker and Morris (1985).

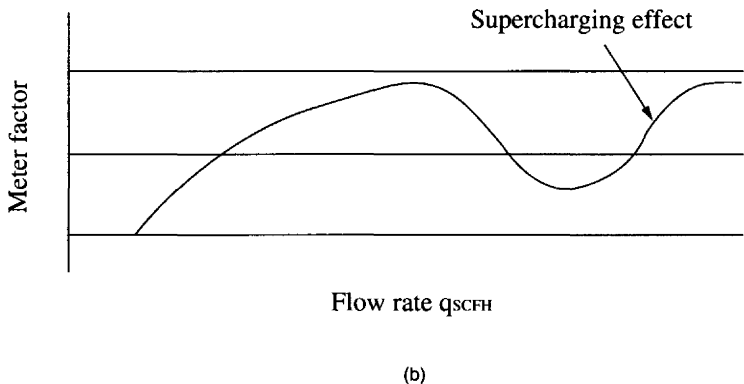
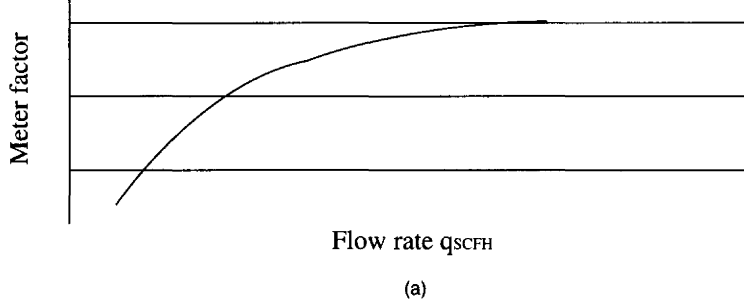


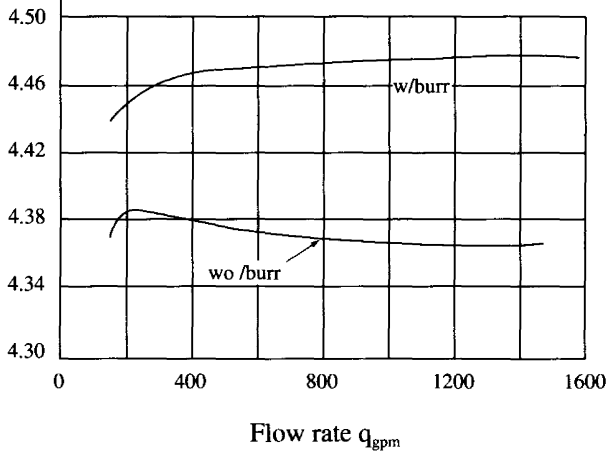
Figure 15.35 Effect of pulsating gas flow on a positive displacement meter. (a) Steady flow. (b) Pulsating flow.

TABLE 15.6 Influence Quantities on Turbine Flowmeters

Design	
Burrs (blades)	Fig. 15.36
Surface finish/blades/bearings	Fig. 15.37
Installation	
Protruding upstream gasket	Fig. 15.38
Double elbows in different planes	Fig. 15.39
Single elbow	Fig. 15.40
Orifice	Fig. 15.40
Tube bundle upstream	Fig. 15.41
Tube bundle with swirl angle changes	Fig. 15.42
Orientation:	Negligible (<0.1%)
Precautions	
Filter fluid with differential pressure across to check filter	
Unshielded bearing filter fluid (max. velocity 2 m/s) with dp to check plugging	
LPG low lubricity; calibrate every 2 months	
Not recommended for multicomponent fluids	
Two phase/multicomponent poor performance even with small quantities of bubbles for <15% air approximately 5%; if rotor speed 200 to 300 radians/s, 10 to 50%	
Caution with LPG; may vaporize if pipes unlagged	
Pumping	
Pulsating Flow	
Pulsating flow	Fig. 15.44
Pulsating flow overestimate	Up to 2%
Bias errors	
Fluid	
Gas bubbles cause overregistration.	
Viscosity change of 1 to 100 cP change may shift K-factor by 1.2%.	
Electronics	
Spurious noise or pulses may be caused by adjacent equipment.	
Stability	
Long-term stability test run of 9000 h increased by 0.86%.	
K-factor change with time	Fig. 15.43
Test with liquid ammonia	<0.1% 416 days

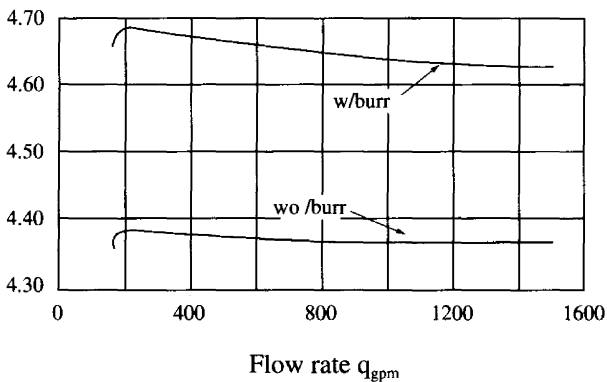
Sources: Akaike et al. (1978), Baker and Deacon (1983), Millington et al. (1986), Nicholl, (1975), Van Der Kam and Van Dellen (1991).

K-Factor



(a)

K-Factor



(b)

Figure 15.36 Effect of burrs on turbine meter blades. (a) Small burrs. (b) Large burrs.

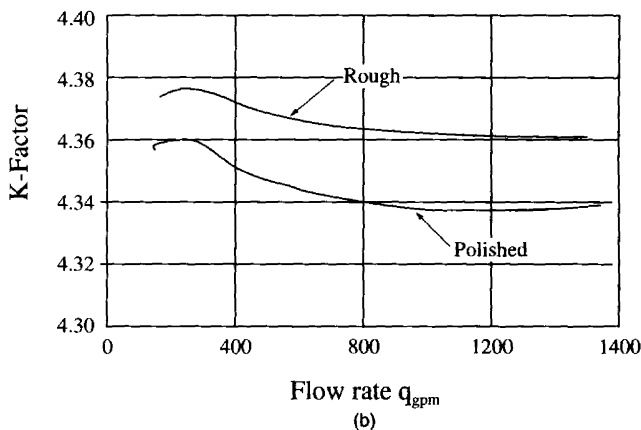
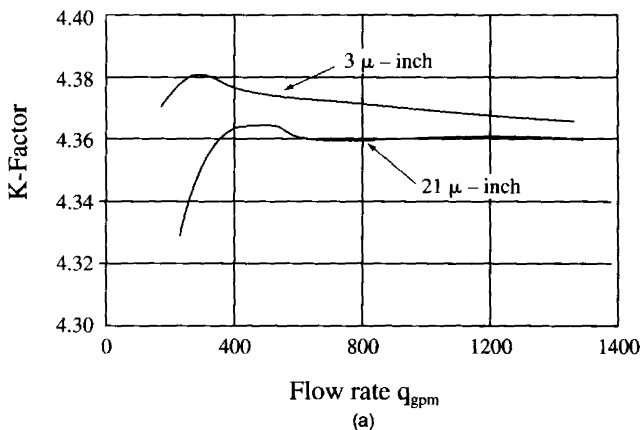


Figure 15.37 Surface finish effects. (a) Blade finish. (b) Rotor bearing.

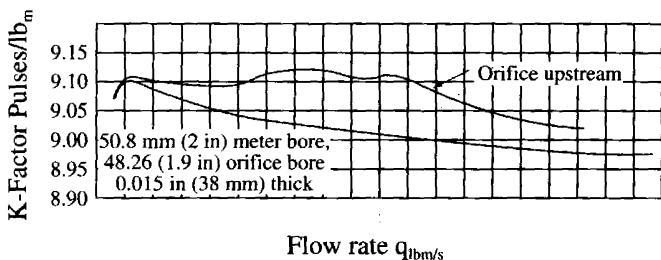


Figure 15.38 Simulated effect of a protruding upstream gasket on a liquid turbine flowmeter.

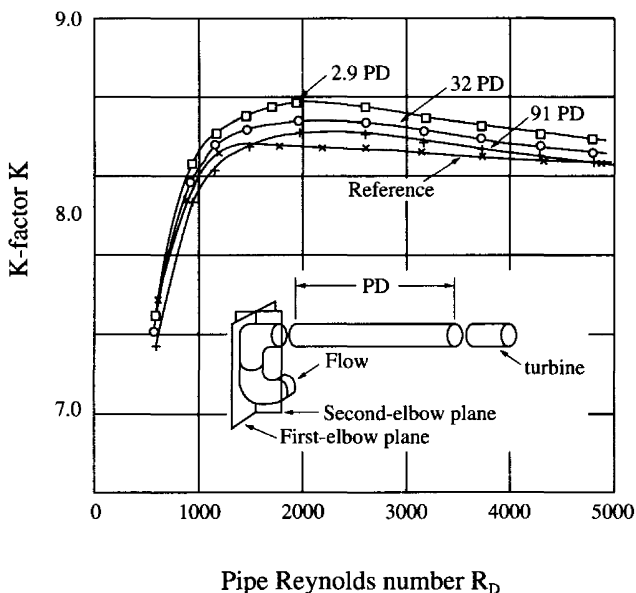


Figure 15.39 Effect of double elbows on a turbine flowmeter.

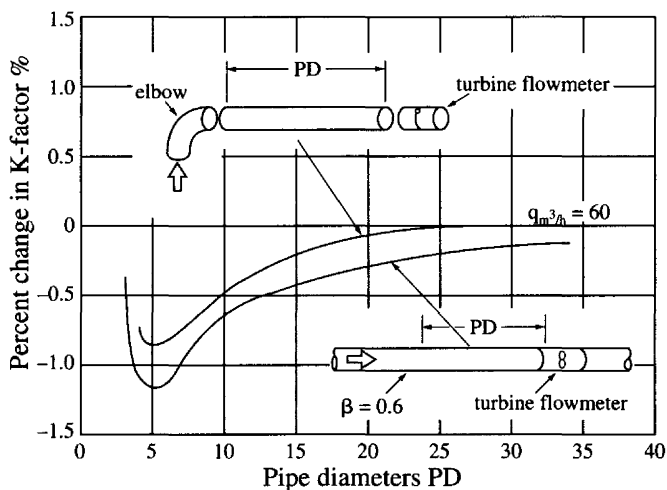


Figure 15.40 Upstream disturbance effect on a turbine flowmeter. (a) Elbow. (b) Orifice.

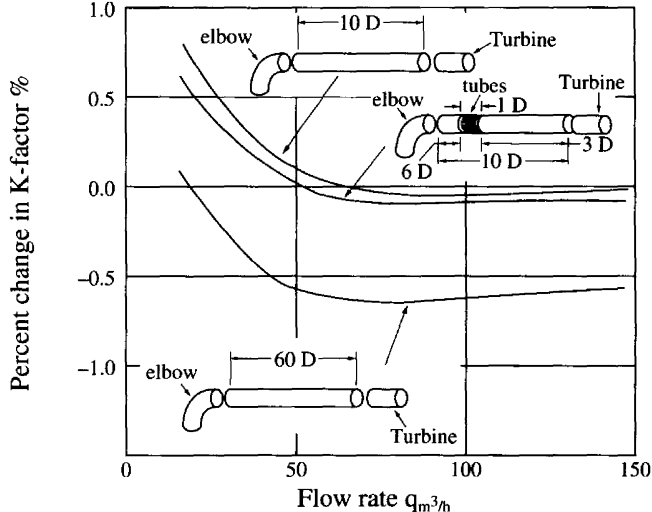


Figure 15.41 Effect of tube bundle on a turbine flowmeter.

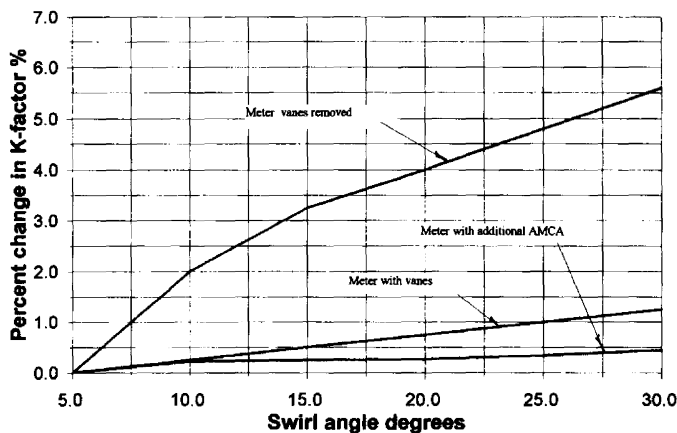


Figure 15.42 Effect of straighteners on a turbine flowmeter with swirl angle.

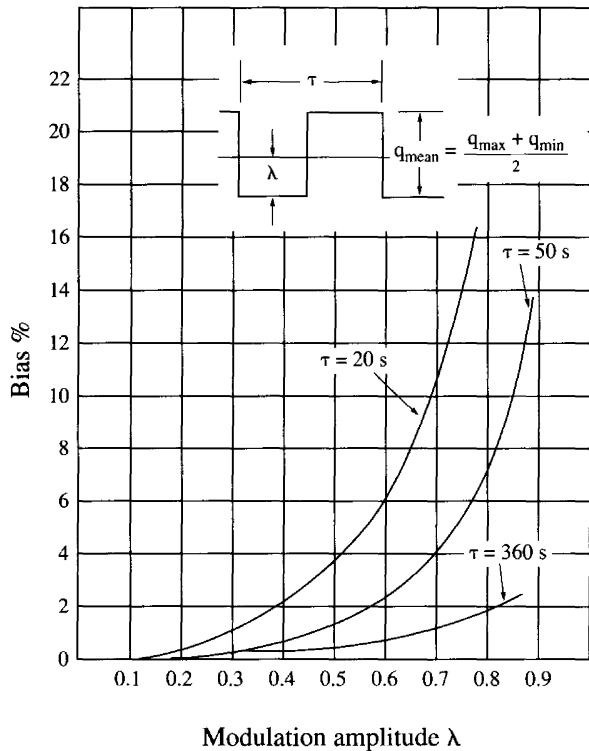
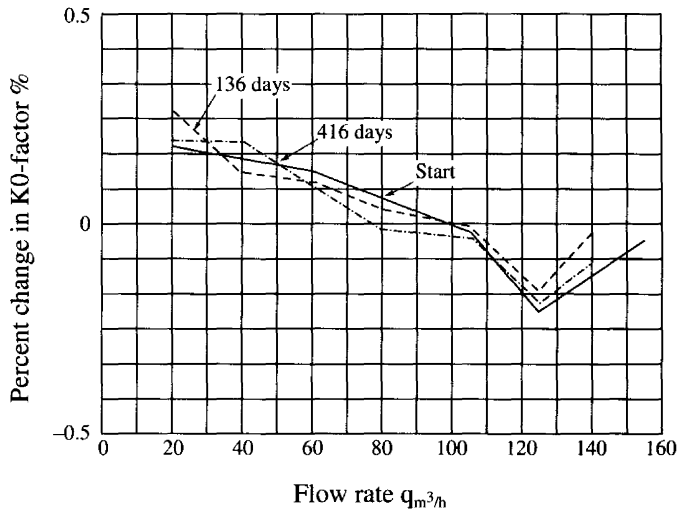
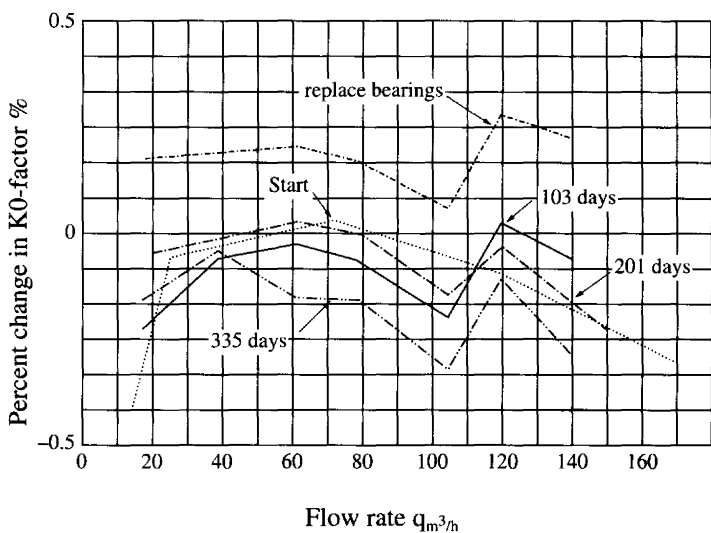


Figure 15.43 Pulsating flow effect on a 4-in turbine flowmeter.



(a)



(b)

Figure 15.44 3 1/2-in (80 mm) turbine K-factor change with time. (a) Meter 1. (b) Meter 2.

TABLE 15.7 Influence Quantities on Ultrasonic Flowmeters**Design**

Pipe thickness effect (clamp-on)

Fig. 15.45

Installation

Acoustic noise from pumps or other machinery may interfere with measurement.

Cavitation noise introduces a high-intensity wide-band acoustic noise.

Particles or other deposits on wetted detectors will reduce sensitivity and lead to failure.

Single elbow (single path)

Fig. 15.46

Single elbow (dual path)

Fig. 15.47

Double elbow differing planes (single path)

Fig. 15.48

Double elbow differing planes (dual path)

Fig. 15.49

Contraction (single path)

Fig. 15.50

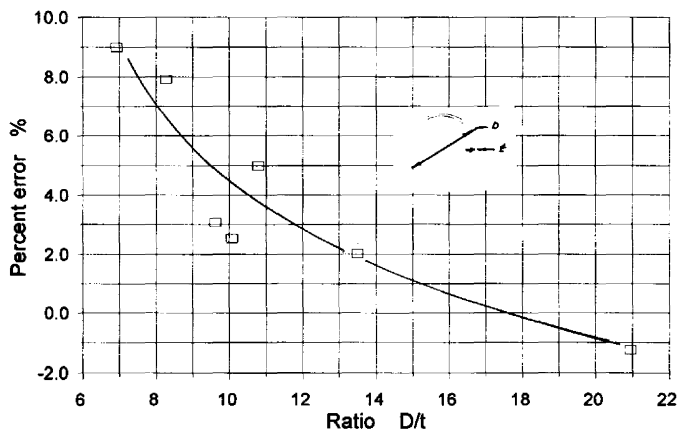
Expander

Fig. 15.51

Multicomponent fluids

Water/air flow (vertically installed)

Fig. 15.52

Sources: Halttunen (1990), Heritage (1989).**Figure 15.45** Effect of pipe thickness on a clamp-on ultrasonic flowmeter.

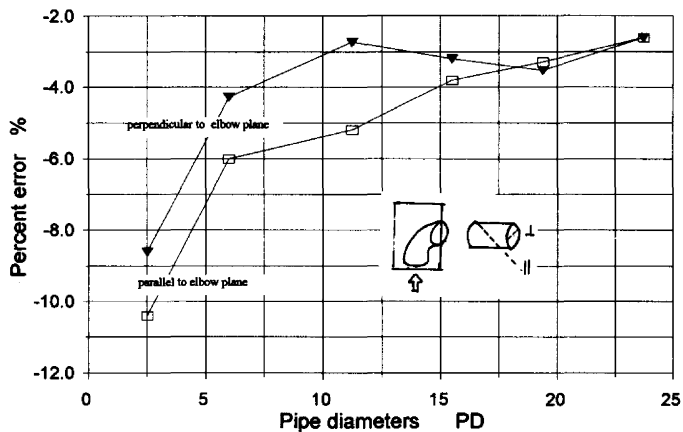


Figure 15.46 Effect of a single elbow on a single path ultrasonic flowmeter.

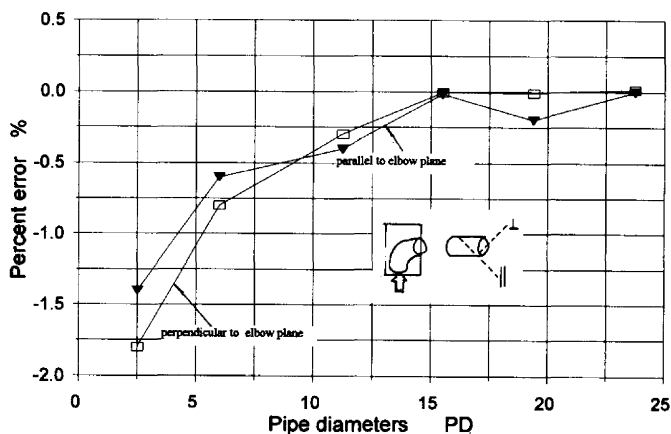


Figure 15.47 Effect of a single elbow on a dual path ultrasonic flowmeter.

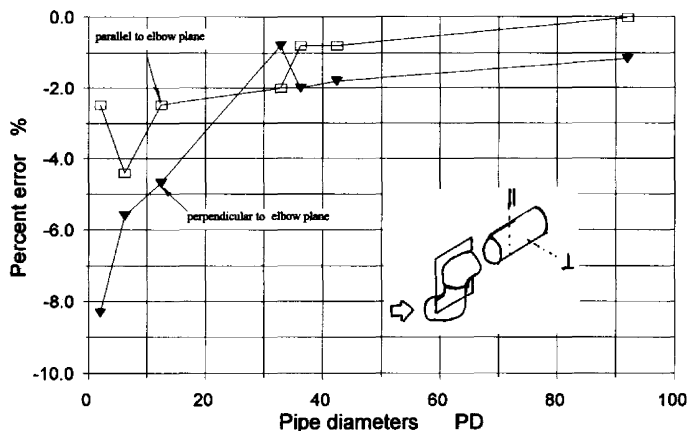


Figure 15.48 Effect of two elbows in perpendicular planes on a single path ultrasonic flowmeter.

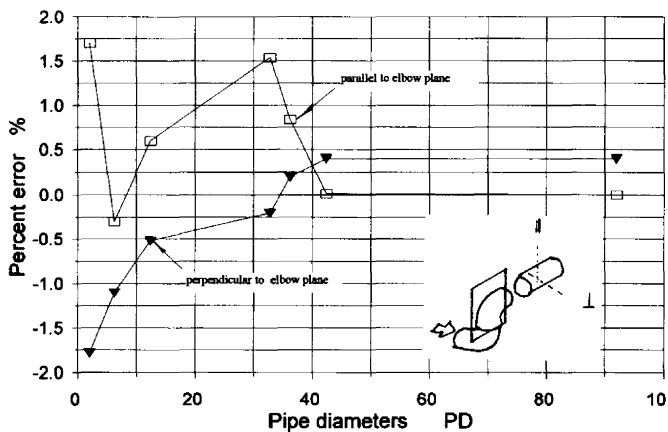


Figure 15.49 Effect of two elbows in perpendicular planes on a dual path ultrasonic flowmeter.

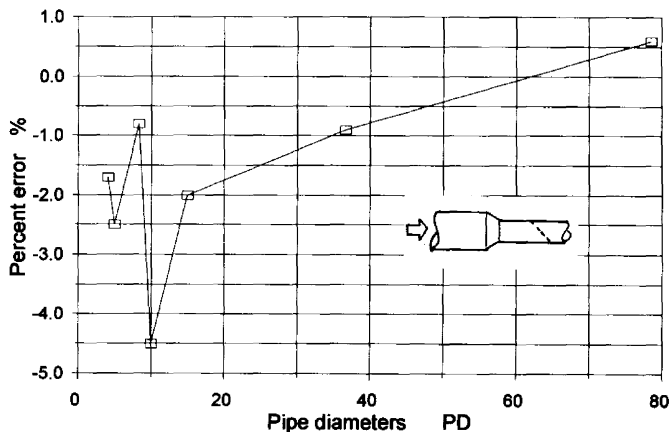


Figure 15.50 Effect of a contraction on a single path ultrasonic flowmeter.

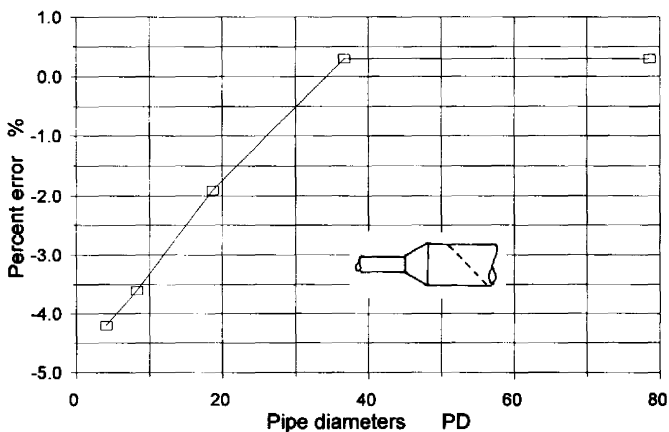


Figure 15.51 Effect of an expander on a single path ultrasonic flowmeter.

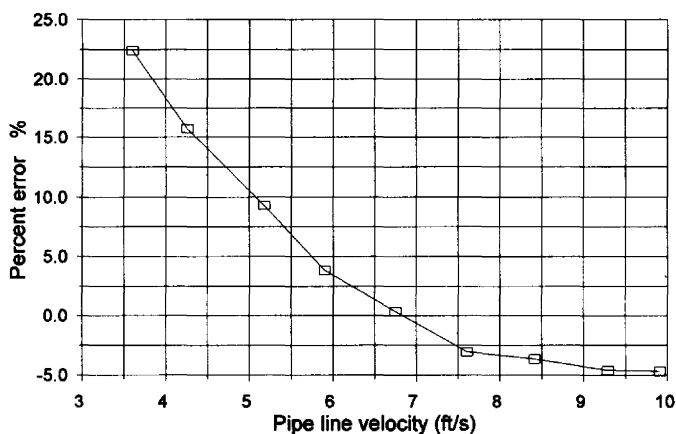


Figure 15.52 Effect of water/air flow on a vertically installed ultrasonic flowmeter.

TABLE 15.8 Influence Quantities on Vortex Flowmeters

Design	
Pressure profile	Fig. 15.53
Installation	
Upstream pipe roughness	Fig. 15.54
Upstream pipe mismatch on wafer body	Fig. 15.55
Single elbow	Fig. 15.56
Double elbows (planar)	Fig. 15.57
Double elbows in perpendicular planes	Fig. 15.58
Reducer	Fig. 15.59
Expander	Fig. 15.60
Pumping	
Pulsating flow	Fig. 15.61
Bias Errors	
Fluid	
Wet (quality) steam correction	Fig. 15.62
Pressure tap location	
Bias error for tap location	Fig. 15.63
Stability	
Test results	Fig. 15.64
Vibration (detector design dependent)	
Repeated hammer blows may introduce spurious pulses.	
5–2 kHz may introduce spurious pulses at zero/or low flow.	

Sources: Baker and Deacon (1983), Hayward and Jelffs (1986), Mottram (1991), Takamoto, et al. (1993).

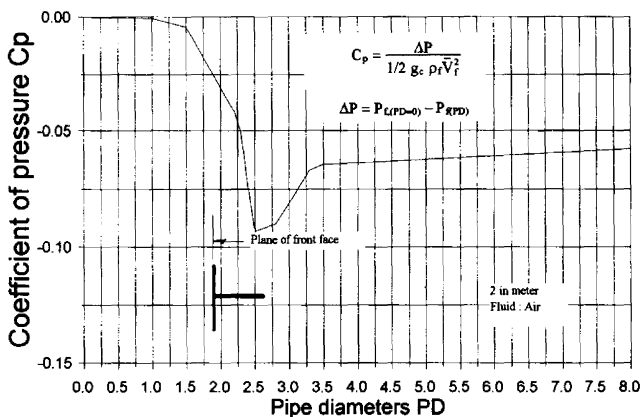
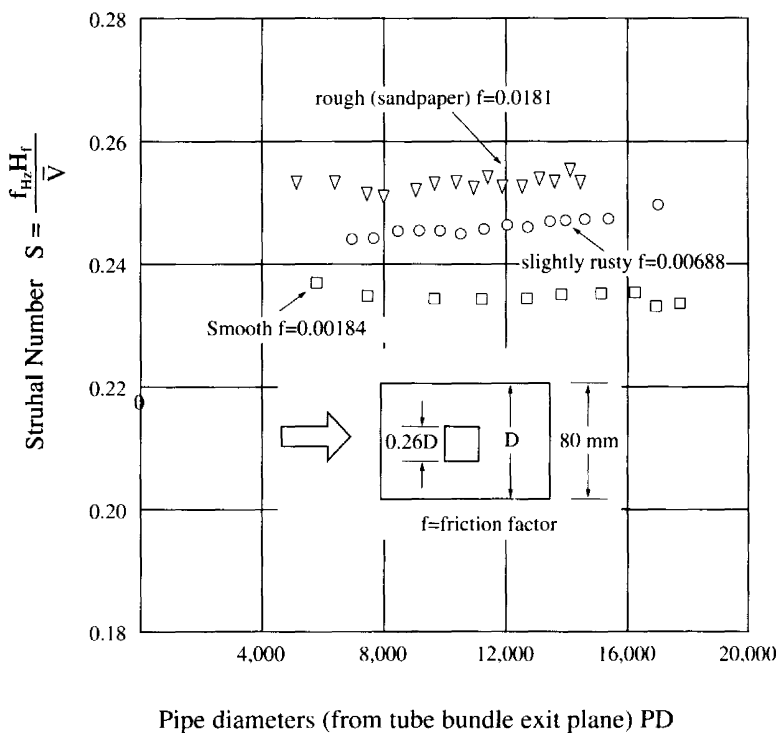


Figure 15.53 Pressure profile along a "T"-shape vortex flowmeter.



Pipe diameters (from tube bundle exit plane) PD

Figure 15.54 Effect of pipe roughness on a 3-in vortex flowmeter.

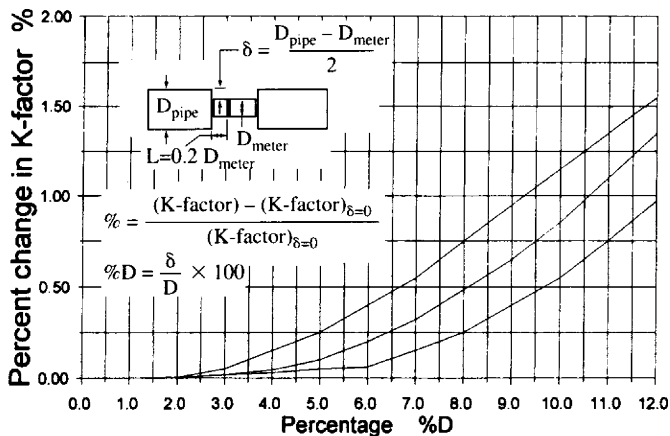


Figure 15.55 Effect of pipe mismatch on a vortex flowmeter.

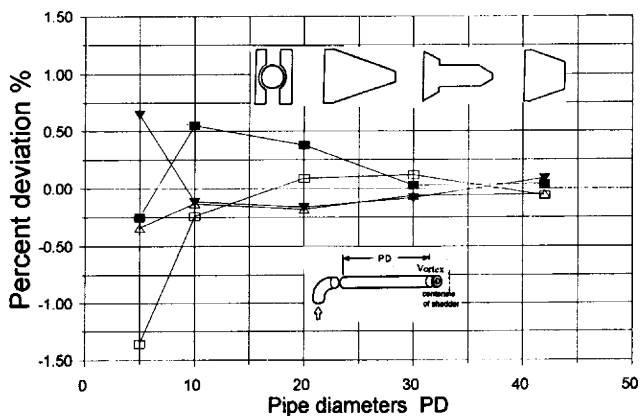


Figure 15.56 Effect of a single upstream elbow on four different vortex flowmeters.

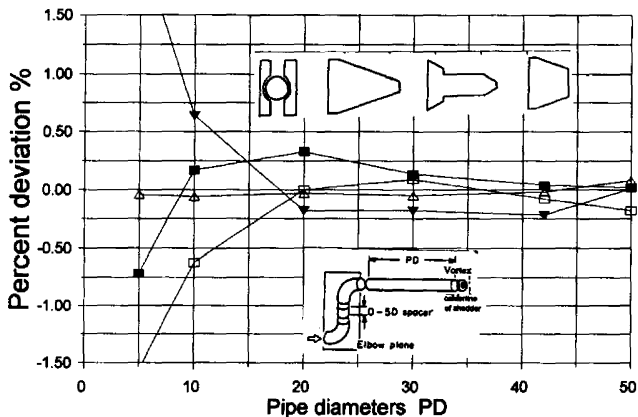


Figure 15.57 Effect of double elbows in different planes on four different vortex flowmeters.

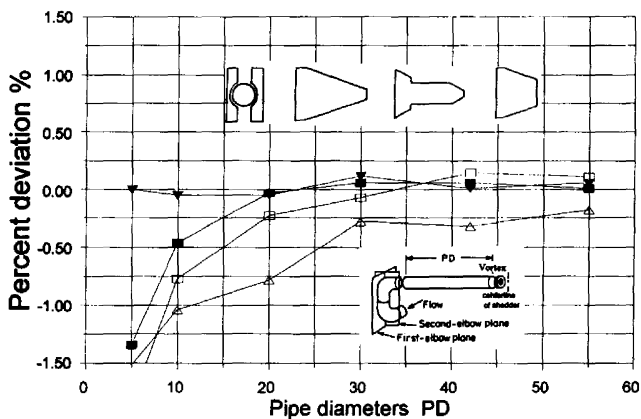


Figure 15.58 Effect of double elbows in same plane on four vortex flowmeter designs.

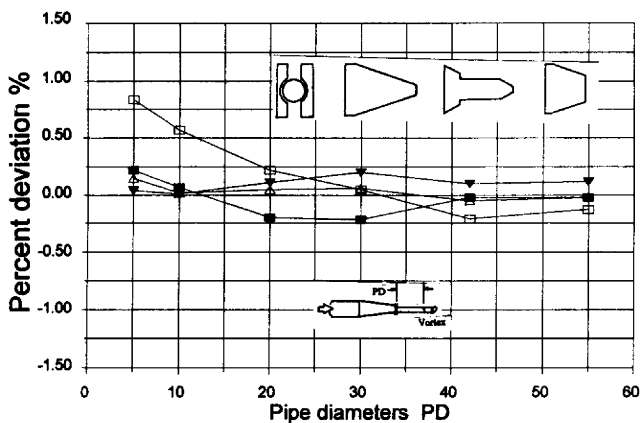


Figure 15.59 Effect of a reducer upstream on four different vortex flowmeters.

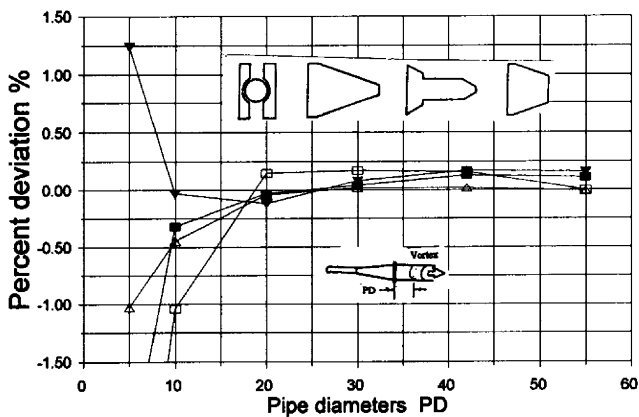


Figure 15.60 Effect of an expander on four different vortex flowmeters.

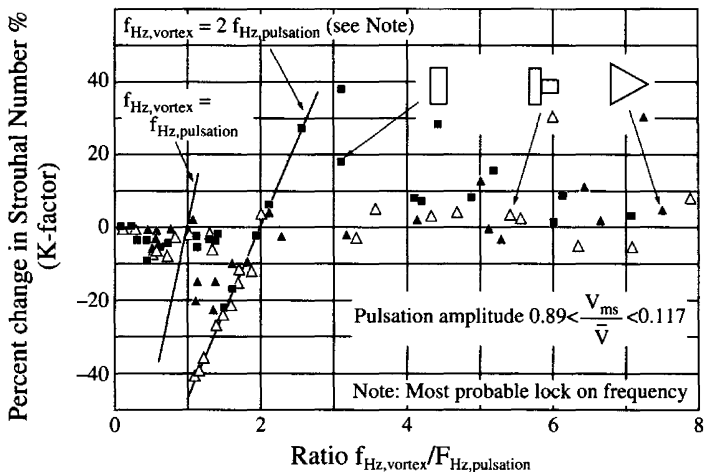


Figure 15.61 Pulsating flow effect on vortex flowmeters.

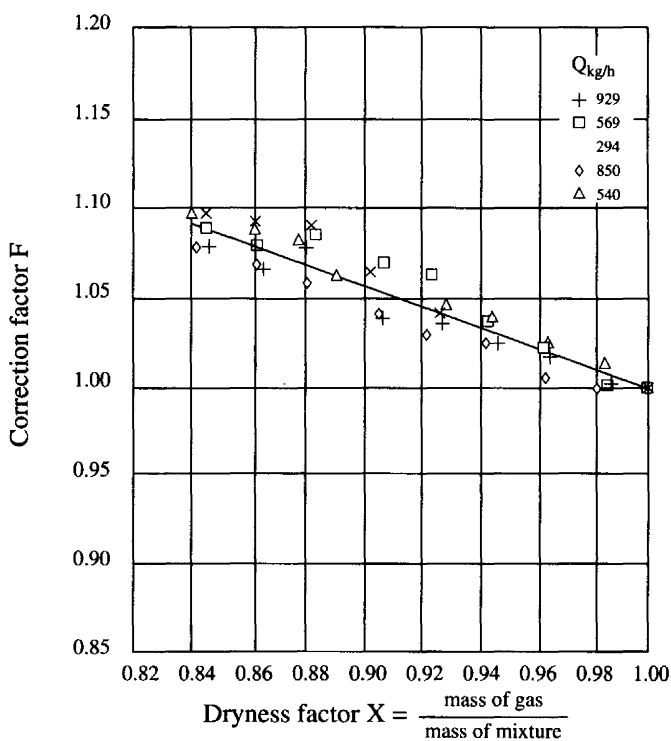


Figure 15.62 Wet-steam correction factor for vortex flowmeters.

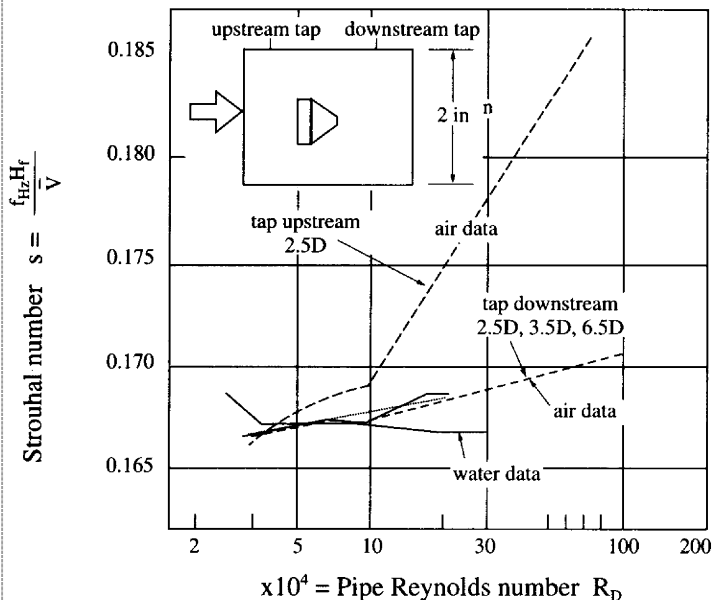


Figure 15.63 Effect of pressure tap location Strouhal number (K-factor).

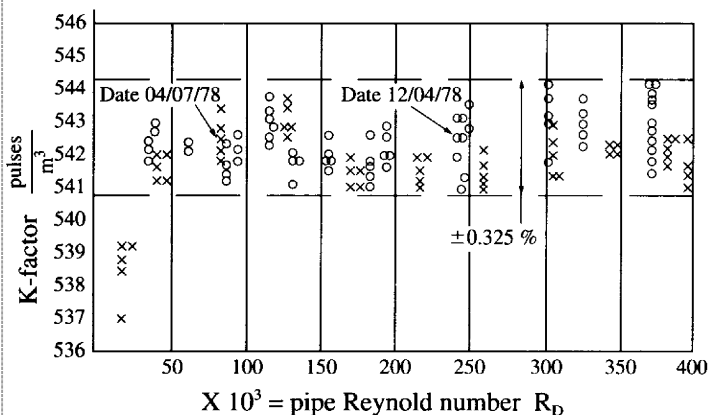


Figure 15.64 Results of on-site calibration of an 8 vortex flowmeter.

REFERENCES

- Akaike, S., T. Toyokura, S. Ugiyama, and H. Amemori: "Study of Flow Straightening of Turbine Flowmeter," JSME (Japanese Society of Mechanical Engineer), vol. 21, no. 157, pp. 1152-1159, 1978.
- Baker, R. C.: "Coriolis Flowmeters: Industrial Practice and Published Information," *Flow Measurement and Instrumentation*, vol. 5, no. 4, pp. 229-246, 1994.
- and J. Deacon: "Test on Turbine, Vortex and Electromagnetic Flowmeters in Two Phase Air/Water Upward Flow," *Int. Conf. on Physical Modeling of Multiphase Flow*, Coventry, 1983.
- and M. V. Morris: "Positive Displacement Meters for Liquids," *Trans. Inst. MC (Measurement and Control)*, no. 4, 1985.
- Birker, B.: "Theory Design and Performance on the Straight Through Mass Flowmeter," *Mass Flow Measurement Direct and Indirect*, London, 1989.
- Frankvoort, W.: "Results of the Evaluation of the Performance of Mass Flowmeters Using a Prover Loop," *Mass Flow Measurement Direct and Indirect, Proc. Int. Conf. Mass Flow Measurement*, IBC Publishing, London, 1989.
- Grumski, J. T., and R. A. Bajura: "Performance of a Coriolis-Type Mass Flowmeter in the Measurement of Two-Phase (Air-Liquid) Mixtures," *Mass Flow Measurements*, FED-vol. 17, pp. 75-83, 1984.
- Halttunen, J.: "Installation Effects on Ultrasonic and Electromagnetic Flowmeters: A Model Based Approach," *Flow Measurement and Instrumentation*, vol. 2, no. 1, pp. 287-292, 1990.
- Hayward, A. T. J., and P. A. M. Jeffs: "The Potential of the Vortex-Shedding Meter as a Custody-Transfer Meter for Liquids," *Conf. on Fluid Flow Measurement in the Mid-1980s*, paper 10.1, pp. 541-559, NEL, 1986.
- Hemp, J., and G. A. H. Sultan: "On the Theory and Performance of Coriolis Mass Flowmeters," *Mass Flow Measurement Direct and Indirect, Proc. Int. Conf. Mass Flow Measurement*, IBC Publishing, London, 1989.
- Heritage, J. E.: "The Performance of Transit Time Ultrasonic Flowmeters Under Good and Disturbed Flow Conditions," *Flow Measurement and Instrumentation*, vol. 1, no. 1, pp. 24-30, 1989.
- Hobbs, J. M., and J. S. Humphreys: "The Effect of Orifice Plate Geometry upon Discharge Coefficient," *Flow Measurement and Instrumentation*, vol. 1, no. 3, pp. 133-140, 1990.
- Hussein, I. B., and I. Owen: "Calibration of Flowmeters in Superheated and Wet Steam," *Flow Measurement and Instrumentation*, vol. 2, no. 4, pp. 209-215, 1991.
- Hutton, S. P.: "Prediction of Venturi Meter Coefficients and Their Variation with Roughness and Age," *Proc. Inst. Civil. Engr., Part 3*, pp. 216-241, London, 1954.
- : "The Effect of Inlet Flow Conditions on the Accuracy of Flowmeters," *Int. J. Mech. Eng. Conf.*, Pub 4, pp. 1-8, 1974.
- ISO 10790, *Measurement of Fluid Flow in Closed Conduits—Coriolis Mass Flowmeters*, ISO, Geneva, 1994.
- Jeannon, J. M.: "Pulsations from Rotary Positive Displacement Gas Meters," Ph.D. thesis, Univ. of Leicester, 1975.
- Jorissen, A. L.: "Discharge Measurements by Means of Venturi Tubes," ASME paper 50-A-71, 1950.
- Kiel, W.: "Difference Measurements Using Coriolis Mass Flowmeters," *Flow Measurement and Instrumentation*, vol. 2, no. 2, pp. 135-138, 1991.
- Mattingly, G. E., T. T. Yeh, B. Robertson, and K. M. Kothari: "NBS Research on Institute Flowmeter Calibrations," *AGA Distribution and Transmission Conf.*, AGA, Arlington, VA, 1987.
- and ———: "Effect of Pipe Elbows and Tube Bundles on Selected Types of Flowmeters," *Flow Measurement and Instrumentation*, vol. 2, no. 1, pp. 4-13, 1991.

- Miller, R. W.: *Calibration Results for Bent Orifices and Effects of Elbows on Various Differential Producers*, Foxboro, Mass., private data summary, 1988.
- Millington, B. C., C. W. Adams, and N. W. King: "The Effect of Upstream Installation Conditions on the Performance of Small Liquid Turbine Meters," *Int. Symp. on Flow Measurement*, AGA, Washington, 1986.
- Mottram, R. C.: "Vortex Flowmeters—Installation Effects," *Flow Measurement and Instrumentation*, vol. 2, no. 1, pp. 56–60, 1991.
- Mottram, R. C., and Spencer, E. A., "Installation Test Show Orifice Plate Deviations", *Symp Flow Metering and Proving Techniques in the Offshore Oil Industry*, Inst. Meas and Control, London, 1983.
- Nicholl, A. J.: "An Investigation into the Factors Affecting the Performance of Turbine Meters," *Conf. on Fluid Flow Measurement in the Mid-1970s*, pp. 541–559, NEL, 1975.
- Norman, R., P. Graham, and W. A. Drew: "Effects of Acoustic Noise on Orifice Meters," *Int. Symp. on Flow Measurement*, AGA, Washington, 1995.
- Shell *Shell Flow Meter Engineering Handbook* McGraw-Hill Book Company (UK) Limited, 1985.
- Starrett, P. S., H. B. Nottage, and P. F. Halfpenny: "Survey of Information Concerning the Effects of Non-standard Approach Conditions upon Orifice and Venturi Meters," ASME WAM paper, 65-WA/FM-5, 1965.
- Takamoto, M., H. Utsumi, N. Wantanabe, and T. Tero: "Installation Effects on Vortex Shedding Flowmeters," *Flow Measurement and Instrumentation*, vol. 4, no. 4, pp. 277–285, 1993.
- Tsuchida, T., Y. Terashima, and T. Machiyama: "The Effects of Flow Velocity Profile on the Electromagnetic Flowmeters," Reprint from *Reports of Researchers*, Nippon Institute of Technology, 1982.
- Van Der Kam, P. M. A., and K. Van Dellen: "The Effect of Double Bends Out of Plane on Turbine Meters," *Flow Measurement and Instrumentation*, vol. 2, no. 1, pp. 56–60, 1991.
- Van Laak, F. A. L.: "Liquid Quantity Meters in Combination with Density Meters, a Realistic Alternative to Weigh-Bridge in Loading Stations for Liquids," *Proc. of FLOMEKO 1978*, pp. 77–95, Goningen, Netherlands, 1978.
- Vetter, G., and S. Notzon: "Effect of Pulsating Flow on Coriolis Mass Flowmeters," *Flow Measurement and Instrumentation*, vol. 5, no. 4, pp. 263–273, 1994.
- Wagner, J. J.: "Effect of Sensor Design and Application Characteristics on Coriolis Mass Meter Performance: An Overview," *2d Int. Conference on Flow Measurement*, London, 1988.

DISCUSSIONS AND PROOFS

A.1 NEWTON'S METHOD FOR THE APPROXIMATE SOLUTION OF NUMERICAL EQUATIONS

Many of the equations used in flow measurement require an iterative solution for the flow rate, compressibility factor, or orifice bore. Newton's method for the approximate solution of numerical equations is a convenient trial-and-error technique that requires fewer estimates than other methods. In many cases the initial solution is sufficiently accurate, and a single calculation can be used. The calculations are readily programmable on hand calculators, dedicated microprocessors, or central computers.

As an example of the use of Newton's method, consider a 2-in (50-mm) orifice flowmeter operating at a Reynolds number of 10,000, for which the flow equation reduces to

$$q = 4.019 + \frac{0.8884}{q^{0.75}} \quad (\text{A.1})$$

In this equation, the first constant (4.019) is the calculated flow rate at an infinite Reynolds number for the measured differential and fluid density. The second constant includes the coefficient correction for Reynolds number, a dimensional term, and any necessary unit conversion.

Equation (A.1) is nonlinear, and to solve it estimates of the flow rate q must be successively substituted until the relationship is satisfied. Instead, Eq. (A.1) can be rearranged into a *function* equation as

$$F = 4.019 + \frac{0.8884}{q^{0.75}} - q \quad (\text{A.2})$$

Then, to solve Eq. (A.2) for the flow rate q , successive estimates of the flow rate are substituted into Eq. (A.2) until F is calculated to be zero.

The values of F for several flow rates are given in Table A.1, beginning with the infinite flow rate. These pairs of values are shown plotted in Fig. A.1. The zero crossing provides the zero root of Eq. (A.2), which is the desired flow rate. Its value can be read as 4.316; when substituted into Eq. (A.1) or (A.2), this value satisfies the equality.

The number of iterations (or estimates or guesses) is reduced if the equation of the tangent to the curve at the initial estimate q_0 is used to calculate the second

TABLE A.1 Values of the Function F of Eq. (A.2) for Various Flow Rates

Flow rate q_{PPS}	F
4.019	+0.313
4.119	+0.207
4.229	+0.091
4.329	-0.014
4.429	-0.119

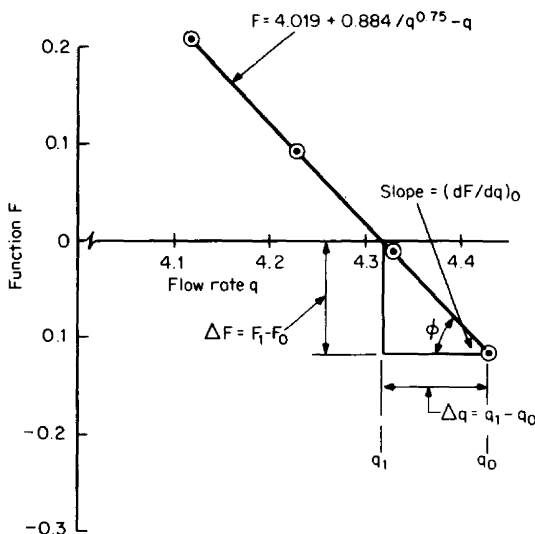


Figure A.1 Plot of the function F .

flow-rate estimate q_1 . For a tangent to the curve shown in Fig. A.1 at the point q_0 , the angle ϕ is approximately given by

$$\tan \phi = \frac{\Delta F}{\Delta q} = \frac{F_1 - F_0}{q_1 - q_0} \quad (\text{A.3})$$

Under the assumption that the second estimate q_1 is the desired zero root, F_1 equals zero. Equation (A.3) then becomes

$$q_1 = q_0 - \frac{F_0}{\tan \phi} \quad (\text{A.4})$$

where F_0 is the value of the function F for the initial flow-rate estimate.

The slope of the function F at any point is calculated by substituting the flow rate at that point into the derivative of the function. In general,

$$\frac{dF}{dq} = F' = -(0.6663q^{-1.75} + 1) \quad (\text{A.5})$$

and at the point where $q = q_0$, the slope is

$$\tan \phi = F'_0 = -(0.6663q_0^{-1.75} + 1) \quad (\text{A.6})$$

Substituting Eq. (A.6) into Eq. (A.4) yields the equation for calculating the second estimate as

$$q_1 = q_0 - \frac{F_0}{F'_0} = q_0 + \frac{4.019 + 0.8884q_0^{-0.75} - q_0}{0.6663q_0^{-1.75} + 1} \quad (\text{A.7})$$

Equation (A.7) can be solved directly to obtain the zero root q_1 , the desired flow rate. In most cases this single equation gives results to within 0.01 percent of the true value, which is sufficient for most flow applications. Subsequent estimates for improved calculation accuracy are obtained as

$$q_2 = q_1 - \frac{F_1}{F'_1} \quad q_3 = q_2 - \frac{F_2}{F'_2} \quad \dots \quad (\text{A.8})$$

and, in general,

$$q_n = q_{n-1} - \frac{F_{n-1}}{F'_{n-1}} \quad (\text{A.9})$$

where n is the estimate number.

Table A.2 lists values of the function F , the derivative F' , and the calculated flow rate for three initial estimates. In the first calculation, the initial assumption

TABLE A.2 Sample Iterations for Calculating the Flow Rate q

Trial n	Flow rate q_{n-1}	F , Eq. (A.2)	F' , Eq. (A.6)	Flow rate q_n Eq. (A.9)	Deviation, %
FOR INITIAL ESTIMATE CLOSE TO ZERO ROOT					
1	4.019	0.3130	-1.0584	4.3147	-0.02
2	4.3147	0.0010	-1.0516	4.3157	0.00
3	4.3157	0.0000	-1.0516	4.3157	0.00
FOR INITIAL GUESS SUBSTANTIALLY DIFFERENT FROM ZERO ROOT					
1	1.000	3.9074	-1.6663	3.3450	-22.49
2	3.3450	1.0332	-1.0805	4.3012	-0.34
3	4.3012	0.0153	-1.0519	4.3157	0.00
1	100	-95.9529	-1.0002	4.0673	-5.76
2	4.0673	0.2619	-1.0572	4.3150	-0.02
3	4.3150	0.0007	-1.0516	4.3157	0.00

of a flow rate equal to the constant 4.019 in Eq. (A.1) gives a calculation accuracy of 0.02 percent; for an initial guess substantially different from the zero root, two or three iterations are required for that accuracy.

Newton's method can be used to solve any nonlinear equation that is first rearranged into the general function form of Eq. (A.2), provided the function F is continuous.

A.2 PROOF THAT THE MEASURED DIFFERENTIAL INCLUDES THE POTENTIAL-ENERGY TERM FOR INCLINED INSTALLATIONS

Shown in Fig. A.2a is a differential producer inclined with respect to the horizontal. Bernoulli's equation along a stream tube can be written as

$$\frac{P_{f1}}{\rho_f} + \frac{\bar{V}_{f1}^2}{2g_c} + \frac{g_l}{g_c} H_{EL,1} = \frac{P_{f2}}{\rho_f} + \frac{\bar{V}_{f2}^2}{2g_c} + \frac{g_l}{g_c} H_{EL,2} \quad (\text{A.10})$$

Rearranging gives

$$\frac{P_{f1} - P_{f2}}{\rho_f} + \frac{g_l}{g_c} (H_{EL,1} - H_{EL,2}) = \frac{\bar{V}_{f2}^2 - \bar{V}_{f1}^2}{2g_c} \quad (\text{A.11})$$

Mass flow continuity requires that

$$q_{PPS} = \rho_{f1} A_1 \bar{V}_{f1} = \rho_{f2} A_2 \bar{V}_{f2} \quad (\text{A.12})$$

Then, for a constant-density fluid,

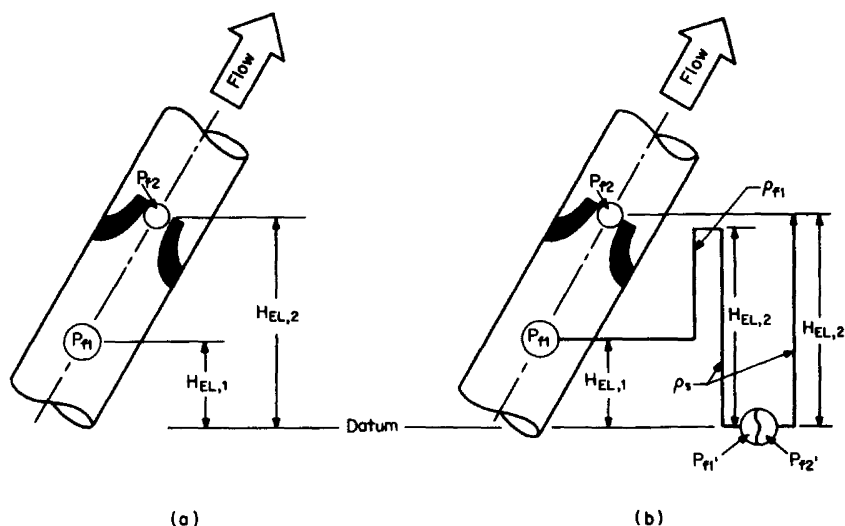


Figure A.2 Bernoulli's equation applied to an inclined differential producer. (a) Stream tube. (b) Lead lines at same elevation.

$$\bar{V}_{f1}^2 = \left(\frac{\rho_f A_2}{\rho_f A_1} \right)^2 \bar{V}_{f2}^2 = \beta^4 \bar{V}_{f2}^2 \quad (\text{A.13})$$

Substitution of Eq. (A.13) into Eq. (A.11) yields

$$\frac{P_{f1} - P_{f2}}{\rho_f} + \frac{g_l}{g_c} (H_{EL,1} - H_{EL,2}) = \frac{1 - \beta^4}{2g_c} \bar{V}_{f2}^2 \quad (\text{A.14})$$

which, when rewritten for mass flow rate using Eq. (A.12), yields

$$\frac{P_{f1} - P_{f2}}{\rho_f} + \frac{g_l}{g_c} (H_{EL,1} - H_{EL,2}) = \frac{1 - \beta^4}{2g_c} \frac{q_{PPS}^2}{\rho_f^2 A_2^2} \quad (\text{A.15})$$

The mass flow equation for an inclined installation thus is

$$q_{PPS} = \frac{\pi}{4} \sqrt{2g_c} \frac{d_F^2}{\sqrt{1 - \beta^4}} \sqrt{\left[P_{f1} - P_{f2} + \frac{g_l}{g_c} (H_{EL,1} - H_{EL,2}) \right] \rho_f} \quad (\text{A.16})$$

For a horizontal installation ($H_{EL,1} = H_{EL,2}$), this reduces to the fundamental mass flow equation (9.17):

$$q_{PPS} = \frac{\pi}{4} \sqrt{2g_c} \frac{d_F^2}{\sqrt{1 - \beta^4}} \sqrt{(P_{f1} - P_{f2}) \rho_f} \quad (\text{A.17})$$

The difference between the equations for a horizontal and an inclined installation is the potential-energy term

$$\frac{g_l}{g_c} (H_{EL,1} - H_{EL,2}) \rho_f \quad (\text{A.18})$$

within the radical.

Shown in Fig. A.2b is a differential-pressure measuring device located at a datum. Upstream lead lines have been brought to the same elevation as the downstream lead lines, so that $H_1 = H_2$. The upstream pressure measured at the datum can be expressed as

$$P_{f1'} = P_{f1} - \frac{g_l}{g_c} (H_{EL,2} - H_{EL,1}) \rho_{f1} + \frac{g_l}{g_c} H_{EL,2} \rho_s \quad (\text{A.19})$$

and the downstream pressure at the datum is

$$P_{f2'} = P_{f2} + \frac{g_l}{g_c} H_{EL,2} \rho_s \quad (\text{A.20})$$

where ρ_s is the density of the seal fluid in the lines.

The differential pressure transmitted to the differential-pressure measuring device, for the same seal-fluid density and provided the lines are at the same elevation, is

$$P_{f1'} - P_{f2'} = P_{f1} - P_{f2} + \frac{g_l}{g_c} (H_{EL,1} - H_{EL,2}) \rho_{f1} \quad (\text{A.21})$$

Equation (A.21) is the measured differential pressure; when it is substituted into Eq. (A.16), the result is

$$q_{PPS} = \frac{\pi}{4} \sqrt{2g_c} \frac{d_F^2}{\sqrt{1 - \beta^4}} \sqrt{(P_{f1'} - P_{f2'})\rho_f} \quad (\text{A.22})$$

Equation (A.22) thus relates the measured differential to the flow rate, and the measured differential adjusts for the potential-energy term in Eq. (A.18).

A.3 USE OF NEWTON'S METHOD FOR SIZING THE BORE OF A DIFFERENTIAL PRODUCER

The relationship between the S_M factor, the beta ratio, the discharge coefficient, and the known sizing information is given by Eq. (9.77). This equation can be written for solution via Newton's method (see Sec. A.1) as

$$F = S_M - \frac{CY\beta^2}{\sqrt{1 - \beta^4}} \quad (\text{A.23})$$

The gas expansion factor Y is not highly sensitive to β and negligible error is introduced by simplifying the derivative of the function to

$$F' = -Y \frac{d}{d\beta} \left(\frac{C\beta^2}{\sqrt{1 - \beta^4}} \right) \quad (\text{A.24})$$

With the substitution of the general form of the discharge-coefficient equation [Eq. (9.49)], the derivative of the function can be written as

$$F' = \frac{-\beta Y}{(1 - \beta^4)^{1.5}} \left[2C_\infty + (\beta - \beta^5)K_1 + \frac{2b + (\beta - \beta^5)K_2}{R_D^n} \right] \quad (\text{A.25})$$

Succeeding estimates for β are then

$$\beta_1 = \beta_0 - \frac{F_0}{F'_0} \quad \beta_2 = \beta_1 - \frac{F_1}{F'_1} \quad \cdots \quad \beta_n = \beta_{n-1} - \frac{F_{n-1}}{F'_{n-1}}$$

A single iteration for β_1 generally yields a calculation accuracy of 0.001 percent or better, and a second iteration is unnecessary.

The function F_0 and its derivative F'_0 are evaluated by substituting β_0 for β into the discharge-coefficient equations given in Table 9.1 to determine C . For liquids, the gas expansion factor Y is 1.0, and for gases (vapors), the expansion factor is calculated by substitution of β_0 for β into the equations given in Table 9.26. With C and Y known, F_0 may be calculated from Eq. (A.23); F'_0 is found using Table A.3.

Example A.1 Use Newton's method to determine the bore for the flange-tapped orifice of Example 9.2.

From Example 9.2,

$$\begin{aligned} (q_{PPH})_{URV} &= 30,000 \text{ lb}_m/\text{h} & (q_{PPH})_N &= 0.8(q_{PPH})_{URV} = 24,000 \text{ lb}_m/\text{h} \\ (h_w)_{URV} &= 100 \text{ in} & (h_w)_N &= 0.64(h_w)_{URV} = 64 \text{ in} \end{aligned}$$

$$(R_D)_{URV} = 1,882,700 \quad (R_D)_N = 0.8(R_D)_{URV} = 1,506,200$$

$$S_M = 0.39759 \quad \beta_0 = 0.74322 \quad D = 5.761 \text{ in}$$

and from Example 9.4,

$$k_i = 1.308$$

The function equation (for the initial estimate) is, by Eq. (A.1),

TABLE A.3 Values of K_1 and K_2 in the Equation $F' = \frac{-\beta Y}{(1 - \beta^4)^{1.5}} \left[2C_x + (\beta - \beta^5)K_1 + \frac{2b + (\beta - \beta^5)K_2}{R_D''} \right]^*$

Primary device	K_1	K_2
Venturi		
Machined inlet	0	0
Rough-cast inlet	0	0
Rough-welded sheet-iron inlet	0	0
Universal Venturi tube ‡	0	0
Lo-Loss Tube §	$-0.471 + 1.128\beta - 1.542\beta^2$	0
Nozzle		
ASME long radius	0	$-3.265\beta^{-0.5}$
ISA	$-0.9274\beta^{3.1}$	$-8936 + 92,961\beta^{3.7}$
Venturi nozzle (ISA inlet)	$-0.882\beta^{3.5}$	0
Orifice		
Corner taps	$0.0655\beta^{1.1} - 1.472\beta^7$	$229.3\beta^{1.5}$
Flange taps		
$D \geq 2.3 \text{ in}$	$0.0655\beta^{1.1} - 1.472\beta^7 + \frac{0.36}{D} \frac{\beta^3}{(1 - \beta^4)^2} - \frac{0.101}{D} \beta^2$	$229.3\beta^{1.5}$
$2 \leq D \leq 2.3 \text{ in}$	$0.0655\beta^{1.1} - 1.472\beta^7 + 0.156 \frac{\beta^3}{(1 - \beta^4)^2} - \frac{0.101\beta^2}{D}$	$229.3\beta^{1.5}$
$D^* > 58.4 \text{ mm}$	$0.0655\beta^{1.1} - 1.472\beta^7 + \frac{9.144}{D^*} \frac{\beta^3}{(1 - \beta^4)^2} - 2.568 \frac{\beta^2}{D^*}$	$229.3\beta^{1.5}$
$50.8 \leq D^* \leq 58.4 \text{ mm}$	$0.0655\beta^{1.1} - 1.472\beta^7 + 0.156 \frac{\beta^3}{(1 - \beta^4)^2} - 2.568 \frac{\beta^2}{D^*}$	$229.3\beta^{1.5}$
D and $D/2$ taps	$0.0655\beta^{1.1} - 1.472\beta^7 + 0.156 \frac{\beta^3}{(1 - \beta^4)^2} - 0.0474\beta^2$	$229.3\beta^{1.5}$
$2\frac{1}{2}D$ and $8D$ taps ¶	$0.9681\beta^{1.1} + 3.84\beta^7 + 0.156 \frac{\beta^3}{(1 - \beta^4)^2}$	$229.3\beta^{1.5}$

* F' is the derivative of the function $F = S_M - CY\beta^2/\sqrt{1 - \beta^4}$.

‡ From BIF CALC-440/441; the manufacturer should be consulted for exact coefficient information.

§ Derived from Badger Meter, Inc., Lo-Loss tube coefficient curve; the manufacturer should be consulted for exact coefficient information.

¶ From Stolz (1978).

$$F_0 = S_M - \frac{C_0(Y_1)_0\beta_0^2}{\sqrt{1 - \beta_0^4}}$$

and, from Table 9.1,

$$C_0 = 0.5959 + 0.0312\beta_0^{2.1} - 0.184\beta_0^8 + 0.09 \frac{\beta_0^4}{D(1 - \beta_0^4)} \\ - 0.0337 \frac{\beta_0^3}{D} + 91.71 \frac{\beta_0^{2.5}}{(R_D)_N^{0.75}}$$

Substituting the initial estimate $\beta_0 = 0.74322$ into this equation gives $C_0 = 0.60097$.

From Eqs. (c) and (h) of Table 9.26,

$$x_1 = \frac{(h_w)_N}{27.73p_{f1}} = \frac{64}{(27.73)(204)} = 0.01131$$

and

$$(Y_1)_0 = 1 - (0.41 + 0.35\beta_0^4) \frac{x_1}{k_i} = 0.99553$$

Substitution into the function equation gives

$$F_0 = 0.39759 - \frac{(0.60097)(0.99553)(0.74322)^2}{\sqrt{1 - (0.74322)^4}} = 0.001142$$

The derivative of the function equation (for the initial estimate) is

$$F'_0 = \frac{-\beta_0(Y_1)_0}{(1 - \beta_0^4)^{1.5}} \left[2C_x + (\beta_0 - \beta_0^5)K_1 + \frac{2b + (\beta_0 - \beta_0^5)K_2}{R_D^{0.75}} \right]$$

From Table 9.1, for $\beta_0 = 0.74322$,

$$C_x = 0.5959 + 0.0312\beta_0^{2.1} - 0.184\beta_0^8 + 0.09 \frac{\beta_0^4}{D(1 - \beta_0^4)} \\ - 0.0337 \frac{\beta_0^3}{D} = 0.59997$$

$$b = 91.71 \beta_0^{2.5} = 43.6555$$

and from Table A.3,

$$K_1 = 0.0655 \beta_0^{1.1} - 1.472 \beta_0^7 + \frac{0.36}{D} \frac{\beta_0^3}{(1 - \beta_0^4)^2} - \frac{0.101}{D} \beta_0^2 = -0.093536$$

$$K_2 = 229.3 \beta_0^{1.5} = 146.92$$

Substitution then gives $F'_0 = -1.4758$, and the second estimate for β is, from Eq. (A.4),

$$\beta_1 = \beta_0 - \frac{F_0}{F'_0} = 0.74322 - \frac{0.001142}{-1.4758} = 0.74399$$

Tabulated below are successive iterations for β , carried to seven places to show the rapid convergence:

	<i>n</i>		
	1	2	3
β_{n-1}	0.7432227	0.7439916	0.7439904
C_{n-1}	0.6009739	0.6009042	0.6009042
$(Y_1)_{n-1}$	0.9955299	0.9955299	0.9955299
F_{n-1}	0.00113475	-0.00000185	1.6×10^{-12}
F'_{n-1}	-1.475	-1.480580	-1.480572
β_n	0.7439916	0.7439904	0.7439904

The orifice bore is then

$$d = \beta_n D = (0.7440)(5.761) = 4.286 \text{ in}$$

Note: There is no justification for seven-place calculations in determining β , other than to maintain calculational accuracy, since the discharge coefficients for primary devices are known, at best, to within ± 0.1 percent under laboratory conditions.

REFERENCES FOR APPENDIXES A TO I

- ASME MFC-3M, *Measurement of Fluid Flow in Closed Conduits Using Orifice, Nozzle, and Venturi*, ASME, New York, 1995.
- ASME: "Fluid Meters: The ASME-ISO Orifice Equation," *Mech. Eng.*, vol. 103, no. 7, 1981.
- ASME: *Steam Tables*, 3d ed., American Society of Mechanical Engineers, New York, 1977.
- ASME/ANSI B36.10, *Welded and Seamless Wrought Steel Pipe*, New York, 1995.
- ASTM E380-79, *Annual Book of ASTM Standards*, pt. 41, American Society for Testing and Materials, Philadelphia, 1980.
- Baumeister, T.: *Marks' Standard Handbook for Mechanical Engineers*, 9th ed., McGraw-Hill, New York, 1988.
- Dieterich Standard Corporation: *Annubar Flow Handbook*, Dieterich publication DS-7300M (1/79), Boulder, Colo., 1979.
- Edmister, Wayne: *Applied Hydrocarbon Thermodynamics*, vol. 1, Gulf, Houston, 1961.
- : *Applied Hydrocarbon Thermodynamics*, vol. 2, Gulf, Houston, 1974.
- Fischer & Porter Company, *Catalog 10-A-54*, Fischer & Porter publication 10355, Warminster, Pa., 1950.
- Fluidic Techniques, Inc.: *Technical Data, Orifice Flange, Pipe*, Mansfield, Texas, 1982.
- Gambill, W. R.: "How P and T Change Liquid Viscosity," *Chem. Eng.*, p. 126, McGraw-Hill, New York, 1959.

- Gas Processors Supplier Association: *Engineering Data Book*, 9th ed., 4th rev., Tulsa, 1979.
- Giles, R. W.: *Fluid Mechanics and Hydraulics*, 2d ed., McGraw-Hill, New York, 1962.
- Hardy, R. C., and R. L. Cottington: *J. Res. Nat. Bur. Stand.*, vol. 42, p. 573, 1949.
- NIST, *Guide for the Use of the International System of Units (SI)*, NIST Special Publication 811, Barry N. Taylor, 1995.
- PEA: *Bulletin T.S. 622-77*, Pacific Energy Association, Los Angeles, 1977.
- Perry, R. H., and D. Green: *Chemical Engineers' Handbook*, 6th ed., McGraw-Hill, New York, 1984.
- Reid, R. C., J. M. Prausnitz, and B. R. Poling: *The Properties of Gases and Liquids*, 4th ed., McGraw-Hill, New York, 1987.
- Schoenthaler, J. L.: Standard Oil of California Technical Reprint, San Francisco, 1966.
- Spink, L. K., *Principles and Practice of Flowmeter Engineering*, 9th ed., The Foxboro Company, Foxboro, Mass., 1967.
- Stolz, J.: *OSU 89 Test Analysis: Interim Report on Pipe Taps Discharge Coefficient*, ISO/TC30/SC2 (France 17) 95E, AFNOR, Paris, 1978.
- Swindells, J. F.: Unpublished results (National Bureau of Standards).
- VDI: Publication 2040, Verein Deutscher Ingenieure, Düsseldorf, 1970.

TABLE B.2 Maximum Permissible Inside Diameters and Minimum Wall Thicknesses for ASTM A106 Pipe

Nominal pipe size, in	Maxi- mum outside diam- eter, in	Wall, ID, in	Nominal wall thickness and inside diameter, in												
			Sched- ule 10	Sched- ule 20	Sched- ule 30	Standard weight	Sched- ule 40	Sched- ule 60	Extra strong	Sched- ule 80	Sched- ule 100	Sched- ule 120	Sched- ule 140	Sched- ule 160	Double extra strong
$\frac{1}{8}$	0.421	Wall				0.060	0.060		0.083	0.083					
		ID				0.302	0.302		0.254	0.254					
$\frac{1}{4}$	0.556	Wall				0.077	0.077		0.110	0.110					
		ID				0.402	0.402		0.335	0.335					
$\frac{3}{8}$	0.691	Wall				0.080	0.080		0.110	0.110					
		ID				0.531	0.531		0.470	0.470					
$\frac{1}{2}$	0.856	Wall				0.095	0.095		0.129	0.129				0.164	0.257
		ID				0.665	0.665		0.598	0.598				0.528	0.341
$\frac{3}{4}$	1.066	Wall				0.099	0.099		0.135	0.135				0.191	0.270
		ID				0.868	0.868		0.796	0.796				0.684	0.527
1	1.331	Wall				0.116	0.116		0.157	0.157				0.219	0.313
		ID				1.098	1.098		1.017	1.017				0.893	0.704

TABLE B.2 Maximum Permissible Inside Diameters and Minimum Wall Thicknesses for ASTM A106 Pipe (*Continued*)

Nominal pipe size, in	Maxi- mum outside diam- eter, in	Wall, ID, in	Nominal wall thickness and inside diameter, in										Sched- ule 140	Sched- ule 160	Double extra strong
			Sched- ule 10	Sched- ule 20	Sched- ule 30	Standard weight	Sched- ule 40	Sched- ule 60	Extra strong	Sched- ule 80	Sched- ule 100	Sched- ule 120			
1½	1.676	Wall				0.123	0.123		0.167	0.167				0.219	0.334
		ID				1.431	1.431		1.341	1.341				1.238	1.007
1½	1.916	Wall				0.127	0.127		0.175	0.175				0.246	0.350
		ID				1.662	1.662		1.566	1.566				1.424	1.216
2	2.406	Wall				0.135	0.135		0.191	0.191				0.300	0.382
		ID				2.138	2.137		2.025	2.025				1.806	1.643
2½	2.906	Wall				0.178	0.178		0.242	0.242				0.328	0.483
		ID				2.551	2.551		2.423	2.423				2.250	1.940
3	3.531	Wall				0.189	0.189		0.263	0.263				0.383	0.525
		ID				3.153	3.153		3.006	3.006				2.765	2.481
3½	4.031	Wall				0.198	0.198		0.278	0.278					0.557
		ID				3.636	3.636		3.475	3.475					2.918
4	4.531	Wall				0.207	0.207		0.295	0.295		0.383		0.465	0.590

		ID	4.117				4.117		3.942		3.942		3.765		3.602		3.352	
5	5.626	Wall	0.226				0.226		0.328		0.328		0.438		0.547		0.656	
		ID	5.174				5.174		4.969		4.969		4.751		4.532		4.313	
6	6.688	Wall	0.245				0.245		0.378		0.378		0.492		0.628		0.756	
		ID	6.198				6.198		5.932		5.932		5.704		5.431		5.176	
8	8.719	Wall	0.219	0.242	0.282	0.282	0.355	0.438	0.438	0.519	0.628	0.711	0.793	0.766				
		ID	8.250	8.203	8.124	8.124	7.977	7.813	7.813	7.650	7.431	7.267	7.102	7.156				
10	10.844	Wall	0.219	0.269	0.319	0.319	0.438	0.438	0.519	0.628	0.738	0.875	0.984					
		ID	10.406	10.307	10.205	10.205	9.969	9.969	9.806	9.587	9.369	9.094	8.875					
12	12.844	Wall	0.219	0.289	0.328	0.355	0.492	0.438	0.601	0.738	0.875	0.984	1.148					
		ID	12.406	12.266	12.188	12.133	11.860	11.969	11.642	11.369	11.094	10.875	10.548					
14	14.094	Wall	0.219	0.273	0.328	0.328	383	0.519	0.438	0.656	0.820	0.956	1.094	1.230				
		ID	13.656	13.548	13.438	13.438	13.327	13.056	13.219	12.781	12.454	12.181	11.906	11.633				
16	16.094	Wall	0.219	0.273	0.328	0.328	0.438	0.574	0.438	0.738	0.902	1.066	1.258	1.394				
		ID	15.656	15.548	15.438	15.438	15.219	14.946	15.219	14.619	14.290	13.962	13.577	13.306				
18	18.094	Wall	0.219	0.273	0.383	0.328	0.492	0.656	0.438	0.820	1.012	1.203	1.367	1.558				
		ID	17.656	17.548	17.327	17.438	17.110	16.781	17.219	16.454	16.071	15.688	15.360	14.977				

TABLE B.2 Maximum Permissible Inside Diameters and Minimum Wall Thicknesses for ASTM A106 Pipe (*Continued*)

Nominal pipe size, in	Maxi- mum outside diam- eter, in	Wall, ID, in	Nominal wall thickness and inside diameter, in												
			Sched- ule 10	Sched- ule 20	Sched- ule 30	Standard weight	Sched- ule 40	Sched- ule 60	Extra strong	Sched- ule 80	Sched- ule 100	Sched- ule 120	Sched- ule 140	Sched- ule 160	Double extra strong
20	20.125	Wall	0.219	0.328	0.438	0.328	0.519	0.711	0.438	0.902	1.121	1.313	1.531	1.722	
		ID	19.688	19.469	19.250	19.469	19.087	18.704	19.250	18.321	17.883	17.500	17.063	16.681	
24	24.125	Wall	0.219	0.328	0.492	0.328	0.601	0.847	0.438	1.066	1.340	1.586	1.804	2.050	
		ID	23.688	23.469	23.142	23.469	22.923	22.431	23.250	21.994	21.446	20.954	20.517	20.025	
30	30.125	Wall	0.273	0.438	0.547	0.328			0.438						
		ID	29.579	29.250	29.031	29.469			29.250						

SOURCE: Fluidic Techniques, Inc. (1982); used with permission.

TABLE B.3 Standard Honed Internal Diameters for Flow-Nozzle Sections

Nominal pipe size D , in	Schedule no.	Bored diameter, in	Tolerance, in		Nominal pipe size D , in	Schedule no.	Bored diameter, in	Tolerance, in	
4	40	4.065	± 0.005		10	20	10.291	+0.005	-0.010
	80	3.881	± 0.005			30	10.186	+0.005	-0.010
	120	3.697	± 0.005			40	10.081	+0.005	-0.010
	160	3.524	± 0.005			60	9.831	+0.005	-0.010
5	40	5.089	± 0.005			80	9.660	+0.005	-0.010
	80	4.874	± 0.005			100	9.431	+0.005	-0.010
	120	4.611	± 0.005			120	9.201	+0.005	-0.010
	160	4.415	± 0.005			140	8.913	+0.005	-0.010
6	40	6.111	± 0.005			160	8.683	+0.005	-0.010
	80	5.831	± 0.005		12	20	12.291	+0.005	-0.015
	120	5.592	± 0.005			30	12.144	+0.005	-0.015
	160	5.306	± 0.005			40	12.004	+0.005	-0.015
8	20	8.166	+0.005	-0.010		60	11.717	+0.005	-0.015
	30	8.116	+0.005	-0.010		80	11.488	+0.005	-0.015
	40	8.033	+0.005	-0.010		100	11.201	+0.005	-0.015
	60	7.879	+0.005	-0.010		120	10.913	+0.005	-0.015
	80	7.706	+0.005	-0.010		140	10.683	+0.005	-0.015
	100	7.535	+0.005	-0.010		160	10.339	+0.005	-0.015
	120	7.306	+0.005	-0.010					
	140	7.133	+0.005	-0.010					
	160	6.960	+0.005	-0.010					

TABLE B.3 Standard Honed Internal Diameters for Flow-Nozzle Sections (*Continued*)

Nominal pipe size D , in	Schedule no.	Bored diameter, in	Tolerance, in		Nominal pipe size D , in	Schedule no.	Bored diameter, in	Tolerance, in	
14	10	13.511	+0.005	-0.020	18	10	17.541	+0.005	-0.030
	20	13.427	+0.005	-0.020		20	17.427	+0.005	-0.030
	30	13.311	+0.005	-0.020		30	17.197	+0.005	-0.030
	40	13.197	+0.005	-0.020		40	16.967	+0.005	-0.030
	60	12.910	+0.005	-0.020		60	16.622	+0.005	-0.030
	80	12.622	+0.005	-0.020		80	16.278	+0.005	-0.030
	100	12.278	+0.005	-0.020		100	15.875	+0.005	-0.030
	120	11.992	+0.005	-0.020		120	15.474	+0.005	-0.030
	140	11.703	+0.005	-0.020		140	15.130	+0.005	-0.030
	160	11.416	+0.005	-0.020		160	14.728	+0.005	-0.030
16	10	15.541	+0.005	-0.020	20	10	19.541	+0.005	-0.030
	20	15.427	+0.005	-0.020		20	19.311	+0.005	-0.030
	30	15.311	+0.005	-0.020		30	19.081	+0.005	-0.030
	40	15.081	+0.005	-0.020		40	18.910	+0.005	-0.030
	60	14.795	+0.005	-0.020		60	18.508	+0.005	-0.030
	80	14.451	+0.005	-0.020		80	18.106	+0.005	-0.030
	100	14.106	+0.005	-0.020		100	17.616	+0.005	-0.030
	120	13.762	+0.005	-0.020		120	17.244	+0.005	-0.030
	140	13.360	+0.005	-0.020		140	16.784	+0.005	-0.030
	160	13.073	+0.005	-0.020		160	16.384	+0.005	-0.030

SOURCE: Fluidic Techniques, Inc. (1982); used with permission.

TABLE B.4 Coefficient of Thermal Expansion†

Material	Coefficient of thermal expansion	
	α , in/(in·°F)	α' , mm/(mm·°C)
Plain carbon steel (SAE 1020)		
70–600°F (21–315°C)	0.0000067	0.000012
–300–70°F (–185–21°C)	0.0000047	0.000009
Stainless steels		
301		
70–600°F (21–314°C)	0.0000097	0.0000175
–300–70°F (–185–21°C)	0.0000076	0.0000137
304		
70–600°F (21–315°C)	0.0000095	0.0000171
–300–70°F (–185–21°C)	0.0000074	0.0000133
310		
70–600°F (21–315°C)	0.0000090	0.0000162
–300–70°F (–185–21°C)	0.0000070	0.0000126
316		
70–600°F (21–315°C)	0.0000096	0.0000173
–300–70°F (–185–21°C)	0.0000071	0.0000128
330		
70–600°F (21–315°C)	0.0000089	0.0000160
–300–70°F (–185–21°C)	0.0000058	0.0000104
347		
70–600°F (21–315°C)	0.0000097	0.0000175
–300–70°F (–185–21°C)	0.0000075	0.0000135
Hastelloy B 32–212°F (0–100°)	0.0000056	0.0000101
Hastelloy C	0.0000063	0.0000113
Inconel X, annealed	0.0000067	0.0000120
Haynes Stellite 25 (L605)	0.0000076	0.0000137
Copper (ASTM B152, B124, B133)	0.0000093	0.0000167
Yellow brass (ASTM B36, B134, B135)	0.0000105	0.0000189
Aluminum bronze (ASTM B169 Alloy A)	0.0000092	0.0000166
Beryllium copper 25 (ASTM B194)	0.0000093	0.0000167
Cupronickel 30%	0.0000085	0.0000154
K-Monel	0.0000074	0.0000133
Nickel	0.0000083	0.0000149
Pyrex glass 32–580°F (0–300°C)	0.0000002	0.0000004
Titanium 70–212°F (20–100°C)	0.0000047	0.0000085
Tantalum 70–212°F (20–100°C)	0.0000036	0.0000065

TABLE B.4 Coefficient of Thermal Expansion† (*Continued*)

**Equations for mean coefficient of thermal expansions for U.S.
units from 70°F to temperature and SI units from 21°C to
temperature**

Carbon steel: carbon-moly, low-carbon steels (<3 Cr)

$$\alpha_{\text{in}/(\text{in}\cdot^{\circ}\text{F})} = 5.877 \times 10^{-6} + 2.538 \times 10^{-9}T_F - 2.575 \times 10^{-13}T_F^2 - 2.042 \times 10^{-16}T_F^3$$

$$\alpha_{\text{mm}/(\text{mm}\cdot^{\circ}\text{C})} = 10.725 \times 10^{-6} + 8.171 \times 10^{-9}T_C - 1.671 \times 10^{-12}T_C^2 - 2.065 \times 10^{-15}T_C^3$$

Stainless steels

300 Series

$$\alpha_{\text{in}/(\text{in}\cdot^{\circ}\text{F})} = 8.949 \times 10^{-6} + 2.009 \times 10^{-9}T_F - 1.043 \times 10^{-12}T_F^2 + 3.381 \times 10^{-16}T_F^3$$

$$\alpha_{\text{mm}/(\text{mm}\cdot^{\circ}\text{C})} = 16.223 \times 10^{-6} + 6.307 \times 10^{-9}T_C - 5.940 \times 10^{-12}T_C^2 + 3.589 \times 10^{-15}T_C^3$$

400 Series

$$\alpha_{\text{in}/(\text{in}\cdot^{\circ}\text{F})} = 5.073 \times 10^{-6} + 2.151 \times 10^{-9}T_F - 6.526 \times 10^{-13}T_F^2 + 3.920 \times 10^{-17}T_F^3$$

$$\alpha_{\text{mm}/(\text{mm}\cdot^{\circ}\text{C})} = 9.255 \times 10^{-6} + 6.841 \times 10^{-9}T_C - 3.825 \times 10^{-12}T_C^2 + 4.517 \times 10^{-16}T_C^3$$

†Ranges of 70 to 600°F (21–315°C) unless otherwise noted.

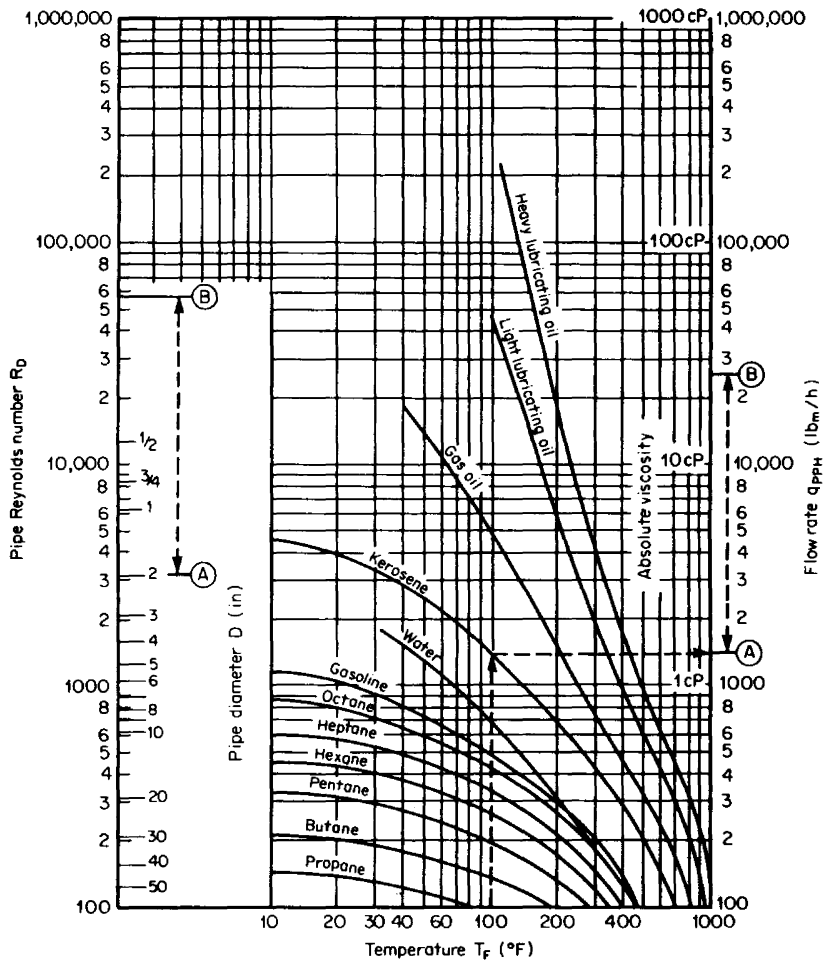


Figure B.1 Reynolds-number alignment curves for liquids. The example is for kerosene ($q_{PPH} = 25,000$, $T_F = 100^\circ\text{F}$, $D = 2$ in): (1) Locate point A using T_F . (2) Determine distance AB to flow-rate value. (3) Lay out distance AB from pipe size. (4) Read Reynolds number $R_D = 57,000$. (From Spink, 1967.)

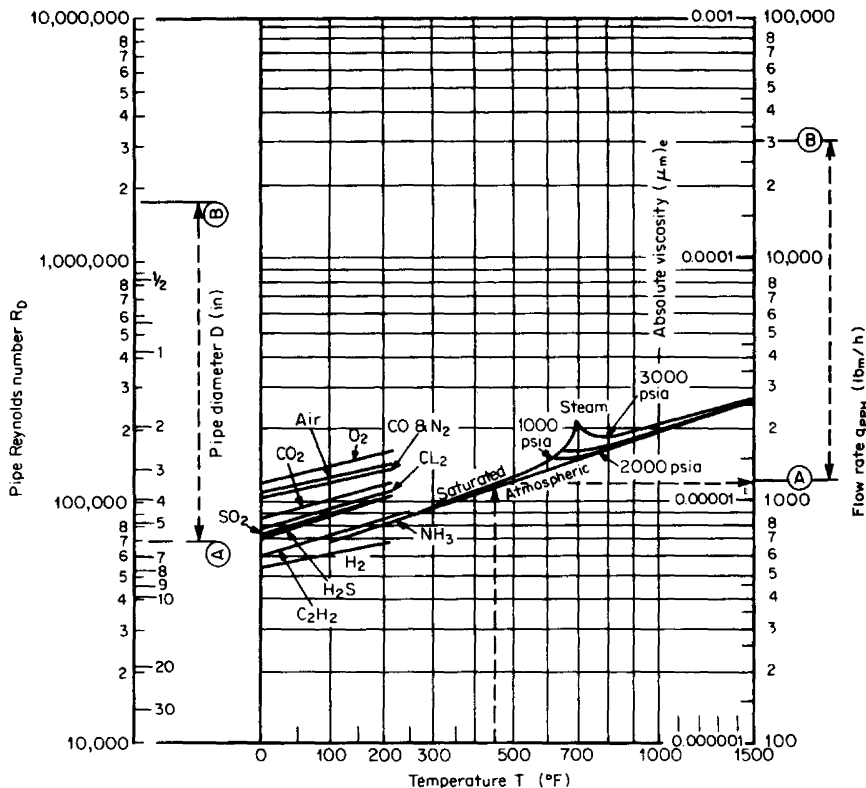


Figure B.2 Reynolds-number alignment curves for gas (vapor). The example is for saturated steam ($q_{PPH} = 30,000$, $T_F = 450^{\circ}\text{F}$, $D = 6$ in): (1) Locate point A using T_F . (2) Determine distance AB to flow-rate value. (3) Lay out distance AB from pipe size. (4) Read Reynolds number $R_D = 1,800,000$. (From Spink, 1967.)

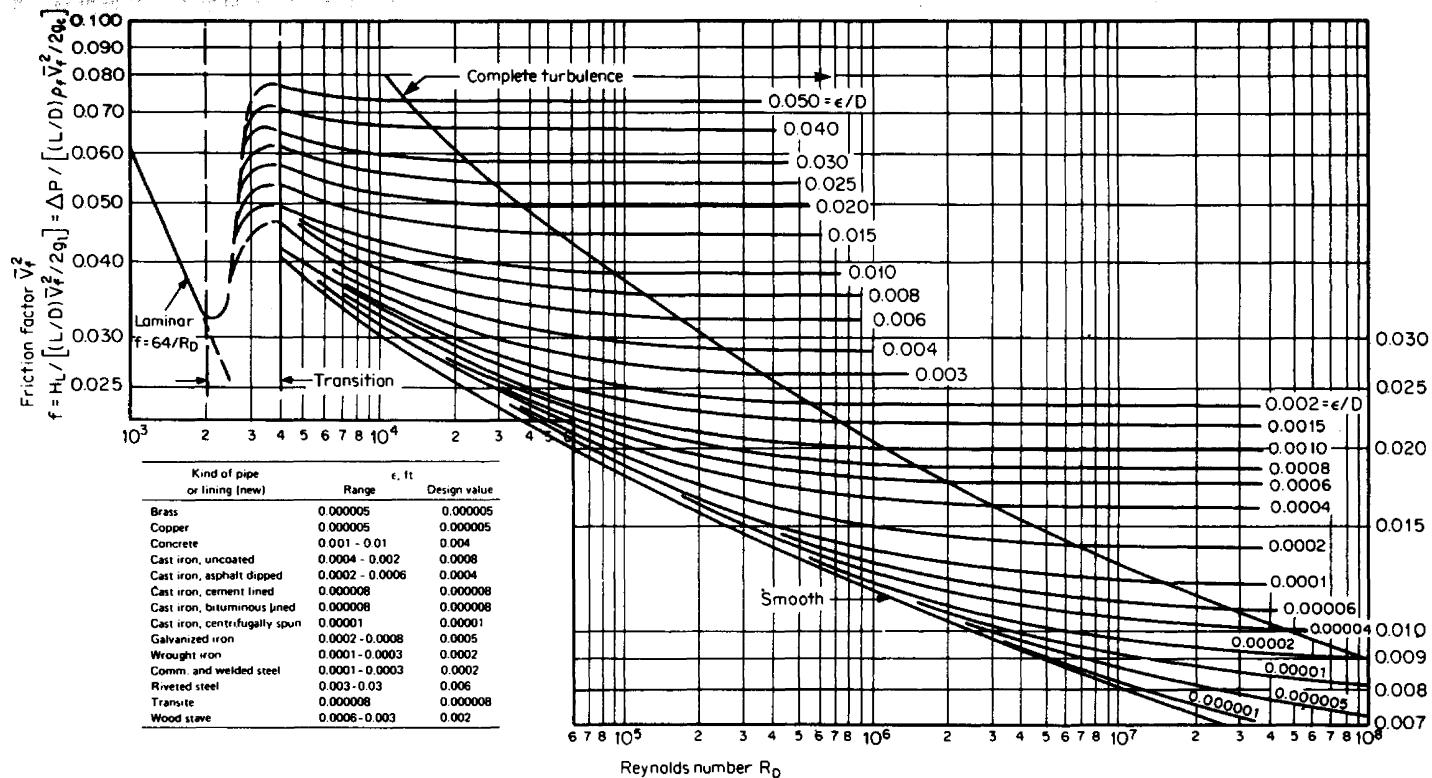


Figure B.3 Moody friction-factor diagram. Curves for relative roughness ϵ/D from 0.000001 to 0.050, where ϵ = size of surface imperfections in inches, D = actual inside diameter in inches. (From Giles, 1962.)

FLOW-RATE, REYNOLDS-NUMBER, AND UNIT CONVERSION TABLES

TABLE C.1 SI-Unit Conversion Factors†

To convert from	To	Multiply by
ACCELERATION		
ft/s ²	meter per second ² (m/s ²)	3.048 000*E - 01
free fall, standard (g)	meter per second ² (m/s ²)	9.806 650*E + 00
in/s ²	meter per second ² (m/s ²)	2.540 000*E - 02
ANGLE		
degree (angle)	radian (rad)	1.745 329 E - 02
minute (angle)	radian (rad)	2.908 882 E - 04
second (angle)	radian (rad)	4.848 137 E - 06
AREA		
ft ²	meter ² (m ²)	9.290 304*E - 02
in ²	meter ² (m ²)	6.451 600*E - 04
mi ² (international)	meter ² (m ²)	2.589 988 E + 06
mi ² (U.S. survey)	meter ² (m ²)	2.589 998 E + 06
BENDING MOMENT OR TORQUE		
dyne · cm	newton meter (N · m)	1.000 000*E - 07
kgf · m	newton meter (N · m)	9.806 650*E + 00
ozf · in	newton meter (N · m)	7.061 552 E - 03
lbf · in	newton meter (N · m)	1.129 848 E - 01
lbf · ft	newton meter (N · m)	1.355 818 E + 00
BENDING MOMENT OR TORQUE PER UNIT LENGTH		
lbf · ft/in	newton meter per meter (N · m/m)	5.337 866 E + 01
lbf · in/in	newton meter per meter (N · m/m)	4.448 222 E + 00
ENERGY (INCLUDES WORK)		
British thermal unit (International Table)	joule (J)	1.055 056 E + 03
British thermal unit (mean)	joule (J)	1.055 87 E + 03
British thermal unit (thermochemical)	joule (J)	1.054 350 E + 03

†Factors with an asterisk are exact.

TABLE C.1 SI-Unit Conversion Factors† (Continued)

To convert from	To	Multiply by
British thermal unit (39°F)	joule (J)	1.059 67 E + 03
British thermal unit (59°F)	joule (J)	1.054 80 E + 03
British thermal unit (60°F)	joule (J)	1.054 68 E + 03
calorie (International Table)	joule (J)	4.186 800*E + 00
calorie (mean)	joule (J)	4.190 02 E + 00
calorie (thermochemical)	joule (J)	4.184 000*E + 00
calorie (15°C)	joule (J)	4.185 80 E + 00
calorie (20°C)	joule (J)	4.181 90 E + 00
calorie (kilogram, International Table)	joule (J)	4.186 800*E + 03
calorie (kilogram, mean)	joule (J)	4.190 02 E + 03
calorie (kilogram, thermochemical)	joule (J)	4.184 000*E + 03
electronvolt	joule (J)	1.602 19 E - 19
erg	joule (J)	1.000 000*E - 07
ft·lb _f	joule (J)	1.355 818 E + 00
ft·poundal	joule (J)	4.214 011 E - 02
kilocalorie (International Table)	joule (J)	4.186 800*E + 03
kilocalorie (mean)	joule (J)	4.190 02 E + 03
kilocalorie (thermochemical)	joule (J)	4.184 000*E + 03
kW·h	joule (J)	3.600 000*E + 06
therm	joule (J)	1.055 056 E + 08
ton (nuclear equivalent of TNT)	joule (J)	4.184 E + 09
W·h	joule (J)	3.600 000*E + 03
W·s	joule (J)	1.000 000*E + 00

MASS PER UNIT TIME

lb _m /h	kilograms per sec (kg/s)	1.259 979 E - 04
lb _m /min	kilograms per sec (kg/s)	7.559 873 E - 03
lb _m /s	kilograms per sec (kg/s)	4.535 924 E - 01
Ton (short)/h	kilograms per sec (kg/s)	2.519 958 E - 01

MASS PER UNIT VOLUME

grain (lb avoirdupois/7000)/gal (U.S. liquid)	kilogram per meter ³ (kg/m ³)	1.711 806 E - 02
g/cm ³	kilogram per meter ³ (kg/m ³)	1.000 000*E + 03
oz (avoirdupois)/gal (U.K. liquid)	kilogram per meter ³ (kg/m ³)	6.236 021 E + 00
oz (avoirdupois)/gal (U.S. liquid)	kilogram per meter ³ (kg/m ³)	7.489 152 E + 00
oz (avoirdupois)/in ³	kilogram per meter ³ (kg/m ³)	1.729 994 E + 03
lb/ft ³	kilogram per meter ³ (kg/m ³)	1.601 846 E + 01
lb/in ³	kilogram per meter ³ (kg/m ³)	2.767 990 E + 04
lb/gal (U.K. liquid)	kilogram per meter ³ (kg/m ³)	9.977 633 E + 01
lb/gal (U.S. liquid)	kilogram per meter ³ (kg/m ³)	1.198 264 E + 02
lb/yd ³	kilogram per meter ³ (kg/m ³)	5.932 764 E - 01
slug/ft ³	kilogram per meter ³ (kg/m ³)	5.153 788 E + 02
ton (long)/yd ³	kilogram per meter ³ (kg/m ³)	1.328 939 E + 03
ton (short)/yd ³	kilogram per meter ³ (kg/m ³)	1.186 553 E + 03

POWER

Btu (International Table)/h	watt (W)	2.930 711 E - 01
Btu (International Table)/s	watt (W)	1.055 056 E + 03
Btu (thermochemical)/h	watt (W)	2.928 751 E - 01
Btu (thermochemical)/min	watt (W)	1.757 250 E + 01
Btu (thermochemical)/s	watt (W)	1.054 350 E + 03
cal (thermochemical)/min	watt (W)	6.973 333 E - 02
cal (thermochemical)/s	watt (W)	4.184 000*E + 00
erg/s	watt (W)	1.000 000*E - 07
ft·lb _f /h	watt (W)	3.766 161 E - 04
ft·lb _f /min	watt (W)	2.259 697 E - 02

†Factors with an asterisk are exact.

TABLE C.1 SI-Unit Conversion Factors† (Continued)

To convert from	To	Multiply by
ft·lb _f /s	watt (W)	1.355 818 E + 00
horsepower (550 ft·lb _f /s)	watt (W)	7.456 999 E + 02
horsepower (boiler)	watt (W)	9.809 50 E + 03
horsepower (electric)	watt (W)	7.460 000*E + 02
horsepower (metric)	watt (W)	7.354 99 E + 02
horsepower (water)	watt (W)	7.460 43 E + 02
horsepower (U.K.)	watt (W)	7.457 0 E + 02
kilocalorie (thermochemical)/min	watt(W)	6.973 333 E + 01
kilocalorie (thermochemical)/s	watt (W)	4.184 000*E + 03
ton (refrigeration)	watt (W)	3.516 800 E + 03

PRESSURE OR STRESS (FORCE PER UNIT AREA)

atmosphere (standard)	pascal (Pa)	1.013 250*E + 05
atmosphere (technical = 1 kg _f /cm ²)	pascal (Pa)	9.806 650*E + 04
bar	pascal (Pa)	1.000 000*E + 05
centimeter of mercury (0°C)	pascal (Pa)	1.333 22 E + 03
centimeter of water (4°C)	pascal (Pa)	9.806 38 E + 01
dyne/cm ²	pascal (Pa)	1.000 000*E - 01
foot of water (39.2°F)	pascal (Pa)	2.988 98 E + 03
gram-force/cm ²	pascal (Pa)	9.806 650*E + 01
inch of mercury (32°F)	pascal (Pa)	3.386 38 E + 03
inch of mercury (60°F)	pascal (Pa)	3.376 85 E + 03
inch of water (60°F)	pascal (Pa)	2.488 429 E + 02
inch of water (68°F)	pascal (Pa)	2.4864107 E + 02
kg _f /cm ²	pascal (Pa)	9.806 650*E + 04
kg _f /m ²	pascal (Pa)	9.806 650*E + 00
kg _f /mm ²	pascal (Pa)	9.806 650*E + 06
kip/in ² (ksi)	pascal (Pa)	6.894 757 E + 06
millibar	pascal (Pa)	1.000 000*E + 02
millimeter of mercury (0°C)	pascal (Pa)	1.333 22 E + 02
poundal/ft ²	pascal (Pa)	1.488 164 E + 00
lb _f /ft ²	pascal (Pa)	4.788 026 E + 01
lb _f /in ² (psi)	pascal (Pa)	6.894 757 E + 03
psi	pascal (Pa)	6.894 757 E + 03
torr (mm Hg, 0°C)	pascal (Pa)	1.333 22 E + 02

TEMPERATURE

degree Celsius	kelvin (K)	$T_K = T_{°C} + 273.15$
degree Fahrenheit	degree Celsius	$T_{°C} = (T_F - 32)/1.8$
degree Fahrenheit	kelvin (K)	$T_K = (T_F + 459.67)/1.8$
degree Rankine	kelvin (K)	$T_R = T_F/1.8$
kelvin	degree Celsius	$T_{°C} = T_K - 273.15$

VELOCITY

ft/h	meter per second (m/s)	8.466 667 E - 05
ft/min	meter per second (m/s)	5.080 000*E - 03
ft/s	meter per second (m/s)	3.048 000*E - 01
in/s	meter per second (m/s)	2.540 000*E - 02

†Factors with an asterisk are exact.

TABLE C.1 SI-Unit Conversion Factors† (*Continued*)

To convert from	To	Multiply by
VISCOSITY		
centipoise	pascal second (Pa·s)	1.000 000*E - 03
centistoke	meter ² per second (m ² /s)	1.000 000*E - 06
ft ² /s	meter ² per second (m ² /s)	9.290 304*E - 02
poise	pascal second (Pa·s)	1.000 000*E - 01
poundal·s/ft ²	pascal second (Pa·s)	1.488 164 E + 00
lb/(ft·h)	pascal second (Pa·s)	4.133 789 E - 04
lb/(ft·s)	pascal second (Pa·s)	1.488 164 E + 00
lb _f ·s/ft ²	pascal second (Pa·s)	4.788 026 E + 01
lb _f ·s/in ²	pascal second (Pa·s)	6.894 757 E + 03
rhe	1 per pascal second [1/(Pa·s)]	1.000 000*E + 01
slug/(ft·s)	pascal second (Pa·s)	4.788 026 E + 01
stokes	meter ² per second (m ² /s)	1.000 000*E - 04
VOLUME		
fluid ounce (U.S.)	meter ³ (m ³)	2.957 353 E - 05
ft ³	meter ³ (m ³)	2.831 685 E - 02
gallon (Canadian liquid)	meter ³ (m ³)	4.546 090 E - 03
gallon (U.K. liquid)	meter ³ (m ³)	4.546 092 E - 03
gallon (U.S. dry)	meter ³ (m ³)	4.404 884 E - 03
gallon (U.S. liquid)	meter ³ (m ³)	3.785 412 E - 03
pint (U.S. dry)	meter ³ (m ³)	5.506 105 E - 04
pint (U.S. liquid)	meter ³ (m ³)	4.731 765 E - 04
quart (U.S. dry)	meter ³ (m ³)	1.101 221 E - 03
quart (U.S. liquid)	meter ³ (m ³)	9.463 529 E - 04
VOLUME PER UNIT TIME		
ft ³ /min	meter ³ per second (m ³ /s)	4.719 474 E - 04
ft ³ /s	meter ³ per second (m ³ /s)	2.831 685 E - 02
gallon (U.S. liquid)/(hp·h) (SFC, specific fuel consumption)	meter ³ per joule (m ³ /J)	1.410 089 E - 09
in ³ /min	meter ³ per second (m ³ /s)	2.731 177 E - 07
gallon (U.S. liquid) per day	meter ³ per second (m ³ /s)	4.381 264 E - 08
gallon (U.S. liquid) per minute	meter ³ per second (m ³ /s)	6.309 020 E - 05

†Factors with an asterisk are exact.

SOURCE: Reprinted/adapted, with permission, from ASTM (1980). Copyright, American Society for Testing and Materials, 1916 Race Street, Philadelphia, Pa. 19103.

TABLE C.3 Conversion Equations for U.S. Flow-Rate Units

	Liquid	Gas	Vapor (steam)
	→	$V_f = 183.3465 \frac{q_{ch}}{D^2}$	←
	→	$q_{ch} = 5.454154 \times 10^{-3} D^2 V_f$	←
Mass flow rate, lb _m /h	→	$q_{PPH} = 19.63495 \rho_f D^2 V_f$	←
	→	$q_{PPH} = 3600 \rho_f q_{ch}$	←
	$q_{PPH} = 500.230 G_f q_{gpm}$	$q_{PPH} = 9715.775 \frac{P_f G}{T_f Z_f} q_{ch}^\dagger$	←
Volumetric flow rate at flowing conditions	$q_{gpm} = 2.447994 D^2 V_f$		
	$q_{gpm} = 1.999082 \times 10^{-3} \frac{q_{PPH}}{G_f}$		
	$q_{gpm} = 448.8312 q_{ch}$		
	$q_{gpm} = \frac{\rho_b}{\rho_f} q_{GPM}$		
	$q_{gpm} = \frac{G_b}{G_f} q_{GPM}$		
Volumetric flow rate at base conditions‡	$q_{GPM} = \frac{\rho_f}{\rho_b} q_{gpm}$	$q_{SCFH} = 35.29340 \frac{P_f Z_b}{T_f Z_f} q_{ach}$	
	$q_{GPM} = \frac{G_f}{G_b} q_{gpm}$		
	$q_{GPM} = 448.8312 \frac{G_f}{G_b} q_{ch}$	$q_{SCFH} = 692.9843 \frac{P_f Z_b}{T_f Z_f} D^2 V_f$	
	$q_{GPM} = 2.447994 \frac{G_f}{G_b} D^2 V_f$	$q_{SCFH} = 13.07732 \frac{Z_b}{G} q_{PPH}$	
	$q_{GPM} = 1.999082 \times 10^{-3} \frac{q_{PPH}}{G_b}$	$q_{SCFH} = \frac{1}{\rho_b} q_{PPH}$	

 †For liquids, q_{ch} ; for gases (vapors), q_{ach} .

‡Liquid base volumes at 60°F and 14.69595 psia; gas base volumes at 59°F and 14.69595 psia.

TABLE C.4 Reynolds-Number Equations for U.S. Flow Units

Flow rate unit	Absolute viscosity				Kinematic viscosity		
	English		cgs Metric		English	cgs Metric	
	$(\mu_f)_e$	$(\mu_m)_e$	Poise μ_P	Centipoise μ_{cP}	ν_e	Stokes ν_{St}	Centistokes ν_{cSt}
	$\text{lb}_f \cdot \text{s}/\text{ft}^2$	$\text{lb}_m/(\text{ft} \cdot \text{s})$	$\text{g}/(\text{cm} \cdot \text{s})$	$\text{g}/(\text{cm} \cdot \text{s})$	ft^2/St	cm^2/St	cm^2/St
Average velocity \bar{V}_f	$\frac{\rho_f \bar{V}_f D}{386.0886(\mu_f)_e}$	$\frac{\rho_f \bar{V}_f D}{12(\mu_m)_e}$	$\frac{1.240137 \rho_f \bar{V}_f D}{\mu_P}$	$\frac{124.0137 \rho_f \bar{V}_f D}{\mu_{cP}}$	$\frac{\bar{V}_f D}{12\nu_e}$	$\frac{77.41920 \bar{V}_f D}{\nu_{St}}$	$\frac{7741.920 \bar{V}_f D}{\nu_{cSt}}$
Mass flow q_{PPS}	$\frac{0.4748820 q_{PPS}}{D(\mu_f)_e}$	$\frac{15.27888 q_{PPS}}{D(\mu_m)_e}$	$\frac{227.3748 q_{PPS}}{D\mu_P}$	$\frac{22,737.47 q_{PPS}}{D\mu_{cP}}$	$\frac{15.27888 q_{PPS}}{\rho_f D \nu_e}$	$\frac{14,194.54 q_{PPS}}{\rho_f D \nu_{St}}$	$\frac{1,419,454 q_{PPS}}{\rho_f D \nu_{cSt}}$
q_{PPH}	$\frac{q_{PPH}}{7580.830 D(\mu_f)_e}$	$\frac{q_{PPH}}{235.6194 D(\mu_m)_e}$	$\frac{q_{PPH}}{15.83288 D\mu_P}$	$\frac{6.315964 q_{PPH}}{D\mu_{cP}}$	$\frac{q_{PPH}}{235.6194 \rho_f D \nu_e}$	$\frac{3.942929 q_{PPH}}{\rho_f D \nu_{St}}$	$\frac{394.2929 q_{PPH}}{\rho_f D \nu_{cSt}}$
Volumetric at flowing conditions q_{cfs}	$\frac{0.4748820 \rho_f q_{cfs}}{D(\mu_f)_e}$	$\frac{15.27888 \rho_f q_{cfs}}{D(\mu_m)_e}$	$\frac{227.3747 \rho_f q_{cfs}}{D\mu_P}$	$\frac{22,737.47 \rho_f q_{cfs}}{D\mu_{cP}}$	$\frac{15.27888 q_{cfs}}{D \nu_e}$	$\frac{14,194.54 q_{cfs}}{D \nu_{St}}$	$\frac{1,419,454 q_{cfs}}{D \nu_{cSt}}$
q_{gpm}	$\frac{\rho_f q_{gpm}}{945.1426 D(\mu_f)_e}$	$\frac{\rho_f q_{gpm}}{29.37593 D(\mu_m)_e}$	$\frac{0.5065929 \rho_f q_{gpm}}{D\mu_P}$	$\frac{50.65929 \rho_f q_{gpm}}{D\mu_{cP}}$	$\frac{q_{gpm}}{29.37593 D \nu_e}$	$\frac{31.62557 q_{gpm}}{D \nu_{St}}$	$\frac{3162.557 q_{gpm}}{D \nu_{cSt}}$
Volumetric at base conditions q_{GPM}	$\frac{G_b q_{GPM}}{15.15470 D(\mu_f)_e}$	$\frac{2.123041 G_b q_{GPM}}{D(\mu_m)_e}$	$\frac{31.59433 G_b q_{GPM}}{D\mu_P}$	$\frac{3159.433 G_b q_{GPM}}{D\mu_{cP}}$	$\frac{G_b q_{GPM}}{29.37593 G_f D \nu_e}$	$\frac{31.62557 G_b q_{GPM}}{G_f D \nu_{St}}$	$\frac{3159.434 G_b q_{GPM}}{G_f \nu_{cSt}}$
q_{SCFH}	$\frac{G q_{SCFH}}{99136.68 Z_b D(\mu_f)_e}$	$\frac{G q_{SCFH}}{3081.289 Z_b D(\mu_m)_e}$	$\frac{G q_{SCFH}}{207.0515 Z_b D\mu_P}$	$\frac{0.4829716 G q_{SCFH}}{Z_b D\mu_{cP}}$	$\frac{T_f Z_f q_{SCFH}}{8315.808 \rho_f Z_b D \nu_e}$	$\frac{0.1117186 T_f Z_f q_{SCFH}}{\rho_f Z_b D \nu_{St}}$	$\frac{11.17186 T_f Z_f q_{SCFH}}{\rho_f Z_b D \nu_{cSt}}$

NOTE: D = pipe size (in); \bar{V}_f = fluid velocity (ft/s); ρ_f = fluid density (lb_m/ft^3).

TABLE C.5 Reynolds-Number Equations for SI Units

Flow-rate unit	Absolute viscosity		Kinematic viscosity	
	μ_P	μ_{cP}	ν_{St}	ν_{cSt}
Average velocity V_f^*	$\frac{\rho_f^* V_f^* D^*}{100 \mu_P}$	$\frac{\rho_f V_f^* D^*}{\mu_{cP}}$	$\frac{10 V_f^* D^*}{\nu_{St}}$	$\frac{1000 V_f^* D^*}{\nu_{cSt}}$
Mass flow q_{KPH}	$\frac{3.536777 q_{KPH}}{D^* \mu_P}$	$\frac{353.6777 q_{KPH}}{D^* \mu_{cP}}$	$\frac{3536.777 q_{KPH}}{\rho_f^* D^* \nu_{St}}$	$\frac{353,677.7 q_{KPH}}{\rho_f^* D^* \nu_{cSt}}$
Volumetric at flowing conditions	$\frac{0.2122066 \rho_f^* q_{lpm}}{D^* \mu_P}$	$\frac{21.22066 \rho_f^* q_{lpm}}{D^* \mu_{cP}}$	$\frac{212.2066 q_{lpm}}{D^* \nu_{St}}$	$\frac{21,220.66 q_{lpm}}{D^* \nu_{cSt}}$
Volumetric at base conditions (liquid)† q_{LPM}	$\frac{211.9970 G_b q_{LPM}}{D^* \mu_P}$	$\frac{21199.70 G_b q_{LPM}}{D^* \mu_{cP}}$	$\frac{212.2070 G_b q_{LPM}}{G_f D^* \nu_{St}}$	$\frac{212,207.0 G_b q_{LPM}}{G_f D^* \nu_{cSt}}$
Volumetric at base conditions‡ (gas) q_{SCMH}	$\frac{4.332211 G q_{SCMH}}{Z_b D^* \mu_P}$	$\frac{433.2211 G q_{SCMH}}{Z_b D^* \mu_{cP}}$	$\frac{1243.671 T_K Z_f q_{SCMH}}{p_f^* Z_b D^* \nu_{St}}$	$\frac{124,367.2 T_K Z_f q_{SCMH}}{p_f^* Z_b d^* \nu_{cSt}}$

†Base temperature = 15.56°C; base pressure = 101.325 kPa.

‡ISO 5024 base: $p_f^* = 101.325$ kPa, $T_{Kb} = 288.15$ K.NOTE: The poise (P) and the stokes (St) are cgs metric units, not SI metric units; 1 P = 0.1 Pa.s; 1 St = 0.0001 m²/s.

TABLE C.6 U.S. Unit Sizing Equations

Mass flow rate (liquid/gas/vapor)			
Density	$S_M = \frac{q_{PPH}}{358.9268 D_f^2 \sqrt{\rho_f h_w}}$	(a)	$R_{Df} = \frac{6.31597 q_{PPH}}{\mu_{cP} D_f}$ (e)
Volumetric flow rate at flowing conditions (liquid)			
Specific gravity	$S_M = \frac{\sqrt{F_p G_F} q_{gpm}}{5.666455 D_f^2 \sqrt{h_w}}$	(b)	$R_{Df} = \frac{3159.43 F_p G_F q_{gpm}}{\mu_{cP} D_f}$ (f)
Volumetric flow rate at base conditions (liquid)			
Specific gravity	$S_M = \frac{G_b q_{GPM}}{5.666455 D_f^2 \sqrt{F_p G_F h_w}}$	(c)	$R_{Df} = \frac{3159.43 G_b q_{GPM}}{\mu_{cP} D_f}$ (g)
Gas			
$p_v T$	$S_M = \frac{p_b \sqrt{Z_{f1} T_{f1} G} (q_{SCFH})_b}{218.4834 Z_b T_b D_f^2 \sqrt{h_w p_{f1}}}$	(d)	$R_{Df} = \frac{17.04569 G p_b (q_{SCFH})_b}{Z_b T_b \mu_{cP} D_f}$ (h)

NOTE: D_f in these equations is defined by $D_f = F_{aD} F_{Dp} D_{meas}$ normally $F_{Dp} = 1.0$

TABLE C.7 SI Unit Sizing Equations

Mass flow rate (liquid/gas/vapor)			
Density	$S_M = \frac{q_{KPH}}{0.126447 D_f^{*2} \sqrt{\rho_{f1}^* \Delta p^*}}$	(a)	$R_{Df} = \frac{353.676 q_{KPH}}{\mu_{cP} D_f^*}$ (e)
Volumetric flow rate at flowing conditions (liquid)			
Specific gravity	$S_M = \frac{\sqrt{F_p G_F} q_{lpm}}{0.06667619 D_f^{*2} \sqrt{\Delta p^*}}$	(b)	$R_{Df} = \frac{21199.7 F_p G_F q_{lpm}}{\mu_{cP} D_f^*}$ (f)
Volumetric flow rate at base conditions (liquid)			
Specific gravity	$S_M = \frac{G_b q_{LPM}}{0.06667619 D_f^{*2} \sqrt{F_p G_F \Delta p^*}}$	(c)	$R_{Df} = \frac{21199.7 G_b q_{LPM}}{\mu_{cP} D_f^*}$ (g)
		Gas	
$p_v T$	$S_M = \frac{p_b \sqrt{Z_{f1} T_{K1}} G (q_{SCMH})_b}{0.06774938 Z_b T_{Kb} D_f^{*2} \sqrt{\Delta p^* \rho_{fa}^*}}$	(d)	$R_{Df} = \frac{1232.003 G p_b^* (q_{SCMH})_b}{Z_b T_{Kb} \mu_{cP} D_f^*}$ (h)

NOTE: D_f^* in these equations is defined by $D_f^* = F_{ad}^* F_{dp}^*$ normally $F_{dp}^* = 1.0$

TABLE C.8 U.S./SI Flow Rate Equations

	U.S.		SI	
Mass flow rate (vapor)				
Density	$q_{PPH} = 358.9268 \frac{CY_1 d_f^2}{\sqrt{1 - (d_f/D_f)^4}} \sqrt{h_w \rho_{f1}}$	(a)	$q_{KPH} = 0.126447 \frac{CY_1 d_f^{*2}}{\sqrt{1 - (d_f^*/D_f^*)^4}} \sqrt{\Delta p^* \rho_{f1}^*}$	(i)
	$R_{Df} = \frac{6.31597 q_{PPH}}{\mu_{cP} D_f}$	(b)	$R_{Df} = \frac{353.676 q_{KPH}}{\mu_{cP} D_f^*}$	(j)
Volumetric flow rate at flowing conditions (liquid)				
Specific gravity	$q_{gpm} = 5.666455 \frac{Cd_f^2}{\sqrt{1 - (d_f/D_f)^4}} \sqrt{F_p G_F} \sqrt{h_w}$	(c)	$q_{lpm} = 0.06667619 \frac{Cd_f^{*2}}{\sqrt{1 - (d_f^*/D_f^*)^4}} \sqrt{F_p G_F} \sqrt{\Delta p^*}$	(k)
	$R_{Df} = \frac{3159.432 F_p G_F q_{gpm}}{\mu_{cP} D_f}$	(d)	$R_{Df} = \frac{21199.697 F_p G_F q_{lpm}}{\mu_{cP} D_f^*}$	(l)
Volumetric flow rate at base conditions (liquid)				
Specific gravity	$q_{GPM} = 5.666455 \frac{Cd_f^2}{\sqrt{1 - (d_f/D_f)^4}} \frac{\sqrt{F_p G_F}}{G_b} \sqrt{h_w}$	(e)	$q_{LPM} = 0.06667619 \frac{Cd_f^{*2}}{\sqrt{1 - (d_f^*/D_f^*)^4}} \frac{\sqrt{F_p}}{G_b} \sqrt{\Delta p^*}$	(m)
	$R_{Df} = \frac{3159.432 G_b q_{GPM}}{\mu_{cP} D_f}$	(f)	$R_{Df} = \frac{21199.697 G_b q_{LPM}}{\mu_{cP} D_f^*}$	(n)
Volumetric flow rate at base conditions (gas)				
pvT equation	$(q_{SCFH})_b = 218.4834 \frac{Cd_f^2}{\sqrt{1 - (d_f/D_f)^4}} \frac{Y_1 Z_b T_b \sqrt{p_{f1}}}{p_b \sqrt{G Z_{f1} T_{f1}}} \sqrt{h_w}$	(g)	$(q_{SCMH})_b = 0.06774938 \frac{Cd_f^{*2}}{\sqrt{1 - (d_f^*/D_f^*)^4}} \frac{Y_1 Z_b T_{kb} \sqrt{p_{f1}^*}}{p_b^* \sqrt{G Z_{f1} T_{k1}}} \sqrt{\Delta p^*}$	(o)
	$R_{Df} = \frac{17.04569 G p_b (q_{SCFH})_b}{Z_b T_b \mu_{cP} D_f}$	(h)	$R_{Df} = \frac{1232.003 G p_b (q_{SCMH})_b}{Z_b T_b \mu_{cP} D_f^*}$	(p)

NOTE: D_f in these equations is defined by $D_f = F_{uD} F_{Dp} D_{meas}$ and $d_f = F_{ud} F_{dp} d_{meas}$ normally $F_{uD} = F_{ud} = 1.0$.

TABLE C.9 U.S./SI Differential Pressure Equations

U.S.		SI			
Mass flow rate (vapor)					
Density	$h_w = \frac{1 - (d_f/D_f)^4}{(358.9268 C d_f^2 Y_1)^2 \rho_{f1}} q_{PPH}^2$ $R_{Df} = \frac{6.31597 q_{PPH}}{\mu_{cP} D_f}$	(a)	$\Delta p^* = \frac{1 - (d_f^*/D_f^*)^4}{(0.126447 C d_f^{*2} Y_1)^2 \rho_{f1}^*} q_{KPH}^2$ $R_{Df} = \frac{353.676 q_{KPH}}{\mu_{cP} D_f^*}$	(i)	(j)
Volumetric at flowing conditions (liquid)					
Specific gravity	$h_w = \frac{1 - (d_f/D_f)^4 F_p G_F}{(5.666455 C d_f^2)^2} q_{gpm}^2$ $R_{Df} = \frac{3159.432 F_p G_F q_{gpm}}{\mu_{cP} D_f}$	(c)	$\Delta p^* = \frac{1 - (d_f^*/D_f^*)^4 F_p G_F}{(0.06667619 C d_f^{*2})^2} q_{lpm}^2$ $R_{Df} = \frac{21199.697 F_p G_F q_{lpm}}{\mu_{cP} D_f^*}$	(k)	(l)
Volumetric at base conditions (liquid)					
Specific gravity	$h_w = \frac{[1 - (d_f/D_f)^4] G_b^2}{(5.666455 C d_f^2)^2 F_p G_F} q_{GPM}^2$ $R_{Df} = \frac{3159.432 G_b q_{GPM}}{\mu_{cP} D_f}$	(e)	$\Delta p^* = \frac{[1 - (d_f^*/D_f^*)^4] G_b^2}{(0.06667619 C d_f^{*2})^2 F_p G_F} q_{LPM}^2$ $R_{Df} = \frac{21199.697 G_b q_{LPM}}{\mu_{cP} D_f^*}$	(m)	(n)
Volumetric at base conditions (gas)					
pvT equation	$h_w = \frac{[1 - (d_f/D_f)^4] p_b^2 G Z_{f1} T_{f1}}{(218.4834 C d_f^2 Y_1 Z_b T_b)^2 p_{f1}} (q_{SCFH})_b^2$ $R_{Df} = \frac{17.04569 G p_b (q_{SCFH})_b}{Z_b T_b \mu_{cP} D_f}$	(g)	$\Delta p^* = \frac{[1 - (d_f^*/D_f^*)^4] p_b^2 G Z_{f1} T_{K1}}{(0.06774938 C d_f^{*2} Y_1 Z_b T_{Kb})^2 p_{f1}} (q_{SCMH})_b^2$ $R_{Df} = \frac{1232.003 G p_b (q_{SCMH})_b}{Z_b T_b \mu_{cP} D_f^*}$	(o)	(p)

NOTE: D_f^* in these equations is defined by $D_f^* = F_{ad}^* F_{dp}^* D_{meas}^*$ and $d_f^* = F_{ad}^* F_{dp}^* d_{meas}^*$ normally $F_{ad}^* = F_{dp}^* = 1.0$.

GENERALIZED FLUID PROPERTIES

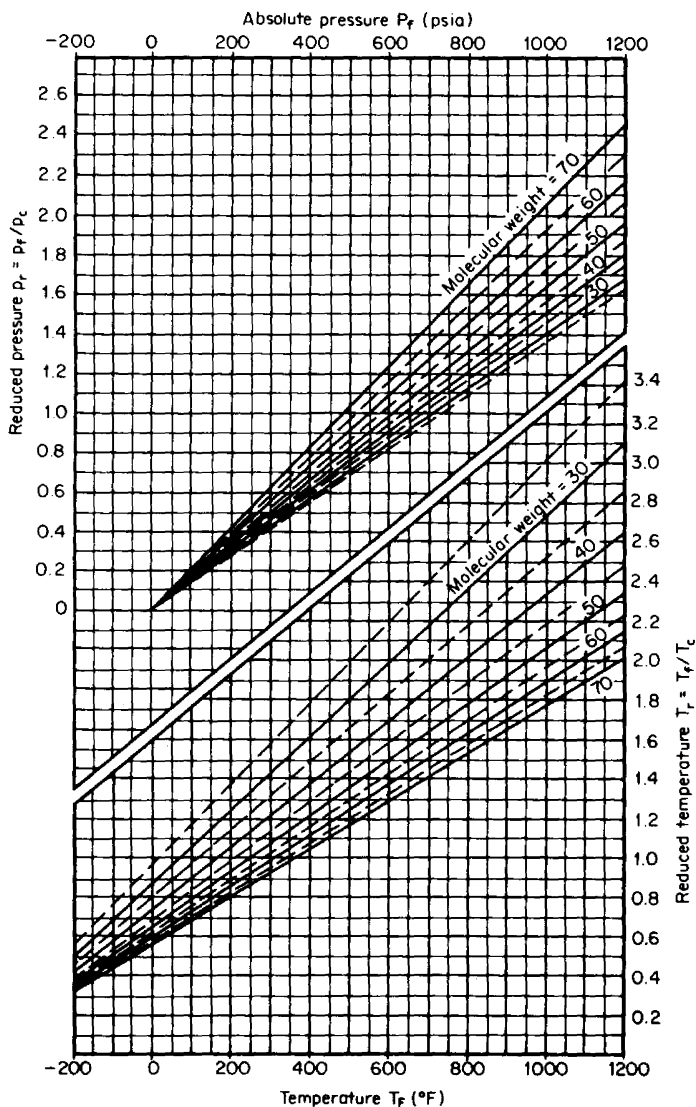


Figure D.1 Estimated reduced pressure and temperature from molecular weight. (From GPSA, 1979; used with permission.)

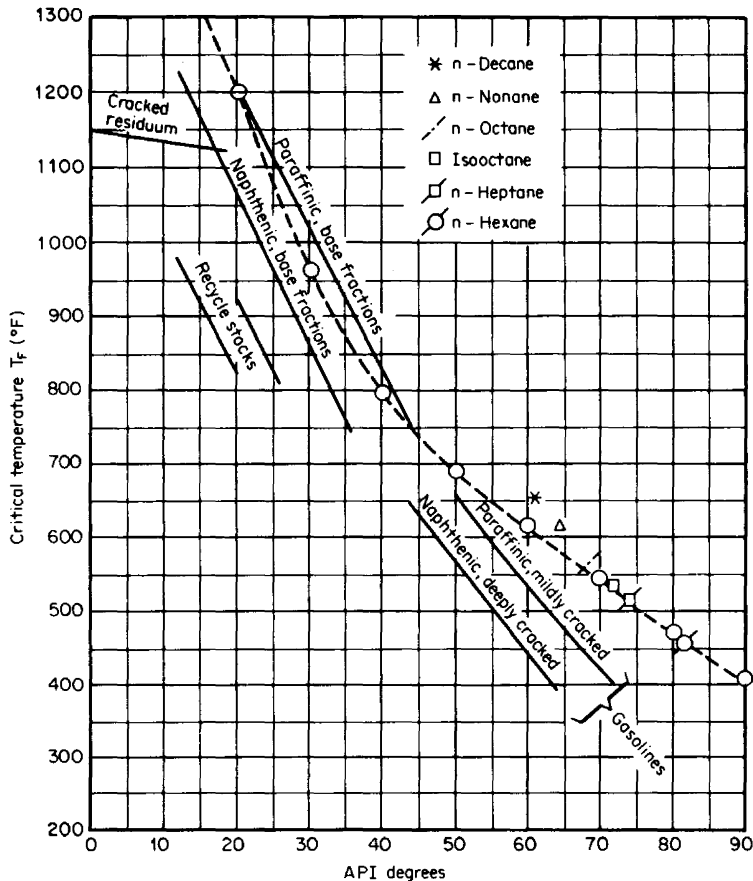


Figure D.2 Estimated critical temperature for typical petroleum oils. (From Spink, 1967.)

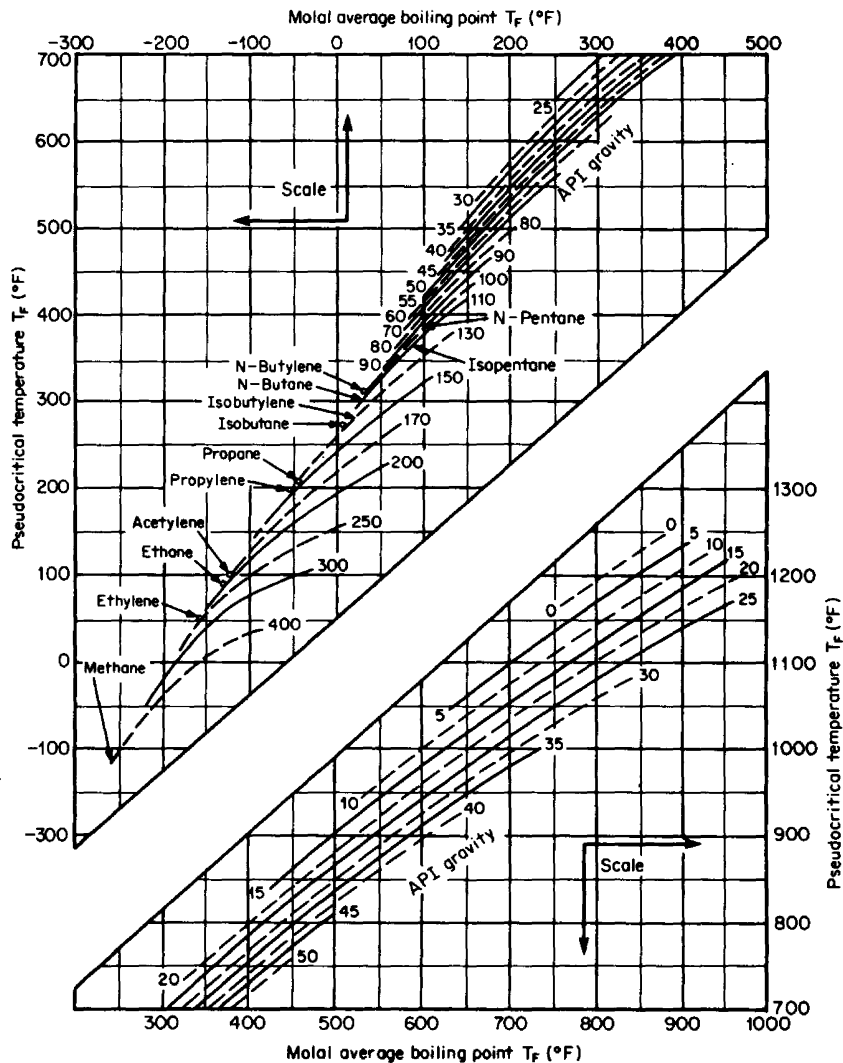


Figure D.3 Chart for estimating pseudocritical temperature from molal average boiling point. (From Spink, 1967.)

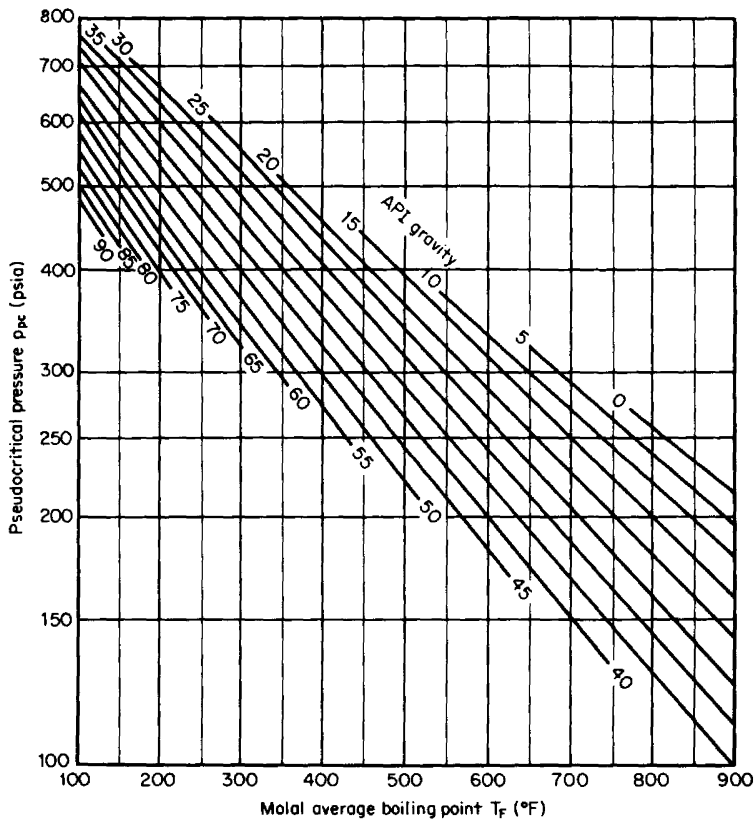


Figure D.4 Chart for estimating critical pressure from molal average boiling point. (From Spink, 1967.)

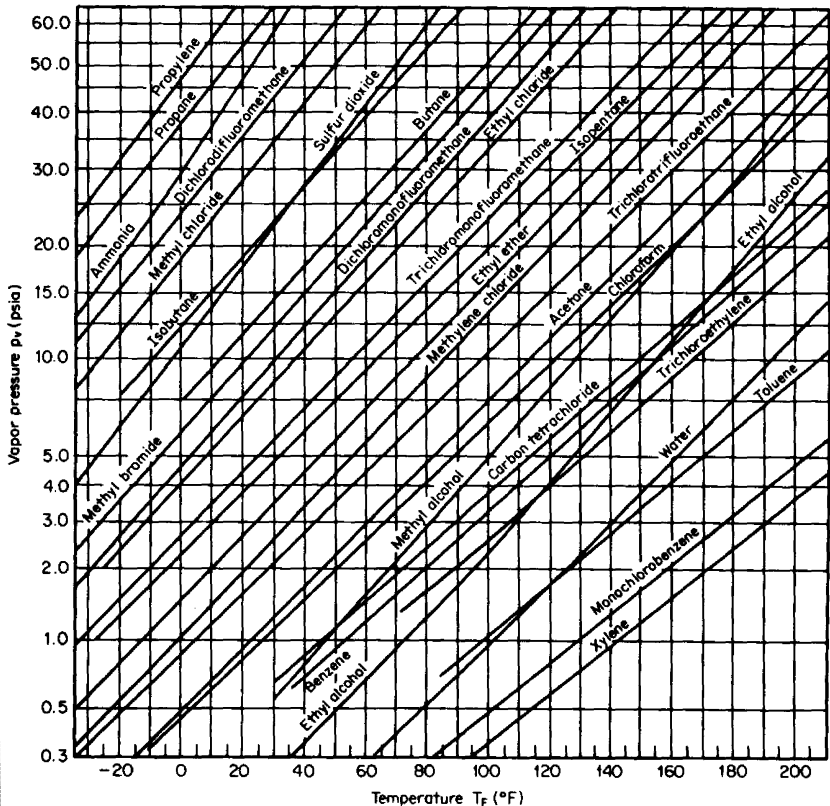


Figure D.5 Vapor-pressure curves for some fluids.

TABLE D.1 Physical Properties

Substance	Molecular weight M_w	Normal boiling point		Critical properties							Isentropic exponent (ideal gas) at 60°F, k_p $= \frac{c_p}{c_v}$
				Temperature T_c		Pressure p_c , psia	Volume		Compress- ibility Z_c , dimension- less	Acentric factor ω	
		°F	°R	°F	°R		V_c , ft ³ / (lb _m ·mol)	v_c , ft ³ /lb			
Acetylene	26.038	-119.1	340.6	95.3	554.9	890.6	1.812	0.0696	0.271	0.184	1.26
Air	28.9625	-317.6	142.1	-220.8	238.9	546.7	1.463	0.0505	0.312	-0.012†	1.400
Ammonia	17.031	-28.2	431.5	270.4	730.1	1635.7	1.159	0.0680	0.242	0.250	1.310
Argon	39.9480	-302.5	157.1	-188.2	271.4	706.9	1.199	0.0300	0.291	-0.004	1.668
Benzene	70.114	176.3	635.9	552.1	1011.8	709.8	4.145	0.0530	0.271	0.212	1.08
1,2-Butadiene	54.092	51.5	511.2	339.0	798.7	652.5	3.507	0.0648	0.267	0.255	1.120
1,3-Butadiene	54.092	24.0	483.7	305.3	765.0	627.5	3.532	0.0653	0.270	0.195	1.120
Isobutane	58.1243	10.67	470.3	274.9	734.6	529.1	4.217	0.0726	0.283	0.176	1.11
<i>n</i> -Butane	58.1243	31.2	490.9	305.7	765.4	551.1	4.0836	0.0703	0.274	0.193	1.10
Isobutylene	56.108	19.7	479.3	292.6	752.2	580.5	3.824	0.0682	0.275	0.190	1.12
1-Butene	56.108	20.8	480.4	295.6	755.3	583.4	3.848	0.0686	0.277	0.187	1.11
Carbon tetrachloride	153.82	169.8	629.5	541.9	1001.5	661.3	4.421	0.0287	0.272	0.194	1.067
Carbon dioxide	44.010	-109.2	350.5	87.9	547.6	1069.9	1.505	0.0342	0.274	0.225	1.295
Carbon monoxide	28.01055	-312.6	147.1	-220.5	239.2	507.0	1.494	0.0533	0.295	0.049	1.395
<i>cis</i> -2-Butene	56.108	38.8	498.4	324.4	784.1	609.9	4.514	0.0805	0.272	0.202	1.121
Chlorine	70.906	-30.0	429.7	290.9	750.6	1116.9	1.983	0.0280	0.275	0.073	1.355

Cyclohexane	84.162	177.4	637.0	536.5	996.1	590.8	4.940	0.0587	0.273	0.213	1.08
Cyclopentane	70.135	120.7	580.3	461.2	920.9	654.0	4.171	0.0595	0.276	0.192	1.117
<i>n</i> -Decane	142.286	345.5	805.1	652.0	1111.7	305.7	9.640	0.0678	0.247	0.490	1.038
2,3-Dimethyl butane	86.178	136.5	596.2	440.2	899.8	454.1	5.742	0.0666	0.270	0.247	1.065
2,2-Dimethyl pentane	100.205	174.7	634.3	477.1	936.7	402.7	6.666	0.0665	0.267	0.289	1.053
2,4-Dimethyl pentane	100.205	177.0	636.7	475.8	935.5	396.8	6.705	0.0669	0.265	0.306	1.053
3,3-Dimethyl pentane	100.205	186.9	646.6	505.7	965.3	427.7	6.637	0.0662	0.274	0.270	1.073
Ethane	30.0701	-127.6	332.1	90.1	549.7	708.4	2.374	0.0789	0.285	0.098	1.18
Ethyl alcohol	46.069	173.0	632.7	469.5	929.2	925.9	2.671	0.0580	0.248	0.635	1.13
Ethylene	28.054	-154.8	304.9	48.7	508.3	730.4	2.061	0.0028	0.276	0.085	1.22
Ethylbenzene	106.168	277.1	736.7	651.1	1110.8	523.2	5.992	0.0564	0.263	0.301	1.072
3-Ethylpentane	100.205	200.2	659.9	513.4	973.1	418.8	6.657	0.0664	0.267	0.310	1.054
Helium-4	4.003	-452.1	7.6	-450.3	9.34	32.9	0.917	0.2290	0.301	0.387	1.660
<i>n</i> -Heptane	100.205	209.2	668.9	512.7	972.4	396.8	6.916	0.0690	0.263	0.351	1.052
<i>n</i> -Hexane	86.178	155.8	615.4	453.7	913.3	430.6	5.918	0.0687	0.260	0.296	1.062
Hydrogen	2.016	-423.0	36.7	-399.9	59.8	188.1	1.040	0.5158	0.305	0.22	1.412
Hydrogen chloride	34.461	-121.1	338.6	124.6	584.3	1205.7	1.295	0.0376	0.249	0.12	1.41
Hydrogen sulfide	34.08	-76.6	383.1	212.1	671.8	1269.2	1.613	0.0473	0.284	0.100	1.32
Methane	16.043	-258.6	201.1	-116.6	343.1	667.2	1.589	0.0991	0.288	0.008	1.315
Methyl alcohol	32.042	148.4	608.4	463.0	922.7	1174.2	1.889	0.0589	0.224	0.559	1.203
Neon	20.183	-411.1	48.6	-379.8	79.9	399.7	0.667	0.0330	0.311	0.000	1.667

TABLE D.1 Physical Properties (*Continued*)

Substance	Molecular weight M_w	Critical properties									Isentropic exponent (ideal gas) at 60°F, k_p $= \frac{c_p}{c_v}$
		Normal boiling point		Temperature T_c		Pressure p_c , psia	Volume		Compress- ibility Z_c , dimension- less	Acentric factor ω	
							V_c , ft ³ / (lb _m · mol)	v_c , ft ³ /lb			
		°F	°R	°F	°R						
Nitrogen	28.0134	−320.4	139.3	−232.5	227.2	492.3	1.436	0.0513	0.290	0.040	1.400
<i>n</i> -Nonane	128.259	303.5	763.2	610.6	1070.3	335.1	8.913	0.0695	0.26	0.444	1.042
Octane (average)	114.2327	258.2	717.9	564.8	1024.5	364.5	7.873	0.0689	0.261	0.399	1.046
<i>n</i> -Octane	114.232	256.7	716.4	564.2	1023.8	360.1	7.904	0.0692	0.259	0.394	1.046
2,2,4-Trimethylpentane†	114.232	210.7	670.3	519.4	979.0	371.8	7.517	0.0658	0.266	0.303	1.046
Oxygen	31.9988	−297.3	162.4	−181.4	278.3	731.9	1.175	0.0367	0.288	0.021	1.397
2-Methyl butane (isopentane)†	72.1514	82.1	541.8	369.1	828.7	490.9	4.910	0.0680	0.271	0.227	1.076
2,2-Dimethyl propane, (neopentane)†	72.151	49.0	508.7	321.2	780.8	464.4	4.854	0.0673	0.269	0.197	1.076
<i>n</i> -Pentane	72.1514	96.9	556.6	385.6	845.3	489.4	4.856	0.0673	0.262	0.251	1.07

Propane	44.0972	-43.7	416	206.0	665.6	615.8	3.260	0.0739	0.281	0.152	1.13
Propylene	42.081	-54.0	405.7	197.3	657.0	670.1	2.893	0.0688	0.275	0.148	1.154
Sulfur dioxide	64.063	13.7	473.4	315.8	775.4	1143.4	1.951	0.0304	0.268	0.251	1.29
Styrene	104.152	293.3	752.9	704.9	1164.6	579.0	5.634	0.0541	0.261	0.257†	1.076
Toluene	92.141	231.2	690.8	605.4	1065.1	596.7	5.057	0.0548	0.264	0.257	1.06
Triptane (2,2,3-trimethylbutane)	100.205	177.5	637.2	496.3	956.0	429.1	6.383	0.0637	0.267	0.251	1.052
Water	18.01534	212.1	671.8	705.5	1165.1	3197.9	0.895	0.0497	0.229	0.344	1.335
<i>m</i> -Xylene	106.168	282.5	742.1	650.9	1110.6	514.4	6.025	0.0567	0.260	0.331	1.072
<i>O</i> -Xylene	106.168	292.0	751.7	674.7	1134.4	540.8	5.920	0.0558	0.263	0.314	1.049
<i>p</i> -Xylene	106.168	281.0	740.7	649.5	1109.2	510.0	6.069	0.0572	0.260	0.324	1.073
Xenon	131.30	-162.7	297.0	61.8	521.5	846.5	1.891	0.0144	0.286	0.002	1.665

†This acentric factor is calculated as

$$\omega = \frac{3 \log (p_c/14.7)}{7 T_c/T_B - 1.0} - 1.0$$

‡Source: Gas Processors Suppliers Association, "Engineering Data Book", Ninth edition, fourth revision, 1979

SOURCE: Reid, et al. (1987).

LIQUID DENSITY AND SPECIFIC GRAVITY

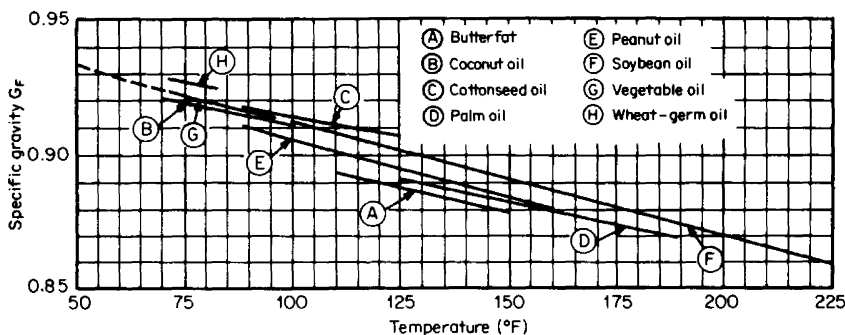


Figure E.1 Specific gravities of fats and oils. (From Fischer & Porter Catalog 10-A-54; used with permission.)

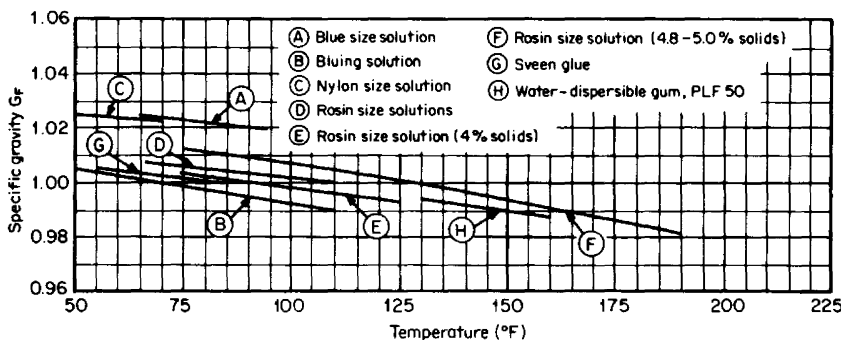


Figure E.2 Specific gravities of liquids related to the paper, leather, and textile industries. (From Fischer & Porter Catalog 10-A-54; used with permission.)

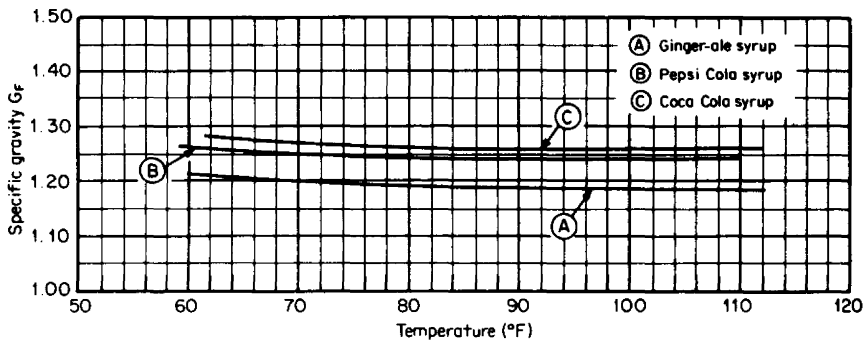


Figure E.3 Specific gravities of syrups. (From Fischer & Porter Catalog 10-A-54; used with permission.)

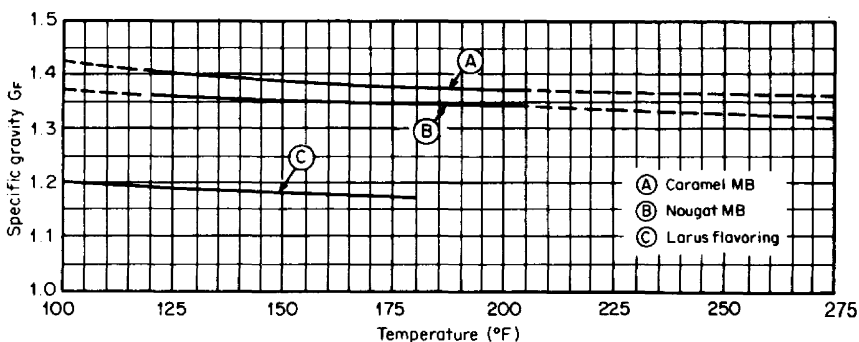


Figure E.4 Specific gravities of liquids related to the candy industry. (From Fischer & Porter Catalog 10-A-54; used with permission.)

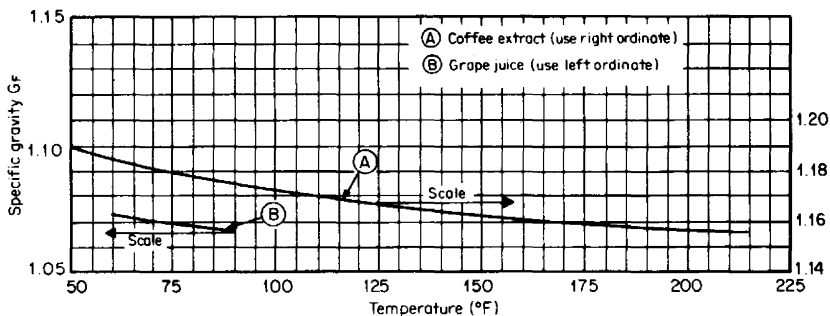


Figure E.5 Specific gravities of liquids related to the food industry. (From Fischer & Porter Catalog 10-A-54; used with permission.)

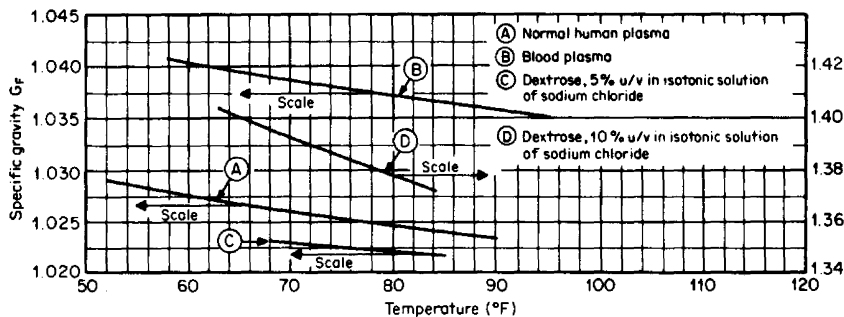


Figure E.6 Specific gravities of intravenous solutions. (From Fischer & Porter Catalog 10-A-54; used with permission.)

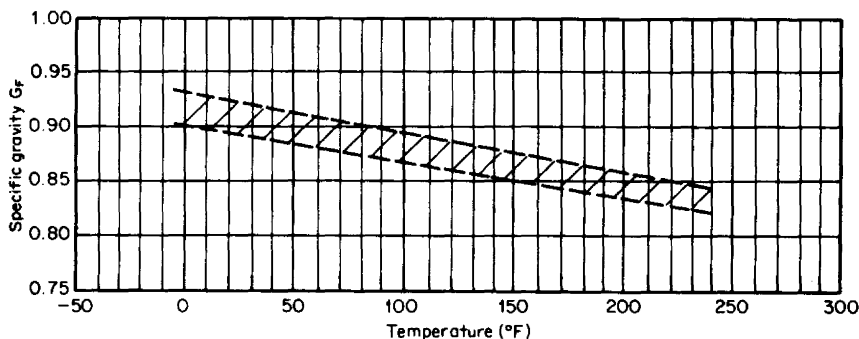


Figure E.7 Specific gravities of Garboyle D.T.E. oils. (From Fischer & Porter Catalog 10-A-54; used with permission.)

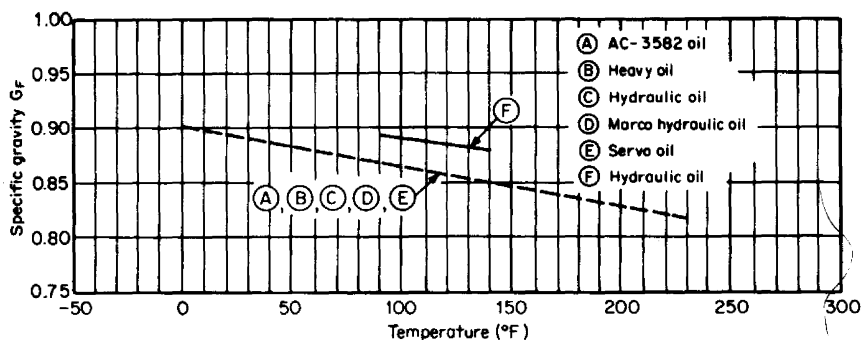


Figure E.8 Specific gravities of hydraulic oils. (From Fischer & Porter Catalog 10-A-54; used with permission.)

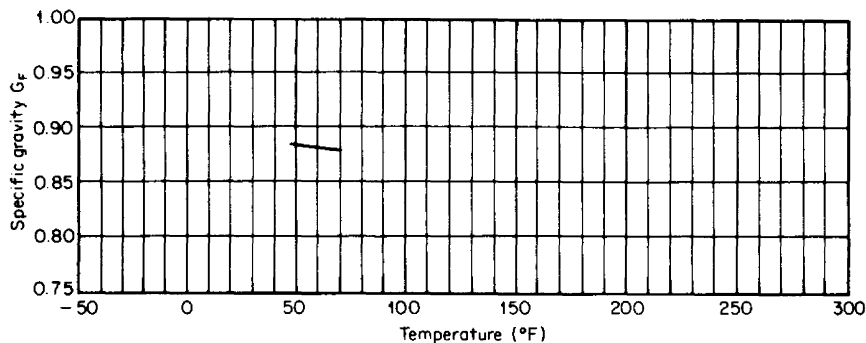


Figure E.9 Specific gravities of Delco lube oil. (From Fischer & Porter Catalog 10-A-54; used with permission.)

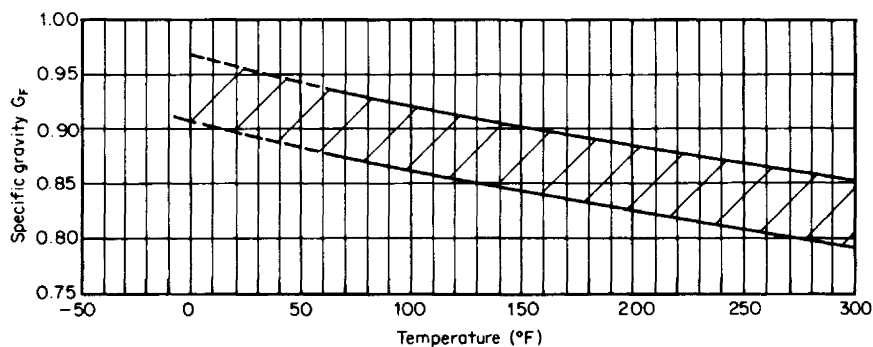


Figure E.10 Specific gravities of S.A.E. (Pennsylvania base) oils. (From Fischer & Porter Catalog 10-A-54; used with permission.)

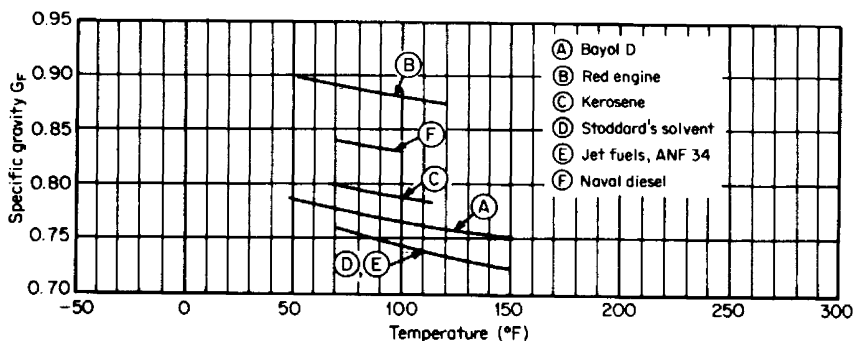


Figure E.11 Specific gravities of miscellaneous fuel oils. (From Fischer & Porter Catalog 10-A-54; used with permission.)

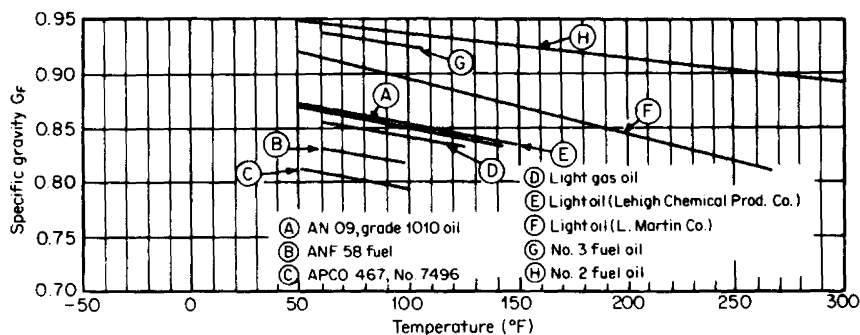


Figure E.12 Specific gravities of miscellaneous fuel oils. (From Fischer & Porter Catalog 10-A-54; used with permission.)

- | | |
|--------------------------------|-----------------------------|
| (A) Typical diesel fuel blends | (F) Heptane |
| (B) Ethane | (G) Decane |
| (C) Propane | (H) Typical kerosene blends |
| (D) Butane | (I) Typical gasoline blends |
| (E) Pentane | |

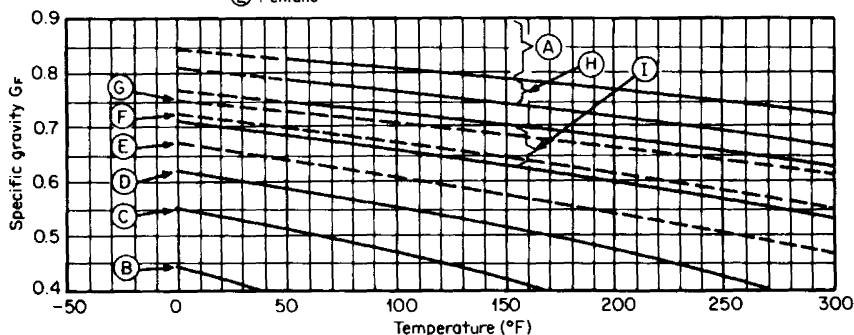


Figure E.13 Specific gravities of typical fuel blends. (From Fischer & Porter Catalog 10-A-54; used with permission.)

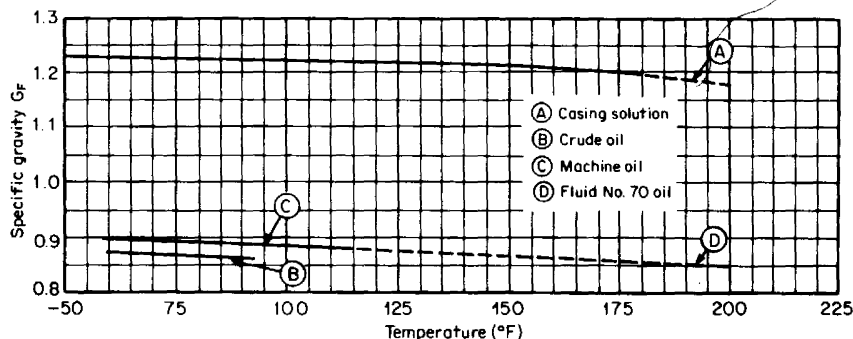


Figure E.14 Specific gravities of miscellaneous oils. (From Fischer & Porter Catalog 10-A-54; used with permission.)

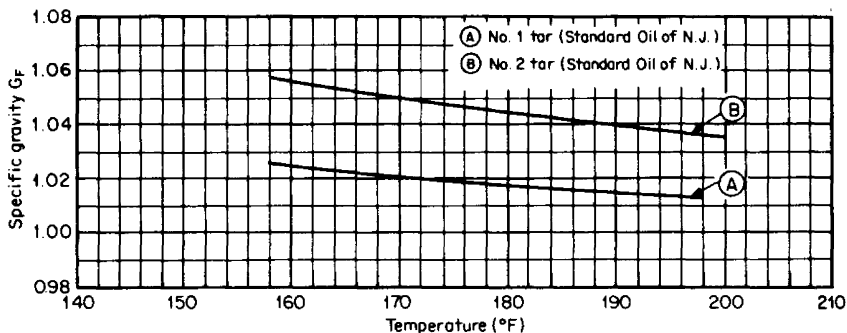


Figure E.15 Specific gravities of high boiling fractions. (From Fischer & Porter Catalog 10-A-54; used with permission.)

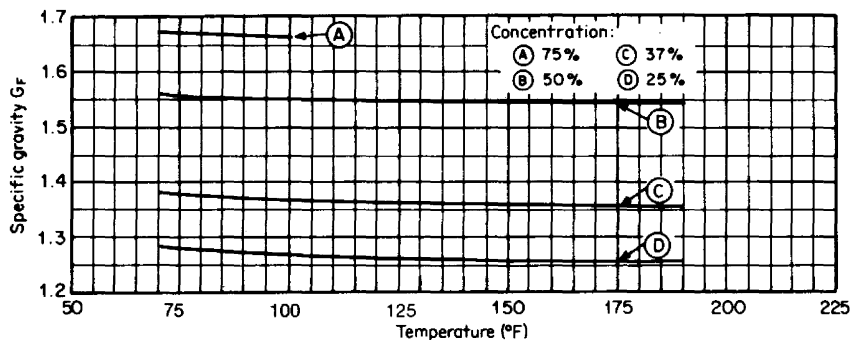


Figure E.16 Specific gravities of phosphoric acid solutions. (From Fischer & Porter Catalog 10-A-54; used with permission.)

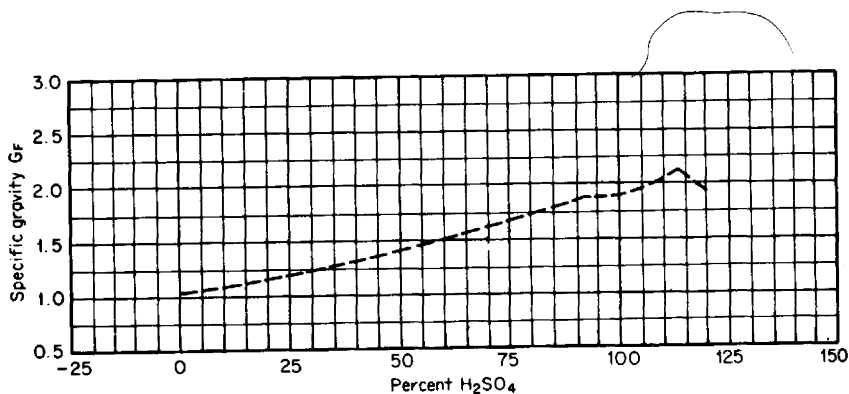


Figure E.17 Specific gravities of sulfuric acid solutions at a temperature T_F of 60°F (15.6°C). (From Fischer & Porter Catalog 10-A-54; used with permission.)

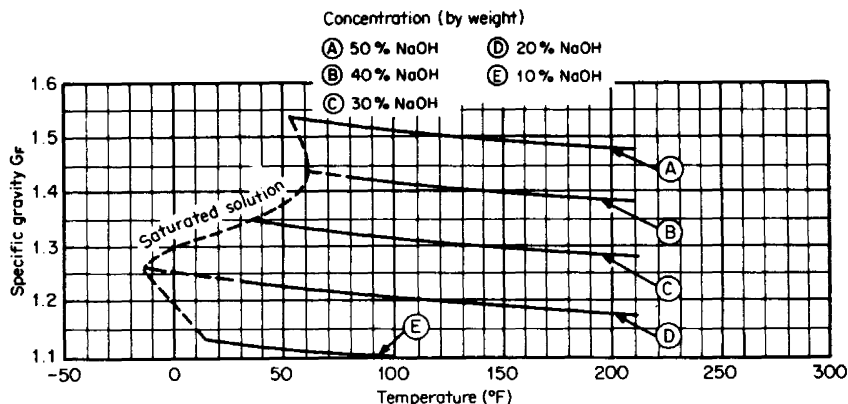


Figure E.18 Specific gravities of sodium hydroxide solutions. (From Fischer & Porter Catalog 10-A-54; used with permission.)

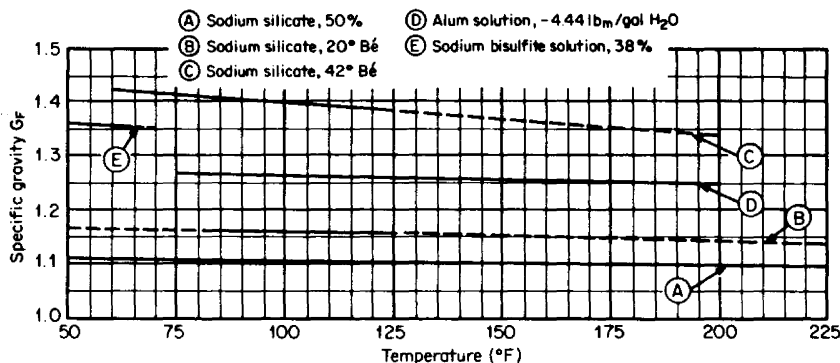


Figure E.19 Specific gravities of inorganic solutions. (From Fischer & Porter Catalog 10-A-54; used with permission.)

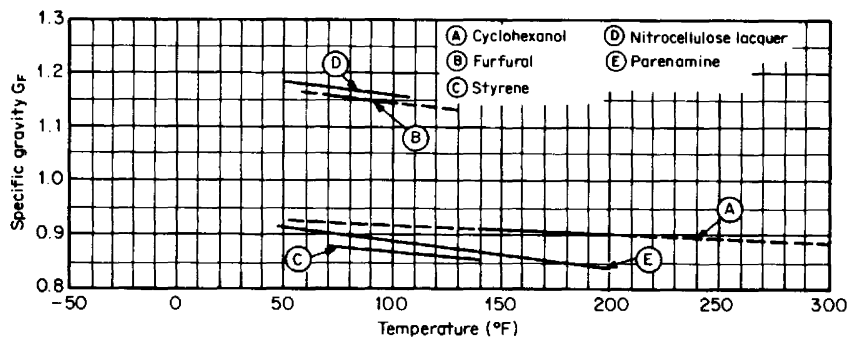


Figure E.20 Specific gravities of miscellaneous organic compounds. (From Fischer & Porter Catalog 10-A-54; used with permission.)

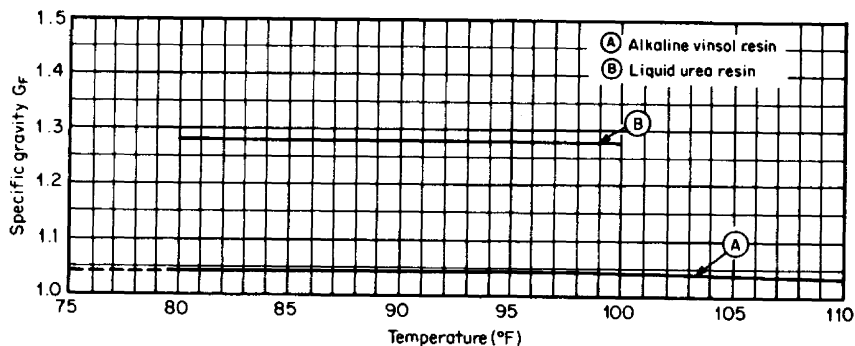


Figure E.21 Specific gravities of resins. (From Fischer & Porter Catalog 10-A-54; used with permission.)

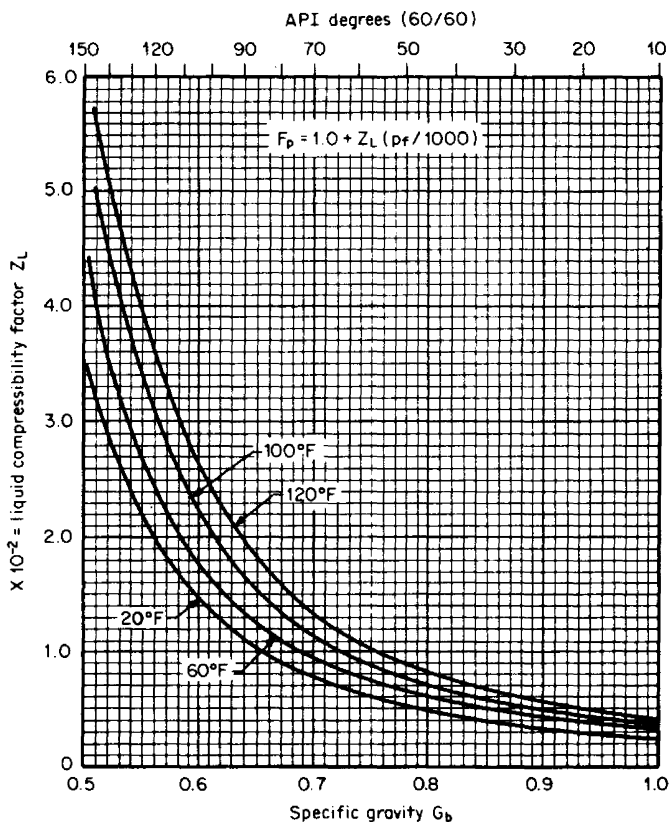


Figure E.22 Average liquid-hydrocarbon compressibility factor.

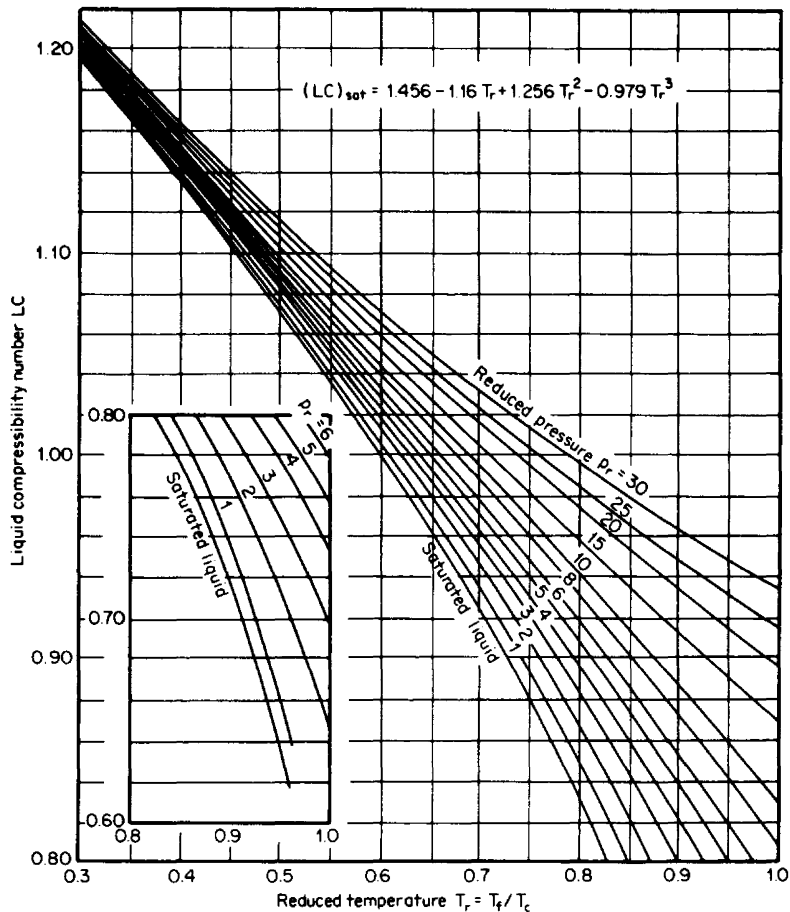


Figure E.23 Lu's generalized liquid compressibility diagram. (From Perry and Green, 1984.)

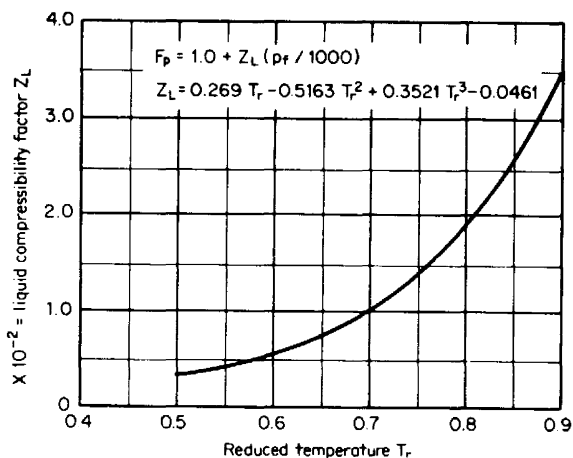


Figure E.24 Generalized liquid compressibility factor.

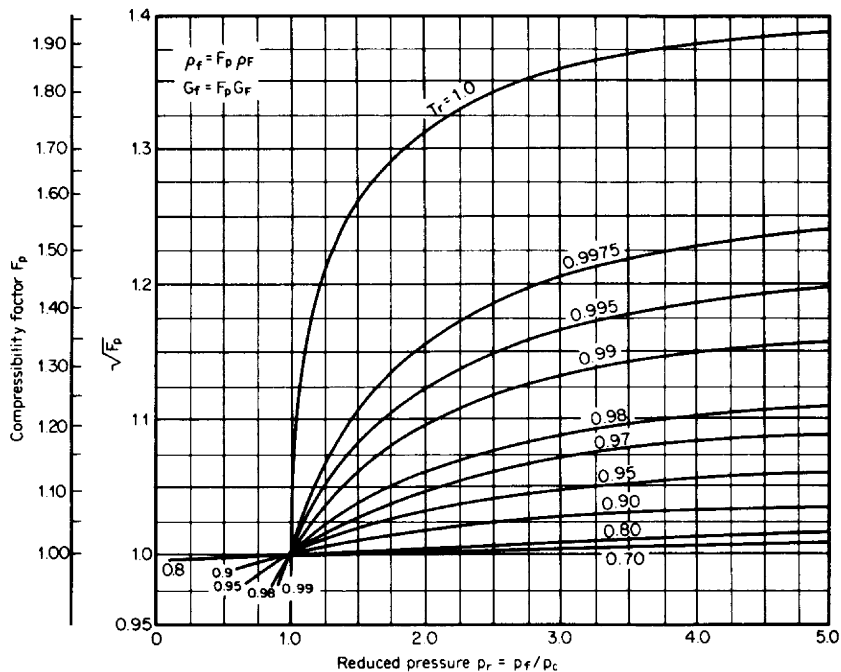


Figure E.25 Generalized petroleum-oil compressibility factor. (From Spink, 1967.)

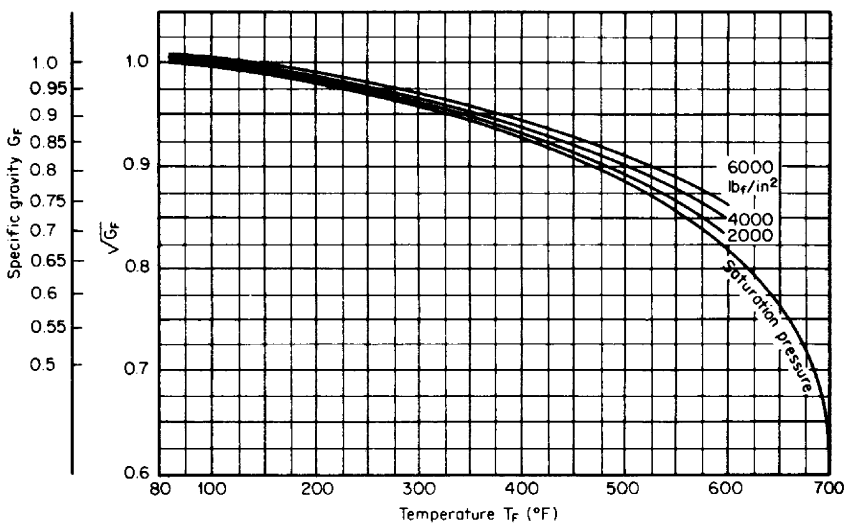


Figure E.26 Specific gravity and the square root of specific gravity for water. (From Spink, 1967.)

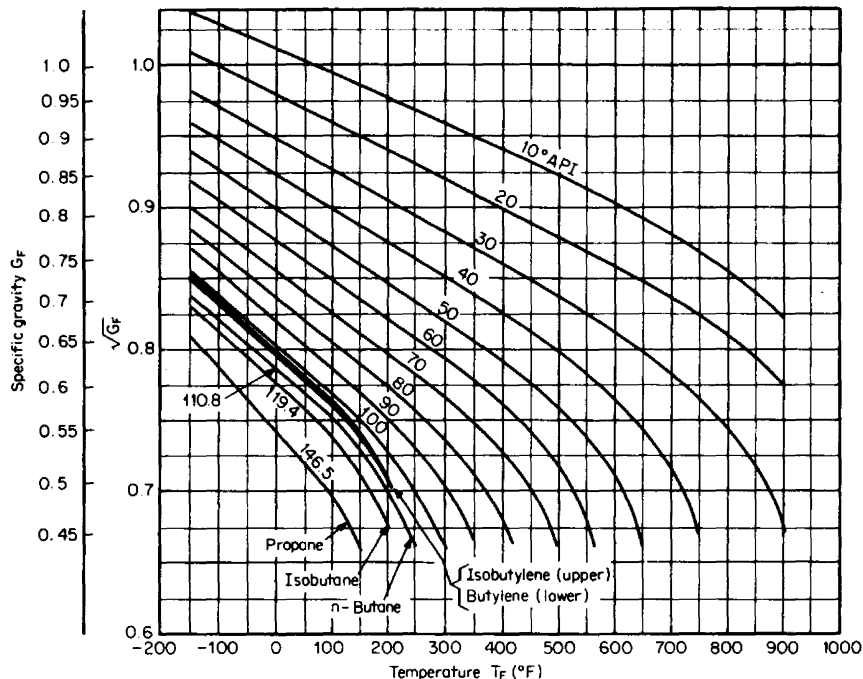


Figure E.27 Specific gravity and the square root of specific gravity for hydrocarbons. (From Spink, 1967.)

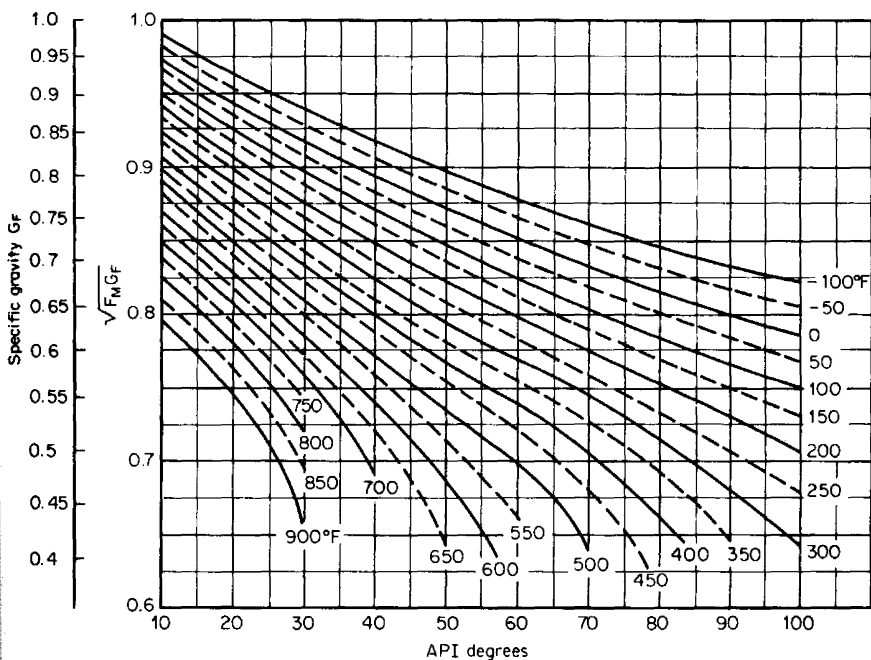


Figure E.28 Specific gravity and the square root of specific gravity for hydrocarbons, based on API-degrees reading. (From Spink, 1967.)

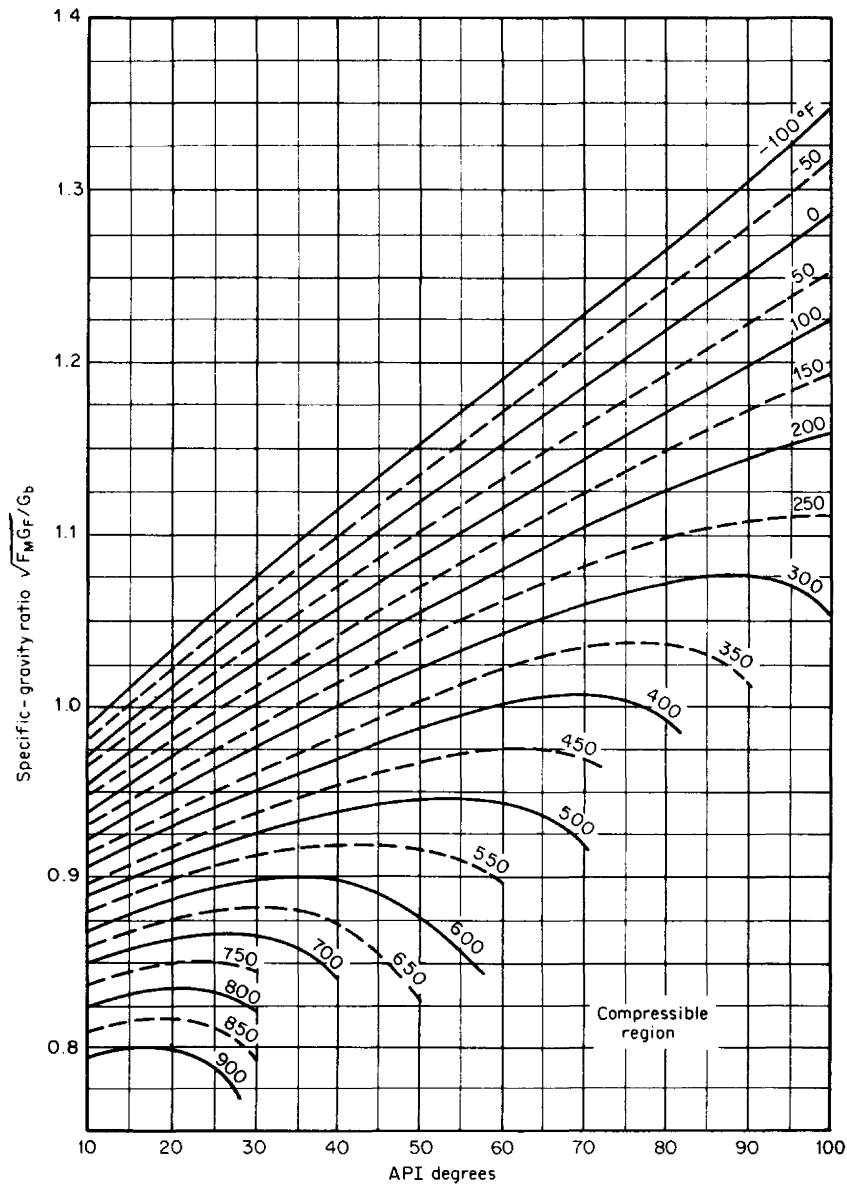


Figure E.29 Square root of specific gravity divided by base specific gravity for petroleum oils. (From Spink, 1967.)

TABLE E.1 Liquid Compressibility Data

Substance	Temperature, °F	Bulk-modulus zero intercept K_{BMO}	Slope b_c	Liquid compressibility factor Z_L
Acetone	68	240,000	5.7	0.00417
Amyl alcohol (iso)	68	172,500	5.95	0.00580
Amyl alcohol (<i>n</i>)	68	240,000	10.7	0.00417
Benzene	68	188,000	9.7	0.00532
Bromine	68	259,000	8.8	0.00386
Butyl alcohol (iso)	68	179,000	16.4	0.00559
Carbon bisulfide	68	254,000	6.6	0.00394
Carbon tetrachloride	68	168,500	10.4	0.00594
Chloroform	68	174,500	11.2	0.00573
Dichloroethyl sulfide	68	426,000	12.3	0.00235
Ethyl acetate	68	161,000	11.1	0.00621
Ethyl alcohol	68	230,000	5.3	0.00435
Ethyl bromide	68	145,000	11.0	0.00690
Ethyl chloride	68	142,000	10.7	0.00704
Ethyl ether	68	172,000	9.0	0.00581
Ethyl iodide	68	179,000	10.7	0.00559
Hexane	68	123,500	29.7	0.00810
Kerosene	68	263,500	8.1	0.00380
Mercury	71.5	3,650,000	7.7	0.000274
Methyl alcohol	68	152,500	9.9	0.00656
Phosphorus trichloride	68	230,000	10.8	0.00435
Propyl alcohol	68	188,000	9.7	0.00532
Toluene	68	196,000	10.6	0.00510
Water	68	337,000	7.8	0.00297
Water	104	381,500	8.0	0.00262

TABLE E.2 Specific Gravities at 60°F/60°F Corresponding to API Degrees and Weights per U.S. Gallon at 60°F†

API degrees	Specific gravity	Pounds per U.S. gallon	API degrees	Specific gravity	Pounds per U.S. gallon	API degrees	Specific gravity	Pounds per U.S. gallon	API degrees	Specific gravity	Pounds per U.S. gallon
10	1.0000	8.328	33	0.8602	7.163	56	0.7547	6.283	79	0.6722	5.595
11	0.9930	8.270	34	0.8550	7.119	57	0.7507	6.249	80	0.6690	5.568
12	0.9861	8.212	35	0.8498	7.076	58	0.7467	6.216	81	0.6659	5.542
13	0.9792	8.155	36	0.8448	7.034	59	0.7428	6.184	82	0.6628	5.516
14	0.9725	8.099	37	0.8398	6.993	60	0.7389	6.151	83	0.6597	5.491
15	0.9659	8.044	38	0.8348	6.951	61	0.7351	6.119	84	0.6566	5.465
16	0.9593	7.989	39	0.8299	6.910	62	0.7313	6.087	85	0.6536	5.440
17	0.9529	7.935	40	0.8251	6.870	63	0.7275	6.056	86	0.6506	5.415
18	0.9465	7.882	41	0.8203	6.830	64	0.7238	6.025	87	0.6476	5.390
19	0.9402	7.830	42	0.8155	6.790	65	0.7201	5.994	88	0.6446	5.365
20	0.9340	7.778	43	0.8109	6.752	66	0.7165	5.964	89	0.6417	5.341
21	0.9279	7.727	44	0.8063	6.713	67	0.7128	5.934	90	0.6388	5.316
22	0.9218	7.676	45	0.8017	6.675	68	0.7093	5.904	91	0.6360	5.293
23	0.9159	7.627	46	0.7972	6.637	69	0.7057	5.874	92	0.6331	5.269
24	0.9100	7.578	47	0.7927	6.600	70	0.7022	5.845	93	0.6303	5.246
25	0.9042	7.529	48	0.7883	6.563	71	0.6988	5.817	94	0.6275	5.222
26	0.8984	7.481	49	0.7839	6.526	72	0.6953	5.788	95	0.6247	5.199
27	0.8927	7.434	50	0.7796	6.490	73	0.6919	5.759	96	0.6220	5.176
28	0.8871	7.387	51	0.7753	6.455	74	0.6886	5.731	97	0.6193	5.154
29	0.8816	7.341	52	0.7711	6.420	75	0.6852	5.703	98	0.6166	5.131
30	0.8762	7.296	53	0.7669	6.385	76	0.6819	5.676	99	0.6139	5.109
31	0.8708	7.251	54	0.7628	6.350	77	0.6787	5.649	100	0.6112	5.086
32	0.8654	7.206	55	0.7587	6.316	78	0.6754	5.622			

†Calculated from the formula specific gravity = $141.5/(131.5 + \text{API degrees})$. The weights in this table are weights in air at 60°F with 50 percent humidity and 760 mm pressure.

SOURCE: Baumeister (1978).

TABLE E.3 Specific Gravities at 60°F/60°F Corresponding to Degrees Baumé for Liquids Lighter than Water and Weights per U.S. Gallon at 60°F†

Degrees Baumé	Specific gravity	Pounds per gallon	Degrees Baumé	Specific gravity	Pounds per gallon	Degrees Baumé	Specific gravity	Pounds per gallon	Degrees Baumé	Specific gravity	Pounds per gallon
10.0	1.0000	8.328	33.0	0.8589	7.152	55.0	0.7568	6.300	78.0	0.6731	5.602
11.0	0.9929	8.269	34.0	0.8537	7.108	56.0	0.7527	6.266	79.0	0.6699	5.576
12.0	0.9859	8.211	35.0	0.8485	7.065	57.0	0.7487	6.233	80.0	0.6667	5.549
13.0	0.9790	8.153	36.0	0.8434	7.022	58.0	0.7447	6.199	81.0	0.6635	5.522
14.0	0.9722	8.096	37.0	0.8383	6.980	59.0	0.7407	6.166	82.0	0.6604	5.497
15.0	0.9655	8.041	38.0	0.8333	6.939	60.0	0.7368	6.134	83.0	0.6573	5.471
16.0	0.9589	7.986	39.0	0.8284	6.898	61.0	0.7330	6.102	84.0	0.6542	5.445
17.0	0.9524	7.931	40.0	0.8235	6.857	62.0	0.7292	6.070	85.0	0.6512	5.420
18.0	0.9459	7.877	41.0	0.8187	6.817	63.0	0.7254	6.038	86.0	0.6482	5.395
19.0	0.9396	7.825	42.0	0.8140	6.777	64.0	0.7216	6.007	87.0	0.6452	5.370
20.0	0.9333	7.772	43.0	0.8092	6.738	65.0	0.7179	5.976	88.0	0.6422	5.345
21.0	0.9272	7.721	44.0	0.8046	6.699	66.0	0.7143	5.946	89.0	0.6393	5.320
22.0	0.9211	7.670	45.0	0.8000	6.661	67.0	0.7107	5.916	90.0	0.6364	5.296
23.0	0.9150	7.620	46.0	0.7955	6.623	68.0	0.7071	5.886	91.0	0.6335	5.272
24.0	0.9091	7.570	47.0	0.7910	6.586	69.0	0.7035	5.856	92.0	0.6306	5.248
25.0	0.9032	7.522	48.0	0.7865	6.548	70.0	0.7000	5.827	93.0	0.6278	5.225
26.0	0.8974	7.473	49.0	0.7821	6.511	71.0	0.6965	5.798	94.0	0.6250	5.201
27.0	0.8917	7.425	50.0	0.7778	6.476	72.0	0.6931	5.769	95.0	0.6222	5.178
28.0	0.8861	7.378	51.0	0.7735	6.440	73.0	0.6897	5.741	96.0	0.6195	5.155
29.0	0.8805	7.332	52.0	0.7692	6.404	74.0	0.6863	5.712	97.0	0.6167	5.132
30.0	0.8750	7.286	53.0	0.7650	6.369	75.0	0.6829	5.685	98.0	0.6140	5.110
31.0	0.8696	7.241	54.0	0.7609	6.334	76.0	0.6796	5.657	99.0	0.6114	5.088
32.0	0.8642	7.196				77.0	0.6763	5.629	100.0	0.6087	5.066

†Calculated from the formula specific gravity $\frac{60^\circ}{60^\circ} F = 140/(130 - \text{Baumé degrees})$.

TABLE E.4 Specific Gravities at 60°F/60°F Corresponding to Degrees Baumé for Liquids Heavier than Water†

Degrees Baumé	Specific gravity	Degrees Baumé	Specific gravity	Degrees Baumé	Specific gravity	Degrees Baumé	Specific gravity	Degrees Baumé	Specific gravity	Degrees Baumé	Specific gravity
0	1.0000	12	1.0902	24	1.1983	36	1.3303	48	1.4948	60	1.7059
1	1.0069	13	1.0985	25	1.2083	37	1.3426	49	1.5104	61	1.7262
2	1.0140	14	1.1069	26	1.2185	38	1.3551	50	1.5263	62	1.7470
3	1.0211	15	1.1154	27	1.2288	39	1.3679	51	1.5426	63	1.7683
4	1.0284	16	1.1240	28	1.2393	40	1.3810	52	1.5591	64	1.7901
5	1.0357	17	1.1328	29	1.2500	41	1.3942	53	1.5761	65	1.8125
6	1.0432	18	1.1417	30	1.2609	42	1.4078	54	1.5934	66	1.8354
7	1.0507	19	1.1508	31	1.2719	43	1.4216	55	1.6111	67	1.8590
8	1.0584	20	1.1600	32	1.2832	44	1.4356	56	1.6292	68	1.8831
9	1.0662	21	1.1694	33	1.2946	45	1.4500	57	1.6477	69	1.9079
10	1.0741	22	1.1789	34	1.3063	46	1.4646	58	1.6667	70	1.9333
11	1.0821	23	1.1885	35	1.3182	47	1.4796	59	1.6860		

†Calculated from the formula specific gravity $\frac{60^\circ}{60^\circ} \text{F} = 145/(145 - \text{Baumé degrees})$.

SOURCE: Baumeister (1978).

TABLE E.5 Density of Mercury: U.S. and SI Units†

Temperature				Temperature			
°F	°C	lb _m /ft ³	kg/m ³	°F	°C	lb _m /ft ³	kg/m ³
32	0.00	848.72	13595.2	56	13.33	846.67	13562.3
33	0.56	848.63	13593.8	57	13.89	846.58	13560.9
34	1.11	848.55	13592.4	58	14.44	846.50	13559.5
35	1.67	848.46	13591.0	59	15.00	846.41	13558.2
36	2.22	848.38	13589.7	60	15.56	846.32	13556.8
37	2.78	848.29	13588.3	61	16.11	846.24	13555.4
38	3.33	848.20	13586.9	62	16.67	846.15	13554.1
39	3.89	848.12	13585.6	63	17.22	846.07	13552.7
40	4.44	848.03	13584.2	64	17.78	845.98	13551.3
41	5.00	847.95	13582.8	65	18.33	845.90	13550.0
42	5.56	847.86	13581.5	66	18.89	845.81	13548.6
43	6.11	847.78	13580.1	67	19.44	845.73	13547.2
44	6.67	847.69	13578.7	68	20.00	845.64	13545.9
45	7.22	847.61	13577.3	69	20.56	845.55	13544.5
46	7.78	847.52	13576.0	70	21.11	845.47	13543.1
47	8.33	847.44	13574.6	71	21.67	845.38	13541.8
48	8.89	847.35	13573.2	72	22.22	845.30	13540.4
49	9.44	847.26	13571.9	73	22.78	845.21	13539.0
50	10.00	847.18	13570.5	74	23.33	845.13	13537.6
51	10.56	847.09	13569.1	75	23.89	845.04	13536.3
52	11.11	847.01	13567.8	76	24.44	844.96	13534.9
53	11.67	846.92	13566.4	77	25.00	844.87	13533.5
54	12.22	846.84	13565.0	78	25.56	844.79	13532.2
55	12.78	846.75	13563.7	79	26.11	844.70	13530.8

TABLE E.5 Density of Mercury: U.S. and SI Units† (*Continued*)

Temperature				Temperature			
°F	°C	lb _m /ft ³	kg/m ³	°F	°C	lb _m /ft ³	kg/m ³
80	26.67	844.61	13529.4	91	32.78	843.67	13514.4
81	27.22	844.53	13528.1	92	33.33	843.59	13513.0
82	27.78	844.44	13526.7	93	33.89	843.50	13511.6
83	28.33	844.36	13525.3	94	34.44	843.42	13510.3
84	28.89	844.27	13523.9	95	35.00	843.33	13508.9
85	29.44	844.19	13522.6	96	35.56	843.25	13507.5
86	30.00	844.10	13521.2	97	36.11	843.16	13506.1
87	30.56	844.02	13519.8	98	36.67	843.08	13504.8
88	31.11	843.93	13518.5	99	37.22	842.99	13503.4
89	31.67	843.85	13517.1	100	37.78	842.91	13502.0
90	32.22	843.76	13515.7	101	38.33	842.82	13500.7

† $\rho_{\text{Hg}} = 846.324[1 - 0.000101(T_F - 60)]$. Equation from AGA Report 3 (ANSI/API 2530, 1985).

TABLE E.6 Density and Viscosity of Water: U.S. and SI Units

Temperature		Density†		Viscosity‡ μ_{cP}
°F	°C	lb _m /ft ³	kg/m ³	
32	0.00	62.41796	999.839	1.7869
33	0.56	62.42014	999.874	1.7536
34	1.11	62.42198	999.904	1.7212
35	1.67	62.42348	999.928	1.6898
36	2.22	62.42465	999.947	1.6592
37	2.78	62.42549	999.960	1.6295
38	3.33	62.42601	999.968	1.6005
39	3.89	62.42622	999.972	1.5724
40	4.44	62.42611	999.970	1.5450
41	5.00	62.42571	999.964	1.5183
42	5.56	62.42500	999.952	1.4923
43	6.11	62.42400	999.936	1.4670
44	6.67	62.42271	999.916	1.4424
45	7.22	62.42114	999.890	1.4184
46	7.78	62.41928	999.861	1.3950
47	8.33	62.41715	999.827	1.3722
48	8.89	62.41476	999.788	1.3499
49	9.44	62.41209	999.746	1.3283
50	10.00	62.40916	999.699	1.3071
51	10.56	62.40598	999.648	1.2865
52	11.11	62.40254	999.592	1.2664
53	11.67	62.39885	999.533	1.2468
54	12.22	62.39491	999.470	1.2276
55	12.78	62.39073	999.403	1.2089
56	13.33	62.38631	999.333	1.1907
57	13.89	62.38165	999.258	1.1729
58	14.44	62.37676	999.180	1.1555
59	15.00	62.37164	999.098	1.1385
60	15.56	62.36630	999.012	1.1219
61	16.11	62.36073	998.923	1.1057
62	16.67	62.35494	998.830	1.0898
63	17.22	62.34893	998.734	1.0743
64	17.78	62.34271	998.634	1.0592
65	18.33	62.33627	998.531	1.0444
66	18.89	62.32963	998.425	1.0299
67	19.44	62.32277	998.315	1.0158
68	20.00	62.31572	998.202	1.0019
69	20.56	62.30846	998.085	0.9884
70	21.11	62.30100	997.966	0.9753
71	21.67	62.29334	997.843	0.9624
72	22.22	62.28549	997.718	0.9498
73	22.78	62.27744	997.589	0.9374
74	23.33	62.26920	997.457	0.9253
75	23.89	62.26078	997.322	0.9134
76	24.44	62.25216	997.184	0.9018
77	25.00	62.24336	997.043	0.8904
78	25.56	62.23438	996.899	0.8793
79	26.11	62.22521	996.752	0.8683

TABLE E.6 Density and Viscosity of Water: U.S. and SI Units (*Continued*)

Temperature		Density†		Viscosity‡ μ_{cP}
°F	°C	lb _m /ft ³	kg/m ³	
80	26.67	62.21587	996.602	0.8576
81	27.22	62.20635	996.450	0.8471
82	27.78	62.19665	996.294	0.8368
83	28.33	62.18678	996.136	0.8267
84	28.89	62.17673	995.975	0.8168
85	29.44	62.16651	995.812	0.8071
86	30.00	62.15612	995.645	0.7975
87	30.56	62.14557	995.476	0.7882
88	31.11	62.13484	995.304	0.7790
89	31.67	62.12396	995.130	0.7700
90	32.22	62.11291	994.953	0.7612
91	32.78	62.10169	994.773	0.7525
92	33.33	62.09032	994.591	0.7440
93	33.89	62.07879	994.407	0.7356
94	34.44	62.06710	994.219	0.7274
95	35.00	62.05525	994.030	0.7194
96	35.56	62.04325	993.837	0.7115
97	36.11	62.03110	993.643	0.7037
98	36.67	62.01880	993.446	0.6960
99	37.22	62.00634	993.246	0.6885
100	37.78	61.99374	993.044	0.6812
101	38.33	61.98099	992.840	0.6739
102	38.89	61.96810	992.633	0.6668
103	39.44	61.95506	992.425	0.6598
104	40.00	61.94188	992.214	0.6529
105	40.56	61.92856	992.000	0.6462
106	41.11	61.91510	991.785	0.6395
107	41.67	61.90151	991.567	0.6330
108	42.22	61.88778	991.347	0.6266
109	42.78	61.87391	991.125	0.6202
110	43.33	61.85992	990.901	0.6140
111	43.89	61.84579	990.674	0.6079
112	44.44	61.83154	990.446	0.6019
113	45.00	61.81716	990.216	0.5960
114	45.56	61.80266	989.983	0.5902
115	46.11	61.78803	989.749	0.5844
116	46.67	61.77329	989.513	0.5788
117	47.22	61.75843	989.275	0.5733
118	47.78	61.74345	989.035	0.5678
119	48.33	61.72836	988.793	0.5624
120	48.89	61.71315	988.550	0.5571
121	49.44	61.69784	988.304	0.5519
122	50.00	61.68243	988.057	0.5468
123	50.56	61.66691	987.809	0.5418
124	51.11	61.65128	987.559	0.5368
125	51.67	61.63556	987.307	0.5319

TABLE E.6 Density and Viscosity of Water: U.S. and SI Units (*Continued*)

Temperature		Density†		Viscosity‡ μ_{cp}
°F	°C	lb _m /ft ³	kg/m ³	
126	52.22	61.61975	987.053	0.5271
127	52.78	61.60384	986.799	0.5223
128	53.33	61.58784	986.542	0.5176
129	53.89	61.57176	986.285	0.5130
130	54.44	61.55559	986.026	0.5085
131	55.00	61.53934	985.765	0.5040
132	55.56	61.52302	985.504	0.4996
133	56.11	61.50662	985.241	0.4953
134	56.67	61.49015	984.977	0.4910
135	57.22	61.47361	984.713	0.4867
136	57.78	61.45701	984.447	0.4826
137	58.33	61.44035	984.180	0.4785
138	58.89	61.42364	983.912	0.4744
139	59.44	61.40687	983.644	0.4705
140	60.00	61.39006	983.374	0.4665
141	60.56	61.37321	983.104	0.4626
142	61.11	61.35632	982.834	0.4588
143	61.67	61.33939	982.562	0.4550
144	62.22	61.32243	982.291	0.4513
145	62.78	61.30545	982.019	0.4477
146	63.33	61.28845	981.747	0.4440
147	63.89	61.27144	981.474	0.4405
148	64.44	61.25441	981.201	0.4370
149	65.00	61.23739	980.929	0.4335
150	65.56	61.22036	980.656	0.4300
151	66.11	61.20334	980.383	0.4267
152	66.67	61.18633	980.111	0.4233
153	67.22	61.16935	979.839	0.4200
154	67.78	61.15238	979.567	0.4168
155	68.33	61.13545	979.296	0.4136
156	68.89	61.11856	979.025	0.4104
157	69.44	61.10170	978.755	0.4073
158	70.00	61.08490	978.486	0.4042
159	70.56	61.06816	978.218	0.4011
160	71.11	61.05148	977.951	0.3981
161	71.67	61.03488	977.685	0.3952
162	72.22	61.01835	977.420	0.3922
163	72.78	61.00191	977.157	0.3893

† $\rho(\text{kg/m}^3) = 999.8395639 + 6.798299989 \times 10^{-2} T_C - 9.10602556 \times 10^{-3} (T_C)^2 + 1.005272999 \times 10^{-4} (T_C)^3 - 1.126713526 \times 10^{-6} (T_C)^4 + 6.591795606 \times 10^{-9} (T_C)^5$

‡If $0 \leq T_C \leq 20^\circ\text{C}$, use $A = 1301/[998.333 + 8.1855(T_C - 20) + 0.00585(T_C - 20)^2] - 3.30233$ and $\mu_{\text{cp}} = (100)(10^4)$. If $20 \leq T_C \leq 100^\circ\text{C}$, use $A = [1.3272(20 - T_C) - 0.001053(T_C - 20)^2]/(T_C + 105)$ and $\mu_{\text{cp}} = (\mu_{\text{cp}} \text{ at } 20^\circ\text{C})(10^4)$. The equations for viscosity are from Hardy and Cottingham (1949) and Swindells (NBS). The density of water is calculated from Eq. (2.172).

Note: Values presented are at atmospheric pressure.

VISCOSITIES OF LIQUIDS

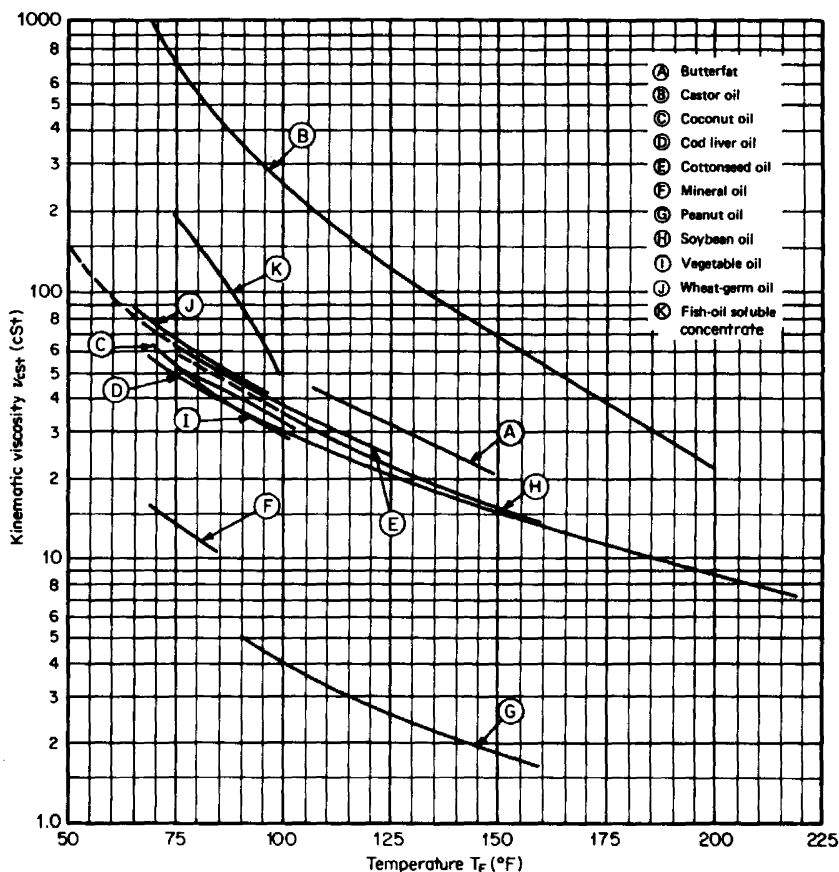


Figure F.1 Kinematic viscosities of fats and oils. (From Fischer & Porter Catalog 10-A-54; used with permission.)

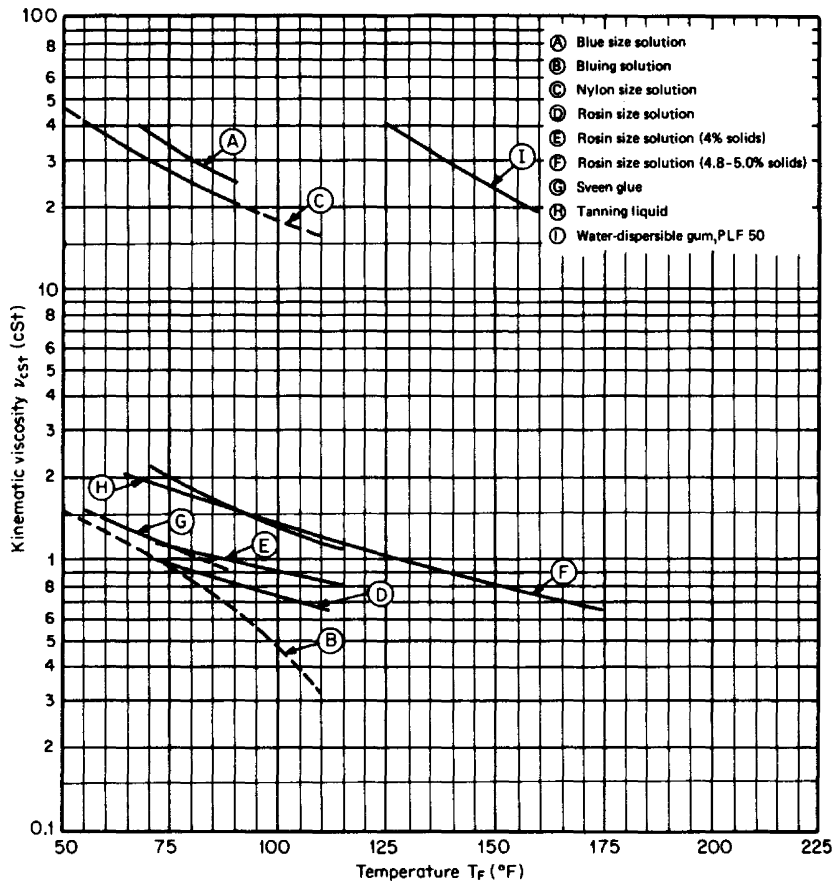


Figure F.2 Kinematic viscosities of liquids related to the paper, leather, and textile industries. (From Fischer & Porter Catalog 10-A-54; used with permission.)

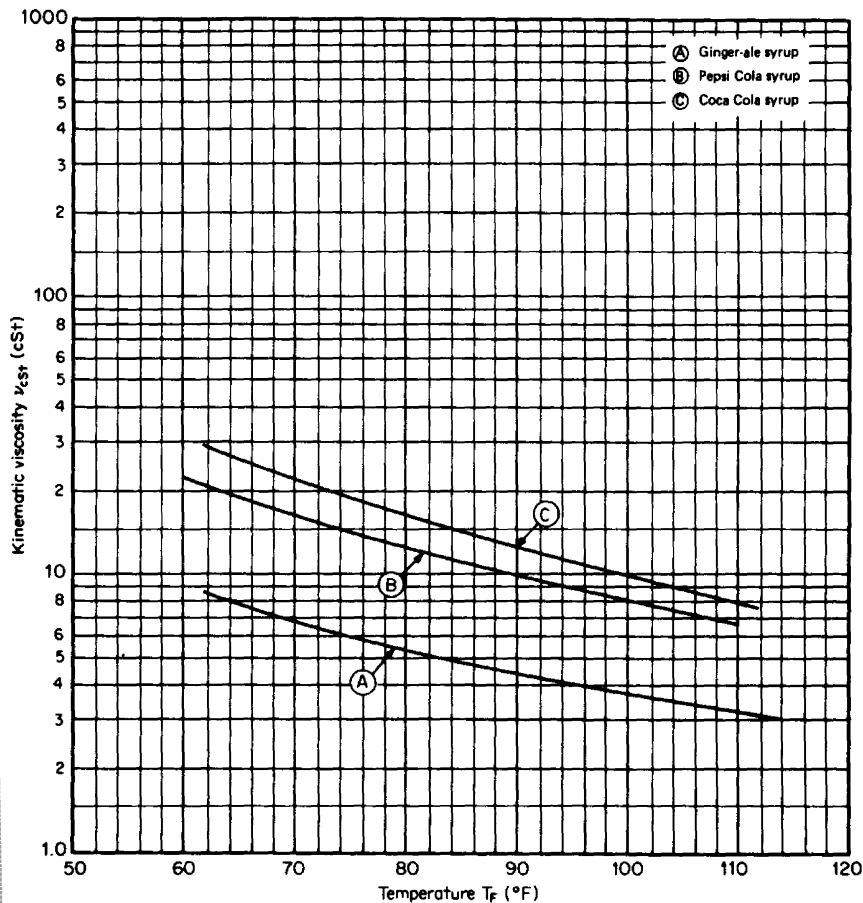


Figure F.3 Kinematic viscosities of syrups. (From Fischer & Porter Catalog 10-A-54; used with permission.)

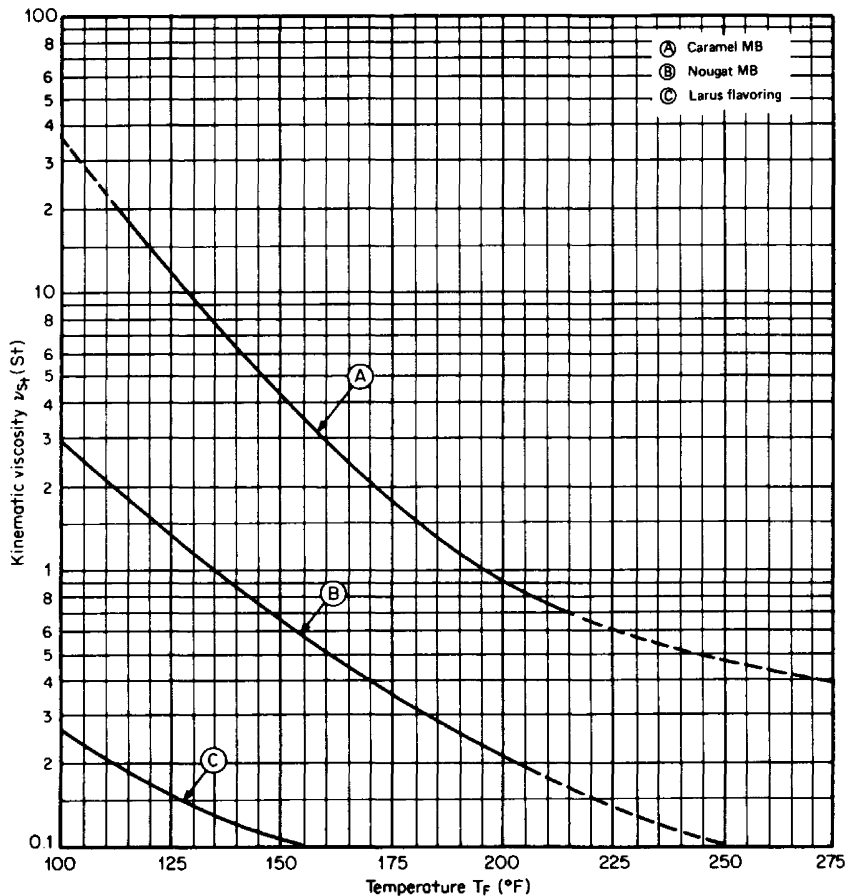


Figure F.4 Kinematic viscosities of liquids related to the candy industry. (From Fischer & Porter Catalog 10-A-54; used with permission.)

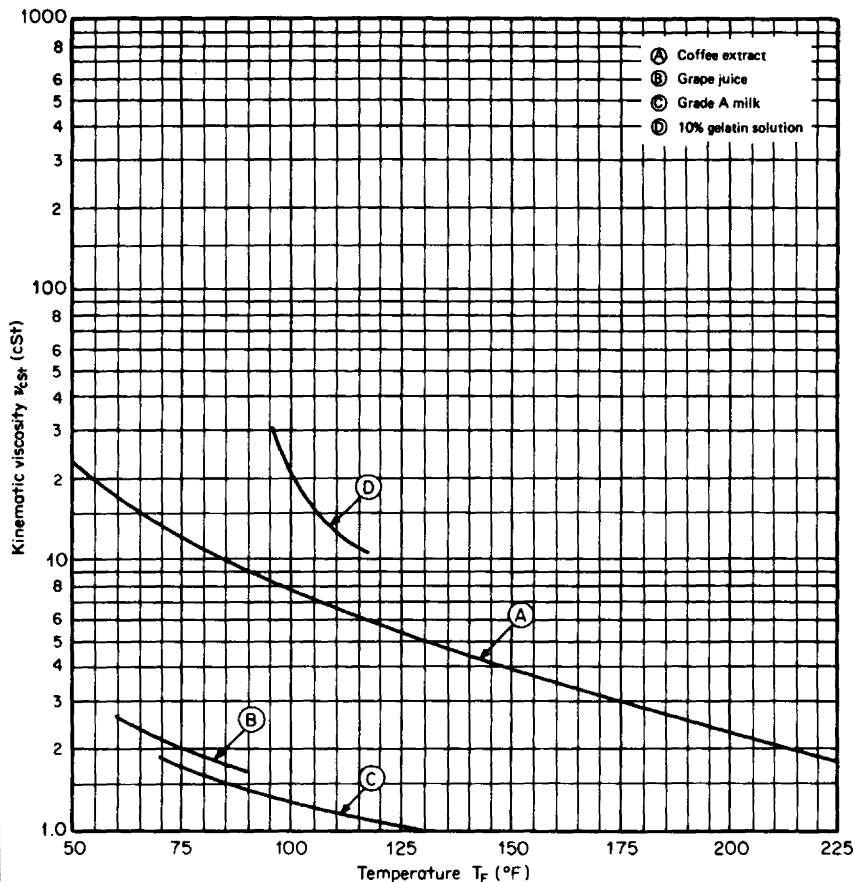


Figure F.5 Kinematic viscosities of miscellaneous liquids related to the food industry. (From Fischer & Porter Catalog 10-A-54; used with permission.)

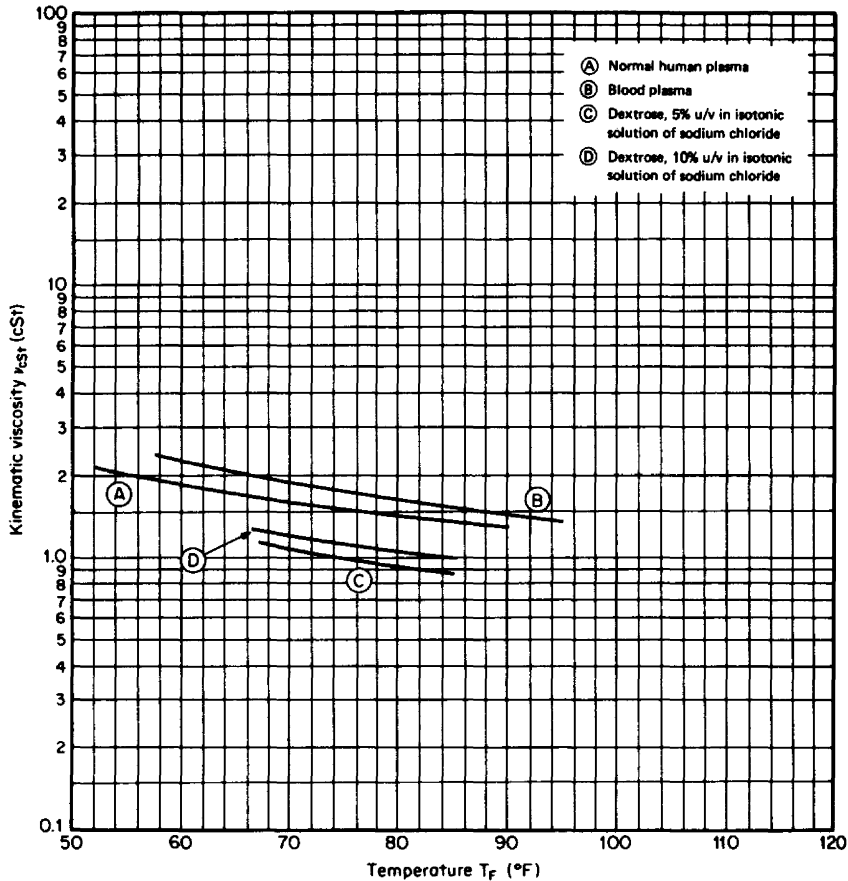


Figure F.6 Kinematic viscosities of intravenous solutions. (From Fischer & Porter Catalog 10-A-54; used with permission.)

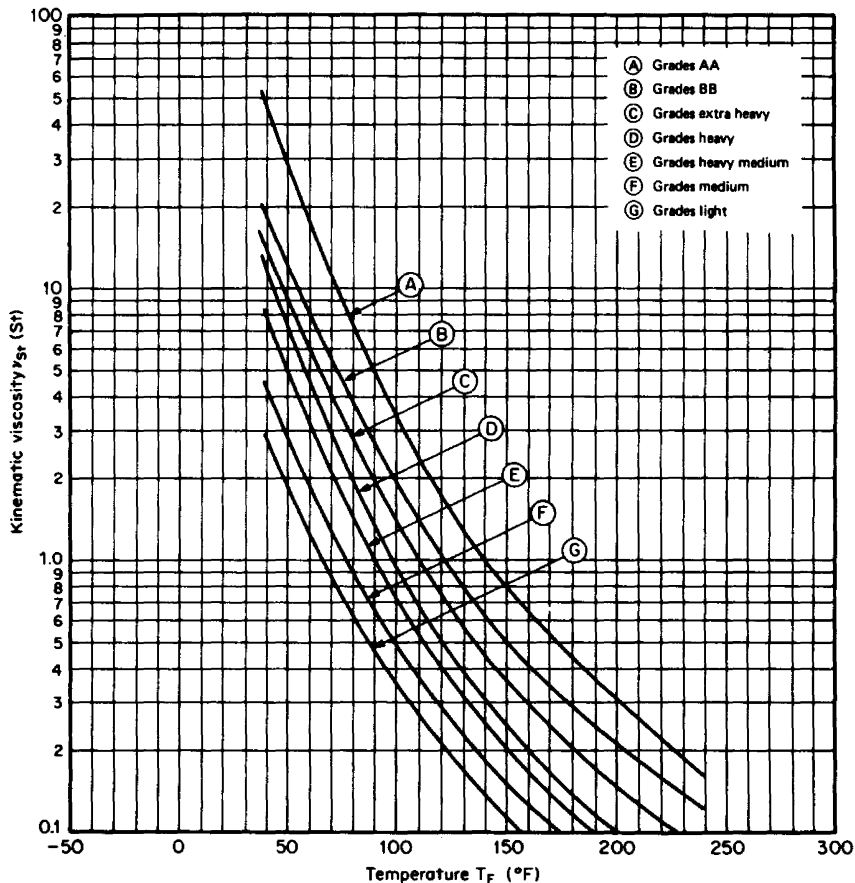


Figure F.7 Kinematic viscosities of Gargoyle D.T.E. oils. (From Fischer & Porter Catalog 10-A-54; used with permission.)

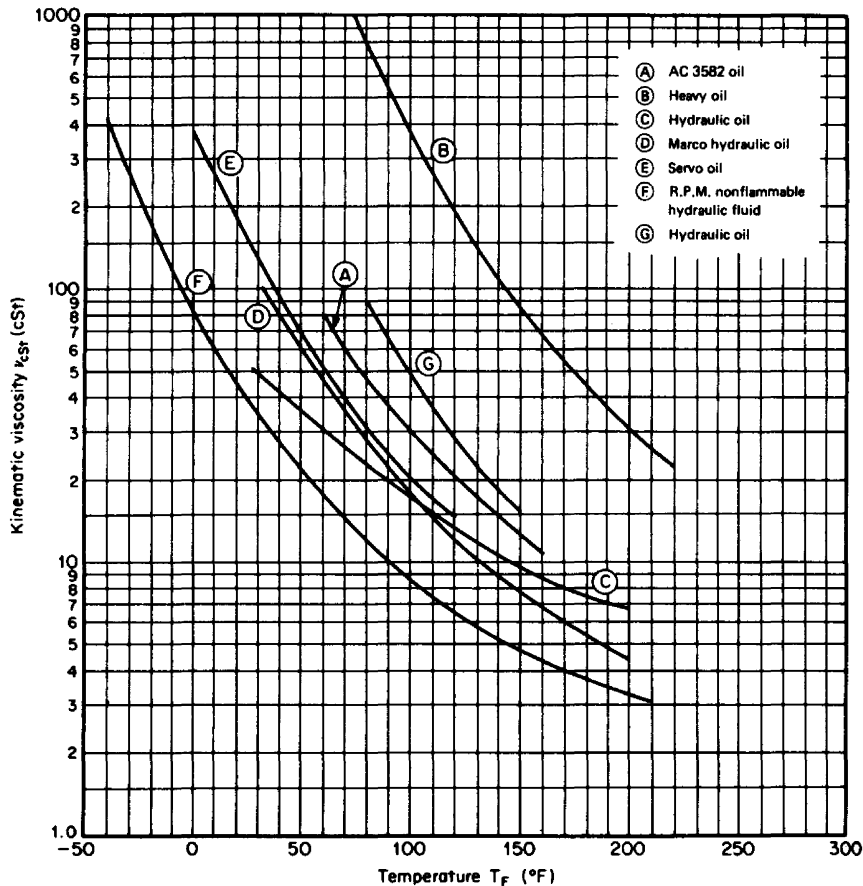


Figure F.8 Kinematic viscosities of hydraulic oils. (From Fischer & Porter Catalog 10-A-54; used with permission.)

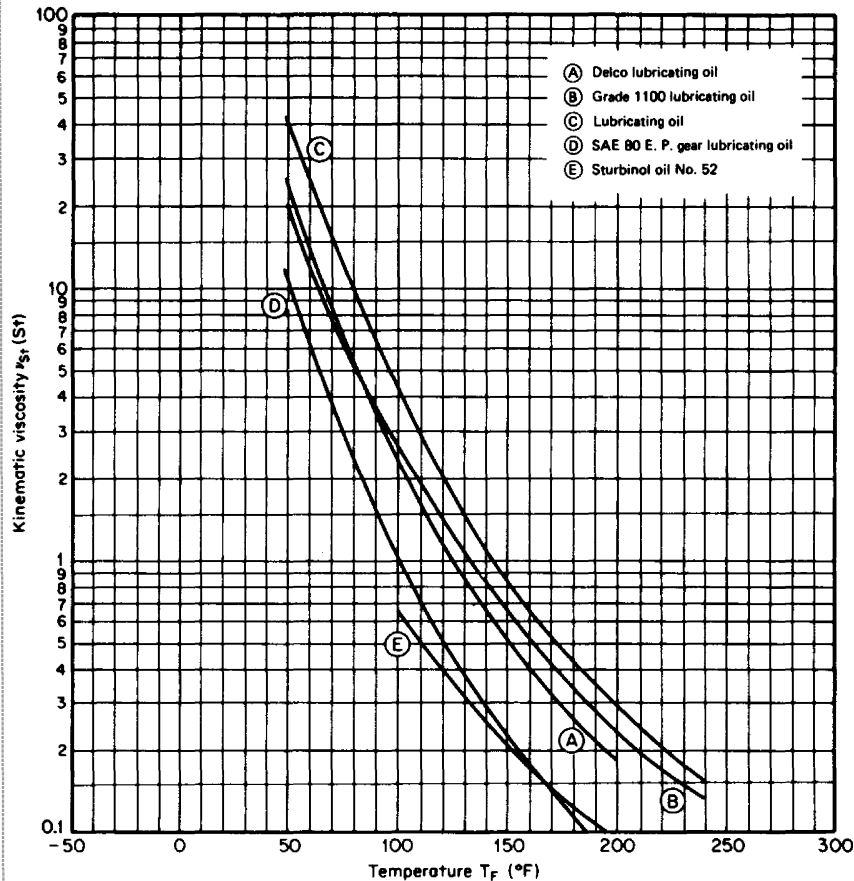


Figure F.9 Kinematic viscosities of lube oils. (From Fischer & Porter Catalog 10-A-54; used with permission.)

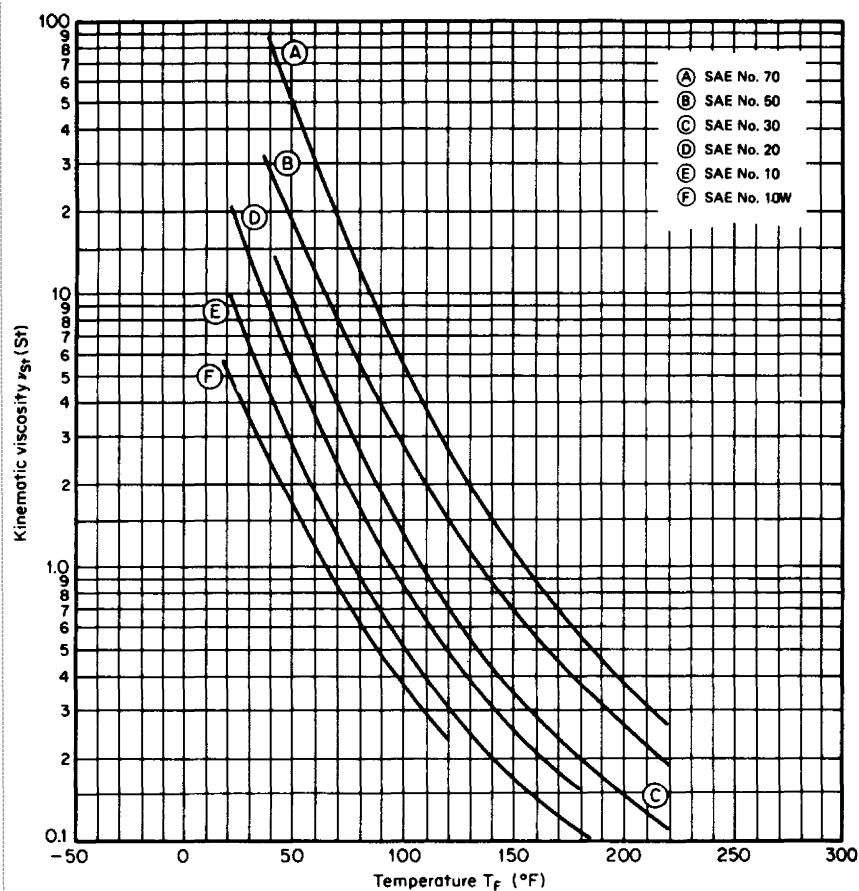


Figure F.10 Kinematic viscosities of SAE (Pennsylvania base) oils. (From Fischer & Porter Catalog 10-A-54; used with permission.)

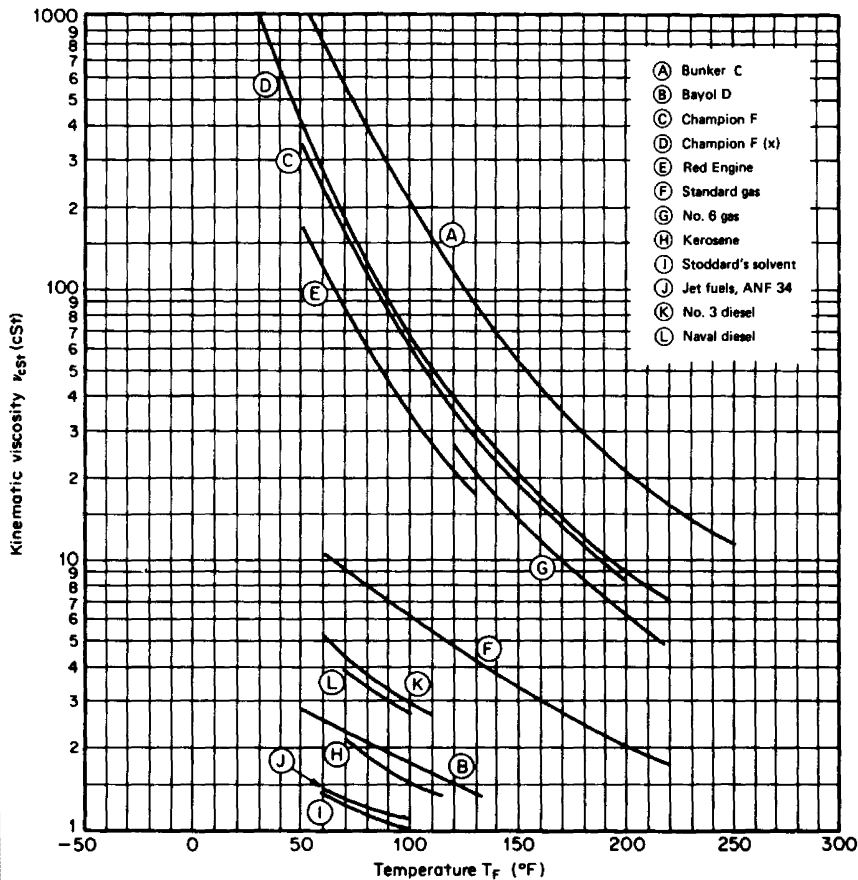


Figure F.11 Kinematic viscosities of miscellaneous fuel oils. (From Fischer & Porter Catalog 10-A-54; used with permission.)

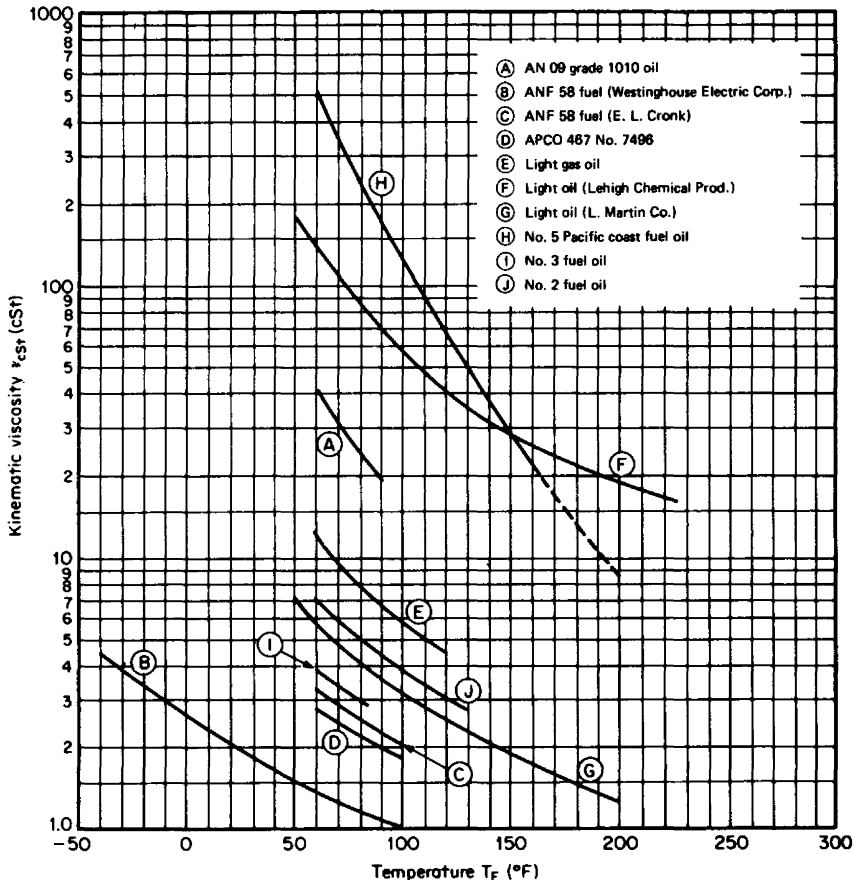


Figure F.12 Kinematic viscosities of miscellaneous fuel oils. (From Fischer & Porter Catalog 10-A-54; used with permission.)

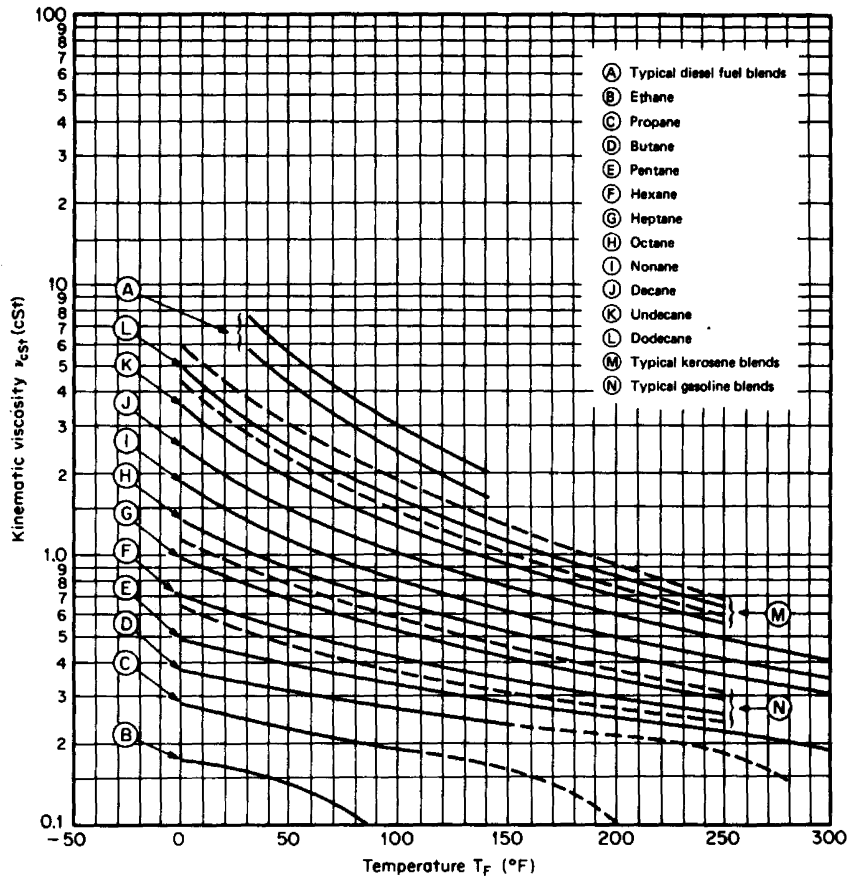


Figure F.13 Kinematic viscosities of typical fuel blends. (From Fischer & Porter Catalog 10-A-54; used with permission.)

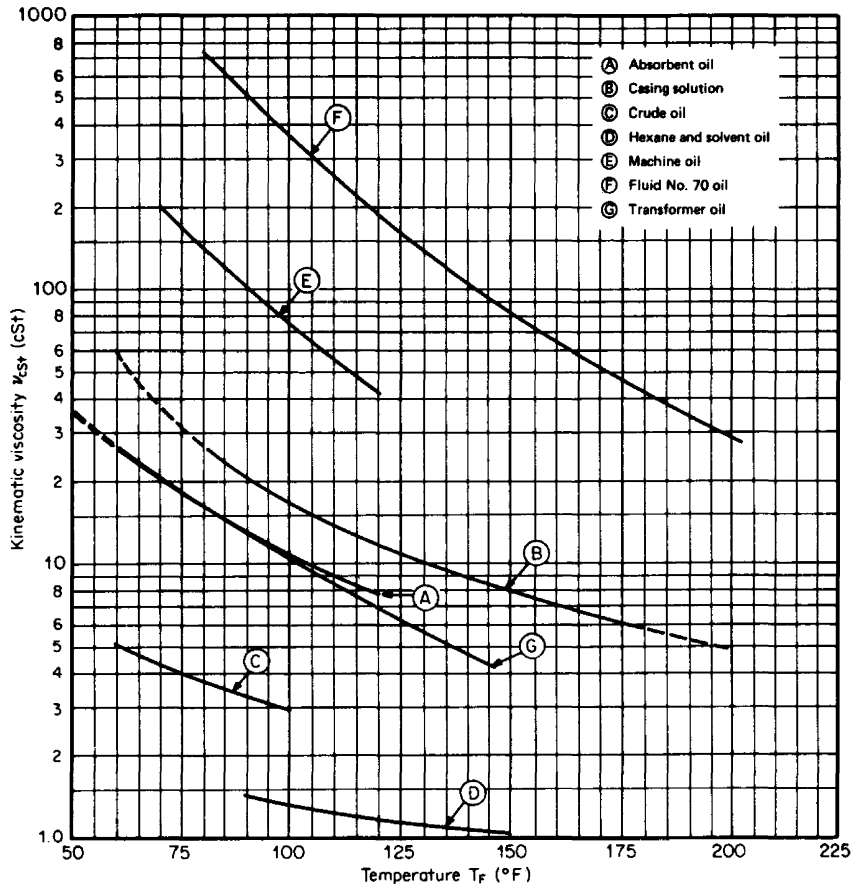


Figure F.14 Kinematic viscosities of miscellaneous oils. (From Fischer & Porter Catalog 10-A-54; used with permission.)

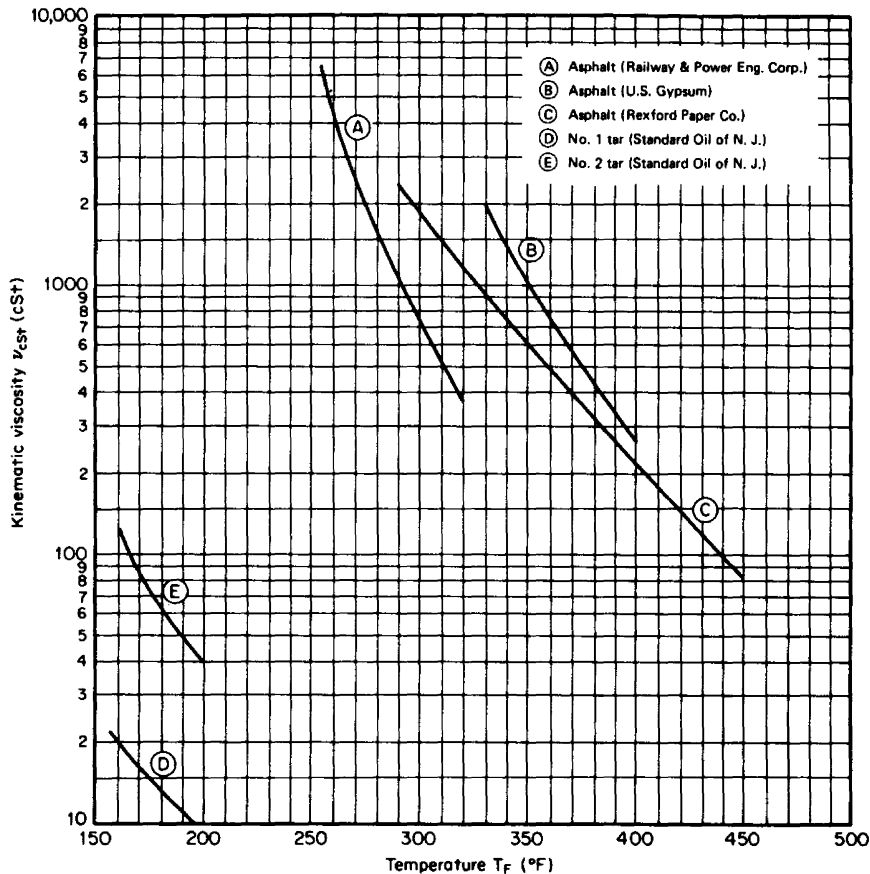


Figure F.15 Kinematic viscosities of high boiling fractions. (From Fischer & Porter Catalog 10-A-54; used with permission.)

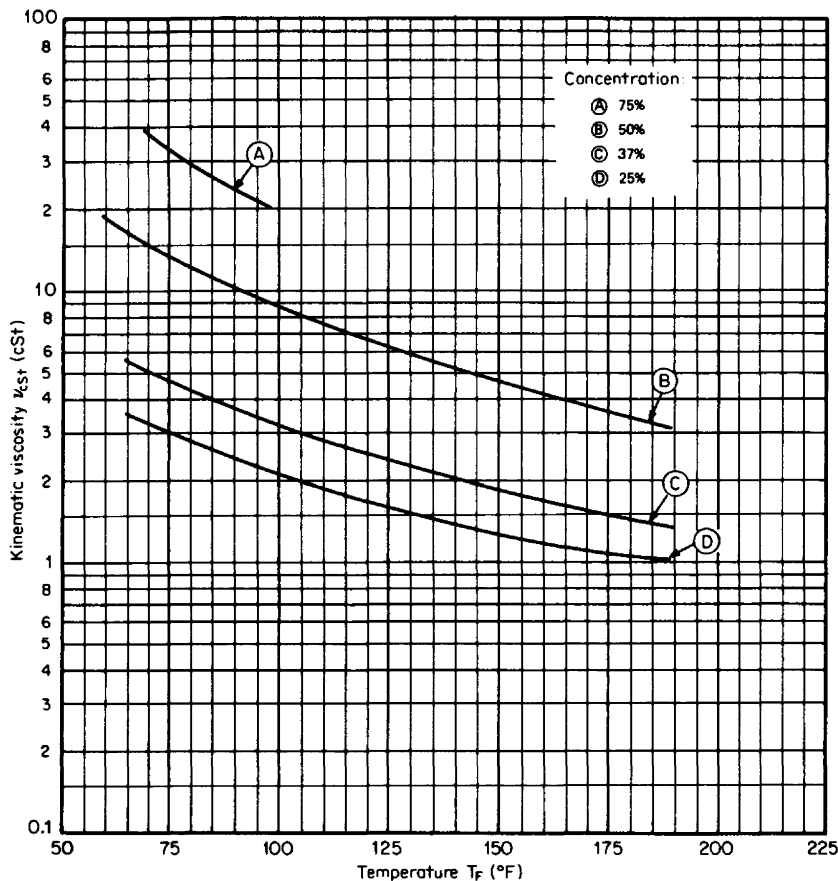


Figure F.16 Kinematic viscosities of phosphoric acid solutions. (From Fischer & Porter Catalog 10-A-54; used with permission.)

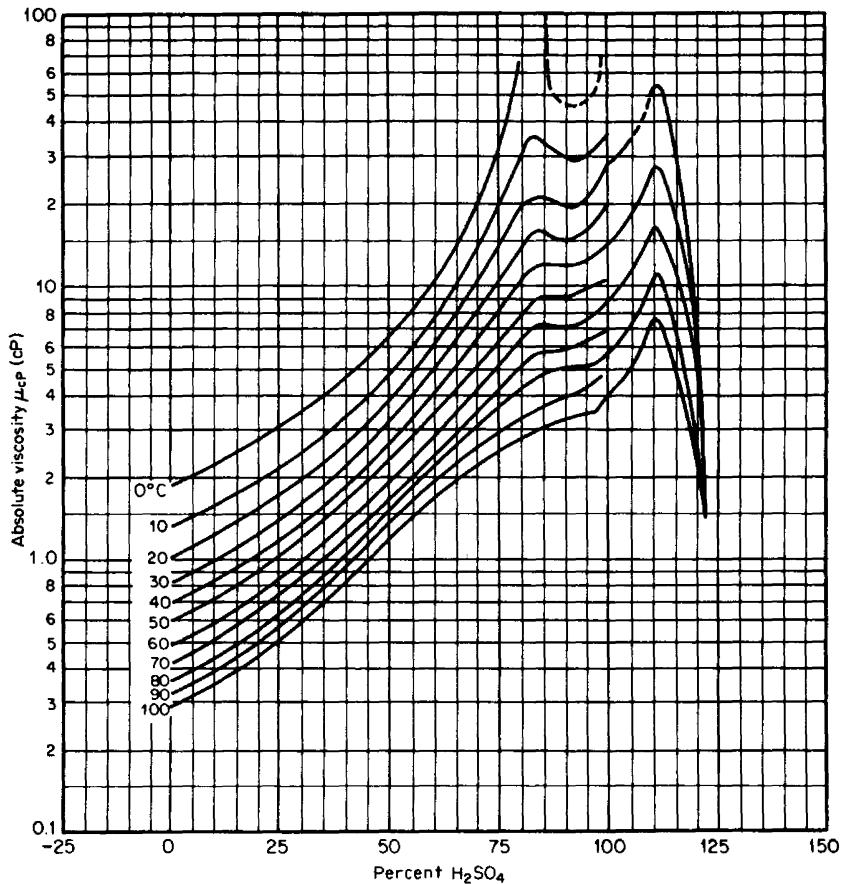


Figure F.17 Absolute viscosities of sulfuric acid solutions. (From Fischer & Porter Catalog 10-A-54; used with permission.)

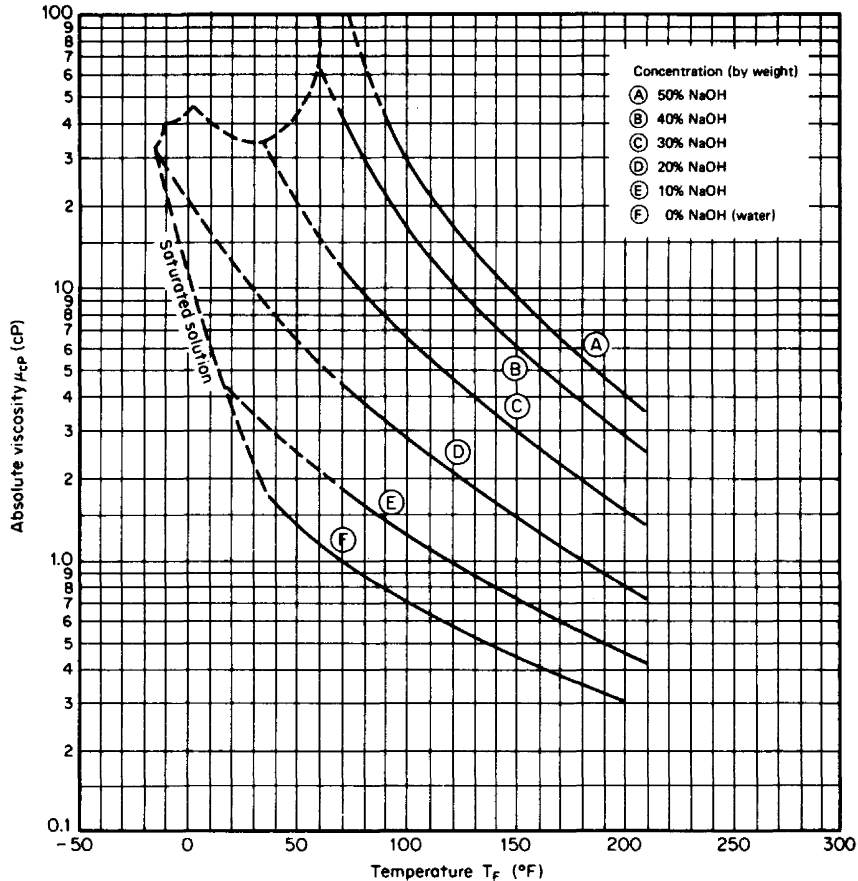


Figure F.18 Absolute viscosities of sodium hydroxide solutions. (From Fischer & Porter Catalog 10-A-54; used with permission.)

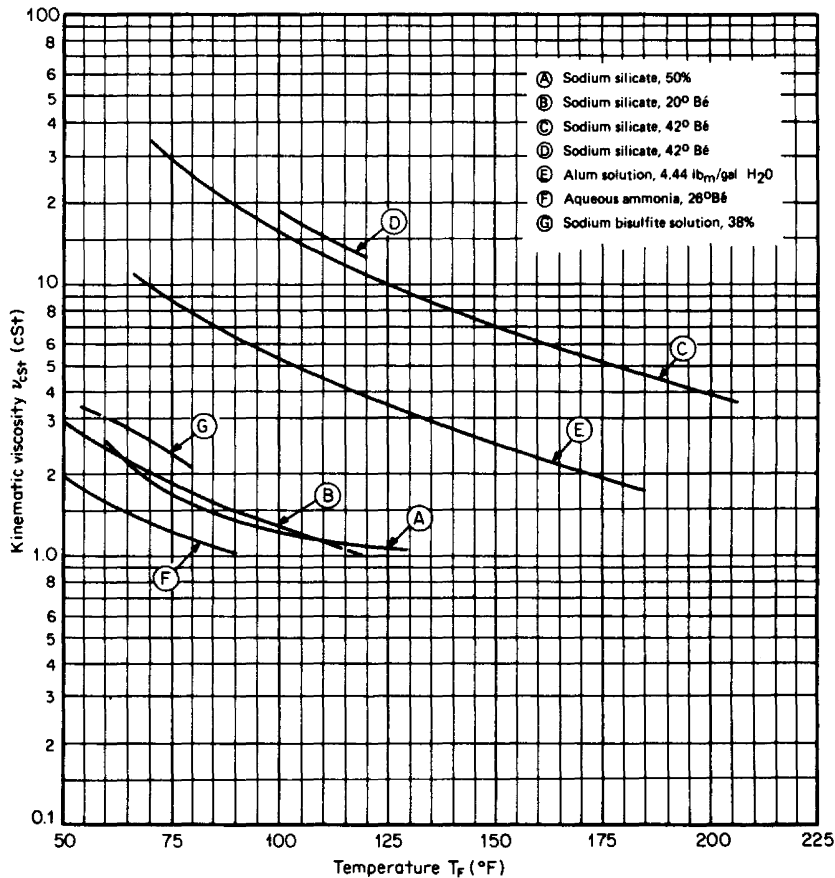


Figure F.19 Kinematic viscosities of inorganic solutions. (From Fischer & Porter Catalog 10-A-54; used with permission.)

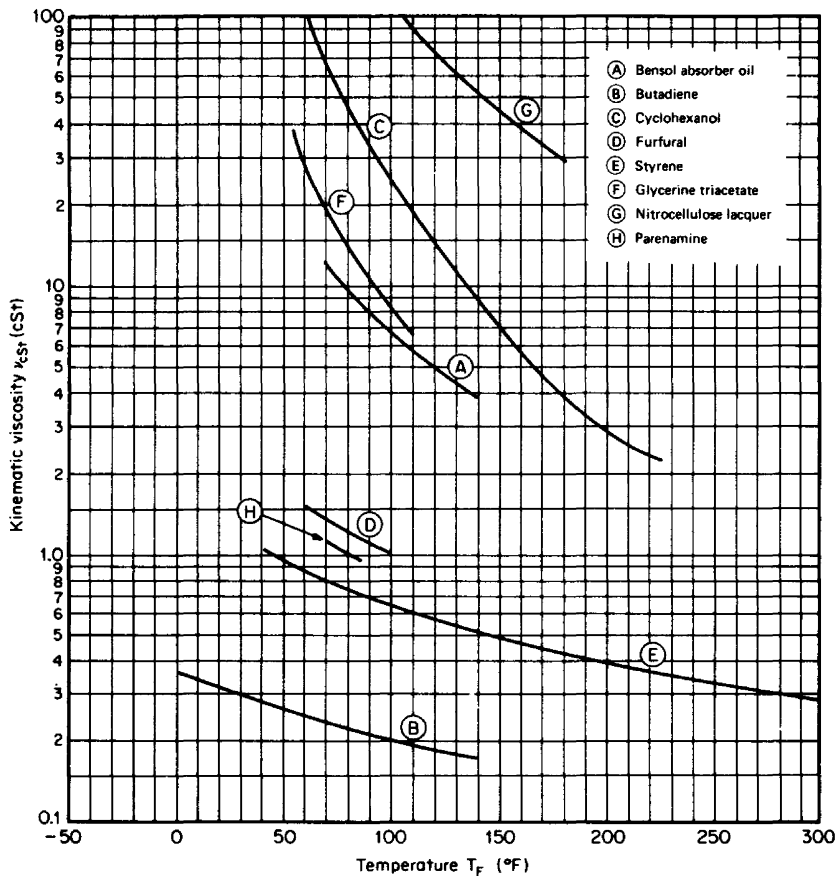


Figure F.20 Absolute viscosities of miscellaneous organic compounds. (From Fischer & Porter Catalog 10-A-54; used with permission.)

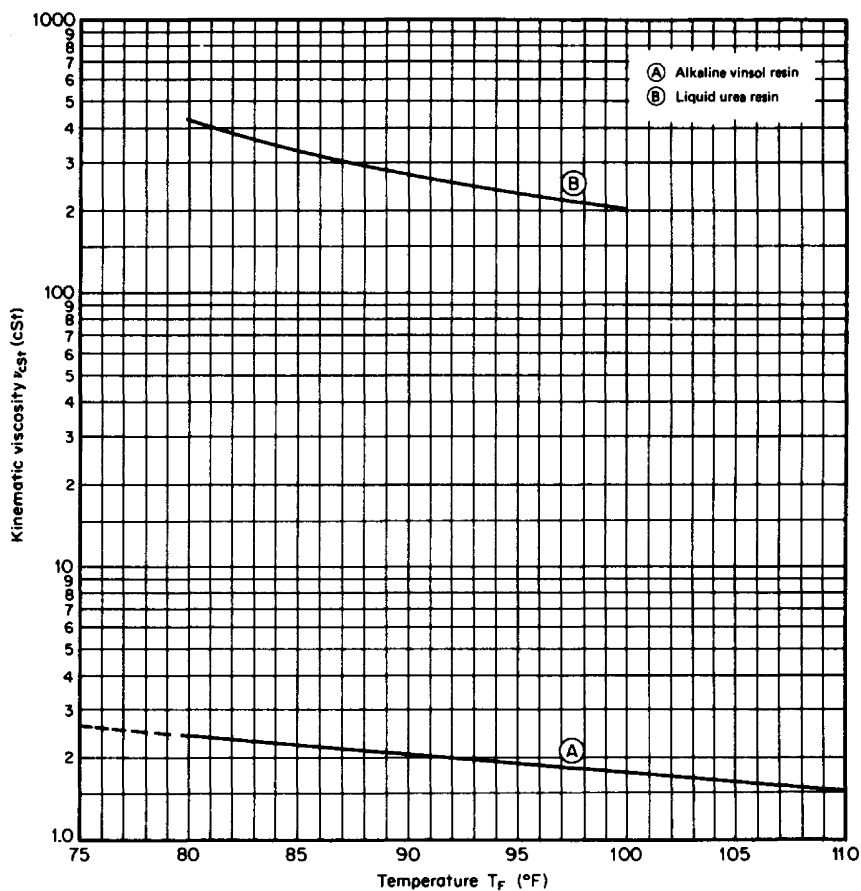


Figure F.21 Kinematic viscosities of resins. (From Fischer & Porter Catalog 10-A-54; used with permission.)

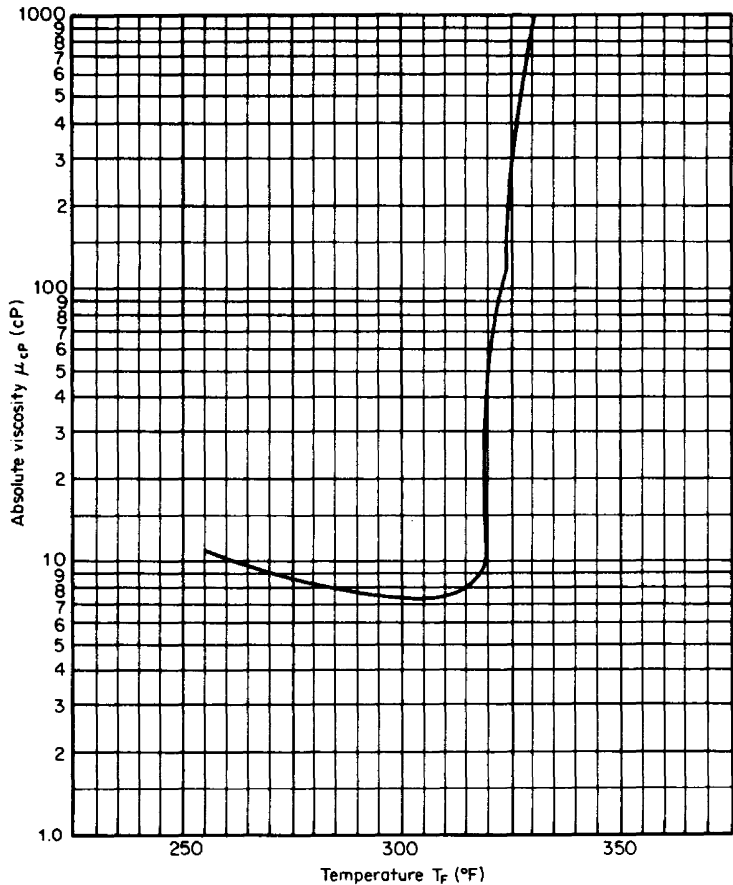


Figure F.22 Absolute viscosities of liquid sulfur. (From Fischer & Porter Catalog 10-A-54; used with permission.)

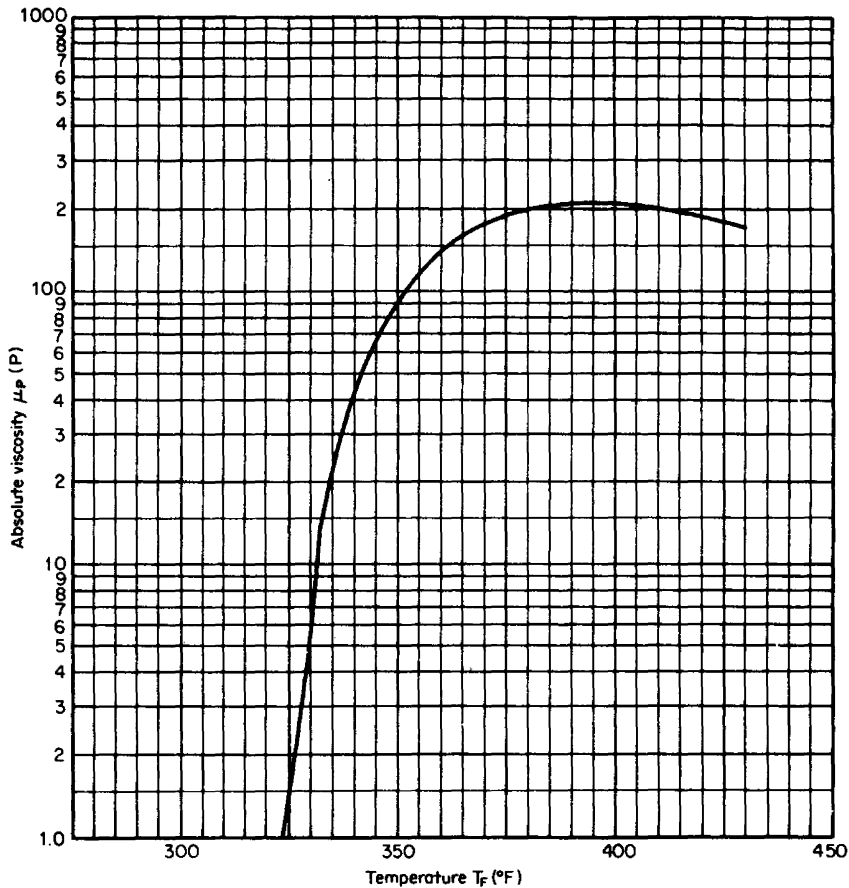


Figure F.23 Absolute viscosities of liquid sulfur. (From Fischer & Porter Catalog 10-A-54; used with permission.)

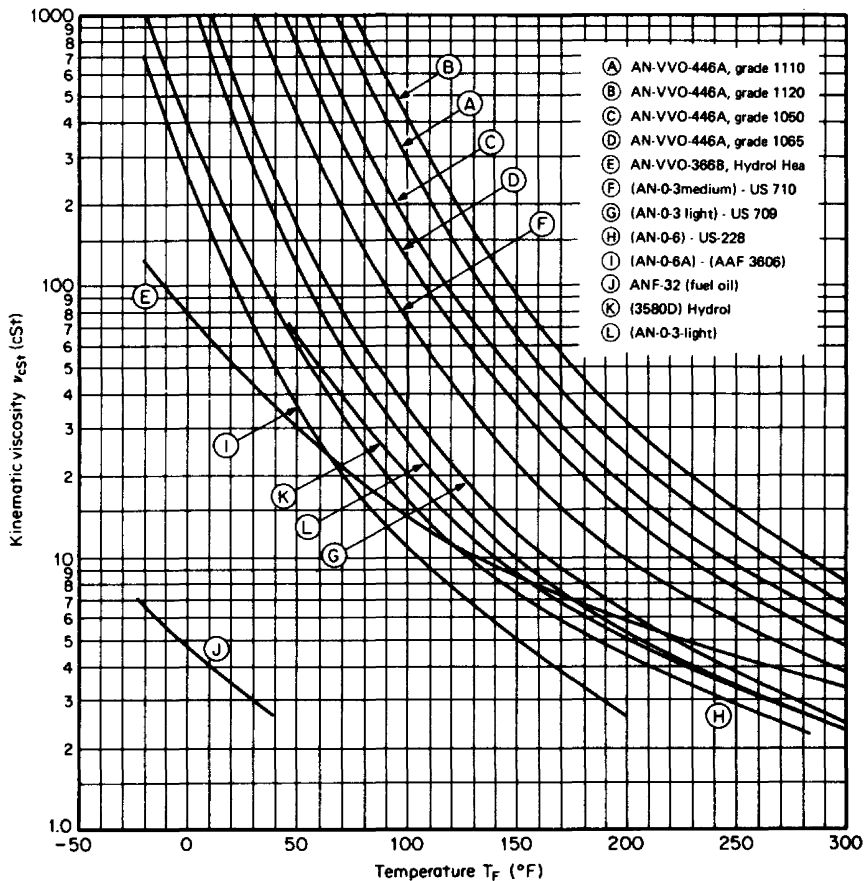


Figure F.24 Kinematic viscosities of Army and Navy lube and hydraulic oils. (From Fischer & Porter Catalog 10-A-54; used with permission.)

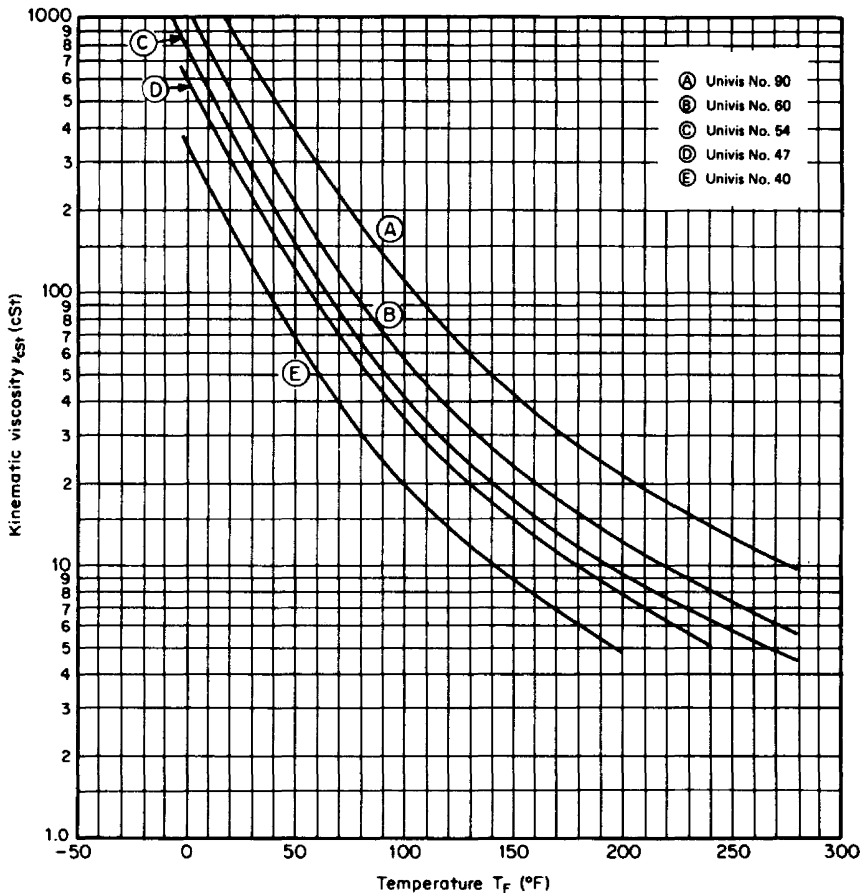


Figure F.25 Kinematic viscosities of Univis oils (Standard Oil of New Jersey.) (From Fischer & Porter Catalog 10-A-54; used with permission.)

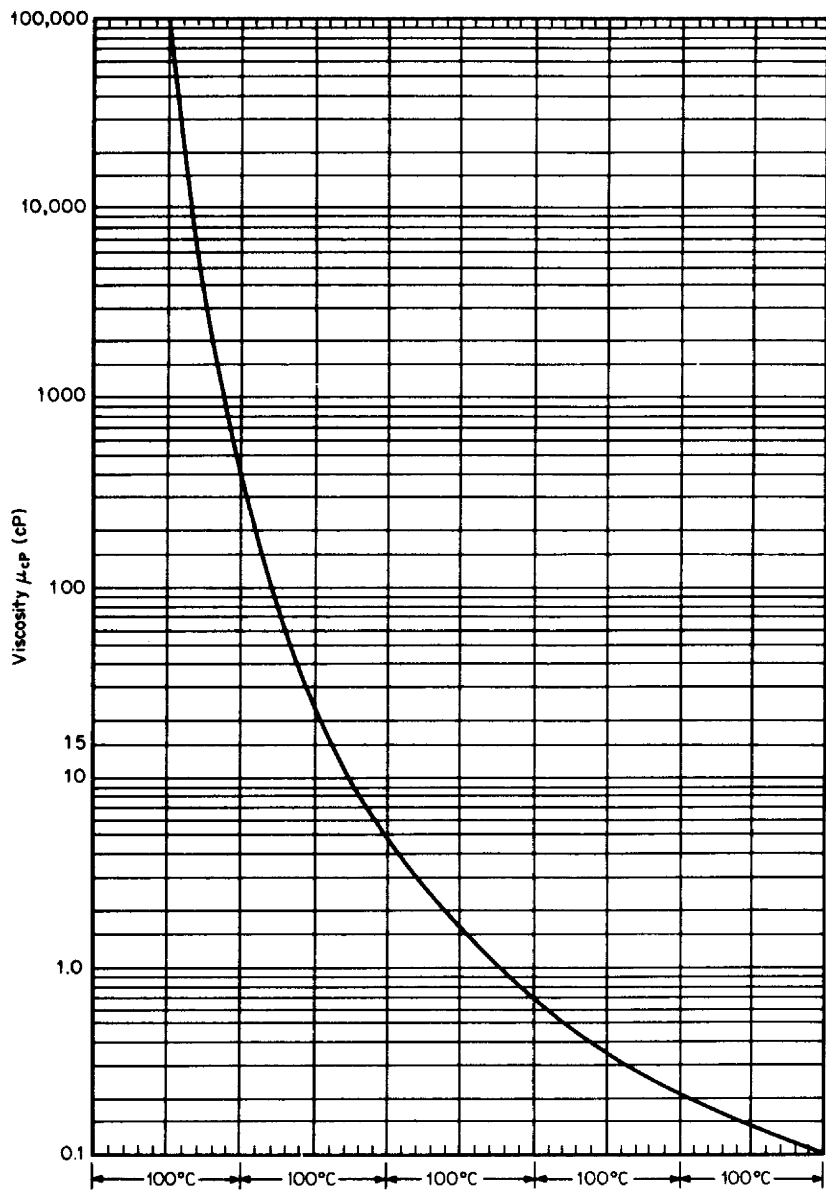


Figure F.26 Curve for estimating viscosity from a single measurement value. (From Gambill, 1959.)

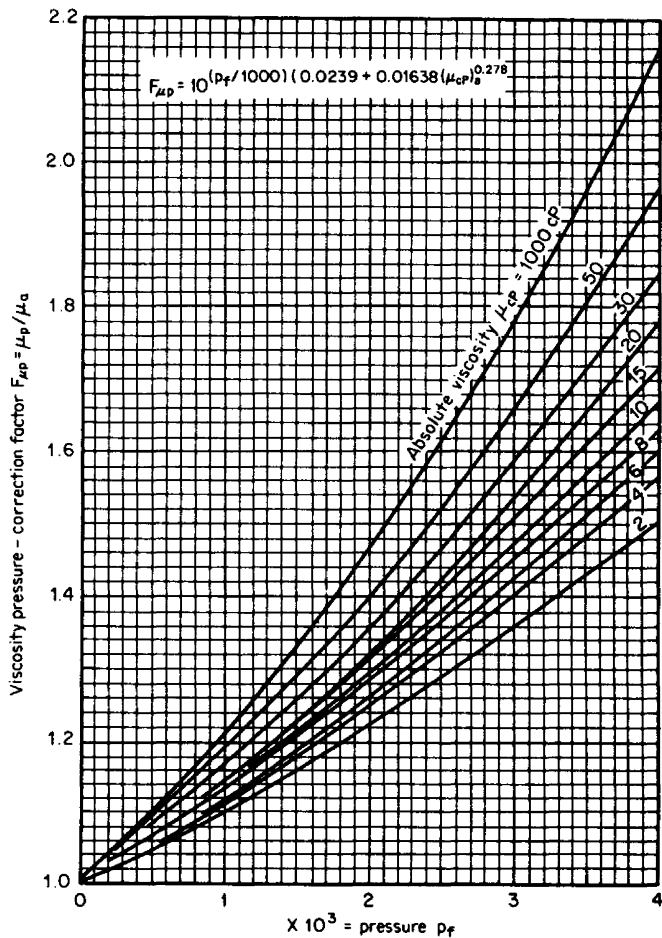


Figure F.27 Viscosity pressure-correction factor for oils.

TABLE G.1 Density (in Pounds-Mass per Cubic Foot) and Absolute Viscosity μ_{CP} (in Centipoises) of Steam and Compressed Water†

	Pressure, psia					
	12.	14.696	16.	18.	20.	22.
Temp., °F	201.96	212.00	216.32	222.41	227.96	233.07
Sat. vap.	0.03087 (0.01208)	0.03732 (0.01228)	0.04040 (0.01236)	0.04511 (0.01248)	0.04978 (0.01258)	0.05443 (0.01268)
Sat. liq.	60.06059 (0.29966)	59.81363 (0.28214)	59.70482 (0.27515)	59.54873 (0.26580)	59.40363 (0.25775)	59.26779 (0.25071)
Temp., °F						
220.	0.03000 (0.01245)	0.03684 (0.01244)	0.04017 (0.01243)	59.61096 (0.26943)	59.61138 (0.26943)	59.61180 (0.26943)
240.	0.02910 (0.01287)	0.03572 (0.01286)	0.03894 (0.01285)	0.04388 (0.01284)	0.04885 (0.01284)	0.05384 (0.01283)
260.	0.02825 (0.01329)	0.03467 (0.01328)	0.03779 (0.01328)	0.04258 (0.01327)	0.04738 (0.01326)	0.05221 (0.01325)
280.	0.02746 (0.01372)	0.03369 (0.01371)	0.03671 (0.01371)	0.04136 (0.01370)	0.04601 (0.01369)	0.05069 (0.01369)
300.	0.02671 (0.01415)	0.03276 (0.01414)	0.03570 (0.01414)	0.04021 (0.01413)	0.04473 (0.01413)	0.04927 (0.01412)
320.	0.02600 (0.01459)	0.03189 (0.01458)	0.03474 (0.01458)	0.03913 (0.01457)	0.04352 (0.01457)	0.04793 (0.01456)
340.	0.02533 (0.01503)	0.03107 (0.01502)	0.03384 (0.01502)	0.03811 (0.01501)	0.04239 (0.01501)	0.04667 (0.01500)
360.	0.02470 (0.01547)	0.03029 (0.01546)	0.03299 (0.01546)	0.03715 (0.01546)	0.04131 (0.01545)	0.04548 (0.01545)
380.	0.02410 (0.01592)	0.02955 (0.01591)	0.03218 (0.01591)	0.03624 (0.01590)	0.04029 (0.01590)	0.04436 (0.01590)
400.	0.02353 (0.01636)	0.02884 (0.01636)	0.03142 (0.01636)	0.03537 (0.01635)	0.03933 (0.01635)	0.04329 (0.01635)
420.	0.02299 (0.01682)	0.02817 (0.01681)	0.03069 (0.01681)	0.03455 (0.01681)	0.03841 (0.01680)	0.04228 (0.01680)
440.	0.02247 (0.01727)	0.02754 (0.01726)	0.02999 (0.01726)	0.03376 (0.01726)	0.03753 (0.01726)	0.04131 (0.01725)
460.	0.02197 (0.01772)	0.02693 (0.01772)	0.02933 (0.01772)	0.03301 (0.01771)	0.03670 (0.01771)	0.04039 (0.01771)
480.	0.02150 (0.01818)	0.02635 (0.01818)	0.02869 (0.01817)	0.03230 (0.01817)	0.03590 (0.01817)	0.03951 (0.01817)
500.	0.02105 (0.01864)	0.02579 (0.01863)	0.02809 (0.01863)	0.03161 (0.01863)	0.03514 (0.01863)	0.03867 (0.01863)
520.	0.02061 (0.01910)	0.02526 (0.01909)	0.02751 (0.01909)	0.03096 (0.01909)	0.03441 (0.01909)	0.03787 (0.01909)
540.	0.02020 (0.01956)	0.02475 (0.01955)	0.02695 (0.01955)	0.03033 (0.01955)	0.03371 (0.01955)	0.03710 (0.01955)
560.	0.01980 (0.02002)	0.02426 (0.02001)	0.02642 (0.02001)	0.02973 (0.02001)	0.03304 (0.02001)	0.03636 (0.02001)

	Pressure, psia					
	12.	14.696	16.	18.	20.	22.
Temp., °F						
600.	0.01905 (0.02094)	0.02333 (0.02094)	0.02541 (0.02094)	0.02859 (0.02093)	0.03178 (0.02093)	0.03497 (0.02093)
650.	0.01818 (0.02209)	0.02227 (0.02209)	0.02426 (0.02209)	0.02729 (0.02209)	0.03033 (0.02209)	0.03338 (0.02209)
700.	0.01739 (0.02325)	0.02131 (0.02325)	0.02320 (0.02325)	0.02611 (0.02325)	0.02902 (0.02325)	0.03192 (0.02325)
750.	0.01667 (0.02440)	0.02042 (0.02440)	0.02224 (0.02440)	0.02502 (0.02440)	0.02781 (0.02440)	0.03059 (0.02440)
800.	0.01601 (0.02556)	0.01961 (0.02556)	0.02135 (0.02555)	0.02402 (0.02555)	0.02670 (0.02555)	0.02937 (0.02555)
850.	0.01539 (0.02670)	0.01886 (0.02670)	0.02053 (0.02670)	0.02310 (0.02670)	0.02567 (0.02670)	0.02824 (0.02670)
900.	0.01483 (0.02784)	0.01816 (0.02784)	0.01977 (0.02784)	0.02225 (0.02784)	0.02472 (0.02785)	0.02720 (0.02785)
950.	0.01430 (0.02898)	0.01751 (0.02898)	0.01907 (0.02898)	0.02146 (0.02898)	0.02384 (0.02898)	0.02623 (0.02898)
1000.	0.01381 (0.03011)	0.01691 (0.03011)	0.01842 (0.03011)	0.02072 (0.03011)	0.02302 (0.03011)	0.02533 (0.03011)
1050.	0.01335 (0.03123)	0.01635 (0.03123)	0.01780 (0.03123)	0.02003 (0.03123)	0.02226 (0.03123)	0.02449 (0.03124)
1100.	0.01292 (0.03235)	0.01583 (0.03235)	0.01723 (0.03235)	0.01939 (0.03235)	0.02154 (0.03235)	0.02370 (0.03235)
1150.	0.01252 (0.03346)	0.01533 (0.03346)	0.01670 (0.03346)	0.01878 (0.03346)	0.02087 (0.03346)	0.02296 (0.03346)
1200.	0.01214 (0.03455)	0.01487 (0.03455)	0.01619 (0.03455)	0.01822 (0.03456)	0.02024 (0.03456)	0.02227 (0.03456)
1250.	0.01179 (0.03564)	0.01444 (0.03564)	0.01572 (0.03564)	0.01768 (0.03565)	0.01965 (0.03565)	0.02161 (0.03565)
1300.	0.01145 (0.03672)	0.01402 (0.03673)	0.01527 (0.03673)	0.01718 (0.03673)	0.01909 (0.03673)	0.02100 (0.03673)
1350.	0.01113 (0.03780)	0.01364 (0.03780)	0.01485 (0.03780)	0.01670 (0.03780)	0.01856 (0.03780)	0.02042 (0.03780)
1400.	0.01083 (0.03886)	0.01327 (0.03886)	0.01445 (0.03886)	0.01625 (0.03886)	0.01806 (0.03886)	0.01987 (0.03886)
1450.	0.01055 (0.03991)	0.01292 (0.03991)	0.01407 (0.03991)	0.01583 (0.03992)	0.01759 (0.03992)	0.01935 (0.03992)
1500.	0.01028 (0.04096)	0.01259 (0.04096)	0.01371 (0.04096)	0.01542 (0.04096)	0.01714 (0.04096)	0.01885 (0.04096)

†Absolute viscosity μ_{cp} is shown in parentheses.

SOURCE: Derived from ASME, 1977.

TABLE G.1 Density (in Pounds-Mass per Cubic Foot) and Absolute Viscosity μ_{cp} (in Centipoises) of Steam and Compressed Water† (*Continued*)

	Pressure, psia					
	24.	26.	28.	30.	32.	34.
Temp. °F	237.82	242.25	246.41	250.34	254.05	257.58
Sat. vap.	0.05904 (0.01277)	0.06364 (0.01286)	0.06821 (0.01294)	0.07276 (0.01301)	0.07729 (0.01309)	0.08181 (0.01315)
Sat. liq.	59.13985 (0.24449)	59.01871 (0.23892)	58.90354 (0.23390)	58.79364 (0.22934)	58.68843 (0.22517)	58.58742 (0.22133)
Temp. °F						
220.	59.61222 (0.26944)	59.61264 (0.26944)	59.61306 (0.26945)	59.61349 (0.26945)	59.61391 (0.26945)	59.61433 (0.26946)
240.	0.05884 (0.01282)	59.08068 (0.24172)	59.08111 (0.24173)	59.08155 (0.24173)	59.08199 (0.24173)	59.08243 (0.24174)
260.	0.05705 (0.01325)	0.06190 (0.01324)	0.06678 (0.01323)	0.07167 (0.01322)	0.07657 (0.01321)	0.08150 (0.01321)
280.	0.05538 (0.01368)	0.06008 (0.01367)	0.06479 (0.01366)	0.06952 (0.01366)	0.07426 (0.01365)	0.07902 (0.01364)
300.	0.05381 (0.01412)	0.05837 (0.01411)	0.06294 (0.01410)	0.06752 (0.01410)	0.07211 (0.01409)	0.07672 (0.01408)
320.	0.05234 (0.01455)	0.05677 (0.01455)	0.06120 (0.01454)	0.06565 (0.01454)	0.07011 (0.01453)	0.07457 (0.01453)
340.	0.05096 (0.01500)	0.05526 (0.01499)	0.05957 (0.01499)	0.06389 (0.01498)	0.06822 (0.01498)	0.07256 (0.01497)
360.	0.04966 (0.01544)	0.05385 (0.01544)	0.05804 (0.01543)	0.06224 (0.01543)	0.06645 (0.01543)	0.07066 (0.01542)
380.	0.04843 (0.01589)	0.05250 (0.01589)	0.05659 (0.01588)	0.06068 (0.01588)	0.06477 (0.01588)	0.06888 (0.01587)
400.	0.04726 (0.01634)	0.05123 (0.01634)	0.05521 (0.01634)	0.05920 (0.01633)	0.06319 (0.01633)	0.06719 (0.01632)
420.	0.04615 (0.01680)	0.05003 (0.01679)	0.05391 (0.01679)	0.05780 (0.01679)	0.06169 (0.01678)	0.06559 (0.01678)
440.	0.04509 (0.01725)	0.04888 (0.01725)	0.05267 (0.01724)	0.05646 (0.01724)	0.06026 (0.01724)	0.06407 (0.01724)
460.	0.04409 (0.01771)	0.04778 (0.01770)	0.05149 (0.01770)	0.05519 (0.01770)	0.05891 (0.01770)	0.06262 (0.01769)
480.	0.04312 (0.01816)	0.04674 (0.01816)	0.05036 (0.01816)	0.05398 (0.01816)	0.05761 (0.01816)	0.06124 (0.01815)
500.	0.04221 (0.01862)	0.04574 (0.01862)	0.04928 (0.01862)	0.05283 (0.01862)	0.05638 (0.01862)	0.05993 (0.01861)
520.	0.04133 (0.01908)	0.04479 (0.01908)	0.04826 (0.01908)	0.05172 (0.01908)	0.05519 (0.01908)	0.05867 (0.01907)
540.	0.04049 (0.01954)	0.04388 (0.01954)	0.04727 (0.01954)	0.05067 (0.01954)	0.05406 (0.01954)	0.05746 (0.01954)
560.	0.03968 (0.02001)	0.04300 (0.02000)	0.04633 (0.02000)	0.04965 (0.02000)	0.05298 (0.02000)	0.05631 (0.02000)

	Pressure, psia					
	24.	26.	28.	30.	32.	34.
Temp., °F						
600.	0.03816 (0.02093)	0.04135 (0.02093)	0.04455 (0.02093)	0.04774 (0.02093)	0.05094 (0.02093)	0.05414 (0.02093)
650.	0.03642 (0.02209)	0.03946 (0.02209)	0.04251 (0.02209)	0.04556 (0.02209)	0.04861 (0.02209)	0.05166 (0.02208)
700.	0.03483 (0.02325)	0.03774 (0.02325)	0.04066 (0.02324)	0.04357 (0.02324)	0.04649 (0.02324)	0.04940 (0.02324)
750.	0.03338 (0.02440)	0.03617 (0.02440)	0.03896 (0.02440)	0.04175 (0.02440)	0.04454 (0.02440)	0.04733 (0.02440)
800.	0.03205 (0.02555)	0.03472 (0.02555)	0.03740 (0.02555)	0.04008 (0.02555)	0.04276 (0.02555)	0.04544 (0.02555)
850.	0.03081 (0.02670)	0.03339 (0.02670)	0.03596 (0.02670)	0.03853 (0.02670)	0.04111 (0.02670)	0.04368 (0.02670)
900.	0.02968 (0.02785)	0.03215 (0.02785)	0.03463 (0.02785)	0.03711 (0.02785)	0.03959 (0.02785)	0.04207 (0.02785)
950.	0.02862 (0.02898)	0.03101 (0.02898)	0.03339 (0.02898)	0.03578 (0.02898)	0.03817 (0.02898)	0.04056 (0.02898)
1000.	0.02763 (0.03011)	0.02994 (0.03011)	0.03224 (0.03011)	0.03455 (0.03011)	0.03686 (0.03011)	0.03916 (0.03011)
1050.	0.02671 (0.03124)	0.02894 (0.03124)	0.03117 (0.03124)	0.03340 (0.03124)	0.03563 (0.03124)	0.03786 (0.03124)
1100.	0.02585 (0.03235)	0.02801 (0.03235)	0.03017 (0.03235)	0.03232 (0.03235)	0.03448 (0.03235)	0.03664 (0.03235)
1150.	0.02505 (0.03346)	0.02714 (0.03346)	0.02923 (0.03346)	0.03132 (0.03346)	0.03341 (0.03346)	0.03550 (0.03346)
1200.	0.02429 (0.03456)	0.02632 (0.03456)	0.02834 (0.03456)	0.03037 (0.03456)	0.03240 (0.03456)	0.03442 (0.03456)
1250.	0.02358 (0.03565)	0.02555 (0.03565)	0.02751 (0.03565)	0.02948 (0.03565)	0.03145 (0.03565)	0.03341 (0.03565)
1300.	0.02291 (0.03673)	0.02482 (0.03673)	0.02673 (0.03673)	0.02864 (0.03673)	0.03055 (0.03673)	0.03246 (0.03673)
1350.	0.02227 (0.03780)	0.02413 (0.03780)	0.02599 (0.03780)	0.02785 (0.03780)	0.02970 (0.03780)	0.03156 (0.03780)
1400.	0.02167 (0.03886)	0.02348 (0.03886)	0.02529 (0.03886)	0.02709 (0.03887)	0.02890 (0.03887)	0.03071 (0.03887)
1450.	0.02111 (0.03992)	0.02286 (0.03992)	0.02462 (0.03992)	0.02638 (0.03992)	0.02814 (0.03992)	0.02990 (0.03992)
1500.	0.02057 (0.04096)	0.02228 (0.04096)	0.02399 (0.04096)	0.02571 (0.04096)	0.02742 (0.04096)	0.02914 (0.04097)

†Absolute viscosity μ_{cP} is shown in parentheses.

SOURCE: Derived from ASME, 1977.

TABLE G.2 Compressibility Factors for Air

Temperature			Pressure, psia (bars)									
°F	°R	K	14.5 (1)	72.5 (5)	145 (10)	290 (20)	580 (40)	870 (60)	1160 (80)	1450 (100)	2175 (150)	2900 (200)
-325	135	75								0.5099	0.7581	1.0025
-316	144	80								0.4887	0.7258	0.9588
-298	162	90	0.9764							0.4581	0.6779	0.8929
-280	180	100	0.9797	0.8872					0.3498	0.4337	0.6386	0.8377
-244	216	120	0.9880	0.9373	0.8660	0.6730			0.3371	0.4132	0.5964	0.7720
-208	252	140	0.9927	0.9614	0.9205	0.8297	0.5856	0.3313	0.3737	0.4340	0.5909	0.7699
-172	288	160	0.9951	0.9748	0.9489	0.8954	0.7803	0.6603	0.5696	0.5489	0.6340	0.7564
-136	324	180	0.9967	0.9832	0.9660	0.9314	0.8625	0.7977	0.7432	0.7084	0.7180	0.7986
-100	360	200	0.9978	0.9886	0.9767	0.9539	0.9100	0.8701	0.8374	0.8142	0.8061	0.8549
-10	450	250	0.9992	0.9957	0.9911	0.9822	0.9671	0.9549	0.9463	0.9411	0.9450	0.9713
80	540	300	0.9999	0.9987	0.9974	0.9950	0.9917	0.9901	0.9903	0.9930	1.0074	1.0326
170	630	350	1.0000	1.0002	1.0004	1.0014	1.0038	1.0075	1.0121	1.0183	1.0377	1.0635
260	720	400	1.0002	1.0012	1.0025	1.0046	1.0100	1.0159	1.0229	1.0312	1.0533	1.0795
350	810	450	1.0003	1.0016	1.0034	1.0063	1.0133	1.0210	1.0287	1.0374	1.0614	1.0913
440	900	500	1.0003	1.0020	1.0034	1.0074	1.0151	1.0234	1.0323	1.0410	1.0650	1.0913

SOURCE: Perry and Green (1984).

TABLE G.3 Compressibility Factors for Argon

Temperature			Pressure, psia (atm)						
°F	°R	K	14.7 (1)	58.8 (4)	103 (7)	147 (10)	588 (40)	1617 (70)	1470 (100)
-280	180	100	0.9782	0.9079					
-190	270	150	0.9930	0.9716	0.950	0.927			
-100	360	200	0.9971	0.9882	0.9792	0.9702	0.8978	0.7838	0.6917
-10	450	250	0.9986	0.9945	0.9905	0.9864	0.9476	0.9141	0.8878
26	486	270	0.9990	0.9960	0.9930	0.9900	0.9622	0.9388	0.9208
44	504	280	0.9991	0.9966	0.9940	0.9915	0.9679	0.9486	0.9340
62	522	290	0.9993	0.9971	0.9949	0.9927	0.9729	0.9570	0.9454
80.3	540	300	0.9994	0.9975	0.9957	0.9938	0.9773	0.9643	0.9553
98	558	310	0.9995	0.9979	0.9963	0.9948	0.9810	0.9706	0.9637
116	576	320	0.9996	0.9982	0.9969	0.9956	0.9843	0.9761	0.9710
170	630	350	0.9998	0.9990	0.9983	0.9977	0.9921	0.9888	0.9879
260	720	400	1.0000	0.9999	0.9999	0.9998	1.0002	1.0022	1.0057
350	810	450	1.0001	1.0004	1.0007	1.0011	1.0050	1.0101	1.0162
440	900	500	1.0002	1.0007	1.0013	1.0018	1.0079	1.0147	1.0224
530	990	550	1.0002	1.0009	1.0016	1.0023	1.0095	1.0174	1.0259

SOURCE: Perry and Green (1984).

TABLE G.4 Compressibility Factors for Carbon Dioxide

Temperature			Pressure, psia (bars)								
°F	°R	°C	14.5 (1)	72.5 (5)	145 (10)	290 (20)	580 (40)	870 (60)	1160 (80)	1450 (100)	2900 (200)
32	492	0	0.9933	0.9658	0.9294	0.8496					
122	582	50	0.9964	0.9805	0.9607	0.9195	0.8300	0.7264	0.5981	0.4239	
212	672	100	0.9977	0.9883	0.9764	0.9524	0.9034	0.8533	0.8022	0.7514	0.5891
302	762	150	0.9985	0.9927	0.9853	0.9705	0.9416	0.9131	0.8854	0.8590	0.7651
392	852	200	0.9991	0.9953	0.9908	0.9818	0.9640	0.9473	0.9313	0.9170	0.8649
482	942	250	0.9994	0.9971	0.9943	0.9886	0.9783	0.9684	0.9593	0.9511	0.9253
572	1032	300	0.9996	0.9982	0.9967	0.9936	0.9875	0.9822	0.9773	0.9733	0.9640
662	1122	350	0.9998	0.9991	0.9983	0.9964	0.9938	0.9914	0.9896	0.9882	0.9895
752	1212	400	0.9999	0.9997	0.9994	0.9989	0.9982	0.9979	0.9979	0.9984	1.0073
842	1302	450	1.0000	1.0000	1.0003	1.0005	1.0013	1.0023	1.0038	1.0056	1.0070

SOURCE: Perry and Green (1984).

TABLE G.5 Compressibility Factors for Carbon Monoxide

Temperature			Pressure, psia (atm)						
°F	°R	K	14.7 (1)	58.8 (4)	103 (7)	147 (10)	588 (40)	1617 (70)	1470 (100)
-100	360	200	0.9973	0.9893	0.9813	0.9734			
-10	450	250	0.9989	0.9957	0.9926	0.9896	0.9632		
80	540	300	0.9997	0.9987	0.9977	0.9968	0.9907	0.9896	0.9935
170	630	350	1.0000	1.0002	1.0003	1.0005	1.0042	1.0112	1.0216
260	720	400	1.0002	1.0010	1.0017	1.0025	1.0042	1.0112	1.0216
350	810	450	1.0003	1.0014	1.0025	1.0035	1.0152	1.0285	1.0433
440	900	500	1.0004	1.0016	1.0029	1.0041	1.0172	1.0314	1.0469
620	1080	600	1.0005	1.0018	1.0032	1.0045	1.0186	1.0332	1.0485

SOURCE: Perry and Green (1984).

TABLE G.6 Compressibility Factors for Hydrogen

Temperature			Pressure, psia (atm)						
°F	°R	K	14.7 (1)	58.8 (4)	103 (7)	147 (10)	588 (40)	1617 (70)	1470 (100)
-370	90	50	0.9919	0.9675	0.9431	0.9186			
-280	180	100	0.9998	0.9992	0.9987	0.9983	1.0029	1.0222	1.0560
-190	270	150	1.0006	1.0024	1.0041	1.0058	1.0260	1.0507	1.0796
-100	360	200	1.0007	1.0028	1.0048	1.0069	1.0283	1.0513	1.0760
-10	450	250	1.0006	1.0025	1.0044	1.0065	1.0264	1.0469	1.0682
80	540	300	1.0006	1.0024	1.0042	1.0059	1.0238	1.0420	1.0607
170	630	350	1.0005	1.0020	1.0036	1.0053	1.0213	1.0376	1.0541
260	720	400	1.0005	1.0020	1.0034	1.0048	1.0193	1.0339	1.0486
350	810	450	1.0004	1.0016	1.0030	1.0044	1.0176	1.0307	1.0439
440	900	500	1.0004	1.0016	1.0028	1.0040	1.0160	1.0280	1.0400

SOURCE: Perry and Green (1984).

TABLE G.7 Compressibility Factors for Methane

Temperature			Pressure, psia (bars)								
°F	°R	K	14.5 (1)	72.5 (5)	145 (10)	290 (20)	580 (40)	870 (60)	1160 (80)	1450 (100)	2900 (200)
-280	180	100								0.4313	0.8498
-190	270	150	0.9856	0.9243	0.8333					0.3405	0.6573
-100	360	200	0.9937	0.9682	0.9350	0.8629	0.6858	0.3755	0.3218	0.3657	0.6148
-10	450	250	0.9972	0.9841	0.9678	0.9356	0.8694	0.8035	0.7403	0.6889	0.6953
80	540	300	0.9982	0.9915	0.9828	0.9663	0.9342	0.9042	0.8773	0.8548	0.8280
170	630	350	0.9988	0.9954	0.9905	0.9821	0.9657	0.9513	0.9390	0.9293	0.9226
260	720	400	0.9995	0.9976	0.9957	0.9908	0.9833	0.9771	0.9721	0.9691	0.9783
350	810	450	0.9999	0.9996	0.9991	0.9965	0.9941	0.9923	0.9917	0.9922	1.0128
440	900	500	1.0000	1.0000	1.0000	1.0003	1.0009	1.0021	1.0043	1.0068	1.0335
620	1080	600	1.0002	1.0010	1.0021	1.0040	1.0083	1.0128	1.0175	1.0227	1.0555

SOURCE: Perry and Green (1984).

TABLE G.8 Compressibility Factors for Nitrogen

Temperature			Pressure, psia (bars)								
°F	°R	K	14.5 (1)	72.5 (5)	145 (10)	290 (20)	580 (40)	870 (60)	1160 (80)	1450 (100)	2900 (200)
-334	126	70						0.3400	0.4516	0.5623	1.1044
-316	144	80	0.9593					0.3122	0.4140	0.5148	1.0061
-298	162	90	0.9722					0.2938	0.3888	0.4826	0.9362
-280	180	100	0.9798	0.8910				0.2823	0.3720	0.4605	0.8840
-244	216	120	0.9883	0.9397	0.8732	0.7059		0.2822	0.3641	0.4438	0.8188
-208	252	140	0.9927	0.9635	0.9253	0.8433	0.6376	0.4251	0.4278	0.4799	0.7942
-172	288	160	0.9952	0.9766	0.9529	0.9042	0.8031	0.7017	0.6304	0.6134	0.8107
-136	324	180	0.9967	0.9846	0.9690	0.9381	0.8782	0.8125	0.7784	0.7530	0.8550
-100	360	200	0.9978	0.9897	0.9791	0.9592	0.9212	0.8882	0.8621	0.8455	0.9067
-10	450	250	0.9992	0.9960	0.9924	0.9857	0.9741	0.9655	0.9604	0.9589	1.0048
80	540	300	0.9998	0.9990	0.9983	0.9971	0.9964	0.9973	1.0000	1.0052	1.0559
170	630	350	1.0001	1.0007	1.0011	1.0029	1.0069	1.0125	1.0189	1.0271	1.0810
260	720	400	1.0002	1.0011	1.0024	1.0057	1.0125	1.0199	1.0283	1.0377	1.0926
350	810	450	1.0003	1.0018	1.0033	1.0073	1.0153	1.0238	1.0332	1.0430	1.0973
440	900	500	1.0004	1.0020	1.0040	1.0081	1.0167	1.0257	1.0350	1.0451	1.0984

SOURCE: Perry and Green (1984).

TABLE G.9 Compressibility Factors for Oxygen

Temperature			Pressure, psia (bars)								
°F	°R	K	14.5 (1)	72.5 (5)	145 (10)	290 (20)	580 (40)	870 (60)	1160 (80)	1450 (100)	2900 (200)
-325	135	75								0.4200	0.8301
-316	144	80								0.4007	0.7912
-298	162	90								0.3696	0.7281
-280	180	100	0.9757							0.3464	0.6798
-244	216	120	0.9855	0.9246	0.8367					0.3173	0.6148
-208	252	140	0.9911	0.9535	0.9034	0.7852	0.1334	0.1940	0.2527	0.3099	0.5815
-172	288	160	0.9939	0.9697	0.9379	0.8689	0.6991	0.3725	0.2969	0.3378	0.5766
-136	324	180	0.9960	0.9793	0.9579	0.9134	0.8167	0.7696	0.5954	0.5106	0.6043
-100	360	200	0.9970	0.9853	0.9705	0.9399	0.8768	0.8140	0.7534	0.6997	0.6720
-10	450	250	0.9987	0.9938	0.9870	0.9736	0.9477	0.9237	0.9030	0.8858	0.8563
80	540	300	0.9994	0.9968	0.9941	0.9884	0.9771	0.9676	0.9597	0.9542	0.9560
170	630	350	0.9998	0.9990	0.9979	0.9961	0.9919	0.9890	0.9870	0.9870	1.0049
260	720	400	1.0000	1.0000	1.0000	1.0000	1.0003	1.0011	1.0022	1.0045	1.0305
350	810	450	1.0002	1.0007	1.0015	1.0024	1.0048	1.0074	1.0106	1.0152	1.0445
440	900	500	1.0002	1.0011	1.0022	1.0038	1.0075	1.0115	1.0161	1.0207	1.0523

SOURCE: Perry and Green (1984).

TABLE G.10 Compressibility Factors for Steam

Pressure, psia	Temperature, °F																		
	400	600	800	1000	1200	1400	1600	1800	2000	2200	2400	2600	2800	3000	3200	3400	3600	3800	4000
10	0.9965	0.9989	0.9992	0.9995	0.9999	0.9999	0.9999	1.0000	1.0000	1.0000	1.0001	1.0006	1.0012	1.0024	1.0053	1.0084	1.0145	1.0211	1.0332
15	0.9943	0.9972	0.9986	0.9993	0.9997	0.9998	0.9999	0.9999	1.0000	1.0000	1.0001	1.0004	1.0012	1.0022	1.0042	1.0072	1.0124	1.0188	1.0295
20	0.9930	0.9970	0.9981	0.9991	0.9995	0.9996	0.9998	0.9999	1.0000	1.0000	1.0001	1.0003	1.0011	1.0020	1.0036	1.0065	1.0112	1.0173	1.0269
40	0.9861	0.9940	0.9967	0.9981	0.9990	0.9994	0.9996	0.9998	0.9999	0.9999	1.0001	1.0003	1.0010	1.0018	1.0028	1.0054	1.0090	1.0139	1.0214
60	0.9788	0.9910	0.9951	0.9973	0.9984	0.9991	0.9924	0.9997	0.9999	0.9999	1.0001	1.0003	1.0009	1.0018	1.0024	1.0048	1.0080	1.0120	1.0186
80	0.9714	0.9878	0.9935	0.9963	0.9979	0.9987	0.9992	0.9996	0.9998	0.9999	1.0001	1.0003	1.0008	1.0016	1.0023	1.0044	1.0073	1.0108	1.0170
100	0.9469	0.9848	0.9919	0.9954	0.9974	0.9985	0.9990	0.9995	0.9998	0.9999	1.0001	1.0004	1.0007	1.0015	1.0022	1.0042	1.0067	1.0099	1.0157
150	0.9435	0.9770	0.9879	0.9931	0.9960	0.9976	0.9985	0.9993	0.9997	0.9998	1.0001	1.0004	1.0006	1.0014	1.0021	1.0039	1.0059	1.0087	1.0137
200	0.9216	0.9690	0.9839	0.9908	0.9947	0.9968	0.9980	0.9991	0.9996	0.9998	1.0001	1.0005	1.0007	1.0015	1.0021	1.0037	1.0055	1.0080	1.0126
400		0.9356	0.9675	0.9817	0.9893	0.9935	0.9960	0.9982	0.9982	0.9998	1.0002	1.0007	1.0011	1.0017	1.0023	1.0033	1.0049	1.0070	1.0105
600		0.8989	0.9509	0.9725	0.9839	0.9904	0.9942	0.9973	0.9988	0.9997	1.0002	1.0008	1.0014	1.0019	1.0026	1.0034	1.0048	1.0066	1.0097
800		0.8586	0.9336	0.9633	0.9790	0.9872	0.9925	0.9964	0.9985	0.9996	1.0003	1.0010	1.0016	1.0022	1.0029	1.0036	1.0049	1.0065	1.0094
1,000		0.8138	0.9162	0.9540	0.9733	0.9841	0.9905	0.9955	0.9981	0.9994	1.0004	1.0012	1.0019	1.0025	1.0032	1.0039	1.0052	1.0066	1.0092
1,500		0.6702	0.8695	0.9305	0.9600	0.9764	0.9859	0.9932	0.9971	0.9992	1.0007	1.0017	1.0026	1.0033	1.0040	1.0048	1.0059	1.0072	1.0096
2,000			0.8188	0.9067	0.9468	0.9687	0.9813	0.9900	0.9958	0.9990	1.0010	1.0023	1.0034	1.0042	1.0049	1.0058	1.0068	1.0082	1.0104
4,000			0.5608	0.8060	0.8942	0.9392	0.9647	0.9836	0.9930	0.9989	1.0024	1.0050	1.0069	1.0082	1.0093	1.0106	1.0118	1.0132	1.0149
6,000				0.7042	0.8442	0.9121	0.9497	0.9771	0.9907	0.9991	1.0048	1.0081	1.0110	1.0128	1.0138	1.0152	1.0165	1.0179	1.0195
8,000				0.6185	0.8003	0.8883	0.9371	0.9714	0.9895	1.0004	1.0075	1.0118	1.0152	1.0172	1.0188	1.0204	1.0216	1.0229	1.0242
10,000				0.5699	0.7657	0.8693	0.9274	0.9668	0.9890	1.0025	1.0105	1.0158	1.0196	1.0220	1.0240	1.0258	1.0271	1.0284	1.0298

SOURCE: Perry and Green (1984).

TABLE G.11 Supercompressibility Factors for Natural Gas of Specific Gravity 0.555 to 0.600†

$$F_{pv} = \left(1 + \frac{2.48p_g \times 10^{5.0+2.02G}}{T_r^{3.825}} \right)^{1/2} \quad G \leq 0.600$$

Gauge pressure‡ psig	Specific gravity G									
	0.555	0.560	0.565	0.570	0.575	0.580	0.585	0.590	0.595	0.600
10	1.001	1.001	1.001	1.001	1.001	1.001	1.001	1.001	1.001	1.001
20	1.001	1.001	1.001	1.001	1.001	1.002	1.002	1.002	1.002	1.002
30	1.002	1.002	1.002	1.002	1.002	1.002	1.002	1.002	1.002	1.002
40	1.003	1.003	1.003	1.003	1.003	1.003	1.003	1.003	1.003	1.003
50	1.003	1.003	1.004	1.004	1.004	1.004	1.004	1.004	1.004	1.004
60	1.004	1.004	1.004	1.004	1.004	1.005	1.005	1.005	1.005	1.005
70	1.005	1.005	1.005	1.005	1.005	1.005	1.005	1.006	1.006	1.006
80	1.005	1.005	1.006	1.006	1.006	1.006	1.006	1.006	1.006	1.007
90	1.006	1.006	1.006	1.006	1.007	1.007	1.007	1.007	1.007	1.007
100	1.007	1.007	1.007	1.007	1.007	1.007	1.008	1.008	1.008	1.008
110	1.007	1.008	1.008	1.008	1.008	1.008	1.008	1.009	1.009	1.009
120	1.008	1.008	1.008	1.009	1.009	1.009	1.009	1.009	1.010	1.010
130	1.009	1.009	1.009	1.009	1.010	1.010	1.010	1.010	1.010	1.011
140	1.009	1.010	1.010	1.010	1.010	1.010	1.011	1.011	1.011	1.011
150	1.010	1.010	1.010	1.011	1.011	1.011	1.011	1.012	1.012	1.012
160	1.011	1.011	1.011	1.011	1.012	1.012	1.012	1.013	1.013	1.013
170	1.011	1.012	1.012	1.012	1.012	1.013	1.013	1.013	1.014	1.014
180	1.012	1.012	1.013	1.013	1.013	1.013	1.014	1.014	1.014	1.015
190	1.013	1.013	1.013	1.014	1.014	1.014	1.015	1.015	1.015	1.016
200	1.103	1.014	1.014	1.014	1.015	1.015	1.015	1.016	1.016	1.016
210	1.014	1.014	1.015	1.015	1.015	1.016	1.016	1.016	1.017	1.017
220	1.015	1.015	1.015	1.016	1.016	1.016	1.017	1.017	1.018	1.018
230	1.015	1.016	1.016	1.016	1.017	1.017	1.018	1.018	1.018	1.019
240	1.016	1.016	1.017	1.017	1.017	1.018	1.018	1.019	1.019	1.020
250	1.017	1.017	1.017	1.018	1.018	1.019	1.019	1.020	1.020	1.020
260	1.017	1.018	1.018	1.018	1.019	1.019	1.020	1.020	1.021	1.021
270	1.018	1.018	1.019	1.019	1.020	1.020	1.021	1.021	1.022	1.022
280	1.019	1.019	1.019	1.020	1.020	1.021	1.021	1.022	1.022	1.023
290	1.019	1.020	1.020	1.021	1.021	1.022	1.022	1.023	1.023	1.024
300	1.020	1.020	2.021	1.021	1.022	1.022	1.023	1.023	1.024	1.024
310	1.021	1.021	1.022	1.022	1.023	1.023	1.024	1.024	1.025	1.025
320	1.021	1.022	1.022	1.023	1.023	1.024	1.024	1.025	1.025	1.026
330	1.022	1.022	1.023	1.023	1.024	1.025	1.025	1.026	1.026	1.027
340	1.023	1.023	1.024	1.024	1.025	1.025	1.026	1.026	1.027	1.028
350	1.023	1.024	1.024	1.025	1.025	1.026	1.027	1.027	1.028	1.028
360	1.024	1.024	1.025	1.026	1.026	1.027	1.027	1.028	1.029	1.029
370	1.024	1.025	1.026	1.026	1.027	1.027	1.028	1.029	1.029	1.030
380	1.025	1.026	1.026	1.027	1.028	1.028	1.029	1.030	1.030	1.031

TABLE G.11 Supercompressibility Factors for Natural Gas of Specific Gravity 0.555 to 0.600† (Continued)

Gauge pressure‡ P_G	Specific gravity G									
	0.555	0.560	0.565	0.570	0.575	0.580	0.585	0.590	0.595	0.600
390	1.026	1.026	1.027	1.028	1.028	1.029	1.030	1.030	1.031	1.032
400	1.026	1.027	1.028	1.028	1.029	1.030	1.030	1.031	1.032	1.032
420	1.028	1.028	1.029	1.030	1.030	1.031	1.032	1.033	1.033	1.034
440	1.029	1.030	1.030	1.031	1.032	1.033	1.033	1.034	1.035	1.036
460	1.030	1.031	1.032	1.032	1.033	1.034	1.035	1.036	1.036	1.037
480	1.032	1.032	1.033	1.034	1.035	1.035	1.036	1.037	1.038	1.039
500	1.033	1.034	1.034	1.035	1.036	1.037	1.038	1.039	1.040	1.040
520	1.034	1.035	1.036	1.037	1.038	1.038	1.039	1.040	1.041	1.042
540	1.036	1.036	1.037	1.038	1.039	1.040	1.041	1.042	1.043	1.044
560	1.037	1.038	1.039	1.039	1.040	1.041	1.042	1.043	1.044	1.045
580	1.038	1.039	1.040	1.041	1.042	1.043	1.044	1.045	1.046	1.047
600	1.039	1.040	1.041	1.042	1.043	1.044	1.045	1.046	1.047	1.048

†Tabulated values are for a temperature $T_f = 520^\circ\text{R}$ (60°F).

‡Gauge pressure is measured at the downstream tap for orifice flowmeters.

SOURCE: Derived from PEA (1977).

TABLE G.12 Supercompressibility Factors for Natural Gas of Specific Gravity 0.605 to 0.650†

$$F_{pv} = \left(1 + \frac{3.32p_G \times 10^{5.0+1.81G}}{T_f^{3.825}} \right)^{1/2} \quad 0.601 \leq G \leq 0.650$$

Gauge pressure‡ P_G	Specific gravity G									
	0.605	0.610	0.615	0.620	0.625	0.630	0.635	0.640	0.645	0.650
10	1.001	1.001	1.001	1.001	1.001	1.001	1.001	1.001	1.001	1.001
20	1.002	1.002	1.002	1.002	1.002	1.002	1.002	1.002	1.002	1.002
30	1.003	1.003	1.003	1.003	1.003	1.003	1.003	1.003	1.003	1.003
40	1.003	1.003	1.004	1.004	1.004	1.004	1.004	1.004	1.004	1.004
50	1.004	1.004	1.004	1.004	1.005	1.005	1.005	1.005	1.005	1.005
60	1.005	1.005	1.005	1.005	1.005	1.006	1.006	1.006	1.006	1.006
70	1.006	1.006	1.006	1.006	1.006	1.007	1.007	1.007	1.007	1.007
80	1.007	1.007	1.007	1.007	1.007	1.007	1.008	1.008	1.008	1.008
90	1.008	1.008	1.008	1.008	1.008	1.008	1.009	1.009	1.009	1.009
100	1.008	1.009	1.009	1.009	1.009	1.009	1.010	1.010	1.010	1.010
110	1.009	1.009	1.010	1.010	1.010	1.010	1.010	1.011	1.011	1.011
120	1.010	1.010	1.011	1.011	1.011	1.011	1.011	1.012	1.012	1.012
130	1.011	1.011	1.011	1.012	1.012	1.012	1.012	1.013	1.013	1.013

†Tabulated values are for a temperature $T_f = 520^\circ\text{R}$ (60°F).

‡Gauge pressure is measured at the downstream tap for orifice flowmeters.

TABLE G.12 Supercompressibility Factors for Natural Gas of Specific Gravity 0.605 to 0.650† (Continued)

Gauge pressure‡ P_G	Specific gravity G									
	0.605	0.610	0.615	0.620	0.625	0.630	0.635	0.640	0.645	0.650
140	1.012	1.012	1.012	1.013	1.013	1.013	1.013	1.014	1.014	1.014
150	1.013	1.013	1.013	1.013	1.014	1.014	1.014	1.015	1.015	1.015
160	1.013	1.014	1.014	1.014	1.015	1.015	1.015	1.016	1.016	1.016
170	1.014	1.015	1.015	1.015	1.015	1.016	1.016	1.016	1.017	1.017
180	1.015	1.015	1.016	1.016	1.016	1.017	1.017	1.017	1.018	1.018
190	1.016	1.016	1.017	1.017	1.017	1.018	1.018	1.018	1.019	1.019
200	1.017	1.017	1.017	1.018	1.018	1.019	1.019	1.019	1.020	1.020
210	1.018	1.018	1.018	1.019	1.019	1.019	1.020	1.020	1.021	1.021
220	1.018	1.019	1.019	1.020	1.020	1.020	1.021	1.021	1.022	1.022
230	1.019	1.020	1.020	1.020	1.021	1.021	1.022	1.022	1.023	1.023
240	1.020	1.020	1.021	1.021	1.022	1.022	1.023	1.023	1.024	1.024
250	1.021	1.021	1.022	1.022	1.023	1.023	1.024	1.024	1.025	1.025
260	1.022	1.022	1.023	1.023	1.024	1.024	1.025	1.025	1.026	1.026
270	1.023	1.023	1.023	1.025	1.024	1.025	1.026	1.026	1.027	1.027
280	1.023	1.024	1.024	1.025	1.025	1.026	1.026	1.027	1.028	1.028
290	1.024	1.025	1.025	1.026	1.026	1.027	1.027	1.028	1.029	1.029
300	1.025	1.026	1.026	1.027	1.027	1.028	1.028	1.029	1.029	1.030
310	1.026	1.026	1.027	1.027	1.028	1.029	1.029	1.030	1.030	1.031
320	1.027	1.027	1.028	1.028	1.029	1.030	1.030	1.031	1.031	1.032
330	1.027	1.028	1.029	1.029	1.030	1.030	1.031	1.032	1.032	1.033
340	1.028	1.029	1.029	1.030	1.031	1.031	1.032	1.033	1.033	1.034
350	1.029	1.030	1.030	1.031	1.032	1.032	1.033	1.034	1.034	1.035
360	1.030	1.031	1.031	1.032	1.033	1.033	1.034	1.035	1.035	1.036
370	1.031	1.031	1.032	1.033	1.033	1.034	1.035	1.036	1.036	1.037
380	1.032	1.032	1.033	1.034	1.034	1.035	1.036	1.036	1.037	1.038
390	1.032	1.033	1.034	1.034	1.035	1.036	1.037	1.037	1.038	1.039
400	1.033	1.034	1.035	1.035	1.036	1.037	1.038	1.038	1.039	1.040
420	1.035	1.036	1.036	1.037	1.038	1.039	1.039	1.040	1.041	1.042
440	1.036	1.037	1.038	1.039	1.040	1.040	1.041	1.042	1.043	1.044
460	1.038	1.039	1.040	1.041	1.041	1.042	1.043	1.044	1.045	1.046
480	1.040	1.041	1.041	1.042	1.043	1.044	1.045	1.046	1.047	1.048
500	1.041	1.042	1.043	1.044	1.045	1.046	1.047	1.048	1.049	1.050
520	1.043	1.044	1.045	1.046	1.047	1.048	1.049	1.050	1.051	1.052
540	1.045	1.046	1.046	1.047	1.048	1.049	1.050	1.051	1.052	1.054
560	1.046	1.047	1.048	1.049	1.050	1.051	1.052	1.053	1.054	1.055
580	1.048	1.049	1.050	1.051	1.052	1.053	1.054	1.055	1.056	1.057
600	1.049	1.050	1.051	1.053	1.054	1.055	1.056	1.057	1.058	1.059

†Tabulated values are for a temperature $T_f = 520^\circ\text{R}$ (60°F).

‡Gauge pressure is measured at the downstream tap for orifice flowmeters.

SOURCE: Derived from PEA (1977).

TABLE G.13 Supercompressibility Factors for Natural Gas of Specific Gravity 0.660 to 0.750†

$$F_{pv} = \left(1 + \frac{4.66p_G \times 10^{5.0+1.6G}}{T_f^{3.825}} \right)^{1/2} \quad 0.651 \leq G \leq 0.750$$

Gauge pressure‡ P_G	Specific gravity G									
	0.660	0.670	0.680	0.690	0.700	0.710	0.720	0.730	0.740	0.750
10	1.001	1.001	1.001	1.001	1.001	1.001	1.001	1.001	1.001	1.002
20	1.002	1.002	1.002	1.002	1.003	1.003	1.003	1.003	1.003	1.003
30	1.003	1.003	1.003	1.004	1.004	1.004	1.004	1.004	1.004	1.005
40	1.004	1.004	1.005	1.005	1.005	1.005	1.005	1.006	1.006	1.006
50	1.005	1.006	1.006	1.006	1.006	1.006	1.007	1.007	1.007	1.008
60	1.006	1.007	1.007	1.007	1.008	1.008	1.008	1.008	1.009	1.009
70	1.008	1.008	1.008	1.008	1.009	1.009	1.009	1.010	1.010	1.011
80	1.009	1.009	1.009	1.010	1.010	1.010	1.011	1.011	1.012	1.012
90	1.010	1.010	1.010	1.011	1.011	1.012	1.012	1.013	1.013	1.013
100	1.011	1.011	1.012	1.012	1.012	1.013	1.013	1.014	1.014	1.015
110	1.012	1.012	1.013	1.013	1.014	1.014	1.015	1.015	1.016	1.016
120	1.013	1.013	1.014	1.015	1.015	1.016	1.016	1.017	1.017	1.018
130	1.014	1.015	1.015	1.016	1.016	1.017	1.017	1.018	1.019	1.019
140	1.015	1.016	1.016	1.017	1.017	1.018	1.019	1.019	1.020	1.021
150	1.016	1.017	1.017	1.018	1.019	1.019	1.020	1.021	1.022	1.022
160	1.017	1.018	1.018	1.019	1.020	1.021	1.021	1.022	1.023	1.024
170	1.018	1.019	1.020	1.020	1.021	1.022	1.023	1.024	1.024	1.025
180	1.019	1.020	1.021	1.022	1.022	1.023	1.024	1.025	1.026	1.027
190	1.020	1.021	1.022	1.023	1.024	1.024	1.025	1.026	1.027	1.028
200	1.021	1.022	1.023	1.024	1.025	1.026	1.027	1.028	1.029	1.030
210	1.022	1.023	1.024	1.025	1.026	1.027	1.028	1.029	1.030	1.031
220	1.024	1.024	1.025	1.026	1.027	1.028	1.029	1.030	1.031	1.033
230	1.025	1.026	1.026	1.027	1.028	1.030	1.031	1.032	1.033	1.034
240	1.026	1.027	1.028	1.029	1.030	1.031	1.032	1.033	1.034	1.036
250	1.027	1.028	1.029	1.030	1.031	1.032	1.033	1.034	1.036	1.037
260	1.028	1.029	1.030	1.031	1.032	1.033	1.035	1.036	1.037	1.038
270	1.029	1.030	1.031	1.032	1.033	1.035	1.036	1.037	1.039	1.040
280	1.030	1.031	1.032	1.033	1.035	1.036	1.037	1.039	1.040	1.041
290	1.031	1.032	1.033	1.034	1.036	1.037	1.038	1.040	1.041	1.043
300	1.032	1.033	1.034	1.036	1.037	1.038	1.040	1.041	1.043	1.044
310	1.033	1.034	1.036	1.037	1.038	1.040	1.041	1.043	1.044	1.046
320	1.034	1.035	1.037	1.038	1.039	1.041	1.042	1.044	1.046	1.047
330	1.035	1.036	1.038	1.039	1.041	1.042	1.044	1.045	1.047	1.049
340	1.036	1.038	1.039	1.040	1.042	1.043	1.045	1.047	1.048	1.050
350	1.037	1.039	1.040	1.041	1.043	1.045	1.046	1.048	1.050	1.051
360	1.038	1.040	1.041	1.043	1.044	1.046	1.048	1.049	1.051	1.053
370	1.039	1.041	1.042	1.044	1.045	1.047	1.049	1.051	1.052	1.054
380	1.040	1.042	1.043	1.045	1.047	1.048	1.050	1.052	1.054	1.056

TABLE G.13 Supercompressibility Factors for Natural Gas of Specific Gravity 0.660 to 0.750† (Continued)

Gauge pressure‡ P_g	Specific gravity G									
	0.660	0.670	0.680	0.690	0.700	0.710	0.720	0.730	0.740	0.750
390	1.041	1.043	1.044	1.046	1.048	1.050	1.051	1.053	1.055	1.057
400	1.042	1.044	1.046	1.047	1.049	1.051	1.053	1.055	1.057	1.059
420	1.044	1.046	1.048	1.050	1.051	1.053	1.055	1.057	1.059	1.061
440	1.047	1.048	1.050	1.052	1.054	1.056	1.058	1.060	1.062	1.064
460	1.049	1.050	1.052	1.054	1.056	1.058	1.060	1.063	1.065	1.067
480	1.051	1.053	1.054	1.056	1.059	1.061	1.063	1.065	1.068	1.070
500	1.053	1.055	1.057	1.059	1.061	1.063	1.065	1.068	1.070	1.073
520	1.055	1.057	1.059	1.061	1.063	1.066	1.068	1.070	1.073	1.076
540	1.057	1.059	1.061	1.063	1.066	1.068	1.070	1.073	1.076	1.078
560	1.059	1.061	1.063	1.066	1.068	1.070	1.073	1.076	1.078	1.081
580	1.061	1.063	1.065	1.068	1.070	1.073	1.076	1.078	1.081	1.084
600	1.063	1.065	1.068	1.070	1.073	1.075	1.078	1.081	1.084	1.087

†Tabular values are for a temperature $T_f = 520^\circ\text{R}$ (60°F).

‡Gauge pressure is measured at the downstream tap for orifice flowmeters.

SOURCE: Derived from PEA (1977).

TABLE G.14 Supercompressibility Factors for Natural Gas of Specific Gravity 0.765 to 0.900†

$$F_{pv} = \left(1 + \frac{7.91 p_g \times 10^{5.0+1.26G}}{T_f^{3.825}} \right)^{1/2} \quad 0.751 \leq G \leq 0.900$$

Gauge pressure‡ P_g	Specific gravity G									
	0.765	0.780	0.795	0.810	0.825	0.840	0.855	0.870	0.885	0.900
10	1.001	1.002	1.002	1.002	1.002	1.002	1.002	1.002	1.002	1.002
20	1.003	1.003	1.003	1.003	1.004	1.004	1.004	1.004	1.004	1.004
30	1.004	1.005	1.005	1.005	1.005	1.006	1.006	1.006	1.006	1.007
40	1.006	1.006	1.006	1.007	1.007	1.007	1.008	1.008	1.008	1.009
50	1.007	1.008	1.008	1.008	1.009	1.009	1.010	1.010	1.010	1.011
60	1.009	1.009	1.010	1.010	1.011	1.011	1.012	1.012	1.013	1.013
70	1.010	1.011	1.011	1.012	1.012	1.013	1.013	1.014	1.015	1.015
80	1.012	1.012	1.013	1.013	1.014	1.015	1.015	1.016	1.017	1.017
90	1.013	1.014	1.014	1.015	1.016	1.017	1.017	1.018	1.019	1.020
100	1.015	1.015	1.016	1.017	1.018	1.018	1.019	1.020	1.021	1.022
110	1.016	1.017	1.018	1.018	1.019	1.020	1.021	1.022	1.023	1.024
120	1.018	1.018	1.019	1.020	1.021	1.022	1.023	1.024	1.025	1.026

TABLE G.14 Supercompressibility Factors for Natural Gas of Specific Gravity 0.765 to 0.900† (Continued)

Gauge pressure‡ P_G	Specific gravity G									
	0.765	0.780	0.795	0.810	0.825	0.840	0.855	0.870	0.885	0.900
130	1.019	1.020	1.021	1.022	1.023	1.024	1.025	1.026	1.027	1.028
140	1.021	1.022	1.022	1.023	1.024	1.026	1.027	1.028	1.029	1.030
150	1.022	1.023	1.024	1.025	1.026	1.027	1.029	1.030	1.031	1.032
160	1.024	1.025	1.026	1.027	1.028	1.029	1.030	1.032	1.033	1.035
170	1.025	1.026	1.027	1.028	1.030	1.031	1.032	1.034	1.035	1.037
180	1.026	1.028	1.029	1.030	1.031	1.033	1.034	1.036	1.037	1.039
190	1.028	1.029	1.030	1.032	1.033	1.035	1.036	1.038	1.039	1.041
200	1.029	1.031	1.032	1.033	1.035	1.036	1.038	1.040	1.041	1.043
210	1.031	1.032	1.034	1.035	1.037	1.038	1.040	1.041	1.043	1.045
220	1.032	1.034	1.035	1.037	1.038	1.040	1.042	1.043	1.045	1.047
230	1.034	1.035	1.037	1.038	1.040	1.042	1.043	1.045	1.047	1.049
240	1.035	1.037	1.038	1.040	1.042	1.043	1.045	1.047	1.049	1.051
250	1.037	1.038	1.040	1.042	1.043	1.045	1.047	1.049	1.051	1.054
260	1.038	1.040	1.041	1.043	1.045	1.047	1.049	1.051	1.053	1.056
270	1.039	1.041	1.043	1.045	1.047	1.049	1.051	1.053	1.055	1.058
280	1.041	1.043	1.044	1.046	1.048	1.050	1.053	1.055	1.057	1.060
290	1.042	1.044	1.046	1.048	1.050	1.052	1.055	1.057	1.059	1.062
300	1.044	1.046	1.048	1.050	1.052	1.054	1.056	1.059	1.061	1.064
310	1.045	1.047	1.049	1.051	1.053	1.056	1.058	1.061	1.063	1.066
320	1.047	1.049	1.051	1.053	1.055	1.058	1.060	1.063	1.065	1.068
330	1.048	1.050	1.052	1.054	1.057	1.059	1.062	1.064	1.067	1.070
340	1.049	1.051	1.054	1.056	1.058	1.061	1.064	1.066	1.069	1.072
350	1.051	1.053	1.055	1.058	1.060	1.063	1.065	1.068	1.071	1.074
360	1.052	1.054	1.057	1.059	1.062	1.064	1.067	1.070	1.073	1.076
370	1.054	1.056	1.058	1.061	1.063	1.066	1.069	1.072	1.075	1.078
380	1.055	1.057	1.060	1.062	1.065	1.068	1.071	1.074	1.077	1.080
390	1.056	1.059	1.061	1.064	1.067	1.070	1.073	1.076	1.079	1.082
400	1.058	1.060	1.063	1.066	1.068	1.071	1.074	1.078	1.081	1.084
420	1.061	1.063	1.066	1.069	1.072	1.075	1.078	1.081	1.085	1.088
440	1.063	1.066	1.069	1.072	1.075	1.078	1.082	1.085	1.089	1.093
460	1.066	1.069	1.072	1.075	1.078	1.082	1.085	1.089	1.093	1.097
480	1.069	1.072	1.075	1.078	1.082	1.085	1.089	1.093	1.096	1.101
500	1.072	1.075	1.078	1.081	1.085	1.089	1.092	1.096	1.100	1.105
520	1.075	1.078	1.081	1.085	1.088	1.092	1.096	1.100	1.104	1.109
540	1.077	1.081	1.084	1.088	1.091	1.095	1.099	1.104	1.108	1.112
560	1.080	1.083	1.087	1.091	1.095	1.099	1.103	1.107	1.112	1.116
580	1.083	1.086	1.090	1.094	1.098	1.102	1.106	1.111	1.115	1.120
600	1.086	1.089	1.093	1.097	1.101	1.105	1.110	1.114	1.119	1.124

†Tabular values are for a temperature $T_f = 520^\circ\text{R}$ (60°F).

‡Gauge pressure is measured at the downstream tap for orifice flowmeters.

SOURCE: Derived from PEA (1977).

TABLE G.15 Supercompressibility Factors for Natural Gas of Specific Gravity 0.920 to 1.100†

$$F_{pv} = \left(1 + \frac{11.63 p_G \times 10^{5.0+1.07G}}{T_f^{3.825}} \right)^{1/2} \quad 0.901 \leq G \leq 1.100$$

Gauge pressure‡ P_G	Specific gravity G									
	0.920	0.940	0.960	0.980	1.000	1.020	1.040	1.060	1.080	1.100
10	1.002	1.002	1.003	1.003	1.003	1.003	1.003	1.003	1.003	1.004
20	1.005	1.005	1.005	1.005	1.006	1.006	1.006	1.006	1.007	1.007
30	1.007	1.007	1.008	1.008	1.008	1.009	1.009	1.010	1.010	1.011
40	1.009	1.010	1.010	1.011	1.011	1.012	1.012	1.013	1.014	1.014
50	1.011	1.012	1.013	1.013	1.014	1.015	1.015	1.016	1.017	1.018
60	1.014	1.014	1.015	1.016	1.017	1.017	1.018	1.019	1.020	1.021
70	1.016	1.017	1.018	1.018	1.019	1.020	1.021	1.022	1.024	1.025
80	1.018	1.019	1.020	1.021	1.022	1.023	1.024	1.026	1.027	1.028
90	1.020	1.021	1.023	1.024	1.025	1.026	1.027	1.029	1.030	1.032
100	1.023	1.024	1.025	1.026	1.028	1.029	1.030	1.032	1.033	1.035
110	1.025	1.026	1.027	1.029	1.030	1.032	1.033	1.035	1.037	1.039
120	1.027	1.028	1.030	1.031	1.033	1.035	1.036	1.038	1.040	1.042
130	1.029	1.031	1.032	1.034	1.036	1.037	1.039	1.041	1.043	1.045
140	1.032	1.033	1.035	1.037	1.038	1.040	1.042	1.044	1.047	1.049
150	1.034	1.035	1.037	1.039	1.041	1.043	1.045	1.047	1.050	1.052
160	1.036	1.038	1.040	1.042	1.044	1.046	1.048	1.051	1.053	1.056
170	1.038	1.040	1.042	1.044	1.046	1.049	1.051	1.054	1.056	1.059
180	1.040	1.042	1.045	1.047	1.049	1.051	1.054	1.057	1.059	1.062
190	1.043	1.045	1.047	1.049	1.052	1.054	1.057	1.060	1.063	1.066
200	1.045	1.047	1.049	1.052	1.054	1.057	1.060	1.063	1.066	1.069
210	1.047	1.049	1.052	1.054	1.057	1.060	1.063	1.066	1.069	1.072
220	1.049	1.052	1.054	1.057	1.060	1.063	1.066	1.069	1.072	1.076
230	1.051	1.054	1.057	1.059	1.062	1.065	1.069	1.072	1.075	1.079
240	1.054	1.056	1.059	1.062	1.065	1.068	1.071	1.075	1.079	1.082
250	1.056	1.058	1.061	1.064	1.068	1.071	1.074	1.078	1.082	1.086
260	1.058	1.061	1.064	1.067	1.070	1.074	1.077	1.081	1.085	1.089
270	1.060	1.063	1.066	1.069	1.073	1.076	1.080	1.084	1.088	1.092
280	1.062	1.065	1.068	1.072	1.075	1.079	1.083	1.087	1.091	1.095
290	1.064	1.068	1.071	1.074	1.078	1.082	1.086	1.090	1.094	1.099
300	1.067	1.070	1.073	1.077	1.081	1.084	1.089	1.093	1.097	1.102
310	1.069	1.072	1.076	1.079	1.083	1.087	1.091	1.096	1.100	1.105
320	1.071	1.074	1.078	1.082	1.086	1.090	1.094	1.099	1.103	1.108
330	1.073	1.077	1.080	1.084	1.088	1.092	1.097	1.102	1.107	1.112
340	1.075	1.079	1.083	1.087	1.091	1.095	1.100	1.105	1.110	1.115
350	1.077	1.081	1.085	1.089	1.093	1.098	1.103	1.107	1.113	1.118
360	1.079	1.083	1.087	1.091	1.096	1.101	1.105	1.110	1.116	1.121
370	1.081	1.085	1.090	1.094	1.098	1.103	1.108	1.113	1.119	1.124
380	1.084	1.088	1.092	1.096	1.101	1.106	1.111	1.116	1.122	1.128

TABLE G.15 Supercompressibility Factors for Natural Gas of Specific Gravity 0.920 to 1.100† (Continued)

Gauge pressure‡ P_G	Specific gravity G									
	0.920	0.940	0.960	0.980	1.000	1.020	1.040	1.060	1.080	1.100
390	1.086	1.090	1.094	1.099	1.104	1.108	1.114	1.119	1.125	1.131
400	1.088	1.092	1.097	1.101	1.106	1.111	1.116	1.122	1.128	1.134
420	1.092	1.096	1.101	1.106	1.111	1.116	1.122	1.128	1.134	1.140
440	1.096	1.101	1.106	1.111	1.116	1.122	1.127	1.133	1.140	1.146
460	1.100	1.105	1.110	1.116	1.121	1.127	1.133	1.139	1.146	1.153
480	1.105	1.110	1.115	1.120	1.126	1.132	1.138	1.145	1.152	1.159
500	1.109	1.114	1.119	1.125	1.131	1.137	1.144	1.150	1.158	1.165
520	1.113	1.118	1.124	1.130	1.136	1.142	1.149	1.156	1.163	1.171
540	1.117	1.123	1.128	1.134	1.141	1.147	1.154	1.162	1.169	1.177
560	1.121	1.127	1.133	1.139	1.146	1.153	1.160	1.167	1.175	1.183
580	1.125	1.131	1.137	1.144	1.151	1.158	1.165	1.173	1.181	1.189
600	1.129	1.135	1.142	1.148	1.155	1.163	1.170	1.178	1.187	1.195

†Tabular values are for a temperature $T_f = 520^\circ\text{R}$ (60°F).

‡Gauge pressure is measured at the downstream tap for orifice flowmeters.

SOURCE: Derived from PEA (1977).

TABLE G.16 Supercompressibility Factors for Natural Gas of Specific Gravity 1.140 to 1.500†

$$F_{pv} = \left(1 + \frac{17.48p_G \times 10^{5.0+0.9G}}{T_f^{3.825}} \right)^{1/2} \quad 1.101 < G < 1.500$$

Gauge pressure‡ P_G	Specific gravity G									
	1.140	1.180	1.220	1.260	1.300	1.340	1.380	1.420	1.460	1.500
10	1.004	1.004	1.004	1.005	1.005	1.006	1.006	1.007	1.007	1.008
20	1.008	1.008	1.009	1.010	1.011	1.011	1.012	1.013	1.015	1.016
30	1.011	1.012	1.013	1.014	1.016	1.017	1.019	1.020	1.022	1.024
40	1.015	1.016	1.018	1.019	1.021	1.023	1.025	1.027	1.029	1.031
50	1.019	1.020	1.022	1.024	1.026	1.028	1.031	1.033	1.036	1.039
60	1.022	1.024	1.026	1.029	1.031	1.034	1.037	1.040	1.043	1.047
70	1.026	1.028	1.031	1.033	1.036	1.039	1.043	1.046	1.050	1.054
80	1.030	1.032	1.035	1.038	1.041	1.045	1.049	1.053	1.057	1.062
90	1.034	1.036	1.039	1.043	1.046	1.050	1.055	1.059	1.064	1.070
100	1.037	1.040	1.044	1.047	1.051	1.056	1.061	1.066	1.071	1.077
110	1.041	1.044	1.048	1.052	1.057	1.061	1.066	1.072	1.078	1.084
120	1.045	1.048	1.052	1.057	1.061	1.067	1.072	1.078	1.085	1.092
130	1.048	1.052	1.057	1.061	1.066	1.072	1.078	1.084	1.091	1.099

TABLE G.16 Supercompressibility Factors for Natural Gas of Specific Gravity 1.140 to 1.500† (Continued)

Gauge pressure‡ P_0	Specific gravity G									
	1.140	1.180	1.220	1.260	1.300	1.340	1.380	1.420	1.460	1.500
140	1.052	1.056	1.061	1.066	1.071	1.077	1.084	1.091	1.098	1.106
150	1.055	1.060	1.065	1.070	1.076	1.083	1.090	1.097	1.105	1.113
160	1.059	1.064	1.069	1.075	1.081	1.088	1.095	1.103	1.112	1.121
170	1.063	1.068	1.073	1.079	1.086	1.093	1.101	1.109	1.118	1.128
180	1.066	1.072	1.078	1.084	1.091	1.098	1.107	1.115	1.125	1.135
190	1.070	1.075	1.082	1.088	1.096	1.104	1.112	1.121	1.131	1.142
200	1.073	1.079	1.086	1.093	1.101	1.109	1.118	1.127	1.138	1.149
210	1.077	1.083	1.090	1.097	1.105	1.114	1.123	1.133	1.144	1.156
220	1.080	1.087	1.094	1.102	1.110	1.119	1.129	1.139	1.151	1.163
230	1.084	1.091	1.098	1.106	1.115	1.124	1.134	1.145	1.157	1.170
240	1.087	1.094	1.102	1.111	1.120	1.129	1.140	1.151	1.163	1.176
250	1.091	1.098	1.106	1.115	1.124	1.134	1.145	1.157	1.170	1.183
260	1.094	1.102	1.110	1.119	1.129	1.139	1.151	1.163	1.176	1.190
270	1.098	1.106	1.114	1.124	1.134	1.144	1.156	1.169	1.182	1.197
280	1.101	1.109	1.118	1.128	1.138	1.150	1.162	1.174	1.188	1.203
290	1.104	1.113	1.122	1.132	1.143	1.154	1.167	1.180	1.194	1.210
300	1.108	1.117	1.126	1.137	1.148	1.159	1.172	1.186	1.201	1.216
310	1.111	1.120	1.130	1.141	1.152	1.164	1.178	1.192	1.207	1.223
320	1.115	1.124	1.134	1.145	1.157	1.169	1.183	1.197	1.213	1.229
330	1.118	1.128	1.138	1.149	1.161	1.174	1.188	1.203	1.219	1.236
340	1.122	1.131	1.142	1.154	1.166	1.179	1.193	1.209	1.225	1.242
350	1.125	1.135	1.146	1.158	1.170	1.184	1.199	1.214	1.231	1.249
360	1.128	1.139	1.150	1.162	1.175	1.189	1.204	1.220	1.237	1.255
370	1.132	1.142	1.154	1.166	1.179	1.194	1.209	1.225	1.243	1.262
380	1.135	1.146	1.158	1.170	1.184	1.198	1.214	1.231	1.249	1.268
390	1.138	1.149	1.161	1.174	1.188	1.203	1.219	1.236	1.255	1.274
400	1.142	1.153	1.165	1.179	1.193	1.208	1.224	1.242	1.260	1.280
420	1.148	1.160	1.173	1.187	1.202	1.217	1.234	1.253	1.272	1.293
440	1.155	1.167	1.181	1.195	1.210	1.227	1.244	1.263	1.284	1.305
460	1.161	1.174	1.188	1.203	1.219	1.236	1.254	1.274	1.295	1.317
480	1.168	1.181	1.196	1.211	1.228	1.245	1.264	1.285	1.306	1.329
500	1.174	1.188	1.203	1.219	1.236	1.255	1.274	1.295	1.318	1.341
520	1.181	1.195	1.211	1.227	1.245	1.264	1.284	1.306	1.329	1.353
540	1.187	1.202	1.218	1.235	1.253	1.273	1.294	1.316	1.340	1.365
560	1.194	1.209	1.225	1.243	1.262	1.282	1.303	1.326	1.351	1.377
580	1.200	1.216	1.233	1.251	1.270	1.291	1.313	1.336	1.361	1.388
600	1.206	1.222	1.240	1.258	1.278	1.299	1.322	1.346	1.372	1.400

†Tabular values are for a temperature $T_f = 520^\circ\text{R}$ (60°F).

‡Gauge pressure is measured at the downstream tap for orifice flowmeters.

SOURCE: Derived from PEA (1977).

TABLE G.17 F_{pv} Correction for Temperature

F_{pv}	Temperature T_F , °F														
	40	50	60	70	80	90	100	110	120	130	140	150	160	170	180
1.001	1.001	1.001	1.001	1.001	1.001	1.001	1.001	1.001	1.001	1.001	1.001	1.001	1.001	1.000	1.000
1.002	1.002	1.002	1.002	1.002	1.002	1.002	1.002	1.001	1.001	1.001	1.001	1.001	1.001	1.001	1.001
1.003	1.003	1.003	1.003	1.003	1.003	1.002	1.002	1.002	1.002	1.002	1.002	1.002	1.002	1.001	1.001
1.004	1.005	1.004	1.004	1.004	1.003	1.003	1.003	1.003	1.003	1.002	1.002	1.002	1.002	1.002	1.002
1.005	1.006	1.005	1.005	1.005	1.004	1.004	1.004	1.004	1.003	1.003	1.003	1.003	1.003	1.002	1.002
1.006	1.007	1.006	1.006	1.006	1.005	1.005	1.005	1.004	1.004	1.004	1.003	1.003	1.003	1.003	1.003
1.007	1.008	1.008	1.007	1.007	1.006	1.006	1.005	1.005	1.005	1.004	1.004	1.004	1.004	1.003	1.003
1.008	1.009	1.009	1.008	1.007	1.007	1.006	1.006	1.006	1.005	1.005	1.005	1.004	1.004	1.004	1.004
1.009	1.010	1.010	1.009	1.008	1.008	1.007	1.007	1.006	1.006	1.006	1.005	1.005	1.005	1.004	1.004
1.010	1.012	1.011	1.010	1.009	1.009	1.008	1.008	1.007	1.007	1.006	1.006	1.005	1.005	1.005	1.005
1.011	1.013	1.012	1.011	1.010	1.010	1.009	1.008	1.008	1.007	1.007	1.006	1.006	1.006	1.005	1.005
1.012	1.014	1.013	1.012	1.011	1.010	1.010	1.009	1.008	1.008	1.007	1.007	1.007	1.006	1.006	1.005
1.013	1.015	1.014	1.013	1.012	1.011	1.011	1.010	1.009	1.009	1.008	1.008	1.007	1.007	1.006	1.006
1.014	1.016	1.015	1.014	1.013	1.012	1.011	1.011	1.010	1.009	1.009	1.008	1.008	1.007	1.007	1.006
1.015	1.017	1.016	1.015	1.014	1.013	1.012	1.011	1.011	1.010	1.009	1.009	1.008	1.008	1.007	1.007
1.016	1.019	1.017	1.016	1.015	1.014	1.013	1.012	1.011	1.011	1.010	1.009	1.009	1.008	1.008	1.007
1.017	1.020	1.018	1.017	1.016	1.015	1.014	1.013	1.012	1.011	1.011	1.010	1.009	1.009	1.008	1.008
1.018	1.021	1.019	1.018	1.017	1.016	1.015	1.014	1.013	1.012	1.011	1.010	1.010	1.009	1.009	1.008
1.019	1.022	1.020	1.019	1.018	1.016	1.015	1.014	1.013	1.013	1.012	1.011	1.010	1.010	1.009	1.009
1.020	1.023	1.022	1.020	1.019	1.017	1.016	1.015	1.014	1.013	1.012	1.012	1.011	1.010	1.010	1.009
1.021	1.024	1.023	1.021	1.020	1.018	1.017	1.016	1.015	1.014	1.013	1.012	1.011	1.011	1.010	1.010
1.022	1.026	1.024	1.022	1.020	1.019	1.018	1.017	1.016	1.015	1.014	1.013	1.012	1.011	1.011	1.010
1.023	1.027	1.025	1.023	1.021	1.020	1.019	1.017	1.016	1.015	1.014	1.013	1.013	1.012	1.011	1.010
1.024	1.028	1.026	1.024	1.022	1.021	1.019	1.018	1.017	1.016	1.015	1.014	1.013	1.012	1.012	1.011
1.025	1.029	1.027	1.025	1.023	1.022	1.020	1.019	1.018	1.017	1.015	1.015	1.014	1.013	1.012	1.011

TABLE G.17 F_{pv} Correction for Temperature (*Continued*)

F_{pv}	Temperature T_p , °F														
	40	50	60	70	80	90	100	110	120	130	140	150	160	170	180
1.026	1.030	1.028	1.026	1.024	1.023	1.021	1.020	1.018	1.017	1.016	1.015	1.014	1.013	1.013	1.012
1.027	1.031	1.029	1.027	1.025	1.023	1.022	1.020	1.019	1.018	1.017	1.016	1.015	1.014	1.013	1.012
1.028	1.032	1.030	1.028	1.026	1.024	1.023	1.021	1.020	1.019	1.017	1.016	1.015	1.014	1.014	1.013
1.029	1.034	1.031	1.029	1.027	1.025	1.023	1.022	1.020	1.019	1.018	1.017	1.016	1.015	1.014	1.013
1.030	1.035	1.032	1.030	1.028	1.026	1.024	1.023	1.021	1.020	1.015	1.017	1.016	1.015	1.015	1.014
1.031	1.036	1.033	1.031	1.029	1.027	1.025	1.023	1.022	1.021	1.019	1.018	1.017	1.016	1.015	1.014
1.032	1.037	1.034	1.032	1.030	1.028	1.026	1.024	1.023	1.021	1.020	1.019	1.018	1.016	1.015	1.015
1.033	1.038	1.036	1.033	1.031	1.029	1.027	1.025	1.023	1.022	1.020	1.019	1.018	1.017	1.016	1.015
1.034	1.039	1.037	1.034	1.032	1.029	1.028	1.026	1.024	1.023	1.021	1.020	1.019	1.017	1.016	1.016
1.035	1.041	1.038	1.035	1.033	1.030	1.028	1.026	1.025	1.023	1.022	1.020	1.019	1.018	1.017	1.016
1.036	1.042	1.039	1.036	1.034	1.031	1.029	1.027	1.025	1.024	1.022	1.021	1.020	1.019	1.017	1.016
1.037	1.043	1.040	1.037	1.034	1.032	1.030	1.028	1.026	1.025	1.023	1.022	1.020	1.019	1.018	1.017
1.038	1.044	1.041	1.038	1.035	1.033	1.031	1.029	1.027	1.025	1.024	1.022	1.021	1.020	1.018	1.017
1.039	1.045	1.042	1.039	1.036	1.034	1.032	1.030	1.028	1.026	1.024	1.023	1.021	1.020	1.019	1.018
1.040	1.046	1.043	1.040	1.037	1.035	1.032	1.030	1.028	1.027	1.025	1.023	1.022	1.021	1.019	1.018
1.041	1.047	1.044	1.041	1.038	1.036	1.033	1.031	1.025	1.027	1.025	1.024	1.022	1.021	1.020	1.019
1.042	1.049	1.045	1.042	1.039	1.036	1.034	1.032	1.030	1.028	1.026	1.025	1.023	1.022	1.020	1.019
1.043	1.050	1.046	1.043	1.040	1.037	1.035	1.033	1.030	1.029	1.027	1.025	1.024	1.022	1.021	1.020
1.044	1.051	1.047	1.044	1.041	1.038	1.036	1.033	1.031	1.029	1.027	1.026	1.024	1.023	1.021	1.020
1.045	1.052	1.048	1.045	1.042	1.039	1.036	1.034	1.032	1.030	1.028	1.026	1.025	1.025	1.022	1.021
1.046	1.053	1.049	1.046	1.043	1.040	1.037	1.035	1.033	1.031	1.029	1.027	1.025	1.024	1.022	1.021
1.047	1.054	1.051	1.047	1.044	1.041	1.038	1.036	1.033	1.031	1.029	1.027	1.026	1.024	1.023	1.022
1.048	1.056	1.052	1.048	1.045	1.042	1.039	1.036	1.034	1.032	1.030	1.028	1.026	1.025	1.023	1.022
1.049	1.057	1.053	1.049	1.046	1.043	1.040	1.037	1.035	1.033	1.031	1.029	1.027	1.025	1.024	1.022
1.050	1.058	1.054	1.050	1.047	1.043	1.041	1.038	1.035	1.033	1.031	1.029	1.027	1.026	1.024	1.023

1.050	1.058	1.054	1.050	1.047	1.043	1.041	1.038	1.035	1.033	1.031	1.029	1.027	1.026	1.024	1.023
1.051	1.059	1.055	1.051	1.047	1.044	1.041	1.039	1.036	1.034	1.032	1.030	1.028	1.026	1.025	1.023
1.052	1.060	1.056	1.052	1.048	1.045	1.042	1.039	1.037	1.035	1.032	1.030	1.029	1.027	1.025	1.024
1.053	1.061	1.057	1.053	1.049	1.046	1.043	1.040	1.038	1.035	1.033	1.031	1.029	1.027	1.026	1.024
1.054	1.062	1.058	1.054	1.050	1.047	1.044	1.041	1.038	1.036	1.034	1.032	1.030	1.028	1.026	1.025
1.055	1.064	1.059	1.055	1.051	1.048	1.045	1.042	1.039	1.037	1.034	1.032	1.030	1.028	1.027	1.025
1.056	1.065	1.060	1.056	1.052	1.049	1.045	1.042	1.040	1.037	1.035	1.033	1.031	1.029	1.027	1.026
1.057	1.066	1.061	1.057	1.053	1.050	1.046	1.043	1.040	1.038	1.036	1.033	1.031	1.029	1.028	1.026
1.058	1.067	1.062	1.058	1.054	1.050	1.047	1.044	1.041	1.039	1.036	1.034	1.032	1.030	1.028	1.027
1.059	1.068	1.063	1.059	1.055	1.051	1.048	1.045	1.042	1.039	1.037	1.035	1.032	1.031	1.029	1.027
1.060	1.069	1.064	1.060	1.056	1.052	1.049	1.046	1.043	1.040	1.037	1.035	1.033	1.031	1.029	1.028
1.061	1.071	1.066	1.061	1.057	1.053	1.049	1.046	1.043	1.041	1.038	1.036	1.034	1.032	1.030	1.028
1.062	1.072	1.067	1.062	1.058	1.054	1.050	1.047	1.044	1.041	1.039	1.036	1.034	1.032	1.030	1.028
1.063	1.073	1.068	1.063	1.059	1.055	1.051	1.048	1.045	1.042	1.039	1.037	1.035	1.033	1.031	1.029
1.064	1.074	1.069	1.064	1.060	1.056	1.052	1.049	1.045	1.043	1.040	1.038	1.035	1.033	1.031	1.029
1.065	1.075	1.070	1.065	1.061	1.056	1.053	1.049	1.046	1.043	1.041	1.038	1.036	1.034	1.032	1.030
1.066	1.076	1.071	1.066	1.061	1.057	1.054	1.050	1.047	1.044	1.041	1.039	1.036	1.034	1.032	1.030
1.067	1.077	1.072	1.067	1.062	1.058	1.054	1.051	1.048	1.045	1.042	1.039	1.037	1.035	1.033	1.031
1.068	1.079	1.073	1.068	1.063	1.059	1.055	1.052	1.048	1.045	1.042	1.040	1.037	1.035	1.033	1.031
1.069	1.080	1.074	1.069	1.064	1.060	1.056	1.052	1.049	1.046	1.043	1.040	1.038	1.036	1.034	1.032
1.070	1.081	1.075	1.070	1.065	1.061	1.057	1.053	1.050	1.047	1.044	1.041	1.039	1.036	1.034	1.032
1.071	1.082	1.076	1.071	1.066	1.062	1.058	1.054	1.050	1.047	1.044	1.042	1.039	1.037	1.035	1.033
1.072	1.083	1.077	1.072	1.067	1.063	1.058	1.055	1.051	1.048	1.045	1.042	1.040	1.037	1.035	1.033
1.073	1.084	1.078	1.073	1.068	1.063	1.059	1.055	1.052	1.049	1.046	1.043	1.040	1.038	1.036	1.034
1.074	1.086	1.079	1.074	1.069	1.064	1.060	1.056	1.053	1.049	1.046	1.043	1.041	1.038	1.036	1.034
1.075	1.087	1.081	1.075	1.070	1.065	1.061	1.057	1.053	1.050	1.047	1.044	1.041	1.039	1.037	1.035
1.076	1.088	1.082	1.076	1.071	1.066	1.062	1.058	1.054	1.051	1.048	1.045	1.042	1.039	1.037	1.035
1.077	1.089	1.003	1.077	1.072	1.067	1.063	1.059	1.055	1.051	1.048	1.045	1.043	1.040	1.038	1.036
1.078	1.090	1.084	1.078	1.073	1.068	1.063	1.059	1.056	1.052	1.049	1.046	1.043	1.041	1.038	1.036
1.079	1.091	1.085	1.079	1.074	1.069	1.064	1.060	1.056	1.053	1.049	1.046	1.044	1.041	1.039	1.036

TABLE G.17 F_{pv} Correction for Temperature (*Continued*)

F_{pv}	Temperature T_F , °F														
	40	50	60	70	80	90	100	110	120	130	140	150	160	170	180
1.080	1.092	1.086	1.080	1.075	1.070	1.065	1.061	1.057	1.053	1.050	1.047	1.044	1.042	1.039	1.037
1.081	1.094	1.087	1.081	1.076	1.070	1.066	1.062	1.058	1.054	1.051	1.048	1.045	1.042	1.040	1.037
1.082	1.095	1.088	1.082	1.076	1.071	1.067	1.062	1.058	1.055	1.051	1.048	1.045	1.043	1.040	1.038
1.083	1.096	1.089	1.083	1.077	1.072	1.067	1.063	1.059	1.055	1.052	1.049	1.046	1.043	1.041	1.038
1.084	1.097	1.090	1.084	1.078	1.073	1.068	1.064	1.060	1.056	1.053	1.049	1.046	1.044	1.041	1.039
1.085	1.098	1.091	1.085	1.079	1.074	1.069	1.065	1.061	1.057	1.053	1.050	1.047	1.044	1.042	1.039
1.086	1.099	1.092	1.086	1.080	1.075	1.070	1.065	1.061	1.057	1.054	1.051	1.048	1.045	1.042	1.040
1.087	1.100	1.093	1.087	1.081	1.076	1.071	1.066	1.062	1.058	1.055	1.051	1.048	1.045	1.043	1.040
1.088	1.102	1.094	1.088	1.082	1.077	1.072	1.067	1.063	1.059	1.055	1.052	1.049	1.046	1.043	1.041
1.089	1.103	1.096	1.089	1.083	1.077	1.072	1.068	1.063	1.059	1.056	1.052	1.049	1.046	1.044	1.041
1.090	1.104	1.097	1.090	1.084	1.078	1.073	1.068	1.064	1.060	1.056	1.053	1.050	1.047	1.044	1.042
1.091	1.105	1.098	1.091	1.085	1.079	1.074	1.069	1.065	1.061	1.057	1.054	1.050	1.047	1.045	1.042
1.092	1.106	1.099	1.092	1.086	1.080	1.075	1.070	1.066	1.061	1.058	1.054	1.051	1.048	1.045	1.043
1.093	1.107	1.100	1.093	1.087	1.081	1.076	1.071	1.066	1.062	1.058	1.055	1.052	1.048	1.046	1.043
1.094	1.108	1.101	1.094	1.088	1.082	1.076	1.072	1.067	1.062	1.059	1.055	1.052	1.049	1.046	1.044
1.095	1.110	1.102	1.095	1.089	1.083	1.077	1.072	1.068	1.064	1.060	1.056	1.053	1.050	1.047	1.044
1.096	1.111	1.103	1.096	1.090	1.084	1.078	1.073	1.068	1.064	1.060	1.057	1.053	1.050	1.047	1.044
1.097	1.112	1.104	1.097	1.090	1.084	1.079	1.074	1.069	1.065	1.061	1.057	1.054	1.051	1.048	1.045
1.098	1.113	1.105	1.098	1.091	1.085	1.080	1.075	1.070	1.066	1.062	1.058	1.054	1.051	1.048	1.045
1.099	1.114	1.106	1.099	1.092	1.086	1.081	1.075	1.071	1.066	1.062	1.058	1.055	1.052	1.049	1.046
1.100	1.115	1.107	1.100	1.093	1.087	1.081	1.076	1.071	1.067	1.063	1.059	1.055	1.052	1.049	1.046

TABLE G.18 Corrections to Supercompressibility Factor F_{pv} for Air

Specific gravity	Percent air	Pressure, psig									
		35		135		235		335		435	
		30-89°	90-149°	30-89°	90-149°	30-89°	90-149°	30-89°	90-149°	30-89°	90-149°
0.50-0.649	1	0.001	0.000	0.001	0.001
	2	0.001	0.001	0.001	0.002	0.001	0.002	0.001
	3	0.001	0.001	0.001	0.002	0.001	0.002	0.002	0.003	0.002
	4	0.001	0.001	0.002	0.001	0.002	0.001	0.003	0.002	0.005	0.003
	5	0.001	0.001	0.002	0.001	0.003	0.002	0.004	0.003	0.006	0.004
	6	0.001	0.001	0.002	0.002	0.004	0.002	0.005	0.004	0.007	0.004
	7	0.001	0.001	0.003	0.002	0.004	0.003	0.006	0.004	0.008	0.005
	8	0.001	0.001	0.003	0.002	0.005	0.003	0.007	0.005	0.009	0.006
0.650-0.749	1	0.001	0.001	0.001	0.001	0.001
	2	0.001	0.001	0.001	0.002	0.001	0.003	0.002
	3	0.001	0.001	0.001	0.002	0.001	0.002	0.002	0.004	0.002
	4	0.001	0.001	0.002	0.001	0.002	0.002	0.003	0.003	0.005	0.003
	5	0.001	0.001	0.002	0.002	0.003	0.002	0.004	0.003	0.006	0.004
	6	0.001	0.001	0.002	0.002	0.004	0.003	0.005	0.004	0.008	0.005
	7	0.001	0.001	0.003	0.002	0.005	0.003	0.006	0.005	0.009	0.006
	8	0.001	0.001	0.003	0.003	0.005	0.004	0.007	0.005	0.010	0.007
0.750-0.849	1	0.001	0.000	0.001	0.001	0.001	0.001
	2	0.001	0.001	0.001	0.001	0.002	0.001	0.003	0.002
	3	0.001	0.001	0.001	0.002	0.001	0.003	0.002	0.004	0.003
	4	0.001	0.001	0.002	0.001	0.003	0.002	0.004	0.003	0.006	0.004
	5	0.001	0.001	0.002	0.002	0.004	0.003	0.005	0.004	0.007	0.005
	6	0.001	0.001	0.003	0.002	0.004	0.003	0.006	0.005	0.009	0.006
	7	0.001	0.001	0.003	0.002	0.005	0.004	0.007	0.005	0.010	0.007
	8	0.001	0.001	0.004	0.003	0.006	0.005	0.009	0.006	0.012	0.008

TABLE G.19 Corrections to Supercompressibility Factor F_{pv} for Carbon Dioxide

Specific gravity	Percent CO ₂	Pressure, psig									
		35		135		235		335		435	
		30-89°	90-149°	30-89°	90-149°	30-89°	90-149°	30-89°	90-149°	30-89°	90-149°
0.550-0.649	1	0.001	0.001	0.001
	2	0.001	0.001	0.001	0.001	0.001	0.001	0.002	0.001
	3	0.001	0.001	0.001	0.001	0.001	0.001	0.002	0.001	0.002	0.002
	4	0.001	0.001	0.001	0.001	0.002	0.002	0.002	0.002	0.003	0.002
	5	0.001	0.001	0.002	0.002	0.002	0.002	0.003	0.002	0.004	0.003
	6	0.001	0.001	0.002	0.002	0.003	0.002	0.003	0.002	0.004	0.003
	7	0.001	0.001	0.003	0.002	0.004	0.002	0.004	0.003	0.005	0.003
	8	0.002	0.001	0.003	0.002	0.004	0.002	0.005	0.003	0.006	0.004
0.650-0.749	1	0.001	0.001	0.001	0.001	0.002	0.001
	2	0.001	0.001	0.001	0.002	0.002	0.003	0.002
	3	0.001	0.001	0.001	0.001	0.002	0.002	0.003	0.002	0.004	0.003
	4	0.001	0.001	0.002	0.001	0.003	0.002	0.004	0.003	0.006	0.004
	5	0.001	0.001	0.002	0.002	0.003	0.003	0.005	0.004	0.007	0.004
	6	0.001	0.001	0.003	0.002	0.004	0.003	0.006	0.004	0.008	0.005
	7	0.002	0.001	0.003	0.002	0.005	0.004	0.006	0.005	0.009	0.006
	8	0.002	0.001	0.004	0.003	0.005	0.004	0.007	0.005	0.010	0.007
0.750-0.849	1	0.001	0.001	0.001	0.001	0.002	0.001
	2	0.001	0.001	0.002	0.001	0.003	0.002	0.004	0.003
	3	0.001	0.001	0.001	0.001	0.003	0.001	0.004	0.003	0.005	0.004
	4	0.001	0.001	0.002	0.002	0.003	0.003	0.005	0.004	0.006	0.005
	5	0.001	0.001	0.002	0.002	0.004	0.003	0.007	0.005	0.008	0.006
	6	0.002	0.001	0.003	0.003	0.005	0.004	0.008	0.006	0.010	0.007
	7	0.002	0.001	0.004	0.003	0.006	0.005	0.009	0.007	0.011	0.008
	8	0.002	0.002	0.004	0.003	0.007	0.005	0.010	0.007	0.013	0.009

0.850-0.949	1	0.001	0.001	0.001	0.001
	2	0.001	0.001	0.001	0.001	0.002	0.002
	3	0.001	0.001	0.002	0.001	0.003	0.002
	4	0.001	0.001	0.003	0.002	0.004	0.003
	5	0.001	0.001	0.004	0.002	0.005	0.004
	6	0.002	0.001	0.004	0.003	0.006	0.005
	7	0.002	0.002	0.005	0.003	0.007	0.005
	8	0.002	0.002	0.006	0.004	0.008	0.006
0.950-1.04	1	0.001	0.001	0.001	0.001
	2	0.001	0.001	0.001	0.001	0.002	0.002
	3	0.001	0.001	0.002	0.002	0.004	0.003
	4	0.001	0.001	0.003	0.002	0.005	0.003
	5	0.002	0.001	0.004	0.003	0.006	0.004
	6	0.002	0.002	0.004	0.003	0.008	0.005
	7	0.002	0.002	0.005	0.004	0.009	0.006
	8	0.003	0.002	0.006	0.004	0.011	0.007
1.05-1.14	1	0.001	0.001		
	2	0.001	0.001	0.002	0.001		
	3	0.001	0.001	0.003	0.002		
	4	0.001	0.001	0.003	0.003		
	5	0.002	0.002	0.004	0.003		
	6	0.002	0.002	0.005	0.004		
	7	0.003	0.002	0.006	0.004		
	8	0.003	0.002	0.007	0.005		
1.15-1.24	1	0.001	0.001		
	2	0.001	0.001	0.002	0.001		
	3	0.001	0.001	0.003	0.002		
	4	0.002	0.001	0.004	0.003		
	5	0.002	0.002	0.005	0.004		

TABLE G.19 Corrections to Supercompressibility Factor F_{pv} for Carbon Dioxide (*Continued*)

Specific gravity	Percent CO ₂	Pressure, psig									
		35		135		235		335		435	
		30-89°	90-149°	30-89°	90-149°	30-89°	90-149°	30-89°	90-149°	30-89°	90-149°
	6	0.002	0.002	0.007	0.004						
	7	0.003	0.002	0.008	0.005						
	8	0.003	0.003	0.009	0.006						
1.25-1.34	1	0.001								
	2	0.001	0.001								
	3	0.001	0.001								
	4	0.002	0.002								
	5	0.002	0.002								
	6	0.003	0.002								
	7	0.003	0.003								
	8	0.004	0.003								
1.35-1.44	1	0.001									
	2	0.001	0.001								
	3	0.001	0.001								
	4	0.002	0.001								
	5	0.002	0.002								
	6	0.003	0.002								
	7	0.003	0.002								
	8	0.004	0.003								

NOTE: The above corrections for given amounts of carbon dioxide are deductible from the corrected supercompressibility factors in Tables G.11 through G.17. Each heading is inclusive to next higher heading. Do not interpolate.

TABLE G.20 Supercompressibility Factors for Natural Gas of 0.6 Specific Gravity:† U.S. Units

P_G , Psig	Flowing temperature T_F , °F													
	-40	-20	0	20	40	60	80	100	120	140	160	180	200	220
0	1.0000	1.0000	1.0000	1.0000	1.0000	1.0000	1.0000	1.0000	1.0000	1.0000	1.0000	1.0000	1.0000	1.0000
100	1.0157	1.0137	1.0119	1.0104	1.0091	1.0079	1.0070	1.0061	1.0054	1.0047	1.0041	1.0036	1.0032	1.0028
200	1.0329	1.0284	1.0245	1.0212	1.0184	1.0160	1.0141	1.0123	1.0108	1.0094	1.0082	1.0072	1.0063	1.0055
300	1.0517	1.0441	1.0378	1.0325	1.0281	1.0243	1.0212	1.0185	1.0161	1.0141	1.0123	1.0108	1.0094	1.0082
400	1.0725	1.0610	1.0518	1.0442	1.0380	1.0327	1.0284	1.0247	1.0215	1.0187	1.0163	1.0142	1.0124	1.0108
500	1.0954	1.0792	1.0665	1.0564	1.0481	1.0413	1.0357	1.0309	1.0268	1.0233	1.0202	1.0176	1.0153	1.0132
600	1.1211	1.0988	1.0821	1.0690	1.0585	1.0499	1.0430	1.0370	1.0320	1.0277	1.0240	1.0208	1.0180	1.0156
700	1.1500	1.1202	1.0986	1.0820	1.0691	1.0587	1.0502	1.0432	1.0372	1.0321	1.0277	1.0240	1.0207	1.0178
800	1.1826	1.1431	1.1158	1.0955	1.0798	1.0674	1.0575	1.0492	1.0423	1.0364	1.0313	1.0270	1.0232	1.0199
900	1.2193	1.1678	1.1337	1.1092	1.0906	1.0761	1.0646	1.0551	1.0472	1.0405	1.0348	1.0299	1.0256	1.0219
1000	1.2597	1.1939	1.1522	1.1231	1.1014	1.0847	1.0716	1.0609	1.0520	1.0445	1.0381	1.0326	1.0279	1.0237
1100	1.3021	1.2211	1.1711	1.1370	1.1120	1.0931	1.0784	1.0665	1.0566	1.0483	1.0413	1.0352	1.0301	1.0255
1200	1.3421	1.2481	1.1898	1.1506	1.1224	1.1013	1.0850	1.0719	1.0610	1.0519	1.0443	1.0377	1.0321	1.0272
1300	1.3754	1.2735	1.2079	1.1639	1.1325	1.1091	1.0912	1.0770	1.0652	1.0554	1.0471	1.0400	1.0339	1.0287
1400	1.4007	1.2959	1.2246	1.1764	1.1421	1.1166	1.0971	1.0818	1.0691	1.0586	1.0497	1.0421	1.0356	1.0300
1500	1.4138	1.3132	1.2393	1.1879	1.1511	1.1235	1.1026	1.0863	1.0728	1.0615	1.0521	1.0440	1.0371	1.0312
1600	1.4175	1.3248	1.2512	1.1978	1.1589	1.1298	1.1076	1.0904	1.0762	1.0643	1.0543	1.0458	1.0385	1.0323
1700	1.4145	1.3311	1.2603	1.2062	1.1658	1.1353	1.1121	1.0941	1.0792	1.0667	1.0563	1.0474	1.0398	1.0333
1800	1.4068	1.3330	1.2663	1.2126	1.1715	1.1400	1.1160	1.0974	1.0819	1.0689	1.0580	1.0487	1.0409	1.0341
1900	1.3959	1.3312	1.2695	1.2173	1.1760	1.1439	1.1194	1.1002	1.0842	1.0708	1.0595	1.0499	1.0417	1.0347
2000	1.3827	1.3264	1.2704	1.2202	1.1793	1.1470	1.1221	1.1026	1.0861	1.0724	1.0607	1.0508	1.0424	1.0352

TABLE G.20 Supercompressibility Factors for Natural Gas of 0.6 Specific Gravity:† U.S. Units (*Continued*)

P_G , Psig	Flowing temperature T_F , °F													
	-40	-20	0	20	40	60	80	100	120	140	160	180	200	220
2100	1.3680	1.3186	1.2677	1.2207	1.1812	1.1493	1.1243	1.1044	1.0876	1.0734	1.0614	1.0513	1.0429	1.0355
2200	1.3527	1.3093	1.2635	1.2199	1.1820	1.1508	1.1258	1.1058	1.0887	1.0741	1.0619	1.0516	1.0431	1.0358
2300	1.3365	1.2988	1.2579	1.2175	1.1816	1.1513	1.1266	1.1066	1.0893	1.0745	1.0621	1.0517	1.0432	1.0359
2400	1.3205	1.2879	1.2511	1.2139	1.1800	1.1508	1.1266	1.1067	1.0894	1.0745	1.0691	1.0515	1.0431	1.0357
2500	1.3059	1.2763	1.2436	1.2095	1.1777	1.1496	1.1261	1.1065	1.0892	1.0741	1.0615	1.0511	1.0427	1.0355
2600	1.2906	1.2646	1.2352	1.2040	1.1742	1.1475	1.1248	1.1056	1.0885	1.0736	1.0610	1.0506	1.0422	1.0350
2700	1.2756	1.2527	1.2265	1.1980	1.1703	1.1450	1.1230	1.1043	1.0875	1.0728	1.0603	1.0499	1.0415	1.0343
2800	1.2608	1.2408	1.2174	1.1915	1.1657	1.1418	1.1208	1.1026	1.0862	1.0717	1.0593	1.0489	1.0407	1.0335
2900	1.2464	1.2289	1.2081	1.1845	1.1606	1.1381	1.1180	1.1005	1.0845	1.0703	1.0580	1.0478	1.0396	1.0324
3000	1.2324	1.2172	1.1987	1.1773	1.1552	1.1341	1.1150	1.0981	1.0825	1.0687	1.0566	1.0464	1.0383	1.0313

NOTE: For expanded tables of supercompressibility factors for natural gas, see A.G.A. Report No. 3 or A.G.A. Supercompressibility Tables (NX-19).

†For specific gravities other than 0.6, adjust pressure and temperature before entering table:

$$(p_G)_{\text{table}} = \frac{156.47 p_G}{160.8 - 7.22G + 100x_{\text{CO}_2} - 39.2x_{\text{N}_2}} \quad (T_F)_{\text{table}} = \frac{226.29}{99.15 + 211.9G - 100x_{\text{CO}_2} - 168.1x_{\text{N}_2}} (T_F + 460) - 460$$

SOURCE: Dieterich Standard Corp.

TABLE G.21 Supercompressibility Factors for Natural Gas of 0.6 Specific Gravity:† SI Units

Gauge press, kPa	Flowing temperature T_c , °C													
	-40	-29	-18	-7	4	16	27	38	49	60	71	82	93	104
0	1.0000	1.0000	1.0000	1.0000	1.0000	1.0000	1.0000	1.0000	1.0000	1.0000	1.0000	1.0000	1.0000	1.0000
689	1.0157	1.0137	1.0119	1.0104	1.0091	1.0079	1.0070	1.0061	1.0054	1.0047	1.0041	1.0036	1.0032	1.0028
1,379	1.0329	1.0284	1.0245	1.0212	1.0184	1.0160	1.0141	1.0123	1.0108	1.0094	1.0082	1.0072	1.0063	1.0055
2,068	1.0517	1.0441	1.0378	1.0325	1.0281	1.0243	1.0212	1.0185	1.0161	1.0141	1.0123	1.0108	1.0094	1.0082
2,758	1.0725	1.0610	1.0518	1.0442	1.0380	1.0327	1.0284	1.0247	1.0215	1.0187	1.0163	1.0142	1.0124	1.0108
3,447	1.0954	1.0792	1.0665	1.0564	1.0481	1.0413	1.0357	1.0309	1.0268	1.0233	1.0202	1.0176	1.0153	1.0132
4,137	1.1211	1.0988	1.0821	1.0690	1.0585	1.0499	1.0430	1.0370	1.0320	1.0277	1.0240	1.0208	1.0180	1.0156
4,826	1.1500	1.1202	1.0986	1.0820	1.0691	1.0587	1.0502	1.0432	1.0372	1.0321	1.0277	1.0240	1.0207	1.0178
5,516	1.1826	1.1431	1.1158	1.0955	1.0798	1.0674	1.0575	1.0492	1.0423	1.0364	1.0313	1.0270	1.0232	1.0199
6,205	1.2193	1.1678	1.1337	1.1092	1.0906	1.0761	1.0646	1.0551	1.0472	1.0405	1.0348	1.0299	1.0256	1.0219
6,895	1.2597	1.1939	1.1522	1.1231	1.1014	1.0847	1.0716	1.0609	1.0520	1.0445	1.0381	1.0326	1.0279	1.0237
7,584	1.3021	1.2211	1.1711	1.1370	1.1120	1.0931	1.0784	1.0665	1.0566	1.0483	1.0413	1.0352	1.0301	1.0255
8,274	1.3421	1.2481	1.1898	1.1506	1.1224	1.1013	1.0850	1.0719	1.0610	1.0519	1.0443	1.0377	1.0321	1.0272
8,963	1.3754	1.2735	1.2079	1.1639	1.1325	1.1091	1.0912	1.0770	1.0652	1.0554	1.0471	1.0400	1.0339	1.0287
9,653	1.4007	1.2959	1.2246	1.1764	1.1421	1.1166	1.0971	1.0818	1.0691	1.0586	1.0497	1.0421	1.0356	1.0300
10,340	1.4138	1.3132	1.2393	1.1879	1.1511	1.1235	1.1026	1.0863	1.0728	1.0615	1.0521	1.0440	1.0371	1.0312
11,030	1.4175	1.3248	1.2512	1.1978	1.1589	1.1298	1.1076	1.0904	1.0762	1.0643	1.0543	1.0458	1.0385	1.0323
11,720	1.4145	1.3311	1.2603	1.2062	1.1658	1.1353	1.1121	1.0941	1.0792	1.0667	1.0563	1.0474	1.0398	1.0333
12,410	1.4068	1.3330	1.2663	1.2126	1.1715	1.1400	1.1160	1.0974	1.0819	1.0689	1.0580	1.0487	1.0409	1.0341
13,100	1.3959	1.3312	1.2695	1.2173	1.1760	1.1439	1.1194	1.1002	1.0842	1.0708	1.0595	1.0499	1.0417	1.0347
13,790	1.3827	1.3264	1.2704	1.2202	1.1793	1.1470	1.1221	1.1026	1.0861	1.0724	1.0607	1.0508	1.0424	1.0352

TABLE G.21 Supercompressibility Factors for Natural Gas of 0.6 Specific Gravity:† SI Units (*Continued*)

Gauge press, kPa	Flowing temperature T_c , °C													
	-40	-29	-18	-7	4	16	27	38	49	60	71	82	93	104
14,480	1.3680	1.3186	1.2677	1.2207	1.1812	1.1493	1.1243	1.1044	1.0876	1.0734	1.0614	1.0513	1.0429	1.0355
15,170	1.3527	1.3093	1.2635	1.2199	1.1820	1.1508	1.1258	1.1058	1.0887	1.0741	1.0619	1.0516	1.0431	1.0358
15,860	1.3365	1.2988	1.2579	1.2175	1.1816	1.1513	1.1266	1.1066	1.0893	1.0745	1.0621	1.0517	1.0432	1.0359
16,550	1.3205	1.2879	1.2511	1.2139	1.1800	1.1508	1.1266	1.1067	1.0894	1.0745	1.0619	1.0515	1.0431	1.0357
17,240	1.3059	1.2763	1.2436	1.2095	1.1777	1.1496	1.1261	1.1065	1.0892	1.0741	1.0615	1.0511	1.0427	1.0355
17,930	1.2906	1.2646	1.2352	1.2040	1.1742	1.1475	1.1248	1.1056	1.0885	1.0736	1.0610	1.0506	1.0422	1.0350
18,620	1.2756	1.2527	1.2265	1.1980	1.1703	1.1450	1.1230	1.1043	1.0875	1.0728	1.0603	1.0499	1.0415	1.0343
19,300	1.2608	1.2408	1.2174	1.1915	1.1657	1.1418	1.1208	1.1026	1.0862	1.0717	1.0593	1.0489	1.0407	1.0335
19,990	1.2464	1.2289	1.2081	1.1845	1.1606	1.1381	1.1180	1.1005	1.0845	1.0703	1.0580	1.0478	1.0396	1.0324
20,680	1.2324	1.2172	1.1987	1.1773	1.1552	1.1341	1.1150	1.0981	1.0825	1.0687	1.0566	1.0464	1.0383	1.0313

NOTE: For expanded tables of supercompressibility factors for natural gas, see A.G.A. Report No. 3 or A.G.A. Supercompressibility Tables (NX-19).

†For specific gravities other than 0.6, adjust pressure and temperature before entering table:

$$(p^\circ)_{\text{table}} = \frac{156.47p^\circ}{160.8 - 7.22G + 100x_{\text{CO}_2} - 39.2x_{\text{N}_2}} \quad (T^\circ\text{C})_{\text{table}} = \frac{226.29}{99.15 + 211.9G - 100x_{\text{CO}_2} - 168.1x_{\text{N}_2}} (T^\circ\text{C} + 273) - 273$$

SOURCE: Dieterich Standard Corp.

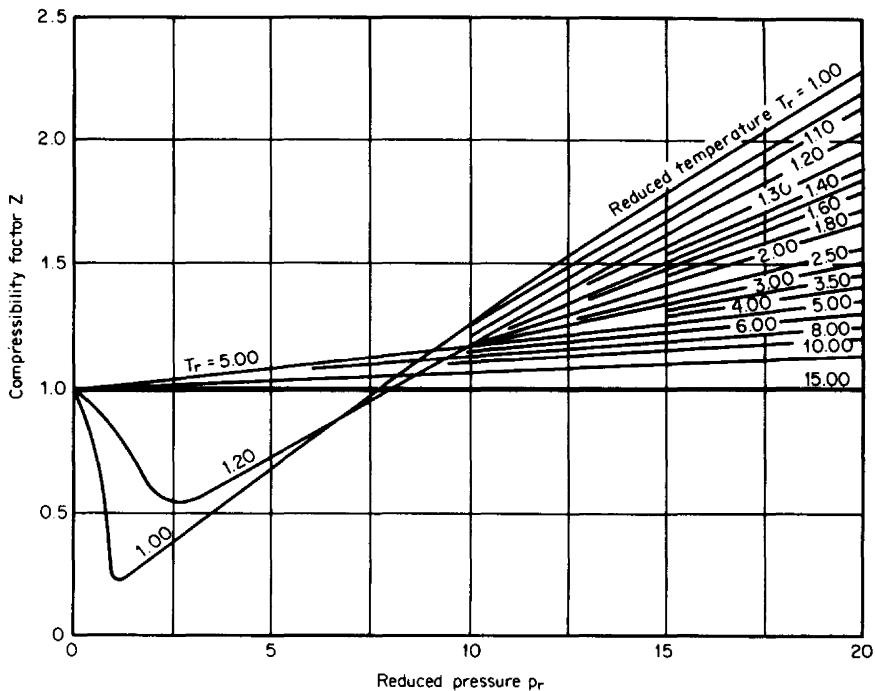


Figure G.1 Nelson-Obert compressibility chart ($p_r = 0$ to 20). (From Spink, 1967.)

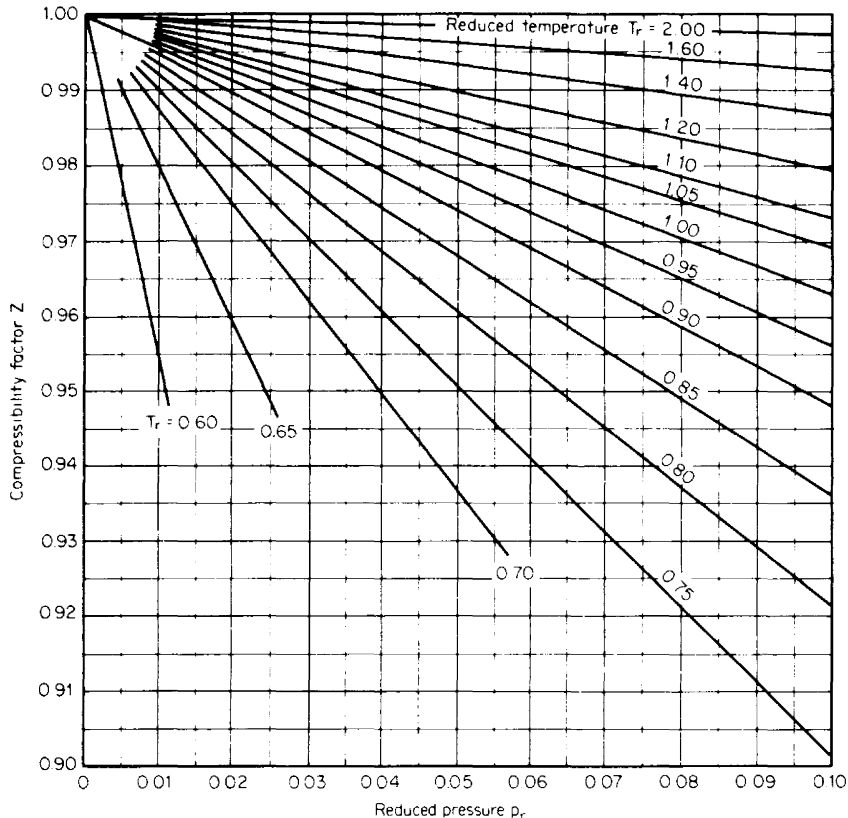


Figure G.2 Nelson-Obert compressibility diagram ($p_r = 0$ to 0.10). (From Spink, 1967.)

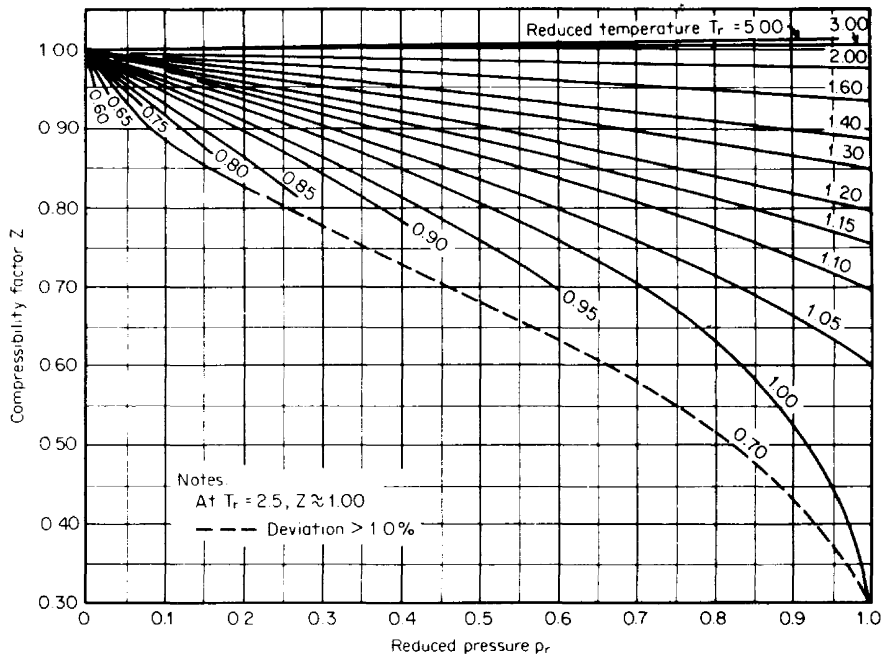


Figure G.3 Nelson-Obert compressibility chart ($p_r = 0$ to 1.0). (From Spink, 1967.)

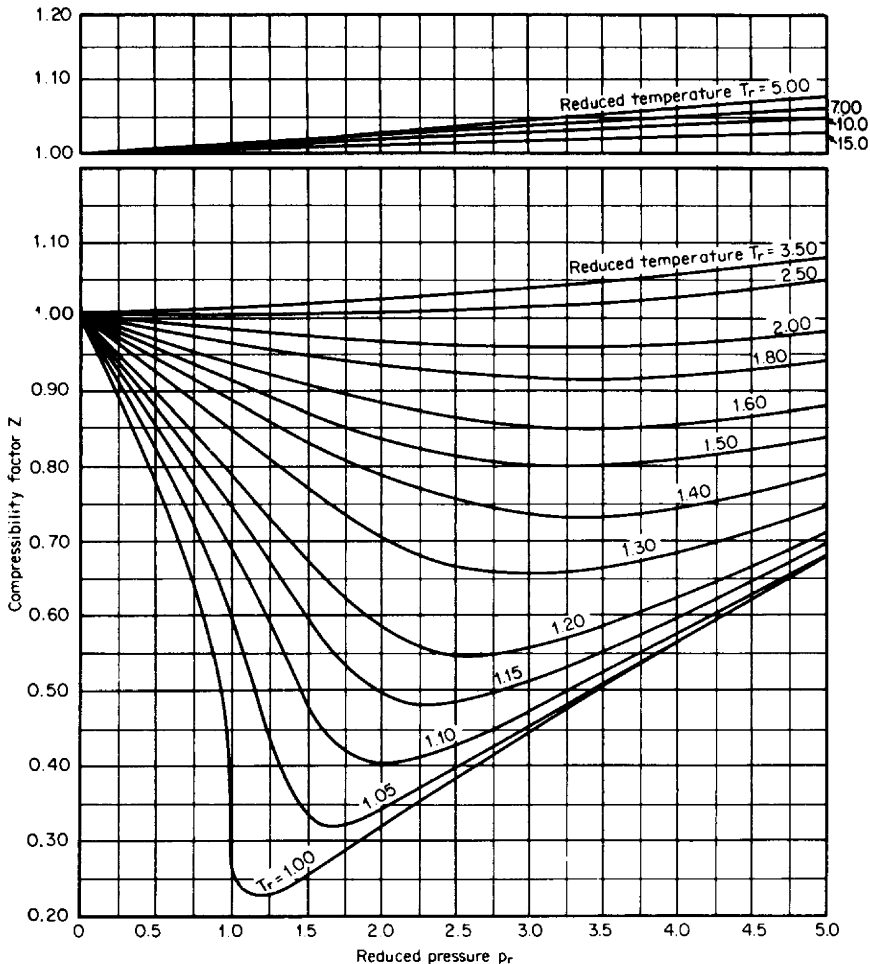


Figure G.4 Nelson-Obert compressibility chart ($p_r = 0$ to 5.00). *Note:* Do not use for ammonia. Do not use for methyl fluoride below $T_r = 1.3$ or for hydrogen or helium below $T_r = 2.5$. For hydrogen or helium above $T_r = 2.5$, use adjusted constants: $T_c + 14.4^\circ\text{F}$ and $p_c + 117.6 \text{ lb}_f/\text{in}^2$. Maximum deviation, when used as above, is less than $2\frac{1}{2}$ percent except near $T_r = 1.0$ and $p_r = 1.0$. (From Spink, 1967.)

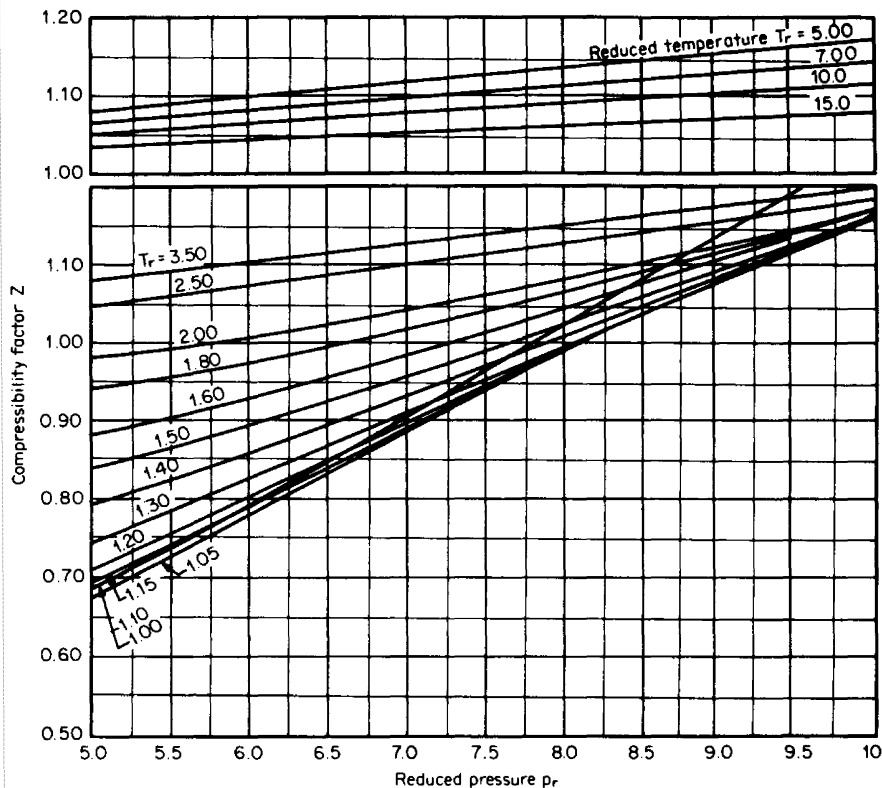


Figure G.5 Nelson-Obert compressibility chart ($p_r = 5$ to 10). *Note:* Do not use for ammonia. Do not use for methyl fluoride below $T_r = 1.3$ or for hydrogen or helium below $T_r = 2.5$. For hydrogen or helium above $T_r = 2.5$, use adjusted constants: $T_c + 14.4^\circ\text{F}$ and $p_c + 117.6 \text{ lb}_f/\text{in}^2$. Maximum deviation, when used as above, is less than $2\frac{1}{2}$ percent except near $T_r = 1.0$ and $p_r = 1.0$. (From Spink, 1967.)

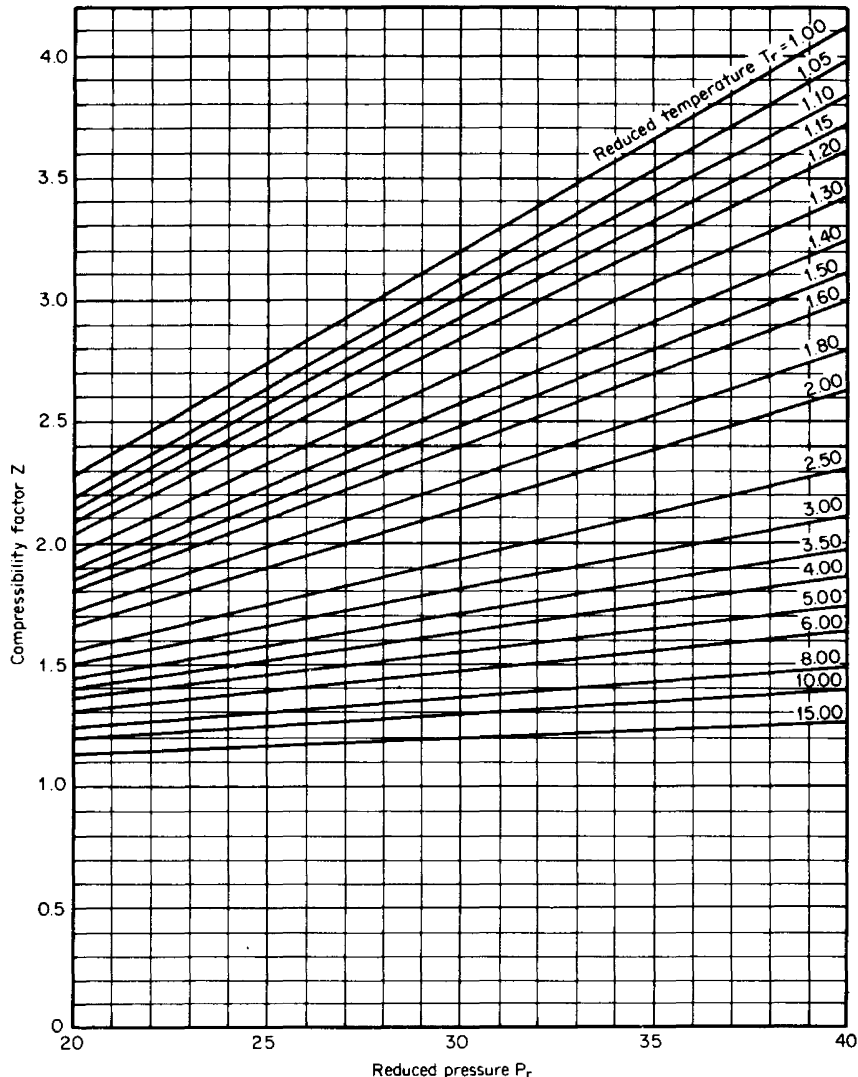


Figure G.6 Nelson-Obert compressibility chart ($p_r = 20$ to 40). *Note:* Maximum deviation for oxygen, argon, air, nitrogen, carbon monoxide, ethane, methane, ethylene, or propane is less than 5 percent. Also, for hydrogen or helium, if adjusted critical constants are used, then $T_c + 14.4^\circ\text{F}$ and $p_c + 117.6 \text{ lb}_f/\text{in}^2$. (From Spink, 1967.)

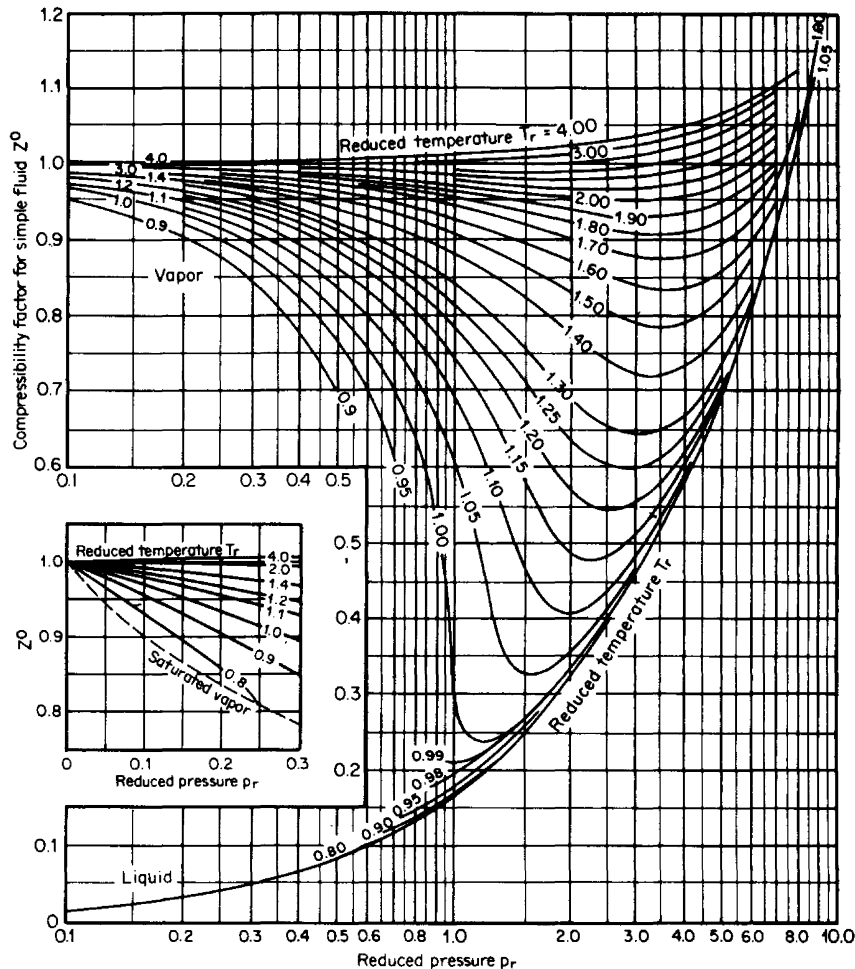


Figure G.7 Generalized compressibility factor for the simple fluids argon, krypton, and xenon. (From Edmister, 1974; used with permission.)

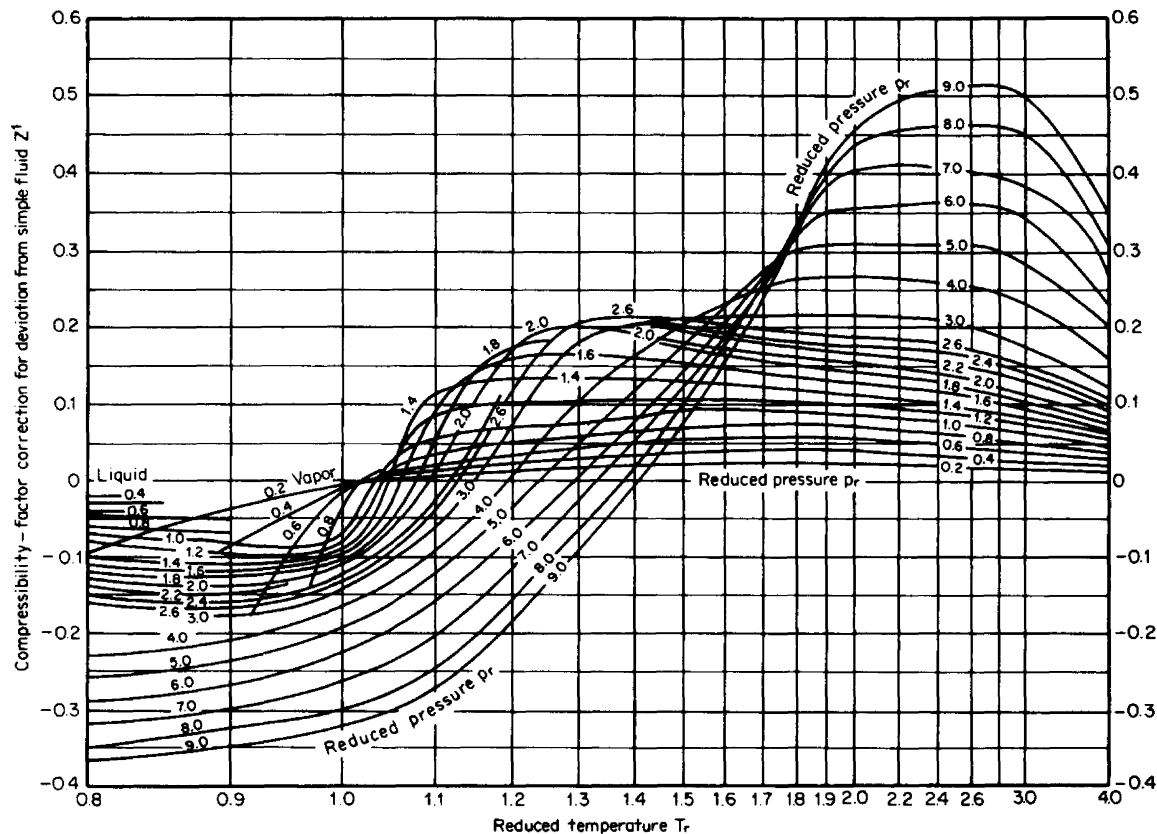


Figure G.8 Generalized compressibility-factor correction for deviation from simple fluid. (From Edmister, 1974; used with permission.)

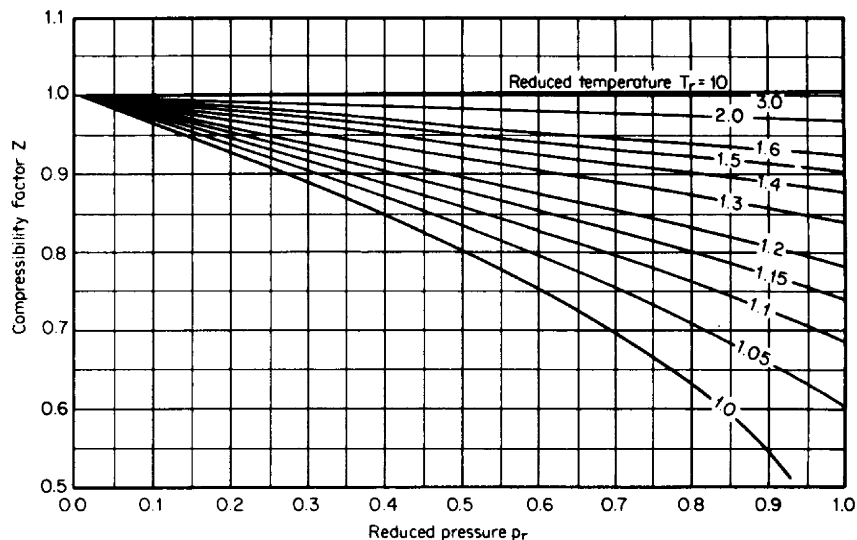


Figure G.9 Redlich-Kwong compressibility factor, based on equation of state ($p_r = 0$ to 1.0).

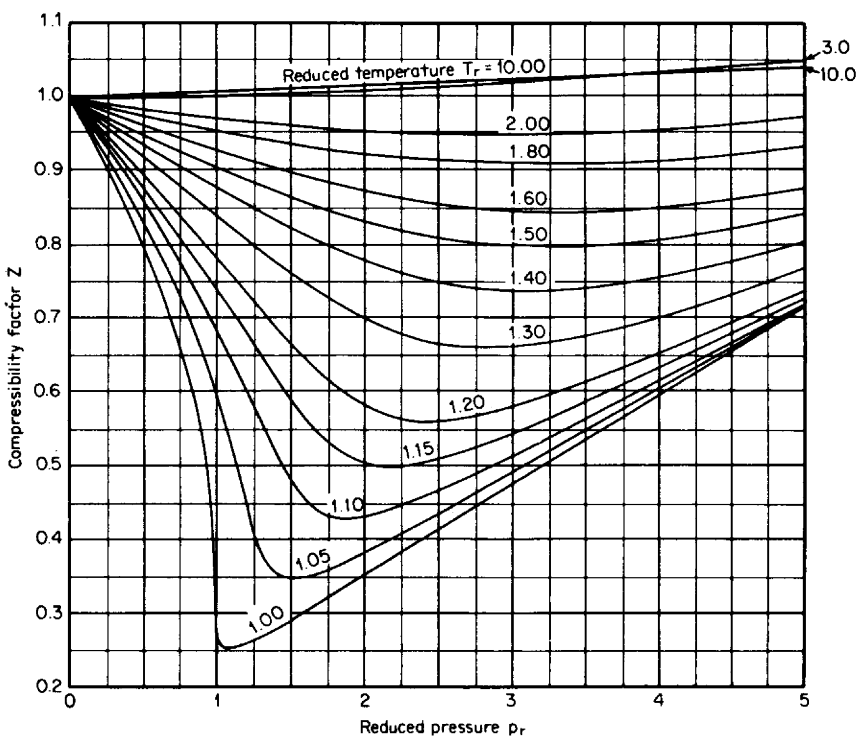


Figure G.10 Redlich-Kwong compressibility factor, based on equation of state ($p_r = 0$ to 5).

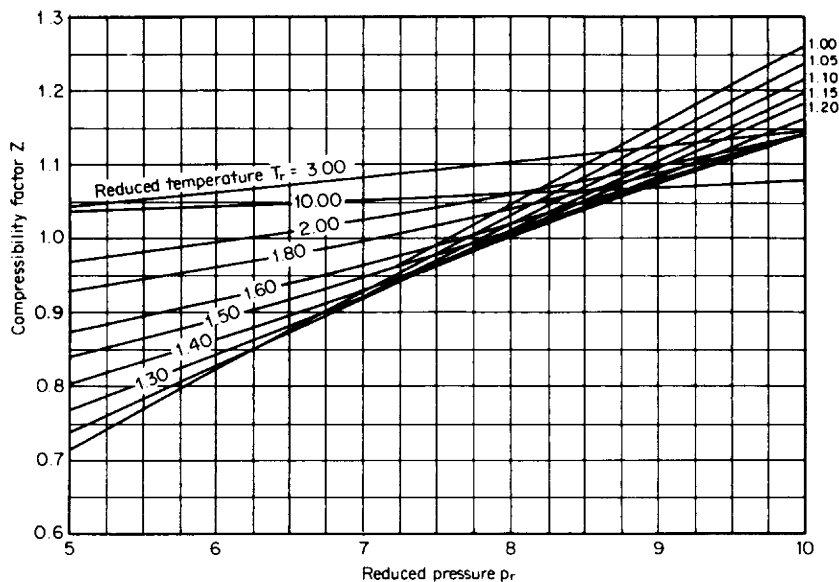


Figure G.11 Redlich-Kwong compressibility factor, based on equation of state ($p_r = 5$ to 10).

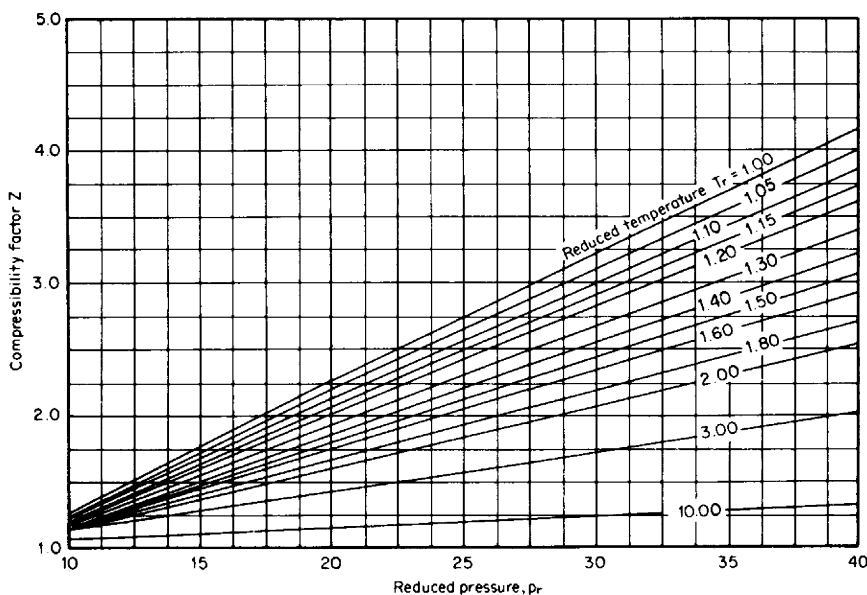


Figure G.12 Redlich-Kwong compressibility factor, based on equation of state ($p_r = 10$ to 40).

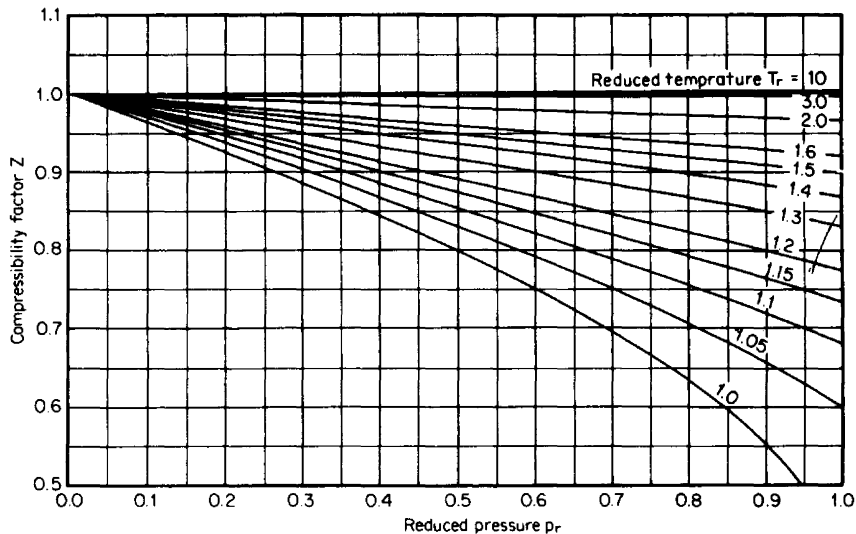


Figure G.13 Hall-Yarborough compressibility diagrams ($p_r = 0$ to 1.0).

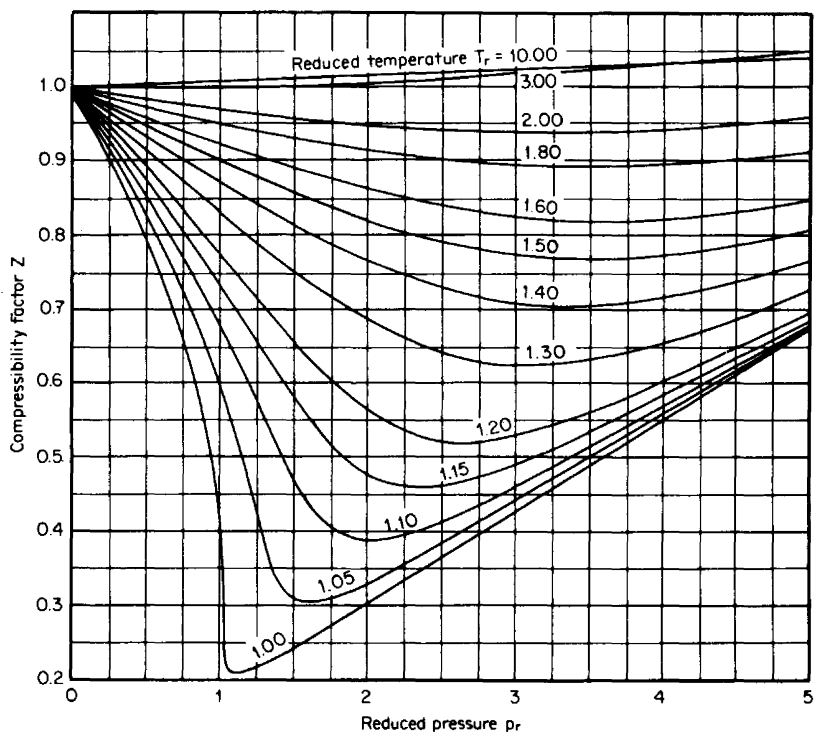


Figure G.14 Hall-Yarborough compressibility diagrams ($p_r = 0$ to 5).

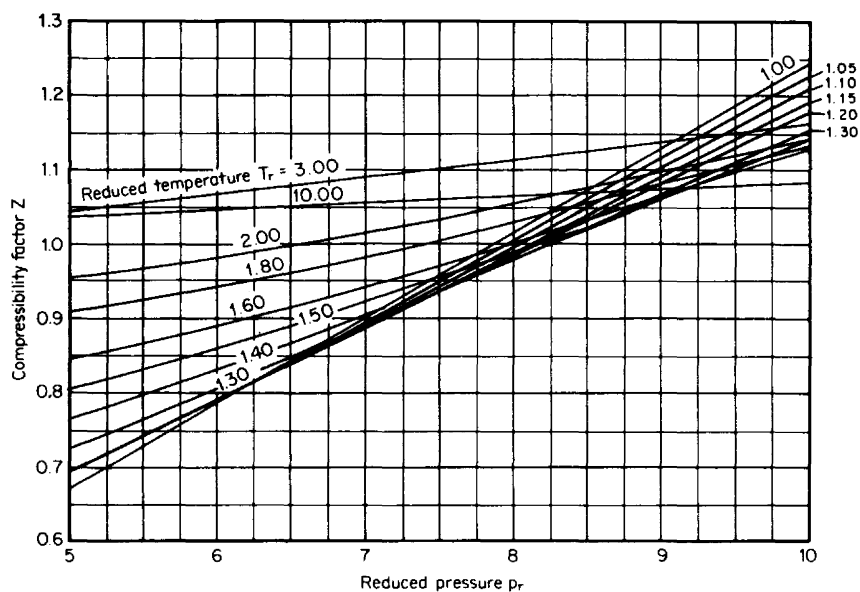


Figure G.15 Hall-Yarborough compressibility diagrams ($p_r = 5$ to 10).

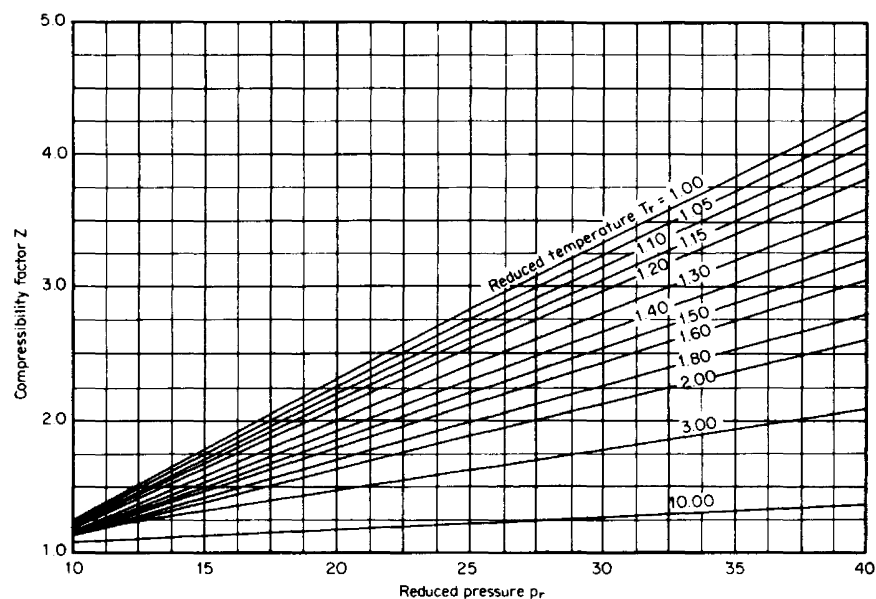
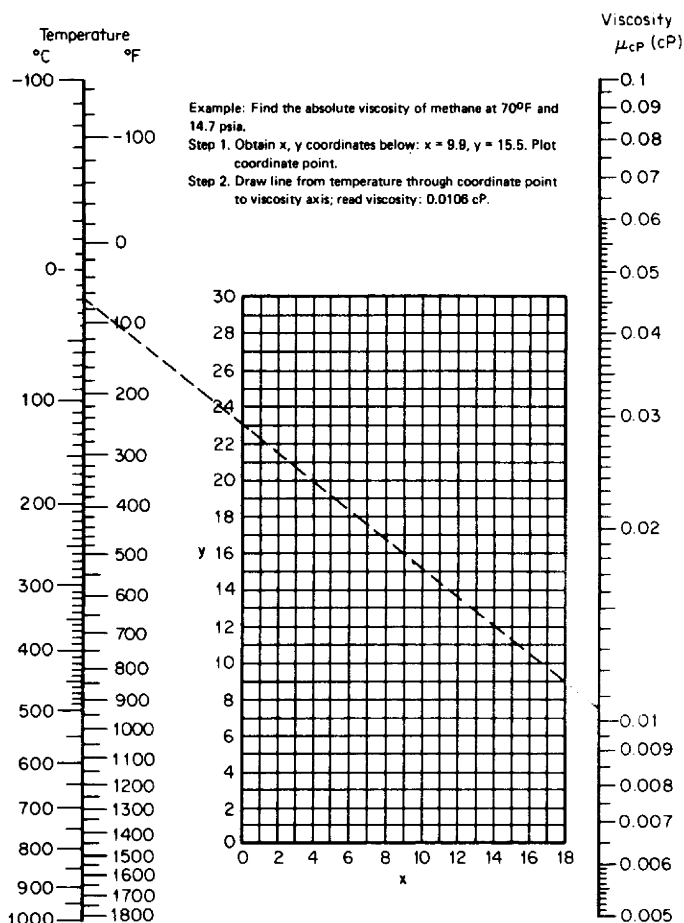


Figure G.16 Hall-Yarborough compressibility diagrams ($p_r = 10$ to 40).



Gas	X	Y	Gas	X	Y
Acetic acid	7.7	14.3	Freon-113	11.3	14.0
Acetone	8.9	13.0	Helium	10.9	20.5
Acetylene	9.8	14.9	Hexane	8.6	11.8
Air	11.0	20.0	Hydrogen	11.2	12.4
Ammonia	8.4	16.0	3H ₂ + 1N ₂	11.2	17.2
Argon	10.5	22.4	Hydrogen bromide	8.8	20.9
Benzene	8.5	13.2	Hydrogen chloride	8.8	18.7
Bromine	8.9	19.2	Hydrogen cyanide	9.8	14.9
Butene	9.2	13.7	Hydrogen iodide	9.0	21.3
Butylene	8.9	13.0	Hydrogen sulfide	8.6	18.0
Carbon dioxide	9.5	18.7	Iodine	9.0	18.4
Carbon disulfide	8.0	16.0	Mercury	5.3	22.9
Carbon monoxide	11.0	20.0	Methane	9.9	15.5
Chlorine	9.0	18.4	Methyl alcohol	8.5	15.6
Chloroform	8.9	15.7	Nitric oxide	10.9	20.5
Cyanogen	9.2	15.2	Nitrogen	10.6	20.0
Cyclohexane	9.2	12.0	Nitrosyl chloride	8.0	17.6
Ethane	9.1	14.5	Nitrous oxide	8.8	19.0
Ethyl acetate	8.5	13.2	Oxygen	11.0	21.3
Ethyl alcohol	9.2	14.2	Pentane	7.0	12.8
Ethyl chloride	8.5	15.6	Propane	9.7	12.9
Ethyl ether	8.9	13.0	Propyl alcohol	8.4	13.4
Ethylene	9.5	15.1	Propylene	9.0	13.8
Fluorine	7.3	23.8	Sulfur dioxide	9.6	17.0
Freon-11	10.6	15.1	Toluene	8.6	12.4
Freon-12	11.1	16.0	2,3,3-Trimethylbutane	9.5	10.5
Freon-21	10.8	15.3	Water	8.0	16.0
Freon-22	10.1	17.0	Xenon	9.3	23.0

Figure H.1 Gas (vapor) absolute-viscosity alignment chart at atmospheric pressure. (From Perry and Green, 1984.)

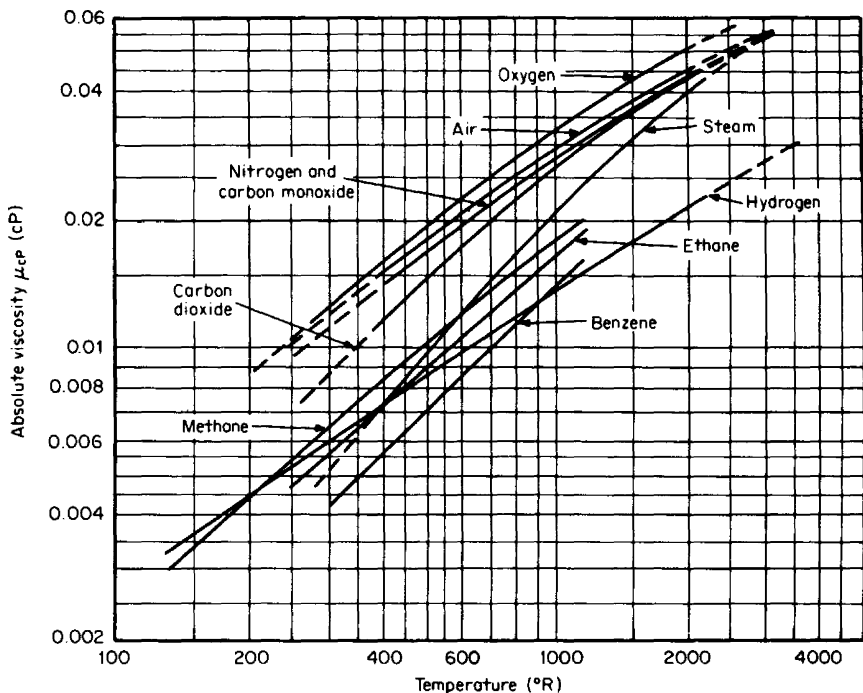


Figure H.2 Viscosities of gases at atmospheric pressure. (From Baumeister, 1978.)

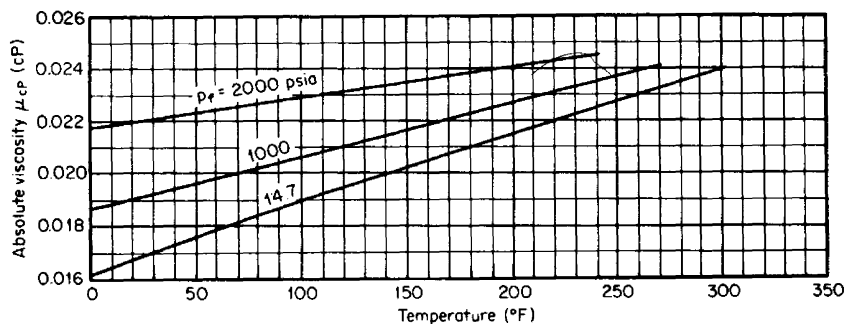


Figure H.3 Absolute viscosity of air. (From Fischer & Porter Catalog 10-A-54; used with permission.)

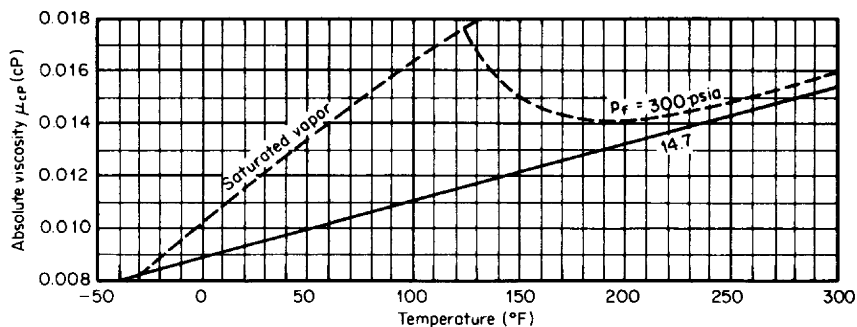


Figure H.4 Absolute viscosity of ammonia. (From Fischer & Porter Catalog 10-A-54; used with permission.)

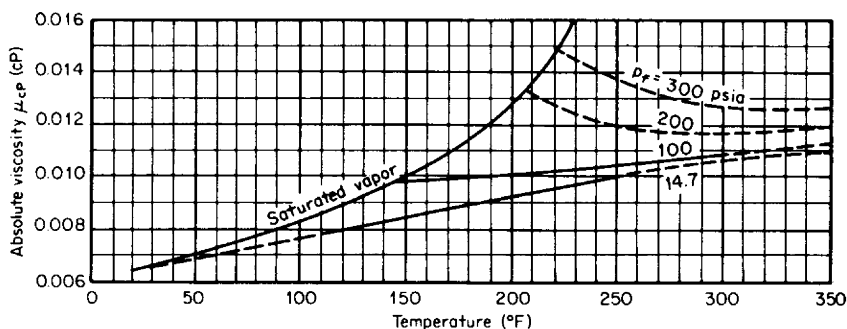


Figure H.5 Absolute viscosity of butane. (From Fischer & Porter Catalog 10-A-54; used with permission.)

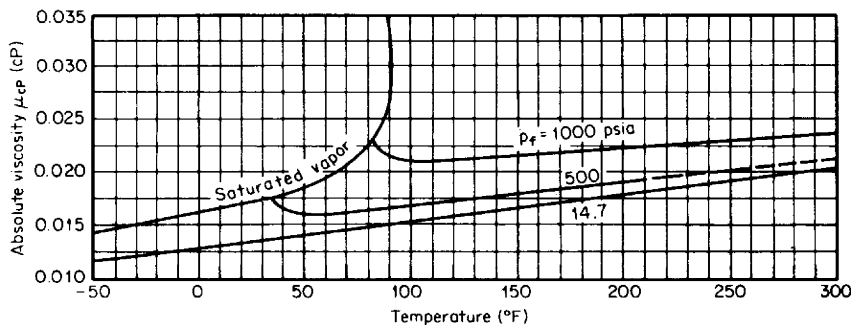


Figure H.6 Absolute viscosity of carbon dioxide. (From Fischer & Porter Catalog 10-A-54; used with permission.)

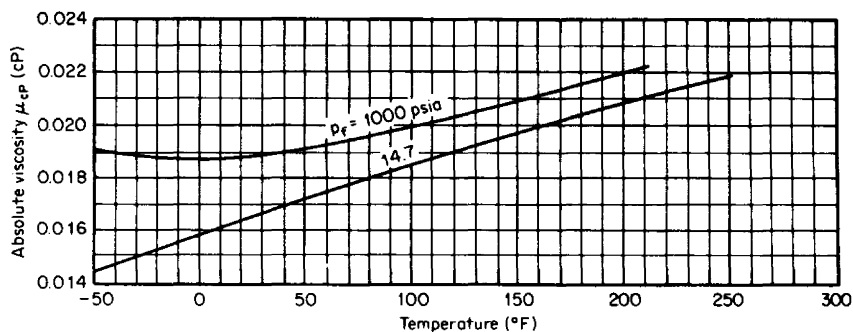


Figure H.7 Absolute viscosity of carbon monoxide. (From Fischer & Porter Catalog 10-A-54; used with permission.)

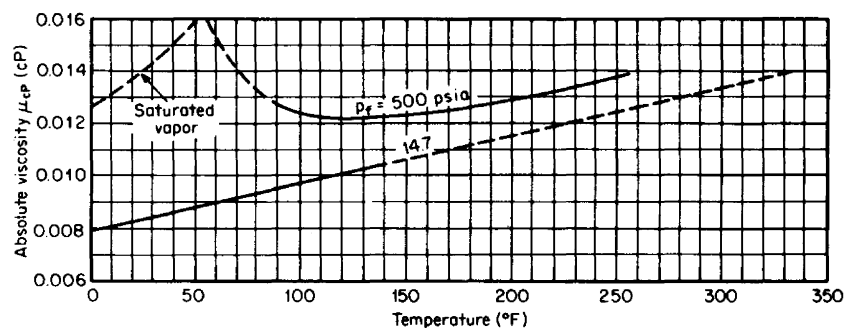


Figure H.8 Absolute viscosity of ethane. (From Fischer & Porter Catalog 10-A-54; used with permission.)

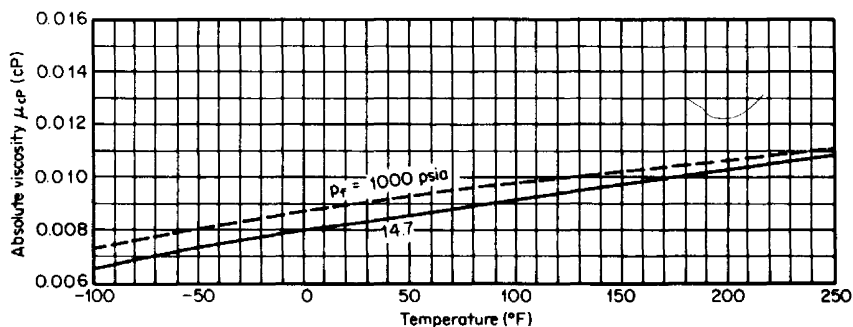


Figure H.9 Absolute viscosity of hydrogen. (From Fischer & Porter Catalog 10-A-54; used with permission.)

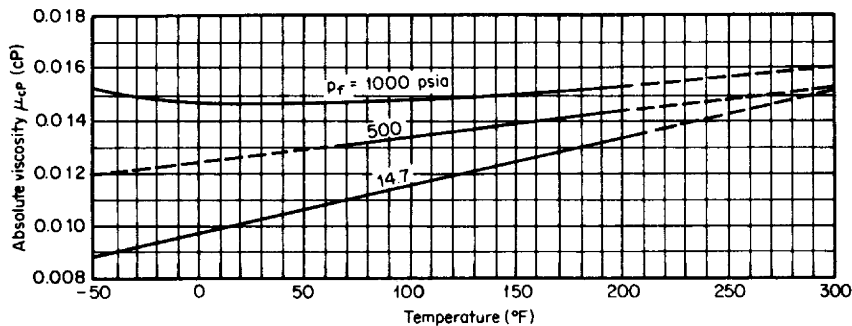


Figure H.10 Absolute viscosity of methane. (From Fischer & Porter Catalog 10-A-54; used with permission.)

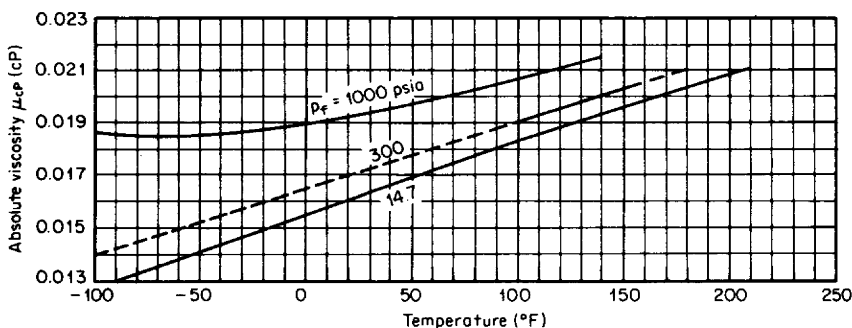


Figure H.11 Absolute viscosity of nitrogen. (From Fischer & Porter Catalog 10-A-54; used with permission.)

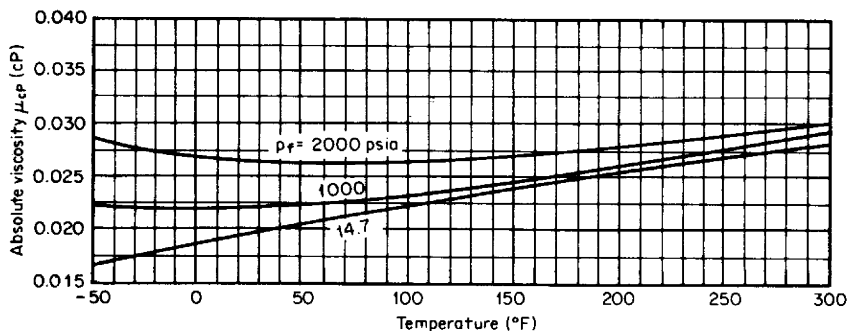


Figure H.12 Absolute viscosity of oxygen. (From Fischer & Porter Catalog 10-A-54; used with permission.)

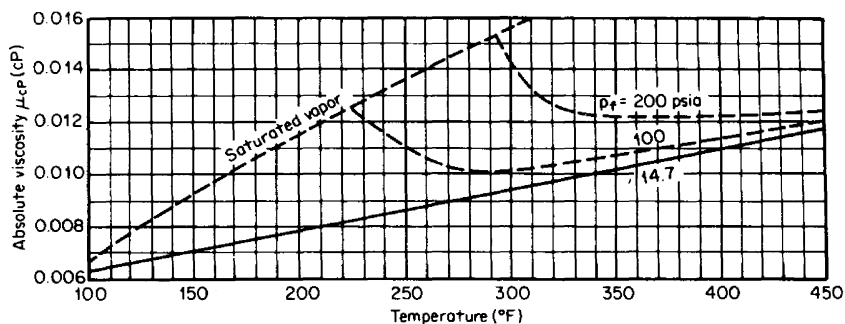


Figure H.13 Absolute viscosity of pentane. (From Fischer & Porter Catalog 10-A-54; used with permission.)

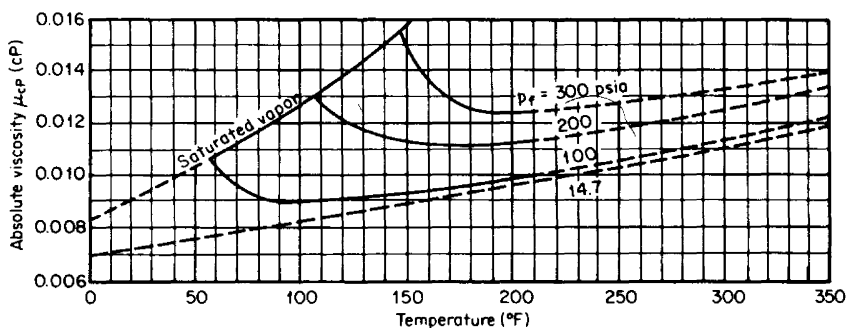


Figure H.14 Absolute viscosity of propane. (From Fischer & Porter Catalog 10-A-54; used with permission.)

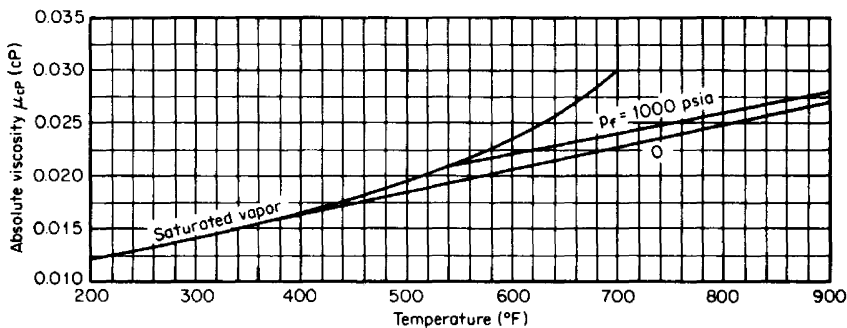


Figure H.15 Absolute viscosity of steam. (From Fischer & Porter Catalog 10-A-54; used with permission.)

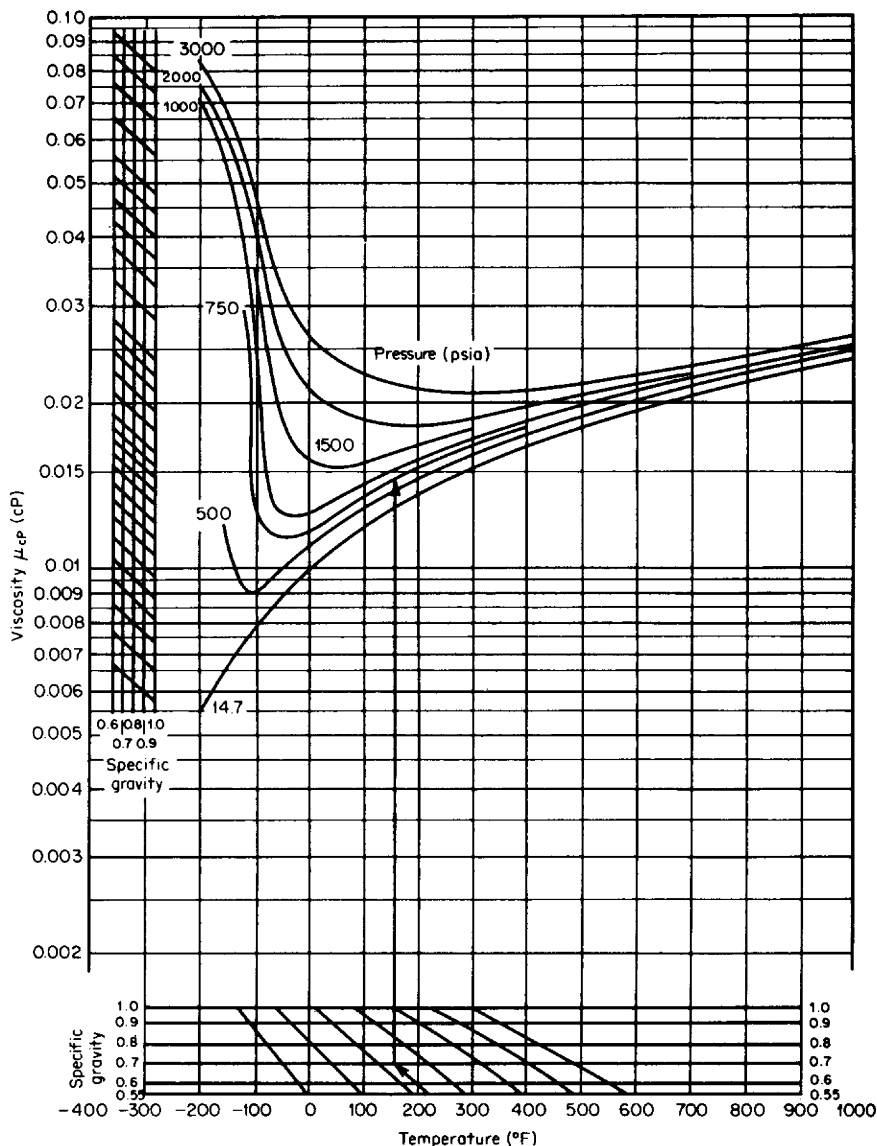


Figure H.16 Absolute viscosity of hydrocarbon gases. (From Gas Processors Supplier Association, 1978.)

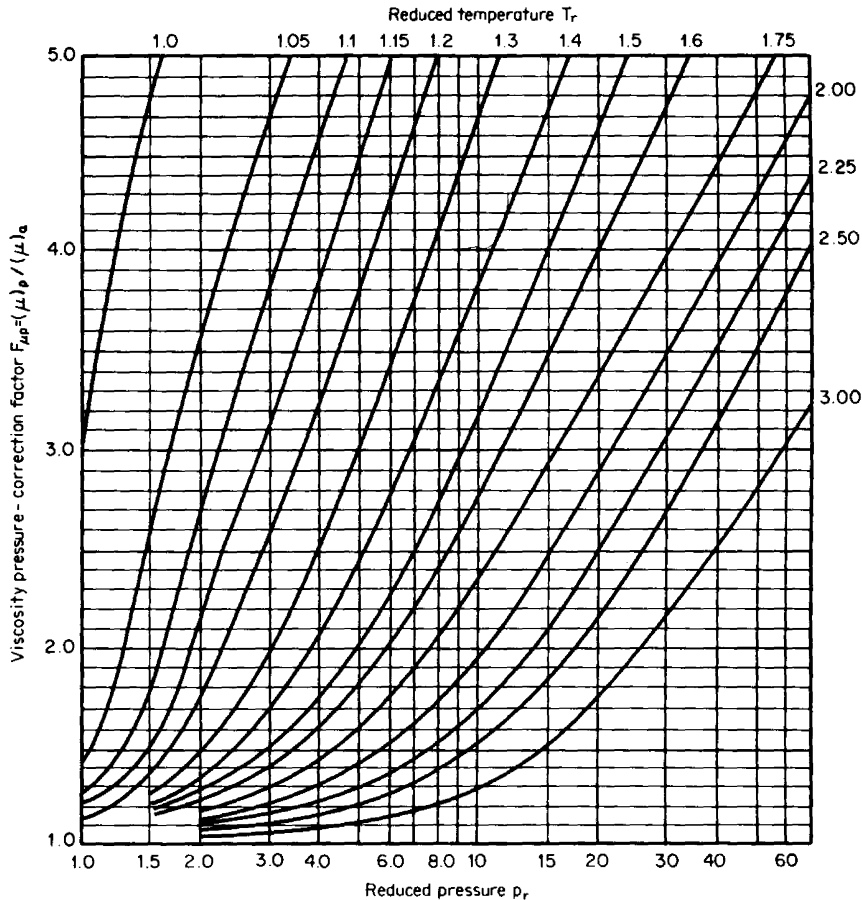


Figure H.17 Viscosity pressure correction factor: $(\mu)_a$ = absolute viscosity at atmospheric pressure; $(\mu)_p$ = absolute viscosity at operating pressure. (From Gambill, 1958.)

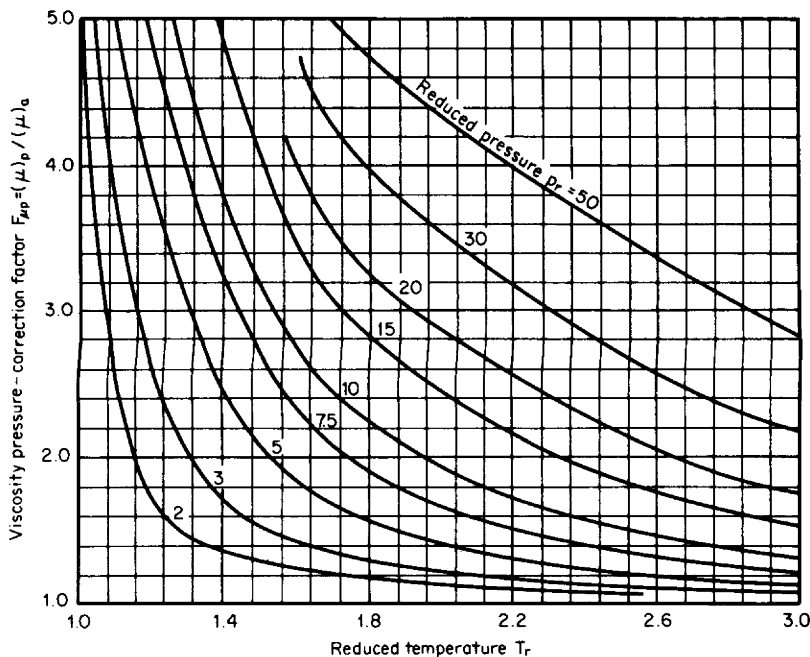


Figure H.18 Viscosity-pressure correction factor (cross-plot of Fig. H.17). (From Gambill, 1958.)

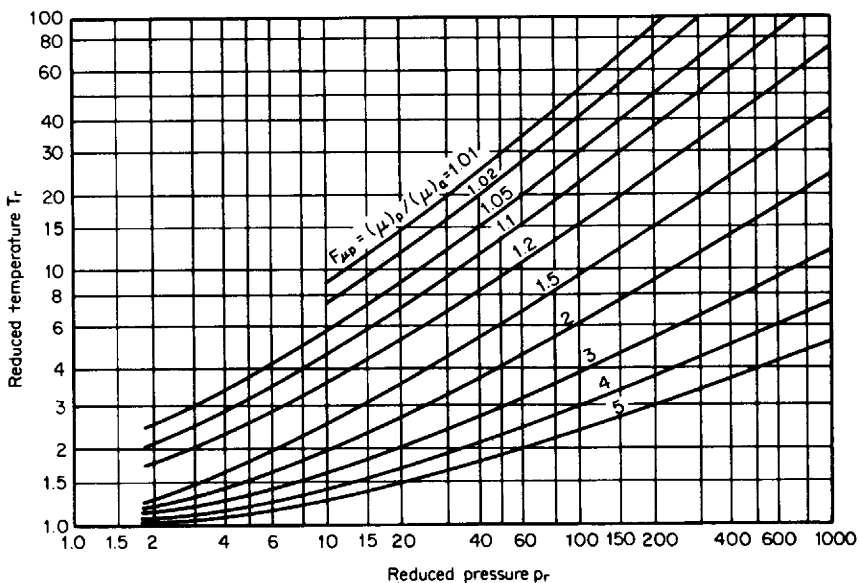


Figure H.19 Viscosity-pressure correction factor—extended pressure range. (From Gambill, 1958.)

ISENTROPIC EXPONENTS

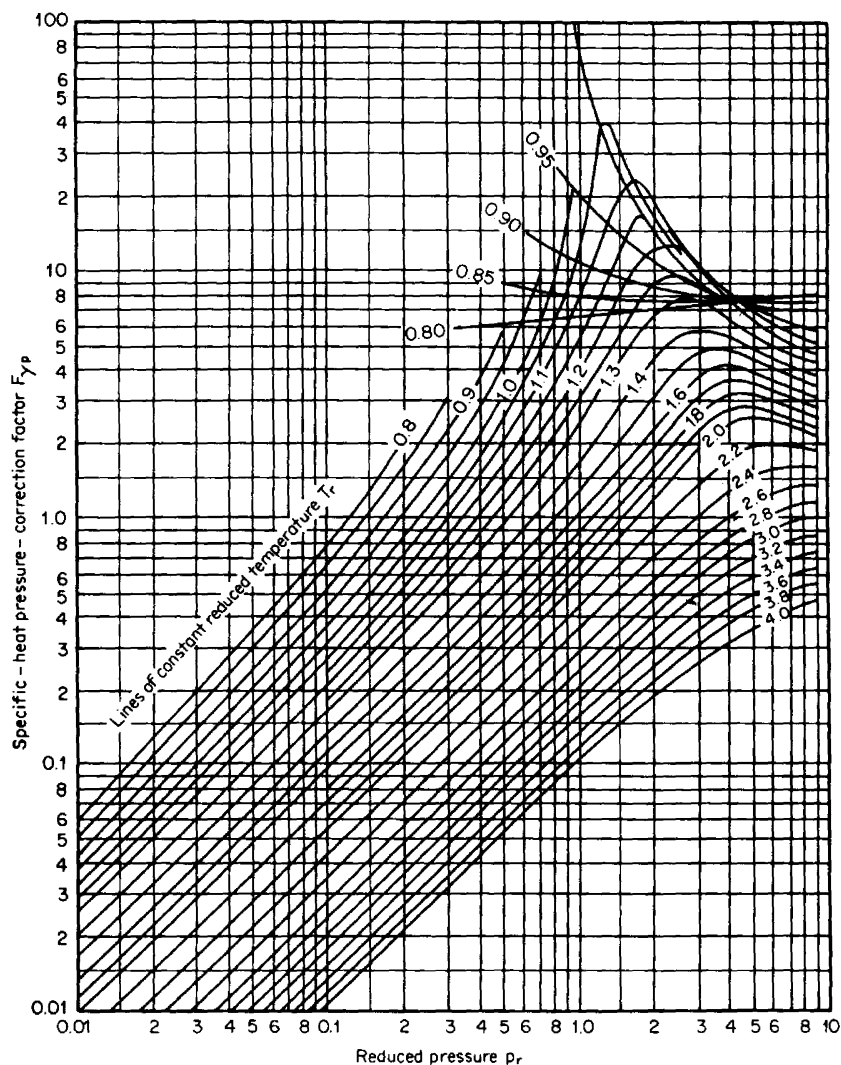
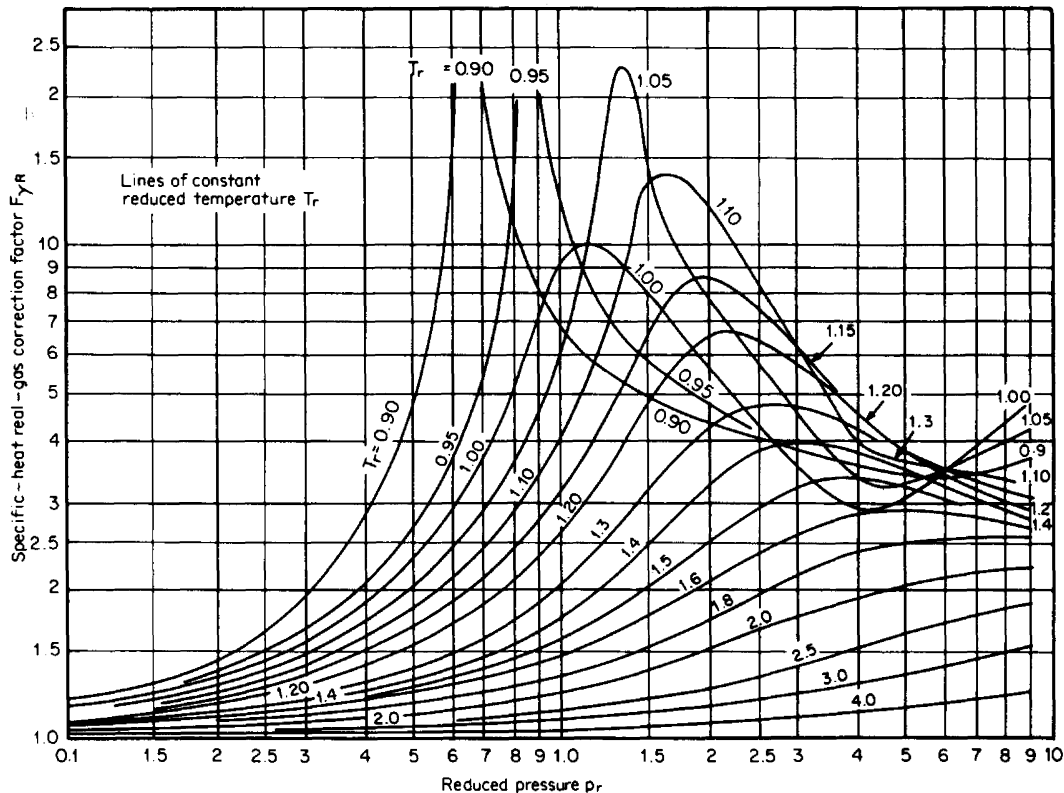


Figure 1.1 Specific-heat pressure-correction factor F_{yp} for simple fluid, $\omega = 0$. (From Edmister, 1974; all rights reserved, used with permission.)

Figure 1.2 Specific-heat real-gas correction factor, F_{yr} ; $\omega = 0$. (From Edmister, 1974; all rights reserved; used with



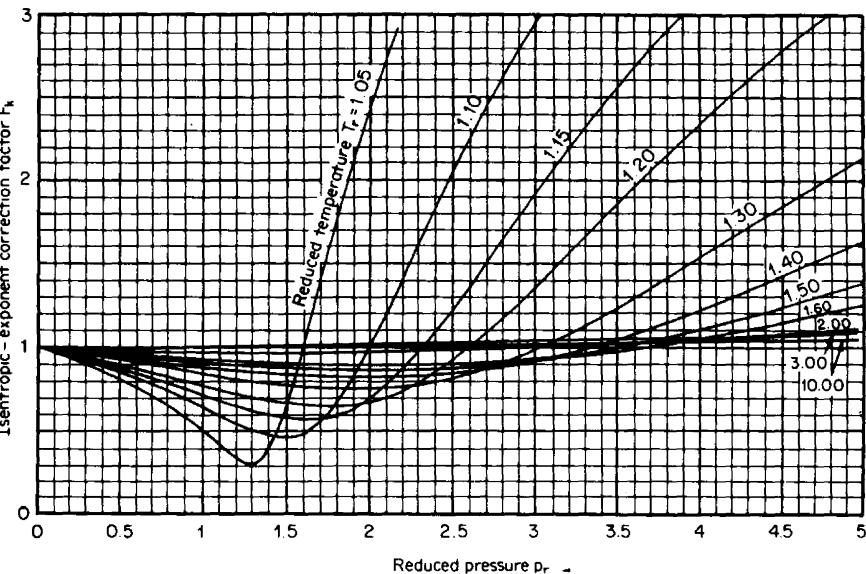


Figure I.3 Isentropic-exponent correction factor F_k .

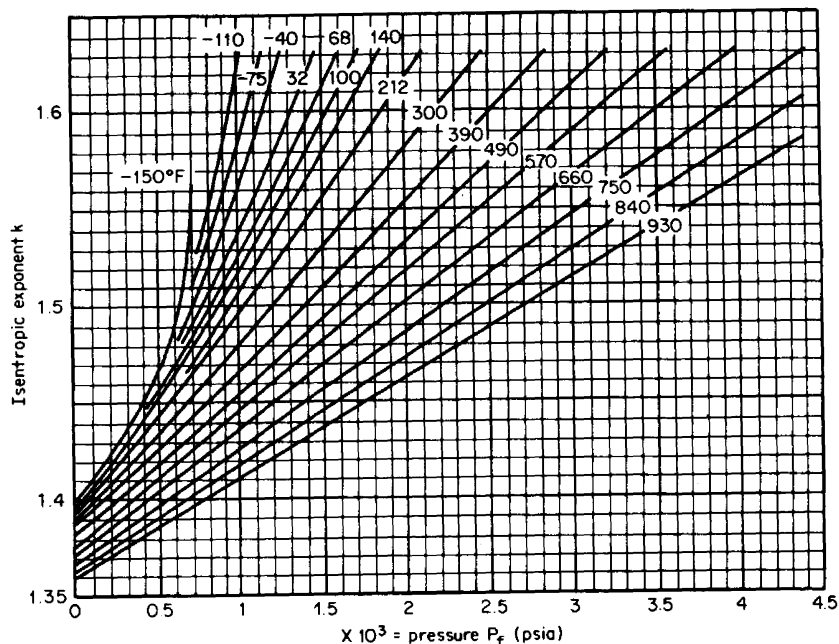


Figure I.4 Isentropic exponent k for air. (Source: VDI, 1970.)

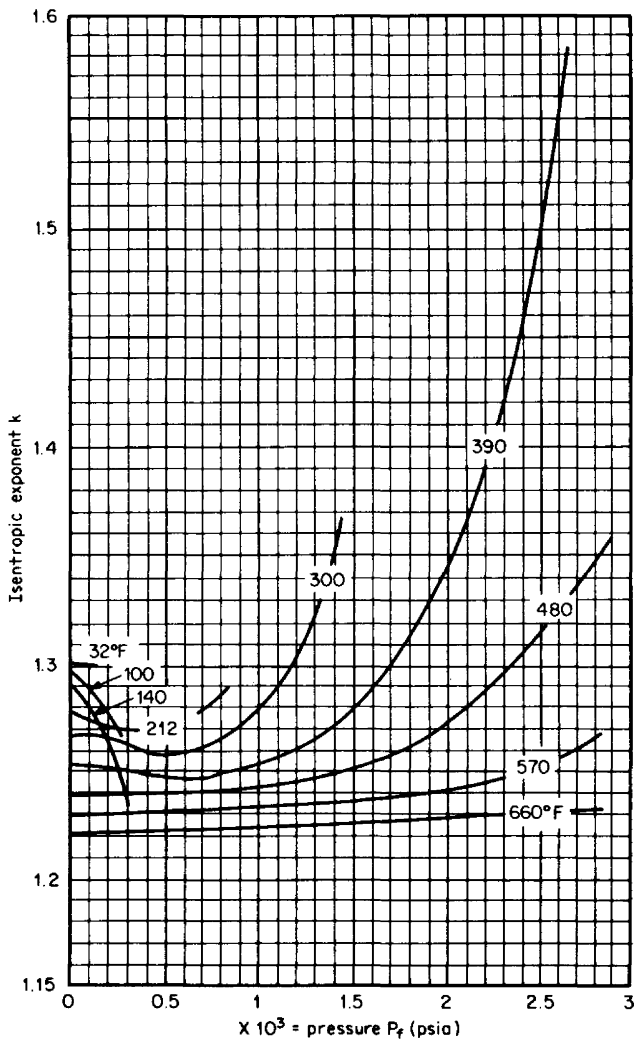


Figure I.5 Isentropic exponent k for ammonia. (Source: VDI, 1970.)

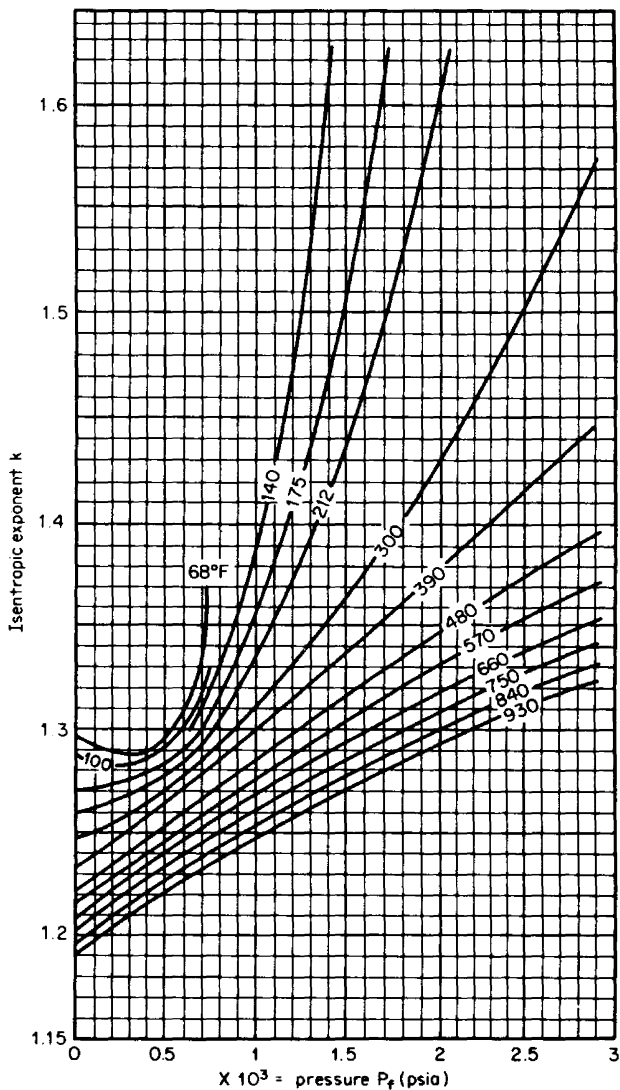


Figure I.6 Isentropic exponent k for carbon dioxide. (Source: VDI, 1970.)

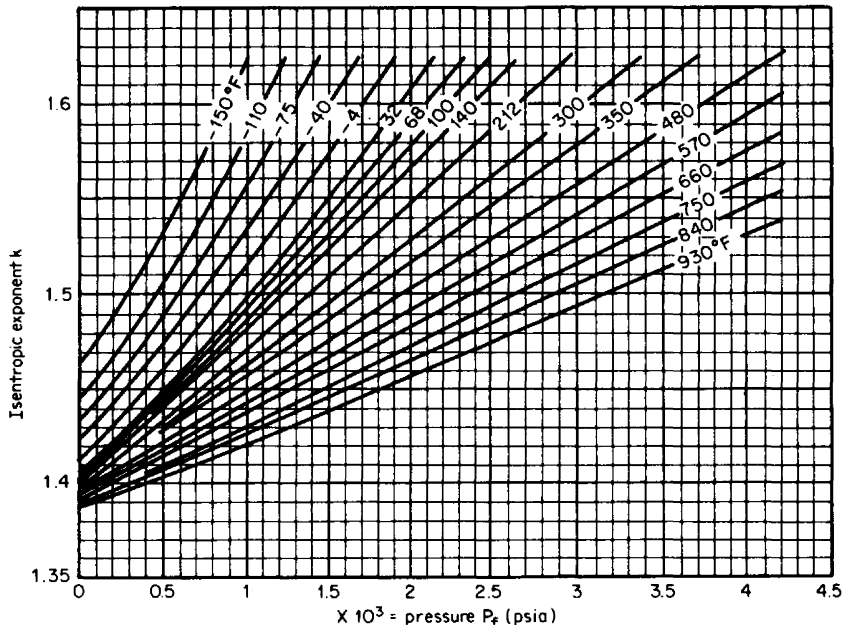


Figure I.7 Isentropic exponent k for hydrogen. (Source: VDI, 1970.)

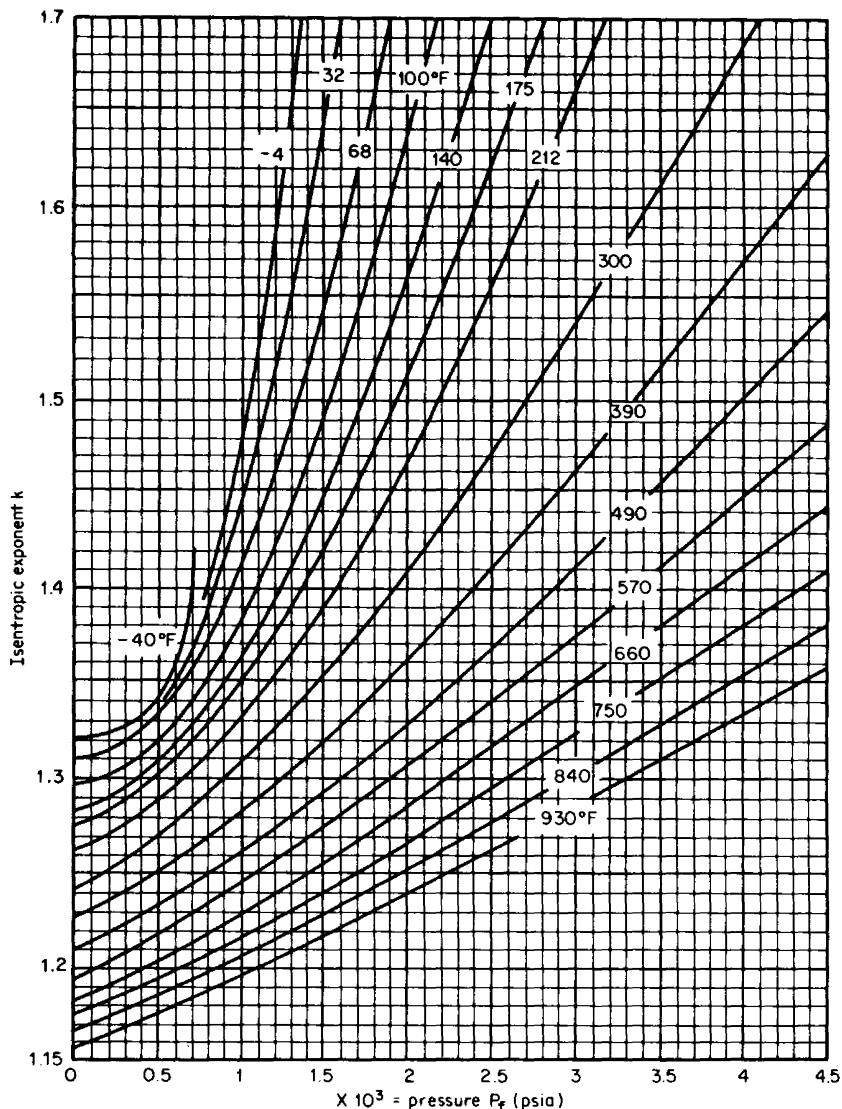


Figure I.8 Isentropic exponent k for methane. (Source: VDI, 1970.)

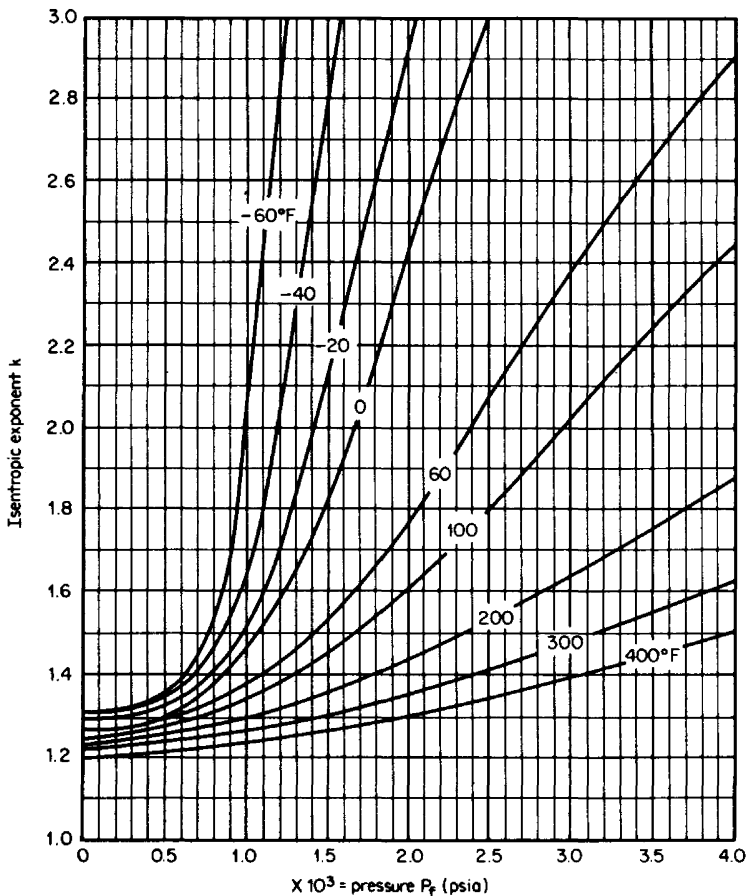


Figure I.9 Isentropic exponent for natural gas: specific gravity $G = 0.6$, $P_{pc} = 672$ psia, $T_{pc} = 360^\circ\text{R}$. (From Schoenthaler, 1966; used with permission.)

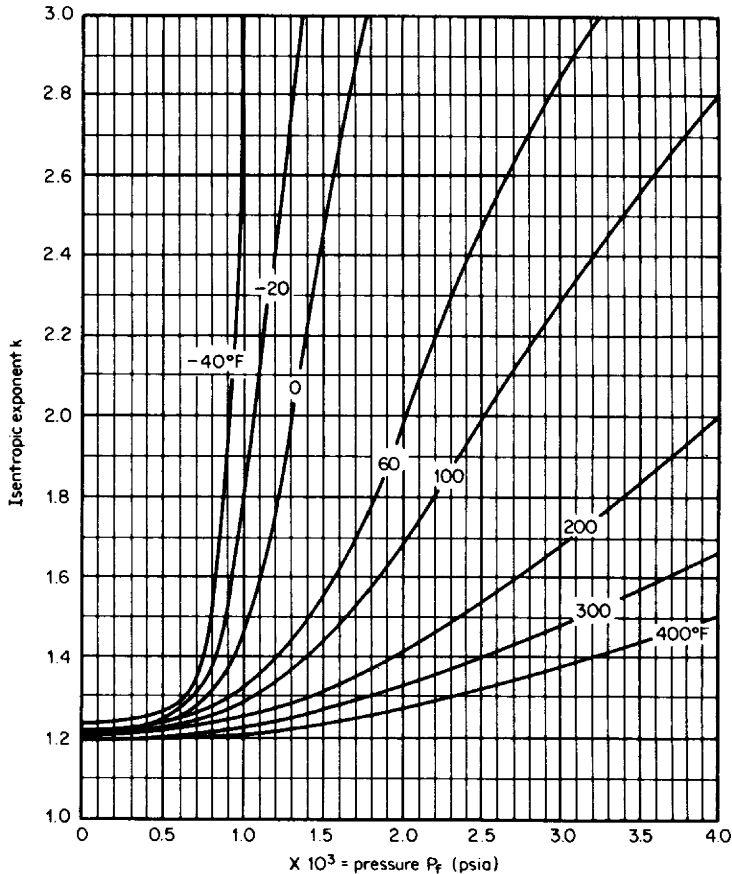


Figure I.10 Isentropic exponent for natural gas: specific gravity $G = 0.7$, $P_{pc} = 667$ psia, $T_{pc} = 382^\circ\text{R}$. (From Schoenthaler, 1966; used with permission.)

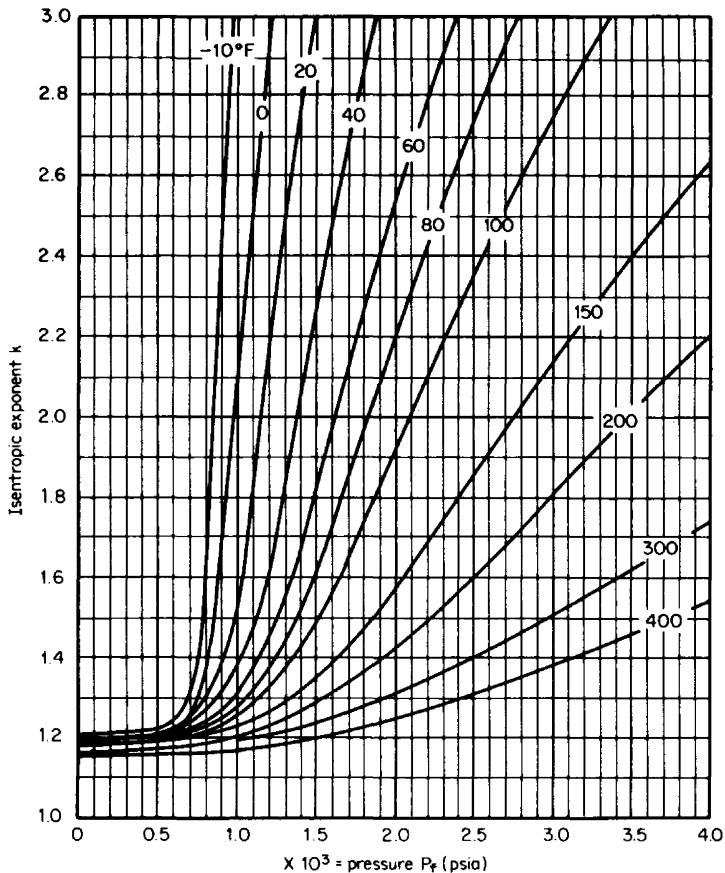


Figure I.11 Isentropic exponent for natural gas: specific gravity $G = 0.8$, $P_{pc} = 662$ psia, $T_{pc} = 424^\circ\text{R}$. (From Schoenthaler, 1966; used with permission.)

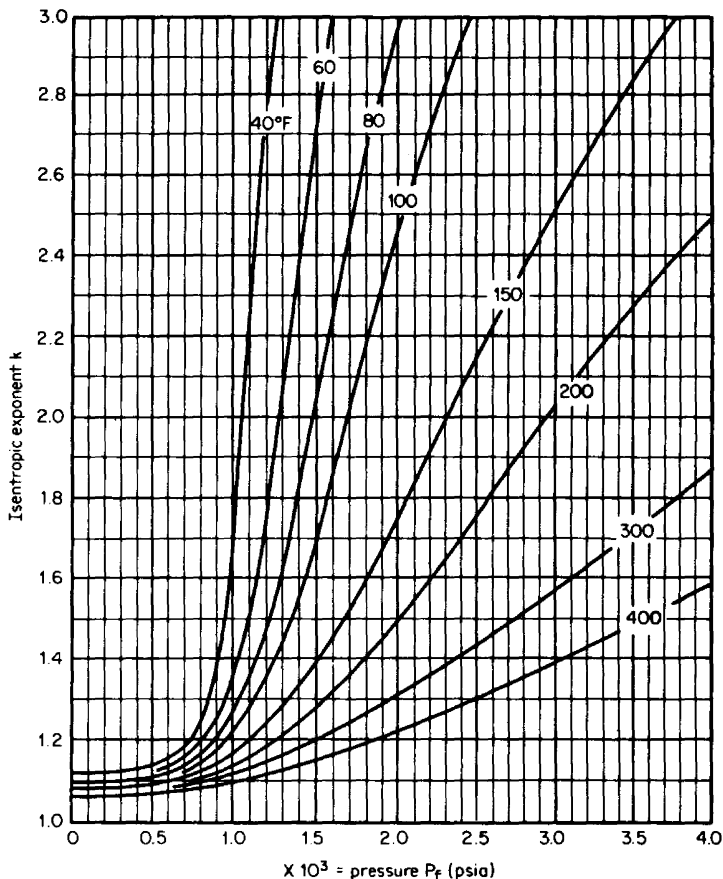


Figure I.12 Isentropic exponent for natural gas: specific gravity $G = 0.9$, $P_{pc} = 657$ psia, $T_{pc} = 456^\circ\text{R}$. (From Schoenthaler, 1966; used with permission.)

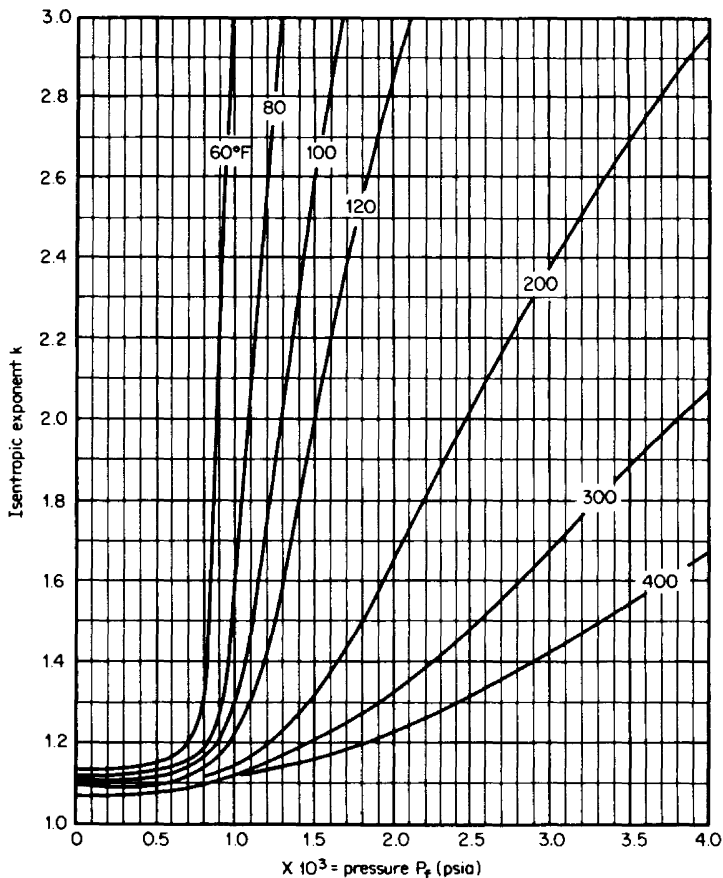


Figure I.13 Isentropic exponent for natural gas: specific gravity $G = 1.0$, $P_{pc} = 652$ psia, $T_{pc} = 486^\circ\text{R}$. (From Schoenthaler, 1966; used with permission.)

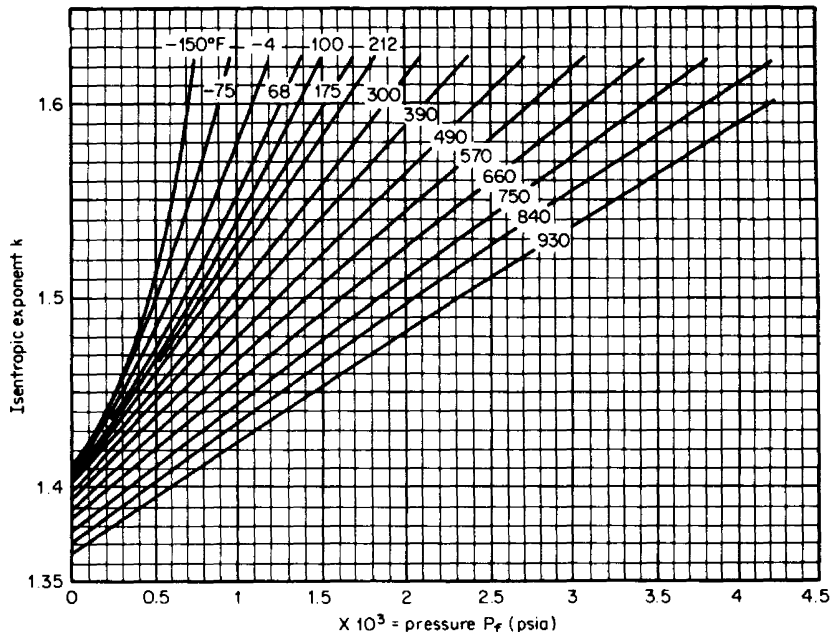


Figure I.14 Isentropic exponent k for nitrogen. (Source: VDI, 1970.)

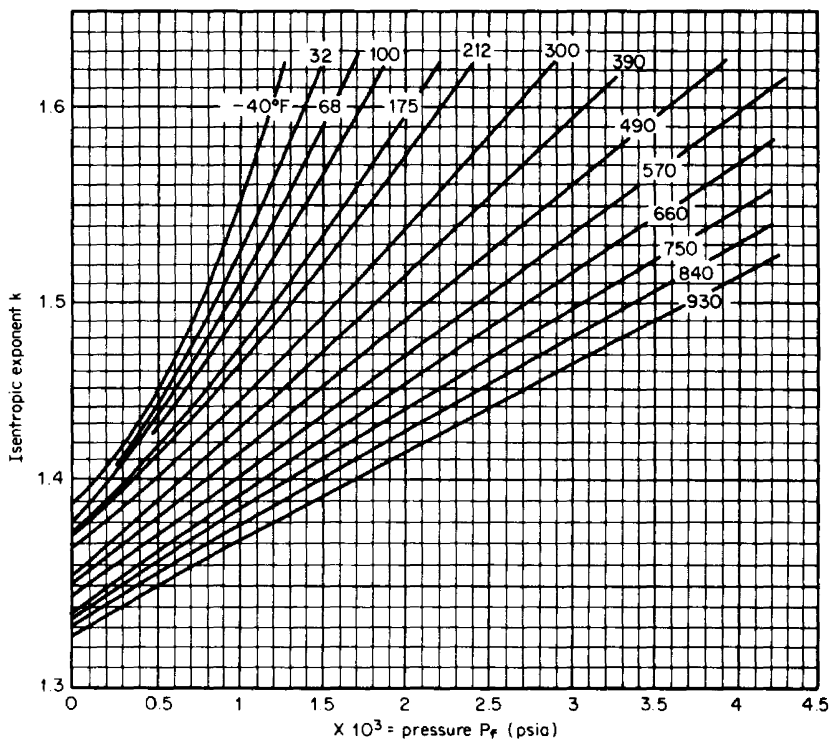


Figure I.15 Isentropic exponent k for oxygen. (Source: VDI, 1970.)

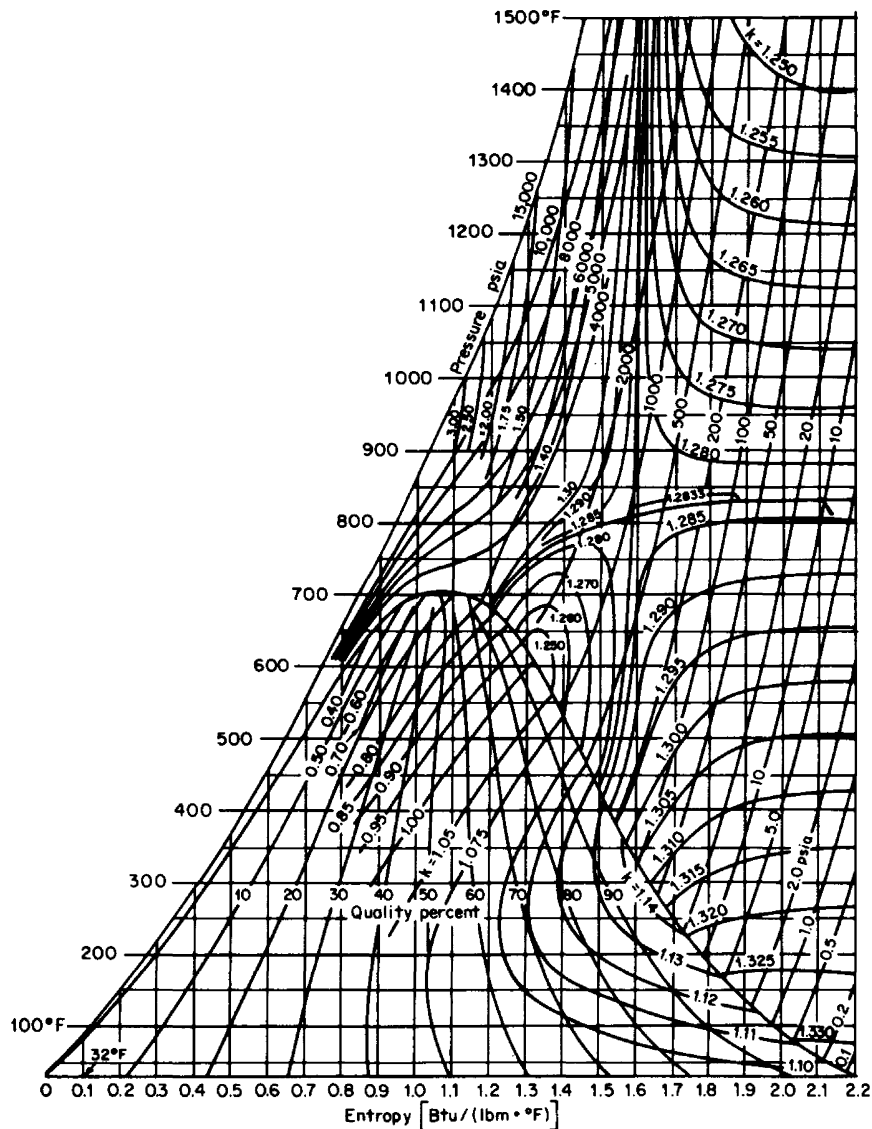


Figure I.16 Isentropic exponent for steam k . (From "ASME Steam Tables," ASME, New York, 1967.)

Specific heat
 C_p [Btu/(lb_m · °F)]

Example: Calculate the ideal isentropic exponent of air at 300°F and 14.7 psia.

Step 1: Find number below. Draw a line from the temperature through the number, and read $C_p = 0.25$. Find $M_w = 28.96$ in Table D.1.

Step 2: Calculate the ideal isentropic exponent, using

$$K_i = \frac{M_w C_p}{M_w C_p - 1.986}$$

$$k_i = \frac{(0.25)(28.96)}{(0.25)(28.96) - 1.986} = 1.38$$

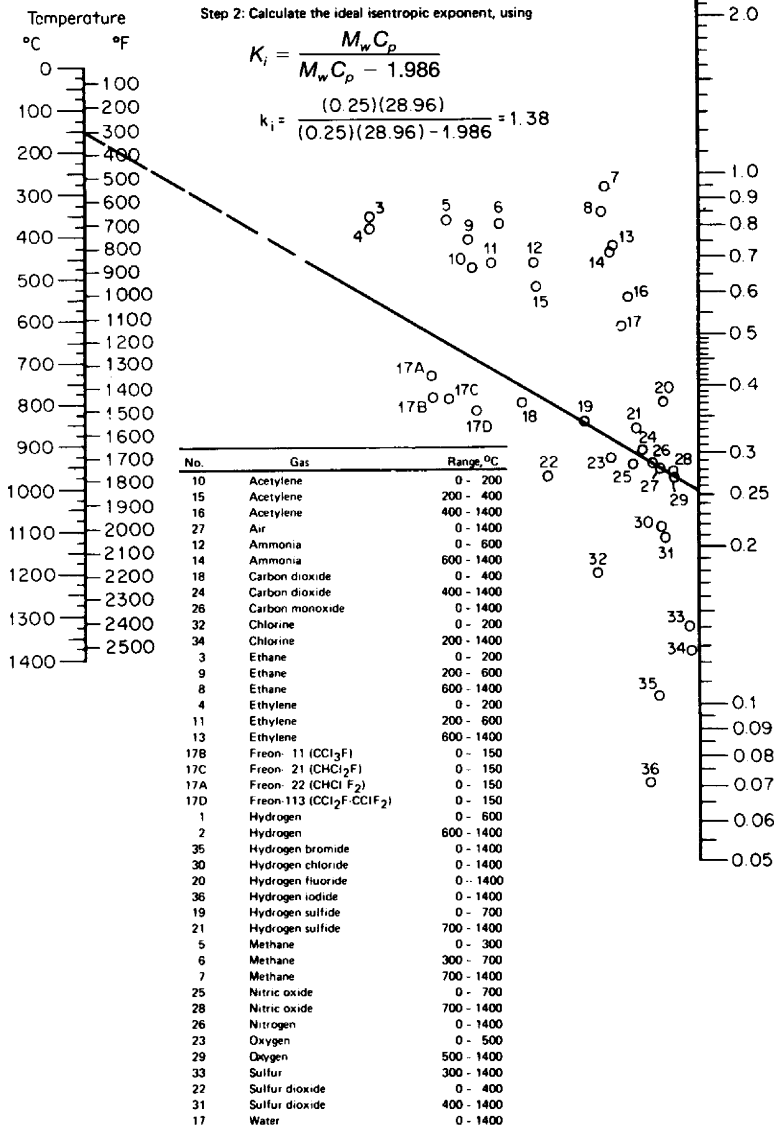


Figure I.17 Specific heats C_p of gases at 1 atm pressure. (From Perry and Green, 1984.)

TABLE I.1 Values of Ideal-Gas State Heat Capacity (C_p), [Btu/(lb_m·mol·°R)] for Paraffins and Olefins

Temperature, °F	Methane, CH ₄	Acetylene, C ₂ H ₂	Ethylene, C ₂ H ₄	Ethane, C ₂ H ₆	Propene, C ₃ H ₆	Propane, C ₃ H ₈	Iso-butane, iC ₄ H ₁₀	i-Butene, iC ₄ H ₈	Iso-butane, iC ₄ H ₁₀	n-Butane, nC ₄ H ₁₀	Iso-pentane, iC ₅ H ₁₂	n-Pentane, nC ₅ H ₁₂	n-Hexane, nC ₆ H ₁₄	n-Heptane, nC ₇ H ₁₆	°F
-100	8.00		8.37	10.2	12.0	13.3	15.8	15.2	17.2	18.3	19.9	20.6	25.1	29.2	-100
-90	8.02		8.42	10.3	12.2	13.6	16.1	15.4	17.5	18.6	20.4	21.1	25.6	29.8	-90
-80	8.04		8.48	10.4	12.4	13.8	16.4	15.6	17.8	18.9	20.9	21.5	26.1	30.4	-80
-70	8.06		8.55	10.5	12.5	14.0	16.7	15.9	18.1	19.2	21.4	22.0	26.6	30.9	-70
-60	8.08		8.54	10.6	12.7	14.2	17.1	16.1	18.4	19.5	21.9	22.5	27.1	31.5	-60
-50	8.09		8.72	10.8	12.9	14.5	17.4	16.4	18.7	19.8	22.3	22.9	27.7	32.1	-50
-40	8.12		8.82	10.9	13.1	14.7	17.7	16.7	19.0	20.1	22.8	23.4	28.2	32.7	-40
-30	8.15		8.93	11.1	13.2	14.9	18.0	17.0	19.4	20.4	23.3	23.8	28.7	33.3	-30
-20	8.17		9.04	11.2	13.4	15.2	18.3	17.3	19.7	20.7	23.8	24.3	29.2	33.9	-20
-10	8.20		9.17	11.3	13.6	15.4	18.6	17.6	20.1	21.0	24.3	24.8	29.7	34.5	-10
0	8.23	9.68	9.32	11.4	13.7	15.6	18.9	18.0	20.4	21.3	24.8	25.2	30.2	35.1	0
10	8.26	9.79	9.46	11.6	13.8	15.9	19.2	18.3	20.7	21.5	25.2	25.7	30.7	35.7	10
20	8.29	9.90	9.60	11.7	14.1	16.1	19.5	18.6	21.1	21.8	25.7	26.2	31.3	36.3	20
30	8.33	10.0	9.74	11.9	14.3	16.4	19.9	19.0	21.5	22.1	26.2	26.6	31.8	36.9	30
40	8.37	10.1	9.88	12.0	14.5	16.6	20.2	19.3	21.8	22.4	26.6	27.0	32.3	37.5	40
50	8.41	10.2	10.0	12.2	14.7	16.9	20.5	19.6	22.2	22.6	27.1	27.5	32.8	38.1	50
60	8.45	10.3	10.2	12.2	14.9	17.1	20.8	19.9	22.5	22.9	27.6	27.9	33.3	38.7	60
70	8.49	10.4	10.3	12.5	15.1	17.4	21.1	20.2	22.9	23.2	28.0	28.4	33.8	39.3	70
80	8.54	10.5	10.4	12.6	15.3	17.6	21.4	20.5	23.2	23.4	28.5	28.8	34.4	39.8	80
90	8.59	10.6	10.6	12.8	15.5	17.9	21.6	20.9	23.6	23.7	28.9	29.3	34.9	40.4	90
100	8.65	10.7	10.7	13.0	15.8	18.2	22.0	21.2	24.0	24.1	29.4	29.7	35.4	41.1	100
110	8.70	10.8	10.9	13.1	16.0	18.4	22.2	21.5	24.3	24.4	29.8	30.1	35.9	41.7	110
120	8.76	10.9	11.0	13.3	16.2	18.7	22.5	21.8	24.7	24.8	30.3	30.6	35.4	42.2	120
130	8.82	11.0	11.1	13.4	16.4	19.0	22.8	22.1	25.0	25.1	30.8	31.0	37.0	42.8	130
140	8.88	11.1	11.3	13.6	16.6	19.2	23.1	22.4	25.4	25.5	31.2	31.5	37.5	43.4	140

150	8.95	11.1	11.4	13.8	16.8	19.5	23.4	22.7	25.8	25.8	31.7	31.9	38.0	44.0	150
160	9.01	11.2	11.5	13.9	17.0	19.8	23.7	23.0	26.1	26.1	32.1	32.3	38.5	44.6	160
170	9.08	11.3	11.7	14.1	17.2	20.1	24.0	23.3	26.5	26.5	32.6	32.7	39.0	45.2	170
180	9.14	11.4	11.8	14.3	17.4	20.4	24.3	23.6	26.9	26.8	33.0	33.2	39.5	45.8	180
190	9.21	11.5	11.9	14.5	17.6	20.6	24.6	24.0	27.2	27.2	33.4	33.6	40.0	46.4	190
200	9.28	11.5	12.1	14.6	17.8	20.9	24.9	24.2	27.6	27.5	33.9	34.0	40.5	46.9	200
210	9.35	11.6	12.2	14.8	18.1	21.2	25.2	24.5	27.9	27.9	34.3	34.5	41.0	47.5	210
220	9.42	11.7	12.4	15.0	18.3	21.4	25.4	24.8	28.3	28.2	34.7	34.9	41.5	48.1	220
230	9.49	11.8	12.5	15.1	18.5	21.7	25.7	25.1	28.7	28.5	35.2	35.3	42.0	48.7	230
240	9.56	11.8	12.6	15.3	18.7	22.0	26.0	25.4	29.0	28.9	35.6	35.7	42.5	49.2	240
250	9.64	11.9	12.8	15.5	18.9	22.2	26.3	25.7	29.4	29.2	36.0	36.1	43.0	49.5	250
260	9.71	12.0	12.9	15.7	19.1	22.5	26.5	26.0	29.7	29.6	36.4	36.5	43.4	50.4	260
270	9.78	12.0	13.0	15.8	19.3	22.8	26.8	26.3	30.1	29.9	36.9	37.0	43.9	50.9	270
280	9.85	12.1	13.1	16.0	19.5	23.0	27.1	26.6	30.4	30.2	37.3	37.4	44.4	51.5	280
290	9.92	12.2	13.3	16.2	19.7	23.3	27.4	26.9	30.8	30.6	37.7	37.7	44.9	52.0	290
300	10.0	12.2	13.4	16.3	19.9	23.6	27.6	27.1	31.1	30.9	38.1	38.2	45.4	52.6	300
310	10.1	12.3	13.5	16.5	20.1	23.8	27.9	27.4	31.5	31.2	38.5	38.6	45.8	53.2	310
320	10.2	12.3	13.7	16.7	20.3	24.1	28.1	27.7	31.8	31.6	38.9	39.0	46.3	53.7	320
330	10.2	12.4	13.8	16.8	20.5	24.3	28.4	28.0	32.1	31.9	39.4	39.4	46.8	54.2	330
340	10.3	12.4	13.9	17.0	20.7	24.6	28.7	28.3	32.5	32.2	39.8	39.8	47.3	54.8	340
350	10.4	12.5	14.0	17.2	20.9	24.8	29.0	29.5	32.8	32.5	40.2	40.2	47.7	55.3	350
360	10.5	12.6	14.2	17.3	21.1	25.1	29.2	28.8	33.1	32.8	40.5	40.5	48.2	55.9	360
370	10.6	12.6	14.3	17.5	21.3	25.3	29.4	29.1	33.4	33.2	40.9	40.9	48.7	56.4	370
380	10.6	12.7	14.4	17.7	21.5	25.6	29.7	29.4	33.7	33.5	41.3	41.3	49.1	56.9	380
390	10.7	12.7	14.5	17.8	21.7	25.8	29.9	29.6	34.0	33.8	41.7	41.7	49.6	57.5	390
400	10.8	12.8	14.7	18.0	21.8	26.0	30.2	29.9	34.4	34.1	42.1	42.1	50.0	58.0	400
410	10.9	12.8	14.8	18.2	22.0	26.3	30.4	30.1	34.7	34.4	42.5	42.4	50.5	58.5	410
420	11.0	12.9	14.9	18.3	22.2	26.5	30.7	30.4	35.0	34.7	42.9	42.8	50.9	59.0	420
430	11.0	12.9	15.0	18.5	22.4	26.8	30.9	30.6	35.3	35.0	43.3	43.2	51.3	59.5	430
440	11.1	13.0	15.2	18.6	22.6	27.0	31.2	30.9	35.6	35.3	43.7	43.6	51.8	60.0	440

TABLE I.1 Values of Ideal-Gas State Heat Capacity (C_p), [Btu/(lb_m·mol·°R)] for Paraffins and Olefins (*Continued*)

Temperature, °F	Methane, CH ₄	Acetylene, C ₂ H ₂	Ethylene, C ₂ H ₄	Ethane, C ₂ H ₆	Propene, C ₃ H ₆	Propane, C ₃ H ₈	Iso-butane, iC ₄ H ₁₀	<i>i</i> -Butene, iC ₄ H ₈	Iso-butane, iC ₄ H ₁₀	<i>n</i> -Butane, nC ₄ H ₁₀	Iso-pentane, iC ₅ H ₁₂	<i>n</i> -Pentane, nC ₅ H ₁₂	<i>n</i> -Hexane, nC ₆ H ₁₄	<i>n</i> -Heptane, nC ₇ H ₁₆	°F
450	11.2	13.0	15.3	18.8	22.8	27.2	31.4	31.2	35.9	35.6	44.0	43.9	52.2	60.5	450
460	11.3	13.1	15.4	19.0	23.0	27.5	31.7	31.4	36.2	35.9	44.4	44.3	52.7	61.0	460
470	11.4	13.1	15.5	19.1	23.1	27.7	31.9	31.6	36.5	36.2	44.7	44.6	53.1	61.5	470
480	11.4	13.1	15.6	19.3	23.3	27.9	32.2	31.9	36.8	36.5	45.1	45.0	53.5	61.9	480
490	11.5	13.2	15.7	19.4	23.5	28.1	32.4	32.2	37.1	36.8	45.5	45.3	53.9	62.4	490
500	11.6	13.2	15.8	19.6	23.7	28.4	32.6	32.4	37.3	37.1	45.8	45.7	54.3	62.9	500
510	11.7	13.3	16.0	19.7	23.8	28.6	32.9	32.6	37.6	37.4	46.2	46.0	54.7	63.4	510
520	11.8	13.3	16.0	19.9	24.0	28.8	33.1	32.8	37.9	37.6	46.5	46.3	55.1	63.8	520
530	11.8	13.4	16.2	20.0	24.2	29.0	33.3	33.1	38.2	37.9	46.8	46.7	55.5	64.3	530
540	11.9	13.4	16.3	20.2	24.4	29.2	33.5	33.3	38.5	38.2	47.2	47.0	55.9	64.7	540
550	12.0	13.4	16.4	20.3	24.5	29.4	33.8	33.5	38.8	38.5	47.5	47.4	56.3	65.2	550
560	12.1	13.5	16.5	20.5	24.7	29.6	34.0	33.8	39.0	38.7	47.9	47.7	56.7	65.6	560
570	12.2	13.5	16.6	20.6	24.9	29.8	34.2	34.0	39.3	39.0	48.2	48.0	57.1	66.1	570
580	12.2	13.6	16.7	20.8	25.0	30.0	34.4	34.2	39.5	39.3	48.5	48.3	57.5	66.5	580
590	12.3	13.6	16.8	20.9	25.2	30.3	34.6	34.4	39.8	39.5	48.9	48.7	57.9	67.0	590
600	12.4	13.6	16.9	21.0	25.4	30.5	34.9	34.7	40.1	39.8	49.2	49.0	58.2	67.4	600
610	12.5	13.7	17.0	21.2	25.5	30.6	35.1	34.9	40.3	40.0	49.5	49.3	58.6	67.8	610
620	12.5	13.7	17.1	21.3	25.7	30.8	35.3	35.1	40.6	40.3	49.9	49.6	59.0	68.3	620
630	12.6	13.8	17.2	21.5	25.9	31.0	35.5	35.3	40.8	40.5	50.2	49.9	59.3	68.7	630
640	12.7	13.8	17.3	21.6	26.0	31.2	35.7	35.5	41.1	40.7	50.5	50.2	59.7	69.1	640
650	12.8	13.8	17.4	21.7	26.2	31.4	35.9	35.7	41.3	41.0	50.8	50.5	60.0	69.5	650
660	12.8	13.9	17.5	21.9	26.3	31.6	36.1	35.9	41.6	41.2	51.1	50.8	60.4	69.9	660
670	12.9	13.9	17.6	22.0	26.5	31.8	36.3	36.2	41.8	41.5	51.4	51.1	60.8	70.3	670
680	13.0	13.9	17.7	22.2	26.6	32.0	36.5	36.4	42.1	41.7	51.7	51.4	61.1	70.7	680
690	13.1	14.0	17.8	22.3	26.8	32.2	36.7	36.5	42.3	42.0	52.0	51.7	61.5	71.1	690

700	13.1	14.0	17.9	22.4	26.9	32.4	36.9	36.8	42.6	42.2	52.3	52.0	61.8	71.5	700
710	13.2	14.0	18.0	22.6	27.1	32.6	37.1	37.0	42.8	42.4	52.6	52.3	62.1	71.9	710
720	13.3	14.1	18.0	22.7	27.2	32.8	37.3	37.2	43.0	42.7	52.9	52.6	62.5	72.3	720
730	13.4	14.1	18.1	22.8	27.4	32.9	37.5	37.4	43.2	42.9	53.2	52.9	62.8	72.7	730
740	13.4	14.2	18.2	23.0	27.5	33.1	37.7	37.5	43.5	43.2	53.5	53.2	63.1	73.1	740
750	13.5	14.2	18.3	23.1	27.6	33.3	37.8	37.7	43.7	43.4	53.8	53.4	63.5	73.5	750
760	13.6	14.2	18.4	23.2	27.8	33.5	38.0	37.9	43.9	43.6	54.0	53.7	63.8	73.9	760
770	13.7	14.3	18.5	23.3	27.9	33.6	38.2	38.1	44.2	43.8	54.3	54.0	64.1	74.2	770
780	13.7	14.3	18.6	23.5	28.1	33.8	38.4	38.3	44.4	44.0	54.6	54.3	64.4	74.6	780
790	13.8	14.3	18.7	23.6	28.2	34.0	38.6	38.5	44.6	44.3	54.9	54.5	64.7	75.0	790
800	13.9	14.4	18.7	23.7	28.4	34.2	38.8	38.7	44.8	44.5	55.2	54.8	65.1	75.3	800
810	13.9	14.4	18.8	23.8	28.5	34.3	39.0	38.9	45.0	44.7	55.4	55.1	65.4	75.7	810
820	14.0	14.4	18.9	23.9	28.6	34.5	39.1	39.1	45.2	45.0	55.7	55.3	65.7	76.0	820
830	14.1	14.4	19.0	24.1	28.8	34.7	39.3	39.2	45.5	45.2	55.9	55.6	66.0	76.4	830
840	14.1	14.5	19.1	24.2	28.9	34.8	39.5	39.4	45.7	45.4	56.2	55.8	66.3	76.7	840
850	14.2	14.5	19.2	24.3	29.0	35.0	39.7	39.6	45.9	45.6	56.4	56.1	66.6	77.1	850
860	14.3	14.6	19.2	24.4	29.2	35.2	39.8	39.8	46.1	45.8	56.7	56.3	66.9	77.4	860
870	14.4	14.6	19.3	24.6	29.3	35.3	40.0	39.9	45.3	46.0	57.0	56.6	67.2	77.8	870
880	14.4	14.6	19.4	24.7	29.4	35.5	40.2	40.1	46.5	46.2	57.2	56.9	67.5	78.1	880
890	14.5	14.6	19.5	24.8	29.5	36.7	40.4	40.3	46.7	46.4	57.5	57.1	67.8	78.5	890

SOURCE: Edmister (1961). Copyright 1961 by Gulf Publishing Company, Houston, Texas; all rights reserved. Used with permission.

TABLE I.2 Values of Ideal-Gas State Heat Capacity (C_p)_i [Btu/(lb_m·mol·°R)] for Miscellaneous Compounds

Temperature, °F	Hydrogen, H ₂	Nitrogen, N ₂	Oxygen, O ₂	Carbon monoxide, CO	Carbon dioxide, CO ₂	Water, H ₂ O	Hydrogen sulfide, H ₂ S	Sulfur dioxide, SO ₂	Sulfur trioxide, SO ₃	°F
-200	6.35	6.95	6.95	6.95	7.20		7.88	8.10	9.00	-200
-190	6.34	6.95	6.95	6.95	7.25		7.88	8.14	9.11	-190
-180	6.35	6.95	6.95	6.95	7.28		7.90	8.20	9.22	-180
-170	6.36	6.95	6.95	6.95	7.32		7.90	8.24	9.33	-170
-160	6.39	6.95	6.95	6.95	7.37		7.91	8.30	9.45	-160
-150	6.42	6.95	6.95	6.95	7.42		7.92	8.35	9.56	-150
-140	6.44	6.95	6.95	6.95	7.47		7.93	8.40	9.67	-140
-130	6.47	6.95	6.95	6.95	7.53		7.94	8.45	9.77	-130
-120	6.50	6.95	6.96	6.95	7.59		7.95	8.50	9.90	-120
-110	6.53	6.95	6.96	6.95	7.65		7.96	8.56	10.0	-110
-100	6.56	6.95	6.96	6.95	7.71		7.97	8.61	10.1	-100
-90	6.58	6.95	6.96	6.95	7.78		7.98	8.56	10.2	-90
-80	6.61	6.95	6.96	6.95	7.84		7.99	8.71	10.3	-80
-70	6.63	6.95	6.95	6.95	7.90		8.00	8.76	10.4	-70
-60	6.66	6.95	6.96	6.95	7.97		8.02	8.81	10.6	-60
-50	6.68	6.95	6.96	6.95	8.03		8.03	8.87	10.7	-50
-40	6.70	6.95	6.97	6.95	8.11		8.04	8.91	10.8	-40
-30	6.72	6.95	6.97	6.95	8.18		8.05	8.97	10.9	-30
-20	6.75	6.95	6.97	6.95	8.25		8.06	9.01	11.0	-20
-10	6.77	6.95	6.97	6.95	8.33		8.08	9.06	11.1	-10
0	6.78	6.95	6.98	6.95	8.38	7.98	8.09	9.12	11.2	0
10	6.80	6.95	6.98	6.95	8.45	7.99	8.10	9.18	11.3	10
20	6.82	6.95	6.98	6.95	8.51	7.99	8.12	9.23	11.4	20
30	6.83	6.95	6.99	6.96	8.58	8.00	8.13	9.28	11.6	30
40	6.85	6.95	6.99	6.96	8.65	8.00	8.15	9.33	11.7	40

50	6.86	6.95	7.00	6.96	8.70	8.00	8.16	9.38	11.8	50
60	6.87	6.95	7.00	6.96	8.76	8.01	8.17	9.43	11.9	60
70	6.88	6.95	7.01	6.96	8.83	8.02	8.19	9.48	12.0	70
80	6.89	6.96	7.02	6.96	8.89	8.02	8.20	9.53	12.1	80
90	6.90	6.96	7.02	6.96	8.95	8.03	8.22	9.59	12.2	90
100	6.90	6.96	7.03	6.96	9.01	8.03	8.24	9.64	12.3	100
110	6.91	6.96	7.03	6.96	9.06	8.04	8.25	9.69	12.4	110
120	6.92	6.96	7.04	6.97	9.12	8.05	8.27	9.74	12.6	120
130	6.92	6.96	7.05	6.97	9.19	8.06	8.28	9.79	12.7	130
140	6.93	6.96	7.06	6.97	9.24	8.06	8.30	9.84	12.8	140
150	6.93	6.96	7.07	6.97	9.30	8.07	8.32	9.89	12.9	150
160	6.94	6.96	7.08	6.97	9.35	8.08	8.34	9.94	13.0	160
170	6.94	6.96	7.09	6.98	9.40	8.09	8.36	9.98	13.1	170
180	6.94	6.96	7.10	6.98	9.46	8.10	8.38	10.0	13.2	180
190	6.95	6.96	7.11	6.98	9.51	8.11	8.39	10.1	13.3	190
200	6.95	6.97	7.12	6.98	9.57	8.12	8.41	10.1	13.4	200
210	6.96	6.97	7.13	6.99	9.62	8.13	8.43	10.2	13.5	210
220	6.96	6.97	7.14	6.99	9.66	8.14	8.45	10.2	13.6	220
230	6.96	6.98	7.15	7.00	9.72	8.15	8.47	10.2	13.7	230
240	6.97	6.98	7.16	7.00	9.77	8.16	8.49	10.3	13.8	240
250	6.97	6.98	7.18	7.00	9.82	8.17	8.51	10.4	13.9	250
260	6.97	6.99	7.19	7.01	9.86	8.18	8.53	10.4	14.0	260
270	6.97	6.99	7.20	7.01	9.91	8.19	8.55	10.4	14.1	270
280	6.97	6.99	7.21	7.02	9.96	8.20	8.57	10.5	14.2	280
290	6.98	6.99	7.22	7.02	10.0	8.22	8.59	10.5	14.3	290

TABLE I.2 Values of Ideal-Gas State Heat Capacity (C_p), [Btu/(lb_m·mol·°R)] for Miscellaneous Compounds (*Continued*)

Temperature, °F	Hydrogen, H ₂	Nitrogen, N ₂	Oxygen, O ₂	Carbon monoxide, CO	Carbon dioxide, CO ₂	Water, H ₂ O	Hydrogen sulfide, H ₂ S	Sulfur dioxide, SO ₂	Sulfur trioxide, SO ₃	°F
300	6.98	7.00	7.24	7.03	10.1	8.23	8.62	10.6	14.4	300
310	6.98	7.00	7.25	7.03	10.1	8.24	8.64	10.6	14.5	310
320	6.98	7.01	7.26	7.04	10.2	8.25	8.66	10.6	14.6	320
330	6.98	7.01	7.28	7.04	10.2	8.26	8.68	10.7	14.7	330
340	6.98	7.02	7.29	7.05	10.2	8.28	8.70	10.7	14.8	340
350	6.98	7.02	7.30	7.05	10.3	8.29	8.72	10.8	14.9	350
360	6.98	7.02	7.32	7.05	10.3	8.30	8.75	10.8	15.0	360
370	6.98	7.02	7.33	7.07	10.4	8.31	8.77	10.8	15.1	370
380	6.98	7.03	7.34	7.07	10.4	8.33	8.79	10.9	15.2	380
390	6.99	7.04	7.36	7.08	10.4	8.34	8.82	10.9	15.2	390
400	6.99	7.05	7.37	7.09	10.5	8.35	8.84	11.0	15.3	400
410	6.99	7.05	7.38	7.09	10.5	8.37	8.87	11.0	15.4	410
420	6.99	7.05	7.40	7.10	10.6	8.38	8.89	11.0	15.5	420
430	6.99	7.06	7.41	7.11	10.6	8.40	8.91	11.1	15.6	430
440	6.99	7.07	7.42	7.12	10.6	8.41	8.93	11.1	15.7	440
450	6.99	7.07	7.44	7.12	10.7	8.42	8.96	11.2	15.7	450
460	6.99	7.08	7.45	7.13	10.7	8.44	8.98	11.2	15.8	460
470	6.99	7.08	7.46	7.14	10.8	8.45	9.00	11.2	15.9	470
480	6.99	7.09	7.48	7.15	10.8	8.46	9.02	11.3	16.0	480
490	6.99	7.10	7.49	7.15	10.8	8.48	9.05	11.3	16.0	490

500	6.99	7.10	7.50	7.16	10.9	8.49	9.07	11.3	16.1	500
510	7.00	7.11	7.52	7.17	10.9	8.51	9.09	11.4	16.2	510
520	7.00	7.11	7.53	7.18	11.0	8.52	9.12	11.4	16.2	520
530	7.00	7.12	7.54	7.19	11.0	8.54	9.14	11.4	16.3	530
540	7.00	7.13	7.56	7.20	11.0	8.55	9.16	11.5	16.4	540
550	7.00	7.14	7.57	7.20	11.1	8.57	9.19	11.5	16.4	550
560	7.00	7.15	7.59	7.21	11.1	8.58	9.21	11.5	16.5	560
570	7.00	7.16	7.60	7.22	11.2	8.60	9.24	11.6	16.6	570
580	7.00	7.16	7.61	7.23	11.2	8.61	9.26	11.6	16.6	580
590	7.00	7.17	7.62	7.24	11.2	8.62	9.28	11.6	16.7	590
600	7.00	7.18	7.64	7.25	11.2	8.64	9.30	11.6	16.8	600
610	7.00	7.19	7.65	7.26	11.3	8.66	9.32	11.7	16.8	610
620	7.00	7.19	7.66	7.27	11.3	8.67	9.35	11.7	16.9	620
630	7.01	7.20	7.68	7.28	11.4	8.69	9.38	11.7	17.0	630
640	7.01	7.20	7.69	7.29	11.4	8.70	9.40	11.8	17.0	640
650	7.01	7.21	7.70	7.30	11.4	8.72	9.42	11.8	17.1	650
660	7.01	7.22	7.71	7.31	11.4	8.73	9.44	11.8	17.1	660
670	7.01	7.23	7.73	7.32	11.5	8.75	9.47	11.8	17.2	670
680	7.01	7.24	7.74	7.33	11.5	8.76	9.49	11.9	17.2	680
690	7.01	7.25	7.75	7.34	11.5	8.78	9.52	11.9	17.3	690

source: Edmister (1961). Copyright 1961 by Gulf Publishing Company, Houston, Texas; all rights reserved. Used with permission.

TABLE 1.3 Specific-Heat Equation for Ideal Gases at 1 Atmosphere†

Gas	Symbol	Equation for C_p , Btu/(lb _m ·mol·°R)	Temperature range, °R
Oxygen	O ₂	$11.515 - \frac{172}{\sqrt{T}} + \frac{1530}{T}$	540–5000
		$11.515 - \frac{172}{\sqrt{T}} + \frac{1530}{T} + \frac{0.05(T - 4000)}{1000}$	5000–9000
Nitrogen	N ₂	$9.47 - \frac{3.47 \times 10^3}{T} + \frac{1.16 \times 10^6}{T^2}$	540–5000
Carbon monoxide	CO	$9.46 - \frac{3.29 \times 10^3}{T} + \frac{1.07 \times 10^6}{T^2}$	540–5000
Hydrogen	H ₂	$5.76 + \frac{0.578T}{1000} + \frac{20}{\sqrt{T}}$	540–4000
		$5.76 + \frac{0.578T}{1000} + \frac{20}{\sqrt{T}} - \frac{0.33(T - 4000)}{1000}$	4000–9000
Water	H ₂ O	$19.86 - \frac{597}{\sqrt{T}} + \frac{7500}{T}$	540–5000
Carbon dioxide	CO ₂	$16.2 - \frac{6.53 \times 10^3}{T} + \frac{1.41 \times 10^6}{T^2}$	540–6300
Methane	CH ₄	$4.22 + 8.211 \times 10^{-3}T$	492–1800
		$27.0 - \frac{14.400}{T}$	1800–5940
Ethylene	C ₂ H ₄	$6.0 + 8.33 \times 10^{-3}T$	720–1400
Ethane	C ₂ H ₆	$6.6 + 13.33 \times 10^{-3}T$	720–1440
Ethyl alcohol	C ₂ H ₆ O	$4.5 + 21.1 \times 10^{-3}T$	680–1120
Methyl alcohol	CH ₄ O	$2.0 + 16.67 \times 10^{-3}T$	680–1100
Benzene	C ₆ H ₆	$6.5 + 28.9 \times 10^{-3}T$	520–1120
Octane	C ₈ H ₁₈	$14.4 + 53.3 \times 10^{-3}T$	720–1440
Dodecane	C ₁₂ H ₂₆	$19.6 + 80.0 \times 10^{-3}T$	720–1440

† The T in this table from Baumeister is the same as T_f used throughout this handbook.

SOURCE: Baumeister (1988).

"Anyone involved in the selection or operation of flowmeters should have access to this book."

—Applied Mechanics Review

Through two previous editions, thousands of international engineers have turned to this handbook for reliable and complete information on the selection, design, specification, and installation of flowmeters to measure liquid, gas, and steam flows within all engineering applications.

Now the Third Edition brings you completely up to date, with new and expanded coverage of:

- The latest ISO, ASME, and ANSI-related standards—including guidelines for implementing them in your designs and installations
- Meter influence quantities for all flowmeters
- Widely used flowmeters around the world, including thermal mass, GILFLO, "V" Cone, wedge flowmeter, Laminar Flow elements, and pitot tubes
- The latest proposed orifice and nozzle equations, complete with examples

As practical as it is authoritative, this handbook serves as a single-source guide for selecting, sizing, and performing pipe flow rate calculations. It features both customary and SI equations throughout ... complete coverage of fluid properties and equations of state ... key information on seven-place equation constants and simplifying equations ... and includes many examples, graphs, tables, and practical applications to aid in decision making, improve job performance, and save time and expense.

This comprehensive reference covers everything from industry-wide standards and practices, to specific descriptions and examples, to physical property data and installation requirements. As a result, the new edition remains the standard reference in the field and is the *only* guide to flowmeter engineering that you'll ever need.

Cover Design: Kay Wannous
Cover Photo: SuperStock, Inc.



McGraw-Hill
1221 Avenue of the Americas
New York, NY 10020

